DTIC FILE COPY

(2)

DNA EM-1
PART II

DEFENSE NUCLEAR AGENCY EFFECTS MANUAL NUMBER 1

CAPABILITIES OF NUCLEAR WEAPONS

1 JULY 1972

Document released under the Freedom of Information Act, DNA Case No. 86-113

HEADQUARTERS
Defense Nuclear Agency
Washington, D.C. 20305

DTIC ELECTE S D
2 MAR 1989
E

AD-A955 385

This document has been approved for public release and sale; its distribution is unlimited.

89 3 02 026

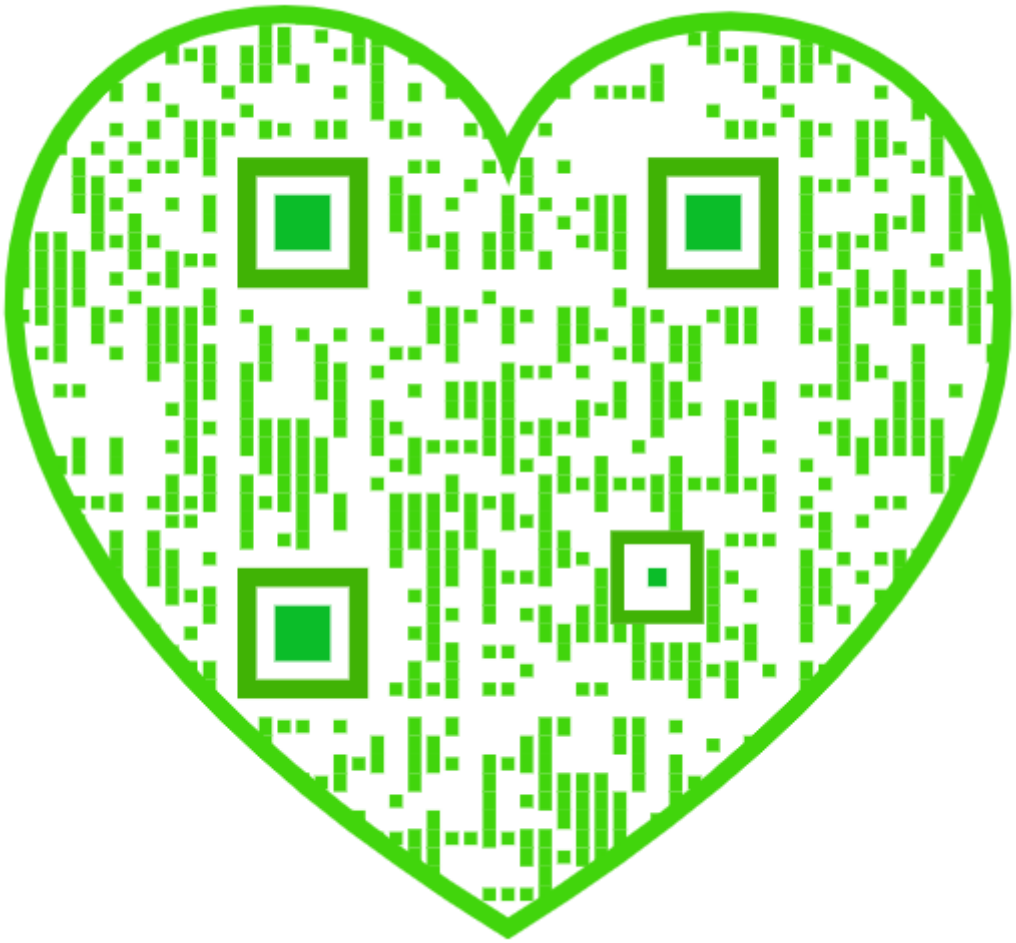

DNA EM-1
PART II
1 JULY 1972

DEFENSE NUCLEAR AGENCY EFFECTS MANUAL NUMBER 1

CAPABILITIES OF NUCLEAR WEAPONS

PART II
DAMAGE CRITERIA

HEADQUARTERS
Defense Nuclear Agency
Washington, D.C. 20305

EDITOR
PHILIP J. DOLAN
STANFORD RESEARCH INSTITUTE

QUALITY INSPECTED 4

UNANNOUNCED

Accession For
NTIS GRA&I
DTIC TAB
Unannounced
Justification
By
Distribution/
Availability Codes
Dist | Avail and/or Special
A-1

DNA EM-1
PART II
CHANGE 1
1 JULY 1978

DEFENSE NUCLEAR AGENCY EFFECTS MANUAL NUMBER 1

CAPABILITIES OF NUCLEAR WEAPONS

PART II
DAMAGE CRITERIA

HEADQUARTERS
Defense Nuclear Agency
Washington, D.C. 20305

EDITOR
PHILIP J. DOLAN
SRI INTERNATIONAL

LIST OF EFFECTIVE PAGES

The following is a list of current pages for Part II, *Damage Criteria*, of DNA Effects Manual Number 1 (DNA EM-1), *Capabilities of Nuclear Weapons*. When applicable, insert latest change pages; dispose of superceded pages in accordance with applicable regulations.

Total number of pages in this part of the Handbook is consisting of the following:

i through ii ..... change 1
iii through xlvi ..... original
9-1 through 9-188 ..... original
10-1 through 10-38 ..... original
11-1 through 11-148 ..... original
12-1 through 12-32 ..... original
13-1 through 13-88 ..... original
14-1 through 14-76 ..... original
15-1 through 15-64 ..... original
16-1 through 16-122 ..... original
17-1 through 17-40 ..... original
A-1 through A-18 ..... original
B-1 through B-8 ..... original
C-1 through C-16 ..... original
D-1 through D-16 ..... change 1
E-1 through E-20 ..... original
F-1 through F-34 ..... original

[redacted]

DNA EM-1

HEADQUARTERS
DEFENSE NUCLEAR AGENCY
WASHINGTON, D.C. 20305

1 July 1972

EFFECTS MANUAL NUMBER 1

CAPABILITIES OF NUCLEAR WEAPONS [redacted]

The Revised Edition January 1968, *Capabilities of Nuclear Weapons* [redacted], DASA EM-1 is hereby superseded and cancelled.

With the concurrence of the Military Services, this document was redesignated DASA Effects Manual Number 1 (DASA EM-1) by action of the Joint Chiefs of Staff on 8 July 1966. With the change of the Defense Atomic Support Agency to the Defense Nuclear Agency on 1 July 1971, this document was redesignated the DNA Effects Manual Number 1 (DNA EM-1). Publication and initial distribution of future changes and revisions of this document will be effected by the Defense Nuclear Agency.

FOR THE DIRECTOR:

John A. Northrop

JOHN A. NORTHROP
Deputy Director (Science & Technology)

[redacted]

[redacted]

FOREWORD

This edition of the *Capabilities of Nuclear Weapons* represents the continuing efforts by the Defense Nuclear Agency to correlate and make available nuclear weapons effects information obtained from nuclear weapons testing, small-scale experiments, laboratory effort and theoretical analysis. This document presents the phenomena and effects of a nuclear detonation and relates weapons effects manifestations in terms of damage to targets of military interest. It provides the source material and references needed for the preparation of operational and employment manuals by the Military Services.

The *Capabilities of Nuclear Weapons* is not intended to be used as an employment or design manual by itself, since more complete descriptions of phenomenological details should be obtained from the noted references. Every effort has been made to include the most current reliable data available on 31 December 1971 in order to assist the Armed Forces in meeting their particular requirements for operational and target analysis purposes.

Comments concerning this manual are invited and should be addressed:

Director
Defense Nuclear Agency
ATTN: STAP
Washington, D. C. 20305

C. H. DUNN
Lt General, USA
Director

[redacted]

TABLE OF CONTENTS

PART I PHENOMENOLOGY

CHAPTER 1 INTRODUCTION

	Page
PURPOSE	1-1
CHARACTERISTICS OF NUCLEAR EXPLOSIONS	1-1
AIR BURST	1-7
THE SURFACE BURST	1-12
THE TRANSITION ZONE BETWEEN AN AIR BURST AND A SURFACE BURST	1-14
THE HIGH-ALTITUDE BURST	1-15
THE UNDERGROUND BURST	1-20
THE UNDERWATER BURST	1-23

CHAPTER 2 BLAST AND SHOCK PHENOMENA

INTRODUCTION	2-1
SECTION I AIR BLAST PHENOMENA	2-1
RELIABILITY	2-2
BLAST-WAVE CALCULATIONS IN FREE AIR	2-4
RELATIONS BETWEEN SHOCK FRONT PARAMETERS	2-21
BLAST-WAVE PHENOMENA AT THE SURFACE	2-38
BLAST-WAVE CALCULATIONS AT THE SURFACE	2-45
THE BLAST WAVE AT HIGH ALTITUDES	2-125
WEAPONS WITH ENHANCED OUTPUTS	2-138
SECTION II CRATERING PHENOMENA	2-147
PREDICTION OF CRATER DIMENSIONS	2-152
EJECTA	2-168
CHARGE STEMMING	2-173
EFFECTS OF GEOLOGICAL FACTORS	2-174
MULTIPLE BURST GEOMETRIES	2-174
SECTION III GROUND SHOCK PHENOMENA	2-176

[redacted]

TABLE OF CONTENTS (Continued)

CHAPTER 2 BLAST AND SHOCK PHENOMENA [redacted] (Continued)

		Page
SECTION IV	UNDERWATER EXPLOSION PHENOMENA	2-193
	WATER SHOCK WAVE AND OTHER PRESSURE PULSES	2-197
	SURFACE EFFECTS OTHER THAN WAVES	2-203
	WATER SURFACE WAVES	2-216
	UNDERWATER CRATERING	2-223

CHAPTER 3 THERMAL RADIATION PHENOMENA [redacted]

	RADIANT EXPOSURE	3-1
	TRANSMITTANCE	3-5
	APPROXIMATE CALCULATIONS OF RADIANT EXPOSURE	3-37
	SURFACE AND SUBSURFACE BURSTS	3-42
	THE THERMAL PULSE	3-46
	FIREBALL BRIGHTNESS	3-55
	THE THERMAL PULSE FROM SPECIAL WEAPONS	3-56
	HIGH ALTITUDE THERMAL PHENOMENA	3-63
	RELIABILITY OF THERMAL SOURCE DATA	3-72
	RELATION OF RADIANT EXPOSURE TO PEAK OVERPRESSURE	3-74
	PHYSICS OF FIREBALL DEVELOPMENT	3-104

CHAPTER 4 X-RAY RADIATION PHENOMENA [redacted]

	INTRODUCTION	4-1
SECTION I	NUCLEAR WEAPONS AS X-RAY SOURCES	4-9
SECTION II	X-RAY ENVIRONMENTS PRODUCED BY NUCLEAR WEAPONS	4-25

CHAPTER 5 NUCLEAR RADIATION PHENOMENA [redacted]

	INTRODUCTION	5-1
SECTION I	INITIAL NUCLEAR RADIATION	5-1

[redacted]

[redacted]

TABLE OF CONTENTS (Continued)

CHAPTER 5 NUCLEAR RADIATION PHENOMENA [redacted] (Continued)

	Page
NEUTRONS	5-2
GAMMA RAYS	5-17
INITIAL RADIATION DOSE TO PERSONNEL	5-24
SECTION II NEUTRON-INDUCED ACTIVITY IN SOILS	5-52
SECTION III RESIDUAL RADIATION	5-65
FALLOUT	5-65
RESIDUAL RADIATION FROM WATER SURFACE AND UNDERWATER BURSTS	5-104
DOSE RECEIVED WHILE FLYING THROUGH A NUCLEAR CLOUD	5-139
PRECIPITATION EFFECTS	5-145

CHAPTER 6 TRANSIENT RADIATION EFFECTS ON ELECTRONICS (TREE) PHENOMENA [redacted]

INTRODUCTION	6-1
ENVIRONMENT	6-3
INTERACTIONS BASIC TO TREE	6-6
MANIFESTATIONS OF TREE IN MATERIALS	6-10

CHAPTER 7 ELECTROMAGNETIC PULSE (EMP) PHENOMENA [redacted]

ENVIRONMENT – GENERAL DESCRIPTION	7-1
ELECTROMAGNETIC FIELD GENERATION	7-5
INTERNAL EMP	7-15
COMPUTER CODE DESCRIPTIONS	7-17
SYSTEMS EFFECTS	7-18

CHAPTER 8 PHENOMENA AFFECTING ELECTROMAGNETIC WAVE PROPAGATION [redacted]

INTRODUCTION	8-1

[redacted]

[redacted]

TABLE OF CONTENTS (Continued)

CHAPTER 8 PHENOMENA AFFECTING ELECTROMAGNETIC WAVE PROPAGATION [redacted] (Continued)

		Page
SECTION I	PHENOMENA AFFECTING RADIO FREQUENCIES	8-2
	IONIZATION AND DEIONIZATION	8-2
	TRAVELING DISTURBANCES IN E AND F REGIONS OF IONOSPHERE	8-15
	ELECTROMAGNETIC RADIATIONS	8-16
	ABSORPTION	8-16
	PHASE CHANGES	8-20
SECTION II	METHODS FOR CALCULATING ABSORPTION OF RADIO FREQUENCIES	8-23

PART II DAMAGE CRITERIA

CHAPTER 9 INTRODUCTION TO DAMAGE CRITERIA [redacted]

SECTION I	CONTENT AND LIMITATIONS OF PART II	9-1
9-1	Introduction to Chapter 9	9-1
9-2	Organization of Part II	9-1
9-3	Limitations in Part II	9-2
SECTION II	BLAST AND SHOCK DAMAGE	9-2
	LOADING	9-3
9-4	Air Blast Loading in the Mach Reflection Region	9-3
9-5	Qualitative Examples of Net Loading	9-4
9-6	Regular and Mach Reflection	9-10
9-7	Target Motion	9-10
9-8	Nonideal Waveforms	9-10
9-9	Underwater Shock Wave Loading	9-10
9-10	Ground Shock Loading	9-11
	RESPONSE AND DAMAGE	9-11
9-11	Surface Structures	9-11
9-12	Shielded Structures	9-13
9-13	Aircraft	9-13
SECTION III	THERMAL RADIATION DAMAGE	9-13
	INTRODUCTION	9-13
9-14	Radiant Exposure	9-14
9-15	Thermal Pulse Duration	9-14

[redacted]

[redacted]

TABLE OF CONTENTS (Continued)

CHAPTER 9 INTRODUCTION TO DAMAGE CRITERIA [redacted] (Continued)

	Page
9-16 Target Response	9-14
9-17 Target Orientation	9-15
9-18 Shielding	9-15
THERMAL RESPONSE OF MATERIALS	9-15
9-19 Thickness Effects	9-16
9-20 Color	9-22
9-21 Transparency	9-23
9-22 Effect of Humidity	9-23
9-23 Response of Metal Sheets	9-25
9-24 Thermal Damage to Various Materials	9-25
SURVIVAL IN FIRE AREAS	9-28
9-25 Causes of Death	9-28
9-26 Shelters	9-29
9-27 Escape from the Fire Areas	9-30
9-28 Safe Areas Within the Fire	9-31
SECTION IV THERMAL RADIATION DEGRADATION OF STRUCTURAL RESISTANCE TO AIR BLAST	9-31
THERMAL ENERGY ABSORBED	9-32
9-29 Absorption	9-32
9-30 Energy Losses	9-35
CHANGES IN MATERIAL STATE AND MATERIALS PROPERTIES	9-38
9-31 Changes in Material State	9-38
9-32 Change in Materials Properties	9-46
RESISTANCE TO LOAD	9-63
SECTION V X-RAY DAMAGE EFFECTS	9-67
INTRODUCTION	9-67
X-RAY ENERGY DEPOSITION CALCULATIONS	9-68
9-33 X-ray Cross Sections	9-68
9-34 X-ray Energy Deposition and Shine Through Fluences	9-69
9-35 X-ray Energy Deposition Summary	9-93
INITIAL PRESSURIZATION OF MATERIALS DUE TO X-RAY DEPOSITION	9-93
9-36 Phase Changes Induced by X-ray Heating	9-93
9-37 The Gruneisen Parameter and the Equation of State	9-101
SHOCK WAVE PROPAGATION AND DAMAGE PREDICTIONS	9-103
9-38 Through-the-Thickness Elastic-Plastic Shock Propagation	9-105

[redacted]

[redacted]

TABLE OF CONTENTS (Continued)

CHAPTER 9 INTRODUCTION TO DAMAGE CRITERIA [redacted] (Continued)

Page

9-39 Through-the-Thickness Material Response 9-107
IMPULSE AND STRUCTURAL RESPONSE ANALYSIS 9-107
9-40 Impulse Calculations 9-107
9-41 Structural Response Analysis 9-115
REENTRY VEHICLE HARDENING 9-115
9-42 Balanced Hardening with Respect to Neutrons and X-rays 9-116
9-43 X-ray Hardening Concepts 9-116
SECTION VI NUCLEAR RADIATION SHIELDING 9-118
SECTION VII TREE – COMPONENT PART AND CIRCUIT RESPONSE 9-121
SEMICONDUCTOR COMPONENT PARTS 9-122
9-44 Transient Effects 9-122
9-45 Permanent Effects 9-132
9-46 Heating and Thermomechanical Damage 9-140
OTHER ELECTRONIC COMPONENT PARTS 9-147
9-47 Electron Tubes 9-147
9-48 Capacitors 9-149
9-49 Resistors 9-151
9-50 Batteries and Cables 9-151
9-51 Quartz Crystals 9-153
9-52 Solder Joints 9-154
9-53 Infrared Detectors 9-154
ELECTRONIC CIRCUITS 9-155
9-54 Radiation Response of Discrete-Component-Part Circuits 9-155
9-55 Radiation Response of Integrated Circuits 9-158
SECTION VIII ELECTROMAGNETIC PULSE (EMP) DAMAGE MECHANISMS 9-170
ENERGY COUPLING 9-170
9-56 Basic Coupling Modes 9-170
9-57 Resonant Configurations 9-171
COMPONENT DAMAGE 9-172
9-58 Types of Damage 9-172
9-59 Damage Levels 9-173
EMP HARDENING 9-175
9-60 System Analysis 9-175
9-61 Recommended Practices 9-176
TESTING 9-178

[redacted]

[redacted]

TABLE OF CONTENTS (Continued)

CHAPTER 9 INTRODUCTION TO DAMAGE CRITERIA [redacted] (Continued)

Page

9-62 Importance of Testing 9-178
9-63 Simulation Facilities 9-179
BIBLIOGRAPHY 9-183

CHAPTER 10 PERSONNEL CASUALTIES [redacted]

INTRODUCTION 10-1
SECTION I AIR BLAST 10-1
MECHANISMS AND CRITERIA FOR INJURY 10-1
10-1 Direct Overpressure Effects 10-1
10-2 Translational Forces and Impact 10-2
10-3 Blast-Energized Debris 10-3
10-4 Miscellaneous Effects 10-3
CASUALTY PREDICTION 10-4
10-5 Personnel in the Open 10-4
10-6 Personnel in a Forest 10-4
10-7 Personnel in Structures 10-5
10-8 Personnel in Vehicles 10-5
SECTION II THERMAL RADIATION 10-10
SKIN BURNS 10-10
CLASSIFICATION OF BURNS 10-10
10-9 First Degree Burns 10-10
10-10 Second Degree Burns 10-10
10-11 Third Degree Burns 10-10
10-12 Reduction in Effectiveness by Burns 10-11
BURN INJURY ENERGIES AND RANGES 10-11
10-13 Personnel Parameters 10-11
10-14 Burn Exposures for Unprotected Skin 10-12
10-15 Burns Under Clothing 10-12
10-16 Body Areas Involved 10-12
10-17 Incapacitation from Burns 10-15
10-18 Modification of Injury 10-15
EFFECTS OF THERMAL RADIATION ON THE EYES 10-15
10-19 Flashblindness 10-15
10-20 Retinal Burns 10-15

[redacted]

TABLE OF CONTENTS (Continued)

CHAPTER 10 PERSONNEL CASUALTIES [redacted] (Continued)

Page

10-21 Modification of Thermal Effects on the Eye 10-17
10-22 Safe Separation Distance Curves 10-17

SECTION III NUCLEAR RADIATION 10-23

INITIAL RADIATION 10-23
10-23 Radiation Sickness 10-23
10-24 Incapacitation 10-24
10-25 Modification of Injury 10-25
10-26 Military Assumptions 10-25

RESIDUAL RADIATION 10-25
10-27 External Hazards 10-25
10-28 Internal Hazards 10-31
10-29 Modification of Injury 10-31

SECTION IV COMBINED INJURY 10-31

10-30 Radiation and Thermal Injuries 10-32
10-31 Mechanical and Radiation Injuries 10-33
10-32 Thermal and Mechanical Injuries 10-33

CASUALTY CRITERIA 10-33

PERSONNEL IN THE OPEN 10-33

PERSONNEL IN STRUCTURES 10-35

TREATMENT 10-35

BIBLIOGRAPHY 10-36

CHAPTER 11 DAMAGE TO STRUCTURES [redacted]

INTRODUCTION 11-1

SECTION I DAMAGE TO ABOVEGROUND STRUCTURES 11-1

AIR BLAST EFFECTS 11-2
11-1 Nature of Loading 11-2
11-2 Nature of Damage 11-3
11-3 Structural Characteristics 11-3
11-4 Isodamage Curves 11-9

[redacted]

TABLE OF CONTENTS (Continued)

CHAPTER 11 DAMAGE TO STRUCTURES [redacted] (Continued)

Page

11-5 Shallow Underground Bursts 11-12
11-6 Ground Shock and Cratering 11-12

SECTION II DAMAGE TO BELOWGROUND STRUCTURES 11-40

STRUCTURES BURIED IN SOIL 11-40
11-7 Definition of Burial Conditions 11-40
11-8 Deeply Buried Structures 11-41
11-9 Structures Buried at Shallow Depths 11-48
11-10 Intermediate Depths of Burial 11-49

LINED AND UNLINED OPENINGS IN ROCK 11-49
11-11 Definition of Damage to Openings in Rock 11-50
11-12 Types of Tunnel Linings 11-51
11-13 Procedures for Tunnel Vulnerability Evaluation 11-52
11-14 Vulnerability Evaluation of Surface Silos in Rock 11-55

SECTION III SHOCK VULNERABILITY OF EQUIPMENT AND PERSONNEL 11-97

11-15 Shock Mounting 11-97
11-16 Nature of Elastic Systems Comprised of Mounted Equipment 11-99
11-17 Design of Mounted Equipment to Resist Shock 11-99
11-18 Vulnerability Analysis 11-100

SECTION IV DAMS AND HARBOR INSTALLATIONS 11-109

AIR BLAST 11-109
11-19 Concrete Gravity Dams 11-109
11-20 Harbor Installations 11-109

WATER SHOCK 11-109
11-21 Concrete Dams and Water Locks 11-109

CRATERING 11-109
11-22 Cratering Earth Dams and Causeways 11-109

WATER WAVES 11-110
11-23 Impact and Hydrostatic Pressure 11-110
11-24 Drag Forces 11-110
11-25 Inundation 11-110

THERMAL-RADIATION DAMAGE 11-110

SECTION V PETROLEUM, OIL, AND LUBRICANT (POL) STORAGE TANKS ... 11-110

11-26 Damage Criteria 11-110
11-27 Loading and Response 11-111
11-28 Damage 11-111

[redacted]

TABLE OF CONTENTS (Continued)

CHAPTER 11 DAMAGE TO STRUCTURES [redacted] (Continued)

Page

SECTION VI FIELD FORTIFICATIONS 11-118
11-29 Air Blast Damage 11-118
11-30 Protection of Fortifications from Air Blast Damage 11-118
11-31 Thermal Radiation Damage 11-121

SECTION VII FIRE IN URBAN AREAS 11-127
INTRODUCTION 11-127
EVOLUTION OF MASS FIRES 11-127
11-32 Ignition Points 11-127
11-33 Room Flashover 11-128
11-34 Active Burning of a Structure 11-128
11-35 Fire Spread Between Structures 11-128
11-36 Mass Fires 11-129
ESTIMATION AND CONTROL OF THERMAL DAMAGE 11-130
11-37 Radiant Exposure Thresholds 11-130
11-38 Fire Radii 11-134
11-39 The San Jose Study 11-134
11-40 The New Orleans Study 11-136
11-41 Effects of Clouds 11-138
11-42 Firestorm Criteria 11-143
11-43 Conflagrations 11-144
11-44 Fire Control 11-144
BIBLIOGRAPHY 11-146

CHAPTER 12 MECHANICAL DAMAGE DISTANCES FOR SURFACE SHIPS AND SUBMARINES SUBJECTED TO NUCLEAR EXPLOSIONS [redacted]

INTRODUCTION 12-1
12-1 Damage Mechanisms 12-1
12-2 Damage Classification 12-1
12-3 Seaworthiness Impairment 12-1
12-4 Mobility Impairment 12-2
12-5 Weapon Delivery Impairment 12-2
SECTION I DAMAGE TO SURFACE SHIPS FROM AIR BURSTS 12-2
BLAST DAMAGE 12-2
12-6 General 12-2

[redacted]

[redacted]

TABLE OF CONTENTS (Continued)

CHAPTER 12 MECHANICAL DAMAGE DISTANCES FOR SURFACE SHIPS AND SUBMARINES SUBJECTED TO NUCLEAR EXPLOSIONS [redacted] (Continued)

Page

12-7 Damage Criteria 12-3
12-8 Damage Distances 12-3
12-9 Capsizing from Blast 12-6

DAMAGE FROM OTHER AIR BURST PHENOMENA 12-6
12-10 Thermal Radiation 12-6
12-11 Damage from Nuclear Radiation and Electromagnetic Pulse 12-8
12-12 (Omitted)

SECTION II SURFACE SHIP DAMAGE FROM UNDERWATER BURSTS 12-8

DAMAGE FROM THE SHOCK WAVE IN THE WATER 12-8
12-13 Damage Criteria 12-8
12-14 Damage Distances 12-9
12-15 Effect of Ocean Environment on Damage Ranges 12-9

DAMAGE FROM OTHER UNDERWATER BURST PHENOMENA 12-17

SECTION III SUBMARINE DAMAGE FROM UNDERWATER BURSTS 12-17

DAMAGE FROM THE SHOCK WAVE IN THE WATER 12-17
12-16 Damage Criteria 12-17
12-17 Damage Distances 12-18
12-18 Effect of Ocean Environment on Damage Ranges 12-18

DAMAGE FROM OTHER UNDERWATER BURST PHENOMENA 12-19

BIBLIOGRAPHY 12-30

CHAPTER 13 DAMAGE TO AIRCRAFT [redacted]

INTRODUCTION 13-1

SECTION I BLAST AND THERMAL EFFECTS ON AIRCRAFT 13-1

13-1 Sure-Safe and Sure-Kill Envelopes 13-2

NUCLEAR WEAPON EFFECTS ANALYSIS 13-4
13-2 Gust Effects 13-4
13-3 Overpressure Effects 13-7
13-4 Thermal Radiation Effects 13-7
13-5 Combined Effects 13-9

SECTION II AIRCRAFT RESPONSE TO BLAST AND THERMAL EFFECTS 13-10

AIRCRAFT RESPONSE TO GUST EFFECTS 13-10
13-6 Aerodynamic Coefficients for Aircraft 13-10

[redacted]

TABLE OF CONTENTS (Continued)

CHAPTER 13 DAMAGE TO AIRCRAFT [redacted] (Continued)

Page

13–7 Gust Effects on In-Flight Aircraft 13–27
13–8 Gust Effects on Parked Aircraft 13–27

AIRCRAFT RESPONSE TO OVERPRESSURE EFFECTS 13–50
13–9 Overpressure Effects on In-Flight and Parked Aircraft 13–50

AIRCRAFT RESPONSE TO THERMAL RADIATION EFFECTS 13–59
13–10 Thermal Effects on In-Flight and Parked Aircraft 13–59

BURST-TIME ENVELOPES 13–67
13–11 Requirement for Burst-Time Envelopes 13–67

BIBLIOGRAPHY 13–86

CHAPTER 14 DAMAGE TO MILITARY FIELD EQUIPMENT [redacted]

INTRODUCTION 14–1

SECTION I AIR BLAST DAMAGE 14–1
14–1 Damage Mechanisms 14–1
14–2 Air Blast Environment 14–2
14–3 Target Characteristics 14–4
14–4 Target Exposure 14–6
14–5 Effects of Ground Surface Conditions 14–12
14–6 Vehicle Status 14–14

SECTION II DAMAGE PREDICTIONS 14–17
14–7 Definitions of Damage Categories 14–17
14–8 Prediction Techniques 14–18
14–9 Untested Equipment 14–52

SECTION III DAMAGE FROM CAUSES OTHER THAN BLAST AND NUCLEAR RADIATION 14–57
14–10 Fire Damage 14–57
14–11 Obscuration of Optical Devices 14–58
14–12 Damage by Missiles 14–58
14–13 The Effects of Time 14–59

SECTION IV TREE DAMAGE CRITERIA 14–59

SYSTEMS ANALYSIS 14–60
14–14 Types of Systems Analysis Used in TREE 14–60

[redacted]

[redacted]

TABLE OF CONTENTS (Continued)

CHAPTER 14 DAMAGE TO MILITARY FIELD EQUIPMENT [redacted] (Continued)

Page

14–15 The Complexity of Performing System Analysis for TREE 14–60
14–16 Characteristics of the Analysis Used in This Section 14–61
REVIEW OF ELECTRONIC SUSCEPTIBILITY TO NUCLEAR RADIATION 14–62
14–17 Component Part Vulnerability 14–62
14–18 Subsystem Vulnerability 14–64
TREE-DAMAGE ESTIMATES 14–64
14–19 Ground Equipment 14–65
14–20 An Example of Ground Equipment Survivability Estimation 14–65
14–21 Aircraft Systems 14–67
14–22 An Example of Aircraft Survivability Estimation 14–67
14–23 Missile Systems 14–70
BIBLIOGRAPHY 14–72

CHAPTER 15 DAMAGE TO FOREST STANDS [redacted]

INTRODUCTION 15–1
SECTION I AIR BLAST 15–1
15–1 Forest Stand Types 15–1
15–2 Damage–Distance Relations 15–3
SECTION II TROOP AND VEHICLE MOVEMENT 15–41
15–3 Blowdown Debris Characteristics 15–42
15–4 Vehicle Movement 15–44
15–5 Troop Movement 15–46
15–6 Predicting Effects on Movement 15–49
SECTION III THERMAL RADIATION 15–52
15–7 Ignitions 15–52
15–8 Kindling Fuels 15–52
15–9 Thermal Radiation on Forests 15–56
15–10 Forest Fire Ignition and Spread 15–58
BIBLIOGRAPHY 15–64

CHAPTER 16 DAMAGE TO MISSILES [redacted]

SECTION I BLAST DAMAGE TO TACTICAL MISSILE SYSTEMS 16–1

[redacted]

[redacted]

TABLE OF CONTENTS (Continued)

CHAPTER 16 DAMAGE TO MISSILES [redacted] (Continued)

Page

SERGEANT WEAPON SYSTEM 16-3
16-1 Description of the SERGEANT Weapon System 16-3
16-2 Vulnerability Levels of the SERGEANT Missile System 16-7
16-3 Reliability of SERGEANT Vulnerability Estimates 16-10

LANCE WEAPON SYSTEM 16-12
16-4 Description of the LANCE Weapon System 16-12
16-5 Vulnerability Levels for the LANCE Missile System 16-12
16-6 Reliability of LANCE Vulnerability Estimates 16-17

HAWK WEAPON SYSTEM 16-19
16-7 Description of the HAWK Weapon System 16-19
16-8 Vulnerability Levels for the HAWK Missile System 16-23
16-9 Reliability of HAWK Vulnerability Estimates 16-24

SAMPLE PROBLEM: AIR BLAST DAMAGE TO A TACTICAL MISSILE SYSTEM 16-26
16-10 Description of the HONEST JOHN System 16-26
16-11 Vulnerability Levels for HONEST JOHN Missile System 16-31

SECTION II BLAST AND THERMAL VULNERABILITY OF IN-FLIGHT STRATEGIC SYSTEMS 16-34

INTRODUCTION 16-34
16-12 Sources of Data 16-38
16-13 Limitations in Application of the Data 16-38

BLAST LOADING ON REENTRY (RV) SYSTEMS 16-39
16-14 Environment Scaling 16-39
16-15 General Intercept Loads and Load Duration 16-47
16-16 Intercept Load Duration 16-51
16-17 Fireball Traversal Time 16-51
16-18 Total Traversal Time 16-52
16-19 Exit Loads 16-57
16-20 Blast Data Generalization 16-57
16-21 Typical RV Aerodynamics 16-57
16-22 Initial Interaction of Vehicle Flow-Field and Blast Wave (Shock-Shock) ... 16-58
16-23 Damage Envelopes 16-58

RESULTS OF SOME RV BLAST AND THERMAL LOAD AND VULNERABILITY CALCULATIONS 16-66
16-24 Blast Loads on the RV 16-66
16-25 Thermal Radiation Loads on the RV 16-70

[redacted]

[redacted]

TABLE OF CONTENTS (Continued)

CHAPTER 16 DAMAGE TO MISSILES [redacted] (Continued)

Page

16-26 Description of a Blast/Thermal Vulnerability Determination 16-75
16-27 Results of the RV Vulnerability Determination 16-77
16-28 Summary and Conclusions Concerning RV Vulnerability Calculations 16-81

ANTIMISSILE (ABM) SYSTEMS 16-81
16-29 Shell Breathing Response 16-86
16-30 Vehicle Bending Response 16-87
16-31 Thermal Radiation Effects 16-87
16-32 ABM Blast/Thermal Vulnerability Envelopes 16-90
16-33 Conclusions 16-91

BLAST AND THERMAL LETHALITY 16-96
16-34 Blast and Thermal Free Field Environments 16-96
16-35 ABM Blast Loads on Threat Vehicles (Point Mass) 16-96
16-36 Blast Loads on the RV Threat Vehicle 16-101
16-37 ABM Blast Kill Radii 16-106
16-38 Fireball Thermal Effects on Threat RV's 16-109

BIBLIOGRAPHY 16-116

CHAPTER 17 RADIO FREQUENCY SIGNAL DEGRADATION RELEVANT TO COMMUNICATIONS AND RADAR SYSTEMS [redacted]

INTRODUCTION 17-1

SECTION I DEGRADATION MECHANISMS 17-2

ATTENUATION 17-2
17-1 Fireball Absorption 17-2
17-2 Absorption in the Region Around the Fireball 17-2
17-3 D-Region Absorption 17-4
17-4 Absorption of Noise 17-4
17-5 Attenuation by Scattering and Beam Spreading 17-4
17-6 Effects of Reflection 17-6

INTERFERENCE 17-6
17-7 Noise 17-6
17-8 Reflection, Refraction, and Scatter 17-6

SIGNAL DISTORTION 17-6

SECTION II SYSTEM CHARACTERISTICS AND EFFECTS 17-7

VLF AND LF SYSTEMS 17-7

[redacted]

[redacted]

TABLE OF CONTENTS (Continued)

CHAPTER 17 RADIO FREQUENCY SIGNAL DEGRADATION RELEVANT TO COMMUNICATIONS AND RADAR SYSTEMS [redacted] (Continued)

Page

17-9 VLF and LF Propagation 17-7
17-10 Effects of Nuclear Bursts on VLF and LF Systems 17-7
17-11 Spread-Debris Environment 17-9
17-12 Effect of a [redacted] 6300-km Burst 17-9
17-13 Effect of Detonations Below About 300 km 17-13

HF SYSTEMS 17-13
17-14 HF Propagation 17-13
17-15 Effect of Nuclear Bursts on HF Systems 17-13
17-16 Effect of Surface or Near-Surface Bursts 17-16
17-17 Effect of a [redacted] 30-km Burst 17-16
17-18 Effects of a [redacted] 50-km Burst 17-17
17-19 Effect of Multiple Multimegaton 150-km Bursts 17-17
17-20 Effect of a 1-Mt, 250-km Burst 17-18
17-21 Effect of a [redacted] 1000-km Burst 17-19

SATELLITE COMMUNICATION SYSTEMS 17-19
17-22 Effects of Nuclear Bursts on Satellite Systems 17-19
17-23 Nuclear Effects on Two Typical Satellite Systems 17-20

TROPOSCATTER COMMUNICATION SYSTEMS 17-22
17-24 Effects of Nuclear Bursts on Troposcatter Systems 17-22
17-25 Nuclear Effects on Three Typical Troposcatter Systems 17-26

IONOSCATTER COMMUNICATION SYSTEMS 17-26
17-26 Effects of Nuclear Bursts on Ionoscatter Systems 17-27
17-27 Nuclear Effects on Typical Ionoscatter Systems 17-28

RADAR SYSTEMS 17-30
17-28 Ballistic Missile Defense Systems 17-32
17-29 Nuclear Effects on Area Defense Systems 17-32
17-30 Nuclear Effects on Hardsite Defense Systems 17-36

BIBLIOGRAPHY 17-40

APPENDIX A SUPPLEMENTARY BLAST DATA [redacted]

SECTION I MATHEMATICAL DESCRIPTION OF THE SHOCK FRONT A-1

A-1 The Rankine-Hugoniot Equations A-1
A-2 Equation of State of an Ideal Gas A-3
A-3 Shock Wave Equations for an Ideal Gas A-3
A-4 Units, Constants, and Conversion Factors A-5

[redacted]

[redacted]

TABLE OF CONTENTS (Continued)

APPENDIX A SUPPLEMENTARY BLAST DATA [redacted] (Continued)

Page

A-5 Equation of State of Air A-5
A-6 Equations for Strong Shock Waves in Air A-5
SECTION II PHYSICAL DESCRIPTION OF SHOCK WAVE BEHAVIOR A-8
A-7 Step Function Shock Wave A-8
A-8 Shock-Front Formation A-9
A-9 Pressure-Momentum Interaction at a Shock Front A-9
A-10 Normal Reflection at a Solid Barrier A-10
A-11 Pressures on Simple Shapes A-12
A-12 The Rankine-Hugoniot Equations (Alternate Analysis) A-14
A-13 Dynamic Pressure A-16

APPENDIX B USEFUL RELATIONSHIPS [redacted]

B-1 General Equivalents B-1
B-2 Constants B-1
B-3 Standard Sea Level Atmosphere B-1
B-4 Conversions B-2
B-5 Fractional Power and Dimension Scaling B-4

APPENDIX C PROBABILITY CONSIDERATIONS [redacted]

C-1 Protective Design and Weapon Selection C-1
SECTION I DAMAGE PROBABILITIES C-2
DAMAGE CAUSED BY MOTION INPUT C-2
C-2 Description of Charts for Damage Caused by Motion Input C-2
C-3 Instructions for Motion Input Analyses C-3
C-4 Illustrative Examples for Motion Inputs C-3
DAMAGE CAUSED BY PRESSURE C-7
C-5 Description of Charts for Damage to Surface Structures Caused by Pressure Input C-7
C-6 Description of Charts for Damage to Underground Structures Caused by Pressure Input C-8
C-7 Instructions for Pressure Input Analyses C-8
C-8 Illustrative Examples for Pressure Inputs C-8
C-9 System Consideration C-9
SECTION II DERIVATION OF EQUATIONS USED IN SECTION I C-14
C-10 Properties of Lognormal Variates C-14
C-11 Probability of Failure or Survival C-14

[redacted]

[redacted]

TABLE OF CONTENTS (Continued)

		Page
APPENDIX D	ABSTRACTS OF DNA HANDBOOKS	D-1
APPENDIX E	GLOSSARY	E-1
APPENDIX F	LIST OF SYMBOLS	F-1

[redacted]

[redacted]

LIST OF ILLUSTRATIONS

PART II

Figure	*Title*	*Page*
9-1	[redacted] Initial Conditions for Loading of a Rigid, Fixed Cube [redacted]	9-5
9-2	[redacted] Target Loading by Overpressure [redacted]	9-6
9-3	[redacted] Net Blast Loading on Representative Structures [redacted]	9-9
9-4	[redacted] Direct and Reflected Shock Waves from an Underwater Burst [redacted]	9-12
9-5	[redacted] Ignition Thresholds for Black α-Cellulose Exposed to a Rectangular Thermal Pulse [redacted]	9-20
9-6	[redacted] Ignition Thresholds for Black α-Cellulose Exposed to a Simulated Weapon Pulse [redacted]	9-21
9-7	[redacted] Dimensionless Temperature Profiles in Opaque and Diathermanous Semi-Infinite Solids Exposed to a Rectangular Thermal Pulse [redacted]	9-24
9-8	[redacted] Exposed Facing Temperature-Time Histories of Aluminum Honeycomb. Facing, 0.016-in. Gray Painted Skin; Core 1/8-in., Cell Size 1/2-in. Thick. 21-24.2 cal/cm^2, 3.8 Mt [redacted]	9-33
9-9	[redacted] Schematic Comparison of Ideal Cosine Law with Function Including Scattering, Reflection, and Refraction [redacted]	9-35
9-10	[redacted] Thin Plate, Thick Plate, and Finite Plate Regions for Exposure to Nuclear Weapons Thermal Radiation [redacted]	9-41
9-11	[redacted] Thermal Response of a Thin Plate to Nuclear Weapons Thermal Radiation Pulse [redacted]	9-45
9-12	[redacted] Coefficient of Linear Expansion as a Function of Temperature for Stainless Steels [redacted]	9-48
9-13	[redacted] Coefficient of Linear Expansion as a Function of Temperature for Titanium Alloys [redacted]	9-49
9-14	[redacted] Coefficient of Linear Expansion as a Function of Temperature for Heat Resistant Alloys [redacted]	9-50
9-15	[redacted] Coefficient of Linear Expansion as a Function of Temperature for Aluminum Alloys [redacted]	9-51
9-16	[redacted] Typical Stress-Strain Curves for Titanium 6Al-4V Alloy at Room and Elevated Temperatures [redacted]	9-52
9-17	[redacted] Typical Stress-Strain Curves for 2014-T6 Aluminum Alloy at Room and Elevated Temperatures [redacted]	9-53
9-18	[redacted] Typical Stress-Strain Curves for 301 Stainless Steel at Room and Elevated Temperatures [redacted]	9-54
9-19	[redacted] Types of Rapid Heating Tensile Tests [redacted]	9-55
9-20	[redacted] Types of Short Time Creep Tests [redacted]	9-56

[redacted]

[redacted]

LIST OF ILLUSTRATIONS (Continued)

Figure	*Title*	*Page*
9-21	[redacted] 2024-T3 Aluminum Alloy Ultimate Strength at Elevated Temperature [redacted]	9-57
9-22	[redacted] 2024-T81 Aluminum Alloy Ultimate Strength at Elevated Temperature [redacted]	9-58
9-23	[redacted] 2014-T6 Aluminum Alloy Yield Strength at Elevated Temperature [redacted]	9-59
9-24	[redacted] Ultimate Strength Test Results for 6Al-4V Titanium Alloy at Elevated Temperature [redacted]	9-61
9-25	[redacted] Ultimate Strength Test Results for Full Hard Stainless Steel at Elevated Temperature [redacted]	9-62
9-26	[redacted] Stress-Strain Approximation for 2014-T6 Aluminum Alloy [redacted]	9-64
9-27	[redacted] Photon Cross Sections in Beryllium [redacted]	9-85
9-28	[redacted] Photon Cross Sections in Aluminum [redacted]	9-86
9-29	[redacted] Photon Cross Sections in Iron [redacted]	9-87
9-30	[redacted] Photon Cross Sections in Copper [redacted]	9-88
9-31	[redacted] Photon Cross Sections in Tungsten [redacted]	9-89
9-32	[redacted] Photon Cross Sections in Uranium [redacted]	9-90
9-33	[redacted] Photon Cross Sections in Carbon Phenolic (CP), $\bar{Z}$ = 6.08 [redacted]	9-91
9-34	[redacted] Photon Cross Sections in Tape Wound Silicon Phenolic (TWSP), $\bar{Z}$ = 9.01 [redacted]	9-92
9-35	[redacted] Energy Deposited in Aluminum by Black Body Spectra [redacted]	9-94
9-36	[redacted] Energy Deposited in Copper by Black Body Spectra [redacted]	9-95
9-37	[redacted] Energy Deposited by Black Body X-ray Spectra in Carbon Phenolic (CP) [redacted]	9-96
9-38	[redacted] Energy Deposited by Black Body X-ray Spectra in Tape Wound Silica Phenolic (TWSP) [redacted]	9-97
9-39	[redacted] Aluminum Isoenergy Lines. Parameter is Energy in cal/gm [redacted]	9-99
9-40	[redacted] Aluminum Isoenergy Lines and Adiabats [redacted]	9-100
9-41	[redacted] Sequence of Spallation Following Radiation Deposition [redacted]	9-104
9-42	[redacted] Equation of State for Elastic-Plastic Material Description [redacted]	9-106
9-43	[redacted] Normalized Vapor Impulses Produced in Aluminum by Various Black Body X-ray Spectra [redacted]	9-109
9-44	[redacted] Normalized Vapor Impulses Produced in Copper by Various Black Body X-ray Spectra [redacted]	9-110
9-45	[redacted] Two-Dimensional Lattice Structure of Silicon [redacted]	9-123
9-46	[redacted] Illustration of a Semiconductor Junction [redacted]	9-124
9-47	[redacted] Relative Shapes of Diffusion Component of Primary Photocurrent [redacted]	9-126

[redacted]

[redacted]

LIST OF ILLUSTRATIONS (Continued)

Figure	*Title*	*Page*
9–48	[redacted] NPN Transistor Illustrating the Primary Photocurrent [redacted]	9–127
9–49	[redacted] Radiation Storage Time [redacted]	9–128
9–50	[redacted] Gamma Ray Exposure Rate as a Function of Pulse Width Switching Thresholds for a 3A60A SCR [redacted]	9–130
9–51	[redacted] Construction of Typical Junction, MOS, and Thin–Film Field–Effect Transistors [redacted]	9–131
9–52	[redacted] An Illustrative Diode Characteristic for Pre– and Post–irradiation by Neutrons [redacted]	9–133
9–53	[redacted] An Illustration of Rise Time and Storage Time [redacted]	9–134
9–54	[redacted] Fast Neutron Bombardment Effect on Voltage–Current Characteristic of a Germanium Tunnel Diode [redacted]	9–135
9–55	[redacted] Fast Neutron Bombardment Effect on Voltage–Current Characteristic of a Silicon Tunnel Diode [redacted]	9–136
9–56	[redacted] Current–Gain Degradation Characteristics for Some Common Transistor Types [redacted]	9–138
9–57	[redacted] Steps in the Fabrication of an NPN Silicon Planar Transistor [redacted]	9–142
9–58	[redacted] Transistor Cross Section and Package [redacted]	9–143
9–59	[redacted] Ball Stitch and Ultrasonic Bonding [redacted]	9–145
9–60	[redacted] Semiconductor Failure Modes [redacted]	9–146
9–61	[redacted] Circuit Response as a Function of Radiation–Pulse Width [redacted]	9–156
9–62	[redacted] Circuit in Which Burnout Could Occur [redacted]	9–157
9–63	[redacted] Load–Terminal I–V Characteristic ("On" Segment) of RD 308 in Neutron Environment [redacted]	9–165
9–64	[redacted] MC1525 Typical Transfer Characteristics [redacted]	9–166
9–65	[redacted] Electric Induction in a Copper Wire [redacted]	9–170
9–66	[redacted] Magnetic Induction in a Simple Loop [redacted]	9–171
9–67	[redacted] Resistive Coupling as a Result of Currents in the Ground [redacted]	9–171
9–68	[redacted] Reflected and Refracted Waves at the Air–Ground Interface [redacted]	9–172
9–69	[redacted] Energy Required to Damage Various Classes of Equipment [redacted]	9–177
10–1	[redacted] Fifty Percent Casualties for the Indicated Blast Effects for Prone Personnel Exposed in the Open or in a Forest to a 1 kt Burst [redacted]	10–8
10–2	[redacted] One Percent Casualties for the Indicated Blast Effects for Prone Personnel Exposed in the Open or in a Forest to a 1 kt Burst [redacted]	10–9
10–3	[redacted] Radiant Exposure Required to Produce Skin Burns for Different Skin Pigmentation [redacted]	10–13
10–4	[redacted] Skin Burn Probabilities for an Average Population Taking No Evasive Action [redacted]	10–14

[redacted]

[redacted]

LIST OF ILLUSTRATIONS (Continued)

Figure	*Title*	*Page*
10-5	[redacted] Distance Thresholds for Second Degree Burns for Various Evasion Times [redacted]	10-16
10-6	[redacted] Safe Separation Distances, for an Observer on the Ground, from Bursts at 10 kft and 50 kft During the Day [redacted]	10-18
10-7	[redacted] Safe Separation Distance, for an Observer at 50 kft, from Bursts at 10 kft and 50 kft During the Day [redacted]	10-19
10-8	[redacted] Safe Separation Distance, for an Observer on the Ground, from Bursts at 10 kft and 50 kft, During the Night [redacted]	10-20
10-9	[redacted] Safe Separation Distance, for an Observer at 50 kft, from Bursts at 10 kft and 50 kft, During the Night [redacted]	10-21
10-10	[redacted] Safe Separation Distance, for an Observer on the Ground, from Low Yield Weapons Exploded at 1,000 ft Height of Burst [redacted]	10-22
10-11	[redacted] Personnel Effectiveness After Exposure to 1,400 rads [redacted]	10-26
10-12	[redacted] Personnel Effectiveness After Exposure to 2,800 rads [redacted]	10-27
10-13	[redacted] Personnel Effectiveness After Exposure to 7,000 rads [redacted]	10-28
10-14	[redacted] Personnel Effectiveness After Exposure to 13,000 rads [redacted]	10-29
10-15	[redacted] Personnel Effectiveness After Exposure to 22,000 rads [redacted]	10-30
10-16	[redacted] Comparison of Effects from Low Altitude Bursts [redacted]	10-34
11-1	[redacted] Idealized Loading Functions [redacted]	11-4
11-2	[redacted] Isodamage Curves for Fifty Percent Probability of Severe Damage to Multistory Blast-Resistant Reinforced Concrete Buildings [redacted]	11-16
11-3	[redacted] Isodamage Curves for Fifty Percent Probability of Severe Damage to Multistory Reinforced Concrete Buildings with Concrete Walls, Small Window Area, Three to Eight Stories [redacted]	11-17
11-4	[redacted] Isodamage Curves for Fifty Percent Probability of Severe Damage to Multistory Wall Bearing Buildings, Brick Apartment House Type, up to Three Stories [redacted]	11-18
11-5	[redacted] Isodamage Curves for Fifty Percent Probability of Severe Damage to Multistory Wall Bearing Building, Monumental Type, up to Four Stories [redacted]	11-19
11-6	[redacted] Isodamage Curves for Fifty Percent Probability of Severe Damage to Wood Frame Buildings, House Type, One or Two Stories [redacted]	11-20
11-7	[redacted] Isodamage Curves for Fifty Percent Probability of Severe Damage to Light Steel Frame Industrial Buildings, Single Story, Frangible Walls, up to 5 Ton Crane Capacity [redacted]	11-21
11-8	[redacted] Isodamage Curves for Fifty Percent Probability of Severe Damage to Heavy Steel Frame Industrial Buildings, Single Story, Frangible Walls, 25 to 50 Ton Crane Capacity [redacted]	11-22

[redacted]

[redacted]

LIST OF ILLUSTRATIONS (Continued)

Figure	*Title*	*Page*
11-9	[redacted] Isodamage Curves for Fifty Percent Probability of Severe Damage to Heavy Steel Frame Industrial Buildings, Single Story, Frangible Walls, 60 to 100 Ton Crane Capacity [redacted]	11-23
11-10	[redacted] Isodamage Curves for Fifty Percent Probability of Severe Damage to Multistory Steel Frame Office Type Buildings, 3- to 10-Stories, Frangible Walls, Earthquake Resistant Construction [redacted]	11-24
11-11	[redacted] Isodamage Curves for Fifty Percent Probability of Severe Damage to Multistory Steel Frame Office Type Buildings, 3- to 10-Stories, Frangible Walls, Non-Earthquake Resistant Construction [redacted]	11-25
11-12	[redacted] Isodamage Curves for Fifty Percent Probability of Severe Damage to Multistory Reinforced Concrete Frame Office Type Buildings, 3- to 10-Stories, Frangible Walls, Earthquake Resistant Construction [redacted]	11-26
11-13	[redacted] Isodamage Curves for Fifty Percent Probability of Severe Damage to Multistory Reinforced Concrete Frame Office Type Buildings, 3- to 10-Stories, Frangible Walls, Non-Earthquake Resistant Construction [redacted]	11-27
11-14	[redacted] Isodamage Curves for Fifty Percent Probability of Severe Damage to Four-Lane Highway Truss Bridges and Double Track Ballast Floor Railroad Truss Bridges, Span 200 ft to 400 ft [redacted]	11-28
11-15	[redacted] Isodamage Curves for Fifty Percent Probability of Severe Damage to Two-Lane Highway Truss Bridges, Spans 200 ft to 400 ft; Single Track Ballast Floors and Double Track Open Floor Railroad Truss Bridges, Spans 200 ft to 400 ft; and Single Track Open Floor Railroad Truss Bridges, Span 400 ft [redacted]	11-29
11-16	[redacted] Isodamage Curves for Fifty Percent Probability of Severe Damage to Single Track Open Floor Railroad Truss Bridges, Span 200 ft [redacted]	11-30
11-17	[redacted] Isodamage Curves for Fifty Percent Probability of Severe Damage to Four-Lane Through Highway Girder Bridges, Spans 75 ft [redacted]	11-31
11-18	[redacted] Isodamage Curves for Fifty Percent Probability of Severe Damage to Two-Lane Deck, Two-Lane Through, and Four-Lane Deck Highway Bridges, Spans 75 ft; Double Track Deck, Open or Ballast Floor Railroad Girder Bridges, Span 75 ft; Single or Double Track Through, Ballast Floor Railroad Girder Bridges, Spans 75 ft [redacted]	11-32
11-19	[redacted] Isodamage Curves for Fifty Percent Probability of Severe Damage to Single Track Deck, Open or Ballast Floor, and Single or Double Track Through, Open Floor Railroad Girder Bridges, Spans 75 ft [redacted]	11-33
11-20	[redacted] Isodamage Curves for Fifty Percent Probability of Severe Damage to Two-Lane Through and Four-Lane Deck or Through Highway Girder	

[redacted]

[redacted]

LIST OF ILLUSTRATIONS (Continued)

Figure	Title	Page
	Bridges, Spans 200 ft; Double Track Deck or Through, Ballast Floor Railroad Girder Bridges, Spans 200 ft [redacted]	11-34
11-21	[redacted] Isodamage Curves for Fifty Percent Probability of Severe Damage to Two-Lane Deck Highway Girder Bridges, Spans 200 ft; Single Track Deck or Through, Ballast Floor, and Double Track Deck or Through, Open Floor Railroad Girder Bridges, Spans 200 ft [redacted]	11-35
11-22	[redacted] Isodamage Curves for Fifty Percent Probability of Severe Damage to Single Track Deck or Through, Open Floor, Railroad Girder Bridges, Spans 200 ft [redacted]	11-36
11-23	[redacted] Isodamage Curves for Fifty Percent Probability of Severe Damage to Floating Bridges, U.S. Army Standard M-2 and M-4, Random Orientation [redacted]	11-37
11-24	[redacted] Damage-Distance Reduction for Surface Structures from 1 kt Bursts in Soil [redacted]	11-39
11-25	[redacted] Depth of Cover Classification for Arches [redacted]	11-42
11-26	[redacted] Buried Arches, Average Depth of Earth Cover [redacted]	11-43
11-27	[redacted] Average Depth of Earth Cover for Buried Domes [redacted]	11-44
11-28	[redacted] Configuration of Mounded Arches [redacted]	11-45
11-29	[redacted] Correction for Attenuation with Depth [redacted]	11-71
11-30	[redacted] Damage Pressure Level [redacted]	11-72
11-31	[redacted] Correction for Arching [redacted]	11-73
11-32	[redacted] Definition of Effective Pulse Duration [redacted]	11-74
11-33	[redacted] Approximate Values of J and r_g for Common Shapes [redacted]	11-77
11-34a	[redacted] Conditions for Moderate Damage by Impulsive Loading [redacted]	11-78
11-34b	[redacted] Conditions for Heavy Damage by Impulsive Loading [redacted]	11-79
11-35	[redacted] Resistance of Deeply Buried Horizontal Reinforced Concrete Arches [redacted]	11-80
11-35a	[redacted] Arch Radius Versus Rise-Span Ratio [redacted]	11-81
11-35b	[redacted] Correction Factor for Material Properties for Deeply Buried Horizontal Reinforced Concrete Arches [redacted]	11-82
11-36	[redacted] Resistance of Deeply Buried Horizontal Steel Arches [redacted]	11-83
11-37	[redacted] Resistance of Deeply Buried Reinforced Concrete Domes [redacted]	11-84
11-37a	[redacted] Dome Radius Versus Rise-Span Ratio [redacted]	11-85
11-37b	[redacted] Correction Factor for Material Properties for Deeply Buried Reinforced Concrete Domes [redacted]	11-86
11-38	[redacted] Resistance of Horizontal One-Way Slabs [redacted]	11-87
11-39	[redacted] Resistance of Horizontal Square Two-Way Slabs — Restrained Edges [redacted]	11-88

[redacted]

[redacted]

LIST OF ILLUSTRATIONS (Continued)

Figure	Title	Page
11-40	[redacted] Resistance of Horizontal Square Two-Way Slabs – Two Adjacent Edges Supported [redacted]	11-89
11-41	[redacted] Aspect Ratio Correction Factor for Strength of Two-Way Slabs [redacted]	11-90
11-42	[redacted] Resistance of Horizontal Square Flat Slabs [redacted]	11-91
11-42a	[redacted] Aspect Ratio Correction Factor for Strength of Rectangular Flat Slabs [redacted]	11-92
11-43	[redacted] Radial Dead Load Soil Pressure on Vertical Cylinder [redacted]	11-93
11-44	[redacted] Interaction Diagram for Reinforced Concrete Beam – Columns [redacted]	11-94
11-45	[redacted] Basic Chart for Vulnerability of Tunnels in Rock [redacted]	11-96
11-46	[redacted] Vulnerability Criteria – Class A Equipment [redacted]	11-101
11-47	[redacted] Vulnerability Criteria for Personnel [redacted]	11-102
11-48	[redacted] Vulnerability Plot for Seismic Velocity (c_p) of 1500 fps – Vertical Motion [redacted]	11-105
11-49	[redacted] Vulnerability Plot for Seismic Velocity (c_p) of 5000 fps – Vertical Motion [redacted]	11-106
11-50	[redacted] Vulnerability Plot for Seismic Velocity (c_p) of 15,000 fps – Vertical Motion [redacted]	11-107
11-51	[redacted] Shock Response Spectra and Vulnerability Calculation [redacted]	11-108
11-52	[redacted] Blast Resistance of Unprotected Floating and Conical-roof Tanks for 20 kt [redacted]	11-114
11-53	[redacted] Blast Resistance of Protected Floating and Conical-roof Tanks for 20 kt [redacted]	11-115
11-54	[redacted] Blast Resistance of Unprotected Floating and Conical-roof Tanks for 500 kt [redacted]	11-116
11-55	[redacted] Blast Resistance of Protected Floating and Conical-roof Tanks for 500 kt [redacted]	11-117
11-56	[redacted] Command Posts and Personnel Shelters (reference Table 11-13) – Damage by 1 kt as Function of Height of Burst and Ground Distance [redacted]	11-125
11-57	[redacted] Machine-gun Emplacements – Damage by 1 kt as a Function of Height of Burst and Ground Distance (reference Table 11-13) [redacted]	11-124
11-58	[redacted] Damage Levels to Foxholes and Trenches in Selected Soils Versus Overpressure Impulse [redacted]	11-126
11-59	[redacted] Ignition Thresholds for Newspaper [redacted]	11-133
11-60	[redacted] Graphical Summary of San Jose Study [redacted]	11-135
11-61	[redacted] Graphical Summary of New Orleans Study [redacted]	11-137
11-62	[redacted] Graphical Analysis of the Thermal and Blast Effects of Two Nuclear Bursts [redacted]	11-142

[redacted]

LIST OF ILLUSTRATIONS (Continued)

Figure	Title	Page
12-1	[redacted]	12-5
12-2		12-7
12-3		12-14
12-4		12-15
12-5		12-16
12-6		12-22
12-7		12-23
12-8		12-24
12-9		12-25
12-10		12-26
12-11		12-27
12-12		12-28
12-13		12-29
13-1	Example Airplane (American) [redacted]	13-16
13-2	Example Helicopter [redacted]	13-17
13-3	Subsonic Wing Lift Curve Slope [redacted]	13-18
13-4a	Wing Supersonic Normal Force Curve Slope [redacted]	13-19
13-4b	Wing Supersonic Normal Force Curve Slope [redacted]	13-20
13-4c	Wing Supersonic Normal Force Curve Slope [redacted]	13-21
13-5	[redacted] Ratio of the Aspect Ratio of the Vertical Tail in the Presence of the Body to That of the Isolated Vertical Tail at Subsonic Speeds [redacted]	13-25
13-6	[redacted] Empirical Factor for Estimating C_{L_α} for Vertical Tails [redacted]	13-26
13-7	[redacted] Dynamic Factor vs Weapon Yield [redacted]	13-34

[redacted]

LIST OF ILLUSTRATIONS (Continued)

Figure	Title	Page
13–8a	[redacted] $w/c \times \Delta L/L$ as a Function of Scaled Range ($N > 0$) [redacted]	13–35
13–8b	[redacted] $w/c \times \Delta L/L$ as a Function of Scaled Range ($N < 0$) [redacted]	13–36
13–9	[redacted] Standard Shapes for Gust Envelopes at Intercept Time [redacted]	13–37
13–10	[redacted] Lethal Ratio vs Weapon Yield [redacted]	13–38
13–11	[redacted] Dynamic Factor vs Weapon Yield [redacted]	13–45
13–12a	[redacted] $\eta \times \Delta L/L$ as a Function of Scaled Range ($N > 0$) [redacted]	13–46
13–12b	[redacted] $\eta \times \Delta L/L$ as a Function of Scaled Range ($N < 0$) [redacted]	13–47
13–13	[redacted] Standard Shapes for Gust Envelopes at Intercept Time [redacted]	13–48
13–14	[redacted] Lethal Ratio vs Weapon Yield [redacted]	13–49
13–15	[redacted] Peak Overpressure from a 1 kt Free Air Burst in a Standard Sea Level Atmosphere [redacted]	13–54
13–16	[redacted] The Range Parameter $\overline{HR}_i$ as a Function of Sea Level Overpressure [redacted]	13–55
13–17a	[redacted] $\overline{BH}_i$ as a Function of $\overline{HR}_i$, Short Ranges [redacted]	13–56
13–17b	[redacted] $\overline{BH}_i$ as a Function of $\overline{HR}_i$, Long Ranges [redacted]	13–57
13–18	[redacted] Overpressure Envelope for Parked Aircraft [redacted]	13–58
13–19	[redacted] Equilibrium Temperature as a Function of Mach Number [redacted]	13–65
13–20	[redacted] Thermal Partition as a Function of Yield and Altitude [redacted]	13–66
13–21	[redacted] Geometry of Burst and Intercept Reference Frames [redacted]	13–76
13–22	[redacted] Time of Arrival of the Shock Front from a 1 kt Free Air Burst in a Standard Sea Level Atmosphere [redacted]	13–77
13–23	[redacted] Intercept-Time Envelope (Front View) [redacted]	13–78
13–24a	[redacted] Intercept-Time Envelope (Side View) [redacted]	13–79
13–24b	[redacted] Slice Through Intercept-Time Volume at Y_I = 2,000 Feet [redacted]	13–79
13–24c	[redacted] Slice Through Intercept-Time Volume at Y_I = 4,000 Feet [redacted]	13–80
13–24d	[redacted] Slice Through Intercept-Time Volume at Y_I = 6,000 Feet [redacted]	13–80
13–24e	[redacted] Slice Through Intercept-Time Volume at Y_I = 8,000 Feet [redacted]	13–81
13–24f	[redacted] Slice Through Intercept-Time Volume at Y_I = 10,000 Feet [redacted]	13–81
13–25a	[redacted] Burst-Time Envelope (Side View) [redacted]	13–82
13–25b	[redacted] Slice Through Burst-Time Volume at Y_B = 2,000 Feet [redacted]	13–82
13–25c	[redacted] Slice Through Burst-Time Volume at Y_B = 4,000 Feet [redacted]	13–83
13–25d	[redacted] Slice Through Burst-Time Volume at Y_B = 6,000 Feet [redacted]	13–83
13–25e	[redacted] Slice Through Burst-Time Volume at Y_B = 8,000 Feet [redacted]	13–84
13–25f	[redacted] Slice Through Burst-Time Volume at Y_B = 10,000 Feet [redacted]	13–84
13–26a	[redacted] Burst-Time Envelope (Front View) [redacted]	13–85
13–26b	[redacted] Burst-Time Envelope (Top View) [redacted]	13–85
14–1	[redacted] Surface Burst Ground Range as a Function of Yield for Constant Total Impulse of 0.50 psi-sec [redacted]	14–3

[redacted]

[redacted]

LIST OF ILLUSTRATIONS (Continued)

Figure	*Title*	*Page*
14–2	[redacted] Target Response Modes [redacted]	14–5
14–3	[redacted] Illustration of the Damage vs Distance Curve [redacted]	14–7
14–4	[redacted] Damage to 1/4 Ton and 2-1/2 Ton Trucks, Side–On Orientation, as a Function of Ground Distance from a 1 kt Surface Burst [redacted]	14–8
14–5	[redacted] Damage to U.S. 57-mm and U.K. 25-Pounder, Side–On Orientation, as a Function of Ground Distance from a 1 kt Surface Burst [redacted]	14–9
14–6	[redacted] Damage to World War II and M38 1/4–Ton Trucks as a Function of Distance from a 1 kt Surface Burst [redacted]	14–10
14–7	[redacted] Illustration of the Effect of Target Orientation: Damage to World War II 1/4–Ton Trucks Oriented Side–On and End–On as a Function of Distance from a 1 kt Surface Burst [redacted]	14–11
14–8	[redacted] The Effect of Shielding [redacted]	14–12
14–9	[redacted] Effect of Weapon Yield on World War II 1/4–Ton Trucks Exposed Side–On in Shielded and Unshielded Conditions to Surface Explosions [redacted]	14–13
14–10	[redacted] Effect of Surface Condition on Damage Category Illustrated by Damage to 1/4–Ton Trucks Oriented Side–On to the Blast Wave from a 1 kt Surface Burst on Two Surfaces [redacted]	14–15
14–11	[redacted] Effect of Vehicle Status on the Distance for a Specified Damage Level from a 1 kt Surface Burst to U.S. 1/4–Ton Trucks (Brakes On, In Gear) and U.K. 1/4–Ton Trucks (Brakes Off, Out–of–Gear) Exposed in an End–On Orientation [redacted]	14–16
14–12	[redacted] Peak Dynamic Pressure as a Function of Peak Overpressure [redacted]	14–26
14–13	[redacted] Damage to *Wheeled Vehicles* as a Function of Height of Burst (HOB) and Ground Distance (GD) for a 1 kt Explosion Over Nonideal and Near–Ideal Surfaces. The curves show HOB and GD at which there is a 50 percent probability that the item of equipment will experience at least the level of damage shown. NOTE: HOB scales as $W^{1/3}$; GD scales as $W^{0.4}$ [redacted]	14–37
14–14	[redacted] Damage to *Artillery* as a Function of Height of Burst (HOB) and Ground Distance (GD) for a 1 kt Explosion Over Nonideal and Near–Ideal Surfaces. The curves show HOB and GD at which there is a 50 percent probability that the item of equipment will experience at least the level of damage shown. NOTE: HOB scales as $W^{1/3}$; GD scales as $W^{0.4}$ [redacted]	14–38
14–15	[redacted] Damage to *Tracked Vehicles (Except Tanks) and Engineer Heavy Equipment* as a Function of Height of Burst (HOB) and Ground Distance	

[redacted]

[redacted]

LIST OF ILLUSTRATIONS (Continued)

Figure	*Title*	*Page*
	(GD) for a 1 kt Explosion Over Nonideal and Near-Ideal Surfaces. The curves show HOB and GD at which there is a 50 percent probability that the item of equipment will experience at least the level of damage shown. NOTE: HOB scales as $W^{1/3}$; GD scales as $W^{0.4}$ [redacted]	14–39
14–16	[redacted] Damage to *Tanks (Light and Heavy)* as a Function of Height of Burst (HOB) and Ground Distance (GD) for a 1 kt Explosion Over Nonideal and Near-Ideal Surfaces. The curves show HOB and GD at which there is a 50 percent probability that the item of equipment will experience at least the level of damage shown. NOTE: HOB scales as $W^{1/3}$; GD scales as $W^{0.4}$ [redacted]	14–40
14–17	[redacted] Damage to *Small Arms* as a Function of Height of Burst (HOB) and Ground Distance (GD) for a 1 kt Explosion Over Nonideal and Near-Ideal Surfaces. The curves show HOB and GD at which there is a 50 percent probability that the item of equipment will experience at least the level of damage shown. NOTE: HOB scales as $W^{1/3}$; GD scales as $W^{0.4}$ [redacted]	14–41
14–18	[redacted] Damage to *Generators* as a Function of Height of Burst (HOB) and Ground Distance (GD) for a 1 kt Explosion Over Nonideal and Near-Ideal Surfaces. The curves show HOB and GD at which there is a 50 percent probability that the item of equipment will experience at least the level of damage shown. NOTE: HOB scales as $W^{1/3}$; GD scales as $W^{0.4}$ [redacted]	14–42
14–19	[redacted] Damage to *Locomotives* as a Function of Height of Burst (HOB) and Ground Distance (GD) for a 1 kt Explosion Over both Nonideal and Near-Ideal Surfaces. The curves show HOB and GD at which there is a 50 percent probability that the item of equipment will experience at least the level of damage shown. NOTE: HOB scales as $W^{1/3}$; GD scales as $W^{0.4}$ [redacted]	14–43
14–20	[redacted] Damage to *Box Cars* as a Function of Height of Burst (HOB) and Ground Distance (GD) for a 1 kt Explosion Over both Nonideal and Near-Ideal Surfaces. The curves show HOB and GD at which there is a 50 percent probability that the item of equipment will experience at least the level of damage shown. NOTE: HOB scales as $W^{1/3}$; GD scales as $W^{0.4}$ [redacted]	14–44
14–21	[redacted] Damage to *Supply Dumps* as a Function of Height of Burst (HOB) and Ground Distance (GD) for a 1 kt Explosion Over both Nonideal and Near-Ideal Surfaces. The curves show HOB and GD at which there is the indicated probability that the dump will experience at least the level of damage shown. NOTE: HOB scales as $W^{1/3}$; GD scales as $W^{0.4}$ [redacted]	14–45
14–22	[redacted] Damage to *Telephone Poles* as a Function of Height of Burst (HOB) and Ground Distance (GD) for a 1 kt Explosion Over both Nonideal and	

[redacted]

[redacted]

LIST OF ILLUSTRATIONS (Continued)

Figure	*Title*	*Page*
	Near-Ideal Surfaces. The curves show HOB and GD at which there is a 50 percent probability that the item of equipment will experience at least the level of damage shown. NOTE: HOB scales as $W^{1/3}$; GD scales as $W^{1/3}$ [redacted]	14–46
14–23	[redacted] Damage to *Water Storage Equipment* as a Function of Height of Burst (HOB) and Ground Distance (GD) for a 1 kt Explosion Over Nonideal and Near-Ideal Surfaces. The curves show HOB and GD at which there is a 50 percent probability that the item of equipment will experience at least the level of damage shown. NOTE: HOB scales as $W^{1/3}$; GD scales as $W^{1/3}$ [redacted]	14–47
14–24	[redacted] Damage to *Shielded Wheeled Vehicles* as a Function of Height of Burst (HOB) and Ground Distance (GD) for a 1 kt Explosion Over both Nonideal and Near-Ideal Surfaces. The curves show HOB and GD at which there is a 50 percent probability that the item of equipment will experience at least the level of damage shown. NOTE: HOB scales as $W^{1/3}$; GD scales as $W^{1/3}$ [redacted]	14–48
14–25	[redacted] Damage to *Shielded Engineer Heavy Equipment* as a Function of Height of Burst (HOB) and Ground Distance (GD) for a 1 kt Explosion Over both Nonideal and Near-Ideal Surfaces. The curves show HOB and GD at which there is a 50 percent probability that the item of equipment will experience at least the level of damage shown. NOTE: HOB scales as $W^{1/3}$; GD scales as $W^{1/3}$ [redacted]	14–49
14–26	[redacted] Damage to *Signal, Electronic Fire Control Equipment, Antennas and Rigid Radomes* as a Function of Height of Burst (HOB) and Ground Distance (GD) for a 1 kt Explosion Over Nonideal and Near-Ideal Surfaces. The curves show HOB and GD at which there is the indicated probability that the item of equipment will experience at least the level of damage shown. NOTE: HOB scales as $W^{1/3}$; GD scales as $W^{0.4}$ except for Radomes. For Radomes use $W^{1/3}$ [redacted]	14–50
14–27	[redacted] Damage to *Wire Entanglements* as a Function of Height of Burst (HOB) and Ground Distance (GD) for a 1 kt Explosion Over Nonideal and Near-Ideal Surfaces. The curves show HOB and GD at which there is a 50 percent probability that the item of equipment will experience at least the level of damage shown. NOTE: HOB scales as $W^{1/3}$ for yields < 1 kt, $W^{0.4}$ for yields > 1 kt [redacted]	14–51
15–1	[redacted] Light Damage to Various Broadleaf Forest Types [redacted]	15–7
15–2	[redacted] Moderate Damage to a Type I Forest [redacted]	15–8
15–3	[redacted] Severe Damage to a Type I Forest [redacted]	15–9
15–4	[redacted] Total Damage to a Type I Forest [redacted]	15–10
15–5	[redacted] Moderate Damage to a Type II Forest [redacted]	15–11

[redacted]

[redacted]

LIST OF ILLUSTRATIONS (Continued)

Figure	Title	Page
15-6	Severe Damage to a Type II Forest	15-12
15-7	Total Damage to a Type II Forest	15-13
15-8	Moderate Damage to a Type III Forest	15-14
15-9	Severe Damage to a Type III Forest	15-15
15-10	Total Damage to a Type III Forest	15-16
15-11	Moderate Damage to a Type IVa-1(f) Forest	15-17
15-12	Severe Damage to a Type IVa-1(f) Forest	15-18
15-13	Total Damage to a Type IVa-1(f) Forest	15-19
15-14	Moderate Damage to a Type IVa-1(d) Forest	15-20
15-15	Severe Damage to a Type IVa-1(d) Forest	15-21
15-16	Total Damage to a Type IVa-1(d) Forest	15-22
15-17	Moderate Damage to a Type IVa-2(f) Forest	15-23
15-18	Severe Damage to a Type IVa-2(f) Forest	15-24
15-19	Total Damage to a Type IVa-2(f) Forest	15-25
15-20	Moderate Damage to a Type IVa-2(d) Forest	15-26
15-21	Severe Damage to a Type IVa-2(d) Forest	15-27
15-22	Total Damage to a Type IVa-2(d) Forest	15-28
15-23	Moderate Damage to a Type IVb(f) Forest	15-29
15-24	Severe Damage to a Type IVb(f) Forest	15-30
15-25	Total Damage to a Type IVb(f) Forest	15-31
15-26	Moderate Damage to a Type IVb(d) Forest	15-32
15-27	Severe Damage to a Type IVb(d) Forest	15-33
15-28	Total Damage to a Type IVb(d) Forest	15-34
15-29	Moderate Damage to a Type IVc(f) Forest	15-35
15-30	Total Damage to a Type IVc(f) Forest	15-36
15-31	Moderate Damage to a Type IVc(d) Forest	15-37
15-32	Total Damage to a Type IVc(d) Forest	15-38
15-33	Moderate Damage to a Type IVd Forest	15-39
15-34	Total Damage to a Type IVd Forest	15-40
15-35	Stem-ft per Acre Comparison Between a Rain Forest and a Coniferous Forest	15-43
15-36	Average Diameter of Stems Down, Comparison Between a Rain Forest and a Coniferous Forest, 1 kt	15-44
15-37	Debris Characteristics Preventing Radial Movement of Vehicles	15-45
15-38	Debris Characteristics Preventing Circumferential Movement of Vehicles	15-46
15-39	Minimum Radiant Exposures of Wildland Kindling Fuels by a 1 Kiloton Explosion	15-55

[redacted]

[redacted]

LIST OF ILLUSTRATIONS (Continued)

Figure	*Title*	*Page*
15–40	[redacted] Probability of Exposure of the Forest Floor ("Standard Northern European Forest") as a Function of Elevation Angle: Examples of a Point Source and a Spherical Source Subtending an Angle of 10 Degrees [redacted]	15–57
15–41	[redacted] Probability of Exposure of Forest Floor for Different Levels of Tree Density [redacted]	15–59
16–1	[redacted] Missile Configurations, SERGEANT, LANCE, and HAWK [redacted]	16–2
16–2	[redacted] SERGEANT System, Semitrailer Transporter with Missile Section Containers [redacted]	16–4
16–3	[redacted] SERGEANT System, Launching Station with Missile in Firing Position [redacted]	16–5
16–4	[redacted] SERGEANT System, Launching Station Firing Set [redacted]	16–6
16–5	[redacted] SERGEANT System, Organizational Maintenance Test Station (OMTS) [redacted]	16–8
16–6	[redacted] SERGEANT, Major Item Blast Vulnerability [redacted]	16–11
16–7	[redacted] LANCE System, Primary Units of the Missile System [redacted]	16–13
16–8	[redacted] LANCE System, Prefire Tester and Fire Pack [redacted]	16–14
16–9	[redacted] LANCE, Major Item Blast Vulnerability [redacted]	16–18
16–10	[redacted] HAWK System, Basic Assault Firing Unit [redacted]	16–20
16–11	[redacted] HAWK System, Auxiliary Components [redacted]	16–21
16–12	[redacted] HAWK, Major Item Blast Vulnerability [redacted]	16–25
16–13	[redacted] HONEST JOHN, Major Components of Rocket [redacted]	16–26
16–14	[redacted] HONEST JOHN, Truck-Mounted Rocket Launcher in Traveling Position [redacted]	16–27
16–15	[redacted] HONEST JOHN Rocket Launcher in Firing Position [redacted]	16–28
16–16	[redacted] HONEST JOHN, Auxiliary Equipment [redacted]	16–29
16–17	[redacted] HONEST JOHN, Major Item Blast Vulnerability [redacted]	16–33
16–18	[redacted] ABM and RV Configuration Comparison [redacted]	16–35
16–19	[redacted] ABM and RV Operating Envelope Comparison [redacted]	16–35
16–20	[redacted] Response Regimes for Interceptor Missile [redacted]	16–36
16–21	[redacted] Nuclear Encounter and Event Sequence for RV and ABM [redacted]	16–37
16–22	[redacted] HARTS Configuration [redacted]	16–40
16–23	[redacted] Blast Intercept Conditions Nomenclature [redacted]	16–41
16–24	[redacted] Scaled Blast Wave Radius for Constant Hardness Level for Configuration A, 5,500 nm Range [redacted]	16–44
16–25	[redacted] Scaled Time of Blast Intercept for Constant Hardness Level for Configuration A, 5,500 nm Range [redacted]	16–45

[redacted]

[redacted]

LIST OF ILLUSTRATIONS (Continued)

Figure	*Title*	*Page*
16–26	[redacted] Variation of Hardness Level with Altitude and Slant Range for [redacted] Configuration A [redacted]	16–46
16–27	[redacted] Normal Reentry Trajectory; Initial Altitude = 400,000 ft, Initial Velocity (V_i) = 23,900 ft/sec, Initial Flight-Path Angle = 20°, Ballistic Coefficient $\beta = W/C_dA$ lb/ft^2 [redacted]	16–48
16–28	[redacted] Normal Reentry Trajectory; Initial Altitude = 400,000 ft, Initial Velocity (V_i) = 24,000 ft/sec, Initial Flight-Path Angle = 30°, Ballistic Coefficient $\beta = W/C_dA$ lb/ft^2 [redacted]	16–49
16–29	[redacted] Normal Reentry Trajectory; Initial Altitude = 400,000 ft, Initial Velocity (V_i) = 24,000 ft/sec, Initial Flight-Path Angle = 30°, Ballistic Coefficient $\beta = W/C_dA$ lb/ft^2 [redacted]	16–50
16–30	[redacted] Scaled Intercept Load Duration Time, 500 g Hardness, Configuration A [redacted]	16–54
16–31	[redacted] Scaled Fireball Traversal Time 500 g Hardness, Configuration A [redacted]	16–55
16–32	[redacted] Scaled Total Blast Traversal Time 500 g Hardness, Configuration A [redacted]	16–56
16–33	[redacted] Flow Pattern Around an Axisymmetric Blunt-Nosed Body [redacted]	16–57
16–34	[redacted] Steady State Flow Field Surface Pressures, Sphere-Cone-Flare Body [redacted]	16–59
16–35	[redacted] Steady State Flow Field Surface Pressures, Cone Sphere Body [redacted]	16–60
16–36	[redacted] Maximum Overpressure and Overpressure Duration for Typical Shock-Shock Interactions [redacted]	16–61
16–37	[redacted] Determination of Locus of Escape [redacted]	16–63
16–38	[redacted] Qualitative Iso-g Contours [redacted]	16–64
16–39	[redacted] In-Flight Intercept [redacted]	16–65
16–40	[redacted]	16–67
16–41	[redacted]	16–68
16–42	[redacted]	16–69
16–43	[redacted]	16–71

[redacted]

[redacted]

LIST OF ILLUSTRATIONS (Continued)

Figure	Title	Page
16–44	[redacted] Thermal Radiation Heat Load on the Cone as a Function of Initial Slant Range for Several Burst Altitudes [redacted]	16–72
16–45	[redacted] Thermal Radiation Heat Load on the Cone as a Function of Initial Slant Range for Several Burst Yields [redacted]	16–73
16–46	[redacted] Thermal Radiation Heat Load on the Cone as a Function of Initial Slant Range for Several Trajectories [redacted]	16–74
16–47	[redacted]	16–78
16–48	[redacted]	16–79
16–49	[redacted] Cone Bulk Temperature After Fly Through as a Function of Initial Slant Range from Burst (Head on Intercept) [redacted]	16–80
16–50	[redacted] Minimum Initial Slant Range for Structural/Thermal Damage at 40 kft Burst Altitude, V_E/γ_E = 17,000 ft/sec/–35° [redacted]	16–82
16–51	[redacted] Inboard Profile of AIRS I Vehicle [redacted]	16–84
16–52	[redacted] Inboard Profile of AIRS II Vehicle [redacted]	16–85
16–53	[redacted] Illustration of Ablation Phenomena [redacted]	16–89
16–54	[redacted]	16–92
16–55	[redacted]	16–93
16–56	[redacted]	16–94
16–57	[redacted]	16–95
16–58	[redacted] Computed Temperature Profile, t = 4.64 msec, 30 kilofeet Altitude [redacted]	16–97
16–59	[redacted] Computed Density Profile, t = 4.64 msec, 30 kilofeet Altitude [redacted]	16–98
16–60	[redacted] Computed Static Pressure Profile, t = 4.64 msec, 30 kilofeet Altitude [redacted]	16–99
16–61	[redacted] Computed Particle Velocity Profile, t = 4.64 msec, 30 kilofeet Altitude [redacted]	16–100
16–62	[redacted] RV Target A, Static Overpressure as a Function of Time, 30° Intercept [redacted]	16–102
16–63	[redacted] RV Target A, Dynamic Pressure as a Function of Time, 30° Intercept [redacted]	16–103

[redacted]

[redacted]

LIST OF ILLUSTRATIONS (Continued)

Figure	*Title*	*Page*
16–64	[redacted] RV Target A, Static Overpressure Impulse as a Function of Time, 30° Intercept [redacted]	16–104
16–65	[redacted] RV Target A, Dynamic Pressure Impulse as a Function of Time, 30° Intercept [redacted]	16–105
16–66	[redacted] Pressure–Impulse Damage Levels, RV Target A Configuration Aft Bay [redacted]	16–108
16–67	[redacted] SPRINT Blast Loads, RV Target A, 30 kilofeet Altitude, Aft Bay [redacted]	16–110
16–68	[redacted] Ablation Rate and Mass Ablated as a Function of Time for Target A Threat RV [redacted]	16–111
16–69	[redacted] Mass Ablated as a Function of Burst Time Standoff Distance for Target A Threat RV [redacted]	16–112
16–70	[redacted] Typical Traverse–Mass Erosion Rate History [redacted]	16–114
16–71	[redacted] Typical Traverse–TML History [redacted]	16–115
17–1	[redacted] Approximate Locations of Ionization Causing Absorption [redacted]	17–3
17–2	[redacted] Attenuation Related to Normal Loss Due to Spread–Debris Environment, 4000–km Path Length [redacted]	17–10
17–3	[redacted] Attenuation Relative to Normal Loss of Nighttime Impulse Disturbance, Path Length = 4000 km [redacted]	17–11
17–4	[redacted] Phase Variation Relative to Normal for Nighttime Impulse Disturbance, Path Length = 4000 km [redacted]	17–12
17–5	[redacted] Examples of Daytime HF Ray–Path Geometry [redacted]	17–14
17–6	[redacted] Example of Signal–to–Noise Ratio and Absorption After a [redacted] 30–km Burst [redacted]	17–23
17–7	[redacted] Example of Signal–to–Noise Ratio and Noise Temperature After Multimegaton 150–km Bursts [redacted]	17–24
17–8	[redacted] Illustration of Troposcatter Geometry [redacted]	17–25
17–9	[redacted] Illustration of Ionoscatter Geometry [redacted]	17–29
17–10	[redacted] Plan View of Radar and Target Geometry [redacted]	17–34
17–11	[redacted] Signal–to–Noise Ratios and Elevation Errors for Radar Located at Target [redacted]	17–35
17–12	[redacted] Signal–to–Noise Ratios and Elevation Errors for Offset Radar [redacted]	17–37
17–13	[redacted] Solid Angle Obscured by 10–kt Intercept [redacted]	17–38
A–1	[redacted] Change in Air Properties Across a Shock Front [redacted]	A–2
A–2	[redacted] Equation of State Data for Air [redacted]	A–6
A–3	[redacted] Idealized Shock Wave [redacted]	A–8
A–4	[redacted] Parameters of a 10 psi Shock Wave [redacted]	A–10

[redacted]

[redacted]

LIST OF ILLUSTRATIONS (Continued)

Figure	*Title*	*Page*
A-5	Reflection of a 10 psi Shock Wave from a Solid Barrier	A-11
A-6	Reflection of a Shock Wave by a Small Object	A-12
B-1	Various Fractional Powers of Numbers	B-6
B-2	Dimension Scaling Nomogram	B-7
B-3	Height of Burst—Horizontal Distance—Slant Range Nomogram	B-8
C-1	Probability Distributions for Failure or for Survival as Function of Ratio of Median Input Motion b_i to Median Vulnerability Level of Motion b_v	C-5
C-2	Coefficient of Variation σ/m as Function of b_i/b_v Ratio for Specified Probability of Failure (or of b_v/b_i for Specified Probability of Survival)	C-6

[redacted]

[redacted]

LIST OF TABLES

PART II

Table	Title	Page
9-1	Thermal Properties of Materials	9-18
9-2	Approximate Radiant Exposures for Ignition of Fabrics	9-26
9-3	Approximate Radiant Exposures for Ignition of Various Materials	9-27
9-4	Minimum Structure Separation for Escape Route	9-31
9-5	Absorption Coefficients for Bare Metals	9-32
9-6	Average Absorption Coefficients for Laser Heated Coated Substrates	9-33
9-7	Representative Values of Absorption Coefficients for Metals with Various Coatings or Surface Treatments	9-34
9-8	Values of h_{cv} Obtained from Various Functions in the Order in Which the Equations are Given Above	9-37
9-9	Allowable Uniform Static Load for Aluminum Plate at Three Temperatures	9-65
9-10	X-ray Cross Sections, Beryllium Z = 4 (cm^2/gm)	9-77
9-11	X-ray Cross Sections, Aluminum Z = 13 (cm^2/gm)	9-78
9-12	X-ray Cross Sections, Iron Z = 26 (cm^2/gm)	9-79
9-13	X-ray Cross Sections, Copper Z = 29 (cm^2/gm)	9-80
9-14	X-ray Cross Sections, Tungsten Z = 74 (cm^2/gm)	9-81
9-15	X-ray Cross Sections, Uranium Z = 92 (cm^2/gm)	9-83
9-16	X-ray Deposition and Shine Through in Aluminum for 10 cal/cm^2 of Incident X-rays	9-93
9-17	Enthalpy Change for Selected Metals	9-98
9-18	Fluence Required to Produce Various Enthalpy Changes at the Surface of Aluminum (cal/cm^2)	9-101
9-19	Enthalpy Changes ϵ (Mb)	9-102
9-20	Pressure Change, P (Mb)	9-103
9-21	X-ray Energy Deposition and Shine Through for Reference RV Shell	9-117
9-22	Estimated Dose Transmission Factors (Interior Dose/Exterior Dose)	9-120
9-23	Representative Radiation-Failure Levels for Digital Junction-Isolated Semiconductor Integrated Circuits	9-163
9-24	Failure Thresholds for Typical Digital Microcircuits	9-167
9-25	Failure Thresholds for Typical Linear Microcircuits	9-168
9-26	Failure Thresholds for Typical MOS Digital Microcircuits	9-169
9-27	Minimum Observed Joule Energy to Cause Burnout	9-174
9-28	Minimum Joule Energy to Cause Permanent Degradation Indicated	9-175
9-29	Minimum Joule Energy to Cause Circuit Upset or Interference	9-176

[redacted]

[redacted]

LIST OF TABLES (Continued)

Table	Title	Page
9-30	[redacted] Comparison of Guided Wave and Radiating Simulators [redacted]	9-181
10-1	[redacted] Estimated Casualty Production in Buildings for Three Degrees of Structural Damage [redacted]	10-6
10-2	[redacted] Response to Single Whole-Body Exposures [redacted]	10-24
11-1	[redacted] Damage to Types of Structures Primarily Affected by Blast Wave Overpressure During the Diffraction Phase [redacted]	11-5
11-2	[redacted] Damage to Types of Structures Primarily Affected by Dynamic Pressure During the Drag Phase [redacted]	11-6
11-3	[redacted] Building Parameter Values [redacted]	11-10
11-4	[redacted] Reference List of Isodamage Curves for Various Types of Bridges [redacted]	11-11
11-5	[redacted] Factors for Obtaining Distances Corresponding to 50 Percent Probability of Moderate Damage to the Indicated Structure Type [redacted]	11-13
11-6	[redacted] Ratio of Horizontal to Vertical Soil Pressures, K_o [redacted]	11-56
11-7	[redacted] Equivalent Friction Angles for Noncranular Cohesive Soils [redacted]	11-57
11-8	[redacted] Typical Tunnel Design Concepts [redacted]	11-58
11-9	[redacted] Limits of Vulnerability in Terms of Overpressure for Surface Silos—1 Mt [redacted]	11-59
11-10	[redacted] Definition of γ and δ for Figures 11-32 and 11-34 [redacted]	11-75
11-11	[redacted] Estimates of Frequency and Vulnerability of Typical Items of Equipment [redacted]	11-98
11-12	[redacted] Light Damage to POL Tanks [redacted]	11-112
11-13	[redacted] Damage Criteria for Field Fortifications [redacted]	11-119
11-14	[redacted] Unified Soil Classification [redacted]	11-120
12-1	[redacted]	12-3
12-2	[redacted]	12-8
12-3	[redacted]	12-10
12-4	[redacted]	12-18
13-1	[redacted] Selected Data Based on U.S. Standard Atmosphere, 1962 English Units [redacted]	13-15
13-2	[redacted] Overpressure Criteria [redacted]	13-51
13-3	[redacted] Average Properties of Selected Engineering Materials [redacted]	13-63
13-4	[redacted] Average Values of Absorptivities, α [redacted]	13-64
14-1	[redacted] Definitions of Damage Categories [redacted]	14-18
14-2	[redacted] Wheeled Vehicle Subsystems [redacted]	14-18

NAVY (k)(1)

[redacted]

[redacted]

LIST OF TABLES (Continued)

Table	Title	Page
14-3	[redacted] Typical Subsystem Damage for Various Damage Categories [redacted]	14-19
14-4	[redacted] List of Equipment and Corresponding Prediction Tables [redacted]	14-22
14-5	[redacted] Equipment Sensitive to Total Impulse [redacted]	14-23
14-6	[redacted] Equipment Sensitive to Overpressure [redacted]	14-24
14-7	[redacted] Equipment Sensitive to Dynamic Pressure [redacted]	14-25
14-8	[redacted] Untested Equipment [redacted]	14-53
14-9	[redacted] Ambient Radiation Levels for "Sure Safe" and "Sure Kill" in Selected Ground Systems [redacted]	14-66
14-10	[redacted] Ambient Radiation Levels for "Sure Safe" and "Sure Kill" for General Aircraft Subsystems [redacted]	14-68
14-11	[redacted] Ambient Radiation Levels for "Sure Safe" and "Sure Kill" for Missile Systems [redacted]	14-71
15-1	[redacted] Average Height of Trees, Diameter, Tree Density, and Length of Tree Stem [redacted]	15-2
15-2	[redacted] Index of Isodamage Curves Showing Forest Stand Type and Applicable Figure Number for Indicated Degree of Damage [redacted]	15-3
15-3	[redacted] Effects of a 1 kt Weapon Burst at a Height of 270 Feet Over a Rain Forest [redacted]	15-41
15-4	[redacted] Effects of a 1 kt Surface Burst on a Coniferous Forest [redacted]	15-42
15-5	[redacted] Comparison of Radial and Circumferential Movement Rates for Troops in a Rain Forest Blowdown Area, Scaled to a 1 kt Nuclear Explosion [redacted]	15-48
15-6	[redacted] Comparison of Circumferential Movement Rates for Troops in a Coniferous Forest Blowdown Area, Scaled to a 1 kt Nuclear Explosion [redacted]	15-48
15-7	[redacted] Influence of Forest Damage on the Movement of Troops and Vehicles [redacted]	15-49
15-8	[redacted] Classes of Thin Wildland Kindling Fuels (Arranged in Order of Decreasing Flammability) [redacted]	15-52
15-9	[redacted] "Standard Northern European Forest" Data [redacted]	15-57
15-10	[redacted] Condition of Wildland Fuels During Fire Season [redacted]	15-60
15-11	[redacted] Criteria of "No-Spread" of Fires [redacted]	15-61
15-12	[redacted] Fire-Out Criteria [redacted]	15-62
15-13	[redacted] Burning Durations by Fuel Type [redacted]	15-63
16-1	[redacted] SERGEANT, Characteristics and Damage Levels for System Components [redacted]	16-9
16-2	[redacted] Blast Vulnerability Summary, SERGEANT Missile System [redacted]	16-10
16-3	[redacted] LANCE, Characteristics and Damage Levels for System Components [redacted]	16-15
16-4	[redacted] Blast Vulnerability Summary, LANCE Missile System [redacted]	16-19

[redacted]

[redacted]

LIST OF TABLES (Continued)

Table	Title	Page
16-5	[redacted] HAWK, Characteristics and Damage Levels for System Components [redacted]	16-22
16-6	[redacted] Blast Vulnerability Summary, HAWK Missile System [redacted]	16-24
16-7	[redacted] Missile System Components – HONEST JOHN [redacted]	16-30
16-8	[redacted] Summary – HONEST JOHN [redacted]	16-31
16-9	[redacted] Range of Basic Parameters for HARTS II [redacted]	16-39
17-1	[redacted] Satellite Communications Link Description, System A [redacted]	17-21
17-2	[redacted] Satellite Communications Link Description, System B [redacted]	17-21
17-3	[redacted] Estimated Outage Times for Fireball Intersection of the Propagation Path [redacted]	17-22
17-4	[redacted] Troposcatter Communication Link Description [redacted]	17-27
17-5	[redacted] Approximate Extent and Duration of Effects on Troposcatter Communications, Assuming Proper Burst Placement [redacted]	17-28
17-6	[redacted] Ionoscatter Communications Link Description [redacted]	17-30
17-7	[redacted] Approximate Outage Times 1000-, 1500-, and 2000-km Ionoscatter Links, Assuming Proper Burst Placement [redacted]	17-31
A-1	[redacted] Shock Wave Equations for an Ideal Gas [redacted]	A-4
A-2	[redacted] English and Metric Systems of Units [redacted]	A-5
A-3	[redacted] Equations for Strong Shock Waves [redacted]	A-7
C-1	[redacted] Standard Deviations for Use in Probability Analyses [redacted]	C-4
C-2	[redacted] Median Vulnerability to Overpressures Corresponding to Severe Damage of Diffraction Sensitive Structures [redacted]	C-10
C-3	[redacted] Median Vulnerability to Dynamic Pressures Corresponding to Severe Damage of Drag Sensitive Structures [redacted]	C-11
C-4	[redacted] Median Vulnerability to Overpressures Corresponding to Moderate Damage of Diffraction Sensitive Structures [redacted]	C-12
C-5	[redacted] Median Vulnerability to Dynamic Pressures Corresponding to Moderate Damage of Drag Sensitive Structures [redacted]	C-13

[redacted]

LIST OF PROBLEMS

PART II

Problem	*Title*	*Page*
9-1	Calculation of Thermal Thickness of a Metal Plate	9-40
9-2	Calculation of Temperature Rise in a Thermally Thin Plate	9-43
9-3	Calculation of X-ray Energy Deposition at the Surface	9-71
9-4	Calculation of X-ray Energy Deposition at a Depth in a Material and the Shine Through Fluence	9-74
9-5	Calculation of Vapor Blowoff Impulse	9-113
9-6	Calculation of the Location of Phase Change Boundaries	9-114
10-1	Calculation of Casualties for Personnel in the Open or in a Forest	10-7
11-1	Calculation of Damage to Aboveground Structures from an Air Burst	11-14
11-2	Calculation of Damage-Distance Reduction for Surface Targets from Shallow Underground Bursts	11-38
11-3	Calculation of the Thickness for a Deeply Buried Reinforced Concrete Dome	11-60
11-4	Calculation of the Vulnerability of the Roof of a Deeply Buried, Reinforced Concrete Rectangular Structure	11-62
11-5	Calculation of the Thickness Required for Shallow Buried Reinforced Concrete Arch	11-65
11-6	Calculation of the Vulnerability of the Near Surface Portion of a Reinforced Concrete Silo	11-68
11-7	Calculation of the Vulnerability of Tunnels Buried in Rock	11-95
11-8	Calculation of the Vulnerability of Equipment Mounted in an Underground Structure	11-103
11-9	Calculation of Damage to POL Storage Tanks	11-113
11-10	Calculation of Damage to Field Fortifications	11-122
11-11	Calculation of the Radiant Exposure to Ignite Combustibles Indoors	11-132
11-12	Estimation of Fire Damage	11-140
12-1	Calculation of Air Blast Damage Distances to Surface Ships as a Result of Air Bursts	12-4
12-2	Calculation of Shock Wave Damage Distances to Surface Ships as a Result of Underwater Bursts	12-12
12-3	Calculation of Damage Distances for Submarines from Underwater Bursts	12-20
13-1	Calculation of the Aerodynamic Coefficient for Wing and Horizontal Tail	13-12
13-2	Calculation of the Aerodynamic Coefficient for the Vertical Tail	13-22

[redacted]

LIST OF PROBLEMS (Continued)

Problem	*Title*	*Page*
13–3	Calculation of Intercept-Time Envelopes that Determine Sure-Safe and Sure-Kill Regions with Respect to Material Velocity on Airplanes in Flight	13–29
13–4	Calculation of Intercept-Time Envelopes Determining Sure-Safe and Sure-Kill Regions with Respect to Gust Effects of the Material Velocity Behind the Blast Wave on Helicopters in Flight	13–39
13–5	Calculation of the Boundaries in Space that Define the Sure-Safe and Sure-Kill Regions with Respect to the Effects of Overpressure Behind the Blast Wave on Aircraft In-Flight or Parked	13–51
13–6	Calculation of Boundaries in Space (Envelopes) that Define the Sure-Safe and Sure-Kill Regions with Respect to Thermal Radiation on Aircraft In-Flight or Parked	13–60
13–7	Calculation of Burst-Time Envelopes for Gust or Overpressure Effects from Intercept-Time Envelopes	13–68
14–1	Calculation of Damage to Wheeled Vehicles	14–27
14–2	Calculation of Damage to Shielded Wheeled Vehicles	14–29
14–3	Calculation of Damage to Wire Entanglement	14–31
14–4	Calculation of Damage to Artillery	14–33
14–5	Calculation of the Advantage in Shielding Engineer Heavy Equipment	14–35
15–1	Calculation of Air Blast Damage to Forest Stands	15–5
15–2	Calculation of the Distance at Which Movement Will Be Impaired	15–50
15–3	Estimation of Movement Difficulty	15–51
15–4	Calculation of the Requirements for Wildland Kindling Fuel Ignition	15–54
16–1	Calculation of Hardness Level	16–43
16–2	Calculation of Load Characteristics, Fireball Traversal Time and Total Traversal Time	16–53
B–1	Use of Fractional Power Curves and Dimension Scaling Nomogram	B–5

[redacted]

[redacted]

Security Classification

DOCUMENT CONTROL DATA - R & D

(Security classification of title, body of abstract and indexing annotation must be entered when the overall report is classified)

1. ORIGINATING ACTIVITY (Corporate author)
Director
Defense Nuclear Agency
Washington, D.C. 20305

2a. REPORT SECURITY CLASSIFICATION
[redacted]

2b. GROUP

3. REPORT TITLE
Capabilities of Nuclear Weapons Effects Manual Number 1

4. DESCRIPTIVE NOTES (Type of report and inclusive dates)
Handbook

5. AUTHOR(S) (First name, middle initial, last name)
N.A.

6. REPORT DATE	7a. TOTAL NO. OF PAGES	7b. NO. OF REFS
1 July 1972	956	

8a. CONTRACT OR GRANT NO.	9a. ORIGINATOR'S REPORT NUMBER(S)
DASA 01-69-C-0022	DNA EM-1, Part 2
b. PROJECT NO. NWER XXAXD	
c. Task and Subtask A002	9b. OTHER REPORT NO(S) (Any other numbers that may be assigned this report)
d. Work Unit 01 and 02	

10. DISTRIBUTION STATEMENT
None

11. SUPPLEMENTARY NOTES	12. SPONSORING MILITARY ACTIVITY
Supersedes and cancels "Capabilities of Nuclear Weapons," DASA EM-1 dated January 1968.	Director Defense Nuclear Agency Washington, D.C. 20305

13. ABSTRACT

[redacted] This edition of the "Capabilities of Nuclear Weapons" represents the continuing efforts by the Defense Nuclear Agency to correlate and make available nuclear weapons effects information obtained from nuclear weapons testing, small-scale experiments, laboratory effort and theoretical analysis. This document presents the phenomena and effects of a nuclear detonation and relates weapons effects manifestations in terms of damage to targets of military interest. It provides the source material and references needed for the preparation of operational and employment manuals by the Military Services.

[redacted] The "Capabilities of Nuclear Weapons" is not intended to be used as an employment or design manual by itself, since more complete descriptions of phenomenological details should be obtained from the noted references. Every effort has been made to include the most current reliable data available on 31 December 1971 in order to assist the Armed Forces in meeting their particular requirements for operational and target analysis purposes.

[redacted] Due to the physical size of the document, it is published in two (2) parts, [redacted]

DD FORM 1 NOV 68 1473

[redacted]

Security Classification

[redacted]

Security Classification

14. KEY WORDS	LINK A		LINK B		LINK C	
	ROLE	WT	ROLE	WT	ROLE	WT
Nuclear Weapon Effects						
Blast and Shock Phenomena						
Air Blast Phenomena						
Cratering Phenomena						
Ground Shock Phenomena						
Water Shock Phenomena						
Underwater Cratering Phenomena						
Water Surface Phenomena						
Thermal Radiation Phenomena						
X-Ray Radiation Phenomena						
Nuclear Radiation Phenomena						
Initial Nuclear Radiation						
Neutron Induced Activity						
Residual Radiation						
Transient Radiation Effects on Electronics Phenomena						
TREE Phenomena						
Electromagnetic Pulse Phenomena						
EMP Phenomena						
Phenomena Affecting Electromagnetic Wave Propagation						
Blast and Shock Damage						
Thermal Radiation Damage						
X-Ray Damage						
Nuclear Radiation Shielding						
TREE Damage Mechanisms						
EMP Damage						
Personnel Casualties						
Blast Injury						
Thermal Injury						
Nuclear Radiation Injury						
Combined Injury						
Damage to Structures						
Shock Vulnerability of Equipment and Personnel						
Damage to Field Fortifications						
Damage to Dam and Harbor Installations						
Damage to POL Tanks						
Fire in Urban Areas						
Damage to Naval Equipment						
Damage to Surface Ships						
Damage to Subsurface Ships						
Damage to Aircraft						
Damage to Military Field Equipment						
Air Blast Damage to Military Field Equipment						
Thermal Damage to Military Field Equipment						
TREE Damage to Military Field Equipment						
Forest Stand Damage						
Air Blast in Forest Stands						
Blowdown						
Thermal Damage in Forests						
Forest Blowdown Effects on Mobility						
Damage to Missiles						
Radio Frequency Signal Degradation Relevant to Communications Systems						
Radio Frequency Signal Degradation Relevant to Radar Systems						

[redacted]

Security Classification

AD-A955 393

PART II

DAMAGE CRITERIA

Chapter 9

INTRODUCTION TO DAMAGE CRITERIA

Part I of this manual describes the basic phenomena associated with a nuclear explosion for various burst conditions. These phenomena include: blast and shock, thermal radiation, X-ray radiation, nuclear radiation, transient radiation effects on electronics (TREE), electromagnetic pulse (EMP) phenomena, and phenomena affecting electromagnetic wave propagation. Part II treats the mechanisms of casualty production and damage to military targets, and describes the response of these targets by correlating the basic physical phenomena with various defined degrees of damage.

SECTION I

CONTENT AND LIMITATIONS OF PART II

9-1 Introduction to Chapter 9

The information in Part I is divided according to the phenomenology, with one chapter being devoted to each of the seven phenomena listed above. This chapter provides a general discussion of the physical damage mechanisms associated with each of the first six phenomena listed above (the last phenomenon does not produce physical damage; the degradation of signals from radio and radar systems is discussed in Chapter 17). Separate sections describe the damage mechanisms associated with each of the six phenomena. In addition, Section IV of this chapter discusses the degradation of equipment by thermal radiation that might affect its response to the blast wave.

9-2 Organization of Part II

Part II of this manual is divided into chapters according to types of targets that exhibit similar response characteristics. Further subdivisions within the chapters separate the types of targets into subtypes, and for each subtype there are frequently further subdivisions according to the phenomena that cause the damage.

The data presented here are interpretations of complex results of the nuclear weapons effects research and test programs of the Department of Defense. A constant effort is made to deduce theoretical models and scaling laws for the various weapons effects that permit a quantitative prediction of the extent of a given effect from a weapon of one yield related to weapons of other yields. Since the initiation of the limited nuclear test ban treaty, a large amount of effort has been devoted to the development of complex computer codes to predict the environments created by the various phenomena resulting from nuclear explosions and the interactions of these environments with personnel and military systems. A large number of scaling laws presented in Part I that are useful in predicting the environment from a given explosion were derived from the calculations performed with these codes. Many additional scaling laws,

89 3 02 032

derived from field and laboratory experiments, and theoretical studies, as well as the codes, are presented in the chapters of Part II to aid in the predictions of the response of personnel and systems to the environment. Graphical presentation is used in preference to tabular or purely computational presentations wherever possible. The damage curves are drawn for a probability of 50 percent of producing the indicated damage. Curves of 90 and 10 percent probability are included when the quantity and quality of the data permit. In addition, Appendix C provides the methodology for estimating any probability of damage, provided that the median values of the response of a given system are known. Estimates of such median values for the equipment discussed in Sections I through III of Chapter 11 are provided in Appendix C. Effort has been made to provide a comprehensive set of data in a readily usable form; however, certain categories of damage are not amenable to generalization. Some limitations in the content of Part II are discussed in paragraph 9-3.

An estimate of the degree of reliability accompanies most of the data presented herein. Statements of the reliability of damage data only pertain to the basic response data, which, for the target analyst represent the "radius of effect." They should not be confused with the terms variability and probability of damage, which pertain to target response; nor do these estimates include operational considerations such as linear, circular, or spherical aiming and fuzing errors, yield variations, and target intelligence.

9-3 Limitations in Part II

As mentioned in paragraph 9-2, the remaining chapters of Part II each contain descriptions of damage to a category of targets that exhibit similar response characteristics. Unfortunately, the response to certain of the phenomena depends so strongly on a specific system design that it is impossible to present response data for a "category" of targets (e.g., communications equipment, aircraft, missiles). These phenomena include X-ray radiation and EMP. Therefore, general discussions of the types of systems that are likely to be affected by these phenomena and the general nature of the responses are given in Sections V and VIII of this chapter. No response criteria are provided in subsequent chapters; however, the potential importance of these phenomena are mentioned where appropriate. TREE response is also very dependent on specific system design. The response of electronic components and circuits is described in Section VII of this chapter. Section IV of Chapter 14 contains a brief review of component and circuit response supplemented with discussions of general electrical responses of classes of systems. This latter discussion is intended to include a cross section of systems that should provide some basis for estimating the radiation damage threshold of other similar equipment.

SECTION II
BLAST AND SHOCK DAMAGE

When a blast or shock wave strikes a target, the target may be damaged (distorted sufficiently to impair usefulness) by the blast or shock wave itself, by being translated by the blast wave and striking another object or the ground, or by being struck by another object translated by the blast wave. For example, the air blast wave can shatter windows, dish in walls, collapse roofs, deflect structural frames of buildings, and bend or rupture aircraft panels and frames. Vehicles, tanks, artillery pieces, and personnel can strike other objects on the ground while being hurled through the air or tumbled along the ground by the blast wave. Ship hulls may be split or crushed by the water shock wave. Buried structures or structural founda-

ssion For
GRA&I
TAB
ounced
fication
By
Distribution/
Availability Co
Dist | Avail and/or Special
A-1 | 23
QUALITY INSPECTED 4
UNANNOUNCED

tions can be displaced, collapsed, or ruptured by the ground shock wave. Usually, the degree of damage sustained by a particular target cannot be correlated specifically to a single blast or shock parameter. The total damage received by the target may depend on a combination of air blast and ground or water shock parameters. The orientation of the target with respect to the blast wave, and the type of surface (the topography or the type of soil) associated with the target also determine damage.

LOADING

The blast loading on an object is a function not only of the blast characteristics of the incident wave (rise time, peak overpressure, peak dynamic pressure, decay, and duration), but also of the size, shape, orientation, and response of the object. The influence of the target characteristics on the loading is discussed below, with emphasis on air blast loading.

9-4 Air Blast Loading in the Mach Reflection Region

The loading on an object exposed to air blast is a combination of the forces exerted by the overpressure and the dynamic pressure of the incident blast wave. The loading at any point on a surface of an object can be described as the sum of the dynamic pressure, multiplied by a local drag coefficient, and the overpressure after any initial reflections have cleared the structure. Since the loading changes rapidly while the blast wave is reflecting from the front surfaces and diffracting around the object, loading generally comprises two distinct phases: the initial diffraction phase; and the phase following diffraction when the object is completely engulfed by the blast wave. This latter phase approaches a steady state and usually is referred to as the drag phase, because during this phase the drag forces (i.e., the forces resulting from the dynamic pressures) are the predominant factors in the production of a net translational force on the object. The following discussion of the loading process is based on an ideal blast wave as described in Section I (Figure 2-1), Chapter 2. Where nonideal blast waves, with slow rise time, irregular shapes, and high dynamic pressures (paragraphs 2-21 through 2-31, Chapter 2) introduce complications into the loading process, further explanation is provided. The loading on an object can be described conveniently in three parts: diffraction loading, drag loading, and net loading. These are discussed separately below.

Diffraction Loading. The side of an object facing the shock front of an air blast wave bears overpressures several times that of the incident overpressure because it both receives and reflects the shock. In the Mach reflection region the overpressure incident on the object is actually that of the original free air blast wave which has been reflected from the ground surface to a higher value. The reflection off the object therefore constitutes a second reflection process. In the regular reflection region, the incident overpressure is that of the free air blast wave (see paragraph 9-6). The magnitude of the reflected overpressure depends on the angle between the shock front and the face of the object, the rise time of the incident blast wave, and the initial incident shock strength. The greatest reflected overpressures occur when the direction of propagation of the shock front is normal to the face of the object, when the rise to the peak overpressure is essentially instantaneous, and when the incident shock strength is high. As the blast wave progresses it bends or diffracts around the object, eventually exerting overpressures on all sides. Before the object is entirely engulfed in the pressure region, however, overpressure is exerted on the front side of the object, whereas only ambient air pressure exists on the back side. During the diffraction phase this pressure differential produces a translational force on the object in the direction of blast wave propaga-

tion. When the blast wave has completely surrounded a small object, the translational force that results from diffraction loading is reduced essentially to zero, because the pressures on the front and on the back are almost equal. In the cases of long objects or short duration blast waves, the net force may actually reverse, because the overpressure on the front face may decay to a value lower than that on the rear face. The importance of this translational loading in the production of damage to the target depends on the duration of the loading or on the time required for the shock front to traverse the target and, therefore, on the size of the target. The effects of the translational load decrease as the duration of the load is decreased until, in some instances, translational load effects can be ignored. The overpressures continue on all sides of the object until the positive phase of the blast wave has passed. These pressures may be sufficient to crush an object (a 55-gallon drum may be damaged in this manner in addition to damage that might be incurred by translation). Thus, the diffraction phase translational loading depends primarily on the object size, pressure pulse duration, and on increases in differential overpressures resulting from reflection on the front face.

Drag Loading. During the time of diffraction and until the blast wave has passed, the wind behind the shock front causes dynamic pressures to be exerted on the object as drag loading. Except in the case where shock strengths are high, these pressures are much lower than the reflected overpressures; however, they produce a translational force that the target component receives for the entire positive phase duration of the blast wave. For a given blast wave, the loading that results from dynamic pressure depends principally on the shape and orientation of the object, ranging from less than four-tenths of the dynamic pressures in the case of a cylinder (when normal to the cylindrical axis), to over twice the dynamic pressures for an irregular, sharp-edged object.

Net Loading. Net loading is the combined load on the element that tends to translate it in the direction of propagation of the blast wave. Thus, it is the difference between the load on the front face and the load on the back face; the loads on the sides are of no effect in producing translation.

9-5 Qualitative Examples of Net Loading

The net load on a target can be developed most simply by considering the idealized case shown in Figure 9-1, in which a classical, sharp fronted blast wave moving along the surface of the ground encounters a simple, rigid, fixed cube. When the blast wave arrives at the front face of the target, this face experiences a sudden rise in overpressure to a value p_r that is greater than the peak overpressure Δp of the incident blast wave (also frequently called "side on" overpressure). As the shock wave moves over the cube, subjecting its top and side faces to side on overpressure, the pressure on the front face of the cube begins to drop as the result of rarefaction waves that are generated at the edges of the front face, and which move across that face. When the wave encounters the back face of the cube, that face experiences a gradual pressure increase. The air behind the front of the incident shock wave is in motion, and as the wave envelopes the cube this air motion also affects the pressures experienced by the various faces of the cube.

After a time that is related to the cube dimensions and to the velocity of the incident shock wave, the pressure on the front face becomes

$$p_f = \Delta p(t) + C_{df} q(t)$$

where

$\Delta p(t)$ = the overpressure in the incident shock wave as a function of time, t,

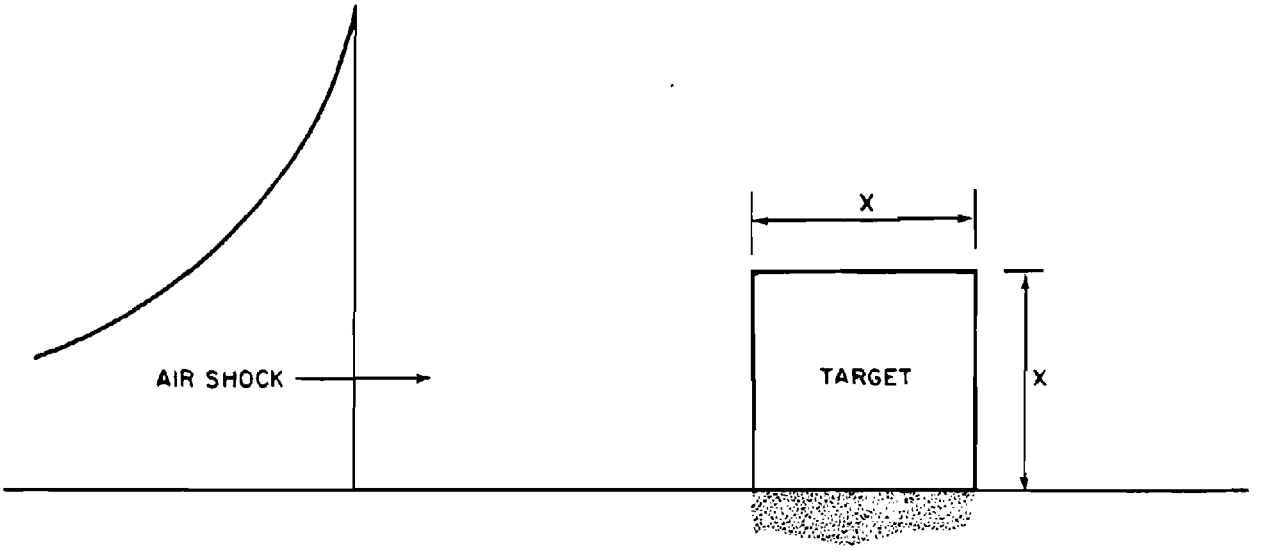

Figure 9-1. Initial Conditions for Loading of a Rigid, Fixed Cube

C_{df} = the drag coefficient of the front face of the cube,

$q(t)$ = the dynamic pressure in the incident shock wave as a function of time, t.

After the shock wave has passed over the cube and has reached the back face, the pressure on that face begins to rise and, at a later time also related to the cube dimensions and the velocity of the incident shock wave, the pressure becomes

$$p_b = \Delta p(t) - C_{db} q(t)$$

where

C_{db} = the drag coefficient of the back face of the cube.

Note that both expressions contain overpressure and dynamic pressure components. As far as the *net* horizontal (translational) loading on the cube is concerned (i.e., the pressures tending to move the cube to the right in Figure 9-1), the overpressure contributions must be subtracted from one another (pressure on the back face tends to move the cube to the left) while the dynamic pressure contributions must be added to each other.

It is convenient to consider the two contributions separately. Figure 9-2 illustrates the overpressure loadings only (dynamic pressure contributions are not included) experienced by the front and back faces of the cube both during the early (diffraction) phases – up to time t_1 on the front face and time t_3 on the back face of the cube – and after the times that the equations given above apply.

The incident shock wave is of the classical (peaked) form with peak overpressure and overpressure duration of Δp and t_p^+ respectively; t_1 is the time after which the total front face loading is represented by the equation for p_f

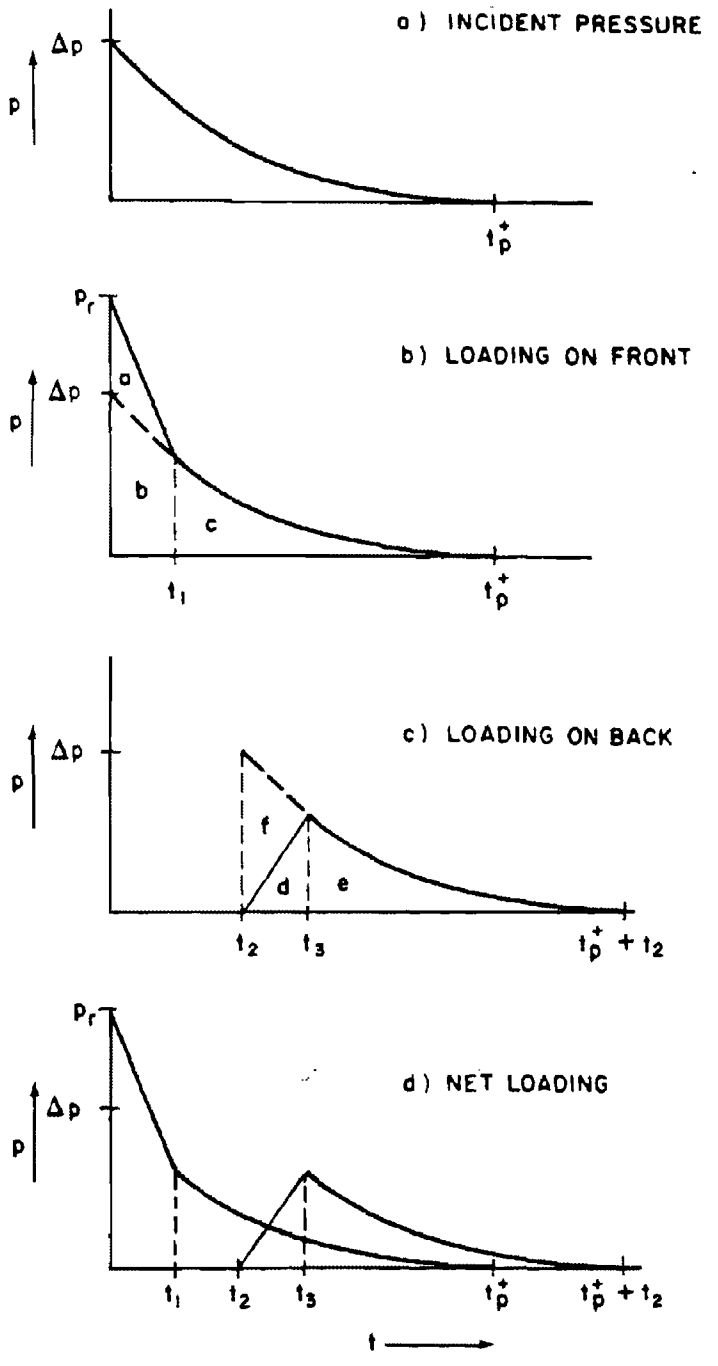

Figure 9-2. [redacted] Target Loading by Overpressure [redacted]

above: t_2 is the time for the shock wave to reach the back face, and t_3 is the time after which the total back face loading is represented by the equation for p_b above.

From Figure 9-2b, the total impulse on the front face, I_F (i.e., the area under the curve multiplied by the area of the cube face, A) is equal to the sum of the areas a, b, and c.

$$I_F = (a + b + c)A$$

The total impulse on the back face, I_B, is (Figure 9-2c)

$$I_B = (d + e)A$$

The net overpressure impulse is $I_F - I_B$. If the cube is not too large compared to the duration of the blast wave, the following approximations hold among the areas:

$$b = d + f,$$

$$c = e,$$

Thus, the net overpressure impulse is

$$I_N = (a + f)A.$$

If the initial drop of pressure on the front face and the build up of pressure on the rear face are assumed to be linear, the net impulse is

$$I_N = A\left[1/2\,(p_r - \Delta p)\,t_1 + 1/2\,\Delta p\,(t_3 - t_2)\right]$$

in which the term containing t_1 is area "a," and the term containing t_2 and t_3 is area "f" of Figure 9-2. Note in particular that the only times are t_1, t_2, and t_3, i.e., those times related to the initial envelopment of the cube by the blast wave. I_N does not, in this simple analysis, depend on overpressure duration t_p^+.

Substitution of commonly accepted values of t_1, t_2, and t_3 for a curve leads to the following expression for the net impulse from *overpressure* diffraction around the target:

$$I_N = A\left[\frac{X}{2U}\,(3p_r + \Delta p)\right]$$

where

X = one-half the width or the height, whichever is smaller,

U = velocity of the shock wave.

These values of t_1, t_2 and t_3 originally were derived from early shock tube experiments and full scale nuclear tests on structures at low pressure levels. Consequently, they are used for illustrative purposes only in this simple analysis. More recent work with two and three dimensional models in the shock tube has shown that the exact values for these times depend strongly on model shape and pressure level as well as sound velocity in the reflected pressure region on the face of the model rather than shock front velocity.

The impulse on the cube due to dynamic pressure I_q is

$$I_q = A\int_o^{t+} q(t)C_d\,dt$$

where

I_q = drag impulse,

q = dynamic pressure,

C_d = drag coefficient of the entire object, a combination of C_{df} and C_{db}.

By expressing p_r in terms of Δp and shock strength ξ, and U in terms of the sound velocity, c and the shock strength ξ, the drag impulse equation may be solved in terms of Δp,

ξ, C_d, and shock wave duration* t^+. The combined impulse is

$$I_T = \left\{\left[\frac{X\Delta p}{2c}\left(\frac{42 + 24\xi}{\xi + 7} + 1\right)\left(1 + \frac{6\xi}{7}\right)^{-1/2}\right] + \left[\frac{0.54\Delta p C_d t^+ \xi}{\xi + 7}\right]\right\}.$$

The first expression in brackets, which is independent of duration, is the overpressure contribution. The second expression is the contribution of dynamic pressure.

If height of burst and ground distance are scaled as the cube root of the yield W for weapons of different yields, Δp remains constant, but the shock wave duration t^+ varies as the cube root of the yield. Thus, the yield dependence is

$$I_T = A\left[B + C\left(W^{1/3}\right)\right]$$

where B, the overpressure contribution (I_N for a 1 kt yield), and C, the dynamic pressure contribution (I_q for a 1 kt yield), are both constants. Thus, the contribution to total impulse from overpressure remains constant, while that from dynamic pressure increases as the cube root of the yield. For very low fractional kiloton yields, the loading is highly impulsive with most of the load coming from the overpressure contribution. As the yield increases, at a constant scaled height of burst and ground distance, the total impulse also increases, with an increasing fraction resulting from dynamic pressure.

Figures 9-3a and b show representative net loadings for two classes of weapon yield and two classes of structures, one small and one large. A small element would be about the size of a telephone pole or a jeep; a large element would be the size of a house or larger. Since the reflected overpressure is more than twice the incident pressure on the front face of the element, the loading displays an initial peak value. The reflected pressure decays or clears the front face at a time that depends on the size of the element. The rapid decay for the small element may make the reflected pressure spike of no significance, whereas the slow decay for the large element creates a load that may govern the response of the target entirely. For the representative cases shown, the diffraction phase terminates at time t_{diff}, the time at which the reflected pressure has decayed to the incident pressure. At this time the drag phase begins. It continues until the end of the positive phase of the incident blast wave. The load during the drag phase is shown to be equal to the dynamic pressure, i.e., the drag coefficients of the elements are equal to 1.0. The characteristics of the target element determine whether the response of the element is governed primarily by the diffraction phase or the drag phase. Figures 9-3a and b show that for medium and high yield weapons and small elements, a much greater impulse (the area under the loading curve) occurs during the drag phase than during the diffraction phase. As the yield increases the drag phase impulse increases in importance. For large elements and large yield weapons, the diffraction phase and drag phase impulses are about equal. In this latter case the drag phase impulse may still be of no importance, because the significant target response may occur during the diffraction phase. The diffraction phase impulses are not changed by the yield of the weapon (this is true for all but very large structures exposed to low yield weapons), whereas the drag phase impulses are directly related to the weapon yield (for the same peak dynamic pressures).

* In this solution it is assumed that the difference between t_p^+ and t_q^+ may be neglected, and $t_p^+ = t_q^+ = t^+$.

[redacted]

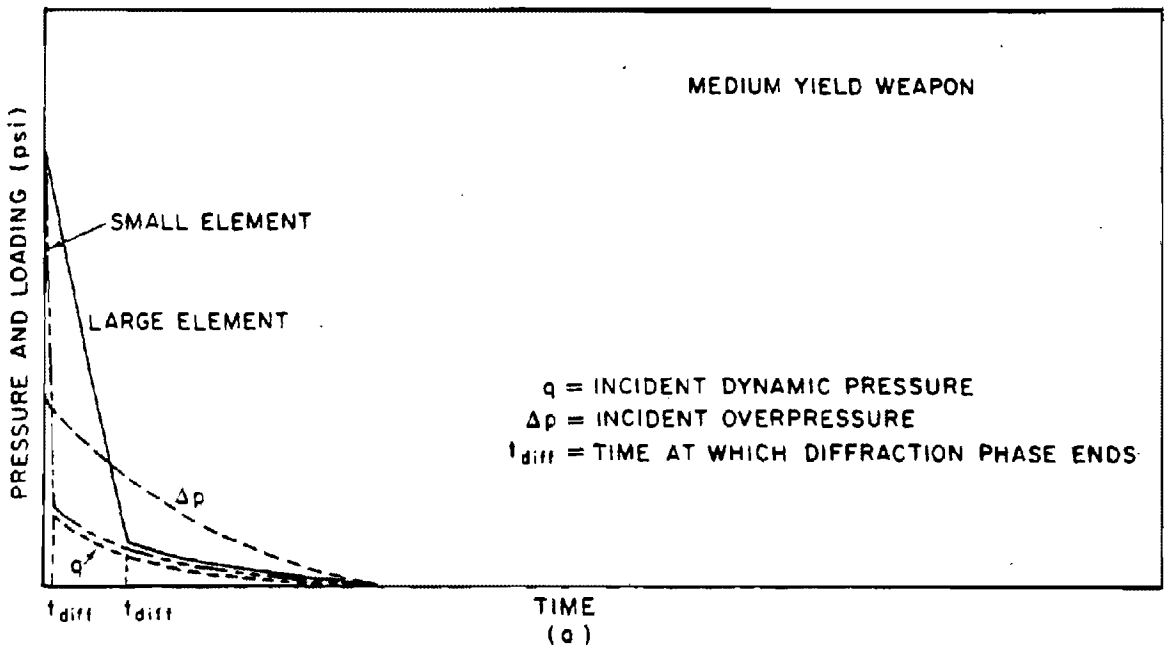

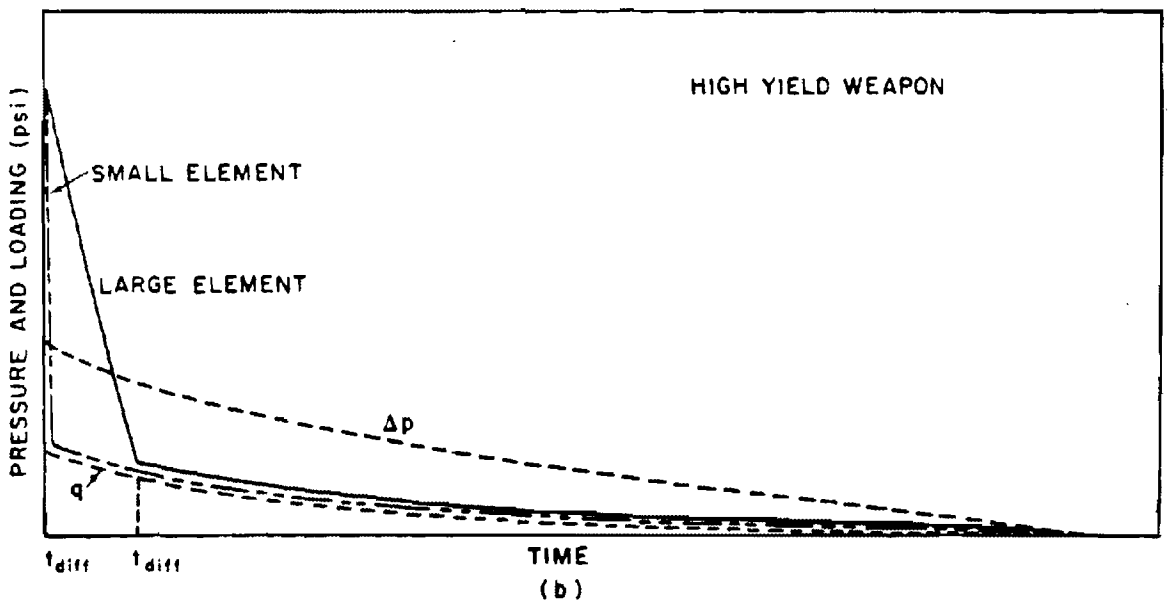

Figure 9-3. [redacted] Net Blast Loading on Representative Structures [redacted]

[redacted]

9-6 Regular and Mach Reflection

Specific aspects of the blast wave propagation must be considered when computing the load on a target. The loading of a surface target in the regular reflection region (pargraph 2-18, Chapter 2) is complicated by the vertical component of the incident blast wave, which causes multiple reflections between the ground and the target and additional reflected pressures on horizontal surfaces. In the Mach reflection region (paragraph 2-18), the loading is simplified because the blast wave propagation is horizontal. Near the surface of the ground, the vertical component of the drag forces in the regular reflection region is cancelled by the reflected wave rapidly; therefore, the brief vertical drag loading is ignored, except when the target is near the ground zero of an air burst. For aircraft in flight, the loading may be a single horizontal shock from a Mach stem or two separate shocks; the first from the free air wave and the second from the ground reflected wave. In establishing the damage curves for surface targets, the loadings on targets in the regular reflection region during the diffraction phase are considered separately from the loadings on similar targets in the Mach reflection region. The surface conditions are assumed to be average unless otherwise indicated in the figures that provide the damage curves. Objects that are primarily susceptible to horizontal drag loading in the Mach reflection region may become primarily susceptible to crushing action if they are in the early regular reflection region.

9-7 Target Motion

When air blast loading is considered, the movement of the target component during loading is assumed to have negligible effect on the loading itself. Aircraft and missiles in flight are exceptions. Their speed, orientation, and movement during loading assume increased importance (see Chapters 13 and 16).

9-8 Nonideal Waveforms

As discussed in paragraphs 2-31 and 2-32, ideal waveforms are seldom found along the surface for overpressure levels above 6 psi. The description of the diffraction and drag phases given in preceding paragraphs is not true in regions of nonideal waveforms. If the overpressure wave has a long rise time (30 to 40 msec) to a peak value, full reflection of the wave from the surface of a structure will not occur. At the same time, the relationship between dynamic pressure and overpressure is different from that described for the ideal blast wave. During the diffraction phase, the drag forces caused by high dynamic pressures may be the predominant damage-producing criteria. Since many conventional surface structures sustain severe damage at low peak overpressure levels, and nonideal waveforms occur only in the higher overpressure regions, such waveforms were not considered in determining damage criteria for such structures. Careful consideration must be given to nonideal waveforms when assessing the vulnerability of protective structures that were designed to withstand high overpressures. The dynamic pressures for such waveforms generally will be higher than would be expected if the blast wave were ideal. There are few data on blast loading in the high pressure regions.

9-9 Underwater Shock Wave Loading

The air blast wave operates in a compressible fluid, while the water shock wave operates in a noncompressible fluid. This difference in medium accounts for the differences in detail betweeen air blast and water shock loading. The peak values in water are higher than they would be at the same distance from an explosion of the same yield in air. However, the duration of the shock wave in water is shorter than in air. When the shock wave strikes a rigid, submerged surface, such as the sea bottom, it is reflected.

[redacted]

When the shock wave reaches the air-water surface (a less rigid medium), however, a refraction (or negative pressure) wave occurs. The combination of the surface reflected shock wave and the direct shock wave produces a sharp decrease or "cutoff" in the water shock overpressure, as shown in Figure 9-4. Incidence of a shock wave on a ship or structure produces damage through the direct mechanism of overpressure (or excess impulse) and by imparting a transitional velocity to the target structure.

9-10 Ground Shock Loading [redacted]

[redacted] The loading of buried structures by ground shock is connected intimately to the response of the structures. For certain underground structures, serious damage will only occur if the ground shock is so intense that the damage area for those structures is confined closely to the crater area of a surface or underground explosion. For structures near the surface, air blast induced ground shock may cause significant damage. The damage to these structures is more closely related to air blast pressures than it is to crater dimensions. Loading pressures are numerically equal to the ground stress normal to the structure. Such pressures do not produce detectable reflected pressures. Internal equipment of a structure may be subjected to ground shock accelerations that will severely damage the equipment without damaging the structure. For a discussion of accelerations resulting from ground shock see Section III, Chapter 2, and Sections II and III, Chapter 11.

[redacted] RESPONSE AND DAMAGE [redacted]

[redacted] Damage to a target is closely related to, and is a direct derivative of, its response. For targets anchored to the ground, damage is usually the result of displacement of one part of the target with respect to another part, resulting in permanent distortion, collapse, or toppling. For movable targets, however, the target may be moved by the loading with or without a resulting damage. In the latter case, the damage to the target is governed primarily by the manner in which the moving target comes to rest. Whether drag phase loading or diffraction phase loading causes the greater damage will depend upon the weapon yield, target characteristics, and the damage level considered.

9-11 Surface Structures [redacted]

[redacted] The predominant cause of failure to large targets, such as buildings that have small window areas compared to wall areas that either support the structure or are as strong as the structural frames, is the pressure differential between the front and rear faces that exists for a relatively long period of time. If the window area is large, the pressure on each wall is equalized quickly by the entry of the blast wave through the windows. The pressures exerted on the inside of the wall reduce the translational force on the wall. This translational force also is reduced because of a smaller wall area on which the pressures can act; however, the force exerted on interior partitions and rear walls tends to offset the reduction in front face loading in the production of total damage. When the overpressures causing translational force on the structural component are equalized quickly as a result of the geometry or construction of the building, the primary damaging forces are those that are significant in damaging structural components that have fairly small cross sections, such as columns and beams. Structures that are normally damaged by drag forces include smoke stacks, telephone poles, truss bridges, and steel or reinforced concrete frame buildings with light walls. These buildings are drag sensitive, because the light walls of corrugated steel, asbestos, or cinder block fail at low reflected pressures, and they do not transmit a significant load to the structure frame. Only the frame is exposed to the blast, and, being composed of small cross

[redacted]

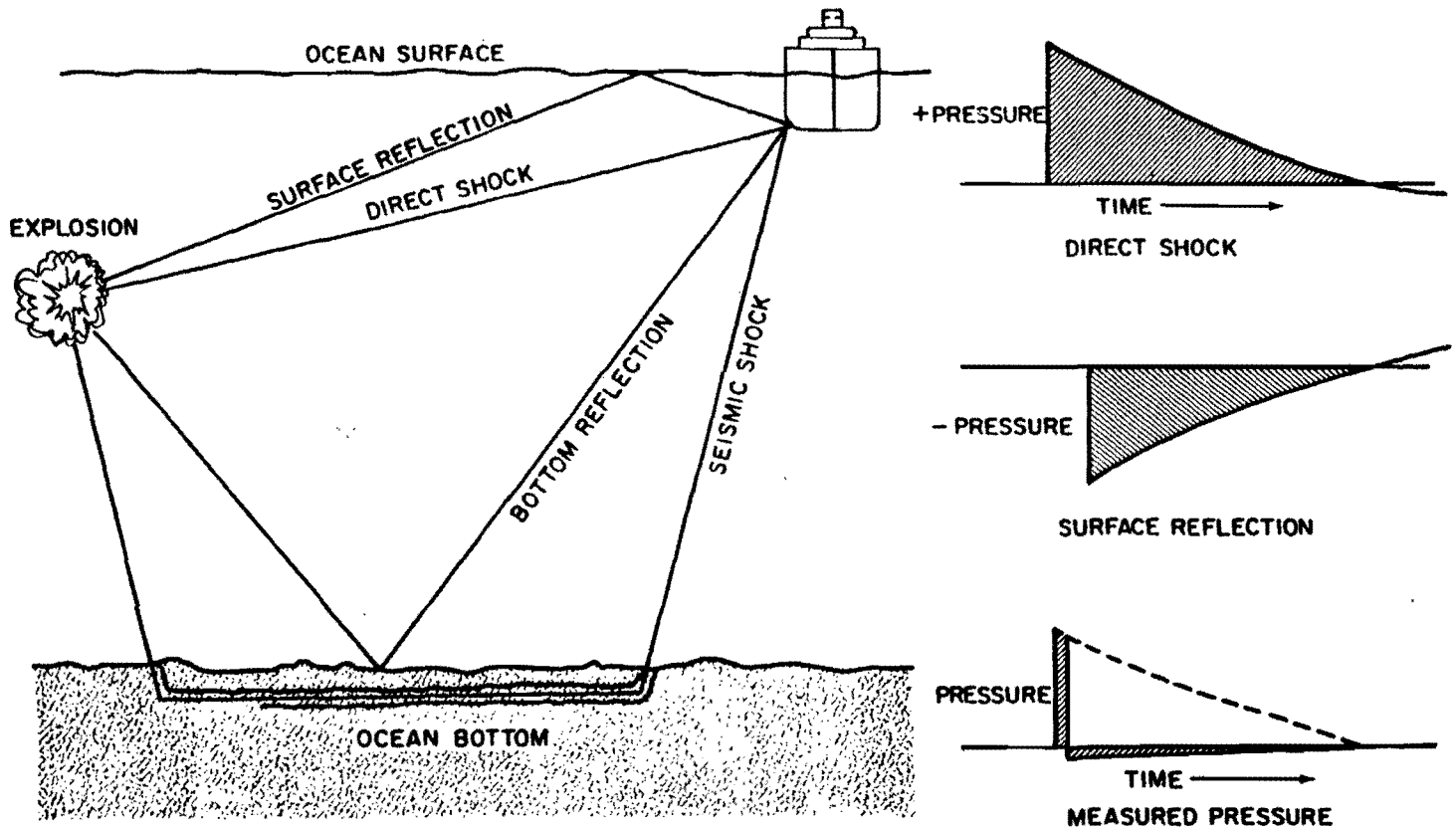

Figure 9-4. Direct and Reflected Shock Waves from an Underwater Burst

section structural elements, it is distorted primarily by drag forces. These buildings are not considered severely damaged unless the structural frame has collapsed or is near the point of collapse. A tree is a good example of a drag sensitive target, because the duration of the diffraction phase is extremely short and there is considerable force applied by the high wind velocity drag loading. Most military field equipment is drag sensitive, because damage generally results from the tumbling or overturning caused by the drag forces.

9-12 Shielded Structures

If the target is shielded from the drag forces, or if it lies within the early regular reflection region, high overpressures may become the damage producing criteria. For blast resistant aboveground structures designed to resist more than 5 to 10 psi overpressure, the distinction between diffraction and drag sensitivity cannot be defined well, because full reflection from the surface of the structure does not occur, and dynamic pressures exceed those expected in the case of the incident waveform. As a result, drag forces may be predominant in producing damage, even during the diffraction phase.

9-13 Aircraft

Aircraft may be damaged by the forces developed in the diffraction phase, in the drag loading phase, or in both. Parked aircraft can receive light, crushing forces corresponding to low overpressures. For example, light skins and frames are easily dished and buckled at relatively low overpressures. At higher overpressure levels, drag loading (referred to as "gust loading" with respect to aircraft) adds to the damage. At these levels, much of the damage may result from translation and overturning of the aircraft. For aircraft in flight, the diffraction and drag forces combine with the existing aerodynamic forces to develop destructive loads on airfoils at low overpressure levels. The diffraction or crushing overpressure effects on the fuselage and other thin skinned components, however, are usually of secondary importance for most in-flight aircraft. Responses of aircraft are discussed in more detail in Chapter 13.

SECTION III
THERMAL RADIATION DAMAGE

INTRODUCTION

Two important effects of thermal radiation are injuries to personnel (burns) and fires that might be ignited in the target area. Burns to personnel are treated in Section II of Chapter 10. Section VII of Chapter 11 discusses fires in urban areas. Section III of Chapter 15 discusses fires in forest stands. The effects of thermal radiation on various classes of equipment are described in other chapters of Part II. This section contains a description of the properties of materials that might result in ignition or degradation of their physical properties. A brief discussion of survival in fire areas is also provided. Section IV describes the degradation of structural resistance to air blast of materials, primarily metals, as a result of thermal radiation.

Chapter 3 provides the data necessary to estimate the thermal environment. In general, thermal damage is likely to be more important than blast damage for surface targets for high yield weapons that are air bursts rather than surface bursts. As discussed in Chapter 3, the influence of weather makes thermal effects much less predictable than blast effects. Clouds or haze can provide a protective screen, and moisture from an earlier rain can reduce the number of fires in outdoor targets. In some cases, cloud cover can enhance thermal effects on the ground. The criteria for thermal damage given in succeeding paragraphs are representative values

for dry materials directly exposed to the thermal source. These values should be applied with the understanding that they can be modified by a variety of factors discussed briefly in the following paragraphs.

9-14 Radiant Exposure

The thermal damage inflicted on a target depends upon the incident energy per unit area. This quantity is called radiant exposure and, as described in Chapter 3, it usually is expressed in calories per square centimeter (cal/cm^2). Radiant exposures below 2 cal/cm^2 will produce little damage other than possible eye injury (Section II, Chapter 10). Radiant exposures above 10 cal/cm^2 usually produce significant damage in unprotected target areas.

9-15 Thermal Pulse Duration

The radiant exposure required to damage a particular target varies with the duration of the thermal pulse. The reason is readily seen from the following example: about 3 to 5 cal/cm^2 from a short thermal pulse, e.g., from a 1 kt detonation, will produce a second degree burn on bare skin, but direct sunlight delivers the same radiant exposure in a little over 2 minutes with no serious effects.

The time scale of the thermal pulse from low altitude nuclear weapon bursts may be characterized by the parameter t_{max}, the time during the final pulse at which the fireball is radiating maximum power. This time increases with increasing yield and decreases with increasing altitude. The relation of t_{max} to pulse duration and the method for calculating t_{max} are given in Chapter 3. As described in Chapter 3, the time scale of the thermal pulse may be specified indirectly in terms of yield for low altitude bursts. The thermal pulse for high altitude bursts (up to about 100,000 feet) may be described in terms of an equivalent sea level burst. Specifying the thermal pulse duration in terms of yield is convenient since it eliminates the necessity to calculate t_{max}; therefore, many damage criteria are given in terms of radiant exposure and yield rather than radiant exposure and time to final maximum.

9-16 Target Response

For most materials, the heat absorbed from the thermal pulse initially is confined to a thin surface layer. Damage usually results from high surface temperatures. The nature and the degree of the damage depend not only on the intensity and duration of the thermal pulse, but also on several properties of the material that are described below.

Thickness. Thick organic materials such as wood, plastics, and heavy fabrics char and may burst into flame while exposed to the thermal pulse; however, this flaming is only a transient effect. As the radiant pulse decays, the absorbed thermal energy continues to penetrate the material. This flow of heat allows the surface to cool to a temperature too low to support combustion.

Thin materials, such as light fabrics, newspaper, dry leaves, and dry grass tend to become hotter than the surfaces of thicker materials since the absorbed thermal energy is confined to a relatively small volume of material. Also, since these materials are heated throughout, they usually continue to burn once they are ignited. Moreover, subsequent arrival of the blast wave frequently will fail to extinguish the fire.

Thermal Conductivity. Most metals allow rapid penetration of thermal energy to depths below the surface as a result of their high values of thermal conductivity. Consequently, the peak surface temperatures induced in thick pieces of metal are considerably less than the peak surface temperatures induced in most nonmetallic materials. Thin pieces of metal may fail as a result of the combined effects of the thermal pulse, which reduces the strength of the metal by heating it, and the blast wave, which causes it to bend or collapse. This effect is dis-

cussed in more detail in Section IV. Dry rotted wood (or punk) has a lower thermal conductivity than sound wood as a result of its porous structure. When the surface of punk is ignited by a thermal pulse, conduction of heat to the interior is too slow to allow significant cooling of the surface, and burning continues.

Color. Light colored objects of a given thickness are more resistant to thermal radiation than dark colored objects, because they reflect more of the incident energy. Color has little effect on the response of materials that blacken (char) early in the thermal pulse, because the energy delivered during the remainder of the pulse is absorbed efficiently by the charred surface.

Transparency. Transparent materials are relatively resistant to thermal damage (even though transparency in the visible region does not assure that the material is transparent to infrared) because the radiant energy that passes through them usually does not contribute to heating. Partially transparent materials are thermally resistant because the incident thermal energy is deposited over a range of depths rather than being confined to a thin surface layer. Peak temperatures induced in partially transparent materials therefore are likely to be lower than the peak temperatures produced at the surfaces of opaque materials.

Moisture Content. Thermal damage to materials that absorb moisture depends on the percentage of water in such materials. Usually, the moisture content varies with the prevailing relative humidity. Exposure to recent rain, however, may alter the moisture content significantly. Scorching or charring of an organic surface by radiant energy is preceded by vaporization of the water. Consequently, more energy is required to produce a given damage effect on wet surfaces or on targets in highly humid atmospheres. Materials located indoors and exposed to thermal radiation through windows are damaged more readily during the latter part of the heating season (late winter and early spring), largely because of decreased interior humidities.

9-17 Target Orientation

In clear atmospheres and in the absence of reflecting surfaces, the amount of energy incident on a unit area of a target surface is greatest when the surface is directly facing the burst. If the target surface is not facing the burst, the energy per unit area depends on the angle between the perpendicular to the surface and the direction of the incoming radiation.

When the atmosphere is hazy, much of the energy received at the target is scattered by atmospheric particles, arrives from all directions, and reaches portions of the target that are not exposed to direct radiation. Scattered energy is likely to be a large fraction of the total energy received when the slant range from the burst to the target exceeds about half the visual range. Reflection from clouds and from the ground can produce similar effects.

9-18 Shielding

Any object that casts a shadow is capable of shielding objects behind it from the direct component of thermal radiation. Trees, buildings, foxholes, hills, etc. offer effective protection except when the scattered component of thermal radiation is large. After leaves have been stripped by the dynamic pressure (wind) of a nuclear burst, the trees offer little shielding from the thermal radiation produced by a second burst. Reflection of thermal radiation from exposed walls of foxholes is about 5 percent.

THERMAL RESPONSE OF MATERIALS

The amount of thermal radiation that a material will absorb depends on the properties of the material discussed in paragraph 9-16. The amount of energy absorbed usually is determined by multiplying the incident energy by an

absorption coefficient. The absorption coefficient cannot be measured directly, but a good estimate can be made by performing spectral measurements of reflectance (the fraction of incident energy reflected from the surface) over the range of wave lengths of the nuclear spectral distribution and by finding an average value of reflectance. The coefficient of absorptance is equal to one minus the average value of the reflectance. The absorptance determined in this manner is valid only as long as the surface does not change as a result of the absorbed thermal energy. Another approach is to divide the quantity of energy absorbed by the incident energy. The absorbed energy is determined from experimentally determined temperature vs time relationships and appropriate theoretical energy balance relationships. Absorptance is a function of time and temperature although an average value is usually employed. This function when known may be found as an input specification for certain computer programs. In the absence of more definitive data for a specific systems, an absorption coefficient of 0.5 is a reasonable value to assume for many materials, particularly metals. For a conservative defensive assumption, the absorption coefficient may be taken to be 1.0 (i.e., total absorption), particularly for dark porous materials.

In many cases, it is appropriate to consider only one or two fuel types, assuming that these fuels are the critical items that will determine whether fires are started in a particular area. In other cases, more detail is required. For example, an estimate of the thermal energy that will ignite a particular type of material used in military uniforms may be desired. The data contained in the succeeding paragraphs is intended as a guide in the solution of more specific problems.

9-19 Thickness Effects

The time required for thermal energy to penetrate very thin materials is short compared to the duration of the thermal pulse. At the end of the pulse, the absorbed thermal energy is distributed more or less uniformly throughout the material. In very thick materials, the end of the pulse finds most of the absorbed thermal energy in a surface layer, with the bulk of the material almost unaffected.

If the terms thermally "thin" and thermally "thick" are used to distinguish between materials that are heated throughout from those that are initially heated only at the surface, it is apparent that physical thickness is not the only parameter involved. For example, as a result of the rapid penetration of heat into metals, a sheet of metal is more likely to be thermally thin than is a sheet of insulating material of the same physical thickness.

The ability of a short pulse of energy to penetrate a target material is most readily measured in the laboratory and most readily treated analytically if the thermal pulse is given a rectangular waveform rather than the more complex waveform produced by a nuclear weapon. A parameter that is useful for calculating thermal response of materials is the characteristic thermal response time τ_o, given by the equation

$$\tau_o = \rho C_p L^2/k \text{ sec},$$

where k is thermal conductivity (cal-sec^{-1} cm^{-1}°C^{-1}), ρC_p is heat capacity per unit volume (ρ = density in g-cm^{-3} and C_p = specific heat at constant pressure in cal-g^{-1} °C^{-1}), and L is the thickness, in centimeters, of the layer of material.

The quantity

$$\alpha = \frac{k}{\rho C_p}$$

is called thermal diffusivity (cm^2/sec). Use of this quantity simplies the previous equation to

$$\tau_o = \frac{L^2}{\alpha} \text{ sec.}^*$$

Thermal diffusivity and other properties of a number of materials are shown in Table 9-1.

Characteristic time may be related in several ways to the thermal response of a target. Most important is that the ignition of thin fuels by a rectangular thermal pulse requires the least radiant exposure when pulse duration is about equal to τ_o.

Two other relations apply to a thick slab of material. For any particular material exposed to a rectangular pulse of length τ, the previous equation can be transformed to give a characteristic thickness

$$\delta = \sqrt{\alpha\tau} \text{ cm.}$$

for which the characteristic time is equal to the pulse duration. If a thick slab of this material is exposed to a pulse of length τ, the temperature rise at the surface is the same as would be produced by uniformly distributing the absorbed thermal energy in a slab of thickness δ, and the peak temperature rise at depth δ in the thick slab is about half as great as the peak temperature rise at the surface.

For example, consider a block of red pine that is exposed to 15 cal/cm^2 from a rectangular pulse of 3 seconds duration. From Table 9-1, the properties of red pine are

$$\rho = 0.51 \text{ g/cm}^3,$$

$$C_p = 0.4 \text{ cal/g} \cdot {}^\circ C,$$

$$\alpha = 24 \times 10^{-4} \text{ cm}^2/\text{sec.}$$

The characteristic depth is

$$\delta = \sqrt{\alpha\tau} = \sqrt{(24 \times 10^{-3})(3)} = 0.085 \text{ cm.}$$

The mass of wood per unit area in a slab of this thickness is

$$\rho\delta = (0.51)(0.085) = 0.043 \text{ g/cm}^2.$$

The heat absorbed by the wood before it begins to scorch is equal to the product of the incident radiant energy, Q, and the absorption coefficient, A. If the absorption coefficient is assumed to be 0.5.

$$QA = (15)(0.5) = 7.5 \text{ cal/cm}^2.$$

Absorption of this amount of energy in a layer of thickness δ would result in an energy density of

$$\frac{QA}{\rho\delta} = \frac{7.5}{0.043} = 174 \text{ cal/g.}$$

If the energy were evenly distributed through this layer, the resulting temperature rise would be

$$\frac{QA}{\rho\delta C_p} = \frac{174}{0.4} = 435^\circ C.$$

and the peak temperature rise at the surface of the wood would be about the same.

The result obtained above may be generalized as follows:

$$\Delta T_s = \frac{QA}{\rho\delta C_p} = \frac{QA}{\rho C_p \sqrt{\alpha\tau}} = \frac{QA}{\rho C_p \sqrt{\tau k/\rho C_p}}.$$

* This equation is useful, but it is by no means exact. The simplified heat-flow analysis from which this equation is derived neglects the effects of radiation and convection heat losses from the surfaces of the exposed sample. It also assumes an isotropic medium, i.e., a medium whose structure and properties in the neighborhood of any point are the same relative to all directions through the point. It also neglects the changes in thermal properties that occur as the exposed material heats, volatilizes, chars, and bursts into flame.

Table 9-1. [redacted] Thermal Properties of Materials [redacted]

Materials	Density, ρ (gm/cm^3)	Specific Heat, C_p ($cal/gm \cdot {}^\circ C$)	Conductivity, k ($cal/sec \cdot cm \cdot {}^\circ C$)	Diffusivity, α (cm^2/sec)
Insulating Materials				
Air	9.46×10^{-4}	0.24	0.55×10^{-4}	0.22
Asbestos	0.58	0.20	4.6×10^{-4}	$40. \times 10^{-4}$
Balsa	0.12	0.4	1.2×10^{-4}	$25. \times 10^{-4}$
Brick (common red)	1.8	0.2	$16. \times 10^{-4}$	$18. \times 10^{-4}$
Celluloid	1.4	0.35	5.0×10^{-4}	$10. \times 10^{-4}$
Cotton, sateen, green	0.70	0.35	1.5×10^{-4}	2.5×10^{-4}
Fir, Douglas-				
spring growth	0.29	0.4	$2. \times 10^{-4}$	$17. \times 10^{-4}$
summer growth	1.00	0.4	$5. \times 10^{-4}$	$12. \times 10^{-4}$
Fir, white	0.45	0.4	2.6×10^{-4}	$14. \times 10^{-4}$
Glass, window	2.2	0.2	$19. \times 10^{-4}$	$43. \times 10^{-4}$
Granite	2.5	0.19	$66. \times 10^{-4}$	$140. \times 10^{-4}$
Leather sole	1.0	0.36	3.8×10^{-4}	$11. \times 10^{-4}$
Mahogany	0.53	0.36	3.1×10^{-4}	$16. \times 10^{-4}$
Maple	0.72	0.4	4.5×10^{-4}	$16. \times 10^{-4}$
Oak	0.82	0.4	5.0×10^{-4}	$15. \times 10^{-4}$
Pine, white	0.54	0.33	3.6×10^{-4}	$18. \times 10^{-4}$
Pine, red	0.51	0.4	$5. \times 10^{-4}$	$24. \times 10^{-4}$
Rubber, hard	1.2	0.5	3.6×10^{-4}	$60. \times 10^{-4}$
Teak	0.64	0.4	4.1×10^{-4}	$16. \times 10^{-4}$
Metals (100°C)				
Aluminum	2.7	0.22	0.49	1.0
Cadmium	8.65	0.057	0.20	0.45
Copper	8.92	0.094	0.92	1.1
Gold	19.3	0.031	0.75	1.2
Lead	11.34	0.031	0.081	0.23
Magnesium	1.74	0.25	0.38	0.87
Platinum	21.45	0.027	0.17	0.29
Silver	10.5	0.056	0.96	1.6
Steel, mild	7.8	0.11	0.107	1.2
Tin	6.55	0.056	0.14	0.38
Miscellaneous Materials				
Ice (0°C)	0.92	0.492	$54. \times 10^{-4}$	$120. \times 10^{-4}$
Water	1.00	1.00	$14. \times 10^{-4}$	$14. \times 10^{-4}$
Skin (porcine, dermis, dead)	1.06	0.77	$9. \times 10^{-4}$	$11. \times 10^{-4}$
Skin (human, living, averaged for upper 0.1 cm)	1.06	0.75	$8. \times 10^{-4}$	$30. \times 10^{-4}$
Polyethylene (black)	0.92	0.55	$8. \times 10^{-4}$	$17. \times 10^{-4}$

[redacted]

where ΔT_s is the peak temperature rise at the surface. The parameters that define the thermal pulse may be separated from those that define the material properties, and

$$\Delta T_s = \left(\frac{Q}{\sqrt{\tau}}\right)\left(\frac{A}{\sqrt{k\rho C_p}}\right).$$

For a fixed rectangular pulse, $Q/\sqrt{\tau}$ is a constant, and the equation may be written

$$\Delta T_s = (K)\left(\frac{A}{\sqrt{k\rho C_p}}\right).$$

In practice, the surface temperature rise produced in a thick material is approximately proportional to $A/\sqrt{k\rho C_p}$ over a wide range of pulse shapes and pulse times. Thus, this parameter may be used as a measure of the relative susceptibility of various materials to surface heating.

Direct measurements of the ignition properties of a representative cellulosic fuel have been reported. The material is α-cellulose, blackened by the addition of carbon, and made into sheets of various thicknesses. This material has the uniformity required to obtain repeatable test results, and its thermal properties are similar to those of common cellulosic fuels, such as paper and dry leaves.

Figure 9-5 shows the results of exposing this material to the idealized rectangular thermal pulse. Figure 9-6 shows the results obtained in the more practical case of a simulated weapon pulse. These curves show data for black α-cellulose sheets of a variety of thicknesses by using normalized coordinates. The ordinate is normalized radiant exposure. One unit on this scale corresponds to the energy per unit area that will raise the temperature of the entire sheet 1°C. Thus, a given value of the ordinate represents a higher radiant exposure for a thicker sheet of cellulose. The abscissa of Figure 9-5 is normalized pulse duration, the duration of the rectangular pulse divided by τ_o, the characteristic thermal response time of the sheet of material. The abscissa of Figure 9-6 is a similar normalized time, t_{max}/τ_o. Normalization fails in the case of long pulses, and the curves break into families of curves for different thicknesses of material.

If the pulse has such a short duration that the exposed surface reaches the ignition temperature while the back surface remains cool, two distinct ignition thresholds appear. Low values of radiant exposure produce high surface temperatures and flames, but the flames do not persist after the end of the thermal pulse. This region is labeled transient ignition in Figures 9-5 and 9-6. Sustained ignition only occurs when higher radiant exposures raise the temperature throughout the thickness of the cellulose to a level that is sufficiently high to sustain the flow of combustible gases from breakdown of the fuel. It is difficult to supply sufficient energy with short pulses, since a large amount of the energy that is deposited is carried away by the rapid ablation of the thin surface layer. This transient flaming phenomenon is typical of the response of sound wooden boards to a thermal pulse.

If the pulse is of long duration, the ignition threshold rises because the exposed material can dissipate an appreciable fraction of the energy while it is being received. For very long rectangular pulses an irradiance of about 0.5 cal · $cm^{-2} sec^{-1}$ is required to ignite the cellulose. Heat supplied to the material at a slow rate is just sufficient to offset radiative and convective heat losses, while maintaining the cellulose at the ignition temperature of about 300°C.

Materials respond to the thermal pulse from a nuclear weapon in much the same way that they respond to a rectangular thermal pulse; however, a number of practical effects make a thorough analysis of ordinary fuels ignited by

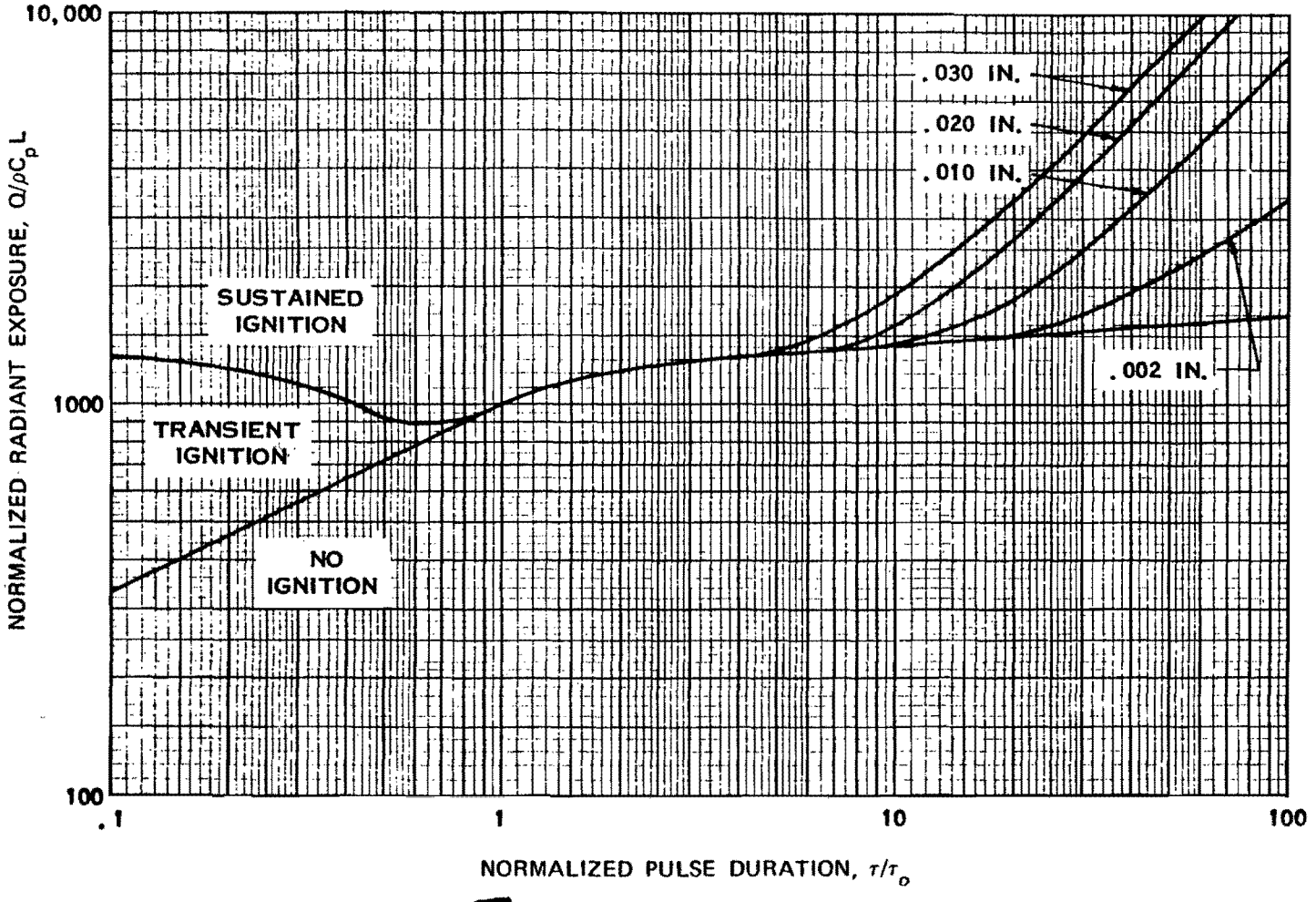

Figure 9-5. [redacted] Ignition Thresholds for Black α-Cellulose Exposed to a Rectangular Thermal Pulse [redacted]

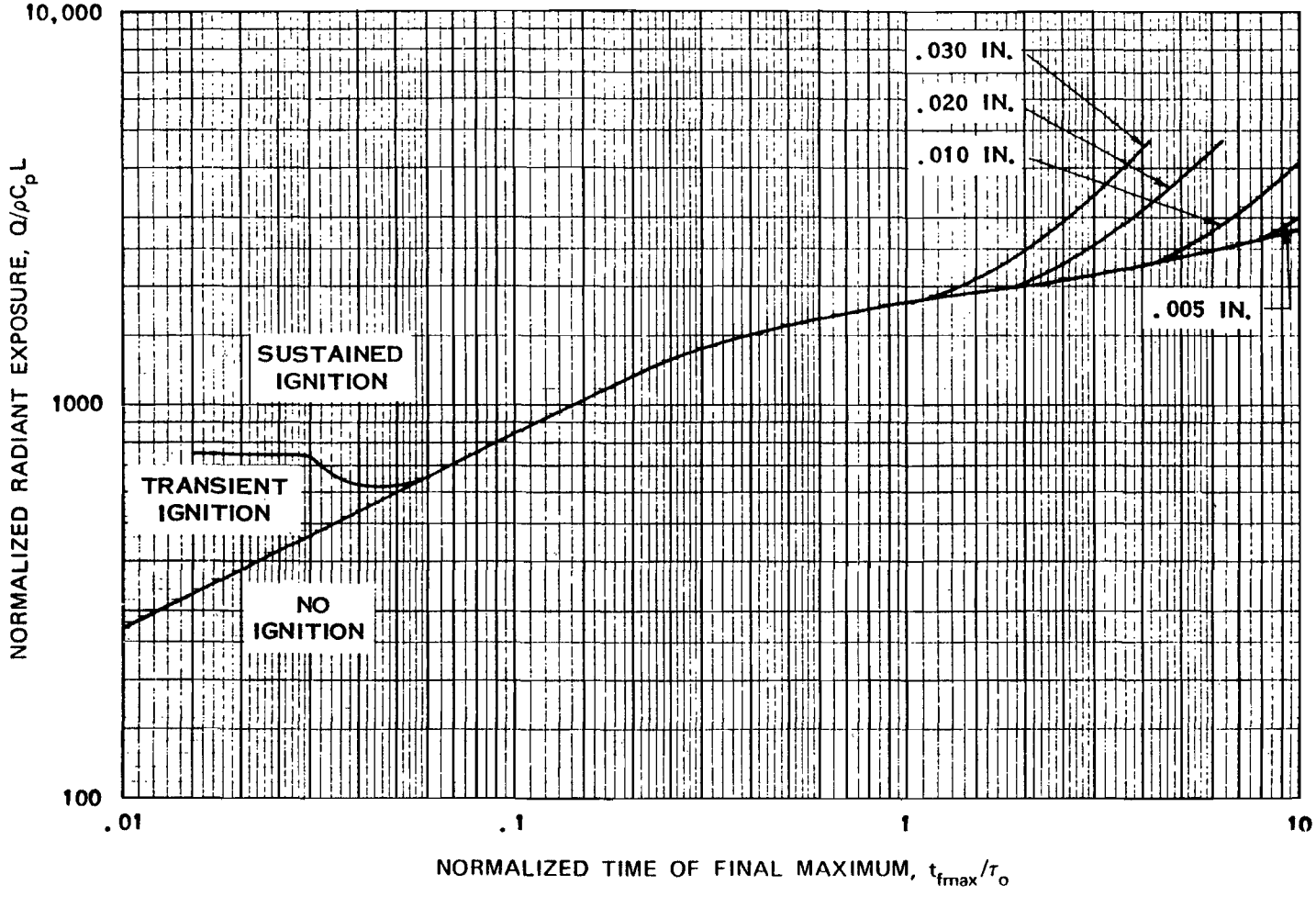

Figure 9-6. [redacted] Ignition Thresholds for Black α-Cellulose Exposed to a Simulated Weapon Pulse [redacted]

weapon pulses difficult. While the fuel absorbs heat and its surface chars, its absorption coefficient changes. As a result, the shape of the energy pulse actually absorbed by the material differs from that of the incident energy pulse (this effect is avoided in the α-cellulose by making the material black initially). A weapon pulse has no single rectangular wave equivalent, since the nature of material response to a thermal pulse varies with pulse shape as well as pulse length. However, for many calculations a rough equivalence may be obtained by assigning between 2.5 and 3 times the irradiance of the rectangular pulse to the weapon pulse.

Both rectangular and weapon pulse data show an optimum pulse length for igniting materials. For the rectangular pulse, this optimum occurs with a pulse length slightly shorter than the characteristic thermal response time of the material. A pulse of this optimum duration lasts long enough to allow an appreciable amount of heat to penetrate to the back face, but it is short enough that only a small heat loss occurs during the pulse.

For example, consider newsprint that is 0.008 cm thick, which has a thermal diffusivity, α, of $10^{-3}\,cm^2/sec$. From the equation given previously

$$\tau_o = \frac{L^2}{\alpha}.$$

From Figure 9-6, the threshold for sustained ignition of black α-cellulose is a minimum when

$$\frac{t_{max}}{\tau_o} = \frac{t_{max}\alpha}{L^2} = 0.045.$$

The properties of newspaper are similar to those of α-cellulose, so the same relation may be assumed to hold for the newsprint. Thus,

$$t_{max} = 0.045\,\frac{L^2}{\alpha} = \frac{(0.045)(0.008)^2}{0.001}$$

$$t_{max} = 2.9 \times 10^{-3} \text{ sec.}$$

From the equation given in Chapter 3

$$t_{max} = 0.043\ W^{0.43}\ (\rho/\rho_o)^{0.42} \text{ sec.}$$

At sea level $\rho = \rho_o$, and

$$W = (t_{max}/0.043)^{2.3}$$

$$W = \left(\frac{2.9 \times 10^{-3}}{4.3 \times 10^{-2}}\right)^{2.3} = 0.002 \text{ kt.}$$

This yield is so small that little confidence may be placed in the result; however, this example demonstrates the general rule that short thermal pulses are more likely to ignite newsprint than long pulses over the range of yields that probably will be of practical importance.

9-20 Color

Although thermal damage depends on the radiant exposure to which a target is subjected, it depends in a much more direct manner on the amount of thermal energy absorbed. Thus color, which indicates the amount and spectral distribution of the visible energy reflected, is one indication of the resistance of a material to thermal damage.

White materials reflect most of the energy in the visible portion of the spectrum that is incident on them, but all cellulosic fuels (which constitute the commonest potential ignition sites) absorb energy in the near infrared region. Cellulosic materials also char in response to high radiant exposures, and once the surface begins to blacken they absorb strongly. The total amount of energy absorbed depends on the absorption coefficient averaged not only over the spectrum of energies contained in the thermal pulse, but also over the interval of time during which the pulse is received. For a thin cellulosic material exposed to a moderately high level of radiant energy (just enough to ignite the ma-

terial) blackening will not occur immediately, and the following rules give an effective average for the absorption coefficient that is roughly correct.

- If the material is white or nearly white, the effective absorption coefficient for the thermal pulse is about the square root of the absorption coefficient for visible light. *Example:* If the visible absorption coefficient is 0.1, the effective absorption coefficient for the thermal pulse is about 0.3.
- If the material has a color that is as dark as or darker than dove gray (a fairly light shade of gray), the effective absorption coefficient for thermal radiation is about equal to the visible absorption coefficient.
- The response of most of the nonwhite materials that provide potential ignition sites may be approximated by assigning an effective absorption coefficient of 0.5.

9-21 Transparency

The energy that passes through a partially transparent material cannot heat it. Thus, the energy deposited in the material is the incident energy minus the reflected energy minus the transmitted energy.

The depth of penetration of thermal energy into a partially transparent material is determined by two mechanisms: heat absorbed at or near the surface penetrates by diffusion; and heat penetrates as radiant energy before it is absorbed. As shown in paragraph 9-19, the diffusion of heat may be associated with a transient thickness δ. Similarly, the penetration of thermal energy due to diathermancy (partial transparency) may be associated with a characteristic depth of $1/\beta$, where β is the extinction coefficient. In a practical situation, both of these mechanisms work simultaneously, and the heat penetrates deeper than it would if only one mechanism were effective.

Usually, one or the other of the two mechanisms is dominant. If the product $\beta\delta$ exceeds 3 or 4, penetration will occur principally by diffusion. If the product is less than about 1/4, penetration will be principally by transmission of radiant energy. Temperature profiles in a semi-infinite solid are shown in Figure 9-7 in terms of dimensionless parameters, where ΔT is temperature rise, k is thermal conductivity, ρ is density, C_p is specific heat, H is energy absorbed (not the incident energy) per unit area, τ is rectangular pulse duration, and δ is characteristic depth defined in paragraph 9-19.

9-22 Effect of Humidity

The water content of thin fuels responds rapidly to changes in humidity. The radiant exposure that is required to ignite a thin cellulosic fuel is approximately

$$Q = Q_0 \ (1 + h/2),$$

where h is relative humidity and Q_0 is the radiant exposure that will ignite the fuel when it is completely dry.

In general, ignition data give radiant exposure thresholds for average rather than extremely dry conditions. If the tabulated value of radiant exposure Q_1 applies to a relative humidity of h_1, the equation given above becomes

$$Q = Q_1 \ \frac{1 + h/2}{1 + h_1/2}.$$

For example, if the radiant exposure from a 1 Mt explosion that is required to ignite new white bond paper is 30 cal/cm^2 when the relative humidity is 65 percent, the ignition threshold for the same explosion when the relative humidity is 15 percent is

$$Q = (30) \left(\frac{1 + 0.15/2}{1 + 0.65/2} \right) = 24 \text{ cal/cm}^2.$$

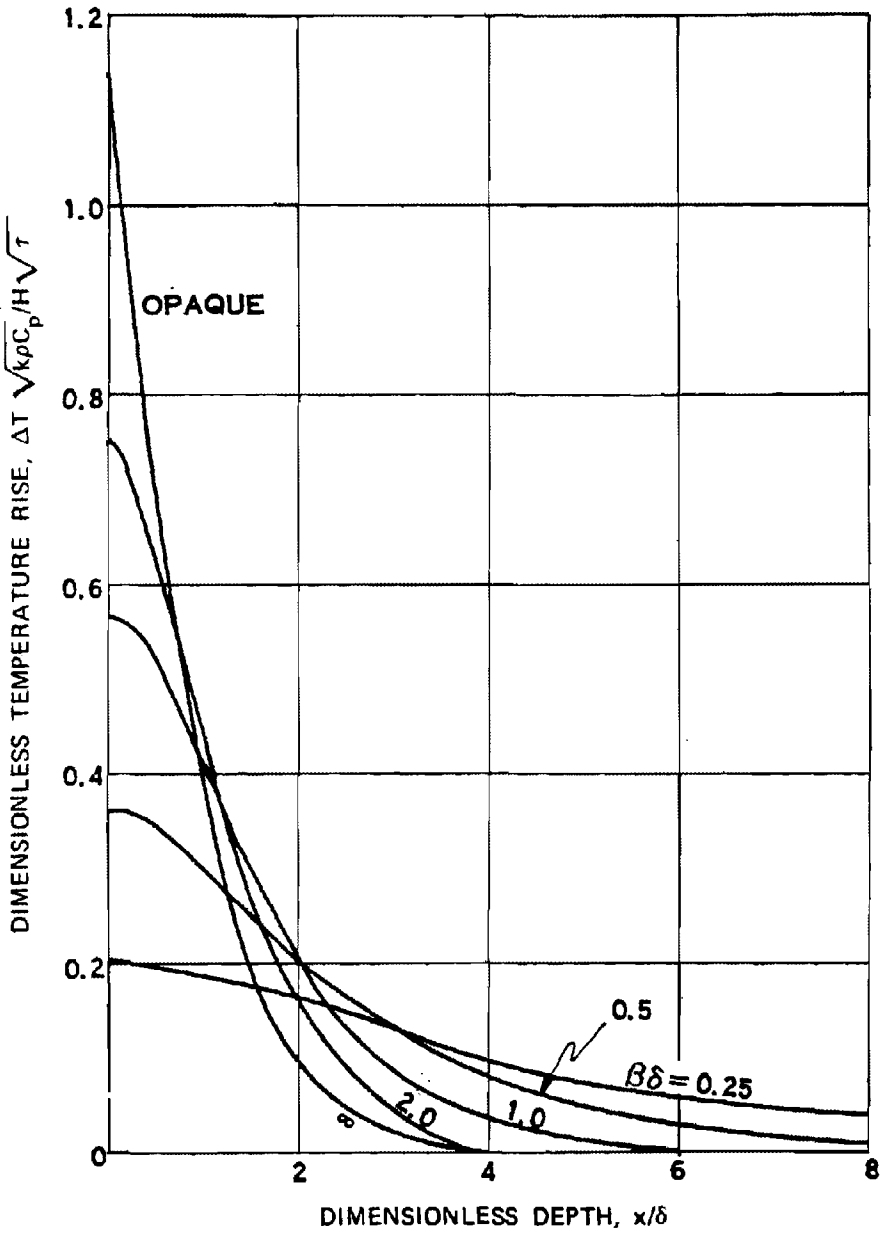

Figure 9-7. [redacted] Dimensionless Temperature Profiles in Opaque and Diathermanous Semi-Infinite Solids Exposed to a Rectangular Thermal Pulse [redacted]

[redacted]

9-23 Response of Metal Sheets [redacted]

[redacted] Both the tensile strength and the elastic modulus of metals tend to decrease with increasing temperature. Thus, thermal energy has the potential to weaken metallic structural members. If exposed metal parts are essential to the strength of a structure or a piece of equipment, weakening the metal by heating it may make the unit more susceptible to damage by the blast wave.

[redacted] Most structural metal is relatively immune to this form of damage in the loading levels of interest. If a heavy part such as a steel I-beam is subjected to a thermal pulse that is sufficiently intense to weaken it appreciably, it is probably so close to the burst that the blast wave could demolish the structure without assistance from the thermal pulse. Walls or roofs usually shield heavy structural members from the thermal pulse.

[redacted] Light weight units are more likely to be vulnerable to this synergistic damage. The outer covering and the materials that give these units mechanical strength are frequently one and the same. The material is likely to be an aluminum alloy, which loses strength at a much lower temperature than steel.

(U) The degradation of the response of metals to the blast wave as a result of thermal exposure is discussed in more detail in Section IV of this chapter.

9-24 Thermal Damage to Various Materials [redacted]

[redacted] The general trends discussed in the preceding paragraphs are illustrated by a number of specific examples in Tables 9-2 and 9-3. These tables show the critical radiant exposures for specified damage to fabrics and to various other materials, respectively. The radiant exposures are shown for three weapon pulse durations. The corresponding yields are shown in the footnote for low air bursts (note that altitude scaling is required for a 24 Mt burst to be considered an air burst (see Chapter 3)). Various yield/altitude combinations that will give the same values of t_{max} may be obtained by the methods described in Chapter 3.

[redacted] The values presented in Table 9-2 for fabrics apply for an ambient relative humidity of 65 percent and an ambient temperature of 20°C. For extremely dry conditions, the values shown for fabrics should be reduced by 25 percent. For extremely high relative humidities, near 100 percent (at 20°C), the values for fabrics should be increased by 25 percent. If the fabrics are water-soaked, the critical radiant exposures should be increased by 300 percent. The values for uniforms in Table 9-2 refer to damage to the material itself. They are not applicable for predicting skin burns under uniforms. However, when the outer garment ignites, the probability of skin burns should be considered.

[redacted] The effect, "tears on flexing," indicates the radiant exposure level at which the outer garment ceases to serve as a reliable barrier to the environment. Under certain environmental conditions the garment would require immediate replacement.

[redacted] Cotton or rayon fabrics generally can be ignited by exposure to thermal radiation. Nylons, dacrons, and similar synthetics generally are not ignited but melt at relatively low radiant exposures. Woolens do not ignite, but the fibers scorch and coalesce. When a sufficient thickness of the woolen fabric is scorched it becomes brittle and can be torn or crumbled readily.

[redacted] Most thick, dense materials that ordinarily are considered inflammable do not ignite to persistent flaming ignition when exposed to transient thermal radiation pulses. Wood, in the form of siding or beams, may flame during the exposure but the flame is extinguished when the exposure ceases.

[redacted]

[redacted]

Table 9-2. [redacted] Approximate Radiant Exposures for Ignition of Fabrics [redacted]

Material	Weight (oz/yd^2)	Color	Effect on Material	Radiant Exposure* (cal/cm^2) t_{max} 0.2 sec	t_{max} 1.0 sec	t_{max} 3.2 sec
Clothing Fabrics						
Cotton	8	White	Ignites	32	48	85
		Khaki	Tears on flexing	17	27	34
		Khaki	Ignites	20	30	39
		Olive	Tears on flexing	9	14	21
		Olive	Ignites	14	19	21
		Dark blue	Tears on flexing	11	14	17
		Dark blue	Ignites	14	19	21
Cotton corduroy	8	Brown	Ignites	11	16	22
Cotton denim, new	10	Blue	Ignites	12	27	44
Cotton shirting	3	Khaki	Ignites	14	21	28
Cotton-nylon mixture	5	Olive	Tears on flexing	8	15	17
	5	Olive	Ignites	12	28	53
Wool	8	White	Tears on flexing	14	25	38
		Khaki	Tears on flexing	14	24	34
		Olive	Tears on flexing	9	13	19
		Dark blue	Tears on flexing	8	12	18
	20	Dark blue	Tears on flexing	14	20	26
Rainwear (double-neoprene-coated nylon twill)	9	Olive	Begins to melt	5	9	13
	9	Olive	Tears on flexing	8	14	22
Drapery Fabrics						
Rayon gabardine	6	Black	Ignites	9	20	26
Rayon-acetate drapery	5	Wine	Ignites	9	22	28
Rayon gabardine	7	Gold	Ignites	**	24†	28†
Rayon twill lining	3	Black	Ignites	7	17	25
Rayon twill lining	3	Biege	Ignites	13	20	28
Acetate-shantung	3	Black	Ignites	10†	22†	35†
Cotton heavy draperies	13	Dark colors	Ignites	15	18	34
Tent Fabrics						
Canvas (cotton)	12	White	Ignites	13	28	51
Canvas	12	Olive drab	Ignites	12	18	28
Other Fabrics						
Cotton chenille bedspread		Light blue	Ignites	**	11†	15†
Cotton venetian blind tape, dirty		White	Ignites	10	18	22
Cotton venetian blind tape		White	Ignites	13†	27†	31†
Cotton muslin window shade	8	Green	Ignites	7	13	19

[redacted] Radiant exposures for the indicated responses (except where marked †) are estimated to be valid to ±25% under standard laboratory conditions. Under typical field conditions the values are estimated to be valid within ±50% with a greater likelihood of higher rather than lower values. For materials marked †, ignition levels are estimated to be valid within ±50% under laboratory conditions and within ±100% under field conditions. For low air bursts, values of t_{max} of 0.2, 1.0, and 3.2 sec correspond roughly to yields of 40 kt, 2 Mt, and 24 Mt, respectively.

** [redacted] Data are not available or appropriate scaling not known.

[redacted]

[redacted]

Table 9-3. [redacted] Approximate Radiant Exposures for Ignition of Various Materials [redacted]

Material	Weight (oz yd^2)	Color	Effect of Material	Radiant Exposure* (cal cm^2) t_{max} 0.2 sec	t_{max} 1.0 sec	t_{max} 3.2 sec
Household Tinder Materials						
Newspaper, shredded	2		Ignites	4	6	11
Newspaper, dark picture area	2		Ignites	5	7	12
Newspaper, printed text area	2		Ignites	6	8	15
Crepe paper	1	Green	Ignites	6	9	16
Kraft paper	3	Tan	Ignites	10	13	20
Bristol board, 3 ply	10	Dark	Ignites	16	20	40
Kraft paper carton used (flat side)	16	Brown	Ignites	16	20	40
New bond typing paper	2	White	Ignites	24†	30†	50†
Cotton rags		Black	Ignites	10	15	20
Rayon rags		Black	Ignites	9	14	21
Cotton string scrubbing mop (used)		Gray	Ignites	10†	15†	21†
Cotton string scrubbing mop (weathered)		Cream	Ignites	10†	19†	26†
Paper book matches, blue head exposed			Ignites	11†	14†	20†
Excelsior ponderosa pit	2 lb ft^3	Light yellow	Ignites		23†	23†
Outdoor Tinder Materials***						
Dry rotted wood punk (fir)			Ignites	4†	6†	8†
Deciduous leaves (beech)			Ignites	4	6	8
Fine grass (cheat)			Ignites	5	8	10
Coarse grass (sedge)			Ignites	6	9	11
Pine needles, brown (ponderosa)			Ignites	10	16	21
Construction Materials						
Roll roofing, mineral surface			Ignites	**	>34	>116
Roll roofing, smooth surface			Ignites	**	30	[illegible]
Plywood, douglas fir			Flaming during exposure	9	16	20
Rubber, pale latex			Ignites	50	80	110
Rubber, black			Ignites	10	20	25
Other Materials						
Aluminum aircraft skin (0.020 in. thick) coated with 0.002 in. of standard white aircraft paint			Blisters	15	30	40
Cotton canvas sandbags, dry filled			Failure	10	18	32
Coral sand			Explodes (popcorning)	15	27	47
Siliceous sand			Explodes (popcorning)	11	19	35

[redacted] Radiant exposures for the indicated responses (except where marked †) are estimated to be valid to ±25% under standard laboratory conditions. Under typical field conditions the values are estimated to be valid within ±50% with a greater likelihood of higher rather than lower values. For materials marked †, ignition levels are estimated to be valid within ±50% under laboratory conditions and within ±100% under field conditions. For low air burst, values of t_{max} of 0.2, 1.0, and 3.2 sec correspond roughly to yields of 40 kt, 2 Mt, and 24 Mt, respectively.

** [redacted] Data are not available or appropriate scaling not known.

*** [redacted] Radiant exposures for ignition of these substances are highly dependent on the moisture content.

[redacted]

SURVIVAL IN FIRE AREAS

The best documented fire storm in history (but not the one causing the greatest loss of life) occurred in Hamburg, Germany during the night of July 27-28, 1943, as a result of an incendiary raid by Allied forces. Factors that contributed to the fire included the high fuel loading of the area and the large number of buildings ignited within a short period of time.

The main raid lasted about 30 minutes. Since the air raid warning and the first high explosive bombs caused most people to seek shelter, few fires were extinguished during the attack. By the time the raid ended, roughly half the buildings in the 5 square-mile fire storm area were burning, many of them intensely. The fire storm developed rapidly and reached its peak in two or three hours.

Many people were driven from their shelters and then found that nearly everything was burning. Some people escaped through the streets; others died in the attempt; others returned to their shelters and succumbed to carbon monoxide poisoning.

Estimates of the number that were killed range from about 40,000 to 55,000. Most of the deaths resulted from the fire storm. Two equally heavy raids on the same city (one occurred two nights earlier; the other, one night later) did not produce fire storms, and they resulted in death rates that have been estimated to be nearly an order of magnitude lower.

More surprising than the number killed is the number of survivors. The population of the fire storm area was roughly 280,000. Estimates have been made that about 45,000 were rescued, 53,000 survived in non-basement shelters, and 140,000 either survived in basement shelters or escaped by their own initiative.

9-25 Causes of Death

The evidence that can be reconstructed from such catastrophes as the Hamburg fire storm indicates that carbon monoxide and excessive heat are the most frequent causes of death in mass fires. Since the conditions that offer protection from these two hazards generally provide protection from other hazards as well, the following discussion is limited to these two causes of death.

Carbon Monoxide. Burning consists of a series of physical and chemical reactions. For most common fuels, one of the last of the reactions is the burning of carbon monoxide to form carbon dioxide near the tips of the flames. If the supply of air is limited, as it is likely to be if the fire is in a closed room or at the bottom of a pile of debris from a collapsed building, the carbon monoxide will not burn completely. Fumes from the fire will contain a large amount of this tasteless, odorless, toxic gas.

During the Hamburg fire, many basement shelters were exposed to fumes. Imperfectly fitting doors and cracks produced by exploding bombs allowed carbon monoxide to penetrate these shelters. The natural positions of many of the bodies recovered after the raid indicated that death had often come without warning, as is frequently the case for carbon monoxide poisoning.

Carbon monoxide kills by forming a more stable compound with hemoglobin than either oxygen or carbon dioxide will form. These latter are the two substances that hemoglobin ordinarily carries through the blood stream. Carbon monoxide that is absorbed by the blood reduces the oxygen carrying capacity of the blood, and the victim dies from oxygen deficiency.

As a result of the manner that carbon monoxide acts, it can contribute to the death of a person who leaves a contaminated shelter to attempt escape through the streets of a burning city. A person recovering from a moderate case of carbon monoxide poisoning may feel well while he is resting, but his blood may be unable

to supply the oxygen his body needs when he exerts himself. After the air raid at Hamburg, victims of carbon monoxide poisoning, apparently in good health, collapsed and died from the strain of walking away from a shelter. It is suspected that many of the people who died in the streets of Hamburg were suffering from incipient carbon monoxide poisoning.

Heat. The body cools itself by perspiration. When the environment is so hot that this method fails, body temperature rises. Shortly thereafter, the rate of perspiration decreases rapidly, and, unless the victim finds immediate relief from the heat, he dies of heat exhaustion. Death from excessive heat may occur in an inadequately insulated shelter; it also may occur in the streets if a safe area cannot be located in a short time.

9-26 Shelters

The results of the Hamburg fire storm illustrate the value of shelters during an intense mass fire. The public air raid shelters in Hamburg had very heavy walls to resist large bombs. Reinforced concrete three feet thick represented typical walls. Some of these shelters were fitted with gas proof doors to provide protection from poison gas. These two features offered good protection from the heat and toxic gases generated by the fire storm.

The public shelters were of three types:

- *Bunkers.* These were large buildings of several shapes and sizes, designed to withstand direct hits by large bombs. The fire storm area included 19 bunkers designed to hold a total of about 15,000 people. Probably twice this number occupied the bunkers during the fire storm, and all of these people survived.
- *Splinterproof Shelters.* These were long single story shelters standing free of other buildings and protected by walls of reinforced concrete at least 2-1/2 feet thick. No deaths resulting from the fire storm were reported among occupants of these shelters. These structures were not gas-proof. Distance from burning structures and low height of the shelters probably provided protection from carbon monoxide.
- *Basement Shelters.* The public shelters that were constructed in large basements had ceilings of reinforced concrete 2 to 5 feet thick. Although reports indicate that some of the occupants of these shelters survived and some did not, statistics to indicate the chance of survival in such structures are not available.
- *Private Basement Shelters.* Private basements were constructed solidly, but most of them lacked the insulating value of very thick walls and the protection of gas-tight construction. Emergency exits (usually leading to another shelter in an adjacent building) could be broken if collapse of the building caused the normal exit to be blocked. As a result of the total destruction in the fire storm area, this precaution was of limited value. Many deaths occurred in these shelters as a result of carbon monoxide poisoning, and the condition of the bodies indicated that intolerable heat followed the carbon monoxide frequently. In some cases, the heat preceded the poisonous gas and was the cause of death. Generally, these shelters offered such a small amount of protection that the occupants were forced out within 10 to 30 minutes. Most of these people were able to move through the streets and escape. Others were forced out later when the fire storm was nearer its peak intensity, and few of these escaped. A few people survived in private basement shelters.

Experience in Hamburg and other mass fire areas suggests the following requirements for

shelters for fire protection:

- *Location.* Shelters should be located as far away from combustible structures as possible. The bottom of a mass of burning debris is very hot and can remain so for days. An open area also may be exposed to considerable heat, but not so much as the basement of a burned-out building. Three feet of earth will provide sufficient insulation for a shelter if no heavy fuels are nearby. However, material scattered by the blast wave could fall on a shelter and render it less safe. The choice of a suitable location for a shelter is most difficult in heavily built-up areas, where mass fires are most likely to occur. Shelters in such areas would have to be designed to withstand the severe environment to which they would be subjected in case of a mass fire. When the shelters in Hamburg were built, the problems of mass fires were not anticipated.
- *Ventilation.* Any shelter that is large enough to house its occupants in reasonable comfort contains sufficient air to sustain life for the duration of a mass fire. The shelter should be constructed so that it can be sealed from the entry of gases from the outside during the period of active burning. After the fire subsides, air will be available inside the shelter if burning debris has not fallen on or near the air intake.
- *Provisions.* If escape from a shelter is necessary, wet coats or blankets would improve the chance of survival in the open. Since any shelter built for protection against a mass fire would logically serve also as a fallout shelter, such items as blankets and water normally would be available.

9-27 Escape from the Fire Areas

A large number of people, chiefly the occupants of basement shelters, escaped from the Hamburg fire simply by leaving while the streets were still passable. In areas where damage is sufficiently light that people can attempt escape, the rate at which the fire builds up is expected to be slow enough to allow 30 minutes or more before movement through the streets will become dangerous.

Escape from the Hamburg fire storm area was simplified by the limited size of the fire. In the event of a mass fire caused by a nuclear attack, the fire area probably will be much larger. Although escape to the edge of the fire may be impossible, parks, bodies of water, or even areas that are not heavily built up may offer relative safety from the fire.

As the fire grows in intensity, selection of a suitable escape route becomes important. Moving through a narrow street, with tall buildings burning intensely on both sides, will subject people to an excessive amount of heat.

Preplanned escape routes are desirable. The safest routes are those that minimize exposure to thermal radiation from burning structures. A safe street would be wide compared to the heights of the buildings facing it. Masonry buildings with few windows would be a lesser threat than buildings with many windows. The solid wall blocks radiant exposure from fires burning inside the building, and it also protects the contents of the building from direct ignition by the thermal pulse from the nuclear weapon.

Simple rules for distinguishing safe from unsafe streets are not available; however, calculations of the street width for which the thermal radiation would be intense enough to ignite clothing in a short time have been made, assuming that buildings on both sides of the street were burning. The results of these calculations are shown in Table 9-4.

Whether or not such streets are safe will depend on many factors, such as fire intensity, percentage of the building fronts occupied by windows, wind speed and direction, protective

clothing, and exposure time. In general, the streets of Hamburg were 45 to 60 feet wide, and the buildings were 3 to 5 stories high. Table 9-4 predicts that such streets would be dangerous, and experience shows that they were. However, even these streets provided escape for some.

Table 9-4. Minimum Structure Separation for Escape Route

Building Height (feet)	Distance Between Buildings (feet)
20	40
30	57
40	67
50	83
60	96

9-28 Safe Areas Within the Fire

Experience indicates that large open areas within a fire storm area probably are safe. A park 1,000 feet in diameter provided adequate protection from the Hamburg fire storm; a similar area of 400 x 400 feet did not.

In Tokyo, during the Kanto earthquake and fire of 1923, fire whirlwinds sweeping across some large open areas killed many who would otherwise have survived. Thus, safety in a particular location depends to some extent on unpredictable aspects of the fire.

SECTION IV
THERMAL RADIATION DEGRADATION OF STRUCTURAL RESISTANCE TO AIR BLAST

Section III of this chapter contains a description of the properties of materials that might result in ignition or degradation of their physical properties. The emphasis of the discussion in Section III concerns the ignition of combustible materials. This section provides a somewhat expanded treatment of the degradation of structural resistance to air blast that is brought about by exposure to thermal radiation.

The problem of integrated thermal/blast effects can be divided into several elements. One element is the free field thermal and air blast environments to which a system element is exposed. Methods of predicting these environments are presented in Chapters 2 and 3. As pointed out in Chapter 3, prediction of the thermal environment is difficult because of the importance of climatic conditions. A statistical or probabilistic description of weather conditions frequently will have to be used to form some estimate of the validity of the results.

The first element of the overall problem treated in this section is the coupling of thermal energy into the structure or system element of interest. The condition of the target surface, its orientation to the detonation, and coatings employed all can affect the amount of thermal energy that is absorbed by the target.

The second element is the mechanisms for the loss of energy from the structure through convective heat losses or reradiation. The third element is the effect of absorbed energy on the state of the target material. The primary effect of this change of state is the fourth element, which is the change in material properties.

The final and fifth element of the problem is the effect of changes in material properties on the structural resistance to air blast loading.

Insufficient data are available concerning the thermophysical properties of nonmetallic materials to provide a realistic discussion of the combined blast/thermal effects on such materials. Any current prediction would be highly uncertain, both with regard to the occurrence of any specific physical phenomena and to the quantitative evaluation of the phenomena. Con-

sequently the discussion in this section will be limited to metallic materials.

THERMAL ENERGY ABSORBED

9-29 Absorption

The amount of thermal radiation that a metallic element will absorb depends on the properties of the metal, color, surface condition, orientation to the burst, the absence or presence of some type of coating (either accidental such as dirt or grease or intentional such as a paint system).* The amount of thermal energy absorbed by a target usually is determined by multiplying the incident energy by an absorption coefficient. The absorption coefficient cannot be directly measured; however, a good estimate can be made by performing spectral measurements of reflectance over the range of wavelengths representative of the nuclear radiation spectral distribution, and finding an average value of reflectance. The coefficient of absorptance then equals one minus this average value of reflectance. The absorptance determined in this manner is valid only as long as the surface does not change as a result of the absorbed thermal energy. Another approach is to divide the quantity of energy absorbed by the incident energy. The absorbed energy is determined from experimentally determined temperature vs time relationships and appropriate theoretical energy balance relationships.† Some typical values for absorption coefficients for bare metals are shown in Table 9-5. A value of 0.5 would be a good value to assume for the absorption coefficient in the absence of more definitive data for a specific system under investigation.

A coating or surface treatment on a metal substrate can alter the effective absorption coefficient significantly, and thereby can alter the amount of energy absorbed by the metal structure. The amount of energy absorbed depends on color, thickness, adhesiveness, and heat transfer characteristics of the coating. The most common type of coating is, of course, paint. The importance of paint in altering the amount of thermal radiation absorbed was noted in early investigations where it was found that the thin aircraft skin under painted insignia had melted, whereas the skin of adjacent areas was not affected. It should not be assumed, however, that paint or other coating is necessarily a detriment. In some instances the smoke that results from the breakdown of the paint can reduce the amount of energy absorbed and thereby reduce the maximum temperature reached by the substrate. Figure 9-8 illustrates this factor. The only true general statement that can be made about coatings is that they can alter the amount of thermal energy absorbed by the substrate. In fact some coatings, even paint systems, can be designed to reduce the amount of energy absorbed. As a general rule, however, most coating systems on present tactical military equipment

Table 9-5. Absorption Coefficients for Bare Metals

Material	Absorption Coefficient
Polished metals	0.25-0.5
Especially clean aluminum	0.2-0.4
Clean aluminum	0.5
Unpolished metals	0.45-0.55
Average over aircraft	0.5

* Implicit in this statement and throughout this discussion is the fact that energy coupling depends on the wavelength of the incident radiation.

† Absorptance is a function of time and temperature, although an average value usually is employed. This function when known may be found as an input specification for certain computer programs.

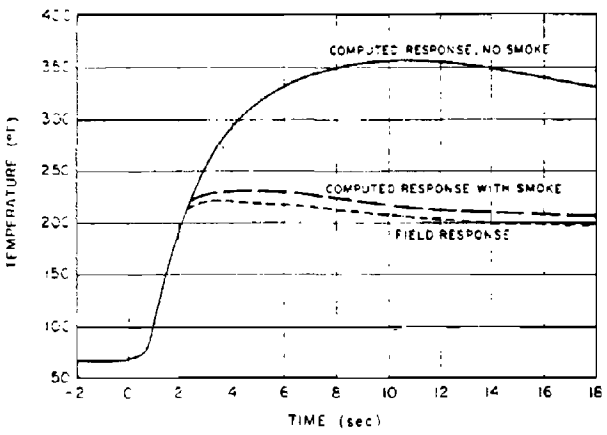

Figure 9-8. [redacted] Exposed Facing Temperature-Time Histories of Aluminum Honeycomb. Facing, 0.016-in. Gray Painted Skin; Core 1/8-in., Cell Size 1/2-in. Thick. 21-24.2 cal/cm^2, 3.8 Mt [redacted]

[redacted] will cause an increase in the amount of energy absorbed. The mechanisms of the response of coatings and the transfer of energy to the substrate are so complex that theoretical descriptions have not been successful. The response of coatings depends upon both the rate at which thermal radiation is received and the total incident energy. A given amount of radiation received at a slow rate may only cause discoloration or slight scorching, whereas if it were received at a very rapid rate it would cause charring or blistering. The latter response is more typical in a nuclear environment. The change in state of the coating reduces the amount of energy available to be transferred to the substrate, because these processes are irreversible. However, the change in state usually increases the absorption coefficient of the coating, and the net result usually is an increase on the amount of energy absorbed by the substrate. An exception occurs if the absorption coefficient was initially high, and energy was absorbed by the smoke layer generated by the decomposing paint. Coatings that respond by physically separating from the surface, i.e., blister, potentially can reduce the amounts of energy transferred to the substrate. Since the response of the coating-substrate system to nuclear weapon thermal radiation is so complex, effective absorption coefficients usually are determined experimentally.

[redacted] The average value of the absorption coefficient, A, depends on the properties of the substrate as the flow of thermal energy from the coating influences the response of the coating. A series of experiments with laser heating provides data to illustrate this point. Various metallic samples were prepared with a Silicon-carbide-synar binder coating (spectrophotometric measurements gave an average absorption coefficient of 0.85 for the coated aluminum sample for equilibrium temperatures of 70 and 600°F for a 10.6 micron wavelength). The average values of the absorption coefficients for a range of irradiances based on temperature vs time data are shown in Table 9-6. The effect of substrate properties is significant.

[redacted] Values of absorption coefficients are shown in Table 9-7. Generally, values range from 0.3 to 0.6 for light or reflective paints, and from

Table 9-6. [redacted] Average Absorption Coefficients for Laser Heated Coated Substrates [redacted]

Substrate	Average Absorption Coefficient
2024-T81 clad aluminum alloy	0.7 ± 0.1
6AL-4V annealed titanium	0.35 ± 0.1*
301 full hard stainless steel	0.80 ± 0.05

[redacted] Evaluation of titanium specimens showed considerable scatter. Erratic behavior probably resulted from improper bonding of the coating and cracking or flaking of the coating during straining.

[redacted]

Table 9-7. [redacted] Representative Values of Absorption Coefficients for Metals with Various Coatings or Surface Treatments [redacted]

Substrate	Coating or Surface Treatment	Absorption Coefficient
Metallic skins	Aluminum paint	0.5
Painted metals (aircraft skins)	White paint	0.3 - 0.5
	White paint (clean)	0.25
	White paint w/oil film	0.30
	Yellow paint	0.4 - 0.55
	Olive paint	0.6 - 0.7
	Gray paint (clean)	0.6
	Black paint	0.65 - 0.95
	Insignia blue	0.9
5032-H32AL	Black paint	0.7 - 1.0
Aluminums	Reflecting white paint	0.32
	Camouflage paint	1.00
6061 Al-Mg alloy	Haze gray Navy paint	0.78 ± 0.04
	Volcanol	0.99 ± 0.05
2024-T3	Anodized black	0.67

[redacted]

0.6 to 1.0 for dark paints or treated surfaces.

[redacted] It is apparent that the selection of an absorption coefficient based on the information in Table 9-7 for use in analyzing the response of a military system could be in error by as much as ±50 percent. Currently, the best solution is to perform upper and lower bound calculations. The upper and lower bound calculations should be based on the best estimate of the condition of the surface at the time of exposure, i.e., dirty, corroded, prior exposures, etc.

[redacted] One additional factor affects the amount of energy absorbed. This factor is the orientation of the surface to the thermal pulse. Ideally, if incident parallel rays are assumed, with no scattering, reflection or refraction, the target surface receives all of the radiation if it is oriented normal to the rays. If the surface is rotated about an axis normal to the rays, it cuts fewer of the rays, and the amount of thermal energy received is reduced. The energy received by a differential area on a curved surface also can be treated in this manner. With such assumptions, the absorbed energy function takes the following form:

$$Q_a = QA_e \cos \theta$$

where

Q = incident energy, usually expressed in cal/cm^2

Q_a = absorbed energy, usually expressed in cal/cm^2

[redacted]

A_e = effective absorption coefficient

θ = incident angle, angle between a line from the source to the surface and a line normal to the plane of the surface.

Under those ideal conditions, the amount of absorbed energy follows the cosine law; however, there will be conditions where scattering, reflection, and refraction, will invalidate the parallel ray assumption in addition to altering Q. This would principally occur at large angles of incidence such as shown schematically in Figure 9-9. A computer program called TRAP has recently been developed to handle these conditions.

Figure 9-9 also illustrates the amount of energy received by the surface of a cylinder with its axis oriented normal to the ray paths. The quantity θ then becomes the distance, in radians, along the circumference, from the point nearest the source.

Both the absorption coefficient and orientation are important in determining the amount of energy absorbed into the target. Errors in orientation are of greater significance at large angles on incidence; however, orientation usually can be inferred, at least for worst cases, whereas the absorption coefficient usually is not well known unless it has been determined experimentally.

9-30 Energy Losses

The absorption of thermal radiation energy into a material has been discussed in the previous paragraph. Before discussing the effect of this absorbed energy on material properties or change in structural resistance, the form and significance of energy losses from the material

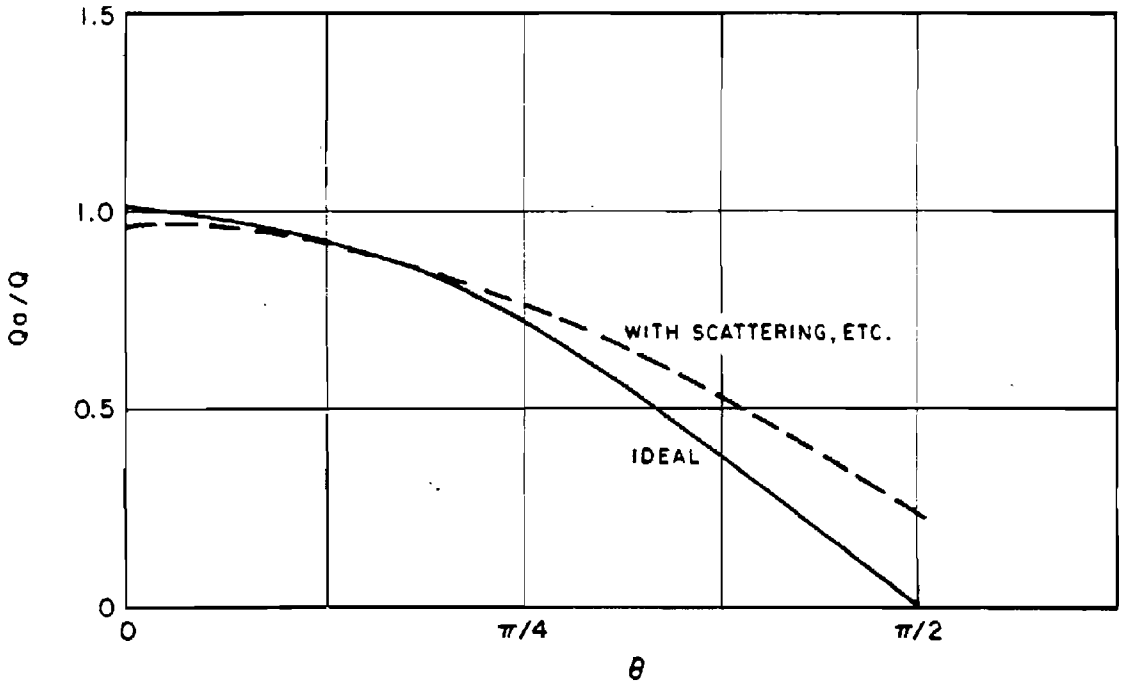

Figure 9-9. Schematic Comparison of Ideal Cosine Law with Function Including Scattering, Reflection, and Refraction

must be discussed. The three ways in which thermal energy can be dissipated are conduction, radiation, and convection. For purposes of this discussion, conductive dissipation is not really a loss, in that energy is redistributed throughout the material system rather than lost from the system. This form of heat dissipation is considered in more detail in the following subsection that discusses the change in material state, and the discussion of temperature profiles.

Radiation losses normally are considered negligible, because the temperature rises in a material are relatively small, even though the radiation heat loss is a function of the fourth power of absolute temperatures. The heat loss through radiation is expressed by:

$$Q_r = \sigma\epsilon(T^4 - T_0^4)$$

where

Q_r = radiative heat loss, cal/cm^2-sec,

σ = Stephan Bolzman Coefficient = 1.36 x 10^{-12} cal/cm^2 sec °K^{-4},

ϵ = emissivity, nondimensional,

T = absolute temperature, °K, of radiator (may be time dependent),

T_0 = absolute temperature, °K, of surrounding air.

If a 200°C temperature difference is assumed, and an emissivity of 0.2 (for oxidized aluminum at temperatures of a few hundred °C), and the ambient air temperature is 300°K, the radiative heat loss becomes:

$$Q_r = (1.36 \times 10^{-12})(0.2)(500^4 - 300^4)$$

$$= 1.48 \times 10^{-2} \text{ cal/cm}^2 \cdot \text{sec}$$

If the temperature rise is 400°C then Q_r becomes equal to 6.3 x 10^{-2} cal/cm^2 sec. Thus, it can be seen that even at high elevated temperatures, the heat loss through radiative processes is small.

Convective heat losses occur when there is a flow of air over the heated surface. This type of heat loss is most important for aircraft in flight and is a weak function of position on the airfoil, and the speed and altitude of the aircraft. The rate of convective heat loss also depends on whether the boundary layer flow is laminar or turbulent. These processes are generally understood, and a number of formulas that are available are given below:

$$h_{cv} = 0.67(10)^{-4} T^{0.3} \frac{(V\rho)^{0.8}}{x^{0.2}}$$

where

h_{cv} = convective heat loss coefficient for turbulent flow,

T = air temperature, °R,

V = flight speed, ft/sec,

ρ = density of air, lb/ft^3,

x = distance from leading edge of airfoil, ft.

$$h_{cv} = 0.176\ \rho V C_p (\log_{10} Re)^{-2.45},$$

$$h_{cv} = 0.01445\ k/x\ (Re)^{0.8}\ (Pr)^{0.33},$$

$$h_{cv} = 0.0282\ k/x\ (Re)^{0.8}\ (Pr)^{0.33},$$

$$h'_{cv} = 0.318\ k/x\ (Pr)^{1/3}\ (Re)^{1/2},$$

$$h'_{cv} = 0.332\ \rho V C_p (Pr)^{-2/3}\ (Re)^{-1/2},$$

where

h_{cv} = convective heat loss coefficient for turbulent flow, cal/cm^2 · sec · °C

h'_{cv} = convective heat loss coefficient for laminar flow, cal/cm^2 · sec · °C

ρ = density of air, gm/cm^3

V = flight speed, cm/sec

C_p = specific heat of air, cal/gm · °C

Re = Reynolds number, $\rho Vx/\mu$, dimensionless

k = thermal conductivity of air, cal/cm · sec · °C

x = distance from leading edge of airfoil, cm

Pr = Prandtl number, $C_p\mu/k$, dimensionless

μ = viscosity of air, gm/sec · cm

These formulas are based on the assumption that a reasonable approximation may be obtained by analysis of airflow over a heated flat plate. Experimental data indicate that the average error in using this approximation may be as much as 30 percent with a mean error of from 10 to 15 percent. The value for h_{cv} ranges from zero to 0.03 cal/cm^2 · sec · °C for a range of reasonable air properties and velocities. Generally, convective heat losses are marginally important for relatively low yield weapons; however, for long duration thermal pulses and under conditions when the temperature difference between the aircraft skin and the air boundary layer is large, the convective heat loss can be significant for high speed aircraft.

Values of h_{cv} have been calculated (see Table 9-8) for purposes of comparing the results of the equations given above, under the following assumed conditions.

Aircraft type = fixed wing

Aircraft speed = 100 mph (4.47 x 10^3 cm/sec)

Aircraft altitude = 1,000 ft

Air temperature = 70°F, 20°C

x = 4 ft, 121.92 cm

$\rho = 7.5(10)^{-2}$ lb/ft^3

Table 9-8. Values of h_{cv} Obtained from Various Functions in the Order in Which the Equations are Given Above

Flow Condition	h_{cv} $\left(\frac{\text{cal}}{\text{cm}^2 \cdot \text{sec} \cdot {}^\circ\text{C}}\right)$
Turbulent	$2.27(10)^{-3}$
	$2.27(10)^{-3}$
	$1.14(10)^{-3}$
	$2.23(10)^{-3}$
Laminar	$2.15(10)^{-4}$
	$2.82(10)^{-4}$

$= 1.2(10)^{-3}$ gm/cm^3

$k = 6.0874(10)^{-5}$ cal/cm · sec · °C

$C_p = 0.2404$ cal/gm · °C

$\mu = 1.798(10)^{-4}$ gm/cm · cm

The use of the convective heat loss coefficient, h_{cv}, is shown below:

$$Q_{cv} = h_{cv} (T_s - T)$$

where

Q_{cv} = convective heat loss, cal/cm^2 · sec

T_s = surface temperature, °C (may be time dependent)

T = surrounding air temperature, °C

For high speed aircraft, it may not be appropriate to assume that the temperature of the surrounding air is the temperature of the air boundary layer next to the heated surface. This

[redacted]

is particularly true if aerodynamic heating occurs. For this situation, the recovery temperature T_r should replace T in the equation given above.

[redacted] For tactical systems of interest to this section, radiative and convective heat losses generally can be neglected. However, these are and normally should be included in detailed analyses and computer calculations for completeness, particularly for high speed aircraft and large yield weapons.

[redacted] CHANGES IN MATERIAL STATE AND MATERIALS PROPERTIES [redacted]

9-31 Changes in Material State

[redacted] The change in material state of primary interest is the change in temperature caused by absorbed thermal radiation. The temperature changes are controlled by the energy absorbed in the material as a function of time and position and by the geometry of the member being analyzed. Geometry can have a significant impact on heat flow through the member as well as heat absorption and losses. There are a number of techniques available for determining temperature changes. These techniques vary from simple formulas to large computer programs depending on the simplifying assumptions that are made and the complexity of the system geometry. The greatest amount of effort has been devoted to the study of temperature changes in flat plates, primarily because of the interest in aircraft safety/survivability problems. Therefore, the following discussion is dominated by analysis of flat plates, although most of what can be learned about the processes affecting plate temperature applies to other geometries because the basic equations describing the processes are the same.

[redacted] Plates can be divided into several types according to the temperature profile through the plate. A thermally "thin" plate usually is defined as a plate where the temperature gradient between the front and back of the plate is small. Thermally thin plates simplify the analysis problem, because, if a significant thermal gradient exists, the thermal stresses become more complex. Plates usually are assumed to be one dimensional, with no heat flow to a supporting structure, so heat sink effects can be neglected, unless the plate is part of a fuel tank.

[redacted] Whether a plate is thermally thin depends not only on the thermophysical properties of the material, but also on the thermal pulse characteristics and the time during the pulse that the criterion is applied. Some materials conduct heat more quickly than others, and the temperature on the back face of these materials will not lag behind the temperature on the front as much as for materials with lower conductivities. For example, the thermal conductivity of aluminum is about 0.4 cal/sec · cm · °C, and that of titanium is about 0.04 cal/sec · cm · °C. Therefore, aluminum conducts 10 times as much heat as titanium in a given amount of time. Other material factors that control the ratio of front to back temperature are specific heat, density, and thickness.

[redacted] The temperature difference also depends on pulse characteristics. For a pulse that is delivered slowly, there may be sufficient time for energy to be conducted to the back face, so the thermal gradient at the time of interest is minimized. Conversely, a pulse that is delivered rapidly may cause a steep thermal gradient. For a given pulse, material, and thickness, the time at which the temperature response is of interest determines whether the thermal gradient is small.

[redacted] A number of techniques have been developed to determine whether a plate can be considered to be thermally thin. One technique that gives a good approximation is illustrated in Figure 9-10. The values of $\eta = t/t_{max}$ and $\alpha t_{max}/b^2$ must be evaluated to use the curves in Figure 9-10. From Chapter 3

[redacted]

[redacted]

[redacted]

$$t_{max} = 0.043\ W^{0.43}\ (\rho/\rho_o)^{0.42}\ \text{sec},*$$

where t_{max} is the time to the principle thermal maximum, W is the weapon yield in kilotons, and ρ/ρ_o is the ratio of the air density at the burst altitude to the air density at sea level. The parameter α is defined as

$$\alpha = k/\rho_m C_p \quad \text{cm}^2/\text{sec}$$

where

k = thermal conductivity of air, cal/cm · sec · °C,

ρ_m = material density, gm/cm^3,

C_p = specific heat of air, cal/gm · °C

and h is the thickness of the plate in centimeters. The point where the values of η and $\alpha t_{max}/h^2$ meet determines whether the plate is thin, finite, or thick. A thin plate is one in which the difference between back and front temperatures is less than 10 percent. A thick plate is one in which there is no temperature rise on the back face. A finite plate falls between the other two criteria.

[redacted] A technique for predicting the temperatures of thermally thin plates uses the relationships shown in Figure 9-11. This technique is believed to provide good results over a fairly wide range of problems of interest. The technique assumes that thermophysical properties and the rate of convective heat loss are constant, that radiation losses are negligible, and that there is no heat loss from the back of the plate.

* [redacted] The examples provided in this section will all be concerned with air bursts that are sufficiently low that the term $(\rho/\rho_o)^{0.42}$ is near enough to 1.0 to be neglected (e.g., at 4,000 feet $(\rho/\rho_o)^{0.42} \approx 0.99$). Therefore, the approximation $t_{max} \approx 0.043\ W^{0.43}$ will be used throughout the remainder of this section.

[redacted]

Problem 9-1. Calculation of Thermal Thickness of a Metal Plate

Figure 9-10 contains curves that define regions where metal plates may be considered thermally thin, finite, and thick, respectively. The curves are plotted as a function of the parameters η and $\alpha t_{max}/b^2$, which are defined in paragraph 9-31. Their use is demonstrated in the following example.

Example

Given: A 5086 Aluminum alloy plate is an important part of a structure under analysis. The plate is 0.875 cm thick and the range of air blast exposures for the system of which it is a part are expected to be from 8 to 15 psi from a 100 kt explosion at a height of burst of 1,000 feet.

Find: Whether the plate can be considered thermally thin.

Solution: The corresponding height of burst for a 1 kt explosion is

$$h_1 = \frac{h}{(W^{1/3})} = \frac{1{,}000}{(100)^{1/3}} = 215 \text{ feet.}$$

From Figures 2-18 and 2-19, Chapter 2, the ground distances from a 1 kt explosion at a height of burst of 215 feet that correspond to 15 and 8 psi overpressure are 895 and 1,250 feet respectively. From Figure 2-28, Chapter 2, the times of arrival of the blast wave from a 1 kt explosion to these distances are 0.37 seconds and 0.61 seconds, respectively. The corresponding times for a 100 kt explosion are

$$t = t_1 W^{1/3}$$

$$t = (0.37)(100)^{1/3} = 1.72 \text{ sec for 15 psi,}$$

and

$$t = (0.61)(100)^{1/3} = 2.83 \text{ sec for 8 psi.}$$

The time to final maximum for a 100 kt low air burst is

$$t_{max} \approx 0.043\ W^{0.43}$$

$$= (0.043)(100)^{0.43} = 0.31 \text{ sec.}$$

Therefore,

$$\eta = t/t_{max}$$

$$\eta = \frac{1.72}{0.31} = 5.5 \text{ for 15 psi,}$$

and

$$\eta = \frac{2.83}{0.31} = 9.1 \text{ for 8 psi.}$$

The properties of the alloy are

$$k = 0.28 \text{ cal/sec} \cdot {}^\circ\text{C},$$

$$C_p = 0.22 \text{ cal/gm} \cdot {}^\circ\text{C},$$

$$\rho = 2.66 \text{ gram/cm}^3.$$

Since

$$\alpha = \frac{k}{\rho C_p},$$

$$\frac{\alpha t_{max}}{b^2} = \frac{k t_{max}}{\rho C_p b^2}$$

$$= \frac{(0.28)(0.31)}{(2.66)(0.22)(0.875)^2}$$

$$= 0.19.$$

Answer: From Figure 9-10, at the 15 psi overpressure level where $\eta = 5.5$, the plate should be considered finite; at the 8 psi overpressure level, where $\eta = 9.1$, the plate can be considered thermally thin.

Related Material: See paragraph 9-31.

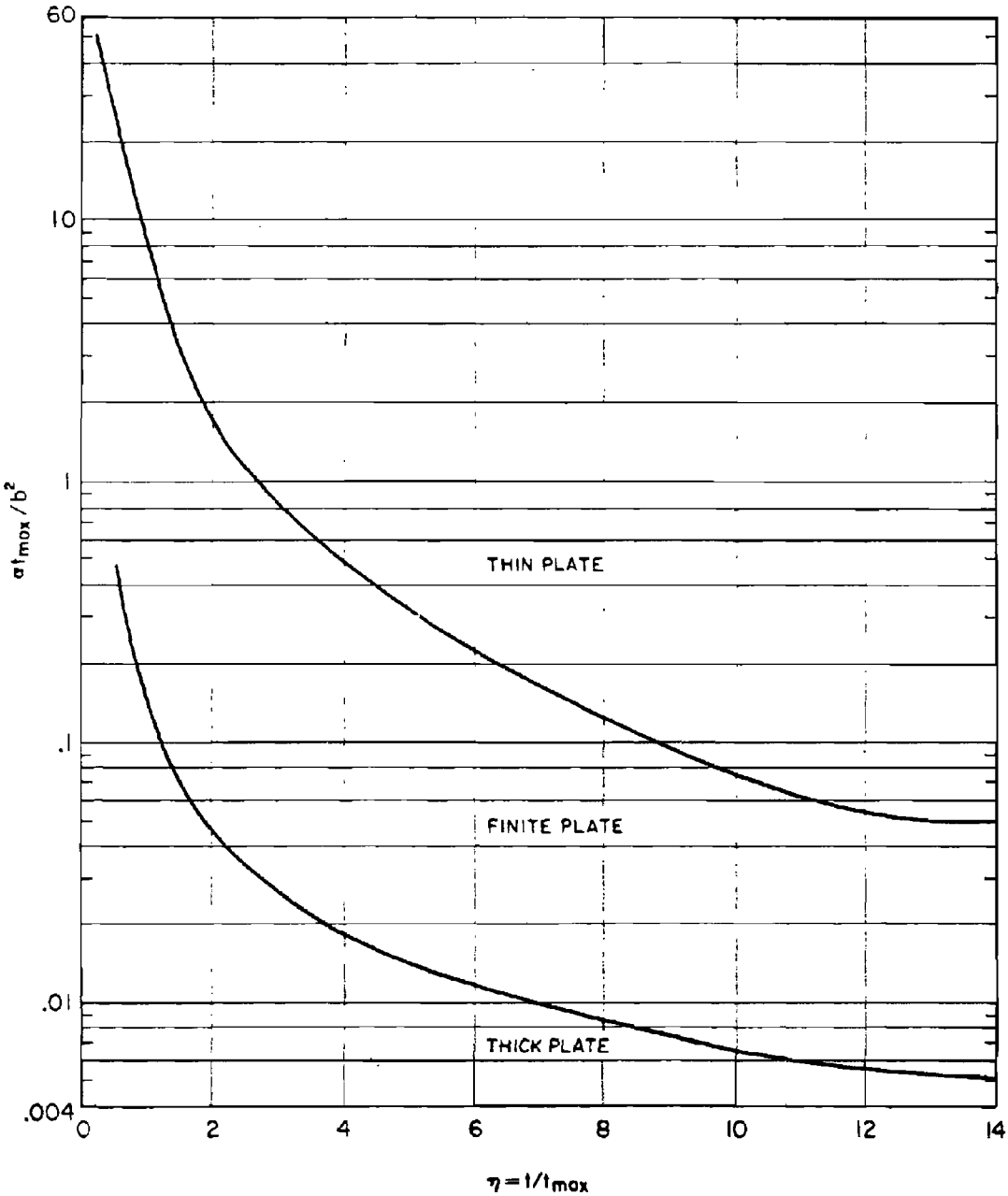

Figure 9-10. [redacted] Thin Plate, Thick Plate, and Finite Plate Regions for Exposure to Nuclear Weapons Thermal Radiation [redacted]

[redacted] The variables used in this technique have units in the cgs system and have been defined previously; however, they are listed below for convenience.

T_o = temperature of the plate prior to exposure,

ΔT = temperature rise, °C,

A = absorption coefficient

Q = thermal exposure, cal/cm^2 (effective thermal exposure may be used where $Q = Q \cos \theta$),

ρ_m = specific gravity of material, gm/cm^3,

C_p = specific heat, cal/gm · °C,

b = plate thickness, cm,

h_{cv} = convective heat loss, cal/cm^2 · sec · °C,

$\eta = t/t_{max}$.

Use of the technique is illustrated in Problem 9-2.

[redacted]

Problem 9-2. Calculation of Temperature Rise in a Thermally Thin Plate

Figure 9-11 contains a family of curves that relate thermophysical properties of a thin metal plate to thermal pulse parameters in a manner that allows calculation of the temperature rise in the plate. The procedures for the calculation are made clear in the following examples. Symbols for the various parameters are listed in paragraph 9-31.

Example 1

Given: A 6061-T6 Aluminum alloy plate is exposed to the thermal pulse from a 100 kt low air burst at a location where the incident radiant energy is 76 cal/cm^2 and arrives at an angle of incidence of 30°. Properties of the plate are

$$T_o = 30°C,$$

$$A = 0.8,$$

$$\rho_m = 2.7 \text{ gm/cm}^3,$$

$$C_p = 0.216 \text{ cal/gm} \cdot °C,$$

$$b = 0.15875 \text{ cm},$$

$$h_{cv} = 0.$$

Find: The temperature of the plate when η = 2, 4, and 6.

Solution: The effective radiant exposure is

$$Q_e = Q \cos \theta = 76 \cos 30° = 65.8 \text{ cal/cm}^2.$$

From Figure 9-11, with

$$\frac{h_{cv} t_{max}}{\rho C_p b} = 0,$$

when

$$\eta = 2, \frac{\Delta T}{AQ/\rho C_p b} = 0.47,$$

when

$$\eta = 4, \frac{\Delta T}{AQ/\rho C_p b} = 0.67,$$

and when

$$\eta = 6, \frac{\Delta T}{AQ/\rho C_p b} = 0.74.$$

The value of $AQ/\rho C_p b$ is

$$\frac{AQ_e}{\rho C_p b} = \frac{(0.8)(65.8)}{(2.7)(0.216)(0.15875)} = 569°C.$$

The temperature rises are

$$\Delta T = (0.47)(569) = 267°C \text{ for } \eta = 2,$$

$$\Delta T = (0.67)(569) = 381°C \text{ for } \eta = 4,$$

and

$$\Delta T = (0.74)(569) = 421°C \text{ for } \eta = 6.$$

Answer: The plate temperatures are

$$T = T_o + \Delta T.$$

Therefore,

$$T_{\eta=2} = 30 + 267 = 297°C$$

$$T_{\eta=4} = 30 + 381 = 411°C$$

$$T_{\eta=6} = 30 + 421 = 451°C.$$

Example 2

Given: The same conditions as Example 1,

except that $h_{cv} = 3.0 \times 10^{-2}$ cal/cm^2 · °C.*

Find: The temperature of the plate when $\eta = 2$, 4, and 6.

Solution:

$$t_{max} = 0.043\ W^{0.43} = (0.043)(100)^{0.43}$$

$$= 0.31 \text{ sec.}$$

$$\frac{h_{cv} t_{max}}{\rho C_p b} = \frac{(3.0 \times 10^{-2})(0.31)}{(2.7)(0.216)(0.15875)} = 0.1.$$

From Figure 9-11, when

$$\eta = 2, \frac{\Delta T}{AQ/\rho C_p b} = 0.44,$$

when

$$\eta = 4, \frac{\Delta T}{AQ/\rho C_p b} = 0.53,$$

and when

$$\eta = 6, \frac{\Delta T}{AQ/\rho C_p b} = 0.51.$$

From Example 1,

$$\frac{AQ}{\rho C_p b} = 569°\text{C}.$$

The temperature rises are

$$\Delta T = (0.44)(569) = 250°\text{C for } \eta = 2,$$

$$\Delta T = (0.53)(569) = 302°\text{C for } \eta = 4,$$

and

$$\Delta T = (0.51)(569) = 290°\text{C for } \eta = 6.$$

Answer: The plate temperatures are

$$T = T_o + \Delta T.$$

Therefore,

$$T_{\eta=2} = 30 + 250 = 280°\text{C},$$

$$T_{\eta=4} = 30 + 302 = 332°\text{C},$$

and

$$T_{\eta=6} = 30 + 290 = 320°\text{C}.$$

Related Material: See paragraph 9-31.

* This value corresponds roughly to an airplane speed of 200 mi/hr.

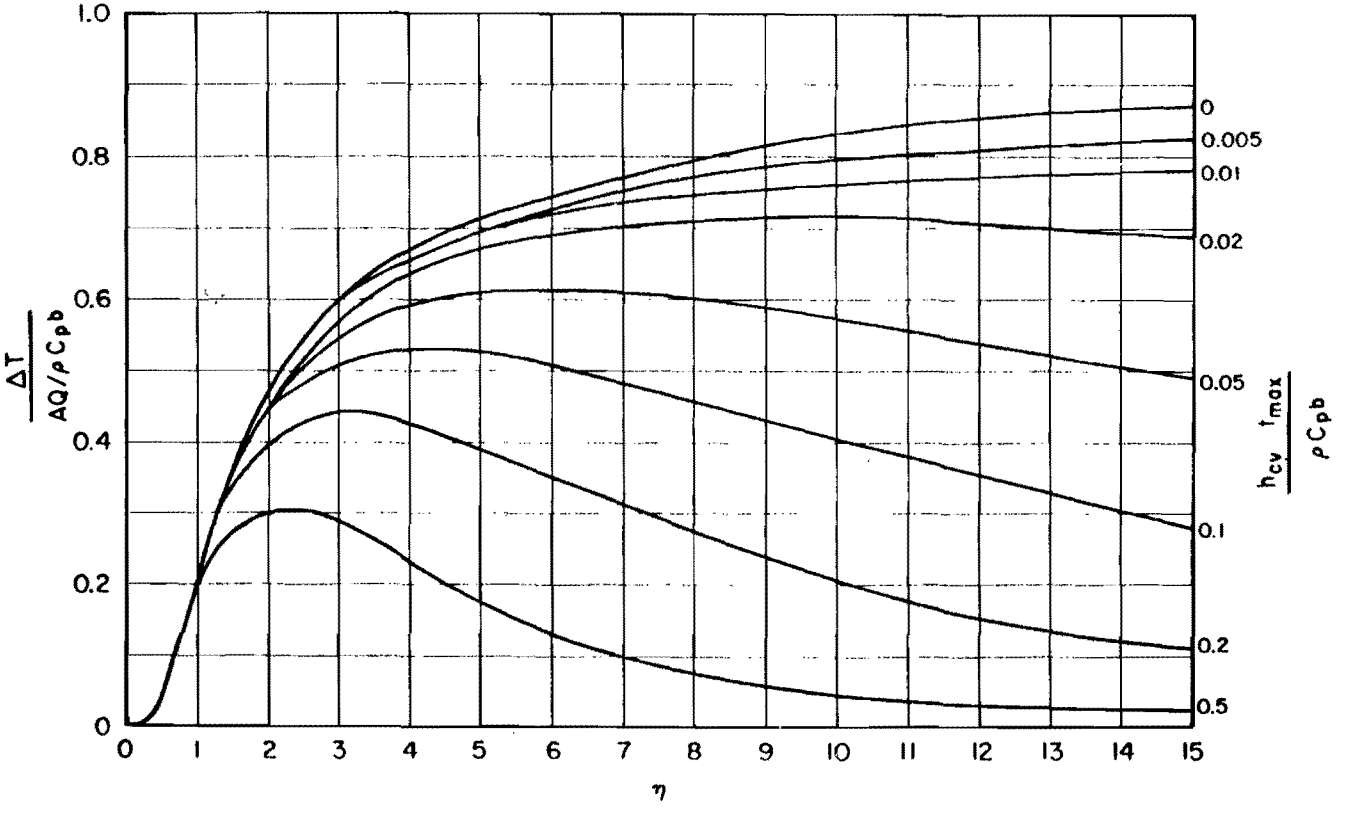

Figure 9-11. [redacted] Thermal Response of a Thin Plate to Nuclear Weapons Thermal Radiation Pulse [redacted]

[redacted]

[redacted] Thermally thick plates are those that do not have a temperature rise on the back surface at the time of interest. Finite plates have a temperature gradient between the front and back surfaces and a temperature rise at both surfaces.

[redacted] Computer codes generally are required to calculate the temperature history of thermally thick and thermally finite plates. Simple graphical techniques have been developed to determine the temperature rise on the front face of a thermally thick plate and on the front face, mid place, and back face of thermally finite plates. These are not included herein because the techniques depend upon thermal source characteristics that are very different from the source characteristics described in Chapter 3.* If graphical techniques that are compatible with the thermal source data of Chapter 3 become available, they will be included in revisions to this manual. In the meantime, users who are interested in the techniques should consult "Thermal Degradation of Structural Resistance to Air Blast" (see bibliography).

[redacted] Requirements to analyze geometries that are more complex than single layer plates (even if they are layered thin plates) or to examine plates with temperature dependent thermophysical properties or heat losses require the use of a computer code. Codes for more complex geometries, such as cylinders and tee beams, have been developed specifically for the types of analysis of concern to this section. As noted previously, the TRAP computer program can calculate temperatures and stresses for two dimensional structures.

[redacted] Honeycomb structures or sandwich construction must be considered as a multi-layered system. A five layer system was used to examine thin sandwich construction. The five layers consisted of the core, the two skins, and the two bonding layers between the skins and core. Most sandwich construction has been found to fail at the bonding layer. Consequently, the temperature of the bond and the thermal stresses in the face sheets (or skins) can be of equal importance. Studies and experiments show that a calculational procedure that includes five layers was required to duplicate experimental results accurately. A code developed for dual layer plates has been used to calculate thick single layer plates by considering both layers to be the same material.

9-32 Change in Materials Properties [redacted]

[redacted] The rise in temperature that occurs when thermal radiation is absorbed can be expected to cause changes in materials prop-

---

[redacted] The important differences in source characteristics are the time to final maximum, where

$$t_{max} = 0.032\ W^{1/2}\ \text{sec}$$

was used in developing the graphical techniques, while a more recent value

$$t_{max} = 0.043\ W^{0.43}\ (\rho/\rho_o)^{0.42}\ \text{sec}$$

is given in Chapter 3, and the power at thermal maximum, where

$$P_{max} = 4\ W^{1/2}\ \text{kt/sec}$$

was used in developing the graphical techniques while a more recent value of

$$P_{max} = \frac{4.3\ W^{0.6}}{(\rho/\rho_o)^{0.44}}\ \text{kt/sec}$$

is given in Chapter 3. The latter determines the maximum irradiance (thermal energy per unit area per unit time) incident on the target. Actually, the procedures described in Problems 9-1 and 9-2 were developed for use with the older expression for t_{max}; however, since the two expressions agree within a few percent for low air bursts and for yields from a few kt to a few Mt, the use of the techniques with the value of t_{max} from Chapter 3 was illustrated. The values of P_{max}, on the other hand, differ widely at all yields. Since the temperature histories presented in the graphical techniques for finite and thick plates depend strongly on irradiance, it is not possible to use the thermal source data with the curves derived for use with the older expression for P_{max}.

[redacted]

erties. Properties of mechanical strength are of greatest concern, since these properties influence structural resistance.

Thermal stresses may be present in either unrestrained or restrained structures or elements thereof if thermal gradients, which usually are caused by increased temperatures, are present. The magnitude of the stresses depends upon the amount of expansion the structure experiences, which depends on the value of the coefficient of thermal expansion, α_e, for the material. The dimensions of this coefficient are length per length per temperature unit, often expressed as in./in.°F or cm/cm/°C. The value of α_e depends on the temperature, as shown in Figures 9-12 through 9-15 for a number of materials. Use of an improper value of α_e can cause serious errors in the estimation of the thermal stress level in some materials. For example, the use of the room temperature value of α_e for AISI 301 stainless steel when the value of 1200°F (~650°C) should have been used, would result in a value of thermal stress that is 20 percent too low. For 2024 Aluminum Alloy, the error would be about 18 percent, whereas for Ti-8Mn Titanium Alloy, the error would be 45 percent. Thus, for large temperature rises, the assumption of a constant value for the coefficient of thermal expansion could lead to significant errors. However, for small temperature rises, on the order of 200°F (110°C), the error would not be significant. For most metallic materials, the error in thermal stress is about 2 percent per 100°F or 3 percent per 100°C temperature rise above room temperature values of α_e. Additional data may be obtained from "Metallic Materials and Elements for Aerospace Vehicle Structures" (see bibliography).

Changes in mechanical strength are the prime reason for concern about the effects of absorbed thermal radiation. Data from several sources are incorporated into Figures 9-16 through 9-18 to provide some indication of the effects of elevated temperature on the tensile strength properties of 2014-T6 Aluminum Alloy, Titanium Alloy 6AL-4V, and 301 full hard stainless steel. The various curves in these figures provide some indication of the effect of elevated temperature and also the effects of the speed at which the sample was heated and the time it remained at a given temperature.

The data that will be discussed comes from several sources. Since the techniques for testing that were used in these sources differ considerably, it will be of value to discuss the various techniques employed.

The four basic types of loading tests that have been used to determine mechanical properties at elevated temperatures are illustrated in Figure 9-19 and 9-20. Figures 9-19a and b illustrate an adaptation of the conventional tensile test for elevated temperature. The sample is heated rapidly to an equilibrium temperature. At some finite time after thermal equilibrium, called the soak time, a conventional tensile loading test is conducted with a constant strain rate loading mechanism. Two loading rates are shown in Figure 9-19a. Figure 9-19b illustrates the type of results that are obtained from the type of test illustrated in Figure 9-19a.

Figures 9-19c and d illustrate another type of tensile test where the sample is loaded with a constant load, then heated at some rate until rupture occurs. Figure 9-19d illustrates the type of results that are obtained from the type of test illustrated in Figure 9-19c. Figure 9-20 illustrates two types of short time creep tests and their results.

Results from these types of tests are shown for three aluminum alloys in Figures 9-21 through 9-23. Some data shown in Figure 9-21 were obtained by the type of the test illustrated in Figure 9-19a. The soak time of the sample was one-half hour before a standard constant strain rate of 0.00033 in./in./sec tensile test was performed. Other data in Figure 9-21 also were

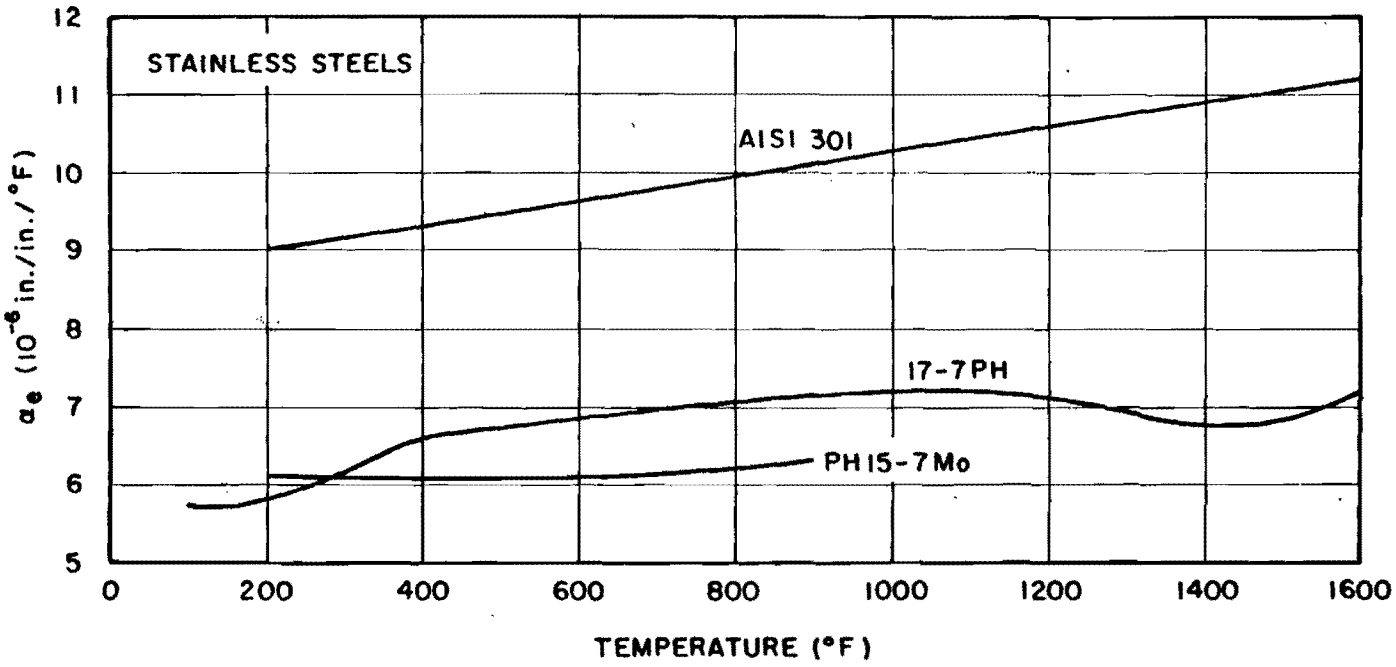

Figure 9-12. Coefficient of Linear Expansion as a Function of Temperature for Stainless Steels

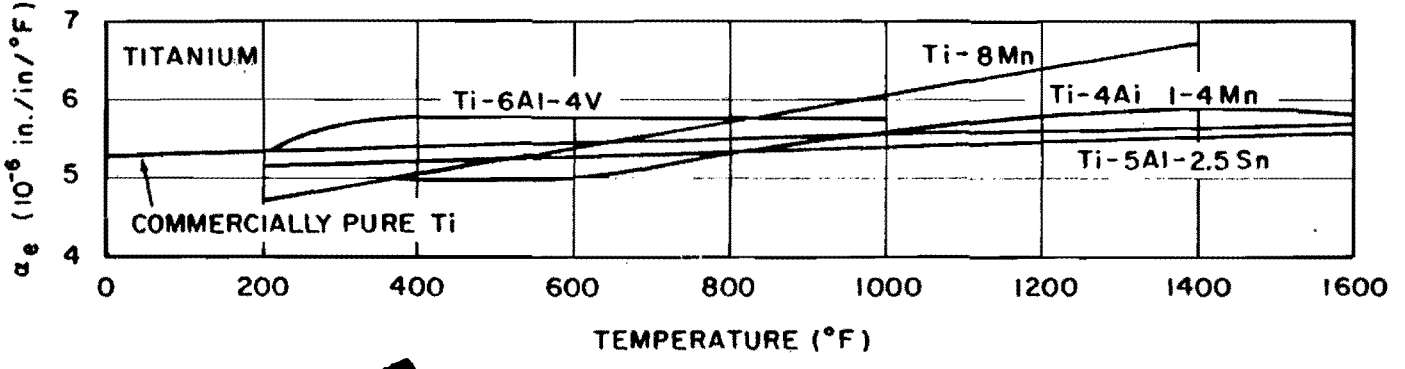

Figure 9-13. Coefficient of Linear Expansion as a Function of Temperature for Titanium Alloys

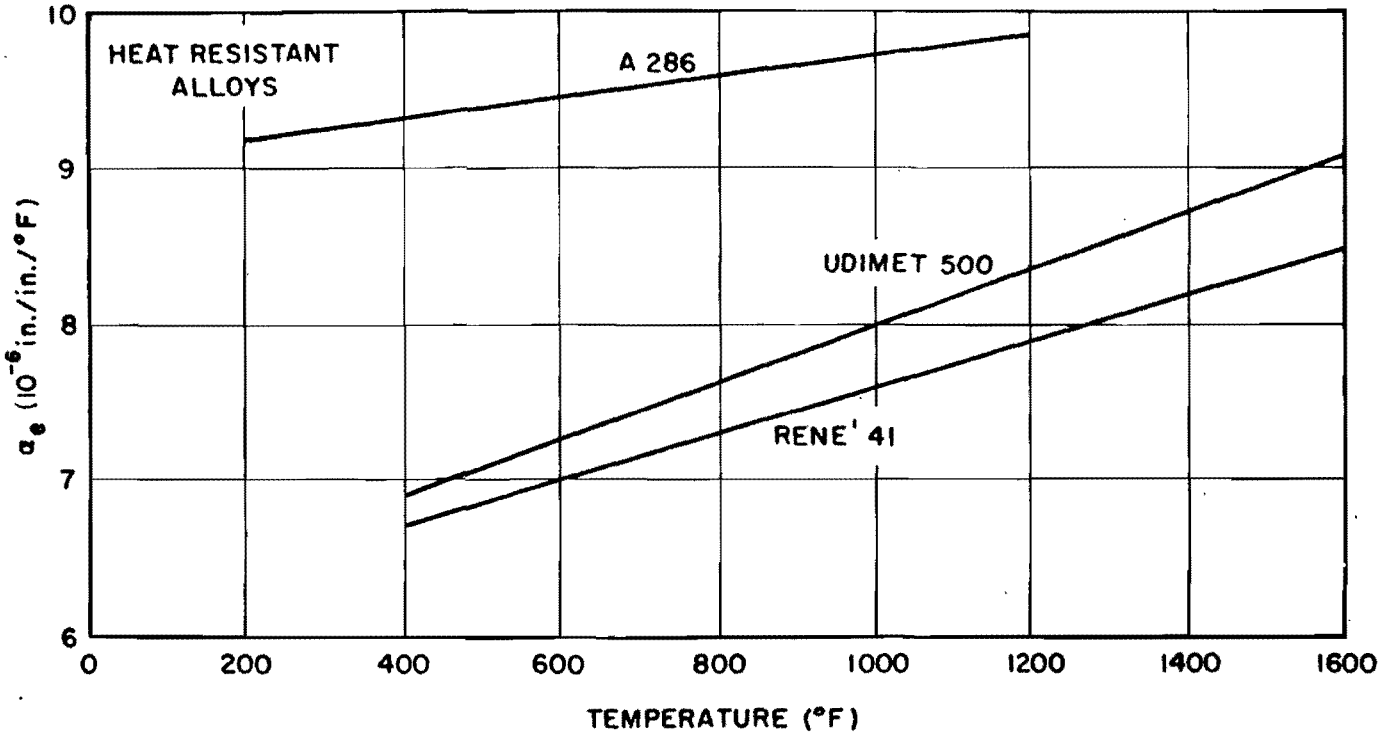

Figure 9-14. [redacted] Coefficient of Linear Expansion as a Function of Temperature for Heat Resistant Alloys [redacted]

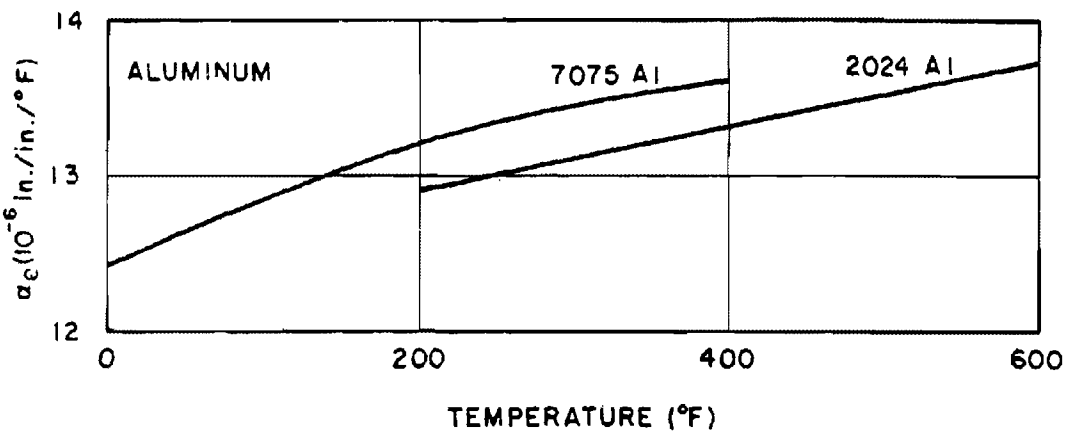

Figure 9-15. [redacted] Coefficient of Linear Expansion as a Function of Temperature for Aluminum Alloys [redacted]

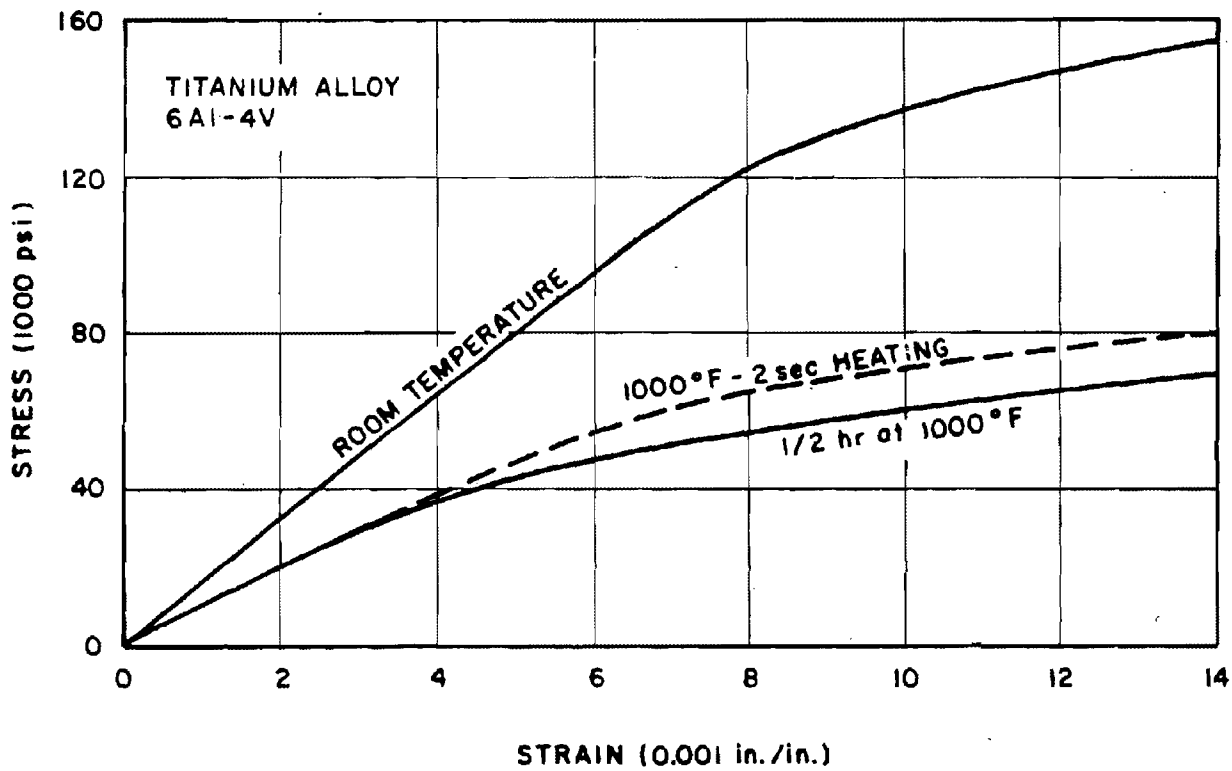

Figure 9-16. [redacted] Typical Stress-Strain Curves for Titanium 6Al-4V Alloy at Room and Elevated Temperatures [redacted]

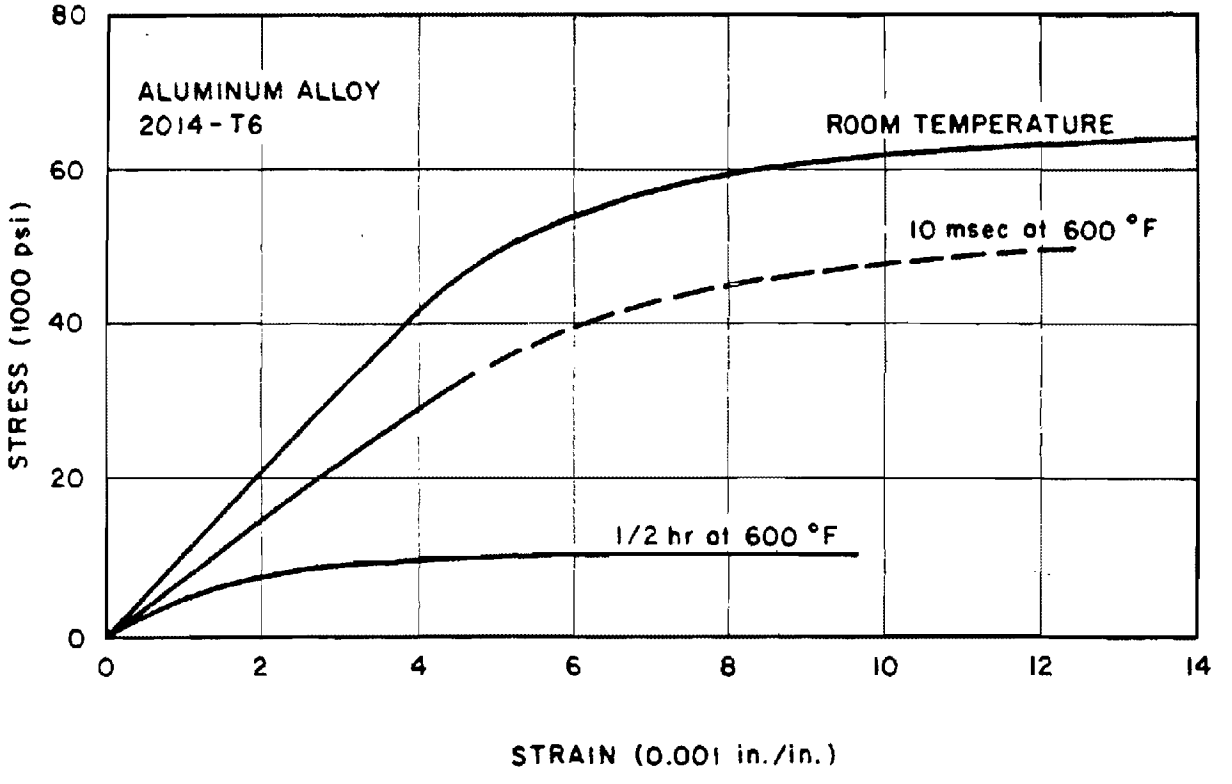

Figure 9-17. [redacted] Typical Stress-Strain Curves for 2014-T6 Aluminum Alloy at Room and Elevated Temperatures [redacted]

[redacted]

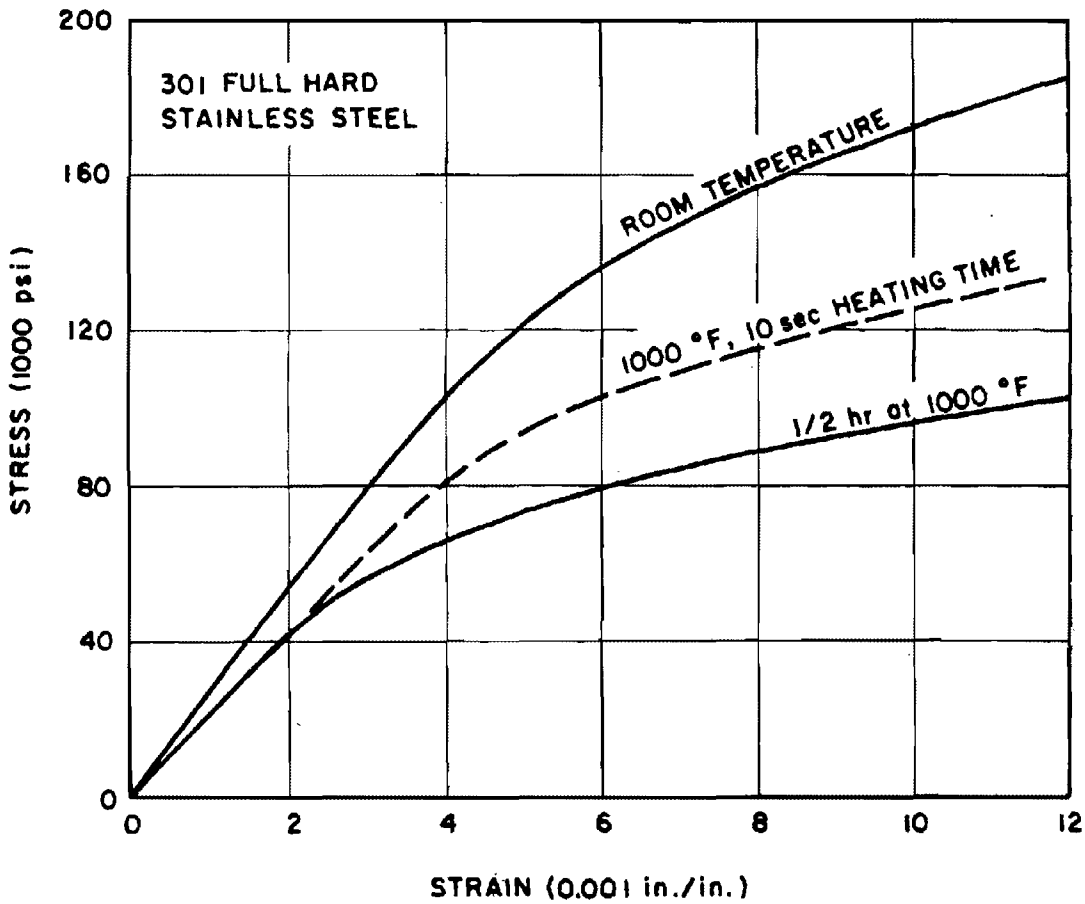

Figure 9-18. [redacted] Typical Stress-Strain Curves for 301 Stainless Steel at Room and Elevated Temperatures [redacted]

[redacted]

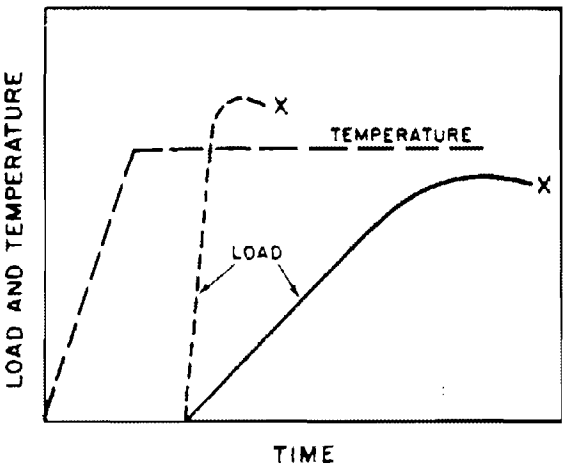

a. Tensile Tests After Rapid Heating

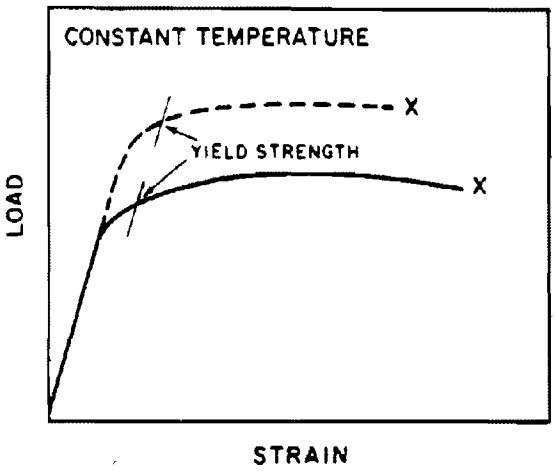

b. Load-Strain Curves from Tests Illustrated in Figure 9-19a.

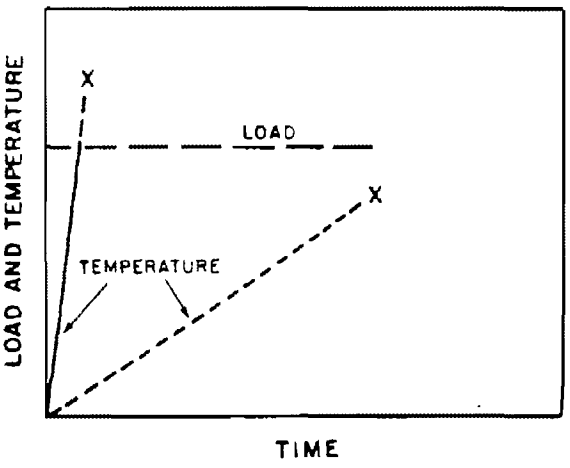

c. Rapid-Heating Constant-Load Tensile Tests

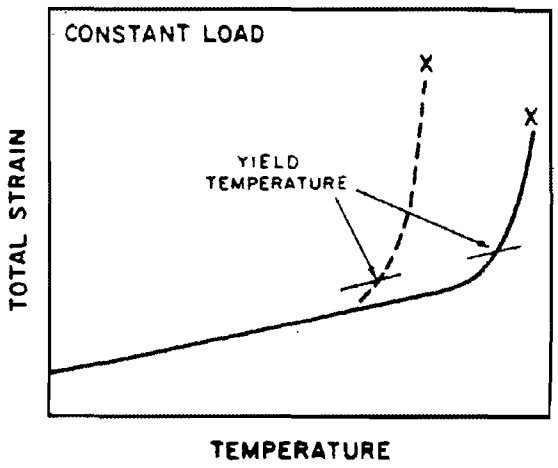

d. Strain-Temperature Curves from Tests Illustrated in Figure 9-19c.

Figure 9-19. [redacted] Types of Rapid Heating Tensile Tests [redacted]

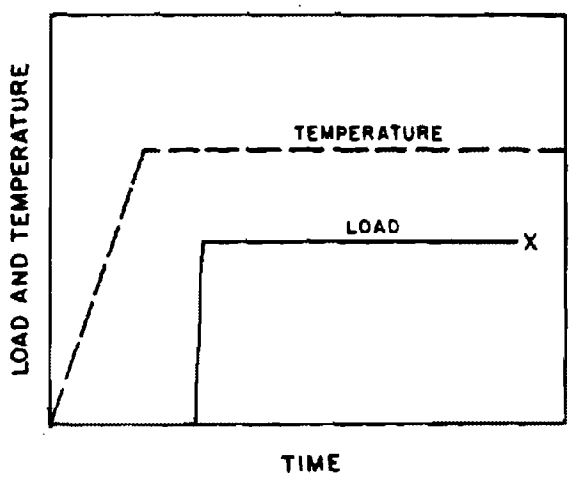

a. Very Short-Time Creep Tests After Rapid Heating

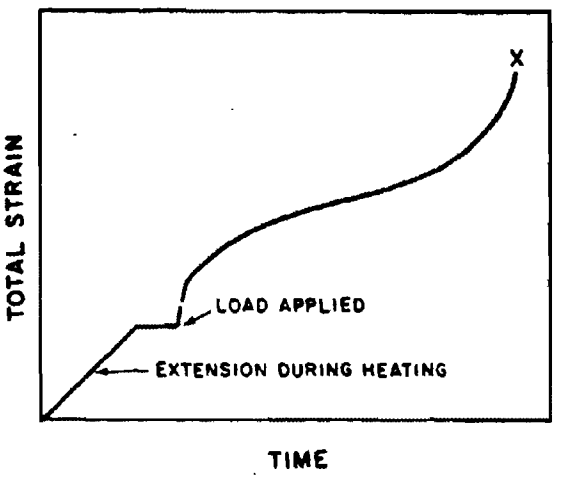

b. Time-Strain Curve

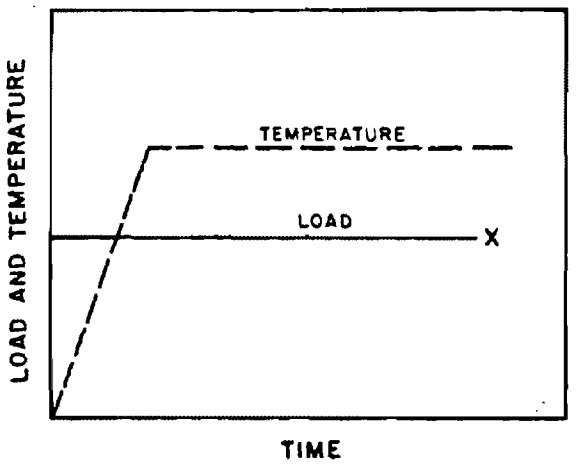

c. Very Short-Time Rapid-Heating Creep Tests

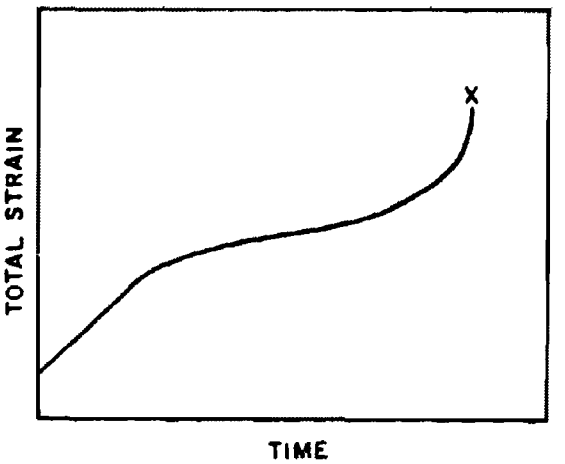

d. Time-Strain Curve

Figure 9-20. [redacted] Types of Short Time Creep Tests [redacted]

[redacted]

[redacted]

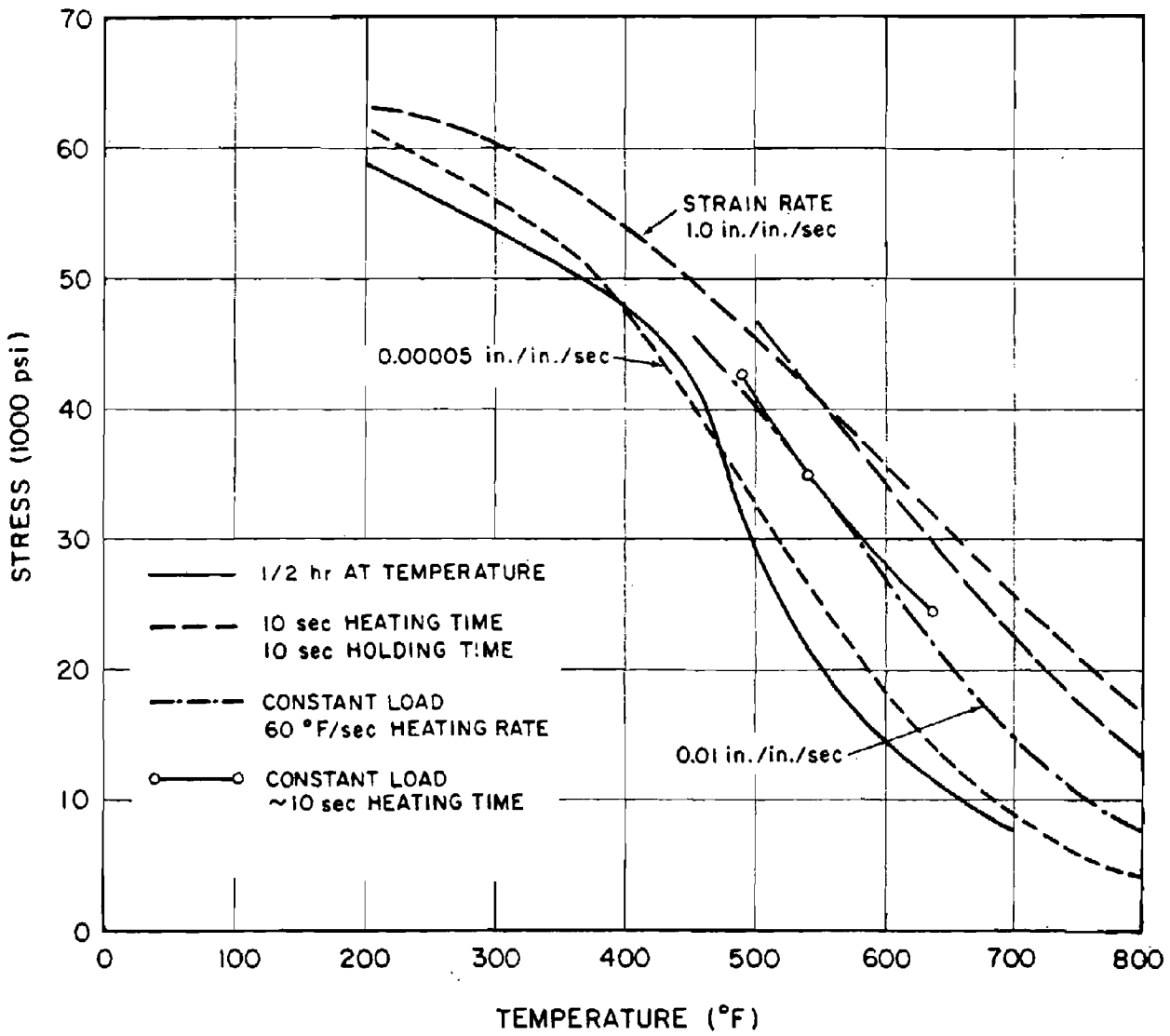

Figure 9-21. [redacted] 2024-T3 Aluminum Alloy Ultimate Strength at Elevated Temperature [redacted]

[redacted]

[redacted]

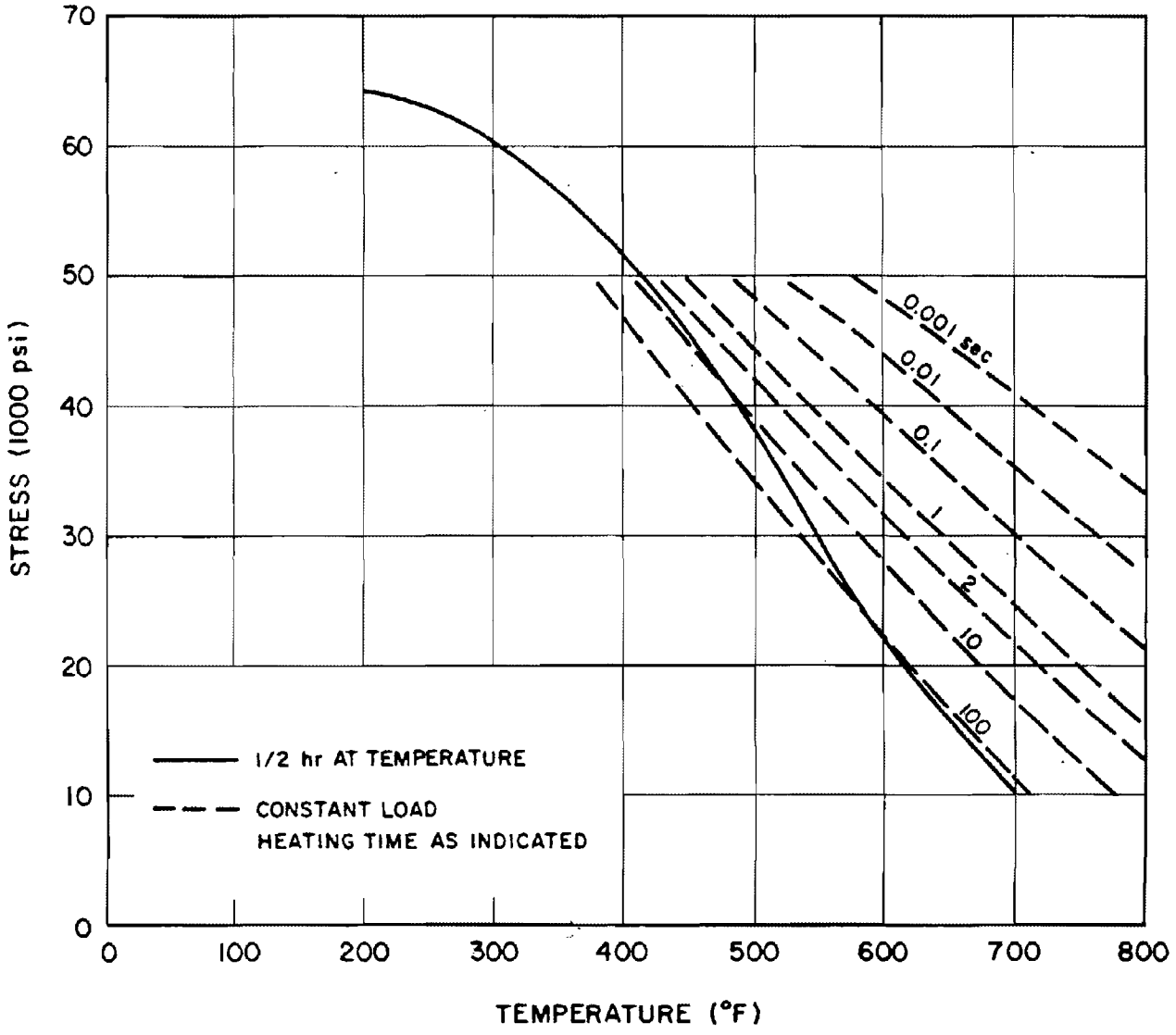

Figure 9-22. [redacted] 2024-T81 Aluminum Alloy Ultimate Strength at Elevated Temperature [redacted]

[redacted]

[redacted]

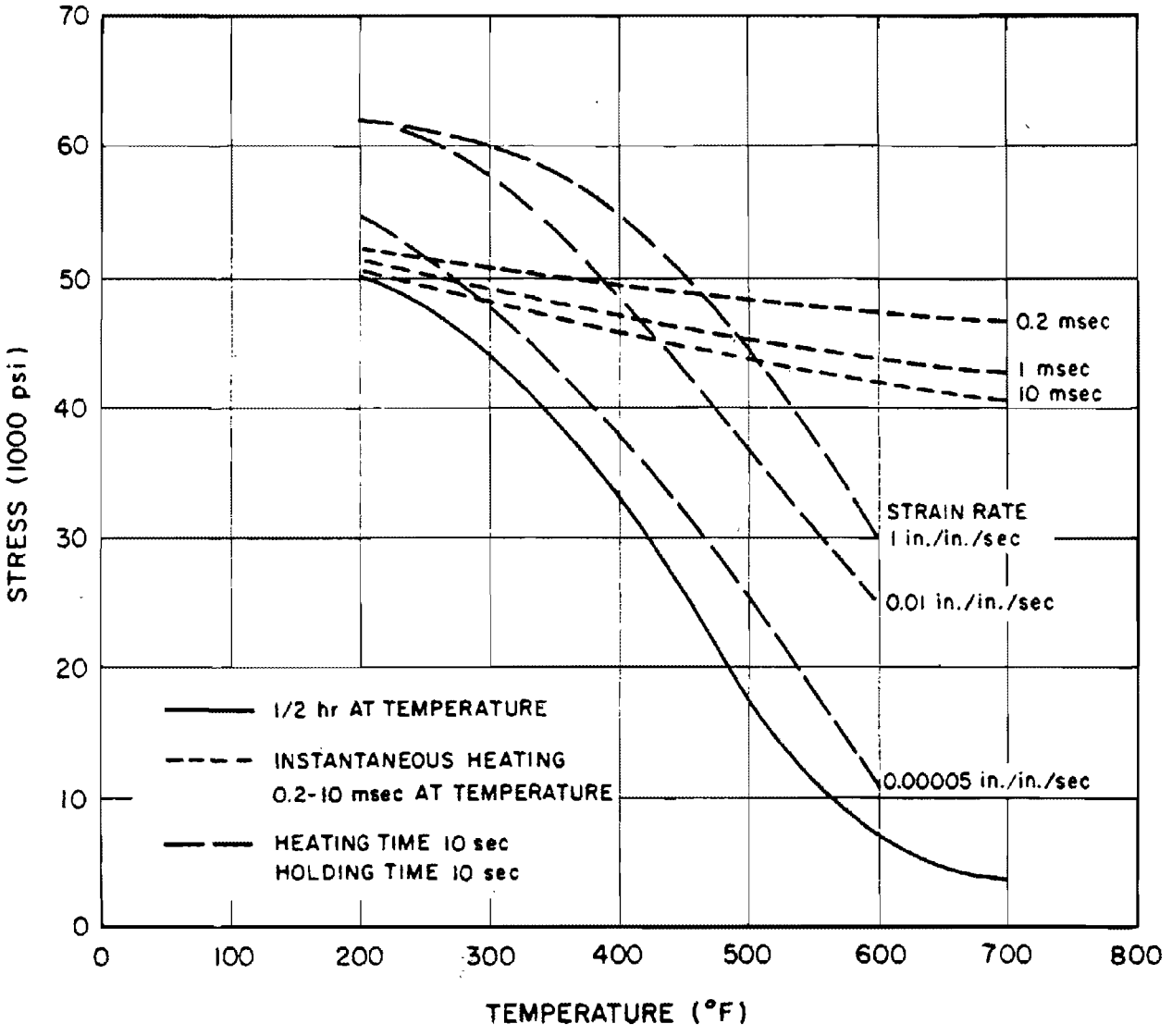

Figure 9-23. [redacted] 2014-T6 Aluminum Alloy Yield Strength at Elevated Temperature [redacted]

[redacted]

obtained in the manner illustrated in Figure 9-19a, but with the equilibrium temperature being reached in 10 sec and with a 10 sec soak time, and with three different strain rates used in the tensile tests. Other data were obtained in the manner illustrated in Figure 9-19c with a heating rate of 60°F/sec. The final data in Figure 9-21 also were obtained in a manner similar to that illustrated in Figure 9-19c with a heating time and time of rupture each approximately 10 sec.

The ultimate strength data in Figure 9-21 tend to show the importance of temperature and strain rate, but the data from the different sources are not consistent and are, therefore, difficult to evaluate. For example, the 0.00005 in./in./sec strain rate curve for 10 sec soak times from one source lies close to the 0.00033 in./in./sec strain rate curve for one-half hour soak times from a different source. Interpolation between the strain rate data for 10 sec soak times would indicate that a 0.00033 in./in./sec strain rate curve for a 10 sec soak time would lie slightly to the right of the 0.00005 in./in./sec curve and, therefore, slightly to the right of the one-half hour soak time curve. However, there are ample data, as shown in Figures 9-16 through 9-18, to justify the expectation that the 10 second curve should fall significantly to the right of the one-half hour curve; that is, for a given temperature and strain rate, the shorter the soak time, the smaller the decrease in tensile strength. It should also be noted that constant load curves should agree more closely.

The ultimate strength data in Figure 9-22 suggest a similar inconsistency although the data were taken from two different types of loading tests. The one-half hour data is from loading tests similar to that shown in Figure 9-19a, and "constant load, heating time as indicated" data is from loading tests similar to that shown in Figure 9-19c. The latter data clearly shows the influence of heating times or heating rates on rapid heating, constant load tensile test results.

The yield strength data shown in Figure 9-23 for 2014-T6 Aluminum Alloy is somewhat more consistent. The instantaneous heating data were obtained in a manner similar to that illustrated in Figure 9-19a, although times are very short. Specimens were heated instantaneously by an electron beam, then a stress wave was sent up the specimen. An analysis of the stress wave characteristics on either side of the heated region provided yield and ultimate strength data as well as elastic modulus data. The times indicated for these data are the delay times between time of heating and the arrival of the stress wave. Thus, the data are for instantaneous heating, very short soak times, and extremely high strain rates ($\sim 10^{-9}\,sec^{-1}$). The comparable strain rate data for 1/2 hour and 10 sec soak times are in the relative positions that would be expected. The one factor that may explain why the comparable strain rate data of Figures 9-21 and 9-23 are relatively close together despite the different soak times is the heating rate.

Similar data from a single source are shown in Figures 9-24 and 9-25 for 6AL-4V Titanium Alloy and full, hard 301 stainless steel. The data in these figures also illustrates the inconsistencies in data discussed for Figures 9-21 through 9-23.

One other mechanical strength property of interest is the elastic or Young's modulus of the material. One source indicates that for soak times of from 1/2 to 10,000 hours, the elastic modulus depends only on temperature and not on soak time for a number of different materials. A separate source indicates that this is true for 6061-T6 and 2014-T6 Aluminum Alloys with soak times of 0.2, 1, and 10 msec. Although this conclusion has not been validated for other materials at small soak times, it appears reasonable to assume that the elastic

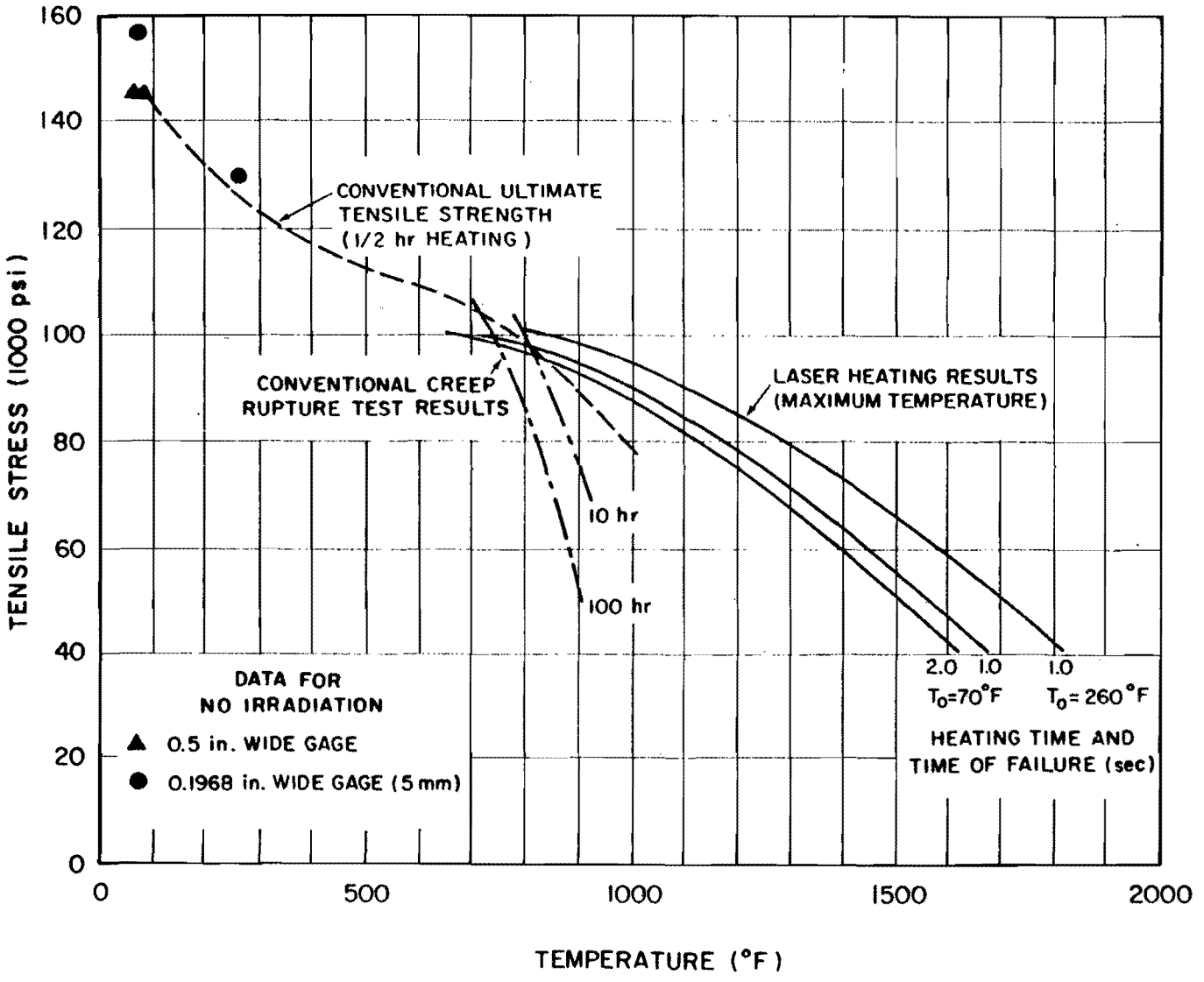

Figure 9-24. [redacted] Ultimate Strength Test Results for 6Al-4V Titanium Alloy at Elevated Temperatures [redacted]

[redacted]

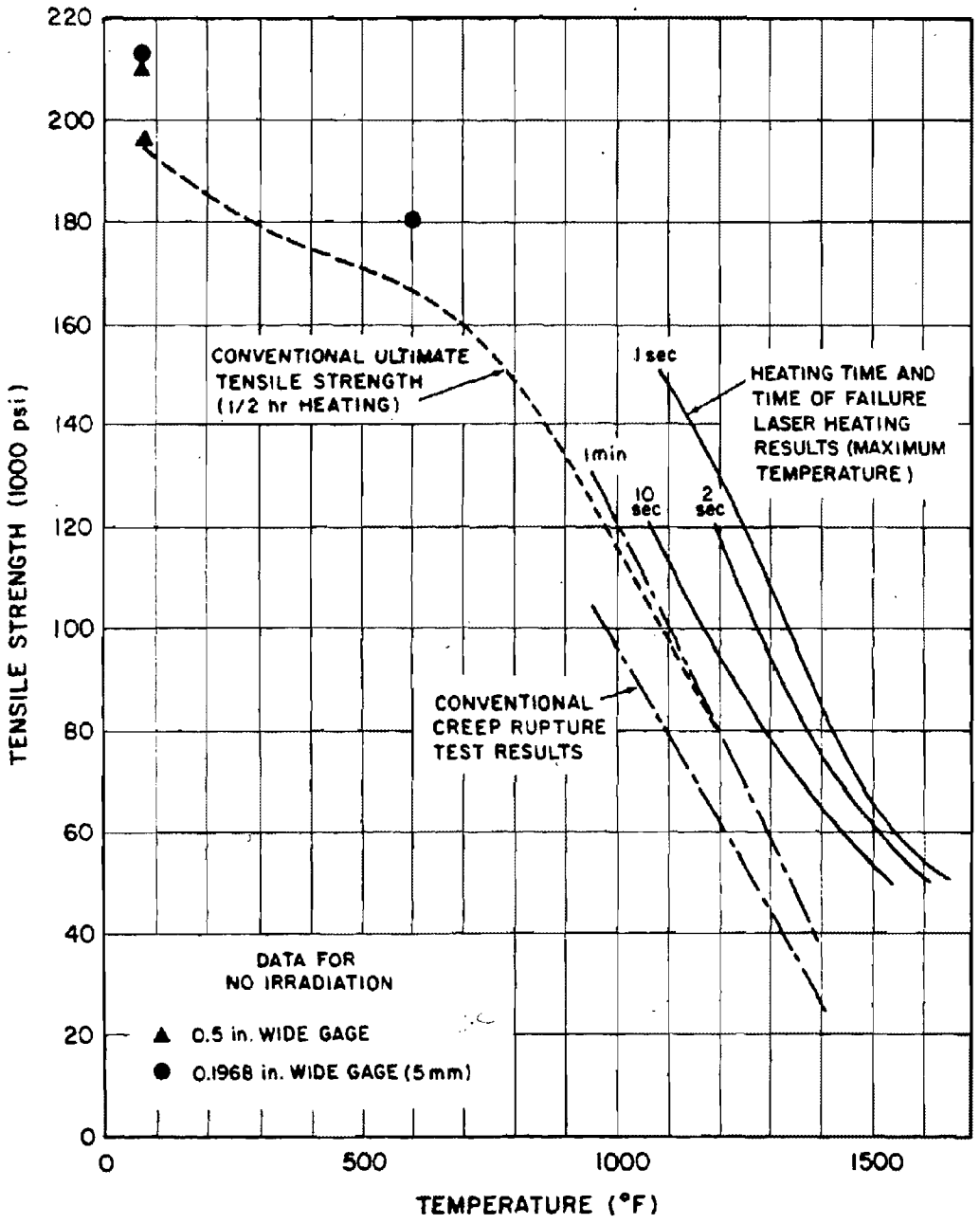

Figure 9-25. [redacted] Ultimate Strength Test Results for Full Hard Stainless Steel at Elevated Temperature [redacted]

[redacted]

modulus only depends on temperature for metallic materials.

In evaluating the information available on changes in mechanical strength properties of materials, it should be reemphasized that a variety of testing techniques have been used to obtain the data presented in this section. Constant strain rate and constant load techniques have both been used. A variety of heating techniques have been used, including ovens, resistance heating, inductive heating, hot-fluid bath heating, radiant heating, lasers, and electron beams. A considerable amount of data have been obtained on a number of different materials.

The data indicate that there are five basic variables that influence the degradation of mechanical strength properties at elevated temperature for particular materials: initial temperature, heating rate, final temperature, soak time, and strain rate. Not much is known about the effect of initial temperature since most data report "room temperature" as the reference temperature. Increases in heating rate, final temperature, or soak times cause a decrease in ultimate and yield strengths. An increase in strain rate at a particular final temperature apparently increases the strength. Because of the different testing techniques employed, the relative importance of these variables in determining material strengths is difficult to determine; however, it appears that soak time and final temperature are most important, followed closely by strain rate, and finally heating rate as long as final temperature is reached in less than one minute.

Although there are considerable data available on rapid heating effects, it is difficult to extrapolate to other than test conditions with any confidence. In any event, in estimating strength, data available on rapid heating and short times appear to be more appropriate than those for slow heating, long soak times for the general class of problems of interest in this manual.

RESISTANCE TO LOAD

The ultimate concern of combined thermal/blast effects is the change, if any, in the vulnerability/survivability of tactical systems compared to vulnerability/survivability to thermal or blast effects separately.

Figure 9-26 illustrates typical experimental stress-strain curves for 2014-T6 Aluminum Alloy with two approximations to this curve: the more or less classical straight line; and the so-called Bell's stress-strain law for dynamic deformation:

$$\sigma = \beta \left(1 - \frac{T}{T_m}\right) \epsilon^{1/2}$$

where

σ = stress, psi,

ϵ = strain, in./in.,

T = temperature of interest, °K,

T_m = melting temperature, °K,

β = parabolic coefficient.

The area under each of these curves is equal to the strain energy absorbed by the material. For the straignt line approximation the area under the room temperature curve equals about 433 in. · lb/in.^{3} to a strain (ϵ) of 0.01 in./in. This compares well with the area of 432 in. · lb/in. under the typical curve to the same ϵ. The Bell stress-strain law gives an area of 441 in. · lb/in.^{3}.

The change in allowable uniform equivalent static load that will give the same maximum deflection as a uniform dynamic load has been determined for degraded 2014-T6 Aluminum alloy properties using elastic theory for large deflections of simply supported square plates.* The allowable load was defined as the maximum

* An air blast loading of long duration, or a flat top wave, was assumed.

[redacted]

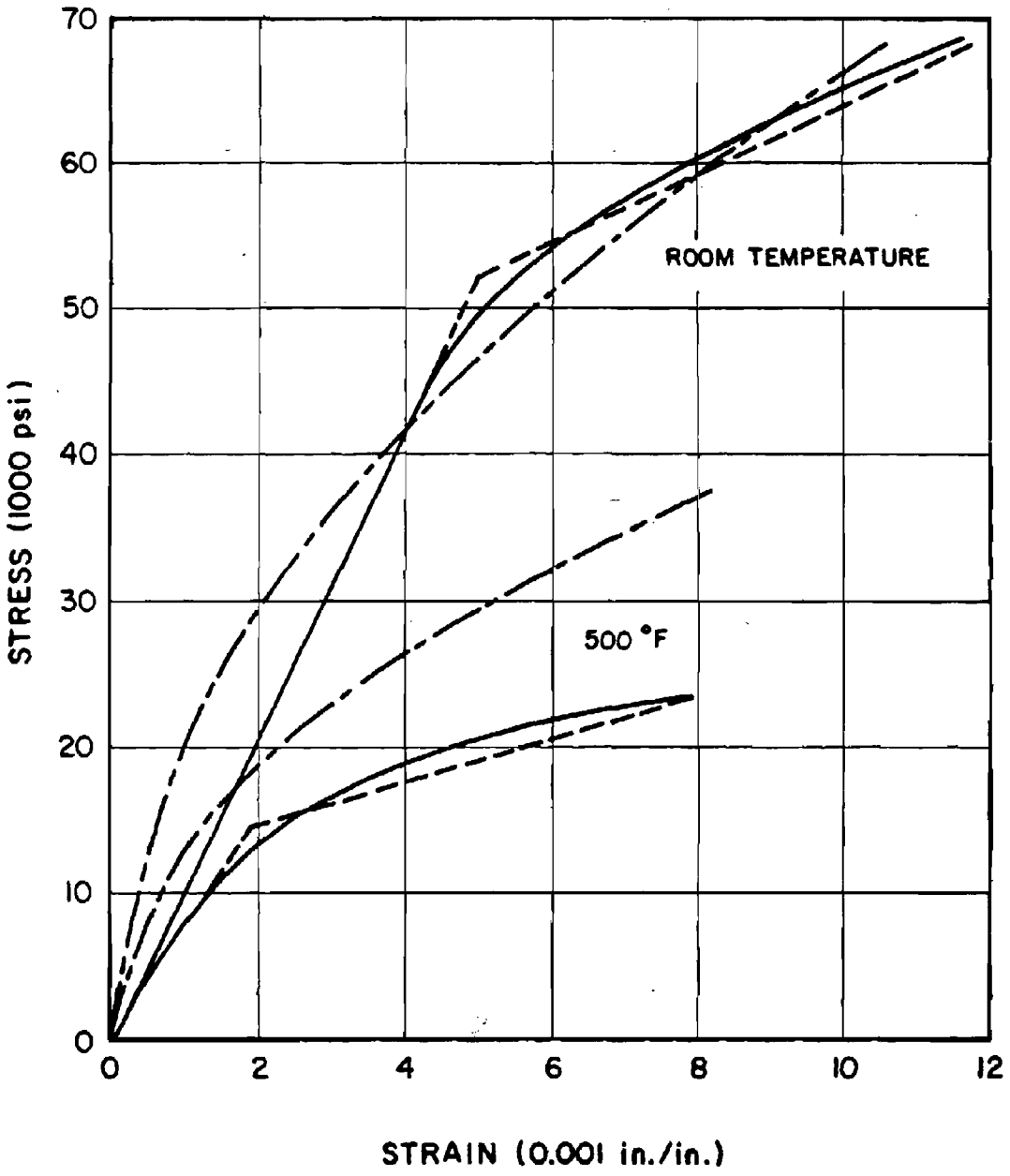

Figure 9-26. [redacted] Stress-Strain Approximation for 2014-T6 Aluminum Alloy [redacted]

[redacted]

[redacted]

[redacted]

static load the plate could carry without exceeding the yield stress. One-half hour soak time data were used to determine the strength properties, and a 20-in. square plate, 1/4-in. thick was assumed. The results are shown in Table 9-9. As can be seen, the maximum allowable load is almost a linear function of allowable stress. The explanation of this can be seen in the following equation, which is the elastic stress equation for the plate under study.

$$\sigma = 7{,}356.8p + 4.632E^{1/3}p^{2/3}.$$

The second term of the equation is for membrane stresses and is the only term that contains the temperature dependent Young's modulus. As the temperature increases, the value of E decreases, so the contribution from the second term is further decreased, and a fairly linear dependence on the pressure, p, remains.

[redacted] The allowable stress in the above example was taken from 1/2 hour soak time data. This provides a lower bound for the allowable load. Examination of Figure 9-21 through 9-25 indicates that the rapid heating, short soak time data generally fall above the 1/2 hour soak time curves. More reliable estimation of allowable loads will depend on the availability and appropriateness of the material data that is required for the type of analysis and calculation techniques being employed by an investigator. [redacted] The truly dynamic case may be analyzed similarly. In both cases, however, the basic factor that influences structural degradation is allowable stress as long as the elastic analysis approach is used.

[redacted] Where deformation or plastic response is responsible for failure, allowable stress no longer can be used to determine allowable load; either total deformation or total energy absorbed must be used.

[redacted] The energy approach consists of stating that the energy absorbed by a structure as it deforms is proportional to the product of the overpressure and the impulse values, ΔpI, of the blast wave that causes the deformation. Thus, for a constant value of absorbed energy used as a measure of damage, any combination of overpressure and impulse that yields the same product will cause the same amount of "damage."

[redacted] The effect of elevated temperature on the damage values has been investigated. One source indicates that for face-centered cubic materials, such as aluminum, the value of the parabolic coefficient of Bell's stress-strain law varies linearly with the temperature. For 2014-T6 Aluminum, the equation would be

$$\sigma = 9.65 \times 10^5 \epsilon^{1/2}$$

Table 9-9. [redacted] Allowable Uniform Static Load for Aluminum Plate at Three Temperatures [redacted]

Temperature (°F)	σy (10^3 psi)	Young's Modulus, E (10^6 psi)	Deflection (in.)	Allowable Load (psi)
70	57	10.5	0.323	7.25
350	43	9.77	0.261	5.45
500	17	8.4	0.117	2.10

[redacted]

where the value of β was obtained by fitting the curve to pass through the room temperature yield stress for the material. The Bell's law equation indicates that the energy under the stress-strain curve is a linear function of temperature by varying values of β linearly. This infers that the damage value, ΔpI, should depend on a linear function of temperature, i.e.,

$$(\Delta pI)_{T_2} = (\Delta pI)_{T_1} \left[\frac{1 - \frac{T_2}{T_m}}{1 - \frac{T_1}{T_m}} \right]$$

where

$(\Delta pI)_{T_1}$ = damage value at temperature T_1

and

$(\Delta pI)_{T_2}$ = damage value at temperature T_2.

If this relation were true, it would be a simple matter to evaluate the vulnerability of a structure. Once the value of ΔpI had been determined for ambient temperatures, the ΔpI value at elevated temperatures could be determined easily.

The Bell's law equation also indicates that yield strength, ultimate strength, and Young's modulus are linear functions of temperature for dynamic deformation. The data that were used to develop the equation were obtained from impact tests of oven heated samples. No information was provided as to what the heating rates or soak times were. The only other comparable data, at least in the dynamic sense, were shown in Figure 9-24, which indicate that data from dynamic tests do seem to approximate a straight line to some degree. Thus, with further testing and research, it may be that a relatively simple approach to assessing structural vulnerability to combined thermal/blast effects will be possible for dynamic deformation damage criteria.

The previous discussion has been concerned primarily with unstressed, unrestrained structural elements. There are three main structural conditions that are encountered in the analysis of structural response to combined thermal/blast effects. These are: unstressed members with no edge or end restraints; unstressed members with restraints; and prestressed members with restraints. These conditions refer to the status of a structure before either thermal or blast loading. The first condition is the easiest to analyze since there are no restraints to dimensional changes during or after heating so the thermal degradation of mechanical strength properties is the main concern. The second condition is more complex since dimension changes are prevented in varying degrees and appreciable thermal stresses may exist at the time of blast loading. The inclusion of these thermal stresses is not uncommon in structural elastic analysis. Thermal stresses caused by thermal gradients in the structural member also are included under this condition. The inclusion of stresses induced by the thermal gradient in an elastic structural analysis generally will require the use of a finite element structural analysis computer code. Unfortunately, it cannot be assumed that either form of thermal stress will be inconsequential, and they should both be addressed specifically in the solution of a particular problem. The final condition is the most difficult to analyze because a member may be stressed prior to thermal or blast loading.

The final factor to consider in determining structural response is the possibility of changes in failure modes, particularly materials rupture. Visual examination of a 1/4-in. by 0.040-in. 2024-T3 Aluminum specimen that fail-

ed indicated little necking down at the failure point. This may be due to the small area (about 17 mm diameter) exposed to thermal radiation. Failure occurred on a 45° plane, with no cupping. Postshot photos of cylindrical/aluminum shells, exposed to HE air blast after rapid heating, indicated an almost brittle-like fracture mode of failure. Failure of similar shells at normal temperature under the same type of loading was of a ductile deformation type. The possibility of a change in failure mode under dynamic loading at elevated temperatures has not been investigated, but is of concern since residual load carrying capabilities of deformed structures are sometimes used in determining vulnerability.

In summary, if elastic criteria are used to determine survivability/vulnerability, and if the necessary materials strength properties are known, a fairly straight forward but not necessarily simple stress analysis may be performed. If dynamic or deformation criteria are necessary, the problem becomes very difficult, if not impossible, because of the lack of validated analysis techniques. A third criterion, material melting, may be used to bound the problem. A temperature criterion may be chosen that is or nearly equal to the melting point of the material with the inference that, at that temperature, the material has no strength, and therefore, no resistance to load. This latter criterion has been used, for example, to establish kill criteria for Army aircraft.

SECTION V
X-RAY DAMAGE EFFECTS

INTRODUCTION

Nuclear weapons as X-ray sources and the environments they produce are described in Chapter 4. This section discusses the interaction of the X-ray environment with aerospace systems and some typical damage mechanisms that result from the interaction. The damage mechanisms depend on the fluence and energy, or temperature, of the X-rays and on the protective and structural materials involved in the interaction. For purposes of discussion the damage mechanisms can be divided conveniently into the effects caused by hot X-rays and those caused by cold X-rays. Some familiarity with the material discussed in Chapter 4 is assumed in the following discussion.

Cold X-rays (typically 1 to 3 keV black body temperatures) are absorbed in a thin surface layer. At sufficiently high fluence, a short pulse of X-rays can heat the surface rapidly and may cause it to vaporize and blow off. This results in: (1) an impulse imparted to the total structure; and (2) generation of a strong shock wave that propagates into the structure, and which may cause spallation of material at free boundaries and internal fracture of materials and bonds. These latter effects are produced by shock wave propagation through the thickness of a surface structure such as the thermal protection shell of a reentry vehicle. The former effects may produce damage by whole vehicle modes of response to the net impulse.

The hot X-rays are more penetrating. They can cause: (1) thermally generated shock waves in the vehicle structural materials and internal components; (2) melting and vaporization of the substructure; (3) internal deposition of energy in electronic components producing transient or permanent damage (see Chapter 6 and Section 7 of this chapter); or (4) produce internal EMP signals (see Chapter 7).

While some nuclear weapons emit only cold X-rays, all hot X-ray weapons have a cold component. Hence, for exoatmospheric events the hot X-ray effects are accompanied by cold X-ray effects. On the other hand, for endoatmospheric explosions, the cold X-rays have short mean free paths, and the X-ray effects beyond distances of a few tens of meters are produced by hot X-rays alone.

[redacted]

[redacted] Damage to a particular system depends on the structural details of the system as well as the X-ray spectrum. Accurate damage prediction even for the simplest geometries, generally require elaborate computer programs to calculate the energy deposition and the response of the system. All vulnerability analyses follow similar computational steps:

1. The X-ray energy deposition is computed using known processes for the materials and structure. This energy is assumed most often to be deposited instantaneously.

2. From the calculated energy deposition and the equation of state for the materials in the structure (if known) for the liquid, solid, and vapor phases of the material, a stress wave, which propagates through the surface structure, is calculated.

3. Damage to the surface structure that results from the stress wave (spallation, internal fracturing, delamination and debonding), is determined. These calculations generally are based on experimentally derived damage response curves. A good deal of progress has been made in the last few years in understanding and predicting fractures in most homogeneous and some composite materials. Even a small amount of fracturing may cause a significant loss in strength of material. One of the most complicating factors involved in making reliable damage predictions is that of in-depth heating prior to stress wave propagation through the material.

4. The response of the whole structure that results from the impulse imparted to it is determined. This response also is generally based on experimentally determined damage or properties degradation measurements. In these computations, the effects of the loss of strength of the structural material as a result of fracturing caused by the immediately preceding stress wave or by in-depth heating must be included. The structure may be broken by the impulse loading, or it may be weakened (buckled) so that it will fail under subsequent stresses, for example, reentry into the atmosphere.

[redacted] X-RAY ENERGY DEPOSITION CALCULATIONS [redacted]

[redacted] The starting point of all X-ray vulnerability analysis is a calculation of the X-ray energy deposition. The determination of the transmitted X-ray fluence, or shine through, into the interior of the aerospace system, is implicit in these calculations. Calculation of X-ray energy deposition involves the use of energy dependent photon absorption cross sections and energy and angle dependent scattering cross sections. Corrections for fluorescence, i.e., reradiation of X-rays, may be significant for high energy photons in certain materials. Sophisticated energy deposition and transport calculations, using detailed energy dependent cross sections and their angular dependence can be made by computers using Monte Carlo techniques. The results serve as an accuracy check and provide "effective" cross section data for simpler techniques. Approximation techniques greatly reduce the amount of effort and time involved in system analysis. Fairly accurate approximate values sometimes can be obtained even by hand calculations, as will be shown with examples.

9-33 X-ray Cross Sections [redacted]

[redacted] The probability of a photon of energy $h\nu$ traversing a distance of absorbing material x is $e^{-\mu x}$, where μ is the linear attenuation coefficient. This probability also can be written as $e^{-(\mu/\rho)\rho x}$, where μ/ρ is the mass attenuation coefficient for the material (see paragraph 4-3). In this representation, μ/ρ is in cm^2/gm and ρx is the thickness in gm/cm^2, i.e., the mass of material in the column of 1 square centimeter cross section and x centimeters long.

[redacted] If the monoenergic X-ray fluence incident normal (perpendicular) to the material sur-

[redacted]

face is φ_o, the direct fluence after traversing a thickness ρx of absorbing material is

$$\varphi_{dir} = \varphi_o e^{-(\mu/\rho)\rho x} \text{ cal/cm}^2.$$

The total mass attenuation coefficient μ/ρ is the sum of several components that represent the various mechanisms that can remove a primary photon from the direct flux, while it traverses a material. These mechanisms are described in paragraph 4-3, Chapter 4, and are: the photoelectric process, Compton inelastic scattering, Compton elastic scattering (incoherent elastic scattering) and Rayleigh elastic scattering (coherent elastic scattering). The first two processes result in photon energy being absorbed and the production of secondary electrons, the photoelectrons and Compton recoil electrons, respectively. The kinetic energy of these electrons is dissipated in the material and heats it. Energy deposition usually is calculated to have occurred at the depth at which the electrons are produced. However, in the case of very thin samples, the range of the freed electrons can exceed the material thickness, and energy deposition cannot be considered to be local. The energy removed from the primary photon beam in the Compton elastic process or the Rayleigh elastic process is not locally absorbed. A clear distinction must be made between attenuation of the primary flux and absorption of energy from the primary flux. For this reason the total linear attenuation coefficient usually is written as $\mu = \mu_a + \mu_s$. Here, μ_a is an absorption coefficient. It represents the first two processes mentioned above, which result in energy absorption. The second term, μ_s, is an elastic scattering coefficient, which contributes to the attenuation of the primary flux but not to local energy absorption. It is sometimes convenient to ignore the Rayleigh coherent scattering coefficient in the total attenuation coefficient. The coherent radiation has the same energy, and nearly the same direction, as the primary photon and cannot be distinguished from it in the "bad" geometry situations that usually occur in nuclear effects applications.*

Mass attenuation coefficients for the elements beryllium, aluminum, iron, copper, tungsten, and uranium are given in Tables 9-10 through 9-15, and Figures 9-27 through 9-32, respectively. These are representative of metallic materials used in aerospace systems. Mass attenuation coefficients for ablator materials, carbon phenolic and tape-wound silicon phenolic are shown in Figures 9-33 and 9-34, respectively. In these tables and figures, Z is the atomic number, μ_{ce}/ρ is the coherent elastic scattering coefficient, μ_{ie}/ρ is the incoherent Compton elastic coefficient, μ_{is}/ρ is the inelastic Compton coefficient, and μ_p/ρ is the photoelectric coefficient. As designated previously, μ_a/ρ and μ/ρ are the energy absorption coefficient and the total attenuation coefficient.†

9-34 X-ray Energy Deposition and Shine Through Fluences

X-ray energy deposition in a thickness δ at a depth x due to direct fluence photons is given by

$$A'_{dir} = \varphi_o \left[1 - e^{-\left(\frac{\mu_a}{\rho}\right)\rho\delta}\right] e^{-\left(\frac{\mu}{\rho}\right)\rho x}.$$

If $\mu_a\delta \ll 1$, and if φ_o is in cal/cm^2, this expression can be written as

$$A'_{dir} = \varphi_o \left(\frac{\mu_a}{\rho}\right) \rho\delta \, e^{-\left(\frac{\mu}{\rho}\right)\rho x} \text{ cal/cm}^2.$$

* A "good" geometry is one in which the distinction between primary and scattered photons can be made accurately.

† The symbols K, L_1, L_2, etc., in the tables and figures indicate the binding energies of the various electron shells (see paragraph 4-3, Chapter 4).

[redacted]

[redacted]

Frequently, the absorption is written in terms of cal/gm by dividing out the thickness $\rho\delta$,

$$A_{dir} = \varphi_o \left(\frac{\mu_a}{\rho}\right) e^{-\left(\frac{\mu}{\rho}\right) \rho x} \text{ cal/gm.}$$

This expression for the absorption is in terms of a dose; however, this assumes that very little of the flux is absorbed in the deposition region at depth x, i.e., the deposition region considered is very thin. Clearly, more energy than is in the incident flux cannot be absorbed.

[redacted] The equation for direct fluence (φ_{dir}) given in paragraph 9-32 can be used to represent a small energy band of photons in X-ray energy spectra such as those tabulated in Table 4-3, Chapter 4, for various black body spectra. The total energy in the direct X-ray fluence after traversing thickness x is obtained by summing over the energy bands.

$$\varphi = \sum_i \varphi_{oi} e^{-\left(\frac{\mu}{\rho}\right)_i \rho x} \text{ cal/cm}^2.$$

In a like manner, the total direct fluence X-ray energy absorption at depth ρx is obtained by summing for each energy band.

$$A = \sum_i \left(\frac{\mu_a}{\rho}\right)_i \varphi_{oi} e^{-\left(\frac{\mu}{\rho}\right)_i \rho x} \text{ cal/cm}^2.$$

[redacted] Problems 9-3 and 9-4 illustrate how these equations can be used to calculate approximate values for energy deposition and shine through.

[redacted]

[redacted]

Problem 9-3. Calculation of X-ray Energy Deposition at the Surface

[redacted] The information contained in Tables 9-10 through 9-15 and Figures 9-27 through 9-34 together with the equation for energy absorption given in paragraph 9-34 provide the means to obtain the approximate X-ray energy absorbed for various spectra and several materials. If the energy deposition at the surface on which the X-rays are incident is desired, the thickness, x, reduces to zero, and the energy deposition equation becomes

$$A = \sum (\mu_a/\rho)_i \, \varphi_{oi} \text{ cal/gm.}$$

[redacted]

[redacted]

Page 9-72 deleted.

[redacted]

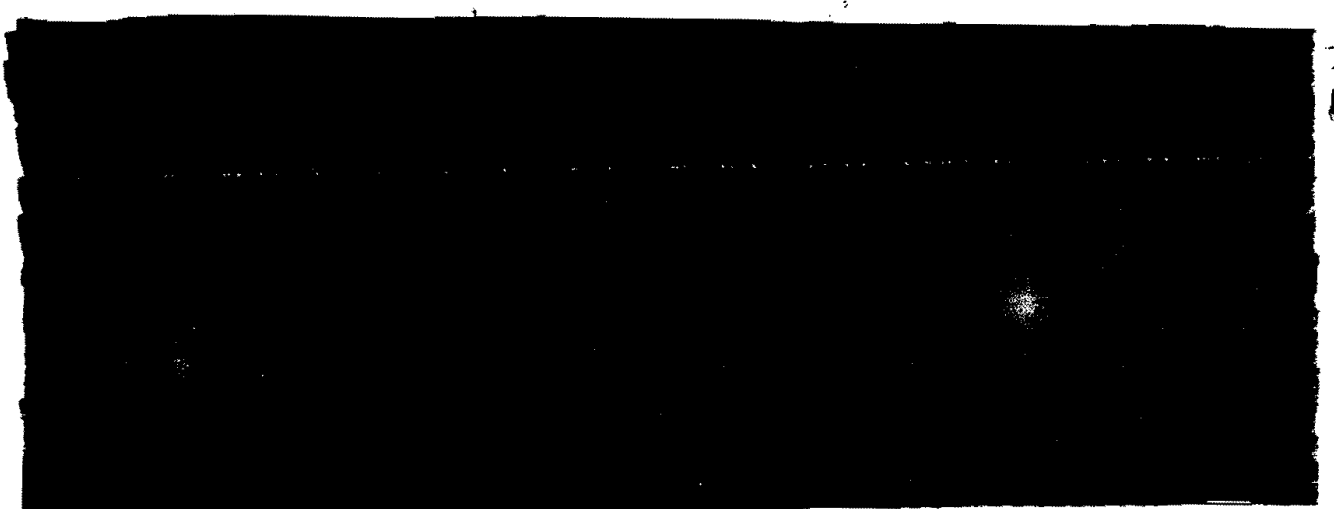

Related Material: See paragraphs 9-33 and 9-34. See also Tables 9-10 through 9-15 and Figures 9-27 through 9-34. See also paragraphs 4-1 through 4-3 and Tables 4-3 and 4-4, Chapter 4.

[redacted]

[redacted]

Problem 9-4. Calculation of X-ray Energy Deposition at a Depth in a Material and the Shine Through Fluence

DNA (L)(2)

[redacted] The information contained in Tables 9-10 through 9-15 and Figures 9-27 through 9-34 together with the equation for energy absorption given in paragraph 9-34 provide the means to obtain the approximate X-ray energy absorbed for various spectra and several materials at a depth x in the materials, as well as the fluence at that depth or the fluence emerging from the back face of the material (shine through).

[redacted]

[redacted] Problem 4-1, Chapter 4, describes the method to obtain energy distributions for various source temperatures from the normalized Planck distributions given in Table 4-1, Chapter 4.

Page 9-75 deleted.

[redacted]

DNA (b)(3)

[redacted]

Reliability: The reliability of the procedures described above depends on the X-ray spectrum and the absorbing material. The accuracy depends primarily on the relative importance of the scattering cross sections, and, for some materials, fluorescence. No definite reliability estimate can be made.

Related Material: See paragraphs 9-33 and 9-34. See also Tables 9-10 through 9-15 and Figures 9-27 through 9-34. See also paragraphs 4-1 through 4-3 and Tables 4-3 and 4-4, Chapter 4.

[redacted]

[redacted]

Table 9-10. [redacted] X-ray Cross Sections, Beryllium Z = 4 (cm^2/gm) [redacted]

Photon Energy keV	μ_{ce}/ρ	μ_{ie}/ρ	μ_{is}/ρ	μ_p/ρ	μ_a/ρ	μ/ρ
0.1	7.097-1*	1.154-3	2.770-7	1.507+4	1.507+4†	1.507+4
0.111K	7.094-1	1.331-3	3.560-7	1.109+4	1.109+4	1.109+4
0.111	7.094-1	1.331-3	3.560-7	2.323+5	2.323+5	2.323+5
0.15	7.079-1	2.007-3	7.257-7	1.105+5	1.105+5	1.105+5
0.2	7.054-1	2.972-3	1.421-6	5.302+4	5.302+4	5.302+4
0.3	6.984-1	5.171-3	3.685-6	1.816+4	1.816+4	1.817+4
0.4	6.889-1	7.660-3	7.223-6	8.292+3	8.292+3	8.292+3
0.5	6.770-1	1.039-2	1.218-5	4.456+3	4.456+3	4.456+3
0.6	6.631-1	1.332-2	1.866-5	2.662+3	2.662+3	2.662+3
0.8	6.306-1	1.972-2	3.650-5	1.165+3	1.165+3	1.165+3
1.0	5.939-1	2.674-2	6.137-5	6.072+2	6.072+2	6.078+2
1.5	4.986-1	4.648-2	1.591-4	1.820+2	1.820+2	1.825+2
2.0	4.153-1	6.151-2	2.771-4	7.626+1	7.626+1	7.674+1
3.0	3.019-1	7.946-2	5.309-4	2.199+1	2.199+1	2.237+1
4.0	2.371-1	9.009-2	7.911-4	9.004	9.004	9.332
5.0	1.968-1	9.831-2	1.066-3	4.481	4.482	4.778
6.0	1.685-1	1.053-1	1.356-3	2.527	2.528	2.802
8.0	1.285-1	1.170-1	1.971-3	1.019	1.021	1.267
10.0	1.003-1	1.261-1	2.613-3	5.024-1	5.050-1	7.314-1
15.0	5.780-2	1.386-1	4.173-3	1.384-1	1.426-1	3.390-1
20.0	3.677-2	1.432-1	5.589-3	5.539-2	6.098-2	2.410-1
30.0	1.844-2	1.433-1	8.064-3	1.525-2	2.331-2	1.851-1
40.0	1.098-2	1.395-1	1.017-2	6.126-3	1.630-2	1.668-1
50.0	7.251-3	1.348-1	1.199-2	3.027-3	1.502-2	1.570-1
60.0	5.132-3	1.299-1	1.357-2	1.705-3	1.528-2	1.503-1
80.0	2.947-3	1.207-1	1.617-2	6.930-4	1.686-2	1.406-1
100.0	1.898-3	1.126-1	1.819-2	3.464-4	1.854-2	1.331-1
150.0	8.554-4	9.646-2	2.164-2	9.953-5	2.174-2	1.191-1
200.0	4.811-4	8.476-2	2.364-2	4.159-5	2.368-2	1.089-1
300.0	2.138-4	6.877-2	2.559-2	1.241-5	2.560-2	9.458-2
400.0	1.203-4	5.830-2	2.630-2	5.346-6	2.631-2	8.473-2
500.0	8.019-5	5.080-2	2.645-2	2.811-6	2.645-2	7.733-2
600.0	5.346-5	4.516-2	2.634-2	1.675-6	2.634-2	7.156-2
800.0	2.807-5	3.708-2	2.571-2	7.501-7	2.571-2	6.282-2
1000.0	1.737-5	3.157-2	2.487-2	4.074-7	2.487-2	5.646-2

[redacted] $7.097 - 1 = 7.097 \times 10^{-1}$.
† $1.507 + 4 = 1.507 \times 10^{4}$.

[redacted]

[redacted]

Table 9-11. [redacted] X-ray Cross Sections, Aluminum Z = 13 (cm^2/gm) [redacted]

Photon Energy keV	μ_{ce}/ρ	μ_{ie}/ρ	μ_{is}/ρ	μ_p/ρ	μ_a/ρ	μ/ρ
0.1	2.504	5.614-4*	1.348-7	4.462+5†	4.462+5	4.462+5
$0.118L_I$	2.503	7.044-4	1.998-7	2.849+5	2.849+5	2.849+5
0.118	2.503	7.044-4	1.998-7	4.273+5	4.273+5	4.273+5
0.15	2.501	9.872-4	3.568-7	2.192+5	2.192+5	2.192+5
0.2	2.496	1.473-3	7.102-7	9.926+4	9.926+4	9.926+4
0.3	2.482	2.591-3	1.874-6	3.250+4	3.250+4	3.250+4
0.4	2.463	3.867-3	3.706-6	1.472+4	1.472+4	1.472+4
0.5	2.439	5.276-3	6.286-6	7.962+3	7.962+3	7.964+3
0.6	2.411	6.799-3	9.696-6	4.819+3	4.819+3	4.822+3
0.8	2.345	1.015-2	1.917-5	2.183+3	2.183+3	2.185+3
1.0	2.269	1.384-2	3.251-5	1.181+3	1.181+3	1.183+3
1.5	2.063	2.431-2	8.474-5	3.866+2	3.866+2	3.887+2
5.560K	2.036	2.533-2	9.169-5	3.473+2	3.473+2	3.493+2
1.560	2.036	2.533-2	9.169-5	4.403+3	4.403+3	4.405+3
2.0	1.869	3.295-2	1.514-4	2.352+3	2.352+3	2.354+3
3.0	1.557	4.629-2	3.164-4	8.087+2	8.087+2	8.103+2
4.0	1.326	5.732-2	5.166-4	3.674+2	3.674+2	3.688+2
5.0	1.143	6.618-2	7.381-4	1.960+2	1.960+2	1.972+2
6.0	9.910-1	7.543-2	1.004-3	1.162+2	1.162+2	1.172+2
8.0	7.482-1	9.132-2	1.598-3	5.004+1	5.004+1	5.088+1
10.0	5.730-1	1.045-1	2.258-3	2.571+1	2.571+1	2.639+1
15.0	3.272-1	1.228-1	3.861-3	7.471	7.475	7.925
20.0	2.133-1	1.319-1	5.390-3	3.057	3.062	3.407
30.0	1.148-1	1.388-1	8.161-3	8.505-1	8.587-1	1.112
40.0	7.319-2	1.394-1	1.052-2	3.394-1	3.499-1	5.625-1
50.0	5.116-2	1.374-1	1.256-2	1.657-1	1.783-1	3.668-1
60.0	3.792-2	1.343-1	1.432-2	9.199-2	1.063-1	2.785-1
80.0	2.209-2	1.268-1	1.719-2	3.625-2	5.344-2	2.024-1
100.0	1.466-2	1.194-1	1.943-2	1.759-2	3.702-2	1.711-1
150.0	6.855-3	1.035-1	2.324-2	4.728-3	2.797-2	1.383-1
200.0	3.935-2	9.131-2	2.549-2	1.868-3	2.736-2	1.226-1
300.0	1.775-3	7.425-2	2.775-2	5.092-4	2.826-2	1.043-1
400.0	1.000-3	6.297-2	2.861-2	2.044-4	2.881-2	9.279-2
500.0	6.384-4	5.490-2	2.880-2	1.014-4	2.890-2	8.444-2
600.0	4.397-4	4.880-2	2.868-2	5.749-5	2.874-2	7.797-2
800.0	2.455-4	4.012-2	2.798-2	2.374-5	2.800-2	6.837-2
1000.0	1.540-4	3.417-2	2.706-2	1.208-5	2.707-2	6.139-2

* [redacted] $5.614 - 4 = 5.614 \times 10^{-4}$.
† [redacted] $4.462 + 5 = 4.462 \times 10^{5}$.

[redacted]

[redacted]

Table 9-12. [redacted] X-ray Cross Sections, Iron Z = 26 (cm^2/gm) [redacted]

Photon Energy keV	μ_{ce}/ρ	μ_{ie}/ρ	μ_{is}/ρ	μ_p/ρ	μ_a/ρ	μ/ρ
0.1	4.842	2.910-4*	6.986-6	1.036+6†	1.036+6	1.036+6
0.15	4.838	5.217-4	1.879-7	3.413+5	3.413+5	3.413+5
0.2	4.833	7.893-4	3.798-7	1.552+5	1.552+5	1.553+5
0.3	4.817	1.415-3	1.023-6	5.115+4	5.114+4	5.115+4
0.4	4.796	2.140-3	2.063-6	2.327+4	2.327+4	2.327+4
0.5	4.769	2.950-3	3.557-6	1.263+4	1.263+4	1.263+4
0.6	4.737	3.835-3	5.522-6	7.665+3	7.665+3	7.670+3
$0.708L_3$	4.696	4.867-3	8.224-6	4.870+3	4.870+3	4.874+3
0.708	4.696	4.867-3	8.224-6	1.741+4	1.741+4	1.742+4
$0.721L_2$	4.691	4.995-3	8.597-6	1.652+4	1.652+4	1.653+4
0.721	4.691	4.995-3	8.597-6	2.479+4	2.479+4	2.479+4
0.8	4.658	5.800-3	1.105-5	1.838+4	1.838+4	1.838+4
0.846	4.638	6.280-3	1.265-5	1.564+4	1.564+4	1.564+4
0.846	4.638	6.280-3	1.265-5	2.346+4	2.346+4	2.346+4
1.0	4.564	7.993-3	1.697-5	1.449+4	1.449+4	1.450+4
1.5	4.288	1.431-2	5.045-5	4.505+3	4.505+3	4.509+3
2.0	3.989	2.022-2	9.432-5	1.966+3	1.966+3	1.970+3
3.0	3.419	3.115-2	2.148-4	6.112+2	6.112+2	6.146+2
4.0	2.917	4.126-2	3.757-4	2.668+2	2.668+2	2.697+2
5.0	2.487	5.035-2	5.713-4	1.402+2	1.402+2	1.428+2
6.0	2.128	5.855-2	7.910-4	8.293+1	8.293+2	8.511+1
$6.404L_3K$	1.994	6.147-2	8.830-4	6.873+1	6.873+1	7.079+1
$7.112K$	1.796	6.649-2	1.055-3	5.081+1	5.081+1	5.267+1
7.112	1.796	6.649-2	1.055-3	4.197+2	4.197+2	4.215+2
8.0	1.594	7.257-2	1.288-3	3.095+2	3.095+2	3.112+2
10.0	1.241	8.321-2	1.852-3	1.714+2	1.714+2	1.727+2
15.0	7.684-1	1.013-1	3.263-3	5.622+1	5.622+1	5.709+1
20.0	5.320-1	1.118-1	4.688-3	2.483+1	2.483+1	2.548+1
30.0	2.931-1	1.211-1	7.311-3	7.632	7.639	8.054
40.0	1.828-1	1.242-1	9.651-3	3.258	3.268	3.575
50.0	1.242-1	1.240-1	1.168-2	1.675	1.687	1.935
60.0	8.974-2	1.223-1	1.341-2	9.709-1	9.843-1	1.196
80.0	5.290-2	1.172-1	1.623-2	4.104-1	4.266-1	5.967-1
100.0	3.479-2	1.114-1	1.843-2	2.108-1	2.292-1	3.754-1
150.0	1.593-2	9.800-2	2.220-2	6.353-2	8.573-2	1.997-1
200.0	9.058-3	8.699-2	2.441-2	2.751-2	5.192-2	1.480-1
300.0	4.053-3	7.124-2	2.665-2	8.699-3	3.535-2	1.106-1
400.0	2.281-3	6.057-2	2.752-2	3.945-3	3.146-2	9.432-2
500.0	1.457-3	5.284-2	2.778-2	2.175-3	2.996-2	8.425-2
600.0	1.008-3	4.698-2	2.770-2	1.354-3	2.905-2	7.704-2
800.0	5.618-4	3.863-2	2.707-2	6.590-4	2.773-2	6.692-2
1000.0	3.548-4	3.291-2	2.619-2	3.863-4	2.658-2	5.984-2

* [redacted] 2.910 - 4 = 2.910 x 10^{-4}.
† [redacted] 1.036 + 6 = 1.036 x 10^{6}.

[redacted]

[redacted]

Table 9-13. [redacted] X-ray Cross Sections, Copper $Z = 29$ (cm^2/gm) [redacted]

Photon Energy keV	μ_{ce}/ρ	μ_{ie}/ρ	μ_{is}/ρ	μ_p/ρ	μ_a/ρ	μ/ρ
0.1	5.295	1.655-4*	3.975-8	3.001+5†	3.001+5	3.001+5
$0.120M_1$	5.294	2.185-4	6.291-8	1.976+5	1.976+5	1.976+5
0.120	5.294	2.185-4	6.291-8	2.174+5	2.174+5	2.174+5
0.15	5.292	3.090-4	1.112-7	1.293+5	1.293+5	1.293+5
0.2	5.288	4.814-4	2.315-7	6.645+4	6.645+4	6.646+4
0.3	5.276	8.992-4	6.502-7	2.602+4	2.602+4	2.602+4
0.4	5.259	1.401-3	1.350-6	1.338+4	1.338+4	1.338+4
0.5	5.238	1.975-3	2.380-6	7.984+3	7.984+3	7.990+3
0.6	5.213	2.615-3	3.774-6	5.238+3	5.238+3	5.243+3
0.8	5.151	4.072-3	7.768-6	2.693+3	2.693+3	2.698+3
$0.931L_3$	5.102	5.145-3	1.138-5	1.896+3	1.896+3	1.901+3
0.931	5.102	5.145-3	1.138-5	8.043+3	8.043+3	8.048+3
$0.951L_2$	5.094	5.314-3	1.201-5	7.593+3	7.593+3	7.598+3
0.951	5.094	5.314-3	1.201-5	1.139+4	1.139+4	1.139+4
1.0	5.074	5.741-3	1.364-5	9.932+3	9.932+3	9.937+3
$1.097L_1$	5.020	6.617-3	1.722-5	7.725+3	7.725+3	7.730+3
1.097	5.020	6.617-3	1.722-5	1.159+4	1.159+4	1.159+4
1.5	4.840	1.071-2	3.782-5	4.935+3	4.935+3	4.940+3
2.0	4.569	1.578-2	7.372-5	2.254+3	2.254+3	2.258+3
3.0	4.006	2.566-2	1.775-4	7.465+2	7.465+2	7.505+2
4.0	3.470	3.499-2	3.191-4	3.409+2	3.409+2	3.444+2
5.0	2.987	4.352-2	4.938-4	1.856+2	1.856+2	1.886+2
6.0	2.571	5.130-2	6.952-4	1.129+2	1.129+2	1.155+2
8.0	1.934	6.489-2	1.155-3	5.156+1	5.156+1	5.356+1
$8.048L_3K$	1.921	6.517-2	1.166-3	5.073+1	5.073+1	5.272+1
8.979K	1.697	7.046-2	1.399-3	3.765+1	3.765+1	3.941+1
8.979	1.697	7.046-2	1.399-3	2.978+2	2.978+2	2.995+2
10.0	1.499	7.607-2	1.676-3	2.234+2	2.234+2	2.250+2
15.0	9.085-1	9.494-2	3.065-3	7.373+1	7.373+1	7.473+1
20.0	6.245-1	1.059-1	4.458-3	3.285+1	3.285+1	3.358+1
30.0	3.479-1	1.166-1	7.071-3	1.026+1	1.026+1	1.073+1
40.0	2.195-1	1.201-1	9.378-3	4.434	4.443	4.783
50.0	1.502-1	1.203-1	1.137-2	2.301	2.312	2.583
60.0	1.090-1	1.187-1	1.309-2	1.344	1.357	1.585
80.0	6.473-2	1.140-1	1.587-2	5.736-1	5.895-1	7.678-1
100.0	4.256-2	1.085-1	1.803-2	2.963-1	3.143-1	4.654-1
150.0	1.958-2	9.568-2	2.172-2	8.966-2	1.114-1	2.267-1
200.0	1.117-2	8.510-2	2.390-2	3.869-2	6.259-2	1.589-1
300.0	5.014-3	6.974-2	2.609-2	1.204-2	2.813-2	1.129-1
400.0	2.821-3	5.933-2	2.696-2	5.346-2	3.231-2	9.466-2
500.0	1.804-3	5.177-2	2.721-2	2.882-3	3.009-2	8.367-2
600.0	1.249-3	4.603-2	2.715-2	1.754-3	2.890-2	7.619-2
800.0	6.967-4	3.785-2	2.654-2	8.161-4	2.736-2	6.590-2
1000.0	4.407-4	3.224-2	2.568-2	4.584-4	2.614-2	5.882-2

*[redacted] $1.655 - 4 = 1.655 \times 10^{-4}$.
†[redacted] $3.001 + 5 = 3.001 \times 10^{5}$.

[redacted]

Table 9-14. [redacted] X-ray Cross Sections, Tungsten Z = 74 (cm^2/gm) [redacted]

Photon Energy keV	μ_{ce}/ρ	μ_{ie}/ρ	μ_{is}/ρ	μ_T/ρ	μ_a/ρ	μ/ρ
0.1	1.191+1*	1.678-4*	4.091-8	3.230+6	3.230+6	3.230+6
0.15	1.191+1	2.957-4	1.070-7	1.089+6	1.089+6	1.089+6
0.2	1.190+1	4.421-4	2.123-7	5.037+5	5.037+5	5.037+5
0.3	1.188+1	7.791-4	5.609-7	1.699+5	1.699+5	1.699+5
0.4	1.184+1	1.165-3	1.120-6	7.857+4	7.857+4	7.858+4
$0.492N_2$	1.181+1	1.553-3	1.841-6	4.520+4	4.520+4	4.522+4
0.492	1.181+1	1.553-3	1.841-6	4.972+4	4.972+4	4.974+4
0.5	1.180+1	1.590-3	1.915-6	4.752+4	4.752+4	4.753+4
$0.595N_1$	1.176+1	2.028-3	2.906-6	2.981+4	2.981+4	2.982+4
0.595	1.176+1	2.028-3	2.906-6	3.279+4	3.279+4	3.280+4
0.6	1.175+1	2.052-3	2.965-6	3.206+4	3.206+4	3.207+4
0.8	1.163+1	3.060-3	5.907-6	1.483+4	1.483+4	1.484+4
1.0	1.149+1	4.186-3	1.008-5	8.152+3	8.152+3	8.164+3
1.5	1.104+1	7.370-3	2.633-5	2.749+3	2.749+3	2.760+3
$1.809M_5$	1.070+1	9.219-3	3.957-5	1.664+3	1.664+3	1.674+3
1.809	1.070+1	9.219-3	3.957-5	4.159+3	4.159+3	4.170+3
$1.872M_4$	1.063+1	9.599-3	4.262-5	3.798+3	3.798+3	3.808+3
1.872	1.063+1	9.599-3	4.262-5	5.696+3	5.696+3	5.707+3
2.0	1.052+1	1.039-2	4.926-5	4.768+3	4.768+3	4.779+3
$2.281M_3$	1.016+1	1.198-2	6.459-5	3.352+3	3.352+3	3.362+3
2.281	1.016+1	1.198-2	6.459-5	4.022+3	4.022+3	4.033+3
$2.575M_2$	9.844	1.368-2	8.289-5	2.907+3	2.907+3	2.916+3
2.575	9.844	1.368-2	8.289-5	3.197+3	3.197+3	3.207+3
$2.820M_1$	9.613	1.510-2	9.999-5	2.507+3	2.507+3	2.516+3
2.820	9.613	1.510-2	9.999-5	2.757+3	2.757+3	2.767+3
3.0	9.457	1.616-2	1.136-4	2.335+3	2.335+3	2.344+3
4.0	8.471	2.164-2	2.013-4	1.080+3	1.080+3	1.088+3
5.0	7.580	2.681-2	3.092-4	5.937+2	5.937+2	6.013+2
6.0	6.791	3.164-2	4.342-4	3.642+2	3.642+2	3.710+2
8.0	5.500	4.012-2	7.259-4	1.684+2	1.684+2	1.740+2
10.0	4.521	4.786-2	1.078-3	9.260+1	1.260+1	9.717+1
$10.207L_3$	4.424	4.849-2	1.114-3	8.766+1	8.766+1	9.213+1
10.207	4.424	4.849-2	1.114-3	1.824+2	1.824+2	1.869+2
$11.544L_2$	3.884	5.238-2	1.351-3	1.300+2	1.300+2	1.339+2
11.544	3.884	5.238-2	1.351-3	1.950+2	1.950+2	1.989+2
$12.100L_1$	3.694	5.392-2	1.453-3	1.713+2	1.713+2	1.751+2
12.100	3.694	5.392-2	1.453-3	2.570+2	2.570+2	2.608+2
15.0	2.936	1.162-2	2.030-3	1.423+2	1.423+2	1.453+2
20.0	2.071	7.112-2	3.079-3	6.448+1	6.448+1	6.663+1
30.0	1.227	8.246-2	5.173-3	2.113+1	2.113+1	2.245+1
40.0	8.196-1	8.822-2	7.145-3	9.575	9.582	1.049+1
50.0	5.854-1	9.076-2	8.918-3	5.182	5.191	5.867

[redacted]

[redacted]

Table 9-14. (Concluded)

Photon Energy keV	μ_{ce}/ρ	μ_{pe}/ρ	μ_{ns}/ρ	μ_p/ρ	μ_a/ρ	μ/ρ
59.318L_3K	4.454-1	9.151-2	1.039-2	3.238	3.248	3.785
60.0	4.373-1	9.150-2	1.050-2	3.138	3.148	3.677
69.525K	3.377-1	9.100-2	1.180-2	2.092	2.104	2.533
69.525	3.377-1	9.100-2	1.180-2	1.020+1	1.021+1	1.064+1
80.0	2.597-1	9.037-2	1.313-2	7.367	7.380	7.730
100.0	1.741-1	8.768-2	1.522-2	4.265	4.280	4.542
150.0	8.216-2	8.022-2	1.884-2	1.471	1.490	1.652
200.0	4.733-2	7.237-2	2.086-2	6.666-1	6.875-1	8.071-1
300.0	2.141-2	6.024-2	2.287-2	2.144-1	2.373-1	3.189-1
400.0	1.209-2	5.160-2	2.365-2	9.661-2	1.203-1	1.839-1
500.0	7.750-3	4.522-2	2.387-2	5.287-2	7.674-2	1.297-1
600.0	5.366-3	4.031-2	2.383-2	3.281-2	5.664-2	1.023-1
800.0	3.014-3	3.323-2	2.334-2	1.606-2	3.940-2	7.565-2
1000.0	1.916-3	2.831-2	2.263-2	9.610-3	3.224-2	6.246-2

[redacted] 1.191 + 1 = 11.91.
[redacted] 1.684 - 4 = 1.684×10^{-4}.

[redacted]

[redacted]

Table 9-15. [redacted] X-ray Cross Sections, Uranium Z = 92 (cm^2/gm) [redacted]

Photon Energy keV	μ_{ce}/ρ	μ_{ie}/ρ	μ_{pp}/ρ	μ_{Γ}/ρ	μ_a/ρ	μ/ρ
0.1	1.423+1*	3.177-5*	7.748-9	1.180+6	1.180+6	1.180+6
0.15	1.422+1	6.810-5	2.473-8	4.701+5	4.701+5	4.701+5
0.2	1.421+1	1.169-4	5.624-8	2.446+5	2.446+5	2.446+5
0.3	1.417+1	2.507-4	1.804-7	9.744+4	9.744+4	9.745+4
0.4	1.413+1	4.307-4	4.138-7	5.071+4	5.071+4	5.072+4
0.5	1.407+1	6.551-4	7.884-7	3.055+4	3.055+4	3.057+4
0.6	1.400+1	9.230-4	1.334-6	2.020+4	2.020+4	2.021+4
0.8	1.383+1	1.585-3	3.054-6	1.051+4	1.051+4	1.052+4
1.0	1.362+1	2.410-3	5.803-6	6.333+3	6.333+3	6.347+3
1.2738$_{L_3}$	1.327+1	3.791-3	1.160-5	3.664+3	3.664+3	3.677+3
1.271	1.327+1	3.791-3	1.160-5	4.030+3	4.030+3	4.043+3	
1.4	1.306+1	4.785-3	1.650-5	3.044+3	3.040+3	3.053+3
1.42	1.306+1	4.785-3	1.650-5	3.344+3	3.344+3	3.358+3
1.5	1.297+1	5.106-3	1.856-5	3.052+3	3.052+3	3.065+3
2.0	1.239+1	8.109-3	3.849-5	1.568+3	1.568+3	1.60 +3
3.0	1.113+1	1.464-2	1.033-4	6.327+2	6.327+2	6.438+2
3.552$1_{L_1}$	1.043+1	1.819-2	1.513-4	4.313+2	4.313+2	4.417+2
3.552	1.043+1	1.819-2	1.513-4	9.717+2	9.717+2	9.822+2
3.728M_4	1.024+1	1.935-2	1.687-4	8.640+2	8.640+2	8.742+2
3.728	1.024+1	1.935-2	1.687-4	1.296+3	1.296+3	1.307+3
4.0	9.966	2.116-2	1.977-4	1.092+3	1.092+3	1.102+3
4.303$3_{L_2}$	9.619	2.277-2	2.281-4	9.140+2	9.140+2	9.236+2
4.303	9.619	2.277-2	2.281-4	1.097+3	1.097+3	1.106+3
5.0	8.944	2.642-2	3.059-4	7.616+2	7.616+2	7.705+2
5.1822M_3	8.763	2.721-2	3.262-4	6.981+2	6.981+2	7.069+2
5.182	8.763	2.721-2	3.262-4	7.679+2	7.679+2	7.767+2
5.548M_2	8.430	2.883-2	3.691-4	6.506+2	6.506+2	6.590+2
5.548	8.430	2.883-2	3.691-4	7.156+2	7.156+2	7.241+2
6.0	8.004	3.078-2	4.249-4	5.916+2	5.916+2	5.997+2
8.0	6.043	3.780-2	6.857-4	2.939+2	2.939+2	3.000+2
10.0	5.504	4.232-2	9.528-4	1.709+2	1.709+2	1.765+2
15.0	3.783	5.184-2	1.718-3	6.377+1	6.377+1	6.707+1
17.166L_3	3.246	5.562-2	2.090-3	4.594+1	4.594+1	4.924+1
17.166	3.246	5.562-2	2.090-3	9.787+1	9.787+1	1.012+2
20.0	2.725	6.021-2	2.611-3	6.586+1	6.586+1	6.865+1
20.948L_2	2.568	6.145-2	2.785-3	5.841+1	5.841+1	6.104+1
20.948	2.568	6.145-2	2.785-3	6.663+1	6.663+1	6.926+1
21.757L_1	2.443	6.247-2	2.935-3	6.030+1	6.030+1	6.281+1
21.757	2.443	6.247-2	2.935-3	9.045+1	9.045+1	9.296+1
30.0	1.601	7.173-2	4.528-3	3.883+1	3.883+1	4.050+1
40.0	1.043	7.894-2	6.444-3	1.821+1	1.821+1	1.933+1
50.0	7.277-1	8.241-2	8.168-3	1.012+1	1.012+1	1.094+1

[redacted]

[redacted]

Table 9-15. (Concluded)

Photon Energy keV	μ_{ce}/ρ	μ_{te}/ρ	μ_{ts}/ρ	μ_{π}/ρ	μ_a/ρ	μ/ρ
60.0	5.339-1	8.375-2	9.690-3	6.261	6.271	6.886
80.0	3.178-1	8.353-2	1.226-2	2.936	2.948	3.349
98.440L_3K	2.176-1	8.189-2	1.416-2	1.700	1.714	2.014
100.0	2.114-1	8.166-2	1.431-2	1.632	1.646	1.939
115.606K	1.646-1	7.956-2	1.560-2	1.114	1.130	1.374
115.606	1.646-1	7.956-2	1.560-2	5.035	5.046	5.295
150.0	9.832-2	7.573-2	1.799-2	2.166	2.184	2.358
200.0	5.627-2	6.872-2	1.999-2	9.940-1	1.013	1.139
300.0	2.533-2	5.625-2	2.150-2	3.873-1	4.088-1	4.904-1
400.0	1.429-2	4.935-2	2.273-2	2.034-1	2.261	2.898-1
500.0	9.149-3	4.340-2	2.299-2	1.196-1	1.426	1.952-1
600.0	6.343-3	3.869-2	2.292-2	7.428-2	9.720-2	1.422-1
800.0	3.557-3	3.128-2	2.200-2	3.107-2	5.307-2	8.792-2
1000.0	2.264-2	2.725-2	2.178-2	1.381-2	3.559-2	6.511-2

[redacted] 1.423 + 1 = 14.23,
† [redacted] 3.177 − 5 = 3.177×10^{-5}.

[redacted]

[redacted]

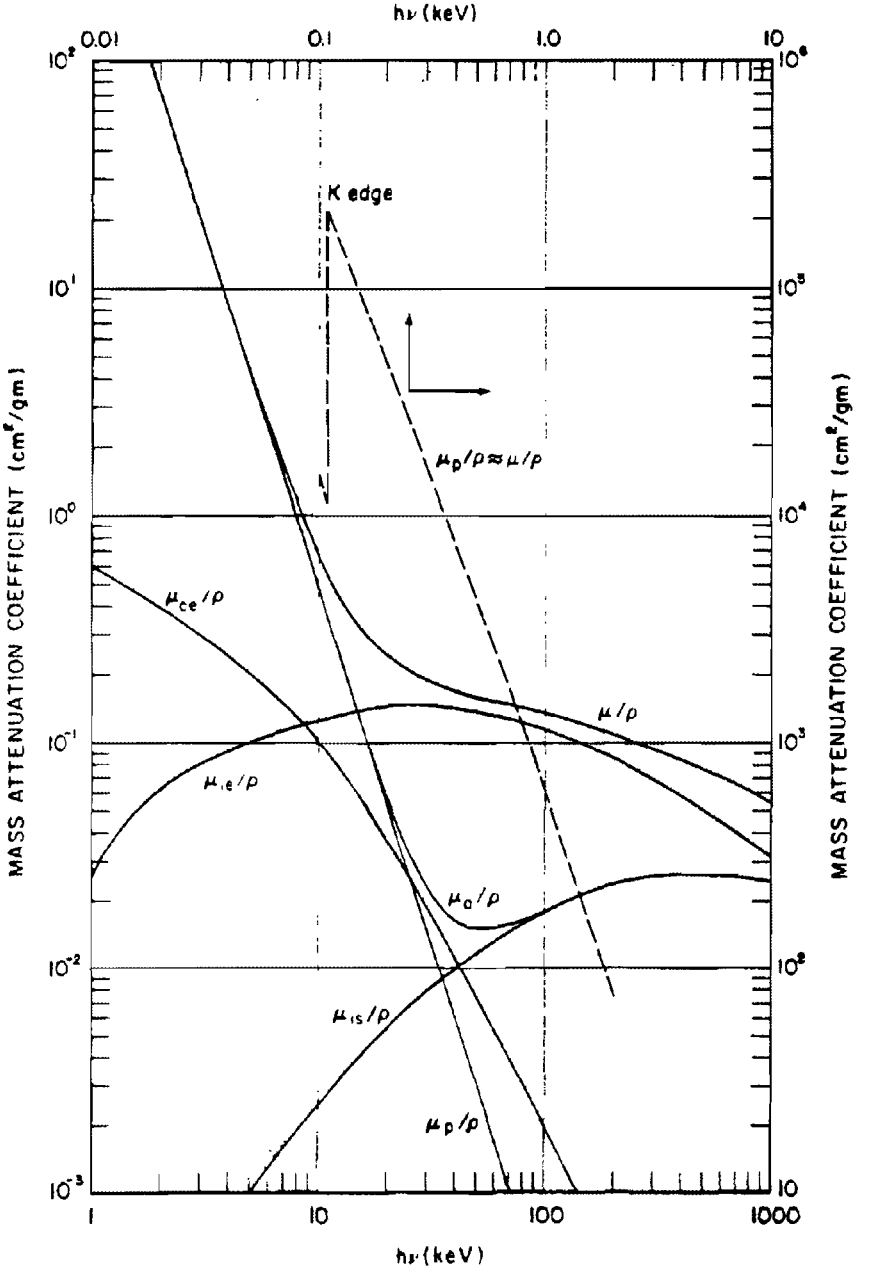

Figure 9-27. [redacted] Photon Cross Sections in Beryllium [redacted]

[redacted]

[redacted]

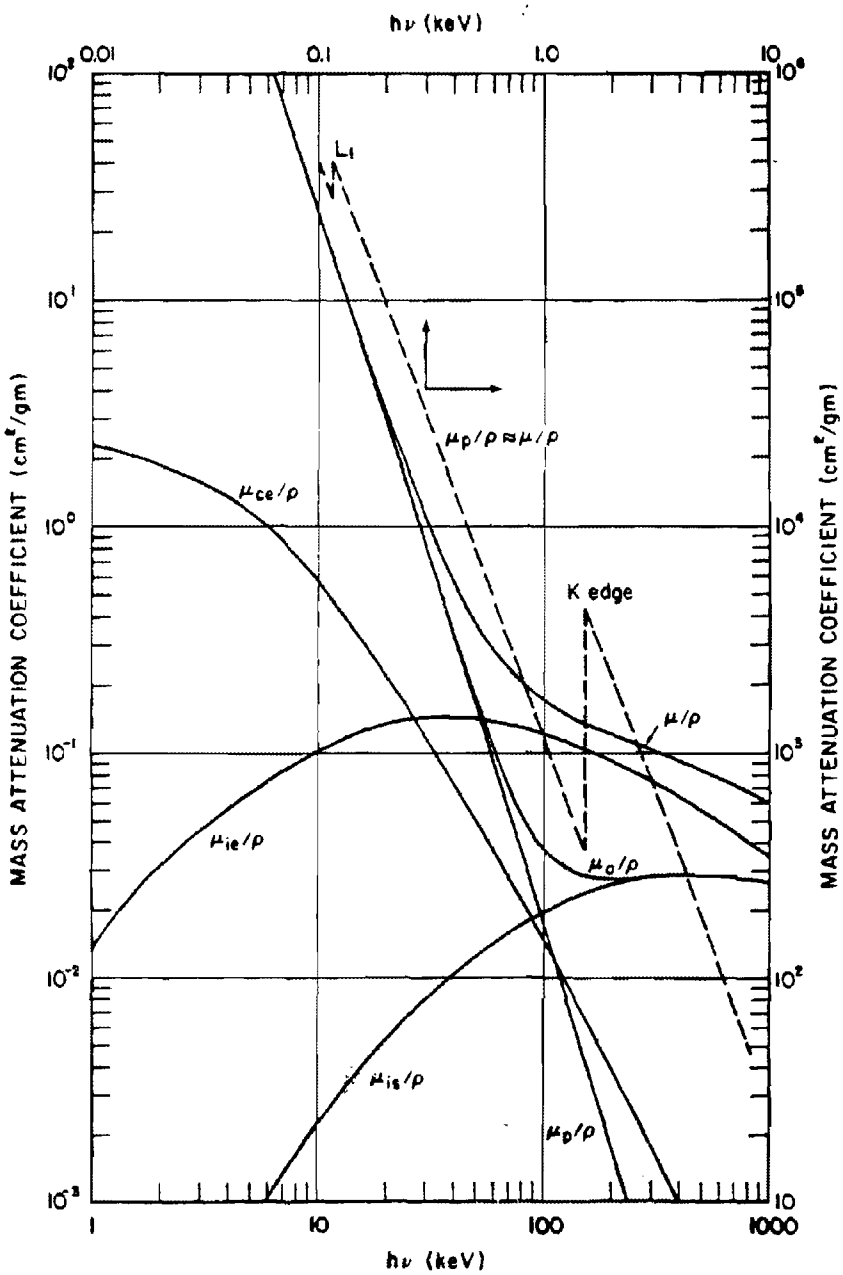

Figure 9-28. [redacted] Photon Cross Sections in Aluminum [redacted]

[redacted]

[redacted]

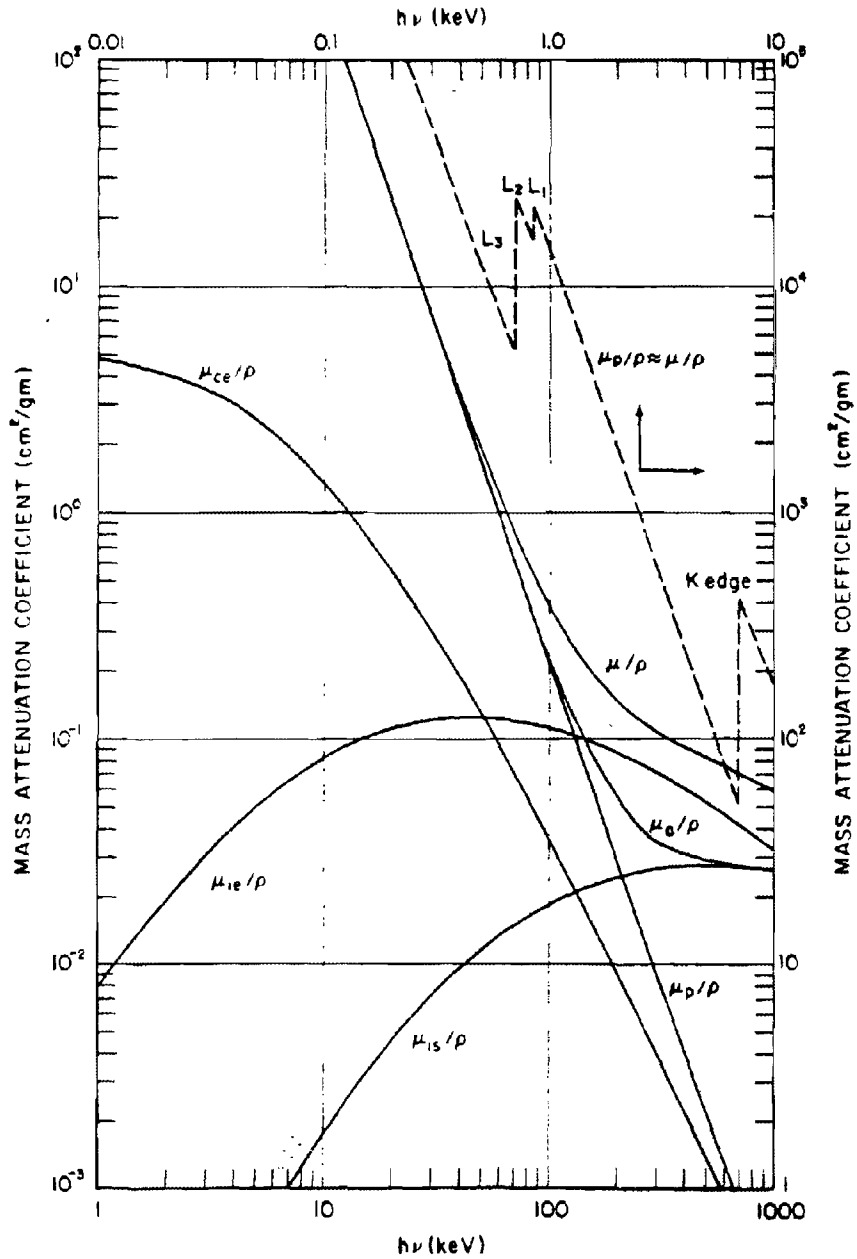

Figure 9-29. [redacted] Photon Cross Sections in Iron [redacted]

[redacted]

[redacted]

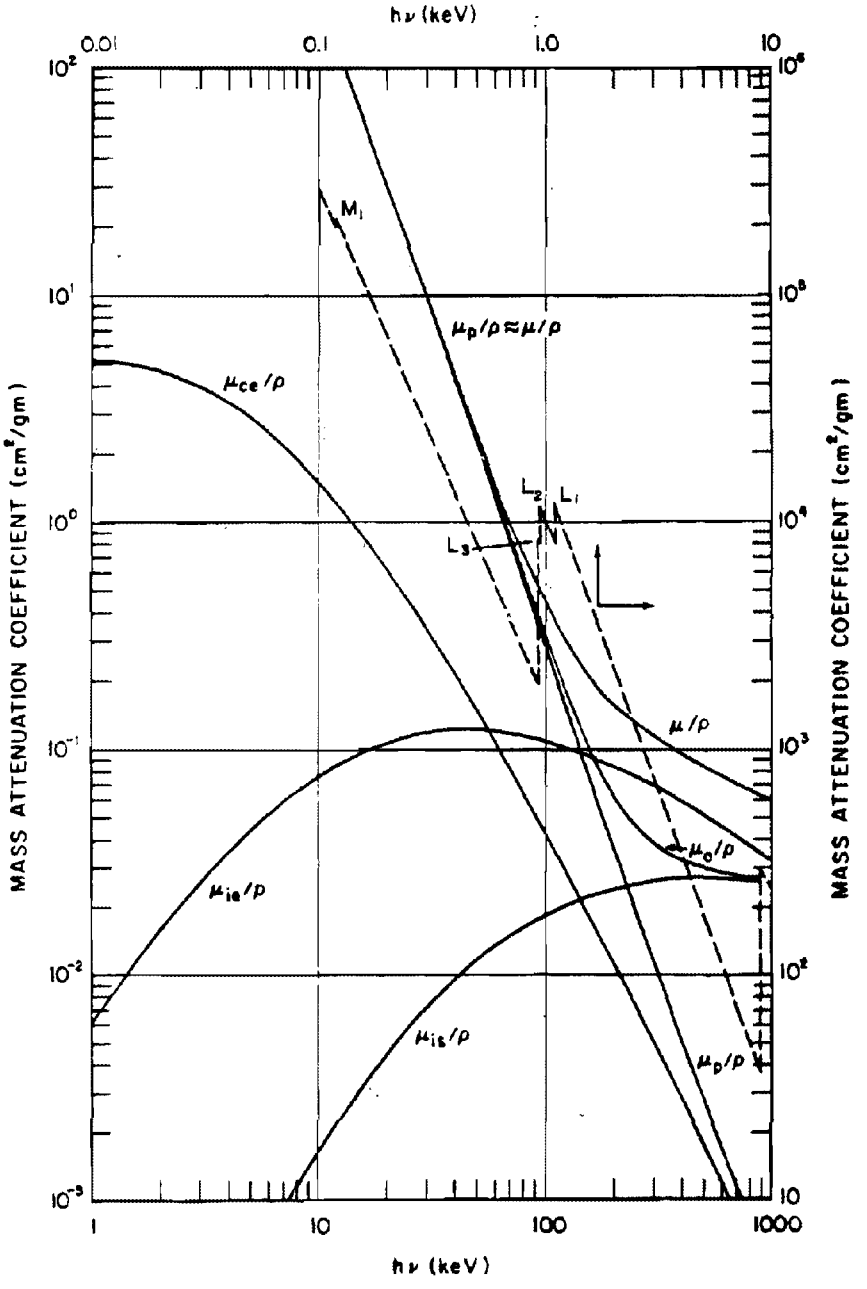

Figure 9-30. [redacted] Photon Cross Sections in Copper [redacted]

[redacted]

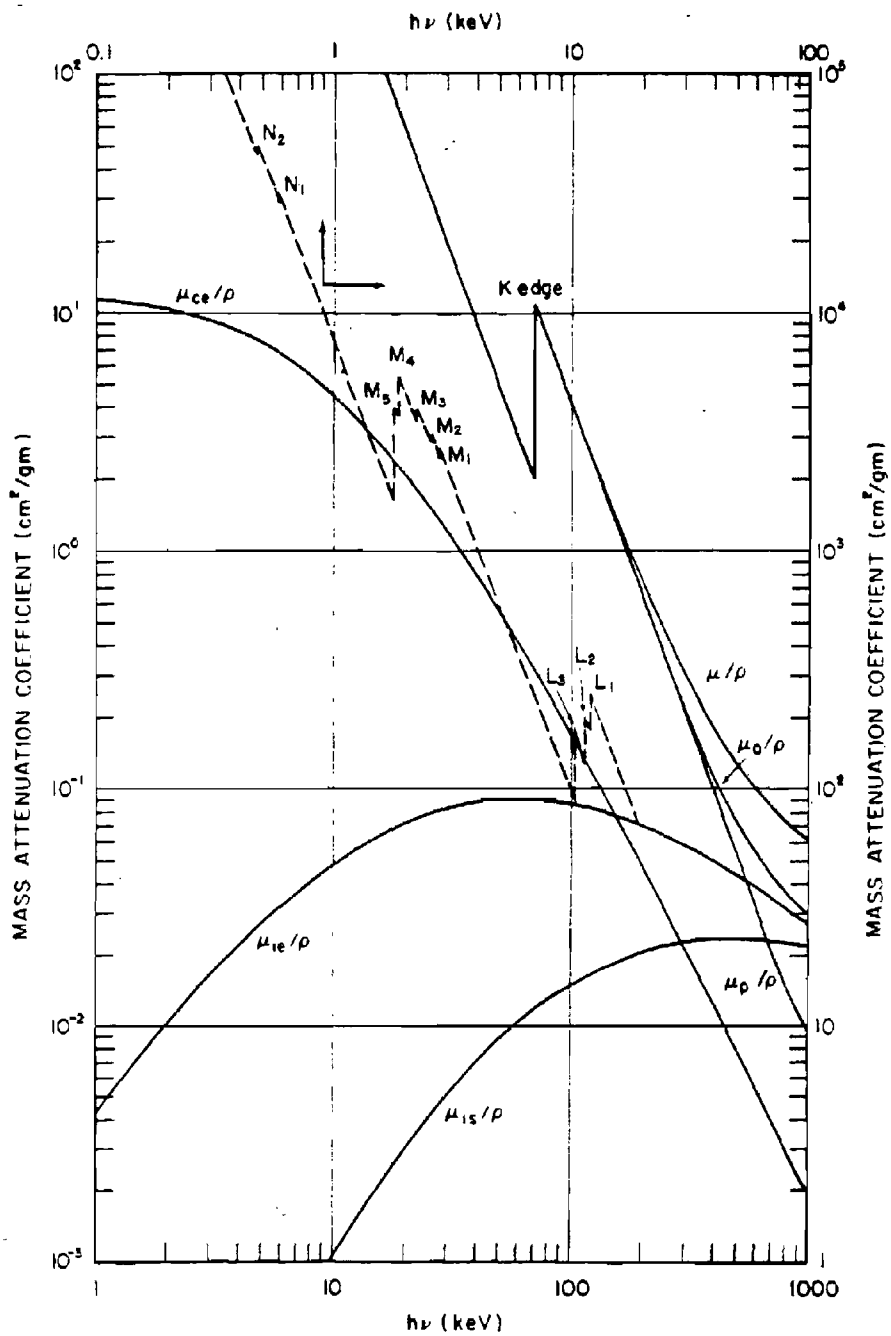

Figure 9-31. [redacted] Photon Cross Sections in Tungsten [redacted]

[redacted]

[redacted]

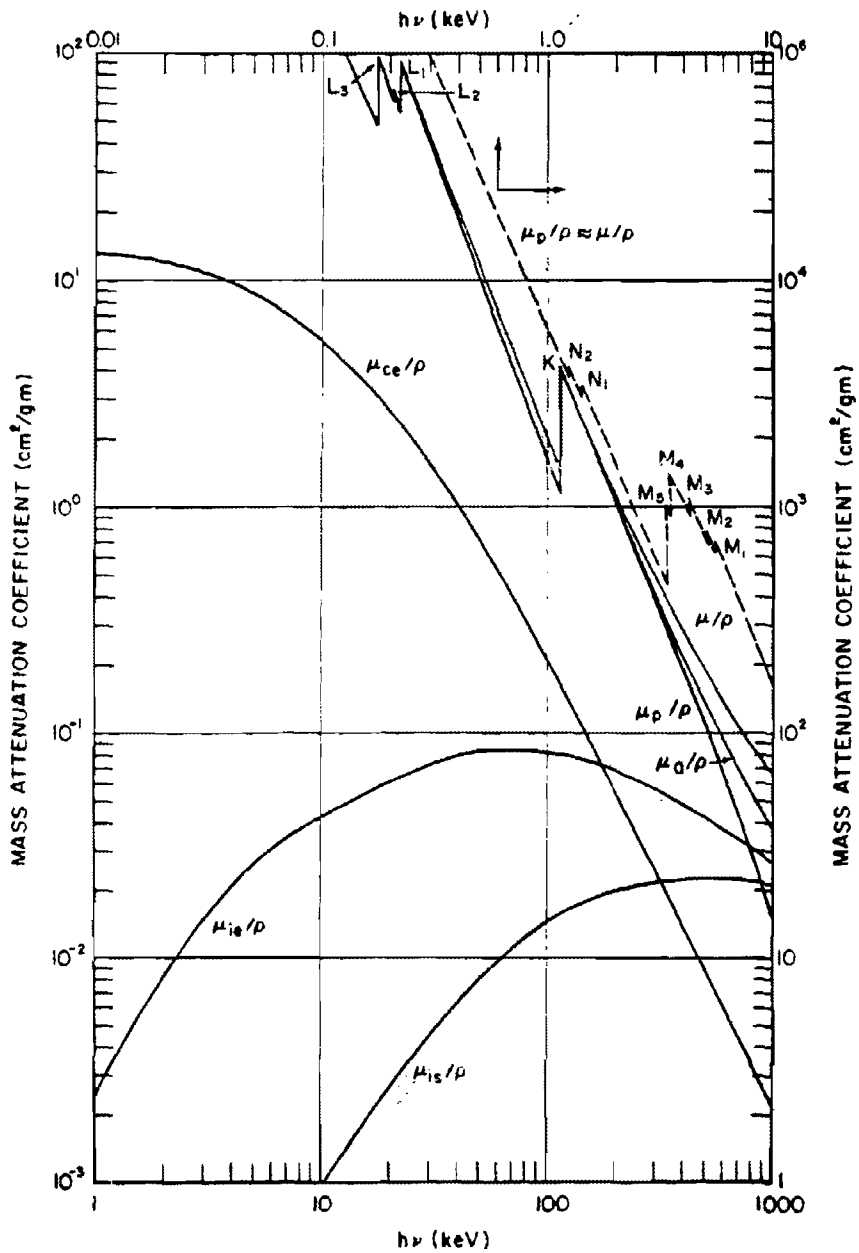

Figure 9-32. [redacted] Photon Cross Sections in Uranium [redacted]

[redacted]

[redacted]

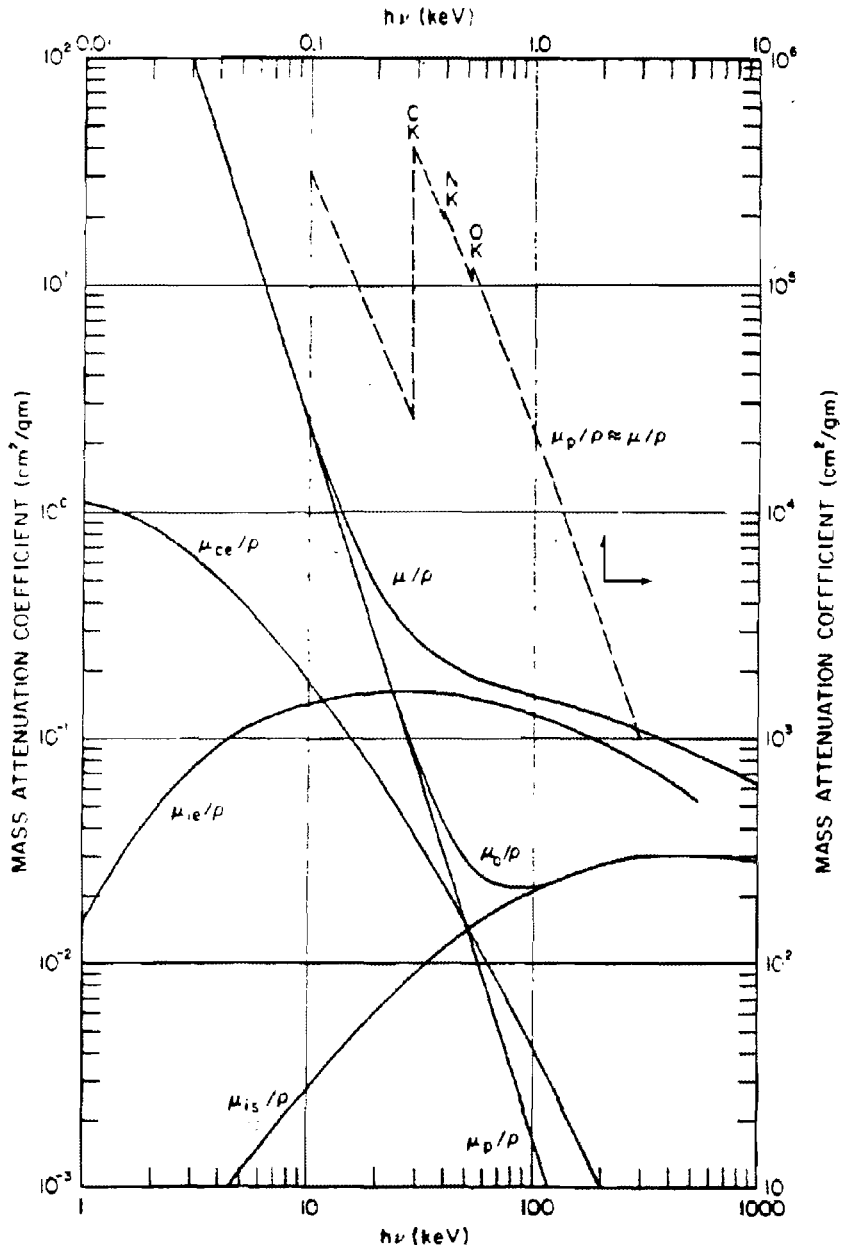

Figure 9-33. [redacted] Photon Cross Sections in Carbon Phenolic (CP), $\bar{Z}$ = 6.08 [redacted]

[redacted]

7

[redacted]

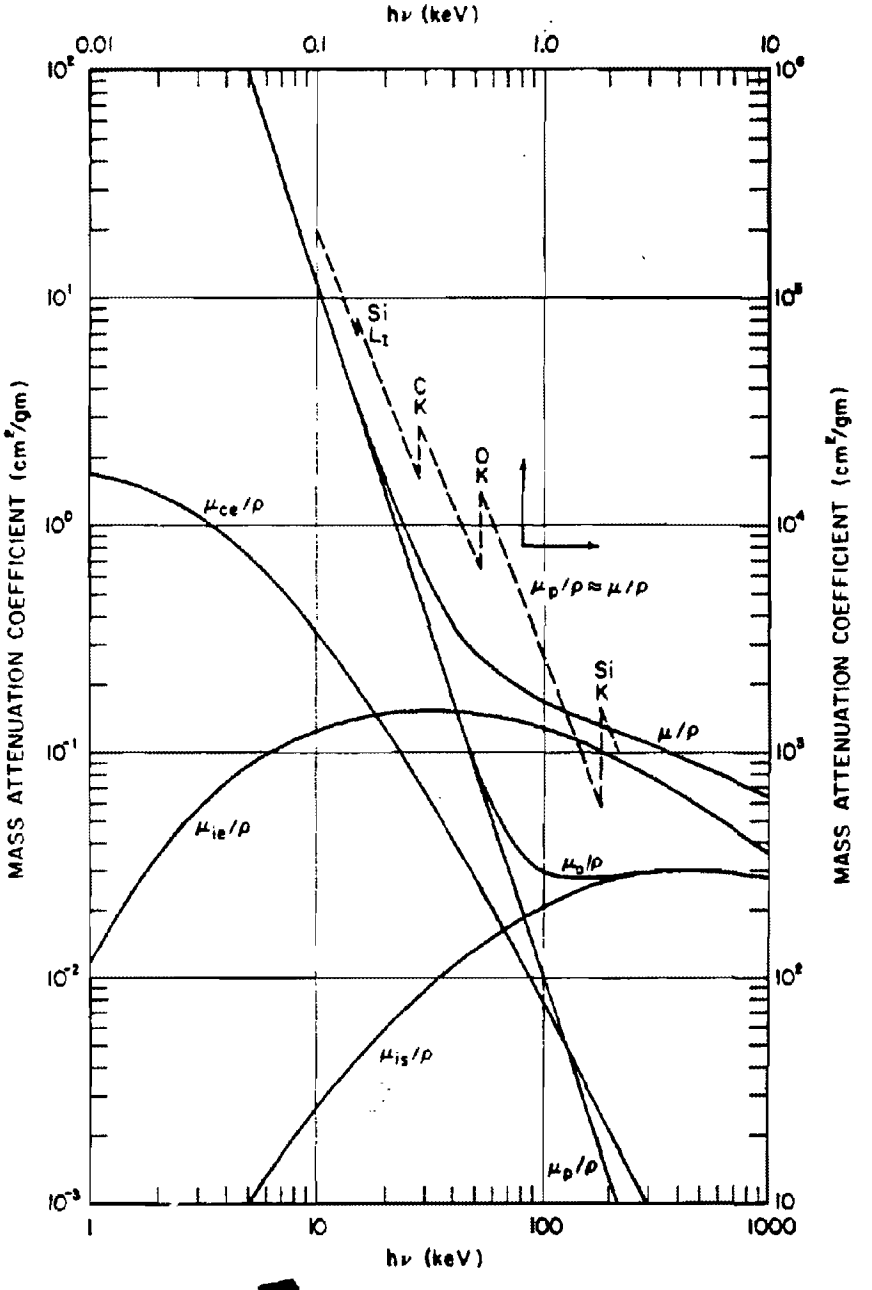

Figure 9-34. [redacted] Photon Cross Sections in Tape Wound Silicon Phenolic (TWSP), $\bar{Z}$ = 9.01 [redacted]

[redacted]

[redacted]

9-35 X-ray Energy Deposition Summary

[redacted] The methods described in paragraphs 9-33 and 9-34 and illustrated in Problems 9-3 and 9-4 allow the calculation of curves that show approximations of energy deposition as a function of depth for black body spectra incident on any material, if the cross sections are known for the material [redacted]

INITIAL PRESSURIZATION OF MATERIALS DUE TO X-RAY DEPOSITION [redacted]

[redacted] An immediate consequence of the deposition of X-ray energy is the rapid heating of the material. This heating causes an initial pressure distribution as a function of depth in the structure. The initial pressurization generates shock waves that propagate through the thickness of the shell of the structure. The heating can result in a solid material changing phase, that is, melting or vaporizing. The melting and vaporization cause blowoff, which imparts an impulse to the structure and excites whole structure modes of response.

9-36 Phase Changes Induced by X-ray Heating [redacted]

[redacted] In most nuclear weapon X-ray environments, the X-ray energy is deposited in a very short time, a few nanoseconds to a few hundred nanoseconds. The material cannot expand appreciably during this time, so the energy deposition process can be considered to occur at a constant volume or at normal material density, ρ_0. Rapid melting and vaporization are accompanied by enormous pressure increases. Values

[redacted]

[redacted]

DNA
(L)(3)

Deleted

Figure 9-35. [redacted] Energy Deposited in Aluminum by Black Body Spectra [redacted]

[redacted]

[redacted]

Deleted

Figure 9-36. [redacted] Energy Deposited in Copper by Black Body Spectra [redacted]

[redacted]

[redacted]

DNA
(L)(3)

Deleted

Figure 9-37. [redacted] Energy Deposited by Black Body X-ray Spectra in Carbon Phenolic (CP) [redacted]

[redacted]

[redacted]

[redacted]

Deleted

Figure 9-38. [redacted] Energy Deposited by Black Body X-ray Spectra in Tape Wound Silica Phenolic (TWSP) [redacted]

[redacted]

[redacted]

for enthalpy changes for melting and vaporization for the metals discussed in the previous subsection are given in Table 9-17. These values are for one atmosphere pressure. In most X-ray problems of interest the material is initially at very high pressure, so these values can be considered to be only approximate. This approach is not correct for ablators as a class although it might apply to carbon phenolic in a cold environment. Confining the discussion to metals will not restrict the transfer of principles.*

[redacted] The rising pressure that results from heating at constant density is illustrated in Figures 9-39 and 9-40 where isoenergy lines of aluminum are shown in pressure-density plots. If the internal energy is above the critical energy, 3,016 cal/gm for aluminum, the material can be considered as a vapor. Figure 9-40 shows the high pressure, high energy intercepts with the normal density abscissa (ρ_o = 2.7 gm/cm^3). The release adiabats for expansion from density ρ_o to low density and pressure also are shown in this figure. Expansion along the adiabat results in decreasing internal or potential energy as the material develops kinetic energy during "blowoff." For example, a 6,000 cal/gm energy deposition in aluminum at ρ_o = 2.7 gm/cm^3 results in a pressure of about 1.5 megabars (Mb). The aluminum would expand from that state to low pressure and density, with final internal energy of about 3,000 cal/gm and about 3,000 cal/gm of kinetic energy. The 3,000 cal/gm of internal or potential energy is used to overcome the physical and chemical forces that bind the atoms together in the solid. This leads to the concept of heat of sublimation. The heat of sublimation at absolute zero, E_{so}, is the energy required to form the saturated vapor from the solid at a temperature of absolute zero. Thus, E_{so} does not include any energy of kinetic motion. The energy of sublimation generally is a function of temperature becoming larger for larger deposition energies (temperatures).

* [redacted] The problem of phase changes in a composite heat shield ablator is more complicated since different deposition profiles, material enthalpy, and thermal conductivities are involved in the calculations. While some materials, e.g., tape-wrapped carbon phenolic, may behave like metals in a cold environment, the techniques described here generally are not applicable to the description of the blowoff process in the broad category of composite materials that use three dimension (3-D) weaves for heat shields or for X-ray shields that use dispersed high Z materials for loading.

Table 9-17. [redacted] Enthalpy Change for Selected Metals [redacted]
(cal/gm)

Metal-Atomic Weight	To Melt	Through Melt	To Vapor	Through Vapor	Sublimation Energy
Be 9.013	876.0	1,187.0	2,147.0	10,040.0	8,682.0
Al 26.98	160.4	255.3	771.1	3,347.0	2,891.0
Fe 55.85	250.8	315.8	573.0	2,071.0	1,782.0
Cu 63.54	110.0	160.0	336.0	1,481.0	1,275.0
W 183.85	153.9	200.0	304.0	1,353.0	1,110.0
U 238.00	49.0	64.5	171.9	596.1	492.1

[redacted]

[redacted]

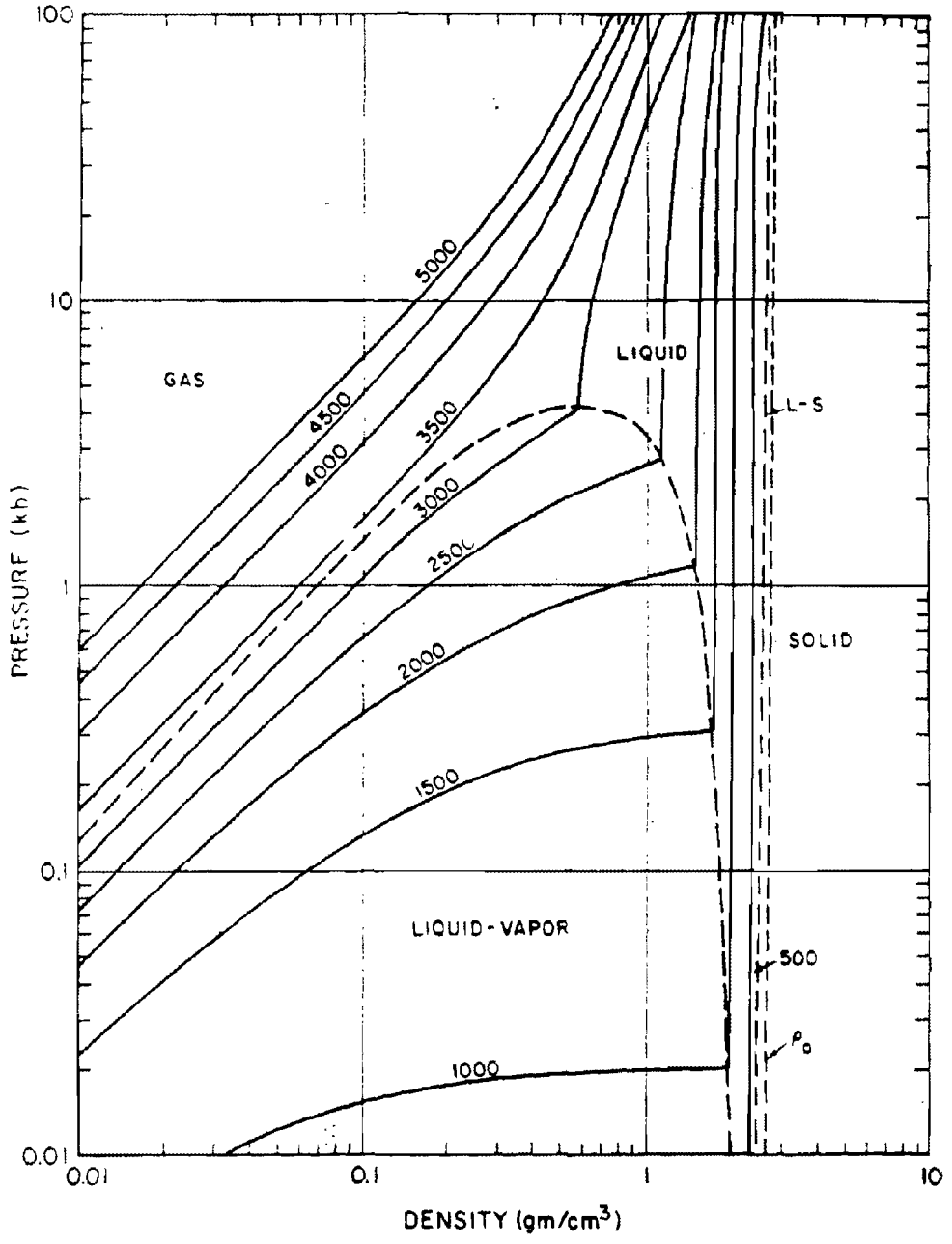

Figure 9-39. [redacted] Aluminum Isoenergy Lines. Parameter is Energy in cal/gm [redacted]

[redacted]

[redacted]

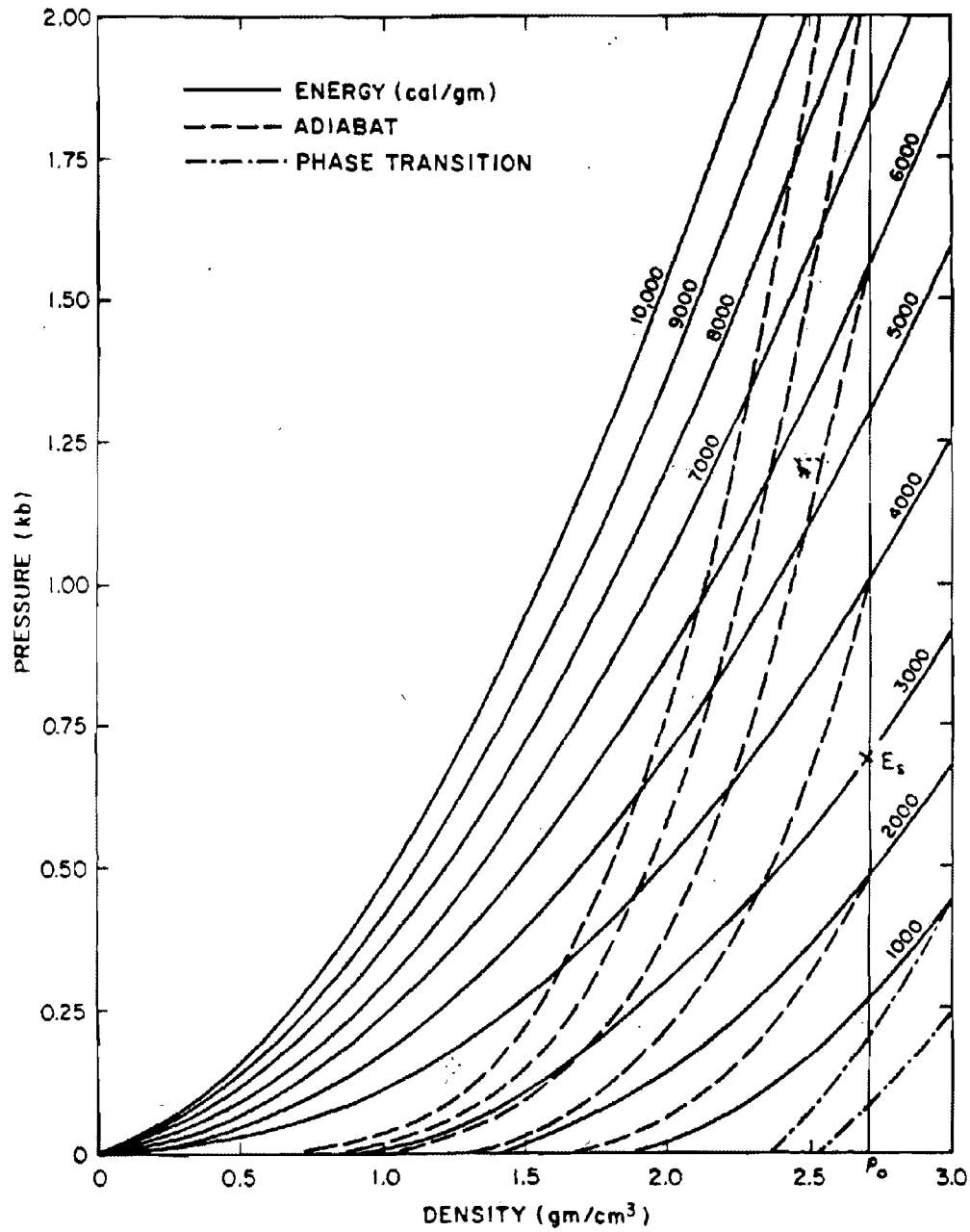

Figure 9-40. [redacted] Aluminum Isoenergy Lines and Adiabats [redacted]

[redacted]

[redacted]

9-37 The Grüneisen Parameter and the Equation of State

As a first approximation to the equation of state of material, it is assumed that the pressure in the material increases linearly with the deposited internal energy per unit volume,

$$P = G\eta\epsilon,$$

where G is the Grüneisen ratio for the material, ϵ is the internal energy per unit volume, and $\eta =$

[redacted]

[redacted]

ρ/ρ_o, the ratio of the density to a normalized density of the material, usually the ambient density. In codes used to calculate shock wave propagation, for example the PUFF type codes, more elaborate equations of state are used to fit the experimentally determined behavior of the solid and vapor phases. The equations used in the PUFF codes reduce to the equation given above when $\eta = 1$, and generally only one value of G is used to specify a material.

[redacted] Although there may be small errors in calculating the X-ray energy deposition as a function of depth, the significant sources of errors in pressure predictions are the accuracy and validity of the Grüneisen parameter for solid and vapor equations of state. Experimental values of G obtained by different methods result in factors of about two uncertainty even for some of the common materials such as aluminum, beryllium, and tungsten. Even though indications are that G is not well known as a function of deposited energy, some very good correlations have been obtained for computed and measured values of pressure waves in X-ray tests, when careful calculations are made employing elastic plastic properties of the materials.

[redacted] Initial pressurization in distended materials such as porous metals and foams present a particularly difficult and uncertain condition for current analytical techniques.

[redacted] The units for ϵ in the equation given above are energy per unit volume, which have the same dimensions as pressure. Therefore, the energy required in cal/gm for a phase change can be expressed in units of pressure, if the density of the material is specified. If the internal energy, E, is given per unit mass, the relation to ϵ is

$$\epsilon \text{ (cal/cm}^3\text{)} = E \text{ (cal/gm)} \ \rho_o \text{(gm/cm}^3\text{)}.$$

The value of ϵ in megabars may then be obtained by the relation

$$\epsilon \text{ (Mb)} = \epsilon \text{ (cal/cm}^3\text{)} \times 4.18 \times 10^7 \left(\frac{\text{erg}}{\text{cal}}\right) \times 1 \left(\frac{\text{dyne} \cdot \text{cm}}{\text{erg}}\right) \times 1 \left(\frac{\text{Mb}}{10^{12} \text{ dyne/cm}^2}\right)$$

$$\epsilon \text{ (Mb)} = 4.8 \times 10^{-5} \ \epsilon \left(\frac{\text{cal}}{\text{cm}^3}\right)$$

$$= 4.18 \times 10^{-5} \ \rho_o E \left(\frac{\text{cal}}{\text{gm}}\right).$$

Thus, the previous equation for pressure may be written

$$P \text{ (Mb)} = G \frac{\rho}{\rho_o} \epsilon \text{ (Mb)},$$

or

$$P \text{ (Mb)} = 4.18 \times 10^{-5} \ G\rho \ E \text{ (cal/gm)}.$$

The enthalpy changes of the metals shown in Table 9-17 in cal/gm are given in Table 9-19.

Table 9-19. [redacted] Enthalpy Changes ϵ (Mb) [redacted]

Metal	ρ_o (gm/cm^3)	To Melt	Through Melt	To Vapor	Through Vapor	Sublimation Energy, E_s
Be	1.85	0.068	0.0918	0.166	0.776	0.671
Al	2.70	0.0181	0.0288	0.087	0.378	0.326
Fe	7.86	0.0824	0.1036	0.188	0.680	0.585
Cu	8.92	0.0410	0.0596	0.125	0.552	0.475
W	19.3	0.124	0.161	0.245	1.092	0.895
U	18.7	0.0383	0.0504	0.134	0.466	0.385

[redacted]

[redacted]

Table 9-20. [redacted] Pressure Change, P (Mb) [redacted]
($\rho = \rho_0$, $\eta = 1$)

Metal	G	To Melt	Through Melt	To Vapor	Through Vapor	Sublimation Energy, E_s
Be	1.45	0.099	0.133	0.241	0.12	0.973
Al	2.13	0.0386	0.0613	0.185	0.805	0.694
Fe	1.69	0.139	0.175	0.318	1.15	0.989
Cu	2.00	0.082	0.119	0.250	1.10	0.950
W	1.43	0.177	0.230	0.350	1.56	1.28
U	2.03	0.078	0.102	0.273	0.946	0.782

[redacted]

The pressures associated with these changes at ambient density, i.e., when $\rho = \rho_0$, and P (Mb) = $G\epsilon$ (Mb), are shown in Table 9-20.

[redacted] From Table 9-20, aluminum has a sublimation pressure of about 0.7 Mb at ambient density, corresponding to sublimation energy of about 2,900 cal gm (Table 9-17). This point is shown in Figure 9-40, labeled E_s at about 3,000 cal gm. Table 9-20 indicates that the pressures associated with vaporization of metals at ambient density are with some exceptions about 1 Mb. A survey of more than 30 common metal elements indicates that an average of 1 Mb for vaporization is a good approximation, especially if the Grüneisen value for the material is uncertain. Since a bar corresponds to 14.7 psi a Mb is the enormous pressure of about 1.45×10^7 psi. Thus, tremendous forces are involved in the pressure gradients associated with metal vaporization at ambient density. Table 9-17 shows that vaporization usually involves several thousand calories per gram of energy. High explosive materials (TNT, etc.) release about 1,000 cal/gm. Therefore, on a mass basis there is more energy associated with metal vaporization than with high explosives. Generally, the thicknesses of material evaporated by X-ray absorption is small, and, the total mass of material that is vaporized generally is small.

[redacted] SHOCK WAVE PROPAGATION AND DAMAGE PREDICTIONS [redacted]

[redacted] The sequence of events for the generation and propagation of a stress wave through the thickness of an aerospace shell and the damage produced is illustrated in Figure 9-41. Cold X-rays are deposited primarily in a relatively thin sheet of material at the front surface (Figure 9-41a). After the energy is deposited a compression wave propagates inward from the front surface, followed by a rarefaction that causes the vapor and liquid to blow off (Figure 9-41b). This rarefaction also may cause a spall of solid material from the front surface (Figure 9-41c). Later the compression wave reflects from the back surface and returns as a rarefaction wave. This rarefaction wave, or the coincidence of this wave with the rearward moving rarefaction may cause the rear surface to spall (Figure 9-41d), or may cause fracturing or debonding. This process occurs within the order of a microsecond and generally is complete before the overall structural motion occurs. The shock effects are

[redacted]

[redacted]

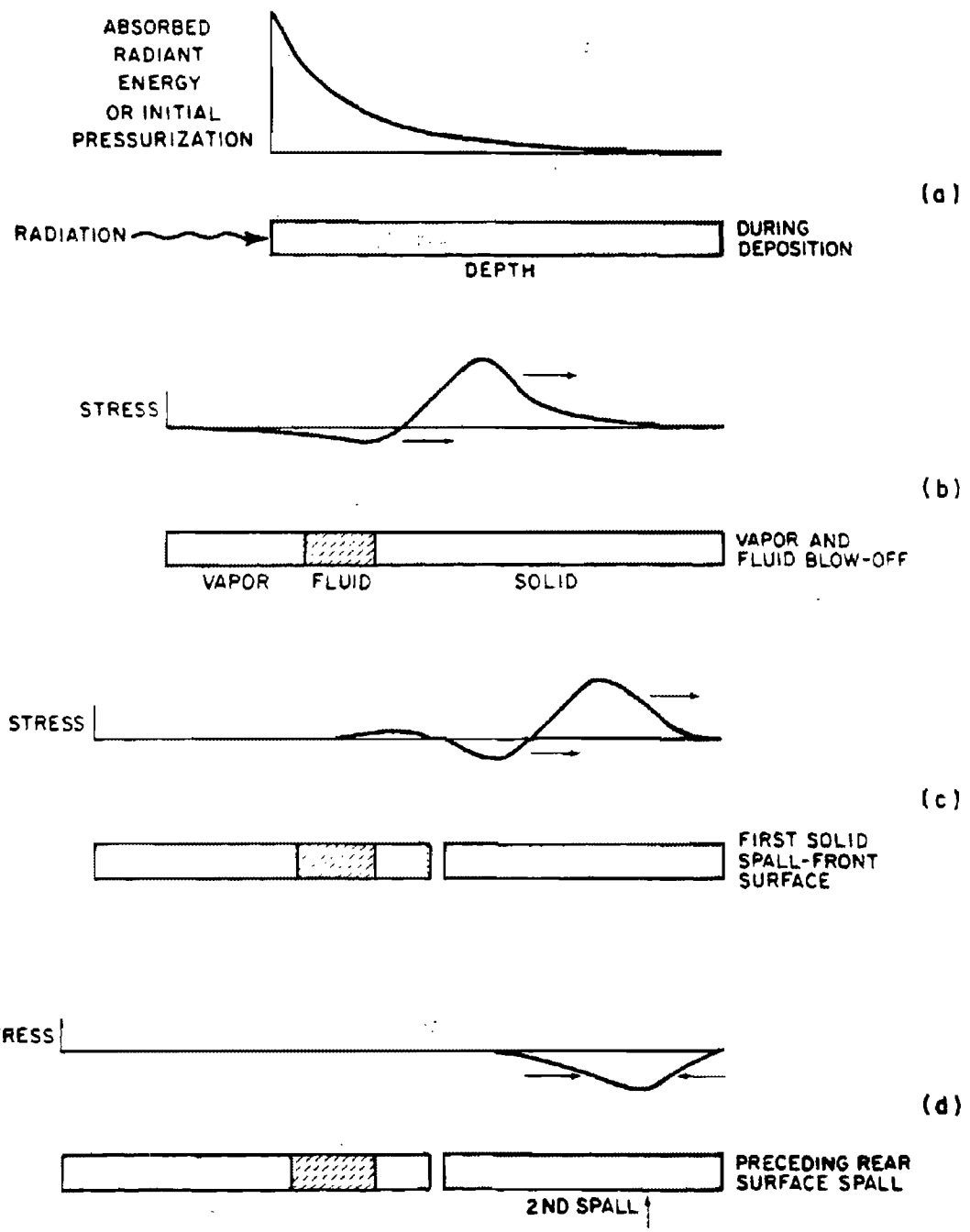

Figure 9-41. [redacted] Sequence of Spallation Following Radiation Deposition [redacted]

[redacted]

extremely local, depending on the sheet thickness and not on the overall geometry of the structure, so spall damage, including fracturing and debonding, usually cannot be scaled according to the laws that govern structural behavior. Since the spall damage occurs early, possibly weakening the structure, it can have a strong effect on the subsequent response to the structure to the impulse that has been imparted.

Propagation of stress waves and the damage predictions are not amenable to hand calculations. Most stress wave propagation calculations are performed on computers using one dimensional (1-D) models to represent a cross section of an aerospace vehicle shell. These stress wave propagation calculations are used routinely in design analysis and are the direct outputs of PUFF-like codes or their variations. The stress wave propagation predictions are used to:

1. Obtain a calculated pressure time history at the rear surface of a 1-D sample for direct comparison to experimental values that are obtained by laboratory simulation or by underground nuclear tests. The agreement or lack of correlation serve as an important criteria for judging the adequacy of analytical techniques. The conclusions are almost universal that the largest sources of error in stress wave propagation codes are associated with the mechanical aspects of the material behavior, such as failure criteria, and the elastic-plastic models, which should include strain rate and temperature dependence.

2. Obtain maximum tension as a function of depth in the materials to indicate regions of potential material failure, debonding, and spalling. Definitions that are required for the materials failure level under these dynamic tensile loads are obtained experimentally.

3. Obtain input data for structural response analysis.

There also are some 2-D shock propagation codes being used for specific calculations involving cylinders, nose tips, etc. Peak pressure predictions using pure hydrodynamic representations of the material in code calculations are generally high by a factor of 2 to 4. If a dynamic elastic-plastic constitutive relationship is included, the predictions are improved significantly.

9-38 Through-the-Thickness Elastic-Plastic Shock Propagation

Considerable progress has been made in correlating measured and calculated through-the-thickness shock propagation in one dimension by using the elastic-plastic materials description in PUFF-type codes. The stress strain diagram shown in Figure 9-42 illustrates a two-wave nature of the elastic-plastic shock wave propagation. The total stress, σ, is the sum of the hydrostatic pressure, P, and an elastic stress offset of $2/3\ Y_o$, where Y_o is the yield strength of the material (its compressive yield strength if that is different from its yield strength in simple tension). The effect of the yield stress path OAB is to propagate two stress waves having different velocities into the undisturbed material. The slope of the elastic portion, OA, is larger than the plastic portion, AB. The propagation speed is larger if the slope of the stress strain curve is larger. Hence, an elastic precursor shock traveling with the elastic velocity, c_E, runs in front of the slower total stress wave which propagates with a bulk sound speed, c_o

$$c_E = \sqrt{\frac{K}{\rho_o} + \frac{4/3S^*}{\rho_o}}$$

$$c_o = \sqrt{\frac{K}{\rho_o}}$$

where K is the bulk modulus and S^* is the shear modulus.

An elastic rarefaction stress ($4/3\ Y_o$ or twice the stress offset) propagates from the rear of the shock wave at velocity c_E and overtakes

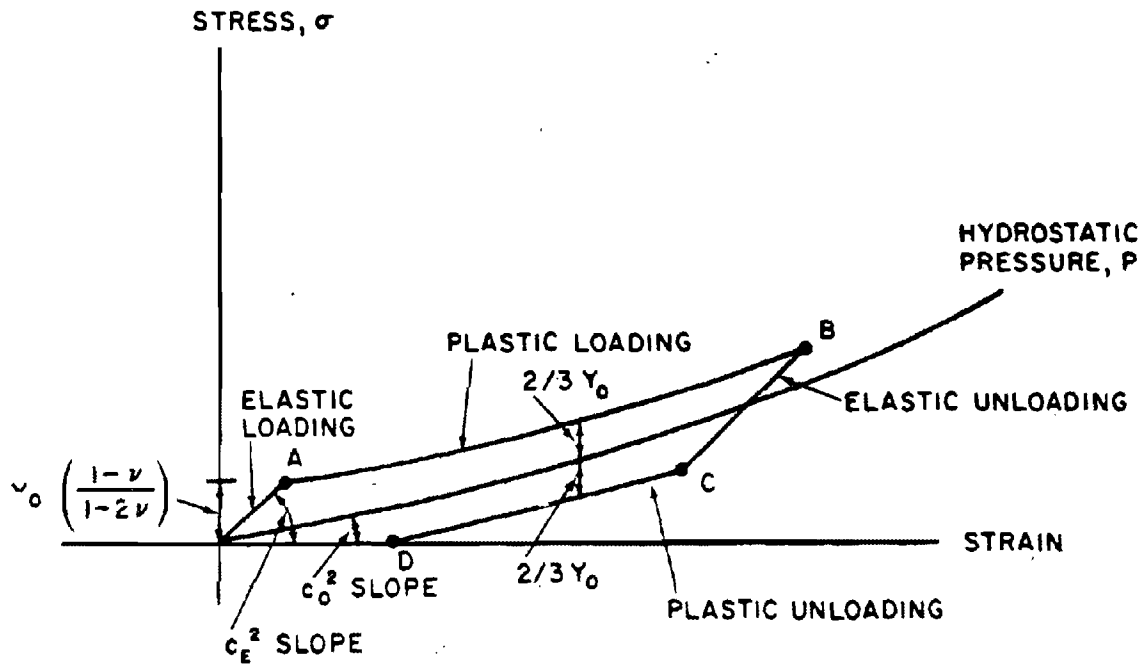

Figure 9-42. [redacted] Equation of State for Elastic-Plastic Material Description [redacted]

[redacted]

the slower plastic wave (path BC). This rarefaction wave causes a greater attenuation of the main stress pressure wave than is obtained in pure hydrodynamic calculations (up and down the Hugoniot). This greater attenuation of the elastic plastic wave propagation compared to purely hydrodynamic calculations results in better correlation with measured values of stress. The plastic unloading to a stress-free condition, path CD in Figure 9-42, also propagates with velocity c_0 and completes the cycle.

[redacted] Although the elastic-plastic code calculations improved the correlation of measured and computed through-the-thickness stresses for some materials, if a material has strong strain rate or temperature dependence these features also must be incorporated into the calculations. Stress wave propagation through materials such as foams require an entirely different constitutive expression, and anisotropic materials such as three-dimensional quartz phenolic, can have quite different material properties in different directions. Similarly, propagation characteristics of inhomogeneous materials or materials that contain small radiation absorbers lead to complicated propagation analysis. Propagation in these materials has not been treated in an analytically satisfactory manner. Most of the current analytical techniques used in the solution of stress wave propagation in the materials are deficient in varying degrees in the following ways.

1. There is incomplete understanding of the material behavior under the types of conditions that result from X-ray energy deposition, so the material representations are inadequate in most cases.

2. Experimental data for verification and modification of the equations of state and con-

[redacted]

[redacted]

stitutive relations in the analytical techniques have been limited and of poor quality.

9-39 Through-the-Thickness Material Response

Simulation tests and underground nuclear weapons tests can identify failure and damage modes that result from shock wave propagation and through-the-thickness material response on samples that are meaningful in terms of the expected response of reentry vehicles or aerospace shells. The experimental results are most meaningful when appropriate analytical techniques are used to correlate the experimental results with the stress wave characteristics producing the response modes. Hundreds of complex aerospace structure composites as well as samples of metals and plastics have been exposed during underground nuclear weapons tests at various X-ray fluence levels with different X-ray spectra and deposition times.

IMPULSE AND STRUCTURAL RESPONSE ANALYSIS

The vapor and/or liquid blowoff following X-ray deposition imparts a reactive impulse to the aerospace structure. The structural response takes place for the most part after the shock wave discussed in the last section has dissipated. This shock wave may have damaged or weakened the structure by spallation, debonding, or fracture. The damage to the structure should be considered in the structural response analysis if an accurate prediction is to be made. Obviously, this is a complicated problem and is not amenable to hand calculation. However, some rough estimates of impulse can be made and serve to illuminate the processes that take place.

9-40 Impulse Calculations

Page 9-108 deleted.

[redacted]

DNP
(1-13)

Deleted

Figure 9-43. [redacted] Normalized Vapor Impulses Produced in Aluminum by [redacted] Various Black Body X-ray Spectra

[redacted]

[redacted]

DNA (L-)13)

Deleted

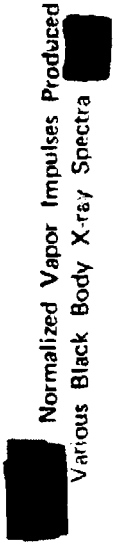

Figure 9-44. [redacted] Normalized Vapor Impulses Produced in Copper by Various Black Body X-ray Spectra

[redacted] [redacted]

Pages 9-111 and 9-112 are deleted.

[redacted]

Problem 9-5. Calculation of Vapor Blowoff Impulse

[redacted] The information presented in the preceding paragraphs provides a means to obtain an approximation of blowoff impulse for certain materials. The following example is presented to illustrate the procedures. In practice, these calculations are performed with computer codes.

DNA (1)(3)

[redacted]

Related Material: See paragraphs 9-34 through 9-37, and 9-40. See also Figures 9-35 through 9-38, 9-43 and 9-44, and Table 9-17.

[redacted]

[redacted]

Problem 9-6. Calculation of the Location of Phase Change Boundaries

[redacted] The preceding paragraphs provide the information necessary to calculate the location of the various phase change boundary layers. The procedure is illustrated in the following example.

DNA (4-)(3)

[redacted]

Related Material: [redacted] paragraphs 9-34 through 9-37, and 9-40. See also Table 9-17 and Figure 9-35.

[redacted]

[redacted]

[redacted]

DNA (U.X(3))

[redacted]

Most of the structure response analyses of reentry vehicles have been developed for survivability. Since low level failure criteria responses have been selected, only elastic deformation has been considered. Such survivability analyses are probably inadequate for the determination of inelastic deformation failure modes and the levels required to define lethality. Essentially all structural response calculations require data on: (1) structural material properties such as stress and strain relations as a function of strain rate and temperature, for yield, stress and strain, fracture points, elastic moduli, and so forth; (2) structural response forcing functions, including asymmetric impulse loads, and in-depth heating and thermal loads applied as distributed and point loads; and (3) structural variation in shell wall thickness and material densities in various layers.

[redacted] **REENTRY VEHICLE HARDENING** [redacted]

DNA (U.X(3))

[redacted]

X-ray hardening refers to techniques

[redacted]

[redacted]

that reduce the susceptibility of reentry vehicles to damage from X-rays.

DNA (G)(3)

[redacted]

DNA (G)(3)

It is beyond the scope of this manual to provide a complete discussion of reentry vehicle hardening techniques. Therefore, a brief general discussion of the techniques, with a few specific examples, is presented in the following paragraphs.

9-42 Balanced Hardening with Respect to Neutrons and X-rays

[redacted]

[redacted]

Page 9-117 deleted.

[redacted]

[redacted]

DNA (b)(3)

[redacted]

SECTION VI

[redacted] NUCLEAR RADIATION SHIELDING [redacted]

[redacted] Any mass of material between a nuclear radiation source and personnel or sensitive equipment will reduce the dose to the personnel or equipment compared to the free field dose at the same location relative to the source. The dose received by a person behind a building, in a building, in a field fortification, in a tank, or in a

[redacted]

[redacted]

ship will be less than that which would be received in an exposed free field position.

In principle, it would be possible to calculate the dose behind a shield by using simplified neutron and gamma ray transport equations similar to those given in Chapter 5; however, several considerations make hand calculations impractical.

- The neutrons and gamma rays will arrive at the shield from many directions after having been scattered during their transport through the atmosphere.
- Calculation of radiation transport from a point source through single geometries can be done with reasonable accuracy by using an exponential factor and a buildup factor similar to those described in Section I, Chapter 5 for transport through homogeneous air, but the geometries of shielding enclosures are seldom simple, and, as mentioned above, the radiation incident on the shield is not unidirectional. This has the effect of making the problem similar to a multi-source problem.
- The attenuation of neutrons by inelastic scatter or radiative capture results in the emission of one or more gamma rays, which can contribute to the dose within the shielded area even though the neutrons are removed from the penetrating radiation beam.
- The specific location of the burst and the receiver can affect the degree of attenuation, e.g., different members of a tank crew will have different degrees of protection from the same explosion, and any particular member of the crew will have a different degree of protection from initial radiation from bursts at different locations relative to the tank. In other words, each location within each shielded structure must be evaluated separately, or at least a sufficient number of locations must be evaluated to determine the overall shielding efficiency of the structure or piece of equipment.

These complexities, and others, make it necessary to use computer codes to determine the shielding efficiency of any structure or piece of equipment. Even when using the codes, some simplification in the description of the shield geometry usually is necessary. However, satisfactory methods for treating fairly complex geometries have been developed. These are described in DASA 1892, "Weapons Radiation Shielding Handbook" (see bibliography). Results of some sample calculations are also provided. Unfortunately, sufficient calculations have not been performed to permit the development of a generalized simple method for shielding calculations that would be suitable for inclusion in this manual.

Table 9-22 provides some estimates of the shielding afforded by various structures and types of military material. These estimates are given in terms of a "dose transmission factor," which is defined as the ratio of the dose measured behind the shield to the dose that would be measured in the absence of the shield. Some of the transmission factors shown in Table 9-22 were obtained by measurements at weapon tests or are extrapolations from such measurements. Other transmission factors were obtained by relatively detailed calculations, while still others are mere estimates. Ranges of values are given for the dose transmission factors for most structures. These ranges result from two causes: uncertainty in the estimates themselves, and variations in the degree of shielding that may be obtained at different locations within a structure. Separate transmission factors are given for initial gamma rays and residual (fallout) gamma rays for two reasons: the average energy of the initial gamma rays is higher than the average energy of the residual gamma rays, and there are different source geometries.

[redacted]

[redacted]

Table 9-22. [redacted] Estimated Dose Transmission Factors (Interior Dose/Exterior Dose) [redacted]

DNA
(1)

Deleted

[redacted]

[redacted]

[redacted] No specific reliability can be attached to the dose transmission factors shown in Table 9-22. They are felt to be reasonable values for generalized applications; however, specific shielding problems should be addressed by methods such as those described in DASA 1892.

SECTION VII

[redacted] TREE – COMPONENT PART AND CIRCUIT RESPONSE [redacted]

[redacted] This section contains a discussion of the effects of nuclear radiation on electronic component parts and circuits. The intent is to provide an introduction to the failure modes and responses that result from ionization, displacement, and thermomechanical shock. A more detailed description of the effects is contained in the TREE Handbook (see bibliography).

[redacted] Since semiconductor devices generally are considered to be the most sensitive devices in an electronic circuit, emphasis is placed on them. However, the discussion does include other electronic component parts.

[redacted] Within the scope of this manual, this section can only aid in establishing levels where electronic equipment might experience failures as a result of the radiation environment and indicate the extent of the problems. The numbers presented are only estimates for a generic grouping or subgrouping. It must be understood that it is very difficult to give accurate radiation effects data for generic types of electronics. For example, transistors can show sufficient amplification loss to be useless after receiving 10^{10} to 10^{15} n/cm^2 ($E > 10$ keV, fission). That is 5 orders of magnitude difference and is relatively useless information. Fortunately, transistors can be subgrouped to improve their characterization. The problem of accurate prediction, however, is not completely solved. Even if one particular type of transistor is considered, the neutron fluence required to reduce the amplification to a particular value can vary more than an order of magnitude. Additionally, the failure threshold for a transistor in one circuit may be greatly different from the failure threshold for that same transistor in a different circuit, i.e., the response of each component part and the circuit configuration must be known to make a reasonable estimate of circuit response.

[redacted] The transient radiation effects are classified into three groups: transient, permanent, and thermomechanical. The transient effects result from nonequilibrium free-charge conditions introduced through the ionization phenomena (see Chapter 6). The permanent effects are attributed to physical property changes of the irradiated materials caused by energetic particles (neutrons and secondary electrons). The thermomechanical effects result primarily from the absorption of low energy photons.

[redacted] The class of effect is defined by the primary effect induced by the radiation. For example, the short term currents that result from ionization may trigger a digital state change or may permanently damage a device in some other manner. This phenomenon is treated as a transient effect, because the permanent consequences result from circuit action and/or device construction rather than from direct radiation induced material property change.

[redacted] The terms "radiation hardened" or "radiation resistance" frequently are connotated incorrectly. These terms mean that someone or some group has examined the component part, circuit, or system, made some modification and/or used part selection criteria and has determined that the electronics will withstand certain levels of certain types of radiation. The experience of the person making the examination as well as the resulting modifications can both vary widely. Consequently, when these terms are used they should be accompanied by the answers to the following questions.

- Hardened to what type of radiation?

[redacted]

- Hardened to what levels of radiation?
- What procedure was used for hardening?
- How has the hardening been verified?

Based on the answers to these questions, the applicability of that "hardened" component part, circuit, or system for his intended use can be judged.

SEMICONDUCTOR COMPONENT PARTS

9-44 Transient Effects

The transient effects observed in semiconductor devices exposed to nuclear radiation result from the creation of excess charge carriers (ionization) that cause current and voltage changes. These changes do not cause permanent damage directly to the semiconductor material. However, their presence may produce permanent changes as a result of current overloads to some components, loss of information stored in memory units, or by the creation of premature signals. Furthermore, such transients can cause saturation of some circuits for times that are long compared to the duration of the ionizing radiation pulse, and may thus cause system failure during a significant and possibly critical period.

Most of the ionization produced in a nuclear weapon environment is due to the photons and 14-MeV-neutrons, although all nuclear radiation can contribute. Because of this predominance of photon excitation of carriers, the observed currents and voltages are often referred to as photocurrents and photovoltages, even though the prefix may not always be proper. The mechanisms whereby this ionization occurs are described in Chapter 6.

Before discussing the transient effects in particular semiconductor devices, it is desirable to review briefly the important basic physical processes responsible for device behavior. These processes are common to all semiconductor devices and must be reasonably well understood before the description of the device response can be followed intelligently.

Current is the manifestation of charge carrier movement within a material. As described in paragraph 6-4, the movement may be random, random with a diffusion from regions of high concentration to regions of low concentration, or, if an electric field is present, the movement may be a drift in the field superimposed on the normal random scattering. Carriers may be trapped by impurities, which are always present in solid state devices. Eventually, the trapped carriers may be annihilated by their mates (oppositely charged carriers) in a process called recombination. The net result of these processes is that the free carriers diffuse and/or drift until they are trapped and are then promptly recombined. Therefore, any electrical currents in the materials are considered to have two components – the drift component and the diffusion component. The time during which a charge carrier is free to move by drift and/or diffusion is called the lifetime of the charge carrier.

The simplest semiconductor device is the diode. The diode is made up of pure semiconductor material doped with impurities so as to be considered to have two regions. Using pure silicon as the example, its atomic structure is considered to have four electrons in the outer orbit. In its crystal form, these outer orbiting electrons are considered to be shared with neighboring silicon atoms (see Figure 9-45). When the pure silicon is doped with an impurity, the impurity atom replaces one of the silicon atoms in the crystal lattice. The impurities are selected to have either three or five outer orbiting electrons. Silicon doped with an impurity having five outer orbiting electrons will have extra electrons that are more or less free to move around, and hence are available for conduction. Silicon doped with impurities with only

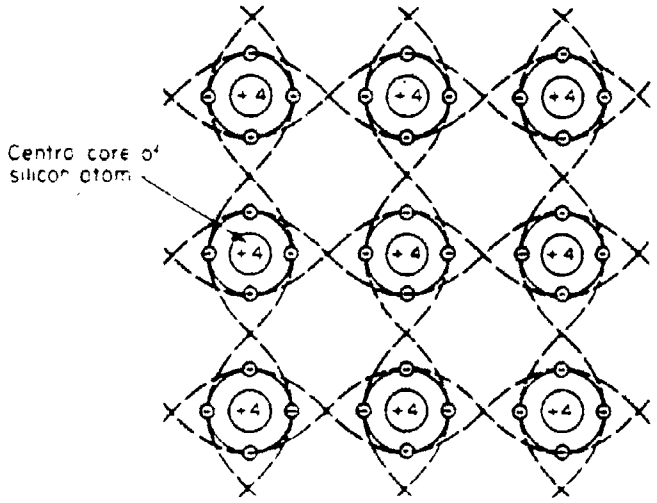

c Pure Silicon

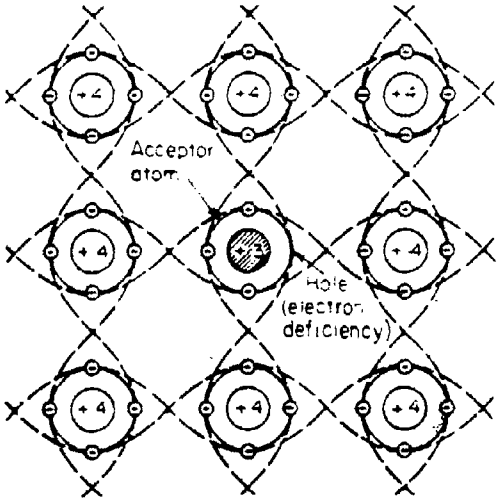

b Silicon with Acceptor Impurity Atom

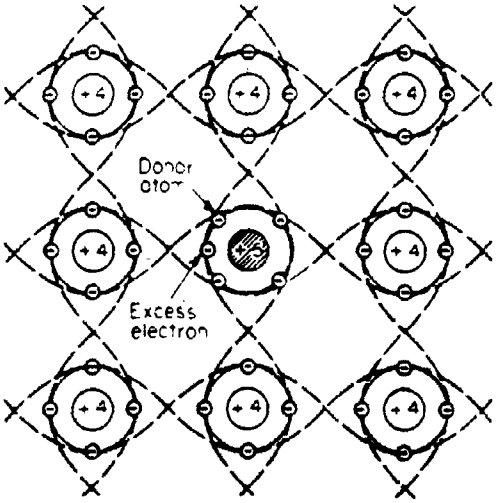

c. Silicon with Donor Impurity Atom

Figure 9-45. [redacted] Two-Dimensional Lattice Structure of Silicon [redacted]

three orbiting electrons does not have sufficient electrons to share with its neighboring silicon atoms. This lack of an electron is called a hole. For conceptual purposes, the hole can be treated like an electron with a positive charge. Consequently, in semiconductor discussion the term charge carriers refers to the electrons and holes made available for the conduction process by the impurity doping.

Figure 9-46 illustrates a semiconductor junction (diode), with the two impurity regions shown separated by a solid line. This represents what conceptually would be the junction of the two materials. However, in reality the silicon is all one crystal, and there is really no physical junction. There are, as illustrated, regions at both ends of the crystal which are predominantly either P type (excess of free holes) or N type (excess of free electrons). A transition region, called the depletion region, exists in the center. Within this region, holes from the P region combine with equal numbers of electrons from the N region. As a result, only a few free charge carriers remain in the region when equilibrium has been reached. Depending on the number of charges removed from each region, a voltage (electric field) will be developed across the depletion region. The voltage across the depletion region under equilibrium is such that any holes (positive charge carriers) introduced into the region would migrate by the drift process to the P region, and a negative charge carrier (electron) introduced into the depletion region would migrate by the drift process to the N region. Under normal conditions conventional current flow* would allow current to flow for ideal diodes only from the P side to the N side. If, however, free carriers were generated in the depletion region, conventional current flow would dictate that a current, proportional to the number of free charge carriers generated, would flow from the N region to the P region. This is in the reverse direction from the normal conventional current flow through an ideal diode. This reverse current, if generated in the depletion region by ionizing radiation, is called the drift component of the photocurrent in a PN junction. The diffusion component of the photocurrent is the result of free carrier generation by the ionizing radiation in the P and N regions near the depletion region. Those hole-electron pairs generated far from the depletion region will be trapped and recombined before they can become effective. The effect of the radiation is to

*In this chapter, normal current flow is considered to be conventional current flow. This is opposite to actual electron flow.

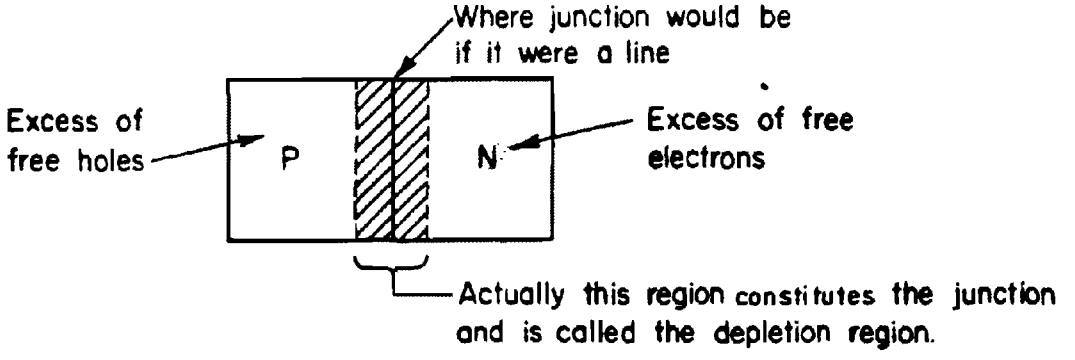
Where junction would be if it were a line
Excess of free holes
P
N
Excess of free electrons
Actually this region constitutes the junction and is called the depletion region.

Figure 9-46. Illustration of a Semiconductor Junction

generate a current in the reverse direction through the diode junction, which tends to forward bias the diode. An expression that generally will predict the photocurrent for many cases of interest is:

$$I_{pp\ max} = qK_g\dot{D}A\ (w + L).$$

where

$I_{pp\ max}$ = the maximum* primary photocurrent for a PN junction

q = electronic charge 1.60 x 10^{-19} coulombs

K_g = the energy-dependent free-charge-carrier-generation constant (electron-hole pairs/ cm^3 · roentgen)

K_g (for silicon) = 4.2 x 10^{13} electron-hole pairs/cm^3 · R

K_g (for germanium) = 1 x 10^{14} electron-hole pairs/cm^3 · R

$\dot{D}$ = the gamma exposure rate, R/sec (The gamma ray photons have energies which would give best results with the K_g constants given above.)

A = junction area in cm^2 (A can typically vary from 0.3 x 10^{-4} to 0.2 x 10^{-1} cm^2)

w = depletion layer width in cm (w varies with applied voltage and is best expressed as $w = w_1\ (V_o - V_j)^{-b}$ where V_o is the built-in junction potential (~0.35 volts for germanium and ~0.72 volts for silicon) w_1 typically varies from 0.5 x 10^{-4} cm to 1 x 10^{-3} cm, V_j is the junction voltage, and b typically varies from 0.05 to 0.5.

L = diffusion length for minority carriers on the side of the junction with the longer diffusion length in cm (L can vary typically from 0.15 x 10^{-1} cm to 0.2 x 10^{-4} cm).

The duration of the photocurrent depends on the time required for free holes and free electrons to be trapped and to recombine. Since these times are short, the photocurrent is a pulse of current of relatively short duration. Typical pulse shapes are shown in Figure 9-47.

Tunnel diodes are at least an order of magnitude more radiation resistant than diodes in general, since they are characterized by small geometry, heavily doped PN regions, and narrow junctions. The short-circuit photocurrent can be estimated from the equations applicable to general diodes. Since the lifetime of minority carriers in tunnel diodes is very short, the response of a tunnel diode to a pulse of radiation is expected to follow the radiation pulse. Normally, the width of the depletion region for tunnel diodes is so narrow that the photocurrent will consist primarily of the diffusion component. The maximum photocurrent under short

* For those more theoretically inclined this equation applies in the case where $\tau < t_p/4$ and is the steady-state value. A more detailed equation and development is the *TREE Handbook*.

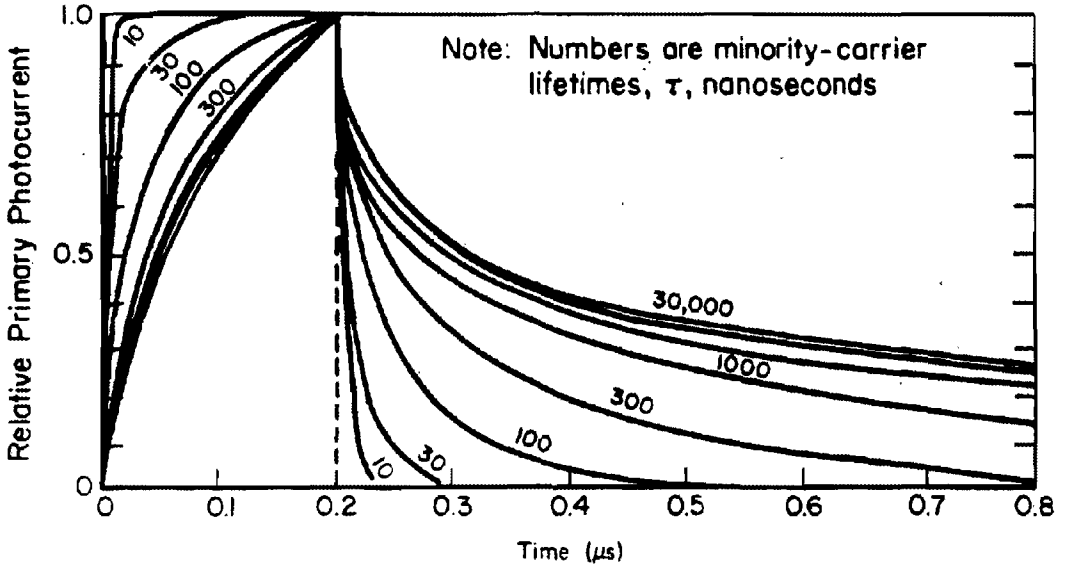

Figure 9-47. [redacted] Relative Shapes of Diffusion Component of Primary Photocurrent [redacted]

[redacted]

circuit conditions can thus be estimated as follows:

$$I_{pp\ max} = qK_g\dot{D}A\ (L_n + L_p)$$

where

q, K_g, $\dot{D}$ and A are defined as in the diode expression, and L_n and L_p are the diffusion lengths in the N and P regions, respectively. Diffusion lengths are comparable on each side of the junction.

[redacted] The radiation induced offset voltage in an open circuited tunnel diode is influenced by the tunneling current at low dose rates, but at higher dose rates a tunnel diode behaves like a conventional diode. This behavior occurs because very little induced voltage is required to set up a tunneling current equal to the diffusion current of excess carriers. When the tunneling current reaches a maximum, the induced voltage rises sharply to the value for a conventional diode.

[redacted] A transistor is a more complicated device than a diode, both structurally and functionally. The main functional advantage of the transistor is the fact the transistor has the ability to amplify its input signal. The transistor has three impurity regions that alternate, i.e., NPN or PNP. When an operating transistor* is exposed to transient ionizing radiation, a current pulse is observed in the external circuit. This current pulse, which may be orders of magnitude larger than that of a diode with comparable dimensions, can reach a peak value at a time later than the radiation peak, and can, in some cases, continue for milliseconds.

* [redacted] The following paragraphs are concerned with bipolar transistors; not to MOS, junction field-effect transistors, or thin-film transistors.

[redacted]

[redacted] This characteristic behavior of transistors is the result of the amplifying properties acting on the primary radiation induced photocurrents. The electrical action of the transistor creates a secondary photocurrent that is typically greater than the primary photocurrent by a factor equal to the gain (a measure of ability of the transistor to amplify) of the transistor. Analysis of the radiation response of a transistor involves the determination of the primary photocurrent, followed by a calculation of the magnitude and duration of secondary photocurrents under the given circuit conditions.

[redacted] In transistors, the primary photocurrent is generated in five regions: in the collector- and emitter-junction depletion regions, in the base, and in the emitter and collector bodies lying within a diffusion length of the junctions. In most cases, the generation of primary photocurrent in the emitter body and within the junctions can be neglected since the emitter body and the junction volumes are a relatively small part of the total generating volume (see Figure 9-48).

[redacted] The secondary photocurrent is produced by the accumulation of excess majority carriers in the base region as a result of the flow of primary photocurrents across the PN junctions of the device. This excess charge, which is confined in the base by the built-in junction fields, is the correct polarity to forward bias the emitter base junction and to cause normal current to flow. The collector current that is produced is called secondary photocurrent. This collector

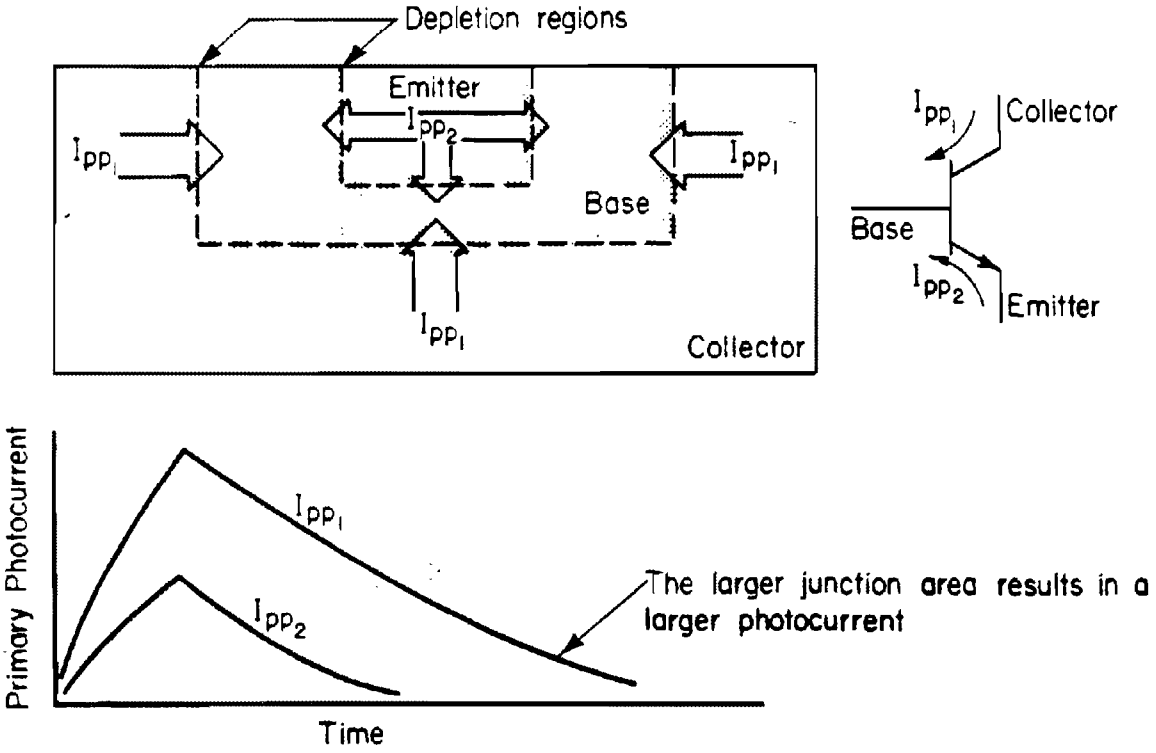

Figure 9-48. [redacted] NPN Transistor Illustrating the Primary Photocurrent [redacted]

current continues to flow until the excess charge stored in the base can either recombine with minority carriers or flow out through the external base lead.

The magnitude of the collector current pulse will depend on the dose rate if the radiation pulse is long compared to the lifetimes of the transistor base and collector, but it will depend on the total dose if the pulse is shorter than those lifetimes. This results from the charge transferred from the collector by the primary photocurrent being stored in the base region. Since many transistors have lifetimes that are as long as or longer than typical nuclear weapon radiation pulses. the prompt dose is quite often the most important factor.

A simplified linear approximation of the primary photocurrent in a transistor can be estimated with the following equation:

$$I_{PP} = \frac{\dot{D}}{CONST.} [t_s + 0.03],$$

where

$\dot{D}$ = the gamma ray exposure rate, R/s

$CONST.$ = 0.83×10^8 for NPN devices and 0.42×10^8 for PNP devices*

t_s = charge storage time (in μs) for the device of interest (t_s typically can vary from a few nanoseconds to hundreds of microseconds).

The duration of the photocurrent response depends on the radiation pulse width, the radiation storage time (which is different than the charge storage time (t_s)), and the time for holes and electrons to recombine. The radiation pulse width is determined by the weapon. The time for holes and electrons to recombine is illustrated for a diode in Figure 9-47, which applies generally for transistors. The radiation storage time, t_{sr}, is defined by Figure 9-49a. The radiation storage times for several dose rates are shown in Figure 9-49b. These latter curves are

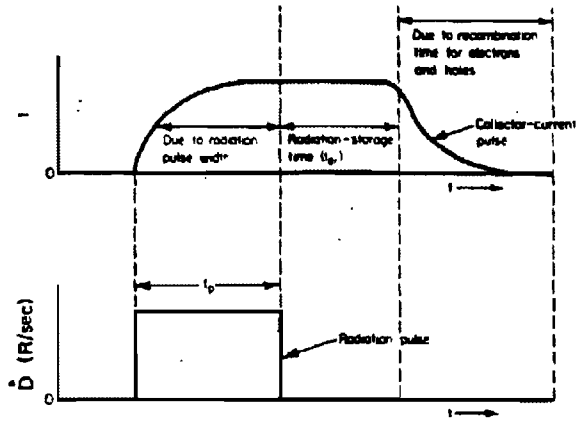

a. Definition of the Device Radiation-Response Times

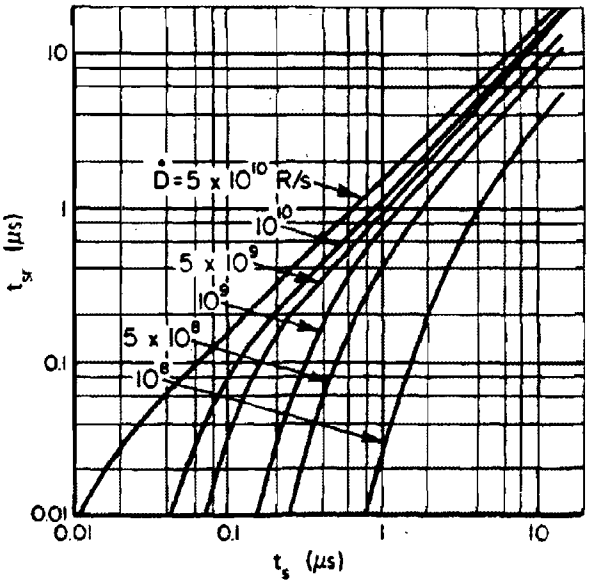

b. t_{sr} vs t_s Curves

Figure 9-49. Radiation Storage Time

*These equations only apply for the steady-state estimate of the primary photocurrent for silicon planar and mesa transistors with rated maximum continuous collector dissipation below 0.8 watt at 250C. More detailed information about prediction is available in the TREE Handbook (see bibliography).

[redacted]

[redacted] for a particular bias and radiation condition during storage. They are presented as being illustrative, and no attempt should be made to generalize from the curves. It is necessary to analyze a transistor or diode in the particular circuit configuration in which it is used to determine the threshold for circuit malfunction. As a result of the many different circuit configurations and bias conditions that can occur for transistors and diodes, failure thresholds that would be of value can not be specified generally for the TREE environment.

[redacted] A silicon controlled rectifier (SCR) is a solid state semiconductor device composed of four layers of alternate-impurity semiconductor material containing three PN junctions. The SCR is an active switching element that will remain in a nonconducting or "off" state until turned on or "fired" by a low-level control signal on the gate. It will then remain "on" without need for a sustaining control signal. The SCR is turned "off" by reducing its output (anode) current below the "dropout" level. Radiation induced currents, like those discussed for diodes and transistors, are a direct function of the junction areas, diffusion lengths, etc., and thus are difficult to predict since values for the parameters usually are not available. Since these currents, above a threshold, can induce changes in the state of an SCR, some method is required to predict the magnitude of the radiation induced currents, or, more specifically, the radiation threshold above which switching occurs.

[redacted] It has been found that the transient radiation switching thresholds (critical radiation exposure rate) for SCR's are functions of the radiation pulse width. The exposure rate required to trigger an SCR becomes constant for pulse widths longer than a critical value. This critical value is a function of the device minority carrier lifetime and the device delay "turn on" time. For pulse widths less than the critical value, the exposure rate required to trigger an SCR increases rapidly as the pulse width approaches zero. The dependence of the switching threshold of a 3A60A SCR on pulse widths and gamma ray exposure rate is shown in Figure 9-50. The critical pulse width for this device is approximately 2 microseconds.

[redacted] Typically the SCR type of device would not be expected to fire below 10^6 rads (Si)/sec. For most cases, however, the pulse width is sufficiently short that the devices are dose dependent. Failures occur typically at prompt doses between 0.1 and 1 rad (Si).

[redacted] Field-effect transistors (FET) are a family of unipolar devices that have pentode-like characteristics. The three major categories within this family are the junction FET, the metal-oxide insulated-gate FET (MOSFET), and the thin-film insulated-gate FET (TFT). The geometry and construction features of typical field-effect transistors are shown in Figure 9-51. The basic structure of the FET devices involves a source, a gate, and a drain in rough functional correspondence to the familiar cathode, grid, and plate of vacuum tube technology.

[redacted] The mechanisms by which radiation generates photocurrents in an FET are not substantially different from those for bipolar transistors and diodes. The important radiation parameters in an FET are the transient gate and drain-to-source currents. Possible sources of transient currents in FET's can be grouped into the following categories:

- Leakage currents across PN junctions that behave like PN junction photocurrents discussed previously.
- Direct modulation of the channel conductivity and mobility (usually applicable at high ($>10^8$ rads (Si)/s) dose rates).
- Leakage currents through the gate oxide layer (applicable to the metal oxide and thin-film FET's).
- Secondary emission (see Chapter 6) and atmosphere ionization currents.

[redacted]

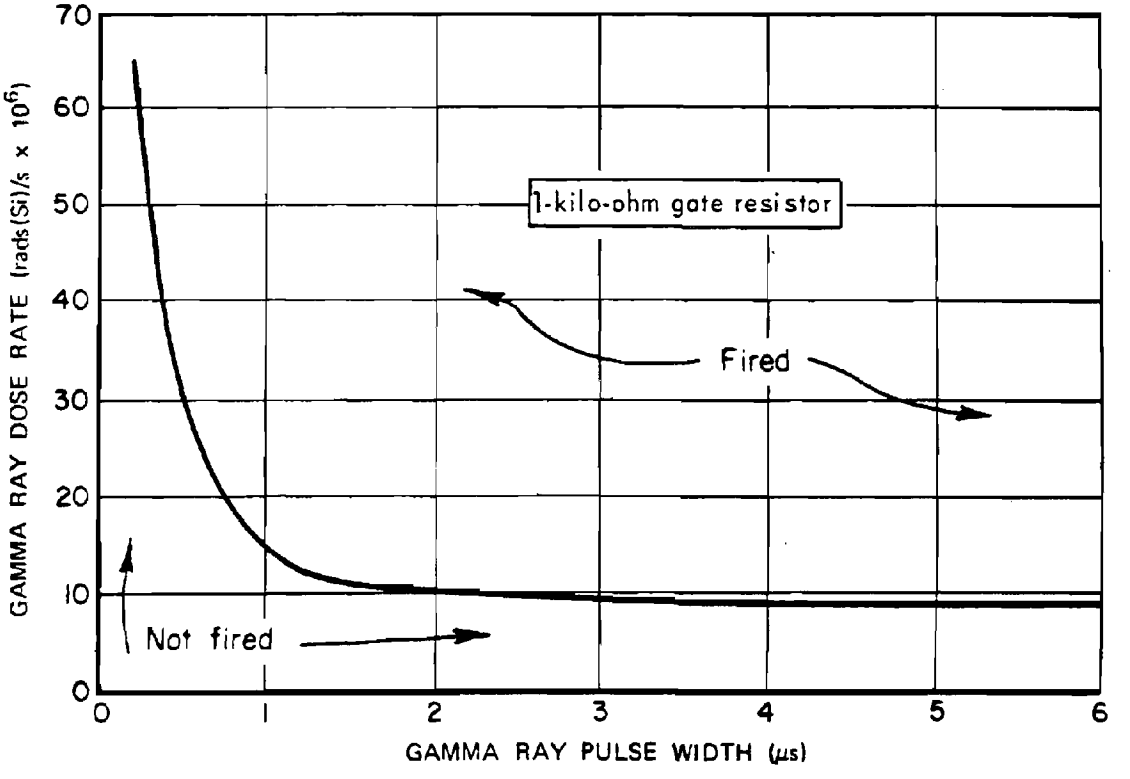

Figure 9-50. [redacted] Gamma Ray Exposure Rate as a Function of Pulse Width Switching Thresholds for a 3A60A SCR [redacted]

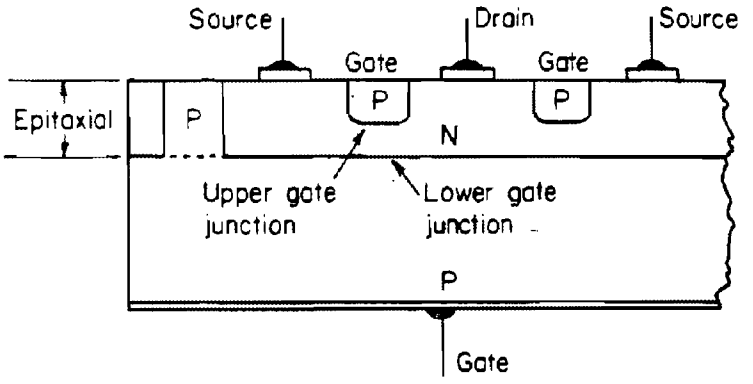

a Junction Field-Effect Transistor

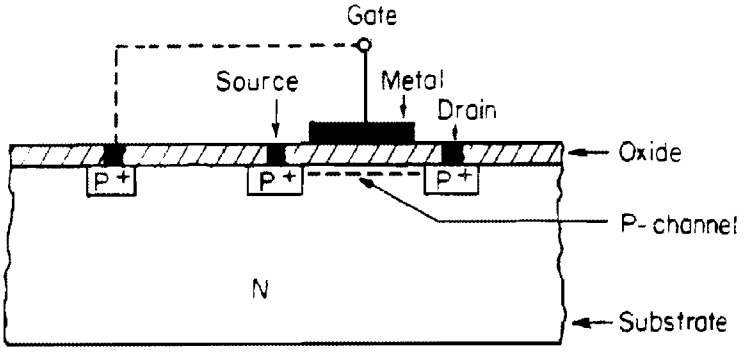

b MOS Field-Effect Transistor

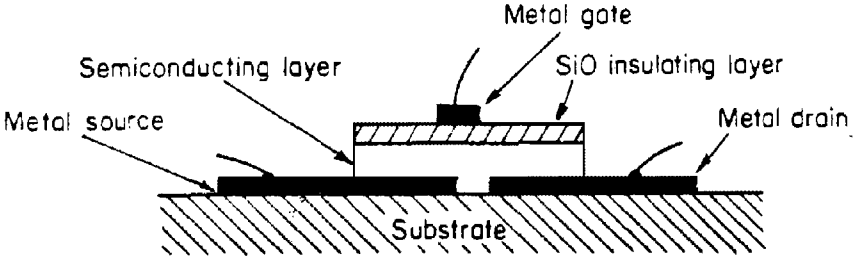

c. Thin-Film Field-Effect Transistor

Figure 9-51. Construction of Typical Junction, MOS, and Thin-Film Field-Effect Transistors

[redacted]

[redacted] Significant problems generally are not caused in field-effect transistors at dose rates below 10^6 rads (Si)/sec.

9-45 Permanent Effects [redacted]

[redacted] Permanent effects in semiconductor devices are those that can be attributed to physical property changes that result from the direct interaction of the radiation with the material of interest. These property changes typically last for periods that are long with respect to the recovery times of the components. These property changes occur in a very short time period and result in a rapid change in the operating characteristics of the device. A closely related effect is called rapid annealing, which is the process by which an initially large change in device parameters recovers very rapidly, approaching the smaller change observed several minutes after the radiation exposure.

[redacted] Most permanent effects in semiconductor devices subjected to a nuclear radiation pulse result from damage to the semiconductor material by energetic neutrons ($E > 10$ keV); however, the effects of gamma rays and secondary electrons must not be underestimated. In certain devices such as MOS field-effect transistors the effects of ionizing radiation can be the principal causes of permanent failure.

[redacted] Permanent effects can be grouped into two categories – bulk, and surface effects. Bulk effects are changes in the device characteristics that can result from damage to the bulk material. Surface effects are changes that are generally caused by radiation induced ionization near the surface of the device. Bulk damage effects from neutron radiation usually can be predicted within a factor of 2, while surface effects are generally unpredictable.

[redacted] Bulk effects result from electron, gamma ray, and neutron induced lattice displacements in the bulk of the material (see Chapter 6). Fast neutrons lose energy primarily by elastic collisions with the semiconductor atoms and cause large disordered clusters to be formed within the material. Gamma radiation loses energy by creating Compton electrons (see Section I, Chapter 5), which may cause lattice displacements. Since electrons have such a small mass, they primarily cause vacancy-interstitial pairs rather than clusters of defects that are typical of neutron damage. Lattice damage that results from gamma radiation usually is of secondary importance, unless a large gamma dose ($>10^5$ rads) is absorbed by the material.

[redacted] Lattice damage degrades the electrical characteristics of semiconductor devices by increasing the number of trapping, scattering, and recombination centers.

- The trapping centers remove carriers from the conduction process.
- The additional scattering centers reduce the mean free path of the free carriers. Since the mobility is directly proportional to the mean free path, radiation exposure reduces the mobility of charge carriers.
- The recombination centers decrease the minority carrier lifetime according to the relationship (see Chapter 6).

$$\frac{1}{\tau_\varphi} = \frac{1}{\tau_o} + K\varphi,$$

where

τ_φ = minority-carrier lifetime at fluence φ in seconds,

τ_o = initial minority-carrier lifetime (bulk lifetime), in seconds,

K = lifetime damage constant, cm^2/(neutron-seconds),

φ = fast neutron fluence, neutrons/cm^2.

[redacted] Permanent effects also can be caused by radiation induced changes in the semiconductor surface. The changes in the surface conditions

[redacted]

attributed to radiation that can cause permanent effects are surface charging mechanisms and changes in the surface recombination velocity. The most likely charging mechanisms are the collection of ions from a gas in the atmosphere surrounding the semiconductor device and the ejection of electrons from dielectric materials which are either deposited on the semiconductor surface or in which the device is encapsulated. These ions migrate under the influence of electric fields. As a result of the collection of these charges, inversion layers can form near the surface, causing large increases in leakage currents. In silicon devices these leakage currents result from recombination-generation in the enlarged depletion region.

[redacted] Ionizing radiation can cause changes in recombination velocity, which has deleterious effects on the effective lifetime according to the relation

$$\frac{1}{\tau_{eff}} = \frac{1}{\tau_{\varphi}} + \frac{1}{\tau_{surf}},$$

where

τ_{eff} = effective lifetime,

τ_{φ} = bulk lifetime,

τ_{surf} = surface lifetime (an inverse function of recombination velocity).

Surface effects usually are negligible compared to bulk lifetime damage for most conventional devices in a transient radiation environment. Field-effect devices, where radiation induced surface changes are the primary damage mechanisms, represent an important exception. [redacted] The general effects of nuclear radiation on semiconductor diodes are summarized below and are illustrated in Figure 9-52 and 9-53.

- The forward voltage of the diode at constant current normally will increase as a

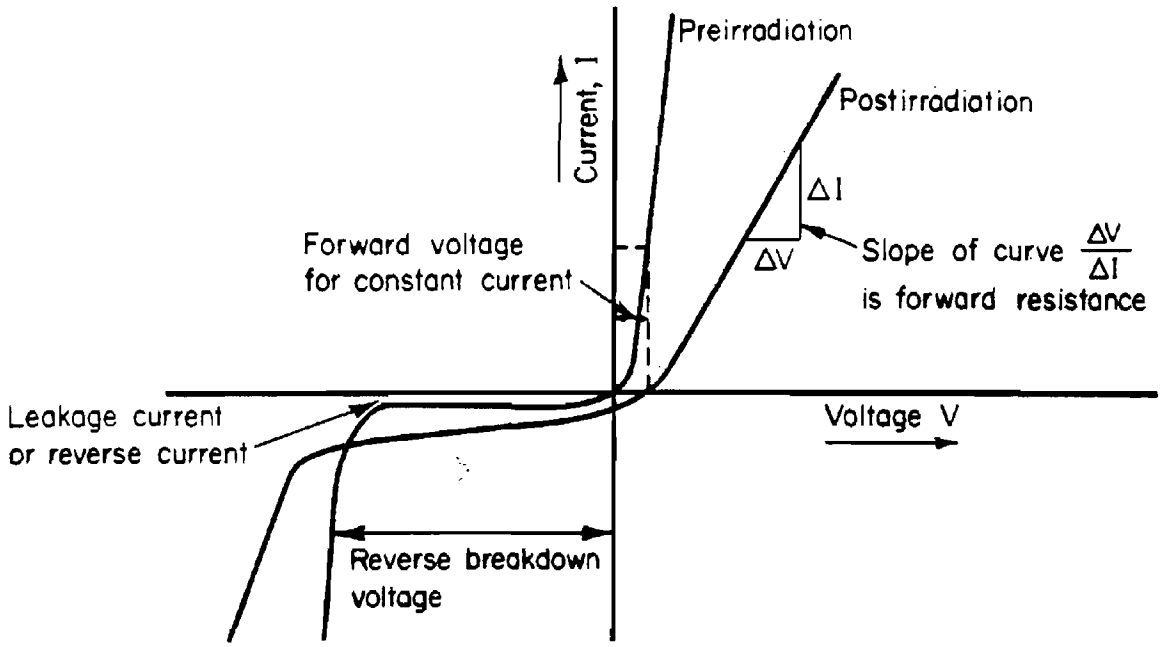

Figure 9-52. [redacted] An Illustrative Diode Characteristic for Pre- and Post-irradiation by Neutrons [redacted]

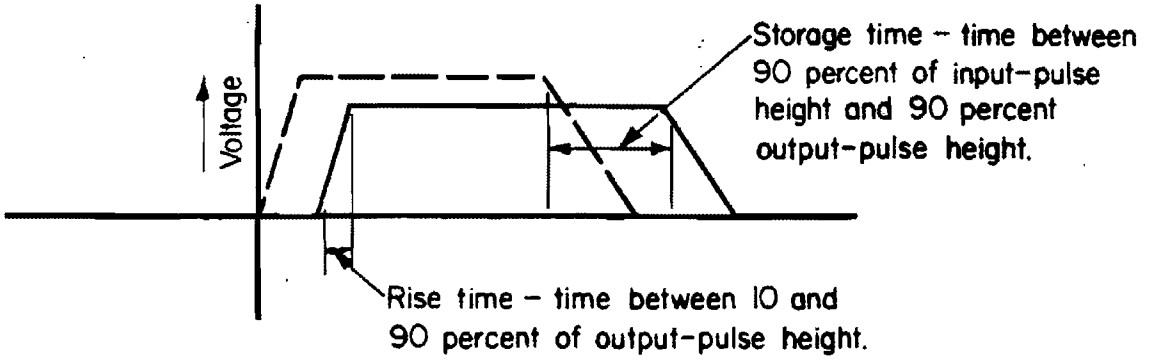
Voltage
Storage time – time between 90 percent of input-pulse height and 90 percent output-pulse height.
Rise time – time between 10 and 90 percent of output-pulse height.

Figure 9-53. An Illustration of Rise Time and Storage Time

result of changes in resistivity and mobility in the bulk material.

- The dynamic forward resistance will increase as a result of changes in resistivity and conductivity modulation.
- The surface effects and increases in carrier generation in the space-charge region will cause the reverse current to increase.
- The reverse breakdown voltage normally will increase because of an increase in resistivity.
- The switching characteristic of the diode generally will be changed. The rise time will increase, and the storage time will decrease as a result of lifetime damage.

Diodes generally are an order of magnitude more resistant to radiation than transistors of similar type. For this reason, theoretical and experimental studies have concentrated on transistors rather than diodes. Prediction techniques for diodes are complicated by the fact that the various bulk and surface damage mechanisms interact in an intricate manner. The wide variety of diode types, i.e., material, doping level and profile, geometry, etc., all tend to make comprehensive prediction schemes difficult and inaccurate. However, some quantitative trends in the changes in diode parameters can be given. The more important changes in diode characteristics, from a circuits point of view, are the increase in forward voltage at constant current and the increase of reverse leakage current. Changes in the dynamic forward resistance, breakdown voltage, and switching characteristics usually are of secondary importance.

The forward voltage at constant current generally starts to increase at a fluence of 10^{13} to 10^{14} n/cm^2 ($E > 10$ keV, fission), though some diodes exhibit changes at fluences as low as 10^{12} n/cm^2 ($E > 10$ keV, fission) while others show no change up to fluences as large as 10^{15} n/cm^2 ($E > 10$ keV, fission). Usually, fluences of about an order of magnitude greater than the fluences required to cause the initial change will double the forward voltage.

The reverse leakage current usually increases with exposure, but decreases also have been observed. Nominally, changes begin at fluences from 10^{13} to 10^{14} n/cm^2 ($E > 10$ keV, fission). Gamma ray doses as low as 5×10^4 rads (Si) have caused significant leakage currents. Germanium devices generally have larger changes in leakage current than silicon devices.

The changes in breakdown voltage are typically the largest for diodes with high breakdown voltage. Reference voltage diodes (zener

[redacted]

diodes) are relatively resistant to radiation with reference voltage changes less than 5 percent at 10^{15} n cm^2 ($E > 10$ keV, fission).

[redacted] The storage time is directly proportional to lifetime. Hence, the fluence at which the storage time will be reduced to one-half the preirradiation value will be

$$\varphi = \frac{1}{\tau_0 K},$$

where

τ_0 is the minority carrier lifetime.

K is the damage constant (see Chapter 6).

[redacted] Other diode types are specifically designed for rectifier application where high breakdown voltage and a low voltage drop are required even at high current. These diodes usually are designed with a PIN junction, which results in a device that is less sensitive to radiation than the standard type diodes.

[redacted] Selenium rectifiers and hot carrier diodes (metal semiconductor junction) appear to be more radiation resistant than either germanium or silicon diodes because of their material and structural differences. Reactor tests conducted on the HPA-2300 series hot carrier diodes confirm the relative radiation hardness of these devices. Most units tested remained within manufacturer's specifications at fluences of 3×10^{15} n/cm^2 ($E > 0.1$ MeV, fission) and 9×10^5 rads (Si).

[redacted] Diodes classified as "tunnel diodes" are easily recognized by their forward current characteristic, which shows a region of negative resistance. The effect of radiation on tunnel diodes is observable on the current-voltage (I-V) characteristic at fluences between 10^{15} and 10^{16} n/cm^2 ($E > 10$ keV, fission), and can be summarized as follows:

- The slope of the primary tunneling current is not changed; however, the peak current is slightly reduced as a result of the redistribution of the electrons in the defect states.
- The valley current at a given voltage increases due to the additional tunneling via defect states.
- For voltages larger than valley voltage, there is an increased current for a given voltage due to the excess current, which predominates over the diminishing normal diode current.

[redacted] Figures 9-54 and 9-55 show representative germanium and silicon tunnel diodes under neutron irradiation. The figures show that tunnel diodes are still operational at 5×10^{15} n/cm^2 ($E > 10$ keV, fission), which indicates the relative radiation hardness of these devices.

[redacted] The general effects of nuclear radiation on bipolar transistors can be summarized as follows:

- The current gain (amplification) of the transistor will be degraded as a result of lifetime damage to the bulk material. Degradation of gain will be greatest immed-

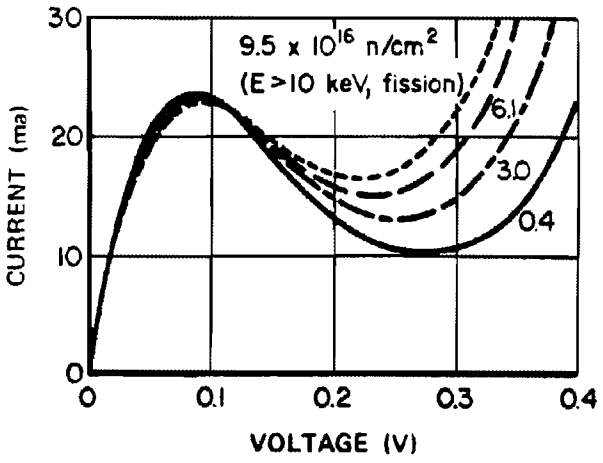

Figure 9-54. [redacted] Fast Neutron Bombardment Effect on Voltage-Current Characteristic of a Germanium Tunnel Diode [redacted]

[redacted]

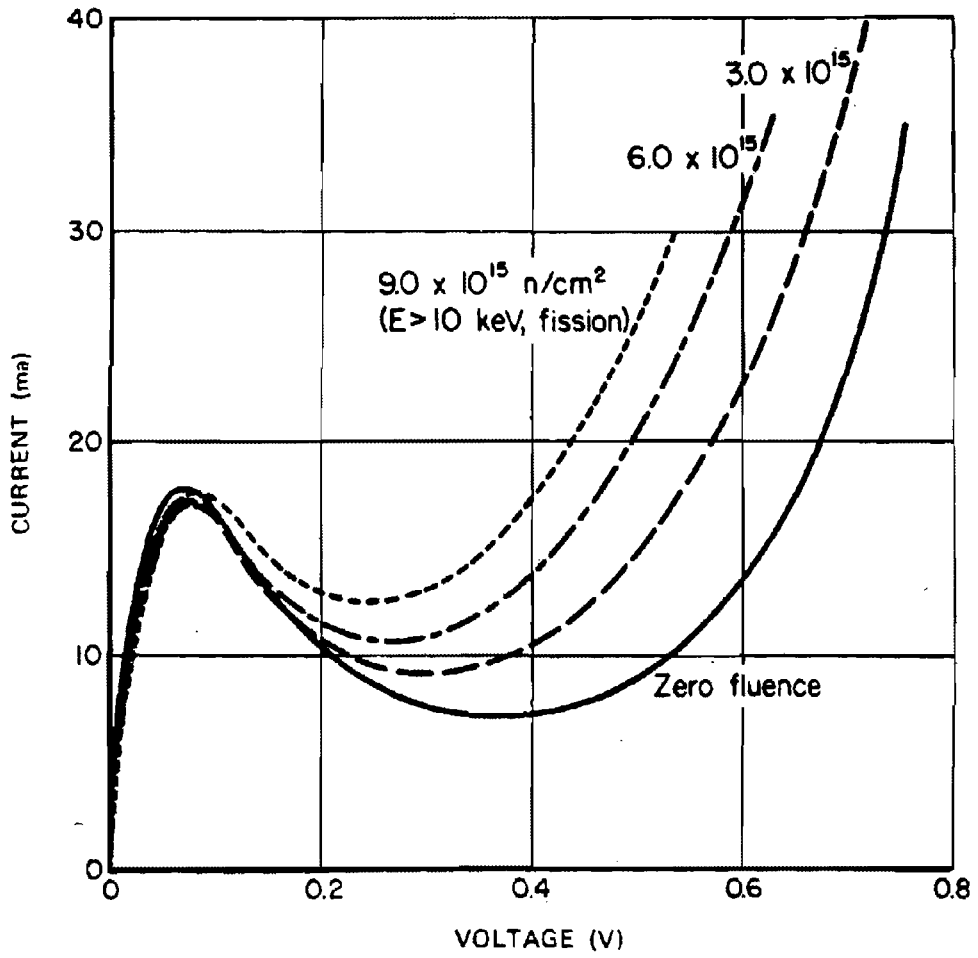

Figure 9-55. [redacted] Fast Neutron Bombardment Effect on Voltage-Current Characteristic of a Silicon Tunnel Diode [redacted]

iately following a burst of nuclear radiation, and the gain will recover rapidly to a quasi steady-state value. The annealing can go on for weeks, but usually the current gain recovery is small or negligible after the initial recovery.

- The reverse leakage current will increase as a result of surface effects and carrier generation in the space-charge region.
- Changes occur in the punch-through voltage, and the base-to-emitter and collector-to-base breakdown voltage as a result of changes in resistivity.
- Increases in base-spreading resistance, collector body resistance, and saturation voltage result from changes in resistivity and conductivity modulation.
- The switching characteristics also are changed slightly – exemplified by decreased storage time and increased turn-on time as a result of changes in lifetime and resistivity.

[redacted] Since transistors usually are the most vulnerable devices used in conventional circuits, predictions of circuit response under radiation conditions will be limited by the accuracy with which transistor behavior can be predicted. The reduction of current gain generally will limit the usefulness of the component before the other factors listed above become a serious problem. Therefore, emphasis is placed on the prediction of current gain degradation. However, in some applications saturation voltages and/or leakage currents across reverse biased junctions may be the limiting factors.

[redacted] The structure of a device is an important factor in determining its radiation resistance. A general rule is that the thinner base, higher frequency, and smaller junction area devices usually have better radiation resistance. For example, the diffused-junction devices usually offer a resistance to radiation about one order of magnitude better than that offered by the alloy-junction devices.

[redacted] Experimental data for conventional transistors in the form of generalized gain degradation curves are shown in Figure 9-56 for some common transistor types. The ratio β_φ/β_o represents the ratio of gain at some fast neutron fluence to the gain prior to irradiation. Figure 9-56 is representative of preliminary data from steady-state reactor experiments. The transistor types have been placed in their respective regions on the basis of where a majority of samples of a given type fell on the graph. Caution should be exercised in using and interpreting the information in the figure, since irradiation temperature, irradiation source, measurement conditions, etc. are not specified.

[redacted] A further word of caution should be injected concerning the interpretation of gain degradation data. A sharp decrease in β occurs during exposure and then rapidly anneals to a final value that is commonly measured. The time dependence of gain degradation can best be interpreted with the use of the annealing factor, F, defined as follows:

$$F(t) = \frac{\dfrac{1}{\beta_\varphi(t)} - \dfrac{1}{\beta_o}}{\dfrac{1}{\beta_\varphi(\infty)} - \dfrac{1}{\beta_o}} = \frac{K(t)}{K(\infty)} ,$$

where

$\beta_\varphi(t)$, $K(t)$ are gain and damage constants as a function of time after a fast burst of nuclear radiation.

$\beta_\varphi(\infty)$, $K(\infty)$ are the steady-state values of gain and damage constants.

[redacted] The magnitude and form of F varies with temperature, injection level, doping level, and impurity content. Typical values for the annealing factor at 1 msec range from approximately two to three for NPN transistors and

[redacted]

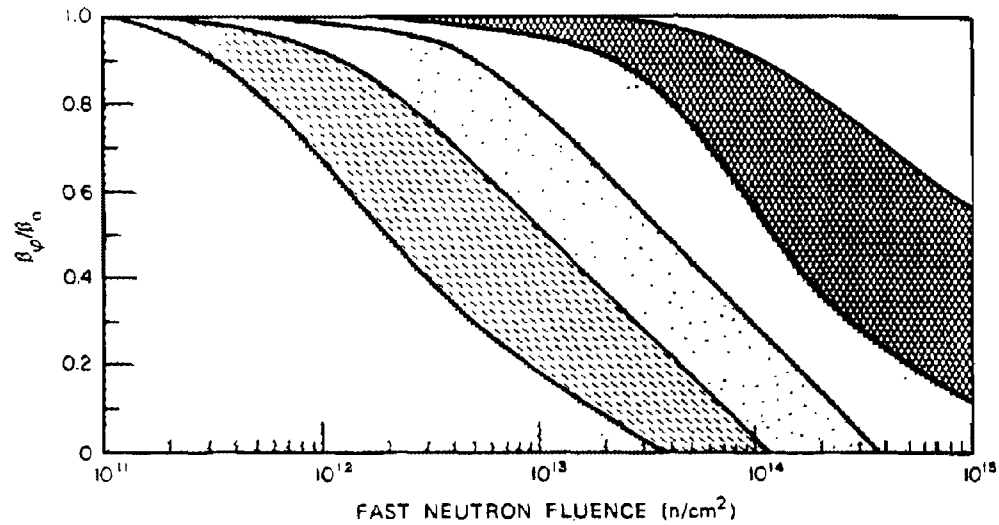

I	II	III		IV			V
2N329A	2N336	2N697	2N3244	2N404	2N2708	S-7241	2N700
2N1016E	2N699	2N708	2N3251	2N585	2N2784	S-7242	2N706B
2N1486	2N861	2N718	2N3252	2N705	2N2808	PT 2600	2N709
2N1653	2N917	2N720A	2N3300	2N706	2N2845	XF 805	2N797
2N1722	2N1016	2N722	2N3444	2N707A	2N2857	4907974	2N918
2N2187	2N1132	2N869	2N3486	2N708	2N2894		2N955A
2N2484	2N1184	2N910	2N3497	2N743	2N3013		2N964
	2N1613	2N1306	2N3499	2N744	2N3017		2N1195
	2N1711	2N1342	2N3509	2N834	2N3119		2N1709
	2N1900	2N1506	3TE240	2N835	2N3209		2N2537
	2N1936	2N1717	BR100A	2N914	2N3227		2N2616
	2N2187	2N1893	7900302	2N915	2N3252		2N2808
	2N2219	2N2192A	7900329	2N916	2N3287		2N3014
	2N2223	2N2193A		2N917	2N3303		2N3263
	2N2243A	2N2217		2N1306	2N3309		2N3287
	2N2297	2N2222		2N1307	2N3327		2N3309
	2N2411	2N2223		2N1506	2N3375		S-6781
	2N2878	2N2368		2N1709	2N3546		
	2N3072	2N2461		2N2218	2N3570		
	2N3439	2N2699		2N2369	2N3633		
	2N3499	2N2801		2N2538	2N3723		
	2N3501	2N2887		2N2540	FT 0040		
	2N3502	2N2907		2N2656			
	2N3637						

Figure 9-56. [redacted] Current Gain Degradation Characteristics for Some Common Transistor Types [redacted]

[redacted]

[redacted]

slightly smaller for PNP transistors. The annealing factor can be as high as 7 for low injection situations and immediately after turning on a device that was off during the neutron pulse.

[redacted] Other transistor parameters also can be degraded. Permanent increases occur in leakage currents across reverse-biased junctions. In general, the discussion of diode leakage is applicable to transistor leakage.

[redacted] Changes in breakdown voltages, punch-through voltage, and collector and emitter body resistances are negligible at fluences where the gain is still usable. The effects of nuclear radiation on these parameters can be analyzed from comments made about diodes.

[redacted] The changes in saturation voltage and in the switching time as a result of nuclear radiation are of interest for switching applications. In many cases the saturation voltage may appear to increase at relatively low levels of radiation, but actually the transistor is losing base drive and is coming out of saturation. The only significant increases in saturation voltage are seen at high collector currents. These increases, however, occur at high neutron fluences.

[redacted] The switching time of a transistor is referred to as the turn-on time and the turn-off time, which consist of the delay time, t_d, the rise time, t_r, the storage time, t_s, and the fall time, t_f. First-order theory indicates that, with the exception of the rise time, these parameters either remain relatively constant or decrease with radiation. Normally, the decreases are larger than the increases in these parameters; thus a net reduction of transistor switching time occurs with radiation, which usually is desirable. The largest changes occur in the storage time, which is proportional to the lifetime. Thus,

$$\varphi = \frac{1}{K\tau_0}$$

is the fluence at which the storage time is reduced by one half.

[redacted] The general effects of nuclear radiation on field-effect transistors can be summarized as follows:

- Changes occur in the threshold voltage, V_T. These changes in threshold voltage affect most of the field-effect transistor parameters.
- Increases in leakage current occur.
- Changes in channel resistivity and carrier mobility occur.

[redacted] Damage in MOS field-effect transistors is due primarily to ionizing radiation. For this reason damage is reported in terms of dose (in rads) or exposure (in Roentgens) rather than fluence (in n/cm^2). The most sensitive parameter to radiation in field-effect transistors is the threshold voltage, V_T. In general, degradation in V_T proceeds rapidly in the range of 10^3 and 10^4 rads (Si), but becomes more gradual above this dose. Complete failures, i.e., complete degradation in transconductance, have been observed at doses of 10^6 to 10^7 rads (Si).

[redacted] Considerable interest has been shown in the use of junction field-effect transistors (JFETS) in a radiation environment, since these are unipolar devices and do not depend on minority-carrier lifetime for operation. The primary effect of radiation on JFET's is the removal of carriers in the channel region. Radiation induced carrier removal is a strong function of resistivity. Thus, increased radiation tolerances is expected from JFET's with a high initial carrier concentration. The planar process has allowed heavily doped JFET's to be manufactured with the necessary control to make them commercially available. These heavily doped JFET's have demonstrated a very significant improvement in radiation hardness, e.g., approximately 15 percent degradation in transconductance after a neutron fluence of 7×10^{14} n/cm^2 ($E > 10$ keV, fission).

[redacted] Thin-film field-effect transistor (TFT) devices have been found to be more radiation

[redacted]

[redacted]

resistant than conventional field-effect transistors. Tests indicate that both the cadmium selenide and the silicon on sapphire type TFT's are operational at 10^6 rads (Si) or 10^{15} n/cm^2 ($E >$ 10 keV, fission).

The negative resistance characteristic of the unijunction transistor depends upon the conductivity modulation of a moderately high resistivity silicon bar by means of injected minority carriers from the rectifying emitter contact. This transistor is highly sensitive to radiation induced changes in minority-carrier lifetime and resistivity. Typical failure thresholds for unijunction transistors are of the order of 5×10^{11} to 5×10^{12} n/cm^2 ($E > 10$ keV, fission). The degradation is manifested by an increase in valley voltage, a decrease in valley current, and increases in the interbase and emitter-base resistances.

The three basic types of silicon PNPN devices are: the silicon-controlled rectifier, SCR; the silicon-controlled switch, SCS, and the Shockley diode. All of these devices may be considered to consist of overlapping NPN and PNP transistors, the primary difference being the external accessibility of the various layers; that is, the Shockley diode provides external access to only the outer P- and N-layers, the SCR has leads to all but the central N-region, and the SCS has leads to all four regions. The "two transistors" of the PNPN structure operate in a positive-feedback configuration, and the current-transfer ratios of the two sections add together for the composite device.

As previously discussed for transistors, radiation induced defects reduce the current gain for both "transistors" so that the required gate current, holding current, and breakover voltage should increase with radiation at fluences comparable to the bulk damage fluence levels in silicon transistors. Theoretical considerations of the mechanisms of PNPN device operation also indicate that excessive leakage currents will cause premature triggering of the devices. Hence, increases in surface and bulk leakage currents induced by radiation may cause the device to conduct continuously. This effect will depend upon the bias level applied in the application.

Since PNPN devices are used in medium- to high-power applications, they cannot be compared to high-frequency transistors in radiation resistance. Typical failure thresholds for PNPN devices range between 10^{12} and 5×10^{14} n/cm^2 ($E > 10$ keV, fission). Some narrow base PNPN devices have performed well at 10^{15} n/cm^2 ($E >$ 10 keV, fission).

9-46 Heating and Thermomechanical Damage

Any electronic component parts in which sufficient energy has been deposited by the electronic system environment will experience a transient rise in its temperature. The performance characteristics of most component parts are sensitive to temperature. Therefore, a temporary perturbation in the response of electronic component parts can be expected. The severity of the perturbation is a function of the deposited energy and the manner in which components are interconnected and mounted. Semiconductor devices are particularly vulnerable to temperature transients.

Fortunately, most of the common circuit design techniques for compensation for temperature rises are directly applicable to the circumvention of heating effects caused by the TREE environment. Consequently, heating effects seldom are emphasized, and other effects predominate. However, in some particularly sensitive components such as inertial-guidance devices, heating effects remain a serious problem.

The thermomechanical-shock effects arise from the deposition of short pulses of high intensity X-ray energy. The component part response differs from the effects discussed so far in that the primary manifestation is the loss of

[redacted]

[redacted]

mechanical integrity. The processes of spallation, blowoff, and delamination combine to produce mechanical damage. In most cases, this mechanical damage results in a permanent, catastrophic electrical failure of the component parts.

[redacted] All electronic components are potentially vulnerable to thermomechanical shock, but semiconductor devices are among the most vulnerable components. The failure modes for transistors exposed to X-rays depend on the materials and geometries employed in their construction. It is, therefore, worthwhile to consider device fabrication in some detail.

[redacted] Transistors are composed of a combination of materials, and the relationship of these materials to each is best illustrated in terms of the processes by which these devices are fabricated. Transistors are produced from single crystal semiconducting material, which is processed into regions of desired type and resistivity to form the junctions necessary for transistor action. The many techniques employed to achieve the required junction configurations include growing the desired material from suitably doped melts and alloying-in the dopant impurities from appropriately metallized surfaces. However, the most prevalent technology being used to fabricate silicon transistors is the so-called "planar" process in which the required dopants are allowed to diffuse through area-defining masks formed on the surface of the silicon. These masks are made of silicon dioxide, which (1) is thermally grown on the surface of the silicon, (2) may be etched to form windows for diffusion, and (3) is a natural barrier to the diffusion of phosphorous and boron (the most commonly employed dopants for producing N- and P-type silicon, respectively). The windows in the silicon dioxide are defined by photoetching techniques initially developed and employed in the fabrication of etched wiring boards and subsequently refined in resolution to permit application in the fabrication of semiconductor devices.

[redacted] Figure 9-57 shows the steps employed in the fabrication of a typical transistor by the planar process. The oxide layer grown in Step (a) is removed in a selected area by photoetching (Step b), and a P-type dopant is allowed to diffuse into the starting N-type silicon to form what will be the base region of the transistor (Step c). A new oxide is grown next (Step d) and is photoetched to form a window over a smaller area, and an N-type dopant in high concentration is allowed to diffuse into this portion of the P-type region (Step e), converting it to (N^+)-type silicon. This forms the emitter region of the transistor. Depth of penetration of the dopant materials is controlled by the times and temperatures at which the diffusion operations are conducted. A final oxide growth (Step f) and selective photoetching (Step g) expose the emitter and base contact points. The whole surface is subsequently coated with aluminum (Step h) and selectively etched to produce the desired current paths and land areas (tabs) for connection (Step i).

[redacted] Since transistors fabricated in the above manner usually are prepared in multiple arrays containing hundreds of identical devices, the next steps are the separation of the individual devices by some technique such as diamond scribing and the mounting of each of the resultant chips (or dice) into a separate package. Typical chips for high-frequency transistors are less than 0.025 x 0.025 in. in area.

[redacted] The transistor package can take many forms (see Figure 9-58a), but in each form there is usually a section of the package that contains the lead wires to which the emitter, base, and collector portions of the device must be connected. This section is called the header. In a typical package this is the bottom section of the can, which contains the three lead wires. A cap is attached to complete the package. The header usually is made of Kovar, a nickel-iron alloy frequently used for glass-to-metal seals because of their comparable thermal-expansion coefficients.

[redacted]

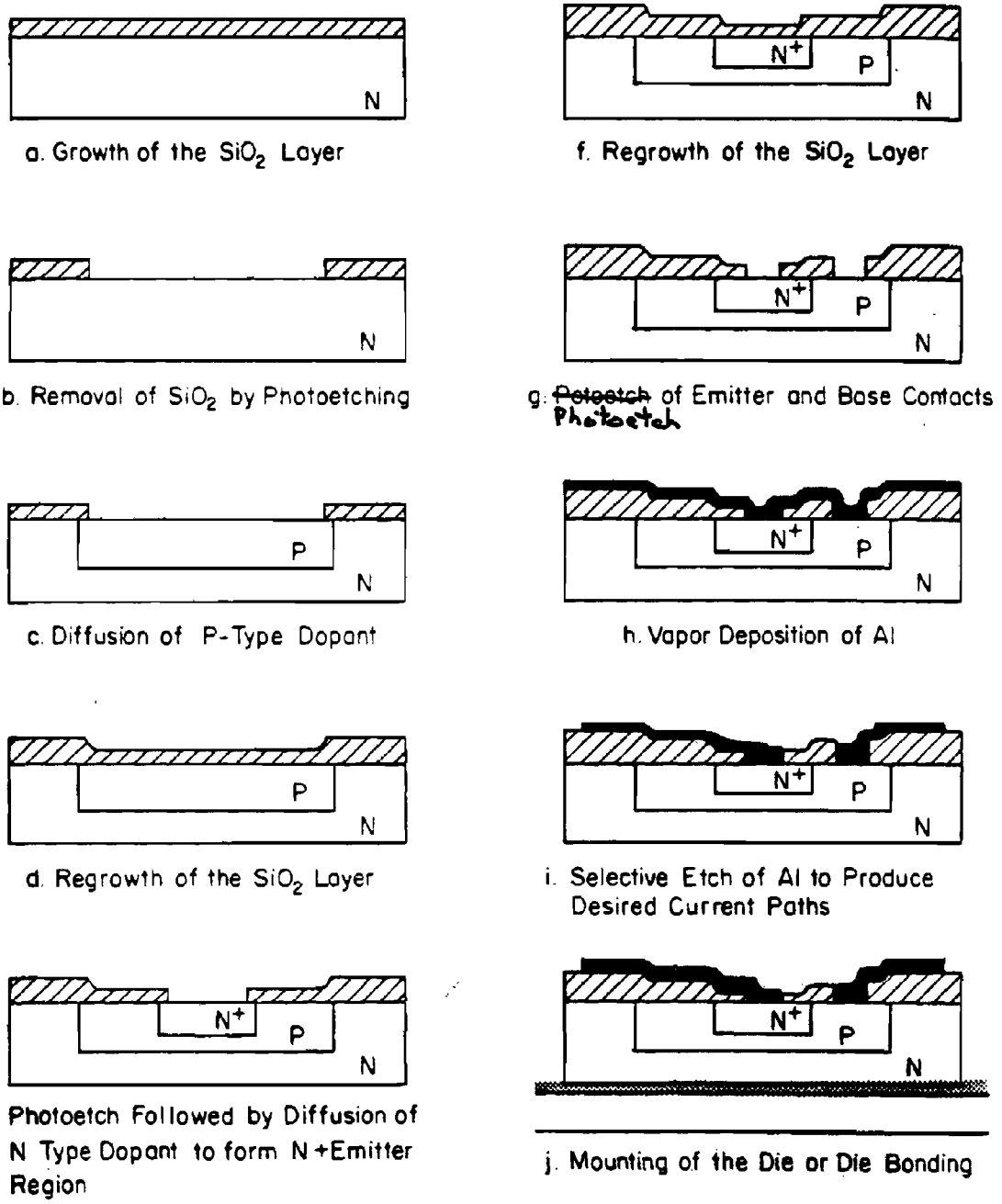

Figure 9-57. [redacted] Steps in the Fabrication of an NPN Silicon Planar Transistor [redacted]

[redacted]

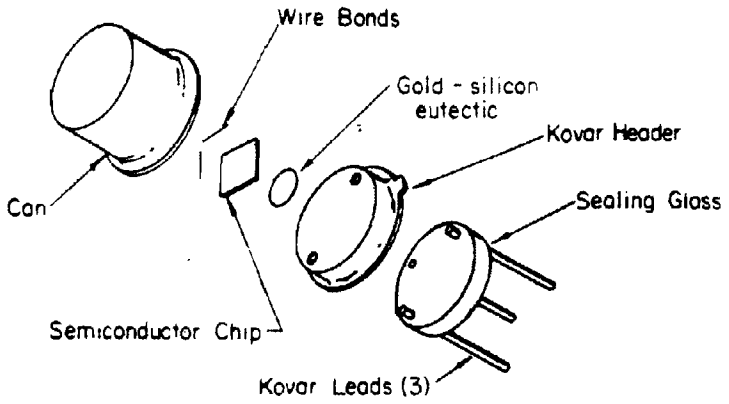

a) Transistor Package

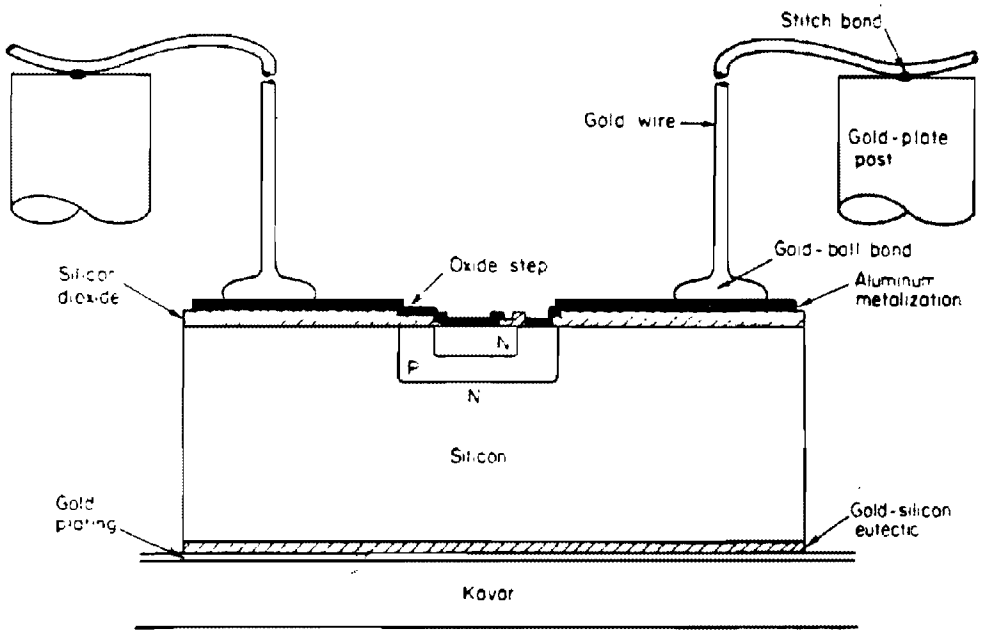

b) Cross-Sectional View of NPN Silicon Planar Transistor

Figure 9-58. Transistor Cross Section and Package

The three Kovar leadout wires are electrically insulated from each other by glass feed-throughs in the Kovar header. Since Kovar oxidizes easily, the external leads, and often the internal leads, on the transistor usually are plated to facilitate subsequent soldering or welding.

The processed semiconductor chip is attached to the header by a fabrication step known as die bonding. Die bonding involves soldering, brazing, or glazing the die to the header. This attachment serves as a mechanical contact, a thermal path, and in some cases (such as the example being employed) an electrical contact. When the connection is to a metal portion of the header, the attachment usually is accomplished by brazing using a eutectic brazing alloy (generally containing gold). This is superior to a soft solder because the high melting point of the eutectic permits use of higher temperatures in sealing the top on the header and in preconditioning the devices if desired. Some disadvantages in the use of eutectic alloys for die bonding are that they generally are expensive, quite brittle, difficult to form into unusual shapes, and they cannot be vacuum evaporated to form thin films. A preform of the eutectic alloy is placed on the header on a platform directly connected to the collector leadout wire. In many applications, a simple gold plating on the Kovar platform suffices as the preform, since on heating in contact with the silicon chip, a gold-silicon eutectic will form. Heat is applied (390°-400°C), the transistor chip is placed on the preform, and the eutectic is chilled with a jet of nitrogen. This operation attaches the chip to header and forms the chip-to-header bond (Step j, Figure 9-57).

Wire bonding makes electrical contact to the emitter and base regions. In some devices this connection is made by attaching the bridging wires directly to suitably metallized etched-open areas on the silicon chip. In many devices, however, these areas are much too small to permit forming quality connections, so the connections are made to extended tabs formed in the aluminum metallization on top of the silicon oxide. This latter configuration is illustrated in Figure 9-58b. The bridging wires, 1/2 to 3 mils in diameter, may be composed of any of a number of materials, but generally they are either gold or aluminum. Gold is used because it forms ohmic contact when alloyed with silicon, is available as extremely fine wire with reasonable strength, and may be bonded by thermocompression. Aluminum wire is used because it provides a one metal system when aluminum metallization is employed for extended tabs and avoids the formation of gold/aluminum alloys ("purple" and "white" plagues), it is available as fine wire, and it makes ohmic contact to both P-type and (N^+)-type silicon.

In thermocompression bonding, the two metals (such as the wire and the bonding pad) are made to seize without a third intermediate phase (such as solder) and without melting. This is accomplished with high pressures and temperatures. The high temperature keeps the metals in the annealing range as they flow into atomic intimacy under the bond. One form of thermocompression bonding (called ball bonding or nail-head bonding) employs gold wire that is heated at the tip with a hydrogen flame to form a ball, which is subsequently driven against the heated chip under pressure to form the bond and concurrently is flattened into a nailhead configuration. In stitch bonding (another form of thermocompression bonding), the wire is bent under pressure from the tool head and forced into the heated pad in such a way that the wire is wedged flat at the point of contact. Either gold or aluminum may be employed in stitch bonding. In ultrasonic bonding, ultrasonic energy is employed to force the two metals into atomic intimacy. The resultant bond resembles a stitch bond. These three bonding techniques are illustrated in Figures 9-59a, b, and c, respectively.

[redacted]

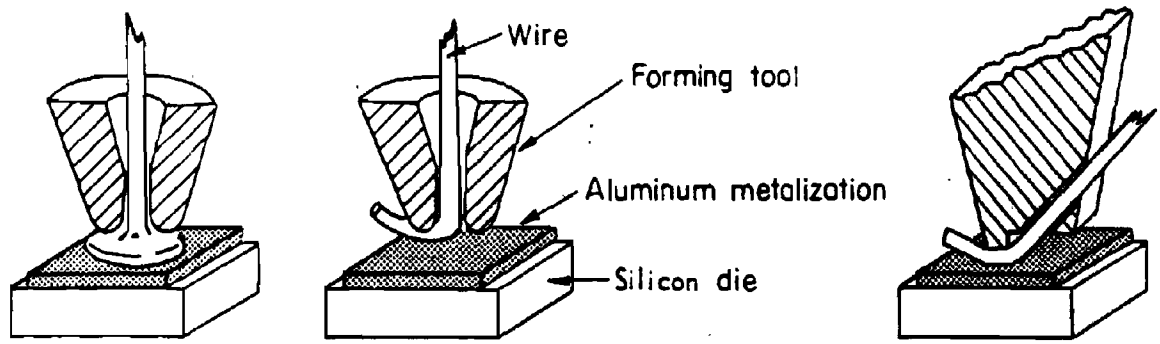

Figure 9-59. [redacted] Ball Stitch and Ultrasonic Bonding [redacted]

DNA (1-3)

[redacted]

Several general modes of failure (see Figure 9-60) are apparent: (a) the wires may break; (b) the emitter or base bonds may separate from the chip; (c) the silicon chip might fracture; (d) the chip may separate from the header; (e) the aluminum metallization constituting the extended tabs might become discontinuous; and (f) the wire bonds at the post may separate.

DNA (1-3)

[redacted]

[redacted]

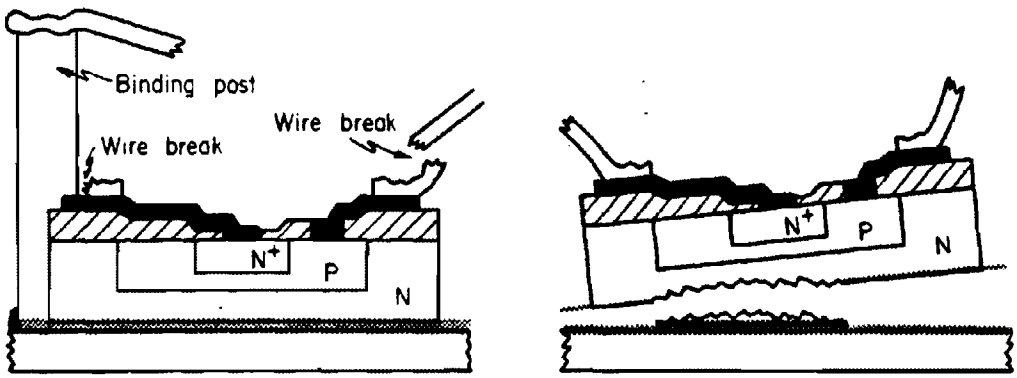

a. Wire Break

d. Chip Separated From Header

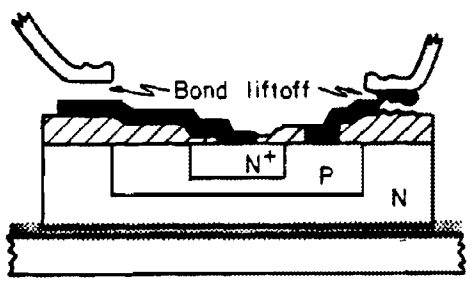

b. Bond Liftoff

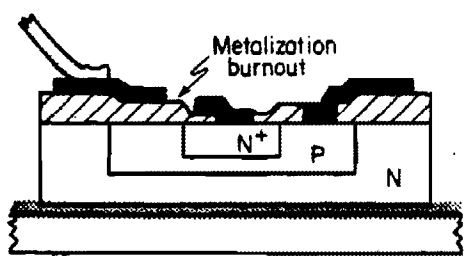

e. Metalization Burnout

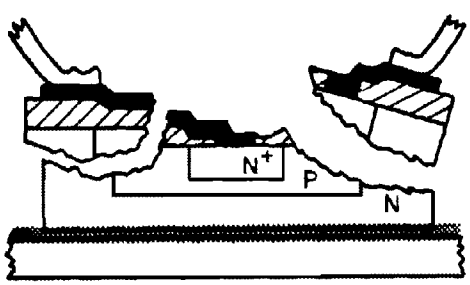

c. Chip Fracture

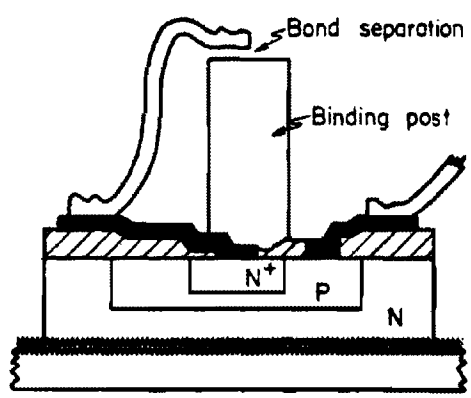

f. Bond-Binding Post Separation

Figure 9-60. [redacted] Semiconductor Failure Modes [redacted]

[redacted]

[redacted]

[redacted]

DNA (1)(3)

[redacted]

OTHER ELECTRONIC COMPONENT PARTS

9-47 Electron Tubes

[redacted] The electron tubes discussed in this subsection are divided into three categories: vacuum tubes, gas-filled tubes, and phototubes. These categories include nearly all types of conventional electron tubes with the exception of microwave tubes. Because of the known differences in interaction of nuclear radiation with metals, gases, and photoemissive materials, as well as with glasses and other ceramics, the observable effects of these interactions might be expected to differ for each category of tube.

[redacted] Permanent damage to vacuum tubes is associated with thermal and fast neutron exposure. No significant permanent damage has been observed in conventional vacuum tubes or Nuvistors exposed to test radiation pulses or to a thermal neutron fluence of less than 10^{13} n/cm^2 (fission). Moderate damage may occur in standard size glass or metal tubes at thermal neutron fluences from 10^{13} to 10^{16} n/cm^2 (fission), and severe damage may occur at fluences greater than 10^{16} n/cm^2 (fission). "Severe damage" is often the failure of the glass envelope, usually at a glass-to-metal seal; "moderate damage" is generally a permanent change in tube operating characteristics. Miniature, subminiature, and ceramic-type tubes are less subject to both moderate and permanent damage than standard size tubes, largely because of the smaller area and mass of the tube parts. However, thermal-neutron fluences sufficient to cause permanent damage to high-vacuum tubes are greater than neutron fluences expected to be encountered in the nuclear weapon environment, e.g., $>10^{16}$ n/cm^2 (fission).

[redacted] The principal transient effect that results from exposure of vacuum tubes, including the Nuvistor, to nuclear radiation is produced by Compton scattering of electrons from structural members by gamma rays. Leakage currents caused by ionization of air between external electrodes, or reduction of resistance of insulating materials such as glass, ceramics, and mica, caused by electron excitation within the material, may have minor effects on tube performance. There is no appreciable radiation induced liberation of gas from tube parts, or ionization of residual gases within the tube.

[redacted] Most of the Compton electrons produced in the structural parts of the tube and ejected into the evacuated region are too energetic to be influenced significantly by the electronic fields in the tube. However, the impact of

[redacted]

[redacted]

[redacted]

high energy electrons on the interior surfaces of the tube assembly produces low energy secondary electrons that can be influenced by the existing electric fields, and thus can alter the normal operating characteristics of the tube. The ejected electrons can be collected by one or more electrodes, depending upon the electrode potential and position. The magnitudes of the resulting transient voltages that appear at the respective electrodes depend on the magnitudes of the transient current and the circuit resistance. The grid circuit is particularly affected by this phenomenon, since it usually suffers a net loss of electrons and therefore may assume a positive charge. The resulting increase in plate current is determined largely by the grid resistance and the gain of the tube.

[redacted] Gas filled tubes (thyratrons), under extensive neutron bombardment, most likely will fail by breaking of the glass envelope or glass-to-metal seals. Such damage occurs at thermal neutron fluences exceeding 10^{16} n/cm^2 (fission).

[redacted] The principal transient effect in a thyratron subjected to a nuclear radiation pulse is spurious firing caused by ionization of the filling gas. The filling gas, in these cases xenon, becomes partially ionized, primarily by gamma rays. Additional ions are created by ion-neutral molecule collisions in the electric field between the plate and the grid. A positive ion sheath can form around the negatively-biased control grid, which will neutralize the grid charge and will permit electrons to be accelerated from the cathode space charge toward the plate. As ion density increases, a sustaining discharge ensues, which can be shut off only by removing the plate voltage.

[redacted] Phototubes are designed to exhibit peak sensitivities to electromagnetic radiation in the visible and near-infrared regions by choosing photosensitive cathodes with low work functions. The presence of photosensitive material in a vacuum tube introduces effects other than those found in receiving type electron tubes in a radiation field.

[redacted] Severe permanent damage to phototubes, as with other vacuum tubes, is attributable to large thermal neutron fluences. Severe damage starts in phototubes at about 10^{15} n/cm^2 (fission). However, moderate permanent damage may occur at thermal neutron fluences two orders of magnitude lower. Moderate damage in some cases is an increase in dark current, or a decrease in anode luminous sensitivity, but in most cases it is a darkening of the glass envelope. This darkening effectively reduces tube sensitivity. The glass discoloration has been observed at fast neutron fluences of 5.5×10^{12} ($E > 10$ keV, fission), and gamma ray doses of 6.3×10^6 rads (C). Thus, both gamma and neutron components of mixed radiation contribute to permanent damage.

[redacted] The principal transient effect in photomultiplier exposed to pulsed X-ray radiation (and presumably to gamma radiation) is an increase in anode current. The increase can be as much as the space-charge-limiting value for a given tube. Furthermore, the duration of the current increase is much greater than that of the radiation pulse. At first, the current increases as a result of currents initiated by luminescence of those areas of the glass envelope that are optically coupled to the cathode of the photomultiplier. This current increase also has been demonstrated in steady-state gamma fields. Glass luminesces at wavelengths and intensities determined by the glass composition and by the dose rate. Since a great deal of the radiant energy is in the visible portion of the light spectrum, where common photomultipliers are sensitive, it would be expected that the degree of photomultiplier response to X-ray and gamma radiation would depend upon both the type of glass used for the envelope and the spectral sensitivity of the cathode material.

[redacted]

[redacted]

[redacted] A second mechanism is required to explain the relatively slow decay of anode current after the radiation field is removed, since glass luminescence decays rapidly. It is believed that decay of anode current may be retarded by electric-field changes in the tube when electrical insulators become charged as a result of large initial current pulses.

DNA (C)(1)

[redacted]

9-48 Capacitors [redacted]

[redacted] Nuclear radiation affects most of the electronic properties of capacitors to some extent. Changes in the capacitance value, dissipation factor, and leakage resistance have been observed during steady-state reactor experiments. These effects generally are not considered severe for fast neutron fluences less than 10^{15} n/cm^2 ($E > 10$ keV, fission), and for most capacitors this limit is about 10^{17} n/cm^2 ($E > 10$ keV, fission).

[redacted] During a high-intensity pulse of nuclear radiation, the most pronounced effect in a capacitor is a transient change in the conductivity of the dielectric material with a corresponding increase in the leakage currents through the capacitor. The most recent concept of ionization effects in insulating and dielectric materials indicates that the ionizing particles create ionizing tracks in the irradiated material. This means that, microscopically, the material is not uniformly ionized (an exception to this occurs at very high dose rates, $\approx 10^{12}$ rads (Si)/sec, where there should be sufficient overlap of the ionized tracks for the material to be considered uniformly ionized).

[redacted] The excess conductivity induced in a material irradiated with a short pulse of ionizing radiation is generally classified in two components: the prompt component, and the delayed component. The prompt component is primarily the result of excess carrier concentration from direct ionization by the radiation and the concurrent recombination and trapping of these carriers. The delayed component is that component of conductivity that remains after the termination of the ionizing pulse. This does not mean to imply that it does not make a small contribution during the radiation pulse. The delayed component is the result of thermal generation of excess carriers from shallow traps, in which they are caught during the prompt pulse, and their concurrent loss to recombination and retrapping. The rate at which these carriers are thermally regenerated depends on the energy level of the trap site, the concentration of filled traps, and the temperature. As there is usually more than one energy level trap in a material, more than one regeneration rate usually is observed in the delayed component.

[redacted] The excess conductivity is proportional to the number of carriers available to drift under the influence of the applied electric field. However, the microscopic nonuniformity of the carrier concentration must be considered for the pulsed irradiation case. For irradiation with ionizing particles with a low specific ionization (the ratio of the number of ion pairs produced per unit path length to the number produced per unit path length by a minimum ionizing particle), the excess prompt conductivity will be the same as if these carriers were generated uniformly throughout the material. However, if the specific ionization is increased (by bombardment with more heavily ionizing particles), a point will be approached where the separation of ionization sites is less than the distance traveled by the electron before it has become thermalized and is able to drift under the influence of

[redacted]

the applied electric field. As this point is approached, the probability that the electron will be captured in the field of a neighboring ion increases, and the contribution to excess conductivity will be reduced. Thus, a plot of prompt conductivity as a function of specific ionization would show the prompt conductivity constant at low specific ionization and decreasing slowly after some threshold values of specific ionization is reached.

The rate at which carriers are lost concurrent with their generation by the ionizing radiation is proportional to the concentration of recombination centers and unfilled trapping centers. While an insignificant number of the total traps in the material might be filled at low doses, the concentration of filled traps within a track depends only on the specific ionization. Thus, the trapping rate is affected by the specific ionization. The result of this effect is to cause an increase in prompt conductivity with specific ionization, which would serve in part to compensate for the decreasing effect mentioned above. However, this effect on the carrier loss rate should be slight, since most of the carriers are lost to recombination rather than trapping.

When the radiation is delivered in a time short compared with the regeneration time of carriers from the traps, and the dose delivered in the pulse is large enough that significant numbers of tracks near the end of the pulse overlap tracks generated earlier, the concentration of filled traps in a track late in the pulse is different from that in a track created earlier in the pulse. When this occurs, the observed prompt conductivity becomes a function of the total dose delivered in the pulse, as well as of the specific ionization of the irradiating particle. It should be noted that a sufficient fraction of traps in a track must be filled to significantly affect the response. Hence, it is quite possible that trap densities in many insulators are high enough so that this condition is not realized in most pulse experiments.

The delayed conductivity component depends on the rates of carrier regeneration and retrapping from trap sites, which depend on the concentration of filled traps and the energy levels of the traps. The concentration of filled traps is a function of the specific ionization of the irradiating particle and, in the case of overlapping tracks, the total dose. As the initial concentration of filled traps within a track is usually a significant fraction of the total concentration of traps, the retrapping probability changes during the time the traps are emptying, thus altering the characteristic time for emptying the remainder of the filled traps. As a result, the decay of the delayed component does not usually follow a simple law. Only in certain cases, where the trapping probability is negligibly perturbed by the radiation, will simple exponential decays be observed.

Neutrons produce ionization by a number of collision processes that give rise to ionizing secondary particles. These processes include:

- Elastic scattering when the recoil atom receives sufficient energy to produce ionization.
- Inelastic scattering, producing a recoil atom that may or may not ionize but that emits a gamma photon that can produce a secondary ionization.
- Capture, resulting in the emission of a photon and/or an ionizing secondary particle (primarily thermal neutrons).
- Reactions resulting in an ionizing particle, e.g., (n,p), or (n,α) reactions (high-energy neutrons).

There are, therefore, many possible different specific ionizations associated with ionized tracks in neutron bombarded materials.

In hydrogenous materials, the principal ionization is caused by recoil protons, which have a high specific ionization. For this reason, neutron induced conductivity in hydrogenous dielectrics has been found to be approximately

[redacted]

one-fifth to one-half that of gamma ray induced conductivity for equal ionization energy deposition rates. For nonhydrogenous dielectrics, the most important contribution to neutron induced ionization is by the interactions of very high-energy neutrons ($E > 2$ MeV).

[redacted] A "polarization effect" that is attributed to space charge buildup within the dielectric material due to nonuniform trapping has been observed with some capacitors, particularly with Mylar, mica, polycarbonate, tantalum oxide and Vitamin Q devices. This effect is manifested in several ways. One is an apparent decrease in the induced conductance with sequential radiation pulsing. Charge transfer across the dielectric during a radiation pulse builds up a space charge field opposing the applied electric field. If the applied electric field is then removed, subsequent radiation pulses result in a current in the external circuit opposite in direction to that observed with the field applied. This is caused by the discharge of the space charge field. Similarly, if the electric field is reversed rather than removed after the space charge has been built up, the space charge field enhances the applied field, and a larger current results than would be observed normally.

[redacted] Saturation of the polarization effect, where no further decrease in the charge transfer is observed with subsequent radiation pulses, occurs after one or more pulses, depending on the capacitor and on the dose delivered in each pulse. Decreases of 50 to 70 percent for mica, 10 to 20 percent for tantalum oxide, and 30 percent for Mylar have been observed due to this space charge buildup during radiation pulsing.

[redacted]

9-49 Resistors [redacted]

[redacted] Radiation effects in resistors are generally small compared with effects in semiconductors and capacitors and are usually neglected. However, in circuits requiring high precision resistors transient effects may be significant at dose rates of as low as 10^7 rads (C)/sec and at neutron fluences of 10^{14} n/cm^2 ($E > 10$ keV, fission).

[redacted] The transient effects are generally attributed to gamma rays that interact with materials to produce electrons, primarily by the Compton process; however, energetic neutrons can also produce significant ionization. Transient effects include (1) a change in the effective resistance due to radiation induced leakage in the insulating material and the surrounding medium, (2) induced current that is the result of the difference between the emission and absorption of secondary electrons by the resistor materials, and (3) change in the conductivity in the bulk material of the resistor. There is no substantial evidence, however, that the third effect is a first-order transient effect.

[redacted] The permanent effects are generally caused by the displacement of atoms by neutrons, causing a change in the resistivity of the material.

[redacted]

9-50 Batteries and Cables

[redacted] Batteries are affected much less by radiation than other component parts. The effects of radiation on nickel-cadmium batteries appear to be insignificant at dose rates up to 10^7 rads (air)/sec. No radiation damage was apparent in a number of batteries and standard cells that were subjected to 10^{13} n/cm^2 ($E > 10$ keV, fission). Transient radiation effects on an ammonia fuze indicated that pulsed gamma ray irradiation of 10^8 rads (air)/sec had no effect on the operation of the battery.

[redacted]

[redacted]

[redacted] It has been recognized for some time that intense pulses of radiation produce significant perturbations in electrical cables and wiring, including coaxial and triaxial signal cables. Even with no voltage applied to a cable, a signal is seen when the cable is exposed to a pulsed radiation environment. The current associated with this signal is defined as a replacement current, since it is most likely a current in an external circuit that is necessary to replace electrons or other charged particles that are knocked out of their usual positions by the radiation. The replacement current definition also applies to the effect of charged carriers associated with the incident radiation embedded in a test sample.

[redacted] The magnitude of the radiation induced signal varies with the voltage applied to the cable. This voltage-dependent portion of the signal, i.e., the total signal exclusive of the replacement current, is called conduction current, thus it is ascribed to the conductivity induced in the insulating dielectric by the radiation. However, it may also contain major contributions from polarization or depolarization processes in the dielectric. These can usually be identified by their gradual disappearance (saturation) after repetitive exposures and by their reappearance in additional "shots" in which the applied voltage is changed greatly, e.g., removed or reversed.

[redacted] Ionizing radiation of any type produces free electrons that contribute to the conductivity of the material. Hence, insulators are expected to have a transient enhanced conductivity in an ionizing radiation environment. Conduction in the insulator is frequently characterized by two components: for very short radiation pulses, a prompt component whose magnitude is a function of only the instantaneous exposure rate, and frequently at the end of the short radiation exposure, a delayed component having approximately exponential decay.

[redacted] Although the replacement, conduction, and polarization currents are fairly well understood in terms of the interactions between the ionizing radiation and the metal-dielectric target system, it is not yet possible to predict quantitatively the response for a given cable in a specified environment. In a mixed neutron-gamma environment, the induced replacement current usually contains positive and negative components, and may therefore assume either polarity. The conduction current sometimes exhibits a rather complicated time dependence consisting of prompt- and delayed-conductivity contributions. The polarization current appears to be greatly affected by the properties of the metal-dielectric interface.

[redacted] Permanent damage effects in cables and wiring are manifested as changes in the physical and electrical properties of the insulating materials. When such damage becomes appreciable, e.g., when the insulation resistance is reduced severely, electrical characteristics may be affected. The extent of the damage to insulating materials is an increasing function of neutron fluence, exposure or dose, humidity, and irradiation temperature. Certain types of wire insulation are quite susceptible to permanent damage. For example, silicon rubber becomes severely cracked and powdered after approximately 2×10^{15} n/cm^2 ($E > 10$ keV, fission). The approximate damage thresholds for three common types of cable insulation are: polyethylene, 1×10^7 rads (C); Teflon TFE, 1×10^4 rads (C); and Teflon FEP, 2×10^6 rads (C). On the other hand, some irradiated polyolefins are capable of withstanding up to 5×10^9 rads (C). A considerable degree of annealing has been observed with respect to insulation resistance, which implies the possibility of adequate electrical serviceability after moderate physical damage.

[redacted] It is not expected that radiation effects on wiring with thin insulation will exhibit the strange behavior observed in coaxial cables. In particular, the very limited measurements that have been performed indicate that the replace-

[redacted]

[redacted]

ment current is primarily a function of the gamma environment. To a good approximation, it can be assumed that the replacement current for a wire or most other objects placed in the radiation environment will amount to the emission of a number of electrons between 1 and 5 x 10^{-3} times the number of gamma photons traversing the object.

[redacted] The conduction current is a very sensitive function of the amount of insulation around the wire and its immediate environment. For a bare wire in air with a ground plane nearby, conduction is due predominantly to the ionization produced in the air. Placing insulation around the wire reduces this conduction, but at the price of increasing the area of the wire and hence the effective replacement current.

9-51 Quartz Crystals [redacted]

[redacted] The radiation response of a quartz crystal oscillator is primarily a function of radiation dose. The type of material from which the oscillator is fabricated, e.g., natural quartz, Z-growth synthetic, Z-growth swept synthetic, etc., and to a lesser extent the type of cut, e.g., AT, BT, etc., and the frequency and mode of operation determine the sensitivity of the oscillator to the radiation. The primary effect of the radiation is a shift in the frequency of the oscillator. Both transient and steady-state shifts have been observed.

[redacted] The steady-state frequency offsets are a result of changes in the elastic stiffness constants of the crystal. For example, perturbations in the crystal bonds due to charge trapping at defects or to formation of new defect complexes will result in steady-state frequency offsets. Of materials tested to date, Z-growth swept-synthetic quartz has been the most radiation tolerant to steady-state frequency offsets. Swept natural quartz is slightly more sensitive and unswept natural quartz and unswept synthetic quartz, respectively, are even more sensitive. The response of a particular crystal also varies with the manner in which the crystal is mounted, the material used for the electrodes, and to a lesser extent differs for each quartz bar grown, even among bars grown under similar conditions. Both swept synthetic and natural quartz crystals can recover 80 percent to 90 percent of their original frequency change after annealing at 500°C for times on the order of 100 to 160 hours.

[redacted] Transient shifts in the frequency of an oscillator and reduction or cessation of the output result from energy deposition and any subsequent temperature rise in the crystal. Temperature gradients in the crystal due to faster removal of heat near the support wires and due to the electrodes absorbing more energy than the crystal, can give rise to frequency shifts induced by the resulting strain.

[redacted] Irradiation of general purpose crystal units has shown that they do not suffer significant permanent effects, within the limits of their stability, at a neutron fluence of 10^{13} n/cm^2 ($E > 10$ keV, fission) and a gamma dose of 4.4 x 10^3 rads (air). Transient phase and amplitude changes resulting from this environment are not of sufficient magnitude to cause concern about their operation under such conditions.

[redacted] Moderate precision crystal units display negligible frequency and amplitude changes when subjected to a reactor pulse. Weapon tests as well as steady-state gamma source tests indicate that a gamma dose greater than 10^4 rads (air) is required to induce significant permanent frequency changes in these devices. Frequency changes up to almost one part in 10^5 were observed after exposure to 7.5 x 10^4 rads (air) and 10^{12} n/cm^2 at a weapon test. The possibility that causes other than radiation contributed to the changes observed at this test cannot be excluded.

[redacted] High precision natural quartz-crystal units either stop oscillating or exhibit appreci-

[redacted]

[redacted]

able decreases in the amplitude of the output signal during nuclear pulses of approximately 10^{12} n/cm^2 ($E > 3$ MeV, fission), and 3 x 10^3 rads (H_2O). If oscillation stops, its cessation persists for minutes. The cessation of oscillation is apparently independent of the voltage, current, or power at which the units are being driven. Resumption of oscillation occurs at a reduced drive current and lower frequency. The drive current is tens of microamperes below the specified rated drive when oscillation resumes. Frequency changes as high as 1 part in 10^7 have been observed when this type of crystal was exposed to 7.9 x 10^{11} n/cm^2 ($E > 3$ MeV, fission), and 2.9 x 10^3 rads (H_2O).

DNA (4)(1)

[redacted]

9-52 Solder Joints

DNA (6)(1)

[redacted]

9-53 Infrared Detectors

[redacted] The infrared detectors that exhibit the greatest sensitivity to infrared radiation are also the most sensitive to nuclear radiation. For radiation pulses that are short compared to the relaxation time, the response of a photoconductive type of infrared detector cell is an excess conductance that is proportional to the radiation exposure. For long pulses the excess conductance is proportional to the radiation intensity and the carrier recombination time. Neutron bombardment causes permanent degradation of output-signal level and signal-to-noise ratio.

[redacted] Irradiation of a lead sulfide device to 1.3 x 10^{14} n/cm^2 ($E > 0.48$ eV, fission) at 134°F revealed a 67 percent reduction of output signal level and greater than 40 percent reduction in the signal-to-noise ratio. Damage was essentially catastrophic after 6.9 x 10^{15} n/cm^2 ($E > 0.48$ eV, fission).

[redacted] Lead selenide devices appear to be somewhat more tolerant to neutron irradiation than lead sulfide detectors. After a neutron fluence of 1.2 x 10^{14} n/cm^2 ($E > 0.48$ eV, fission) at 135°F, the output signal level of a lead selenide cell was reduced by 36 percent, and the signal-to-noise ratio was down more than 46 percent. The output level was down by 96 percent after 1.8 x 10^{16} n/cm^2 ($E > 0.48$ eV, fission). Lead selenide cells that are designed to operate at low temperatures are more sensitive to radiation than those that are not designed for low temperatures.

[redacted] Indium antimode photovoltaic cells that operate at liquid nitrogen temperature showed significant voltage signals at doses less than 0.88 rads (air). The cells exhibited radiation induced voltages roughly proportional to the logarithm of the dose when the radiation was delivered in short pulses. Recovery to within 2 percent of the maximum voltage occurred within 175 μsec after the highest intensity radiation pulses. A complete loss of output from these cells has been observed after a neutron fluence of 2 x 10^{16} n/cm^2 ($E > 0.48$ eV, fission).

[redacted] Thermistor-bolometer infrared detectors are the most neutron tolerant of the devices that have been tested. After 9.6 x 10^{13} n/cm^2 ($E >$

[redacted]

[redacted]

0.48 eV, fission), the output signal level was down by 28 percent, and the signal-to-noise ratio was down about 11 percent. After 1.6 x 10^{16} n/cm^2 ($E > 0.48$ eV, fission), the output level was down 57 percent, and the signal-to-noise ratio was down 66 percent. The detector may be usable for some applications under these conditions.

[redacted] Thermomechanical shock effects in infrared detectors will be similar to those discussed for semiconductor devices, and will occur at about the same levels.

[redacted] ELECTRONIC CIRCUITS [redacted]

9-54 Radiation Response of Discrete-Component-Part Circuits [redacted]

[redacted] Determination of the response of a circuit is complex because of the large variations in circuit configuration and in the component parts that can be used within a circuit configuration. Therefore, determining circuit response becomes a problem of detailed circuit analysis and/or testing. The radiation effects material necessary for this kind of analysis and testing are beyond the scope of this manual. Guidance may be obtained from the *TREE Handbook* and the *TREE Preferred Procedures* (see bibliography). General circuit effects and typical analysis techniques are discussed in this manual.

[redacted] The transient effects that can cause a system to malfunction can result in circuit responses that, like component-part responses, can be both dose and dose rate dependent. If the radiation pulses are short with respect to component-part recovery times the circuit time constants, the circuits will integrate the effects and will be sensitive to the total dose rather than the dose rate. However, when the pulse widths are wide, the circuits are dose rate sensitive. This can be illustrated by reference to Figure 9-61. Assume that for the circuit response plotted, the malfunction threshold is 1.5 volts. Therefore, a 0.15 μs pulse at 1 x 10^9 rad (Si)/sec will cause a malfunction. It is obvious from the curve that the malfunction dose rate is much lower for wider pulses.

[redacted] Discrete digital circuits and circuits that contain silicon controlled rectifiers (SCR's) have displayed failure at doses as low as 0.1 to 1.0 rad (Si) for short pulse widths. It is difficult to design a circuit specially that will not malfunction above a prompt dose of 100 rads (Si).

[redacted] Another effect that can result from the ionizing radiation is the initiation of a catastrophic action or catastrophic failure. An example would be the firing of a pyrotechnic device or the premature initiation of a firing signal. A second type of catastrophic action occurs if a circuit destroys itself as a result of the effects caused by ionization (burnout). Figure 9-62 shows an output stage of a power supply inverter. In normal operation, Q1 and Q2 are turned on alternately. The output at the transformer secondary is a square wave. Ionizing radiation may cause Q1 and Q2 to turn on simultaneously. After the radiation pulse, the transistors will recover to normal operation, and one of the transistors will attempt to turn off. At this time a large voltage will be induced across the transistor that is attempting to turn off. If this voltage exceeds the breakdown voltage, the transistor may be damaged.

[redacted] General statements applicable to both permanent and transient effects include:

- Circuits that use low frequency, thick base semiconductors usually are more susceptible to radiation effects than those circuits that contain high frequency, thin base devices
- Germanium devices generally will show larger photocurrents and leakage currents than comparable silicon devices
- High impedance circuitry generally will be more susceptible to radiation effects than low impedance circuitry

[redacted]

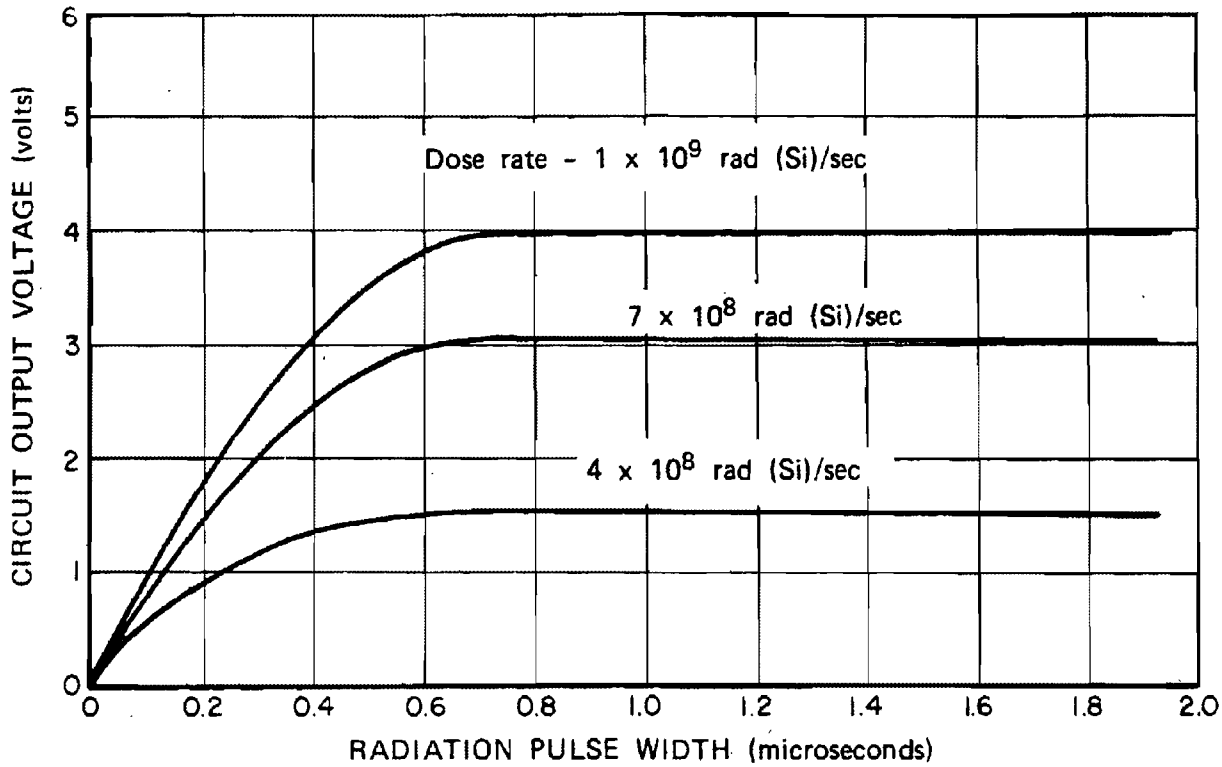

Figure 9-61. [redacted] Circuit Response as a Function of Radiation-Pulse Width [redacted]

[redacted]

- Magnetic memory devices will not be sensitive to the neutron and gamma environments typically specified as the environment in which an electronic system must survive.

[redacted] The primary permanent effects on circuits will be the degradation of semiconductor devices. The solid-state power supplies and regulators with their low frequency transistors will fail to perform their required function when exposed to fluence between 10^{11} and 10^{13} n/cm^2 ($E > 10$ keV, fission) depending on the circuit configuration, component parts, and design margins in the system. Circuits that use MOSFET can fail at gamma doses between 10^3 and 10^5 rads (Si).

[redacted] The failure threshold for thermomechanical shock will be established by the threshold of the component parts.

[redacted] It is desirable to have a method of analysis that can be used to predict the response of components, circuits, and systems. The analysis methods that are used consist of established techniques to calculate circuit and system responses by replacing radiation effects by their corresponding electrical effects. Thus, the problem that is solved eventually is wholly electrical in character. A major advantage of analysis as a simulation tool is that it is not necessary for a circuit or system to exist in a physical state before it can be analyzed. In addition, the analyst has control over the "environment," and it is theoretically possible to simulate the total

[redacted]

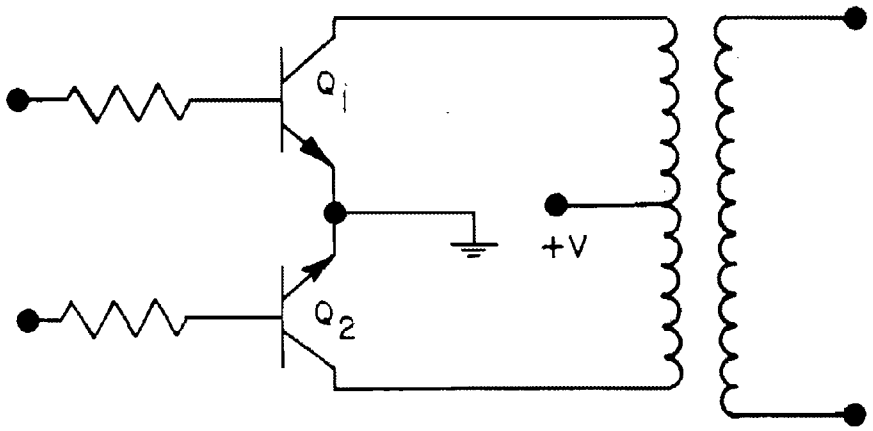

Figure 9-62. [redacted] Circuit in Which Burnout Could Occur [redacted]

[redacted] environment during a single (but complicated) analysis. Perhaps the major disadvantage of analysis (for TREE) is the relatively low confidence in the results. This low confidence level usually arises from the simplifying assumptions that are often made to expedite the analysis and which, themselves, are subject to verification, typically by environmental testing.

[redacted] Certain requirements or inputs are needed for any circuit or system analysis. First, an accurate mathematical description of the electrical characteristics must be obtained. Such a description usually is checked by comparing the computed electrical response to the measured electrical response of a circuit or system. Second, the radiation effects on electronic materials and devices must be represented, or modeled, by electrical effects. For example, displacement effects may be modeled by making transistor current gain a function of time. This step generally requires environmental testing and/or sound analytical procedures to obtain the required radiation effects data. Third, an analysis method must be employed to make an accurate calculation of the steady-state and transient responses of the electronic network of interest. This may be done by hand or with the aid of a computer.*

[redacted] Hand analysis techniques are useful for a quick qualitative and, to a limited degree, quantitative appraisal of the sensitivity of linear circuits and logic circuits to radiation environments. Manual techniques are valuable in the prediction of permanent effects of transient radiation, particularly when the relevant electrical parameters assume constant, degraded values after irradiation. The hand analysis techniques are often quite adequate to establish the initial estimate of radiation induced voltage and current transients and of the steady-state performance degradation. This type of analysis is suitable for a rough estimate of the peak-amplitude radiation response. In practice, only small, simple circuits can be handled.

[redacted] In doing analysis, there is an inevitable choice between time (man-hours) and accuracy. If great confidence in the results is not required (e.g., when the analysis results are to be used to

* [redacted] A more detailed discussion of hand and computer analysis techniques is contained in the "TREE Handbook" (see bibliography).

[redacted]

plan further environmental tests), a large number of simplifying assumptions can be made, and the analysis can be carried out quickly by hand.

If the results of an analysis are to be used directly in a survivability assessment, high accuracy is desirable. This implies that few simplifying assumptions may be made. If a circuit contains more than one or two active devices (e.g., transistors), the circuit model will be complex, and the speed and accuracy of a digital computer should be used. Both hand analysis and computer aided analysis require an equivalent-circuit model that represents electrical and radiation induced phenomena. A notable difference is that the computer can handle an equivalent circuit model in its entirety and can generate the desired response function without making engineering approximations.

Both analog and digital computers have been used for response predictions, and each has advantages and disadvantages; however, recently developed mathematical techniques and programming capabilities make the digital computer preferable for most problems. Several digital programs are available for circuit analysis. These are described in some detail in the "TREE Handbook" (see bibliography). These codes do not do the analysis. They do perform the tedious, error-prone calculations. The individual who uses them must provide the accurate description of the equivalent circuit model and must interpret the results.

Two factors control the accuracy of the results of any TREE analysis method. The first factor is the accuracy and completeness of the description of the response of individual components to a particular radiation environment. This information is basic to the success of any analysis technique and frequently has been the major stumbling block for analysis attempts.

The second factor that affects the accuracy of the analysis results is the assumptions that are made to simplify the analysis problem. Certain aspects of the radiation response of individual components generally are neglected by assuming that they will contribute only a small or negligible portion to the radiation response of the circuit. These assumptions are made on the basis of general experience with the radiation response of circuits and with knowledge of the limits over which they might be valid. Although these assumptions are generally correct, there are specific instances and specific circuit configurations for which they may not hold, and care must be taken in making such assumptions.

In practice most of the analysis approaches result in a fairly reasonable correlation with experimental results. However, it is common knowledge that any experimental result can be explained by a theory, but the theory will not always predict the correct result in a new situation. Therefore, caution should be exercised when accepting a component representation or an analysis technique that predicts the results for a pulsed reactor environment reasonably accurately, if these results are to be applied to a nuclear weapon environment. It is also possible that techniques applicable to switching circuits or nonlinear circuits will not apply to all linear circuit analysis.

9-55 Radiation Response of Integrated Circuits

Integrated circuits include many circuit types differing in construction materials and methods. The four construction types are the monolithic semiconductor, thin film, multichip, and hybrid integrated circuits. The scope of this section will be limited to monolithic and thin film circuits since the radiation response of both multichip and hybrid circuits can be inferred from the discussion of monolithic and film circuits or discrete devices. The discussion includes junction isolated, dielectrically isolated, and air isolated integrated circuits.

[redacted]

[redacted] In junction isolated circuits, the components are defined within a single crystalline substrate by regions of alternate doping that are electrically isolated by reverse biased PN-junction boundaries. The doped regions are formed by the geometrically controlled diffusion of appropriate impurities into the substrate. One or more uniformly doped, epitaxial layers may be grown upon the substrate prior to diffusion (planar epitaxial). The dielectric-isolated circuit is distinguished by the use of a dielectric (silicon dioxide or ceramic) instead of a PN-junction isolation between critical components. A single component or a small number of components are formed within individual single crystalline islands (called tubs) that are imbedded in a polycrystalline substrate. The active elements in both the junction and dielectric isolated circuits can be bipolar transistors, junction FET's, or insulated gate (MOS) FET's. The air isolated circuit usually employs aggregates of unipolar (i.e., field effect) transistors of metal-oxide-silicon construction.* Since this type of transistor may be used as a bias-dependent resistor, complete designs usually are constructed without the use of other circuit elements. Air isolated MOS integrated circuits are fabricated by growing silicon on sapphire (SOS). Portions of the silicon are etched away, leaving isolated islands of silicon upon which transistors are fabricated.

[redacted] Thin-film integrated circuits employ geometrically controlled surface films of conductive and dielectric materials upon a glass or ceramic substrate to define passive circuit elements and interconnections. The active elements may be formed as an integral part of the process (thin film, insulated gate, field effect transistors) or welded to the circuit (conventional, discrete transistors). Circuits of the latter type are referred to as hybrid thin film circuits.

[redacted] The categorization of circuit types given above is somewhat arbitrary. It is based on the present developments in the integrated circuit industry, rather than on strict lines of variance between the types. The categorization is used for convenience of discussion with respect to the effects of transient radiation, where distinctly different effects may occur. For example, the PN junction used for isolation is a source of photocurrents during an ionizing radiation pulse, and may result in large substrate (and hence, power-supply) currents in junction isolated monolithic circuits. This effect is absent in either the air or dielectric-isolated monolithic circuit or the thin film, hybrid circuit.

[redacted] Transient radiation may cause both transient, permanent and thermomechanical shock effects. On a qualitative basis, the primary electrical effects introduced in integrated circuits by transient radiation are similar to the effects described for conventional solid-state circuitry. The magnitude, duration, and electrical consequences of these effects, however, do not follow directly from conventional circuit experience.

[redacted] The effects of radiation on an integrated circuit are more closely related to its geometrical and physical characteristics than to its electrical function or circuit configuration. The proximity of circuit elements within the device, and in some cases its integral structure, make several modes of secondary interaction possible. This is especially important in the case of junction isolated integrated circuits.

[redacted] The transient effects observed in integrated circuits result from the generation of excess charge carriers that cause photocurrents and voltage changes. As previously described for transistors, the motion of excess carriers is governed by the response of carriers to electric fields and concentration gradients. The charge carriers will cause currents to occur until they

* [redacted] Air-isolated bipolar integrated circuits have also been constructed.

[redacted]

[redacted]

[redacted] are swept out by external fields and electron-hole recombination. The peak photocurrents can be a function of either dose rate or dose depending on the duration of the radiation pulse. As a result, if the radiation pulse is long compared to the circuit radiation response time, the microcircuit response is dose rate dependent. However, for radiation pulses that are short compared to the circuit radiation response time, microcircuit response will be dose dependent. Thus, the width of the radiation pulse can be of considerable significance, since the peak photocurrent generated can be a function of the duration of the pulse as well as its amplitude.

[redacted] In a transient-radiation environment, the semiconductor integrated circuit reacts to several mechanisms that have been discussed in connection with conventional circuitry. One point of departure that is made necessary by the monolithic nature of the circuit, is the significant and often predominant interelement effects that occur in addition to the intraelement effects. It is important to consider current paths between as well as within component parts of the microcircuit.

[redacted] Quite generally, the transient effects in any integrated electronic device are a consequence of a sequence of events that may be described as follows:

- The radiation interacts with the circuit material and surrounding encapsulant to introduce charge carriers and to establish a nonequilibrium charge distribution.
- Acting under nonequilibrium electric fields and concentration gradients, mobile carriers flow in the direction that restores equilibrium and thereby produce primary electrical currents. These electrical currents may be semiconductor-junction photocurrents, replacement currents, dielectric-leakage currents, gas-ionization currents, etc.
- The nonequilibrium charge distribution and the primary electrical currents may interact with the electrical circuit to produce secondary effects, e.g., secondary photocurrents. Under certain circumstances, the secondary effects may be sufficiently regenerative to be self-sustaining, and a new stable circuit state will result. In addition, localized electrical stresses may introduce permanent damage.
- The cumulative effects of the radiation induced currents and circuit action are voltage, current, and impedance changes of variable duration at the terminals of the integrated circuit.

[redacted] In junction isolated circuits, the predominant effect is PN-junction photocurrents resulting from ionization in the semiconductor material. Important secondary effects include secondary photocurrents produced by transistor action in any three adjacent doped regions, potentially large substrate currents, and "latchup."

[redacted] The predominant effect in dielectric isolated circuits is also PN-junction photocurrents. The major difference from other monolithic structures is the absence of the extra PN-junction between the components and the substrate and its associated photocurrent. Also, current paths are more restrictive.

[redacted] In air isolated integrated circuits, the important primary transient effects are PN-junction photocurrents, replacement currents resulting from charge scattered from device lead wires and the case, and ionization currents through the surrounding encapsulant. The predominant secondary effect is a secondary photocurrent resulting from the radiation induced gate current and transistor action. In addition, photocurrent is generated in the Zener diode employed for protection in the gate lead of MOS circuits.

[redacted] In MOS integrated circuits, the important primary transient effects are drain-substrate and source-substrate PN-junction photocurrents,

[redacted]

[redacted]

[redacted] replacement currents resulting from charge scattered from device lead wires and the case, and ionization currents through the surrounding encapsulant. The predominant secondary effect is a secondary drain current resulting from the radiation induced gate current. In addition, photocurrent is generated in the Zener diode employed for protection in the gate load.

[redacted] For the most part, thin film circuits may be treated as conventional circuits with extremely small geometries. Ionization currents within and between elements have specific importance, especially in the high-impedance circuitry associated with thin film circuits that employ field effect transistors. Nevertheless, in most cases of interest, the transistor is the predominant element that determines the transient radiation response of the circuit.

[redacted] Semiconductor integrated circuits of the planar-diffused (or planar-epitaxial) type experience transient effects that may be attributed to the interaction of the circuit elements through the active substrate. Two predominant interelement effects that must be considered are the presence of large substrate currents and the occurrence of latchup.

[redacted] In practice, the high packing density of elements on a substrate chip results in the presence of isolation diodes over most of the area of the chip. Thus, a chip 40 x 40-mils may have 1,500 mils^2 of effective isolation-diode area. The total substrate photocurrent may be 100 times that of a typical diode in the circuit. Since the substrate is connected to the power supply system, the substrate currents will be reflected in large currents appearing in the power supply leads. Radiation induced power supply currents of the order of 1 ampere, with durations of a few microseconds have been observed at prompt doses of approximately 10 rads (Si). The potential hazards to the power supply system, which must supply many such circuits, are evident.

[redacted] Present evidence indicates that the very large power supply currents occur primarily in those circuits where transistor action through the substrate is possible. In circuits of this type, radiation thresholds above which the current increases suddenly have been observed. The thresholds have been attributed to the turning on of an equivalent four layer device. Other possibilities include second breakdown and sustaining voltage breakdown.

[redacted] Transients induced in integrated circuits by pulsed ionizing radiation last from less than a microsecond in high speed digital circuits to several tens of microseconds in slower circuits. Occasionally, pulsed-radiation effects with considerably longer recovery times can be explained by circuit time constants. In the extreme case, the abnormal state persists until the dc power is interrupted. When this occurs, normal circuit operation is inhibited and latchup has occurred. In some cases, which are referred to as incipient latchup, the condition lasts only for periods that are long with respect to normal recovery times of the circuits. Latchup can be induced in three ways: by exposure to ionizing radiation; by particular sequences of applying voltage to circuits employing more than one power supply; and other electrical stimulations such as high voltage pulses. Only radiation induced latchup is considered here. Radiation induced latchup has been observed in only a small percentage of the device types that have been irradiated with pulsed ionizing radiation, and of these device types usually only a small percentage of the samples exhibit latchup. In a few cases, a majority of the samples of a certain part from a manufacturer of integrated circuit part types have exhibited latchup.

[redacted] Integrated circuit latchup is always caused by one or more normally reverse biased PN junctions becoming conductive, either by the initiation of a breakdown mechanism or by becoming forward biased. In either case, a sustain-

[redacted]

[redacted]

[redacted]

ing mechanism must act to maintain the breakdown or forward bias condition, once it has been initiated. Three latchup mechanisms have been postulated and observed in junction isolated integrated circuits. These are: PNPN action, second breakdown, and transistor sustaining voltage breakdown. No other mechanisms for sustaining latchup are known, although several others have been postulated.

[redacted] Latchup is normally associated with junction isolation since it usually involves some type of interaction with the silicon substrate through an isolating PN junction. Dielectric isolation is effective in isolating elements from one another and from the silicon substrate and, thus, is an important step in reducing the latchup vulnerability of integrated circuits. However, analyses of the structural characteristics of certain dielectric-isolated circuit types have indicated that the possibility of latchup cannot be ruled out in dielectric-isolated circuits. It is possible that some of the same mechanisms that are responsible for latchup in junction-isolated circuits also can exist in a dielectric-isolated circuit. These mechanisms include second breakdown, sustaining voltage breakdown of transistors and PNPN action if 4 layer structures are included within a dielectrically-isolated region.

[redacted] No latchup mechanisms have been found that are peculiar to dielectric isolation. While photocurrents can be generated in dielectric isolation, there are no sustaining mechanisms for these currents unless the isolation is defective or is subjected to destructively high voltages.

[redacted] Hybrid thin film circuits may be expected to be as tolerant of radiation as their conventional circuit counterparts. The radiation response is determined primarily by the active elements in the circuits.

[redacted] Undoubtedly, dielectric isolated circuits are much less vulnerable to latchup than are their junction isolated counterparts. However, dielectric isolated circuits probably are more latchup-prone than discrete component circuits because: dielectric isolated process limitations occasionally permit four layer structures; diffused resistors are present in some dielectric isolated circuits; and protective surface coatings occasionally are used in special purpose potting compounds or encapsulants, which might compromise the isolation. Component isolation in a dielectric isolated circuit, while much superior to that in a junction-isolated circuit, is still somewhat less complete than that in a discrete component circuit because of photocurrents through the dielectric.

[redacted] A large number of integrated circuits have been irradiated, but the testing has been concentrated on specific microcircuit types, and a broad base of experimental data on the response of microcircuits to radiation is not available. This lack of data is especially true for linear circuits. Representative radiation failure levels for some common digital junction-isolated types are shown in Table 9-23. The levels are listed either in terms of gamma dose or of dose rate, depending upon whether the circuit is normally dose or dose rate dependent. Design and production changes in integrated circuits are common in the industry. The broad ranges given reflect highly variable experimental results and indicate the necessity of considering each circuit as a separate problem.

[redacted] The proximity and intercoupling of elements do not assume importance in the production of permanent effects by nuclear radiation. Integrated circuits may be treated as conventional circuits of small dimensions. The primary factor that determines the tolerance of the circuits to radiation induced permanent effects is the degradation of the active elements with accumulated radiation exposure.

[redacted] Changes in the electrical parameters of diodes and transistors that result from radiation have been discussed. Experiments have shown that the circuits will experience failure when the

[redacted]

[redacted]

Table 9-23. [redacted] Representative Radiation-Failure Levels* for Digital Junction-Isolated Semiconductor Integrated Circuits [redacted]

Type†	Radiation-Failure Level
Large area, slow speed	5 -20 rads (Si)
Large area, moderate speed	10^6-10^7 rads (Si)/sec 20 -60 rads (Si)
Small area, moderate or high speed	10^7-10^9 rads (Si)/sec

* [redacted] Here, the "failure" level corresponds to exceeding the circuit's noise margin.

† [redacted] Type designations defined as follows: Large area - chip area > 5,000 mil^2. Small area - chip area < 5,000 mil^2, Slow speed - propagation delay > 100 nsec, Moderate speed - propagation delay between 25 and 100 nsec, High speed - propagation delay < 25 nsec.

[redacted] gain of the transistors has dropped to the point that they will no longer support proper circuit action. The radiation resistance of the circuits is determined by the stability of the gain of the transistor elements with respect to radiation exposure and the tolerance of the circuit design with respect to gain degradation. Although no class of integrated circuits has been shown to be inherently superior to another, those circuits employing faster transistors usually can withstand a greater neutron fluence. Epitaxial transistors usually, but not exclusively, represent the faster transistor types. Radiation failure levels have been shown to vary from 10^{12} to 10^{15} n/cm^2 ($E > 10$ keV, fission), with the faster circuit types at the high end. The normally conservative design and digital function of most integrated circuits accounts for the circuit longevity beyond what would be considered the minimum useful transistor gain point.

[redacted] The radiation induced circuit response of microcircuits is manifested by changes in both the dc and switching characteristics. The effect on the integrated circuit parameters of changes in components after irradiation will, of course, depend on the specific circuit configuration involved. Frequently, the radiation sensitivity of the circuit is determined by the tolerance of the circuit design with respect to gain degradation.

[redacted] The most radiation sensitive circuit parameter of digital gates and flip-flop circuits is the output low voltage. Circuit failures result when normally ON transistors leave saturation. The amount of current that an output transistor can sink is directly proportional to the current gain. The changes in the output transistor current gain are reflected directly in the current-drive capability (fan-out) of both digital gates and flip-flops.

[redacted] Changes resulting from radiation are observed for other digital-circuit parameters. The saturation voltage of transistors, V_{SAT}, increases with neutron fluence, even though sufficient base drive is supplied to maintain the transistor in saturation, as a result of an increase in the saturation resistance. These changes in saturation resistance usually are negligible at threshold fluences applicable for maximum fan-out. The input threshold voltage of gate circuits normally will increase with radiation exposure as a result of changes in the base-emitter voltage of the output transistor and increased diode forward voltage. Changes in this parameter, however, are not considered significant. Increases in leakage currents also have been observed with radiation exposure, but the changes in this parameter usually will not affect circuit performance.

[redacted] The switching characteristics of typical digital circuits also are affected by radiation.

[redacted]

[redacted]

[redacted]

The rise and fall times of the transistor elements of the microcircuit are increased and its storage time is decreased after neutron exposure. These effects combine, and usually a small net increase of switching time is observed.

[redacted] A good estimate of the radiation tolerance (at different fan-out conditions) of digital circuits can be made by measuring the output current-voltage characteristics. The gain degradation can be calculated, and the degraded characteristics can be plotted with the measured characteristic. An example prediction with experimental results is shown in Figure 9-63 for the RD 308 flip-flop.*

[redacted] Failure in MOS logic circuits results from changes in the threshold voltage of the transistors caused by ionizing radiation. Since a large, negative supply voltage permits greater degradation in threshold voltage before circuit failure occurs, the radiation failure threshold of MOS circuits depends on the maximum supply voltage rating. Experiments indicate that MOS digital microcircuits fail at radiation levels from 10^5 to 6 x 10^7 rads (Si) at manufacturer's rated supply voltages. Such an exposure can be associated with a neutron fluence of 1 to 2 x 10^{14} n/cm^2 ($E > 10$ keV, fission) for the mixed neutron-gamma flux of a typical fast-burst reactor. The characteristics of a particular MOS integrated circuit must be established with reasonable confidence before meaningful predictions can be made.

[redacted] As with digital circuits, the primary cause of linear-microcircuit failure is transistor gain degradation. The degradation of performance of a linear circuit is characterized by radiation induced changes in the transfer characteristics. In linear circuits, the functional dependence of the overall circuit performance on individual transistor elements can be determined only by a detailed circuit analysis. This analysis usually is frustrated by circuit complexity and the inability to measure individual microcircuit elements as a result of the lack of accessible terminals. Therefore, prediction of the performance of linear circuits under irradiation is difficult. The large variety of linear circuits precludes a discussion of each type; however, some general comments can be made concerning the performance of some devices.

[redacted] The radiation responses of both differential and operational amplifiers have been studied. A typical transfer characteristic of a differential amplifier is shown in Figure 9-64. The gain of the circuit began to decrease at a fluence of 3 x 10^{13} n/cm^2 ($E > 10$ keV, fission) and was degraded to roughly 50 percent of its initial value after an order-of-magnitude-larger fluence. These amplifiers were found to maintain their balance during irradiation significantly better than amplifiers made from discrete devices.

[redacted] The largest changes in operational amplifiers induced by radiation were observed in the open loop voltage gain and input bias current. The reduction in the open loop gain is a direct consequence of degradation of transistor gain. The use of lateral and substrate PNP transistors results in a relatively low radiation tolerance of these amplifiers compared to logic circuits. These PNP transistors are widebase units that are degraded at lower fluences than vertical NPN transistors. Changes in voltage gain begin to be observed (5 percent changes) at fluence levels near 10^3 n/cm^2 ($E > 0.1$ MeV, fission) for 709-type operational amplifiers. The neutron fluence where the voltage gain has decreased by 50 percent is about 8 x 10^{13} n/cm^2 ($E > 10$ keV, fission) for units with lateral and substrate transistors. Amplifiers that have eliminated lateral and substrate transistors show improved performance in the presence of radiation. The degradation in gain that is induced by radiation in operational amplifiers depends on the elec-

* [redacted] More details are given in the "TREE Handbook" (see bibliography).

[redacted]

[redacted]

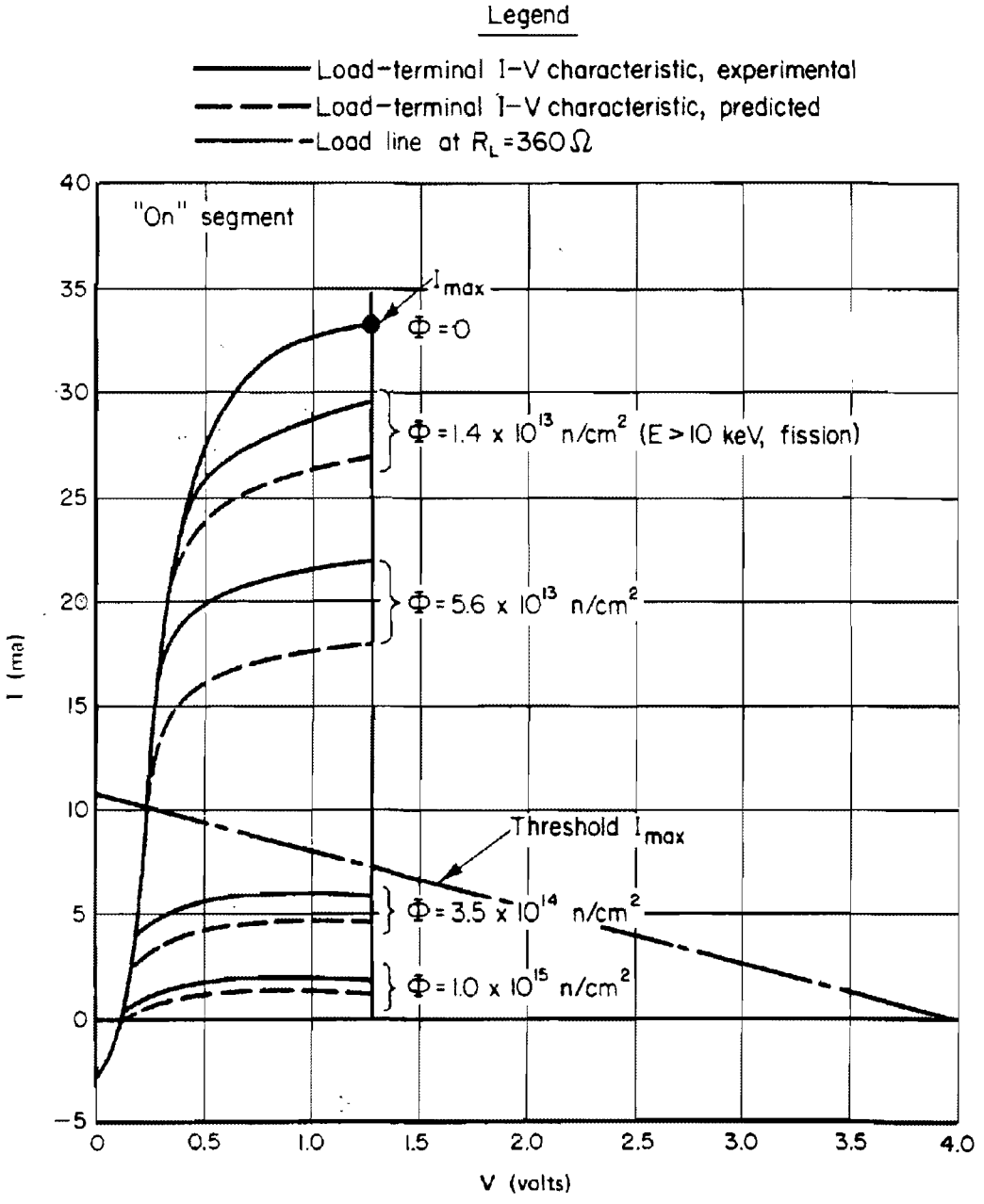

Figure 9-63. [redacted] Load-Terminal I-V Characteristic ("On" Segment) of RD 308 in Neutron Environment [redacted]

[redacted]

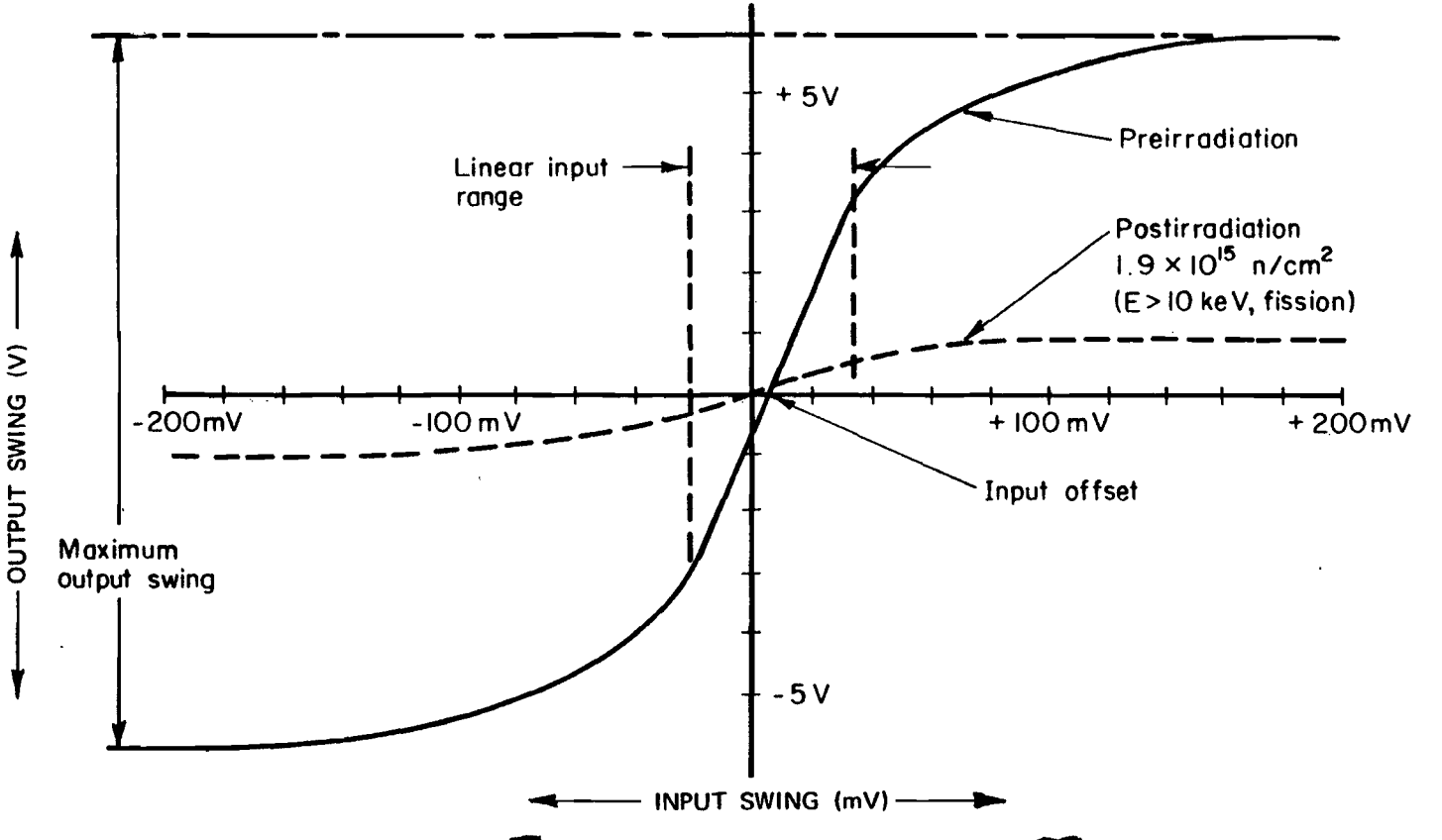

Figure 9-64. MC1525 Typical Transfer Characteristics

[redacted]

trical design. For example, it is important to determine whether the open-loop gain is determined by resistor ratios or by transistor gains. The changes in the input bias current can be correlated directly with changes in the common base current gain of the input transistors. It should be noted that the input transistors of operational amplifiers operate at very low currents (high input impedance), thus degradation of the base-transport factor is accompanied by degradation of the emitter efficiency as well. Factor-of-two increases in bias current have been observed for 709 amplifiers after 3×10^{13} n/cm^2 ($E > 10$ keV, fission). Offset voltage and offset current were found to increase after irradiation. These changes result from emitter-base-voltage and current-gain mismatches after irradiation. The changes in both current and voltage offsets were small at fluences where the gain and the bias current were degraded appreciably, which indicates the uniformity of active elements on the same chip.

[redacted] Even though a large number of integrated microcircuits have been tested, data on the effects of neutron irradiation on microcircuits are still sparse. This is especially true for the linear types of integrated circuits. Radiation experiments indicate that the failure threshold of digital microcircuits is fairly independent of the construction technique. For buffered circuits the failure threshold, at unity fan-out, is near 10^{15} n/cm^2 ($E > 10$ keV, fission), while it is somewhat lower for the nonbuffered circuit types; however, the failure level at rated fan-out (~10) usually occurs over an order of magnitude lower in fluence than the failure level at unity fan-out. Representative radiation failure levels for some common digital microcircuits are shown in Table 9-24. The failure level is specified when the output voltage of the test circuit

Table 9-24. [redacted] Failure Thresholds for Typical Digital Microcircuits [redacted]

Designation	Function	Construction	Failure Level, (n/cm^2)	
MC 201	DTL Gate	Junction Isolation	1.5×10^{15}*	1.2×10^{14}†
DT μL 932	DTL Gate	Junction Isolation	3.0×10^{15}	1.5×10^{14}
RD 209	DTL Gate	Oxide Isolation	3.0×10^{15}	1.5×10^{14}
MC 507	TTL Gate	Junction Isolation	0.8×10^{15}	0.8×10^{14}
SN 54932	TTL Gate	Junction Isolation	1.5×10^{15}	1.2×10^{14}
DT μL 945	DTL Flip-Flop	Junction Isolation	1.5×10^{15}	1.2×10^{14}
SE 124	DTL Flip-Flop	Junction Isolation	0.85×10^{15}	0.8×10^{14}
RD 208	DTL Flip-Flop	Oxide Isolation	0.85×10^{15}	0.8×10^{14}

*[redacted] Failure level at fan-out of 1; neutron fluence specified as ($E > 10$ keV, fission).
†[redacted] Failure level at fan-out of 10; neutron fluence specified as ($E > 10$ keV, fission).

[redacted]

[redacted]

exceeds the noise margin of the following circuit. Typical radiation failure levels for some linear circuits are shown in Table 9-25. Table 9-26 contains irradiation test results for some representative MOS integrated circuits. The failure level is specified as the point when the circuit would not operate or when the threshold voltage exceeded the supply voltage.

[redacted] The test results presented are only intended to provide a broad range of failure levels for order-of-magnitude reference purposes and should be treated with appropriate caution. It should be borne in mind that design and production changes in integrated circuits are common in industry. For this reason, each circuit should be considered a separate problem.

[redacted] The thermomechanical shock effects for all integrated circuit types are the same as those effects on discrete semiconductor parts. The only difference to consider is the increased number of bonds used in each device package, which increases the change of bond failure.

Table 9-25. [redacted] Failure Thresholds for Typical Linear Microcircuits [redacted]

Designation	Function	Construction	Failure Level* (n/cm^2)†
μA 709	Operational Amplifier	Junction Isolation	0.8×10^{14}
RA 909	Operational Amplifier	Oxide Isolation	0.8×10^{14}
Ph 709	Operational Amplifier	Oxide Isolation	3.0×10^{14}
MC 1709	Operational Amplifier	Oxide Isolation	3.0×10^{14}
MC 1525	Differential Amplifier	Junction Isolation	3.0×10^{14}
NM 1024	Differential Amplifier	Oxide Isolation	3.0×10^{14}
NM 1006	Differential Amplifier	Junction Isolation	4.0×10^{14}
RA 138	Amplifier	Oxide Isolation	1.5×10^{14}

[redacted] Failure level – gain degradation 50 percent.
† [redacted] Neutron fluence specified as ($E > 10$ keV, fission).

[redacted]

[redacted]

Table 9-26. [redacted] Failure Thresholds for Typical MOS Digital Microcircuits [redacted]

Designation	Function	Failure Level	
		Gamma, (rads (Si))	Neutron,* (n/cm^2)
SC 1171	NAND gate	2×10^5†	–
MEM 529	Binary element	1.4×10^5‡	–
SC 1171	Binary element	$1. \quad 10^5$‡	–
MEM 501	Shift register	$1. \times 10^5$§	–
MEM 590	Chopper	Not measured**	3×10^{14}
SC 1149	Flip-Flop	Not measured**	8×10^{14}
MC 1155	AND/OR gate	2×10^5 (Cobalt-60)††	
3300	25-bit static shift register	$>5 \times 10^3$ (FXR)‡‡ $>8 \times 10^4$ (TRIGA)‡‡	
3003	100-bit shift register	$>2 \times 10^4$ (FXR)‡‡ $>5 \times 10^4$ (TRIGA)‡‡	
1406	100-bit shift register	$>10^5$ (FXR)‡‡ $<2.5 \times 10^4$ (TRIGA)	
1101	256-random access memory	4×10^4 (FXR) 2×10^4 (TRIGA)	3×10^{11}

* [redacted] Neutron fluence specified as (E > 10 keV, fission).
† [redacted] Supply voltage – 20 volts.
‡ [redacted] Supply voltage – 15 volts.
§ [redacted] Clock voltage – 10 volts.
** [redacted] Supply voltage – 10 volts.
†† [redacted] Type of facility in which test was performed.
‡‡ [redacted] No failures at these levels.

[redacted]

SECTION VIII

ELECTROMAGNETIC PULSE (EMP) DAMAGE MECHANISMS

As described in Chapter 7, the nuclear electromagnetic pulse (EMP) is part of a complex environment produced by a nuclear environment. The EMP contains only a very small part of the total energy produced by a nuclear explosion; however, under the proper circumstances, EMP is capable of causing severe disruption and sometimes damage to electrical and electronic systems at distances where all other effects are absent.

As with the EMP generation described in Chapter 7, the complexity of the calculation of EMP damage mechanisms requires that heavy reliance be placed on computer code calculations for specific problems, and even these calculations must be supplemented by testing in most cases. Consequently, the information presented herein is largely qualitative and will only serve as an introduction to the subject. More complete treatments of EMP damage mechanisms may be found in the "DNA EMP (Electromagnetic Pulse) Handbook" (see bibliography).

Figure 7-18, Chapter 7, provides a matrix that provides some indication of whether EMP constitutes a threat in a given situation relative to the hardness of a system to blast overpressure. This section provides a brief description of EMP energy coupling, component damage, EMP hardening, and testing.

ENERGY COUPLING

9-56 Basic Coupling Modes

There are three basic modes of coupling the energy contained in an electromagnetic wave into the conductors that make up an electric or electronic system: electric induction, magnetic induction, and resistive coupling.

Electric induction arises as the charges in a conductor move under the influence of the tangential component of an impinging electric field. The overall result is that of a voltage source distribution along the conductor. One such point-voltage source is shown in Figure 9-65 for a simple conducting wire, where the current I is produced as a result of the tangential component $E_{i\ tan}$ of the incident electric field $\bar{E}_i$.

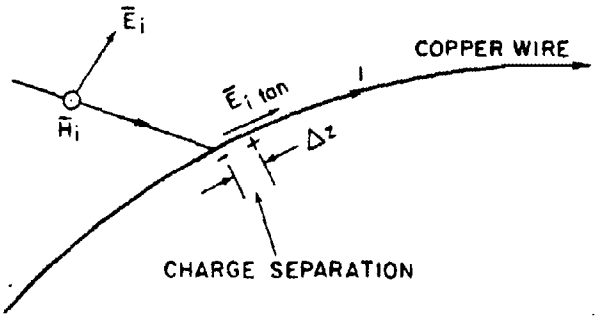

Figure 9-65. Electric Induction in a Copper Wire

Magnetic induction occurs in conductors shaped to form a closed loop when the component of the impinging magnetic field perpendicular to the plane of the loop varies in time, causing charges to flow in the loop. This effect is illustrated in Figure 9-66 for a simple wire loop. Here the magnetic field is shown coming out of the plane of the loop. The loop need not be circular, and magnetic induction may occur with any set of conducting components assembled so as to form a loop.

Resistive coupling comes about indirectly as a conductor that is immersed in a conducting medium, such as ionized air or the ground, is influenced by the currents induced in the medium by the other coupling modes. In effect the conductor shares part of the current as an alternate conducting path. This effect is illustrated in Figure 9-67 for the simple case of a

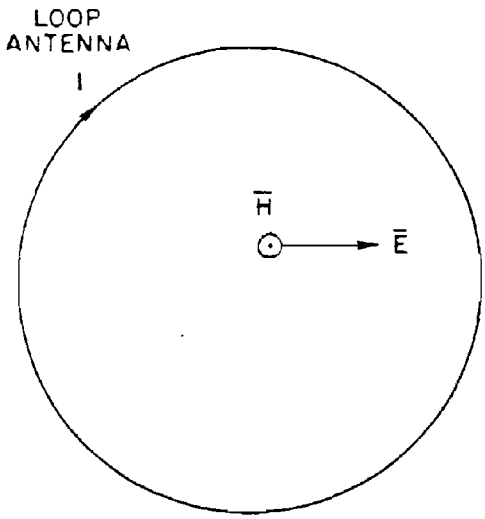

Figure 9-66. [redacted] Magnetic Induction in a Simple Loop [redacted]

[redacted]

conductor immersed in the ground. The tangential component of the incident electric field $\bar{E}_i$ induces a current density $\bar{J}$ in the ground. A distributed voltage drop appears along the wire as a result of the current flow in the ground, and this incremental voltage causes current flow I in the wire. Current also may be induced in the wire directly by the tangential component of the refracted electric field, shown as $\bar{E}_g$. The reflected EMP, $\bar{E}_r$, $\bar{H}_r$, is also shown in Figure 9-67. The potential importance of these reflected fields is discussed below.

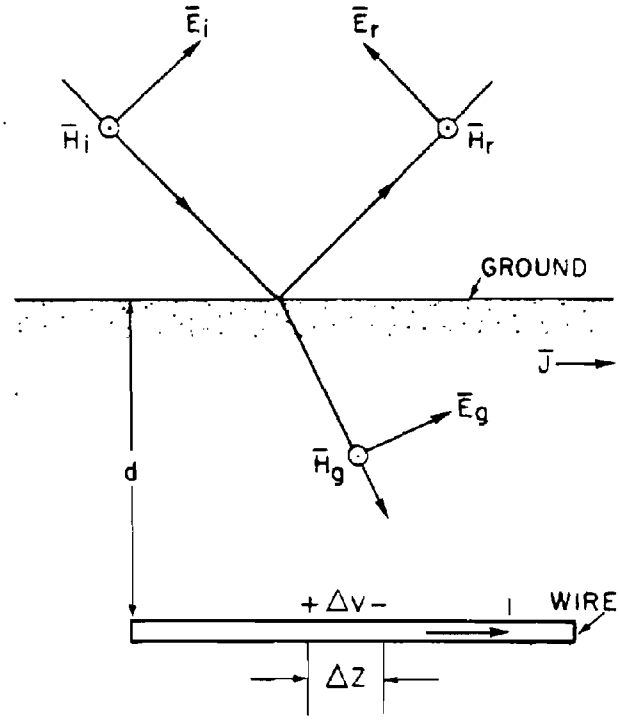

Figure 9-67. [redacted] Resistive Coupling as a Result of Currents in the Ground [redacted]

9-57 Resonant Configurations [redacted]

[redacted] The coupling of energy to a conductor is particularly efficient when the maximum dimension of the conductor configuration is about the same size as the wavelength of the radiation. In this event the voltages that are induced along the conductor at various points are all approximately in phase, so the total voltage induced on the conductor is a maximum. The conductor is said to be resonant, or to behave as an antenna, for frequencies corresponding to near this wavelength. Since EMP has a broad spectrum of frequencies (see Chapter 7), only a portion of this spectrum will couple most efficiently into a specific conductor configuration. Thus, a particular system of interest must be examined with regard to its overall configuration as well as its component configuration. Eash aspect will have characteristic dimensions that determine what part of the pulse (strength and frequencies) constitutes the principal threat.

[redacted] Gross system features that are not normally considered antennas, such as structural features, beams, girders, buried cable, overhead conduit or ducting, wings, fuselage, missile skins, and any wall apertures, must be considered to be potential collectors and conductors of energy into the system. In particular, radiation that

[redacted]

enters through an aperture is analogous to radiation that originates from a plate of the same size and shape as the aperture. Thus, it is resonant, and the aperture is resonant, and it admits a maximum of energy from the pulse for those frequencies near its resonance.

When the EMP strikes the ground, a portion of the pulse will be transmitted through the interface, inducing currents in the ground or any system components buried there, and a portion normally will be reflected as shown in Figure 9-68. Thus, a system that is above the ground will receive the reflected pulse as well as the direct pulse. These may cancel one another partially, but in the worst case they may reinforce and may constitute a greater threat level.

It can be seen that most practical systems in their operational environment present exceedingly complex coupling problems for an arbitrary explosion. The solution for any combination of system and environment is probably unique and will be very sensitive to even minor changes in the parameters. Two approximate approaches have been tried: computer studies as mentioned in Chapter 7, and threat simulation, which will be discussed in succeeding paragraphs.

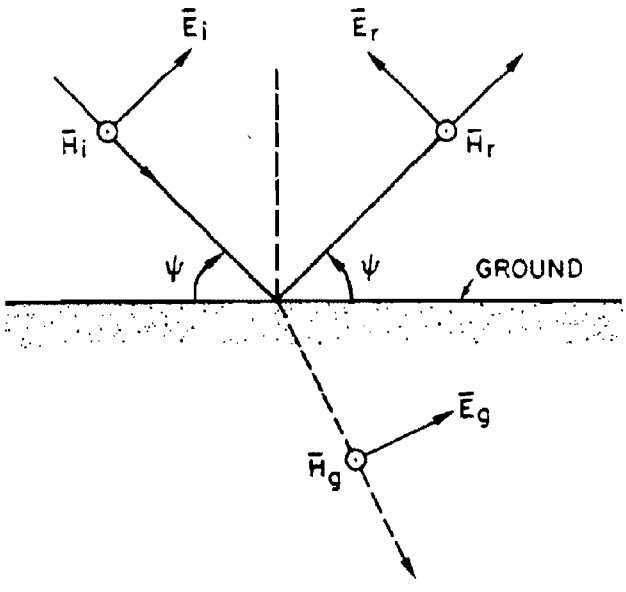

Figure 9-68. Reflected and Refracted Waves at the Air-Ground Interface

COMPONENT DAMAGE

9-58 Types of Damage

Degradation of system performance may occur as a result of functional damage or operational upset. A system will suffer damage if it is damaged permanently as a result of a large electrical transient. For example, a catastrophic failure of a device or component will render its operation unsatisfactory in any circuit. A parametric failure of a device occurs when degradation of some parameter has proceeded to a point where the circuit will continue to operate but at reduced efficiency. These latter failures are classed as functional damage. On the other hand, a system suffering operational upset is only impaired temporarily.

Electronic components that are sensitive to functional damage or burnout are listed below in the order of decreasing sensitivity to damage effects:

microwave semiconductor diodes,

field-effect transistors,

radio-frequency transistors,

audio transistors,

silicon-controlled rectifiers,

power rectifier semiconductor diodes,

vacuum tubes.

Thus, on the basis of components alone, vacuum tubes are less susceptible to EMP damage effects than transistors.

Electronic or electrical systems that are subject to malfunction include:

Most susceptible:

- Low power, high speed digital computer

[redacted]

(upset) either transistorized or vacuum tube

- Systems employing transistors or semiconductor rectifiers (eitner silicon or selenium), such as

  computers

  computer power supplies

  transistorized components terminating long cable runs, especially between sites

  alarm systems

  intercom systems

  life-support system controls

  some telephone equipment which is partially transistorized

  transistorized receivers

  transistorized transmitters

  transistorized 60 to 400 cps converters

  transistorized process control systems

  power system controls; communication links

Less susceptible.

- Vacuum tube equipment (does not include high speed digital equipment and equipment with semiconductor or selenium rectifiers)

transmitters	intercoms
receivers	teletype-telephone
alarm systems	power supplies

- Equipment employing low current switches, relays, meters

alarms	panel indicators, status boards
life-support systems	process controls
power system control panels	

- Hazardous equipment containing

detonators	explosive mixtures
squibs	rocket fuels
pyrotechnical devices	

- Other

  Long power cable runs employing dielectric insulation, equipment associated with high energy storage capacitors or inductors

Least susceptible:

- High-voltage 60 cps equipment

transformers, motors	rotary converters
lamps, filament	heavy duty relays, circuit breakers
heaters	air-insulated power cable runs

[redacted] The less susceptible equipment or components would be made more susceptible if they are connected to long exposed cable runs, such as intersite wiring or overhead exposed power or telephone cables. The equipment can be made less vulnerable if it is protected.

9-59 Damage Levels [redacted]

[redacted] The nature of a circuit has a strong bearing on the transients that cause damage; however, in general pulse lengths of microsecond and submicrosecond duration are required to cause problems. Table 9-27 shows a list of common active devices and the approximate energy required to cause functional damage. The wide range of energies should be noted.

[redacted] The minimum energy required to damage meters or to ignite fuel vapors is about the same as that required to damage semiconductors as shown in Table 9-28. Good composition resistors can withstand pulse powers more than 10,000 times their power rating for micro-

[redacted]

[redacted]

Table 9-27. [redacted] Minimum Observed Joule Energy to Cause Burnout [redacted]

Type	Minimum Joule Energy	Material	Other Data
2N36	4.0×10^{-2}	Ge	PNP Audio Transistor
2N327A	1.6×10^{-2}	Si	PNP Audio Transistor
2N1041	2.0×10^{-2}	Ge	PNP Audio Transistor
2N1308	5.0×10^{-5}	Ge	NPN Switching Transistors
2N706	6.0×10^{-5}	Si	NPN Switching Transistors
2N594	6.0×10^{-3}	Ge	NPN Switching Transistors
2N398	8.0×10^{-4}	Ge	PNP Switching Transistors
2N240	1.0×10^{-2}	Ge	PNP Switching Transistors
MC715	8.0×10^{-5}	Si	Data Input Gate Integrated Circuit
2N4220	1.0×10^{-5}	Si	RF General Purpose FET
2N4224	3.0×10^{-5}	Si	VHF Amp and Mixer FET
1N3659	8.0×10^{-3}	Si	Automotive Rectifier Diode
1N277	2.0×10^{-5}	Ge	High Speed Switching Diode
1N3720	5.0×10^{-4}		Tunnel Diode
1N238	1.0×10^{-7}	Si	Microwave Diode
2N3528	3.0×10^{-3}	Si	Silicon Controlled Rectifier
67D-5010	1.0×10^{-4}		G.E. Varistar (30-joule Rating)
6AF4	1.0×10^{0}		UHF Oscillator Vacuum Tube
66N8	2.0×10^{0}		General Purpose Triode Vacuum Tube

[redacted]

[redacted]

Table 9-28. [redacted] Minimum Joule Energy to Cause Permanent Degradation Indicated [redacted]

Designation	Minimum Joule Energy	Malfunction	Other Data
Relay	2×10^{-3}	Welded Contact	Potter-Brumfield (539) low-current relay
Relay	1×10^{-1}	Welded Contact	Sigma (IIF) one-ampere relay
Microammeter	3×10^{-3}	Slammed Meter	Simpson Microammeter (Model 1212C)
Explosive Bolt	6×10^{-4}	Ignition	EBW 8 amp for 10 μsec detonator, MK1
Squib	2×10^{-5}	Ignition	Electric Squib, N8 3.5 watts for 5 μsec detonator
Fuel Vapors	3×10^{-3}	Ignition	Propane-air mixture 1.75 mm ignition gap

[redacted] second pulses. Capacitors are also fairly hard components. The approximate energies required for degradation of several common components are shown in Table 9-28.

[redacted] The minimum energy necessary for operational upset is a factor of 10 to 100 less than that which is required to damage the most sensitive semiconductor component. Table 9-29 shows the levels required to cause operational upset to some common components to illustrate this factor.

[redacted] A gross comparison of the energy required to damage several classes of electrical equipment is provided in Figure 9-69.

[redacted] The large range of damage levels emphasizes the fact that it is important to consider EMP damage criteria early during the design stage of any piece of equipment that might be susceptible. It is also important to realize that energy collected in one part of a system may be transmitted to other parts of the system as a result of the currents that are induced. Thus, it is not necessary that the EMP couple directly to a sensitive component; energy coupled to various parts of a system may ultimately reach a particular component in sufficient quantity to cause malfunction. With the current state of the art in EMP vulnerability evaluation, the design and hardening of complicated systems requires the joint efforts of systems engineers and professional EMP effects personnel.

[redacted] EMP HARDENING [redacted]

9-60 System Analysis [redacted]

[redacted] A general approach to the examination

[redacted]

[redacted]

Table 9-29. [redacted] Minimum Joule Energy to Cause Circuit Upset or Interference [redacted]

Designation	Minimum Joule Energy	Malfunction	Other Data
Logic Card	3×10^{-9}	Circuit Upset	Typical logic transistor inverter gate
Logic Card	1×10^{-9}	Circuit Upset	Typical flip-flop transistor assembly
Integrated Circuit	4×10^{-10}	Circuit Upset	Sylvania J-K flip-flop monolithic integrated circuit (SF50)
Memory Core	2×10^{-9}	Core Erasure Via Wiring	Burroughs fast computer core memory (FC2001)
Memory Core	5×10^{-8}	Core Erasure Via Wiring	Burroughs medium speed computer core memory (FC8001)
Memory Core	3×10^{-9}	Core Erasure Via Wiring	RCA medium speed, core memory (269M1)
Memory Core	2×10^{-8}		Minimum observable energy in a typical high-gain subsystem
Amplifier	4×10^{-21}	Interference	Minimum observable energy in a typical high-gain amplifier

[redacted]

of a system with regard to its EMP vulnerability could include the following steps. First information concerning the system components and devices is collected. The information is categorized methodically into physical zones based on the susceptibility and worst case exposure for these items. Using objective criteria, problem areas are identified, analyzed, and tested. Suitable changes are made as necessary to correct deficiencies, and the modified system is examined and tested. The approach may be followed on proposed systems or those already in place, although experience indicates that the cost of retrofitting EMP protection is usually overwhelming.

9-61 Recommended Practices [redacted]

[redacted] Within the scope of this manual it is only possible to mention a few of the practices that may be employed in hardening a system to EMP. The following discussion is intended to convey some impression of the extra effort involved in hardening a system to the EMP rather than to provide a comprehensive treat-

[redacted]

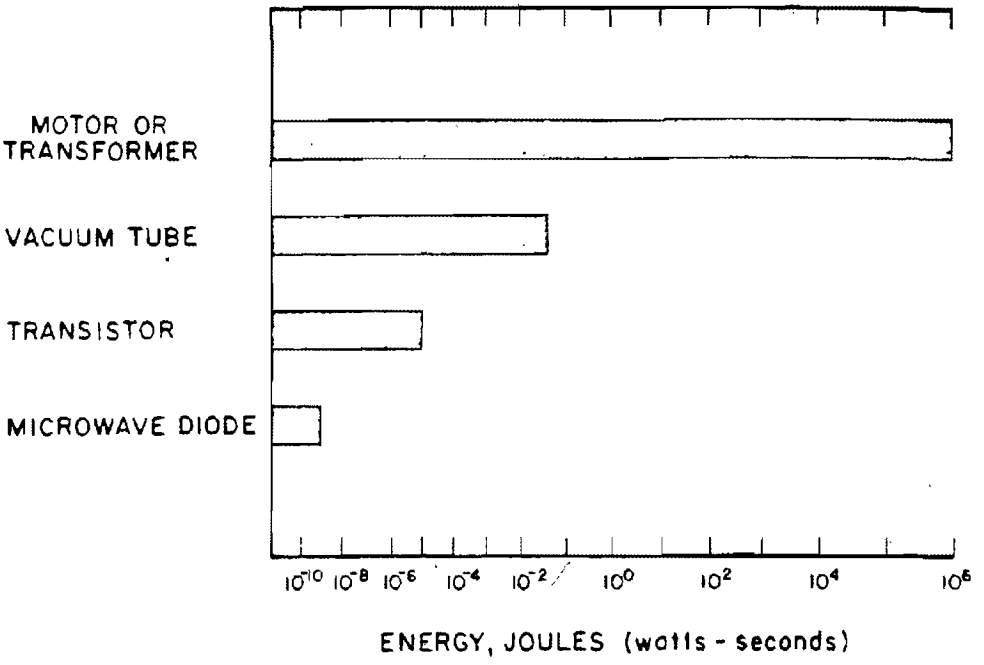

Figure 9-69. [redacted] Energy Required to Damage Various Classes of Equipment [redacted]

[redacted]

ment of what is a highly technical and specialized field.

[redacted] Some general methods for reduction of the EMP environment include geometric arrangement of the equipment, shielding, geographic relocation, and proper grounding.

[redacted] Circuit layout recommendations include the use of common ground points, twisted cable pairs, system and intrasystem wiring in "tree" format (radial spikes) avoiding loop layouts and circuit routes coupling to other circuits, use of conduit or cope trays, and shielded isolated transformers. Avoiding ground return in cable shields is also recommended. Many specific practices carry over from communications and power engineering while many do not. Each must be examined carefully.

[redacted] Good shielding practices include the use of independent zone shields, several thin shields to replace a thick one, continuous shield joints, and keeping sensitive equipment away from shield corners. Avoiding shield apertures, and avoiding the use of the shield as a ground or return conductor is also recommended. The shielding effectiveness of many enclosures frequently is defeated by energy carried by cables or pipes (including water pipes, sewage lines, etc.) into the enclosure.

[redacted] Cabling recommendations include the use of deeply buried intersystem cables (more than 3 feet), shield layer continuity at splices, and good junction box contact. Ordinary braid shielding should be avoided. Cable design represents an extension of shielding and circuit practices from the viewpoint of EMP protection. It is an area where compromises frequently are made in the interests of economy, and thus is an area where professional EMP effects personnel can be

[redacted]

of considerable assistance.

Good grounding practices must be employed. In general, a "ground" is thought of as a part of a circuit that has a relatively low impedance to the local earth surface. A particular ground arrangement that satisfies such a definition may not be optimum, and may be worse than no ground from the EMP viewpoint. A ground can be identified as: the chassis of an electronic circuit, the "low" side of an antenna system, a common bus, or a metal rod driven into the earth. The last depends critically on local soil conditions, and it may result in resistive induced currents in the ground circuit. A good starting point is to provide a single point ground for a circuit cluster, usually at the lowest impedance element – the biggest piece of the system that is electrically immersed in the earth, e.g., the water supply system. It is beyond the scope of this manual even to list all of the grounding recommendations. Once again, this is an area where professional EMP effects personnel can be of considerable assistance.

Finally, various protective devices represent a means to counter other protective shortcomings indirectly. Filters, absorbers, limiters, decouplers, switching devices, arc arresters, fuses, etc., are part of this class of components. When other design practices cannot be used or are not adequate, such devices must be added. Typically they are found in an "EMP room" at the cable entrance to underground installations, in aircraft antenna feeds, in telephone lines, at power entry panels to shielded rooms, etc. On a smaller scale, diodes, nonlinear resistors, SCR clamps, and other such items are built into circuit boards or cabinet entry panels. Few of these devices by themselves are sufficient as a complete solution to a specific problem area, because each has some limitation in speed of response, voltage rating, power dissipation capacity or reset time. Thus, most protective devices are hybrids. A few prepackaged hybrids are available for the protection of audio and power lines from lightning strokes and power surges and, if modified, may be used for EMP protection. No such packages are readily available for high frequency lines, multiple wire cables, antennas, etc., and usually must be custom designed for each application.

TESTING

9-62 Importance of Testing

Even with present day sophistication in analytic techniques, it is clear from the complexities described above that sole reliance cannot be placed in analysis and prediction alone. Testing has a number of important functions.

Testing is essential to verify prior analysis of devices, components, and complete systems early in the design stage. Testing also is the only known method that can be used to identify surprises. Surprises can be unexpected coupling or interaction modes or weaknesses that were overlooked during the design. Nonlinear effects in interaction are a form of surprise that only can be found by testing. After the test, many of the original approximations made in analysis can be refined and improved for future analysis, and the data can improve the analytic capability for more complex problems.

Testing quickly locates weak or susceptible points in components or systems early enough for economic improvement. After the improvements, testing quickly verifies that the improvements bring the performance up to standards.

Testing provides assurance and confidence that the complete system is actually hardened to EMP to the specified threat level. Actual certification can only be obtained by providing the actual nuclear threat environment. Further, periodic testing insures that system hardness is not degraded as a result of environmental or human factors.

[redacted]

9-63 Simulation Facilities [redacted]

[redacted] As a result of the limited test ban treaty, heavy reliance must be placed on simulation to test the EMP hardness of systems. A brief description of generic simulation techniques is given below. A more thorough description of these techniques is contained in the "DNA EMP (Electromagnetic Pulse) Handbook, Volume 2, Analysis and Testing" (see bibliography).

[redacted] The classes of EMP tests are:

- Low level current mapping,
- High level current mapping,
- High level fields.

Low level current mapping is a good test for the beginning of any program. With the system power turned off and a low-level field, the magnitudes and signatures on internal cables are determined. This provides an insight on the work that must follow. After this test and the indicated improvements are made, a high-level current can be injected directly into the system with the system power on to explore for nonlinearities, and to uncover initial indications of system effects. If subsystems malfunction, it may be desirable to conduct extensive subsystem tests in the laboratory. Finally, a high level field test is essential.

[redacted] The type of excitation must be defined in any type of test. The two principle choices are:

- Waveform simulations (time-domain data),
- Continuous wave signals (frequency-domain data).

If the intent is to match a system analysis in the frequency domain to measured system response, continuous wave (CW) signals may be more suitable. If the desire is to compare the test results to known electronic thresholds, it is frequently necessary to test in the time domain. For a complete analysis, it is advisable to consider both types of tests.

[redacted] Large-scale simulators are required for the final test of large systems. The two principal kinds of large simulators are:

- Metallic structures that guide an EM wave past a test object,
- Antennas that radiate an EM field to a test object.

Guided wave simulators use pulse generators that simulate EMP waveforms and operate in the time domain. Radiating antennas use either pulse generators (time domain) or continuous wave (CW) signal generators (frequency domain). Pulse generators themselves can be either high level single shot or low level repetitive.

(U) The essential elements of a guided wave or transmission line simulator include:

- Pulser
- Transition section
- Working volume
- Termination.

An electromagnetic wave of suitable amplitude and waveshape is generated by the pulser. This wave is guided by a tapered section of transmission line (the transition section) from the small cross sectional dimension of the pulser otuput to the working volume. The working volume, where the test object is located, should be large enough to provide a certain degree of field uniformity over the test object. A test object dimension one-fifth that of the working volume satisfies this condition. The termination region prevents the reflection of the guided wave back into the test volume, and consists of a transition section that guides the incident wave to a geometrically small resistive load whose impedance is equal to the characteristic impedance of the transmission line structure.

[redacted] The basic types of radiating simulators are:

- Long wire
- Biconic dipole or conical monopole.

The long wire is usually a long dipole oriented

[redacted]

parallel to the earth's surface. It is supported above the ground by nonconducting poles with high-voltage insulators. The two arms of the dipole are symmetric about the center and constructed from sections of light weight cylindrical conductor, such as irrigation pipe. Pipe sections decrease in diameter with increasing distance from the center, and resistors are placed between the pipe sections to shape the current wave and reduce resonances. The two arms of the dipole are oppositely charged, and when the voltage across the spark gap at the dipole center reaches the breakdown voltage, the gap begins conducting and a current wave front propagates away from the gap.

Conical and biconical antennas use pulsers, such as Marx generators, or CW transmitters instead of relying on the discharge of static surface charges. The antennas are fabricated out of lightweight conducting surfaces or wire grids.

Differences between guided wave and radiating simulators are listed in Table 9-30.

Electromagnetic scale modeling is an important alternative to full scale testing under the following conditions:

- Test facilities or available equipment are at a premium,
- The system to be tested is very large,
- The system dedication cost for full scale testing is high.

In addition to the advantages of modeling under these conditions, benefits can be derived as follows:

- Perhaps sensors can be placed better during full scale testing as a result of model experiments,
- Design modifications or cable reroutes can be made prior to full scale testing,
- EM angles-of-arrival can be determined for worst- and best-case conditions,
- Effects of changes in the conductivity of the surrounding media can be explored to an extent,
- Estimates can be made of some of the responses of a complex system prior to full scale testing,
- Design confirmation of costly systems can be made prior to system fabrication and costs can be reduced,
- Quantitative data can be obtained to validate analysis.

It should be pointed out that because of the difficulty in introducing minute openings or poor bonds into models, and since these often control interior fields, the usefulness of modeling ordinarily is limited to the measurement of external fields, voltages, and currents. Once the exterior fields, voltages, and currents are known for a complex structure, perhaps having cable runs, analysis can often provide internal field quantities of interest.

In actually setting up a scale model test, the following should be kept in mind:

- Broadband pulse response determination involves much more than a steady-state, single-frequency response test does.
- Special EM illumination sources that are coherent, have uniform time delay, and use antennas with constant effective height are required.
- Special modeling techniques are required to study exposed conductors that pass over or within a lossy dielectric, such as earth.

A pulse-type waveform theoretically can be replaced by a continuous wave (CW) source with a sensing system which references the sensed CW signal to a reference phase from the source. Complex Fourier transfer functions can be developed by processing the recorded data on a computer. However, long sweep times are required to ensure that all narrow band responses are explored adequately, and the actual physical implementation of such an approach in the

[redacted]

Table 9-30. [redacted] Comparison of Guided Wave and Radiating Simulators [redacted]

	Guided Wave	Radiating
Energy use	Efficient – mostly directed toward test object	Energy radiated symmetrically about axis – only fraction directed toward test object
Test volume	Limited by size of simulator – difficult to construct large enough for sizable test objects	Limited by desired field intensity
Polarization	Fixed (or bipolar, e.g., ARES)	Variable*
Angle of incidence	Fixed†	Variable*
Earth reflection effects	No	Yes
Geometric attenuation of EM wave amplitude	No – relatively uniform within test volume	Yes (1/R)
Planar wave capability	Yes	Only at distance
Interference with nearby electronics	Limited	Yes

*[redacted] These are, however, limited by the height of the antenna unless it is airborne.

†[redacted] Polarization is fixed relative to earth coordinates; however, a range of polarizations and angles of incidence can be provided in some facilities by changing the position and orientation of the object that is being tested. For example, a missile can be rotated on several axes in ARES to change these to items relative to the missile.

[redacted]

[redacted]

[redacted]

microwave band poses additional difficulties. On the other hand, the use of scaled real time waveforms allows quick development of actual responses, from which complex Fourier transfer functions also can be developed with the aid of computers.

[redacted] Several variations of each type of simulation technique described above are currently operational. Each has some advantages and disadvantages when compared to others. As mentioned previously, it is beyond the scope of this manual to describe individual facilities. The interested user should consult the "DNA EMP (Electromagnetic Pulse) Handbook, Volume 2, Analysis and Testing," (see bibliography), and the references listed therein.

[redacted]

[redacted]

[redacted] BIBLIOGRAPHY [redacted]

Abbott, L. S., H. C. Claiborne, and C. E. Clifford, Eds., *Weapons Radiation Shielding Handbook* [redacted] DASA 1892-1, through 1892-6, Oak Ridge National Laboratory, Oak Ridge, Tennessee, December 1966 through March 1972 (Vols. I, II, III, V, [redacted] Vol. VI, [redacted] Vol. IV [redacted]

Barash, R. M., and J. A. Goertner, *Refraction of Underwater Explosion Shock Waves: Pressure Histories Measured at Caustics in a Flooded Quarry*, NOLTR-67-9, U.S. Naval Ordnance Laboratory, White Oak, Silver Spring, Maryland, 19 April 1967 [redacted]

Batter, J. F., *Transient Effects of a Time Varying Thermal Pulse*, Part II, AFSWP1058, TOI Report No. 58-7, Technical Operations Incorporated, Burlington, Massachusetts, March 1958 [redacted]

Bell, J. F., *Single Temperature-Dependent Stress-Strain Law for Dynamic Plastic Deformation of Annealed Face-Centered Cubic Metals*, Journal of Applied Physics, Vol. 34, No. 1, January 1963 [redacted]

Bergman, P., and N. Griff, *A Method for Evaluation of the Response of Coatings to Thermal Radiation from a Nuclear Weapon*, Naval Applied Science Laboratory Project 940-105, Progress Report 9, November 12, 1968 [redacted]

Bergman, P., et al., *Temperature Response Charts for Opaque Plates Exposed to the Thermal Radiation Pulse from a Nuclear Detonation*, Naval Applied Science Laboratory Project 940-105, Progress Report 10, July 10, 1969 [redacted]

Bethe, H. A., and W. L. Bade, *Theory of X-Ray Effects of High Altitude Nuclear Bursts and Proposed Vehicle Hardening Method* [redacted] RAD-TR-9(7)-60-2, AVCO Corporation, Wilmington, Massachusetts, 8 April 1960 [redacted]

Bothell, L. E., *PUFF IV-EP Code Comparisons to Test Results* [redacted] KN-664-67-2, Kaman Nuclear, Colorado Springs, Colorado, 16 January 1967 [redacted]

Bothell, L. E., and C. E. Archuleta, *PUFF V-EP Code* [redacted] Parts I and II, KN-703-67-101(R), Kaman Nuclear, Colorado Springs, Colorado, December 1967 (Part I, [redacted] Part II [redacted]

Bridges, J. E., *DNA EMP Awareness Course Notes*, DNA 2772T, Illinois Institute of Technology Research Institute, Chicago, Illinois, August 1971 [redacted]

Chandler, C. C., et al., *Prediction of Fire Spread Following Nuclear Explosions*, U.S. Forest Service Research Paper PSW-5, Pacific Southwest Forest and Range Experiment Station, Berkeley, California, 1963 [redacted]

[redacted]

Clarke, T. C., *Interaction Study, Vol. IV, Structural Degradation by Short Time Heating,* AFWL TR-70-157, Boeing Company, Seattle, Washington, December 1970

Cohen, M. L., *A Numerical Technique to Determine the Thermal Histories of Two-Dimensional Solids in the Nuclear Environments,* Naval Applied Science Laboratory Project 940-105, Progress Report 5, June 1958

Cole, R. H., *Underwater Explosions,* Dover Publications, Inc., New York, N.Y., 1965

Davis, G. T., et al., *Project TROIKA, Re-Entry Vehicle Vulnerability Assessment for Advanced Planning for Underground Tests* DASA 2230, AVCO Corporation, Wilmington, Massachusetts, January 1969

Derkesen, W. L., *Ship Vulnerability to Nuclear Attack-Thermal Radiation Effects,* Technical Briefing to the Chief of Naval Material, 2 March 1967.

DNA EMP (Electromagnetic Pulse) Handboo DNA 2114H1-2114H4, DASIAC, General Electric TEMPO, Santa Barbara, California, Volume 1, Design Principles, November 1971, Volume 2, Analysis and Testing, November 1971, Volume 3, Environment and Applications, to be distributed during early calendar year 1973, Volume 4, Resources, November 1971 (Volumes 1, 2, and 4, Volume 3,

Electromagnetic Pulse Sensor and Simulation Notes, Volumes 1-10, AFWL EMP 1-1 through EMP 1-10, Air Force Weapons Laboratory, Kirtland Air Force Laboratory, New Mexico, April 1967 through 1972

Goodwin, L. K., et al., *An Equation of State for Metals,* DASA 2286, Aeroneutronics Division of Philco-Ford, Newport Beach, California, April 1969

Hall. W. J., and N. M. Newmark, *Interpretation of Event Pile Driver Tunnel Liner Results* DASA 2374, University of Illinois, Urbana, Illinois, February 1970

Hall, W. J., and N. M. Newmark, *Supplemental Studies of Event Pile Driver Backpacked Tunnel Liner Results* DASA 2374-1, University of Illinois, Urbana, Illinois, October 1970

Harrison, G., *A Plan for the Development and Evaluation of an Advanced Re-Entry Vehicle* DASA 2208-I, General Electric Corporation, Philadelphia, Pennsylvania, June 1969

Hillendahl, R. W., *Theoretical Models for Nuclear Fireball* DASA 1589-1 through 1589-39, Lockheed Missiles and Space Company, Sunnyvale, California, 1965-68

Julian, A., and C. E. Eves, *Thermal Effects on Strength of Aircraft Structural Sandwich-Type Panels,* WT 1341, Project 8.4, Operation REDWING, Cook Research Laboratories, Skokie, Illinois, 30 April 1958

Julian, A. N., *In-Flight Structural Response of FJ-4 Aircraft to Nuclear Detonations,* WT 1432, Project 5.3, Operation PLUMBBOB, Bureau of Aeronautics, Washington, D.C., 10 February 1960

Kalinowski, J. J., *A Management Guide to Transient-Radiation Effects on Electronics (TREE)* DNA 2051H, Battelle's Columbus Laboratories, Columbus, Ohio, February 1972

Kaplan, K., and C. Wiehle, *Air Blast Loading in the High Shock Strength Region* Part II, Prediction Methods and Examples, URS 633-3, DASA 1460-1, URS Corporation, Burlingame, California, February 1965

Kaufmann, R., and R. J. Heilferty, *Equations and Computer Program to Calculate the Temperature Distribution and History in a Cylinder Subject to Thermal Radiation from a Nuclear Weapon,* NASL Project 940-105, PR-8, U.S. Naval Applied Science Laboratory, Brooklyn, New York, 18 July 1968

Kaufmann, R., and R. J. Heilferty, *Equations and Computer Program to Calculate the Temperature Distribution and History in a Tee Beam Subject to Thermal Radiation from a Nuclear Weapon,* NASL Project 940-105, PR-6, U.S. Naval Applied Science Laboratory, Brooklyn, New York, 20 February 1968

Larin, F., *Radiation Effects in Semiconductor Devices,* John Wiley and Sons, Inc., New York, 1968

Martin, S. B., and S. Holton, *Preliminary Computer Program for Estimating Primary Ignition Ranges for Nuclear Weapons,* USNRDL-TR-866, U.S. Naval Radiological Defense Laboratory, San Francisco, California, 3 June 1965

Melin, J. W., and S. Sutcliff, *Development of Procedures for Rapid Computation of Dynamic Structural Response,* University of Illinois Final Report on Contract AF33(600)-24994 for Physical Vulnerability Division of Intelligence, USAF

Moon, D. P., and W. F. Simmons, *Methods for Conducting Short-Time Tensile, Creep, and Creep-Rupture Tests under Conditions of Rapid Heating,* Defense Metals Information Center Report 121, December 28, 1959

Moon, D. P., and W. F. Simmons, *Selected Short-Time Tensile and Creep Data Obtained under Conditions of Rapid Heating,* Defense Metals Information Report 130, June 17, 1960

Morris, P. J., *Proposed Addition to Chapter 7, DASA EM-1, Section 7.6, Thermal Radiation Degradation of Structural Resistance to Air Blast* URS 7029-6, URS Research Company, San Mateo, California, December 1971

Newmark, N. M., et al., *Analysis of Design of Flexible Underground Structures*, DA-22-079-eng-255, University of Illinois; Urbana, Illinois; 31 October 1962

Newmark, N. M., *An Engineering Approach to Blast Resistant Design*, Paper No. 2786, Transactions, ASCE, *121*, 45-64, 1956

Nuclear Weapons Blast Phenomena, DASA 1200-I, -II, -III, -IV, Defense Atomic Support Agency, Washington, D.C., Vol. I, March 1971, Vol. II, December 1970, Vol. III, March 1970, Vol. IV to be issued during calendar year 1972 (Vol. I, Vol. II Vol. III,

Old, C. C., et al., *TROIKA Study Final Report* DASA 2191-I, -II, -III, and -IV, Lockheed Missiles and Space Company, Sunnyvale, California, August 1968 (Vols. I and II, Vols. III and IV,

Reaugh, J., *Equation-of-State Evaluation Predix Topical Report* PITR-239-1, DASA 2596, Physics International Co., San Leandro, California, April 1972

Seaman, L., et al., *Dynamic Fracture Criteria of Homogeneous Materials*, AFWL-TR-71-156, Stanford Research Institute, Menlo Park, California, February 1972

Seaman, L., *Spall and Fracture Phenomena in the Response of Materials to Nuclear Effects* Third Annual Meeting of Nuclear Survivability Working Group on Propulsion and Ordnance, Stanford Research Institute, Menlo Park, California, 29-30 August 1971

Shelton, F., *Nuclear Weapons as X-Ray Sources, the Environments They Produce, and Some Effects on Aerospace Systems Volume II, Some Effects on Aerospace Systems*, DASA 2397-2, KN-770-69-30, Kaman Nuclear, Colorado Springs, Colorado, September 1969

Snay, H. G., *Underwater Explosion Phenomena: The Parameters of Migrating Bubbles*, NAVORD Report 4185, U.S. Naval Ordnance Laboratory, White Oak, Silver Spring, Maryland, 12 October 1962

Snay, H. G., *Hydrodynamic Concepts Selected Topics for Underwater Nuclear Explosions*, NOLTR 65-52, DASA 1240-1(2), U.S. Naval Ordnance Laboratory, White Oak, Silver Spring, Maryland, 15 September 1966

Staff of Kaman Avidyne, *Handbook for Analysis of Nuclear Weapon Effects on Aircraft* KA-TR-50A, DASA-2048, Kaman Avidyne, Burlington, Massachusetts, April 1970

Staff of Kaman Avidyne, *Handbook of Computer Programs for Analysis of Nuclear Weapon Effects on Aircraft* KA-TR-50S, DASA-2048S, Kaman Avidyne, Burlington, Massachusetts, April 1970

Timoshenko, S., and S. Woinowsky-Krieger, *Theory of Plates and Shells*, McGraw-Hill Book Company, 1959

TREE (Transient-Radiation Effects on Electronics) Handbook DNA 1420H-1, Vol. 1, Edition 3, Battelle's Columbus Laboratories, Columbus, Ohio, December 1971

TREE (Transient-Radiation Effects on Electronics) Handbook DASA 1420-1, Edition 2, Revision 2, Battelle Memorial Institute, Columbus, Ohio, September 1970 (to be replaced by DNA 1420H-2 during early calendar year 1973).

TREE Preferred Procedures (Selected Electronic Parts), DNA-2028H, Battelle's Columbus Laboratories, Columbus, Ohio, June 1972

TREE Simulation Facilities, DASA 2432, Edition 1, Battelle Memorial Institute, Columbus, Ohio, September 1970

Veigele, W. J., et al., *X-Ray Cross Section Compilation from 0.1 keV to 1 MeV*, DNA 2433F Vols. 1 and 2, Revision 1, KN-71-431(R), Kaman Nuclear, Colorado Springs, Colorado, 31 July 1971

Whitaker, W. A., and R. A. Deliberis, *Aircraft Thermal Vulnerability to Large High-Altitude Detonations* AFWL-TR 67-85, Air Force Weapons Laboratory, Kirtland Air Force Base, New Mexico, August 1967

Whitener, J. E., *Deflection of Ballistic Missiles by Nuclear Weapons* RM-2345, RAND Corporation, Santa Monica, California, April 1959

[redacted]

(This page intentionally left blank)

[redacted]

AD-A955 394

Chapter 10
PERSONNEL CASUALTIES

INTRODUCTION

The three principal phenomena associated with nuclear explosions that result in casualties to personnel are blast and shock, thermal radiation, and nuclear radiation. Blast injuries may be direct or indirect; the former are caused by the high air pressure (overpressure), while the latter may be caused by missiles or by displacement of the body.

The frequency of burn injuries resulting from a nuclear explosion is exceptionally high. Most of these are flash burns caused by direct exposure to the thermal radiation, although personnel trapped by spreading fires may be subjected to flame burns. In addition, personnel in buildings or tunnels close to ground zero may be burned by hot gases and dust entering the structure even though they are shielded adequately from direct or scattered radiation.

The harmful effects of the nuclear radiations appear to be caused by ionization and excitation (see paragraph 6-4, Chapter 6) produced in the cells composing living tissue. As a result of ionization, some of the constituents, which are essential to the normal functioning of the cells, are altered or destroyed. As described in Section III, these changes may result in sickness that may terminate with death in some cases.

The effects of these three phenomena on personnel are described in the succeeding three sections. A brief discussion of the effects of combinations of the phenomena is provided in Section IV.

SECTION I
AIR BLAST

MECHANISMS AND CRITERIA FOR INJURY

Injury that results from exposure of personnel to air blast may occur from sudden changes in environmental pressure acting directly on the exposed subject, from displacement of personnel involving decelerative tumbling or impact against a rigid object, from blast-energized debris striking the individual, and from a variety of miscellaneous changes in the immediate environment. Individuals who are injured to such an extent that they are unable to perform assigned tasks are designated casualties. Such a condition typically starts almost immediately following airblast trauma and it can be expected to last from hours to several days, depending on the nature and severity of the injury. The biological effects which may result from exposure to a blast wave are divided into four categories: (1) direct overpressure effects, (2) effects from translational forces and impact, (3) effects of blast energized debris, and (4) miscellaneous effects. These effects are discussed separately in the following paragraphs.

10-1 Direct Overpressure Effects

Casualties that result from direct overpressure effects are those that result from man's inability to withstand rapid changes in his environmental pressure. The body is relatively resistant to the crushing forces from air blast loading; however, large sudden pressure differences resulting from blast wave overpressure may cause serious injury. Anatomic localization of such injury occurs predominantly in air-bearing organ systems such as the lungs, gastroenteric tract, ears and perinasal sinuses. At high overpressures both early (less than 30 minutes) and delayed (30 minutes to several days) lethality will occur as a result of disruption of lung tissue. Early lethality is generally caused by interruption in the blood supply to the heart or brain as a result of air emboli entering the circulatory system

This document has been approved for public release and sale; its distribution is unlimited.

from the damaged lung. Delayed lethality occurs as a result of suffocation caused by continuing hemorrhage within the lung or the development of pulmonary edema. Delayed appearance of casualties also may occur at high overpressures as a result of internal hemorrhage from ruptured organs or as a result of infection due to perforation of the intestine.

Experiments conducted with animals indicate that direct overpressure effects depend upon the peak overpressure, duration and shape of the incident blast wave, and the orientation of the subject. Both the peak overpressure and the duration appear to be important for fast-rising blast waves that have durations less than 50 msec, whereas peak overpressure predominates for positive phase air-blast durations greater than 50 msec. If the time to peak overpressure is greater than a few milliseconds, there is a lower probability of injury because the anatomic structures will be subjected to pressure differences that occur less rapidly. This effect can take place in a structure where the pressure rises gradually due to a long fill time or it may occur near a reflecting surface where the pressure rises in "steps" as a result of a separation in the arrival times of the incident and reflected waves. In general, personnel who are oriented with the feet or head toward the oncoming blast wave will be injured less than those who are oriented with the long axis perpendicular to the blast wave. This is apparently caused by the action of the dynamic pressure to increase the load on the thorax in the latter case. A potentially more hazardous exposure condition occurs when personnel are situated against a flat surface, since normal reflection of a blast wave results in pressures two or more times the magnitude of the incident wave.

Current criteria for direct overpressure effects, based on extrapolations from animal data, predict 50-percent casualties and one percent mortality for randomly oriented, prone personnel exposed to a long-duration fast-rising blast wave of 41 psi and one percent casualties for those exposed to 12 psi. Animal experiments and human accident cases have shown that a 50-percent incidence of eardrum rupture may be expected to occur at 16 psi, whereas one percent might be anticipated at 3.4 psi. Although in certain situations auditory acuity is imperative, eardrum rupture currently is not considered to be a disabling injury in terms of overall effectiveness to individuals in military units.

10-2 Translational Forces and Impact

Injuries caused by translational impact occur as a result of whole body displacement of personnel by blast winds. Anatomic localization of such injuries is not as readily definable as the case for direct overpressure effects. In instances where head impact occurs, concussion, skull fractures, and intracranial hemorrhage may result in rapid loss of consciousness and, in many cases, early lethality. By contrast, impact in which the head is not involved results in a variety of traumatic injuries such as skeletal fractures, ruptured internal organs, blood loss and, in more serious cases, the development of shock. Recovery following such injuries may be more delayed than recovery from direct overpressure effects.

The translational and rotational velocities that are attained by personnel during the accelerative phase of blast-induced displacement depend upon the geometry of exposure and the shape and magnitude of the dynamic-pressure wave. In general, a longer duration of the positive phase of the blast wave will result in a lower peak overpressure being required to produce a given translational velocity. Therefore, larger yields will produce injuries at lower pressures (see Section I, Chapter 2). The severity of the injuries caused by displacement depends to a large extent on the nature of the decelerative phase of the motion. If deceleration occurs by an "impact" with a rigid object, resulting in a stopping distance of less than a few inches, the

QUALITY INSPECTED 4

UNANNOUNCED

probability of a serious injury is much greater than if deceleration occurs by "tumbling" over open terrain, which will result in much longer stopping distances.

Because of the limited data available, casualty criteria for translational impact are far less certain than those for direct overpressure effects. In addition, there are marked differences in impact velocities that are associated with serious injury following head trauma compared with those for noncranial impact. Human cadaver studies indicate that 50 percent mortality may occur following head impact at velocities of 18 ft/sec, whereas large animal studies and human free-fall experience suggest that 54 ft/sec is required for 50 percent mortality when head impact is minimized. Decelerative tumbling experiments involving a limited number of animals suggest that significant mortality does not occur at translational velocities below 88 ft/sec.

Although tentative in nature, estimates based on human accidents and animal experiments predict that a peak translational velocity of 70 ft/sec will result in 50 percent casualties for personnel when deceleration occurs by tumbling over open terrain. If translation occurs where 50 percent of the personnel impact against structures (buildings, vehicles, trees or other rigid objects) the peak translational velocity for 50 percent casualties is expected to be near 35 ft/sec. Similar figures for one percent casualties are 13 ft/sec for decelerative tumbling and 8.5 ft/sec for translation near structures.

10-3 Blast-Energized Debris

The effects of blast-energized debris include injuries that result from the impact of penetrating or nonpenetrating missiles energized by winds, blast overpressures, ground shock, and, in some cases, gravity. The wounding potential of blast-energized debris depends upon the nature and velocity of the moving object and the portion of the body where impact occurs. The types of injuries range from simple contusions and lacerations to more serious penetrations, fractures, crushing injuries, and critical damage to vital organs. The physical factors that determine the velocity attained by debris and thereby determine the severity of potential injury, are similar to those described for translation of personnel. When small light objects are displaced by a blast wave, they reach their maximum velocity quite rapidly, often after only a small portion of the wave has passed; therefore, the maximum velocity is not as dependent on duration as it is for large heavy objects. There are too many variables to establish definitive criteria for injury from debris.

In the specific instance of personnel in forests, tentative casualty criteria are available based on the probability of being struck by falling trees. These criteria are related to the amount of forest damage. Fifty percent casualties are predicted at ranges where the forest damage is moderate to severe, and one percent casualties are anticipated where the damage is light (see Forest Damage Data, Chapter 15).

10-4 Miscellaneous Effects

Miscellaneous blast injuries are those that result from non-line-of-sight thermal phenomena, ground shock, blast-induced fires and high concentrations of dust,

- Non-line-of-sight thermal burns have been observed on animals located in open underground shelters in close proximity to nuclear explosions. Although this phenomenon is not well understood, it has been suggested that the burns resulted from contact with hot dust-laden air that was carried into the structures by the blast wave.
- Ground shock may be a serious problem for personnel in blast-hardened underground structures at close ranges. The magnitude of this hazard may be estimated from the horizontal and vertical motions of the structure, which in turn may be estimated from

the predicted ground motions discussed in Chapter 2.

- Blast-induced fires are primarily a problem for urban areas. The likelihood of such fires depends on the amount of burning and combustible materials in the vicinity of an explosion.
- The evidence indicates that a high concentration of dust represents more of a discomfort than a serious hazard to personnel.

With the possible exception of ground shock, currently there is inadequate information to predict the hazards associated with these miscellaneous effects reliably.

CASUALTY PREDICTION

10-5 Personnel in the Open

For most burst conditions casualties from whole body translation of personnel in the open will extend farther than those from direct overpressure hazards, excluding eardrum rupture. This is especially true for larger yield weapons because of the increased duration of the blast wave. The translation hazard will be less for personnel located in relatively open terrain than for personnel located where they may be blown against buildings, vehicles, trees or other structures. Warned personnel can reduce the translation risks by assuming a prone position, and in the case of larger yields there will be sufficient time for the fireball flash to serve as a warning. It should be noted, however, that for overhead bursts, the direct overpressure effects would be less severe for a standing man than for a prone man because of the "step" loading of the thorax in the former case.

Unless the target area is cluttered with materials subject to fragmentation with displacement, blast-energized debris is not expected to be an overriding hazard for personnel in the open. For small yield surface bursts, however, crater ejecta may extend beyond the other blast effects, although nuclear or thermal radiation may produce casualties at greater distance. In general, the probability of being struck by flying missiles can be reduced by lying down; however crater ejecta, which is likely to be falling nearly vertically at the greater distances may strike more prone personnel than those who are standing. As in the case of blast-energized debris, the miscellaneous air blast effects are not generally expected to represent major hazards for personnel in the open.

If a precursor form of blast wave should develop, personnel located in its proximity would probably be subjected to greater translation and debris hazards than would be expected otherwise because of the increased dynamic pressures. Burst conditions associated with precursor development are discussed in Section 1 of Chapter 2.

Figures 10-1 and 10-2 show the ground distances for 50 percent and one percent casualties, respectively, from the indicated air blast effects as a function of height of burst for randomly oriented, prone personnel exposed in the open to a one kt burst. These figures were derived on the basis of the criteria and assumptions discussed earlier in this section, with the added conditions that crater ejecta was not present and no precursor formed. Since a man with a ruptured eardrum may or may not be considered a casualty depending on the tasks he is expected to perform, this effect has been removed from the other direct overpressure effects, and separate curves are provided. Two translation curves are shown in each figure and the one that is more appropriate to the existing conditions should be used. The figures show the effects for one kt, but they may be scaled to other yields by the scaling rules provided in Problem 10-1.

10-6 Personnel in a Forest

For personnel in a relatively dense forest, the hazard of being struck by falling and translating trees generally will override that resulting from any other air-blast effect. In addition, for

[redacted]

[redacted]

most burst conditions a forest will provide significant protection from thermal radiation and will provide some shielding from nuclear radiation. Therefore, casualties resulting from forest blowdown generally will extend to greater ranges than those from any other weapon effect (direct overpressure, translation, thermal radiation, nuclear radiation, etc.). Exceptions to this general rule are casualties resulting from initial nuclear radiation associated with low yield weapons, and casualties resulting from forest fires ignited by the thermal radiation pulse.

[redacted] Casualty prediction curves for forest blowdown are given in Figures 10-1 and 10-2 as a function of height of burst and ground range for randomly oriented, prone personnel exposed to a one kt burst. These curves may be scaled to other yields by multiplying both the burst heights and the ground ranges by the four-tenths power of the yield. In general, a forest does not greatly reduce or otherwise modify a blast wave. For this reason the other curves in Figures 10-1 and 10-2, which were developed to predict air-blast casualties for personnel in the open, also may be used for personnel in a forest. A description of the particulars concerning these curves has been given in the above discussion for personnel in the open.

10-7 Personnel in Structures [redacted]

[redacted] In addition to providing shielding against thermal and nuclear radiations, blast-resistant structures such as bomb shelters, permanent gun emplacements and, to a certain extent, foxholes usually reduce the blast hazards unless personnel are located directly in the entryway of the structure. The design of these structures may, however, permit the buildup of blast overpressures to a value in excess of the overpressures outside the structure as a result of multiple reflections. Nevertheless, there is generally a lower probability of injury from direct overpressure effects inside a structure than at equivalent distances on the outside, particularly if personnel do not lean against the walls of the structure or sit or lie on the floor. This results from alterations in the pattern of the overpressure wave upon entering the structure.

[redacted] Structural collapse and damage are the major causes of casualties for personnel located in buildings subjected to air blast; for this reason, the number of such casualties can be estimated from the extent of the structural damage. Table 10-1 shows estimates of casualties in two types of buildings for three damage levels. Data from Chapter 11 may be used to predict the ground distances at which specified structural damage will occur for various yields. Collapse of a brick house is expected to result in approximately 25 percent mortality, 20 percent serious injury and 10 percent light injury to the occupants. Reinforced concrete structures, though much more resistant to blast forces, will produce almost 100 percent mortality on collapse. Casualty percentages in Table 10-1 for brick homes are based on data from British World War II experience. They may be assumed to be reasonably reliable for cases where the population expects bombing and most personnel have selected the safest places in the buildings. If there were no warning or preparation, the number of casualties would be expected to be considerably higher. To estimate casualties in structures other than those listed in Table 10-1, the type of structural damage that occurs, and the characteristics of the resultant flying objects must be considered. Broken glass may produce large numbers of casualties, particularly to an unwarned population, at overpressures where personnel would be relatively safe from other effects. Overpressures as low as one or two psi may result in penetrating wounds to bare skin.

10-8 Personnel in Vehicles [redacted]

[redacted] Personnel in vehicles may be injured as a result of the response of the vehicle to blast forces. Padding, where applicable, and the use of safety belts, helmets and harnesses can reduce

[redacted]

[redacted]

Table 10-1 [redacted] Estimated Casualty Production in Buildings for Three Degrees of Structural Damage [redacted]

Structural Damage	Percent of Personnel*		
	Killed Outright	Serious Injury (hospitalization)	Light Injury (no hospitalization)
1-2 story brick homes (high-explosive data from England):			
Severe damage	25	20	10
Moderate damage	<5	10	5
Light damage	–	<5	<5
Reinforced-concrete buildings (nuclear data from Japan):			
Severe damage	100	–	–
Moderate damage	10	15	20
Light damage	<5	<5	15

*These percentages do not include the casualties that may result from fires, asphyxiation, and other causes from failure to extricate trapped personnel. The numbers represent the estimated percentages of casualties expected at the maximum range where a specified structural damage occurs. See Chapter 11 for the distances at which these degrees of damage occur for various yields.

[redacted] this source of casualties significantly, at least within armored vehicles that are strong enough to resist collapse. Serious injury may result to personnel in ordinary wheeled vehicles from flying glass as well as from impact with the vehicle's interior. Comparative numbers of casualties are almost impossible to assess because of the many variables involved.

[redacted]

Problem 10-1 Calculation of Casualties for Personnel in the Open or in a Forest

[redacted] Figures 10-1 and 10-2 are families of curves that show 50 percent and 1 percent casualties, respectively, from the indicated air-blast effects, as a function of height of burst and distance from ground zero. The curves apply to randomly oriented, prone personnel exposed in the open to a 1 kt burst.

[redacted] *Scaling.* For yields other than 1 kt, scale as follows:

1. For the direct overpressure and eardrum rupture curves

$$\frac{d}{d_1} = \frac{h}{h_1} = W^{1/3}$$

where d_1 and h_1 are the distance from ground zero and height of burst respectively, for 1 kt; and d and h are the corresponding distance and height of burst for a yield of W kt.

2. For the translation and forest blowdown curves

$$\frac{d}{d_1} = \frac{h}{h_1} = W^{0.4}$$

where d_1 and h_1 are the distance from ground zero and height of burst, respectively, for 1 kt; and d and h are the corresponding distance and height of burst for a yield of W kt.

[redacted] *Example* [redacted]

Given: A 50 kt weapon burst at an altitude of 860 feet over open terrain.

Find: The distance from ground zero at which translational effects would produce 50 percent casualties among prone personnel.

Solution: The corresponding height of burst for 1 kt is

$$h_1 = \frac{h}{W^{0.4}} = \frac{860}{(50)^{0.4}} = 180 \text{ ft.}$$

From Figure 10-1, at a height of burst of 180 feet, the distance from ground zero at which 50 percent casualties among personnel in the open will occur for a 1 kt burst is 660 feet.

Answer: The corresponding distance for a 50 kt weapon is

$$d = d_1 \times W^{0.4} = 660 \times (50)^{0.4} = 3150 \text{ ft.}$$

Reliability: The distances obtained from Figures 10-1 and 10-2 are estimated to be reliable to within ±15 percent for the indicated effects; however, in view of the uncertainties discussed in paragraphs 10-5 and 10-6 (e.g., the presence of debris, crater ejecta, etc.) no precise estimate of the reliability can be made for a specific situation.

Related Material: See paragraphs 10-1 through 10-6.

[redacted]

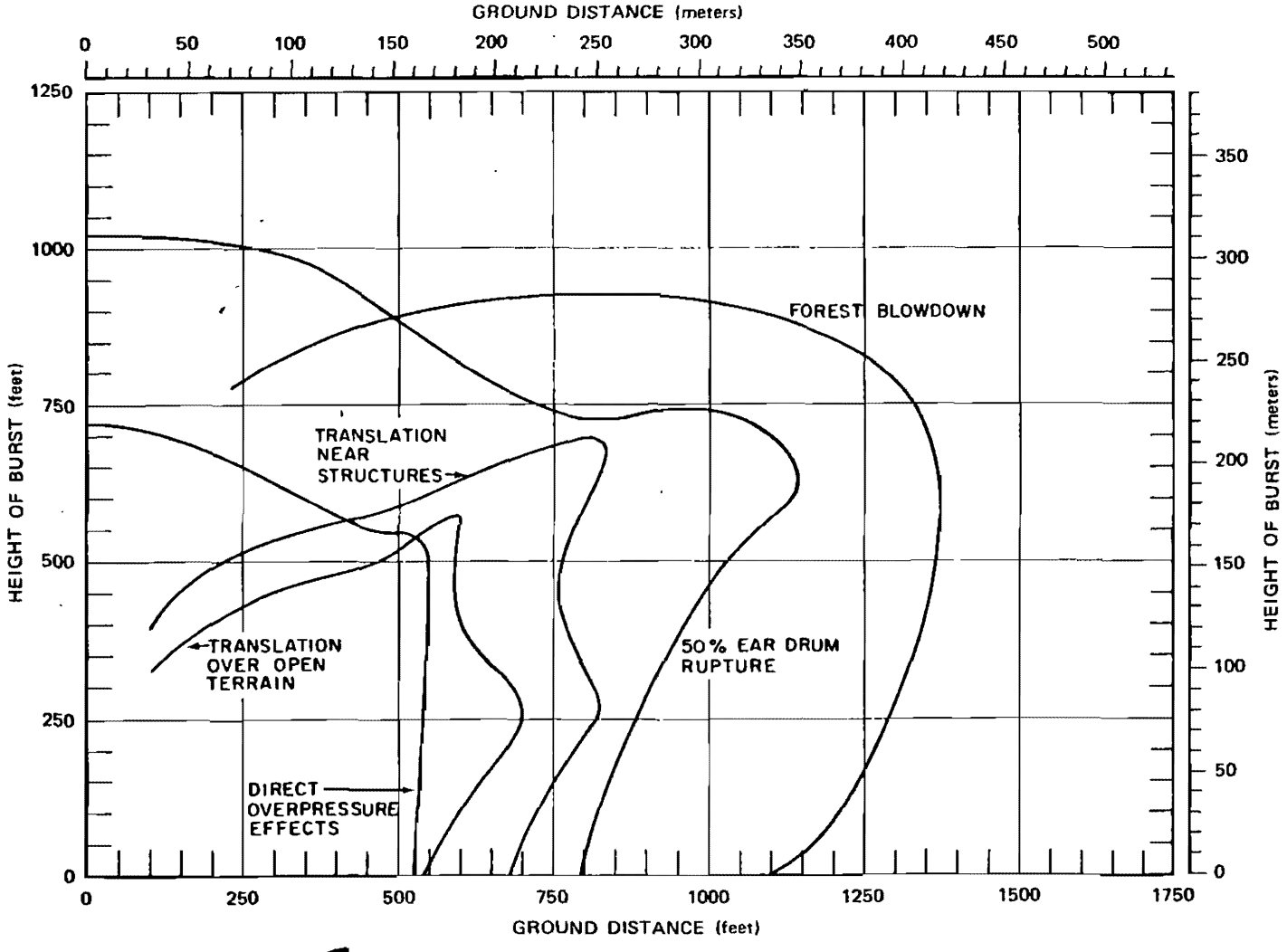

Figure 10-1. Fifty Percent Casualties for the Indicated Blast Effects for Prone Personnel Exposed in the Open or in a Forest to a 1 kt Burst

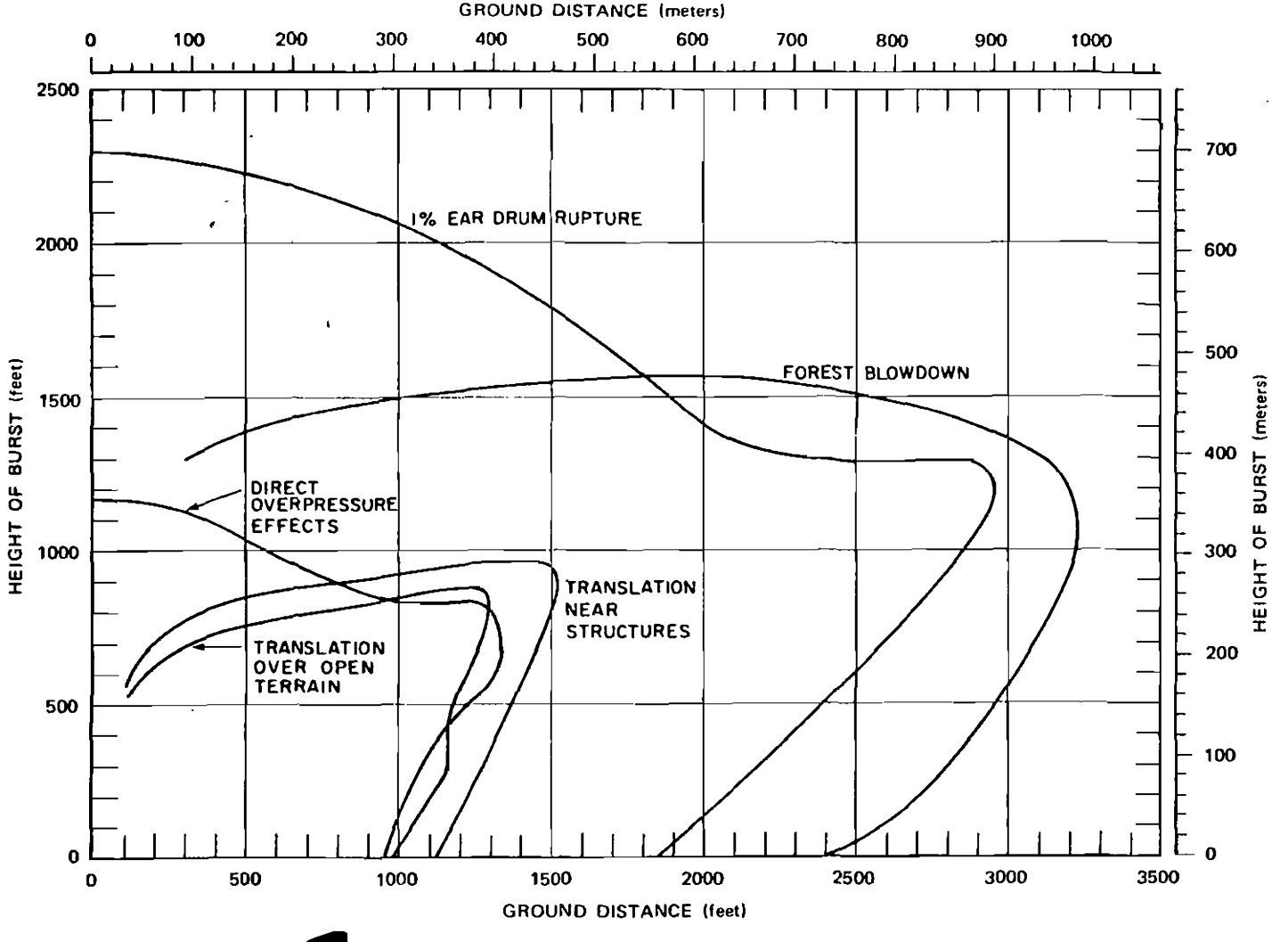

Figure 10-2. [redacted] One Percent Casualties for the Indicated Blast Effects for Prone Personnel Exposed in the Open or in a Forest to a 1 kt Burst [redacted]

SECTION II

THERMAL RADIATION

SKIN BURNS

When a nuclear weapon detonates, personnel will sustain skin burns at distances that may be larger than those distances at which injury occurs as a result of blast or nuclear radiation. These burns may be produced directly by the absorption of radiant energy by the skin, or indirectly by heat transference through clothing or by ignition of the clothing. Thermal radiation is composed of light in the ultraviolet, visible and infrared regions of the spectrum and travels in a straight line at the speed of light. It is emitted within periods of a few milliseconds to several tens of seconds.

If there is substantial material between the individual and the nuclear burst, the thermal radiation will be absorbed and no burns will be produced. Thus, persons in or behind buildings, vehicles, etc., will be shielded from the thermal pulse either partially or completely. In some instances, burns may be avoided or reduced if evasive action is taken during the delivery of the thermal pulse, since heating takes place only during direct exposure. These and other protective measures will be discussed later.

CLASSIFICATION OF BURNS

Burn severity is related to the degree of elevation of skin temperature and the length of time of this elevation. Pain, a familiar warning sensation, occurs when the temperature of certain nerve cells near the surface of the skin is raised to 43°C (109°F) or more. If the temperature is not elevated to a high enough degree or for a sufficient period of time, pain will cease and no injury will occur. The amount of pain is not related to burn severity as is the classification of first degree (1°), second degree (2°) or third degree (3°) burns but it is a useful tool in warning an individual to evade the thermal pulse.

10-9 First Degree Burns

A skin burn is an injury to skin caused by temperature elevation following application of heat by absorption of direct thermal radiation or by transference through cloth. First degree burns are characterized by immediate pain which continues after exposure and by ensuing redness of the exposed area. The first degree burn is a reversible tissue injury; the classic example is sunburn.

10-10 Second Degree Burns

Second degree burns are caused by temperatures that are higher and/or of longer duration than those necessary for first degree skin burns. The injury is characterized by pain and may be accompanied by either no immediate visible effect or by a variety of skin changes including blanching, redness, loss of elasticity, swelling and blisters. After 6 to 24 hours, a scab will form over the injured area. The scab may be flexible, tan or brown, if the injury is moderate, or it may be thick, stiff and dark, if the injury is more severe. Second degree burn wounds will heal within one to two weeks unless they are complicated by infection. Second degree burns do not involve the full thickness of the skin, and the remaining uninjured cells may be able to regenerate normal skin without scar formation.

10-11 Third Degree Burns

Third degree burns are caused by temperatures of a higher magnitude and/or longer duration than second degree burns. The injury is characterized by pain at the peripheral, less injured areas only, since the nerve endings in the centrally burned areas are damaged to the extent that they are unable to transmit pain impulses. Immediately after exposure, the skin may appear normal, scalded, or charred, and it may lose its elasticity. The healing of third degree burns takes several weeks and always results in scar formation unless new skin is grafted over the

[redacted]

burned area. The scar results from the fact that the full thickness of the skin is injured, and the skin cells are unable to regenerate normal tissue.

10-12 Reduction in Effectiveness by Burns

The distribution of burns into three groups obviously has certain limitations since it is not possible to draw a sharp line of demarcation between first- and second-degree, or between second- and third-degree burns. Within each class the burn may be mild, moderate, or severe, so that upon preliminary examination it may be difficult to distinguish between a severe burn of the second degree and a mild third-degree burn. Subsequent pathology of the injury, however, will usually make a distinction possible. In the following discussion, reference to a particular degree of burn should be taken to imply a moderate burn of that type.

The depth of the burn is not the only factor in determining its effect on the individual. The extent of the area of the skin which has been affected is also important. Thus, a first-degree burn over the entire body may be more serious than a third-degree burn at one spot. The larger the area burned, the more likely is the appearance of symptoms involving the whole body. Furthermore: there are certain critical, local regions, such as the hands, where almost any degree of burn will incapacitate the individual.

Persons exposed to a low or intermediate yield nuclear weapon burst may sustain very severe burns on their faces and hands or other exposed areas of the body as a result of the short pulse of directly absorbed thermal radiation. These burns may cause severe superficial damage similar to a third degree burn, but the deeper layers of the skin may be uninjured. This would result in rapid healing similar to a mild second degree burn. Thermal radiation burns occurring under clothing or from ignited clothing or other tinder will be similar to those ordinarily seen in burn injuries of nonnuclear origin. Because of the longer duration of the thermal pulse, the differences between flash burns on exposed skin from air burst high yield weapons and burns of nonnuclear origin may be less apparent.

BURN INJURY ENERGIES AND RANGES

The critical radiant exposure for a skin burn changes as the thermal radiation pulse duration and spectrum change; therefore, the critical distance cannot be determined simply from the calculated radiant exposure. The effective spectrum shifts with yield and altitude; the thermal radiation pulse is shorter for smaller yields or higher burst altitudes (see Chapter 3).

10-13 Personnel Parameters

The probability and severity of an individual being burned will depend upon many factors including: pigmentation, absorptive properties, thickness, conductivity and initial temperature of the skin; distance from the detonation and the amount of shielding; clothing, orientation with respect to the burst, and voluntary evasive action.

Severity of the burn cannot be determined by temperature elevation and pulse duration alone. The energy absorbed by the skin in a normal population may vary by as much as 50 percent because of the variance in skin pigmentation. It is known that depths in skin of 0.001 to 0.002 centimeter are the sites of the initial damage that results in a burn from thermal radiation pulses and that skin temperatures of 70°C (158°F) for a fraction of a second or temperatures of 48°C (118°F) for minutes can result in burns. Skin temperatures for first degree and third degree burns are roughly 25 percent lower and higher, respectively, than those for second degree burns.

For pulses of 0.5 second duration and longer, the amount of energy absorbed is an im-

[redacted]

portant factor. Figure 10-3 shows the effect of absorptive differences of human skin as calculated from measurements of the spectral absorptance and the spectral distribution of the peak power of nuclear weapons bursts in the lower atmosphere. As shown in Figure 10-3, very dark skinned people will receive burns from approximately two-thirds the energy required to produce the same degree of burns on very light skinned people.

10-14 Burn Exposures for Unprotected Skin

Figure 10-4 shows ranges of radiant exposures for the probabilities of burn occurrence. The solid lines represent 50 percent probability for an average population taking no evasive action to receive the indicated type of burns. The dotted lines divide the burn probability distributions into ranges for the three burn levels with average burn probabilities of 18 percent and 82 percent assigned within these exposure ranges.

For example, from Figure 10-4, it can be predicted that, if a normal population is exposed to the thermal pulse at distances producing between 4.5 and 6.0 calories per square centimeter from a 1 megaton weapon, 18 percent of the population will receive second degree burns and 82 percent will receive first degree burns.

A radius from ground zero that produces areas of equal burn probability may be obtained by employing the radiant exposures for skin burn probability from Figure 10-5 and the weapon yield-distance relationship for radiant exposures from Chapter 3.

10-15 Burns Under Clothing

Skin burns under clothing are produced several ways: by direct transmittance through the cloth if the cloth is thin and merely acts as an attenuating screen; by heating the cloth and causing steam or volatile products to impinge on the skin; by conduction from the hot fabric to the skin; or the fabric may ignite, and consequent volatiles and flames will cause burns where they impinge on the skin.

Heat transfer mechanisms cause burns beneath clothing as a result of heat transfer for some time after the thermal pulse ends. These burns generally involve deeper tissues than those that result from the direct thermal pulse on bare skin. Burns caused by ignited clothing also result from longer heat application, and thus will be more like burns occurring in nonnuclear weapon situations.

10-16 Body Areas Involved

The pattern of body area involved in thermal radiation burns from nuclear weapons will differ from the areas injured from conventional means. For weapons of 100 kt or less, where effective evasive action cannot be taken, burns would occur primarily on the directly exposed parts of the body unless the clothing ignites. First and second degree burns of the uncovered skin, and burns through thin clothing occur at lower radiant exposures than those which ignite clothing. Because of these factors, first and second degree burns for this low yield range would involve limited body area and would occur only on one side of the body. For closer distances where the direct thermal pulse produces burns and clothing ignition takes place, persons wearing thin clothing would have third degree burns over that area of the body facing the burst. This phenomenon is typically seen in persons whose clothing catches fire by conventional means.

For the yield range 100 kt and less, persons wearing heavy clothing (in the third degree bare skin burn and clothing ignition zone) will have third degree burns on one exposed body surface and third degree burns on other areas resulting from the burning clothes prior to its removal, or full body third degree burns if the clothing cannot be removed.

[redacted]

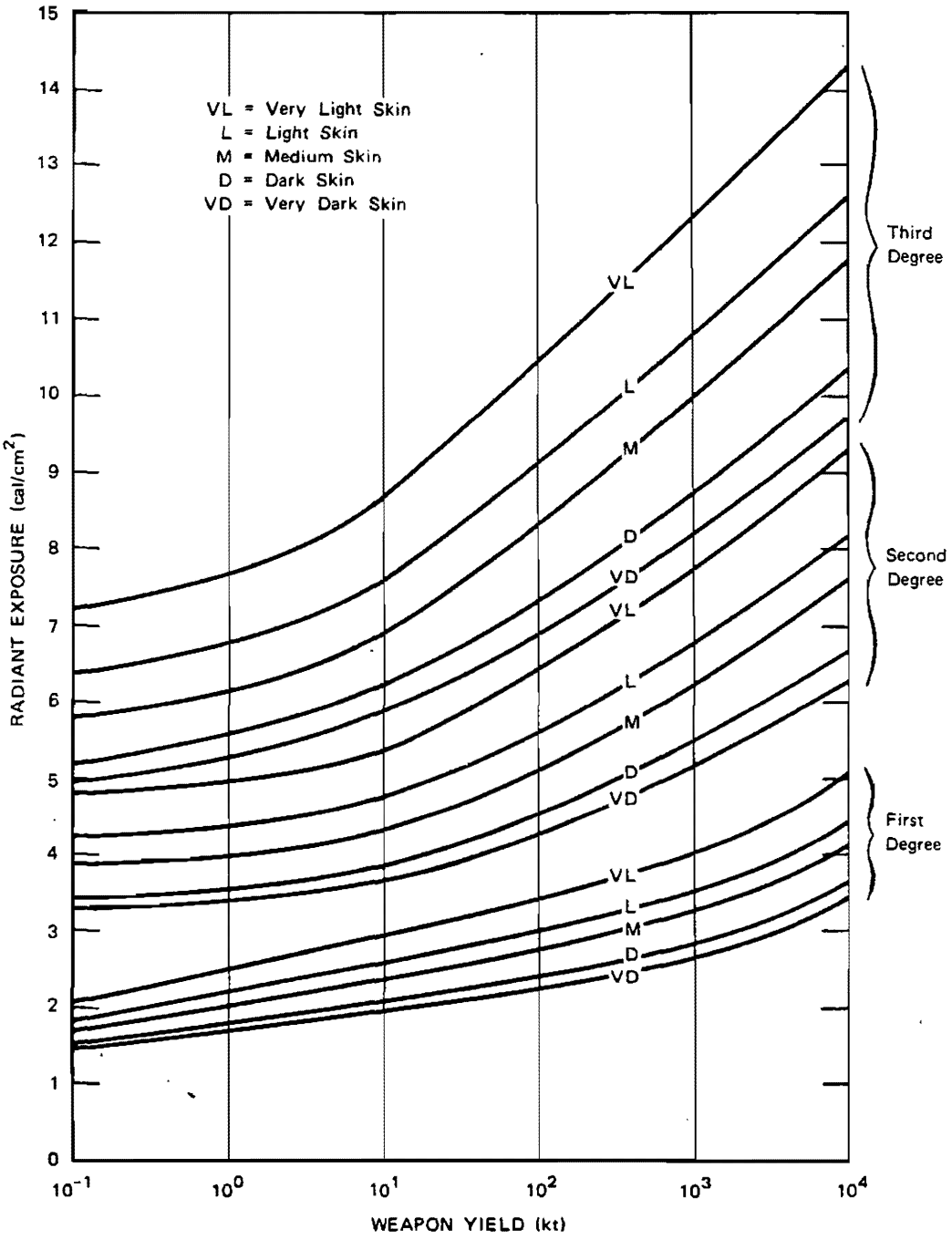

Figure 10-3. [redacted] Radiant Exposure Required to Produce Skin Burns for Different Skin Pigmentation [redacted]

[redacted]

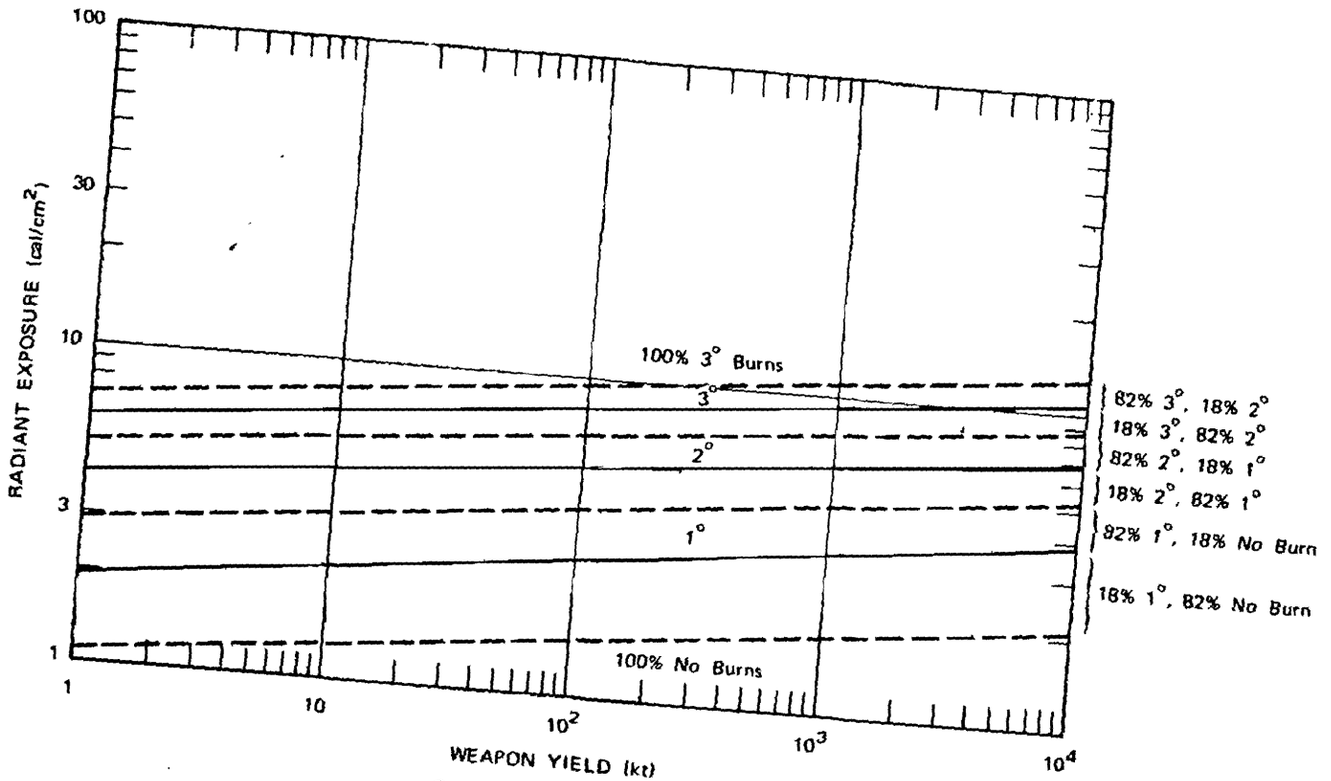

Figure 10-4. [redacted] Skin Burn Probabilities for an Average Population Taking No Evasive Action [redacted]

[redacted]

10-17 Incapacitation from Burns [redacted]

[redacted] Burns to certain anatomical sites of the body, even if only first degree, will frequently cause ineffectiveness because of their critical location. Any burn surrounding the eyes that causes occluded vision because of the resultant swelling of the eyelids, will be incapacitating. Burns of the elbows, knees, hands and feet produce immobility or limitation of motion as the result of swelling, pain or scab formation, and will cause ineffectiveness in most cases. Burns of the face and upper extremity areas are most likely to occur because these areas will more frequently be unprotected. Second or third degree burns in excess of 20 percent of the surface area of the body should be considered a major burn and will require special medical care in a hospital.

[redacted] Shock is a term denoting a generalized state of severe circulatory inadequacy. It will result in ineffectiveness and if untreated may cause death. Third degree burns of 25 percent of the body and second degree burns of 30 percent of the body will generally produce shock within 30 minutes to 12 hours and require prompt medical treatment. Such medical treatment is complicated and causes a heavy drain on medical personnel and supply resources.

10-18 Modification of Injury [redacted]

[redacted] Timely evasion can be effective in reducing burns with weapons yields of 100 kt and greater. The length of time between the burst and the point at which critical radiant exposure occurs increases with increasing yields, permitting personnel to react prior to receiving severe burns. With yields of less than about 100 kt, or for high altitude bursts of larger yields, the thermal pulse is too short for personnel to react and take cover. Since pain occurs at low radiant exposures and at lower temperatures than those that cause first degree burns, it is the initial sensation that occurs, and involuntary action due to pain can be expected instinctively. More effective action can be expected with proper training. Figure 10-5 illustrates the effect of evasion on the production of burns.

[redacted] Personnel in the shadow of buildings, vehicles, or other objects at the time of detonation will be shielded from the pulse and will not be burned.

[redacted] EFFECTS OF THERMAL RADIATION ON THE EYES [redacted]

[redacted] Exposure of the eye to a bright flash of a nuclear detonation produces two possible effects; flashblindness and/or retinal burns.

10-19 Flashblindness [redacted]

[redacted] Flashblindness (dazzle) is a temporary impairment of vision caused by the saturation of the light sensitive elements (rods and cones) in the retina of the eye. It is an entirely reversible phenomena which will normally blank out the entire visual field of view with a bright afterimage. Flashblindness normally will be brief, and recovery is complete.

[redacted] During the period of flashblindness (several seconds to minutes) useful vision is lost. This loss of vision may preclude effective performance of activities requiring constant, precise visual function. The severity and time required for recovery of vision are determined by the intensity and duration of the flash, the viewing angle from the burst, the pupil size, brightness necessary to perform a task and the background, and the visual complexity of the task. Flashblindness will be more severe at night since the pupil is larger and the object being viewed and the background are usually dimly illuminated.

[redacted] Flashblindness may be produced by scattered light and does not necessarily require eye focusing on the fireball.

10-20 Retinal Burns [redacted]

[redacted] A retinal burn is a permanent eye injury that occurs whenever the retinal tissue is heated.

[redacted]

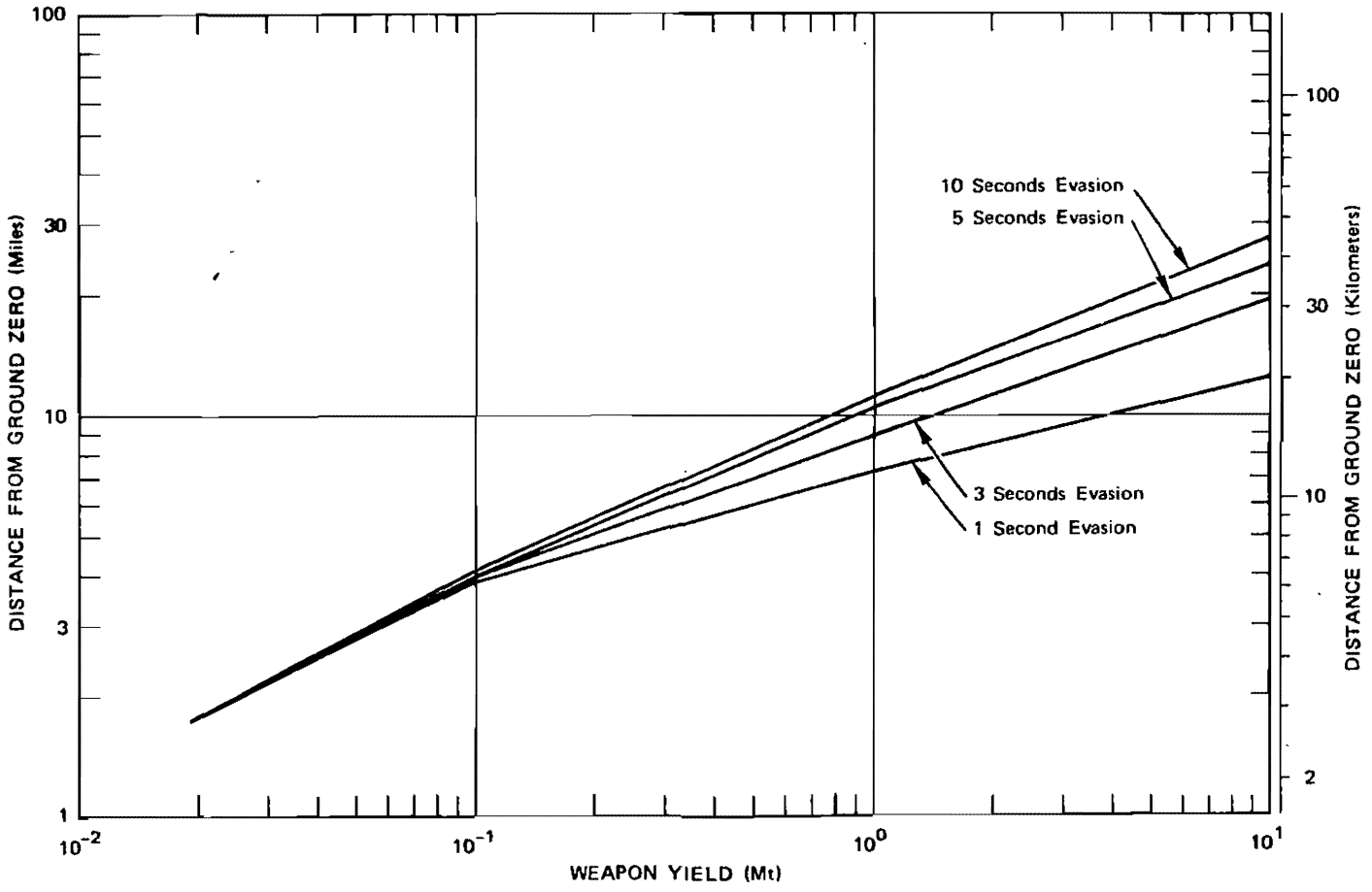

Figure 10-5. Distance Thresholds for Second Degree Burns for Various Evasion Times

[redacted]

excessively by the focused image of the fireball within the eye. The underlying pigmented cells absorb much of the light and raise the temperature in that area. A temperature elevation of 12–20°C (22–36°F) in the eye produces a thermal injury which involves both the pigmented layer and the adjacent rods and cones, so the visual capacity is permanently lost in the burned area. The natural tendency of personnel to look directly at the fireball tends to increase the incidence of retinal burns.

[redacted] Retinal burns can be produced at great distances from nuclear detonations, because the probability of eye burns does not decrease as the square of the distance from the detonation as is true of many other nuclear weapons effects. Theoretically, the optical process of image formation within the eye negates the inverse square law and keeps the intensity per unit area on the retina a constant, regardless of the distance. However, meteorological conditions and the fact that the human eye is not a perfect lens, all contribute toward reducing the retinal burn hazard as the distance is increased between the observer and the detonation.

[redacted] Explosion yields greater than one megaton, and at heights of burst greater than about 130 kilofeet may produce retinal burns as far out as the horizon on clear nights. Bursts above 490 kilofeet probably will not produce any retinal burns in personnel on the ground unless the weapon yield is greater than 10 Mt.

(U) A retinal burn normally will not be noticed by the individual concerned if it is off the central axis of vision; however, very small burned areas may be noticeable if they are centrally located. Personnel generally will be able to compensate for a small retinal burn by learning to scan around the burned area.

10-21 Modification of Thermal Effects on the Eye [redacted]

[redacted] The thermal pulse from a nuclear weapon is emitted at such a rapid rate that any device designed to protect the eye must close extremely fast (<100 μsec) to afford a sure degree of protection for all situations. During the daytime, when the pupil is smaller and objects are illuminated brightly, the 2 percent transmission gold goggle/visor will reduce flashblindness recovery times to acceptable levels. At present, this goggle is unsatisfactory for use at night, and there is no protective device that is adequate for night use.

[redacted] The blink reflexes of the eye are sufficiently fast (~0.2 second) to provide some protection against weapons greater than 100 kt detonated below about 130 kilofeet. The blink time is too slow to provide any appreciable protection for smaller weapon yields or higher burst altitudes.

[redacted] When personnel have adequate warning of an impending nuclear burst, evasive action including closing or shielding the eyes will prevent flashblindness and retinal burns.

10-22 Safe Separation Distance Curves [redacted]

[redacted] Figures 10–6 through 10–10 present flashblindness and retinal burn curves for a number of burst heights as a function of weapon yields and safe separation distance, e.g., that distance where personnel will not receive incapacitating eye injuries. The retinal burn curves show distances that current data show to be safe. The curves for flashblindness were specifically designed for pilots of strategic bombers, where a pilot can effectively read his instruments and complete his mission after a temporary 10 second complete loss of vision. These curves are also applicable to any task where the same criteria of dim task lighting, visual demands, and the 10 second visual loss can be applied. Data are not available for specific distances at which flashblindness will not occur.

[redacted] It should be noted that the flashblindness and the retinal burn safe separation distances do not bear the same relationship to one another as the yield changes. In circumstances that require determination of complete eye safety (realizing

[redacted]

[redacted]

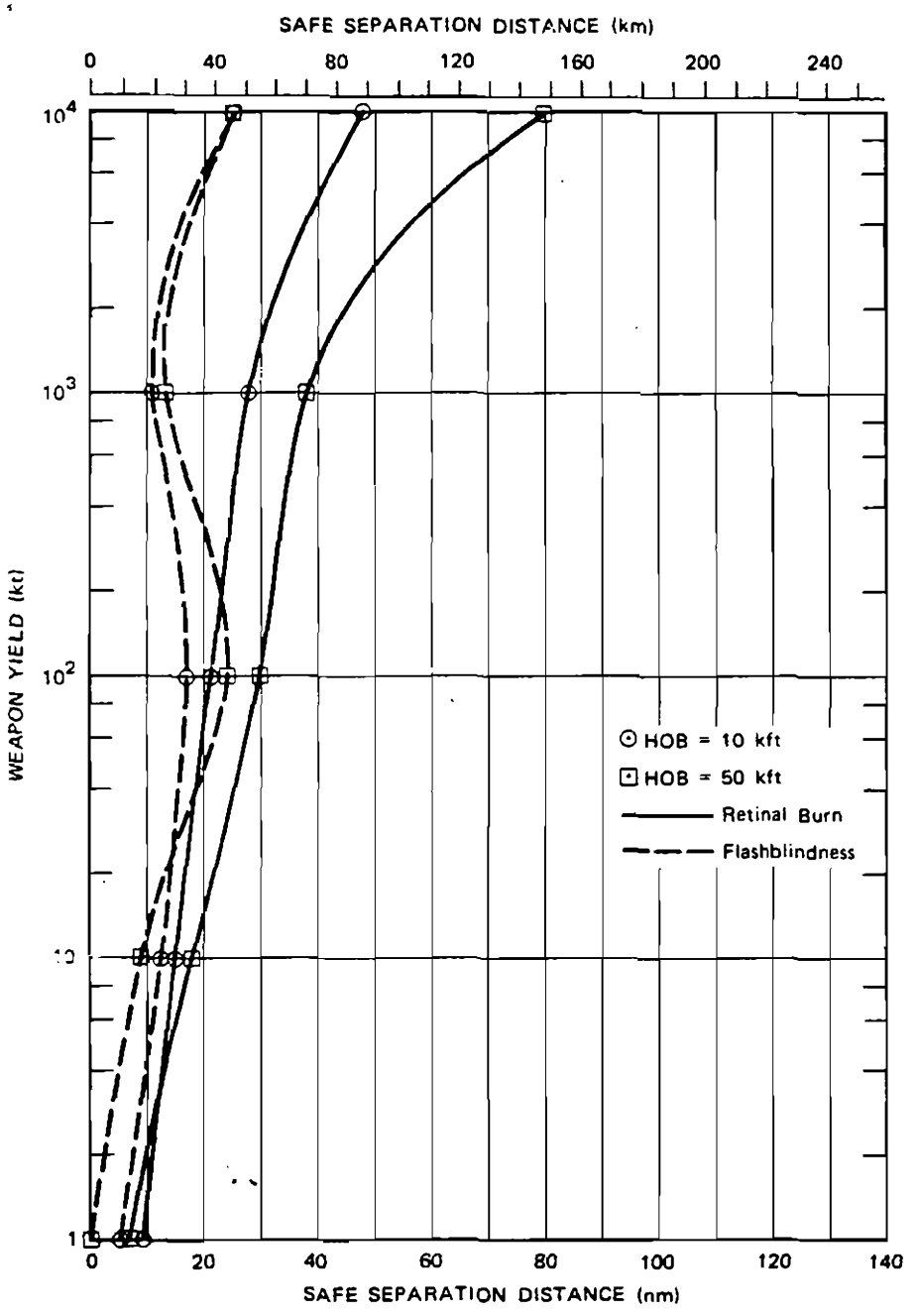

Figure 10-6. [redacted] Safe Separation Distances, for an Observer on the Ground, from Bursts at 10 kft and 50 kft During the Day [redacted]

[redacted]

[redacted]

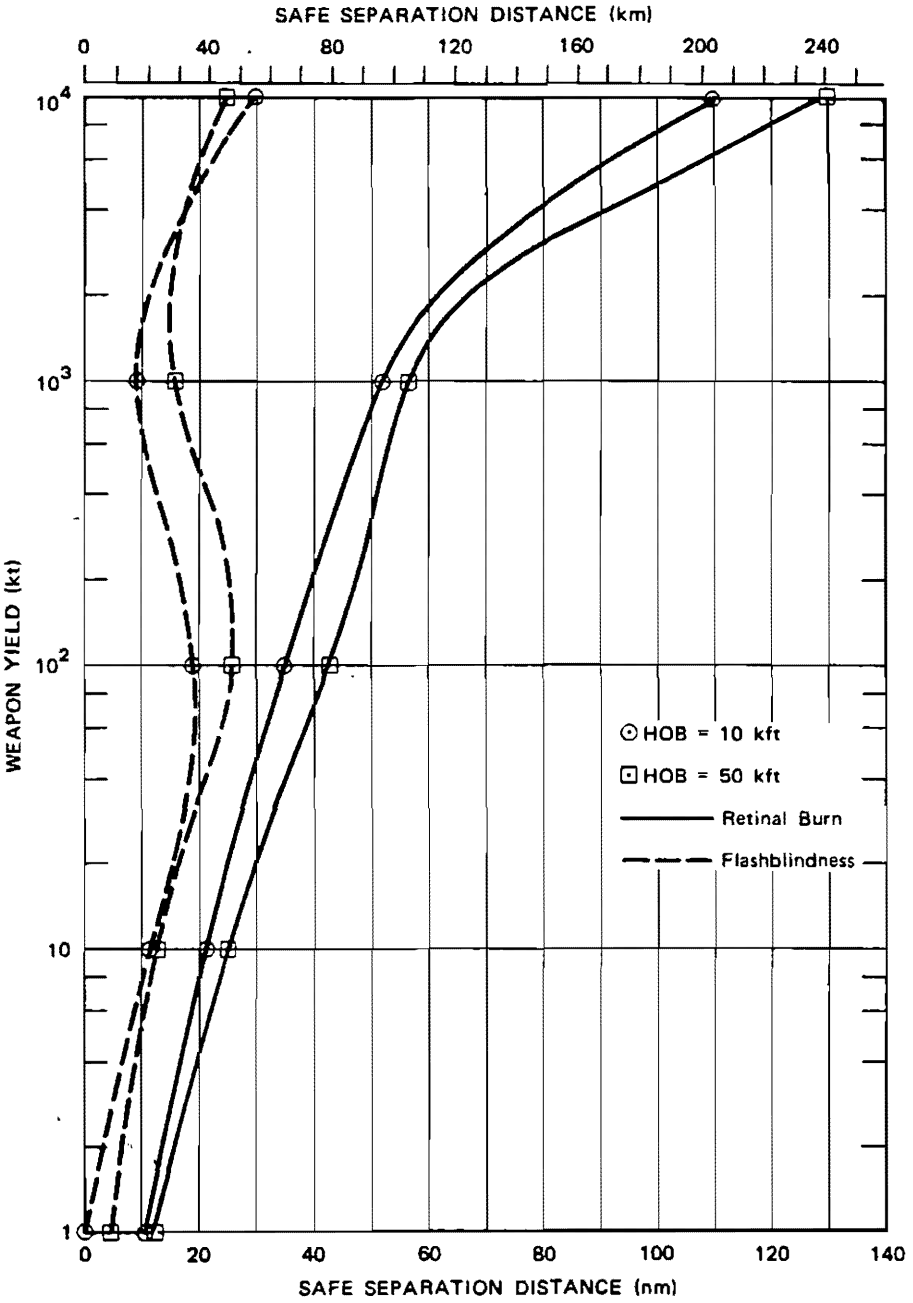

Figure 10-7. [redacted] Safe Separation Distance, for an Observer at 50 kft, from Bursts at 10 kft and 50 kft During the Day [redacted]

[redacted]

[redacted]

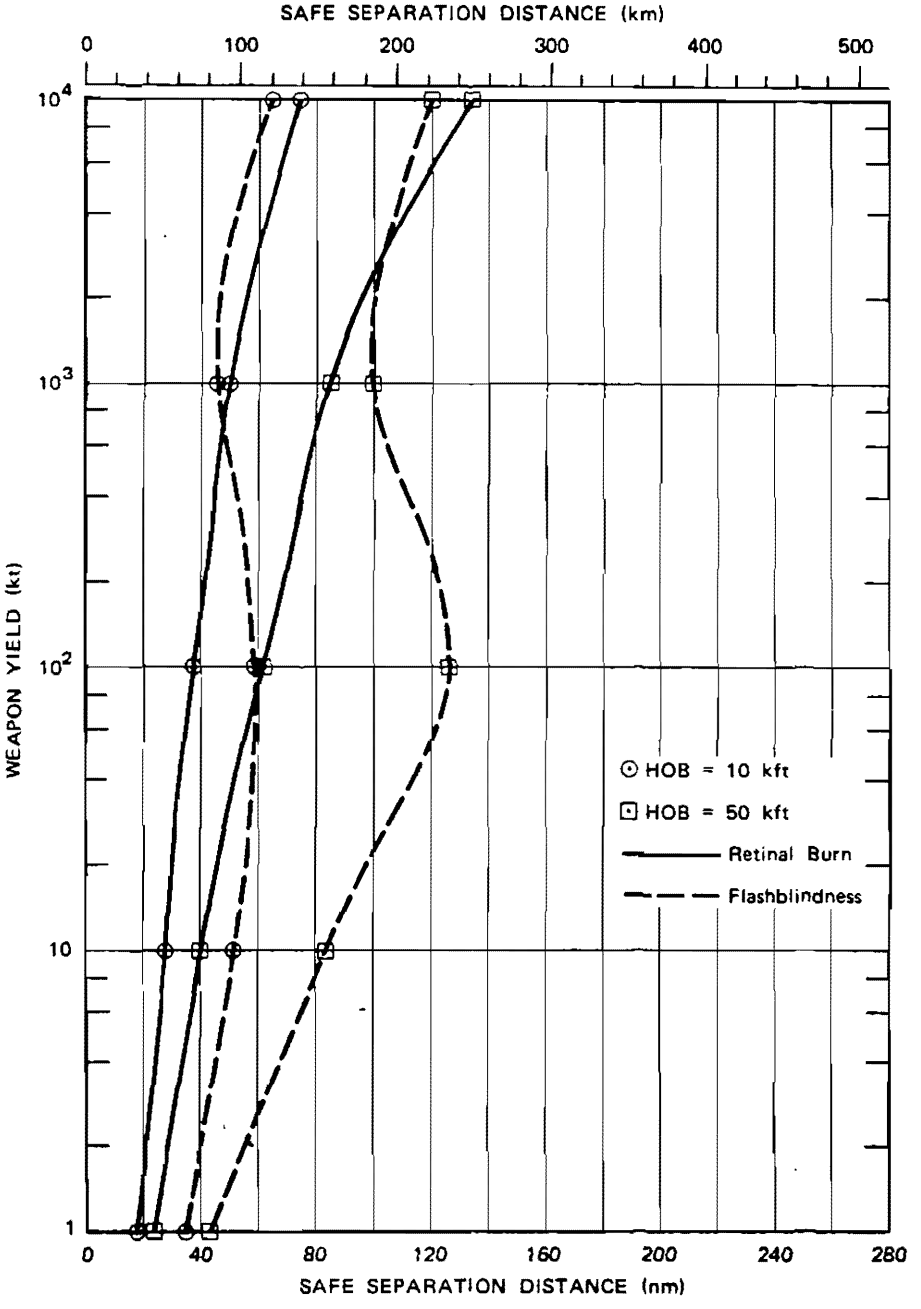

Figure 10-8. [redacted] Safe Separation Distance, for an Observer on the Ground, from Bursts at 10 kft and 50 kft, During the Night [redacted]

[redacted]

[redacted]

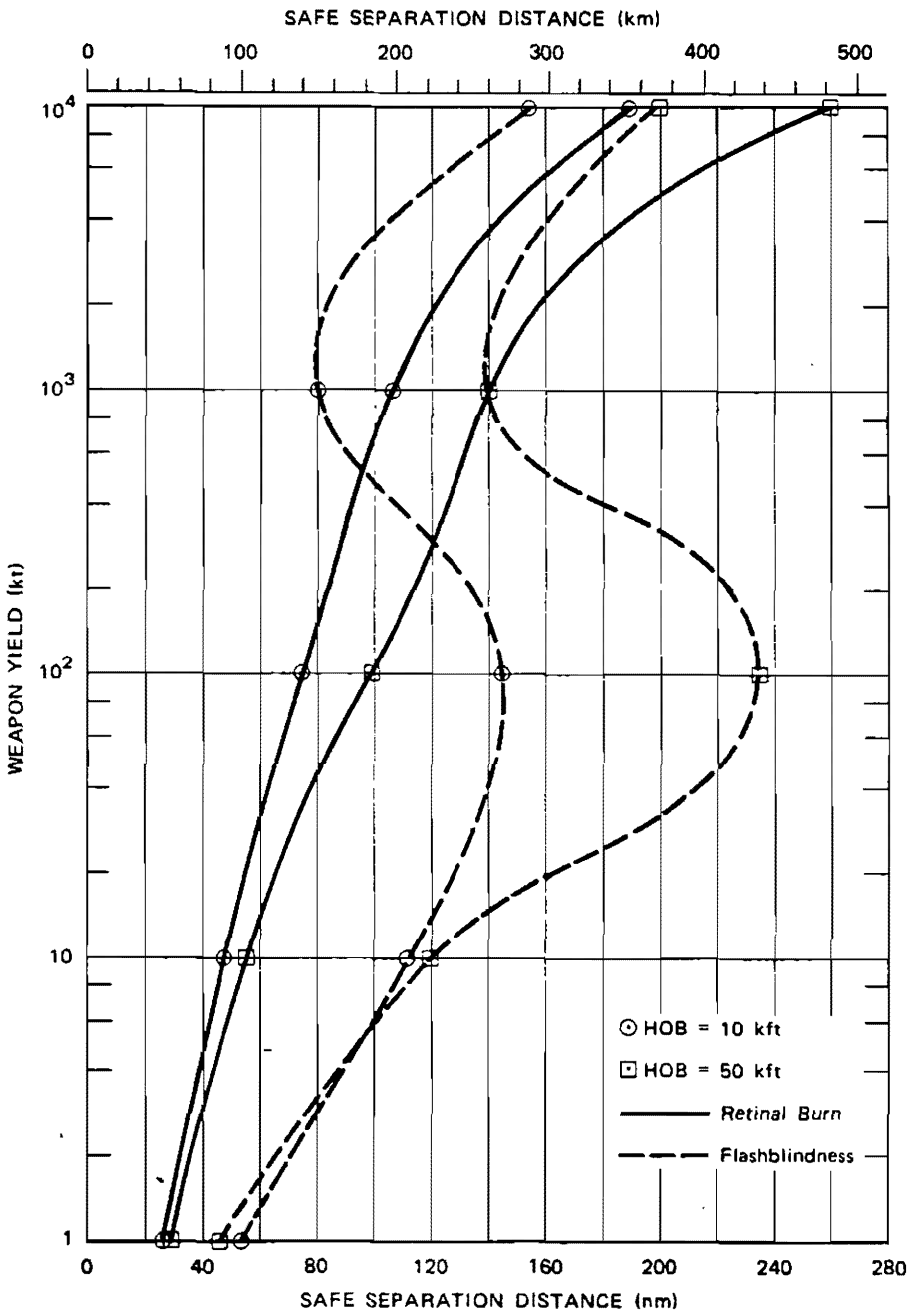

Figure 10-9. [redacted] Safe Separation Distance, for an Observer at 50 kft, from Bursts at 10 kft and 50 kft, During the Night [redacted]

[redacted]

[redacted]

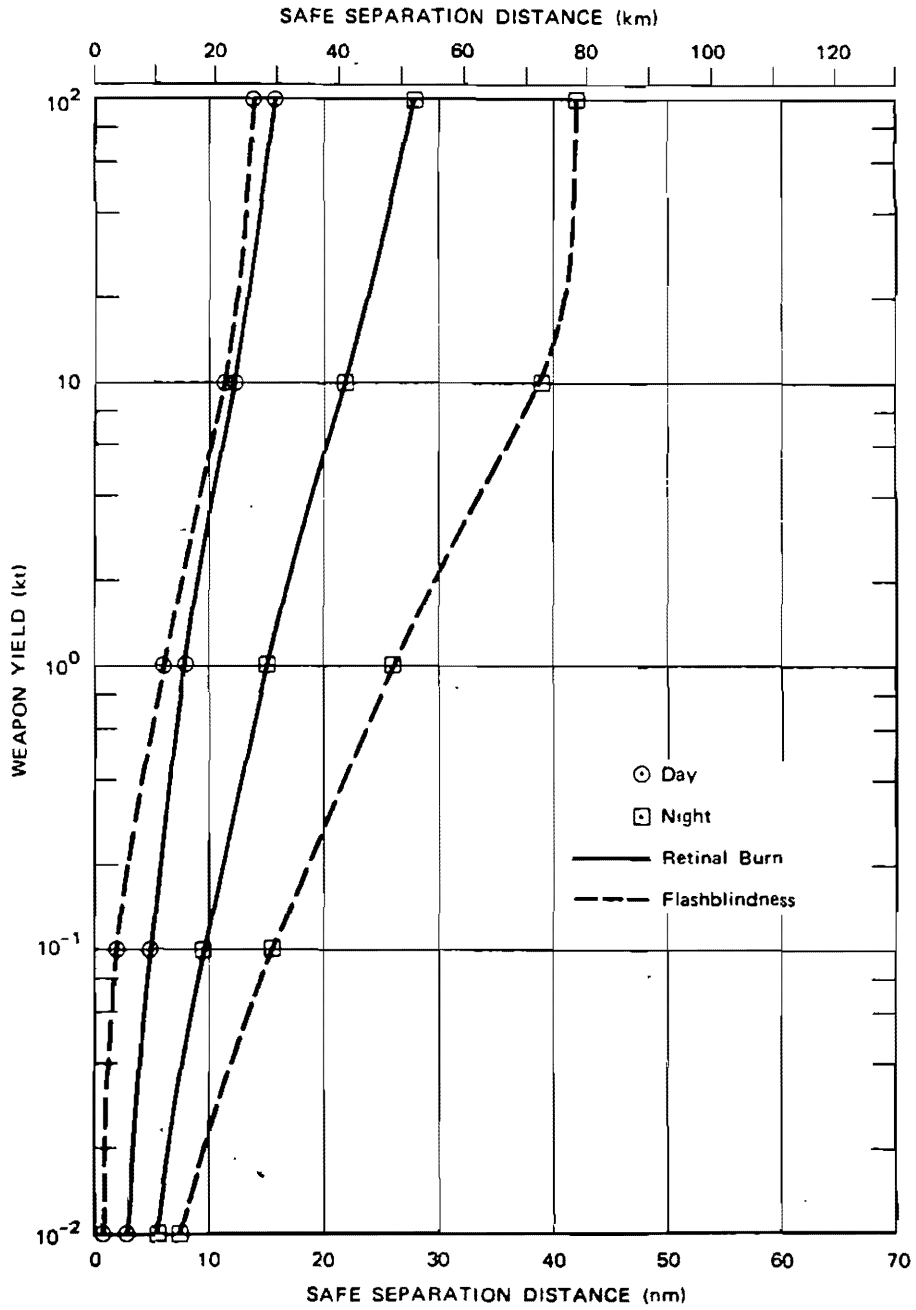

Figure 10-10. [redacted] Safe Separation Distance, for an Observer on the Ground, from Low Yield Weapons Exploded at 1,000 ft Height of Burst [redacted]

[redacted]

the 10 second loss of vision criterion in the flashblindness curves), the retinal burn or flashblindness curve that shows the effect that occurs at the greatest distance from the burst should be used. For example, using Figure 10–8 and a 50 kilofeet height of burst, to determine the distance from a nuclear detonation where there will be no incapacitating eye effects, the flashblindness curve is the limiting factor up to about 3 megatons, then the retinal burn curve becomes the limiting factor.

In instances where only permanent eye damage is of interest, and the temporary loss of vision from flashblindness is not of concern, only the retinal burn curves should be used.

The retinal burn curves show distances at which a nuclear burst will not produce retinal burns provided the eye can blink within 250 milliseconds. A faster blink time would not change the distances appreciably. The curves are based on a very clear day (60 mile visual range). For a cloudy day with a 5 mile visual range, the safe separation distances would be reduced by about 50 percent.

SECTION III
NUCLEAR RADIATION

The injurious effects of nuclear radiations (gamma rays, neutrons, beta particles and alpha particles) on the human target represent a phenomenon that is completely absent from conventional explosives. Since there has not been sufficient experience with humans in the exposure ranges of military interest, the material presented below is based largely on animal experimentation that has been extrapolated to the area of human response. Even if sufficient human data were available, they would be expected to show similar responses and the same wide range of biological variability within species as is seen in animals. Data are presented in terms of absorbed dose at or near the body surface in order to relate to source and transport factors given in Chapter 5. Current radiobiological research results are frequently reported as *midline tissue dose* in rad, a dose significantly lower than doses measured by radiac instruments and absorbed within those volumes near the surface of the body that faces toward the source. For nuclear weapon radiation, the midline tissue doses would be approximately 70 percent of the body surface doses presented in the following paragraphs.

INITIAL RADIATION

Neutrons and gamma rays in various proportions are responsible for biological injury from initial radiation. For military purposes, and until further animal experimentation provides evidence to the contrary, it must be assumed that damage to tissue is directly proportional to the absorbed dose regardless of whether it is delivered by neutrons or gamma rays. For effects of military interest, it is assumed that injury from a neutron rad is equal to that from a gamma rad, and that one rad absorbed dose results from exposure to one roentgen.

10-23 Radiation Sickness

Individuals exposed to whole body ionizing radiation may show certain signs and symptoms of illness. The time interval to onset of these symptoms, their severity, and their duration generally depend on the amount of radiation absorbed, although there will be significant variations among individuals. Within any given dose range, the effects that are manifested can be divided conveniently into three time phases: initial, latent, and final.

During the initial phase, individuals may experience nausea, vomiting, headache, dizziness and a generalized feeling of illness. The onset time decreases and the severity of these symptoms increases with increasing doses. During the latent phase, exposed individuals will experience few, if any, symptoms and most likely will be able to perform operational duties. The final phase is characterized by frank illness that re-

[redacted]

quires hospitalization after exposure to the higher doses. In addition to the recurrence of the symptoms noted during the initial phase, skin hemorrhages, diarrhea and loss of hair may appear, and, at high doses, seizures and prostration may occur. The final phase is consummated by recovery or death. At doses above 1000 rad, death may be expected in all cases. Maximum recovery of survivors exposed to lower doses may require as much as three to six months time. With the foregoing in mind, Table 10-2 is presented as the best available summary of the effects of various whole-body dose ranges of ionizing radiation in human beings.

10-24 Incapacitation [redacted]

[redacted] Direct effects of high doses of external radiation administered over a short time period may result in loss of ability to perform purposeful actions. At doses greater than 2,000 rads, an acute collapse may occur in a short time. The collapse may persist from several minutes to a few hours. A period of relatively normal performance capability will then occur; however, after some time permanent incapacitation and death will result. This early incapacitation, followed by a temporary period of recovery, is defined as early transient incapacitation (ETI). Following this transient incapacitation, exposed personnel *may* be reasonably well oriented, lucid, and able to perform tasks requiring coordination of visual and auditory sensory input. The duration of early transient incapacitation is believed to be dose dependent, i.e., the greater the dose, the longer the transient incapacitation phase. The duration of the temporary period of effec-

Table 10-2 [redacted] Response to Single Whole-Body Exposures [redacted]

	100-200 Rad	200-400 Rad	400-600 Rad	600-1000 Rad	1000-2500 Rad
Initial Phase					
1. Onset of symptoms after irradiation	3-6 hrs	1-6 hrs	1/2 to 6 hrs	1/4 to 4 hrs	5-30 min
2. Duration of phase	≤1 day	1-2 days	1-2 days	≤2 days	≤1 day
Latent Phase					
1. Onset after irradiation	≤1 day	1-2 days	1-2 days	≤2 days	≤1 day
2. Duration of phase	≤2 weeks	2-4 weeks	1-2 weeks	5-10 days	0-7 days*
Final Phase					
1. Onset of symptoms after irradiation	10-14 days	2-4 weeks	7-14 days	5-10 days	4-8 days
2. Duration of phase	4 weeks	2-8 weeks	1-8 weeks	1-4 weeks	2-10 days
3. Time from irradiation to death	—	4-12 weeks	2-10 weeks	1-6 weeks	4-14 days
4. Deaths (% of those exposed)	No deaths	0-30%	30-90%	90-100%	100%

*At the higher doses within this range there may be no latent period.

[redacted]

[redacted]

tiveness is inversely related to the dose. At doses in excess of 15,000 rads, most individuals will experience permanent complete incapacitation within a few minutes post-irradiation, followed by death within 2 to 24 hours.

[redacted] Figures 10-11 through 10-15 list estimated personnel effectiveness at various times following acute radiation doses of 1,400 rads and greater. It should be noted that incapacitation, or performance, decrement, and not death, is the endpoint of interest in these figures.

10-25 Modification of Injury [redacted]

[redacted] When only a portion of the body is exposed to radiation, the effects are significantly less than those described in the preceding two sections. The reduction of the effects depends on the magnitude of exposure and the particular portion of the body that is exposed. Thus, partial shielding afforded by natural or man-made structures can be expected to decrease the severity of radiation injury.

[redacted] Considerable effort has been expended in searching for compounds that will reduce the extent and seriousness of radiation injury when they are administered prior to exposure. At present, there is no satisfactory compound available for issue, although research continues in this area.

[redacted] Treatment of radiation injury is supportive in nature. The treatment is based primarily on symptomology rather than measured or estimated dose received by the individual.

10-26 Military Assumptions [redacted]

[redacted] In order to apply the material above to other than single exposures, it may be assumed that multiple exposures within any 24-hour period are arithmetically additive. This assumption is necessary because the information concerning the results of multiple exposures is limited.

[redacted] Although there is reason to believe that recovery from radiation exposure(s) is never really complete (i.e., some residual injury not necessarily affecting effectiveness remains), it may be assumed for military planning purposes that recovery is complete in approximately 30 days following a single sublethal exposure. Table 10-2 lists more specific information regarding durations of ineffectiveness under varying exposure conditions.

[redacted] RESIDUAL RADIATION [redacted]

[redacted] The importance of residual radiation as a source of injury to personnel depends upon the necessity for military operations in or near areas of local fallout. Time of arrival, weathering, and decay of the deposited fallout all result in a constantly changing rate of external protracted exposure to personnel in contrast to the almost instantaneous exposure to initial radiation. An added hazard results from the presence of small, finely divided, radioactive particulate sources that can contribute to injury by both external and internal irradiation.

10-27 External Hazards [redacted]

[redacted] Gamma rays present the major militarily significant external hazard from residual radiation. Effects on personnel will range from those described previously for initial radiation exposures (in new, high dose-rate, fallout fields) to lesser effects for the same total exposure in low dose-rate fields.

[redacted] Beta burns can occur if fallout particles remain on the skin for periods of hours or more. They will occur most frequently when the fallout particles are deposited on moist skin areas, body crevices, in the hair, or when the particles are held in contact by clothing. While minor skin symptoms may occur during the first 48 hours following exposure, the appearance of burns will be delayed two weeks or more after exposure. Severity of the burns is a function of the radioactivity of the fallout particles and the time period during which they adhere to the body. Personnel ineffectiveness will depend on the severity of the burn and its location on the body.

[redacted]

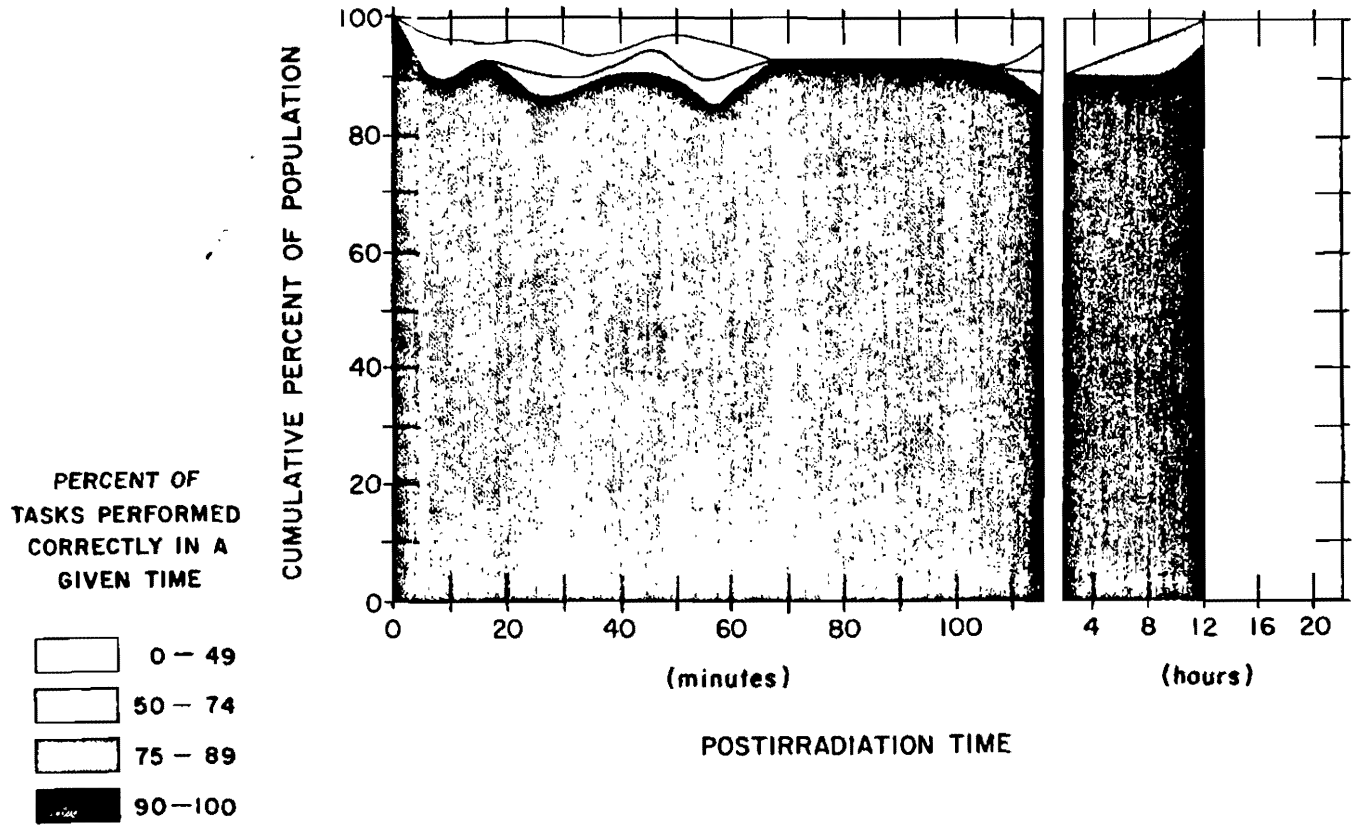

Figure 10-11. Personnel Effectiveness After Exposure to 1,400 rads

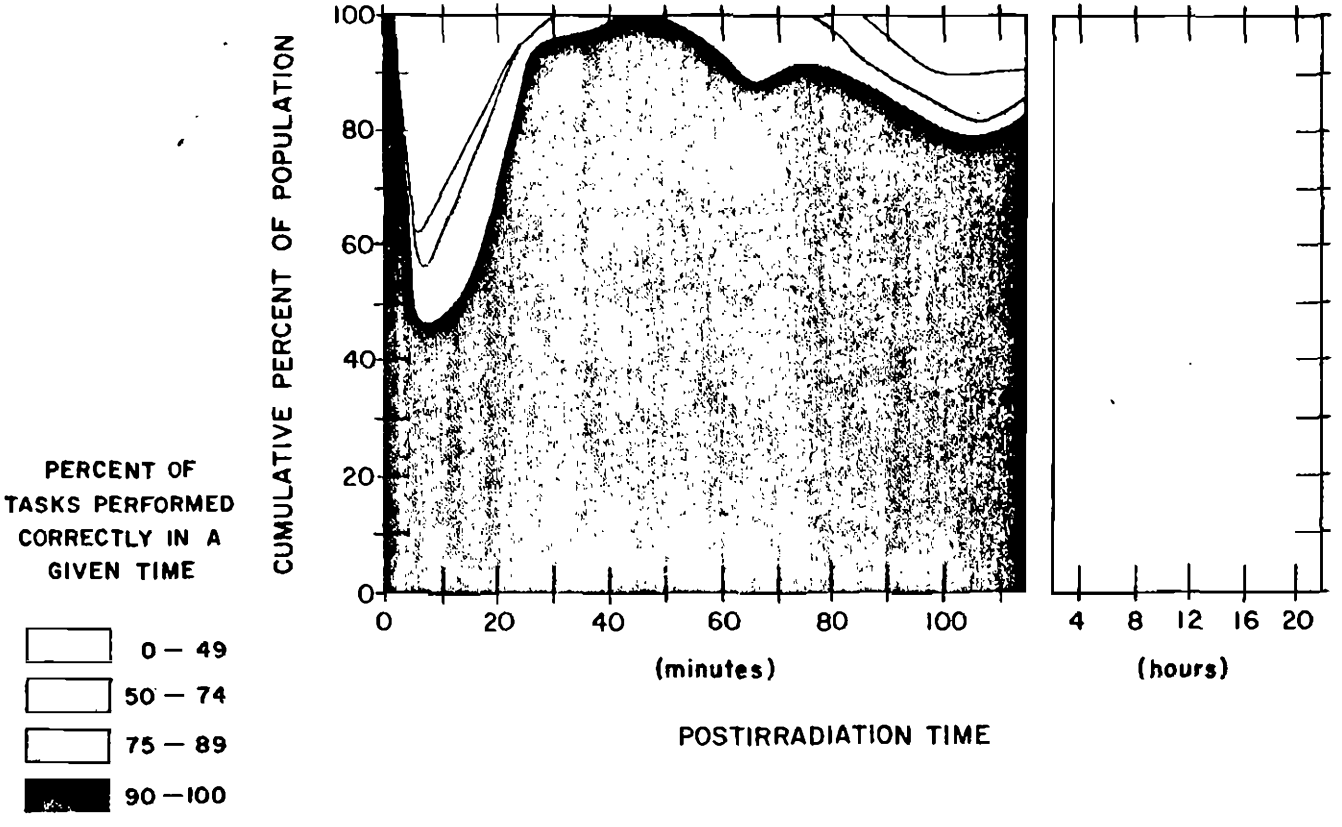

Figure 10-12. Personnel Effectiveness After Exposure to 2,800 rads

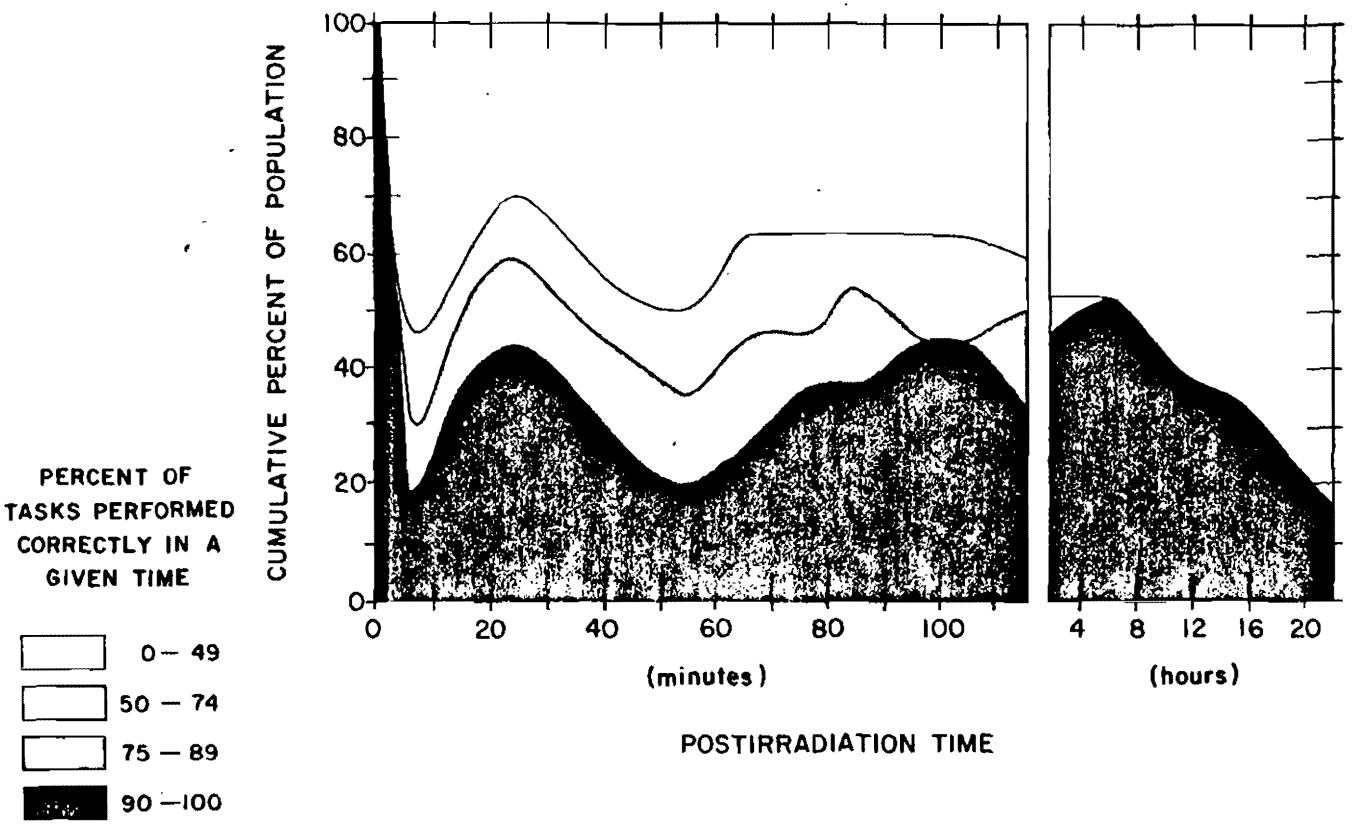

Figure 10-13. Personnel Effectiveness After Exposure to 7,000 rads

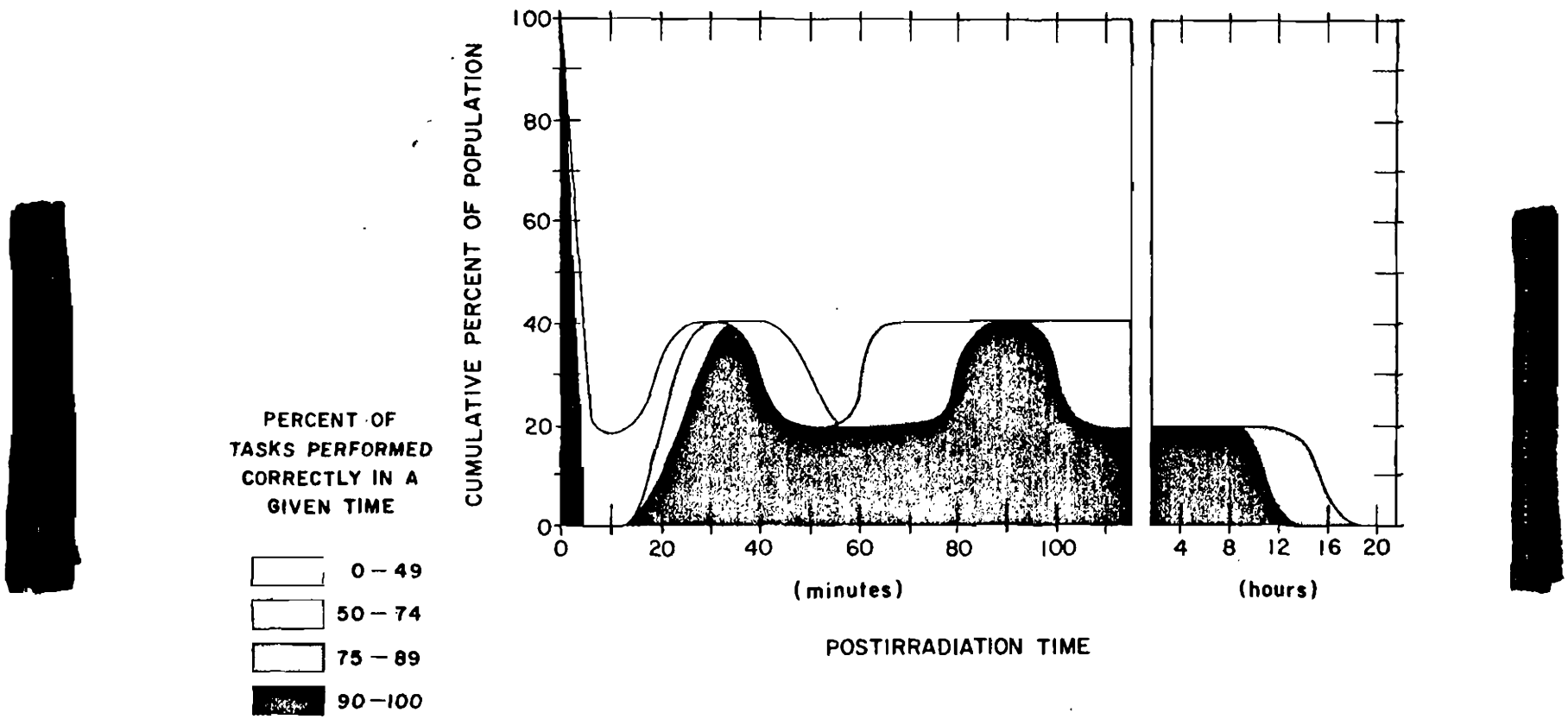

Figure 10-14. Personnel Effectiveness After Exposure to 13,000 rads

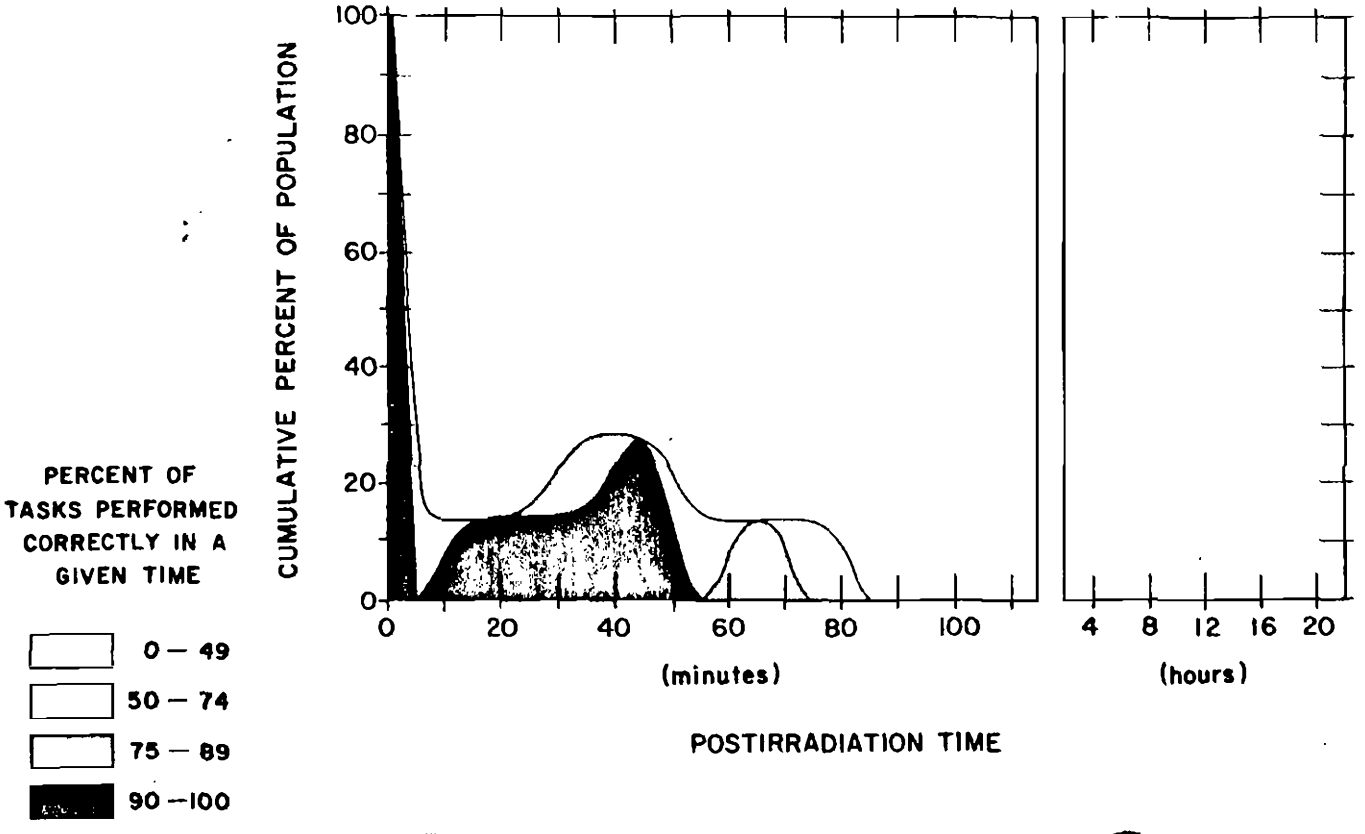

Figure 10-15. Personnel Effectiveness After Exposure to 22,000 rads

[redacted]

10-28 Internal Hazards [redacted]

[redacted] Radioactive materials entering the body by inhalation, eating, or through wounds or breaks in the skin may be deposited in the body where alpha particles, beta particles or gamma rays continue to bombard adjacent tissues. Once fixed within the body, removal is almost impossible, except through natural processes. Effects of internal emitters usually become apparent after a period of years, so, while of not immediate concern insofar as personnel effectiveness is concerned, this deposition may eventually be of great concern to the individual.

[redacted] Inhalation as a route of entry can be expected as the result of resuspension of radioactive materials from dust-producing activities, such as the operations of helicopter and fast-moving vehicles. Handling of contaminated equipment, supplies, and clothing may result in the hands becoming contaminated. The contamination then may enter the body while eating. Ingestion of contaminated foodstuffs and water supplies is another source of internal emitters.

10-29 Modification of Injury [redacted]

[redacted] External residual radiation can be reduced by shielding, i.e., interposition of dense material between personnel and the source of radiation, as described previously for initial radiation. Protection is afforded to varying degrees by armored vehicles, foxholes, buildings and underground shelters. However, in a residual radiation environment, it is probable that radioactive materials will be brought into the protected areas as a result of their adherence to clothing, skin, hair, and equipment. Thus, to reduce exposure, it is necessary to decontaminate both the individual and his equipment. Additionally, as much time as is militarily feasible should be spent in protected environments while the residual radiation is decaying to lower levels. Decontamination of the outer surfaces of structures also will reduce the total dose to personnel.

[redacted] If the outer packaging of foodstuffs is undamaged, they may be consumed without hazard, provided care is taken to insure that the food is not contaminated during removal of the protective covering. Cans should be washed before opening. Normal water filtration procedures will remove a majority of the fallout radioactive materials.

[redacted] Treatment of individuals showing radiation sickness symptoms from exposure to residual radiation is similar to the treatment of sickness caused by initial radiation. Burns caused by prolonged contact of beta emitters with the skin can be reduced in severity, or prevented, by early removal of the fallout material. Burns which do occur respond to conventional methods of treatment for similar burns resulting from other causes.

[redacted] Medical management of conditions arising at later times as a result of fixed internal emitters depends on the organ(s) in which the material is fixed, the number of demonstrated lesions, and the threat of this damage to life.

SECTION IV
[redacted] COMBINED INJURY [redacted]

[redacted] Thus far in this chapter little has been said about the possibility of personnel receiving multiple types of injury; however, such injuries probably would be a common occurrence in the advent of a nuclear war. Multiple injuries might be received nearly simultaneously (e.g., from exposure to a single detonation without fallout radiation) or separated in time by minutes to days (e.g., from exposure to a single detonation followed by fallout radiation, or exposure to multiple detonations). These injuries may consist of any combination of radiation, blast and thermal injuries from nuclear weapons as well as wounds from conventional weapons. Furthermore, such injuries may be influenced by other conditions that might be expected during or after a nuclear attack, such as malnutrition, poor

[redacted]

[redacted]

[redacted]

sanitation, fatigue, and various other environmental factors. Since there are insufficient quantitative data to indicate the manner in which casualty production might be influenced by these latter factors, only combinations of pairs of the following three categories will be discussed in this section: (1) ionizing radiation injuries, (2) thermal injuries, and (3) mechanical injuries (e.g., injuries that result from blast effects).

[redacted] Most of our current knowledge concerning combined injuries is derived from studies of Japanese bomb victims in Hiroshima and Nagasaki and from laboratory and field test experiments involving a variety of animals. In Hiroshima and Nagasaki, 50 percent of the injured 20-day survivors within about 2,200 yards of ground zero received combined injuries whereas an incidence of 25 percent was observed in those located between 2,200 and 5,500 yards. The contribution of such injuries to overall mortality and morbidity has never been determined adequately, but two general impressions have emerged: the combination of mechanical and thermal injury was responsible for the majority of deaths that occurred within the first 48 hours; delayed mortality was higher and complications were more numerous among burned people who had received radiation than what would be anticipated in a burned population where no radiation exposure had occurred. It should be recognized that the stated incidences of combined injuries apply only to the conditions existing in the two Japanese cities at the time of attack and that the number and types of combined injuries are sensitive to yield, burst height, and conditions of exposure. Yields smaller than 10 kilotons probably would result in a significant number of casualties with combinations of prompt-radiation, thermal, and mechanical injuries. On the other hand, larger yields would be expected to result in a marked increase in the number of people with burns associated with mechanical injuries, and prompt-radiation injuries would be relatively insignificant in the surviving population. A weapon detonated at a burst height where fallout is minimized would result in a large number of thermal and mechanical injuries, and, depending upon yield, might also produce a significant number of prompt-radiation injuries. A weapon detonated near (above or below) the surface would maximize the number of injuries due to fallout and would produce a large number of casualties where such injuries would be combined with mechanical and thermal trauma. Personnel outside and unshielded would have a greater likelihood of sustaining prompt and/or fallout radiation in combination with thermal burns than would be the case for personnel inside of any form of structure. In the latter case, thermal burns would be minimized, whereas combinations of mechanical and radiation injury might dominate.

[redacted] Combined injuries may result in synergistic effects, additive effects, or antienergistic effects. That is, the resultant response, whether measured as percent combat ineffectiveness (CI) or mortality, may be greater than, equal to, or less than what would be predicted based on the assumption that the various injuries act independently of one another in producing casualties. Quantitative data from laboratory experiments suggests that, in situations where a combined effect has been observed, the interaction of the various forms of trauma has resulted in enhanced delayed mortality, with little apparent effect on early mortality.

10-30 Radiation and Thermal Injuries [redacted]

[redacted] Depending upon the radiation dose and the severity of burn, mortality has been found to increase by as much as a factor of six above that which might be expected from the two injuries administered singly. Thus, burns which serve as a portal of entry for infection may be considerably more hazardous to a person whose resistance to infection has been lowered by ioniz-

[redacted]

[redacted]

ing radiation. However, enhanced mortality has not been observed when low radiation doses have been administered in combination with minimal burn injuries. Very little information is available on fallout radiation in combination with thermal or any other form of injury.

10-31 Mechanical and Radiation Injuries [redacted]

[redacted] Mechanical and radiation injuries can be expected to be frequent, particularly if fallout is present. Studies indicate that a delay in wound healing is observed with doses in excess of 300 rads, and that wounds in irradiated subjects are considerably more serious if treatment is delayed for more than 24 hours. In addition, missile and impact injuries that result in disruption of the skin and damage to the soft tissues would provide a portal of entry for infection, and thus may be extremely hazardous to irradiated people. Injuries that are associated with significant blood loss would be more serious in personnel who have received a radiation dose large enough to interfere with normal blood clotting mechanisms.

10-32 Thermal and Mechanical Injuries [redacted]

[redacted] Burns and mechanical injuries in combination are often encountered in victims of conventional explosions and increased delayed complications, shorter times-to-death and enhanced mortality are frequent occurrences. However, little quantitative data are available on this form of combined injury.

[redacted] CASUALTY CRITERIA [redacted]

[redacted] No reliable criteria for combat ineffectives are known for personnel receiving combined injuries. The available data do indicate, however, that individuals receiving combined injuries that occur nearly simultaneously are unlikely to become casualties within a few hours, provided the individual injuries would not produce casualties if administered separately. Consequently, it is not unreasonable to make early casualty predictions for a single nuclear detonation on the basis of the most far-reaching effect. In regard to troop-casualty predictions, combined effects can be considered as a bonus, helping to assure the attainment of predicted CI levels, especially since there is a reasonable amount of uncertainty in the predictions for individual effects. If exposure exceeds any "minimal" risk level, that effect could contribute to combined injury and could result in increased casualties at later times. This becomes an important factor in terms of troop safety.

[redacted] PERSONNEL IN THE OPEN [redacted]

[redacted] Figure 10-16 indicates expected burn levels, prompt ionizing-radiation doses, and peak translational velocities as functions of yield and ground distance for randomly-oriented, prone personnel exposed in the open. The curves were derived, assuming a visual range of 16 miles and a burst height such that the fireball would just touch the surface. This is the minimum height of burst which would result in negligible early, or local, fallout. The curves, which are presented for illustrative purposes only, form the limits of a band for each effect. These limits correspond to 50 percent early casualties and "minimal" early risk. The ionizing-radiation dose required to produce 50 percent CI within one hour, e.g., approximately 5,000 rads, is so large that it will result in 100 percent mortality within several days. For this reason, a 500-rad curve, which would correspond to approximately 50 percent mortality within 60 days, is included in Figure 10-16. Direct overpressure effects are not included in the figure since, except for eardrum rupture, which is not normally considered to produce CI, translational effects extend to greater ranges for all of the yields considered.

[redacted] In the case of troop-casualty predictions, prompt-radiation predominates for yields less

[redacted]

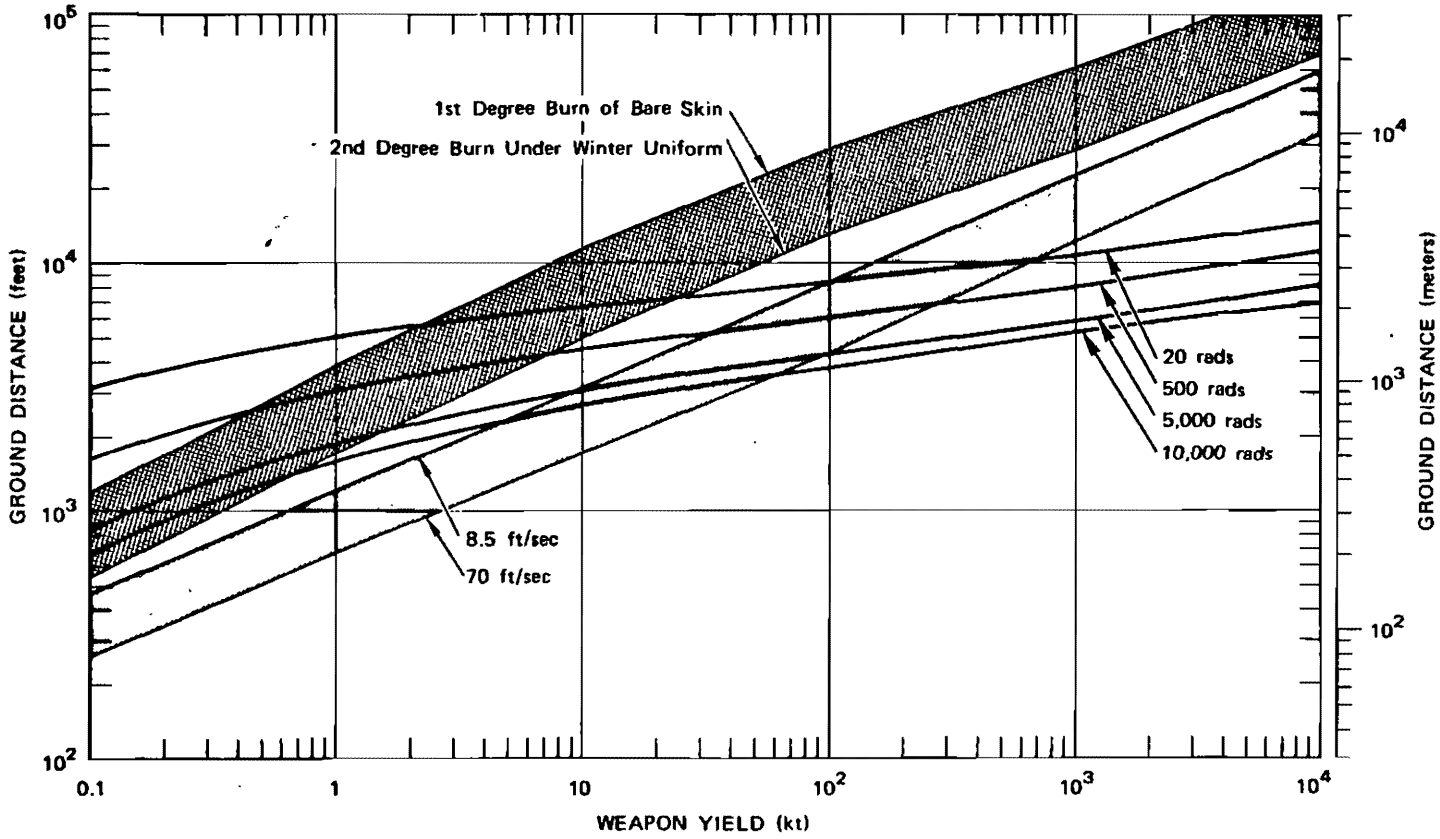

Figure 10-16. Comparison of Effects from Low Altitude Bursts

[redacted]

than 2 kt whereas thermal radiation is the most far-reaching hazard for yields greater than 2 kt. In situations where thermal exposure is neglected as a casualty-producing factor, ionizing radiation is the major effect in producing a 50 percent CI level for yields below 100 kt, while for larger yields, blast effects (translation) predominate.

[redacted] With regard to troop safety, ionizing radiation is the major hazard below 1 kt, while thermal radiation predominates for larger yields. If the troops can be shielded adequately from the thermal pulse, ionizing radiation is the major hazard for yields up to 100 kt, above which blast effects are the most far-reaching hazard.

[redacted] PERSONNEL IN STRUCTURES [redacted]

[redacted] In order to predict casualty levels for troops in situations other than open terrain, for example, inside armoured vehicles or field fortifications, the amount of nuclear radiation, thermal radiation, and blast shielding, as well as the degree of blast hardness of the surrounding materials must be taken into account for each geometry of exposure. As was the case for personnel in the open, casualty predictions must be made on the basis of the most far-reaching single effect rather than on the basis of combined effects. In general, for troops in structures, the major effect producing early casualties is likely to be ionizing radiation for small yields and blast effects for larger yields, with the cross-over point depending on the degree of hardness of the structure. While the hazards from thermal and ionizing radiation levels are reduced in a structure, the hazards from air blast may be magnified as a result of structural collapse, whole-body impact, and falling debris. This is particularly true for relatively soft structures at greater distances.

[redacted] In the case of personnel in field fortifications, severe damage to the structure (Section VI [redacted], Chapter [redacted]) should be taken as representative of 50 percent early CI from blast. Shielding factors (Section VI, Chapter 9) must be considered when estimating nuclear radiation responses of personnel in such structures.

[redacted] TREATMENT [redacted]

[redacted] The triage and treatment of combined injuries present special problems, particularly if significant radiation exposure has occurred. Certain modifications in accepted medical and surgical practices must be considered since radiation exposure, depending upon dose, is known to increase susceptibility to infection, to decrease the efficiency of wound and fracture healing, to increase the likelihood of hemorrhage, to decrease tolerance to anesthetic agents, and to decrease the immune response.

[redacted] It is imperative that primary closure of wounds be accomplished at the earliest possible time and that patients be treated with a broad spectrum antibiotic throughout the period of maximum bone marrow depression. Secondary closure of small soft-tissue wounds should be accomplished by the second or third day. Reparative surgery of an extensive nature should not be performed later than four to five days after injury since skin and soft-tissue healing should have occurred before the effects of ionizing radiation occur. If reparative surgery is not performed within this limited period of time, it must be postponed until the bone marrow has recovered (one to two months post-exposure). Wounds of injuries that require longer than three weeks for healing, such as severe burns and most fractures, should not be definitively treated until radiation recovery is evident. Although reconstructive surgery in the absence of radiation exposure might be performed within the second month or earlier after conventional trauma, it must be postponed for at least three months in instances where radiation exposure is a significant contributory factor. In all instances, extra precaution must be taken to avoid infection and blood loss.

[redacted]

[redacted]

[redacted] BIBLIOGRAPHY [redacted]

Allen, R. G., et al., *The Calculation of Retinal Burn and Flashblindness Safe Separation Distances,* U.S. Air Force School of Aerospace Medicine, Brooks Air Force Base, Texas, September 1968, SAM-TR-68-106 [redacted]

Anderson, R. S., F. W. Stemler, and E. B. Rogers, *Air Blast Studies with Animals,* Chemical Research and Development Laboratories, Army Chemical Center, Maryland, April 1961, DASA 1193 [redacted]

Behrens, C. F., *Atomic Medicine,* Williams & Wilkins, Baltimore, 1959. *Biological and Environmental Effects of Nuclear War,* Hearings before the Special Subcommittee on Radiation of the Joint Committee on Atomic Energy, Congress of the United States, June 1959. U.S. Government Printing Office, Washington, D.C [redacted]

Blatz, H., *Radiation Hygiene Handbook,* McGraw-Hill Book Co., Inc., New York, 1959 [redacted]

Bowen, I. G., A. F. Strehler, and M. B. Wetherbe, *Distribution of Missiles from Nuclear Explosions,* Lovelace Foundation for Medical Education and Research, Albuquerque, New Mexico, December 1956, WT-1168 [redacted]

Bowen, I. G., et al., *Biophysical Mechanisms and Scaling Procedures Applicable in Assessing Responses of the Thorax Energized by Air-Blast Overpressures or Non-Penetrating Missiles,* Lovelace Foundation for Medical Education and Research, Albuquerque, New Mexico, November 1966, DASA 1857 [redacted]

Bowen, I. G., F. R. Fletcher, and D. R. Richmond, *Estimate of Man's Tolerance to the Direct Effects of Air Blast,* Lovelace Foundation for Medical Education and Research, Albuquerque, New Mexico, October 1968, DASA 2113 [redacted]

Brucer, M., *The Acute Radiation Syndrome: Y-12 Accident,* Oak Ridge Institute of Nuclear Studies, April 1959, ORINS-25 [redacted]

Bryant, F. J., et al., U.K. Atomic Energy Authority Report AERE HP/R 2353 (1957); *Strontium in Diet,* Brit. Medical Journal, *1*, 1371 (1958) [redacted]

Claus, W. D. (Ed.), *Radiation Biology and Medicine,* Addison-Wesley Publishing Co. Inc., Reading, Mass., 1958 [redacted]

Conard, R. A., et al., *Medical Survey of Rongelap People Five and Six Years After Exposure to Fallout,* Brookhaven National Laboratory, September 1960, BNL-609 [redacted]

Fletcher, E. R., et al., *Determination of Aerodynamic-Drag Parameters of Small Irregular Objects by Means of Drop Tests,* Lovelace Foundation for Medical Education and Research, Albuquerque, New Mexico, October 1961, CEX-59.14 [redacted]

[redacted]

Fletcher, E. R., and I. G. Bowen, *Blast Induced Translational Effects*, Lovelace Foundation for Medical Education and Research, Albuquerque, New Mexico, November 1966, DASA 1859

Gerstner, H. B., *Acute Radiation Syndrome in Man*, U.S. Armed Forces Medical Journal, *9*, 313 (1958)

Hayes, D. F., *A Summary of Accidents and Incidents Involving Radiation in Atomic Energy Activities*, TID-5360, August 1956; Supplement No. 1, August 1957; Supplement No. 2, September 1959. U.S. Atomic Energy Commission, Washington, D.C.

Hirsch, F. G., *Effects of Overpressure on the Ear – A Review*, Lovelace Foundation for Medical Education and Research, Albuquerque, New Mexico, November 1966, DASA 1858

Kulp, J. L., A. R. Schulert, and E. J. Hodges, *Strontium-90 in Man IV*, Science, *132*, 448 (1960)

Lappin, P. W., and C. F. Adams, *Analysis of the First Thermal Pulse and Associated Eye Effects*, Aerospace Medical Research Laboratories, Wright Patterson Air Force Base, Ohio, December 1968, AM RL-TR-67-214

Loutit, J. F., and R. S. Russell, (Eds.), *The Entry of Fission Products into Food Chains*, Progress in Nuclear Energy, Series VI, Vol. 3, Pergamon Press, Inc., New York, 1961

Miller, R. W., *Delayed Radiation Effects in Atomic Bomb Survivors*, Science, *166*, 569 (1969)

National Academy of Sciences-National Research Council, *The Biological Effects of Atomic Radiation*, 1956; *Pathological Effects of Atomic Radiation*, Publication No. 452, 1961; *Long-Term Effects of Ionizing Radiations from External Sources*, Publication No. 849, 1961; *Effects of Ionizing Radiation on the Human Hematopoietic System*, Publication No. 875, 1961; *Effects of Inhaled Radioactive Particles*, Publication No. 848, 1961, Washington, D.C.

National Council on Radiation Protection and Measurements, *Basic Radiation Protection Criteria*, NCRP Report No. 39, 1971, Washington, D.C

Oughterson, A. W., and S. Warren, *Medical Effects of the Atomic Bomb in Japan*, National Nuclear Energy Series VIII, McGraw-Hill Book Co., Inc., New York, 1956

Proceedings of the International Conferences on the Peaceful Uses of Atomic Energy, Geneva, *Biological Effects of Radiation*, Volume 11, 1956; Vol. 22, 1958; United Nations, New York

Richmond, D. R., I. G. Bowen, and C. S. White, *Tertiary Blast Effects: The Effects of Impact on Mice, etc.* Aerospace Medicine, *32*, 789 (1961)

Richmond, D. R., and C. S. White, *Biological Effects of Blast and Shock*, Lovelace Foundation and Research, Albuquerque, New Mexico, April 1966, DASA 1777

Richmond, D. R., et al., *The Relationship Between Selected Blast Wave Parameters and the Response of Mammals Exposed to Air Blast*, Lovelace Foundation for Medical Education and Research, Albuquerque, New Mexico, November 1966, DASA 1860

Symposium on Radioactive Fallout in Foods, *Agricultural and Food Chemistry*, *9*, 90 (1961)

United Nations General Assembly, *Report of the United Nations Scientific Committee on the Effects of Atomic Radiation*, UN A/3838 Suppl. 17, (13th Sess.) w/Annexes A through I, 1958, United Nations, New York

Wald, N., and G. E. Toma, Jr., *Radiation Accidents through December 1958*, Oak Ridge National Laboratory, March 1961, ORNL-2748, Part B

White, C. S., et al., *Comparative Nuclear Effects of Biomedical Interest*, Civil Effects Study, January 1961, CEX-58.8

White, C. S., and D. R. Richmond, *Blast Biology*, Lovelace Foundation for Medical Education and Research, September 1959, TID-5764

White, C. S., I. G. Bowen, and D. R. Richmond, *A Comparative Analysis of Some of the Immediate Environmental Effects at Hiroshima and Nagasaki*, Health Physics, Pergamon Press, *10*, 89 (1964)

White, C. S., *Tentative Biological Criteria for Assessing Potential Hazards from Nuclear Explosions*, Lovelace Foundation for Medical Education and Research, Albuquerque, New Mexico, December 1963, DASA 1462

White, C. S., *The Scope of Blast and Shock Biology and Problem Areas in Relating Physical and Biological Parameters*, Lovelace Foundation for Medical Education and Research, Albuquerque, New Mexico, November 1966, DASA 1856

White, C. S., *The Nature of Problems Involved in Estimating Immediate Casualties from Nuclear Explosions*, Lovelace Foundation for Medical Education and Research, Albuquerque, New Mexico, November 1968

White, C. S., I. G. Bowen, and D. R. Richmond, *The Environmental Medical Aspects of Nuclear Blast*, Lovelace Foundation for Medical Education and Research, Albuquerque, New Mexico, November 1962, DASA 1341

White, C. S., et al., *The Biodynamics of Air Blast*, Lovelace Foundation for Medical Education and Research, Albuquerque, New Mexico, July 1971, DNA 2738T

CHAPTER V

STRUCTURAL DAMAGE FROM AIR BLAST

INTRODUCTION

GENERAL OBSERVATIONS

5.01 The two preceding chapters have dealt with general principles of air blast and the loads on structures produced by the action of the air blast wave. In the present chapter, the actual damage to buildings of various types, bridges, utilities, and vehicles caused by nuclear explosions will be considered. In addition, criteria of damage to various targets will be discussed and quantitative relationships will be given between the damage and the distances over which such damage may be expected from nuclear weapons of different yields.

5.02 Direct damage to structures attributable to air blast can take various forms. For example, the blast may deflect structural steel frames, collapse roofs, dish-in walls, shatter panels, and break windows. In general, the damage results from some type of displacement (or distortion) and the manner in which such displacement can arise as the result of a nuclear explosion will be examined.

5.03 Attention may be called to an important difference between the blast effects of a nuclear weapon and those due to a conventional high-explosive bomb. In the former case, the combination of high peak overpressure, high wind (or dynamic) pressure, and longer duration of the positive (compression) phase of the blast wave results in "mass distortion" of buildings, similar to that produced by earthquakes and hurricanes. An ordinary explosion will usually damage only part of a large structure, but the blast from a nuclear weapon can surround and destroy whole buildings in addition to causing localized structural damage.

5.04 An examination of the areas in Japan affected by nuclear explosions (§ 2.24) shows that small masonry buildings were engulfed by the oncoming pressure wave and collapsed completely. Light structures and residences were totally demolished by blast and subsequently destroyed by fire. Industrial buildings of steel construction were denuded of roofing and siding, and only twisted frames remained. Nearly everything at close range, except structures and smokestacks of strong reinforced concrete, was destroyed. Some buildings leaned away from ground zero as though struck by a wind of stupendous proportions. Telephone poles were

snapped off at ground level, as in a hurricane, carrying the wires down with them. Large gas holders were ruptured and collapsed by the crushing action of the blast wave.

5.05 Many buildings, which at a distance appeared to be sound, were found on close inspection to be damaged and gutted by fire. This was frequently an indirect result of blast action. In some instances the thermal radiation may have been responsible for the initiation of fires, but in many other cases fires were started by overturned stoves and furnaces and by the rupture of gas lines. The loss of water pressure by the breaking of pipes, mainly due to the collapse of buildings, and other circumstances arising from the explosions, contributed greatly to the additional destruction by fire (Chapter VII).

5.06 A highly important consequence of the tremendous power of the nuclear explosions was the formation of enormous numbers of flying missiles consisting of bricks (and other masonry), glass, pieces of wood and metal, etc. These caused considerable amounts of secondary damage to structures and utilities, and numerous casualties even in the lightly damaged areas. In addition, the large quantities of debris resulted in the blockage of streets, thus making rescue and fire-fighting operations extremely difficult (Fig. 5.06).

5.07 Many structures in Japan were designed to be earthquake resistant, which probably made them stronger than most of their counterparts in the United States. On the other hand, some construction was undoubtedly lighter than in this country. However, contrary to popular belief concerning the flimsy character of Japanese residences, it was the considered opinion of a group of architects and engineers, who surveyed the nuclear bomb damage, that the resistance to blast of American residences

Figure 5.06. Debris after the nuclear explosion at Hiroshima.

in general would not be markedly different from that of the houses in Hiroshima and Nagasaki. This has been borne out by the observations on experimental structures exposed to air blast at nuclear weapons tests in Nevada.

FACTORS AFFECTING RESPONSE

STRENGTH AND MASS

5.08 There are numerous factors associated with the characteristics of a structure which influence the response to the blast wave accompanying a nuclear explosion. Those considered below include various aspects of the strength and mass of the structure, general structural design, and ductility (§ 5.14) of the component materials and members.

5.09 The basic criterion for determining the response of a structure to blast is its strength. As used in this connection, "strength" is a general term, for it is a property influenced by many factors some of which are obvious and others are not. The most obvious indication of strength is, of course, massiveness of construction, but this is modified greatly by other factors not immediately visible to the eye, e.g., resilience and ductility of the frame, the strength of the beam and column connections, the redundancy of supports, and the amount of diagonal bracing in the structure. Some of these factors will be examined subsequently. If the building does not have the same strength along both axes, then orientation with respect to the burst should also be considered.

5.10 The strongest structures are heavily framed steel and reinforced-concrete buildings, particularly those designed to be earthquake resistant, whereas the weakest are probably certain shed-type industrial structures having light frames and long beam spans. Some kinds of lightly built and open frame construction also fall into the latter category, but well-constructed frame houses have greater strength than these sheds.

5.11 The resistance to blast of structures having load-bearing, masonry walls (brick or concrete block), without reinforcement, is not very good. This is due to the lack of resilience and to the moderate strength of the connections which are put under stress when the blast load is applied laterally to the building. The use of steel reinforcement with structures of this type greatly increases their strength.

STRUCTURAL DESIGN

5.12 Except for those regions in which fairly strong earthquake shocks may be expected, most structures in the United States are designed to withstand only the lateral (sideways) loadings produced by moderately strong winds. For design purposes, such loading is assumed to be static (or stationary) in character because natural winds build up relatively slowly and remain fairly steady. The blast from a nuclear explosion, however, causes a lateral dynamic (rather than static) loading; the load is applied extremely rapidly and it lasts for a second or more with continuously decreasing strength. The inertia, as measured by the mass of the structure or

member, is an important factor in determining response to a dynamic lateral load, although it is not significant for static loading.

5.13 Of existing structures, those intended to be earthquake resistant and capable of withstanding a lateral load equal to about 10 percent of the weight, will probably be damaged least by blast. Such structures, often stiffened by diaphragm walls and having continuity of joints to provide additional rigidity, may be expected to withstand appreciable lateral forces without serious damage.

DUCTILITY

5.14 The term ductility refers to the ability of a material or structure to absorb energy inelastically without failure; in other words, the greater the ductility, the greater the resistance to failure. Materials which are brittle have poor ductility and fail suddenly after passing their elastic (yield) loading.

5.15 There are two main aspects of ductility to be considered. When a force (or load) is applied to a material so as to deform it, as is the case in a nuclear explosion, for example, the initial deformation is said to be "elastic." Provided it is still in the elastic range, the material will recover its original form when the loading is removed. However, if the "stress" (or internal force) produced by the load is sufficiently great, the material passes into the "plastic" range. In this state the material does not recover completely after removal of the load; that is to say, some deformation is permanent, but there is no failure. Only when the stress reaches the "ultimate strength" does failure occur.

5.16 Ideally, a structure which is to suffer little damage from blast should have as much ductility as possible. Unfortunately, structural materials are generally not able to absorb much energy in the elastic range, although many common materials can take up large amounts of energy in the plastic range before they fail. One of the problems in blast-resistant design, therefore, is to decide how much permanent (plastic) deformation can be accepted before a particular structure is rendered useless. This will, of course, vary with the nature and purpose of the structure. Although deformation to the point of collapse is definitely undesirable, some lesser deformation may not seriously interfere with the continued use of the structure.

5.17 It is evident that ductility is a desirable property of structural materials required to resist blast. Structural steel and steel reinforcement have this property to a considerable extent. They are able to absorb large amounts of energy, e.g., from a blast wave, without failure and thus reduce the chances of collapse of the structure in which they are used. Structural steel has the further advantage of a higher yield point (or elastic limit) under dynamic than under static loading; the increase is quite large for some steels.

5.18 Although concrete alone is not ductile, when steel and concrete are used together properly, as in reinforced-concrete structures, the ductile behavior of the steel will usually predominate. The structure will then have considerable ductility and, consequently, the ability to absorb energy. Without reinforcement, masonry walls are completely lacking in ductility and readily suffer brittle failure, as stated above.

COMMERCIAL AND ADMINISTRATIVE STRUCTURES

INTRODUCTION

5.19 In this and several subsequent sections, the actual damage to various types of structures caused by the air blast from nuclear explosions will be described. First, commercial, administrative, and similar buildings will be considered. These buildings are of substantial construction and include banks, offices, hospitals, hotels, and large apartment houses. Essentially all the empirical information concerning the effects of air blast on such multistory structures has been obtained from observations made at Hiroshima and Nagasaki. The descriptions given below are for three general types, namely, reinforced-concrete frame buildings, steel-frame buildings, and buildings with load-bearing walls. As is to be expected from the preceding discussion, buildings of the first two types are more blast resistant than those of the third type; however, even light to moderate damage (see Table 5.139a) to frame-supported buildings can result in casualties to people in these buildings.

MULTISTORY, REINFORCED-CONCRETE FRAME BUILDINGS

5.20 There were many multistory, reinforced-concrete frame buildings of several types in Hiroshima and a smaller number in Nagasaki. They varied in resistance to blast according to design and construction, but they generally suffered remarkedly little damage externally. Close to ground zero, however, there was considerable destruction of the interior and contents due to the entry of blast through doors and window openings and to subsequent fires. An exceptionally strong structure of earthquake-resistant (aseismic) design, located some 640 feet from ground zero in Hiroshima, is seen in Fig. 5.20a. Although the exterior walls were hardly damaged, the roof was depressed and the interior was destroyed. More typical of reinforced-concrete frame construction in the United States was the building shown in Fig. 5.20b at about the same distance from ground zero. This suffered more severely than the one of aseismic design.

5.21 A factor contributing to the blast resistance of many reinforced-concrete buildings in Japan was the construction code established after the severe earthquake of 1923. The height of new buildings was limited to 100 feet and they were designed to withstand a lateral force equal to 10 percent of the vertical load. In addition, the recognized principles of stiffening by diaphragms and improved framing to provide continuity were specified. The more important buildings were well designed and constructed according to the code. However, some were built without regard to the earthquake-resistant requirements and these were less able to withstand the blast wave from the nuclear explosion.

5.22 Close to ground zero the vertical component of the blast was more significant and so greater damage to the roof resulted from the downward force (Fig. 5.22a) than appeared farther away. Depending upon its strength, the roof

Figure 5.20a. Upper photo: Reinforced-concrete, aseimic structure; window fire shutters were blown in by blast and the interior gutted by fire (0.12 mile from ground zero at Hiroshima). Lower photo: Burned out interior of similar structure.

Figure 5.20b. Three-story, reinforced-concrete frame building; walls were 13-inch thick brick panel with large window openings (0.13 mile from ground zero at Hiroshima).

was pushed down and left sagging or it failed completely. The remainder of the structure was less damaged than similar buildings farther from the explosion because of the smaller horizontal (lateral) forces. At greater distances, from ground zero, especially in the region of Mach reflection, the consequences of horizontal loading were apparent (Fig. 5.22b).

5.23 In addition to the failure of roof slabs and the lateral displacement of walls, numerous other blast effects were observed. These included bending and fracture of beams, failure of columns, crushing of exterior wall panels, and failure of floor slabs (Fig. 5.23). Heavy damage to false ceilings, plaster, and partitions occurred as far out as 9,000 feet (1.7 miles) from ground zero, and glass windows were generally broken out to a distance of 3¾ miles and in a few instances out to 8 miles.

5.24 The various effects just described have referred especially to reinforced-concrete structures. This is because the buildings as a whole did not collapse, so that other consequences of the blast loading could be observed. It should be pointed out, however, that damage of a similar nature also occurred in structures of the other types described below.

MULTISTORY, STEEL-FRAME BUILDINGS

5.25 There was apparently only one steel-frame structure having more than two stories in the Japanese cities exposed to nuclear explosions. This was a five-story structure in Nagasaki at a distance of 4,500 feet (0.85 mile) from

Figure 5.22a. Depressed roof of reinforced-concrete building (0.10 mile from ground zero at Hiroshima).

Figure 5.22b. Effects of horizontal loading on wall facing explosion (0.4 mile from ground zero at Nagasaki).

Figure 5.23. Reinforced-concrete building showing collapsed roof and floor slabs (0.10 mile from ground zero at Nagasaki).

ground zero (Fig. 5.25). The only part of the building that was not regarded as being of heavy construction was the roof, which was of 4-inch thick reinforced concrete supported by unusually light steel trusses. The downward failure of the roof, which was dished 3 feet, was the only important structural damage suffered.

5.26 Reinforced-concrete frame buildings at the same distance from the explosion were also undamaged, and so there is insufficient evidence to permit any conclusions to be drawn as to the relative resistance of the two types of construction. An example of damage to a two-story, steel-frame structure is shown in Fig. 5.26. The heavy walls of the structure transmitted their loads to the steel frame, the columns of which collapsed. Weakening of unprotected steel by fire could have contributed significantly to the damage to steel-frame structures (§ 5.31).

BUILDING WITH LOAD-BEARING WALLS

5.27 Small structures with light load-bearing walls offered little resistance to the nuclear blast and, in general, collapsed completely. Large buildings of the same type, but with cross walls and of somewhat heavier

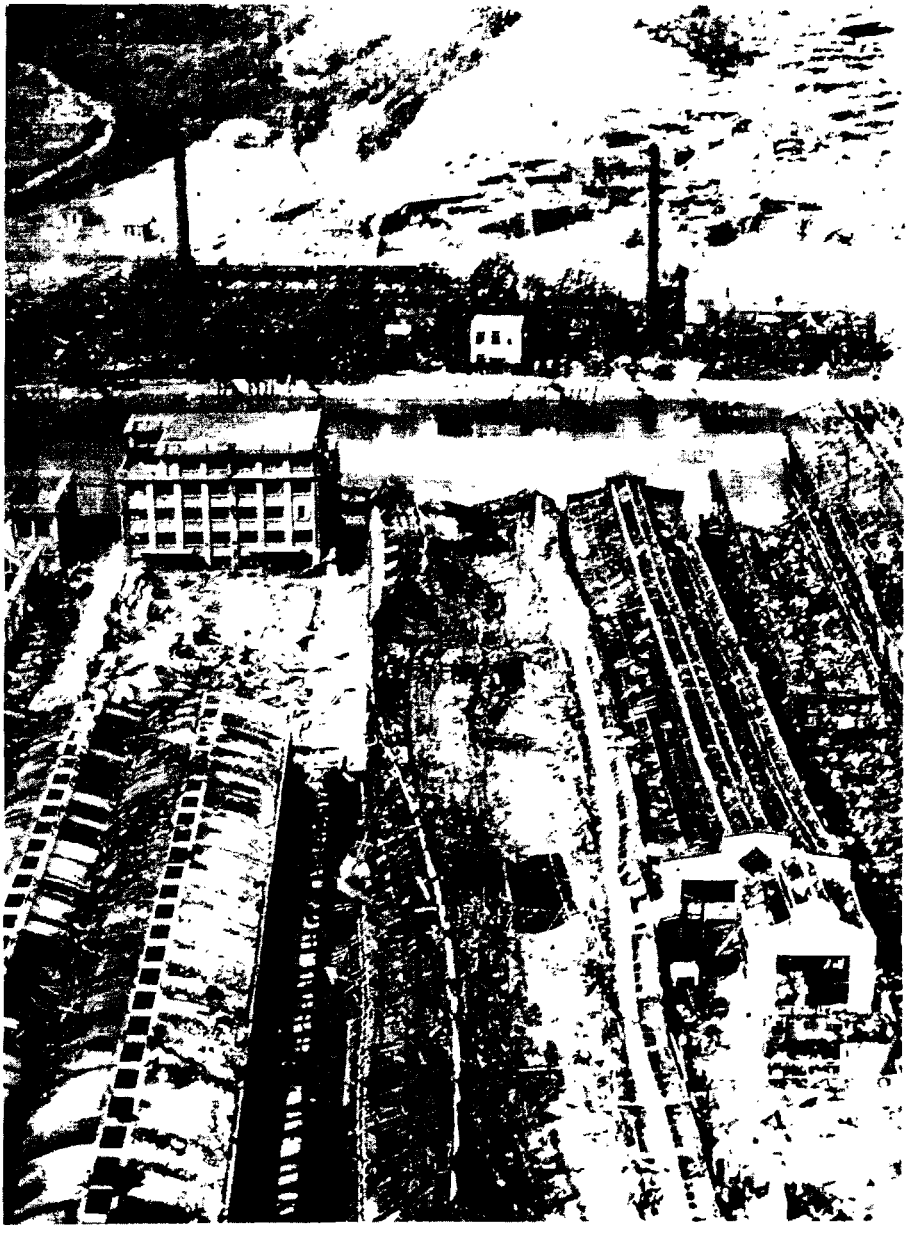

Figure 5.25. At left and back of center is a multistory, steel-frame building (0.85 mile from gound zero at Nagasaki).

Figure 5.26. Two-story, steel-frame building with 7-inch reinforced-concrete wall panels (0.40 mile from ground zero at Hiroshima). The first story columns buckled away from ground zero dropping the second story to the ground.

construction, were more resistant but failed at distances up to 6,300 feet (1.2 miles) from ground zero. Cracks were observed at the junctions of cross walls and sidewalls when the building remained standing. It is apparent that structures with load-bearing walls possess few of the characteristics that would make them resistant to collapse when subjected to large lateral loads.

INDUSTRIAL STRUCTURES

JAPANESE EXPERIENCE

5.28 In Nagasaki there were many buildings of the familiar type used for industrial purposes, consisting of a steel frame with roof and siding of corrugated sheet metal or of asbestos cement. In some cases, there were rails for gantry cranes, but the cranes were usually of low capacity. In general, construction of industrial-type buildings was comparable to that in the United States.

5.29 Severe damage of these structures occurred up to a distance of about 6,000 feet (1.14 miles) from ground zero. Moderately close to ground zero, the buildings were pushed over bodily, and at greater distances they were generally left leaning away from the source of the blast (Fig. 5.29). The columns being long and slender offered little resistance to the lateral loading. Sometimes columns failed due to a lateral force causing flexure, combined with a simultaneous small increase in the downward load coming from the impact of the blast on the roof. This caused buckling and, in some instances, complete collapse. Roof trusses were buckled by compression resulting from lateral blast loading on the side of the building facing the explosion.

5.30 A difference was noted in the effect on the frame depending upon whether a frangible material, like asbestos cement, or a material of high tensile strength, such as corrugated sheet-iron, was used for roof and siding. Asbestos cement broke up more readily permitting more rapid equalization of pressure and, consequently, less structural damage to the frame.

5.31 Fire caused heavy damage to unprotected steel members, so that it was impossible to tell exactly what the

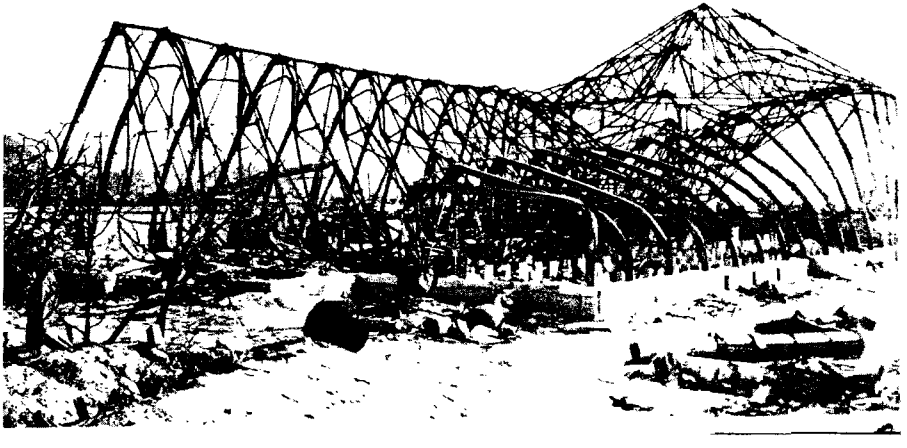

Figure 5.29. Single-story, light steel-frame building (0.80 mile from ground zero at Hiroshima); partially damaged by blast and further collapsed by subsequent fire.

blast effect had been. In general, steel frames were badly distorted and would have been of little use, even if siding and roofing material had been available for repairs.

5.32 In some industrial buildings wood trusses were used to support the roof. These were more vulnerable to blast because of poor framing and connections, and were readily burned out by fire. Concrete columns were employed in some cases with steel roof trusses; such columns appeared to be more resistant to buckling than steel, possibly because the strength of concrete is decreased to a lesser extent by fire than is that of steel.

5.33 Damage to machine tools was caused by debris, resulting from the collapse of roof and siding, by fire in wood-frame structures, and by dislocation and overturning as a result of damage to the building. In many instances the machine tools were belt-driven, so that the distortion of the building pulled the machine tool off its base, damaging or overturning it.

5.34 Smokestacks, especially those of reinforced concrete, proved to have considerable blast resistance (Fig. 5.34a). Because of their shape, they are subjected essentially to drag loading only and, if sufficiently strong, their long period of vibration makes them less sensitive to blast than many other structures. An example of extreme damage to a reinforced-concrete stack is shown in Fig. 5.34b. Steel smokestacks performed reasonably well, but being lighter in weight and subject to crushing were not comparable to reinforced concrete. On the whole, well-constructed masonry stacks withstood the blast somewhat better than did those made of steel.

NEVADA TESTS

5.35 A considerable amount of information on the blast response of structures of several different kinds was obtained in the studies made at the Nevada Test Site in 1953 and in 1955. The nuclear device employed in the test of March 17, 1953, was detonated at the top of a 300-foot tower; the energy yield was about 16 kilotons. In the test of May 5, 1955, the explosion took place on a 500-foot tower and the yield was close to 29 kilotons. In each case, air pressure measurements made possible a correlation, where it was justified, between the blast damage and the peak overpressure.

5.36 Three types of metal buildings of standard construction, such as are used for various commercial and industrial purposes, were exposed at peak overpressures of 3.1 and 1.3 pounds per square inch. The main objectives of the tests, made in 1955, were to determine the blast pressures at which such structures would survive, in the sense that they could still be used after moderate repairs, and to provide information upon which could be based improvements in design to resist blast.

STEEL FRAME WITH ALUMINUM PANELS

5.37 The first industrial type building had a conventional rigid steel frame, which is familiar to structural engineers, with aluminum-sheet panels for roofing and siding (Fig. 5.37a). At a blast overpressure of 3.1 pounds per square inch this building was severely damaged. The welded and bolted steel frame

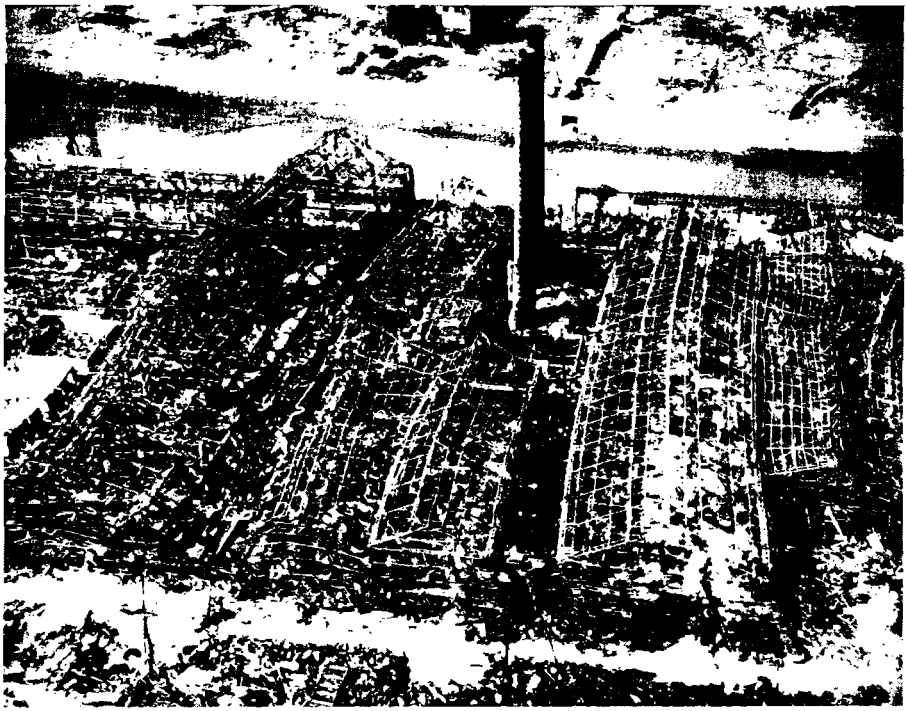

Figure 5.34a. Destroyed industrial area showing smokestacks still standing (0.51 mile from ground zero at Nagasaki).

remained standing, but was badly distorted and pulled away from the concrete footings. On the side facing the explosion the deflection was about 1 foot at the eaves (Fig. 5.37b).

5.38 At a peak overpressure of 1.3 pounds per square inch the main steel frame suffered only slight distortion. The aluminum roofing and siding were not blown off, although the panels were disengaged from the bolt fasteners on the front face of the steel columns and girts (horizontal connecting members). Wall and roof panels facing the explosion were dished inward. The center girts were torn loose from their attachments to the columns in the front of the building. The aluminum panels on the side walls were dished inward slightly, but on the rear wall and rear slope of the roof, the sheeting was almost undisturbed.

5.39 As presently designed, structures of this type may be regarded as being repairable, provided they are not exposed to blast pressures exceeding 1 pound per square inch. Increased blast resistance would probably result from improvement in the design of girts and purlins (horizontal members supporting rafters), in particular. Better fastening between sill and wall footing and increased resistance to transverse loading would also be beneficial.

Figure 5.34b. A circular, 60 feet high, reinforced-concrete stack (0.34 mile from ground zero at Hiroshima). The failure caused by the blast wave occurred 15 feet above the base.

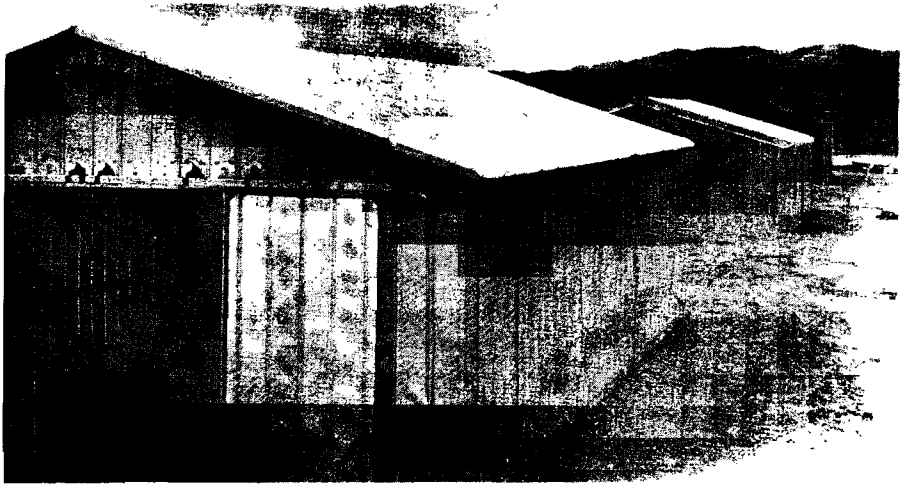

Figure 5.37a. Rigid steel-frame building before a nuclear explosion, Nevada Test Site.

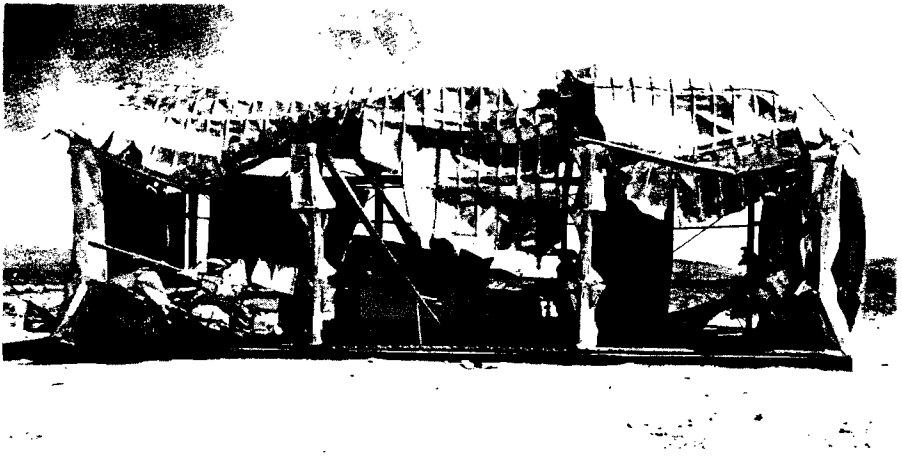

Figure 5.37b. Rigid steel-frame building after a nuclear explosion (3.1 psi peak overpressure).

SELF-FRAMING WITH STEEL PANELS

5.40 A frameless structure with self-supporting walls and roof of light, channel-shaped, interlocking, steel panels (16 inches wide) represented the second standard type of industrial building (Fig. 5.40a). The one subjected to 3.1 pounds per square inch peak overpressure (and a dynamic pressure of 0.2 pound per square inch) was completely demolished (Fig. 5.40b). One or two segments of wall were blown as far as 50 feet away, but, in general, the bent and twisted segments of the building remained approximately in their original locations. Most of the wall sections were still attached to their foundation bolts on the side and rear walls of the

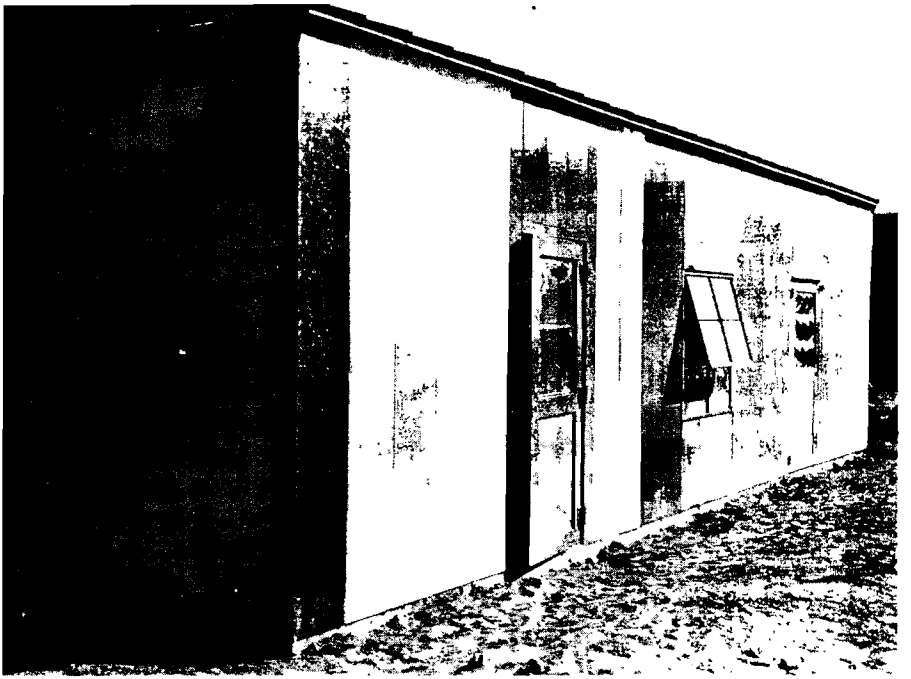

Figure 5.40a. Exterior of self-framing steel panel building before a nuclear explosion, Nevada Test Site.

Figure 5.40b. Self-framing steel panel building after a nuclear explosion (3.1 psi peak overpressure).

building. The roof had collapsed completely and was resting on the machinery in the interior.

5.41 Although damage at 1.3 pounds per square inch peak overpressure was much less, it was still considerable in parts of the structure. The front wall panels were buckled inward from 1 to 2 feet at the center, but the rear wall and rear slope of the roof were undamaged. In general, the roof structure remained intact, except for some deflection near the center.

5.42 It appears that the steel panel type of structure is repairable if exposed to overpressures of not more than about ¾ to 1 pound per square inch. The buildings are simple to construct but they do not hold together well under blast. Blast-resistant improvements would seem to be difficult to incorporate while maintaining the essential simplicity of design.

SELF-FRAMING WITH CORRUGATED STEEL PANELS

5.43 The third type of industrial building was a completely frameless structure made of strong, deeply-corrugated 43-inch wide panels of 16-gauge steel sheet. The panels were held together with large bolt fasteners at the sides and at the eaves and roof ridge. The wall panels were bolted to the concrete foundation. The entire structure was self-supporting, without frames, girts, or purlins (Fig. 5.43).

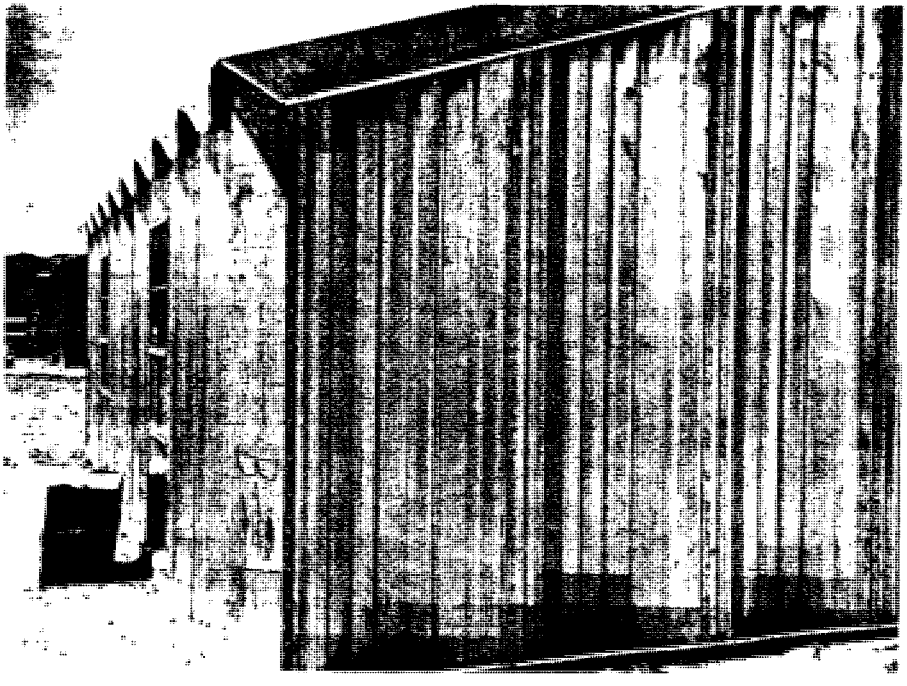

Figure 5.43. Self-framing corrugated steel panel building before a nuclear explosion, Nevada Test Site.

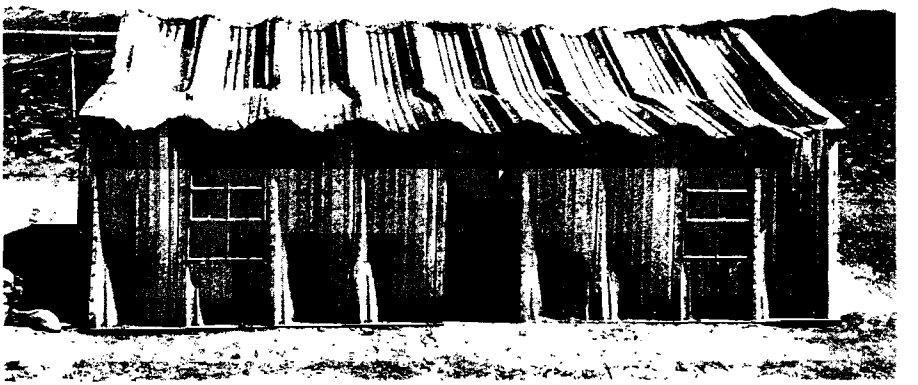

Figure 5.44. Self-framing corrugated steel panel building after a nuclear explosion (3.1 psi peak overpressure).

5.44 At a peak overpressure of 3.1 and a dynamic pressure of 0.2 pound per square inch a structure of this type was badly damaged, but all the pieces remained bolted together, so that the structure still provided good protection from the elements for its contents. The front slope of the roof was crushed downward, from 1 to 2 feet, at midsection, and the ridge line suffered moderate deflection. The rear slope of the roof appeared to be essentially undamaged (Fig. 5.44).

5.45 The front and side walls were buckled inward several inches, and the door in the front was broken off. All the windows were damaged to some extent, although a few panes in the rear remained in place.

5.46 Another building of this type, exposed to 1.3 pounds per square inch peak overpressure, experienced little structural damage. The roof along the ridge line showed indications of downward deflections of only 1 or 2 inches, and there was no apparent buckling of roof or wall panels. Most of the windows were broken, cracked, or chipped. Replacement of the glass where necessary and some minor repairs would have rendered the building completely serviceable.

5.47 The corrugated steel, frameless structure proved to be the most blast-resistant of those tested. It is believed that, provided the overpressure did not exceed about 3 pounds per square inch, relatively minor repairs would make possible continued use of the building. Improvement in the design of doors and windows, so as to reduce the missile hazard from broken glass, would be advantageous.

POSITIVE PHASE DURATION TESTS

5.48 Tests were carried out at Nevada in 1955 and at Eniwetok Atoll in the Pacific in 1956 to investigate the effect of the duration of the positive overpressure phase of a blast wave on damage. Typical drag-type structures were exposed, at approximately the same overpressure, to nuclear detona-

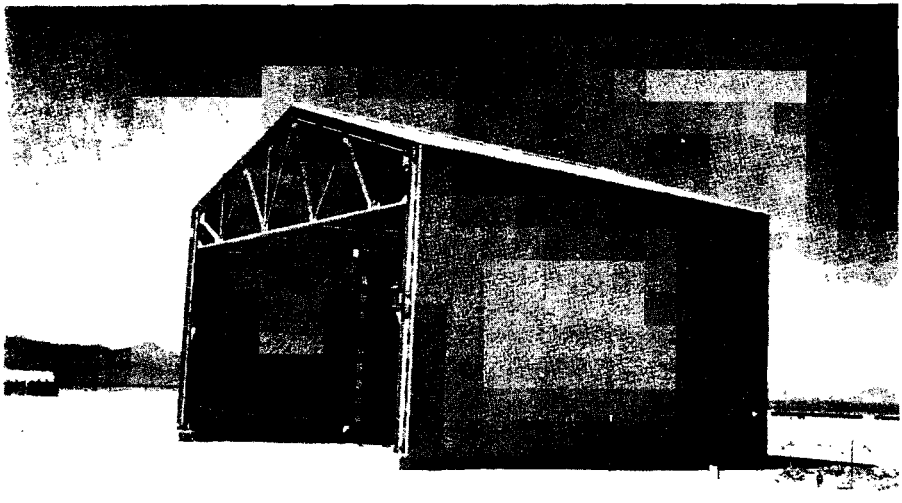

Figure 5.48a. Steel-frame building with siding and roof of frangible material.

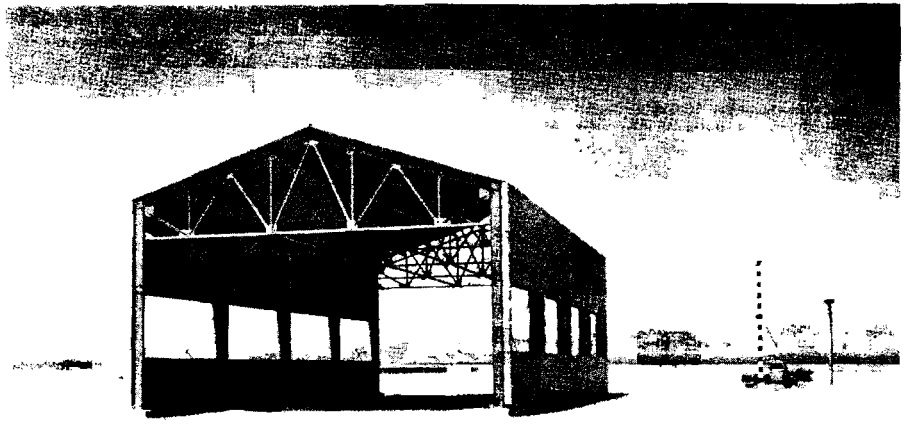

Figure 5.48b. Steel-frame building with concrete siding and window openings of 30 percent of the wall area.

tions in the kiloton and megaton ranges. Two representative types of small industrial buildings were chosen for these tests. One had a steel frame covered with siding and roofing of a frangible material and was considered to be a drag-type structure (Fig. 5.48a). The other had the same steel frame and roofing, but it had concrete siding with a window opening of about 30 percent of the wall area; this was regarded as a semidrag structure (Fig. 5.48b).

5.49 In the Nevada tests, with kiloton yield weapons, the first structure was subjected to a peak overpressure of about 6.5 and a dynamic pressure of 1.1 pounds per square inch; the positive phase duration of the blast wave was 0.9 second. A permanent horizontal deflection of about 15 inches occurred at the top of the columns. The column anchor bolts failed, and yielding was found between the lower chord (horizontal member of the roof truss) and column connections. The girts on the windward side were severely damaged and all of the siding was completely blown off (Fig. 5.49).

5.50 The second building, with the stronger siding, was exposed in Nevada to a peak overpressure loading of about 3.5 and a dynamic pressure of 0.3 pounds per square inch, with a positive phase duration of 1 second. Damage to this structure was small (Fig. 5.50). Although almost the whole of the frangible roof was blown off, the only other damage observed was a small yielding at some connections and column bases.

5.51 Structures of the same type were subjected to similar pressures in the blast wave from a megaton range

Figure 5.49. Structure in Figure 5.48a after exposure to 6.5 psi peak overpressure and 1.1 psi dynamic pressure; positive phase duration 0.9 second.

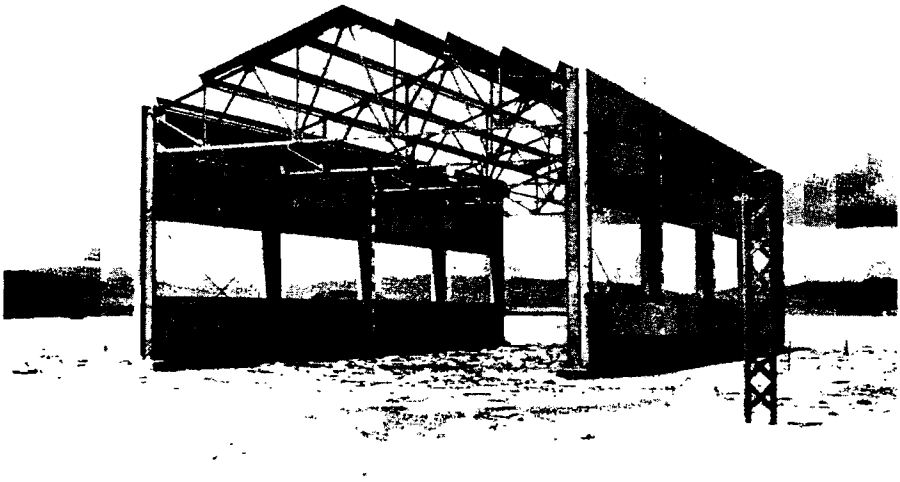

Figure 5.50. Structure in Figure 5.48b after exposure to 3.5 psi peak overpressure and 0.3 psi dynamic pressure; positive phase duration 1 second.

explosion at Eniwetok; namely, a peak overpressure of 6.1 and a dynamic pressure of 0.6 pounds per square inch for the drag-type building, and 5 and 0.5 pounds per square inch, respectively, for the semidrag structure. However, the positive phase now lasted several seconds as compared with about 1 second in the Nevada tests. Both structures suffered complete collapse (Figs. 5.51a and b). Distortion and breakup occurred throughout, particularly of columns and connections. It was concluded, therefore, that damage to drag-sensitive structures can be enhanced, for a given peak overpressure value, if the duration of the positive phase of the blast wave is increased (cf. § 4.13).

RESIDENTIAL STRUCTURES

JAPANESE EXPERIENCE

5.52 There were many wood-framed residential structures with adobe walls in the Japanese cities which were subjected to nuclear attack, but such a large proportion were destroyed by fire that very little detailed information concerning blast damage was obtained. It appeared that, although the quality of the workmanship in framing was usually high, little attention was paid to good engineering principles. On the whole, therefore, the construction was not well adapted to resist wracking action (distortion). For example, mortise and tenon joints were weak points in the

Figure 5.51a. Structure similar to Figure 5.48a after exposure to 6.1 psi peak overpressure and 0.6 psi dynamic pressure; positive phase duration several seconds.

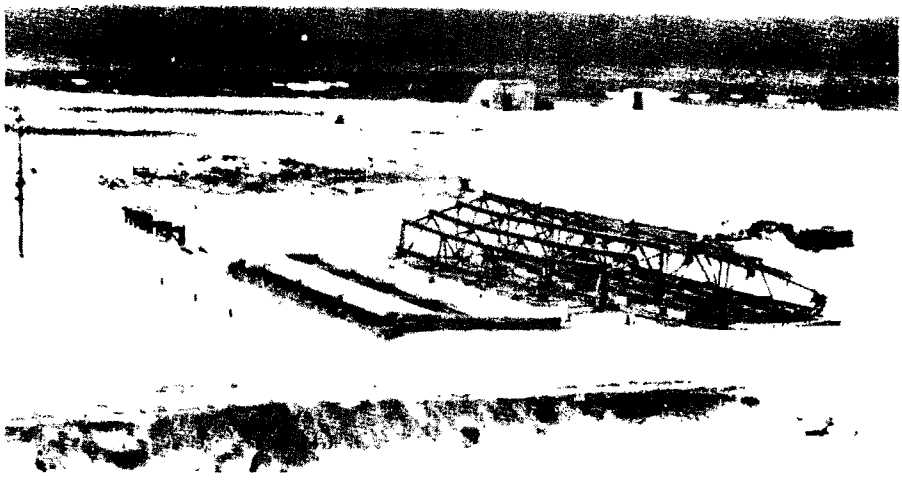

Figure 5.51b. Structure similar to Figure 5.48b after exposure to 5 psi peak overpressu and 0.5 psi dynamic pressure; positive phase duration several seconds.

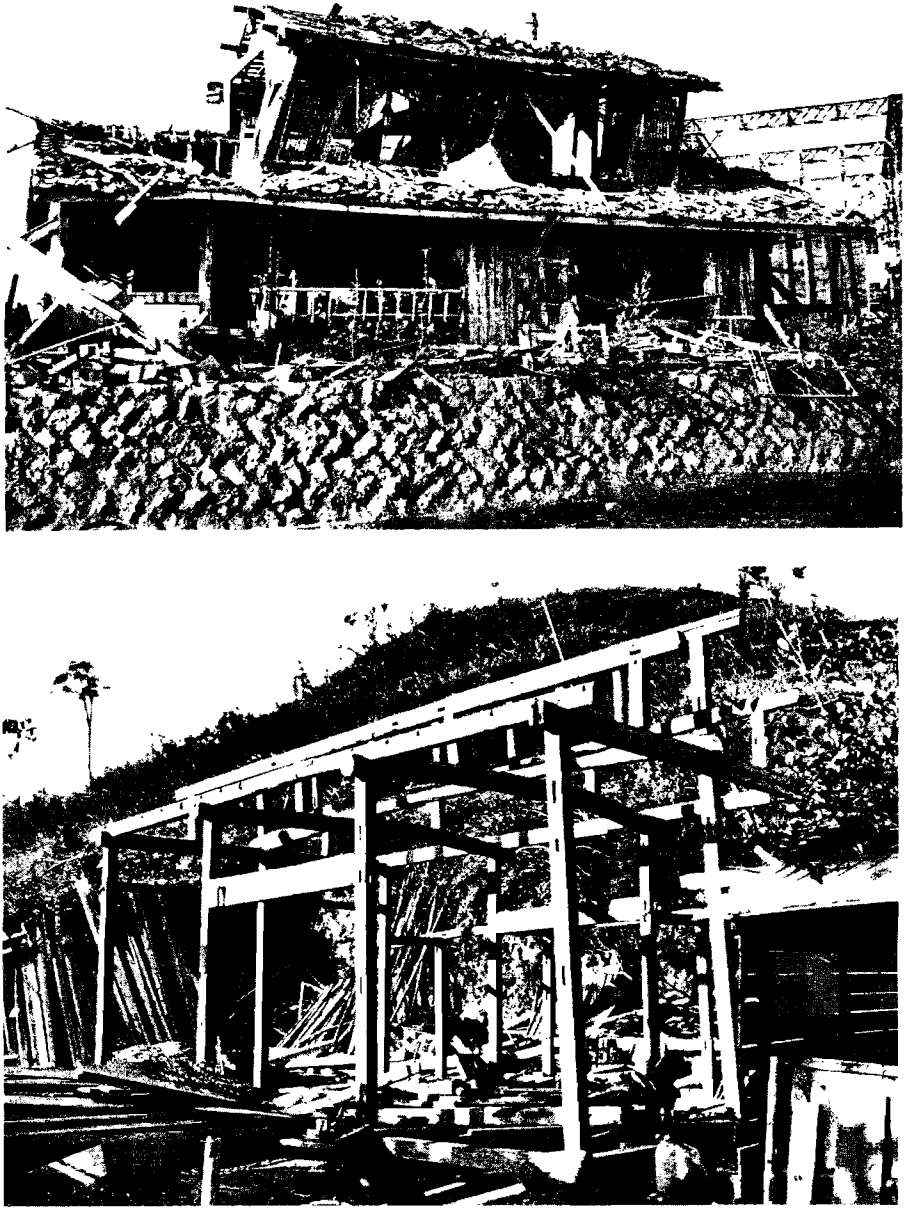

Figure 5.52. Upper photo; Wood-frame building; 1.0 mile from ground zero at Hiroshima. Lower photo: Frame of residence under construction, showing small tenons.

structure and connections were in general poor. Timbers were often dapped (cut into) more than was necessary or slices put in improper locations, result-

ing in an overall weakening (Fig. 5.52).

5.53 In Nagasaki, dwellings collapsed at distances up to 7,500 feet (1.4 miles) from ground zero, where the peak overpressure was estimated to be about 3 pounds per square inch, and there was severe structural damage up to 8,500 feet (1.6 miles). Roofs, wall panels, and partitions were damaged out to 9,000 feet (1.7 miles), where the overpressure was approximately 2 pounds per square inch, but the buildings would probably have been habitable with moderate repairs.

NEVADA TESTS

5.54 The main objectives of the tests made in Nevada in 1953 and 1955 (§ 5.35) on residential structures were as follows: (1) to determine the elements most susceptible to blast damage and consequently to devise methods for strengthening structures of various types; (2) to provide information concerning the amount of damage to residences that might be expected as a result of a nuclear explosion and to what extent these structures would be subsequently rendered habitable without major repairs; and (3) to determine how persons remaining in their houses during a nuclear attack might be protected from the effects of blast and radiations. Only the first two of these aspects of the tests will be considered here, since the present chapter deals primarily with blast effects.

TWO-STORY, WOOD-FRAME HOUSE: 1953 TEST

5.55 In the 1953 test, two essentially identical houses, of a type common in the United States, were placed at different locations. They were of typical wood-frame construction, with two stories, basement, and brick chimney (Fig. 5.55). The interiors were plastered but not painted. Since the tests were intended for studying the effects of blast, precautions were taken to prevent the houses from burning. The exteriors were consequently painted white (except for the shutters), to reflect the thermal radiation. For the same purpose, the windows facing the explosion were equipped with metal venetian blinds having an aluminum finish. In addition, the houses were roofed with light-gray shingles; these were of asbestos cement for the house nearer to the explosion where the chances of fire were greater, whereas asphalt shingles were used for the other house. There were no utilities of any kind.

5.56 One of the two houses was located in the region of Mach reflection where the peak incident overpressure was close to 5 pounds per square inch. It was expected, from the effects in Japan, that this house would be almost completely destroyed—as indeed it was—but the chief purpose was to see what protection might be obtained by persons in the basement.

5.57 Some indication of the blast damage suffered by this dwelling can be obtained from Fig. 5.57. It is apparent that the house was ruined beyond repair. The first story was completely demolished and the second story, which was very badly damaged, dropped down on the first floor debris. The roof was blown off in several sections which landed at both front and back of the house. The gable end walls were blown apart and outward, and the brick chimney was broken into several pieces.

Figure 5.55. Wood-frame house before a nuclear explosion, Nevada Test Site.

Figure 5.57. Wood-frame house after a nuclear explosion (5 psi peak overpressure).

Figure 5.59. Wood-frame house after a nuclear explosion (1.7 psi peak overpressure).

5.58 The basement walls suffered some damage above grade, mostly in the rear, i.e., away from the explosion. The front basement wall was pushed in slightly, but was not cracked except at the ends. The joists supporting the first floor were forced downward probably because of the air pressure differential between the first floor and the largely enclosed basement, and the supporting pipe columns were inclined to the rear. However, only in limited areas did a complete breakthrough from first floor to basement occur. The rest of the basement was comparatively clear and the shelters located there were unaffected.

5.59 The second house, exposed to an incident peak overpressure of 1.7 pounds per square inch, was badly damaged both internally and externally, but it remained standing (Fig. 5.59). People in the main and upper floors would have suffered injuries ranging from minor cuts from glass fragments to possible fatal injuries from flying debris or as a result of translational displacement of the body as a whole. Some damage would also result to the furnishings and other contents of the house. Although complete restoration would have been very costly, it is believed that, with the window and door openings covered, and shoring in the basement, the house would have been habitable under emergency conditions.

5.60 The most obvious damage was suffered by doors and windows, including sash and frames. The front door was broken into pieces and the kitchen and basement entrance doors were torn off their hinges. Damage to interior doors varied; those which were open before

Figure 5.64. Strengthened wood-frame house after a nuclear explosion (4 psi peak overpressure).

the explosion suffered least. Window glass throughout the house was broken into fragments, and the force on the sash, especially in the front of the house, dislodged the frames.

5.61 Principal damage to the first-floor system consisted of broken joists. The second-story system suffered relatively little in structural respects, although windows were broken and plaster cracked. Damage to the roof consisted mainly of broken rafters (2 × 6 inches with 16-inch spacing).

5.62 The basement showed no signs of damage except to the windows, and the entry door and frame. The shelters in the basement were intact.

TWO-STORY, WOOD-FRAME HOUSE: 1955 TEST

5.63 Based upon the results described above, certain improvements in design were incorporated in two similar wood-frame houses used in the 1955 test. The following changes, which increased the estimated cost of the houses some 10 percent above that for normal construction, were made: (1) improved connection between exterior walls and foundations; (2) reinforced-concrete shear walls to replace the pipe columns in the basement; (3) increase in size and strengthening of connections of first-floor joists; (4) substitution of plywood for lath and plaster; (5) increase in size of rafters (to 2 × 8 inches) and wall studs; and (6) stronger nailing of window frames in wall openings.

5.64 Even with these improvements, it was expected that almost complete destruction would occur at 5 pounds per square inch peak overpressure, and so one of the houses was located where the overpressure at the Mach front would be 4 pounds per square inch. Partly because of the increased strength and partly because of the lower air blast pressure the house did not collapse (Fig. 5.64). But the superstructure was so badly damaged that it could not have been occupied without expensive repair which would not have been economically advisable.

Figure 5.65. Strengthened wood-frame house after a nuclear explosion (2.6 psi peak overpressure).

5.65 The other strengthened two-story frame house was in a location where the incident peak overpressure was about 2.6 pounds per square inch; this was appreciably greater than the lower overpressure of the 1953 test. Relatively heavy damage was experienced, but the condition of the house was such that it could be made available for emergency shelter by shoring and not too expensive repairs (Fig. 5.65). Although there were differences in detail, the overall damage was much the same degree as that suffered by the corresponding house without the improved features at an overpressure of 1.7 pounds per square inch.

TWO-STORY, BRICK-WALL-BEARING HOUSE: 1955 TEST

5.66 For comparison with the tests on the two-story, wood-frame structures made in Nevada in 1953, two brick-wall-bearing houses of conventional construction, similar in size and layout, were exposed to 5 and 1.7 pounds per square inch peak overpressure, respectively, in the 1955 tests (Fig. 5.66). The exterior walls were of brick veneer and cinder block and the foundation walls of cinder block; the floors, partitions, and roof were wood-framed.

5.67 At an incident peak overpressure of 5 pounds per square inch, the brick-wall house was damaged beyond

Figure 5.66. Unreinforced brick house before a nuclear explosion, Nevada Test Site.

Figure 5.67. Unreinforced brick house after a nuclear explosion (5 psi peak overpressure).

repair (Fig. 5.67). The side and back walls failed outward. The front wall failed initially inward, but its subsequent behavior was obscured by dust. The final location of the debris from the front wall is therefore uncertain, but very little fell on the floor framing. The roof was demolished and blown off, the rear part landing 50 feet behind the house. The first floor had partially collapsed into the basement as a result of fracturing of the floor joists at the center of the spans and the load of the second floor which fell upon it. The chimney was broken into several large sections.

5.68 Farther from the explosion, where the peak overpressure was 1.7 pounds per square inch, the corresponding structure was damaged to a considerable extent. Nevertheless, its condition was such that it could be made available for habitation by shoring and some fairly inexpensive repairs (Fig. 5.68).

ONE-STORY, WOOD-FRAME (RAMBLER TYPE) HOUSE: 1955 TEST

5.69 A pair of the so-called "rambler" type, single-story, wood-frame houses were erected at the Nevada Test Site on concrete slabs poured in place at grade. They were of conventional design except that each contained a shelter, above ground, consisting of the bathroom walls, floor, and ceiling of reinforced concrete with blast door and shutter (Fig. 5.69).

Figure 5.68. Unreinforced brick house after a nuclear explosion (1.7 psi peak overpressure).

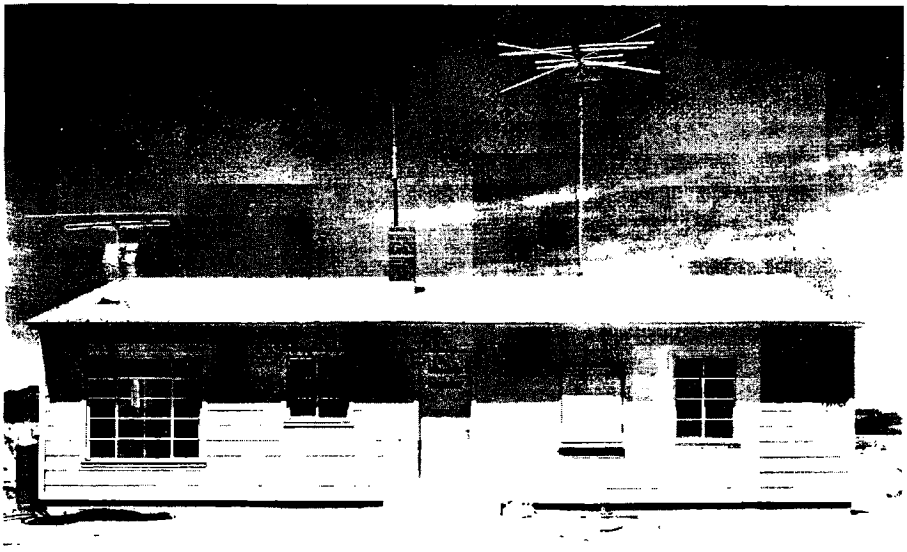

Figure 5.69. Rambler-type house before a nuclear explosion, Nevada Test Site. (Note blast door over bathroom window at right.)

5.70 When exposed to an incident peak overpressure of about 5 pounds per square inch, one of these houses was demolished beyond repair. However, the bathroom shelter was not damaged at all. Although the latch bolt on the blast shutter failed, leaving the shutter unfastened, the window was still intact. The roof was blown off and the rafters were split and broken. The side walls at gable ends were blown outward, and fell to the ground. A portion of the front wall remained standing, although it was leaning away from the direction of the explosion (Fig. 5.70).

5.71 The other house of the same type, subjected to a peak overpressure of 1.7 pounds per square inch, did not suffer too badly and it could easily have been made habitable. Windows were broken, doors blown off their hinges, and plaster-board walls and ceilings were badly damaged. The main structural damage was a broken midspan rafter beam and distortion of the frame. In addition, the porch roof was lifted 6 inches off its supports.

ONE-STORY, PRECAST CONCRETE HOUSE: 1955 TEST

5.72 Another residential type of construction tested in Nevada in 1955 was a single-story house made of precast, lightweight (expanded shale aggregate) concrete wall and partition panels, joined by welded matching steel lugs. Similar roof panels were anchored to the walls by special countersunk and grouted connections. The walls were supported on concrete piers and a concrete floor slab, poured in place on a tamped fill after the walls were erected. The floor was anchored securely to the walls by means of perimeter reinforcing rods held by hook bolts screwed into

Figure 5.70. Rambler-type house after a nuclear explosion (5 psi peak overpressure).

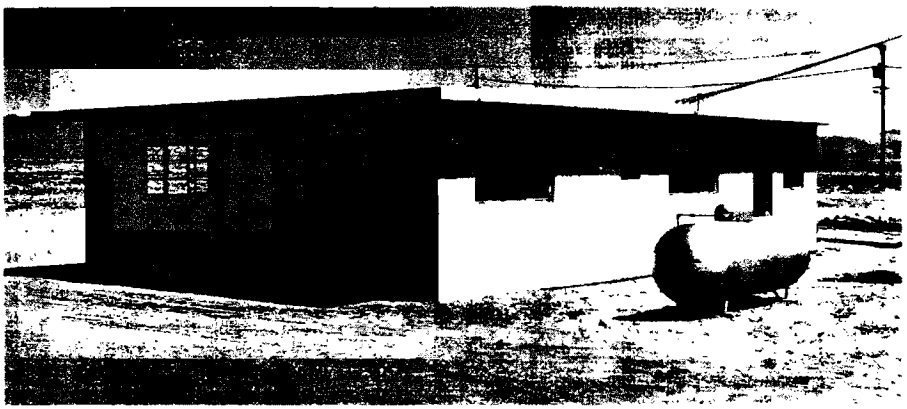

Figure 5.72. Reinforced precast concrete house before a nuclear explosion, Nevada Test Site.

inserts in the wall panels. The overall design was such as to comply with the California code for earthquake-resistant construction (Fig. 5.72).

5.73 This house stood up well, even at a peak overpressure of 5 pounds per square inch. By replacement of demolished or badly damaged doors and windows, it could have been made available for occupancy (Fig. 5.73).

5.74 There was some indication that the roof slabs at the front of the house were lifted slightly from their supports, but this was not sufficient to break any connections. Some of the walls were cracked slightly and others showed indications of minor movement. In certain areas the concrete around the slab connections was spalled, so that the connectors were exposed. The steel

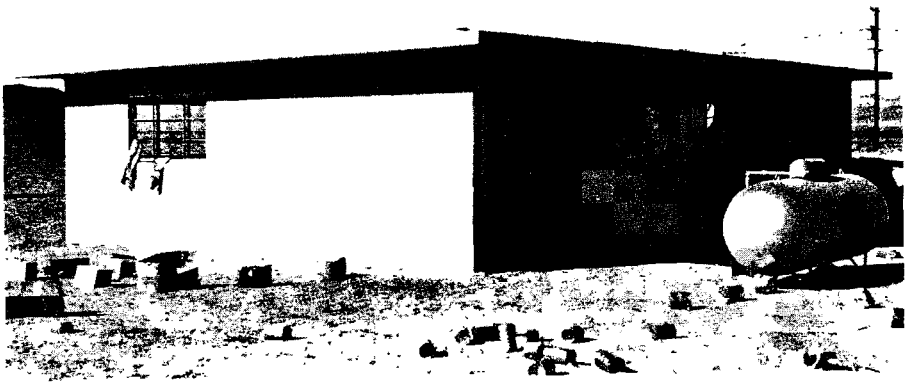

Figure 5.73. Reinforced precast concrete house after a nuclear explosion (5 psi peak overpressure). The LP-gas tank, sheltered by the house, is essentially undamaged.

window-sash was somewhat distorted, but it remained in place.

5.75 At a peak overpressure of 1.7 pounds per square inch, the precast concrete-slab house suffered relatively minor damage. Glass was broken extensively, and doors were blown off their hinges and demolished, as in other houses exposed to the same air pressure. But, apart from this and distortion of the steel window-sash, the only important damage was spalling of the concrete at the lug connections, i.e., where the sash projected into the concrete.

ONE-STORY, REINFORCED-MASONRY HOUSE: 1955 TEST

5.76 The last type of house subjected to test in 1955 was also of earthquake-resistant design. The floor was a concrete slab, poured in place at grade. The walls and partitions were built of lightweight (expanded shale aggregate) 8-inch masonry blocks, reinforced with vertical steel rods anchored into the floor slab. The walls were also reinforced with horizontal steel rods at two levels, and openings were spanned by reinforced lintel courses. The roof was made of precast, lightweight concrete slabs, similar to those used in the precast concrete houses described above (Fig. 5.76).

5.77 At a peak overpressure of about 5 pounds per square inch, windows were destroyed and doors blown in the demolished. The steel window-sash was distorted, but nearly all remained in place. The house suffered only minor structural damage and could have been made habitable at relatively small cost (Fig. 5.77).

5.78 There was some evidence that the roof slabs had been moved, but not sufficiently to break any connections. The masonry wall under the large window (see Fig. 5.77) was pushed in about 4 inches on the concrete floor slab; this appeared to be due to the omission of dowels between the walls and the floor beneath window openings. Some cracks developed in the wall above the same window, probably as a result of improper installation of the reinforced lintel course and the substitution of a pipe

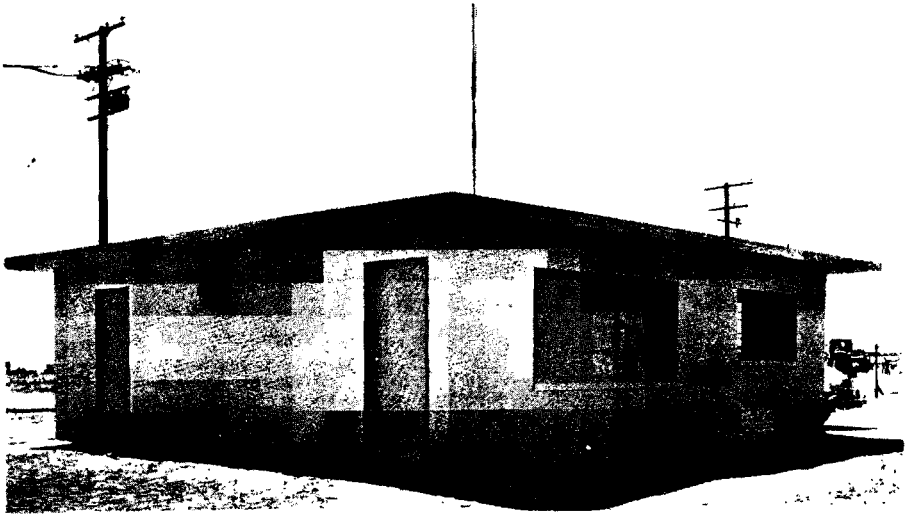

Figure 5.76. Reinforced masonry-block house before a nuclear explosion, Nevada Test Site.

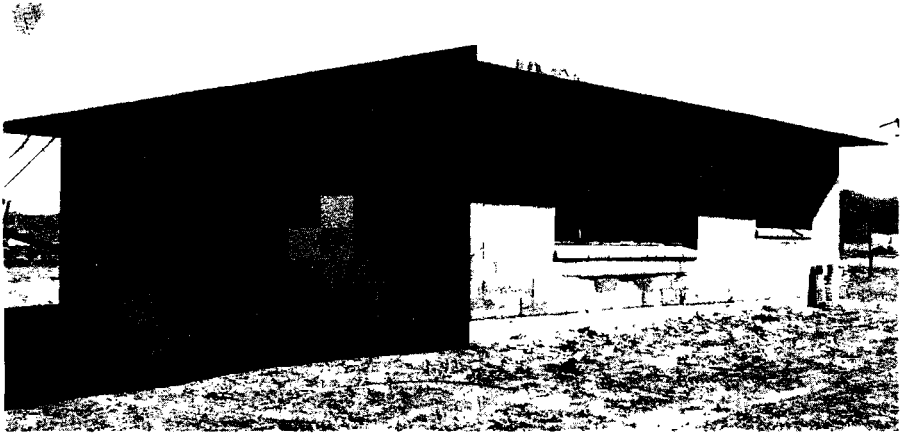

Figure 5.77. Reinforced masonry-block house after a nuclear explosion (5 psi peak overpressure).

column in the center span of the window.

5.79 A house of the same type exposed to the blast at a peak overpressure of 1.7 pounds per square inch suffered little more than the usual destruction of doors and windows. The steel window-sash remained in place but was distorted, and some spalling of the concrete around lug connections was noted. On the whole, the damage to the house was of a minor character and it could readily have been repaired.

TRAILER-COACH MOBILE HOMES: 1955 TEST

5.80 Sixteen trailer-coaches of various makes, intended for use as mobile homes, were subjected to blast in the 1955 test in Nevada. Nine were located where the peak blast overpressure was 1.7 pounds per square inch, and the other seven where the peak overpressure was about 1 pound per square inch. They were parked at various angles with respect to the direction of travel of the blast wave.

5.81 At the higher overpressure two of the mobile homes were tipped over by the explosion. One of these was originally broadside to the blast, whereas the second, at an angle of about 45°, was of much lighter weight. All the others at both locations remained standing. On the whole, the damage sustained was not of a serious character.

5.82 From the exterior, many of the mobile homes showed some dents in walls or roof, and a certain amount of distortion. There were, however, relatively few ruptures. Most windows were broken, but there was little or no glass in the interior, especially in those coaches having screens fitted on the inside. Where there were no screens or venetian blinds, and particularly where there were large picture windows, glass was found inside.

5.83 The interiors of the mobile homes were usually in a state of disorder due to ruptured panels, broken and upset furniture, and cupboards, cabinets, and wardrobes which had been torn loose and damaged. Stoves, refrigerators, and heaters were not displaced, and the floors were apparently unharmed. The plumbing was, in general, still operable after the explosion. Consequently, by rearranging the displaced furniture, repairing cabinets, improvising window coverings, and cleaning up the debris, all trailer-coaches could have been made habitable for emergency use.

5.84 At the 1 pound per square inch overpressure location some windows were broken, but no major damage was sustained. The principal repairs required to make the mobile homes available for occupancy would be window replacement or improvised window covering.

TRANSPORTATION

LIGHT LAND TRANSPORTATION EQUIPMENT

5.85 In Japan, trolley-car equipment was heavily damaged by both blast and fire, although the poles were frequently left standing. Buses and automobiles generally were rendered inoperable by blast and fire as well as by damage caused by flying debris. However, the damage decreased rapidly with distance. An American made automobile was badly damaged and burned at 3,000 feet (0.57 mile) from ground zero, but a similar vehicle at 6,000 feet (1.14 miles) suffered only minor damage.

5.86 Automobiles and buses have been exposed to several of the nuclear test explosions in Nevada, where the conditions, especially as regards dam-

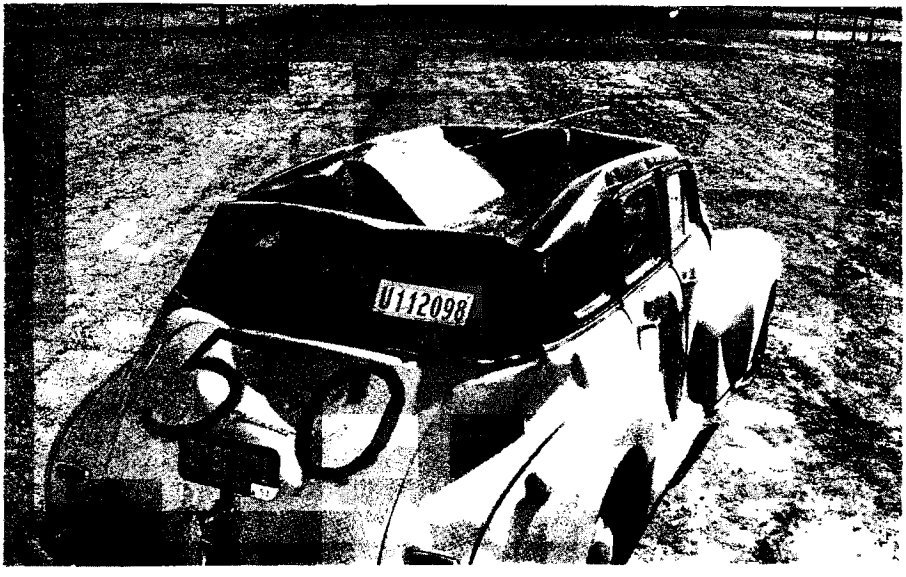

Figure 5.87a. Damage to automobile originally located behind wood-frame house (5 psi peak overpressure); the front of this car can be seen in Figure 5.57. Although badly damaged, the car could still be driven after the explosion.

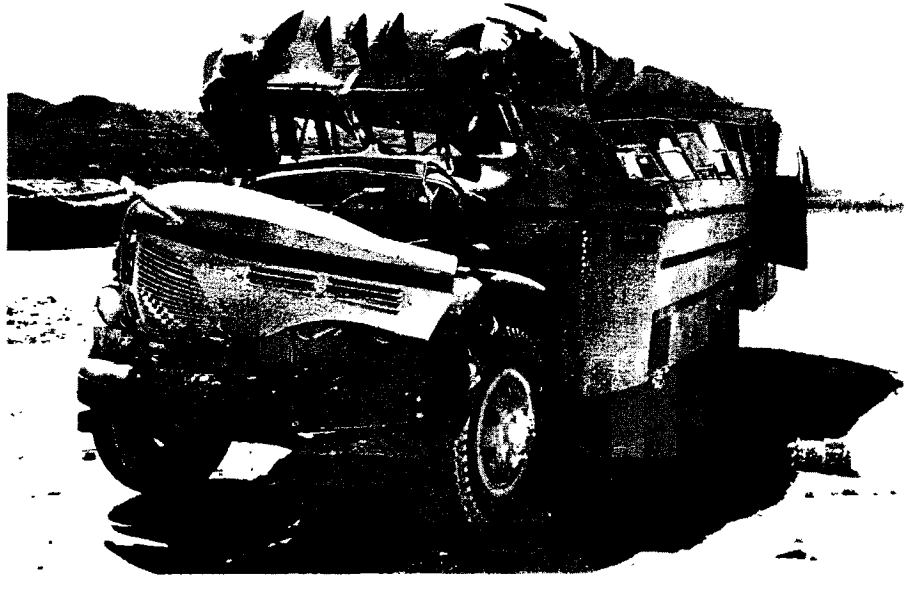

Figure 5.87b. Typical public bus damaged by a nuclear explosion, Nevada Test Site; this bus, like the one in the left background, was overturned, coming to rest as shown after a displacement of 50 feet.

age by fire and missiles, were somewhat different from those in Japan. In the descriptions that follow, distance is related to peak overpressure. In most cases, however, it was not primarily overpressure, but drag forces, which produced the damage. In addition, allowance must be made for the effect of the blast wave precursor (§ 3.79 *et seq.*). Hence, the damage radii cannot be determined from overpressure alone.

5.87 Some illustrations of the effects of a nuclear explosion on motorized vehicles are shown in Figs. 5.87a and b. At a peak overpressure of 5 pounds per square inch motor vehicles were badly battered, with their tops and sides pushed in, windows broken, and hoods blown open. But the engines were still operable and the vehicles could be driven away after the explosion. Even at higher blast pressures, when the overall damage was greater, the motors appeared to be intact.

5.88 During the 1955 tests in Nevada, studies were made to determine the extent to which various emergency vehicles and their equipment would be available for use immediately following a nuclear attack. The vehicles included a rescue truck, gas and electric utility service or repair trucks, telephone service trucks, and fire pumpers and ladder trucks. One vehicle was exposed to a peak overpressure of about 30 pounds per square inch, two at 5 pounds per square inch, two at 1.7 pounds per square inch, and six at about 1 pound per square inch. It should be emphasized, however, that, for vehicles in general, overpressure is not usually the sole or even the primary damage mechanism.

5.89 The rescue truck at the 30 pounds per square inch location was completely destroyed, and only one wheel and part of the axle were found after the blast. At 5 pounds per square inch peak overpressure a truck, with an earth-boring machine bolted to the bed, was broadside to the blast. This truck was overturned and somewhat damaged, but still operable (Fig. 5.89). The earth-boring machine was knocked loose and was on its side leaking gasoline and water. At the same location, shown to the left of the overturned truck in Fig. 5.89, was a heavy-duty electric utility truck, facing head-on to the blast. It had the windshield shattered, both doors and cab dished in, the hood partly blown off, and one tool-compartment door dished. There was, however, no damage to tools or equipment and the truck was driven away without any repairs being required.

5.90 At the 1.7 pounds per square inch location, a light-duty electric utility truck and a fire department 75-foot aerial ladder truck sustained minor exterior damage, such as broken windows and dished-in panels. There was no damage to equipment in either case, and both vehicles would have been available for immediate use after an attack. Two telephone trucks, two gas utility trucks, a fire department pumper, and a Jeep firetruck, exposed to a peak overpressure of 1 pound per square inch, were largely unharmed.

5.91 It may be concluded that vehicles designed for disaster and emergency operation are substantially constructed, so that they can withstand a peak overpressure of about 5 pounds per square inch and the associated dynamic pressure and still be capable of operation. Tools and equipment are protected

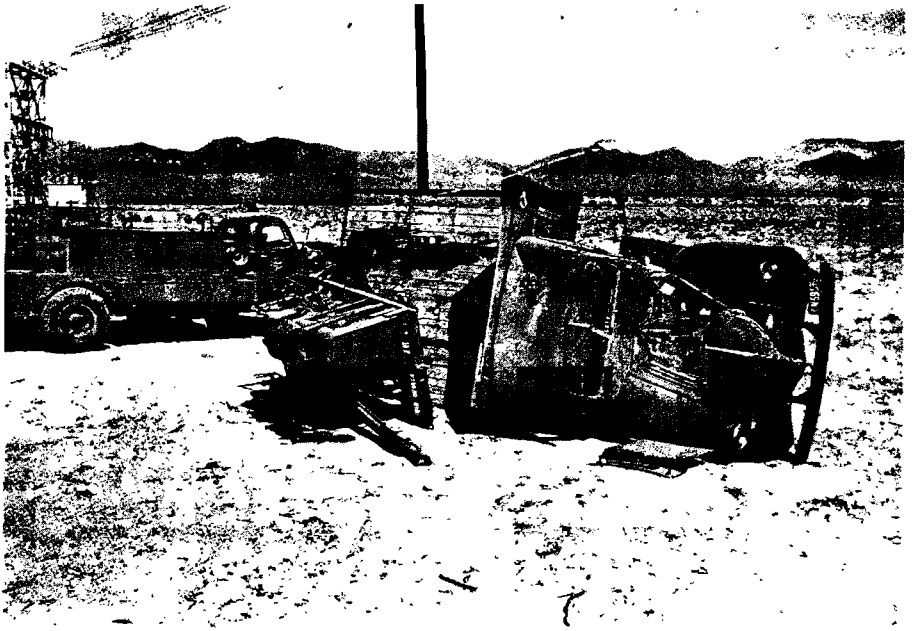

Figure 5.89. Truck broadside to the blast wave (5 psi peak overpressure) overturned; electric utility truck in background head-on to blast was damaged but remained standing.

from the blast by the design of the truck body or when housed in compartments with strong doors.

RAILROAD EQUIPMENT

5.92 Railroad equipment suffered blast damage in Japan and also in tests in Nevada. Like motor vehicles, these targets are primarily drag sensitive and damage cannot be directly related to overpressure. At a peak overpressure of 2 pounds per square inch from a kiloton-range weapon, an empty wooden boxcar may be expected to receive relatively minor damage. At 4 pounds per square inch overpressure, the damage to a loaded wooden boxcar would be more severe (Fig. 5.92a). At a peak overpressure of 6 pounds per square inch the body of an empty wooden boxcar, weighing about 20 tons, was lifted off the trucks, i.e., the wheels, axles, etc., carrying the body, and landed about 6 feet away. The trucks themselves were pulled off the rails, apparently by the brake rods connecting them to the car body. A similar boxcar, at the same location, loaded with 30 tons of sandbags remained upright (Fig. 5.92b). Although the sides were badly damaged and the roof demolished, the car was capable of being moved on its own wheels. At 7.5 pounds per square inch peak overpressure, a loaded boxcar of the same type was overturned, and at 9 pounds per square inch it was completely demolished.

5.93 A Diesel locomotive weighing 46 tons was exposed to a peak over-

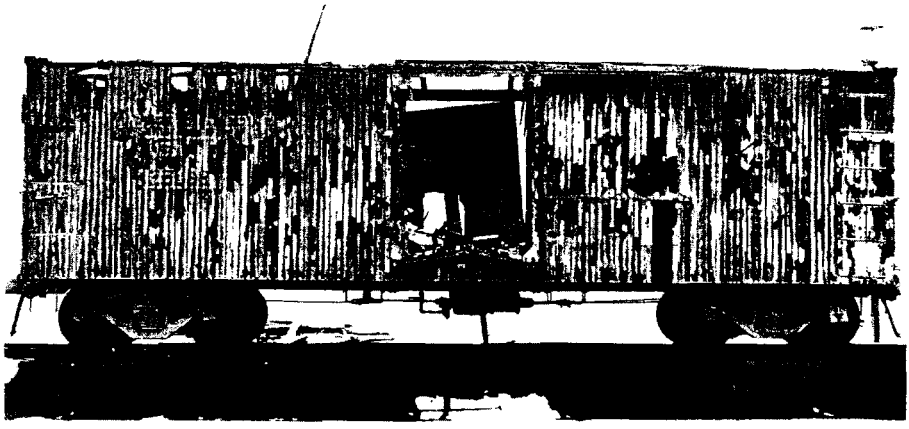

Figure 5.92a. Loaded wooden boxcar after a nuclear explosion (4 psi peak overpressure).

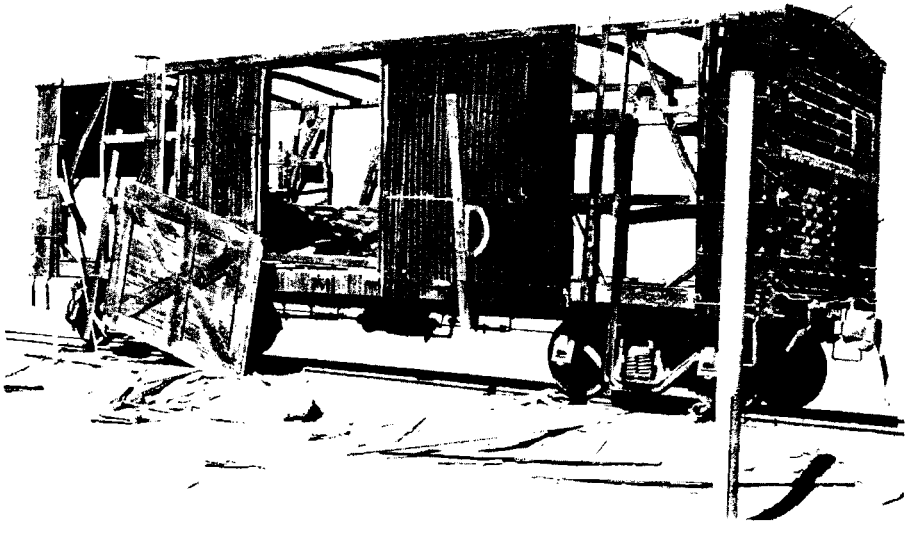

Figure 5.92b. Loaded wooden boxcar after a nuclear explosion (6 psi peak overpressure).

pressure of 6 pounds per square inch while the engine was running. It continued to operate normally after the blast, in spite of damage to windows and compartment doors and panels. There was no damage to the railroad track at this point.

AIRCRAFT

5.94 Aircraft are damaged by blast effects at levels of peak overpressure as low as 1 to 2 pounds per square inch. Complete destruction or damage beyond economical repair may be expected at peak overpressures of 4 to 10 pounds per square inch. Within this range, the peak overpressure appears to be the main criterion of damage. However, tests indicate that, at a given overpressure, damage to an aircraft oriented with the nose toward the burst will be less than damage to one with the tail or a side directed toward the explosion.

5.95 Damage to an aircraft exposed with its left side to the blast at a peak overpressure of 3.6 pounds per square inch is shown in Fig. 5.95a. The fuselage of this aircraft failed completely just aft of the wing. The skin of the fuselage, stabilizers, and engine cowling was severely buckled. Figure 5.95b shows damage to an aircraft oriented with its tail toward the burst and exposed to 2.4 pounds per square inch peak overpressure. Skin was dished in on the vertical stabilizer, horizontal stabilizers, wing surface above the flaps, and outboard wing sections. Vertical stabilizer bulkheads and the fuselage frame near the cockpit were buckled.

SHIPPING

5.96 Damage to ships from an air or surface burst is due primarily to the air blast, since little pressure is transmitted through the water. At closer ranges, air blast can cause hull rupture resulting in flooding and sinking. Such rupture appears likely to begin near the waterline on the side facing the burst. Since the main hull generally is stronger than the superstructure, structures and equipment exposed above the waterline may be damaged at ranges well beyond that at which hull rupture might occur. Masts, spars, radar antennas, stacks, electrical equipment, and other light objects are especially sensitive to air blast. Damage to masts and stacks is apparent in Fig. 5.96; the ship was approximately 0.47 mile from surface zero at the ABLE test (about 20-kiloton air burst) at Bikini in 1946. Air blast may also roll and possibly capsize the ship; this effect would be most pronounced for the air blast wave from a large weapon striking the ship broadside.

5.97 Blast pressures penetrating through openings of ventilation systems and stack-uptake systems can cause damage to interior equipment and compartments, and also to boilers. Damage to the latter may result in immobilization of the ship. The distortion of weather bulkheads may render useless interior equipment mounted on or near them. Similarly, the suddenly applied blast loading induces rapid motion of the structures which may cause shock damage to interior equipment. Equipment in the superstructure is most susceptible to this type of damage, although shock motions may be felt throughout the ship.

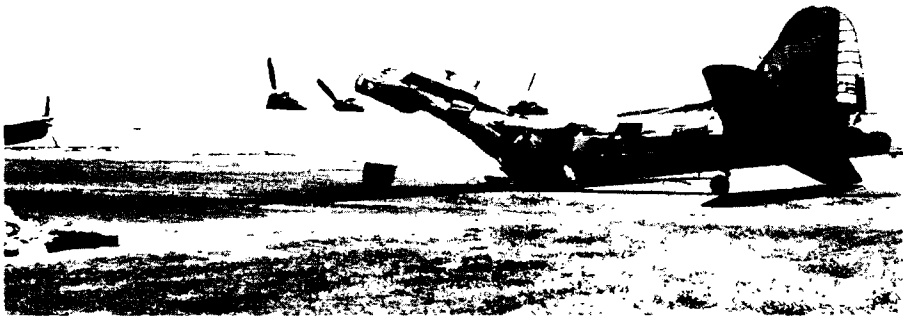

Figure 5.95a. Aircraft after side exposed to a nuclear explosion (3.6 psi peak overpressure).

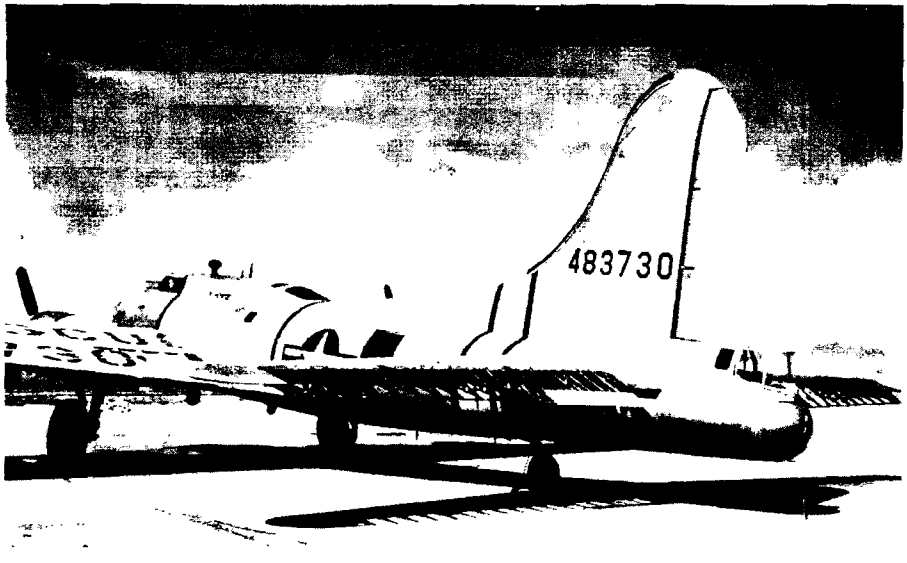

Figure 5.95b. Aircraft after tail exposed to a nuclear explosion (2.4 psi peak overpressure).

UTILITIES

ELECTRICAL DISTRIBUTION SYSTEMS

5.98 Because of the extensive damage caused by the nuclear explosions to the cities in Japan, the electrical distribution systems suffered severely. Utility poles were destroyed by blast or fire, and overhead lines were heavily damaged at distances up to 9,000 feet (1.7 miles) from ground zero (Fig. 5.98).

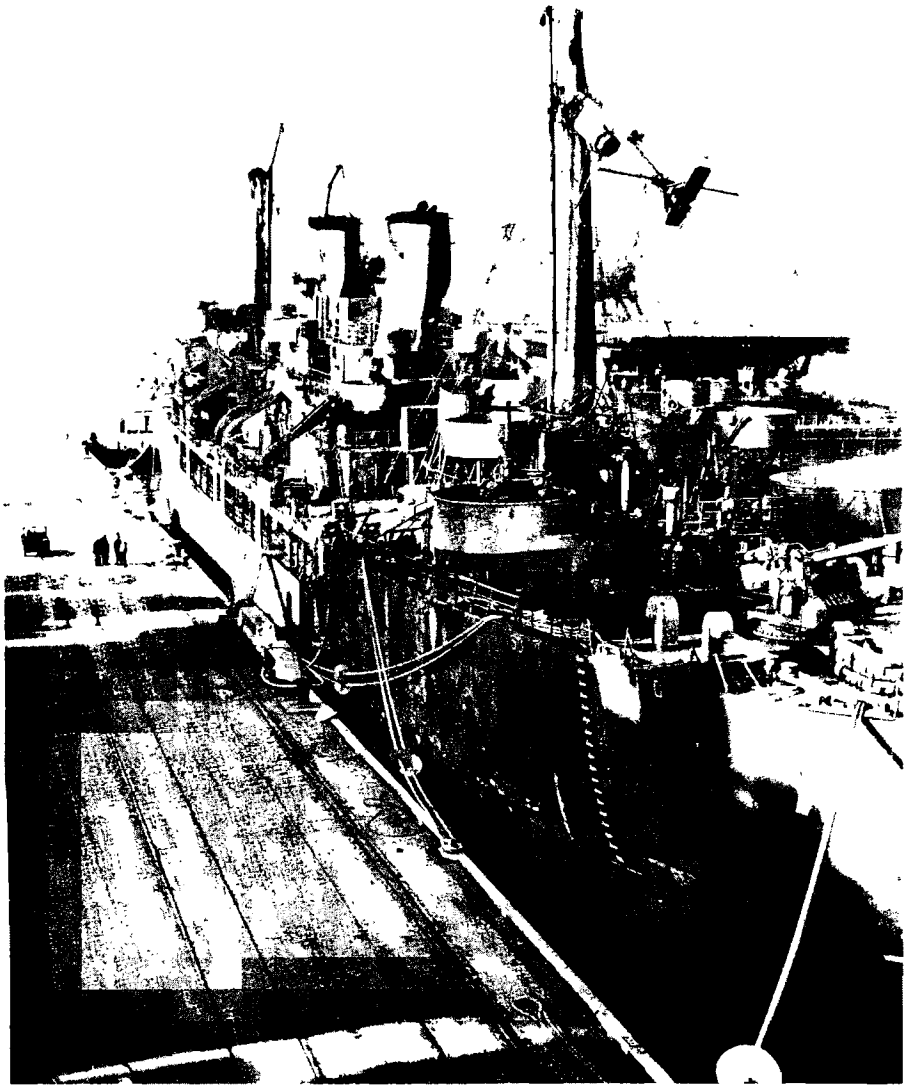

Figure 5.96. The U.S.S. Crittenden after ABLE test; damage resulting was generally serious (0.47 mile from surface zero).

Underground electrical circuits were, however, little affected. Switchgear and transformers were not damaged so much directly by blast as by secondary effects, such as collapse of the structure in which they were located or by debris. Motors and generators were damaged by fire.

5.99 A fairly extensive study of the effects of a nuclear explosion on electric utilities was made in the Nevada tests in 1955. Among the purposes of these tests

Figure 5.98. Damage to utility pole (0.80 mile from ground zero at Hiroshima).

were the following: (1) to determine the blast pressure at which standard electrical equipment might be expected to suffer little or no damage; (2) to study the extent and character of the damage that might be sustained in a nuclear

attack; and (3) to determine the nature of the repairs that would be needed to restore electrical service in those areas where homes and factories would survive sufficiently to permit their use after some repair. With these objectives in mind, two identical power systems were erected; one to be subjected to a peak overpressure of about 5 and a dynamic pressure of 0.6 pounds per square inch and the other to 1.7 and 0.1 pounds per square inch, respectively. It will be recalled that, at the lower overpressure, typical American residences would not be damaged beyond the possibility of further use.

5.100 Each power system consisted of a high-voltage (69-kV) transmission line on steel towers connected to a conventional, outdoor transformer substation. From this proceeded typical overhead distribution lines on 15 wood poles; the latter were each 45 feet long and were set 6 feet in the ground. Service drops from the overhead lines supplied electricity to equipment placed in some of the houses used in the tests described earlier. These installations were typical of those serving an urban community. In addition, the 69-kV transmission line, the 69-kV switch rack with oil circuit-breakers, and power transformer represented equipment of the kind that might supply electricity to large industrial plants.

5.101 At a peak overpressure of 5 and a dynamic pressure of 0.6 pounds per square inch the power system suffered to some extent, but it was not seriously harmed. The type of damage appeared, on the whole, to be similar to that caused by severe wind storms. In addition to the direct effect of blast, some destruction was due to missiles.

5.102 The only damage suffered by the high-voltage transmission line was the collapse of the suspension tower, bringing down the distribution line with it (Fig. 5.102a). It may be noted that the dead-end tower, which was much stronger and heavier, and another suspension tower of somewhat stronger design were only slightly affected (Fig. 5.102b). In some parts of the United States, the suspension towers are of similar heavy construction. Structures of this type are sensitive to drag forces which are related to dynamic pressure and positive phase duration, so that the overpressure is not the important criterion of damage.

5.103 The transformer substation survived the blast with relatively minor damage to the essential components. The metal cubicle, which housed the meters, batteries, and relays, suffered badly, but this substation and its contents were not essential to the emergency operation of the power system. The 4-kV regulators had been shifted on the concrete pad, resulting in separation of the electrical connections to the bus. The glass cells of the batteries were broken and most of the plates were beyond repair. But relays, meters, and other instruments were undamaged, except for broken glass. The substation as a whole was in sufficiently sound condition to permit operation on a nonautomatic (manual) basis. By replacing the batteries, automatic operation could have been restored.

5.104 Of the 15 wood poles used to carry the lines from the substation to the houses, four were blown down completely and broken, and two others were extensively damaged. The collapse of the poles was attributed partly to the

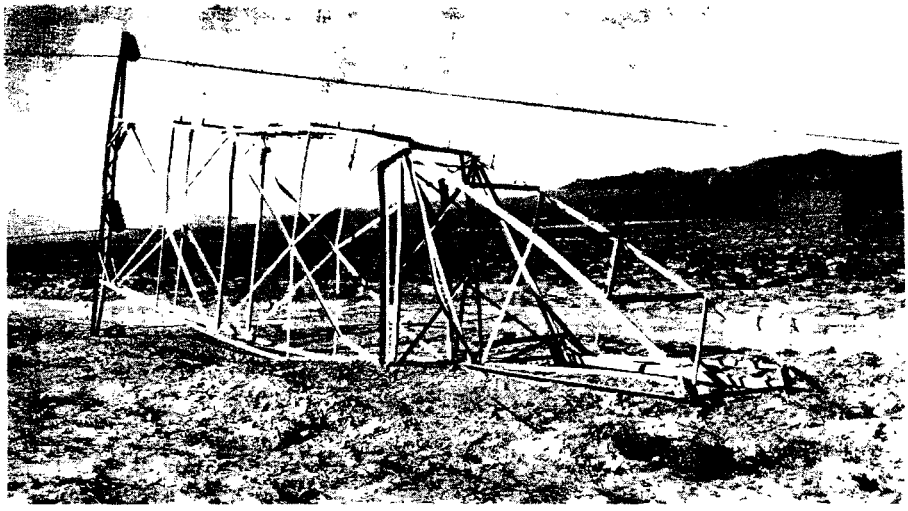

Figure 5.102a. Collapsed suspension tower (5 psi peak overpressure, 0.6 psi dynamic pressure from 30-kiloton explosion), Nevada Test Site.

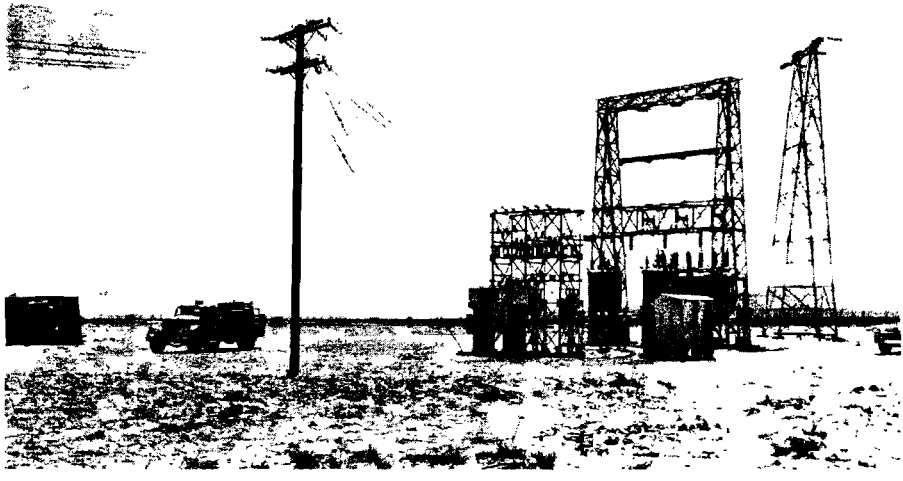

Figure 5.102b. Dead-end tower, suspension tower, and transformers (5 psi peak overpressure, 0.6 psi dynamic pressure from 30-kiloton explosion), Nevada Test Site. The trucks at the left of the photograph are those in Figure 5.89.

weight and resistance of the aerial cable (Fig. 5.104). Other damage was believed to be caused by missiles.

5.105 Several distributor transformers had fallen from the poles and secondary wires and service drops were down (Fig. 5.105). Nevertheless the transformers, pot heads, arresters, cutouts, primary conductors of both aluminum and copper, and the aerial cables

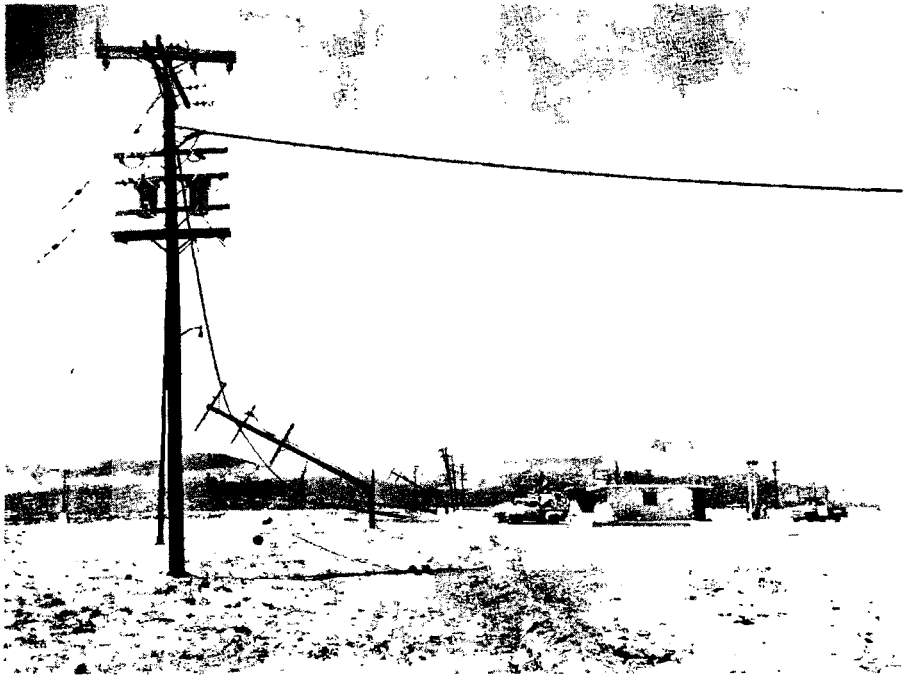

Figure 5.104. Collapse of utility poles on line (5 psi peak overpressure, 0.6 psi dynamic pressure from 30-kiloton explosion), Nevada Test Site.

were unharmed. Although the pole line would have required some rebuilding, the general damage was such that it could have been repaired within a day or so with materials normally carried in stock by electric utility companies.

GAS, WATER, AND SEWERAGE SYSTEMS

5.106 The public utility system in Nagasaki was similar to that of a somewhat smaller town in the United States, except that open sewers were used. The most significant damage was suffered by the water supply system, so that it became almost impossible to extinguish fires. Except for a special case, described below, loss of water pressure resulted from breakage of pipes inside and at entrances to buildings or on structures, rather than from the disruption of underground mains (Figs. 5.106a and b). The exceptional case was one in which the 12-inch cast iron water pipes were 3 feet below grade in a filled-in area. A number of depressions, up to 1 foot in depth, were produced in the fill, and these caused failure of the underground pipes, presumably due to unequal displacements.

5.107 There was no appreciable damage to reservoirs and water-treatment plants in Japan. As is generally the case, these were located outside the cities, and so were at too great a distance from the explosions to be damaged in any way.

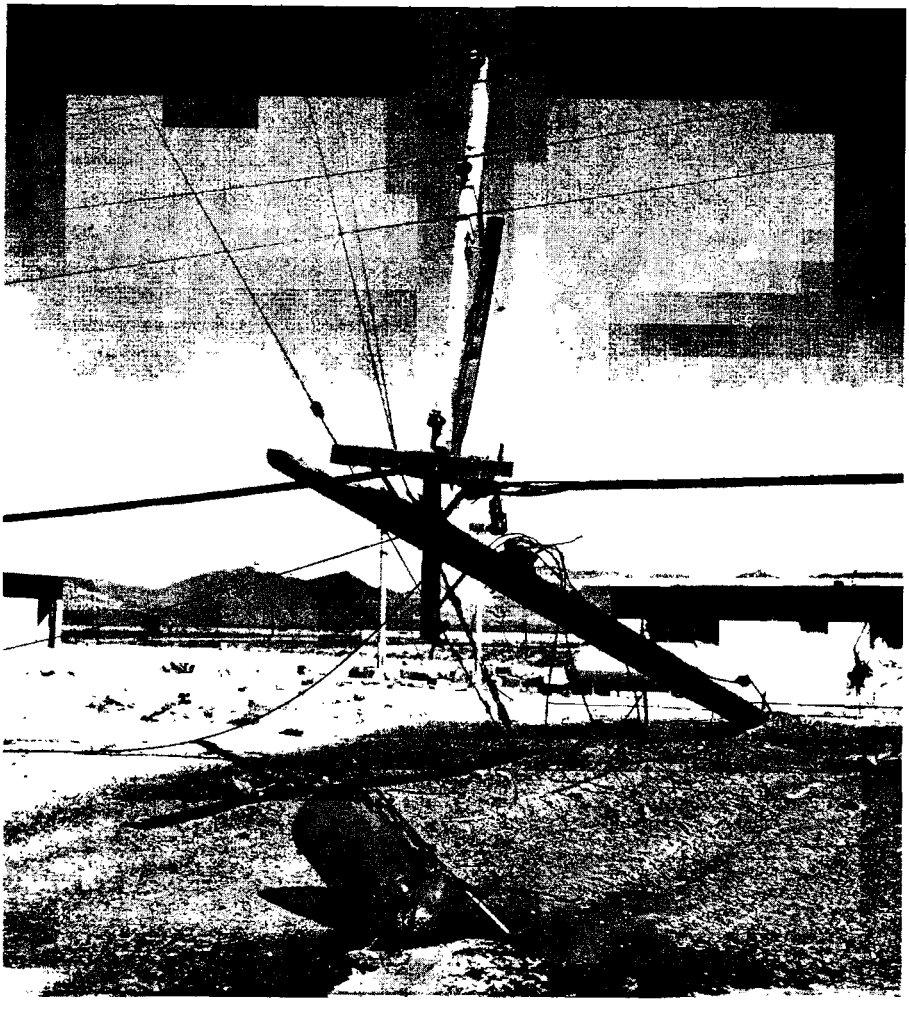

Figure 5.105. Transformer fallen from collapsed utility pole (5 psi peak overpressure), Nevada Test Site.

5.108 Gas holders suffered heavily from blast up to 6,000 feet (1.1 miles) from ground zero and the escaping gas was ignited, but there was no explosion. Underground gas mains appear to have been little affected by the blast.

NATURAL AND MANUFACTURED GAS INSTALLATIONS

5.109 One of the objectives of the tests made in Nevada in 1955 was to determine the extent to which natural and manufactured gas utility installations might be disrupted by a nuclear explosion. The test was intended, in particular, to provide information concerning the effect of blast on critical underground units of a typical gas distribution system.

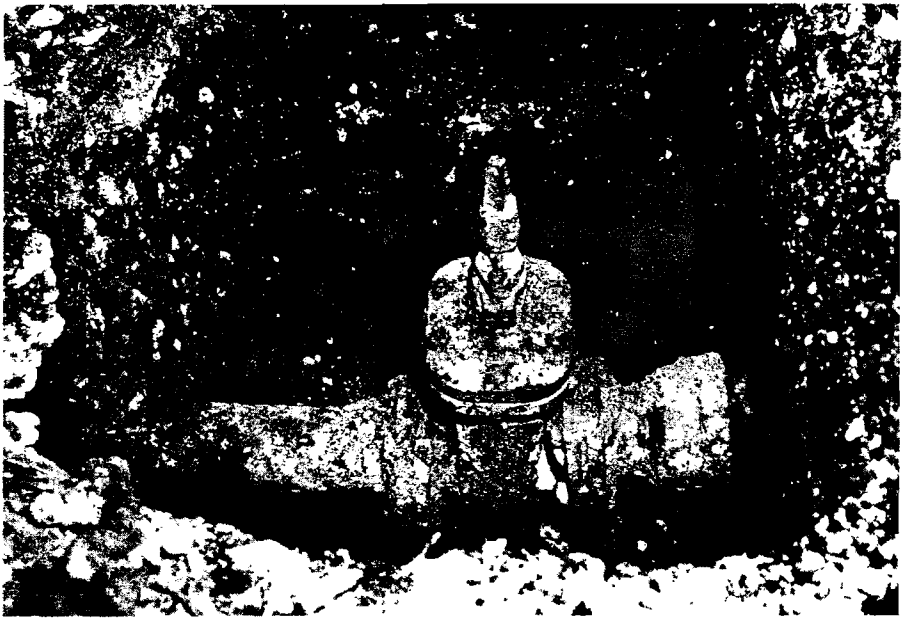

Figure 5.106a. Four-inch gate valve in water main broken by debris from brick wall (0.23 mile from ground zero at Hiroshima).

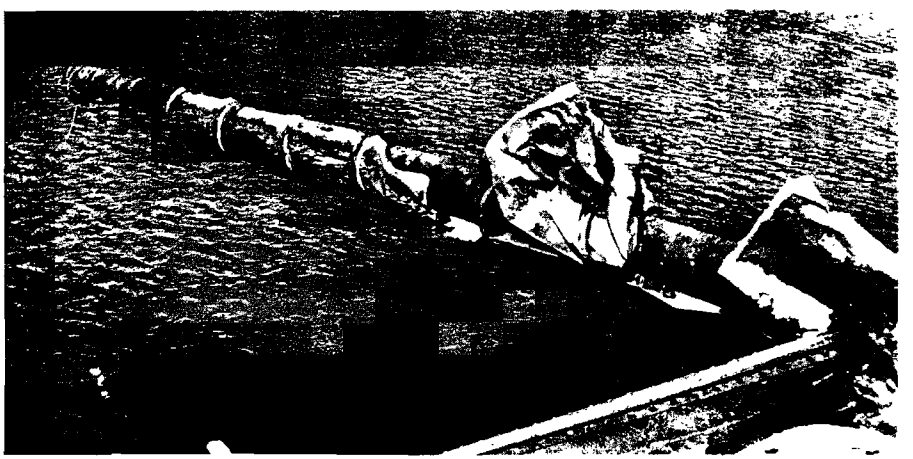

Figure 5.106b. Broken portion of 16-inch water main carried on bridge (0.23 mile from ground zero at Hiroshima).

5.110 The installations tested were of two kinds, each in duplicate. The first represented a typical underground gas-transmission and distribution main of 6-inch steel and cast iron pipe, at a depth of 3 feet, with its associated ser-

vice pipes and attachments. Valve pits of either brick or concrete blocks contained 6-inch valves with piping and protective casings. A street regulator-vault held a 6-inch, low-pressure, pilot-loaded regulator, attached to steel piping projecting through the walls. One of these underground systems was installed where the blast overpressure was about 30 pounds per square inch and the other at 5 pounds per square inch. No domestic or ordinary industrial structures at the surface would have survived the higher of these pressures.

5.111 The second type of installation consisted of typical service lines of steel, copper, and plastic materials connected to 20-foot lengths of 6-inch steel main. Each service pipe rose out of the ground at the side of a house, and was joined to a pressure regulator and meter. The pipe then entered the wall of the house about 2 feet above floor level. The copper and plastic services terminated inside the wall, so that they would be subject to strain if the house moved on its foundation. The steel service line similarly terminated inside the wall, but it was also attached outside to piping that ran around the back of the house at ground level to connect to the house piping. This latter connection was made with flexible seamless bronze tubing, passing through a sleeve in the wall of the building. Typical domestic gas appliances, some attached to the interior piping, were located in several houses. Duplicate installations were located at peak overpressures of 5 and 1.7 pounds per square inch, respectively.

5.112 Neither of the underground installations was greatly affected by the blast. At the 30 pounds per square inch peak overpressure location a 1½-inch pipe pressure-test riser was bent to the ground, and the valve handle, stem, and bonnet had blown off. At the same place two 4-inch ventilating pipes of the street regulator-vaults were sheared off just below ground level. A few minor leaks developed in jute and lead caulked cast iron bell and spigot joints because of ground motion, presumably due to ground shock induced by air blast. Otherwise the blast effects were negligible.

5.113 At the peak overpressure of 1.7 pounds per square inch, where the houses did not suffer severe damage, (§ 5.59), the service piping both inside and outside the houses was unharmed, as also were pressure regulators and meters. In the two-story, brick house at 5 pounds per square inch peak overpressure, which was demolished beyond repair (§ 5.57), the piping in the basement was displaced and bent as a result of the collapse of the first floor. The meter also became detached from the fittings and fell to the ground, but the meter itself and the regulator were undamaged and still operable. All other service piping and equipment were essentially intact.

5.114 Domestic gas appliances, such as refrigerators, ranges, room heaters, clothes dryers, and water heaters suffered to a moderate extent only. There was some displacement of the appliances and connections which was related to the damage suffered by the house. However, even in the collapsed two-story, brick house (§ 5.67), the upset refrigerator and range were probably still usable, although largely buried in debris. The general conclusion is, therefore, that domestic gas (and also electric) appliances would be operable

in all houses that did not suffer major structural damage.

LIQUID PETROLEUM (LP) GAS INSTALLATIONS

5.115 Various LP-gas installations have been exposed to air blast from nuclear tests in Nevada to determine the effects of typical gas containers and supply systems such as are found at suburban and farm homes and at storage, industrial, and utility plants. In addition, it was of interest to see what reliance might be placed upon LP-gas as an emergency fuel after a nuclear attack.

5.116 Two kinds of typical home (or small commercial) LP-gas installations were tested: (1) a system consisting of two replaceable ICC-approved cylinders each of 100-pound capacity; and (2) a 500-gallon bulk storage type system filled from a tank truck. Some of these installations were in the open and others were attached, in the usual manner, by means of either copper tubing or steel pipe service line, to the houses exposed to peak overpressures of 5 and 1.7 pounds per square inch. Others were located where the peak overpressures were about 25 and 10 pounds per square inch. In these cases, piping from the gas containers passed through a concrete wall simulating the wall of a house.

5.117 In addition to the foregoing, a complete bulk storage plant was erected at a point where the peak overpressure was 5 pounds per square inch. This consisted of an 18,000-gallon tank (containing 15,400 gallons of propane), pump compressor, cylinder-filling building, cylinder dock, and all necessary valves, fittings, hose, accessories, and interconnecting piping.

5.118 The dual-cylinder installation, exposed to 25 pounds per square inch peak overpressure, suffered most; the regulators were torn loose from their mountings and the cylinders displaced. One cylinder came to rest about 2,000 feet from its original position; it was badly dented, but was still usable. At both 25 and 10 pounds per square inch peak overpressure the components, although often separated, could generally be salvaged and used again. The cylinder installations at 5 pounds per square inch peak overpressure were mostly damaged by missiles and falling debris from the houses to which they were attached. The component parts, except for the copper tubing, suffered little and were usable. At 1.7 pounds per square inch, there was neither damage to nor dislocation of LP-gas cylinders. Of those tested, only one cylinder developed a leak, and this was a small puncture resulting from impact with a sharp object.

5.119 The 500-gallon bulk gas tanks also proved very durable and experienced little damage. The tank closest to the explosion was bounced end-over-end for a distance of some 700 feet; nevertheless, it suffered only superficially and its strength and serviceability were not impaired. The filler valve was damaged, but the internal check valve prevented escape of the contents. The tank exposed at 10 pounds per square inch peak overpressure was moved about 5 feet, but it sustained little or no damage. All the other tanks, at 5 or 1.7 pounds per square inch, including those at houses piped for service, were unmoved and undamaged (Fig. 5.73).

5.120 The equipment of the

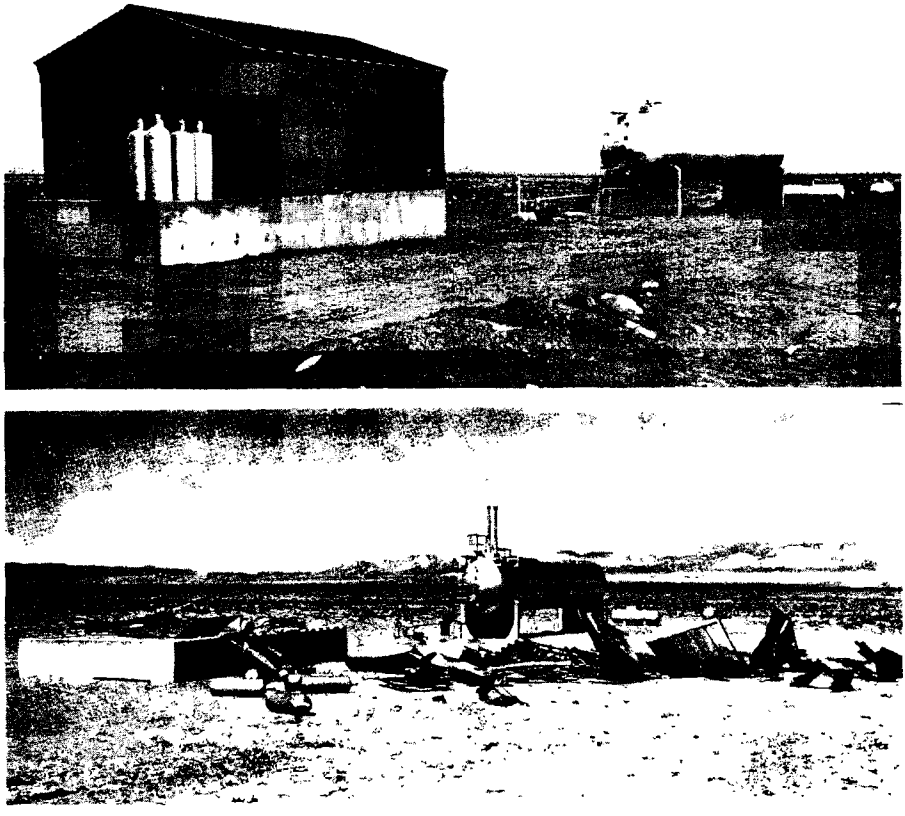

Figure 5.120. Upper photo: LP-gas bulk storage and filling plant before a nuclear explosion. Lower photo: The plant after the explosion (5 psi peak overpressure).

18,000-gallon bulk storage and filling plant received only superficial damage from the blast at 5 pounds per square inch peak overpressure. The cylinder-filling building was completely demolished; the scale used for weighing the cylinders was wrecked, and a filling line was broken at the point where it entered the building (Fig. 5.120). The major operating services of the plant would, however, not be affected because the transfer facilities were outside and undamaged. All valves and nearly all piping in the plant were intact and there was no leakage of gas. The plant could have been readily put back into operation if power, from electricity or a gasoline engine, were restored. If not, liquid propane in the storage tank could have been made available by taking advantage of gravity flow in conjunction with the inherent pressure of the gas in the tank.

5.121 The general conclusion to be drawn from the tests is that standard LP-gas equipment is very rugged, except for copper tubing connections. Disruption of the service as a result of a

nuclear attack would probably be localized and perhaps negligible, so that LP-gas might prove to be a very useful emergency fuel. Where LP-gas is used mainly for domestic purposes, it appears that the gas supply would not be affected under such conditions that the house remains habitable.

MISCELLANEOUS TARGETS

COMMUNICATIONS EQUIPMENT

5.122 The importance of having communications equipment in operating condition after a nuclear attack is evident and so a variety of such equipment has been tested in Nevada. Among the items exposed to air blast were mobile radio-communication systems and units, a standard broadcasting transmitter, antenna towers, home radio and television receivers, telephone equipment (including a small telephone exchange), public address sound systems, and sirens. Some of these were located where the peak overpressure was 5 pounds per square inch, and in most cases there were duplicates at 1.7 pounds per square inch. The damage at the latter location was of such a minor character that it need not be considered here.

5.123 At the higher overpressure region, where typical houses were damaged beyond repair, the communications equipment proved to be very resistant to blast. This equipment is drag sensitive and so the peak overpressure does not determine the extent of damage. Standard broadcast and television receivers, and mobile radio base stations were found to be in working condition, even though they were covered with debris and had, in some cases, been damaged by missiles, or by being thrown or dropped several feet. No vacuum or picture tubes were broken. The only mobile radio station to be seriously affected was one in an automobile which was completely crushed by a falling chimney.

5.124 A guyed 150-foot antenna tower was unharmed, but an unguyed 120-foot tower, of lighter construction, close by, broke off at a height of about 40 feet and fell to the ground (Fig. 5.124). This represented the only serious damage to any of the equipment tested.

5.125 The base station antennas, which were on the towers, appeared to withstand blast reasonably well, although those attached to the unguyed tower, referred to above, suffered when the tower collapsed. As would have been expected from their lighter construction, television antennas for home receivers were more easily damaged. Several were bent both by the blast and the collapse of the houses upon which they were mounted. Since the houses were generally damaged beyond repair at a peak overpressure of 5 pounds per square inch, the failure of the television antennas is not of great significance.

5.126 Some items, such as power lines and telephone service equipment, were frequently attached to utility-line poles. When the poles failed, as they did in some cases (§ 5.104), the communi-

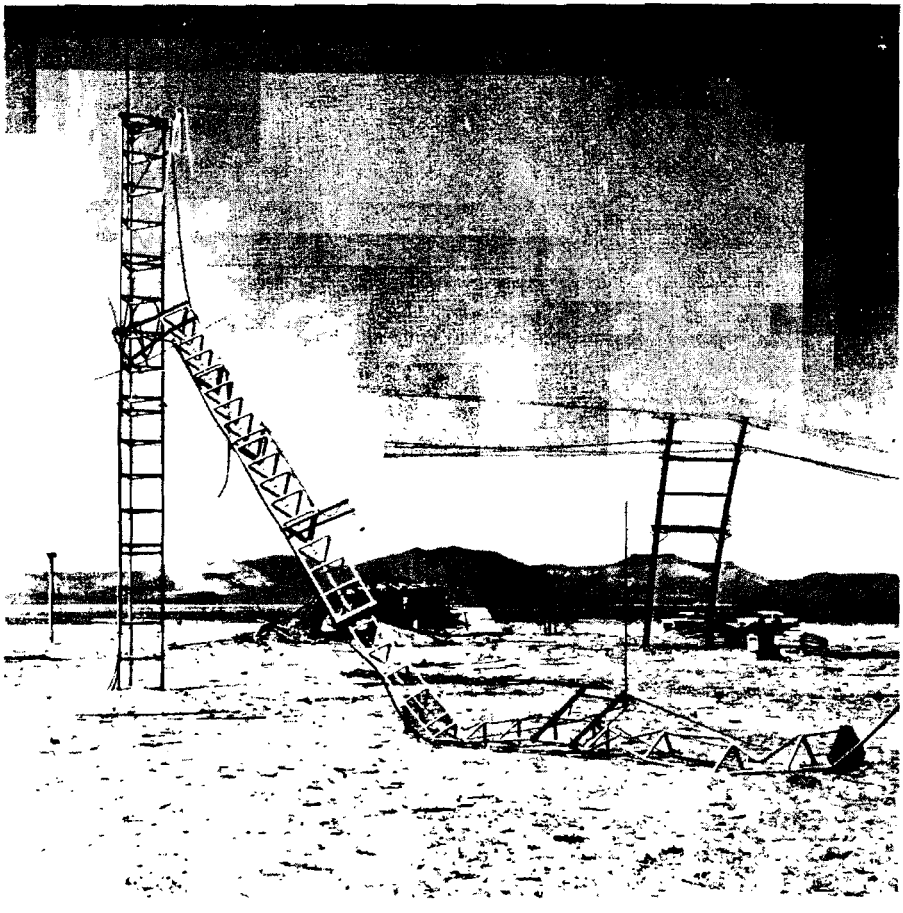

Figure 5.124. Unguyed lightweight 120-foot antenna tower (5 psi peak overpressure, 0.6 psi dynamic pressure from 30-kiloton explosion), Nevada Test Site.

cations systems suffered accordingly. Although the equipment operated satisfactorily after repairs were made to the wire line, it appears that the power supply represents a weak link in the communications chain.

BRIDGES

5.127 There were a number of different kinds of bridges exposed to the nuclear explosions in Hiroshima and Nagasaki. Those of wood were burned in most cases, but steel-girder bridges suffered relatively little destruction (Figs. 5.127a and b). One bridge, only 270 feet from ground zero, i.e., about 2,100 feet from the burst point, which was of a girder type with a reinforced-concrete deck, showed no sign of any structural damage. It had, apparently, been deflected downward by the blast force and had rebounded, causing only a slight net displacement. Other bridges,

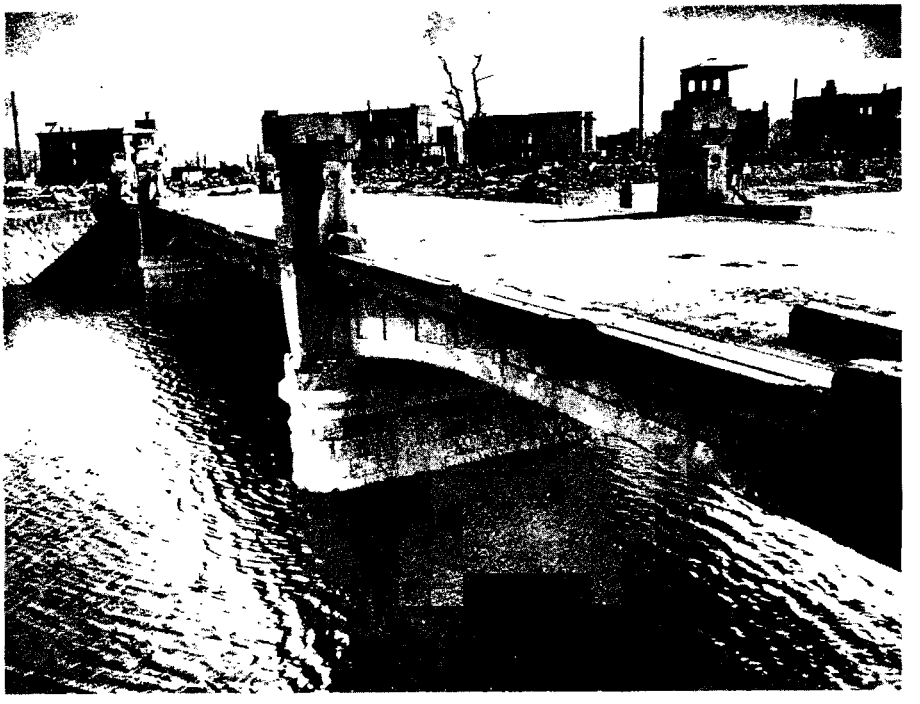

Figure 5.127a. Bridge with deck of reinforced concrete on steel-plate girders; outer girder had concrete facing (270 feet from ground zero at Hiroshima). The railing was blown down but the deck received little damage so that traffic continued.

at greater distances from ground zero, suffered more lateral shifting. A reinforced-concrete deck was lifted from the supporting steel girder of one bridge, apparently as a result of reflection of the blast wave from the surface of the water below.

HEAVY-DUTY MACHINE TOOLS

5.128 The vulnerability of heavy-duty machine tools and their components to air blast from a nuclear explosion was studied at the Nevada Test Site to supplement the information from Nagasaki (§ 5.33). A number of machine tools were anchored on a reinforced-concrete slab in such a manner as to duplicate good industrial practice. Two engine lathes (weighing approximately 7,000 and 12,000 pounds, respectively), and two horizontal milling machines (7,000 and 10,000 pounds, respectively) were exposed to a peak overpressure of 10 pounds per square inch. A concrete-block wall, 8 inches thick and 64 inches high, was constructed immediately in front of the machines, i.e., between the machines and ground zero (Fig. 5.128). The purpose of this wall was to simulate the exterior wall of the average industrial plant and to provide debris and missiles.

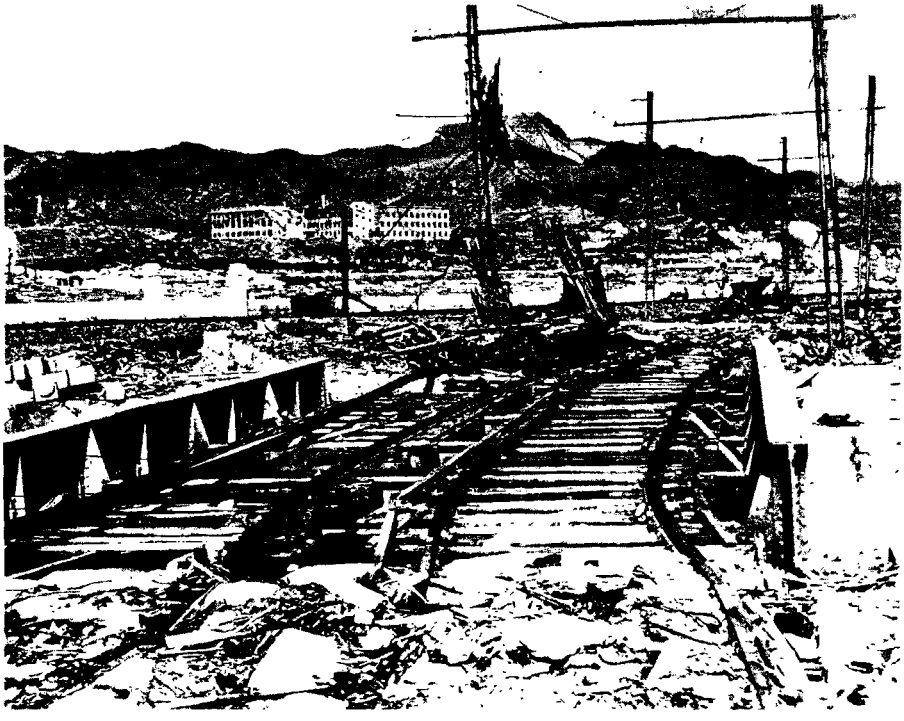

Figure 5.127b. A steel-plate girder, double-track railway bridge (0.16 mile from ground zero at Nagasaki). The plate girders were moved about 3 feet by the blast; the railroad track was bent out of shape and trolley cars were demolished, but the poles were left standing.

5.129 Of the four machines, the three lighter ones were moved from their foundations and damaged quite badly (Fig. 5.129a). The fourth, weighing 12,000 pounds, which was considered as the only one to be actually of the heavy-duty type, survived (Fig. 5.129b). From the observations it was concluded that a properly anchored machine tool of the true heavy-duty type would be able to withstand peak overpressures of 10 pounds per square inch or more without substantial damage.

5.130 In addition to the direct effects of blast, considerable destruction was caused by debris and missiles, much of which resulted from the expected complete demolition of the concrete-block wall. Delicate mechanisms and appendages, which are usually on the exterior and unprotected, suffered especially severely. Gears and gear cases were damaged, hand valves and control levers were broken off, and drive belts were broken. It appears, however, that most of the missile damage could be easily repaired if replacement parts were available, since major dismantling would not be required.

5.131 Behind the two-story brick house in the peak overpressure region of 5 pounds per square inch (§ 5.67), a

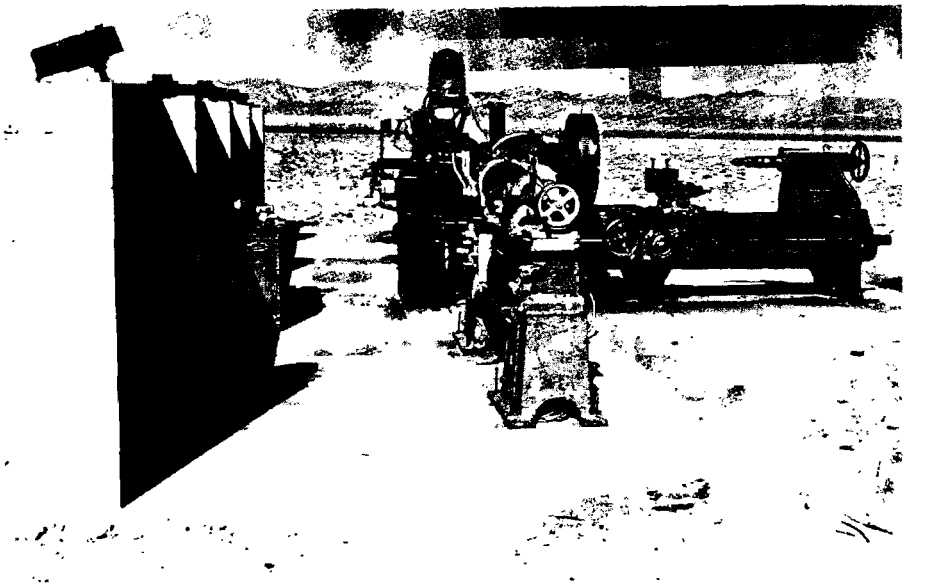

Figure 5.128. Machine tools behind masonry wall before a nuclear explosion, Nevada Test Site.

200-ton capacity hydraulic press weighing some 49,000 pounds was erected. The location was chosen as being the best to simulate actual factory conditions. This unusually tall (19 feet high) and slim piece of equipment showed little evidence of blast damage, even though the brick house was demolished. It was probable that the house provided some shielding from the blast wave. Moreover, at the existing blast pressure, missiles did not have high velocities. Such minor damage as was suffered by the machine was probably due to debris falling from the house.

5.132 At the 3-pounds per square inch peak overpressure location, there were two light, industrial buildings of standard type. In each of these was placed a vertical milling machine weighing about 3,000 pounds, a 50-gallon capacity, stainless-steel, pressure vessel weighing roughly 4,100 pounds, and a steel steam oven approximately 2½ feet wide, 5 feet high, and 9 feet long. Both buildings suffered extensively from blast, but the equipment experienced little or no operational damage. In one case, the collapsing structure fell on and broke off an exposed part of the milling machine.

5.133 The damage sustained by machine tools in the Nevada tests was probably less than that suffered in Japan at the same blast pressures (§ 5.33). Certain destructive factors, present in the latter case, were absent in the tests. First, the conditions were such that there was no damage by fire; and, second, there was no exposure to the elements after the explosion. In addition, the total amount of debris and missiles produced in the tests was probably less than in the industrial buildings in Japan.

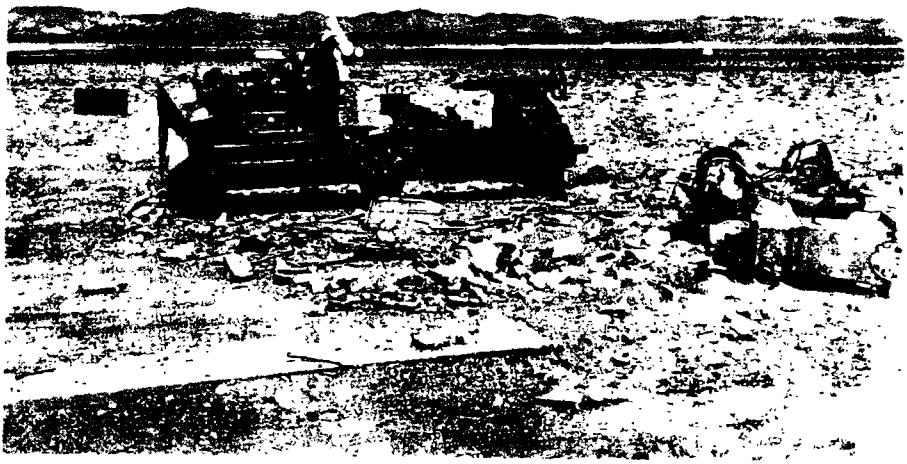

Figure 5.129a. Machine tools after a nuclear explosion (10 psi peak overpressure).

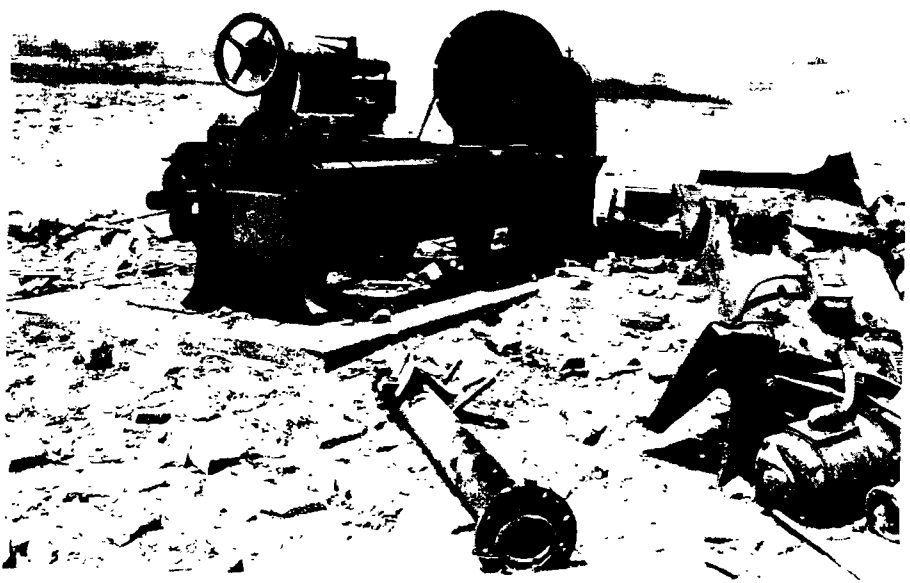

Figure 5.129b. Heavy-duty lathe after a nuclear explosion (10 psi peak overpressure).

ANALYSIS OF DAMAGE FROM AIR BLAST

INTRODUCTION

5.134 The remainder of this chapter is concerned with descriptions of air-blast damage criteria for various types of targets and with the development of damage–distance relationships for predicting the distances at which damage may be expected from nuclear explosions of different energy yields. The nature of any target complex, such as a city, is such, however, that exact predictions are not possible. Nevertheless, by application of proper judgment to the available information, results of practical value can be obtained. The conclusions given here are considered to be applicable to average situations that might be encountered in an actual target complex.

5.135 Damage to structures and objects is generally classified in three categories: severe, moderate, and light. In several of the cases discussed below, the specific nature of each type of damage is described, but the following broad definitions are a useful guide.

Severe Damage

A degree of damage that precludes further use of the structure or object for its intended purpose without essentially complete reconstruction. For a structure or building, collapse is generally implied.

Moderate Damage

A degree of damage to principal members that precludes effective use of the structure or object for its intended purpose unless major repairs are made.

Light Damage

A degree of damage to buildings resulting in broken windows, slight damage to roofing and siding, blowing down of light interior partitions, and slight cracking of curtain walls in buildings. Minor repairs are sufficient to permit use of the structure or object for its intended purpose.

5.136 For a number of types of targets, the distances out to which different degrees of damage may be expected from nuclear explosions of various yields have been represented by diagrams, such as Figs. 5.140 and 5.146. These are based on observations made in Japan and at various nuclear tests, on experiments conducted in shock tubes in laboratories and with high-explosives in field tests, and on theoretical analyses of the loading and response of structures (see Chapter IV). As a result of these studies, it is possible to make reasonably accurate predictions of the response of interior as well as exterior wall panels and complete structures to the air-blast wave. These predictions, however, must take into account constructional details of each individual structure. Moreover, observations made during laboratory tests have indicated a large scatter in failure loadings as a result of statistical variations among wall and material properties. The data in Figs. 5.140 and 5.146 are intended, however,

to provide only gross estimates for the categories of structures given in Tables 5.139a and b. The response of a particular structure may thus deviate from that shown for its class in the figures.

5.137 For structures that are damaged primarily by diffraction loading (§ 4.03), the peak overpressure is the important factor in determining the response to blast. In some instances, where detailed analyses have not been performed, peak overpressures are given for various kinds of damage. Approximate damage–distance relationships can then be derived by using peak overpressure–distance curves and scaling laws from Chapter III. For equal scaled heights of burst, as defined in § 3.62, the range for a specified damage to a diffraction-sensitive structure increases in proportion to the cube root, and the damage area in proportion to the two-thirds power, of the energy of the explosion. This means, for example, that a thousand-fold increase in the energy will increase the range for a particular kind of diffraction-type damage by a factor of roughly ten; the area over which the damage occurs will be increased by a factor of about a hundred, for a given scaled burst height.

5.138 Where the response depends mainly on drag (or wind) loading, the peak overpressure is no longer a useful criterion of damage. The response of a drag-sensitive structure is determined by the length of the blast wave positive phase as well as by the peak dynamic pressure (§ 4.12 *et seq.*). The greater the energy of the weapon, the farther will be the distance from the explosion at which the peak dynamic pressure has a specific value and the longer will be the duration of the positive phase. Since there is increased drag damage with increased duration at a given pressure, the same damage will extend to lower dynamic pressure levels. Structures which are sensitive to drag loading will therefore be damaged over a range that is larger than is given by the cube root rule for diffraction-type structures. In other words, as the result of a thousand-fold increase in the energy of the explosion, the range for a specified damage to a drag-sensitive structure will be increased by a factor of more than ten, and the area by more than a hundred.

ABOVE-GROUND BUILDINGS AND BRIDGES

5.139 The detailed nature of the damage in the severe, moderate, and light categories to above-ground structures of various types are given in Tables 5.139a and b. For convenience, the information is divided into two groups. Table 5.139a is concerned with structures of the type that are primarily affected by the blast wave during the diffraction phase, whereas the structures in Table 5.139b are drag sensitive.

5.140 The ranges for severe and moderate damage to the structures in Tables 5.139a and b are presented in Fig. 5.140, based on actual observations and theoretical analysis. The numbers (1 to 21) in the figure identify the target types as given in the first column of the tables. The data refer to air bursts with the height of burst chosen so as to maximize the radius of damage for the particular target being considered and is not necessarily the same for different targets. For a surface burst, the respective ranges are to be multiplied by three-fourths. An example illustrating the use of the diagram is given.

(Text continued on page 220.)

Table 5.139a

DAMAGE CRITERIA FOR STRUCTURES PRIMARILY AFFECTED BY DIFFRACTION LOADING

Structural Type	Description of Structure	Description of Damage		
		Severe	Moderate	Light
1	Multistory reinforced concrete building with reinforced concrete walls, blast resistant design for 30 psi Mach region pressure from 1 MT, no windows.	Walls shattered, severe frame distortion, incipient collapse.	Walls breached or on the point of being so, frame distorted, entranceways damaged, doors blown in or jammed, extensive spalling of concrete.	Some cracking of concrete walls and frame.
2	Multistory reinforced concrete building with concrete walls, small window area, three to eight stories.	Walls shattered, severe frame distortion, incipient collapse.	Exterior walls severely cracked. Interior partitions severely cracked or blown down. Structural frame permanently distorted, extensive spalling of concrete.	Windows and doors blown in, interior partitions cracked.
3	Multistory wall-bearing building, brick apartment house type, up to three stories.	Collapse of bearing walls, resulting in total collapse of structure.	Exterior walls severely cracked, interior partitions severely cracked or blown down.	Windows and doors blown in, interior partitions cracked.
4	Multistory wall-bearing building, monumental type, up to four stories.	Collapse of bearing walls, resulting in collapse of structure supported by these walls. Some bearing walls may be shielded by intervening walls so that part of the structure may receive only moderate damage.	Exterior walls facing blast severely cracked, interior partitions severely cracked with damage toward far end of building possibly less intense.	Windows and doors blown in, interior partitions cracked.
	Wood frame building, house type, one or two stories.	Frame shattered resulting in almost complete collapse.	Wall framing cracked. Roof severely damaged, interior partitions blown down.	Windows and doors blown in, interior partitions cracked.

Table 5.139b

DAMAGE CRITERIA FOR STRUCTURES PRIMARILY AFFECTED BY DRAG LOADING

Structural Type	Description of Structure	Description of Damage		
		Severe	Moderate	Light
6	Light steel frame industrial building, single story, with up to 5-ton crane capacity; low strength walls which fail quickly.	Severe distortion or collapse of frame.	Minor to major distortion of frame; cranes, if any, not operable until repairs made.	Windows and doors blown in, light siding ripped off.
7	Heavy steel-frame industrial building, single story, with 25 to 50-ton crane capacity; lightweight, low strength walls which fail quickly.	Severe distortion or collapse of frame.	Some distortion to frame; cranes not operable until repairs made.	Windows and doors blown in, light siding ripped off.
8	Heavy steel frame industrial building, single story, with 60 to 100-ton crane capacity; lightweight low strength walls which fail quickly.	Severe distortion or collapse of frame.	Some distortion or frame; cranes not operable until repairs made.	Windows and doors blown in, light siding ripped off.
9	Multistory steel-frame office-type building, 3 to 10 stories. Lightweight low strength walls which fail quickly, earthquake resistant construction.	Severe frame distortion, incipient collapse.	Frame distorted moderately, interior partitions blown down.	Windows and doors blown in, light siding ripped off, interior partitions cracked.
10	Multistory steel-frame office-type building, 3 to 10 stories. Lightweight low strength walls which fail quickly, non-earthquake resistant construction.	Severe frame distortion, incipient collapse.	Frame distorted moderately, interior partitions blown down.	Windows and doors blown in, light siding ripped off, interior partitions cracked.

Table 5.139b (continued)

Structural Type	Description of Structure	Description of Damage		
		Severe	Moderate	Light
11	Multistory reinforced concrete frame office-type building, 3 to 10 stories; lightweight low strength walls which fail quickly, earthquake resistant construction.	Severe frame distortion, incipient collapse.	Frame distorted moderately, interior partitions blown down, some spalling of concrete.	Windows and doors blown in, light siding ripped off, interior partitions cracked.
12	Multistory reinforced concrete frame office type building, 3 to 10 stories; lightweight low strength walls which fail quickly, non-earthquake resistant construction.	Severe frame distortion, incipient collapse.	Frame distorted moderately, interior partitions blown down, some spalling of concrete.	Windows and doors blown in, light siding ripped off, interior partitions cracked.
13	Highway truss bridges, 4-lane, spans 200 to 400 ft; railroad truss bridges, double track ballast floor, spans 200 to 400 ft.	Total failure of lateral bracing or anchorage, collapse of bridge.	Substantial distortion of lateral bracing or slippage on supports, significant reduction in capacity of bridge.	Capacity of bridge not significantly reduced, slight distortion of some bridge components.
14	Highway truss bridges, 2-lane, spans 200 to 400 ft; railroad truss bridges, single track ballast or double track open floors, spans 200 to 400 ft; railroad truss bridges, single track open floor, span 400 ft.	(Ditto)	(Ditto)	(Ditto)
15	Railroad truss bridges, single track open floor, span 200 ft.	(Ditto)	(Ditto)	(Ditto)
16	Highway girder bridges, 4-lane through, span 75 ft.	(Ditto)	(Ditto)	(Ditto)

Table 5.139b (concluded)

Structural Type	Description of Structure	Description of Damage		
		Severe	Moderate	Light
17	Highway girder bridges, 2-lane deck, 2-lane through, 4-lane deck, span 75 ft; railroad girder bridges, double-track deck, open or ballast floor, span 75 ft; railroad girder bridges, single or double track through, ballast floors, span 75 ft.	(Ditto)	(Ditto)	(Ditto)
18	Railroad girder bridges, single track deck, open or ballast floors, span 75 ft; railroad girder bridges, single or double track through, open floors, span 75 ft.	(Ditto)	(Ditto)	(Ditto)
19	Highway girder bridges, 2-lane through, 4-lane deck or through, span 200 ft; railroad girder bridges, double track deck or through, ballast floor, span 200 ft.	(Ditto)	(Ditto)	(Ditto)
20	Highway girder bridges, 2-lane deck, span 200 ft; railroad girder bridges, single track deck or through, ballast floors, span 200 ft; railroad girder bridges, double track deck or through, open floors, span 200 ft.	(Ditto)	(Ditto)	(Ditto)
21	Railroad girder bridges, single track deck or through, open floors, span 200 ft.	(Ditto)	(Ditto)	(Ditto)

The various above-ground structures in Fig. 5.140 are identified (Items 1 through 21) and the different types of damage are described in Tables 5.139a and b. The "fan" from each point indicates the range of yields for which the diagram may be used. For a surface burst multiply the damage distances obtained from the diagram by three-fourths. The results are estimated to be accurate within ±20 percent for the average target conditions specified in § 5.141.

Example

Given: Wood-frame building (Type 5). A 1 MT weapon is burst (*a*) at optimum height, (*b*) at the surface.

Find: The distances from ground zero to which severe and moderate damage extend.

Solution: (*a*) From the point 5 (at the right) draw a straight line to 1 MT (1000 KT) on the severe damage scale and another to 1 MT (1000 KT) on the moderate damage scale. The intersections of these lines with the distance scale give the required solutions for the optimum burst height; thus,

Distance for severe damage = 29,000 feet. *Answer.*

Distance for moderate damage = 33,000 feet. *Answer.*

(*b*) For a surface burst the respective distances are three-fourths those obtained above; hence,

Distance for severe damage = 22,000 feet. *Answer.*

Distance for moderate damage = 25,000 feet. *Answer.*

(The values have been rounded off to two significant figures, since greater precision is not warranted.)

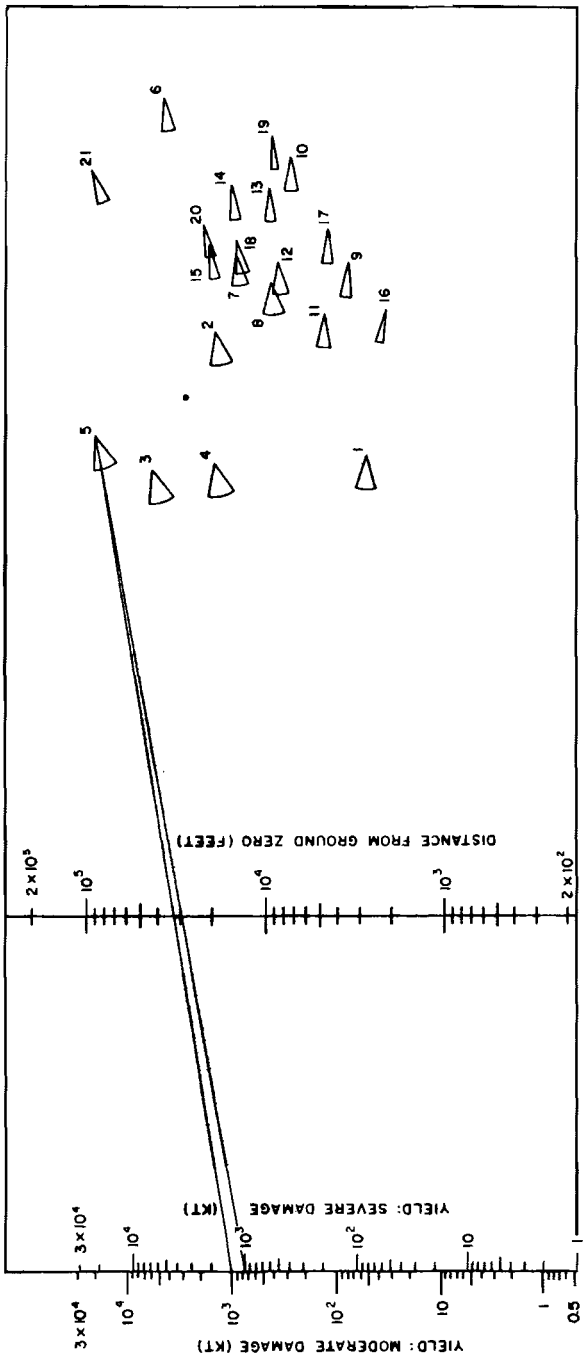

Figure 5.140. Damage-distance relationships for above ground structures.

5.141 The data in Fig. 5.140 are for certain average target conditions. These are that (1) the target is at sea level (no correction is necessary if the target altitude is less than 5,000 feet); (2) the terrain is fairly flat (rugged terrain would provide some local shielding and protection in certain areas and local enhancement of damage in others); and (3) the structures have average characteristics (that is, they are of average size and strength and that orientation of the target with respect to the burst is no problem, i.e., that the ratio of loading to resistance is relatively the same in all directions from the target).

5.142 The "fan" from each point in the figure designating a target type delineates the range of yields over which theoretical analyses have been made. For yields falling within this range, the diagram is estimated to be accurate within ± 20 percent for the average conditions discussed above. The significance of results obtained by applying the diagram to conditions that depart appreciably from the average or to yields outside the limits of the fans must be left to the judgment of the analyst.

5.143 Figure 5.140 gives the distances from ground zero for severe and moderate damage. Light damage to all targets except blast-resistant structures and bridges can be expected at the range at which the overpressure is 1 pound per square inch. For the blast-resistant structure (Type 1) described in Table 5.139a, a peak overpressure of 10 pounds per square inch should be used to estimate the distance for light damage. Light damage to bridges can be expected at the range at which 0.6 pound per square inch dynamic pressure occurs.

5.144 The foregoing results do not take into consideration the possibility of fire. Generally speaking, the direct effects of thermal radiation on the structures and other targets under consideration are inconsequential. However, thermal radiation may initiate fires, and in structures with severe or moderate damage fires may start because of disrupted gas and electric utilities. In some cases, as in Hiroshima (§ 7.71), the individual fires may develop into a mass fire which may exist throughout a city, even beyond the range of significant blast damage. The spread of such a fire depends to a great extent on local weather and other conditions and is therefore difficult to predict. This limitation must be kept in mind when Fig. 5.140 is used to estimate the damage to a particular city or target area.

STRUCTURAL ELEMENTS

5.145 For certain structural elements, with short periods of vibration (up to about 0.05 second) and small plastic deformation at failure, the conditions for failure can be expressed as a peak overpressure without considering the duration of the blast wave. The failure conditions for elements of this type are given in Table 5.145. Some of these elements fail in a brittle fashion, and thus there is only a small difference between the pressures that cause no damage and those that produce complete failure. Other elements may fail in a moderately ductile manner, but still with little difference between the pressures for light damage and complete failure. The pressures are side-on blast overpressures for panels that face

Table 5.145

CONDITIONS OF FAILURE OF OVERPRESSURE-SENSITIVE ELEMENTS

Structural element	Failure	Approximate side-on peak overpressure (psi)
Glass windows, large and small.	Shattering usually, occasional frame failure.	0.5– 1.0
Corrugated asbestos siding.	Shattering.	1.0– 2.0
Corrugated steel or aluminum paneling.	Connection failure followed by buckling.	1.0– 2.0
Brick wall panel, 8 in. or 12 in. thick (not reinforced).	Shearing and flexure failures.	3.0–10.0
Wood siding panels, standard house construction.	Usually failure occurs at the main connections allowing a whole panel to be blown in.	1.0– 2.0
Concrete or cinder-block wall panels, 8 in. or 12 in. thick (not reinforced).	Shattering of the wall.	1.5– 5.5

ground zero. For panels that are oriented so that there are no reflected pressures thereon, the side-on pressures must be doubled. The fraction of the area of a panel wall that contains windows will influence the overpressure required to damage the panel. Such damage is a function of the net load, which may be reduced considerably if the windows fail early. This allows the pressure to become equalized on the two sides of the wall before panel failure occurs.

DRAG-SENSITIVE TARGETS

5.146 A diagram of damage–distance relationships for various targets which are largely affected by drag forces is given in Fig. 5.146. The conditions under which it is applicable and the limits of accuracy are similar to those in § 5.141 and § 5.142, respectively; the possibility of fire mentioned in § 5.144 must also be kept in mind. The targets (Items 1 to 13) in the figure are enumerated on the page facing Fig. 5.146 and the different types of damage are described in the following paragraphs.

Transportation Equipment

5.147 The damage criteria for various types of land transportation equipment, including civilian motor-driven vehicles and earth-moving equipment, and railroad rolling stock are given in Table 5.147a. The various types of damage to merchant shipping from air blast are described in Table 5.147b.

(Text continued on page 225.)

The drag-sensitive targets in Fig. 5.146 are identified as follows:

1. Truck mounted engineering equipment (unprotected).
2. Earth moving engineering equipment (unprotected).
3. Transportation vehicles.
4. Unloaded railroad cars.
5. Loaded boxcars, flatcars, full tank cars, and gondola cars (side-on orientation).
6. Locomotives (side-on orientation).
7. Telephone lines (radial).
8. Telephone lines (transverse).
9. Unimproved coniferous forest stand.
10. Average deciduous forest stand.
11. Loaded boxcars, flatcars, full tank cars, and gondola cars (end-on orientation).
12. Locomotives (end-on orientation).
13. Merchant shipping.

Subscript "m" refers to moderate damage and subscript "s" refers to severe damage.

For a surface burst multiply the distance by three-fourths for Items 1 through 8 and by one-half for Items 9 and 10. For Items 11 through 13, the distances are the same for a surface burst as for the optimum burst height. Estimated accuracy ± 20 percent for average targets.

Example

Given: A transportation type vehicle (Item 3). A 10 KT weapon is burst at (*a*) the optimum height, (*b*) at the surface.

Find: The distances from ground zero to which severe and moderate damage extend.

Solution: (*a*) Draw straight lines from the points 3_s and 3_m, at the right, to 10 KT on the yield scale at the left. The intersections of these lines with the distance scale give the solutions for severe and moderate damage, respectively, for the optimum burst height; thus,

Distance for severe damage = 1,400 feet. *Answer.*

Distance for moderate damage = 1,600 feet. *Answer.*

(*b*) For a surface burst the distances in this case are three-fourths those obtained above; thus,

Distance for severe damage = 1,000 feet. *Answer.*

Distance for moderate damage = 1,200 feet. *Answer.*

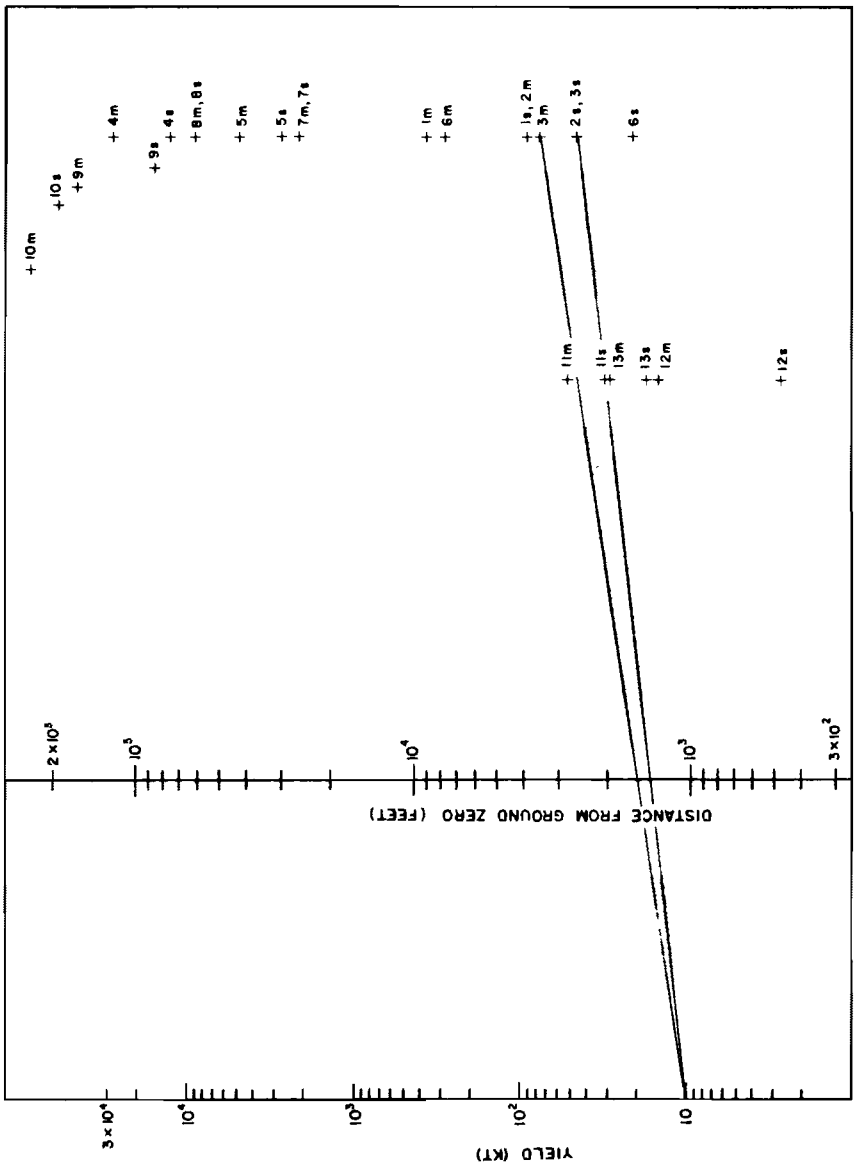

Figure 5.146. Damage–distance relationships for drag-sensitive targets.

Table 5.147a

DAMAGE CRITERIA FOR LAND TRANSPORTATION EQUIPMENT

Description of equipment	Damage	Nature of damage
Motor equipment (cars and trucks).	Severe	Gross distortion of frame, large displacements, outside appurtenances (doors and hoods) torn off, need rebuilding before use.
	Moderate	Turned over and displaced, badly dented, frames sprung, need major repairs.
	Light	Glass broken, dents in body, possibly turned over, immediately usable.
Railroad rolling stock (box, flat, tank, and gondola cars).	Severe	Car blown from track and badly smashed, extensive distortion, some parts usable.
	Moderate	Doors demolished, body damaged, frame distorted, could possibly roll to repair shop.
	Light	Some door and body damage, car can continue in use.
Railroad locomotives (Diesel or steam).	Severe	Overturned, parts blown off, sprung and twisted, major overhaul required.
	Moderate	Probably overturned, can be towed to repair shop after being righted, need major repairs.
	Light	Glass breakage and minor damage to parts, immediately usable.
Construction equipment (bulldozers and graders).	Severe	Extensive distortion of frame and crushing of sheet metal, extensive damage to caterpillar tracks and wheels.
	Moderate	Some frame distortion, overturning, track and wheel damage.
	Light	Slight damage to cabs and housing, glass breakage.

Table 5.147b

DAMAGE CRITERIA FOR SHIPPING FROM AIR BLAST

Damage type	Nature of damage
Severe	The ship is either sunk, capsized, or damaged to the extent of requiring rebuilding.
Moderate	The ship is immobilized and requires extensive repairs, especially to shock-sensitive components or their foundations, e.g., propulsive machinery, boilers, and interior equipment.
Light	The ship may still be able to operate, although there will be damage to electronic, electrical, and mechanical equipment.

Communication and Power Lines

5.148 Damage to telephone, telegraph, and utility power lines is generally either severe or light. Such damage depends on whether the poles supporting the lines are damaged or not. If the poles are blown down, damage to the lines will be severe and extensive repairs will be required. On the other hand, if the poles remain standing, the lines will suffer only light damage and will need little repair. In general, lines extending radially from ground zero are less susceptible to damage than are those running at right angles to this direction.

Forests

5.149 The detailed characteristics of the damage to forest stands resulting from a nuclear explosion will depend on a variety of conditions, e.g., deciduous or coniferous trees, degree of foliation of the trees, natural or planted stands, and favorable or unfavorable growing conditions. A general classification of forest damage, applicable in most cases, is given in Table 5.149. Trees are primarily sensitive to the drag forces from a blast wave and so it is of interest that the damage in an explosion is similar to that resulting from a strong, steady wind; the velocities of such winds that would produce comparable damage are included in the table.

5.150 The damage–distance results derived from Fig. 5.146 apply in particular to unimproved coniferous forests which have developed under unfavorable growing conditions and to most deciduous forests in the temperate zone when foliation is present. Improved coniferous forests, with trees of uniform height and a smaller average tree density per acre, are more resistant to blast than are unimproved forests which have grown under unfavorable conditions. A forest of defoliated deciduous trees is also somewhat more blast resistant than is implied by the data in Fig. 5.146.

Table 5.149

DAMAGE CRITERIA FOR FORESTS

Damage type	Nature of damage	Equivalent steady wind velocity (miles per hour)
Severe	Up to 90 percent of trees blown down; remainder denuded of branches and leaves. (Area impassable to vehicles and very difficult on foot.)	130–140
Moderate	About 30 percent of trees blown down; remainder have some branches and leaves blown off. (Area passable to vehicles only after extensive clearing.)	90–100
Light	Only applies to deciduous forest stands. Very few trees blown down; some leaves and branches blown off. (Area passable to vehicles.)	60–80

PARKED AIRCRAFT

5.151 Aircraft are relatively vulnerable to air blast effects associated with nuclear detonations. The forces developed by peak overpressures of 1 to 2 pounds per square inch are sufficient to dish in panels and buckle stiffeners and stringers. At higher overpressures, the drag forces due to wind (dynamic) pressure tend to rotate, translate, overturn, or lift a parked aircraft, so that damage may then result from collision with other aircraft, structures, or the ground. Aircraft are also very susceptible to damage from flying debris carried by the blast wave.

5.152 Several factors influence the degree of damage that may be expected for an aircraft of a given type at a specified range from a nuclear detonation. Aircraft that are parked with the nose pointed toward the burst will suffer less damage than those with the tail or either side directed toward the oncoming blast wave (§ 5.94). Shielding of one aircraft by another or by structures or terrain features may reduce damage, especially that caused by flying debris. Standard tiedown of aircraft, as used when high winds are expected, will also minimize the extent of damage at ranges where destruction might otherwise occur.

5.153 The various damage categories for parked transport airplanes, light liaison airplanes, and helicopters are outlined in Table 5.153 together with the approximate peak overpressures at which the damage may be expected to occur. The aircraft are considered to be parked in the open at random orientation with respect to the point of burst. The

Table 5.153

DAMAGE CRITERIA FOR PARKED AIRCRAFT

Damage type	Nature of damage		Overpressure (psi)
Severe	Major (or depot level) maintenance required to restore aircraft to operational status.	Transport airplanes	3
		Light liaison craft	2
		Helicopters	3
Moderate	Field maintenance required to restore aircraft to operational status.	Transport airplanes	2
		Light liaison craft	1
		Helicopters	1.5
Light	Flight of the aircraft not prevented, although performance may be restricted.	Transport airplanes	1.0
		Light liaison craft	0.75
		Helicopters	1.0

data in the table are based on tests in which aircraft were exposed to detonations with yields in the kiloton range. For megaton yields, the longer duration of the positive phase of the blast wave may result in some increase in damage over that estimated from small-yield explosions at the same overpressure level. This increase is likely to be significant at pressures producing severe damage, but will probably be less important for moderate and light damage conditions.

5.154 Aircraft with exposed ignitable materials may, under certain conditions, be damaged by thermal radiation at distances beyond those at which equivalent damage would result from blast effects. The vulnerability to thermal radiation may be decreased by protecting ignitable materials from exposure to direct radiation or by painting them with protective (light colored) coatings which reflect, rather than absorb, most of the thermal radiation (see Chapter VII).

POL STORAGE TANKS

5.155 The chief cause of failure of POL (petroleum, oil, lubricant) storage tanks exposed to the blast wave appears to be the lifting of the tank from its foundation. This results in plastic deformation and yielding of the joint between the side and bottom so that leakage can occur. Severe damage is regarded as that damage which is associated with loss of the contents of the tank by leakage. Furthermore, the leakage can lead to secondary effects, such as the development of fires. If failure by lifting does not occur, it is expected that there will be little, if any, loss of liquid from the tank as a consequence of sloshing. There is apparently no clear-cut overall structural collapse which initially limits the usefulness of the tank. Peak overpressures required for severe damage to POL tanks of diameter D may be obtained from Figs. 5.155a and b. Figure 5.155a is applicable to nuclear explosions with energy yields from 1 to 500 kilotons and Fig. 5.155b to yields over 500 kilotons. For yields less than 1 kiloton, the peak overpressure for severe damage may be taken to be 1 pound per square inch.

LIGHTWEIGHT, EARTH COVERED AND BURIED STRUCTURES

5.156 Air blast is the controlling factor for damage to lightweight earth covered structures and shallow buried underground structures. The earth cover provides surface structures with substantial protection against air blast and also some protection against flying debris. The depth of earth cover above the structure would usually be determined by the degree of protection from nuclear radiation required at the design overpressure or dynamic pressure (see Chapter VIII).

5.157 The usual method of providing earth cover for surface or "cut-and-cover" semiburied structures is to build an earth mound over the portion of the structure that is above the normal ground level. If the slope of the earth cover is chosen properly, the blast reflection factor is reduced and the aerodynamic shape of the structure is improved. This results in a considerable reduction in the applied translational forces. An additional benefit of the earth cover is the stiffening or resistance to

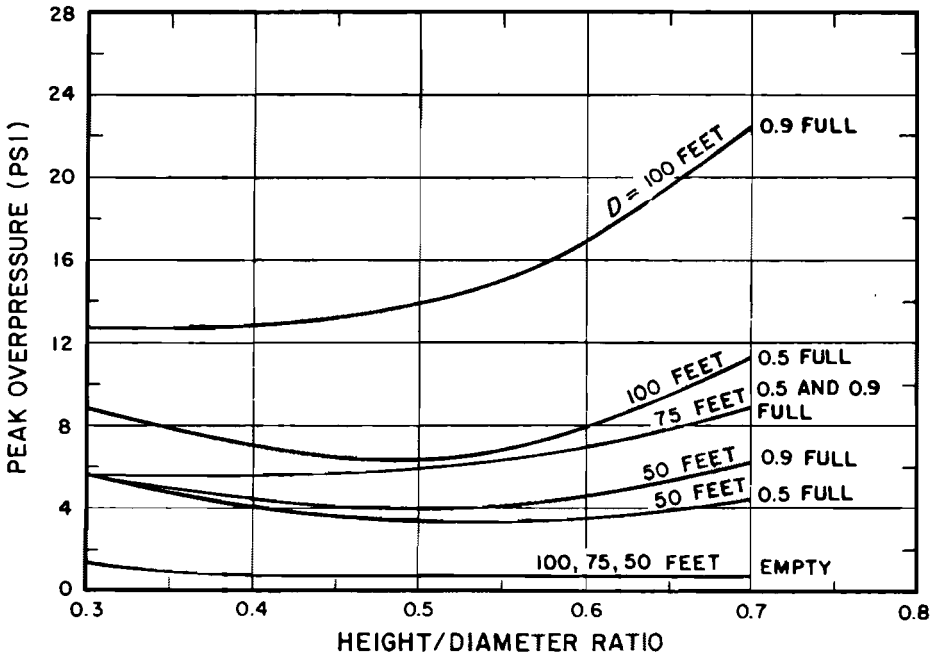

Figure 5.155a. Peak overpressures for severe blast damage to floating- or conical-roof tanks of diameter D for explosions from 1 to 500 kilotons.

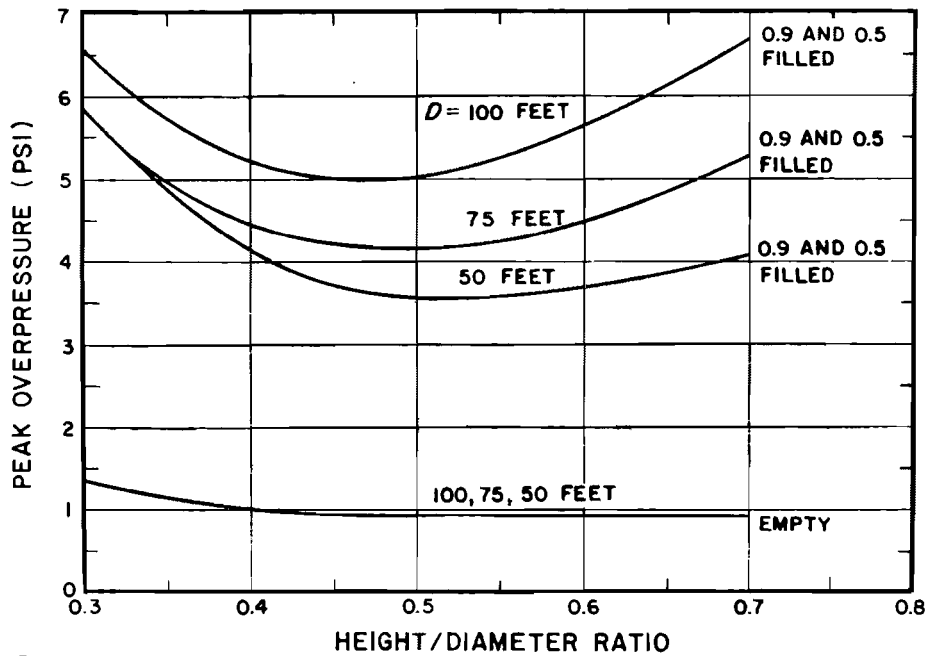

Figure 5.155b. Peak overpressures for severe blast damage to floating- or conical-roof tanks of diameter D from explosions of 500 kilotons or more.

deformation that the earth provides to flexible structures by the buttressing action of the soil.

5.158 For lightweight, shallow buried underground structures the top of the earth cover is at least flush with the original grade but the depth of cover is not more than 6 percent of the span. Such structures are not sufficiently deep for the ratio of the depth of burial to the span to be large enough to obtain the benefits described in § 5.161. The soil provides little attenuation of the air blast pressure applied to the top surface of a shallow buried underground structure. Observations made at full-scale nuclear tests indicate that there is apparently no increase in pressure on the structure as a result of ground shock reflection at the interface between the earth and the top of the structure.

5.159 The lateral blast pressures exerted on the vertical faces of a shallow buried structure have been found to be as low as 15 percent of the blast pressure on the roof in dry, well-compacted, silty soils. For most soils, however, this lateral blast pressure is likely to be somewhat higher and may approach 100 percent of the roof blast pressure in porous saturated soil. The pressures on the bottom of a buried structure, in which the bottom slab is a structural unit integral with the walls, may range from 75 to 100 percent of the pressure exerted on the roof.

5.160 The damage that might be suffered by a shallow buried structure

Table 5.160

DAMAGE CRITERIA FOR SHALLOW BURIED STRUCTURES

Type of structure	Damage type	Peak overpressure (psi)	Nature of damage
Light, corrugated steel arch, surface structure (10-gage corrugated steel with a span of 20–25 ft), central angle of 180°; 5 ft of earth cover at the crown.*	Severe	45– 60	Collapse
	Moderate	50– 50	Large deformations of end walls and arch, also major entrance door damage.
	Light	30– 40	Damage to ventilation and entrance door.
Buried concrete arch 8-in. thick with a 16 ft span and central angle of 180°; 4 ft of earth cover at the crown.	Severe	220–280	Collapse.
	Moderate	100–220	Large deformations with considerable cracking and spalling.
	Light	120–160	Cracking of panels, possible entrance door damage.

*For arched structures reinforced with ribs, the collapse pressure is higher depending on the number of ribs.

will depend on a number of variables, including the structural characteristics, the nature of the soil, the depth of burial, and the downward pressure, i.e., the peak overpressure and direction of the blast wave. In Table 5.160 are given the limiting values of the peak overpressure required to cause various degrees of damage to two types of shallow buried structures. The range of pressures is intended to allow for differences in structural design, soil conditions, shape of earth mound, and orientation with respect to the blast wave.

5.161 Underground structures, buried at such a depth that the ratio of the burial depth to the span approaches (or exceeds) a value of 3.0, will obtain some benefit from the attenuation with depth of the pressure induced by air blast, and from the arching of the load from more deformable areas to less deformable ones. Limited experience at nuclear tests suggests that the arching action of the soil effectively reduces the loading on flexible structures.

BIBLIOGRAPHY

JACOBSEN, L. S. and R. S. AYRE, "Engineering Vibrations," McGraw-Hill Book Co., Inc., 1958.

*JOHNSTON, B. G., "Damage to Commercial and Industrial Buildings Exposed to Nuclear Effects," Federal Civil Defense Administration, February 1956, WT-1189.

*MITCHELL, J. H., "Nuclear Explosion Effects on Structures and Protective Construction—A Selected Bibliography," U.S. Atomic Energy Commission, April 1961, TID-3092.

NEWMARK, N. M., "An Engineering Approach to Blast Resistant Design," *Trans. Amer. Soc. of Civil Engineers*, **121**, 45 (1956).

NORRIS, C. H., *et al.*, "Structural Design for Dynamic Loads," McGraw-Hill Book Co., Inc., 1959.

PICKERING, E. E., and J. L. BOCKHOLT, "Probabilistic Air Blast Failure Criteria for Urban Structures," Stanford Research Institute, Menlo Park, California, November 1971.

*RANDALL, P. A., "Damage to Conventional and Special Types of Residences Exposed to Nuclear Effects," OCDM, FHA, and HHFA, March 1961, WT-1194.

RODGERS, G. L., "Dynamics of Framed Structures," John Wiley and Sons, Inc., 1959.

*SHAW, E. R. and F. P. MCNEA, "Exposure of Mobile Homes and Emergency Vehicles to Nuclear Explosions," Federal Civil Defense Administration, July 1957, WT-1181.

*SPARKS, L. N., "Nuclear Effects on Machine Tools," U.S. Atomic Energy Commission, December 1956, WT-1184.

*TAYLOR, B. C., "Blast Effects of Atomic Weapons Upon Curtain Walls and Partitions of Masonry and Other Materials," Federal Civil Defense Administration, August 1956, WT-741.

*TUCKER, P. W. and G. R. WEBSTER, "Effects of a Nuclear Explosion on Typical Liquefied Petroleum Gas (LP-Gas) Installations and Facilities," Liquefied Petroleum Gas Association, December 1956, WT-1175.

TUNG, T. P. and N. M. NEWMARK, "A Review of Numerical Integration Methods for Dynamic Response of Structures," University of Illinois Structural Research Series No. 69, 1954.

*WILLIAMSON, R. H., "Effects of a Nuclear Explosion on Commercial Communications Equipment," Federal Civil Defense Administration, May 1955, ITR-1193.

WILLOUGHBY, A. B., *et al.*, "A Study of Loading, Structural Response, and Debris Characteristics of Wall Panels," URS Research Co., Burlingame, California, July 1969.

WILTON, C., *et al.*, "Final Report Summary, Structural Response and Loading of Wall Panels," URS Research Co., Burlingame, California, July 1971.

*These publications may be purchased from the National Technical Information Service, U.S. Department of Commerce, Springfield, Virginia, 22161.

AD-A955 396

DTIC ELECTE S 2 MAR 1989 D

Chapter 12

MECHANICAL DAMAGE DISTANCES FOR SURFACE SHIPS AND SUBMARINES SUBJECTED TO NUCLEAR EXPLOSIONS

INTRODUCTION

12-1 Damage Mechanisms

An air burst nuclear weapon may cause mechanical damage to surface ships by air burst, thermal radiation, ionizing radiation, and the electromagnetic pulse. Ship operations may also be affected by personnel casualties; however, only mechanical damage is considered in this chapter.

An underwater burst may cause damage to surface ships by the shock wave in the water, by the water column or plumes thrown up by the burst, by the surface gravity waves produced, or by the ionizing radiation from the base surge, fallout, or contaminated water pool. As for an air burst, the ship status may be affected by personnel casualties; however, only mechanical damage is considered in this chapter.

An underwater burst may cause damage to submerged submarines by the shock wave in the water, and, in special shallow water cases, by collision with the ocean bottom induced by the waves.

12-2 Damage Classification

Damage to surface ships and submarines is described by the degree of impairment of three major ship capabilities: seaworthiness, mobility, and weapon delivery. Complete loss of a capability is characterized as 100-percent impairment; no impairment is considered 0 percent. Levels of impairment of 90 percent and 10 percent are intended to signify nearly complete and slight impairment, respectively. These degrees of impairment should be interpreted as being the midpoints of a band of percent impairments.

The concept of degree of capability impairment is closely related to the fact that, for any given burst condition, a continuous spectrum of degrees of damage would be inflicted on ships of the same type located over a continuous spread of ranges from the burst. A ship is so complex a system that it is not possible to predict damage precisely for any given attack situation. Another consideration is that the crew of a damaged ship will attempt to repair damage; i.e., to decrease the degree of impairment of capability as quickly as possible. The time consumed by such repair is a vital aspect of the total damage assessment, but available knowledge does not justify an attempt to consider it in detail.

Damage ranges are given in this chapter in terms of zones within which varying degrees of impairment of each capability are to be expected. The outer boundary of a given zone corresponds to slight, and possibly temporary, impairment of the indicated capability; the inner boundary corresponds to nearly complete impairment that would require shipyard facilities for repair. The locations of the boundaries are determined by damage criteria derived from experimental data. There are, however, uncertainties involved as a result of a lack of sufficient experimental data. It is estimated that uncertainties concerning damage criteria cause uncertainties in the boundary locations on the order of 15 to 30 percent.

12-3 Seaworthiness Impairment

The degrees of seaworthiness impairment are defined as follows:

- 100 percent: The ship or submarine is sunk.
- 90 percent: The ship is in danger of sinking,

This document has been approved for public release and sale; its distribution is unlimited.

89 3 02 038

capsizing, or breaking up as a result of widespread, uncontrollable flooding or the loss of girder strength. Danger is present even in normal weather, but there is some chance of saving the ship. As a result of damage to its structure or to its buoyancy-control gear, a submarine will be in danger of settling to the bottom.

- 10 percent: Slight plastic deformation of the structure that may cause minor leakage. Hogging or sagging, or topside structural damage can occur, but not to an extent sufficient to endanger the ship in stormy weather. For submarines, this degree of impairment includes that damage that can at worst reduce the maximum safe diving depth slightly, but otherwise allows the submarine to submerge in a controlled manner.
- 0 percent: No plastic deformation of structure and no leakage.

12-4 Mobility Impairment

The degrees of mobility impairment are defined as follows:

- 100 percent: The ship or submarine lacks any ability to operate its propulsion devices.
- 90 percent: The ship can at best just barely maintain steerageway in a desired direction, either as a result of damage to main propulsion machinery and control gear, or as a result of personnel casualties.
- 10 percent: Slight loss of ability to achieve top speed and/or to maneuver normally, as a result of damage or personnel casualties.
- 0 percent: No impairment of mobility.

12-5 Weapon Delivery Impairment

The degrees of weapon delivery impairment are defined as follows:

- 100 percent: The ship or submarine cannot release its weapons.
- 90 percent: Weapons can be released, but it is almost impossible to deliver them effectively because the ship's target-acquisition and communication equipment are inoperative, either as a result of damage to equipment or to topside structure, or as a result of personnel casualties.
- 10 percent: Slight reduction in weapon-delivery efficiency as a result of damage to equipment or topside-structure or as a result of personnel casualties.
- 0 percent: No loss.

SECTION I
DAMAGE TO SURFACE SHIPS FROM AIR BURSTS

BLAST DAMAGE

12-6 General

Air blast damage may be significant for surface ships when the burst is at or above the water surface. The following general description of air blast effects on ships is applicable to existing Navy ships.

At close ranges, air blast can cause hull rupture that can result in flooding and sinking. Hull rupture appears likely to begin near the waterline on the side facing the blast. The main hull of existing Navy ships is, however, stronger than the superstructure and equipment. At ranges beyond those at which hull rupture is likely to occur the main effect of air blast is to distort, rupture, or carry away light structures and equipment vulnerably exposed above the waterline, and to cause casualties among topside personnel. Such damage can cause complete impairment of the weapon delivery capability. Blast pressures penetrating through weather openings of ventilation systems and stack-uptake systems can cause damage to interior equipment and compartments, and also to boilers; the latter may result in immobilization. The distortion of weather bulkheads may cause fracture or render interior equip-

ment mounted on or near them useless. Similarly, the suddenly applied blast loading induces rapid motion of the structures that in turn may cause shock damage to interior equipment. Equipment in the superstructure is most vulnerable to these types of damage, although shock motions may be felt throughout the ship. Air blast also may cause the ship to roll and possibly capsize; this effect is most pronounced for broadside attack by large weapons (multimegaton).

12-7 Damage Criteria

Peak overpressure is used as the sole parameter to describe attack severity, except for the capsizing effect. This criterion is acceptable for most existing surface ship structures, since the effects of the blast wave are practically independent (within predictive accuracies) of the blast wave duration, i.e., weapon yield, for weapons larger than a certain size. Mechanical damage criteria in terms of peak overpressure for some existing Navy ships are given in Table 12-1. The estimates shown in Table 12-1 are derived from CROSSROADS ABLE and SAILOR HAT data, as well as from some structural analyses.

12-8 Damage Distances

Distances at which damage is expected to occur from a 1-Mt air burst are shown in Figure 12-1. The curves define zones in which impairment of a stated capability occurs. The outer boundary of the zone indicates slight (10 percent) impairment; the inner boundary indicates almost complete (90 percent) impairment. At distances beyond the outer boundary of a zone there is essentially no impairment of the stated capability. At ranges within the inner boundary of a zone the impairment is essentially complete.

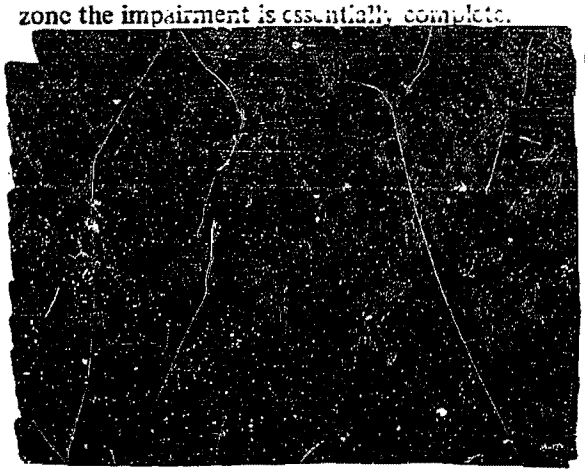

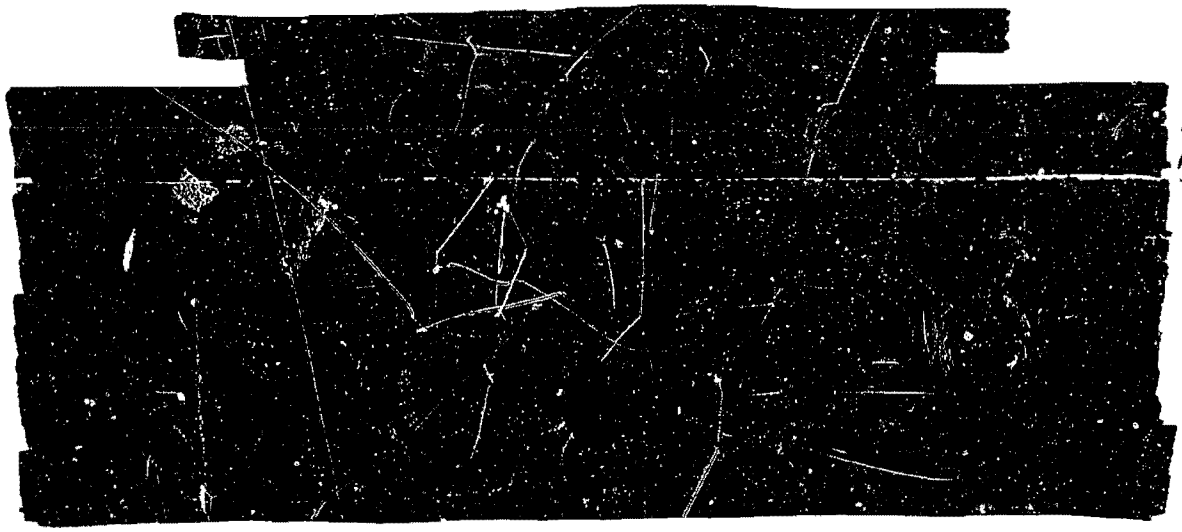

Problem 12-1 Calculation of Air Blast Damage Distances to Surface Ships as a Result of Air Bursts

[redacted] Figure 12-1 shows families of curves that define zones within which a stated degree of impairment is expected to occur to representative Naval ships from a 1 Mt air burst.

[redacted] *Scaling.* Air blast damage distances for yields other than 1 Mt as follows:

$$\frac{d_1}{d_2} = \frac{h_1}{h_2} = \frac{W_1^{1/3}}{W_2^{1/3}}$$

where d_1 (yd) is the distance from surface zero (SZ) for a given degree of damage for yield W_1 (kt) at a height h_1 (ft), and d_2 (yd) is the range for a given degree of damage for a yield W_2 (kt) at height h_2 (ft). This scaling law is applicable within predictive accuracies, provided the weapon yield is larger than about 1 kt.

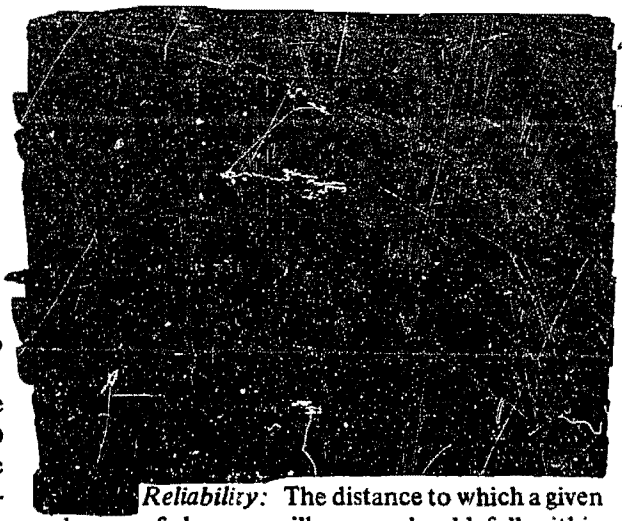

NAVY (6-X-1)

[redacted] *Reliability:* The distance to which a given degree of damage will occur should fall within the bands indicated in Figure 12-1 for the classes of ships listed in Table 12-1. The damage-distance bands provide a rough estimate for ships of similar types.

[redacted] *Related Material:* See paragraphs 12-6 through 12-8 and Section I, Chapter 2.

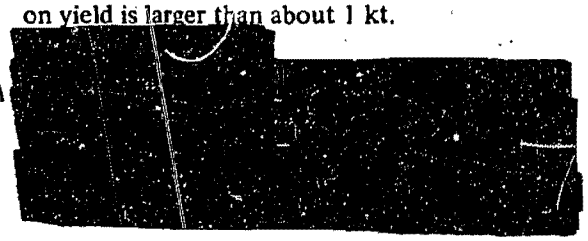

NAVY (6-X-1)

Accession For
NTIS GRA&I
DTIC TAB
Unannounced
Justification
By
Distribution/
Availability Codes
Dist | Avail and/or Special
A-1

QUALITY INSPECTED 4

UNANNOUNCED

PAGE 12-5 DELETED

12-9 Capsizing from Blast

Figure 12-2 shows estimates of ranges for capsizing various types of ships as a result of air blast from surface bursts. The distances are shown as functions of weapon yield, since cube-root scaling does not apply. The estimates are based on theoretical calculations alone, since experimental data are not available on capsizing. The width of the bands in Figure 12-2 corresponds to the difference between two sets of theoretical calculations. The ranges are valid for broadside attack only. Air blast will not capsize a ship in a fore-and-aft attack direction. For an attack direction of 45 degrees off the bow or stern, it is roughly estimated that capsizing ranges are 5 to 10 percent smaller. The capsizing distances from an air burst may be greater than those shown for a surface burst in Figure 12-2. For a given yield the increase in range can be determined approximately by assuming that the capsizing overpressure is independent of burst height (within the Mach region), and then by referring to curves of range versus height of burst for constant overpressures (see Section I, Chapter 2).

DAMAGE FROM OTHER AIR BURST PHENOMENA

12-10 Thermal Radiation

Material exposed to thermal radiation may be charred, scorched, ignited, melted, or otherwise changed. In addition, the heat may affect the mechanical properties of structural metals by annealing (reduction of strength). The rapid rate of delivery of thermal energy may induce large temperature gradients, and the resulting thermal stresses may produce effects such as surface spalling or cracking, and/or permanent distortions of structures or structural elements. Weakening of structural elements may cause weapon system and superstructure components to be more vulnerable to the air blast, which arrives after most of the thermal exposure has been received. Distortion of radar antennas and other superstructure components may cause functional impairment.

Thermal radiation can affect only the exposed topside personnel and material of a surface ship. Any opaque object along the fireball-to-target line of sight will furnish protection from thermal radiation. Topside personnel or material in the shadow or the ship's structural or topside gear would be shielded from thermal radiation.

Fires are not likely to originate except perhaps when severe, and probably overriding, blast damage is also sustained. Normally there is insufficient combustible material topside on combatant ships to sustain fire. Possible exceptions may be vessels carrying inflammable liquids, which may spill as a result of the blast (aircraft carriers), and vessels carrying combustible deck loads (cargo ships). Water washdown systems, installed primarily for protection against deposited radioactive debris, should reduce fire hazards and thermal radiation damage, provided they are turned on prior to the burst.

The main steel hulls of naval ships are not likely to be weakened by thermal radiation, except when severe, and probably overriding, blast damage is also sustained. Of the metallic components in use on present ships, those made of aluminum may be most susceptible to thermal radiation effects (annealing, melting). The effect will be greatest on thin aluminum components. Aluminum plates of alloy 5456-H321 less than 5/16 inch in thicknesses may suffer more than 50-percent loss of strength prior to the arrival of the blast at the 10-psi range from a 1-Mt burst. Lightweight aluminum-alloy components, which have been used extensively in radar antennas as support members, reflector elements, and wave guides, appear to be susceptible to melting, sagging, and buckling when exposed to free-field thermal radiation at the 10 psi overpressure

PAGE 12-7 DELETED

range. Thicker aluminum-alloy materials, which have been used for main superstructures, could be weakened significantly prior to blast arrival.

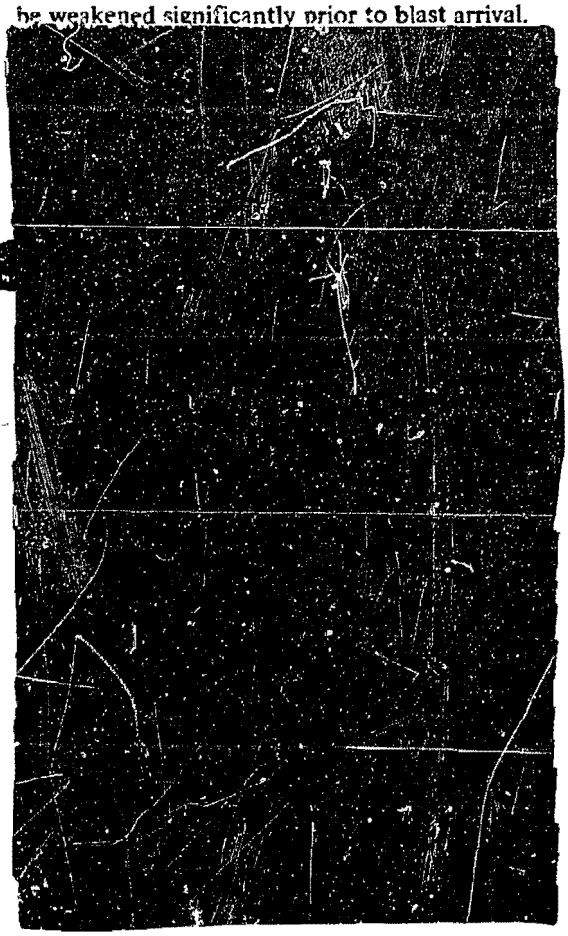

NAVY (4)(1)

12-11 Damage from Nuclear Radiation and Electromagnetic Pulse

Electronic system components are the only pieces of equipment subject to damage from nuclear radiation or the electromagnetic pulse (EMP). General effects of these phenomena on electronic systems are discussed in Sections VII and VIII of Chapter 9. References to more specific treatments of the effects of these phenomena are provided in the same sections of Chapter 9.

SECTION II
SURFACE SHIP DAMAGE FROM UNDERWATER BURSTS

DAMAGE FROM THE SHOCK WAVE IN THE WATER

The shock wave can affect surface ships by deforming hulls plastically, by inducing damaging shock motions in equipment, and by subjecting personnel to injurious shock motions. The degree of hull deformation determines the degree of impairment of seaworthiness, whereas equipment failures determine the degree of impairment of the mobility and weapon delivery capabilities. The principal shock motions induced in surface ships are in the vertical direction. For current surface ships, personnel injuries caused by shock motions probably are not a significant feature in the overall impairment, and no attempt is made herein to estimate the number of personnel casualties or the effect of these casualties on the impairment of capability.

12-13 Damage Criteria

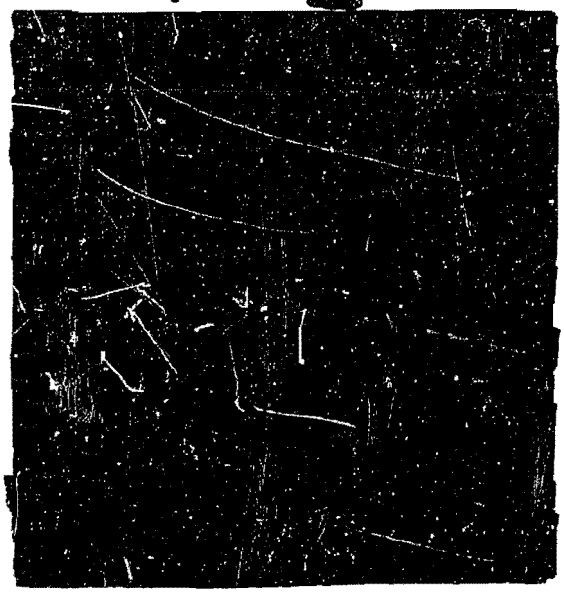

NAVY (4)(1)

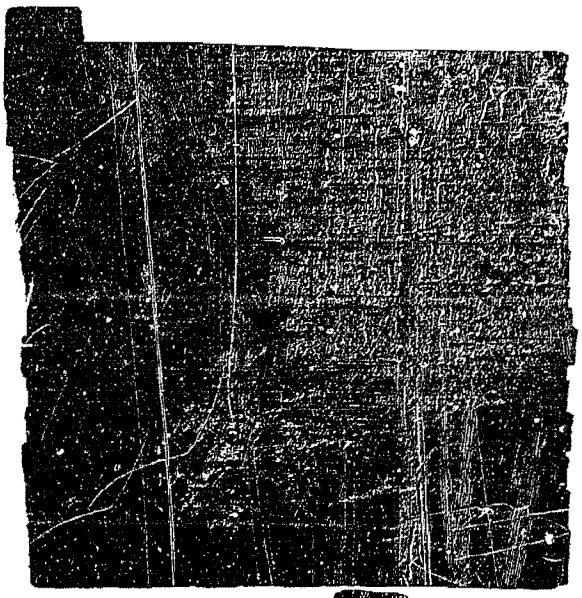

12-14 Damage Distances

The damage distances resulting from the use of the above criteria are shown in Figures 12-3 through 12-5 for 1 kt, 10 kt, and 1 Mt underwater bursts respectively. The distances are given by bands defining zones in which impairment of a stated capability occurs. The outer boundary of the zone indicates slight (10 percent) impairment; the inner boundary of the zone indicates almost complete (90 percent) impairment. At distances beyond the outer boundary of a zone there is essentially no impairment of the stated capability. At distances within the inner boundary of a zone, the impairment is essentially complete.

The damage distances were computed for calm isovelocity water, i.e., no variation of temperature with depth. Allowance was made for anomalous surface reflection (nonlinear reflection occurring when the shock wave propagates nearly parallel to the surface). The possible effect of ship orientation with respect to the direction of shock wave propagation was not considered, nor was the possible effect of different drafts of vessels fully considered.

12-15 Effect of Ocean Environment on Damage Ranges

The shock wave propagating along the direct "line-of-sight" path between the burst point and the surface ship target may not be the governing damage phenomenon in all cases. When the water depth is greater than the burst depth, it is possible, in some cases, for the shock wave reflected from the bottom to produce more severe damage to equipment than the direct shock wave. Although the peak pressure of the reflected shock wave is less than that of the direct shock wave, it propagates in a more nearly vertical direction and, hence, is more effective in producing the vertical shock motions that control the degree of damage to equipment. The reflected wave is most likely to control damage distances for weapon delivery and mobility capabilities when the burst occurs fortuitously at a certain depth. The bottom reflected wave is not likely to control ranges for impairment of seaworthiness.

It is not possible to predict the effects of the reflected shock wave without extensive knowledge of the configuration and structure of the bottom in the vicinity of the detonation. However, certain general statements can be made. If the sea bottom profile is concave, the reflected shock wave will be focused, and ships in certain local areas may sustain a higher degree of damage than would otherwise be expected. Since this will be true only for local areas of the water surface and since the effect depends on the exact bottom configuration, such an event is regarded as a freak occurrence. The sea bottom may be plane, with no appreciable curvature, but nevertheless may slope. If a surface ship is down-slope from surface zero, damage will tend to be less than for a flat bottom at a depth equal to the water depth below the ship. If a surface ship is up-slope from surface zero, damage will tend to be greater than for a flat bottom at a depth equal to the water depth below the ship.

[redacted]

[redacted] Even if the sea bottom is essentially flat, the strength of the reflected shock wave will depend on the composition of the bottom. The shock may be less for mud than for sand, but it may be greater for rock than for sand. Figures 12-3 through 12-5 provide means for estimating distances at which impairment of weapon delivery and mobility may occur as a result of the bottom reflected wave. The estimates are based on the assumption of a flat sea bottom with a reflection coefficient and a relation between reflection coefficient and incident angle similar to that observed at the site of the WAHOO test of Operation HARDTACK. In Figures 12-3 through 12-5, the reflected wave damage distances are shown as functions of the image burst depth. As illustrated in Figure 12-3, the image burst depth is obtained by adding the depth of the bottom to the height of the burst above the bottom, or, equivalently, doubling the depth of the bottom and subtracting the depth of the burst. When determining the distances for impairment of weapon delivery and mobility when the burst and water depths are within the limits given in Table 12-3, the ranges should be found for both the direct shock wave and the bottom reflected shock wave, and the larger value should be used.

[redacted]

NAVY (b)(1)

[redacted]

NAVY (b)(1)

[redacted]

NAVY (E)(1)

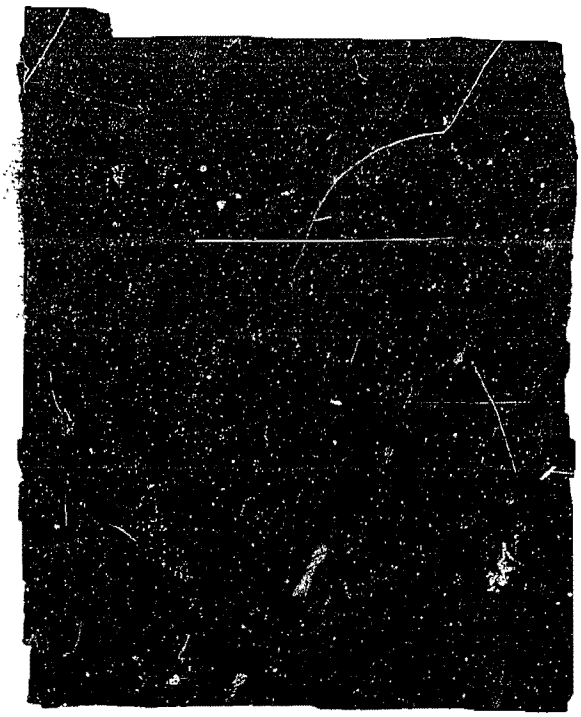

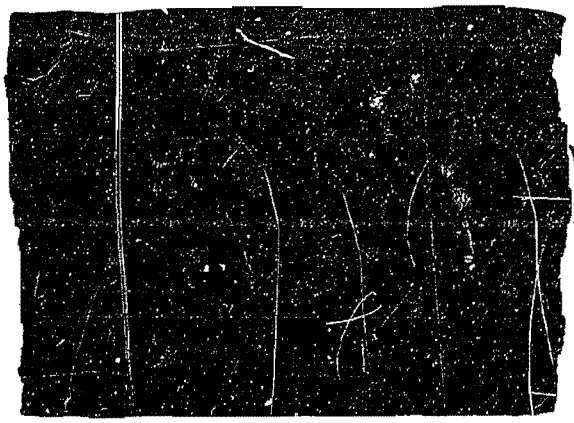

NAVY (E)(1)

[redacted] The ambient sea waves existing just prior to the burst may decrease the damage caused by the shock wave. Although evidence of this effect is too inconclusive to allow quantitative estimates, it appears likely that for otherwise identical conditions, ship damage caused by the shock wave will decrease somewhat as the height of the ambient sea wave increases.

[redacted]

Problem 12-2 Calculation of Shock Wave Damage Distances to Surface Ships as a Result of Underwater Bursts

[redacted] Figures 12-3 through 12-5 show families of curves that define zones within which a stated degree of impairment is expected to occur to representative Naval ships from the indicated weapon yields burst underwater. Each figure has an "a" portion that shows the damage distance relations for the direct shock wave and a "b" portion that shows the relations for the bottom-reflected shock wave.

[redacted] *Scaling.* Water shock damage distances for yields other than those indicated in Figures 12-3 through 12-5 scale as follows (note that the range of yield applicability is shown on each figure):

$$\frac{d_1}{d_2} = \frac{h_1}{h_2} = \frac{W_1^{1/3}}{W_2^{1/3}}$$

where d_1 (yd) is the distance from surface zero (SZ) for a given degree of damage for yield W_1 (kt) at a depth of h_1 (ft), and d_2 (yd) is the distance for the same degree of damage for yield W_2 (kt) at depth h_2 (ft). Image-burst depths and sea bottom depths should be scaled in the same manner as burst depth h.

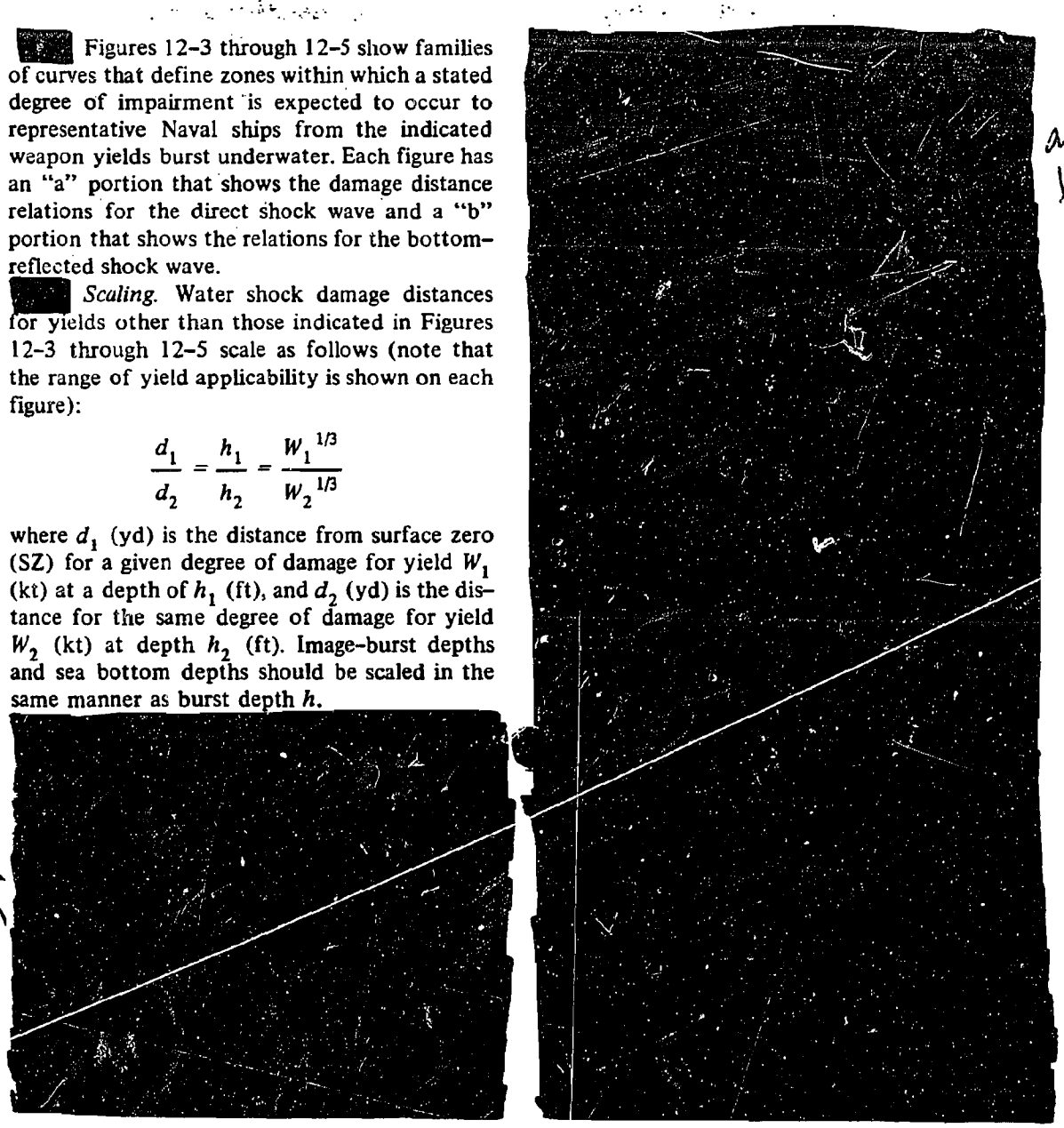

[redacted]

NAVY (b)(1)

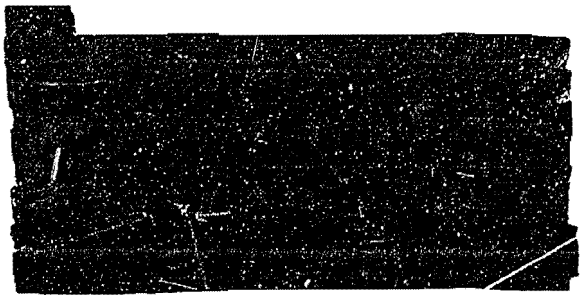

NAVY (b)(1)

Related Material: See paragraphs 12-13 through 12-15, and Section IV, Chapter 2.

PAGES 12-14 THRU 12-16 DELETED

[redacted]

DAMAGE FROM OTHER UNDERWATER BURST PHENOMENA

Water waves (gravity waves produced by a burst) can conceivably be a contributing factor in causing mechanical damage to surface ships, especially to a ship already weakened by air and water shock. Waves might cause flexural (bending of the ship's longitudinal girder) damage to ships oriented end-on to the burst, or capsizing of ships oriented beam-on to the burst. Wave damage has not been observed experimentally in connection with bursts in deep water, but some wave damage appears to have occurred in the shallow water CROSSROADS BAKER test. A complete theoretical investigation of ship response to explosively generated waves has not been carried out. Ship response will depend on the wave periods and heights as well as ship characteristics, heading, and speed. Present indications are that the significance of waves in deep water will be minor relative to other damage phenomena (water shock wave for underwater bursts, air blast for surface bursts.) Waves in shallow water may be more significant in producing damage, since such waves may be steeper, particularly if the water depth is shoaling in the direction of wave propagation.

The water column or plumes thrown up by an underwater burst are not likely to cause significant mechanical damage to surface ships, since, for present ships, the water shock wave damage distances are greater. The highly radioactive base surge associated with the column or plume may be a hazard to personnel in some cases.

SECTION III

SUBMARINE DAMAGE FROM UNDERWATER BURSTS

DAMAGE FROM THE SHOCK WAVE IN THE WATER

The types of damage caused to submarines by the shock wave are generally similar to those caused to surface ships, i.e., they can be classified as hull damage and as shock damage. The hull damage can range from slight plastic deformation of hull plating to rupture of the pressure hull, with subsequent sinking of the submarine. Shock damage to interior equipment, caused by the sudden motion, may result in impairment of the mobility and weapon delivery capabilities. Best available evidence indicates that present operational submarines (submerged) will be lost or severely impaired mechanically before significant levels of personnel casualties are produced among the crew.

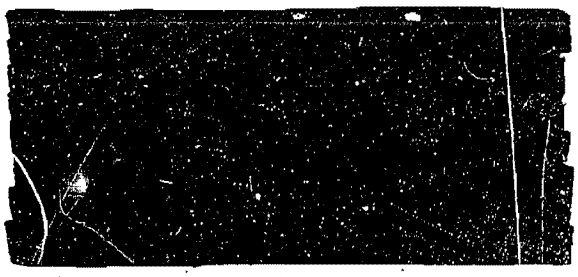

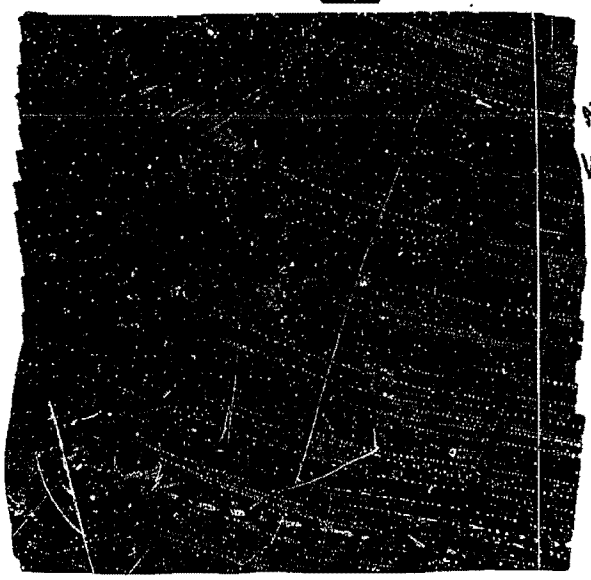

[redacted]

[redacted]

NAVY (b)(1)

[redacted]

NAVY (b)(1)

[redacted]

NAVY (b)(1)

[redacted]

NAVY (b)(1)

[redacted] The damage ranges were computed for calm isovelocity water, i.e., no variations of temperature. Allowance was made for anomalous surface reflection (nonlinear reflection occurring when the shock wave propagates nearly parallel to the surface). The possible effect of submarine orientation with respect to the direction of shock wave propagation was not considered.

12-18 Effect of Ocean Environment on Damage Ranges [redacted]

[redacted] The shock wave reflected from the sea bottom is less significant for submarines than for surface ships. In most cases, submarine damage ranges are not affected by the reflected wave. This is because the reflected wave will always be of lower pressure than the direct wave since it has to travel over a longer distance and suffer reflection losses. The fact that it impinges on the submarine at a different angle is in itself irrelevant (unlike the situation for surface ships), because the damaging effect is essentially independent of the angle of attack.

[redacted]

NAVY (b)(1)

[redacted]

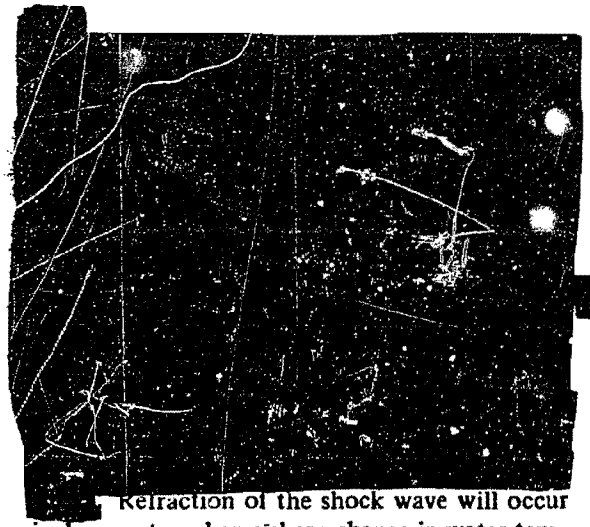

Refraction of the shock wave will occur in deep water when a sharp change in water temperature with depth exists (thermocline). Refraction may affect damage ranges for submerged submarines more significantly than it will for surface ships, since, under certain conditions, damage ranges can be increased appreciably. Although information on the effects of refraction is limited, certain generalizations can be made, which are believed to hold true under most conditions. If the submarine is above the thermocline, the situation is similar to that of a surface ship, i.e., the range at which a certain level of damage is produced is likely to be reduced (see Section III). If both the submarine and the burst are below the thermocline, damage ranges may be increased appreciably under some conditions. The effect of refraction is most significant in local areas where focusing occurs. Outside these areas, the effect is generally small and can be ignored in many cases. In general, the effects of refraction will increase with range from the burst and thus with weapon yield.

DAMAGE FROM OTHER UNDERWATER BURST PHENOMENA

The shock wave usually will be the controlling damage phenomena for submarines. However, gravity waves generated by the underwater burst in some cases conceivably could cause damage. In deep water a submarine should more or less follow the wave motion, and since relatively small accelerations are involved in this case, no damage should result in addition to that caused by the shock wave. In shallow water a submarine close to the bottom could be carried by the wave motion into collision with boulders or protrusions from the sea bed. The worst danger from gravity waves such as those that could be produced if the water depth is shoaling in the direction of wave propagation. The turbulent water involved in this case could cause the submarine to impact against the bottom. Quantitative information is not presently available concerning the damage potential of gravity waves against submarines.

Problem 12-3 Calculation of Damage Distances for Submarines from Underwater Bursts

Scaling. Damage distances for shock wave damage to submarines can be obtained for yields intermediate between those shown in Figures 12-6 through 12-13 by employing the following approximate scaling laws. Ranges for weapon delivery and mobility impairment can, within the range of yield indicated in each figure, be obtained from

$$\frac{d_1}{d_2} = \frac{h_1}{h_2} = \frac{W_1^{1/3}}{W_2^{1/3}}$$

where d_1 (yd) is the damage distance for yield, W_1 (kt) burst at a depth h_1 (ft) and d_2 (yd) is the corresponding damage distance for yield W_2 (kt) at a burst depth of h_2 (ft). During this scaling process the submergence depth of the submarine is kept constant.

(U) The above indicated cube root scaling law applies to distances for impairment of seaworthiness also, provided the yield is greater than 100 kt. For yields smaller than 100 kt in the indicated ranges, it is more accurate to use a square root scaling law for seaworthiness impairment

$$\frac{d_1}{d_2} = \frac{h_1}{h_2} = \frac{W_1^{1/2}}{W_2^{1/2}}$$

where the nomenclature is the same as that used previously. Again, the depth of submergence of the submarine is kept constant during the scaling process.

[redacted]

NAVY (2X1)

NAVY (2X1)

[redacted] *Reliability:* Figures 12-6 through 12-13 provide reasonable estimates for submarine damage criteria described in paragraph 12-16 for the specific submergence depths and yields for which the figures are provided. In view of the approximate nature of the scaling of damage distance with both yield and submergence depth, no firm estimate of overall reliability can be made.

[redacted] *Related Material:* See paragraphs 12-16 through 12-18 and Section IV, Chapter 2.

PAGES 12-22 THRU 12-29 DELETED

[redacted]

[redacted]

[redacted] BIBLIOGRAPHY [redacted]

Hansen, I. S., *Handbook of Underwater Nuclear Explosions, Part II – Effects, Chapter 2 – Surface Ship Structural Response and Damage Development – Section 2.2 – The Effects of Air Blast* [redacted] DASA 1240 (2.2), David Taylor Model Basin Report C-2023, August 1965 [redacted]

Hansen, I. S., *Handbook of Underwater Nuclear Explosions, Part II – Effects, Chapter 3 – Surface Ship Equipment, Section 3.2 – The Effects of Air Blast on Surface Ship Equipment* [redacted] DASA 1240 II (3.2), David Taylor Model Basin Report C-2096, October 1965 [redacted]

Hansen, I. S., *Weapon Delivery Impairment Ranges for DLG-16 and DDG-2 Class Ships Subjected to Air Blast – Preliminary SAILOR HAT Results* [redacted] Proceedings, DASA Conference on SAILOR HAT, DASA 1775, p. 190, May 1966 [redacted]

Hirsch, A. E., *Handbook of Underwater Nuclear Explosions, Part II – Effects, Chapter 8 – Submarine Personnel Casualties, Section 8.1 – Underwater Shock Effects* [redacted] DASA-1240 II (8.1), David Taylor Model Basin Report C-2148, January 1966 [redacted]

Irick, J. T., S. Silverman, and W. E. Baker, *The Rigid-Body Response of Naval Surface Vessels to Air Blast* [redacted] Final Report, Southwest Research Institute, prepared for Naval Ship Research and Development Center, September 1967 [redacted]

Manny, P. A., *Damage Criteria for Naval Ships and Submarines Subjected to Nuclear Explosions* [redacted] Naval Ship Research and Development Center (in preparation) [redacted]

Murray, W. W., *Engineering Predictions of the Early Bodily Response of Submarines to Underwater Explosion Attacks*, Underwater Explosions Research Division, Norfolk Naval Shipyard, Portsmouth, Va., UERD Report 7-58, October 1958.

Murray, W. W., *Ship Damage Classification and Prediction Methods* [redacted] David Taylor Model Basin Report C-1230, September 1961 [redacted]

Murray, W. W., *Loading and Response of Surface-Ship Hull Structures from Underwater Bursts* [redacted] Project 3.4, Operation HARDTACK, WT-1628, December 196[redacted] [redacted]

Murray, W. W., and R. M. Santamaria, *Handbook of Underwater Nuclear Explosions, Part II – Effects, Chapter 2 – Surface Ship Structural Response and Damage Development, Section 2.1 – The Effects of Underwater Phenomena* [redacted] DASA 1240-II (2.1), David Taylor Model Basin Report C-2261, December 1966 [redacted]

[redacted]

Parnell, U. C., and H. M. Schauer, *Handbook of Underwater Nuclear Explosions, Part II – Effects, Chapter 6 – Submarine Hull Response and Damage Development* DASA 1240 II (6), David Taylor Model Basin Report C-2188, June 1966

Rich, H. L., et al., *Shock Loading in Ships from Underwater Bursts and Response of Shipboard Equipment* Project 3.3, Operation HARDTACK, WT-1627, September 1959

Shrider, P. W., *The Interaction of Surface Ships with the Thermal and Radiological Environment* Chapter IV of DASA Handbook of Underwater Nuclear Explosions, Part II, Effects, DASA 1240-II (4), U.S. Naval Radiological Defense Laboratory Report USNRDL-475, January 1964

Weinberger, F., and R. M. Santamaria, *Mechanical Damage Ranges for Surface Ships and Submarines Subjected tc Nuclear Underwater and Air Bursts* David Taylor Model Basin, Report C-1323, November 1961

Zagorites, H. A., and R. L. Hopton, *Survey of the EMP in Shipboard Systems* U.S. Naval Radiological Defense Laboratory Report USNRDL-LR-190, July 1966

PAGE 12-32 INTENTIONALLY LEFT BLANK

AD-A955 397

Chapter 13

DAMAGE TO AIRCRAFT

INTRODUCTION

This chapter treats the damage to aircraft that results from the environment produced by the air blast wave and the thermal radiation from a nuclear explosion. The effects of nuclear radiation on electronic components and circuits are discussed in Section VII, Chapter 9, and some general vulnerability estimates for electronic systems in aircraft are given in Section IV, Chapter 14.

Section I of this chapter describes the blast and thermal effects on aircraft in general terms. Section II describes the response of the aircraft to the various categories of effects, largely in the form of illustrative problems, most of which contain numerical examples. Both in-flight and parked aircraft are considered.

A wide range of test data and a variety of analytical methods have been accumulated over the years to predict both the safe delivery of nuclear weapons and aircraft kill. Criteria for safety and for kill also have been developed; however, all of the aspects of the problems have not been treated in equal depth. The range of available methods that have been developed vary from relatively simple techniques to complex analyses requiring large, high-speed digital computers to obtain the solution. Unfortunately, there is very little information available concerning the relative accuracy and reliability of the various methods.

The discussion provided herein attempts to provide a clear description of the overall problem of aircraft exposed to blast and thermal effects of nuclear explosions. This description provides a means for those who are concerned with, but who do not have an extensive technical background in this area, to obtain an appreciation of the effects and to obtain first order approximations for the problems of aircraft safety and kill. A comprehensive review of a large body of data pertinent to vulnerability and safety analyses of aircraft subjected to the effects of nuclear explosions is contained in "Handbook for Analysis of Nuclear Effects on Aircraft (U)," DASA 2048 (see bibliography). As shown in DASA 2048, assessment of damage to aircraft is a strong function of the detailed characteristics of the specific aircraft of interest. Thus, it is impossible to provide a simple, short method to determine vulnerability in a general manner. DASA 2048 provides several methods for analyzing various classes of aircraft, arranged in order of increasing complexity. The simplest method described in DASA 2048 for each class of aircraft was selected to illustrate the analysis of that class of aircraft in Section II of this chapter. A brief abstract of DASA 2048, including a methodology matrix, is contained in Appendix D of this manual.

The term aircraft, as used in this chapter, applies to both airplanes and helicopters. Where differentiation between the two types of aircraft is intentional, the terms airplane and helicopter are used.

SECTION I

BLAST AND THERMAL EFFECTS ON AIRCRAFT

The problem of determining the effects of nuclear weapon explosions on aircraft has been recognized since the development of the

[redacted]

first nuclear weapons during the mid 1940s. For many years, aircraft represented the only means of delivering nuclear weapons to their targets; hence, it was natural to investigate the capabilities of aircraft with respect to delivering nuclear weapons. Nuclear weapons posed new and vital questions to military planners. Previously, when considering the delivery of conventional bombs by aircraft, the limitations on the capabilities of the aircraft were imposed by factors such as the range and payload of the aircraft and enemy defensive actions. With the emergence of nuclear weapons, a new factor was imposed. The energy output of these new weapons was so great that the delivery aircraft was in danger of being damaged by the explosion of the weapon it had delivered.

Subsequently, military planners became interested in the effects of a nuclear explosion on parked aircraft. Early efforts to understand this problem were largely experimental.

Finally, the possibility of nuclear antiaircraft weapons prompted analysis of the conditions under which an aircraft could be killed by the effects of nuclear weapons. Thus, the complete gamut of nuclear weapon effects on aircraft is of interest, from sure-safe conditions to sure-kill conditions, for both in-flight and parked aircraft.

This section provides background concerning nuclear weapon blast and thermal effects on aircraft, discusses the type, scope and format of the methods of weapon effects analysis presented in Section II, and explains how the results of the analyses may be used together with prescribed criteria to obtain either sure-safe or sure-kill regions for aircraft exposed to blast and thermal effects.

13-1 Sure-Safe and Sure-Kill Envelopes [redacted]

The terms "sure-safe" and "sure-kill" are self explanatory with respect to their general meaning; however, the terms must be examined more explicitly to provide a basis for understanding the analyses that are described in succeeding paragraphs. If the response of an aircraft to one of the effects of nuclear weapons is known, this response must be compared to some criterion to determine whether the aircraft is "safe" or "killed." For example, the aircraft may be termed safe with respect to that weapon effect as long as the particular weapon effect does not degrade the performance of the aircraft or crew in any way. The specification of a sure-kill, or lethal, criterion is more complex, because it is difficult to define the amount of response that will result in a sure-kill. The response must be sufficient to produce some kind of damage to the aircraft or crew. It could be stated that a sure-kill manifests itself by virtually "immediate loss" of the aircraft, but the relation of immediate loss to an amount of damage is difficult. Although some effort has been devoted to this problem, it still remains a major source of error in determining sure-kill conditions. The best available lethal criteria, with the sample response prediction methods, are presented in Section II.

If both response prediction methods and criteria that relate response to sure-safe and sure-kill conditions are available, the particular geometry that defines the relative positions of the nuclear explosion and the aircraft must be defined. The direction and flight path of the aircraft is an important part of the geometry. Two terms, "orientation" and "range," must be defined. For example, if the aircraft were directly above the burst and in straight and level flight, the orientation would be completely defined; however, the distance between the burst and the aircraft, which is range, would not be defined. The complete geometry of the problem, at the time of burst, is described by giving the range and the orientation.

For a specified orientation and range, the aircraft response to some nuclear effect can be determined. This response can be compared

[redacted]

QUALITY INSPECTED 4
UNANNOUNCED

[redacted]

to the maximum response to that effect that can be tolerated without degradation of the performance of the aircraft or crew, i.e., the criterion for sure-safe response. If the calculated response is less than the sure-safe criterion, the aircraft is safe for that range and orientation. Since weapon effects, and hence aircraft response to weapon effects, decrease with increasing range, a shorter range at the same orientation must be considered to find the range at which the calculated response matches the sure-safe criterion. When this range, which is called the sure-safe range, is determined, this range and the orientation assumed define a point on a sure-safe envelope.

[redacted] If the sure-safe range is determined for *all* orientations, a surface in space is defined. If the aircraft is placed at the origin of that surface, any nuclear burst, of the specified yield, which takes place on that surface will produce an aircraft response that matches the sure-safe criterion. Any burst outside of that surface will produce a lesser response; the aircraft will be safe for any burst outside of the surface. Conversely, the aircraft may be unsafe for any burst inside the surface.

[redacted] The surface described above is sometimes referred to as the "sure-safe volume," since it describes the volume in space outside of which a nuclear burst will produce a level of response that is safe for the aircraft and crew. If a plane is passed through this surface, the intersection of the plane and the surface defines a closed line called an "envelope." A sure-safe envelope is simply a plane section of a sure-safe volume.

[redacted] The sure-kill surface or volume may be defined in a similar manner. The sure-kill volume, often called the lethal volume, defines the volume in space inside of which a nuclear burst will produce a level of response that will result in an aircraft kill. A sure-kill envelope is a plane section of a sure-kill volume.

[redacted] For in-flight aircraft, the range and orientation with respect to a given burst point are functions of time as a result of the motion of the aircraft. The time must be specified to specify the geometry completely. In defining the time, it is important to distinguish between types of weapon effects: those effects that take place or at least begin to take place immediately after the burst; and those that do not take place until some time after the burst. Nuclear and thermal radiation, whose effects begin to be felt virtually immediately fall into the first category. Gust and overpressure effects, which are not felt by the aircraft until the arrival of the blast wave are in the second category. Two times of significance are associated with the problem. The first is the burst time and the second is the intercept time, or the time at which the blast wave reaches, or intercepts, the aircraft. For effects in the first category, only the burst time is significant; hence, the orientations and ranges are those corresponding to the burst-time position of the aircraft. For effects in the second category, both the burst time and the intercept time are significant.

[redacted] In calculating response, it is convenient to use the intercept time, because it is at intercept time that the response begins. Hence, application of the response methods results directly in intercept-time volumes and envelopes. The military planner, however, is generally interested in burst-time envelopes, since he wants to know what the effects of a nuclear burst occurring at some point relative to the aircraft will be on an aircraft. He generally is not interested in where the aircraft will be when it is intercepted by the blast wave, but only that some given response will be achieved when it is intercepted. Thus, it becomes necessary to transform intercept-time envelopes into burst-time envelopes. This transformation can be accomplished rather easily. Each range on an intercept-time envelope represents the distance which the blast wave must

[redacted]

travel in order to reach the aircraft. For a given yield and altitude, a time of arrival of the blast wave may be associated with any distance traveled. Hence, the time, measured from burst time, corresponding to any point on the intercept-time envelope may be calculated from weapon characteristics. Using this time, and knowing the aircraft velocity and maneuver condition, a position occupied by the aircraft at burst time may be calculated for each point on an intercept-time envelope. These positions define the burst-time envelopes.

In determining the burst-time envelopes, the assumption is made implicitly that the aircraft maintains a constant speed and maneuver between the time of burst and the time of interception by the blast wave. Within the scope of this manual, the assumption has been made that the airplane velocity does not exceed Mach 2. For an airplane velocity exceeding Mach 2, certain effects that have been ignored in transforming intercept-time envelopes into burst-time envelopes become important. This assumption is valid for low yield weapons, because of the small distances and times involved. For large yield weapons, however, when the blast wave arrival time may be on the order of several seconds, there is time for a pilot to change his course. It would be impossible to guess the course changes; hence, assumption of an unaltered flight path cannot be avoided reasonably. At the same time, this assumption must be considered as a source of error in the case of large yield weapons.

NUCLEAR WEAPON EFFECTS ANALYSIS

A basic description of nuclear weapon blast and thermal phenomena is contained in Chapters 2 and 3 of this manual. The effects of these weapon phenomena on an aircraft are described in the following paragraphs. These effects include material velocity (gust) effects, overpressure effects, thermal radiation effects, and combinations of these effects.

13-2 Gust Effects

The blast wave and the associated material velocity and overdensity are described in Section I of Chapter 2. As the blast wave engulfs an aircraft, the angle of attack of the aircraft is changed by the material velocity. The effect is similar to that produced by atmospheric gusts, and the term gust has become associated with this effect.

Another parameter that is important in determining aerodynamic loads is the dynamic pressure. The dynamic pressure is the product of the air density and the square of the velocity of the aircraft relative to the surrounding air. Since both the density and the relative velocity are changed by the blast wave, the dynamic pressure is changed.

The changes in angle of attack and dynamic pressure produce changes in the aerodynamic loads on the aircraft. Several methods may be used to predict the resulting aerodynamic loads. The simplest is the so-called quasi-steady state method. In this method, the angle of attack and dynamic pressure existing at each instant of time are considered to have existed for a time that is sufficiently long that a steady-state condition has been attained. The aerodynamic forces are then the steady-state forces corresponding to the instantaneously-existing conditions. Since the instantaneously-existing conditions actually are changing rapidly as the blast wave engulfs the aircraft and subsequently decays, the method is called quasi-steady. More sophisticated methods account for the truly transient nature of the response to the aerodynamic loads under the rapidly changing conditions. Such methods are called unsteady aerodynamic methods.

One more complication arises in predicting aerodynamic loads. Aerodynamic loads gen-

erally are assumed to be proportional to the angle of attack, i.e., the loads are assumed to be linear with angle of attack. In the sure-kill case, however, severe loadings are required to produce damage corresponding to a sure-kill condition. These severe loadings generally can occur only if the gust induced angle of attack is large, often well beyond the angle of attack range for which linearity can be assumed reasonably, and nonlinear aerodynamics are of interest. The coupling of unsteady and nonlinear aerodynamics is an extremely complex problem that has been solved only semi-empirically.

The aerodynamic loads described above produce rigid-body accelerations of the aircraft, both in translation and rotation. These accelerations result in translational and rotational velocities and displacements. The translational velocity and the rotational displacement are particularly important in the production of additional aerodynamic loads. If an aircraft is intercepted by a blast wave from directly below, the material velocity is upward. This increases the angle of attack of the aircraft and causes an upward translational velocity, so the aircraft tends to "ride" with the gust. The tendency to ride with the gust causes a reduction in the angle of attack of the aircraft and alleviates the aerodynamic loads. The alleviation that results from riding with the gust is a function of the wing loading for an airplane. The wing loading is the ratio of the airplane weight to the airplane wing area. An airplane with a high wing loading is heavy with respect to its aerodynamic loading; it rides very little with the gust and produces very little load alleviation. Conversely, an airplane with a low wing loading will produce considerable load alleviation by riding with the gust.

The rotational displacement that results from rotational acceleration also alleviates the loading, although the effect is more complex. Roughly, a stable aircraft will rotate into the gust, which reduces the angle of attack and alleviates the loads. Generally, the translational load alleviation is more important than the rotational load alleviation during the time period of interest.

The aerodynamic loads also produce accelerations and displacements in the elastic modes of the aircraft, e.g., the fuselage bends. The elastic displacements and velocities also change the angle of attack and hence the aerodynamic loads. There is thus an interaction between the elastic motion and the aerodynamic loads; this interaction is called the aeroelastic effect. The aeroelastic effect is generally of secondary importance, but there are cases in which it can be of considerable importance.

One more type of motion interacts with the aerodynamic loading. If the sure-kill problem for an in-flight aircraft is considered, the inelastic response often must be considered. A major component, such as the fuselage, ordinarily will fail in an instability, or buckling, type of mode; however, a buckling failure does not necessarily produce a catastrophic failure of the aircraft, i.e., a sure-kill condition. A structure that has undergone a major buckling failure will be weaker than it was prior to the failure; however, it may maintain the capability of carrying a substantial load. The load carrying capability may be sufficient to permit the aircraft to complete its mission. This situation has been demonstrated analytically, in simulation experiments, and in a full-scale test during Operation TEAPOT, a nuclear test in Nevada in 1955.

As the inelastic deformation of the structure increases, its load carrying capability decreases. At some point, the load carrying capability becomes sufficiently low that a sure-kill condition exists. Inelastic deformations required to produce a sure-kill condition may be very large when compared to elastic deformations; the aerodynamic loads induced by inelastic motions may be much larger than the aeroelastic effect described previously.

[redacted]

The final influence on the aerodynamic loadings for in-flight aircraft is pilot or autopilot action upon interception of the aircraft by the blast wave. Pilot action would be too slow to influence the situation substantially during the time period of interest. Autopilot response has been ignored in all known approaches to the problem, presumably because of the low probability that the aircraft would be on autopilot for realistic engagement conditions. It might be noted, however, that an autopilot that is maintaining constant barometric altitude could react violently to the change in pressure accompanying the blast wave.

The concepts of rigid-body, elastic, and inelastic motion have been introduced in outlining the various influences on the aerodynamic loads. Each of these types of motion is important for some type of sure-safe or sure-kill envelope. For example, parked aircraft may be lifted from the ground. This is a rigid-body mode, which must be considered for both sure-safe and sure-kill conditions for parked aircraft.

Parked aircraft also may be damaged by bending of the fuselage or vertical tail as a result of aerodynamic loading of the vertical tail. For sure-safe conditions, this bending will be elastic; for sure-kill conditions, inelastic response also may be important.

Rigid-body motions generally are not important for in-flight aircraft. These motions enter the problem in two ways: (1) their influence on the aerodynamic loads is significant; (2) rigid-body translational accelerations are rough indices of the amount of elastic or inelastic deformation of the major aircraft components, and they may be used in crude methods instead of such deformations, which are the quantities of real interest. More realistic analyses should consider elastic response for sure-safe conditions and inelastic response for sure-kill conditions.

Most of the preceding remarks apply both to airplanes and to helicopters. The only new facets added by helicopters are the rotors. There are three types of helicopter main rotor blades: hinged, rigid (hingeless), and teetering. Each type must be considered separately, because each has its own characteristics.

The important characteristic of a hinged rotor is the hinge, which is offset somewhat from the center of rotation. This permits free rotation of the blade outboard of the hinge in an up-and-down, or flapping, direction. Analysis of this type of blade has shown that bending of the blade is not an important mechanism for either sure-safe or sure-kill conditions. Flapping of the blade about the hinge seems to be more important. Extreme flapping could result in a collision between the blade and the fuselage and/or the flapping stops. Even blade flapping appears to be less important than overpressure damage to the overall system, so gust effects are not considered for hinged blade helicopters in this chapter.

Rigid, or hingeless blades, do not use a flapping hinge. Bending may be important for these blades, and it is considered in this chapter.

Finally, a teetering blade roughly combines the characteristics of the hinged and hingeless blades. A teetering blade is essentially a seesaw about a hinge at the center of rotation. The two blades on the two sides of the hinge are connected rigidly. If there is a loading on the two blades, this loading can always be divided into a symmetrical and an anti-symmetrical component. The loadings on the two blades are identical for the symmetrical component; the loadings on the two blades are exactly opposite for the anti-symmetrical component. The response to the anti-symmetrical component is exactly the same as if each blade were separately hinged at the center of rotation, rather than being connected rigidly. The anti-symmetrical gust loading component on teetering blades can therefore be ignored for the same reasons that gust loading on hinged blades was ignored.

The teetering blade responds to sym-

[redacted]

metric loading as if there were no hinge at the center of rotation, i.e., the teetering blade responds to a symmetric loading as if it were a hingeless blade, and the symmetric component of the gust loading must be considered.

In general, gust effects are only of minor importance for parked aircraft, but they are of primary importance for in-flight aircraft.

13-3 Overpressure Effects

The gust effects influence the major components of the aircraft, such as the wings and/or the blades, the fuselage, the horizontal tail, and the vertical tail. The overpressure, on the other hand, influences smaller elements of the structure, i.e., the skin, the stringers, and the frames, particularly on the fuselage.

When an aircraft is struck by a blast wave, the pressure on the side of the fuselage facing the burst point is increased above the incident value by reflection, and a local loading of short duration is generated (see Figure 9-3). As the blast wave continues to engulf the aircraft, the pressure on the side of the fuselage facing the burst point decays to the pressure behind the blast wave. The characteristic loading is a high reflected pressure (from two to eight times the overpressure associated with the blast wave), which decays very rapidly, in a few milliseconds, to the value of pressure behind the blast wave. This high pressure, short duration pulse is followed by the much longer duration, but lower pressure, pulse that is characteristic of the blast wave.

It is primarily the high reflected pressure, short duration pulse that is responsible for damage to skin panels, stringers, and frames. These structural elements are vulnerable to such short duration loadings because of their high frequencies. For the converse reason, the much lower frequency major components are not influenced to a great extent by the short duration loading.

The short duration pulse produces dishing-in of skin panels and buckling of stringers and frames or portions of stringers and frames. As in the case of analysis of response to gust effects, analysis of overpressure response only requires consideration of the elastic response for the sure-safe case, but inelastic response should be included for sure-kill conditions.

Early efforts to determine overpressure damage relied virtually entirely on experimental results. Simple approaches were advanced later, which analyze the response of skin panels, stringers, and frames to static loadings, and then modify the results by some dynamic factor to account for the true dynamic character of the loading.

With regard to overpressure damage, airplanes and helicopters may be analyzed in the same way. The distinguishing feature of the helicopter, the rotor blade, is virtually invulnerable to overpressure effects, so the helicopter is no different from an airplane in this regard.

Overpressure damage is generally the predominant effect for parked aircraft; however, overpressure damage is usually of minor importance in comparison with gust effects for in-flight aircraft. Overpressure only becomes important for in-flight aircraft in those regions where gust effects are small, i.e., for bursts almost directly in front of or directly behind the aircraft.

13-4 Thermal Radiation Effects

In considering the effects of the thermal radiation from a nuclear explosion, two distinct problems must be addressed: (1) the portion of the thermal radiation emitted by the explosion that reaches the aircraft; and (2) the effect on the aircraft that is produced by the incident radiation.

The radiant exposure of an aircraft in flight varies widely with atmospheric conditions,

orientation of the aircraft with respect to the burst, aircraft velocity, the ground reflecting surfaces, and the location of clouds (see Chapter 3). Scatter and reflection add to the direct radiation, and, under some circumstances, the thermal energy incident on an aircraft in space may be two to three times as great as would be computed at a given slant range for direct radiation only. Conversely, when a heavy cloud layer is between the burst and the aircraft, the radiant exposure may be only a fraction of the predicted value of direct radiation for a given range. In other situations, reflected radiation from clouds may contribute significant thermal energy to areas of the aircraft shaded from direct radiation. During weapon effects tests of an aircraft flying in a cloud above the burst, the radiant exposure at the top of the aircraft and its cockpit area was observed to be as much as one-fourth of the direct radiation on the lower surfaces. This experiment demonstrated the need for protection of weapon delivery aircraft from radiant exposure from any direction.

The motion of the aircraft during the time in which significant thermal radiation is being emitted by the fireball can exert an important influence on the thermal radiation incident upon the aircraft. Obviously, this is particularly true for high-speed aircraft. "Fly-away factors" have been devised which are first order corrections for aircraft motion.

The absorptivity of the aircraft skin and the angle of incidence of the thermal radiation affect the amount of energy that will be absorbed by the structure; the boundary layer in the air flow adjacent to the structure leads to convective cooling. Very thin skins are heated to damaging temperatures rapidly, because the energy is absorbed by the skin much more rapidly that it can be dissipated by conduction and convective cooling. In recent years, designers of military aircraft have reduced aircraft vulnerability to thermal effects by coating materials with low absorptivity paints, by eliminating ignitable materials from exposed surfaces, and by substitution of thicker skins for very thin skins.

An aircraft thin skin panel, supported by internal structure, which is usually much cooler, can be heated sufficiently that it may be buckled by thermal stresses in the sure-safe case, or it may melt in the case of sure-kill. In either case, there will be essentially no change in temperature through the thickness of a thin skin. The thick skin case is a step higher in complexity. The temperature distribution across the thickness of the skin must be considered in determining thermal stresses. A still more complex temperature distribution occurs in built-up structures, with air gaps acting as insulators between spars, stringers, and skin. For all but the simplest configurations, computer programs are necessary to define these temperature distributions accurately.

Analyses of thermal radiation effects on aircraft generally only concern themselves with temperature rather than with stresses, since buckling of thin skin is generally of little or no consequence. Sure-safe envelopes usually are based upon a rather arbitrary temperature, or temperature rise, in the thinnest skin. The temperature chosen is based roughly upon some percentage reduction in strength or stiffness that results from the increased temperature. Sure-kill envelopes are based upon melting of the skin.

Biological injury to the crew from intense thermal radiation, and damage to nonstructural elements that would affect mission performance adversely also must be considered when dealing with thermal criteria. In many cases, these problems can be minimized by adequate protective measures such as cockpit curtains.

A military weapon delivery aircraft properly prepared for its delivery mission with reflective paint and with the crew and all vulner-

[redacted]

able materials shielded from direct thermal radiation will not be damaged by thermal radiation at distances where damage from air blast would be severe. Other aircraft not so prepared may sustain serious damage at very low thermal levels as a result of ignition of items such as rubber and/or fabric seals, fixed landing gear tires, cushions, and headrest covers. Aircraft painted with dark paint are especially vulnerable to thermal radiation damage, because the dark painted surfaces absorb three to four times the thermal energy that is absorbed by polished aluminum surfaces or surfaces protected with reflective paint.

[redacted] As in the case of overpressure effects, there is no difference between helicopters and airplanes with regard to the analysis of thermal radiation effects. The importance of thermal radiation effects relative to the other effects depends upon the yield of the weapon being considered. Relative to other effects, the importance of thermal radiation increase with increasing yield. For small yields, thermal radiation is generally of secondary importance for both parked and in-flight aircraft; thermal radiation from high yield weapons may be dominant for both.

13-5 Combined Effects [redacted]

[redacted] The effects of combinations of various weapon phenomena have been examined, but relatively little has been accomplished in the generation of methods for analyzing combined effects. One reason for this is the difficulty in analyzing each effect individually with adequate accuracy. In general, only qualitative comments may be made concerning combined effects.

[redacted] The first possibility is the interaction between gust and overpressure effects. For in-flight aircraft, the levels of overpressure required to produce a given response are well above the levels associated with significant response to gust effects, and little coupling is expected. For parked aircraft, the gust effects of most importance are lift-off and crushing of the landing gear; overpressure damage will not influence these phenomena significantly. Thus, gust-overpressure coupling appears to be of secondary importance.

[redacted] In considering the thermal interactions with either overpressure or gust, it should be recalled that the usual thermal analyses are concerned with temperatures and not with stresses. To examine the interaction between thermal stresses and gust or overpressure effects would require a combined analysis of a higher level of sophistication than is usually employed for the individual effect. Moreover, the few exploratory investigations indicate that transient thermal stresses seem to be less important as a coupling factor than degradation in material properties that result from elevated temperature. Degradation of material properties generally will be of minor importance at ranges associated with significant gust effects for in-flight aircraft, except in the case of high yield weapons. For high yield weapons, the time period between heating of the structure and interception of the aircraft by the blast wave may permit considerable cooling to take place, and thus minimize interaction effects even in this case.

[redacted] For parked aircraft, the interaction between thermal and overpressure effects could be significant. The state of the art in overpressure effects analysis, however, is such that inclusion of anything more than the effect of degraded material properties (see Section IV, Chapter 9) would be unreasonable.

[redacted] In summary, the only interactions between effects that seem to be of much importance are those between thermal effects and gust or overpressure effects. In those cases, any consideration of interactions should be restricted to use of material properties in the gust or overpressure analyses corresponding to the elevated temperatures produced by the thermal radiation.

[redacted]

Furthermore, consideration of even this interaction should be restricted to the most sophisticated methods of gust and overpressure analysis, and is not recommended for users of this manual.

SECTION II

AIRCRAFT RESPONSE TO BLAST AND THERMAL EFFECTS

AIRCRAFT RESPONSE TO GUST EFFECTS

13-6 Aerodynamic Coefficients for Aircraft

When the blast wave arrives and commences to envelop the aircraft, a complicated pattern of shocks passes over the surfaces of the aircraft very quickly. During this period, frequently called the "diffraction period" (see Section II, Chapter 9), the transient airloads are difficult to predict, and sophisticated methods are required even for the simplest combination of aircraft configuration and blast orientation. However, for many cases of blast loading, such as a supersonic airplane enveloped by a blast from below, the lift and normal force during the diffraction period are nearly the same as during the early post-diffraction period. In other cases, the duration of the diffraction loading is so short that the influence on the response of major aircraft components is very small. Hence, it is reasonable to make first estimates of the transient airloads on a quasi-steady basis by using instantaneous quantities (angle of attack, density, etc.) and steady-state coefficients to compute steady state forces. This simplification is adopted in the aerodynamics methods presented in this chapter.

Methods for calculating gust loadings are presented for two orientations: symmetric loading, with the gust velocity from directly above or below the aircraft; and lateral loading, with the gust velocity directly from the side.

When a wing (tail) is added to a fuselage, certain mutual interference effects may arise between the components. For example, a body induces high upwash velocities near the wing-body (tail-body) juncture, which is commonly termed body-induced wing (tail) interference. The local body flow properties such as Mach number and dynamic pressure also affect the wing (tail) loading. The wing (tail) in turn affects the loads on the body.

Another interference effect, normally considered in stability and control, is that on the tail that results from a wing set at an angle of attack. The downwash that is caused by the trailing vortices from the wing generally reduces the lift on the horizontal tail surfaces during straight and level flight. The magnitude of the reduction depends on the span of the wing relative to the span of the tail, the lift distribution on the wing, and a number of other factors. A blast wave changes the loading in the wing, which alters the strength of the vortex sheet behind the wing, but the change in the strength of the vortex sheet that results from the blast wave does not affect the lift on the tail at early times after blast arrival to any great extent. The blast wave also deflects the vortex sheet away from the plane of the wing. The effect of the vortex sheet on the lift on the tail depends strongly upon the position of the sheet relative to the tail surface. Methods to predict the transient location of the vortex sheet have not been demonstrated for strong blasts; therefore, the interference of the wing on the tail is not included in transient load estimates.

The airloads on the vertical tail produced by lateral blasts are more difficult to predict than the airloads on the wing, because, in addition to the body and the wing, the horizontal tail influences the flow field at the vertical tail. At an angle of attack, the downwash from the wing could influence the vertical tail. The lateral flow over the body has a maximum

velocity at the top where the vertical tail is located. Also, at large angles of attack or sideslip, there are vortices shed from the body that could affect the loads on the vertical tail; presumably the effect of the vortices would be most severe at combined angles of attack and sideslip, a combination which is outside the cases considered here. The horizontal tail interacts with the flow field about the vertical tail, serving to some extent as a reflection plane, so that aerodynamically the vertical tail appears to have an aspect ratio that is larger than the geometric aspect ratio (this is the so-called "end-plating" effect). At supersonic speeds, shocks emanate from the wing and horizontal tail and provide further influence on the vertical tail loads.

Problem 13-1. Calculation of the Aerodynamic Coefficient for Wing and Horizontal Tail

The transient airloads may be obtained on a quasi-steady basis using the instantaneous quantities (angle of attack, density, etc.) and steady-state coefficients. Typically, the theoretical methods predict a lift for a swept wing-body combination which is about 10 percent greater than for an isolated wing without a body, provided that the wing and body are at the same incidence. In wind tunnel tests, however, the lift on a swept wing-body combination was found to be the same as on an isolated wing. In these cases, the area of the isolated wing includes the area submerged within the body. Other methods indicate that the lift on a delta wing-body combination with a typical ratio of body diameter to wing span and traveling at supersonic speeds is within 2 percent of the lift for the same delta wing alone. In view of these results, the lift on the wing (tail)-body combinations is computed for an isolated wing (tail) having the same wing area, including the wing (tail) area submerged within the fuselage.

The calculation of the aerodynamic coefficient for wings and/or horizontal tails, C_{L_α}, is presented in the following series of steps.

1. Using the silhouette profile of the aircraft (for example, see Figures 13-1 and 13-2), from which lengths and surfaces may be found, determine the following:

S = wing/horizontal tail area (sq ft), defined as the extension of the leading and trailing edges of both wings/horizontal tail to the aircraft centerline.

c_r = wing/horizontal tail root chord, i.e., the length along the fuselage centerline (ft) subtended by extensions of the leading and trailing edges.

c_t = wing/horizontal tail tip chord (ft), defined as the length along the fuselage centerline subtended by the wing tip.

b = wing/horizontal tail span, tip to tip (ft).

Λ_{LE} = sweepback angle at wing/horizontal tail leading edge, measured from a line perpendicular to the fuselage centerline (deg).

M = Mach Number = V/c, where V is the aircraft velocity and c is the ambient speed of sound.

2. Calculate the taper ratio λ:

$$\lambda = \frac{c_t}{c_r}$$

and the aspect ratio AR:

$$AR = \frac{b^2}{S}.$$

3. Calculation of the slope of the lift coefficient depends on the value of the Mach number, M. Three regions are defined as follows:

Region 1: $M \leq 0.85$,

Region 2: $M \geq 1.2$,

Region 3: $0.85 < M < 1.2$.

Region 1. Steps a through d present the calculation of the slope C_{L_α} for $M \leq 0.85$.

a. Calculate the value of β^2:

$$\beta^2 = 1 - M^2.$$

[redacted]

b. Determine the tangent of the sweep angle of the mid-chord line, tan $\Lambda_{c/2}$:

$$\tan \Lambda_{c/2} = \tan \Lambda_{LE} - \frac{2}{AR}\left[\frac{1 - \lambda}{1 + \lambda}\right].$$

c. Compute the parameter,

$$AR\left[\beta^2 + \tan^2 \Lambda_{c/2}\right]^{1/2},$$

and enter Figure 13-3, with the value of the parameter to obtain the corresponding value of C_{L_α}/AR.

d. Calculate the slope of the lift coefficient curve as follows:

$$C_{L_\alpha} = \left[\frac{C_{L_\alpha}}{AR}\right] AR.$$

Region 2. Calculation of C_{L_α} for $M \geq 1.2$ is performed by the following steps.

a. Calculate the value of β:

$$\beta = (M^2 - 1)^{1/2}.$$

b. Calculate the values of the parameters:

$$\frac{\beta}{\tan \Lambda_{LE}},$$

and

$$(AR) \tan \Lambda_{LE}.$$

c. Enter Figure 13-4 and select the figure corresponding to the taper ratio λ. Select the curve corresponding to the value of the parameter $(AR) \tan \Lambda_{LE}$. If

$$\frac{\beta}{\tan \Lambda_{LE}} < 1,$$

use the left side of the figure to obtain the value of $\tan \Lambda_{LE} C_{N_\alpha}$. Calculate C_{L_α} as follows:

$$C_{L_\alpha} = \frac{\tan \Lambda_{LE} C_{N_\alpha}}{\tan \Lambda_{LE}},$$

where the normal force coefficient C_{N_α} and C_{L_α} are taken to be equal within the scope of this method.

If

$$\frac{\beta}{\tan \Lambda_{LE}} > 1,$$

determine its reciprocal,

$$\frac{\tan \Lambda_{LE}}{\beta},$$

and use the right side of the figure to obtain the value of βC_{N_α}.

The slope is calculated by:

$$C_{L_\alpha} = \frac{\beta C_{N_\alpha}}{\beta},$$

where C_N is represented as C_L within the scope of this method.

Region 3. The following steps a through c, are used to calculate C_{L_α} for $0.85 < M < 1.2$.

a. Calculate C_{L_α} at $M = 0.85$ following the method in Region 1.

b. Calculate C_{L_α} at $M = 1.2$ following the method in Region 2.

c. Interpolate linearly for the slope at the actual Mach number:

$$C_{L_\alpha} = C_{L_\alpha}(\text{at } M = 0.85) + \frac{M - 0.85}{0.35}\left[C_{L_\alpha}(\text{at } M = 1.2) - C_{L_\alpha}(\text{at } M = 0.85)\right].$$

[redacted]

[redacted]

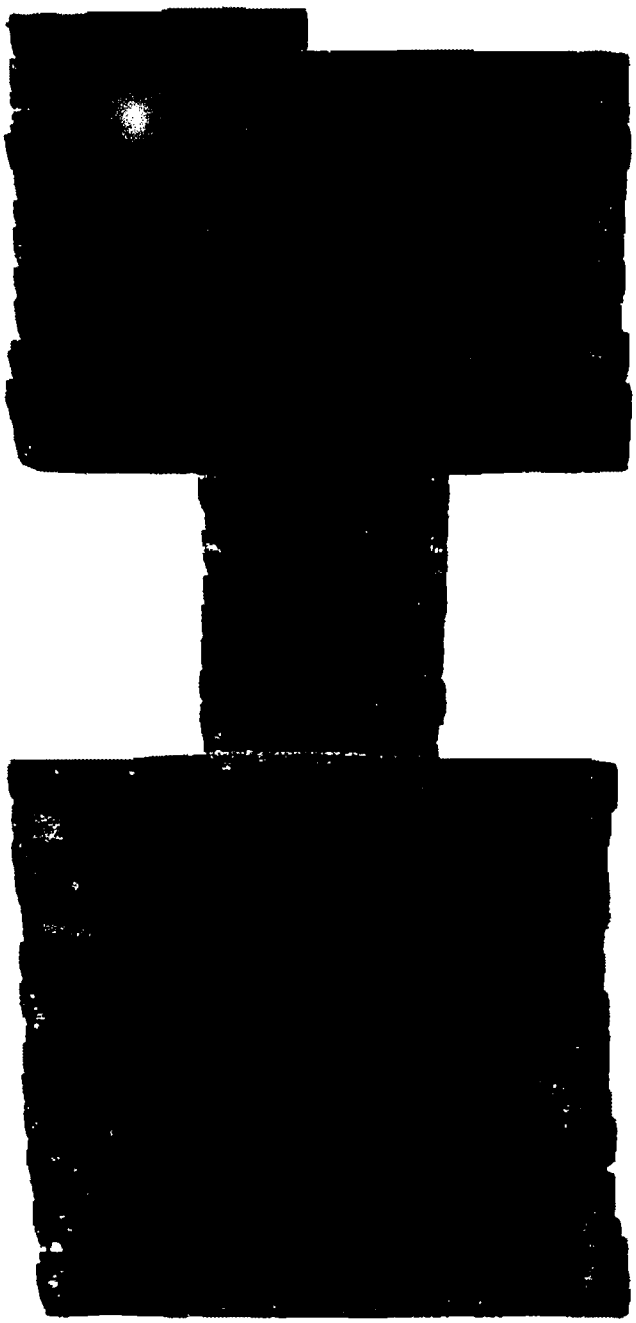

DNA
(4)(1)

[redacted] *Reliability:* The aircraft is assumed to be in a symmetric maneuver prior to blast interception. Blast origin is in the aircraft plane of symmetry. Interference effects of wing on tail, body on wing, and body on tail are neglected. A quasi-steady approach is assumed to be adequate to define blast-induced loads.

[redacted] *Related Material:* See paragraphs 13-1 and 13-2. See also Table 13-1.

[redacted]

[redacted]

Table 13-1. [redacted] Selected Data Based on U.S. Standard Atmosphere, 1962 English Units [redacted]

Altitude feet	Temperature °F	Pressure psi	Density Ratio* ρ/ρ_0	Temperature Ratio T/T_0	Sound Speed ft/sec
0	59.0	14.696	1.0000	1.000	1116
1 000	55.4	14.17	.9711	.993	1113
2 000	51.9	13.66	.9428	.986	1109
3 000	48.3	13.17	.9151	.979	1105
4 000	44.7	12.69	.8881	.973	1101
5 000	41.2	12.23	.8617	.966	1097
10 000	23.4	10.11	.7386	.931	1077
15 000	5.5	8.297	.6295	.897	1057
20 000	-12.3	6.759	.5332	.863	1037
25 000	-30.0	5.461	.4486	.828	1016
30 000	-47.8	4.373	.3747	.794	995
35 000	-65.6	3.468	.3106	.760	973
40 000	-69.7	2.730	.2471	.752	968
45 000	-69.7	2.149	.1945	.752	968
50 000	-69.7	1.692	.1531	.752	968
55 000	-69.7	1.332	.1206	.752	968
60 000	-69.7	1.049	.09492	.752	968
65 000	-69.7	.826	.07475	.752	968
70 000	-67.4	.651	.05857	.756	971
75 000	-64.7	.514	.04591	.762	974
80 000	-62.0	.406	.03606	.767	978
85 000	-59.3	.322	.02837	.772	981
90 000	-56.5	.255	.02236	.777	984
95 000	-53.8	.203	.01765	.782	988
100 000	-51.1	.162	.01396	.788	991
110 000	-41.3	.103	8.692-3	.807	1003
120 000	-26.1	.0667	5.428	.836	1021
130 000	-10.9	.0438	3.446	.865	1038
140 000	4.3	.0292	2.222	.894	1056
150 000	19.4	.0197	1.454	.924	1073
160 000	27.5	.0135	9.770-4	.939	1082
170 000	27.5	9.23-3	6.690	.939	1082
180 000	18.9	6.31	4.652	.923	1072
190 000	8.1	4.27	3.225	.902	1060
200 000	-2.7	2.87	2.217	.881	1048

NOTE: 7.011-3 means 7.011×10^{-3}

*$\rho_0 = 2.38 \times 10^{-3}$ slugs/ft^3
$= 7.65 \times 10^{-2}$ lbs/ft^3

[redacted]

[redacted]

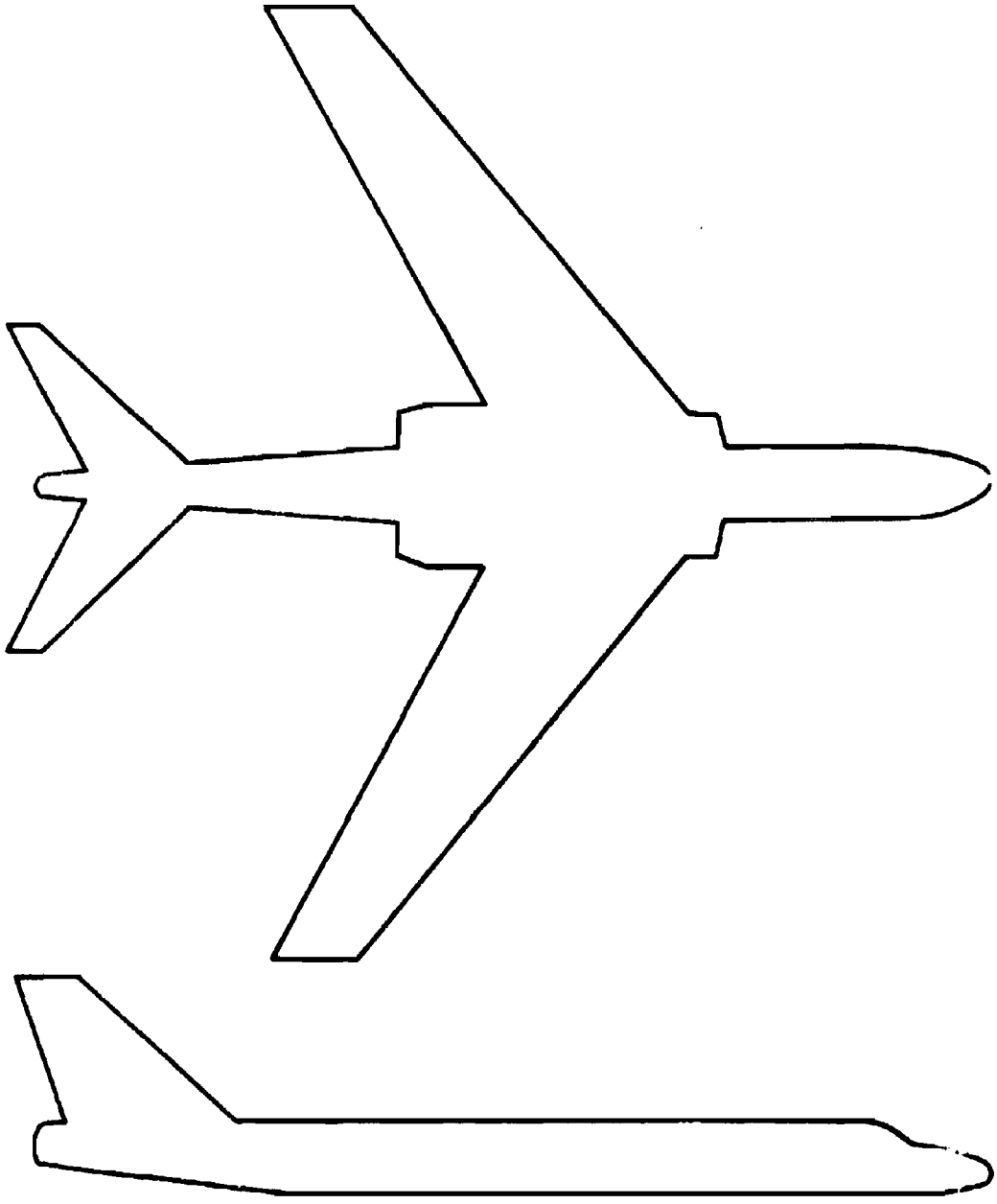

SCALE: 1" = 30'

Figure 13-1. [redacted] Example Airplane (American) [redacted]

[redacted]

[redacted]

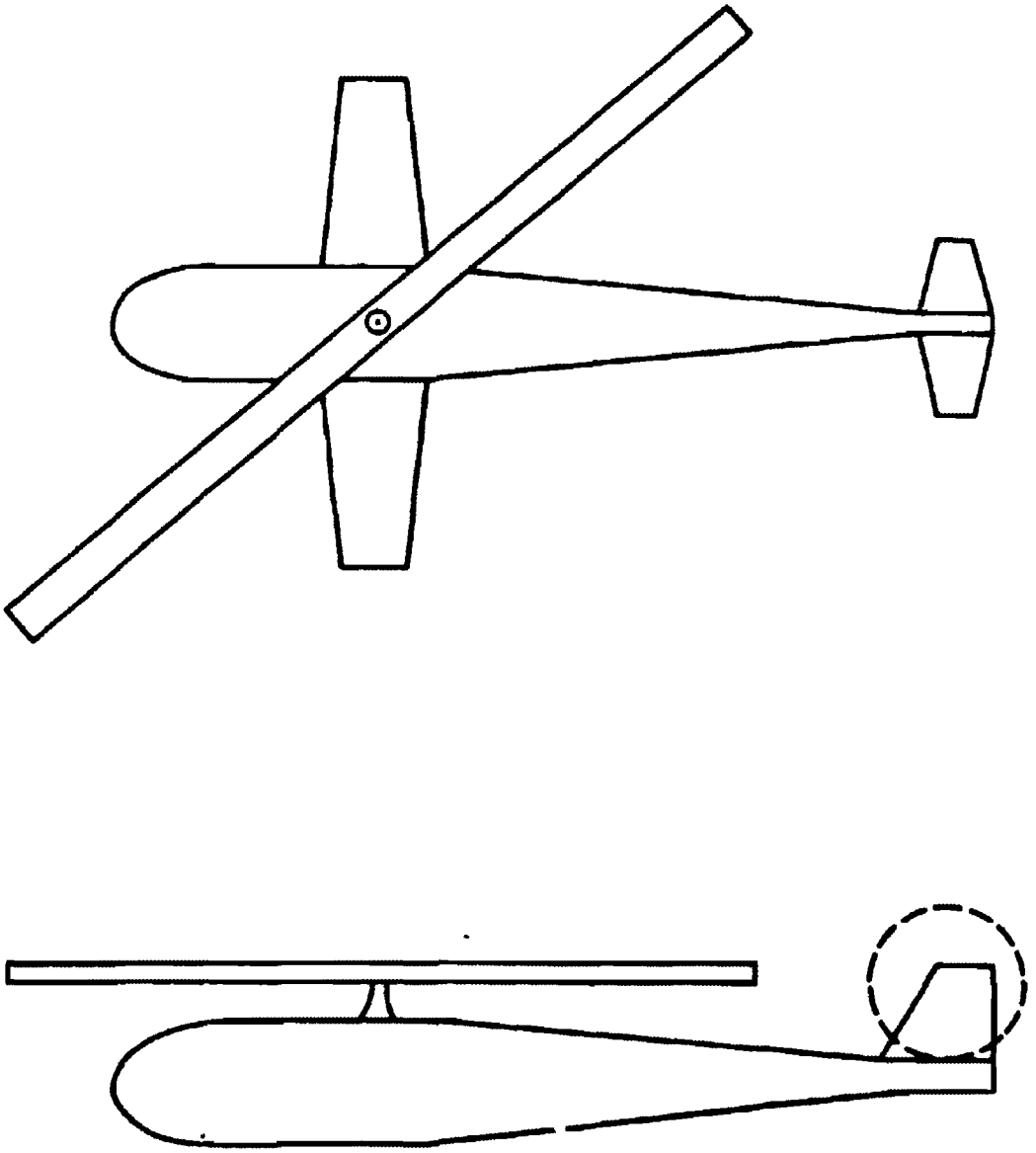

SCALE: 1" = 10'

Figure 13-2. [redacted] Example Helicopter [redacted]

[redacted]

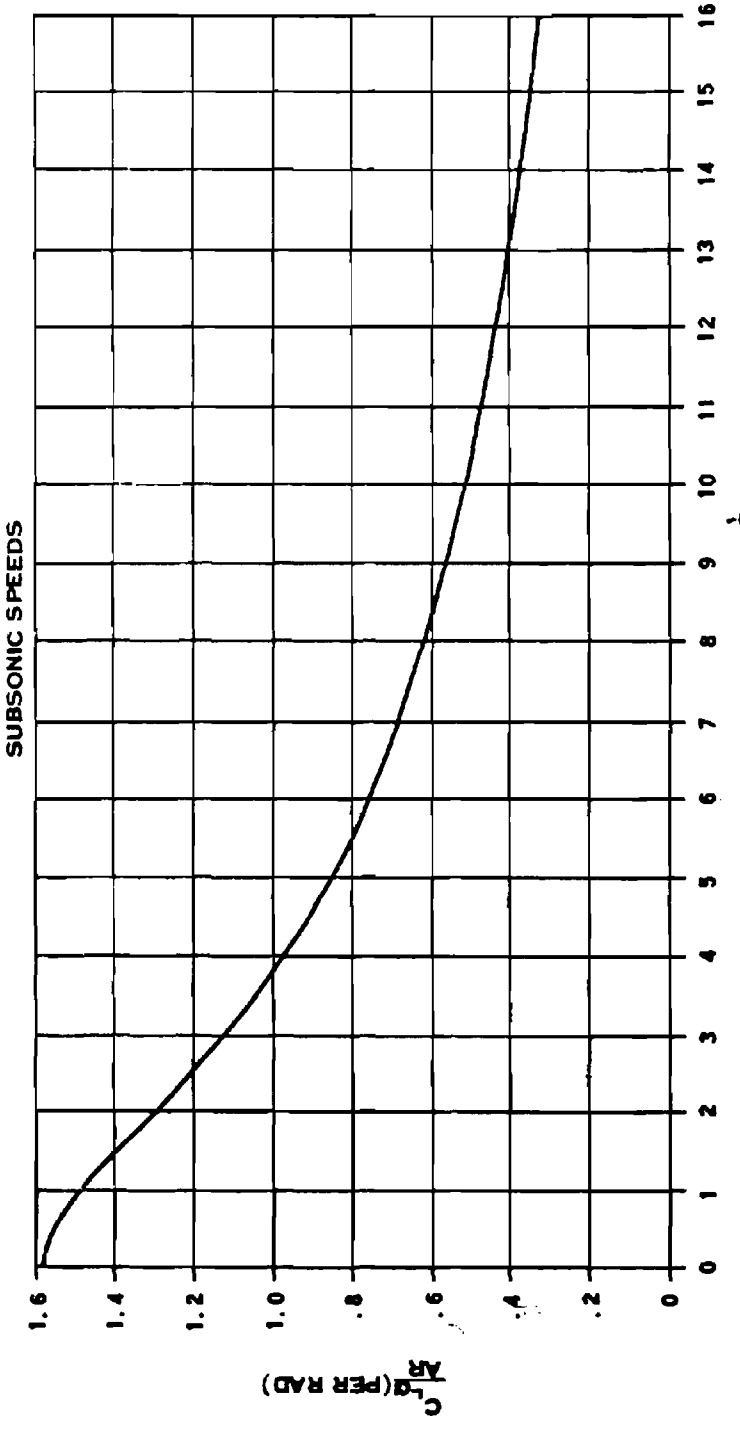

Figure 13-3. [redacted] Subsonic Wing Lift Curve Slope

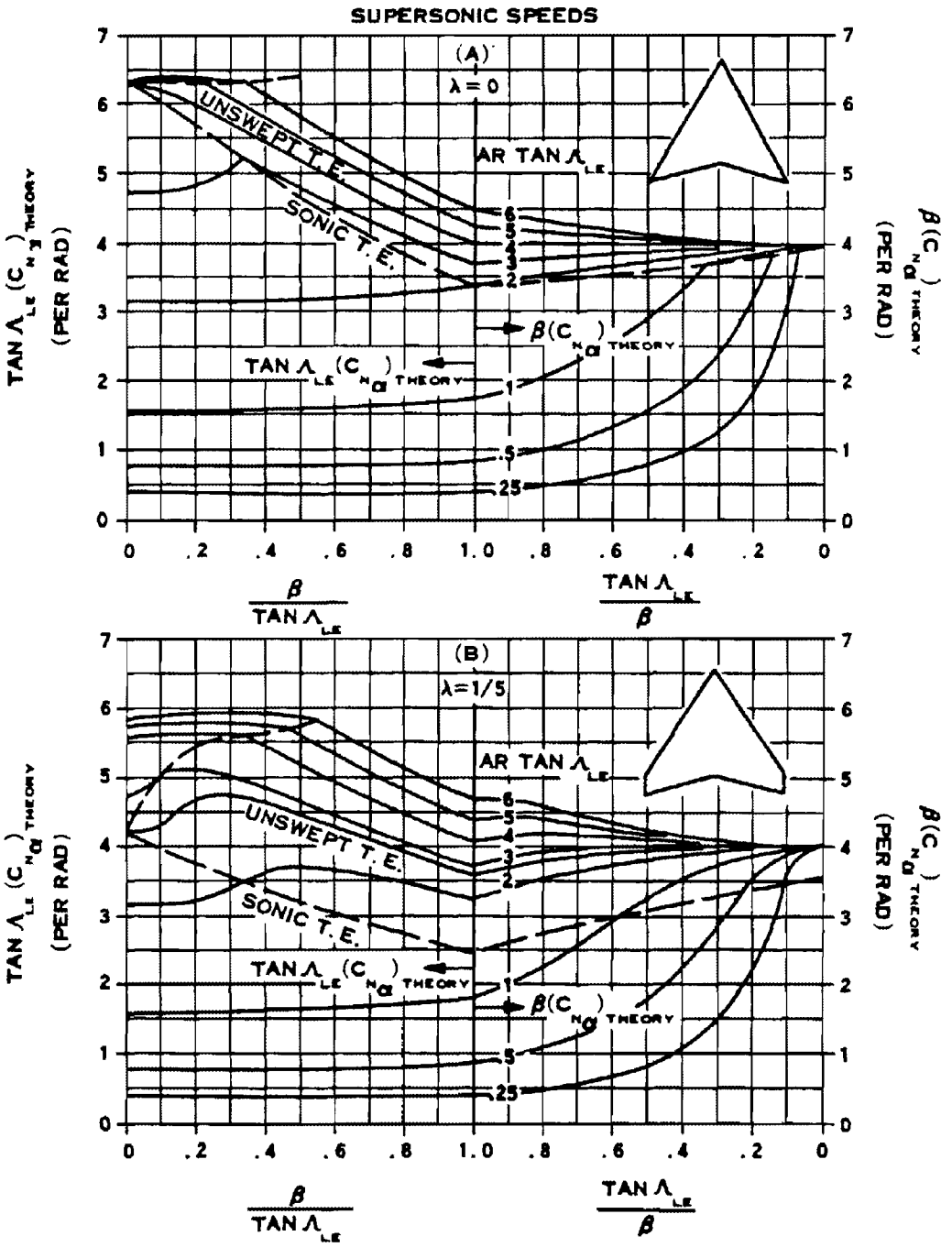

Figure 13-4a. [redacted] Wing Supersonic Normal Force Curve Slope [redacted]

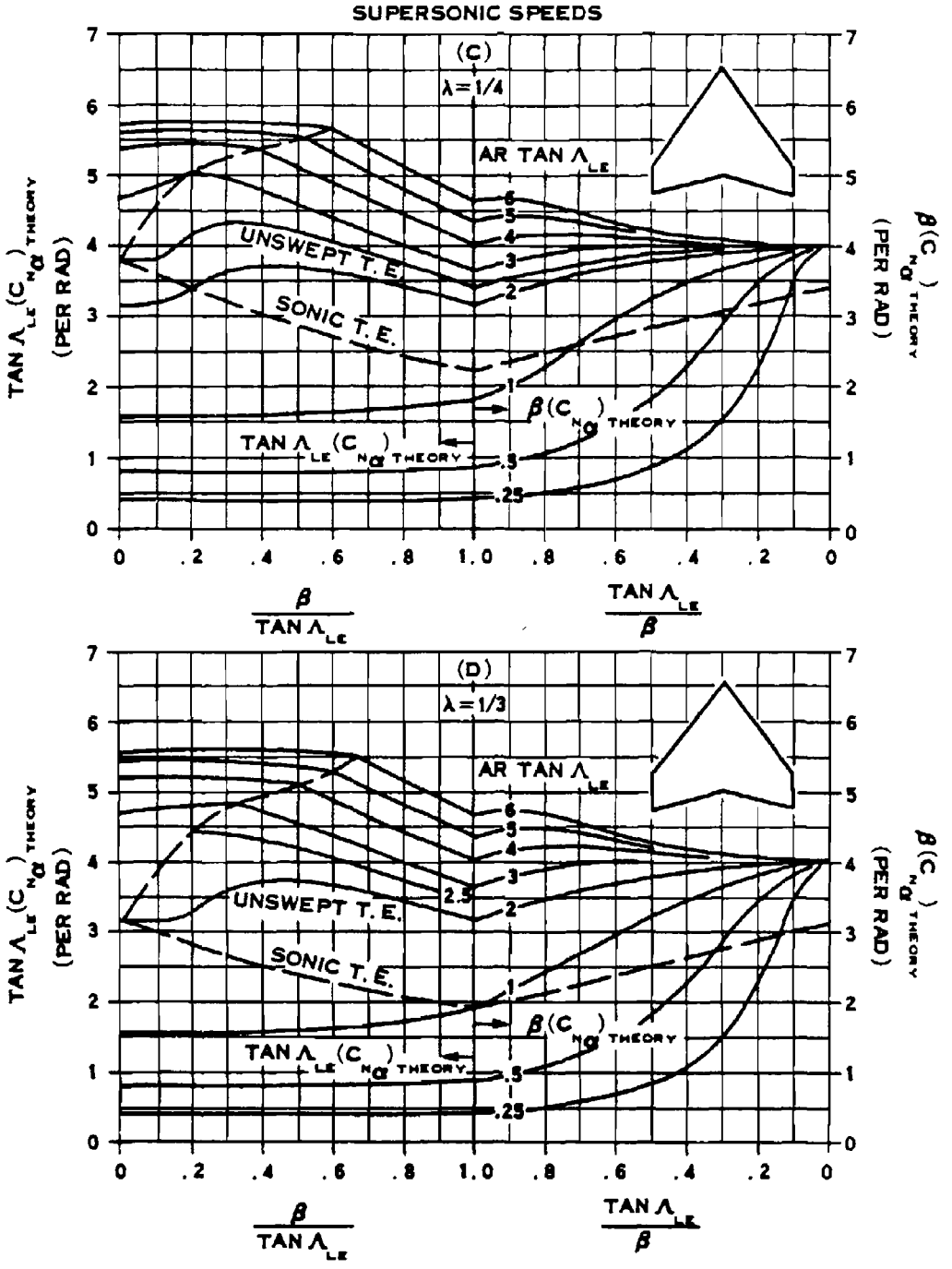

Figure 13-4b. [redacted] Wing Supersonic Normal Force Curve Slope [redacted]

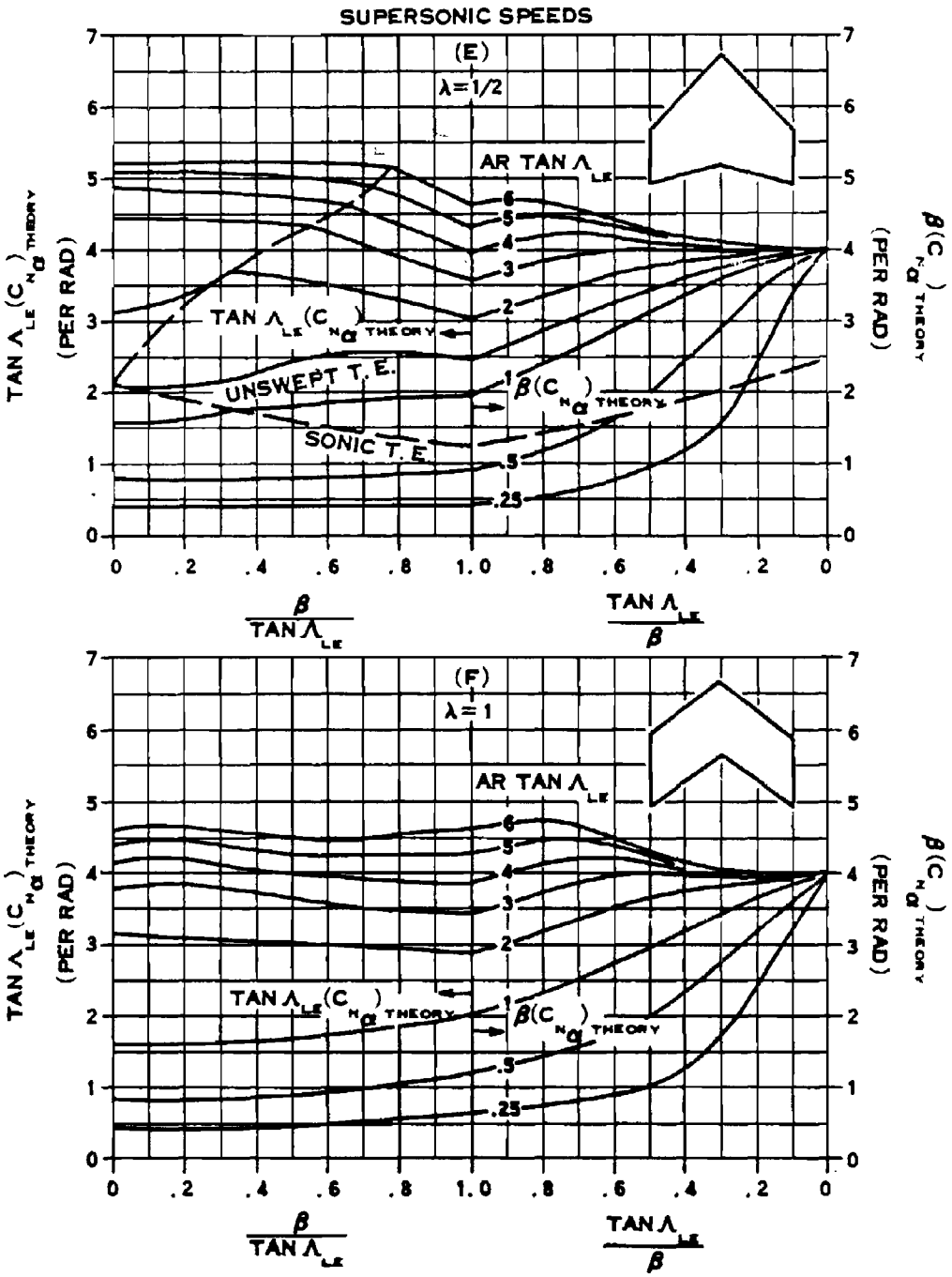

Figure 13-4c. [redacted] Wing Supersonic Normal Force Curve Slope [redacted]

Problem 13-2. Calculation of the Aerodynamic Coefficient for the Vertical Tail

An effective aspect ratio is derived to account for interference effects from the body and the horizontal tail to predict the lateral force on the vertical tail at subsonic speed:

$$AR_{\text{eff}} = \left\{\frac{(AR)_B}{AR}\right\}\left\{1 + K_H\left[\frac{(AR)_{HB}}{(AR)_B} - 1\right]\right\}(AR),$$

where AR is the aspect ratio of the isolated vertical tail, with the span and area of the vertical tail measured to the fuselage centerline; the factor $(AR)_B/AR$ is the ratio of the aspect ratio of the vertical tail in the presence of the fuselage to the aspect ratio of the isolated tail (this ratio is shown in Figure 13-5); the factor K_H accounts for the relative size of the horizontal and vertical tails, and it varies from 0 to about 1.1; and the factor $(AR)_{HB}/(AR)_B$ is the ratio of the vertical tail aspect ratio in the presence of *both* the horizontal tail and body to that of the vertical tail in the presence of the body alone, which varies from 0.9 to 1.2 for typical configurations. Within the accuracy goals of the present calculations, it is reasonable to take this ratio as unity, which gives

$$(AR)_{\text{eff}} = \left(\frac{(AR)_B}{AR}\right) AR.$$

A first approximation for the lift coefficient for the vertical tail, $\bar{C}_{L_\alpha}$, is determined from the wing lift curve slopes shown in Figures 13-3 and 13-4, using the effective aspect ratio $(AR)_{\text{eff}}$. The value of C_{L_α} should be corrected by an empirical factor k, which is a function of the vertical tail span and the body diameter:

$$C_{L_\alpha} = k\,\bar{C}_{L_\alpha}.$$

The diameter k may be obtained from Figure 13-6. All coefficients are based on the dynamic pressure and the elevation area of the isolated vertical tail.

For *direct* side-on blast orientation cases for parked aircraft, the normal force coefficient is obtained from drag data for flat plates in streams normal to the plates. Data indicate that a drag coefficient of 1.2 would apply to plates having an aspect ratio from unity to about 10, which essentially encompasses the range of aspect ratios for vertical tails of current aircraft. Therefore, for analysis of effects on side-on gusts on parked aircraft, a coefficient of 1.2 has been used.

The drag force on the fuselage also becomes important for parked aircraft subjected to side-on gusts. Values of the steady-state drag coefficient vary from about 0.35 to 1.2, depending upon the Reynolds number, which dictates whether the flow is laminar or turbulent. In the case of unsteady drag, a drag coefficient slightly below the laminar value of 1.2 appears to be applicable at early times. Therefore, a drag coefficient of 1.2 has been used for the fuselage for the analysis of the effects of side-on gusts on parked aircrafts.

For supersonic speeds, the slope of the lift coefficient curve C_{L_α} is estimated by the normal force slope for similar wings. In this calculation, C_{L_α} is computed for a wing having a planform of the isolated vertical tail plus its image about the fuselage centerline, using the method given in Problem 13-1, e.g., C_{L_α} is computed for the isolated vertical tail with its image as if it were a wing. The isolated vertical tail which extends from the tip to the fuselage centerline is considered; its area includes, in addition to the exposed part, that area within

the fuselage bounded by the extensions of the leading and trailing edges and the fuselage centerline.

The calculation of the aerodynamic coefficient for vertical tails is presented in the following steps. Several of the lengths and areas that are required already will have been determined in the particular response method being followed, which requires the calculation of C_{L_α} (see Problem 13-1).

1. Using the silhouette profile of the aircraft (for example, see Figures 13-1 and 13-2), from which lengths and surfaces may be found, determine the following:

S = vertical tail area (sq ft), defined by the extensions of the leading and trailing edges to the fuselage centerline.

c_r = vertical tail root chord (ft), i.e., the length along the fuselage centerline subtended by the leading and trailing edges.

c_t = vertical tail tip chord (ft), defined as the length along the fuselage centerline subtended by the vertical tail tip.

b = vertical tail span, fuselage centerline to tip (ft).

Λ_{LE} = sweepback angle of vertical tail leading edge, measured from the vertical (deg).

d = fuselage depth at the intersection of the vertical tail leading edge and the fuselage (ft).

M = Mach Number = V/c, where V is the velocity of the aircraft, and c is the ambient speed of sound.

2. Calculate the taper ratio λ:

$$\lambda = \frac{c_t}{c_r}$$

and the aspect ratio AR:

$$AR = \frac{b^2}{S}.$$

3. Calculation of the aerodynamic coefficient for the vertical tail depends on the value of the Mach number, M. Three regions are defined as follows:

Region 1: $M \leqslant 0.85$,

Region 2: $M \geqslant 1.2$,

Region 3: $0.85 < M < 1.2$.

Region 1. Steps a through g present the calculation of the aerodynamic coefficient for the vertical tail C_{L_α} for $M \leqslant 0.85$.

a. Calculate the value of β^2:

$$\beta^2 = 1 - M^2.$$

b. Determine the tangent of the sweep angle of the mid-chord line, $\tan \Lambda_{c/2}$:

$$\tan \Lambda_{c/2} = \tan \Lambda_{LE} - \frac{2}{AR}\left[\frac{1 - \lambda}{1 + \lambda}\right].$$

c. Calculate the parameter b/d. With the value of this parameter and the value of λ from step 2, enter Figure 13-5 to obtain the value of AR_B/AR.

d. Calculate the effective aspect ratio

$$(AR)_{eff} = \left(\frac{(AR)_B}{AR}\right) AR.$$

e. Compute the parameter

$$(AR)_{eff}\left[\beta^2 + \tan^2 \Lambda_{c/2}\right]^{1/2},$$

and enter Figure 13-3 with this parameter to obtain the value of C_{L_α}/AR.

f. With the value of b/d from step c, enter Figure 13-6 to obtain the value of k, an empirical factor, which is a function of the vertical tail span and the body diameter.

g. Calculate the aerodynamic coefficient for the vertical tail C_{L_α}:

$$C_{L_\alpha} = k \left(\frac{C_{L_\alpha}}{AR}\right) (AR)_{\text{eff}}.$$

Region 2. The calculation of C_{L_α} is the same as that given for Region 2, in Problem 13-1, except that AR is twice that calculated in step two of Problem 13-1, i.e.,

$$AR = 2\left(\frac{b^2}{S}\right).$$

The remaining steps are described once again below.

a. Calculate the value of β:

$$\beta = (M^2 - 1)^{1/2}.$$

b. Calculate the values of the parameters:

$$\frac{\beta}{\tan \Lambda_{LE}}$$

$$(AR) \tan \Lambda_{LE}.$$

c. Enter Figure 13-4 and select the figure corresponding to the taper ratio λ. Select the curve corresponding to the value of the parameter $(AR) \tan \Lambda_{LE}$. If

$$\frac{\beta}{\tan \Lambda_{LE}} < 1,$$

use the left side of the figure to obtain the value of $\tan \Lambda_{LE} C_{N_\alpha}$. Calculate C_{L_α} as follows:

$$C_{L_\alpha} = \frac{\tan \Lambda_{LE} C_{N_\alpha}}{\tan \Lambda_{LE}},$$

where the normal force coefficient C_{N_α} and C_{L_α} are taken to be equal within the scope of this method.

If

$$\frac{\beta}{\tan \Lambda_{LE}} > 1,$$

determine its reciprocal,

$$\frac{\tan \Lambda_{LE}}{\beta},$$

and use the right side of the figure to obtain the value of βC_{N_α}. The slope is calculated by:

$$C_{L_\alpha} = \frac{\beta C_{N_\alpha}}{\beta},$$

where C_N is represented as C_L within the scope of this method.

Region 3. The following steps, a through c, are used to calculate C_{L_α} for $0.85 < M < 1.2$.

a. Calculate C_{L_α} at $M = 0.85$ following the method in Region 1.

b. Calculate C_{L_α} at $M = 1.2$ following the method in Region 2.

c. Interpolate linearly for the slope at the actual Mach number:

$$C_{L_\alpha} = C_{L_\alpha} (\text{at } M = 0.85) + \frac{M - 0.85}{0.35}\left[C_{L_\alpha} (\text{at } M = 1.2) - C_{L_\alpha} (\text{at } M = 0.85)\right].$$

[redacted] No numerical example is provided with this problem since the procedures are so similar to those of Problem 13-1, and since the calculation of the aerodynamic coefficient for the vertical tail is not required for the calculation of the simplified gust loading sure-safe and sure-kill envelopes described in succeeding problems.

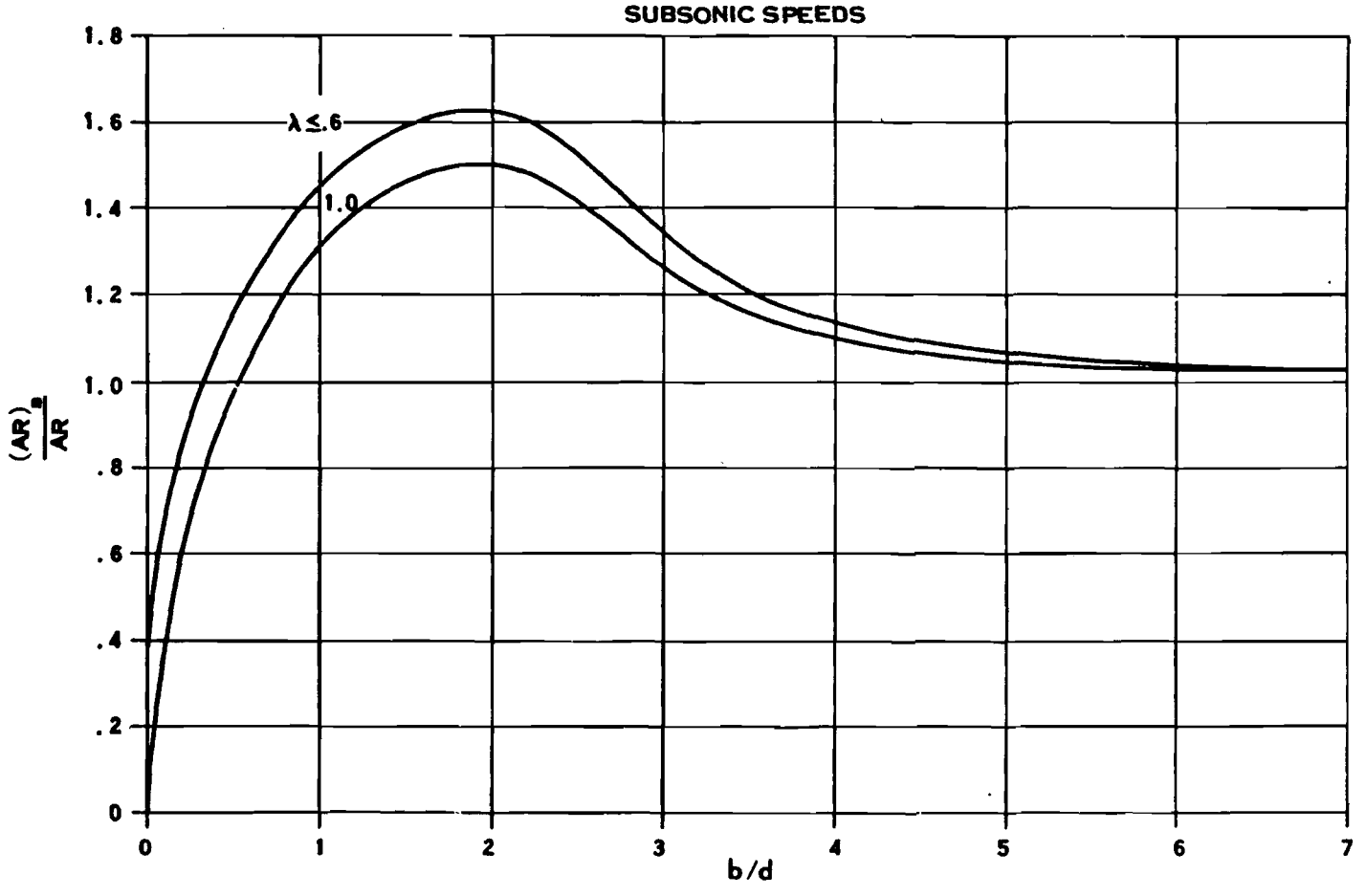

Figure 13-5. Ratio of the Aspect Ratio of the Vertical Tail in the Presence of the Body to That of the Isolated Vertical Tail at Subsonic Speeds

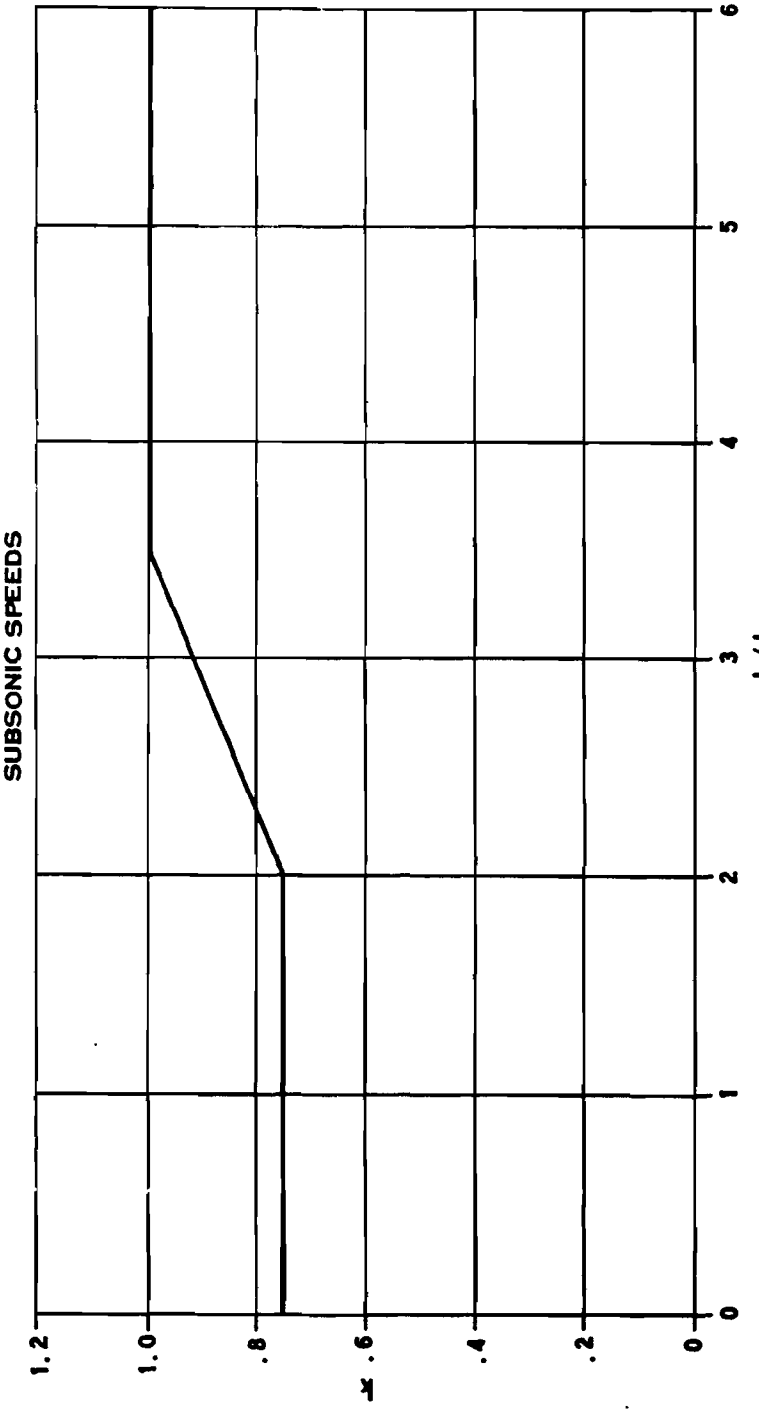

Figure 13-6. [redacted] Empirical Factor for Estimating C_{L_α} for Vertical Tails [redacted]

13-7 Gust Effects on In-Flight Aircraft

A nuclear explosion produces a blast wave that travels outward from the explosion, decaying in strength as it travels. The blast wave induces a flow velocity in the material (in this case, air), through which it passes. This material velocity, or gust, produces changes in the dynamic pressure and the angle of attack of an airplane that is intercepted by the blast wave. An increase in air density also is associated with the blast wave, and this increase in density also contributes to changing the dynamic pressure. The changes in angle of attack and dynamic pressure result in changes in the aerodynamic forces acting on the airplane. These changes in aerodynamic forces produce rigid-body and elastic motions of the airplane. In the sure-kill case, inelastic motions also are important. These motions produce additional aerodynamic forces. The aerodynamic forces and inertia forces may be summed to determine structural loads (such as bending moments) acting on the structure. Comparison of these structural loads with the allowable loads determines the safety of the airplane.

Gust effects on helicopters must be considered in two categories; first, the effects on the main rotor blades, and second, the effects on major components other than the main rotor blades. The second category of effects is very similar to the gust effects on airplanes. The only difference lies in the introduction of rotors as lift-producing devices. Helicopters have fuselages, horizontal tails, vertical tails, and, in some cases, even wings. These components may be analyzed in substantially the same way that the corresponding airplane components are analyzed.

The main rotor blades on the other hand, are unique to helicopters, and thus require special techniques. Three different types of blades must be considered: hinged, rigid (hingeless), and teetering. In the hinged version, a hinge somewhat offset from the center of rotation permits free rotation of the blade outboard of the hinge in an up-and-down, or flapping, direction. The rigid, or hingeless, blade does not use a flapping hinge. The teetering blade roughly combines the characteristics of the hinged and hingeless blades. A teetering blade is essentially a seesaw about a hinge at the center of rotation. The blades on each side of the hinge are rigidly connected.

Problems 13-3 and 13-4 describe the calculation of intercept-time envelopes for sure-safe and sure-kill regions for airplanes and helicopters, respectively.

13-8 Gust Effects on Parked Aircraft

The material velocity and the increased density behind the blast wave give rise to a dynamic pressure that may be sufficiently high to impose large aerodynamic forces on a parked vehicle. For purposes of damage analysis, dynamic pressure effects are classified in two categories:

1. Direct damage to structural components that result from aerodynamic loading.

2. Gross aircraft motions that might produce indirect damage to structural components as a result of lifting the aircraft from the ground and the subsequent impact, or as a result of overturning the aircraft or crushing the landing gear.

The possibility of lifting the aircraft exists whenever the vehicle is subjected to lift forces that are comparable to the vehicle weight, even if tie-downs are employed. An aircraft with a low wing loading (gross weight divided by the wing area, GW/S) is particularly susceptible to this type of damage since, in the parked position, the wing is set at a large angle of attack relative to the ground. Head-on encounter presents the most severe loading condition for this case.

[redacted]

[redacted] Skidding is possible whenever the drag, coupled with the lift, can overcome the frictional forces between the ground and the vehicle tires. With a large lift force, the normal force between ground and tire is reduced. The side force required to cause the vehicle to skid may thus be quite small compared with the weight of the vehicle. Vehicle orientations somewhere between head-on and side-on to the gust are expected to present the worst situation for this type of motion. No definitive criteria can be given for damage from skidding, because the damage criteria depend upon the distance of the aircraft from other objects.

[redacted] In some cases, the vehicle will overturn before skidding. Overturning will occur whenever the aerodynamic moments (about an axis joining appropriate wheel contact points) are of sufficient magnitude to overcome the stabilizing gravity moment and the frictional forces are sufficiently large to prevent skidding. A gust orientation somewhere between head-on and side-on is expected to provide the most severe condition. Other effects will almost always be predominant compared to overturning, and it is exceedingly difficult to devise a meaningful overturning solution that does not involve a substantial computer program.

[redacted] Negative lift results from tail-on encounters (blast approaching from the rear). The negative lift produces downward forces on the wheels, which, if sufficiently large, will damage the landing gear and perhaps the main supporting structure.

[redacted] Tie-downs would be expected to reduce the likelihood of lift-off, skidding, and overturning; however, tests have indicated that tie-downs are not very effective in reducing damage induced by motion when aircraft encounter high strength blast waves.

[redacted] Since helicopters do not have the large lifting surfaces that are present on airplanes, the problems of lift-off and crushing of the landing gear are much less severe for helicopters than for airplanes.

[redacted] Overpressure usually dictates the largest envelopes among all of the damage modes for parked aircraft. No calculation methodology is presented for gust effects on parked aircraft. The sure-safe and sure-kill overpressure envelopes may be accepted as the complete envelopes (see paragraph 13-9 and Problem 13-5).

[redacted]

[redacted]

Problem 13-3. Calculation of Intercept-Time Envelopes that Determine Sure-Safe and Sure-Kill Regions with Respect to Material Velocity on Airplanes in Flight

[redacted] The analysis of gust effects on airplanes in flight is based upon determining the load factor produced on the airplane during the blast encounter, accounting roughly for the fact that this load factor is dynamically applied, and comparing the resultant effective load factor with the critical load factor. For sure-safe conditions, the critical load factor is based upon design limit conditions. For sure-kill conditions, the critical load factor is based upon design ultimate conditions and a lethal ratio factor. The lethal ratio factor is determined from a simple representation of post-failure response by a single degree of freedom system.

[redacted] Standard shapes for the gust envelopes at intercept time are assumed applicable for all airplanes, weapon yields, and altitudes. Each point on the envelope shows the critical position of the airplane relative to the burst point at the time when the airplane is intercepted by the blast wave. The size of the envelopes is determined by evaluating the critical slant ranges, or distances from the burst point, associated with intercepts of the airplane from directly above, below and to the side.

[redacted] The three slant ranges R_a, R_b, and R_s that represent critical distances from above, below and to the side of the airplane, respectively, from which intercept-time envelopes are determined, must be calculated. The data required for the calculations include:

h = airplane altitude (ft),

W = weapon yield (kt),

GW = airplane gross weight at time of interest (lbs),

V = preblast airplane velocity (ft/sec),

n = airplane preblast load factor (for a level flight, $n = 1$) (dimensionless),

N^+ = up-loading airplane limit load factor corresponding to gross weight condition being considered (dimensionless),

N^- = down-loading airplane limit load factor corresponding to gross weight condition being considered (N^- should be used as a negative number) (dimensionless),

Wing planform (see Figure 13-1).

Calculation of the three slant ranges for sure-safe conditions is performed by the following series of steps.

1. Enter Table 13-1 with the airplane altitude, h, to obtain P, the ambient pressure (psi), ρ, the ambient density (slugs/ft^3), and c, the ambient speed of sound (ft/sec).

2. Calculate the Mach number, M:

$$M = \frac{V}{c}.$$

With M, and data defining wing planform, calculate the slope of the lift coefficient curve for the wing, C_{L_α}, using the method described in Problem 13-1.

3. Enter Figure 13-7 and select the curve corresponding to GW, airplane gross weight. Obtain the value of DF, the dynamic factor corresponding to the weapon yield, W.

4. To determine the slant range, R_a, for a burst from above

$$N = N^-,$$

where N is the critical load factor.

[redacted]

5. If

$$n < 0 \text{ and } N < 0,$$

or

$$n < 0 \text{ and } N > 0,$$

reverse the signs of both n and N. Otherwise, leave the signs as they were calculated. If

$$n < 0.01,$$

set

$$n = 0.01.$$

Thus, n will become positive in this step, regardless of its original sign.

6. Calculate $\Delta L/L$, ratio of the incremental lift due to blast to the preblast value of lift as follows:

$$\frac{\Delta L}{L} = \left[\frac{N}{n} - 1\right]\left[\frac{1}{(DF)}\right].$$

7. Calculate w/c, the ratio of the component of the airplane velocity normal to the wing (w) to the speed of sound:

$$\frac{w}{c} = \frac{2n\ (GW)}{\rho\ VSC_{L_\alpha}c},$$

where S is the airplane wing area, and the other symbols have been defined.

8. Calculate the product of $\Delta L/L$ and w/c.

9. Select the curve in Figure 13-8 corresponding to the value of w/c obtained in step 7. Enter the graph with the value of $(w/c)\ (\Delta L/L)$ obtained in step 8, and read the corresponding value of the range parameter $\bar{R}$. If N is positive, use Figure 13-8a. If N is negative, use Figure 13-8b.

10. Compute R_a, the range (ft), which defines the distance at which a nuclear explosion would produce critical effects, as follows:

$$R_a = \bar{R}\left[\frac{14.7\ W}{P}\right]^{1/3}.$$

11. Repeat steps 4 through 10 to calculate R_b. In step 4, set

$$N = N^+$$

for bursts from below, and replace R_a with R_b in the equation of step 10.

12. Set

$$N = N^+,$$

and $n = 1$ (corresponding to straight on level flight). Repeat steps 6 through 10 to calculate R_s (R_s replaces R_a in the equation of step 10). A burst from the side is taken to be equivalent to a burst from below with the airplane in straight and level flight.

13. The ranges R_a, R_b, and R_s define the size of the standard sure-safe envelopes as illustrated in Figure 13-9. R_a represents the diameter of a sphere above the airplane; R_b is the diameter of a sphere below; and R_s is the diameter of a sphere to the side of the airplane. The X-Y plane is the plane of symmetry of the airplane, with the preblast velocity vector pointing in the direction of the positive X-axis; the Y-axis points in the direction of the right wing; the Z-axis is directed upward, thus determining an orthogonal, left-handed system. The envelopes are symmetric with respect to the X-Z plane.

[redacted] Calculation of the slant ranges R_a, R_b, and R_s, that define the size of the standard envelopes at intercept time for sure-kill conditions is performed by the following series of steps:

1. Follow steps 1 through 3 in the calculation of the ranges for sure-safe conditions.

[redacted]

2. Enter Figure 13-10 and select the curve corresponding to GW, airplane gross weight. With weapon yield, W, obtain the value of LR, the lethal ratio.

3. To determine R_a, the slant range for burst from above, calculate N, the critical load factor:

$$N = (1.5)(N^-)(LR),$$

where the factor 1.5 is the usual factor between limit load and ultimate load. Follow steps 5 through 10 in the calculation for sure-safe conditions.

4. To determine R_b for burst from below, calculate N:

$$N = (1.5)(N^+)(LR),$$

and follow steps 5 through 10 in the calculation for sure-safe conditions.

5. To determine R_s, the slant range for burst from the side, calculate N:

$$N = (1.5)(N^+)(LR)$$

and let $n = 1$ since burst from the side is taken as burst from below corresponding to a straight and level flight. Repeat steps 6 through 10 in the calculation for sure-safe conditions.

6. Construct the sure-kill envelopes as described in step 13 in the calculation for sure-safe conditions.

[redacted]

DNA (4)(1)

[redacted]

PAGE 13-32 DELETED

[redacted]

[redacted]

[redacted]

[redacted]

DNA (6)(1)

The resulting intercept time envelopes are illustrated in Figure 13-9.

[redacted] *Reliability:* A typical airplane is used to represent each airplane class for purposes of defining a dynamic factor and a lethal ratio factor. The airplane is in a symmetric flight prior to blast intercept. This definition includes a straight and level flight. All degrees of freedom are ignored except for the two previously mentioned. The atmosphere is assumed homogeneous, having characteristics associated with the altitude at which the airplane is flying. The standard shapes for the gust envelopes at intercept time are assumed to be applicable for all airplanes, weapon yields, and altitudes. The maximum error in the calculation is estimated to be a factor of 2.

[redacted] *Related Material:* See paragraphs 13-1, 13-2, 13-6, and 13-7. See also Table 13-1.

[redacted]

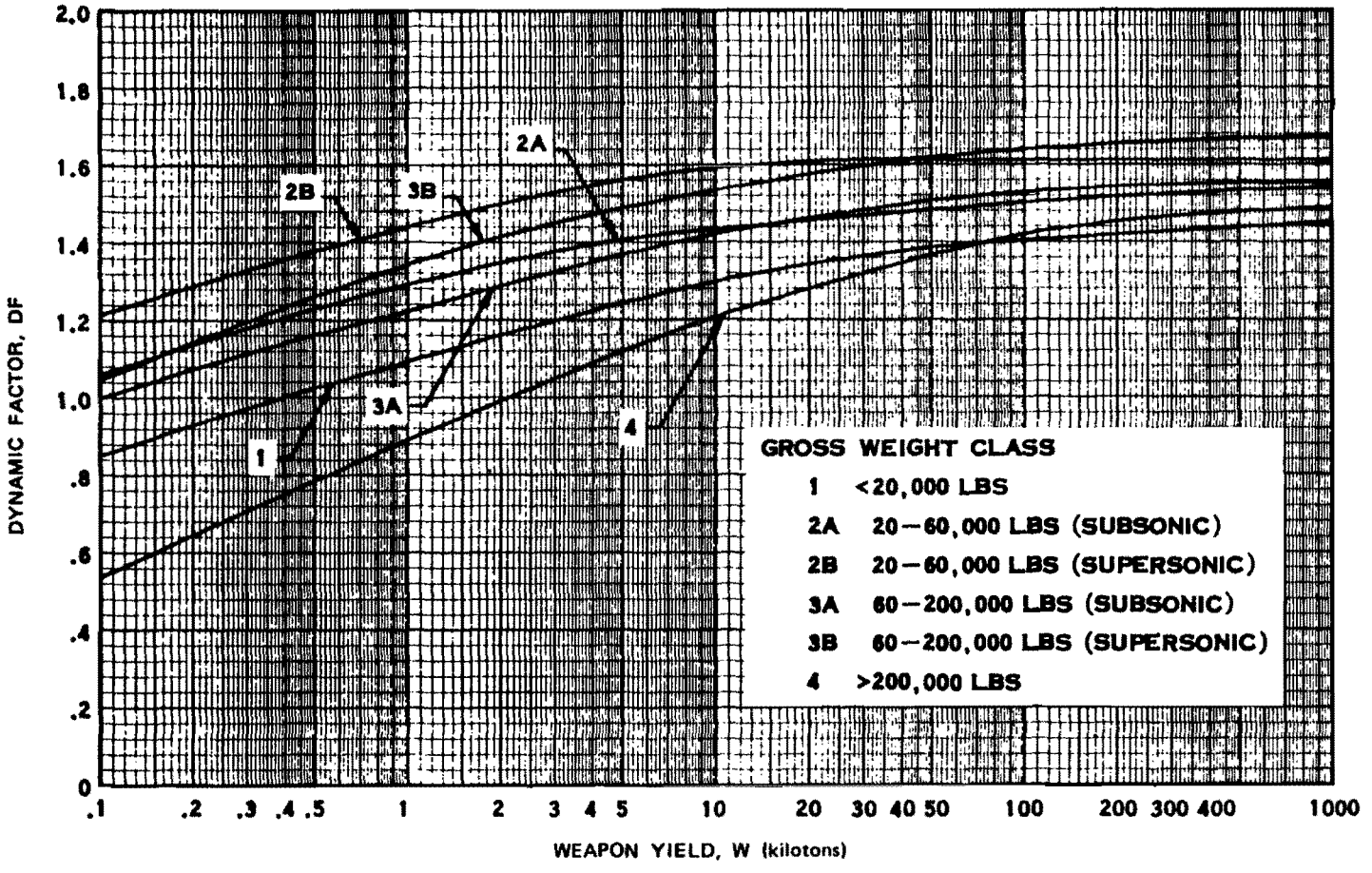

Figure 13-7. [redacted] Dynamic Factor vs Weapon Yield [redacted]

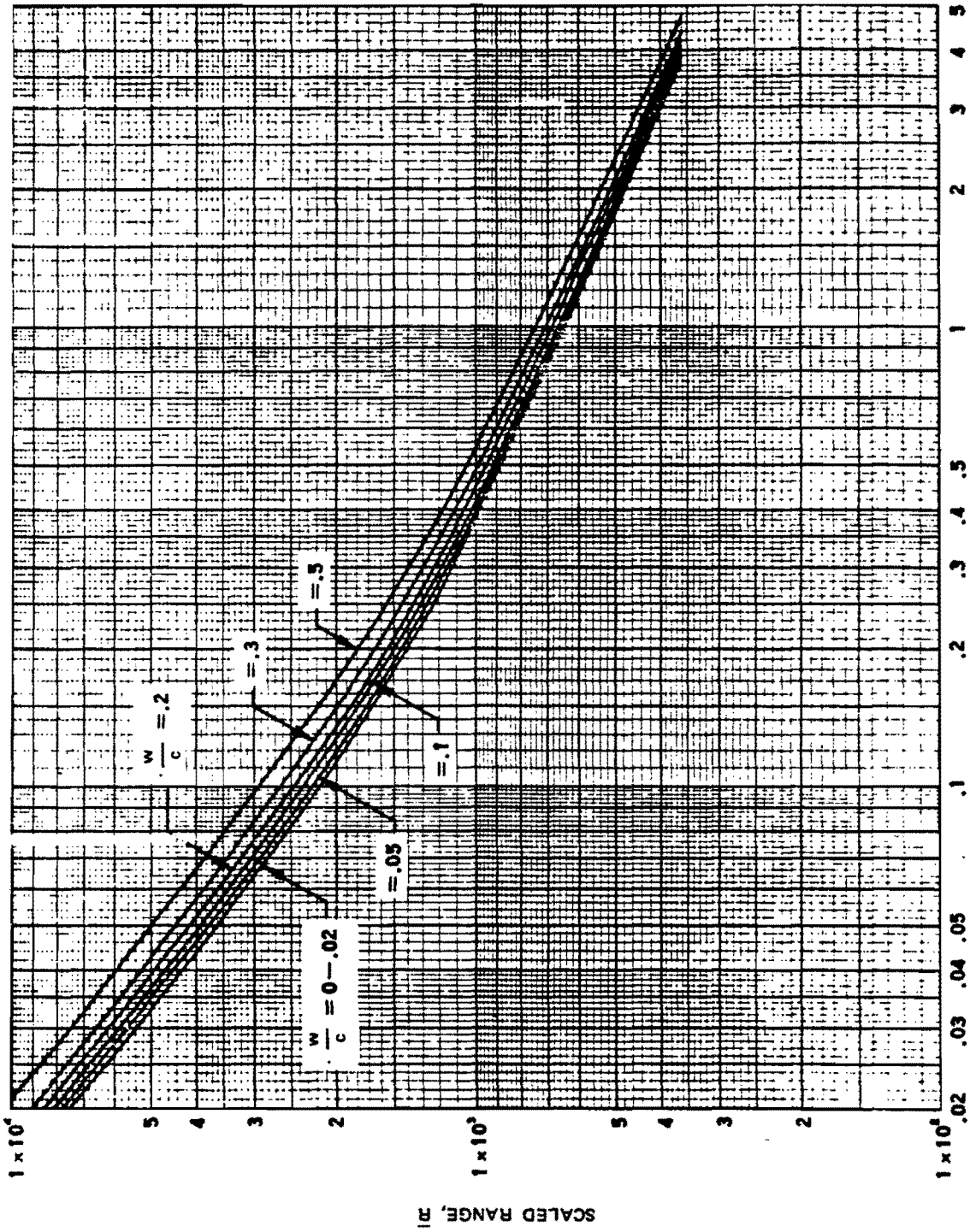

Figure 13-8a. $\frac{w}{c} \times \frac{\Delta L}{L}$ as a Function of Scaled Range (N > 0)

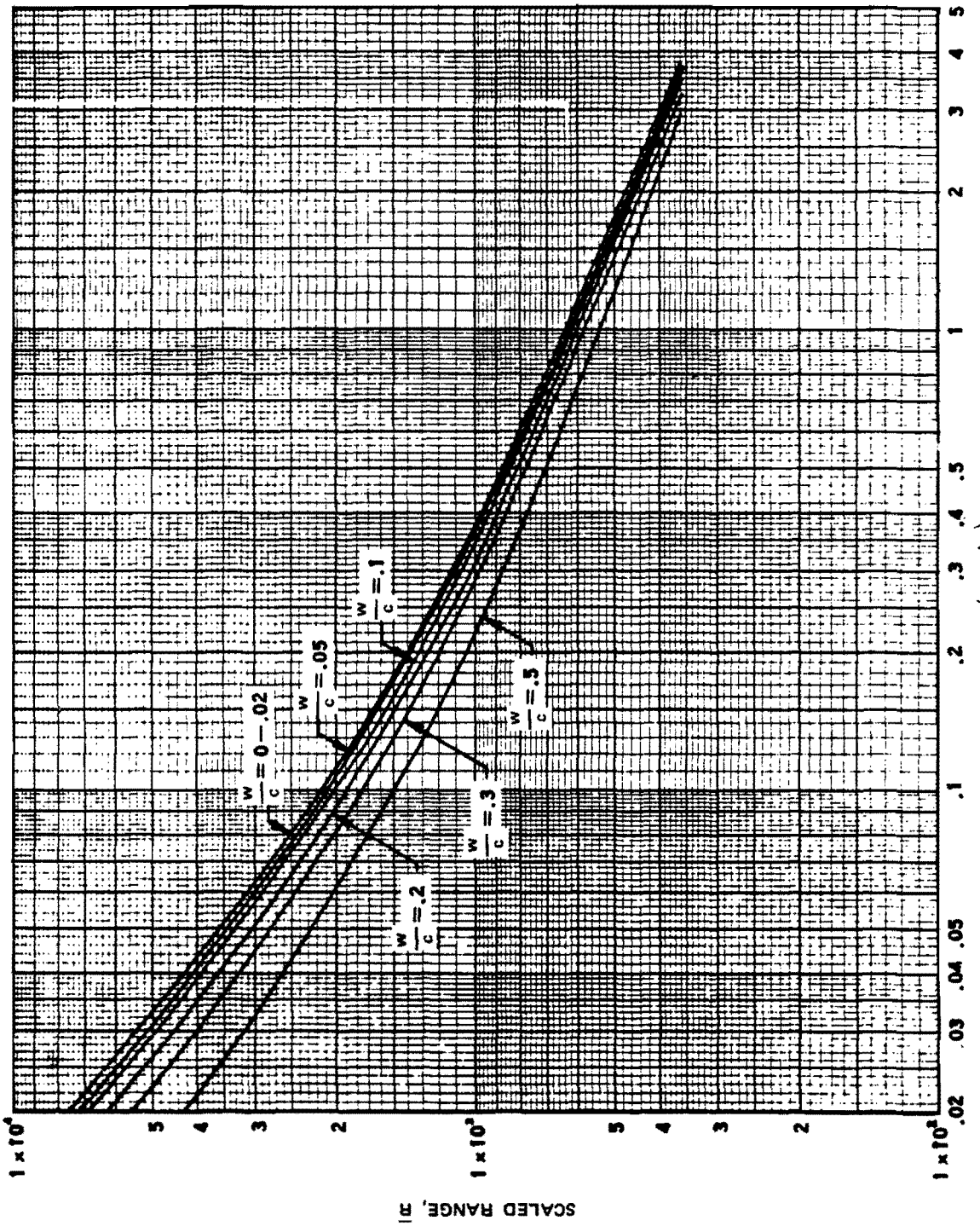

Figure 13-8b. [redacted] $\frac{w}{c} \times \frac{\Delta L}{L}$ as a Function of Scale I Range ($N < 0$) [redacted]

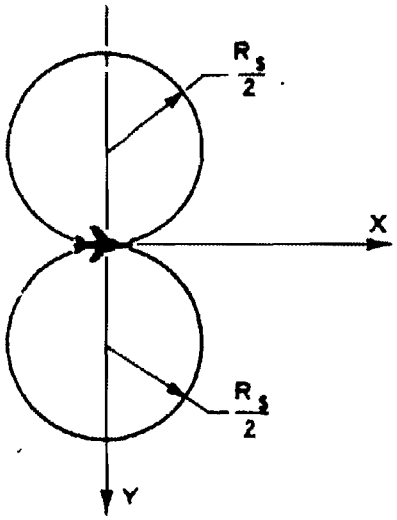

TOP VIEW (SECTION IN X–Y PLANE)

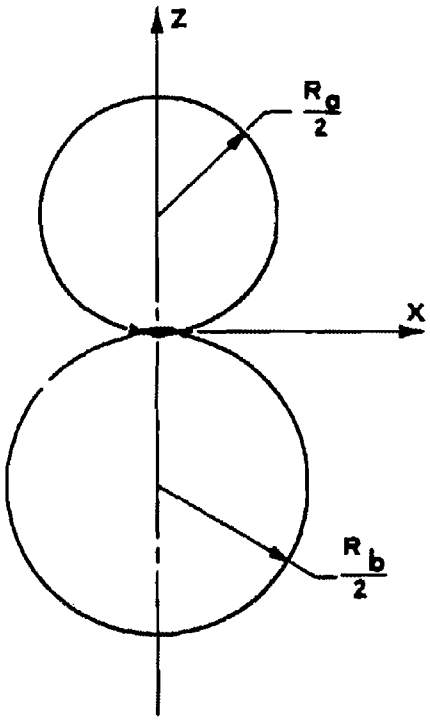

SIDE VIEW (SECTION IN X–Z PLANE)

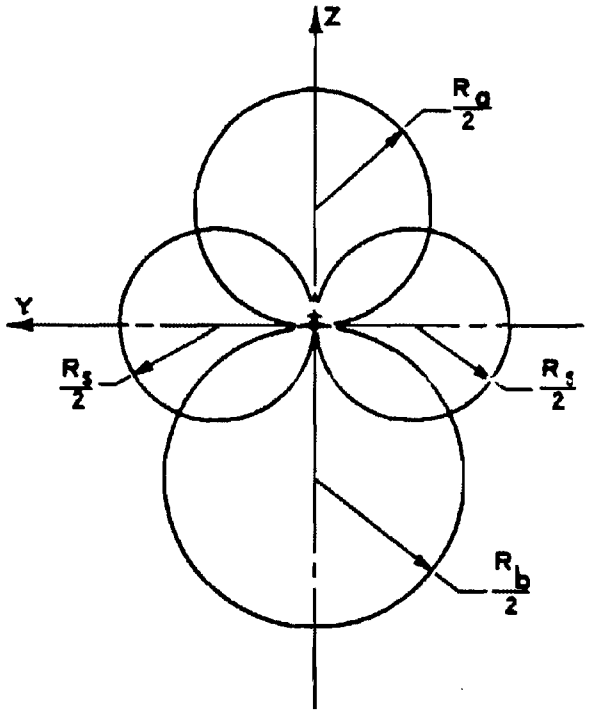

FRONT VIEW (SECTION IN Y–Z PLANE)

Figure 13-9. [redacted] Standard Shapes for Gust Envelopes at Intercept Time [redacted]

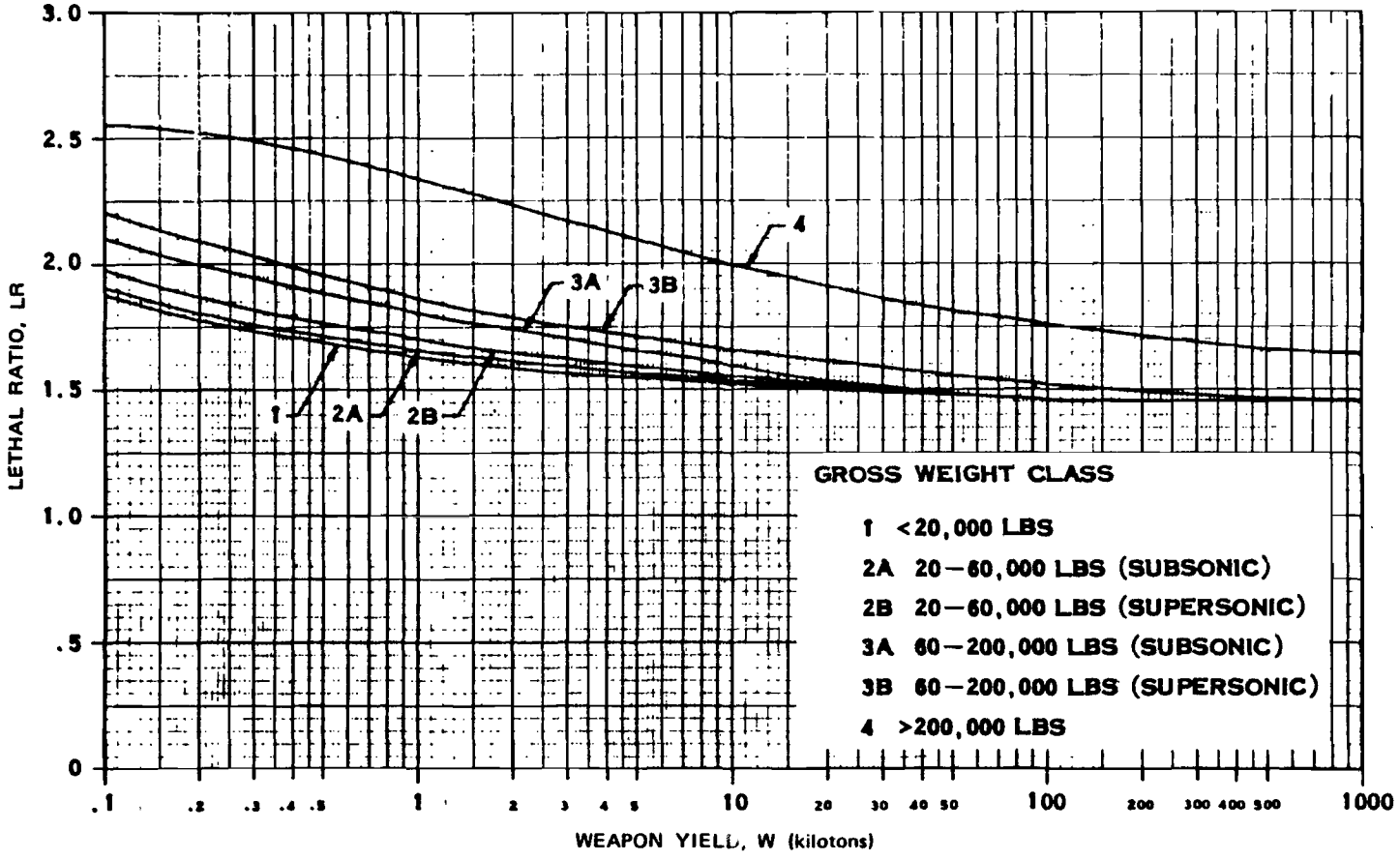

Figure 13-10. [redacted] Lethal Ratio vs Weapon Yield [redacted]

Problem 13-4. Calculation of Intercept-Time Envelopes Determining Sure-Safe and Sure-Kill Regions with Respect to Gust Effects of the Material Velocity Behind the Blast Wave on Helicopters in Flight

The analysis of gust effects on helicopters is based upon determining the load factor produced during the blast encounter, accounting roughly the fact that this incremental load factor is dynamically applied, and comparing the resultant effective load factor with the critical load factor. For sure-safe conditions, the critical load factor is based upon design limit conditions. For sure-kill conditions, the critical load factor is based upon design ultimate conditions and a lethal ratio factor.

Gust effects on helicopters must be considered in two categories: first, the effects on the main rotor blades (hinged, rigid and teetering); and second, the effects on major components other than the main rotor blades, which are very similar to the gust effects on airplanes.

The constraints in the calculation are as follows:

- Representative values of helicopter parameters can be used in defining a dynamic factor and a lethal ratio factor. All other calculations involve the actual helicopter characteristics.
- The helicopter is in a symmetric maneuver prior to blast intercept. This definition includes straight and level forward or hovering flight.
- For a hinged blade, blade response to gust is not considered in this problem; the flapping of a teetering rotor is not considered in the calculation.
- The lift distribution along the blade is linear, starting at zero at the hub and fitted to the actual running lift at the 3/4 blade span position.
- Rigid-body motions of the helicopter are neglected, and the rotor tilt angle is ignored.
- Inflow resulting from the gust is considered to occur too late to influence the response. The effect of the preblast inflow on dynamic pressure is ignored.
- The preblast atmosphere is homogeneous, having characteristics associated with the altitude at which the helicopter is flying.
- Standard shapes for the gust envelopes at intercept time are applicable for all helicopters, weapon yields, and altitudes.

The envelopes calculated in this problem are intercept-time envelopes. The size of the envelopes is determined by evaluating the critical slant ranges, or distances from the burst point, associated with intercepts of the helicopter from directly above, below and to the side.

The three slant ranges R_a, R_b, and R_s representing the critical distances from above, below and to the side, respectively, are calculated first for sure-safe conditions in the following series of steps. The data that are required for the calculations include:

h = helicopter altitude (ft)

W = weapon yield (kt)

GW = helicopter gross weight at time of interest (lbs)

V = preblast helicopter velocity (ft/sec)

Ω_{MR} = main rotor angular velocity (rad/sec)

R_{MR} = main rotor blade radius (ft)

c_{MR} = main rotor blade chord (ft)

b_{MR} = number of blades in main rotor (dimensionless)

n = helicopter preblast load factor; for straight and level flight, $n = 1$ (dimensionless)

N^+ = up-loading helicopter limit load factor corresponding to gross weight condition being considered (dimensionless)

N^- = down-loading helicopter limit load factor corresponding to gross weight condition being considered. Note: N^- should be used as a negative number (dimensionless)

Wing planform (if helicopter has wings).

1. Determine the ambient atmospheric conditions at helicopter altitude h from Table 13-1; P, the ambient pressure (psi); ρ, the ambient density (slugs/ft^3); and c, ambient speed of sound (ft/sec).

2. If the helicopter has no wings, or if a helicopter having wings is hovering, i.e., $V = 0$, go to step 4. Otherwise, calculate the total wing area, S_W, which is defined as the extension of the leading and trailing edges of both wings to the helicopter centerline (ft^2).

3. Using the wing planform (Figure 13-2), with the Mach Number, M, equal to zero, calculate the slope of the lift coefficient curve for the wing, $C_{L_\alpha}^W$, using the method described in Problem 13-1. Let $C_{L_\alpha}^{MR} = 5.7$, where $C_{L_\alpha}^{MR}$ is the lift curve slope for the main rotor.

4. Enter Figure 13-11 with the weapon yield, W, and obtain the corresponding value of DF, the dynamic coefficient.

5. To determine the slant range, R_a, for a burst from above

$$N = N^-,$$

where N is the critical load factor.

6. If

$$n < 0 \text{ and } N < 0,$$

or

$$n < 0 \text{ and } N > 0,$$

reverse the signs of both n and N. Otherwise, leave the signs as they were calculated. If

$$n < 0.01,$$

set

$$n = 0.01.$$

Thus, n will become positive in this step, regardless of its original sign.

7. Calculate $\Delta L/L$, the ratio of the incremental lift due to blast to the preblast value of lift as follows:

$$\frac{\Delta L}{L} = \left[\frac{N}{n} - 1\right]\left[\frac{1}{(DF)}\right].$$

8. Calculate the parameter η:

a. If the helicopter has wings,

$$\eta = \frac{2n\,(GW)}{\rho c\left[\frac{1}{2}C_{L_\alpha}^{MR}\left(b_{MR}R_{MR}c_{MR}\right)\Omega_{MR}R_{MR} + C_{L_\alpha}^{W}VS_W\right]}.$$

b. If the helicopter has no wings,

$$\eta = \frac{2nGW}{\rho c\left[\frac{1}{2}C_{L\alpha}^{MR}\left(b_{MR}R_{MR}c_{MR}\right)\Omega_{MR}R_{MR}\right]}$$

9. Obtain the product

$$\left[\frac{\Delta L}{L}\right]\eta.$$

10. Enter Figure 13-12a if $N > 0$ or 13-12b if $N < 0$, and select the curve corresponding to the value of η from step 8. With the value of

$$\left[\frac{\Delta L}{L}\right]\eta$$

from step 9, obtain the range parameter $\bar{R}$.

[redacted]

[redacted]

11. Compute R_a, the range (ft), which defines the distance at which a nuclear explosion would produce critical effects, as follows:

$$R_a = \bar{R}\left[\frac{14.7\ W}{P}\right]^{1/3}.$$

12. Repeat steps 5 through 11 to calculate R_b. In step 5, set

$$N = N^+$$

for bursts from below, and replace R_a with R_b in the equation of step 10.

13. Set

$$N = N^+,$$

and $n = 1$ (corresponding to straight on level flight). Repeat steps 7 through 11 to calculate R_s (R_s replaces R_a in the equation of step 10). A burst from the side is taken to be equivalent to a burst from below with the helicopter in straight and level flight.

14. The ranges R_a, R_b, and R_s define the size of the standard sure-safe envelopes as illustrated in Figure 13-13. R_a represents the diameter of a sphere above the helicopter; R_b is the diameter of a sphere below; and R_s is the diameter of a sphere to the side of the helicopter. The X-Y plane is the plane of symmetry of the helicopter with the preblast velocity vector pointing in the direction of the positive X-axis; the Y-axis points to the right side of the helicopter; the Z-axis is directed upward, thus determining an orthogonal, left-handed system. The envelopes are symmetric with respect to the X-Z plane.

(U) Calculation of the slant ranges R_a, R_b, and R_s, that define the size of the standard envelopes at intercept time for sure-kill conditions is performed by the following series of steps.

1. Follow steps 1 through 4 in the calculation of the ranges for sure-safe conditions.

2. Enter Figure 13-14 with weapon yield, W, and obtain the value of LR, the lethal ratio.

3. To determine R_a, the slant range for burst from above, calculate N, the critical load factor:

$$N = (1.5)(N^-)(LR),$$

where the factor 1.5 is the usual factor between limit load and ultimate load. Follow steps 6 through 11 in the calculation for sure-safe conditions.

4. To determine R_b for burst from below, calculate N:

$$N = (1.5)(N^+)(LR),$$

and follow steps 6 through 11 in the calculation for sure-safe conditions.

5. To determine R_s, the slant range for burst from the side, calculate N:

$$N = (1.5)(N^+)(LR)$$

and let $n = 1$ since burst from the side is taken as burst from below corresponding to a straight and level flight. Repeat steps 7 through 11 in the calculation for sure-safe conditions.

6. Construct the sure-kill envelopes as described in step 14 in the calculation for sure-safe conditions.

[redacted]

PAGES 13-42 THRU 13-43 DELETED

[redacted]

[redacted]

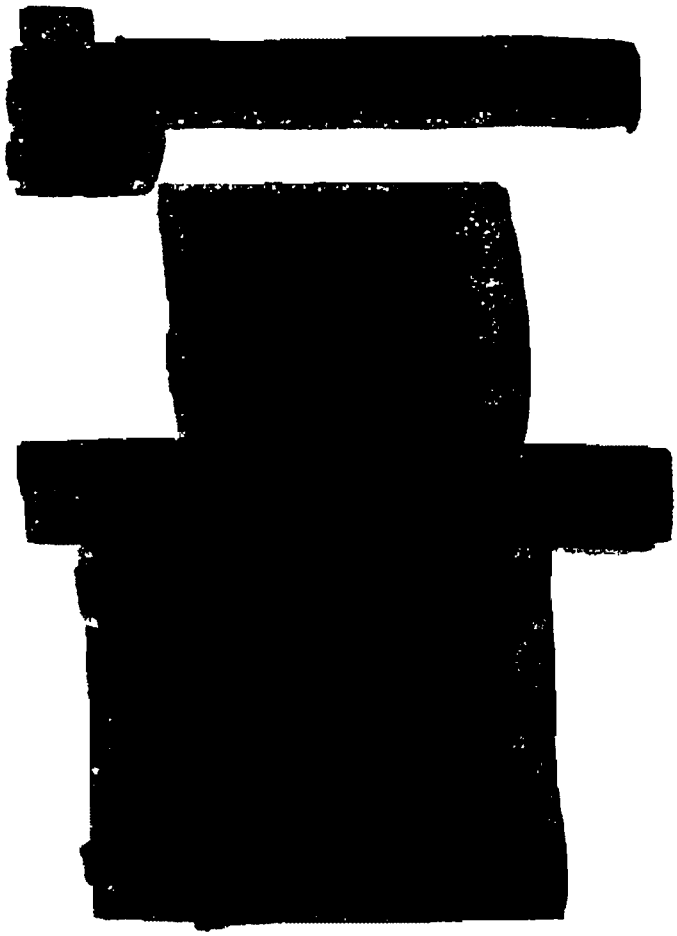

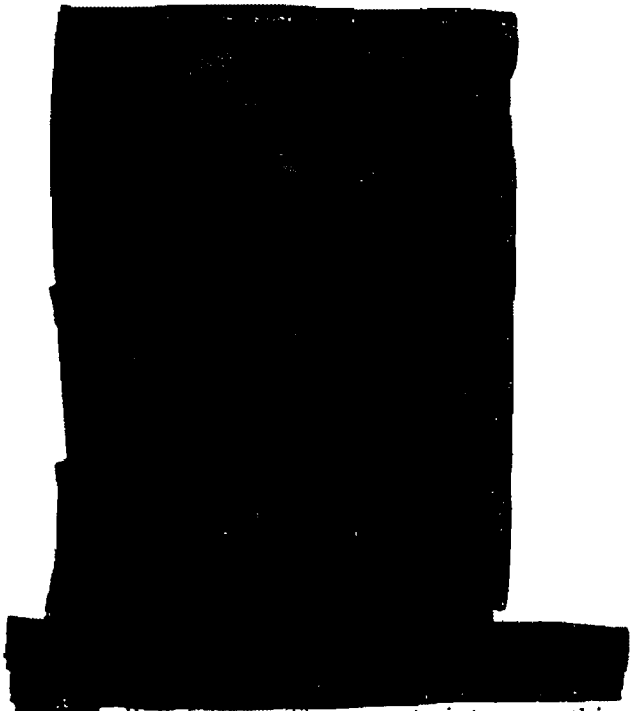

DNA
(4-X1)

[redacted] *Reliability:* The constraints on this method of calculation were described in the introductory paragraphs of this problem. The maximum error is a factor of 2.5.

[redacted] *Related Material:* See paragraphs 13-6 and 13-7, and Problem 13-1. See also Table 13-1.

[redacted]

[redacted]

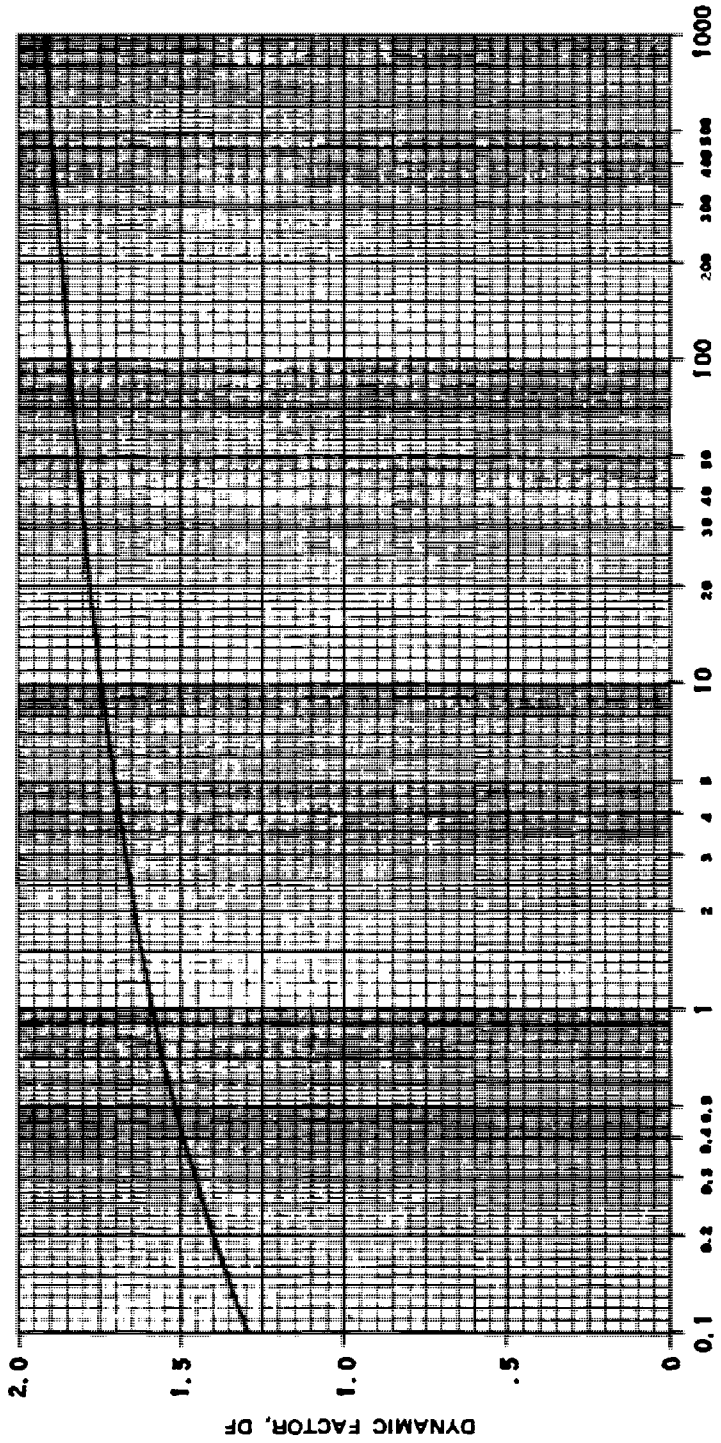

Figure 13-11. [redacted] Dynamic Factor vs Weapon Yield

[redacted]

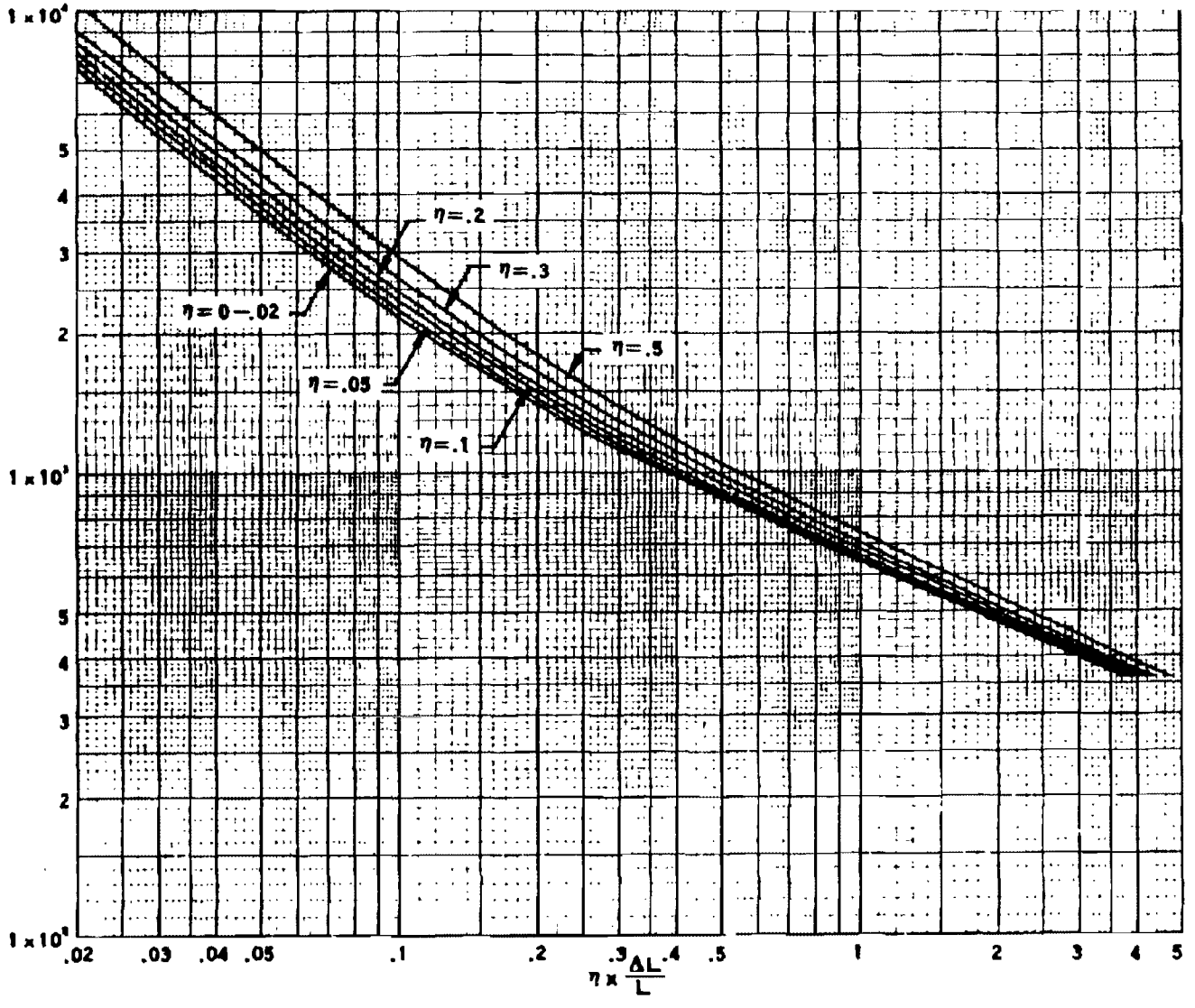

Figure 13-12a. $\eta \times \frac{\Delta L}{L}$ as a Function of Scaled Range (N > 0)

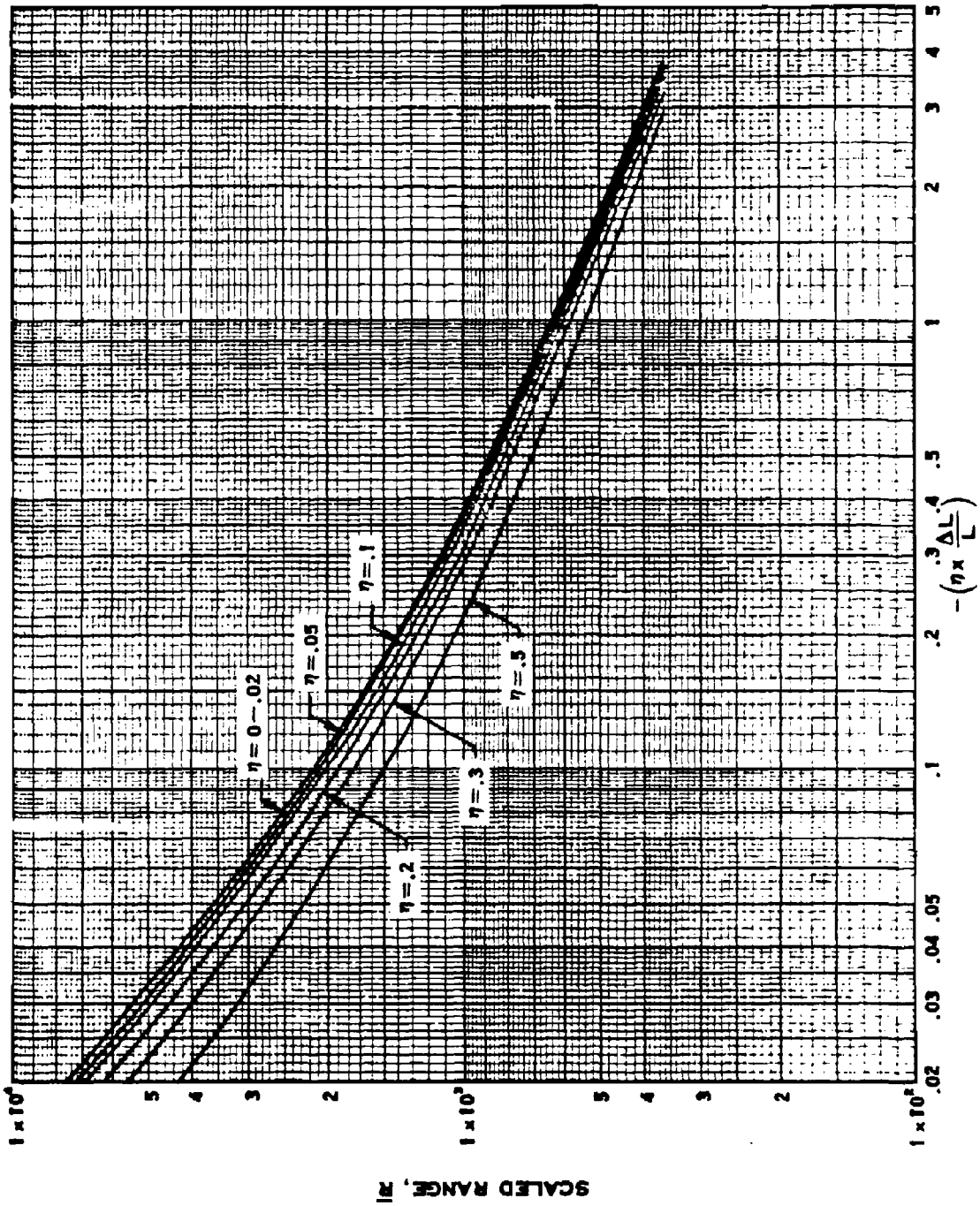

Figure 13-12b. [redacted] $\eta \times \frac{\Delta L}{L}$ as a Function of Scaled Range ($N < 0$)

[redacted]

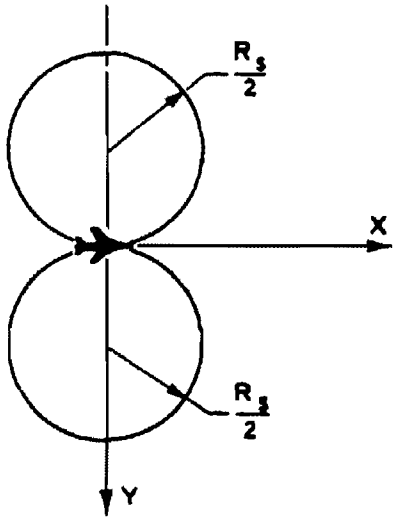

TOP VIEW (SECTION IN X–Y PLANE)

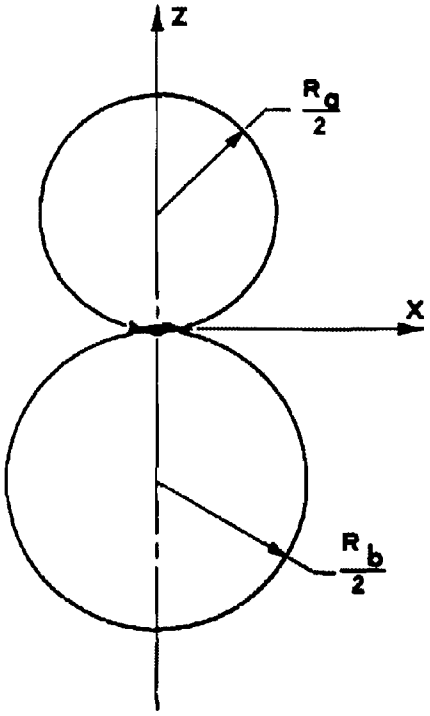

SIDE VIEW (SECTION IN X–Z PLANE)

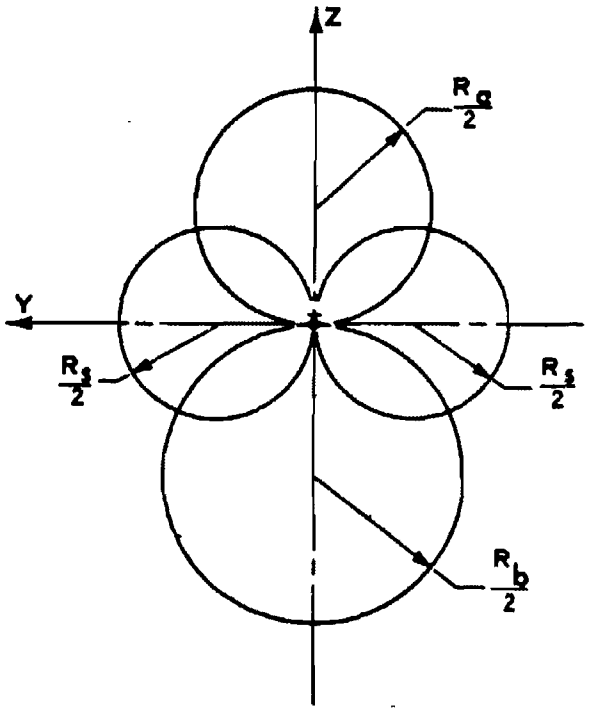

FRONT VIEW (SECTION IN Y–Z PLANE)

Figure 13-13. [redacted] Standard Shapes for Gust Envelopes at Intercept Time [redacted]

[redacted]

[redacted]

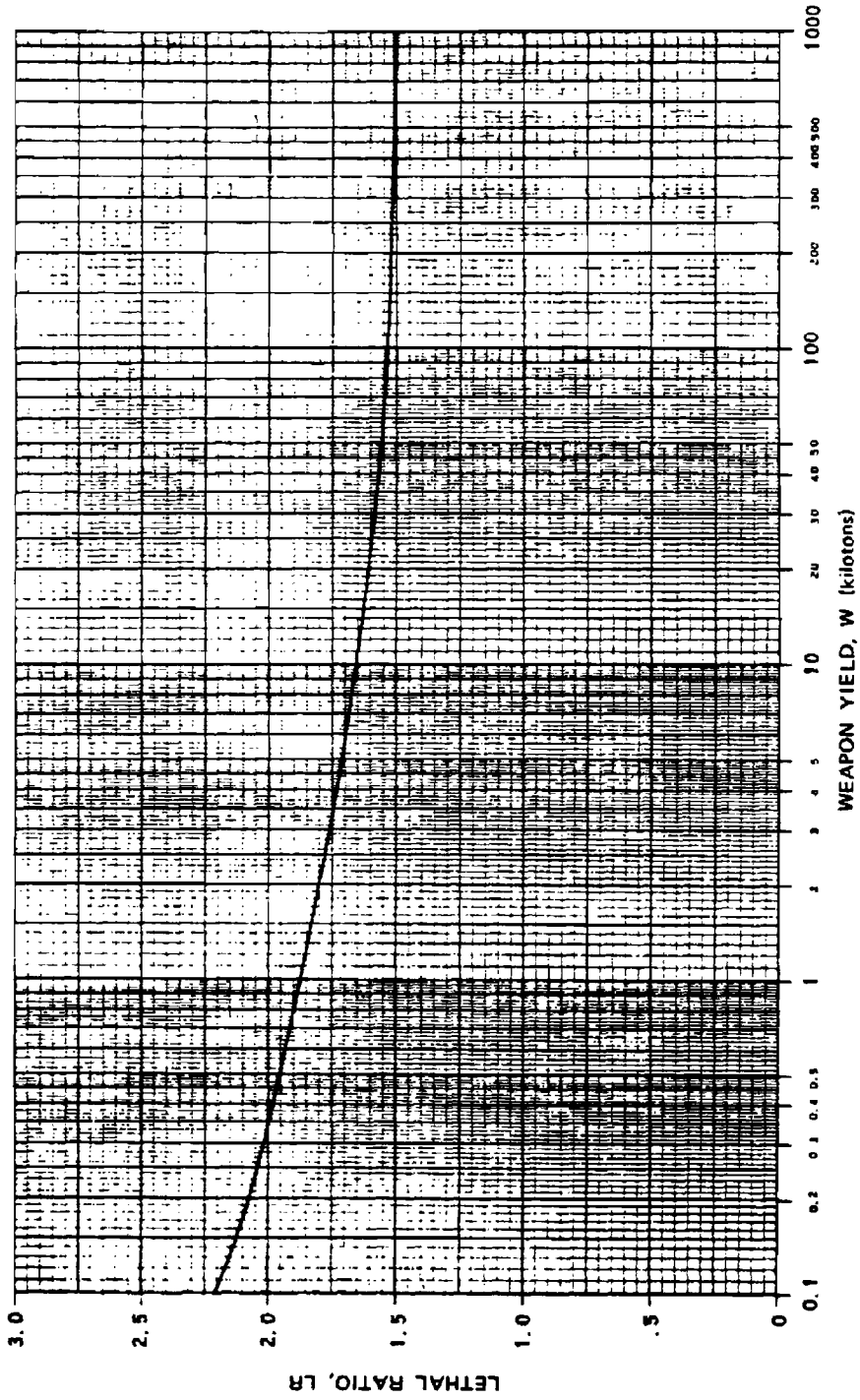

Figure 13-14. [redacted] Lethal Ratio vs Weapon Yield

[redacted]

[redacted]

[redacted] AIRCRAFT RESPONSE TO OVERPRESSURE EFFECTS [redacted]

13-9 Overpressure Effects on In-Flight and Parked Aircraft [redacted]

[redacted] If an aircraft is located in the vicinity of the nuclear explosion, the expanding blast wave eventually engulfs the aircraft. Depending on the distance of the aircraft from the burst, the pressure rise, or overpressure, experienced by an aircraft can be of a sufficient magnitude to damage the structural components.

[redacted] An aircraft subjected to an overpressure loading can experience structural damage in several ways. Skin panels may yield or rupture; longerons, stringers, and frames may fail by compressive yielding or local buckling. The fuselage generally is the most susceptible to these types of damage; hence, *only the fuselage is examined for overpressure effects.* The method presented in this section for analyzing overpressure damage is applicable to all types of aircraft and helicopters both in-flight and parked. Methods for performing the analysis are given in Problem 13-5.

[redacted]

[redacted]

Problem 13-5. Calculation of the Boundaries in Space that Define the Sure-Safe and Sure-Kill Regions with Respect to the Effects of Overpressure Behind the Blast Wave on Aircraft In-Flight or Parked

[redacted] As discussed in paragraph 13-9, overpressure loading can produce structural damage in several ways: however, since the fuselage generally is the most susceptible item, only fuselage damage is considered in the following analysis.

[redacted] The major constraints in the analysis are:

- Overpressure damage to an aircraft is the same for all aircraft in a given class.
- The preblast atmosphere is homogeneous, having characteristics associated with the aircraft altitude.

[redacted] The data required for the analysis are aircraft altitude (ft), weapon yield, and aircraft class. Table 13-2 lists various aircraft classes and corresponding overpressure limits for sure-safe and sure-kill conditions.

[redacted]

[redacted]

[redacted] The overpressure analysis is performed in a series of steps as described below.

1. Determine the ambient pressure P at the aircraft altitude, h, from Table 13-1.

2. Knowing the class of aircraft being considered, obtain the critical overpressure level, Δp, for either sure-safe or sure-kill conditions from Table 13-2.

3. Using the value of the critical overpressure, determine the corresponding value of sea level overpressure by the scaling law given in paragraph 2-14, i.e.,

$$\Delta p_o = \frac{P_o \Delta p}{P} = \frac{14.7\ \Delta p}{P},$$

where the subscript zero indicates sea level values of overpressure and ambient pressure, and the absence of a subscript indicates the corresponding values at altitude h.

4. Enter Figure 13-15* with Δp_o, and determine the corresponding slant range, R_1, from a 1 kt explosion in a sea level atmosphere.

5. Calculate the corresponding slant range, R, for a yield of W kt,

$$R = R_1 \left[\frac{14.7\ W}{P}\right]^{1/3}.$$

6. The critical volume is defined by a sphere of radius R centered on the aircraft. For in-flight aircraft, continue to step 7; for parked aircraft, go to step 8.

7. The volume defined in step 6 is an intercept-time volume; that is, each point on the surface shows the critical position of the aircraft relative to the burst point at the time when the aircraft is intercepted by the blast wave. Ordi-

* [redacted] Figure 13-15 is identical to Figure 2-2, Chapter 2. It is reproduced here for convenience of the user.

[redacted]

narily, burst-time volumes are desired for in-flight aircraft, rather than intercept-time volumes. A point on a burst-time volume defines the critical position of the aircraft relative to the burst point at the time of burst. Thus, a sure-kill burst-time volume shows the regions in space, relative to the airplane, in which the explosion of a given size nuclear weapon will result in the destruction of the aircraft. This is the information that ordinarily is desired. To obtain the burst-time volume, it is necessary to transform the intercept-time volume obtained in step 6 into a burst-time volume. This transformation is demonstrated in Problem 13-7. This concludes the analysis for in-flight aircraft.

8.* For parked aircraft only, the sphere found in step 6 (more properly, the hemisphere) must be modified for ground reflection effects. Enter Figure 13-16 with sea level overpressure determined in step 3, and read three horizontal range parameters, $\overline{HR}_i$ ($i = 1, 2, 3$).

9. Enter Figure 13-17 with $\overline{HR}_i$ and read three corresponding burst height parameters, $\overline{BH}_i$ ($i = 1, 2, 3$). (Note $\overline{BH}_1$ is always zero.)

10. Calculate the burst heights and horizontal ranges, in feet.

$$BH_i = \overline{BH}_i \left[\frac{14.7\ W}{P}\right]^{1/3}$$

$$HR_i = \overline{HR}_i \left[\frac{14.7\ W}{P}\right]^{1/3}.$$

11. Plot the burst height versus horizontal range, by connecting the three points determined in step 10. Draw a radial line from the origin to point 3. The volume defined by rotating this envelope about a vertical axis through the aircraft is the ground-effects volume, which is to be combined with the hemisphere already found. Ground reflection effects are seen to add a "collar" around the base of the hemisphere.

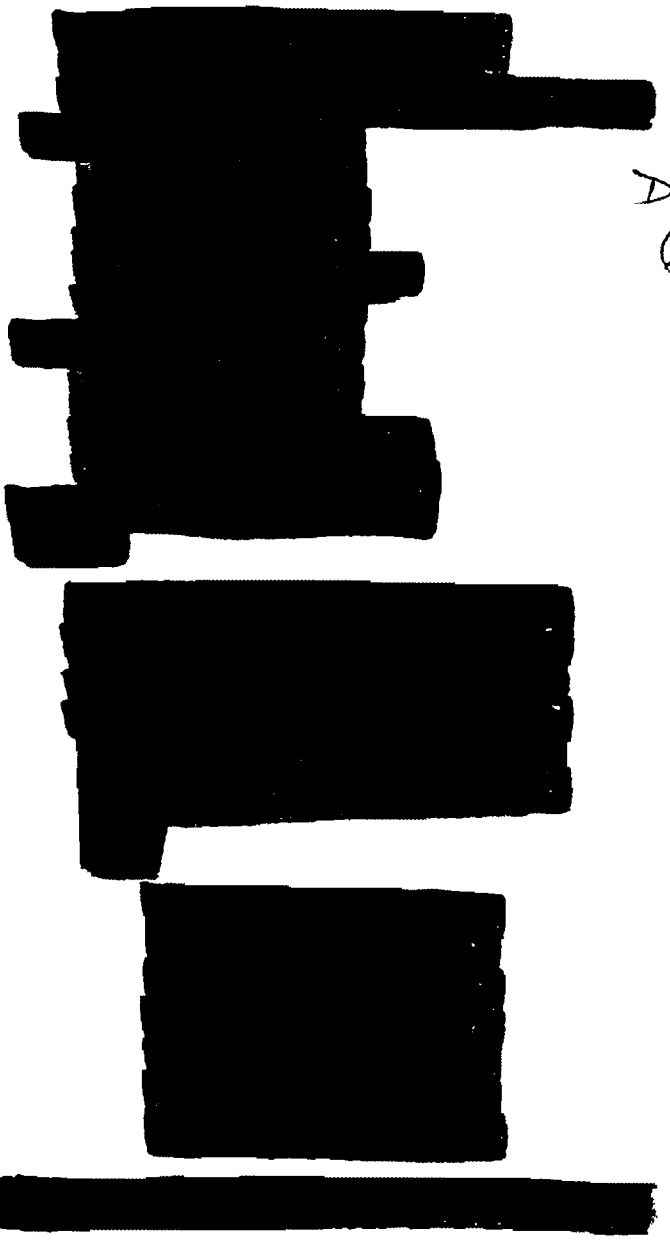

* The envelope generated by following steps 8 through 11 could be obtained by using the air blast height of burst curves in Chapter 2; however, these steps (and the accompanying figures) present the information in a more convenient form that is suitable to the accuracy of this analysis.

[redacted]

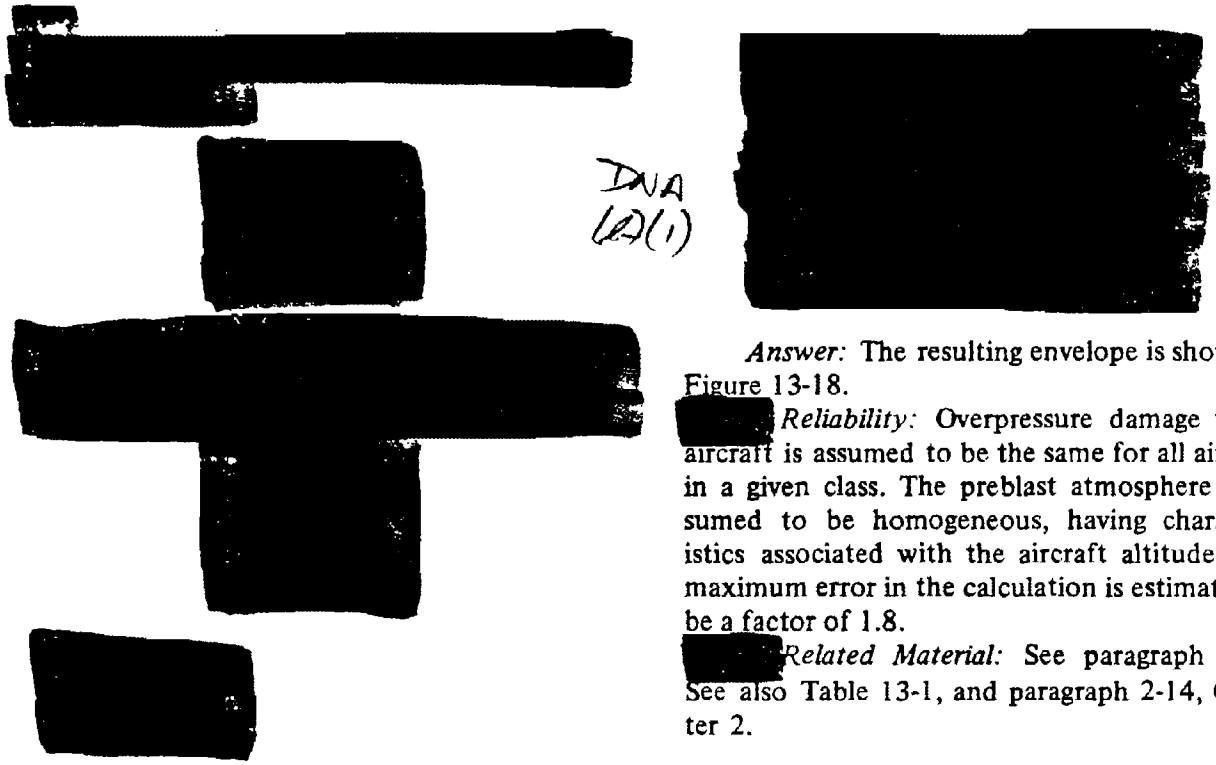

Answer: The resulting envelope is shown in Figure 13-18.

[redacted] *Reliability:* Overpressure damage to an aircraft is assumed to be the same for all aircraft in a given class. The preblast atmosphere is assumed to be homogeneous, having characteristics associated with the aircraft altitude. The maximum error in the calculation is estimated to be a factor of 1.8.

[redacted] *Related Material:* See paragraph 13-9. See also Table 13-1, and paragraph 2-14, Chapter 2.

[redacted]

[redacted]

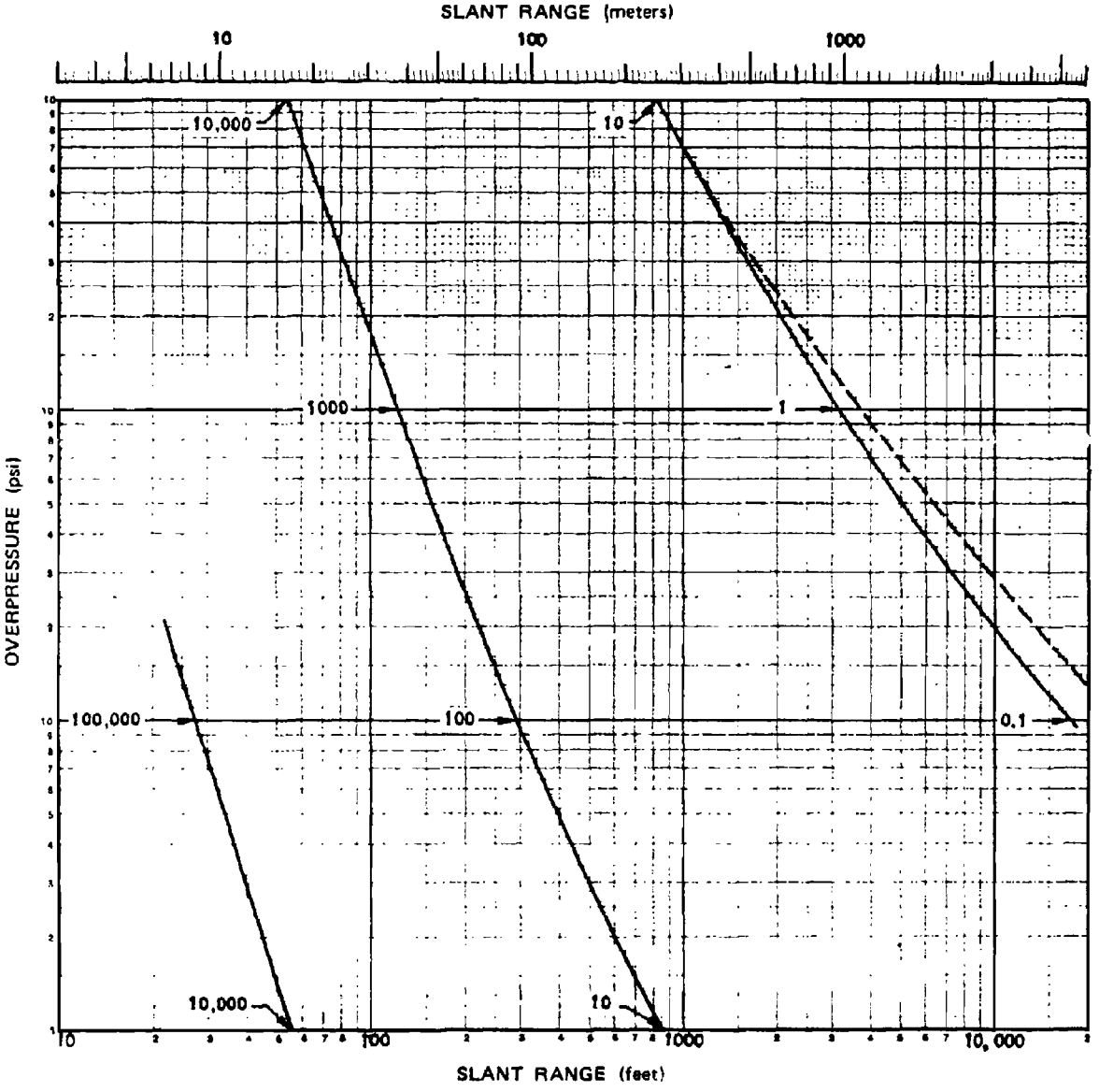

Figure 13-15. [redacted] Peak Overpressure from a 1 kt Free Air Burst in a Standard Sea Level Atmosphere [redacted]

[redacted]

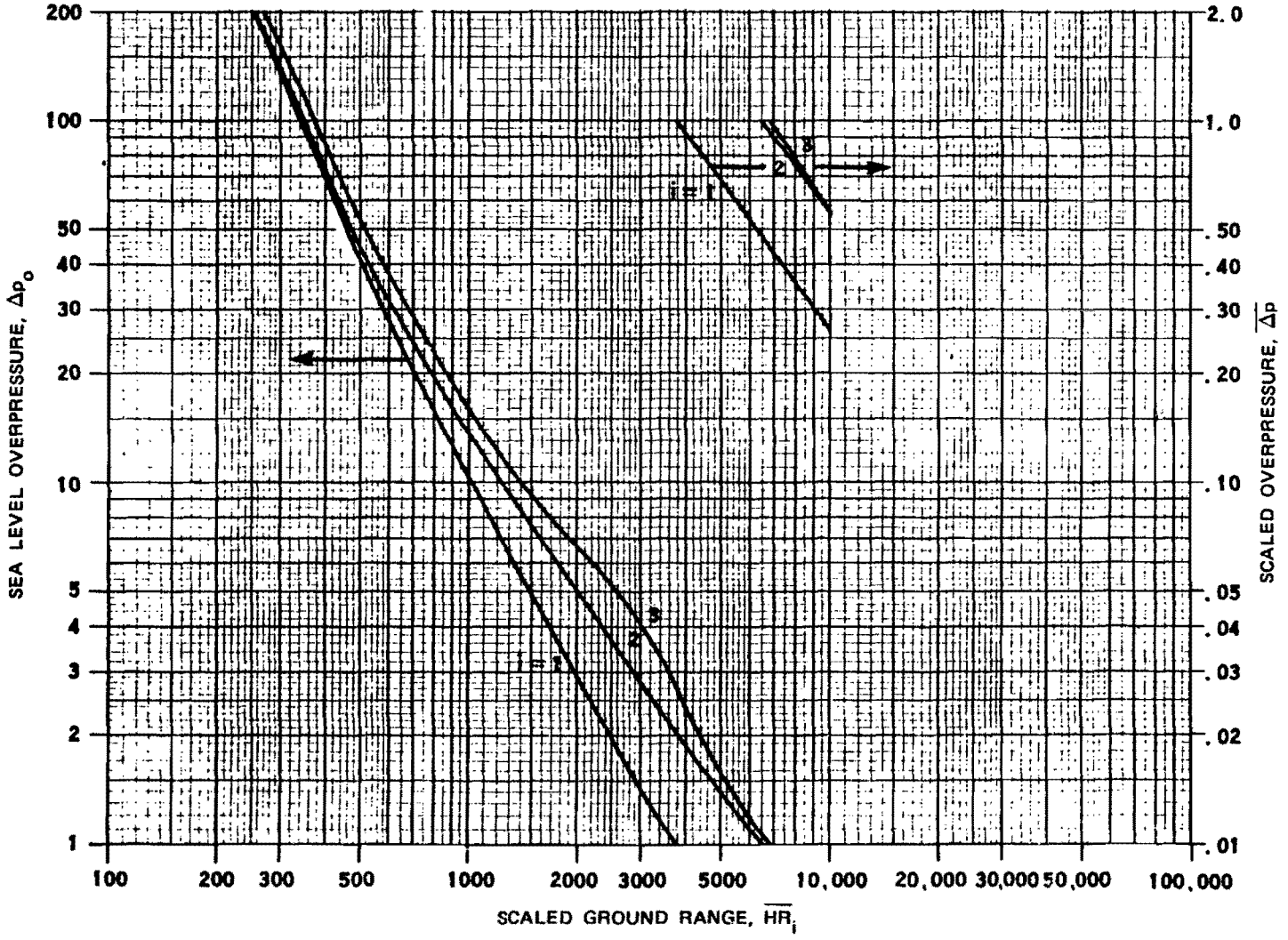

Figure 13-16. [redacted] The Range Parameter $\overline{HR}_i$ as a Function of Sea Level Overpressure [redacted]

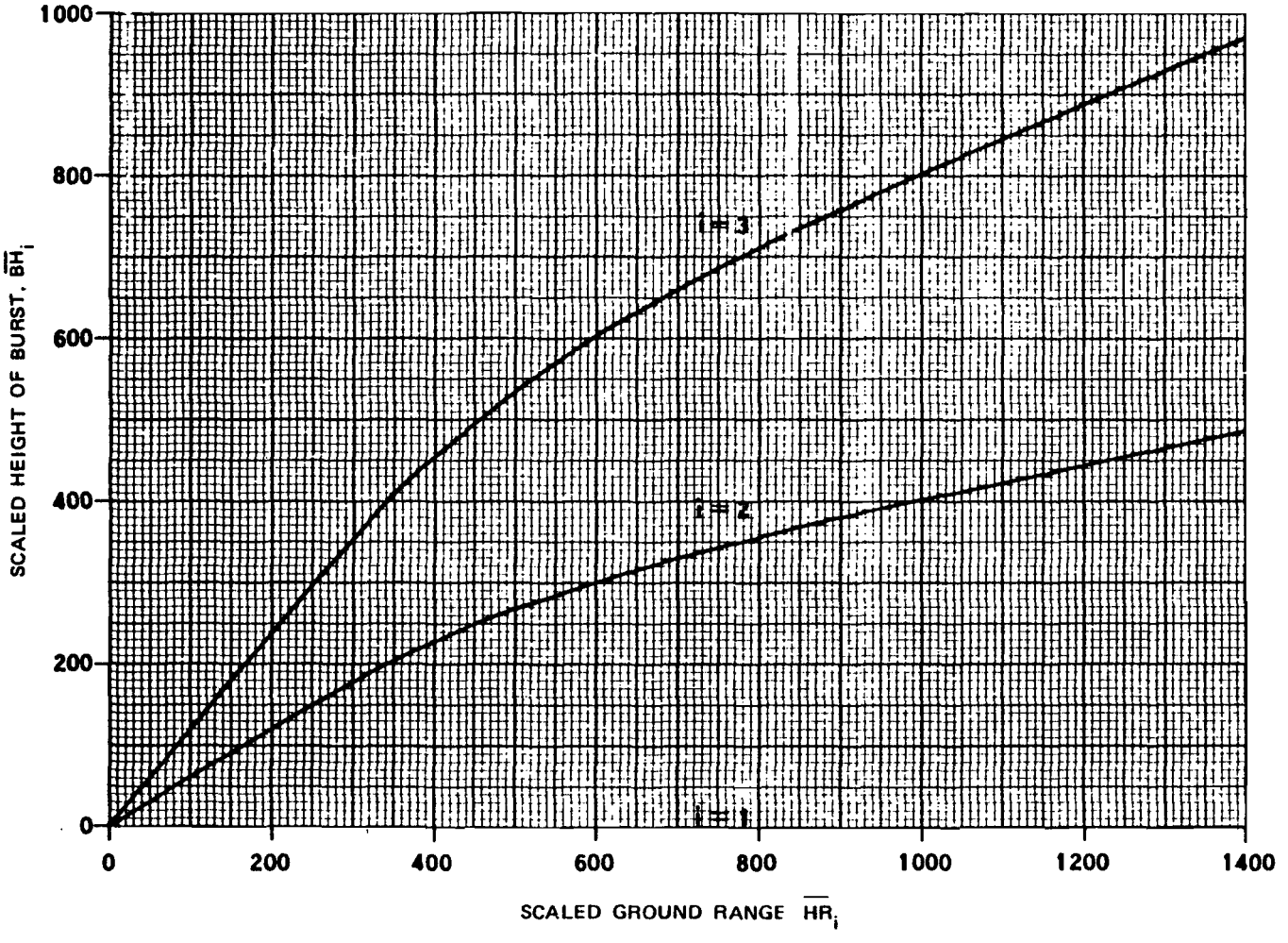

Figure 13-17a. [redacted] $\overline{BH}_i$ as a Function of $\overline{HF}_i$, Short Ranges [redacted]

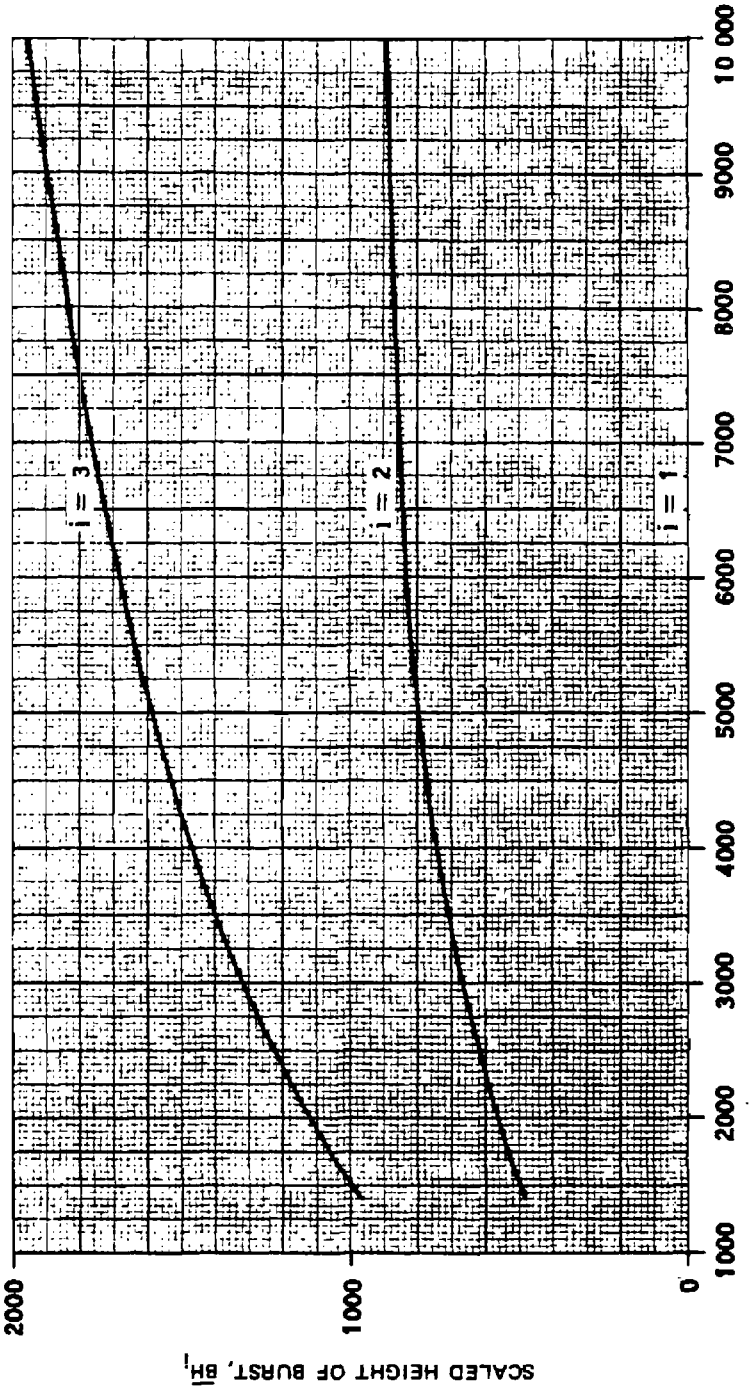

Figure 13-17b. [redacted] $\overline{BH}_i$ as a Function of $\overline{HR}_i$, Long Ranges [redacted]

[redacted]

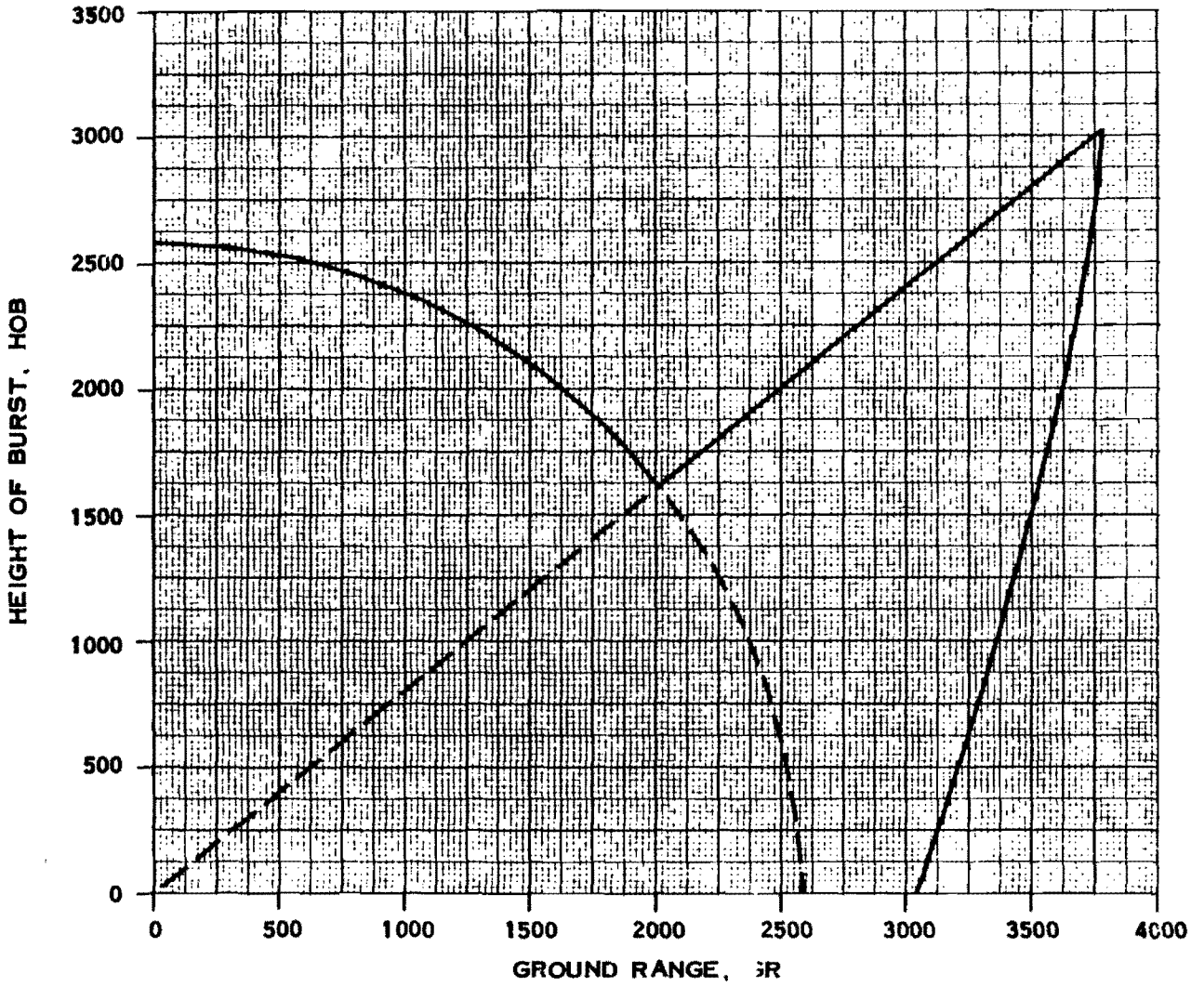

Figure 13-18. Overpressure Envelope for Marked Aircraft

AIRCRAFT RESPONSE TO THERMAL RADIATION EFFECTS

13-10 Thermal Effects on In-Flight and Parked Aircraft

The response of an aircraft to thermal energy is exhibited as a temperature rise in the aircraft skin. Several parameters influence the magnitude of the temperature rise. The most important parameters are skin thickness, skin material, surface condition, cooling effect of the air flowing over the outer surface of the aircraft, reradiation of thermal energy to the atmosphere, and conduction of the incident energy to the inner layers of the skin and substructure.

Sure-safe conditions are based on an allowable temperature rise of the aircraft skin; however, melting of the skin is required for sure-kill. To produce kill, the temperature must increase to the melt temperature, and further heat must be applied to cause melting. The method for analysis of thermal effects on aircraft that is described in Problem 13-6 applies to both airplanes and helicopters.

[redacted]

Problem 13-6. Calculation of Boundaries in Space (Envelopes) that Define the Sure-Safe and Sure-Kill Regions with Respect to Thermal Radiation on Aircraft In-Flight or Parked

[redacted] The analysis is based on calculating the amount of heat required to produce some specified effect. For sure-safe, this effect is raising the temperature of a skin panel to a value which produces a 20 percent reduction in the modulus of elasticity. This criterion is applied to the thinnest structural skin on the fuselage. For sure-kill, the specified effect is melting of the thickest skin on the fuselage. The critical amount of heat, Q_c, which is the heat required to produce the specified effect is assumed to be equal to the thermal energy absorbed by the skin, Q_a. The critical heat, Q_c, is

$$Q_c = \rho_m C_p t \Delta T,$$

where ρ_m is the weight density of the material, C_p is the specific heat of the material, t is the skin thickness, and ΔT is the effective critical temperature rise.

(U) The constraints in the calculation are:

- The aircraft skin is thermally thin, i.e., the incident thermal energy heats the skin uniformly throughout its depth.
- The equilibrium temperature is based on an average set of conditions for turbulent flow.
- At the equilibrium temperature, all degradations of material properties from room temperature values are negligible.
- Cooling effects resulting from airflow over the aircraft are negligible.
- Reradiation is negligible.
- Aircraft motion is neglected.
- Attenuation of the thermal energy by the atmosphere is negligible.
- Reflected radiation from the ground is negligible.
- The fireball is a point source.

(U) Under the constraints

$$Q_a = \alpha Q,$$

where Q is the radiant exposure, i.e., the energy received per unit area (normal to the direction of propagation under the assumed constraints), and α is the absorptivity coefficient for the aircraft surface being considered.

(U) From Chapter 3,

$$Q = \frac{10^{12} Wf}{4\pi R^2} \text{ cal/cm}^2,$$

where

W = weapon yield (kt),

f = thermal partition of energy (dimensionless),

R = distance (cm),

Since 39 cal/cm^2 = 1 Btu/in.^{2}, and 929 cm^2 = 1 ft^2,

$$Q = \frac{10^{12} Wf}{4\pi R^2 (39)(929)} \text{ Btu/in.}^2$$

or

$$Q = \frac{2.19 \times 10^6 Wf}{R^2} \text{ Btu/in.}^2$$

where R is now expressed in feet. Since

[redacted]

$$Q_a = \alpha Q,$$

$$Q_a = \frac{2.19 \times 10^6 Wf\alpha}{R^2},$$

and

$$R = \left[\frac{2.19 \times 10^6 Wf\alpha}{Q_a}\right]^{1/2},$$

or

$$R = 1{,}480\sqrt{\frac{Wf\alpha}{Q_a}},$$

which can be solved directly for the critical range R. If Q_c is taken to be equal to Q_a,

$$R = 1{,}480\sqrt{\frac{Wf\alpha}{Q_c}}$$

$$= 1{,}480\sqrt{\frac{Wf\alpha}{\rho_m C_p t \Delta T}}.$$

[redacted] The data required for solution include:

h = aircraft altitude (ft),

W = weapon yield (kt),

V = preblast aircraft velocity (ft/sec),

Detailed layout drawings of the fuselage, showing skin thickness,

Material of the skin, and

Surface condition of the skin.

[redacted] The analysis is performed in a series of steps.

1. Select the critical skin panels on the fuselage. Three panels should be selected, one each for bursts occurring directly below, directly above, and directly to the side of the aircraft. For each burst orientation, skin panels located in the following regions should be considered:

a. For a burst directly below the aircraft, the lower surface of the fuselage, within 45° of the normal to the bottom of the fuselage.

b. For a burst directly above the aircraft, the upper surface of the fuselage, within 45° of the normal to the top of the fuselage.

c. For a burst directly to the side of the aircraft, the side surface of the fuselage not covered by a and b above.

The selection of the critical skin panel from the locations defined above is based primarily on the thickness of the skin and depends upon whether sure-safe or sure-kill envelopes are sought.

- For sure-safe, select the *thinnest* structural skin. Nonstructural skin, such as access panels, should not be selected. If more than one material is used for the fuselage, investigate the thinnest skin for each material and base the envelopes on the *most* vulnerable.
- For sure-kill, select the *thickest* skin at a fuselage station near the forward end of the tail cone. If more than one material is used for the fuselage, investigate the thickest skin for each material and base the envelopes on the *least* vulnerable.

For a parked aircraft, skip steps 2 and 3 and proceed to step 4. For an in-flight aircraft, proceed to step 2.

2. Determine the ambient speed of sound c (ft/sec) at altitude h from Table 13-1.

3. Calculate the Mach Number,

$$M = \frac{V}{c}.$$

4. Determine the equilibrium temperature, T_e, of the skin.

a. For in-flight aircraft, enter Figure 13-19 with the Mach number, M, and the altitude, h, and read T_e.

b. For parked aircraft, use T_e = 60°F.

[redacted]

[redacted]

5. Determine the material properties for each of the skin panels selected from Table 13-3.

T_c = critical temperature (°F)

C_p = specific heat (Btu/lb°F)

ρ_m = weight density (lb/in.^{3})

For sure-kill only, determine

H = heat of fusion (Btu/lb)

6. Calculate the effective critical temperature rise, ΔT:

a. For sure-safe,

$$\Delta T = T_c - T_e.$$

b. For sure-kill,

$$\Delta T = T_c - T_e + \frac{H}{C_p}.$$

7. Determine the effective absorptivity coefficient, α, from Table 13-4.

8. Determine f from Figure 13-20*, and calculate the critical range in feet,

$$R = 1{,}480 \sqrt{\frac{Wf\alpha}{\rho_m C_p t \Delta T}}.$$

When steps 5 through 8 have been completed for a burst directly below the aircraft, they should be repeated for bursts directly above and directly to the side of the aircraft. Three ranges will have been determined, R_b, R_a, and R_s, where subscripts *"b," "a,"* and *"s"* designate below, above, and side, respectively. Note that, if the critical skin panels for R_a and R_s are of the same material and have the same surface conditions as the skin panel analyzed for R_b, only step 8 need be repeated, introducing the proper value of skin thickness, t.

9. Calculate the average of the three ranges, R_b, R_a, and R_s,

$$R_{av} = \frac{1}{3}\left(R_b + R_a + R_s\right).$$

10. The critical volume is defined by a sphere of radius R_{av} centered on the aircraft.

[redacted]

DNA (A)(1)

[redacted]

* [redacted] Note that Figure 13-20 is identical to Figure 3-1. It is reproduced here for convenience.

[redacted]

[redacted]

Reliability: The constraints on this analysis are described in the introductory paragraphs of this problem. The maximum error is between a factor of 1.5 and 3.

Related Material: See paragraphs 13-1, 13-4, and 13-10. See also Table 13-1.

Table 13-3. [redacted] Average Properties of Selected Engineering Materials [redacted]

Material	Critical Temperature, T_c (°F)		Specific Heat, C_p (Btu/lb°F)		Weight Density ρ_m (lb/in.^{3})	H (Btu/lb)
	Sure-Safe	Sure-Kill	Sure-Safe	Sure-Kill		
Steel	800	2,550	0.13	0.15	0.28	117
Inconel X	1,000	2,550	0.12	0.13	0.30	117
Aluminum	480	1,076	0.22	0.24	0.10	170
Magnesium	200	1,120	0.25	0.26	0.064	160
Titanium	500	2,850	0.13	0.24	0.17	187

[redacted]

[redacted]

Table 13-4. [redacted] Average Values of Absorptivities, α [redacted]

	Sure-Safe	Sure-Kill
Polished Metals	0.25	0.50
Unpolished metals	0.45	0.55
Painted metals		
Paint color		
White	0.30	0.50
Yellow	0.40	0.55
Olive	0.70	0.60
Black	0.90	0.65

[redacted]

[redacted]

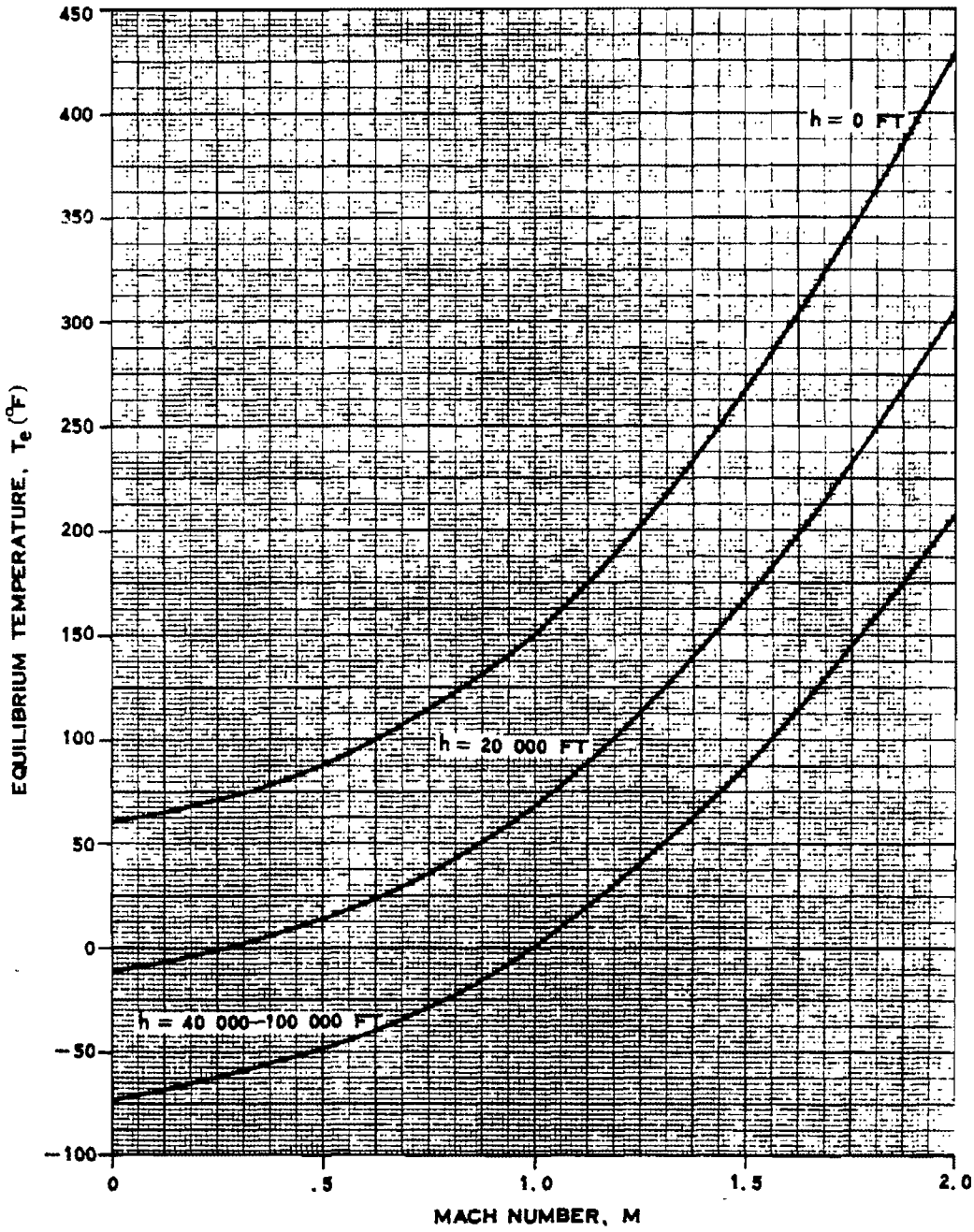

Figure 13-19. [redacted] Equilibrium Temperature as a Function of Mach Number [redacted]

PAGE 13-66 DELETED

[redacted]

[redacted]

[redacted] BURST-TIME ENVELOPES [redacted]

13-11 Requirement for Burst-Time Envelopes [redacted]

[redacted] The envelopes that are obtained by the methods described in Problems 13-3 through 13-6 define the locus of the center of burst relative to the *position of the aircraft at intercept,* for a specified criterion. It usually is preferable to define the corresponding envelope relative to the *position of the aircraft at burst time.* For parked aircraft and for those envelopes corresponding to thermal radiation, which reaches the aircraft almost instantaneously, the two envelopes are the same, i.e., the methodology presented in Problem 13-5 for overpressure effects on parked aircraft and that presented in Problem 13-6 for thermal effects on in-flight or parked aircraft apply equally well to intercept-time and to burst-time envelopes. When considering the response of in-flight aircraft to gust or overpressure, however, the relative positions of the aircraft and the burst center are different at the time of burst than at the time of intercept as a result of the distance traveled by the aircraft during the finite time required for the blast wave to propagate to the intercept point. Methods for transforming the intercept-time envelopes obtained by the methods described in Problems 13-3 through 13-5 for in-flight aircraft into burst-time envelopes for the same aircraft are described in Problem 13-7.

[redacted]

[redacted]

Problem 13-7. Calculation of Burst-Time Envelopes for Gust or Overpressure Effects from Intercept-Time Envelopes

[redacted] As discussed in paragraph 13-1, the assumption must be made that the aircraft is following an unaltered flight path when transforming intercept-time envelopes into burst-time envelopes. This assumption is necessary, since it would be impossible to guess the course changes. The assumption is valid for low yield weapons because of the small distances and times between burst and intercept. In the case of high yield weapons, the blast wave arrival time may be of the order of seconds, and the pilot may have time to change his course, so, for these weapons, the assumption must be considered as a source of error.

[redacted] Two major assumptions, arising from the limitations discussed above, are included in the simplified calculation method described below.

- The aircraft is represented by a point mass traveling at a constant velocity.
- The aircraft is performing a constant symmetric maneuver. As a result of this assumption, the flight path of the aircraft is circular (or straight, for the special case of no maneuver).

[redacted] Two left-handed, body-centered coordinate systems employed in the analysis are shown in Figure 13-21.

- The intercept reference frame (X_I, Y_I, Z_I), the origin of which is located at the aircraft's center of mass at intercept, with the X_I axis collinear with the velocity vector, positive forward, and the Z_I axis in the aircraft plane of symmetry, positive upward.
- The burst reference frame (X_B, Y_B, Z_B), the origin of which is located at the aircraft's center of mass at burst time, with the X_B axis collinear with the velocity vector, positive forward, and the Z_B axis in the aircraft plane of symmetry, positive upward.

[redacted] The $X_I - Z_I$ and $X_B - Z_B$ planes coincide, hence the Y_I and Y_B coordinates of any point are the same.

[redacted] If the center of burst has coordinates (X_I, Y_I, Z_I) in the intercept frame, its position in the burst frame is given by the coordinates (X_B, Y_B, Z_B), where

$$X_B = X_I \cos \Phi + (r - Z_I) \sin \Phi$$

$$Y_B = Y_I,$$

$$Z_B = X_I \sin \Phi - (r - Z_I) \cos \Phi + r,$$

and

r = radius of turn,

Φ = angular change in flight path between burst and intercept times.

The parameters r and Φ are obtained from the relations

$$r = \frac{V^2}{Ng},$$

$$\dot{\Phi} = \frac{V}{r},$$

where

V = preblast aircraft velocity,

N = maneuver normal load factor,

g = acceleration of gravity,

and a dot indicates differentiation with respect to time. It should be noted that N is the *maneuver* normal load, and not the load factor, n, used to calculate the intercept envelopes. N is related to the load factor n by

$$N = n - 1.$$

[redacted]

If the equation for $\dot{\Phi}$ is integrated from burst time to intercept time, the result is,

$$\Phi = \frac{Vt_a}{r}$$

where

t_a = time of arrival of the blast wave at the intercept point; i.e., the time required for the blast front to propagate to the intercept point.

For the special case when the aircraft is not performing a maneuver ($N = 0$), the equations for the position of the burst point in the burst frame simplify to

$$X_B = X_I + Vt_a$$

$$Y_B = Y_I$$

$$Z_B = Z_I.$$

By means of the above equations, the burst frame coordinates (X_B, Y_B, Z_B) may be found for any point on an intercept-time envelope (X_I, Y_I, Z_I). Unfortunately, a general planar burst-time envelope cannot be obtained by merely transforming an intercept envelope point by point. For maneuvering aircraft, only those envelopes in the X_I - Z_I plane (side view) or parallel to the X_I - Z_I plane, may be resolved directly into corresponding planar envelopes in the X_B - Z_B plane or parallel to it. All other intercept-time envelopes will transform into three-dimensional surfaces in the burst frame. In the case of no maneuver, any intercept-time envelope parallel to the X_I axis may be resolved directly into a burst-time envelope in the same plane. This includes envelopes in both the X_I - Z_I plane (side view), and the X_I - Y_I plane (top view). However, in neither case can the Y_B - Z_B plane (front view) envelope be obtained directly. In order to find the burst envelopes for side, front, and top views (or in any arbitrary plane), it is necessary to adopt an indirect procedure. Since the intercept-time envelopes define a volume in space, this entire volume may be transformed into an equivalent volume in the burst frame. The burst-time envelopes then may be determined as the intersection of this volume with the planes in which burst-time envelopes are desired.

The most convenient way of performing this volume transformation is to take "slices" through the intercept-time volume parallel to the X_I - Z_I plane, for selected values of Y_I. Each of these slices may be resolved directly into a slice of the burst-time volume in a plane corresponding to the same value of Y_B. Definition of the burst-time envelopes in several Y_B planes is equivalent to defining the burst-time volume.

The data required to perform the analysis include:

V = preblast aircraft velocity (ft/sec)

h = aircraft altitude (ft)

W = weapon yield (kt)

n = aircraft preblast load factor; for straight and level flight, $n = 1$ (dimensionless)

X_I, Y_I, Z_I = coordinates of points on intercept-time envelopes, as defined in Figure 13-21 (ft).

The analysis is performed in a series of steps, as follows.

1. Determine the ambient atmospheric conditions at altitude h from Table 13-1.

2. Calculate the maneuver normal load factor, N,

$$N = n - 1.$$

3. Calculate the radius of turn, r (not required if $N = 0$.),

$$r = \frac{V^2}{32.2N}.$$

4.* Select a point on the X_I - Z_I plane (side view) intercept-time envelope. Its coordinates are (X_I, Y_I, Z_I), with $Y_I = 0$.

5. Determine the slant range, R, from the center of burst to the selected intercept point.

$$R = \left(X_I^2 + Y_I^2 + Z_I^2\right)^{1/2}.$$

6. Calculate the equivalent range for a 1 kt burst in a sea level atmosphere by the scaling procedures described in paragraph 2-14, Chapter 2,

$$R_1 = R\left(\frac{P}{P_o W}\right)^{1/3} = R\left(\frac{P}{14.7W}\right)^{1/3}.$$

7. Enter Figure 13-22 with R_1, and read the time of arrival, t_1, for a 1 kt burst in a sea level atmosphere.† Calculate the time of arrival of the blast wave at a range R from a yield W at altitude h by the scaling procedures given in paragraph 2-14,

$$t_a = t_1\left(\frac{WP_o}{P}\right)^{1/3}\left(\frac{T_o}{T}\right)^{1/2}.$$

A satisfactory expression for the time of arrival within the accuracy of the methodology presented herein is

$$t_a = t_1\left(\frac{WP_o}{P}\right)^{1/3}\left(\frac{c_o}{c}\right)$$

$$= t_1\left(\frac{14.7W}{P}\right)^{1/3}\left(\frac{1{,}116}{c}\right).$$

8. Calculate the turn angle, Φ, in degrees (not required if $N = 0$),

$$\Phi = 57.3\,\frac{Vt_a}{r}.$$

9. Calculate the coordinates of the point in the burst frame (X_B, Y_B, Z_B).

a. If $N = 0$,

$$X_B = X_I + Vt_a,$$

$$Y_B = Y_I,$$

$$Z_B = Z_I.$$

b. If $N \neq 0$,

$$X_B = X_I \cos\Phi + (r - Z_I)\sin\Phi,$$

$$Y_B = Y_I,$$

$$Z_B = Z_I \sin\Phi - (r - Z_I)\cos\Phi + r.$$

10. Repeat steps 5 through 9 for other points on the intercept-time envelope, until the burst-time envelope has been defined satisfactorily.

11. Determine the intercept-time envelope for a "slice" parallel to the X_I - Z_I plane, with $Y_I \neq 0$. Repeat steps 5 through 10 for points on this envelope.

12. Repeat step 11 for as many "slices" as necessary to define the burst-time volume adequately. Note that only positive values of Y_I need be used since the envelopes are symmetric about the X_I - Z_I or X_B - Z_B plane.

[redacted] At this point, the problem is essentially solved, since the burst-time volume effectively has been defined. The burst-time envelope in any desired plane may be determined from the burst-time volume. The calculation of the burst-

* [redacted] In certain special cases, simpler procedures may be used, although the procedures given above are general and will work in all cases. A description of the special cases is given at the end of the Stepwise Calculation Procedure.

† [redacted] Note that Figure 13-22 is identical to Figure 2-5, Chapter 2. It is reproduced here for convenience.

time envelopes in three planes, The X_B - Z_B plane (side view), the Y_B - Z_B plane (front view), and the X_B - Y_B plane (top view) is described for illustration.

13. The side-view burst-time envelope is the intersection of the X_B - Z_B plane with the burst-time volume. This is just the transformed side-view intercept-time envelope (Y_I = 0), which was the first burst-time envelope defined in the steps given above.

14. The front-view burst-time envelope is the intersection of the Y_B - Z_B plane with the burst-time volume. For each of the burst-time volume "slices," determine the values of Z_B corresponding to X_B = 0, and plot these using the value of Y_B for the slice being considered.

15. The top-view burst-time envelope is the intersection of the X_B - Y_B plane with the burst-time volume. For each of the burst-time volume "slices," determine the values of X_B corresponding to Z_B = 0, and plot these using the value of Y_B for the slice being considered.

16. *Special Cases.* In certain cases, simpler procedures may be used. The methodology of Problem 13-5 results in a spherical intercept-time volume for overpressure effects on in-flight aircraft. The sphere is centered at the origin of the intercept frame (X_I, Y_I, Z_I). Hence, R, R_1, r, and Φ (steps 5-8) are the same for *all* points on the intercept-time volume, and the sphere transforms into a sphere of the same radius in the burst frame. The coordinates of the center of the sphere are

a. If $N = 0$,

$$X_B = Vt_a,$$

$$Y_B = 0,$$

$$Z_B = 0.$$

b. If $N \neq 0$,

$$X_B = r \sin \Phi,$$

$$Y_B = 0,$$

$$Z_B = r(1 - \cos \Phi).$$

Another special case occurs for the gust effects on in-flight aircraft (see Problems 13-3 and 13-4). The complete intercept-time volumes are made up of four spheres. The intersection of any plane with a sphere is a circle. Consider the intersection of a plane parallel to the X_I - Z_I plane and defined by constant Y_I with the sphere at the side of the aircraft. The intersection is a circle on the Y_I axis. All points on this circle are equidistant from the origin; hence, the circle transforms into a circle of the same radius in the burst frame. The coordinates of the center of the circle are

a. If $N = 0$,

$$X_B = Vt_a,$$

$$Y_B = Y_I,$$

$$Z_B = 0.$$

b. If $N \neq 0$,

$$X_B = r \sin \Phi,$$

$$Y_B = Y_I,$$

$$Z_B = r(1 - \cos \Phi).$$

For the case of $N = 0$ only, the intersection of a plane parallel to the X_I - Y_I plane and defined by constant Z_I with the sphere above or below the aircraft transforms into a circle of the same radius in the burst frame. The coordinates of the center of the circle are

$$X_B = Vt_a$$

[redacted]

$$Y_B = 0$$

$$Z_B = Z_I.$$

In all of the above transformations, it should be emphasized that t_a corresponds to a point on the intercept-time envelope being considered, *not* to the center of the circle.

[redacted]

DNA (G)(1)

PAGES 13-73 THRU 13-74 DELETED

[redacted]

[redacted]

[redacted] *Reliability:* The aircraft is assumed to be represented by a point mass traveling at a constant velocity and performing a constant symmetric maneuver. As a result of this assumption, the flight path of the aircraft is circular (or straight for the special case of no maneuver). The maximum error is estimated to be a factor of 1.1.

[redacted] *Related Material:* See paragraphs 13-1, 13-2, 13-6, 13-7, and 13-11. See also Problems 13-3 and 13-4, and Table 13-1.

[redacted]

[redacted]

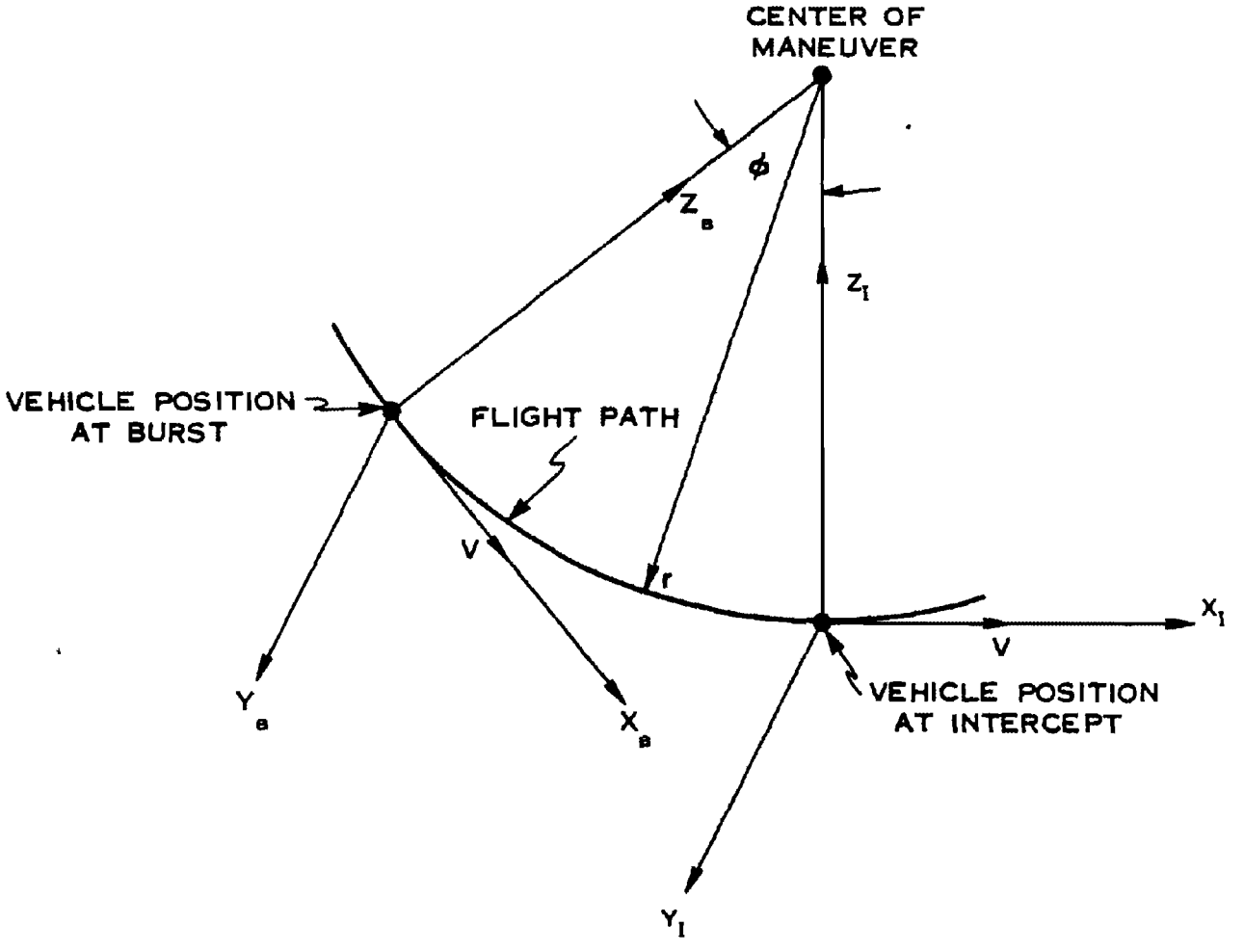

Figure 13-21. [redacted] Geometry of Burst and Intercept Reference Frames [redacted]

[redacted]

[redacted]

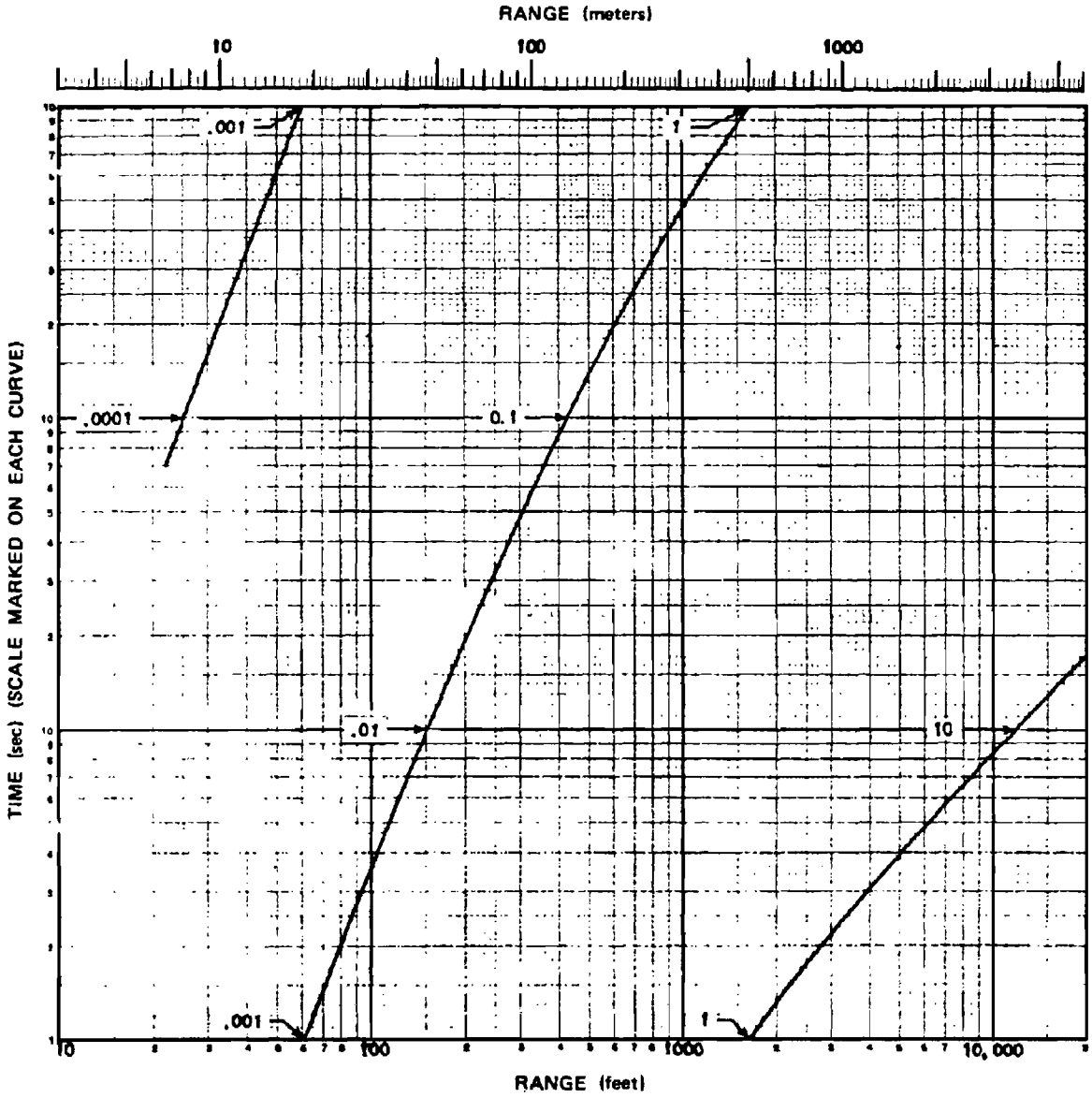

Figure 13-22. [redacted] Time of Arrival of the Shock Front from a 1 kt Free Air Burst in a Standard Sea Level Atmosphere [redacted]

[redacted]

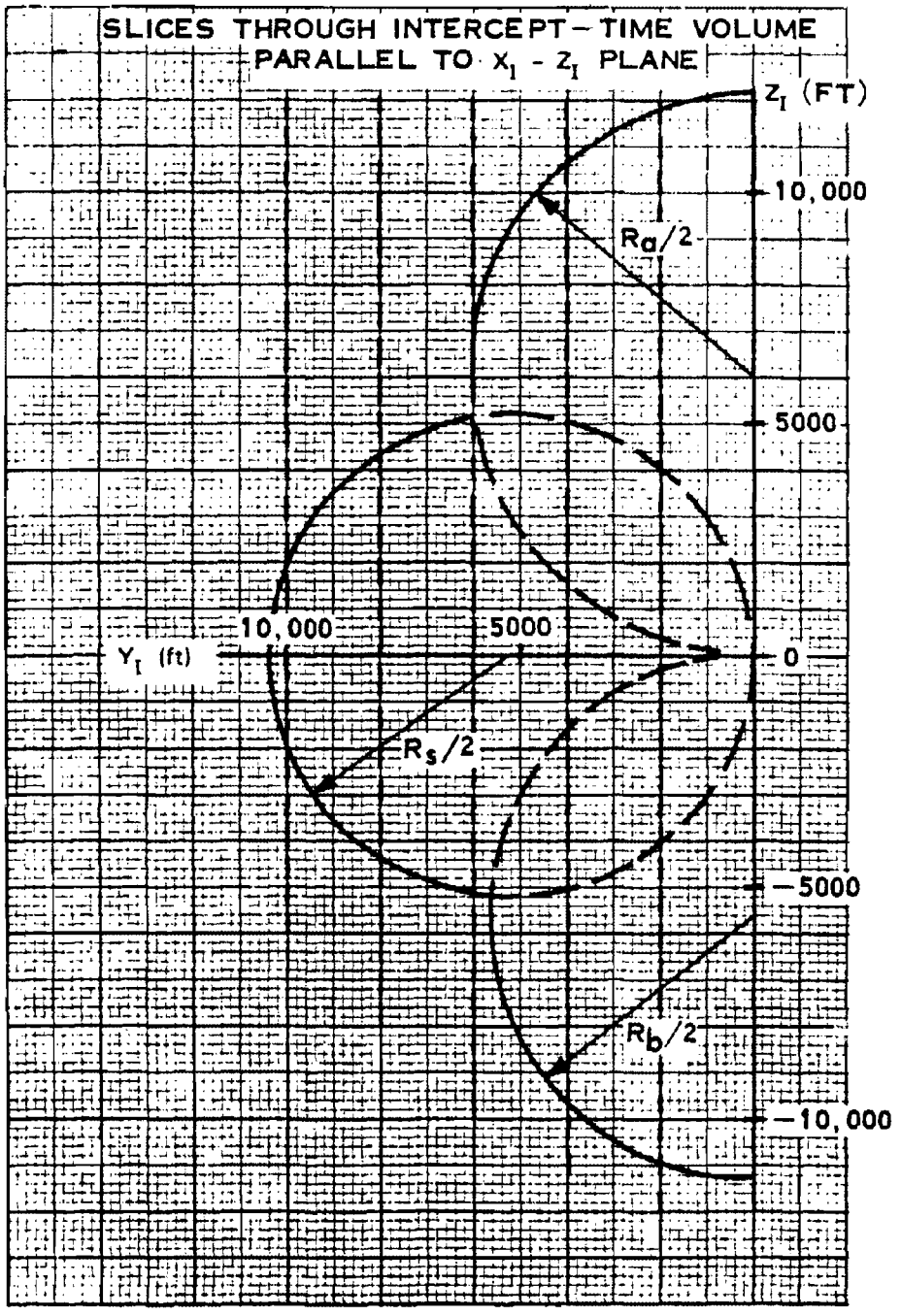

Figure 13-23. [redacted] Intercept-Time Envelope (Front View) [redacted]

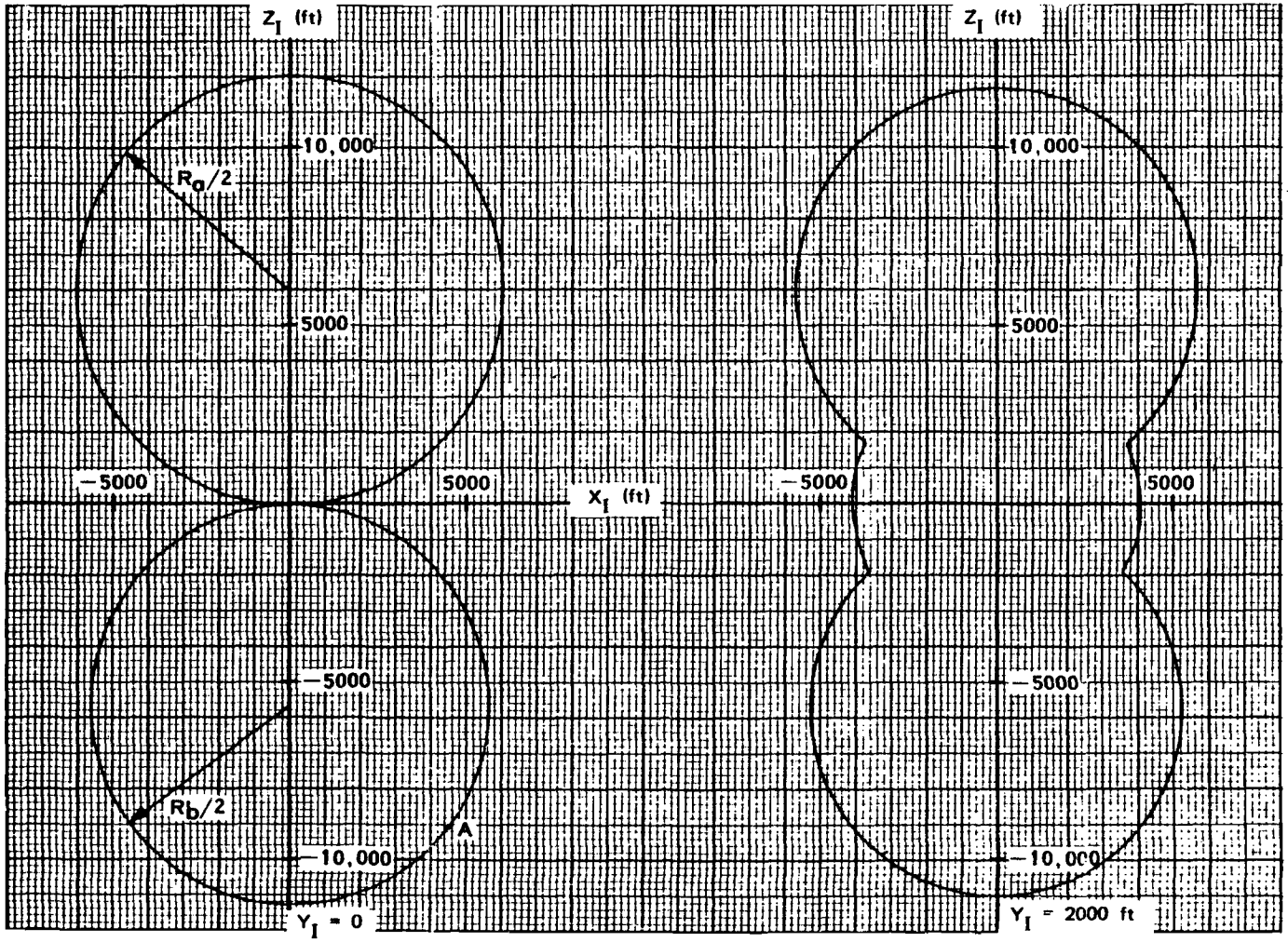

Figure 13-24a. [redacted] Intercept-Time Envelope (Side View) [redacted]

Figure 13-24b. [redacted] Slice Through Intercept-Time Volume at Y_I = 2,000 Feet [redacted]

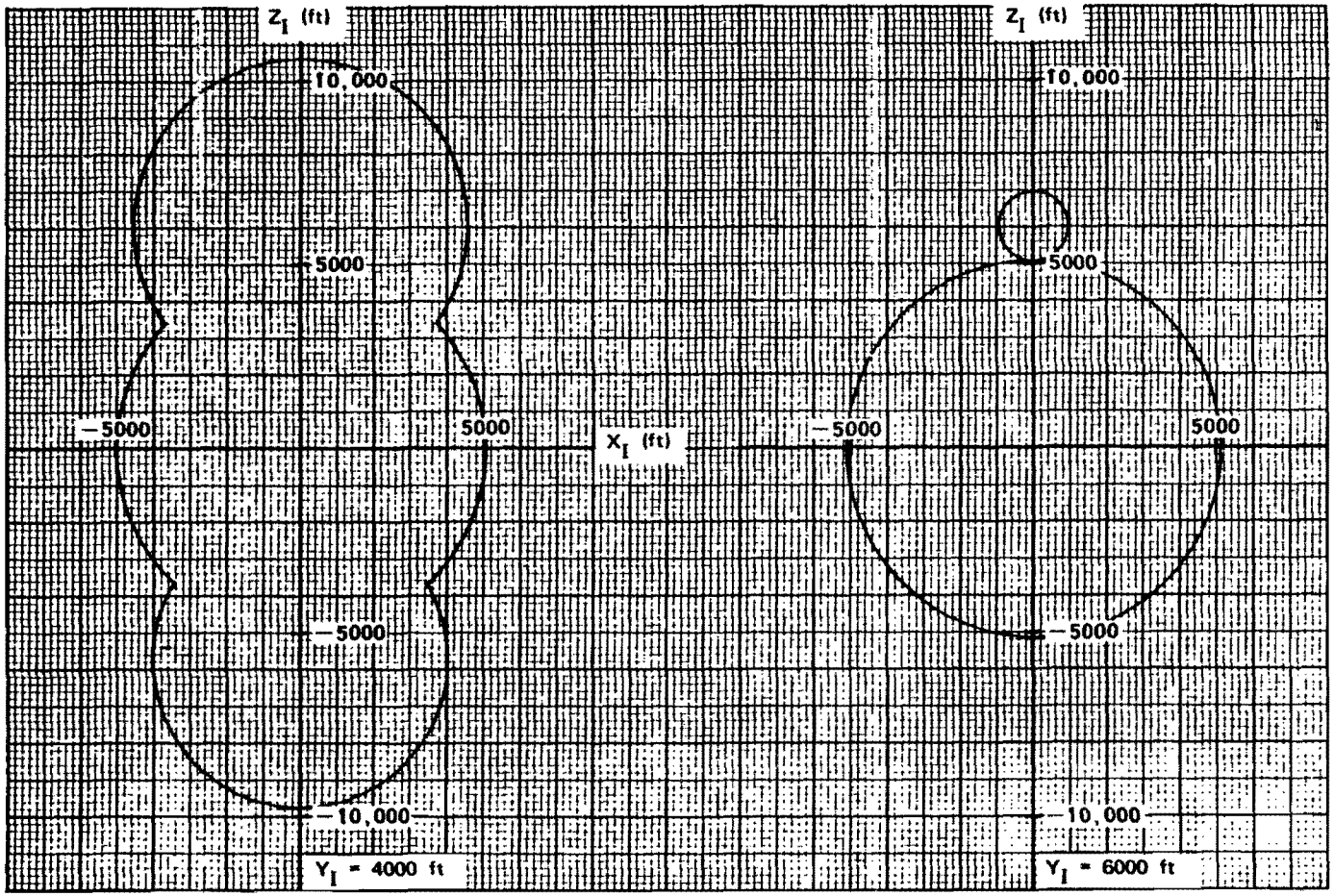

Figure 13-24c. [redacted] Slice Through Intercept-Time Volume at Y_I = 4,000 Feet [redacted]

Figure 13-24d. [redacted] Slice Through Intercept-Time Volume at Y_I = 6,000 Feet [redacted]

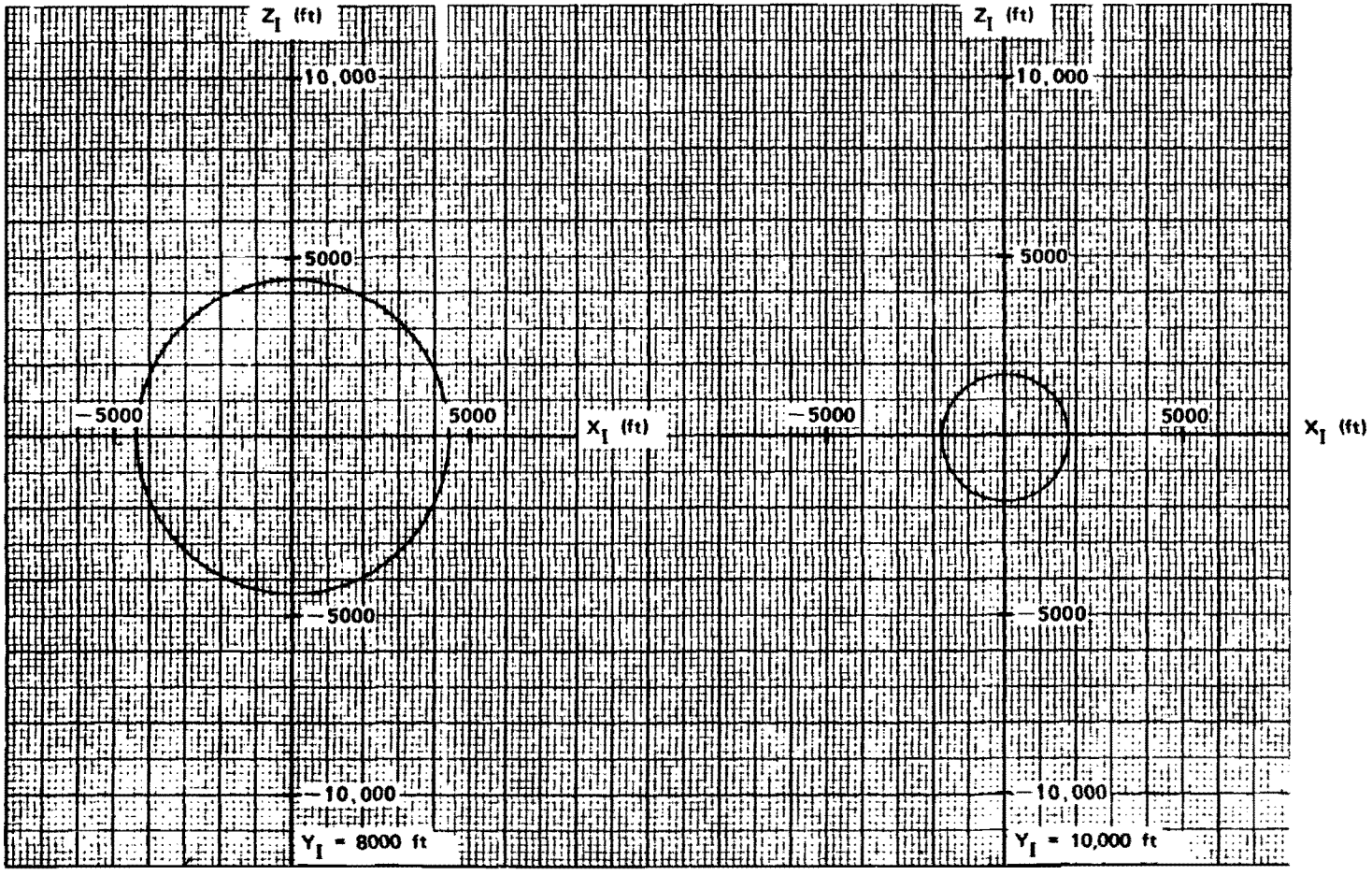

Figure 13-24e. [redacted] Slice Through Intercept-Time Volume at Y_I = 8,000 Feet [redacted]

Figure 13-24f. [redacted] Slice Through Intercept-Time Volume at Y_I = 10,000 Feet [redacted]

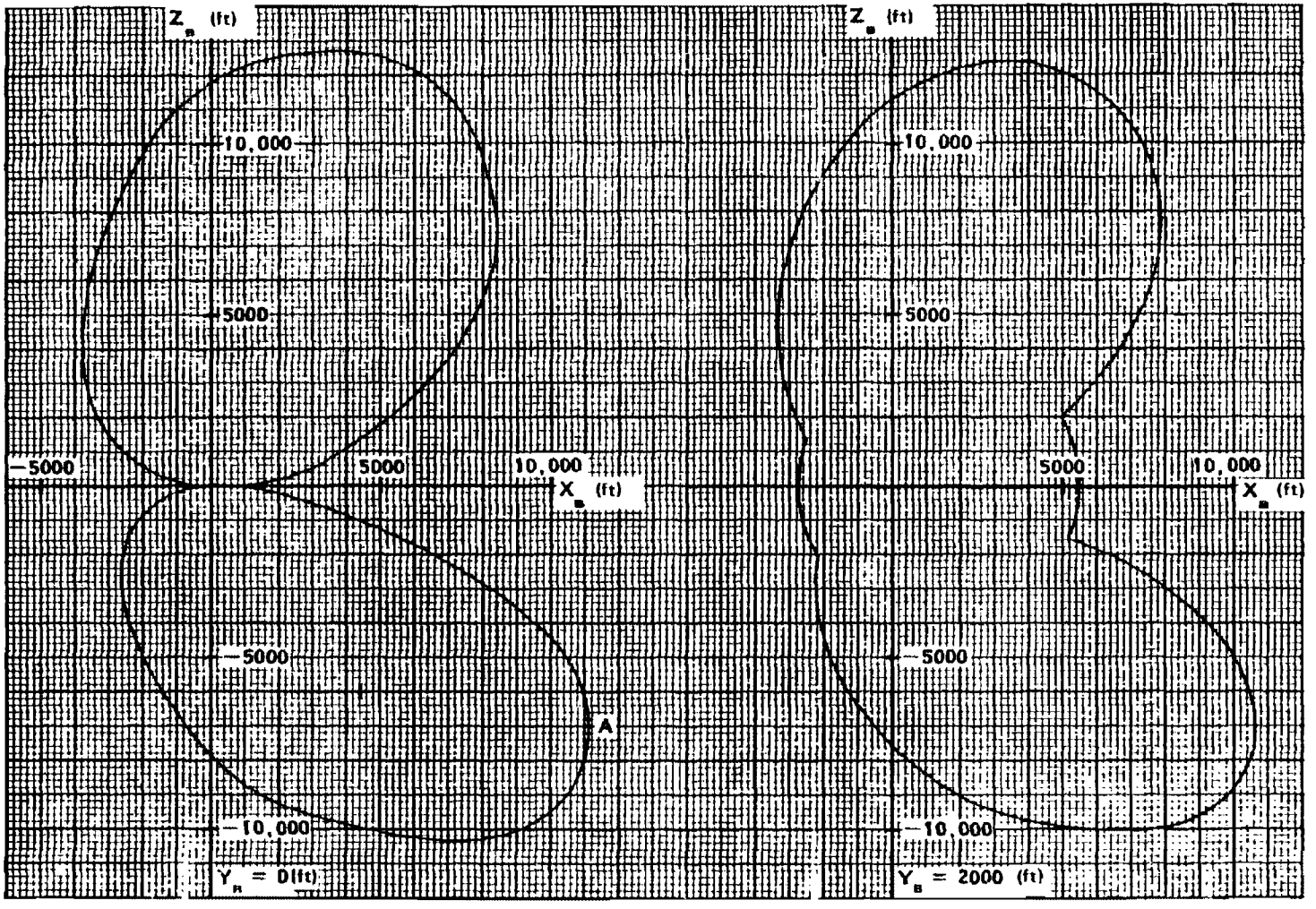

Figure 13-25a. [redacted] Burst-Time Envelope (Side View) [redacted]

Figure 13-25b. [redacted] Slice Through Burst-Time Volume at Y_B = 2,000 Feet [redacted]

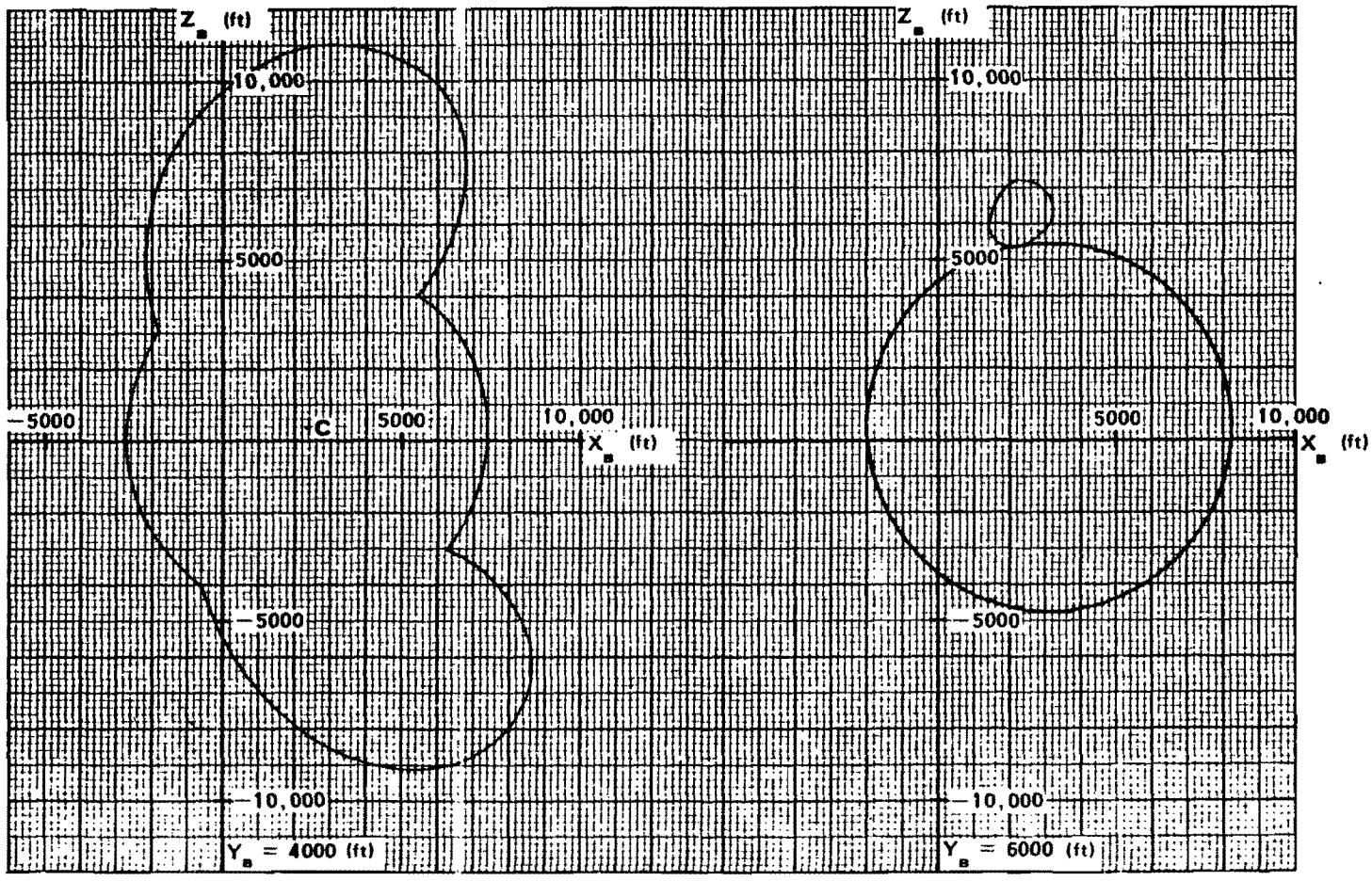

Figure 13-25c. [redacted] Slice Through Burst-Time Volume at Y_B = 4,000 Feet [redacted]

Figure 13-25d. [redacted] Slice Through Burst-Time Volume at Y_B = 6,000 Feet [redacted]

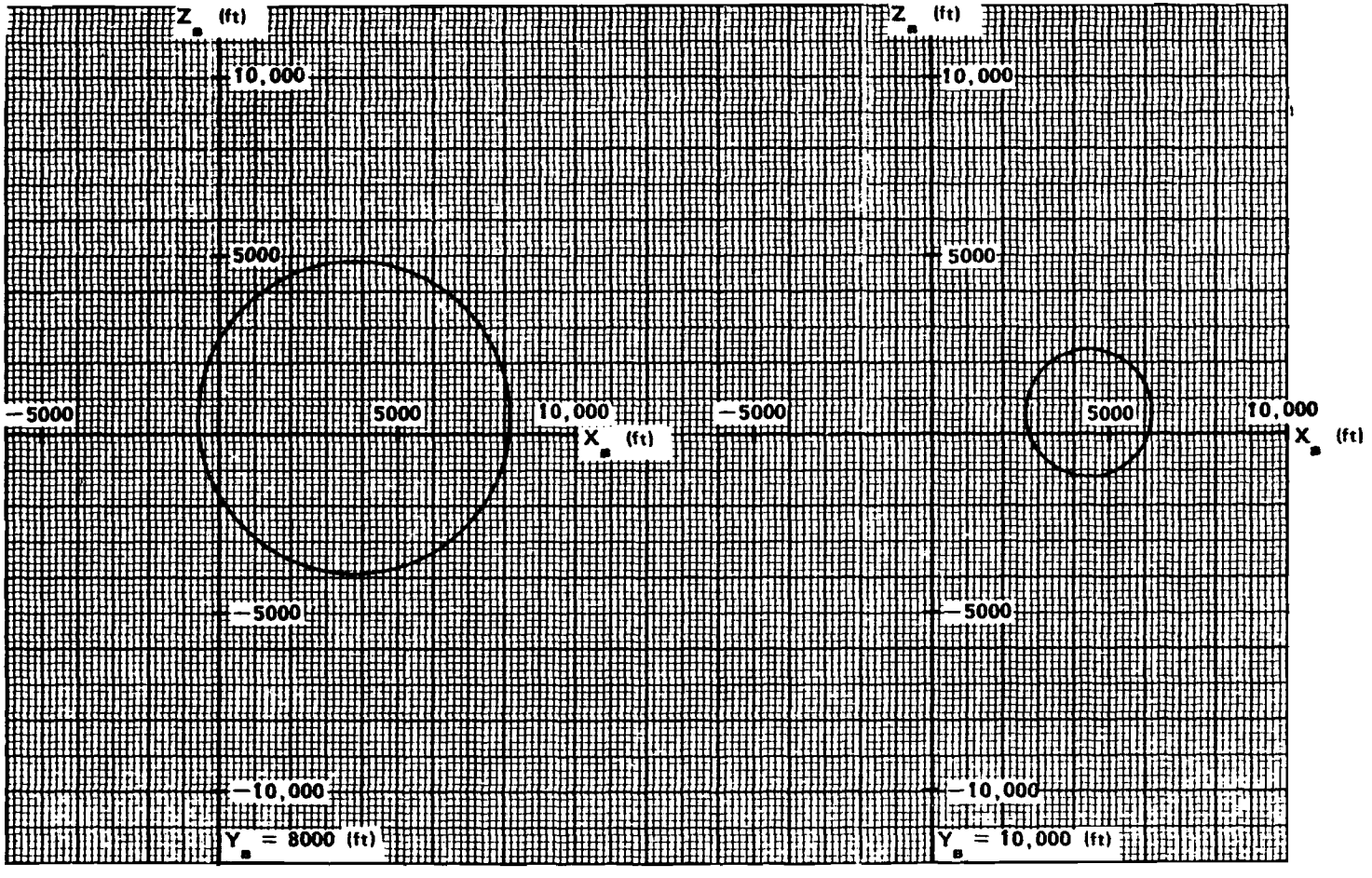

Figure 13-25e. [redacted] Slice Through Burst-Time Volume at Y_B = 8,000 Feet [redacted]

Figure 13-25f. [redacted] Slice Through Burst-Time Volume at Y_B = 10,000 Feet [redacted]

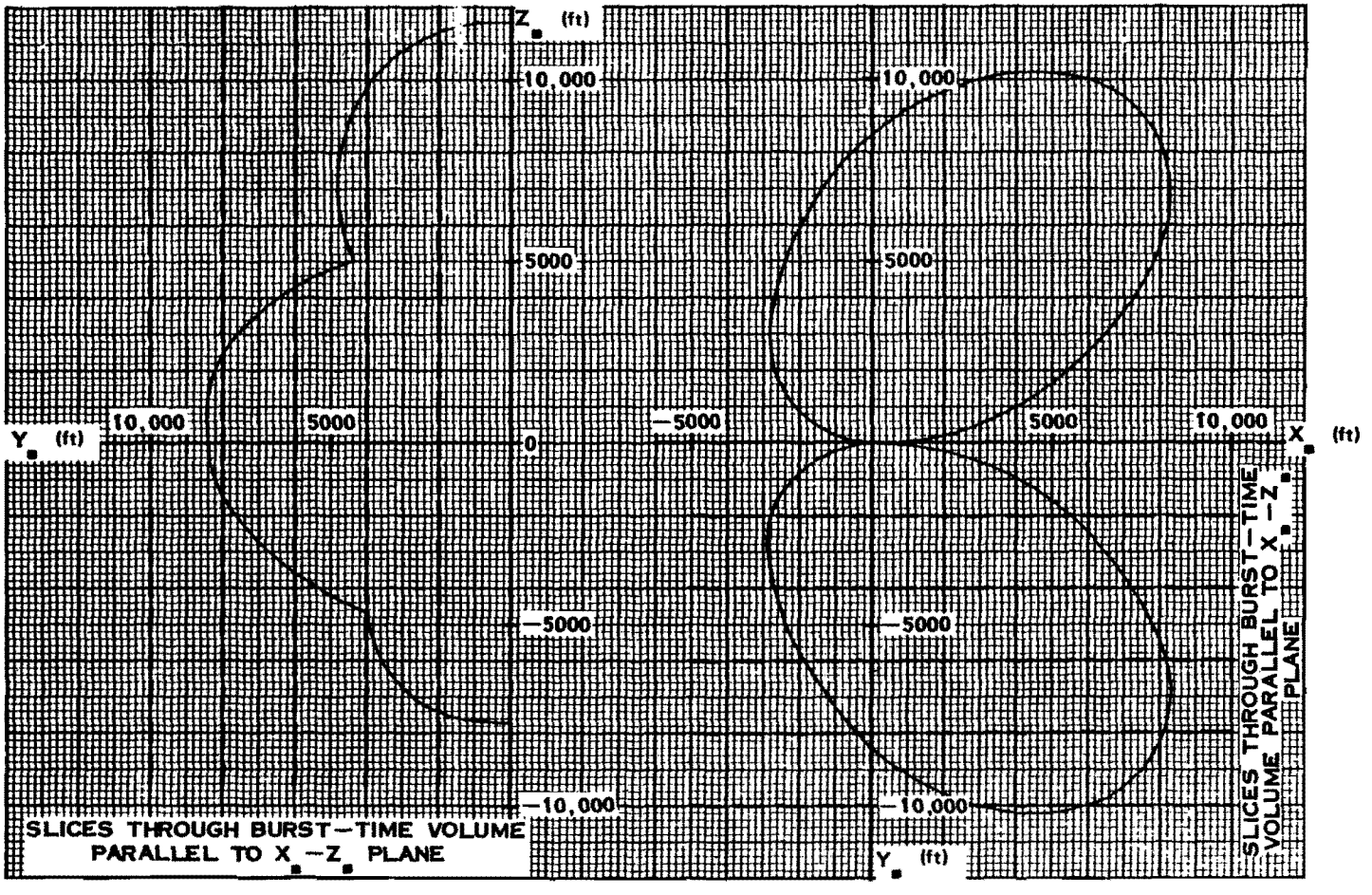

Figure 13-26a. [redacted] Burst-Time Envelope (Front View) [redacted]

Figure 13-26b. [redacted] Burst-Time Envelope (Top View) [redacted]

[redacted]

BIBLIOGRAPHY

Atkinson, G. W., and H. G. Laursen, *Nomographs for Determining the Relationships Between Pressure, Range, Altitude, and Yield in the Shock Front Resulting from a Nuclear Detonation* [redacted] NAVWEPS Report 8295, Naval Weapons Evaluation Facility, Albuquerque, New Mexico, 31 January 1965 [redacted]

Ayvazian, M., E. S. Criscione, and N. P. Hobbs, *Comparison Between Predicted and Measured Structural Responses of a Supersonic Delta Wing to Blast Loads*, AFFDL-TR-65-212, Kaman AviDyne, Burlington, Massachusetts, March 1966 [redacted]

Criscione, E., and J. Putukian, *Preliminary Estimates of the Effect of Blast-Thermal Interaction on the Vulnerability of High-Speed Aircraft in the Vicinity of a Nuclear Detonation* [redacted] ASD-TR-61-135, AviDyne Research Inc., Burlington, Massachusetts, January 1962 [redacted]

Davis, H. T., W. C. Kaufman, *An Experimental Determination of the Maximum Safe Thermal Radiation Loads for a Fighter-Bomber Cockpit*, ASRMDS-TM-63-4, Flight Dynamics Laboratory, Wright-Patterson, Ohio, January 1963 [redacted]

De Hart, R. C., N. L. Basdekas, *Response of Aircraft Fuselages and Missile Bodies to Blast Loading*, ASD TDR-62-458, Southwest Research Institute, San Antonio, Texas, January 1963 [redacted]

Donovan, A. F., and H. R. Lawrence, eds., *Aerodynamic Components of Aircraft at High Speeds, Volume VII of High Speed Aerodynamics and Jet Propulsion*, Princeton University Press [redacted]

Friedman, M. D., and J. R. Ruetenik, *An Analysis of Measured Blast Loads on Swept Wings at High Subsonic Speeds*, AFFDL-TR-65-170, MIT/ASRL TR-102-1, Massachusetts Institute of Technology, Cambridge, Massachusetts, March 1966 [redacted]

Handbook for Analysis of Nuclear Weapon Effects on Aircraft [redacted] DASA 2048, KA-TR-50A, Kaman AviDyne, Burlington, Massachusetts, April 1970 [redacted]

Hobbs, N. P., and K. R. Wetmore, *Lethality Criteria for Aircraft Exposed to Nuclear Blasts* [redacted] AFFDL-TR-66-221, Kaman AviDyne, Burlington, Massachusetts, April 1967 [redacted]

Hobbs, N. P., G. J. Frassinelli, and E. S. Criscione, *Effects of Variations in Aircraft Parameters on Blast Lethality Envelopes* [redacted] RTD-TDR-63-4087, AviDyne Research Inc., Burlington, Massachusetts, February 1964 [redacted]

Nuclear Weapons Blast Phenomena, Volume I, Source and Development of Blast Waves in Air [redacted] DASA 1200-I, DASIAC, Santa Barbara, California, 1 March 1971 [redacted]

Nuclear Weapons Blast Phenomena, Volume II, Blast Wave Interaction [redacted] DASA 1200-II, DASIAC, Santa Barbara, California, 1 December 1970 [redacted]

[redacted]

[redacted]

Nuclear Weapons Blast Phenomena, Volume III, Air and Subsurface Burst Explosions [redacted] DASA 1200-III, DASIAC, Santa Barbara, California, 1 March 1970 [redacted]

Pugh, E. J., and G. B. Bennett, *Vulnerability of Aeronautical Systems to Nuclear Effects, Volume I – Methods of Structural Analysis* [redacted] RTD-TDR-64-1, January 1965 [redacted]

Schlei, E. J., and D. H. Whitford, *The Vulnerability of Parked Army Aircraft to Nuclear Detonations* [redacted] WADC-TR-56-354, University of Dayton, Dayton, Ohio, June 1956 [redacted]

Sears, W. R., ed., *General Theory of High Speed Aerodynamics, Volume VI of High Speed Aerodynamics and Jet Propulsion,* Princeton University Press [redacted]

Witmer, E. A., J. F. Duvivier, and M. Ayvazian, *The Effects of Atomic Explosions on the Main Rotor of Helicopters in Flight* [redacted] WADC-TR-58-301, MIT/ASRL, November 1958 [redacted]

Whitaker, W. A., and R. A. Deliberis, Jr., *Aircraft Thermal Vulnerability to Large High-Altitude Detonations* [redacted]. AFWL-TR-67-85, Air Force Weapons Laboratory, Kirtland Air Force Base, New Mexico, August 1967 [redacted]

PAGE 13-88 INTENTIONALLY LEFT BLANK

[redacted]

Chapter 14

DAMAGE TO MILITARY FIELD EQUIPMENT

INTRODUCTION

One of the primary uses of nuclear weapons would be for the destruction of military field equipment. This chapter describes how a nuclear explosion can damage military field equipment and provides techniques for estimating certain types and categories of damage. Section I provides a description of the mechanisms of air blast damage to military field equipment, and some examples of variations in damage with weapon yield and exposure conditions. Section II provides the techniques for estimating the various categories of air blast damage to military material. Section III provides a brief description of damage that might be caused by missile (objects translated by the blast wave), fire, and other secondary effects. Section IV discusses transient radiation effects on electronic systems (TREES).

SECTION I

AIR BLAST DAMAGE

The military equipment that is included in this section generally can be described as that material that is used by ground forces in the field. The major types include vehicles (wheeled and tracked), artillery, small arms, communications, field radars, mines, railroad rolling stock, generators, and other miscellaneous items. Types of equipment that are specifically excluded are stationary structures, aircraft, and missile systems. The blast and thermal effects on these three types are discussed in Chapters 11, 13, and 16, respectively. This section discusses the causes and categories of blast-induced damage to the types of equipment listed above, while techniques for predicting the damage are given in Section II.

14-1 Damage Mechanisms

Most damage to military equipment is caused by the deforming action of blast overpressure or by target movement associated with the air in motion within a blast wave, i.e., the dynamic pressure. The sudden application of high pressure to the surface of a target as a blast wave envelops it can cause crushing, distortion, or buckling of components and subsystems. These may be either closed components and subsystems whose strengths are less than the forces imposed by the differential pressure between the outside and the inside of the element (e.g., fuel tanks), or open elements on which differential forces occurring during the time taken for the blast wave to envelop the element are large enough to cause failure. This type of damage predominates for very low yield weapons or for short duration pulses.

If the weapon yield is greater than several hundred tons, however, the predominant type of damage to targets in the open results from the drag force caused by dynamic pressures. These drag forces may be large enough to move properly oriented, unshielded targets great distances. They may slide, roll, or bounce along the ground surface and may be damaged seriously by the violent motions. There have been instances in which heavy equipment has been picked up and thrown dozens of feet, and then has hit the ground with sufficient force to be dismembered. Stresses induced by dynamic pressure on other types of equipment, e.g., radar or

radio antennas, can be large enough to cause failure even though the target is not crushed and no gross movement occurs prior to failure.

The preceding discussion shows that the three most important parameters involved in damage to equipment from air blast are the air blast environment, the characteristics of the target, i.e., those factors that influence its reactions to blast loadings, and the target exposure, i.e., those factors, principally target orientation and shielding, that influence the target loading and the reaction of a target to a particular blast loading.

14-2 Air Blast Environment

The various means by which air blast can damage a target can be developed most simply by considering the idealized case in which a classical, sharp fronted blast wave moving over the ground encounters a rigid, fixed cube, as previously described in Section II of Chapter 9. If the height of burst (HOB) and ground distance are scaled as the cube root of the yield, the overpressure Δp remains constant, but the shock wave duration t^+ (as in Chapter 9, the positive phase overpressure duration t_p^+ and the positive phase dynamic pressure duration t_q^+ are assumed to be equal and are designated t^+) varies as the cube root of the yield. Thus, as shown in Chapter 9, the total impulse is represented by

$$I_T = A\left[B + C\,(W^{1/3})\right],$$

where A is the area of the face of the cube normal to the blast wave, B is the overpressure contribution to the impulse, and C is the dynamic pressure contribution to the impulse. Thus, the contribution to total impulse from overpressure remains constant, while that from dynamic pressure increases as the cube root of the yield. For very low fractional kiloton yields, the loading is highly impulsive with most of the load coming from the overpressure contribution. As the yield increases, at a constant scaled HOB and ground distance, the total impulse also increases, with an increasing portion resulting from the dynamic pressure contribution.

To maintain the *same* loading on a target as the yield increases (with a constant $W^{1/3}$ scaled HOB), the actual ground distance must increase at a faster rate than would be necessary to maintain peak overpressure constant, that is, faster than the cube root of the yield. In other words, if HOB is scaled as $W^{1/3}$, ground distance must be scaled as W^n, where $n > 1/3$, to maintain the same loading on the target.

This fact has been demonstrated by theoretical calculations of the relationships between yield and ground distance for a particular target, and a particular total impulse. Typical of such calculations is that performed for the blast wave from surface burst incident on a 20 foot fixed cube at distances such that the total impulse would be 0.5 psi-sec. The results of the calculation are shown in Figure 14-1.

An excellent fit to the curve shown in Figure 14-1 was achieved with an equation of the form

$$\text{Ground Distance} = (\text{constant})(\text{yield})^n,$$

where $n = 0.4138$.

For many years, it has been observed that experimental data concerning damage to military equipment required ground distance scaling of about $W^{0.4}$. The closeness of this exponent to that derived above suggests strongly that the reason for the observed scaling is that the damage was related closely to total impulse. This hypothesis was confirmed by curve-fitting analyses of the relationships between damage to various types of equipment and various air blast parameters. Typical of the results of these analyses is one for damage to 1/4-ton trucks whose sides were exposed to blast waves from weapons ranging in yield from 0.01 kt to 10 Mt. Damage

[redacted]

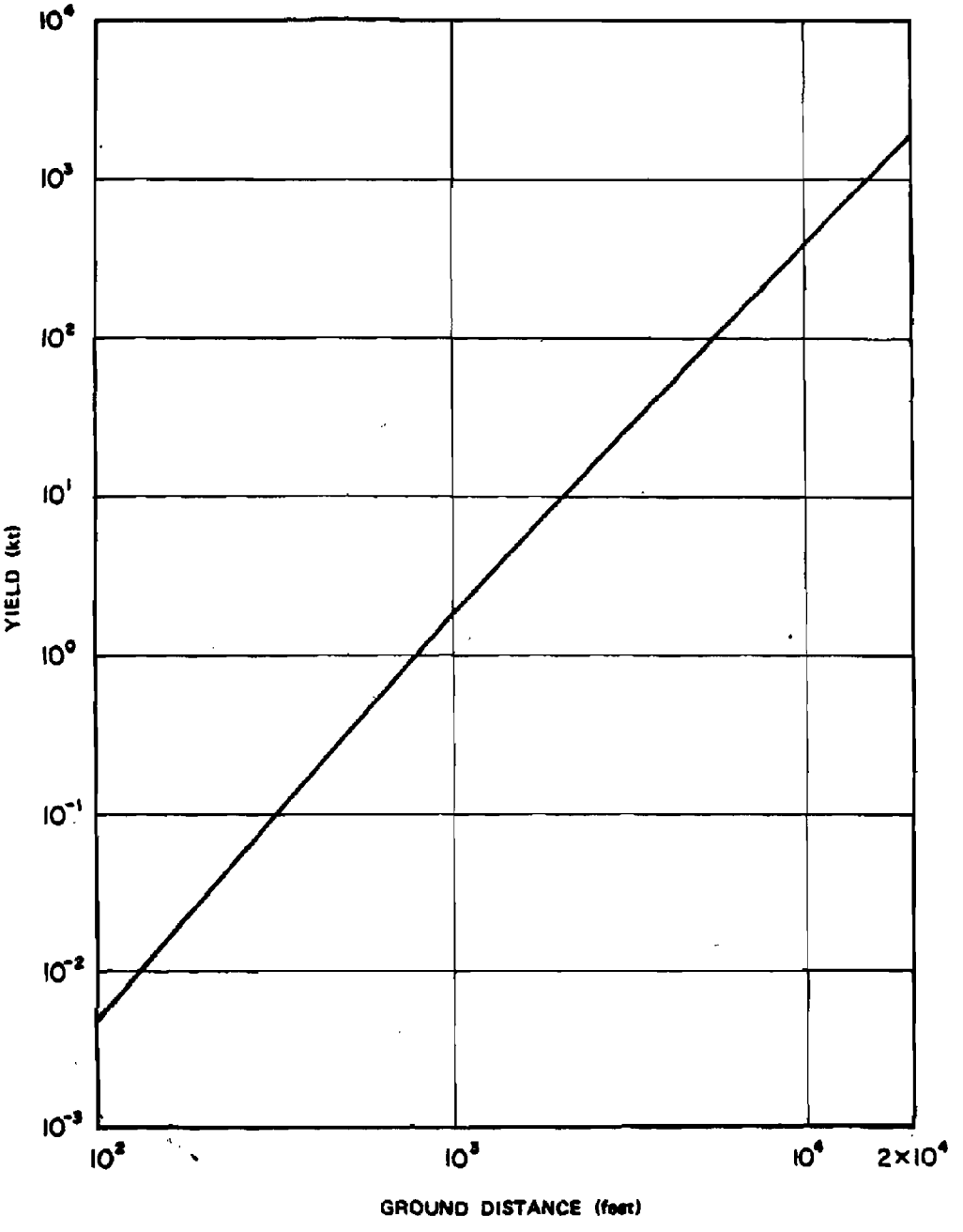

Figure 14-1. [redacted] Surface Burst Ground Range as a Function of Yield for Constant Total Impulse of 0.50 psi-sec [redacted]

[redacted]

correlation was best with total impulse (with an index of determination, I.D., of 0.77),* but the correlation was almost as good with dynamic pressure impulse (I.D. = 0.74). Much poorer correlation was achieved with dynamic pressure, diffraction impulse, and overpressure (with I.D.'s of 0.26, 0.24 and 0.22 respectively).

Most of the foregoing discussion is concerned with air blast phenomena in the Mach reflection region, where the majority of targets usually are found. In the regular reflection region, the overpressure portion of the total impulse usually dominates. This is because the target is exposed to both the incident and reflected air shock, and the horizontal components of dynamic pressure for the two shocks are small, largely because the horizontal component of dynamic pressure is proportional to the square of the sine of the angle θ that the shock front makes with the surface. For example, if θ is 45-deg, the horizontal component of dynamic pressure would be about one-half as much as the dynamic pressure for a shock making an angle of 90-deg with the surface (which is essentially the case in the Mach region). For 30-deg, the horizontal component would be only about one-fourth as much.

In this review of the discussion of the response of a simple cube to air blast a classical, sharp fronted shock wave was assumed to be incident on the cube. The influence of disturbed or non-classical wave shapes on the impulse delivered to a target can be extensive. If the wave form is not sharp-fronted, a considerable rise time may occur before the peak pressure is observed (see the wave shapes in Figures 2-40 and 2-41 of Chapter 2). If the peak overpressure is not at the front of the wave, the relationships between reflected pressure, shock velocity, sound speed, and overpressure are not valid. Furthermore, such nonideal shock waves usually are associated with precursors, within which peak dynamic pressure is not related to peak overpressure as it is with sharp fronted waves, and the dynamic pressure impulse contribution to total impulse given in Section II of Chapter 9 for a simple cube is not valid. Damage still can be related to observed air blast parameters (observed overpressures and dynamic pressures) for such wave shapes, but these parameters are not interrelated as they are for ideal waves.

14-3 Target Characteristics

Two types of target characteristics generally are of importance: the overall geometry of the target, on which blast loadings depend; and the distribution of mass in the target, which determines the kind of motions induced by the blast loading. (These can be interrelated in cases when the response of a target during loading changes its geometry and therefore its loading.)

The influence of geometry can be illustrated by considering two targets with the same cross-sectional area, one of which is composed of flat surfaces and sharp edges while the other has curved surfaces and a more streamlined shape. The target with flat surfaces and sharp edges will have a higher load because its shape will result in higher reflected pressures and drag coefficients than will occur on the smoother target. Consequently, the level of air blast required to induce motion in the non-streamlined target will be less than for the streamlined target.

The influence of mass distribution in a target can be seen by noting that for two targets of the same shape, mass, and area, but with different centers of gravity, the one with the higher center of gravity is more likely to sustain damaging motions than the one with the lower center of gravity. Furthermore, a target with a low mass will undergo greater motions than one with a high mass, if the two have the same area, shape, and location of the center of gravity. Figure 14-2 illustrates some of the types of blast-induced motion that may occur, depending

* The index of determination (ID) is used as a measure of goodness of fit of a curve. The closer the ID is to the number one, the better the fit of the curve.

[redacted]

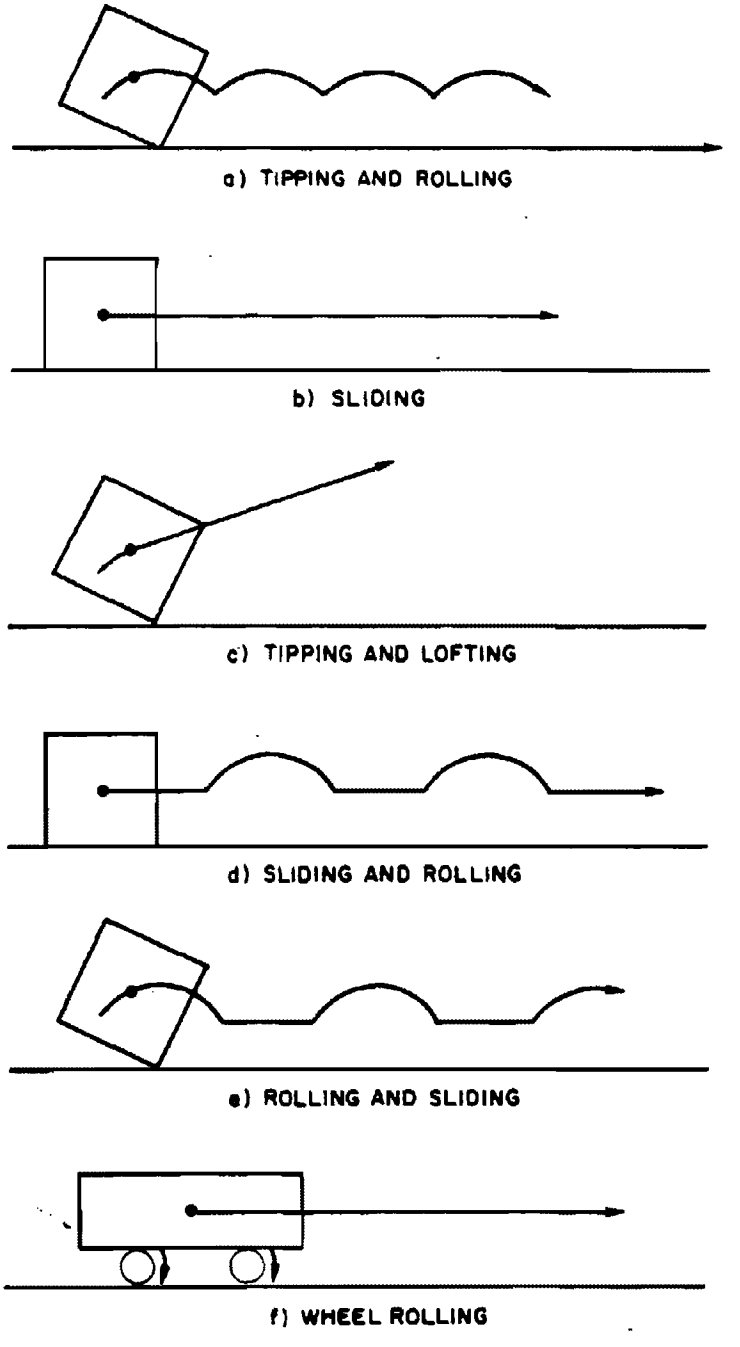

Figure 14-2. [redacted] Target Response Modes [redacted]

[redacted]

upon geometry and mass distribution.

A detailed assessment of the influences of geometry and mass distribution for each piece of equipment is not presented in this chapter. The damage assessment techniques that are presented in Section II for a variety of equipment types (e.g., wheeled vehicles, artillery pieces, tanks) and for a number of items of equipment within each type, are all based on experimental observations. One purpose of this paragraph is to emphasize the fact that different items of equipment within a single type, and even different production runs of the same item of equipment, can exhibit significant differences in damage from the same blast loadings, but they also can exhibit similarities. These differences and similarities are illustrated by several curves that show damage as a function of distance in a manner similar to Figure 14-3, in which damage on an increasing scale from none to severe is the vertical coordinate (the meanings of the damage categories shown in Figure 14-3 are described in Section II), and distance from a 1 kt surface burst at which the various categories of damage have been observed is the horizontal coordinate.* Increasing distance implies decreasing values of blast parameters, so the curve indicates that damage decreases with an increase in distance from the burst point. There are infrequent exceptions to this rule, which generally occur in the regular reflection region for large heights of burst.

Figure 14-4 shows a comparison of the damage-distance curves for two types of wheeled vehicles. Although the two vehicles differ markedly in their characteristics, the ground distances at which they sustain moderate and severe damage are not very different; however, the difference in the distances for light damage is large. Figure 14-5 shows larger differences in the damage-distance curves for the similar artillery pieces. Finally, Figure 14-6 shows fairly substantial differences in the distances at which severe and light damage occurs for two different production runs of the same vehicle.

These comparisons illustrate the difficulties that can be expected to be encountered in making damage predictions for new items of equipment for which little or no information is available.

14-4 Target Exposure

The orientation of the target with respect to the direction of travel of the blast wave, and shielding afforded by nearby terrain features can affect the response of the target significantly. The effects that differences in target exposure can have on damage may be illustrated by curves similar to the schematic presentation in Figure 14-3.

The terminology that is usually used when discussing target orientation describes which side faces the oncoming blast wave, i.e., side-on,† front-on, or rear-on to the blast. A flat surface oriented obliquely or normal to the blast will receive substantially different loads than it would if it were parallel to the blast wave. Little difference in damage is observed for front-on and rear-on orientations for many targets; in this chapter the two orientations are grouped into a single category, end-on orientation. Figure 14-7 illustrates the importance of target orientation to the extent of damage.

A target may be shielded from some of the air blast and thermal radiation effects when some substantial object or terrain feature (natural or man-made) is in the vicinity of the

* Curves were drawn by finding the horizontal scaled distances (d1, d2, etc.) at which changeover from each category of damage to the next higher category occurred. The points so derived were connected by smooth curves.

† The term "side-on" is also used in an alternate designation for incident pressure in a blast wave, i.e., "side-on overpressure" is the overpressure in an incident blast wave before it interacts with a target or object.

[redacted]

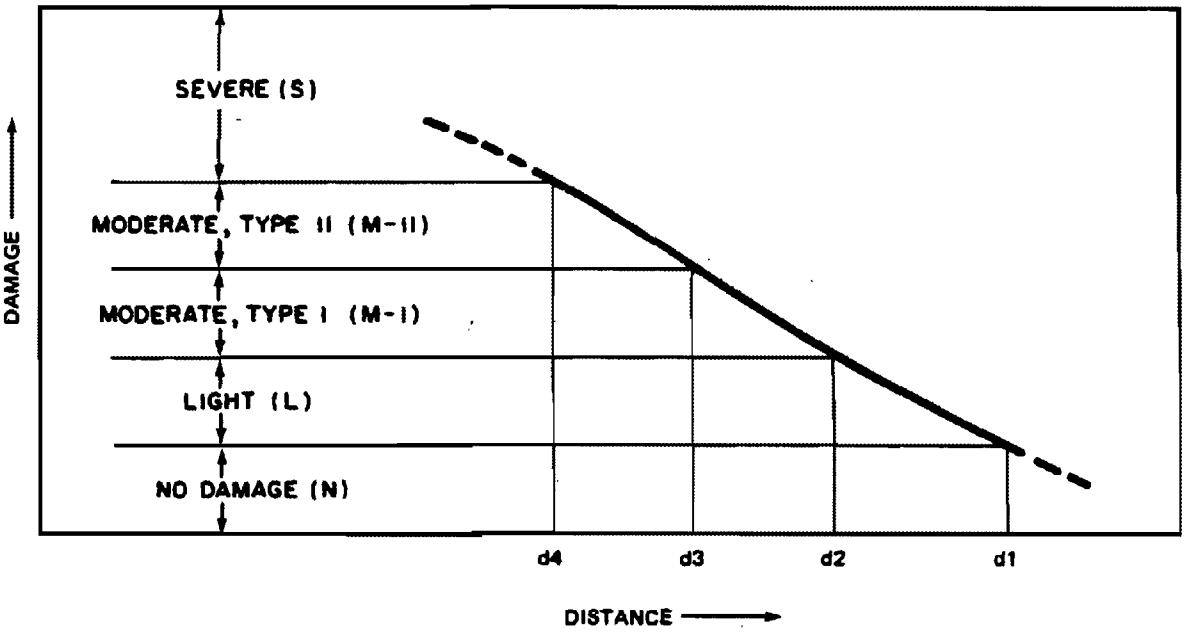

Figure 14-3. [redacted] Illustration of the Damage vs Distance Curve [redacted]

Figures 14-5 through 14-7
(Pages 14-8 through 14-11)
Deleted USANCA (L)(1)

[redacted]

[redacted]

target. Shielding is most effective when the obstacle is between the target and ground zero.

[redacted] Obstacles that are considered in the assessment of the effects of shielding from air blast are local obstacles, such as ravines, constructed slots, or revetments (the effects of large terrain features on blast waves are discussed in paragraphs 2-38 through 2-41 of Chapter 2). The importance of shielding is well documented. Comparisons of damage between shielded and unshielded vehicles exposed to blast from both nuclear and chemical explosions are available. The effectiveness of an obstacle in shielding a target generally results as much from its capability to reduce the target movement as from its ability to modify the blast environment. Figure 14-8 illustrates this point. When the obstacle is between the blast wave and the target most of the impulse or translational force that induces motion (drag loading) does not act on the target. When the obstacle is "behind" the target, the translational force initially applied to the target is the same as it would have been without an obstacle, but the obstacle not only can modify later translational forces (as a result of shock wave reflection), but it can restrict movement, the major cause of damage. The overpressure effects of crushing and fracturing still occur in both cases, and these effects provide lower limits for damage ground distances.

[redacted] Most damage resulting from low yield weapons is caused by overpressure impulse rather than translation, even for unshielded targets, and, since overpressure impulse is not altered drastically by shielding, the effects of shielding are relatively minor for such weapons. However, most damage caused to non-shielded targets by higher yield weapons results from the translational effects of dynamic pressure. Since shielding can reduce translational effects substantially, it can be quite effective as a protection from large yield weapons. Damage to shielded targets results largely from overpressure effects, for which damage distances scale as the cube root of the yield ($W^{1/3}$), while damage to unshielded targets results largely from total impulse effects (including those of dynamic pressure), for which damage distances generally scale as $W^{0.4}$. The effects of shielding are illustrated in Figure 14-9, in which damage distances for shielded targets have been scaled as $W^{1/3}$, and those for unshielded targets by $W^{0.4}$.

14-5 Effects of Ground Surface Conditions [redacted]

[redacted] Ground surface conditions affect damage in two ways: by modification of the blast parameters; and by modification of target response. The former is discussed in paragraphs 2-20 through 2-22 and 2-37 through 2-41 of

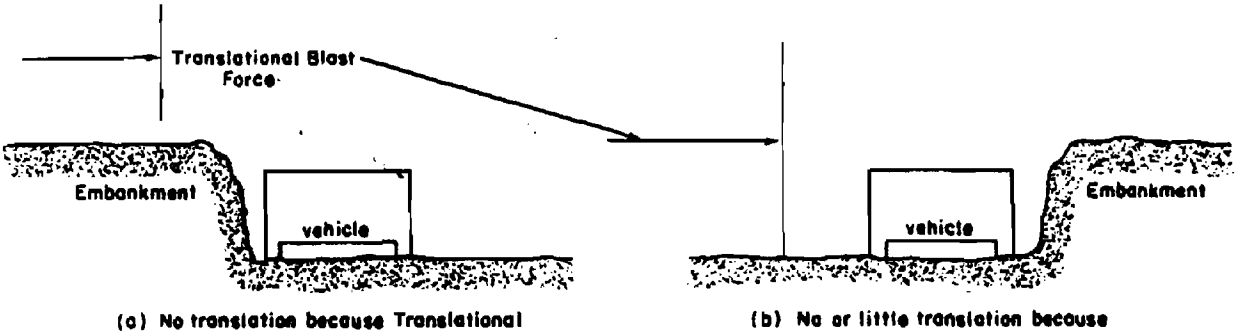

(a) No translation because Translational Force is not applied

(b) No or little translation because embankment restricts movement

Figure 14-8. [redacted] The Effect of Shielding [redacted]

[redacted]

Fig 14-9 Page 14-13 Deleted. USANCA (4)(1)

[redacted]

Chapter 2. The latter is discussed here. Information on the effects of ground condition comes from available test data on vehicles exposed on test surfaces constructed to investigate precursor phenomena. These surfaces were desert, asphalt, and desert covered with water. An analysis of these data concluded that there was a significant difference in damage to vehicles on "hard" (non-yielding, non-deforming) and "soft" (yielding, deforming) surfaces. This is illustrated by the curves in Figure 14-10. Blast wave characteristics were different at comparable scaled distances over the two surfaces. Therefore, a scale showing comparable blast wave conditions, dynamic pressure impulse, was substituted for the distance scale shown in previous figures in order to remove the influence of surface conditions on the blast wave from the comparison.

[redacted] Figure 14-10 shows that surface conditions can influence damage substantially, particularly in the moderate-to-severe categories. This is believed to result from the difference in the target response caused by the difference between the two surfaces shown in Figure 14-10. A soft surface will yield and can be deformed. These surface reactions produce resistive forces against the wheels, which tend to cause the vehicle to tip over. The same vehicle would tend to slide on a hard surface and would not necessarily overturn. The response of a vehicle on a soft surface is likely to resemble the response modes illustrated in Figure 14-2a, c, or e, whereas the same vehicle exposed on a hard surface would be more likely to exhibit the response modes illustrated in Figure 14-2b and d.

[redacted] Data, such as shown in Figure 14-10, are insufficient to incorporate the effects of surface conditions in the damage prediction techniques given in Section II, except as a source of error that degrades the reliability.

14-6 Vehicle Status [redacted]

[redacted] The response of a vehicle to the air blast wave can be influenced by whether or not the brakes are on and/or the transmission is in gear at the time of exposure. Information concerning these influences is available [redacted] Data (6)(1)

[redacted] Differences in the resulting damage occur primarily for end-on orientation of vehicles. Figure 14-11 illustrates the differences between the damage categories for two comparable [redacted] vehicles. A similar comparison for side-on orientation showed very good agreement, thus the difference shown in Figure 14-11 can be attributed chiefly to differences in vehicle status and not to difference of configuration between [redacted] 1/4-ton trucks.

[redacted] When a vehicle is exposed end-on with the brakes off and the transmission out of gear, the primary response is rolling on its wheels rather than sliding or overturning. As shown in Figure 14-11, there appears to be an upper limit on the blast forcing function, above which the vehicle will overturn because the forces are too great to be absorbed by rolling or sliding, or because the probability of encountering an obstacle to substantial movement is high. The status of the vehicle at the time of exposure may be as significant in determining the resulting damage as the orientation or even shielding; however, there are insufficient data to include this factor in the damage prediction techniques with any degree of confidence.

Fig 14-10 + 14-11 on Pages 14-15 + 14-16 Deleted. HSANCA (6)(1)

[redacted]

SECTION II

DAMAGE PREDICTIONS

14-7 Definitions of Damage Categories

The causes of damage to military field equipment by the air blast wave were described in Section I. The description of the various levels of damage (ranging from none to total) must be defined before damage predictions can be made. Various descriptors have been employed over the years by informed and experienced appraisers of damage to describe what they considered to be the degradation of the military effectiveness of various items of equipment. These descriptors, while useful, tend to be somewhat subjective, and they could result in different appraisals of the importance of damage to various items of equipment by different people.

An attempt has been made throughout this manual to describe the damage categories in sufficient detail to indicate the specific damage that applies to a given descriptor (e.g., Tables 11-1 and 11-2, Chapter 11, and Table 12-1, Chapter 12). In this chapter, an attempt has also been made to make the definitions of the damage descriptors less subjective in terms of the availability of a target to perform its intended military functions than descriptor definitions that have been used previously. The definitions that will be presented below include descriptions of the type and level of effort that would be required to restore a target to a condition in which it could perform its intended function, i.e., the definitions provide some insight into the time that would be required to perform essential repairs, although they do not include a measure of any effects that might arise as a result of a time lag before repair (see paragraph 14-13).

To arrive at less subjective definitions, the various items of equipment, which have been examined subsequent to exposure to nuclear and H.E. tests, were divided into functional subsystems. This was done for two reasons: (1) more precise descriptions of damage could be obtained by considering subsystems than could be obtained by considering the item as a whole; (2) different subsystems can have different degrees of impact on the ability of a particular item of equipment to perform its basic function. Four damage levels were defined for each subsystem: no damage; damaged, but functional; damaged, nonfunctional, but repairable; damaged, nonfunctional, and not repairable.

Damage categories for the entire piece of equipment were then defined *in terms of damage sustained by the subsystem.* The damage categories that were adopted are defined in Table 14-1.

The subsystems that were identified for wheeled vehicles are shown in Table 14-2 to illustrate the type of system divisions that were employed.

Of the subsystems listed in Table 14-2, the engine, power train, wheels, and chassis were designated critical subsystems which, if they sustain any damage – even easily repairable damage – so as to render them nonfunctional, would render the entire piece of equipment nonfunctional. Operator appliances and parts of the body generally can sustain some degree of damage that might make the individual element nonfunctional (a windshield may be broken, for example, or the hood could be torn off) but would not prevent the vehicle from performing its basic function.

Although the system for identifying damage categories described above reduces the chances of differences in making damage appraisals, some subjectivity is unavoidable, especially in the determination of whether an element of a subsystem can be repaired. A bent steering column, for example, (part of a noncritical subsystem – operator appliances) is deemed to be non-repairable, i.e., normal prac-

[redacted]

Table 14-1. [redacted] Definitions of Damage Categories [redacted]

Damage Category	Explanation
Light	Damaged, functional (no critical subsystems – and less than half of all subsystems – are nonfunctional)
Moderate Type I	Damaged, nonfunctional, repairable with little or no special tools, parts or skills (at least one *critical* subsystem is nonfunctional, but repairable)
Moderate Type II	Damaged, nonfunctional, repairable with special tools, skills, and parts (at least half of all subsystems are nonfunctional but repairable)
Severe	Damaged, nonfunctional, very difficult to repair (at least one subsystem is nonfunctional and not repairable)*

* [redacted] An exception to this rule could occur if an otherwise not repairable subsystem could be made functional by replacing it with an immediately available spare.

[redacted]

tice would be to replace it although with difficulty, and with appropriate tools, it could be repaired.

[redacted] Some typical descriptions of damage to various subsystems of a variety of items of equipment that have been assigned to the four damage categories are shown in Table 14-3. For obvious reasons this table is by no means complete (many equipment items have five or more subsystems). It is included to make the meanings of the damage categories clearer.

14-8 Prediction Techniques [redacted]

[redacted] Two types of prediction techniques are presented in this section. For individual pieces of equipment, tables are used to relate (directly or indirectly) the damage categories described in the previous paragraphs to the air blast parameter that results in a particular level of damage.

[redacted] To determine ground distance for a particular level of damage, the tables are consulted first, then air blast height of burst curves in Chapter 2 are used to find the scaled (1 kt) ground distance associated with the particular air blast parameter. Finally, appropriate scaling

Table 14-2. [redacted] Wheeled Vehicle Subsystems [redacted]

Subsystem	Name and Description
A	Operator Appliances – such as instruments, driving controls, windshield
B	Body – sheet metal work such as fenders, hood, etc.
C	Engine – including fuel, electrical, and cooling systems
D	Power Train – transmission, drive shaft, axles
E	Wheels – tires, suspension, brakes
F	Chassis – basic frame of vehicle

[redacted]

[redacted]

Table 14-3. [redacted] Typical Subsystem Damage for Various Damage Categories [redacted]

Type of Equipment	Damage Category							
	Light		Moderate Type I		Moderate Type II		Severe	
	Subsystem	Damage Description	Subsystem	Damage Description	Subsystem	Damage Description	Subsystem	Damage Description
Wheeled vehicles	Body	Glass breakage, bent fenders.	Engine	Air cleaner blown off.	Power train	Transmission broken.	Chassis	Gross frame distortion.
Artillery	Sighting	Glass breakage in optics.	Aiming	Traversing mechanism jammed.	Tube	Recoil mechanism inoperable.	Aiming	Elevating mechanism destroyed.
Tanks	External fittings Gun tube	Bent fenders. Some dirt in tube.	Aiming	Elevating mechanism jammed.	Tracks	Idlers broken, tracks bent and twisted.	Hull	Turret torn off.
Small arms	Stock/Grip	Cracked stock.			Stock/Grip	Broken stock.	Receiver/-barrel	Dismembered.
Supply dumps*	Packaging	Packaging not ruptured, items may be scattered.					Packaging	Packaging ruptured.

*POL in 5 and 55 gal. drums; ammunition and rations in standard packages; other items in small containers.

[redacted]

factors are applied to the scaled ground distance to find the actual ground distance. For broader classes of equipment, "Damage-HOB" curves are presented. These are curves that give scaled distances for particular damage categories as a function of scaled height of burst.

[redacted] The first technique, though it incorporates one additional step to find damage ranges, provides the user with some knowledge of the air blast parameters that cause damage and, by inference for certain pieces of equipment, some insight into how the equipment is damaged. For shielded equipment, for example, where, as has been discussed, the principle agents of damage are overpressure effects, the tables show this dependence as well as the need for $W^{1/3}$ scaling. Similarly, some items of equipment (antenna masts, wire entanglements subjected to bursts from medium or large weapons) are particularly susceptible to wind loading (dynamic pressure) damage, with little or no damage due to overpressure effects. Again the tables show this as well as the required $W^{1/3}$ scaling which is appropriate for dynamic pressures.

[redacted] The largest variety of equipment should be sensitive (for reasons given in Section I) to total impulse delivered to the target. Unfortunately, actual total impulse is very difficult to determine. The overpressures portion of total impulse is sensitive to the particular geometry of

[redacted]

the item of equipment being examined. It was demonstrated in paragraph 14-2 that, at least for 1/4-ton trucks oriented side-on to the blast, dynamic pressure impulse ranked second only to total impulse as an air blast parameter to which damage could be related. Thus, with a relatively small loss in accuracy (which would be largest for low yield weapons, for which overpressure effects tend to dominate), dynamic pressure impulse could be employed as an air blast parameter to correlate damage levels.

Unfortunately, height of burst curves are not readily available for dynamic pressure impulse (which would be employed in the second step in the analysis). Therefore, the tables give values of "equivalent overpressure" (Δp_{eq}) or "equivalent dynamic pressure" (q_{eq}), defined as that overpressure under near-ideal conditions, or that dynamic pressure under nonideal conditions (see paragraph 2-20 for a discussion of near-ideal and nonideal surfaces) for a particular yield and height of burst at which the dynamic pressure impulse that would cause a particular level of damage would be experienced. Where Δp_{eq} or q_{eq} are listed as damage causing parameters, ground distance scaling of $W^{0.4}$ should be used.

The damage prediction technique for individual items of equipment uses three tables and a single graph. Table 14-4 lists the equipment and identifies the appropriate table (14-5, 14-6, or 14-7) from which damage information may be obtained. Table 14-5 is for equipment that is damaged principally by total impulse (as measured by Δp_{eq} or q_{eq}), with which $W^{0.4}$ scaling should be used; Table 14-6 is for equipment that is sensitive to overpressure (Δp), with which $W^{1/3}$ scaling should be used; and Table 14-7 is for equipment that is sensitive to dynamic pressure (q), with which $W^{1/3}$ scaling should be used. Tables 14-5 and 14-6 are for use in the Mach shock region only. Table 14-7 can be used in both the Mach and regular reflection region (see paragraph 2-18 for a discussion of Mach and regular reflection regions).

The graph used in the prediction technique, Figure 14-12, relates peak dynamic pressure q to peak overpressure Δp for sharp fronted shock waves. It is useful for determining ground distances for damage to equipment that is sensitive to either equivalent dynamic pressure (q_{eq}) or actual dynamic pressure (q) for values of q below those shown in the dynamic pressure height of burst curves in Chapter 2 (distances beyond about 1,200 to 1,400 feet for a 1 kt burst). Beyond these distances, the shock waves generally are of classical form, and dynamic pressure at the wave front can be related to peak overpressure (see paragraph 2-17). The peak overpressure height of burst curves of Chapter 2 extend to about 12,000 ft from a 1 kt surface burst, and to about 25,000 feet for a 1 kt air burst (where overpressure is as low as 0.25 psi and dynamic pressure as low as 0.0015 psi).

Tables 14-5 through 14-7 generally show the value of the air blast parameter at which there is a 50 percent probability that the item of equipment will experience the indicated damage or greater. In those cases where sufficient information is available to determine the effect of orientation, values are shown for side-on (SO), end-on (EO), and random orientation. If sufficient information is not available, values are only shown for random orientation.

Figures 14-13 through 14-27 show isodamage – height of burst curves for broad classes of equipment as listed below:

Figure	Equipment
14–13	Wheeled Vehicles,
14–14	Artillery,
14–15	Tracked Vehicles (Except Tanks and Engineer Heavy Equipment),
14–16	Tanks (Light and Heavy),
14–17	Small Arms,

14-18 Generators,
14-19 Locomotives,
14-20 Box Cars,
14-21 Supply Dumps,
14-22 Telephone Poles,
14-23 Water Storage Equipment,
14-24 Shielded Wheeled Vehicles,
14-25 Shielded Engineer Heavy Equipment,
14-26 Signal, Electronic Fire Control Equipment, Antennas, and Rigid Radomes
14-27 Wire Entanglements.

A discussion of damage to untested equipment that is not included in Tables 14-5 through 14-7 or in Figures 14-13 through 14-27 is provided in paragraph 14-9 together with estimates of some damage levels.

Scaling procedures for use with Figures 14-13 through 14-27 are described in Problems 14-4 and 14-5 as well as on each figure. Strictly speaking, the damage-distance relationship does not scale as a simple power of yield for the classes of equipment included in this family of figures. The yield dependence of the scaling should be reflected by the curves in a manner similar to the presentations of damage to structures in Figures 11-2 through 11-23. Such a family of curves is in preparation; however, they are not available for inclusion in this manual. It is anticipated that such curves will be incorporated in a future change.

[redacted]

Table 14-4. [redacted] List of Equipment and Corresponding Prediction Tables [redacted]

Equipment Item	Air Blast Parameter		Table
	Near-Ideal	Nonideal	
Unshielded Equipment			
Wheeled Vehicles			
U.S. WW II 1/4-ton truck	Δp_{eq}	q_{eq}	14-5
U.S. M-38 1/4-ton truck	"	"	"
U.S. 2-1/2-ton truck	"	"	"
U.K. scout car	"	"	"
U.K. 1/4-ton truck	"	"	"
Artillery			
Towed U.S. 57-mm anti-tank gun	"	"	"
Towed U.K. 25-pounder gun	"	"	"
Self-propelled guns	q	q	14-7
Landing Vehicle, Tracked	Δp_{eq}	q_{eq}	14-5
Armored Personnel Carrier, M-59	"	"	"
Construction Equipment			
Crawler tractor	"	"	"
Road grader	"	"	"
Tanks	Δp_{eq}	q_{eq}	14-5
Generators	"	"	"
Railroad Cars	"	"	"
Radio Sets	"	"	"
Radio Aerials			
Antenna masts	q	q	14-7
Whip antennas	"	"	"
Wire Entanglements			
Yields < 1 kt	Δp	Δp	14-6
Yields > 1 kt	q	q	14-7
Small Arms	Δp_{eq}	q_{eq}	14-5
Water Storage Equipment			
Lyster bag, 36 gal	Δp	Δp	14-6
Tank, cylindrical, open top	"	"	"
Shielded Equipment			
1/4-ton Trucks	Δp	Δp	14-6
Crawler Tractors	"	"	"
Road Graders	"	"	"
Lightweight Radios	"	"	"

Tables 14-5 through 14-7
Pages 14-23 through 14-25
[redacted] Deleted. USADCA (b)(1)

[redacted]

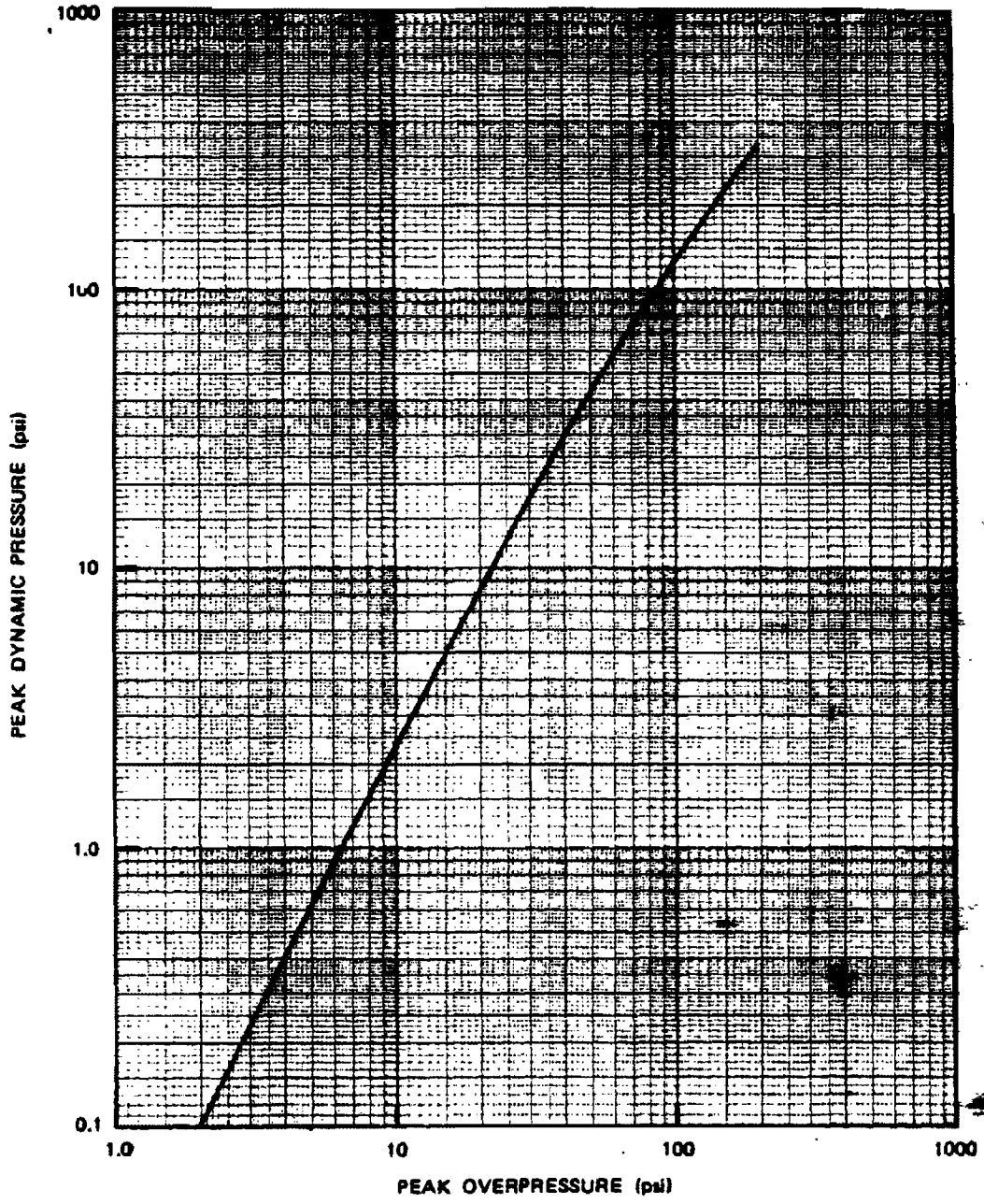

Figure 14-12. [redacted] Peak Dynamic Pressure as a Function of Peak Overpressure [redacted]

[redacted]

Problem 14-1. Calculation of Damage to Wheeled Vehicles

[redacted] Tables 14-5 through 14-7 show values of equivalent overpressure (Δp_{eq}) and dynamic pressure (q_{eq}) necessary to produce a 50 percent probability of at least the damage category indicated to items of equipment listed in Table 14-4. Ground distances must be obtained from Figures 2-18 or 2-19 for Δp_{eq}, and from Figure 2-25 for q_{eq}. In those cases where q_{eq} is lower than shown in Figure 2-25, the corresponding overpressure may be obtained from Figure 14-12. The ground distance corresponding to this overpressure may then be obtained from Figure 2-19 or Figure 2-20.

[redacted] *Scaling.* The height of burst curves of Chapter 2 must be entered with the height of burst or ground distance for a 1 kt explosion. For yields other than 1 kt, the height of burst and ground distance scale as follows:

For equipment listed in Table 14-5,

$$\frac{h}{h_1} = W^{1/3},$$

$$\frac{d}{d_1} = W^{0.4},$$

For equipment listed in Tables 14-6 and 14-7,

$$\frac{h}{h_1} = \frac{d}{d_1} = W^{1/3},$$

where d_1 and h_1 are the distance from ground zero and height of burst, respectively, for 1 kt, and d and h are the corresponding distance and height of burst for a yield of W kt.

[redacted] *Example* [redacted]:

Given: A 10 kt explosion at a height of burst of 200 feet.

Find: The ground distances for each damage category for randomly oriented 2-1/2 ton trucks for both near-ideal and nonideal (light dust) surface conditions.

Solution: From Table 14-4, the equipment is sensitive to total impulse and Table 14-5 is the appropriate table from which to obtain the damage category blast parameters. From Table 14-5, the equivalent overpressures and dynamic pressures for a 1 kt explosion over near-ideal and nonideal surfaces are:

[redacted]

[redacted]

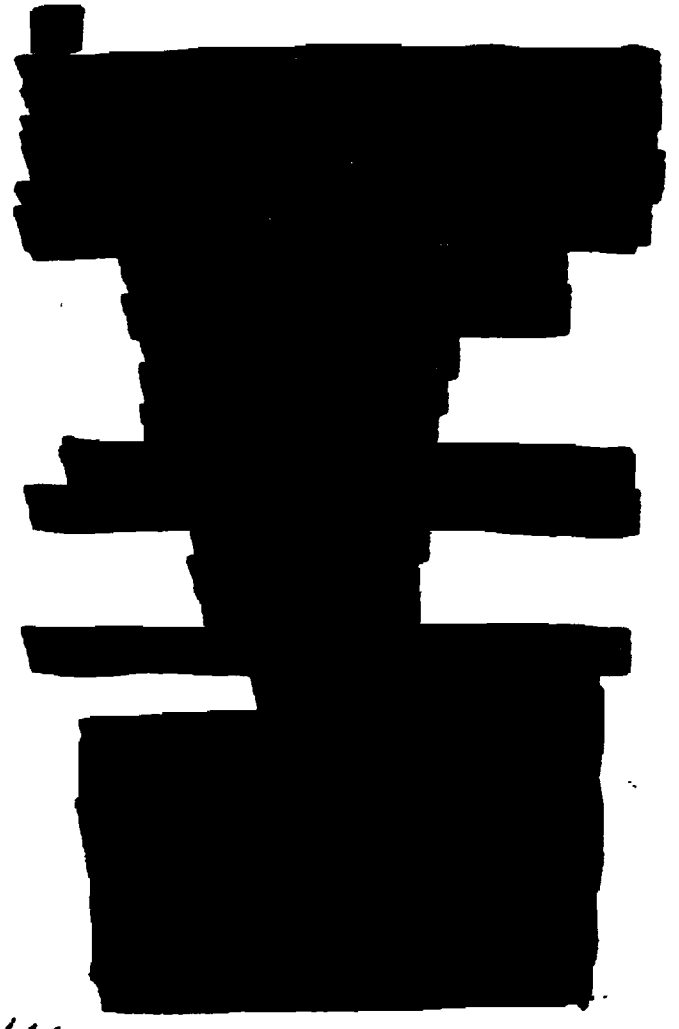

[redacted] *Reliability:* Two factors affect the reliability of damage predictions: the accuracy with which the air blast environment can be predicted; and the accuracy of the damage values or comparable data. The accuracy of the predictions of the overpressure and dynamic pressure environments is discussed in Chapter 2. The values shown in Tables 14-5 through 14-7 are for 50 percent probability with an accuracy of ±25 percent, i.e., the value for a change in damage level is for a 50 percent probability that the greater damage will occur, and the value shown in the table is accurate to within ±25 percent. These reliability and accuracy values are estimates because there are rarely sufficient data to justify a statistical analysis. The damage values with asterisks, signifying limited data, are estimated to be accurate to within ±50 percent. The loss in accuracy resulting from modifications for random orientation and shielding are believed to be small and would have little effect on the overall reliability of the damage prediction.

[redacted] *Related Material:* See paragraphs 14-7 and 14-8, Tables 14-4 through 14-7, and Figure 14-12. See also paragraphs 2-20 through 2-22, Figures 2-18 through 2-20, and Figure 2-25.

[redacted]

[redacted]

Problem 14-2. Calculation of Damage to Shielded Wheeled Vehicles

[redacted] Tables 14-5 through 14-7 show values of equivalent overpressure (Δp_{eq}) and dynamic pressure (q_{eq}) necessary to produce a 50 percent probability of at least the damage category indicated to items of equipment listed in Table 14-4. Ground distances must be obtained from Figures 2-18 or 2-19 for Δp_{eq}, and from Figure 2-25 for q_{eq}. In those cases where q_{eq} is lower than shown in Figure 2-25, the corresponding overpressure may be obtained from Figure 14-12. The ground distance corresponding to this overpressure may then be obtained from Figure 2-19 or Figure 2-20.

[redacted] *Scaling.* The height of burst curves of Chapter 2 must be entered with the height of burst or ground distance for a 1 kt explosion. For yields other than 1 kt, the height of burst and ground distance scale as follows:

For equipment listed in Table 14-5,

$$\frac{h}{h_1} = W^{1/3},$$

$$\frac{d}{d_1} = W^{0.4},$$

For equipment listed in Tables 14-6 and 14-7,

$$\frac{h}{h_1} = \frac{d}{d_1} = W^{1/3},$$

where d_1 and h_1 are the distance from ground zero and height of burst, respectively, for 1 kt, and d and h are the corresponding distance and height of burst for a yield of W kt.

[redacted] *Example* [redacted]:

Given: A 20 kt explosion at a height of burst of 500 feet.

Find: The ground distances for each damage category for 1/4-ton trucks within revetments, i.e., shielded on two sides.

Solution: From Table 14-4, shielded vehicles are overpressure sensitive and Table 14-6 is the appropriate table from which to obtain the damage category blast parameters. Since no particular orientation was specified, random orientation is assumed. From Table 14-6, overpressures for a 1 kt burst over a near-ideal surface are:

[redacted]

USAMICA
14-29

[redacted]

[redacted]

USANCA (b)(1)

[redacted] *Reliability:* Two factors affect the reliability of damage predictions: the accuracy with which the air blast environment can be predicted; and the accuracy of the damage values or comparable data. The accuracy of the predictions of the overpressure and dynamic pressure environments is discussed in Chapter 2. The values shown in Table 14-5 through 14-7 are for 50 percent probability with an accuracy of ±25 percent, i.e., the value for a change in damage level is for a 50 percent probability that the greater damage will occur, and the value shown in the table is accurate to within ±25 percent. These reliability and accuracy values are estimates because there are rarely sufficient data to justify a statistical analysis. The damage values with asterisks, signifying limited data, are estimated to be accurate to within ±50 percent. The loss in accuracy resulting from modifications for random orientation and shielding are believed to be small and would have little effect on the overall reliability of the damage prediction.

[redacted] *Related Material:* See paragraphs 14-7 and 14-8, Tables 14-4 through 14-7, and Figure 14-12. See also paragraphs 2-20 through 2-22, Figures 2-18 through 2-20, and Figure 2-25.

[redacted]

[redacted]

Problem 14-3. Calculation of Damage to Wire Entanglement

[redacted] Tables 14-5 through 14-7 show values of equivalent overpressure (Δp_{eq}) and dynamic pressure (q_{eq}) necessary to produce a 50 percent probability of at least the damage category indicated to items of equipment listed in Table 14-4. Ground distances must be obtained from Figures 2-18 or 2-19 for Δp_{eq}, and from Figure 2-25 for q_{eq}. In those cases where q_{eq} is lower than shown in Figure 2-25, the corresponding overpressure may be obtained from Figure 14-12. The ground distance corresponding to this overpressure may then be obtained from Figure 2-19 or Figure 2-20.

[redacted] *Scaling.* The height of burst curves of Chapter 2 must be entered with the height of burst or ground distance for a 1 kt explosion. For yields other than 1 kt, the height of burst and ground distance scale as follows:

For equipment listed in Table 14-5,

$$\frac{h}{h_1} = W^{1/3},$$

$$\frac{d}{d_1} = W^{0.4},$$

For equipment listed in Tables 14-6 and 14-7,

$$\frac{h}{h_1} = \frac{d}{d_1} = W^{1/3},$$

where d_1 and h_1 are the distance from ground zero and height of burst, respectively, for 1 kt, and d and h are the corresponding distance and height of burst for a yield of W kt.

[redacted] *Example* [redacted]

Given: A 15 kt explosion at a height of burst of 400 feet.

Find: The damage-distance relations for a concertina wire entanglement.

Solution: Table 14-4 indicates that wire entanglements are sensitive to dynamic pressure for yields greater than 1 kt, and that Table 14-7 is the appropriate table from which to obtain the damage category blast parameters. [redacted] The equivalent height of burst for a 1 kt explosion is

$$h_1 = \frac{h}{W^{1/3}} = \frac{400}{(15)^{1/3}} = 162 \text{ ft.}$$

[redacted]

[redacted] *Reliability:* Two factors affect the reliability of damage predictions: the accuracy with which the air blast environment can be predicted; and the accuracy of the damage values or comparable data. The accuracy of the predic-

[redacted]

[redacted]

[redacted]

tions of the overpressure and dynamic pressure environments is discussed in Chapter 2. The values shown in Tables 14-5 through 14-7 are for 50 percent probability with an accuracy of ±25 percent, i.e., the value for a change in damage level is for a 50 percent probability that the greater damage will occur, and the value shown in the table is accurate to within ±25 percent. These reliability and accuracy values are estimates because there are rarely sufficient data to justify a statistical analysis. The damage values with asterisks, signifying limited data, are estimated to be accurate to within ±50 percent. The loss in accuracy resulting from modifications for random orientation and shielding are believed to be small and would have little effect on the overall reliability of the damage prediction.

[redacted] *Related Material:* See paragraphs 14-7 and 14-8, Tables 14-4 through 14-7, and Figure 14-12. See also paragraphs 2-20 through 2-22, Figures 2-18 through 2-20, and Figure 2-25.

[redacted]

[redacted]

Problem 14-4. Calculation of Damage to Artillery

[redacted] Figures 14-13 through 14-27 show families of curves that define the damage categories as functions of height of burst and ground distance from a 1 kt explosion for the several classes of equipment listed in paragraph 14-8. Separate curves are shown for near-ideal and nonideal surface conditions.

[redacted] *Scaling.* For yields other than 1 kt the height of burst and ground distance scale as follows:

For Figures 14-13 through 14-21,

$$\frac{h}{h_1} = W^{1/3},$$

$$\frac{d}{d_1} = W^{0.4},$$

For Figures 14-22 through 14-25, and 14-27,

$$\frac{h}{h_1} = \frac{d}{d_1} = W^{1/3},$$

For Figure 14-26,

$$\frac{h}{h_1} = W^{1/3},$$

$$\frac{d}{d_1} = W^{0.4}, \textit{ except Radomes, for}$$

which distance scales as,

$$\frac{d}{d_1} = W^{1/3},$$

where h_1 and d_1 are the height of burst and ground distance for 1 kt, and h and d are the corresponding height and distance for a yield of W kt. For convenience, the proper scaling is indicated on each figure.

[redacted] *Example* [redacted]:

Given: A 250 kt explosion at a height of burst of 1,250 feet.

Find: The distance to which severe damage occurs to artillery located on a nonideal surface.

Solution: The corresponding height of burst for 1 kt is

$$h_1 = \frac{h}{W^{1/3}} = \frac{1{,}250}{(250)^{1/3}} = 198 \text{ ft.}$$

The listing given in paragraph 14-8 shows that Figure 14-14 is the appropriate figure to determine damage relationships for artillery. [redacted]

[redacted]

[redacted] *Reliability:* The ground distances for the various damage categories shown in Figures 14-13 through 14-18 and 14-22 through 14-27 are estimated to be accurate generally within ±25 percent, although wide variations might occur for individual items within a class (see paragraph 14-3). These reliability values are estimates because there are rarely sufficient data to justify a statistical analysis. The ground distances obtained from Figure 14-19 through 14-21 are estimated to be accurate within ±50

[redacted]

[redacted]

percent because of the even more limited data and because of the difficulty in aggregating all supply dumps into one class. As described in paragraph 14-8, curves that reflect the yield dependence of the scaling might be expected to provide somewhat more reliable predictions; however, such curves are not available at present.

[redacted] *Related Material:* See paragraphs 14-3, 14-7, and 14-8. See also paragraphs 2-20 through 2-22.

[redacted]

Problem 14-5. Calculation of the Advantage in Shielding Engineer Heavy Equipment

Figures 14-13 through 14-27 show families of curves that define the damage categories as functions of height of burst and ground distance from a 1 kt explosion for the several classes of equipment listed in paragraph 14-8. Separate curves are shown for near-ideal and nonideal surface conditions.

Scaling. For yields other than 1 kt the height of burst and ground distance scale as follows:

For Figures 14-13 through 14-21,

$$\frac{h}{h_1} = W^{1/3},$$

$$\frac{d}{d_1} = W^{0.4},$$

For Figures 14-22 through 14-25, and 14-27,

$$\frac{h}{h_1} = \frac{d}{d_1} = W^{1/3},$$

For Figure 14-26,

$$\frac{h}{h_1} = W^{1/3},$$

$$\frac{d}{d_1} = W^{0.4}, \text{ except Radomes, for}$$

which distance scales as,

$$\frac{d}{d_1} = W^{1/3}$$

where h_1 and d_1 are the height of burst and ground distance for 1 kt, and h and d are the corresponding height and distance for a yield of W kt. For convenience, the proper scaling is indicated on each figure.

Example

Given: A 250 kt explosion at a height of burst of 1,000 feet over a nonideal surface.

Find: The advantage in shielding engineer heavy equipment at a distance of one mile from the expected ground zero.

Solution: The corresponding height of burst for 1 kt is

$$h_1 = \frac{h}{W^{1/3}} = \frac{1{,}000}{(250)^{1/3}} = 159 \text{ ft.}$$

The listing given in paragraph 14-8 shows that Figure 14-15 is the appropriate figure to determine damage relationships for unshielded engineer heavy equipment, and Figure 14-25 is appropriate for shielded engineer heavy equipment. The corresponding ground distance from a 1 kt explosion for use with Figure 14-15 is (see *Scaling* above)

$$d_1 = \frac{d}{W^{0.4}}$$

$$d_1 = \frac{5{,}280}{(250)^{0.4}} = 580 \text{ ft.}$$

The corresponding ground distance from a 1 kt explosion for use with Figure 14-25 is (see *Scaling* above)

$$d_1 = \frac{d}{W^{1/3}}$$

$$d_1 = \frac{5{,}280}{(250)^{1/3}} = 838 \text{ ft.}$$

[redacted]

Reliability: The ground distances for the various damage categories shown in Figures 14-13 through 14-18 and 14-22 through 14-27 are estimated to be accurate generally within ±25 percent, although wide variations might occur for individual items within a class (see paragraph 14-3). These reliability values are estimates because there are rarely sufficient data to justify a statistical analysis. The ground distances obtained from Figure 14-19 through 14-21 are estimated to be accurate within ±50 percent because of the even more limited data and because of the difficulty in aggregating all supply dumps into one class. As described in paragraph 14-8, curves that reflect the yield dependence of the scaling might be expected to provide somewhat more reliable predictions; however, such curves are not available at present.

[redacted] *Related Material:* See paragraphs 14-3, 14-7 and 14-8. See also paragraphs 2-20 through 2-22.

Figures 14-13 through 14-27 on Pages 14-37 through 14-51 are deleted.
USAMCA (L)(1)

[redacted]

[redacted]

14-9 Untested Equipment [redacted]

[redacted] Although a wide variety of equipment is included in Tables 14-5 through 14-7, many items are not listed, principally because they were never subjected to the air blast environment of nuclear or large HE tests. In some cases it is possible to deduce an approximate set of damage criteria, either because the untested equipment is comparable in some degree to some item that was tested, or because subsystems of the new equipment are similar to subsystems on tested equipment. The principles and the damage agents described in paragraphs 14-1 through 14-6 should aid in predicting damage to untested equipment, although familiarity with subsystem response (a subject beyond the scope of this chapter) would be more satisfactory.*

[redacted] Table 14-8 lists a number of items of equipment for which approximate levels of damage were deduced from the principles outlined previously. The response information shown in Table 14-8 is generally considered to be accurate to within ±50 percent, unless otherwise stated. This is caused by the inherent inaccuracies associated with the use of the comparability principle, which is primarily useful for obtaining estimates. The remainder of this section describes how the damage levels were determined.

[redacted] *Bridges, Mobile Assault:* A specific example of this equipment is the "Bridge, Floating: Mobile Assault, 36-ft." This item should be examined for its response when on the road, and when in the water. Unfortunately no information about its response in the water exists.

[redacted] When on the road and side-on, the critical angle† for overturning is about 45 degrees, which is comparable with a 2-1/2-ton truck. The area of the side-on vehicle is at least twice that of a 2-1/2-ton truck, and the weight is about four times as much. Because the moment of inertia about an overturning axis would be large, the primary response mode is expected to be sliding. However, because of the box-like configuration and the large, flat-topped surface, a large lifting force is quite possible. In addition, the large weight force on each of four wheels is likely to cause a buildup of resistive force during sliding. It therefore appears reasonable to assume that overturning occurs shortly after sliding begins.

[redacted] In the end-on configuration, the sloping surface of the vehicle will cause a significant vertical force. However, the extremely large moment of inertia in this orientation should provide resistance to overturning. The construction of the item, in addition to the flotation gear, may make it vulnerable to low overpressures. A rupture of the hull or flotation gear would make the item useless until repairs are made. In this instance, whether the item was made of steel or aluminum, the thickness of hull, and whether of riveted or welded construction, would be significant. Thermal effects on flotation gear are not expected to cause rupture or burning except at high yields, although the flotation gear may be torn loose in the end-on configuration.

[redacted] Additional information concerning this item would increase the reliability of damage predictions. Until such time as more information becomes available, the following values are recommended.

[redacted]

USANCA (k)(1)

* [redacted] P. J. Morris, *Study of Military Field Equipment Response to Air Blast and Prediction of Damage (U)* describes predictions based on subsystem response (see bibliography).

† [redacted] Angle through which the item must rotate for the center of mass to be placed over the center of rotation.

‡ [redacted] Use $W^{0.4}$ scaling for ground range.

[redacted]

Table 14-8 Page 14-53 is deleted.
USANCA (k)(1)

[redacted]

[redacted] *Camouflage Nets.* These items are rarely considered in damage predictions. They are included in Table 14-8 primarily as a possible source of fires. Very low dynamic pressures, on the order of 2 psi, are sufficient to destroy their effectiveness for concealment. Cloth netting generally is destroyed by a thermal exposure of 15 cal/cm^2. Cloth nets can be a considerable fire hazard if this amount of thermal energy is received prior to the arrival of a low overpressure blast of about 5 psi, which may be insufficient to extinguish pre-blast flames. Plastic netting is not as susceptible to burning, but it will melt and char at a thermal exposure of approximately 10 cal/cm^2.

[redacted] *Carriers, Full Tracked.* Some data are available on equipment that predates present equipment, e.g., the Armored Infantry Vehicle, M59. So few data are available on similar current equipment, however, that any attempt to apply M59 information to current equipment could be misleading. Present vehicles are significantly different from the M59 since they are constructed of aluminum, whereas the M59 was constructed of steel. The response of carriers is believed to be similar to that of wheeled vehicles in that a boxlike construction and large areas make it susceptible to overturning. It appears that the damage values for 1/4-ton trucks may be appropriate until actual response information becomes available.

[redacted] *Engineer Construction Equipment.* Tabulated values for road grader and tracked tractors are probably appropriate for the present equipment; however, these response tables are based on very few data points, which undoubtedly affects their reliability. The characteristics of the equipment exposed in nuclear tests are not known, and comparisons with present items cannot be made. It is believed, however, that differences will be relatively small.

[redacted] No test information is available for wheeled scoop loader type equipment. Since it is a four-wheeled, rubber-tired vehicle, comparison with other wheeled vehicles is inevitable.

[redacted]

USAMC (L)(1)

[redacted] *Howitzers, Self-Propelled.* The M108 105-mm, M109 155-mm, and M110 8-in. self-propelled howitzers are examples of this equipment type. The M108 and M109 howitzers are more similar in mass distribution and geometry to tanks than to the howitzers exposed during nuclear tests. Their somewhat higher profile and more "bulky" construction of the turret indicate they would be more susceptible to overturning than tanks. Nevertheless, the damage values for tanks should provide a good estimate until a closer examination of these items is made. The 8-in. howitzer on the other hand has a configuration similar to howitzers that were exposed at tests; thus, the damage values for the T97 self-propelled howitzer should provide a good estimate.

[redacted] Damage values for self-propelled howitzers are based on very little data, and care should be exercised in using the tank damage values for the M108 and M109. One major consideration not previously mentioned with regard to these items is the lack of data or analysis for howitzers exposed with their gun tubes in a firing position. Such a configuration could change the response of these items materially as a result of a change in the dispositions of blast forces and resisting moments.

[redacted] *Howitzer, Towed.* Three examples of this category of equipment are the M101A1 105-mm light howitzer, M114A1 155-mm medium howitzer, and M115 8-in. heavy howitzer. Damage values are available for the 57-mm antitank gun and the U.K. 25 pounder. The damage values for the 57-mm AT gun probably can be used for the M101A1 105-mm light how-

[redacted]

[redacted]

itzer, but insufficient information is available for the M114A1 155-mm medium howitzer, and M115 8-in. heavy howitzer.

[redacted] *Radar Sets.* The AN/MPQ-4A radar set is used primarily to locate hostile mortars and to adjust low-velocity artillery fire. When this equipment is in transit, the antenna group and power supply are each mounted on two-wheeled trailers. The antenna trailer has outriggers for stability. The control unit for the radar and power supply can be removed for remote operation from the power supply trailer, which contains a gasoline generator. When in remote operation the control unit is mounted on a tripod-type stand and weighs about 575 pounds. The only response tables which deal with items that resemble any of this equipment are the ones for skid- and trailer-mounted generating sets. The vulnerability of the power supply trailer might be correlated with a trailer-mounted generator, and the antenna group with a skid-mounted generator. The antenna group is difficult to analyze because of its uniqueness, plus the fact that the trailer outriggers should significantly reduce its vulnerability to overturning. The antenna reflector should be the most vulnerable subsystem of this group, and damage to it would probably determine the overall damage category of the radar system. Thus the damage values for generators may be used as an estimate if the antenna reflector is added as another subsystem, which results in the following approximate damage values for both near-ideal and non-ideal blast conditions.

[redacted]

[redacted] Another radar set that may be used as an example is the AN/TPS-25. This is a combat surveillance, night vision, target acquisition radar. There are three major groupings of components in the system. The antenna, antenna mast, radar modulator, and receiver-transmitter are grouped together and connected by cable to the shelter that contains the radar controls and plot board, and houses operating personnel. The system is powered by a remotely located gasoline generator. The shelter may be located either on the ground or on its transporting vehicle, a 2-1/2-ton cargo truck or 3/4-ton or 1-1/2-ton two-wheeled trailer. All components are packed in the shelter during transit or when not in use. The antenna mast comes in three 6-1/2 foot tubular sections, one, two, or three of which may be used. The antenna mounted on the mast weighs about 150 pounds. The modulator rests on the ground next to the antenna mast. [redacted]

[redacted] *Radio Sets and Terminal Telegraph.* The radio sets AN/GRC-26D, AN/GRC-50, AN/MRC-80, and terminal telegraph-telephone

[redacted] Use $W^{0.4}$ scaling for ground range.

[redacted]

[redacted]

[redacted] AN/MCC-6 are normally located in electrical shelters mounted on a 2-1/2-ton cargo truck. These shelters have sheet metal walls, metal frames, and wooden interior walls, ceiling and floor. [redacted]

[redacted] The last example of radio sets is the AN/VRC-12. This is the basic means of communication for vehicles and crew-served weapons upon or within which it is mounted. Its power comes from the vehicle or weapon electrical system. These radios use a whip antenna; they are transistorized except for two tubes in the transmitter driver and power-output stages. The VRC-12 is constructed with printed circuit boards. Therefore, vulnerability should differ considerably from the damage values given for lightweight radios in Table 14-5. Printed circuit boards generally are more vulnerable to shock and vibration than wired circuits. Since these radios are located on or in vehicles and crew-served weapons, the response of the carrier controls the response of the radios to some degree. [redacted] For low yields and shielded vehicles, the following values apply for damage to radios from overpressure.

[redacted] *Wheeled Vehicles.* An example of how untested wheeled vehicles might be analyzed is given by this analysis of the M51A2 5-ton dump truck. Few data exist for a 5-ton dump truck (no vehicles exposed at nuclear tests were loaded). The response of a loaded vehicle could be significantly different because the overturning forces would have to be increased. In fact, the possibility of a sliding response would have to be closely examined. The gross unloaded weight of this vehicle is quite large, about 23,000 lb with a center of gravity that is undoubtedly below the center of pressure, so the vehicle probably would overturn were it not for the high overturning moment and angle required. It is not possible to state categorically how this vehicle will respond. Test data do indicate that when it does overturn, the dump body is separated from the chassis, resulting in serious damage. Therefore, the application of the Table 14-5 damage values for 2-1/2-ton trucks will quite likely result in an overestimation of the low-damage-category ground ranges and an underestimation of the high-damage-category ground ranges.

[redacted] A truck-mounted water purification set is an example of a special-purpose wheeled vehicle. This item is quite likely to have different responses, depending on whether the water purification set is in operation or the equipment is closed down for transport. In operation, side

[redacted] Use $W^{1/3}$ scaling for ground range.

[redacted]

panels of the truck body are opened, exposing the purification equipment directly to blast. In addition, the open compartment would increase the clearing times for the reflected pressure and increase the drag coefficient for dynamic pressure. The weight of this item is not known, but it is obvious that the center of gravity would be relatively high. Coupled with the high surface areas, this virtually assures overturning at relatively low blast values. The response of the purification equipment mounted on the truck chassis cannot be estimated without detailed analysis. However, the response of the item as a whole is believed to be quite similar to a 1/4-ton truck.

Supply Dumps. Damage to supply dumps should be considered in a functional sense. The purpose of a supply dump is to serve as a collection, storage, and dispensing point for materiel. Available information indicates the effect of a blast wave is to scatter containers, at times rupturing the containers and spilling the contents. If the contents are not in bulk form, such as fuel, the contents generally are not damaged. Thus the collection and storage of materiel is not significantly affected. However, the scattering of supplies and blocking of access aisles can degrade the effectiveness of the dump in issuing supplies. The size of the stacks of supplies appears to influence the amount of scattering through some type of volume-vs-area ratio. The blast winds remove boxes, etc., from outer layers in an unravelling process. Since, for a given volume, the area exposed to blast winds depends upon the number of stacks, shielding of supply dumps, such as placing them below ground level, is quite effective in that dynamic pressures have much less area to act on. Overpressure then becomes the dominant factor causing damage. Since contents of supply dumps generally are resistant to crushing forces, an overpressure level of 30 psi is recommended for shielded supply dumps. A dynamic pressure of 5 psi is recommended for unshielded supply dumps. These values are expected to cause major disruption of the supply dump either through damage to or loss of contents or scattering and mixing of containers.

SECTION III
DAMAGE FROM CAUSES OTHER THAN BLAST AND NUCLEAR RADIATION

14-10 Fire Damage

Damage to equipment by fire is referred to in some damage reports. Although some 20 occurrences have been noted, they involved only a very small percentage of the equipment exposed. Most fires appeared to be secondary in nature, that is, they were not started by direct thermal radiation ignition. Two equipment items were burned during nuclear tests under exposure conditions in which they could have received virtually no thermal radiation. In addition, a 1/4-ton truck exposed at a 100-ton high explosive test (in which thermal radiation was negligible) also burned.

The damage to a 6-kVA generator exposed on a U.K. test is particularly interesting. In the damage report the notation is made, "Fire may have started from fuel from broken carburetor spilling on hot muffler." U.K. practice at nuclear tests was to expose running equipment, that is, the engines were running at the time of the explosion. The six recorded occurrences of fires on U.K. tests represents a considerably larger percentage (about 10 percent) of all U.K. equipment exposed than does the number of fires recorded on U.S. tests. Since this may be due to the U.K. practice of running engines during a test, the incidence of secondary fires in an operational situation may be higher than the U.S. test data indicate.

Although it is believed that most fires in the U.S. tests were from secondary rather than

[redacted]

primary thermal ignitions, the source of some of these secondary ignitions is not clear. The two 1/4-ton trucks that burned on one U.S. test were believed to have been ignited by burning asphalt. In one case of a tank exposed to a very low yield burst, personnel reentered the area of the burst shortly after detonation, approaching within 2,000 ft of ground zero at H + 1 hour. No smoke or open flames were observed. However, approximately 1/2 hour later some smoke was observed, although its cause is not known.

[redacted] Shielding from direct thermal radiation occurs when the target is below a line from the burst point to the top of any obstacle, that is when the target is in the shadow cast by the obstacle. The obstacle blocks essentially all thermal radiation. Some thermal radiation will still reach the target via the scattering of radiation by the atmosphere. This scattered radiation can be substantial for large yields because the long distances traveled by the radiation increase the opportunities for scattering. Considerable radiation can also be backscattered from clouds. There is not, however, enough information on scattering to be able to predict damage resulting from thermal radiation to shielded targets.

[redacted] Because the incidence of fires was so low in the U.S. tests (though limited British experience suggests that fires could more frequently occur in operational situations), fire damage is not normally considered in assessing damage to military equipment.

14-11 Obscuration of Optical Devices [redacted]

[redacted] Obscuration of optical devices can be an important type of damage. Evidently, the thermal radiation impinging on coated or painted surfaces near an optical surface together with blast winds, results in the deposit of sufficient sooty material that the optical surface would have to be cleaned prior to use. Most of the information on this phenomenon was obtained from U.S. and U.K. damage reports on exposed tanks, and some scattered data are available on the artillery optics. Although there is no physical damage to the optics, the obscuration is sufficient to preclude their use, and some remedial action must be taken to make them useful.

[redacted] USAMCA (E)(1)

[redacted] Little is discernible in the data about the effect that orientation has on which surfaces become sooted, but it seems wise to develop criteria for sooting of all surfaces. Since most nuclear tests were conducted under nearly ideal atmospheric conditions, and there probably was little scattering of thermal radiation, sooting was probably limited to those surfaces more directly facing GZ.

[redacted] USAMCA (A-X)(1)

[redacted] The data from the exposure of tanks at nuclear tests are sufficiently extensive that obscuration of optics is included in damage estimates for tanks; however, there is insufficient information to apply this process to other optical systems with any reliability.

14-12 Damage by Missiles [redacted]

[redacted] Missiles are objects that are picked up and translated by the blast wave with sufficient velocity that, upon impact with an item of equipment, the stem may be damaged. Examples of such objects are rocks, gravel, sticks, structural debris, battlefield debris, etc. Instances of missile damage are scattered throughout the damage reports of nuclear tests. Some examples are the puncturing of a tire, fuel tank, or radiator by a stick or stone.

[redacted] Missile damage usually has not been included in damage analysis and prediction tech-

[redacted]

niques because its frequency of occurrence is quite low, and it is rarely possible to predict when an item of equipment would be damaged by a missile. Missile damage, therefore, generally is not considered in damage analysis. (An exception for sand and gravel missiles is the chipping and cracking of glass surfaces by blast-wind-transported material. This phenomenon is mentioned in damage reports with sufficient regularity to include it as a damage mechanism even though it rarely makes optical systems completely inoperable.)

Another possible agent of damage that falls under the general category of missile damage is the deposit of dirt, sand, and gravel in gun tubes and in some cases machine-gun barrels. Although there are several specific references to this problem in the test reports, there are no references for dynamic pressures above 10 psi. The more spectacular physical damage that occurred at high dynamic pressures may have caused this effect to be neglected in the examination of the equipment. There are rare references to sand and dirt getting into the breech mechanism, making it difficult to operate.

Deposition of foreign matter in gun tubes does not seem to depend upon orientation of the tubes, which may be explained by the fact that material is transported by both the positive and negative phase of dynamic pressure. In actual combat, there might not be as much sand and gravel as on the desert where nuclear tests were conducted, but there could be other sources of particulate matter available. A little dirt in a gun tube may only mean an increased rate of wear if the gun is fired before cleaning, but it could also lead to more catastrophic damage. Consequently, the possible effects of material deposition within gun tubes should be considered in assessing damage to equipment with such tubes.

14-13 The Effects of Time

Time itself is not a damage mechanism. However, the time lag between occurrence of damage and efforts to repair the damage may alter the damage level of one or more subsystems of military equipment significantly. For example, hydrostatic lock may develop in overturned engines; fuel, water, and oil may leak, and require replacement before the equipment is functional; the corrosive action of spilled battery acid or solvents can render subsystems inoperable; soft systems, such as electronics, may be exposed to weather, making them inoperable. Such events can not only increase damage levels but also can increase the amount and nature of effort necessary to repair the damage.

The damage reported on nuclear tests frequently included some effects of time, although damage reports attempted to compensate for time delays. Test areas often were not reentered nor damage assessments made until many days after the explosion. In an operational situation, particularly if personnel are in a warned protected status at detonation time, recovery efforts would probably start in a matter of hours rather than days. Since the significance of time after damage is extremely difficult to assess quantitatively (because of unknowns in the disposition and capability of repair or recovery efforts soon after detonation) damage assessments included herein do not include the effects of time before repairs can be made.

SECTION IV

TREE DAMAGE CRITERIA

The phenomena associated with transient radiation effects on electronics (TREE) are discussed in Chapter 6. Section VII of Chapter 9 discusses component part and circuit response to nuclear radiation. This section provides estimates of nuclear radiation levels sufficient to cause moderate to severe effects in military equipment. The discussion in this section is limited to electronics, without regard to the system structure or the operator.

[redacted]

SYSTEMS ANALYSIS

14-14 Types of Systems Analysis Used in TREE

Two approaches may be used in systems analysis with respect to TREE, and each leads to a different result. The first approach to survivability analysis addresses the question of whether the system will malfunction during or after exposure to a specifically defined threat or a given set of radiation hardness criteria. The end result is that a system can be classified as vulnerable, questionable, or hard to that specified radiation threat. The survivability of the system can then be improved by redesign of the more vulnerable circuits or subsystems. Although the system may be classified as hard to the specified radiation threat, there is no certainty that the vulnerability levels of the system will have been identified. This approach to survivability analysis may be adequate in some instances, but changes in threat environment, system mission or tactics will require another complete analysis.

The second approach to survivability analysis differs from the analysis described above in two major respects. First, it includes a detailed vulnerability assessment which defines the susceptibility level of each circuit or subsystem to all types of radiation threats, not just a particular one. Second, it is concerned with the statistics of failure for any component or subsystem variations in failure level for all radiation threats. With these data, the system may be evaluated for a specifically defined threat and any variations in the threat resulting from changes in system employment or tactics. In this section interest centers on the expanded survivability analysis approach.

14-15 The Complexity of Performing System Analysis for TREE

The complexity of circuit and system analysis is increased when it becomes necessary to understand the system response during and after exposure to nuclear radiation. This environmental constraint can change or modify the characteristics of the electronics in a very time dependent manner. The level of understanding and the accuracy in prediction of individual component part response often is not sufficient to allow accurate analysis. Therefore testing (in many cases extensive testing) is necessary to establish component part response and to verify circuit analysis. This, however, is not the complete answer to the additional complexity. The radiation response of component parts can vary widely. For example, samples of a certain transistor type can sustain significant variations in percentage of gain degradation for a given neutron exposure. Component part response can also depend on the particular bias conditions under which the part is being operated. That is, the component part could be most vulnerable to a particular radiation component (e.g., gamma rays) in one bias condition while in another bias condition it may be most vulnerable to a different radiation component (e.g., neutrons). The degree of susceptibility can change with bias conditions. As stated in Section VII of Chapter 9, the response of component parts can depend on prompt dose or dose rate. In survivability analysis, both cases must be considered. This possibility of double dependence also applies at the circuit and subsystem levels of response.

The circuit and subsystem design also are critical with respect to radiation susceptibility. The fact that a component has a significant response to a certain level of radiation does not mean that the circuit that uses that component will be susceptible to the same level of radiation. The radiation susceptibility level of the circuit could be higher or lower than the levels of any of the component parts used in the circuit. The tolerances within which each component part and circuit has to perform in order for the system to achieve its function is a factor

[redacted]

[redacted]

in establishing the susceptibility of the circuit. Information of this nature, however, usually is only available during the design phase and frequently must be obtained through a detailed circuit analysis. The tolerances of the critical component parts and circuits, once obtained, are typically so narrow that another complete analysis of the component response and circuit interactions is required to establish the survivability of the system.

[redacted] For similar reasons a problem occurs in the analysis of generic functions, such as an amplifier, flip-flop, or clock circuit. Circuit functions can be performed by a large number of circuit configurations using a very large variety of component part types. Thus, it would be necessary to review all pertinent configurations and component part types that would accomplish the desired function in order to determine the survivability of the generic function. Also, the level of confidence associated with a specific vulnerability level for a generic function would be much lower than that for a specific circuit with specific component parts.

[redacted] The last factor that affects the accuracy of the system analysis is the determination of the environment. That is, the environment that is used to generate the TREE response data (for use in the analysis) has to be correlated to the actual use environment. This correlation may be in error by as much as an order of magnitude unless care is taken to include all factors that may affect the correlation.

[redacted] All these influences are in addition to the normal circuit and systems analysis problems. The resultant analysis becomes a complex manipulation of many interactions. Hence this type of analysis requires skill and understanding in order to approach a reasonably good characterization of the system response to a nuclear-weapon threat.

14-16 Characteristics of the Analysis Used in This Section [redacted]

[redacted] A primary concern of this section is to provide an appreciation for the survivability levels of military electronic equipment exposed to radiation from nuclear weapons. For the purposes of this section, only two levels of survival are used – a "sure safe" level and a "sure kill" level. The term "sure safe" implies a zero percent probability of failure while the "sure kill" implies a 100 percent probability of failure. A great deal of generalizing has taken place in this section (i.e., the discussion is by generic term, and each generic term, such as radio, has hundreds of variations). As a result very low confidence levels are necessarily placed on the "sure safe" and "sure kill" terms. Even with a particular system it is difficult to establish a particular probability of failure with a high degree of confidence because of the problems involved in evaluation of circuit and system responses.

[redacted] These levels of "sure safe" and "sure kill" were established without regard as to whether the system was operating or not operating at the time of the explosion. The levels were established on the basis of system analyses that have been performed on systems in each of the categories. Where analysis information was lacking, estimates were made on the basis of the component parts typically used in that particular generic class and worst-case circuit conditions were assumed. No consideration was given to the aging of the equipment.

[redacted] Utilization of the estimates presented in the latter portion of this section requires that the system be considered to be divided into subsystems according to function. The relative vulnerability of each subsystem can then be estimated on the basis of the subsystem levels presented in the text of this section. If by chance a subsystem does not fit the generic functions listed, the best estimate would have to be based on

[redacted]

[redacted]

[redacted]

the susceptibility of the component parts used in that system. Component part susceptibility is reviewed in the following subsection and is discussed in more detail in Section VII of Chapter 9.

[redacted] THE SURVIVABILITY LEVELS PROVIDED IN LATER PARTS OF THIS SECTION ARE MEANT TO BE USED ONLY AS GUIDES. THEY *SHOULD NOT* BE USED TO FULFILL A REQUIREMENT OR TO ESTABLISH THE VULNERABILITY OR SURVIVABILITY OF A PARTICULAR SYSTEM. More detailed information may be obtained from the TREE (Transient-Radiation Effects on Electronics) Handbook (see bibliography) as well as other references listed in the bibliography.

[redacted] REVIEW OF ELECTRONIC SUSCEPTIBILITY TO NUCLEAR RADIATION [redacted]

14-17 Component Part Vulnerability [redacted]

[redacted] Any discussion of vulnerability or survivability is ultimately based on some definition of failure. In keeping with the scope of this manual, two cases of failure are considered. First, any condition which renders the electronic equipment inoperable following exposure to a nuclear burst constitutes a system failure. The second definition of failure involves those cases where it is critical that the equipment function during the radiation exposure in order to complete a critical mission. In the latter case, a system malfunction initiated during the exposure that causes loss of the mission objective is classified as a failure.

[redacted] Under the first definition of failure, consideration is given primarily to permanent damage in the electronics. The loss of one or more bits of information within a computer as a result of transient effects would not constitute a failure by this definition, if, after reinitialization, the computer functioned satisfactorily, and if the system operation was not critical during the time of the weapon burst.

[redacted] Permanent damage to electronics can result from (see Section VII, Chapter 9):

[redacted]

USAMC (R)(1)

[redacted] Collectively speaking, burnout problems from voltage and current transients normally are not a problem with [redacted] Infrequent exceptions may occur by gate breakdown in MOS transistors, or in poorly designed circuitry. Since gamma rays are not attenuated appreciably in their passage through the electronics package, [redacted] The internal and external X-ray environments can differ considerably, depending on packaging, and other shielding, and the X-ray spectrum (hot or cold, see Chapter 4). [redacted]

USAMC (R)(3)

[redacted] This assumes roughly 98 percent attenuation of X-rays in transit through packaging, which implies a relatively cold source or effective shielding.

[redacted] Neutrons normally affect semiconductor component parts long before they affect other component parts such as capacitors, resistors, and transformers. Among the semiconductor types, unijunction transistors, silicon-controlled

[redacted]

rectifiers, low-frequency and power-type transistors are notably poor performers. The maximum tolerable neutron fluence (or range of fluences) for various semiconductor types are listed below.

[redacted]

Thus, in analyzing systems for hardness, the subsystems containing sensitive semiconductors are likely to be the most vulnerable.

The third type of permanent damage, likely to occur during a nuclear burst is X-ray induced thermomechanical shock. Thermomechanical-shock effects are such that, for a specific device type, there is no unique radiation level that will cause a specific effect.

[redacted]

These levels are the values *at* the component part. Because of the variation in X-ray spectra for various conditions, it is not possible to suggest general X-ray levels external to the systems that will result in these effects.

[redacted]

The second type of failures (failures during exposure) typically are caused by the ionization (gamma and X-ray) dose rate. In component parts, the typical effect is the introduction of potentially large photocurrents that result in a temporary malfunction of the component. This effect could result in a system malfunction if, for example, the extraneous current pulse fired a pyrotechnic device prematurely, or changed a bit of data in a logic circuit required for critical guidance functions. Devices particularly susceptible to large photocurrents are large-area, and/or high-gain devices. Typically the photocurrents generated below 10^6 rads (Si)/s are not sufficient to cause malfunction. Failures resulting from prompt dose effects are closely associated with the dose rate effects. Prompt dose is that dose accumulated during the initial gamma pulse (~0.1 microseconds, see Chapter 5) whereas the total dose is that accumulated over seconds or up to a minute (or longer, if the equipment is in a residual radiation field). Prompt doses as low as 0.1 rad (Si) can

[redacted] To a first approximation, n/cm^2 ($E > 10$ keV, fission) $\simeq$ n/cm^2 (1 MeV silicon damage equivalent).

[redacted] Some quartz resonator crystals and MOS field-effect transistors are very sensitive to gamma radiation.

cause silicon control rectifiers to malfunction, and, normally, prompt doses over 100 rads (Si) will perturb most component parts sufficiently to cause all unhardened circuits to malfunction.

14-18 Subsystem Vulnerability

Generally it is those subsystems that use the more vulnerable semiconductor component parts that will limit the hardness of a system to radiation. The relative sensitivity of semiconductor devices to radiation was outlined in paragraph 14-3. Some of the more common circuits that are likely to use these component parts, and the attendant approximate hardness levels will now be described.*

Unijunction transistors commonly are employed in time-delay circuits, pulse generators, clocks, pulse-shaping circuits, and as a trigger device driving SCR's.

Power transistors generally are of two types: low-frequency types, such as those used in power supply dc-dc convertors or series regulators; and radio frequency (rf) power-amplifier types.

Linear integrated circuits (amplifiers, etc.) are more susceptible to permanent damage than digital types, but the former are not used widely in military equipment.

Possibly the most critical part of a system is its power source. Power supplied from a motor-generator, dynamotor or battery is least likely to fail in a radiation environment.

Failure levels are typical of those listed for power transistors.

Circuits that must retain information are susceptible to transient damage. That is, transient photocurrents can introduce erroneous information into the memory system or even change the information in the memory system.

Integrated circuits can be triggered into a malfunction called "latchup" by the prompt ionizing dose at levels from 10 to 100 rads (Si). Latchup can be important because this particular condition may burn out the circuit or just simply not allow recovery to proper operation for periods long compared to the normal circuit-recovery times.

Section VII, Chapter 9 provides more detailed information concerning circuit response to radiation.

TREE-DAMAGE ESTIMATES

Estimates of system damage from nuclear-burst radiation are based on two factors. First is the likelihood that a given system type contains a susceptible circuit or subsystem as described in paragraph 14-18. Second is the probable environment in which the equipment will be used. Differences in shielding afforded by aircraft, missile, ship, or jeep installations could be significant for some components of nuclear burst radiations.

The estimates that are given in succeeding paragraphs are not all inclusive in the types

* Estimates are based on the assumption that the equipment was not designed with radiation hardness as a parameter, i.e., they are unhardened.

[redacted]

of systems or installations covered. The cross section of systems should provide some basis for estimating the radiation damage threshold of other similar equipment.

[redacted] Radiation levels given in the following paragraphs are considered to be external ambient levels. The gamma environment assumes monoenergetic photons having an energy of approximately 1 to 1.5 MeV. A slightly degraded fission spectrum is assumed for neutrons. The X-ray sources postulated for these estimates are blackbody spectra [redacted]

DNA (L)(3)

[redacted]

14-19 Ground Equipment [redacted]

[redacted] Estimates of radiation levels sufficient to cause failures as previously discussed are shown in Table 14-9 for typical ground installations or ground support equipment under the heading "sure kill." A lower threshold for failure, below which the equipment in question may be considered operable is referred to as "sure safe." All radiation levels are external ambient values that have meaning only for *unhardened* systems. For hardened systems, the hardening specifications should be consulted. It should be borne in mind that the fact that a system has been hardened does *not* mean that it will survive all radiation environments. It should, however, survive at least those to which it was hardened. It is further assumed that for most reasonable surface encounters, [redacted]

USAMCA (L)(1)

[redacted] No ambient exposures are given for X-rays (cal/cm^2), since these depend strongly on the X-ray spectrum, which in turn, is extremely dependent on the weapon type and the degradation of the spectrum through the intervening space. [redacted]

USAMCA (L)(1)

[redacted] Except under unusual circumstances, X-rays probably do not pose a significant threat for ground equipment.

14-20 An Example of Ground Equipment Survivability Estimation [redacted]

[redacted] The Lance support system provides an illustration of the use of Table 14-9. The missile itself is found under the heading "Ground and Sea Support Equipment"; however, the levels listed for the Lance are associated only with the missile and not with the launch support equipment or the communications equipment necessary to direct the launch. The associated critical electronic equipment for launch can be listed as follows:

1. Radio receiver and transmitter, or transceiver
2. Batteries to fire the missile and to operate the launch vehicle
3. Fire control system for the missile.

[redacted] The survivability levels for most of these subsystems can also be found in Table 14-9 and are listed on page 14–67. The firing system, not being listed in the table, must be estimated. A basic description of this system implies that it is a box of electrical toggle switches and lights; which apply power and indicate operation. These component parts are not particularly susceptible to radiation. Therefore, they should be at least as hard as the systems with semiconductor devices. Therefore, they will be considered as part of the communication electronics without affecting the analysis.

[redacted] With this summarized information any of three possible situations can be visualized for analysis:

[redacted]

USAMC (L)

[redacted] The critical factors affecting mission completion in the first case are:

Page 14-66 with Table 14-9 Deleted. USAMCA (L)(1)

[redacted]

[redacted]

USANCA (L)(1)

[redacted]

USANCA (L)(1)

[redacted] For this case the gamma rate would not be critical, since the missile is not in operation and the other equipment does not have to function during the burst.

USANCA (L)(1)

[redacted]

Either the neutrons or gamma rays specified for the sure-kill level could cause significant problems, and both should be considered.

[redacted] The second case [redacted]

USANCA (L)(1)

[redacted]

[redacted] The sure-safe and sure-kill levels for this situation appear to be the same as the previous case. However, the gamma dose rate could cause problems and should be considered in the sure-safe level.

[redacted] For the third case the missile is dependent solely on itself for control and the levels of survivability are the same as those shown for the missile alone.

14-21 Aircraft Systems [redacted]

[redacted] Estimates of sure safe and sure kill radiation levels in aircraft systems are shown in Table 14-10. These levels are considered to represent external ambient conditions. As was the case for ground equipment, the total dose is not considered to be a problem, and thermomechanical shock from X-rays is not considered important. However, the ionization rate includes both the X-ray and gamma-ray rates.

[redacted] The functional breakdown for aircraft systems is more complex than that for ground systems, since many mission functions require several generic functions within the subsystems. As an example, penetration aids, such as terrain clearance radars, include power sources, radars, computers, flight control links and crew station data display consoles. A brief listing of subsystems that are considered to be part of a mission function are shown in the table. Depending on the type and mission of the aircraft of interest, some of these functions may not be critical or may not even be present in the system. For specific equipment it may be necessary to refer to the levels presented in the previous Table 14-9.

14-22 An Example of Aircraft Survivability Estimation [redacted]

[redacted] To clarify the process of analysis, two cases are considered. The first case is a single-engine spotter plane and the second is a jet fighter similar to the F-111A.

[redacted] Considering first, the spotter aircraft, the generic functions are:

Pages 14-68 and 14-69 with Table 14-10 deleted.
USANCA (L)(1)

[redacted]

[redacted]

1. Flight control
2. Crew station
3. Propulsion system
4. Mission and traffic control.

Of these, one function that might be critical to the mission is the Mission and Traffic Control. The crew may not be able to communicate their observations at a critical time, even though they may be able to escape if other generic functions failed. [redacted] If all functions except the crew station were considered, the survivability levels would still be the same. [redacted] Considering the modern fighter aircraft, it would appear that all generic functions listed in Table 14-10 might be associated with the aircraft. Depending on the mission of the plane, various combinations of these generic functions might be critical. For example, if the fighter was used for battlefield support, penetration aids would not be critical. The worst-case survivability levels would occur if both penetration aids and either the air-to-air or air-to-surface missiles were critical for mission completion. [redacted]

14-23 Missile Systems [redacted]

[redacted] The missile systems included in Table 14-11 are categorized according to mission and guidance type. Thus, the damage criteria, in general, are not representative of a specific system, but reflect the mean susceptibility of systems within each category. Furthermore, unless otherwise specified, all systems are assumed to be unhardened. The categories are not all-encompassing. Where no information was available, estimates were made as noted. Sure-safe and sure-kill levels are given in terms of radiation levels external to the system. Although not a great problem for ground or aircraft systems, X-rays represent a much more formidable threat to missile systems operating at altitudes above 20 kilometers, hence, this information is included. The sources of X-rays postulated for these estimates are blackbody spectra [redacted] No problems are anticipated with the total gamma dose effects unless the dose exceeds 10^5 rads (Si). The prompt dose effects are taken into consideration in the dose rate terms. The dose rate estimates include both the X-ray and gamma ray rates. The dose-rate estimates are based on the damage caused by ionization effects, whereas the column head the "X-ray Exposure" includes estimates based on the damage caused by the thermomechanical effects. No example is provided since it is only necessary to select the correct classification for the missile to establish its survivability levels. There are basically three phases critical to the flight of missiles:

1. Storage
2. Powered flight
3. Reentry.

A prime factor that would influence the survivability of a missile in storage is not necessarily the electronics vulnerability associated with the missile but, rather, the shielding effectiveness provided by the storage area (e.g., missile silo). The activation and ground-control electronics would be evaluated by using Table 14-9. The powered flight would be concerned with both the missile and the reentry vehicle. And, last, the reentry would be concerned only with the reentry vehicles.

[redacted]

Page 14-71 with Table 14-11 deleted.

[redacted]

[redacted]

[redacted] BIBLIOGRAPHY [redacted]

Analysis of Atomic Weapons Effects Upon Army Ground Operations Equipment [redacted], Project Attack, Third Phase Report, ORO-S-200, Armour Research Foundation, Chicago, Illinois, 18 June 1951 [redacted]

Analysis of Atomic Weapons Effects Upon Army Ground Operations Equipment [redacted], Project Attack, Fourth Phase Report, Vol. I, ORO-S-208, Armour Research Foundation, Chicago, Illinois, 9 October 1951 [redacted]

Analysis of Atomic Weapons Effects Upon Army Ground Operations Equipment [redacted] Technical Memo ORO-T-223, Vol. I, Blast Effects, Armour Research Foundation, Chicago, Illinois, 16 March 1953 [redacted]

Berning, W. W., *Predicted Effects of Atomic Weapons Upon Ordnance Equipment* [redacted], BRL 847, U.S. Army Ballistic Research Laboratories, Aberdeen Proving Ground, Maryland, January 1953 [redacted].

Berning, W. W. and N. W. Arnold, *Combat Vehicle Exposure* [redacted] Operation Greenhouse, Annex 6.3, WT 90, U.S. Army Ballistic Research Laboratories, Aberdeen Proving Ground, Maryland, August 1952 [redacted]

Bowen, I. G., et al., *A Model Designed to Predict the Motion of Objects Translated by Classical Blast Waves* [redacted], Civil Effects Study CEX-58-9, Lovelace Foundation for Medical Research, Albuquerque, New Mexico, 29 June 1961 [redacted]

Brode, H. L., *Point Source Explosion in Air*, RM-1824-AEC, The RAND Corporation, Santa Monica, California, 3 December 1956 [redacted]

Bryant, E. J. and F. E. Grubbs, *Statistical Estimation of Damage to Ordnance Equipment Exposed to Nuclear Blast* [redacted], BRL 657-RD, U.S. Army Ballistic Research Laboratories, Aberdeen Proving Ground, Maryland, April 1953 [redacted]

Bryant, E. J., N. H. Ethridge, and J. L. McCoy, *Statistical Estimation of Damage to Ordnance Equipment Exposed to Nuclear Blasts* [redacted], Operation UPSHOT-KNOTHOLE, Project 3.21, WT-733, U.S. Army Ballistic Research Laboratories, Aberdeen Proving Ground, Maryland, February 1955 [redacted]

Bryant, E. J., and J. D. Day, *Effects of Rough Terrain on Drag-Sensitive Targets* [redacted] Operation PLUMBBOB, Project 1.8b Final Report, WT-1408, U.S. Army Ballistic Research Laboratories, Aberdeen Proving Ground, Maryland, 9 November 1959 [redacted]

Bryant, E. J., N. H. Ethridge, and M. R. Johnson, *Response of Drag-Type Equipment Targets in the Precursor Zone* [redacted] Operation TEAPOT, Project 3.1 Final Report, WT-1123, U.S. Army Ballistic Research Laboratories, Aberdeen Proving Ground, Maryland, 28 October 1959 [redacted]

[redacted]

Burden, H. S. and J. D. Day, *Transient Drag Loading of Actual and Idealized Shapes from High-Yield Detonations* Operation REDWING, Project 1.5, WT-1305, U.S. Army Ballistic Research Laboratories, Aberdeen Proving Ground, Maryland, 15 March 1960

Calvin, R. L. et al., *The Effects of Atomic Blast on Military Field Equipment* Armour Research Foundation Report M041, Armour Research Foundation, Chicago, Illinois, 28 February 1955

Deeds, F. E., et al., *Mine Field Clearance by Nuclear Weapons* Operation PLUMBBOB, Project 6.1 Final Report, WT-1435, Midwest Research Institute, Kansas City, Missouri, and U.S. Army Engineer Research and Development Laboratories, Fort Belvoir, Virginia, 16 August 1960

Effects of the Atomic Bomb on Nagasaki, Japan, U.S. Strategic Bombing Survey, Physical Damage Division, Vol. I, II, III, June 1947

Effects of the Atomic Bomb on Hiroshima, Japan, U.S. Strategic Bombing Survey, Physical Damage Division, Vol. I, II, III, May 1947

Ethridge, N. H., *Blast Effects on Simple Objects and Military Vehicles* Operation SUN BEAM, Project 1.3, POR-2261, U.S. Army Ballistic Research Laboratories, Aberdeen Proving Ground, Maryland, 18 September 1964

Gwyn, C. W., D. L. Scharfetter, and J. L. Wirth, *The Analysis of Radiation Effects in Semiconductor Junction Devices*, SC-R-67-1158, Sandia Corporation, Albuquerque, New Mexico, July 1967

Hearn, J. N. W., Lt. Col., *Operation BUFFALO: Interim Report of the Target Response Ordnance Group* FWE-142, AWRE Report T25/57, Atomic Weapons Research Establishment, Aldermaston, Berks, England, June 1957

Henderson, J. E., *Vulnerability of Radar to Nuclear Explosions* AWEC/P(57)44, FWE-136, Air Ministry, Ministry of Defence, U.K., August 1957

Heyman, R. J. and H. G. Myer, *Transient Drag and Its Effects on Structures* AFSWC-TR-56-46, American Machine and Foundry, Chicago, Illinois, November 1956

Kalionowski, J. J., *A Management Guide to Transient-Radiation Effects on Electronics (TREE)* DNA 2051H, Battelle Columbus Laboratories, Columbus, Ohio, February 1972

Kaplan, K., and C. Wiehle, *Air Blast Loading in the High Shock Strength Region Part I – Analysis and Correlation, Part II – Prediction Methods and Examples*, URS 633-3, DASA 1460, URS Corporation, Burlingame, California, February 1965,

Larin, F., *Radiation Effects in Semiconductor Devices*, John Wiley and Sons, Inc., New York, 1968

Martin, A. R. F., *The Effects of Blast on Dummies and Scout Cars*, Operation ANTLER, Target Response Group, AWRE Report T6/59, FWE 238, Atomic Weapons Research Establishment, Aldermaston, Berks, England, August 1959.

McCoy, J. L., *Damage Reports on Exposed Ordnance Equipment*, Operation UPSHOT-KNOTHOLE, Supplement to Project 3.21, WT-821, U.S. Army Ballistic Research Laboratories, Aberdeen Proving Ground, Maryland, December 1954

Morris, P. J., *Study of Military Field Equipment Response to Air Blast and Prediction of Damage*, DASA 2005-1 and 2005-2, URS 660-9, URS Research Company, San Mateo, California, 2005-1, October 1971, 2005-2, January 1972

Morris, W. E., et al., *Air Blast Measurements*, Operation UPSHOT-KNOTHOLE, Projects 1.1a and 1.2, WT-710, U.S. Naval Ordnance Laboratory, White Oak, Silver Spring, Maryland, August 1955

Nelson, R. C., Capt., *The Effects of Atomic Weapons on Engineer Heavy Equipment*, ERDL Report 1443, U.S. Army Engineer Research and Development Laboratories, Fort Belvoir, Virginia, 25 April 1956

Nuclear Weapons Blast Phenomena: Volume I, Source and Development of Blast Waves in Air, DASA 1200-I, Defense Atomic Support Agency, Washington, D.C., 1 March 1971

Nuclear Weapons Blast Phenomena: Volume II, Blast Wave Interaction, DASA 1200-II, Defense Atomic Support Agency, Washington, D.C., 1 December 1970

Nuclear Weapons Blast Phenomena: Volume III, Air and Subsurface Explosions, DASA 1200-III, Defense Atomic Support Agency, Washington, D.C., 1 March 1970

Olesen, H. L., *Radiation Effects on Electronic Systems*, General Electric Systems, General Electric Company, Missile and Space Division, Philadelphia, Pennsylvania, Plenum Press, New York, 1966

Operation CROSSROADS Atomic Bomb Tests, Army Ground Group (Task Group 1.4), Report Number XRD-149, Volume I, 27 January 1946 to 27 September 1946

Operation CROSSROADS Atomic Bomb Tests, Report of Commander, Task Unit 1.4.3 (Ordnance), Report Number XRD-152, Volume IV, Appendix VII, January 27 to September 30, 1946

Seager, E. R. Drake, R. F. C. Butler, *Operation TOTEM Group 12 Report: Effects on a Landrover (car, 5 CWT, 4x4) and Generating Sets* AWRE Report T 79/54(x), FWE-131, Atomic Weapons Research Establishment, Aldermaston, Berks, England, September 1956

TREE (Transient-Radiation Effects on Electronics) Handbook Volume 1, Edition Number 3, DNA 1420 H-1, Battelle Columbus Laboratories, Columbus, Ohio, December 1971

TREE (Transient-Radiation Effects on Electronics) Handbook Edition 2, Revision 2, DASA 1420-1, Battelle Memorial Institute, Columbus, Ohio, September 1970, (to be replaced by DNA 1420 H-2 during calendar year 1972).

TREE Preferred Procedures (Selected Electronic Parts), DASA 2028, Battelle Memorial Institute, Columbus, Ohio, May 1968, (to be replaced by DNA 2028H during calendar year 1972).

Vook, F. L., Editor, *Radiation Effects in Semiconductors*, Proceedings of the Santa Fe Conference on Radiation Effects in Semiconductors, Plenum Press, New York, 1968

Willoughby, A. B., K. Kaplan, and R. I. Condit, *Effects of Topography on Shock Waves in Air* AFSWC TR-57-9, Broadview Research and Development, Burlingame, California, March 1956

[redacted]

This page intentionally left blank

[redacted]

AD-A955 399

DTIC ELECTE 2 MAR 1989 S D E

Chapter 15
DAMAGE TO FOREST STANDS

INTRODUCTION

Forest stands may protect personnel from some effects of nuclear weapon explosions, for example, the direct effects of thermal radiation; however, the trees themselves are quite vulnerable to breaking, uprooting, and ignition. Falling limbs and trees may be a hazard, and the debris on the forest floor may impede troop and vehicle movement. In dry, windy weather a nuclear explosion may ignite forest fires, and the smoke and flame may extend the range of hazardous effects many times. The vulnerability of forests depends upon recent local weather history, and upon the type of tree stand involved.

This chapter is divided into three sections. Section I provides data concerning air blast damage to various types of forest stands. Section II contains a discussion of the effects of tree blowdown on troop and vehicle movement and provides methods to predict the degree to which movement might be impaired as a result of tree blowdown. Section III provides information concerning the effects of thermal radiation on forests and the fire hazards that might arise therefrom.

SECTION I
AIR BLAST

15-1 Forest Stand Types

Forest stands may be divided into four general types for the purpose of discussing air blast effects. Types I through IV as well as the subtypes of Type IV are described in the following discussion.

TYPE I: IMPROVED NATURAL OR PLANTED CONIFER FORESTS OF EUROPEAN TYPE. Stands of this type generally occur in Western Europe. They either have been planted or are natural stands that have been cultivated. Characteristics of this type of forest include uniform tree spacing, uniform height and diameter, and a dense crown canopy. Low stumps usually will be found within the stand as a result of thinning. Lower limbs will be clear as a result of pruning, and there will be little or no underbrush. All of these characteristics combine to provide good visibility and easy passage through the forest. Damage to these stands generally is caused by breaking the trunks rather than by uprooting.

TYPE II. UNIMPROVED NATURAL CONIFER FORESTS THAT HAVE DEVELOPED UNDER UNFAVORABLE GROWING CONDITIONS. This type of forest is found in Western Europe and Southeast Asia. Random tree spacing, height, and diameter together with irregular crown canopy characterize this type of stand. The forest floor is partially covered with dead fallen trees, and where clearings occur there is usually heavy underbrush. Visibility is generally poor and passage through the forest is difficult. Damage usually results from uprooting rather than breaking.

TYPE III. UNIMPROVED NATURAL CONIFER FORESTS THAT HAVE DEVELOPED UNDER FAVORABLE GROWING CONDITIONS. This type of forest occurs in Western Europe and Southeast Asia. These forests are characterized by random tree spacing and diameter, uneven crown canopy, and irregular clearings. Visibility and passage through these stands are difficult in Western Europe, although the underbrush generally is light, since dead fallen trees clutter the forest floor.

This document has been approved for public release and sale; its distribution is unlimited.

89 3 02 035

In Southeast Asia, dense shrub undergrowths usually cover the forest floor. Damage to this type of forest usually results from uprooting.

TYPE IV. ALL TYPES OF DECIDUOUS FORESTS. The trees in these stands are similar to the deciduous trees of Western Europe and Southeast Asia. Since damage to these trees depends on the condition of the foliage, two categories must be considered: IV (f) is category type IV with foliation, and IV (d) is type IV without foliation. In both cases extensive crown damage and breakage of limbs will occur. In most ground, trunk damage will be caused mainly by uprooting. This class of forests is broken down into four subtypes:

TYPE IVa. This subtype includes two further subtypes that have different characteristics but produce similar blowdown obstacles equidistant from a particular nuclear burst. Two categories are required as a result of the difference in time required to clear away blowdown obstacles.

TYPE IVa-1. This subtype occurs in Western Europe and Southeast Asia. It includes most temperate zone deciduous forests, such as the shorter, more open parts of the dry season deciduous forests of Northern Southeast Asia and the evergreen oak forests at elevations of 3,000 to 7,000 feet in Southeast Asia. The trees

Table 15-1 Average Height of Trees, Diameter, Tree Density, and Length of Tree Stem

Forest Stand Type	Tree Diameter	Average Height of Trees* (feet)	Average Tree Density per Acre*	Average Total Tree Stem-feet per Acre*
I	up to 24 in.	130	75	9,750
II	up to 20 in.	50	260	13,000
III	up to 40 in.	80	200	16,000
IVa†	up to 40 in.	80	200	16,000
IVa‡	24-in. average	100	140	14,000
IVb‡	40-in. average	100	850	85,000
IVc§	up to 18 in.	35	40	1,400
IVd	up to 18 in.	40	100	4,000

* Stem-feet per acre is determined by multiplying average tree height by tree density.

† Considers only trees 6 in. or larger in diameter.

‡ Height varies up to 200 ft in rain forest and up to 150 ft in dry season deciduous forest for about 10 percent of trees. Diameter varies up to 80 in. for 10 percent of rain forest trees and up to 60 in. for 10 percent of dry season deciduous forests.

§ Height varies from 10–50 ft.

of this subtype are defoliated in the winter in the temperate zone with the exceptions of the evergreen oak (not defoliated) and the dry season forests of Northern Southeast Asia, which are defoliated in the summer.

TYPE IVa-2. Teak plantations and the denser, taller cloud forests that occur at lower elevations are included in this type. The teak plantation trees are planted 15 to 20 feet apart and produce a continuous canopy when foliated. No foliation is present during the dry season. The cloud forests start at an elevation of about 3,500 feet on the mountain slopes of Southeast Asia. The canopy of these forests gives a matted appearance from the air.

TYPE IVb. This subtype includes rain forests of Southeast Asia and the majority of the dry season deciduous forests of Northern Southeast Asia. Although no data are available concerning attenuation of the air blast wave, it is probable that these forests are sufficiently dense to decrease the radius of blast effect, thereby reducing the damage distance of a nuclear explosion.

TYPE IVc. This type includes cloud forests at high elevations, savannas, and low open forests that are made up of small scattered trees. This type of forest, when defoliated, is a good approximation for open deciduous wooded areas, such as orchards, in temperate zones.

TYPE IVd. This type consists of rubber plantation trees that occur mainly in Southeast Asia. The characteristics include little underbrush and dense, overlapping crowns.

[redacted] Table 15-1 shows the characteristic dimensions, tree densities, and tree stem-feet per acre for the forest stand types described above.

Table 15-2 [redacted] Index of Isodamage Curves Showing Forest Stand Type and Applicable Figure Number for Indicated Degree of Damage [redacted]

Forest Stand Type	Light Damage	Moderate Damage	Severe Damage	Total Damage
I	NA	15- 2	15- 3	15- 4
II	NA	15- 5	15- 6	15- 7
III	NA	15- 8	15- 9	15-10
IVa-1(f)	*	15-11	15-12	15-13
IVa-1(d)	15-1	15-14	15-15	15-16
IVa-2(f)	*	15-17	15-18	15-19
IVa-2(d)	15-1	15-20	15-21	15-22
IVb(f)	*	15-23	15-24	15-25
IVb(d)	*	15-26	15-27	15-28
IVc(f)	*	15-29	†	15-30
IVc(d)	15-1	15-31	†	15-32
IVd	*	15-33	†	15-34

* [redacted] The ground range for Light Damage, 50% branch breakage, is less than the ground range for Moderate Damage, 750 stem-feet down per acre.

† [redacted] Forest is of insufficient density and/or height to produce 7,500 stem-feet down per acre.

15-2 Damage-Distance Relations [redacted]

[redacted] Isodamage curves that are functions of weapon yield, distance, and height-of-burst are shown in Figures 15-1 through 15-34 for the forest stand types described in paragraph 15-1. Table 15-2 provides an index of the figures as a function of forest stand type and degree of damage. The degrees of damage shown in Table 15-2 are defined as follows:

TOTAL DAMAGE: 90 percent or more of trees are uprooted.

SEVERE DAMAGE: 9,000 feet of tree stem down per acre for coniferous forests and 7,000 feet of tree stem down per acre for deciduous forests.

MODERATE DAMAGE: 1,500 feet of tree stem down per acre for coniferous forests and 750 feet of tree stem down per acre for deciduous forests.

LIGHT DAMAGE: 50 percent breakage of crowns and branches for deciduous forests. Does not exist for coniferous forests.

Accession For	
NTIS GRA&I	X
DTIC TAB	
Unannounced	
Justification	Basis for doc
By	
Distribution/	
Availability Codes	
Dist	Avail and/or Special
A-1	

QUALITY INSPECTED 4

UNANNOUNCED

Problem 15-1 Calculation of Air Blast Damage to Forest Stands

[redacted] Figures 15-1 through 15-34 show total, severe, moderate, and light isodamage curves for different types of forest stands. Definitions of the degrees of damage are provided in paragraph 15-2. Decreases in the damage distances for shallow subsurface bursts may be estimated from Figure 11-24 by the methods described in Problem 11-2.

[redacted] *Scaling.* For yields between those for which isodamage curves are provided, scale as follows:

$$\frac{d}{d_i} = \frac{h}{h_i} = \left(\frac{W}{W_i}\right)^{1/3}$$

where d_i and h_i are the distance from ground zero and the height of burst, respectively, for yield W_i, which is the nearest yield to the desired yield for which a curve is provided; and d and h are the corresponding distance and height of burst for a (desired) yield of W kt or Mt (W and W_i must be in the same units).

For yields greater than 10 Mt this scaling becomes

$$\frac{d}{d_{10}} = \frac{h}{h_{10}} = \frac{[W(Mt)]^{1/3}}{(10)^{1/3}} = \frac{[W(Mt)]^{1/3}}{2.15}$$

where d_{10} and h_{10} are the distance from ground zero and height of burst, respectively, for 10 Mt; and d and h are the corresponding distance and height of burst for a yield of W Mt.

[redacted] *Example* [redacted]

Given:

a. A 5 kt weapon burst at a height of 400 feet above a Type IVa-1(f) forest stand.

b. A 20 Mt weapon burst at a height of 1,000 feet above a Type I forest stand.

Find:

a. The distance to which severe damage extends for the Type IVa-1(f) forest stand.

b. The distance to which moderate damage extends for the Type I forest stand.

Solution:

a. Table 15-2 shows that Figure 15-12 contains the isodamage curves appropriate for a Type IVa-1(f) forest stand. Examination of Figure 15-12 shows that the yield nearest 5 kt for which an isodamage curve is provided is 3 kt. The corresponding height of burst for a 3 kt weapon is

$$h_3 = h\left(\frac{3}{W}\right)^{1/3} = 400 \times \left(\frac{3}{5}\right)^{1/3} = 340 \text{ ft.}$$

From Figure 15-12, at a height of burst of 340 feet, the distance from ground zero to which severe damage will occur to a Type IVa-1(f) forest stand is 3,000 feet.

b. Table 15-2 shows that Figure 15-2 contains isodamage curves appropriate for moderate damage to a Type I forest stand. The corresponding height of burst for a 10 Mt weapon is

$$h_{10} = \frac{2.15\ h}{(W)^{1/3}} = \frac{2.15 \times 1{,}000}{(20)^{1/3}} = 790 \text{ ft.}$$

From Figure 15-2, at a height of burst of 790 feet, the distance from ground zero to which moderate damage to a Type I forest stand occurs from a 10 Mt weapon is 42,000 feet.

Answer:

a. The corresponding distance for severe damage to a Type IVa-1(f) forest stand from a 5 kt weapon burst at a height of 400 feet is

$$d = d_3\left(\frac{W}{3}\right)^{1/3} = 3{,}000 \times \left(\frac{5}{3}\right)^{1/3} = 3{,}560 \text{ ft.}$$

b. The corresponding distance for moderate damage to a Type I forest stand from a 20 Mt

[redacted]

[redacted]

weapon at a height of 1,000 feet is

$$d = \frac{d_{10}[W(Mt)]^{1/3}}{2.15} = \frac{42{,}000 \times (20)^{1/3}}{2.15}$$

$$= 53{,}000 \text{ ft.}$$

Reliability: The curves of Figures 15-1 through 15-34 are based on observed results of limited full scale tests, limited high explosive field tests, and extensive laboratory experiments. No definite estimate of the reliability of the scaling for yields above about 30 Mt can be made.

Related Material: See paragraphs 15-1 and 15-2. See also Figure 11-24 and Problem 11-2.

[redacted]

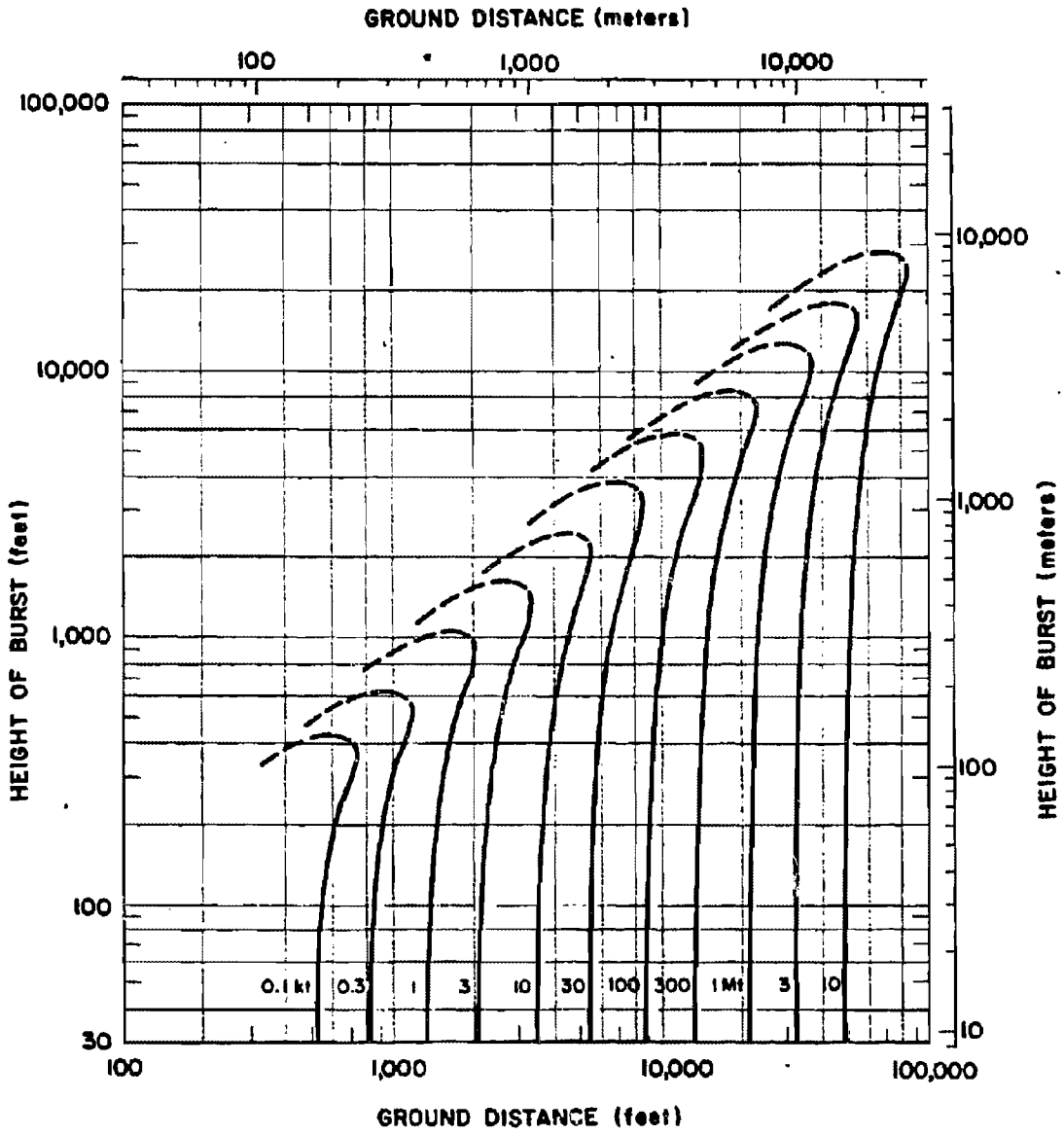

Figure 15-1. [redacted] Light Damage to Various Broadleaf Forest Types (see Table 15-2) [redacted]

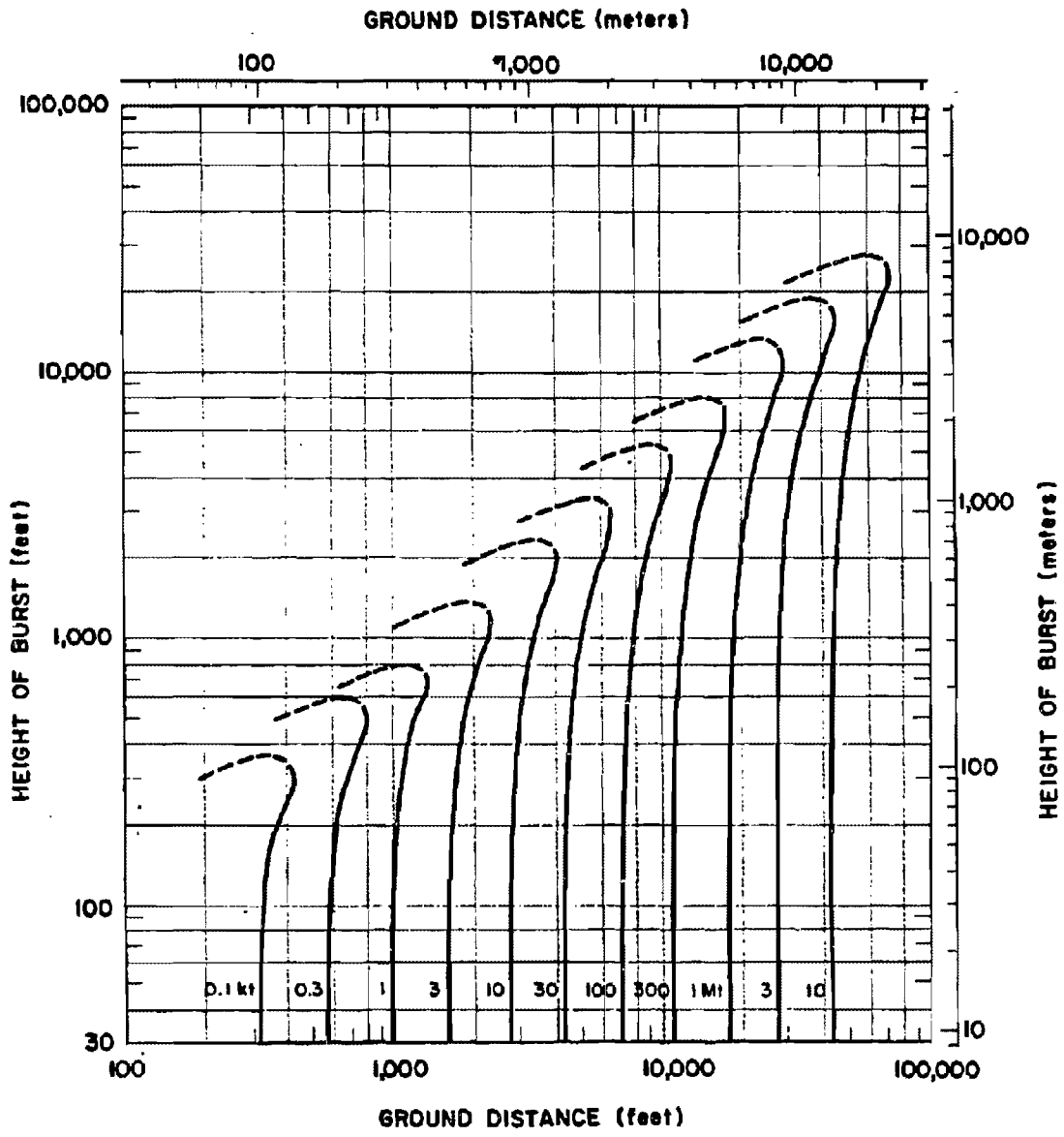

Figure 15-2. [redacted] Moderate Damage to a Type I Forest [redacted]

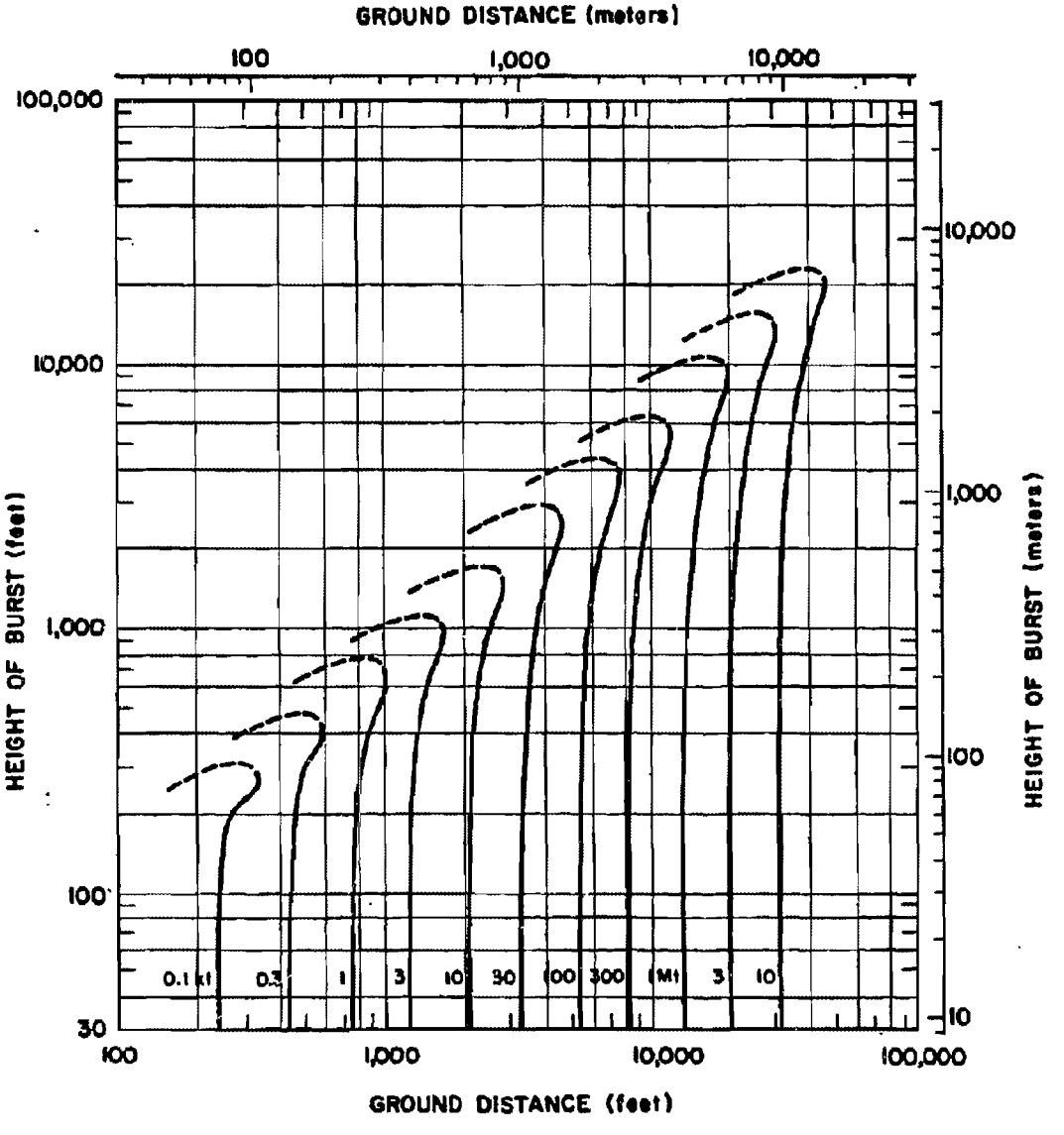

Figure 15-3. [redacted] Severe Damage to a Type I Forest [redacted]

[redacted]

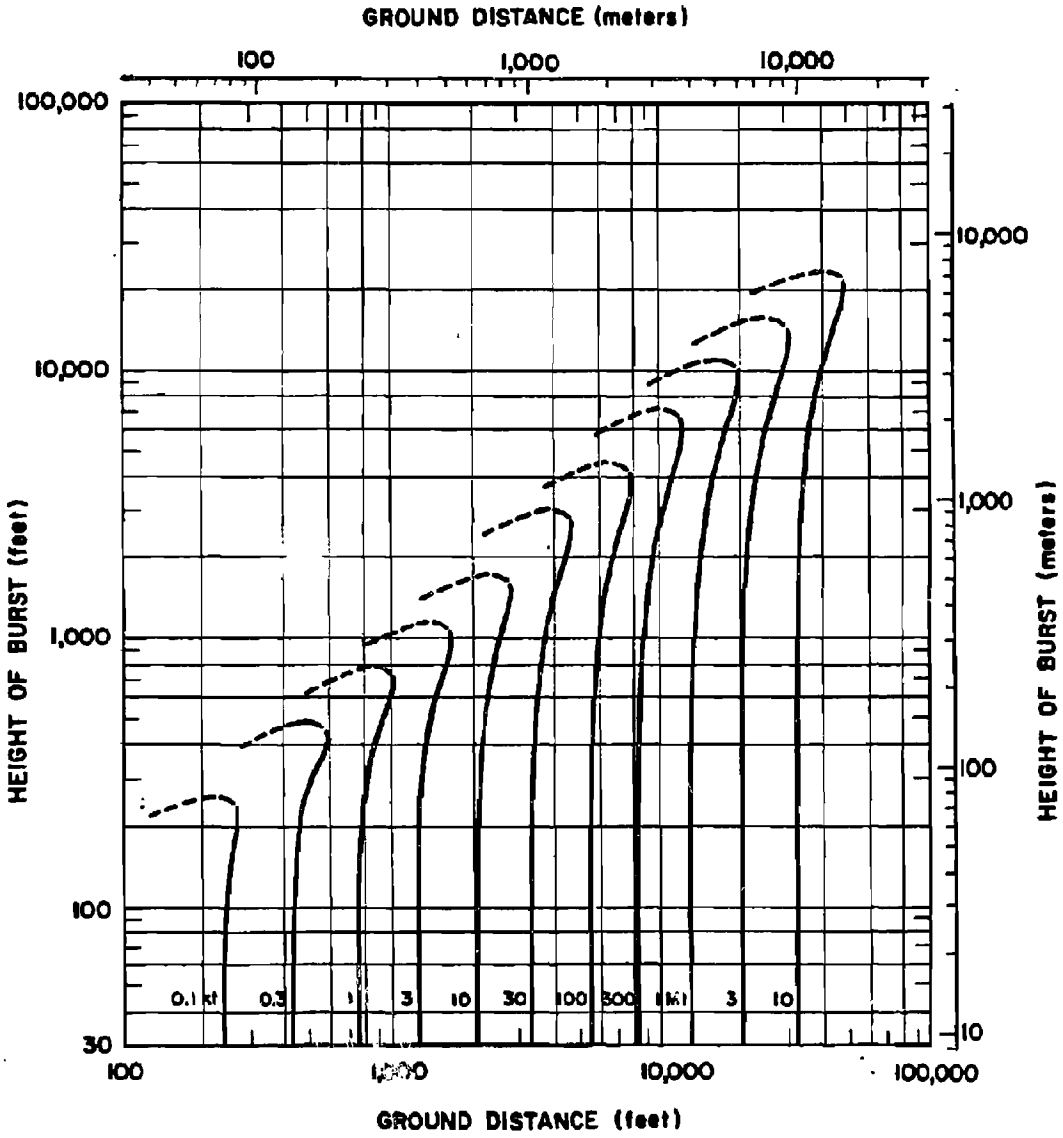

Figure 15-4. [redacted] Total Damage to a Type I Forest [redacted]

[redacted]

[redacted]

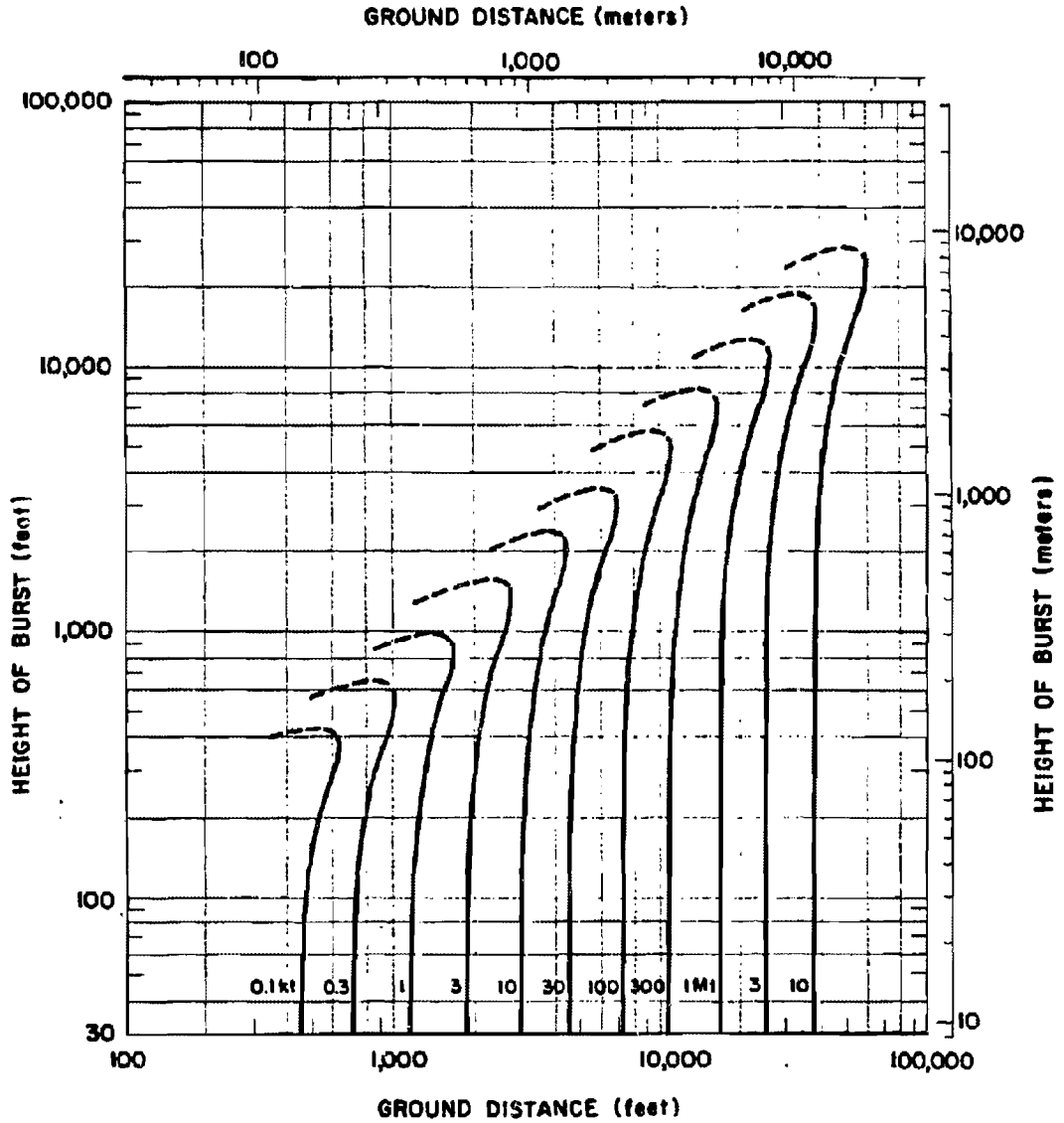

Figure 15-5. [redacted] Moderate Damage to a Type II Forest [redacted]

[redacted]

[redacted]

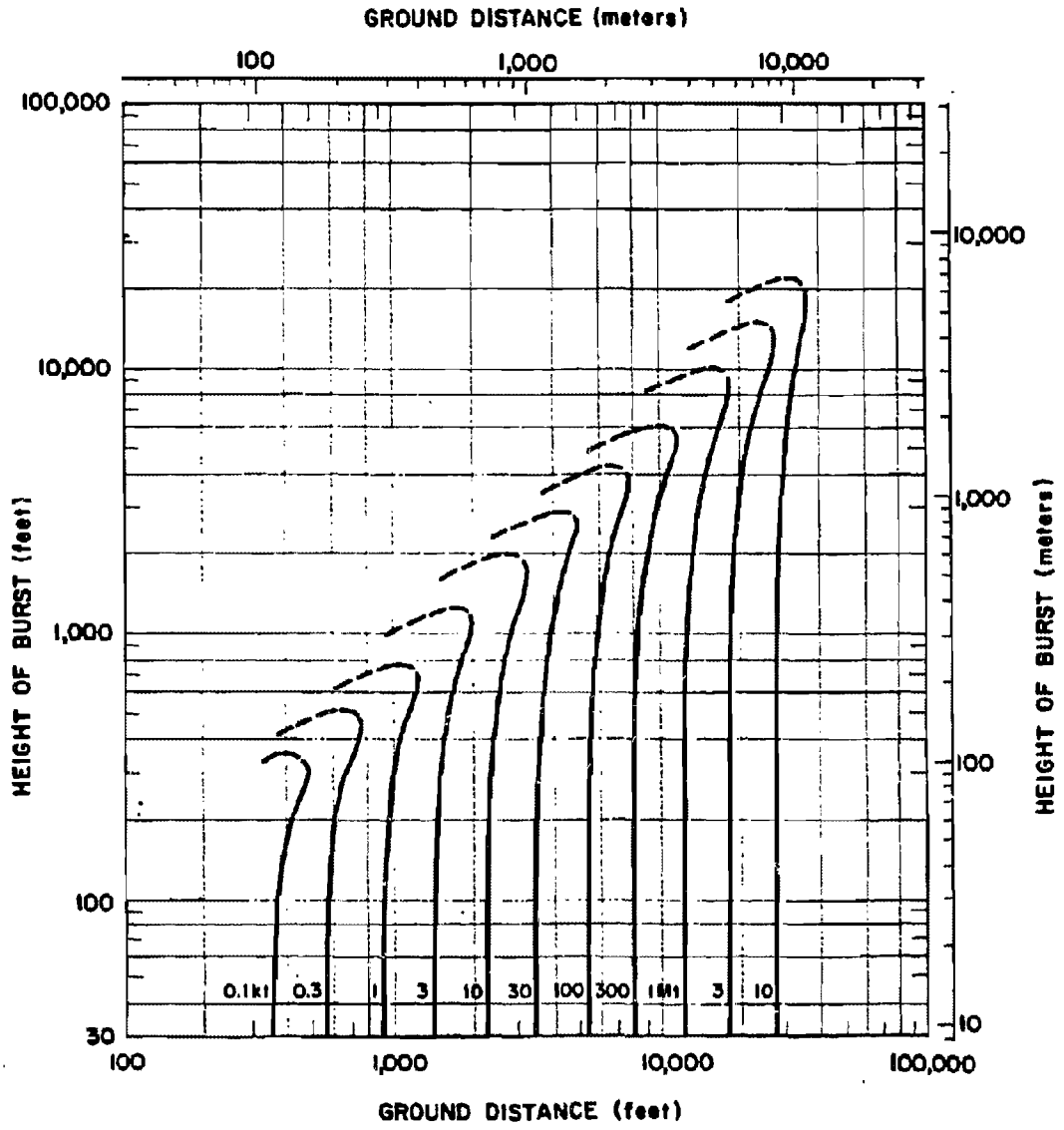

Figure 15-6. [redacted] Severe Damage to a Type II Forest [redacted]

[redacted]

[redacted]

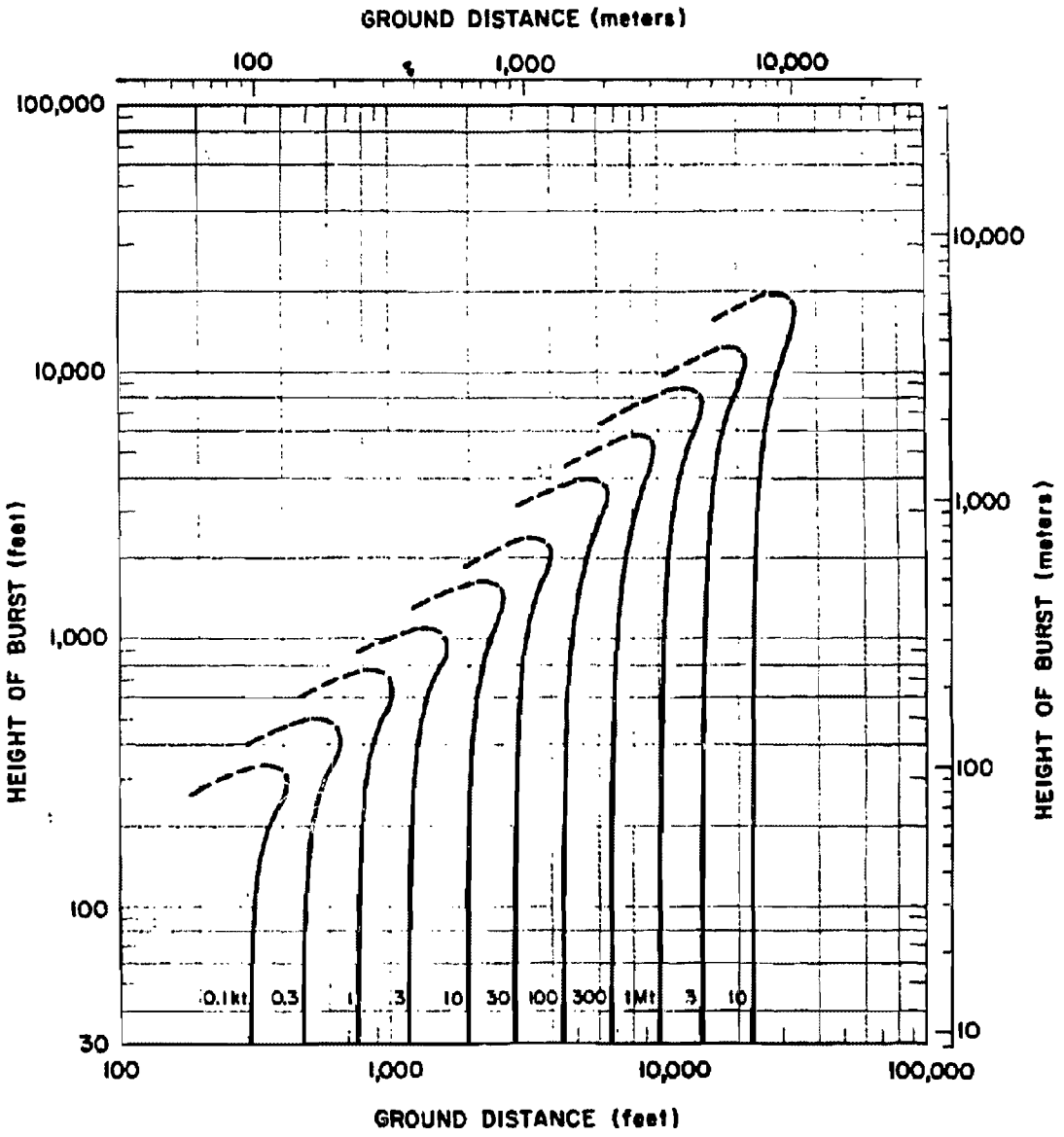

Figure 15-7. [redacted] Total Damage to a Type II Forest [redacted]

[redacted]

[redacted]

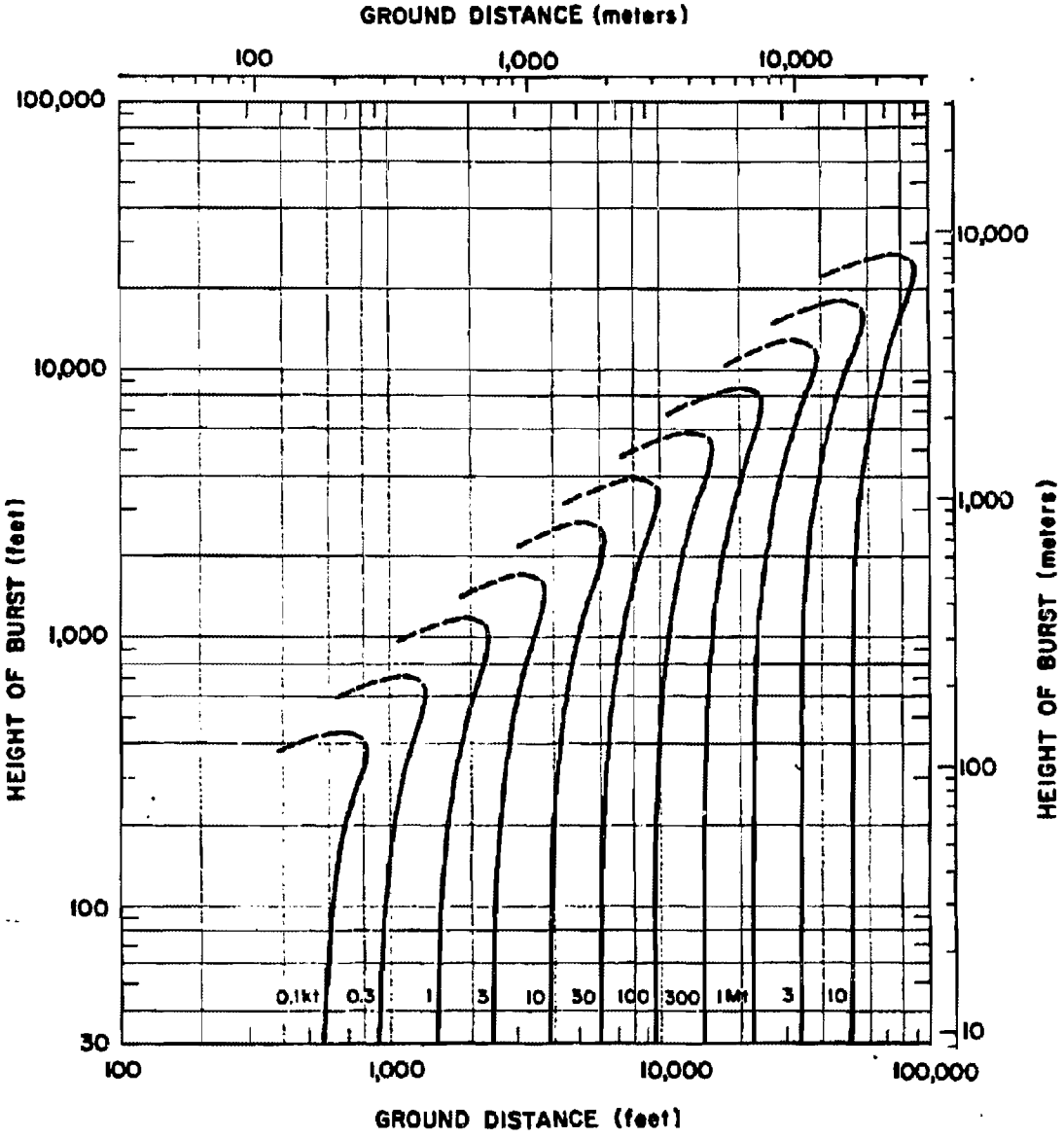

Figure 15-8. [redacted] Moderate Damage to a Type III Forest [redacted]

[redacted]

[redacted]

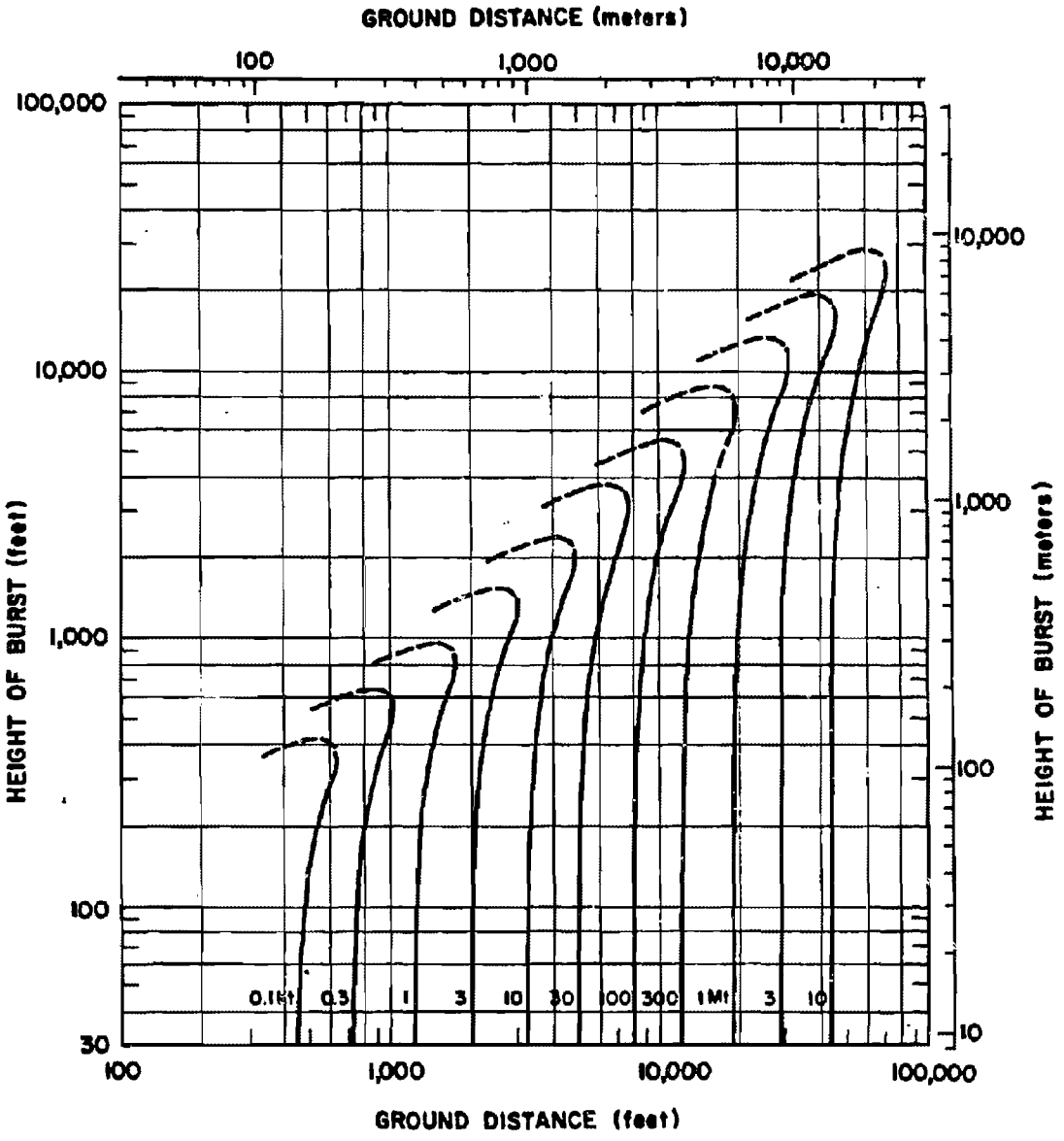

Figure 15-9. [redacted] Severe Damage to a Type III Forest [redacted]

[redacted]

[redacted]

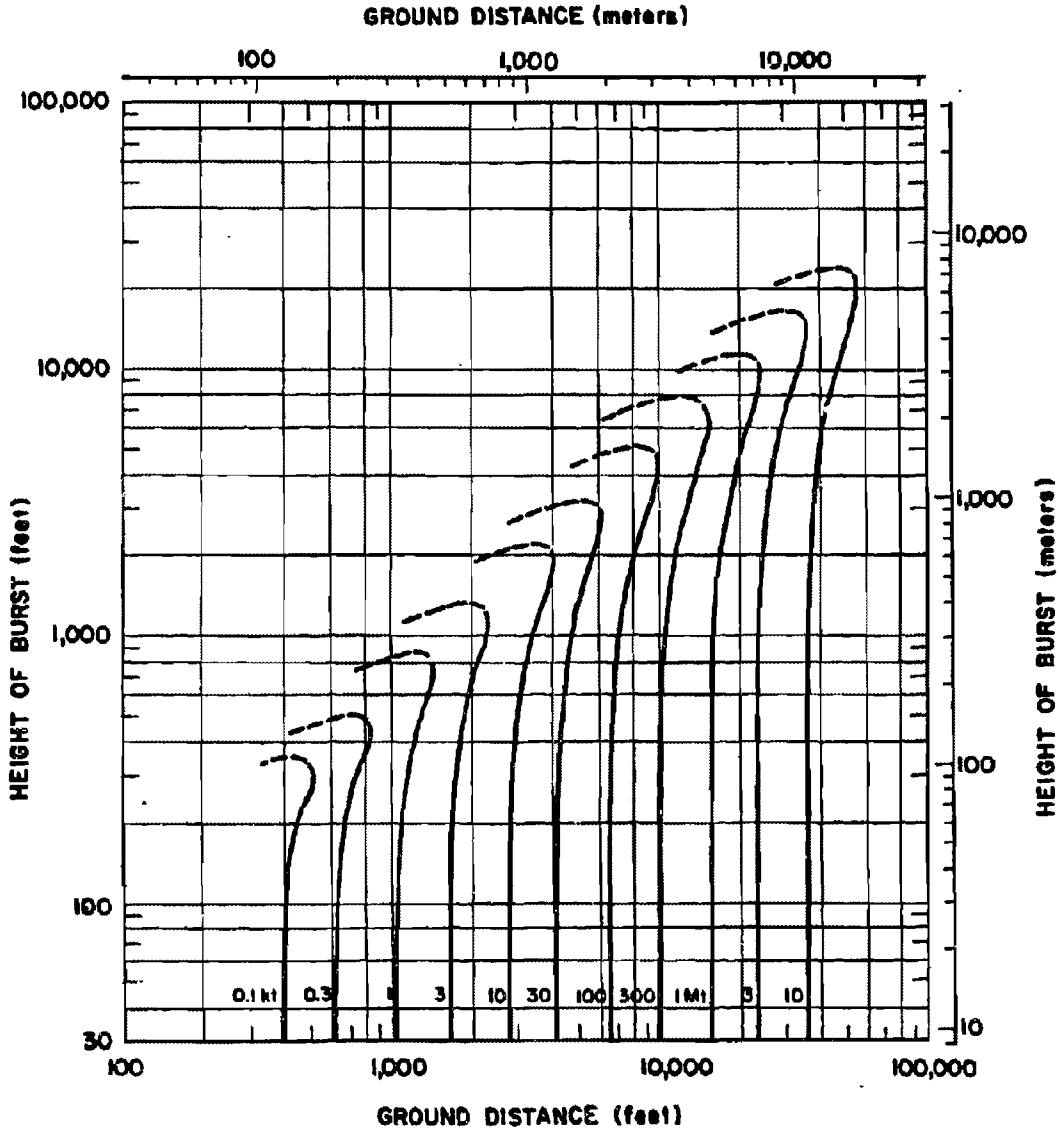

Figure 15-10. [redacted] Total Damage to a Type III Forest [redacted]

[redacted]

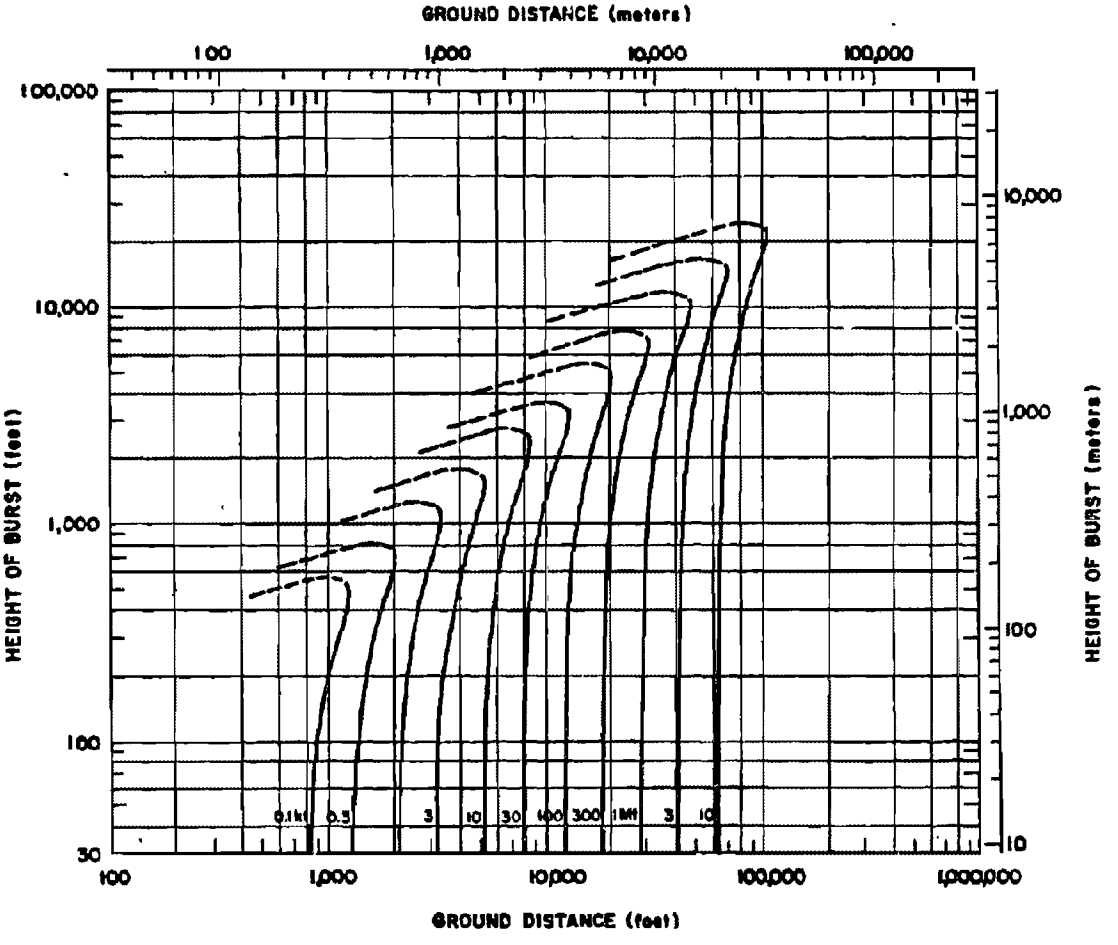

Figure 15-11. [redacted] Moderate Damage to a Type IVs-1(f) Forest [redacted]

[redacted]

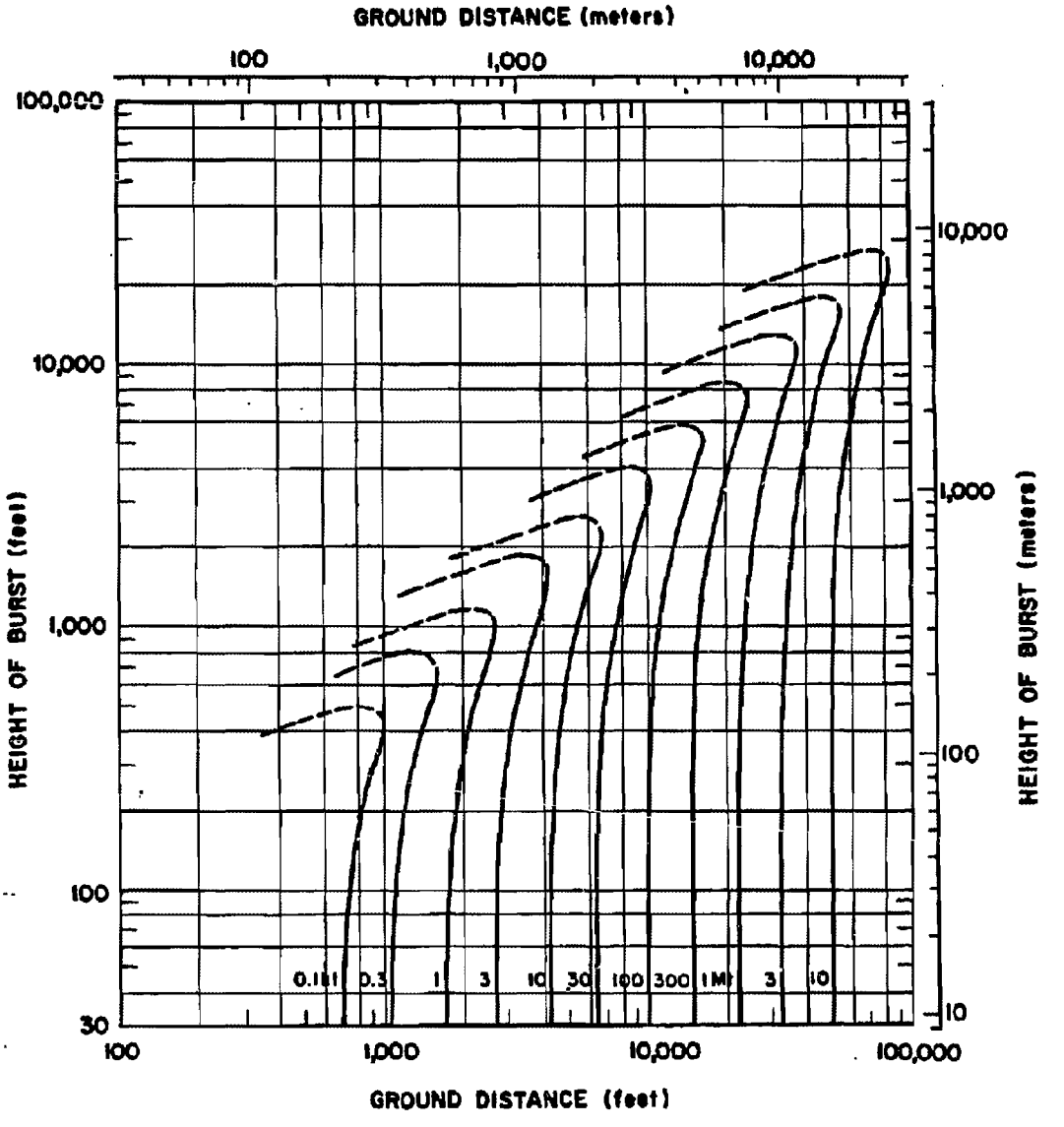

Figure 15-12. [redacted] Severe Damage to a Type IVa-1(f) Forest [redacted]

[redacted]

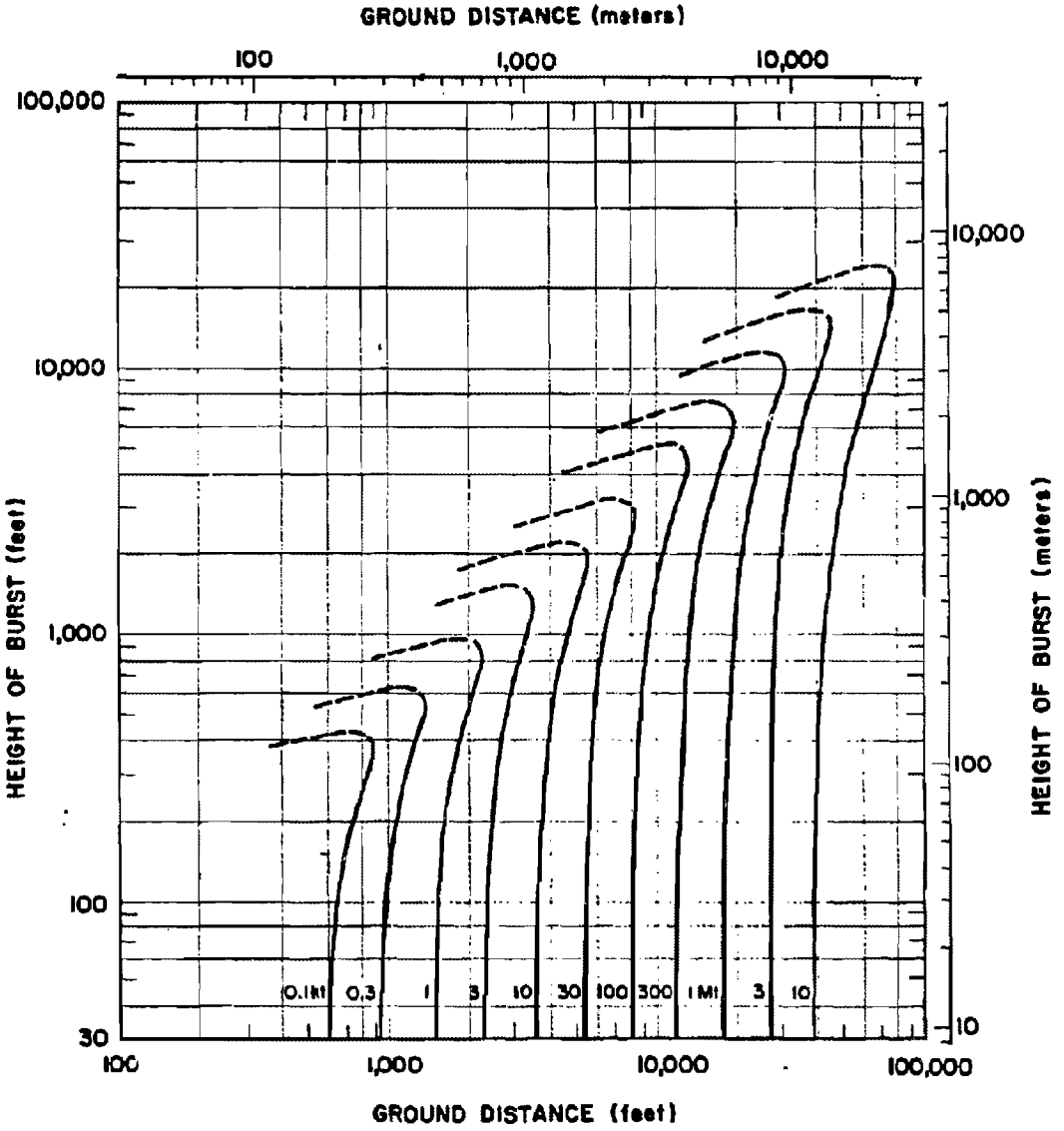

Figure 15-13. [redacted] Total Damage to a Type IVa-1(f) Forest [redacted]

[redacted]

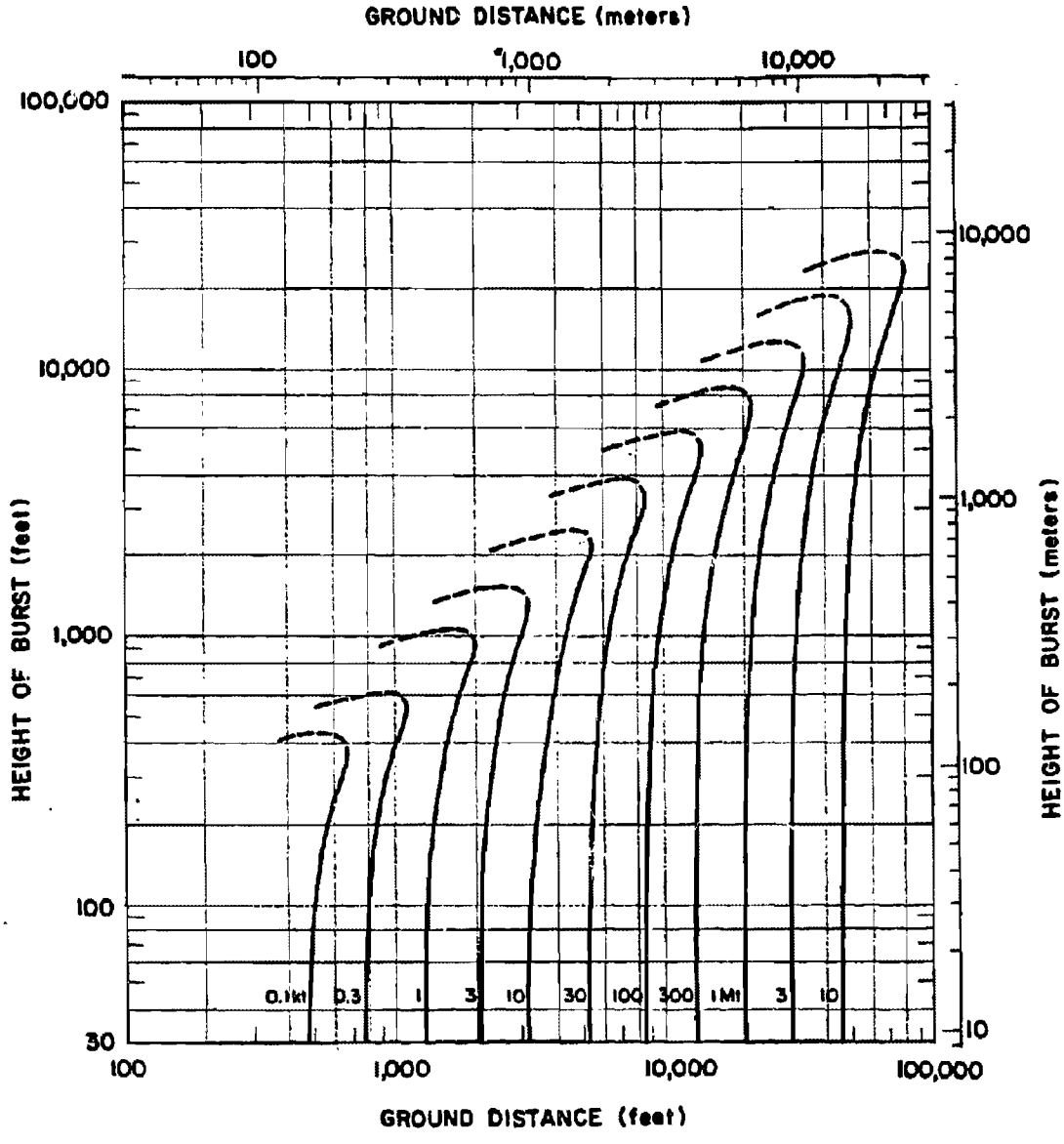

Figure 15-14. [redacted] Moderate Damage to a Type IVa-1(d) Forest [redacted]

[redacted]

[redacted]

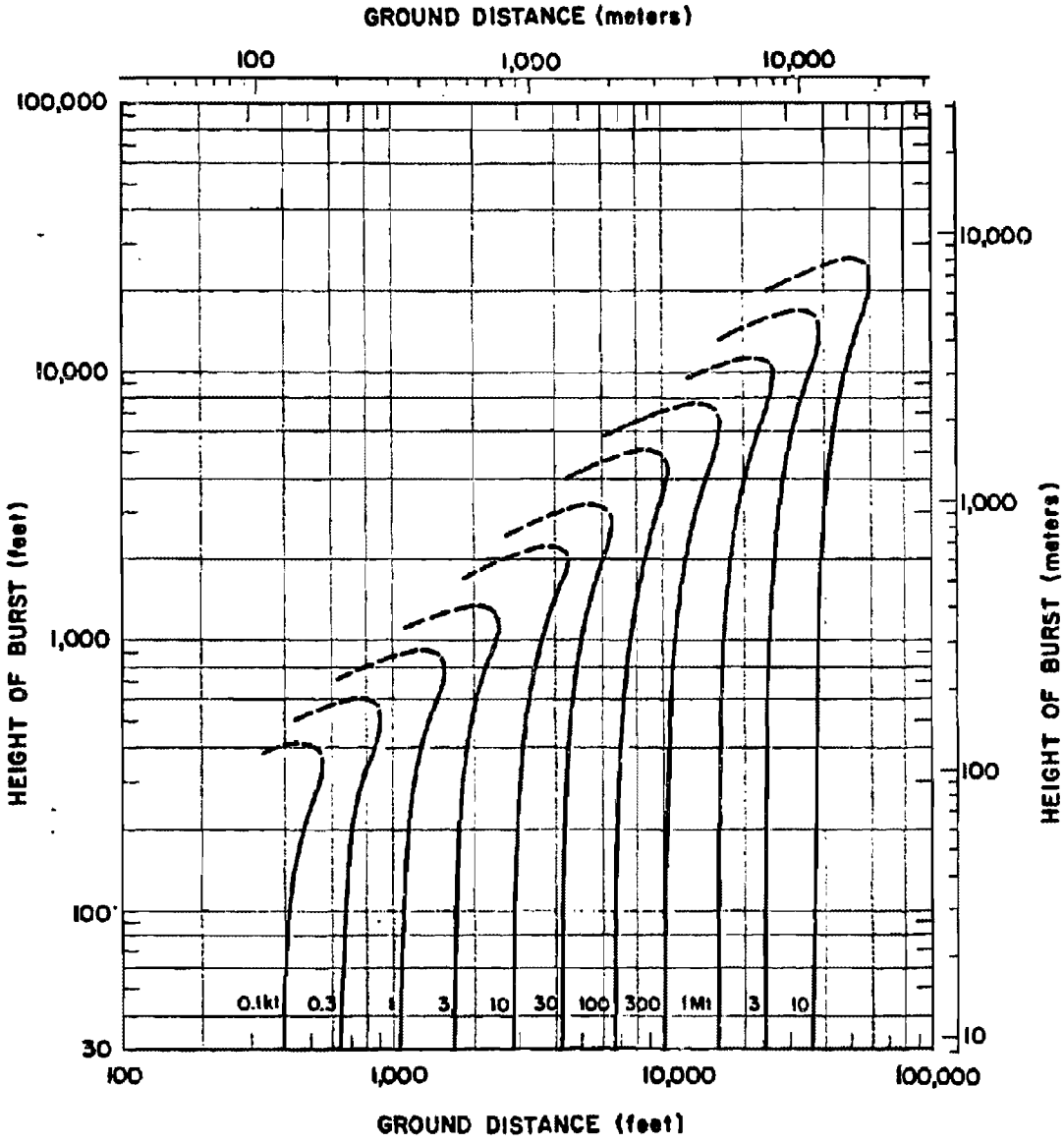

Figure 15-15. [redacted] Severe Damage to a Type IVa-1(d) Forest [redacted]

[redacted]

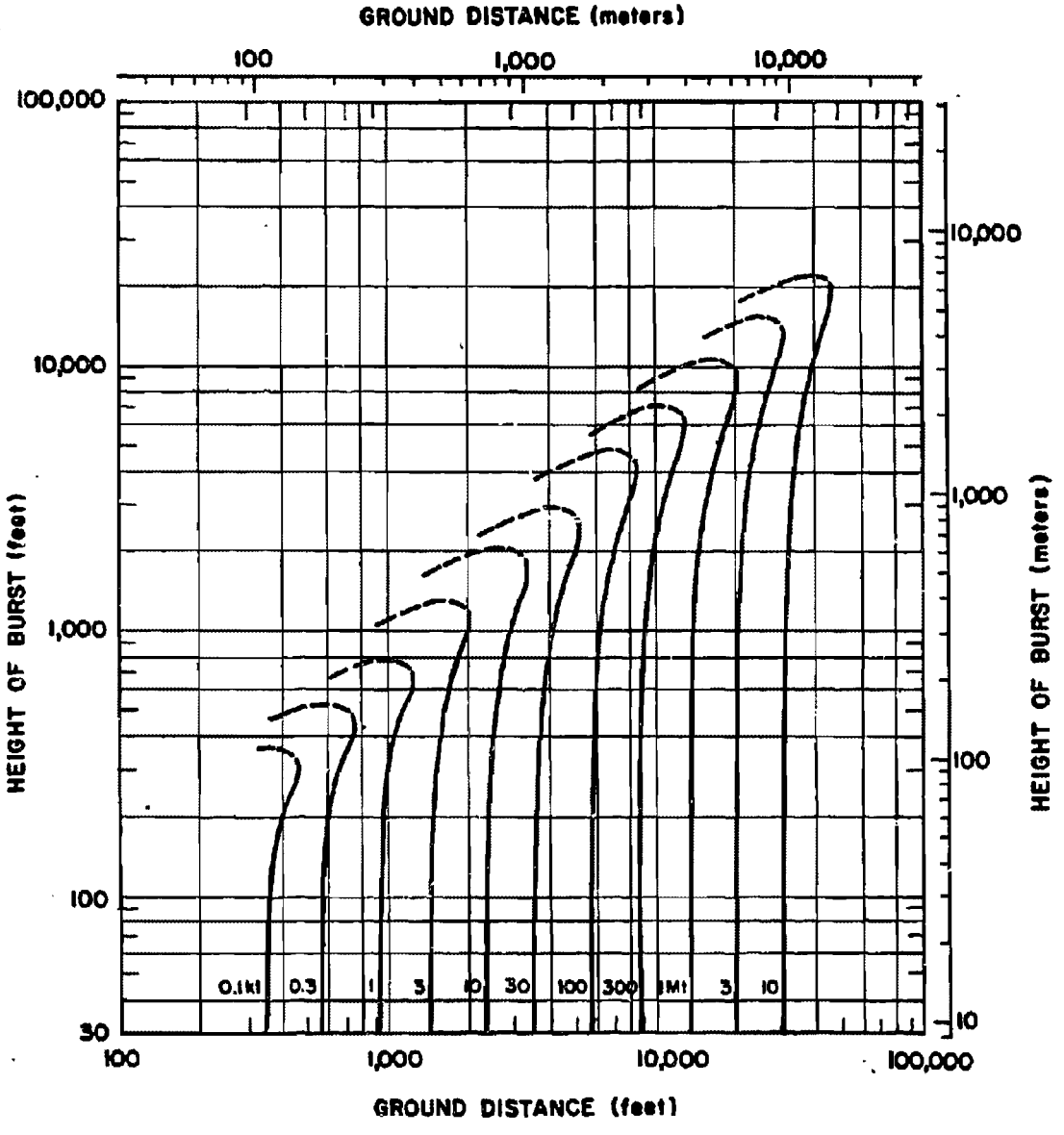

Figure 15-16. [redacted] Total Damage to a Type IVa-1(d) Forest [redacted]

[redacted]

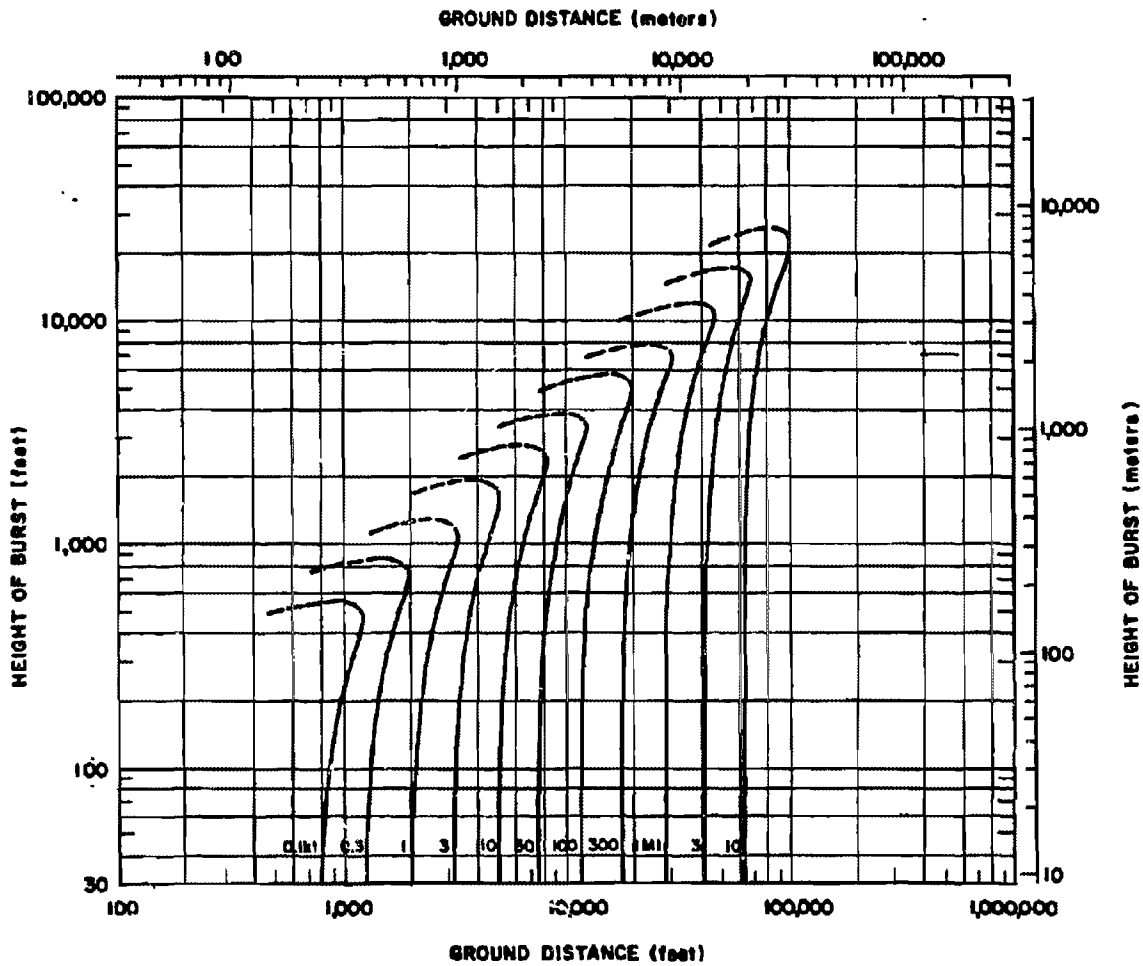

Figure 15-17. [redacted] Moderate Damage to a Type IVa-2(f) Forest [redacted]

[redacted]

[redacted]

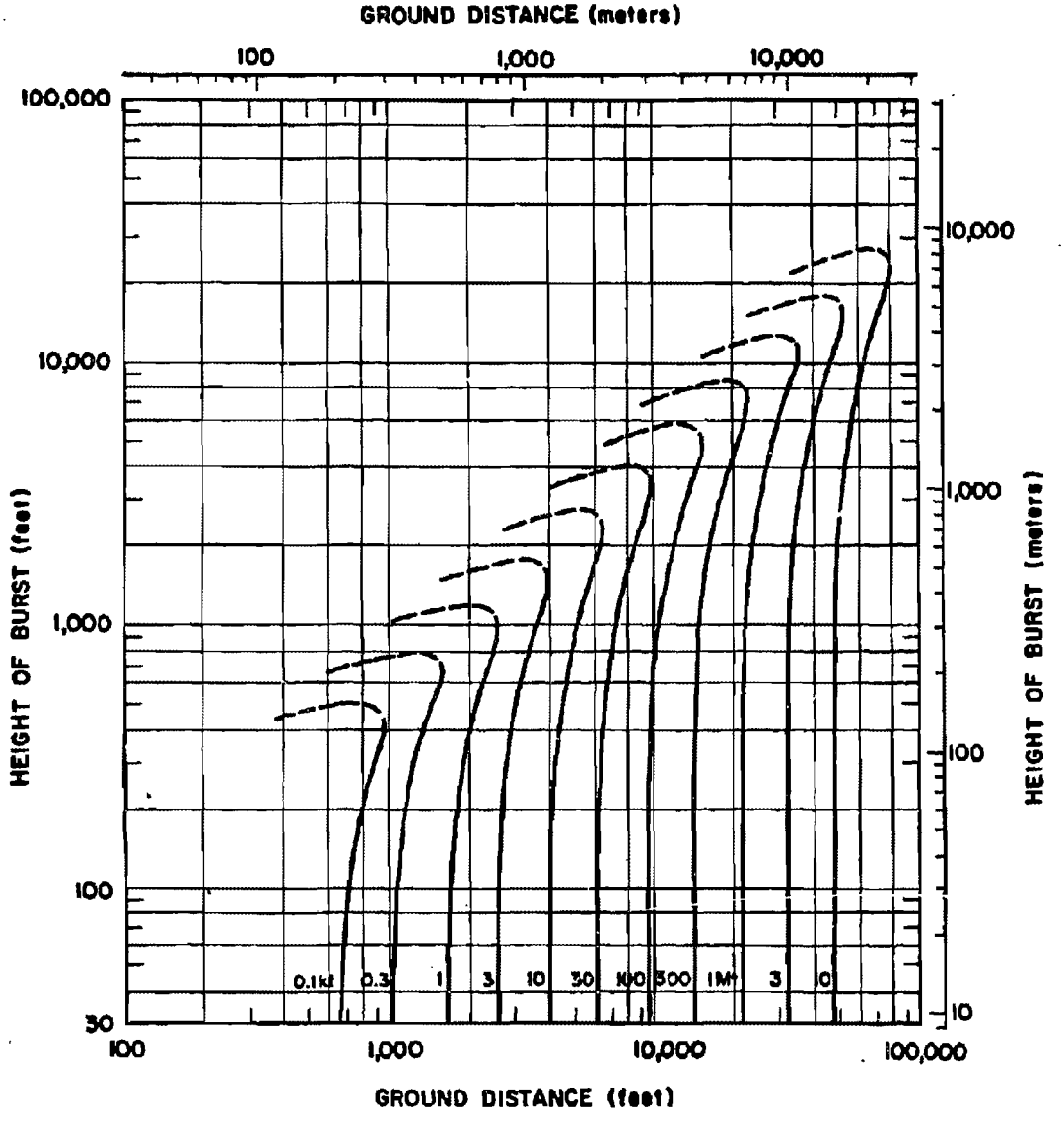

Figure 15-18. [redacted] Severe Damage to a Type IVa-2(f) Forest [redacted]

[redacted]

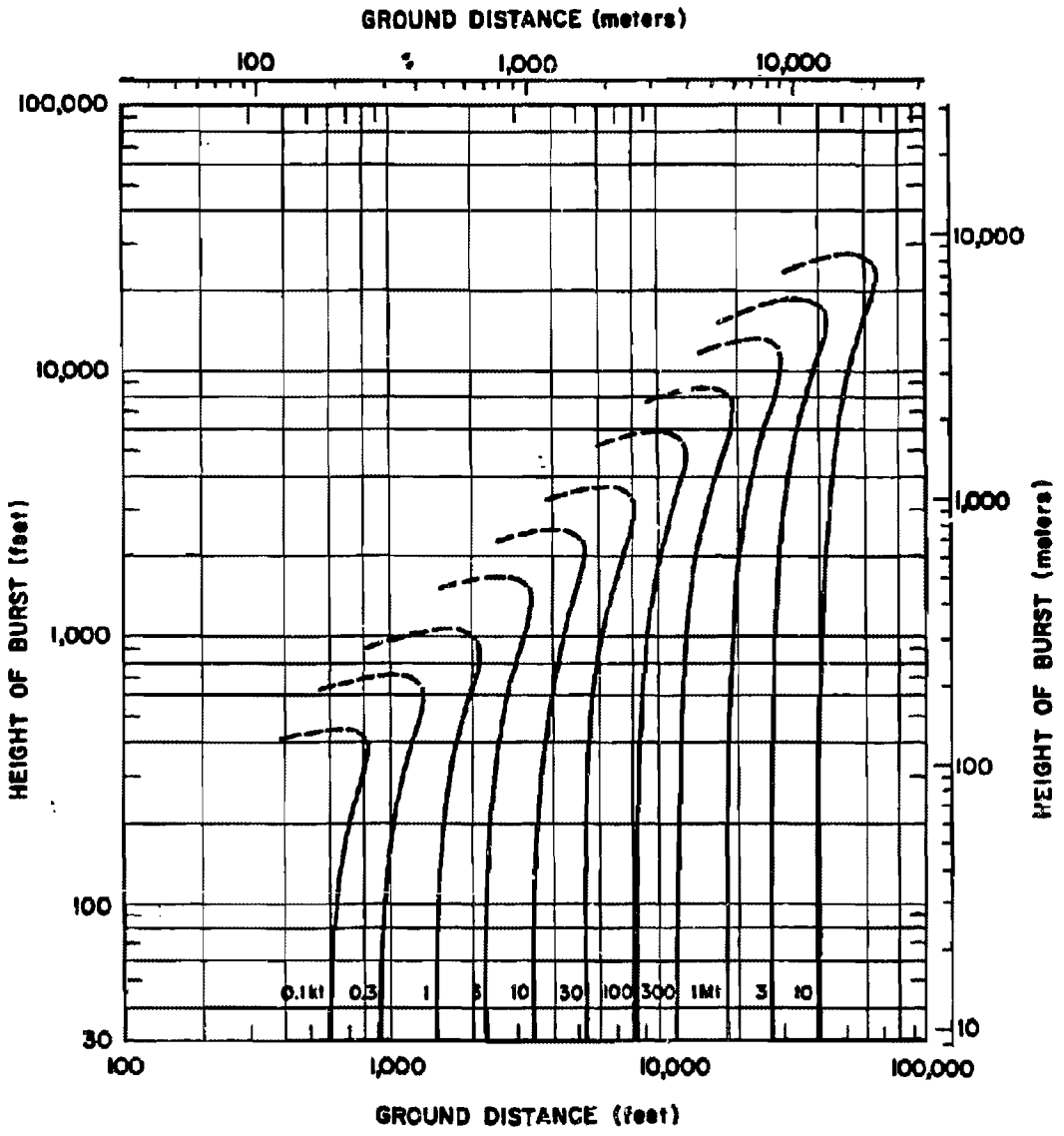

Figure 15-19. [redacted] Total Damage to a Type IVa-2(f) Forest [redacted]

[redacted]

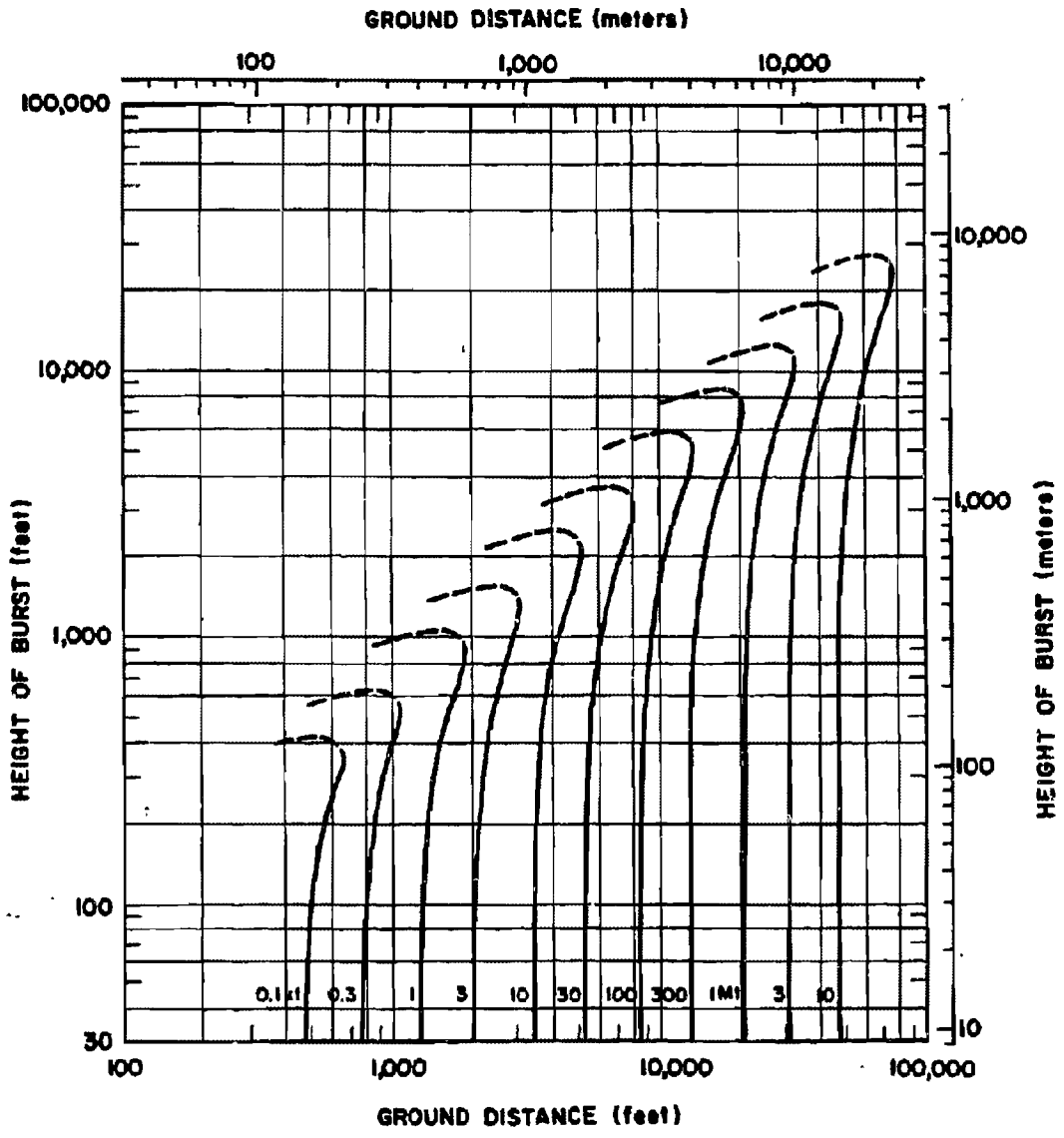

Figure 15-20 [redacted] Moderate Damage to a Type IVa-2(d) Forest [redacted]

[redacted]

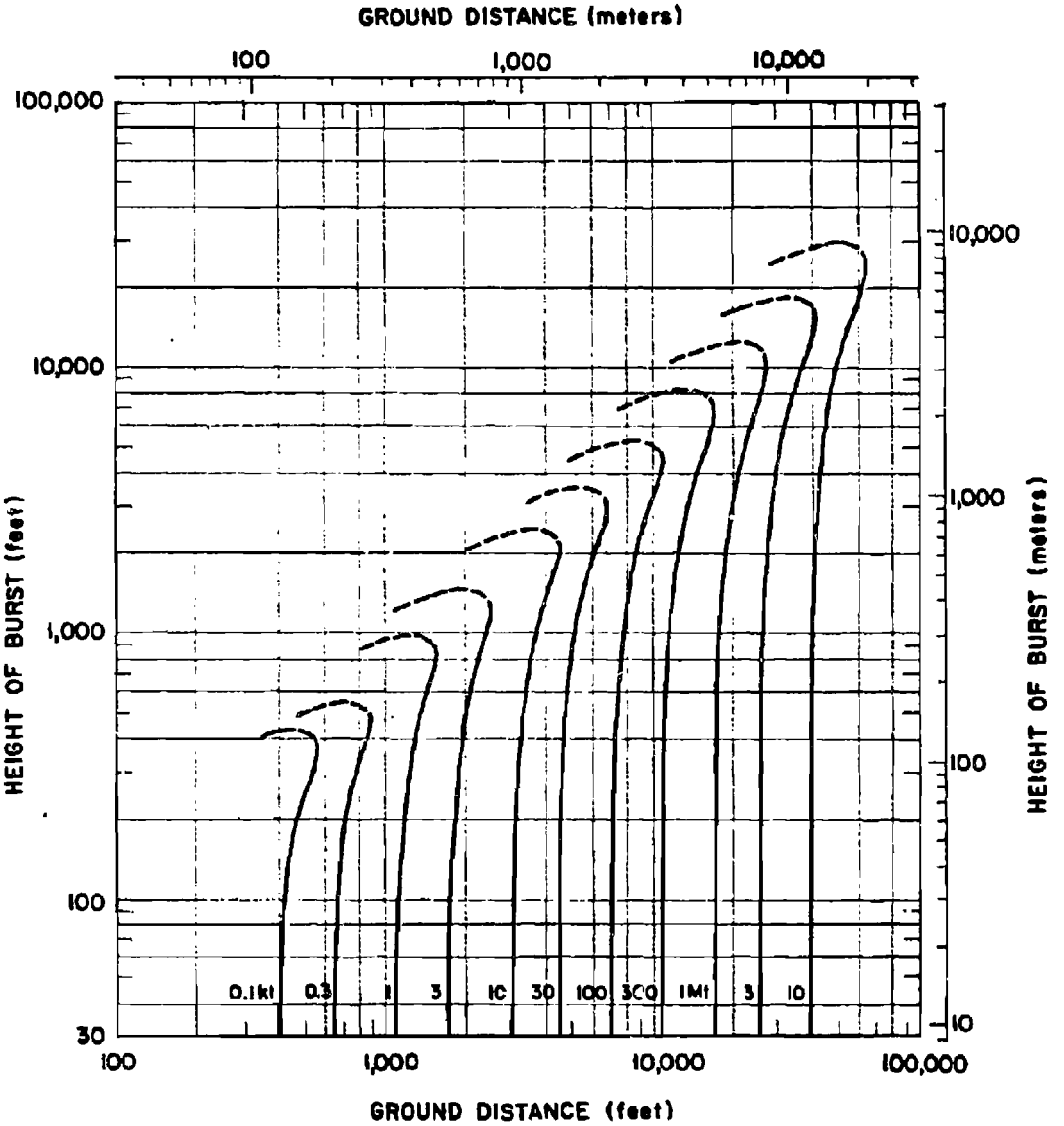

Figure 15-21. [redacted] Severe Damage to a Type IVa-2(d) Forest [redacted]

[redacted]

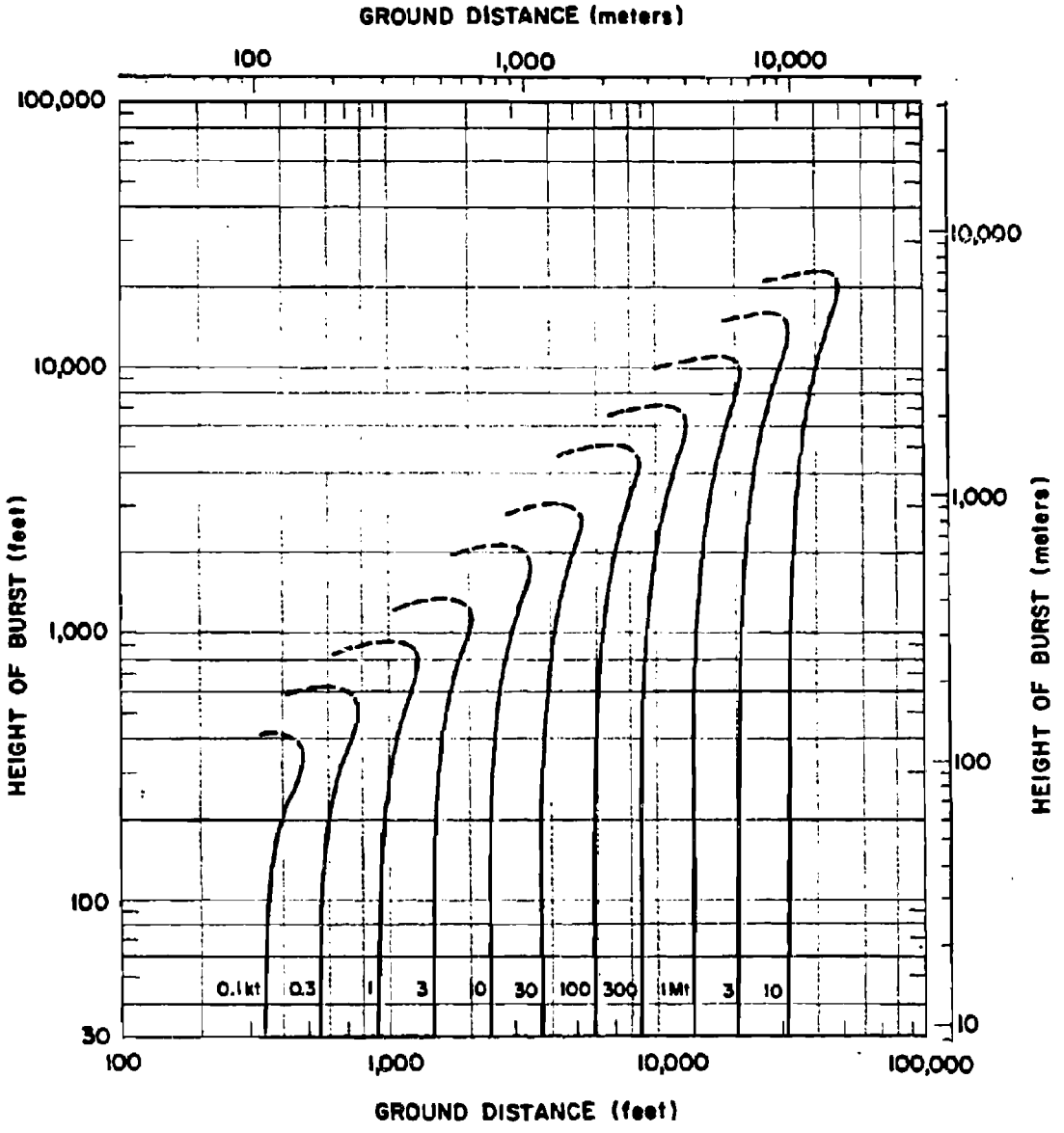

Figure 15-22. [redacted] Total Damage to a Type IVa-2(d) Forest [redacted]

[redacted]

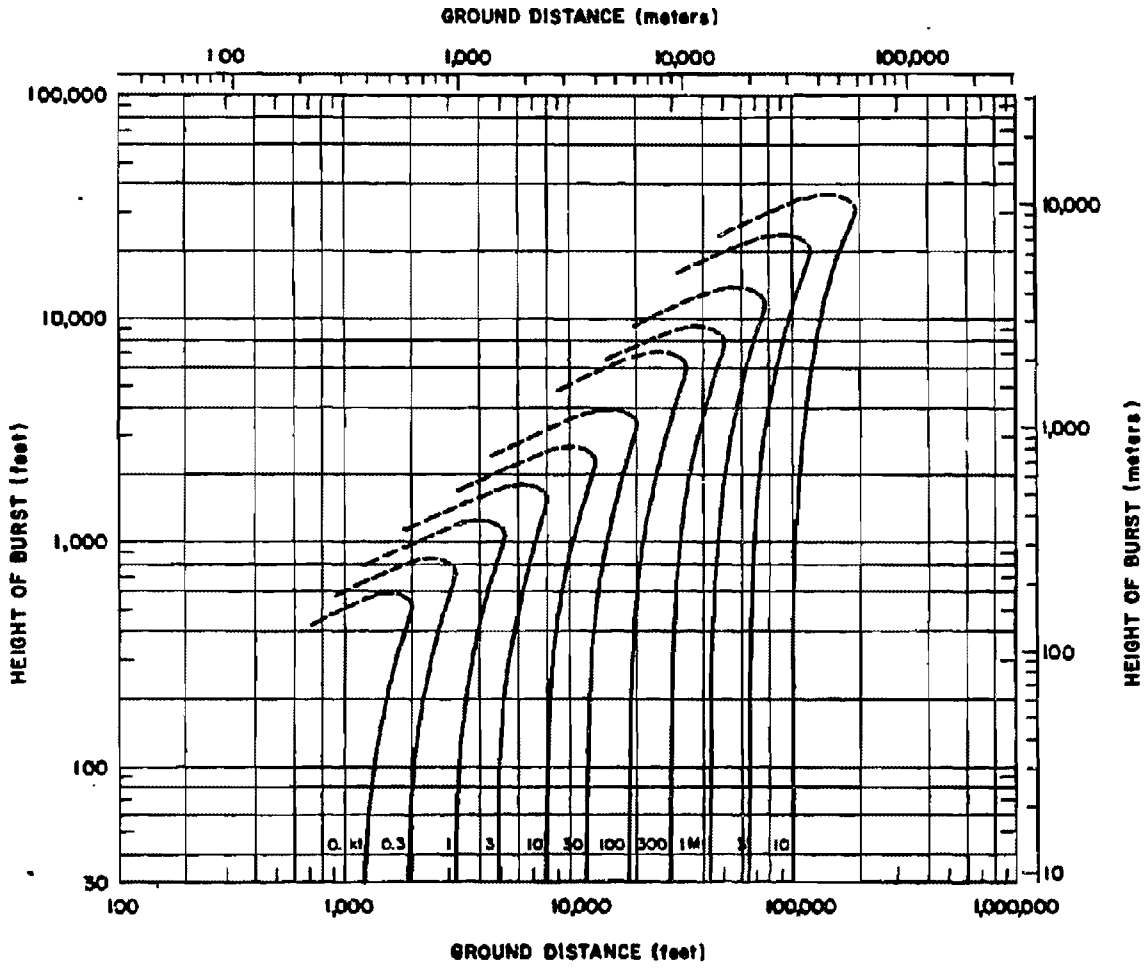

Figure 15-23. [redacted] Moderate Damage to a Type IVb(f) Forest [redacted]

[redacted]

[redacted]

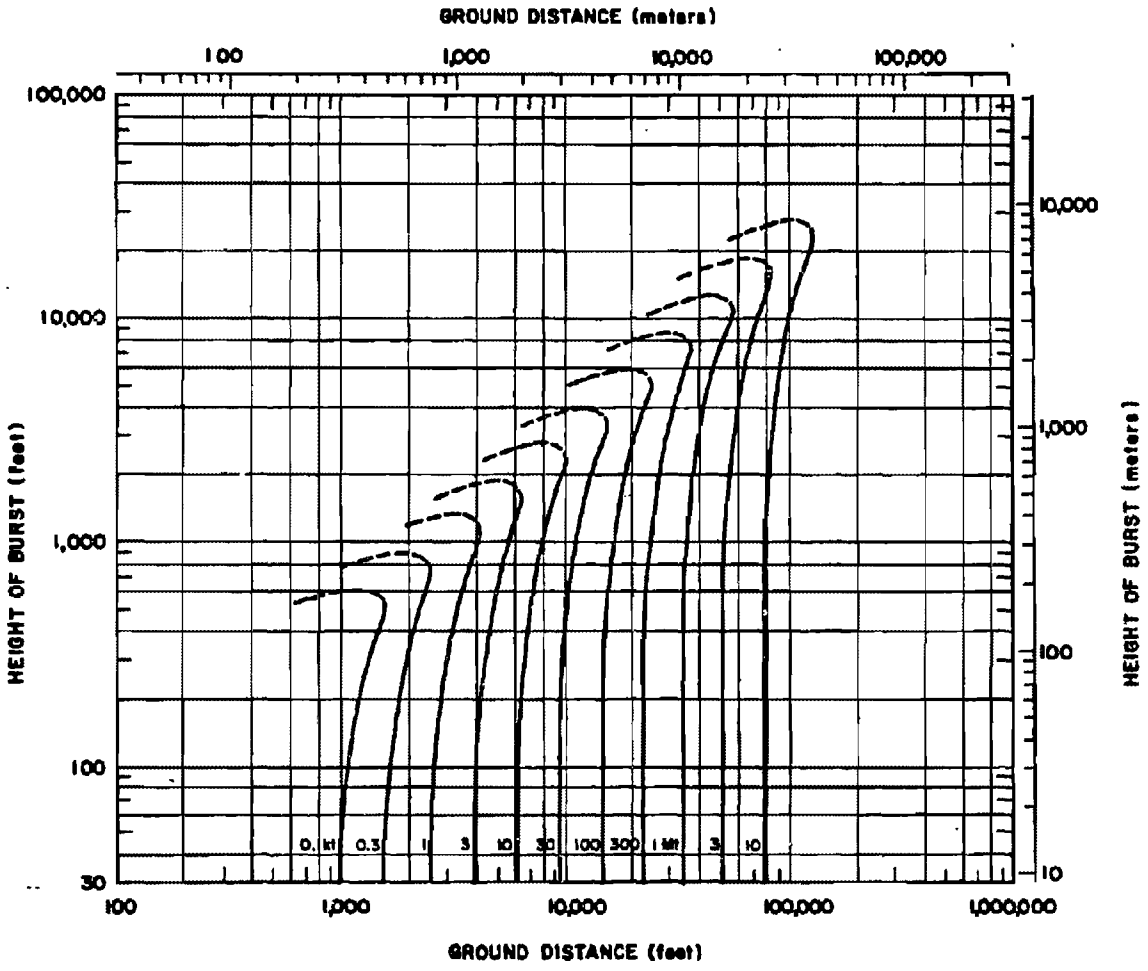

Figure 15-24. [redacted] Severe Damage to a Type IVb(f) Forest [redacted]

[redacted]

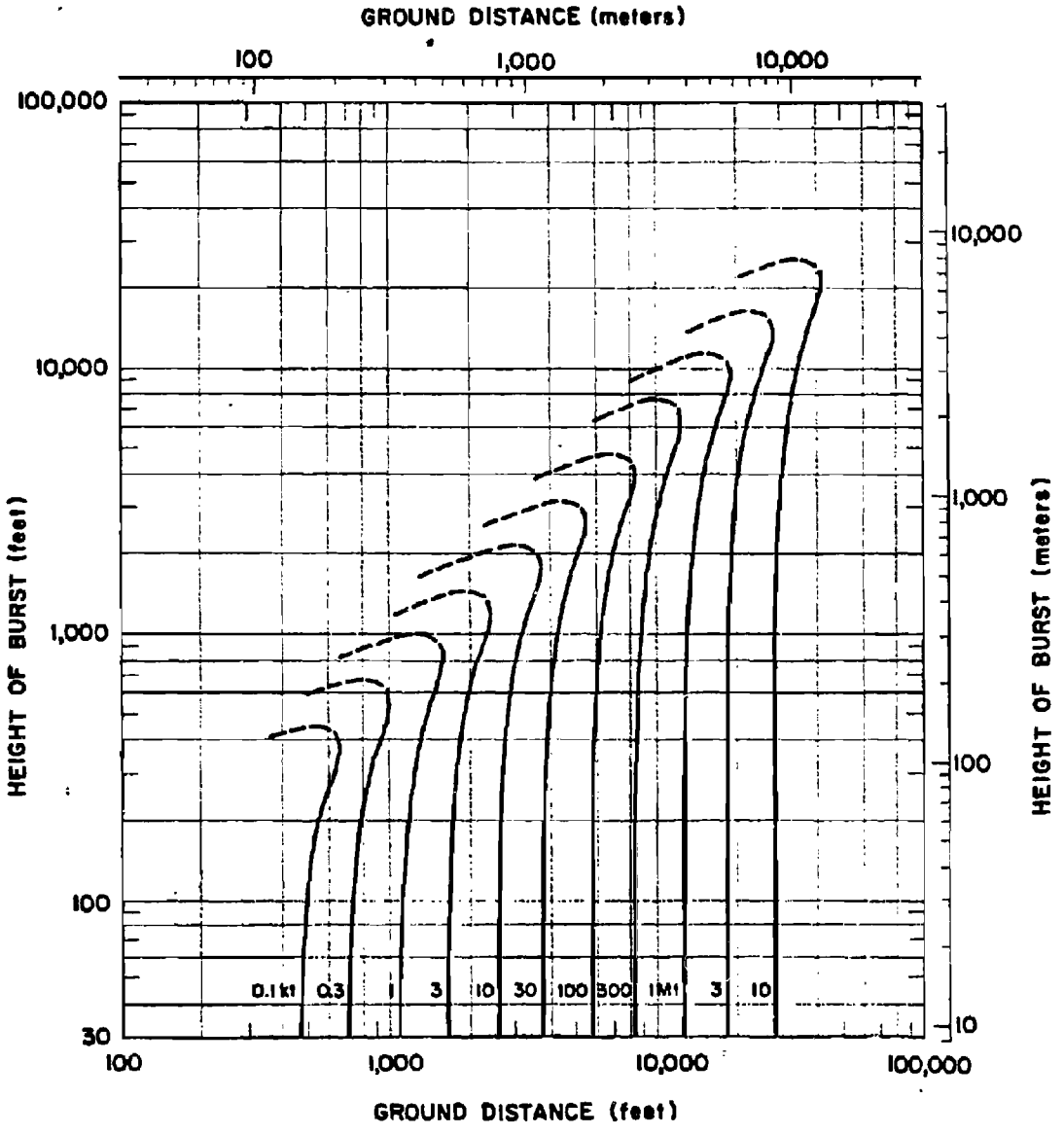

Figure 15-25. [redacted] Total Damage to a Type IVb(f) Forest [redacted]

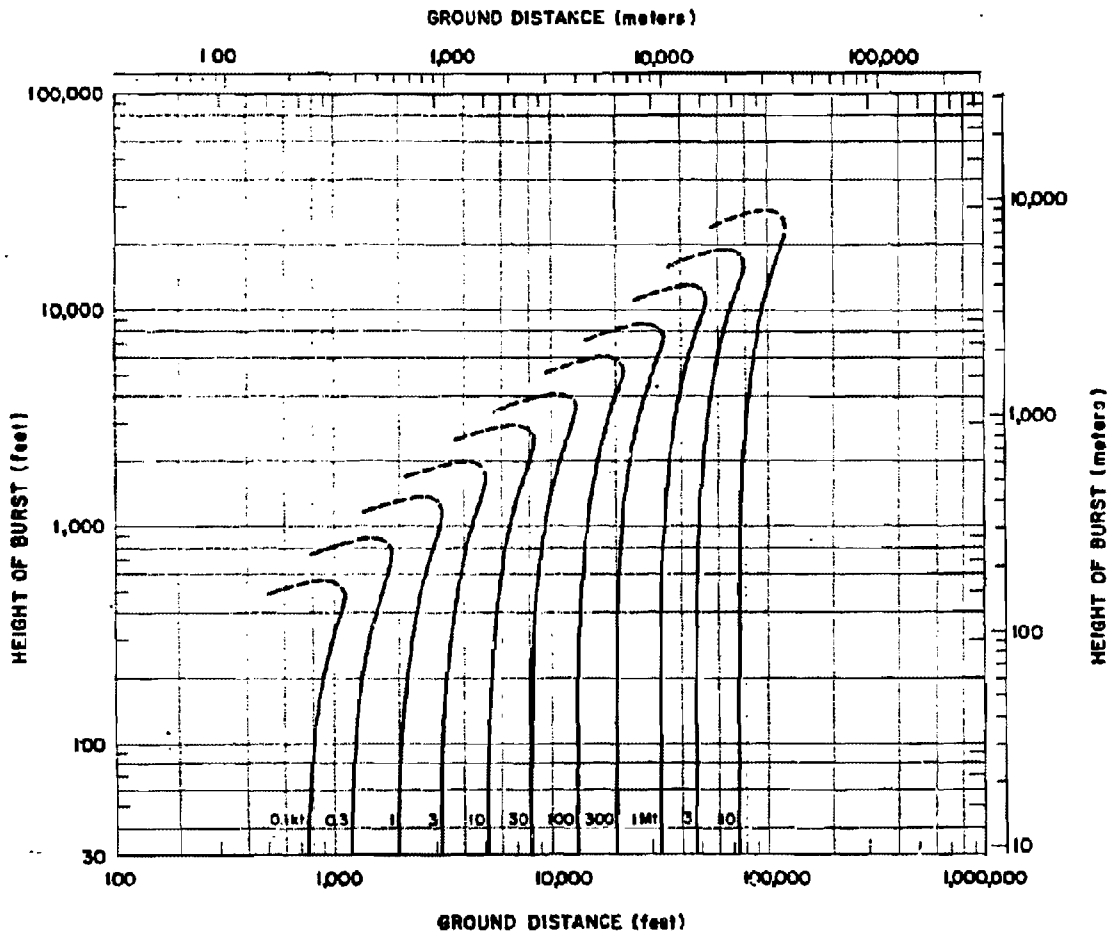

Figure 15-26. [redacted] Moderate Damage to a Type IVb(d) Forest [redacted]

[redacted]

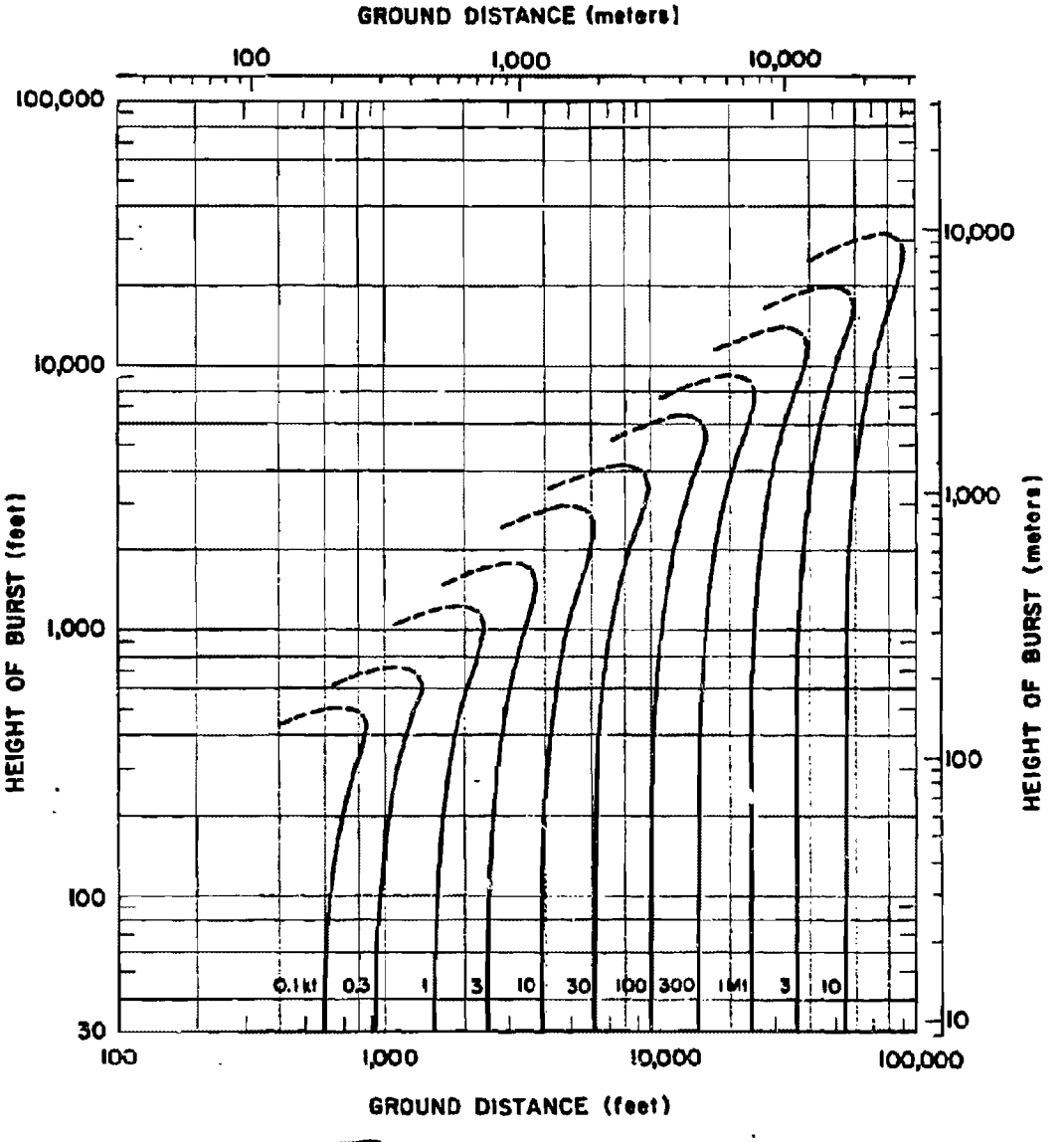

Figure 15-27. [redacted] Severe Damage to a Type IVb(d) Forest [redacted]

[redacted]

[redacted]

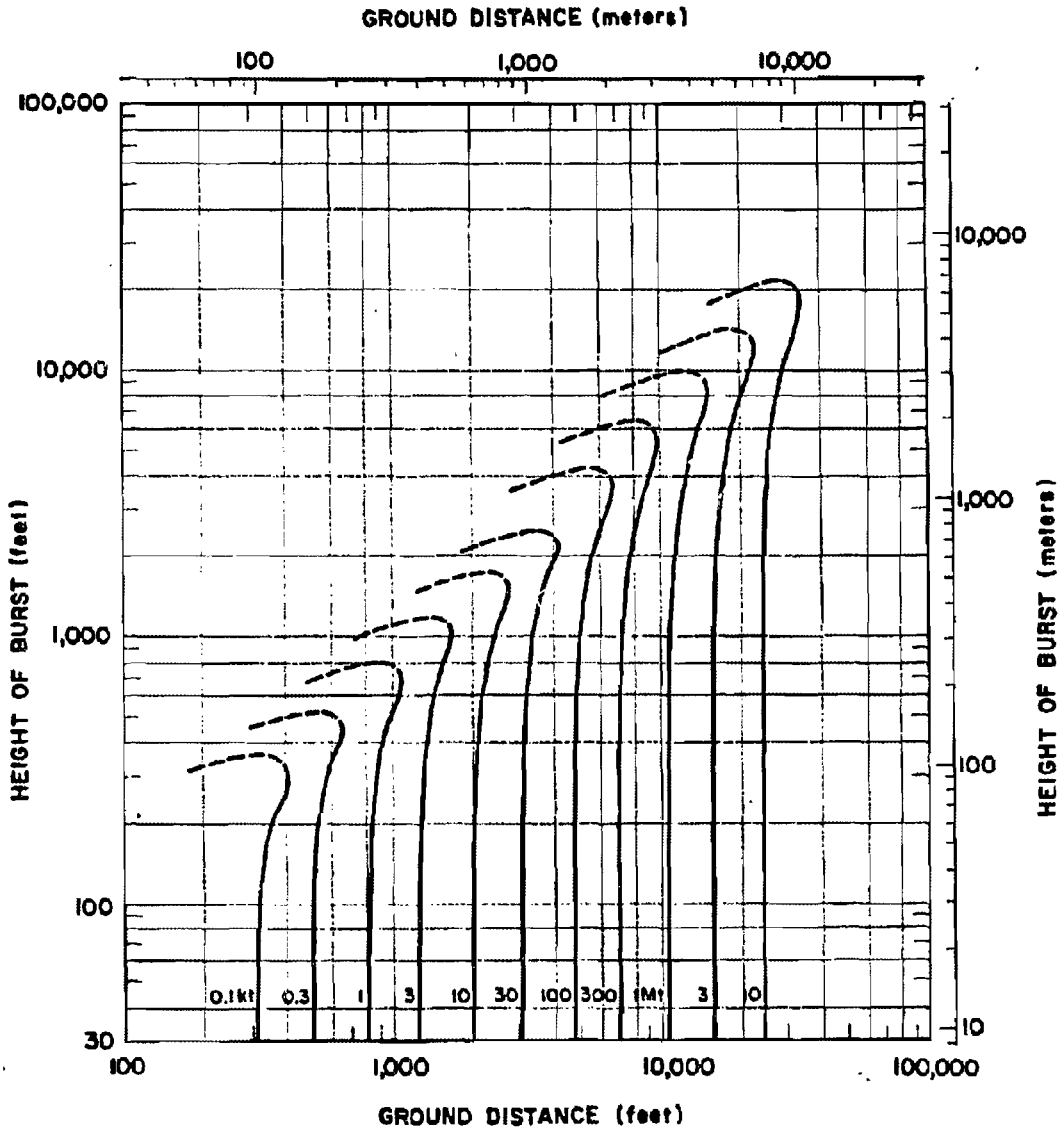

Figure 15-28. [redacted] Total Damage to a Type IVb(d) Forest [redacted]

[redacted]

[redacted]

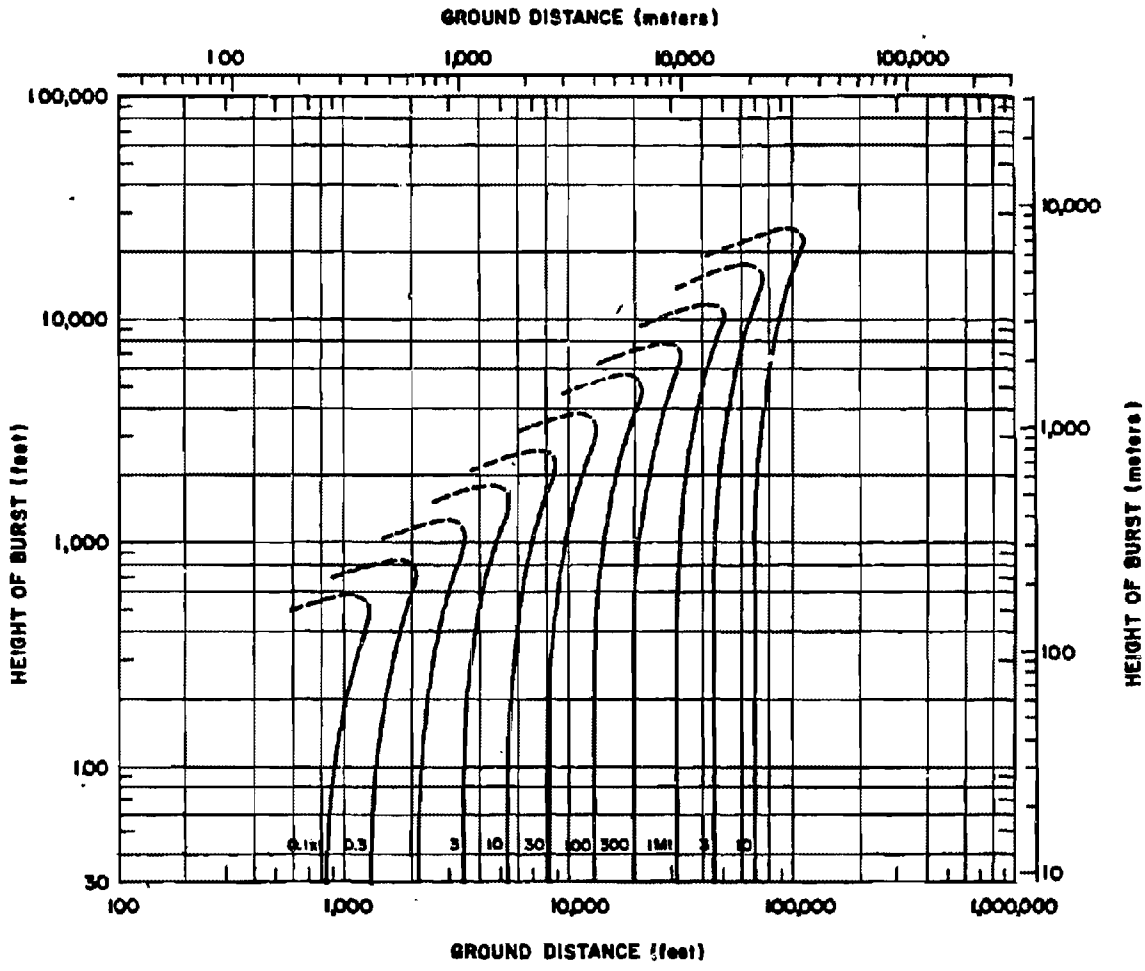

Figure 15-28. [redacted] Moderate Damage to a Type IVc(f) Forest [redacted]

[redacted]

[redacted]

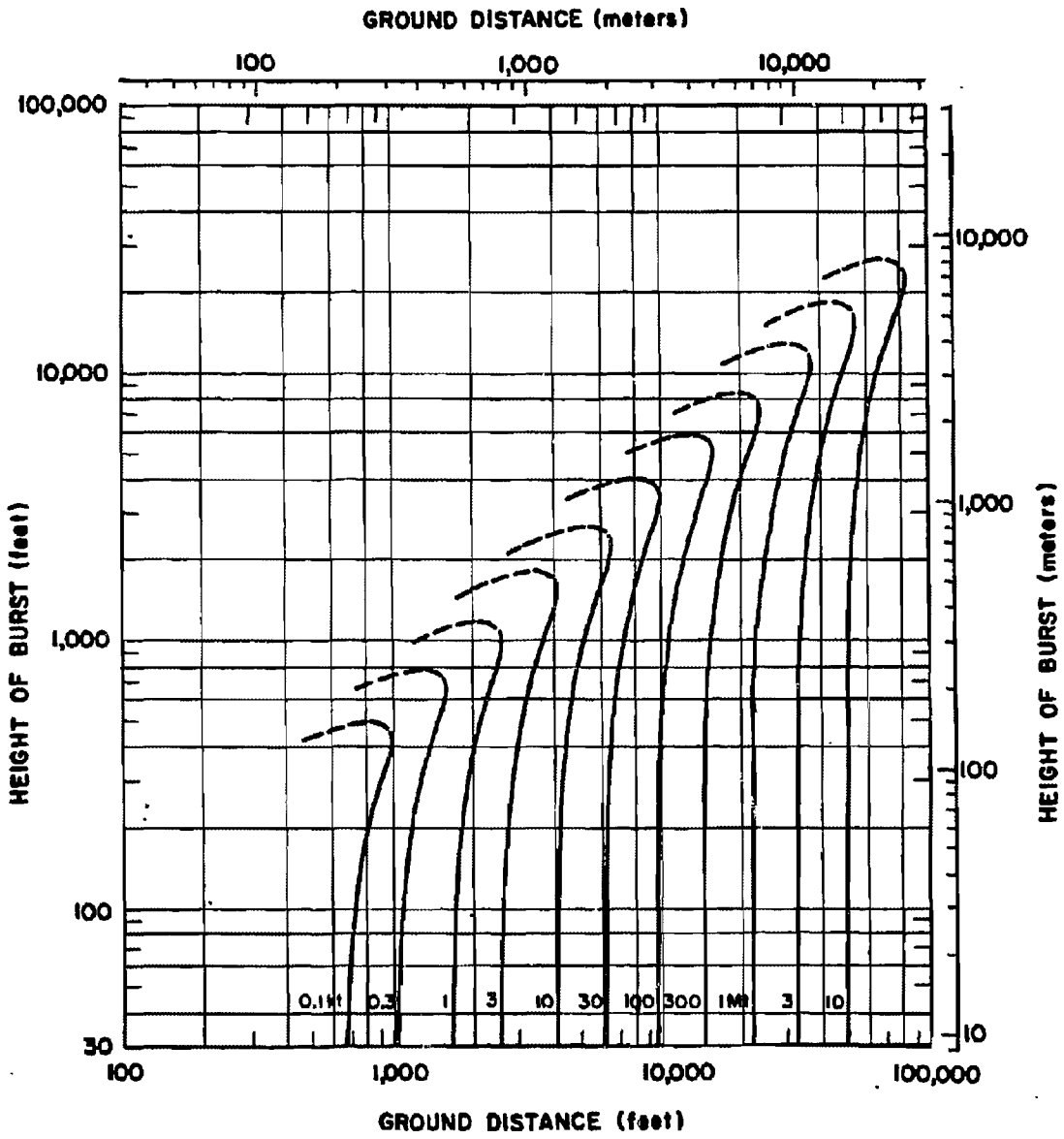

Figure 15-30. [redacted] Total Damage to a Type IVc(f) Forest [redacted]

[redacted]

[redacted]

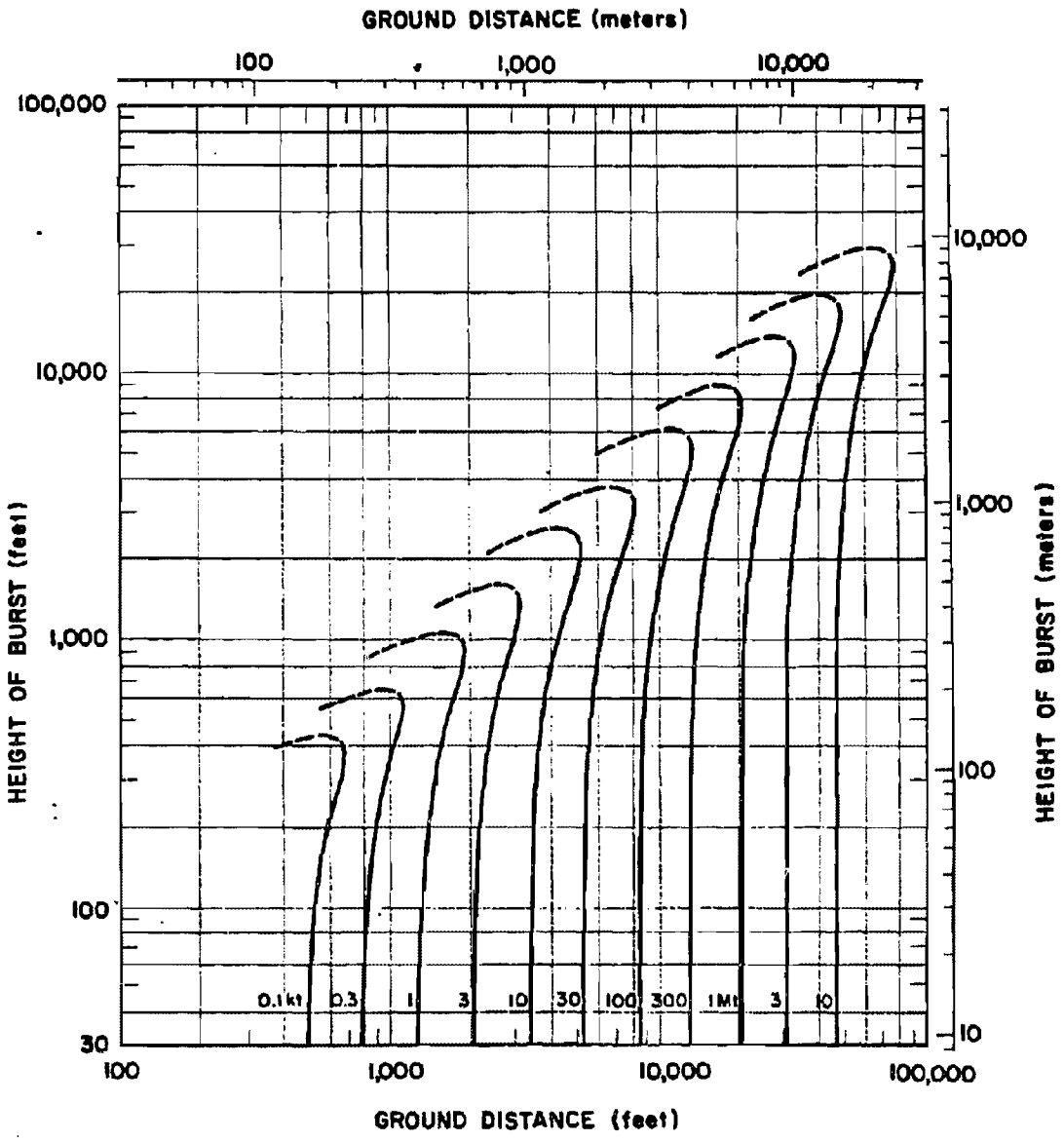

Figure 15-31. [redacted] Moderate Damage to a Type IVc(d) Forest [redacted]

[redacted]

[redacted]

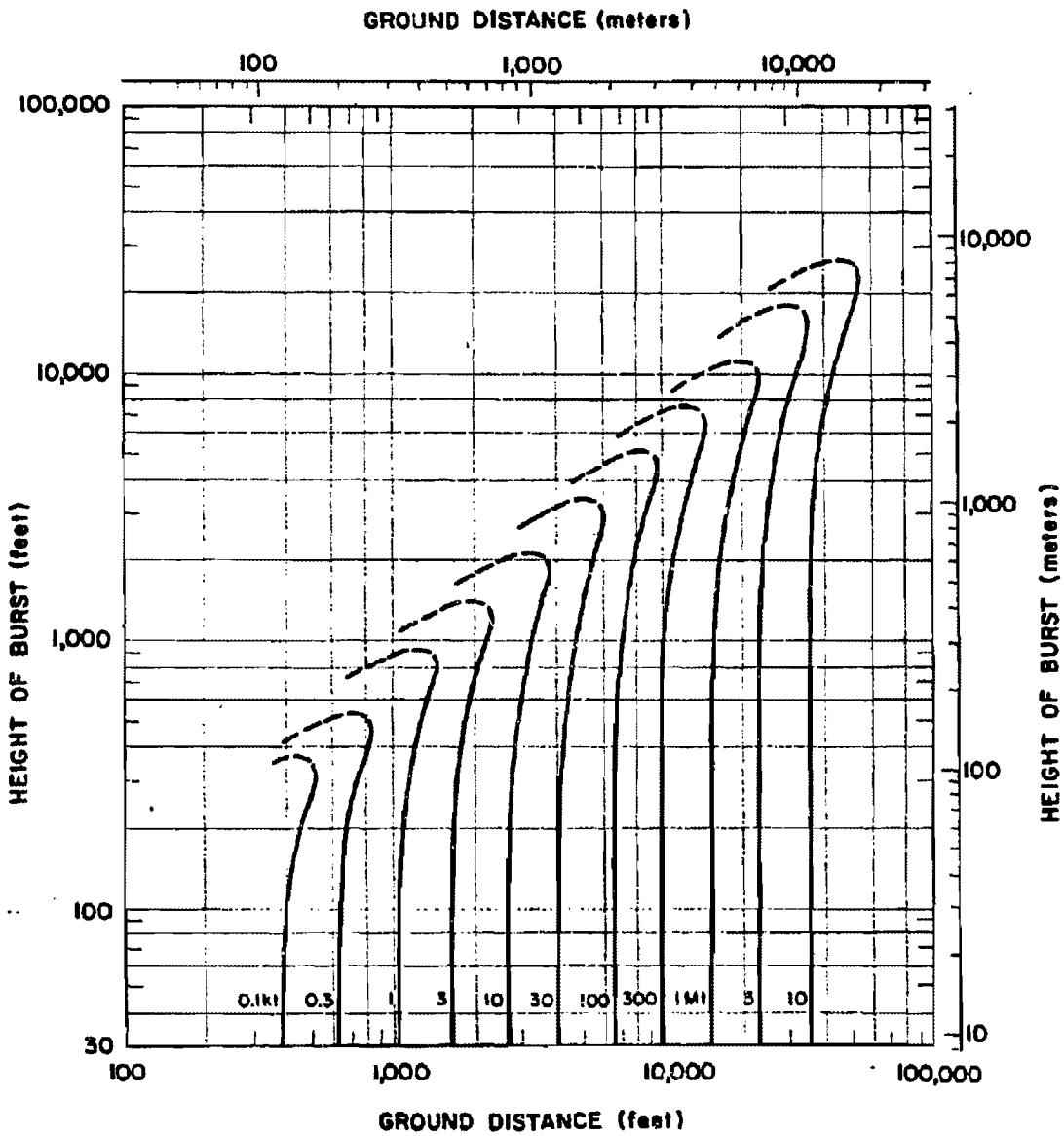

Figure 15-32. [redacted] Total Damage to a Type IVc(d) Forest [redacted]

[redacted]

[redacted]

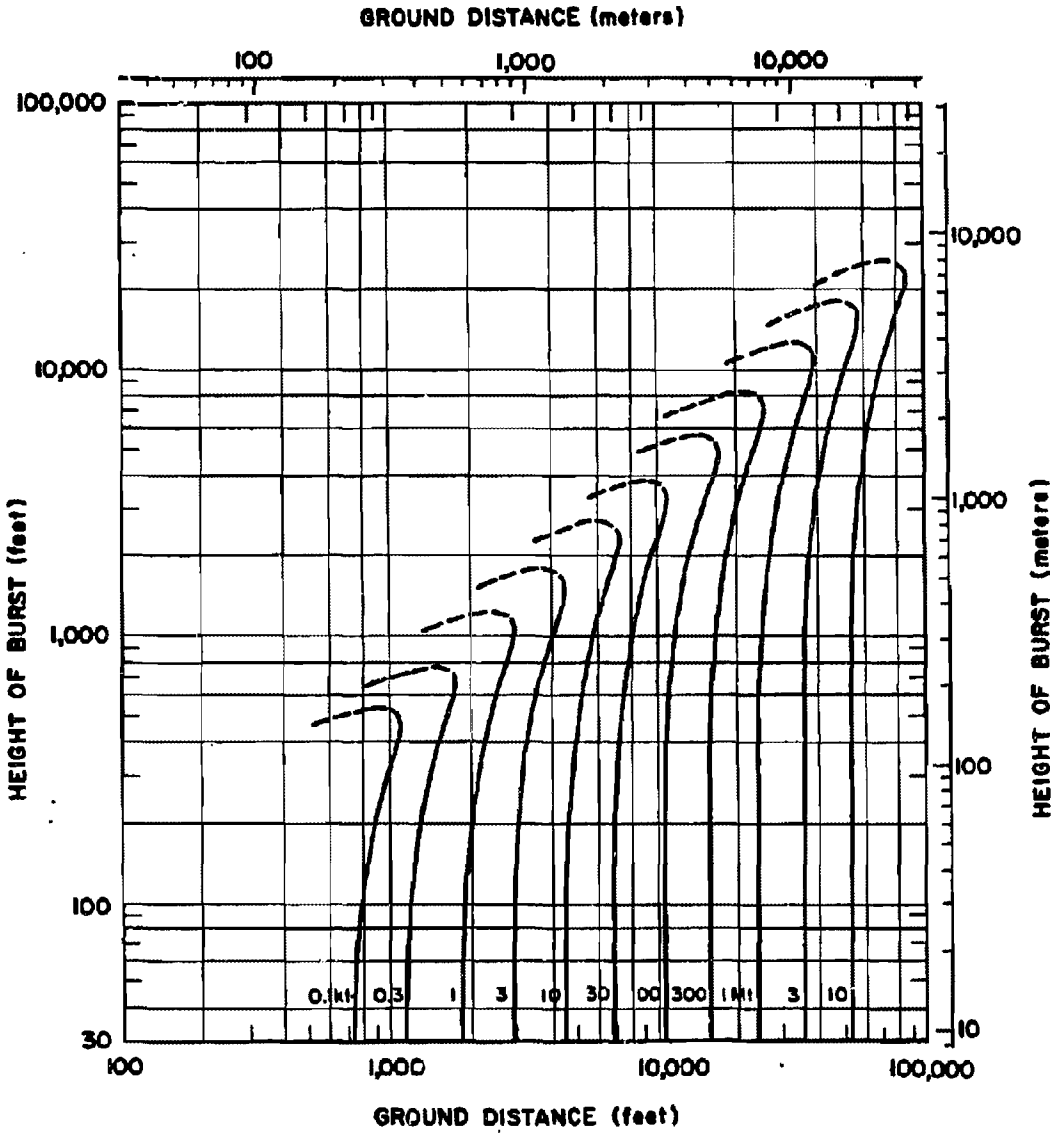

Figure 15-33. [redacted] Moderate Damage to a Type IVd Forest [redacted]

[redacted]

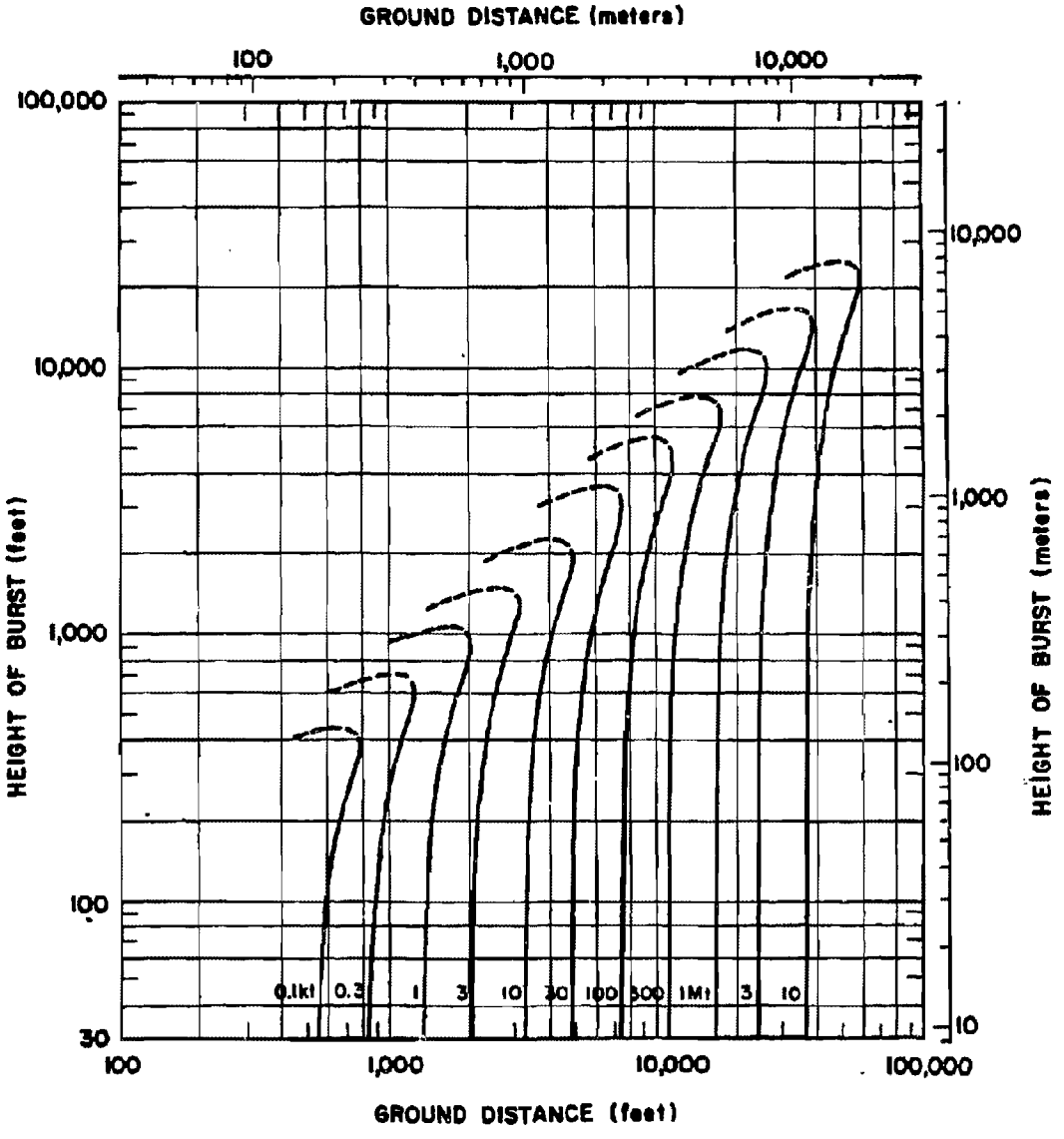

Figure 15-34. [redacted] Total Damage to a Type IVd Forest [redacted]

[redacted]

SECTION II

[redacted] TROOP AND VEHICLE MOVEMENT [redacted]

[redacted] The effects of a nuclear explosion on a forest may have a significant influence on military operations within the region of the forest that is affected by the burst.

[redacted] Two H.E. tests have provided information concerning the character of the region that is damaged and the effect on vehicular and troop movement that the damage will cause. [redacted]

DNA (b)(1)

[redacted] An important difference between the ef-

*[redacted] The information in these tables may be used for yields ≤ 20 kt by determining the ground ranges for equivalent dynamic pressure impulses.

Table 15-3 [redacted] Effects of a 1 kt Weapon Burst at a Height of 270 Feet Over a Rain Forest [redacted]*

DNA (b)(1)

[redacted]	[redacted]
[redacted]	[redacted]
[redacted]	[redacted]
[redacted]	[redacted]
[redacted]	[redacted]
[redacted]	[redacted]
[redacted]	[redacted]
[redacted]	[redacted]
[redacted]	[redacted]

[redacted]

[redacted]

[redacted]

fects on broadleaf and coniferous forests is the nature of the debris.

DNA (b)(1)

[redacted]

15-3 Blowdown Debris Characteristics

[redacted] The impact of the damaged region of a forest on movement is determined by the number and diameter of stems in the path of the vehicles or troops. The variation in these parameters throughout various regions of damage are discussed in the following paragraphs.

[redacted] Data from the two TNT detonations that were mentioned previously are presented in Figures 15-35 and 15-36. Figure 15-35 shows the relation between stem-feet per acre* and ground range for a rain forest and for a coniferous forest. [redacted] The difference in maximum stem-feet per acre between the two forests results from the difference in average tree density and tree height of the

DNA (b)(1)

[redacted] See footnote to Table 15-1.

Table 15-4 [redacted] Effects of a 1 kt Surface Burst on a Coniferous Forest [redacted]

[redacted]

DNA (b)(1)

[redacted]

[redacted]

[redacted]

DNA (b)(1)

[redacted]

Figure 15-35. [redacted] Stem-ft per Acre Comparison Between a Rain Forest and a Coniferous Forest [redacted]

[redacted]

forests. The curve for the rain forest is based on data gathered by observation, while the curve for the coniferous forest is based on calculations, using preshot and postshot tree surveys. Figure 15-36 shows the relation between ground range and average diameter of the debris.

DNA (b)(1)

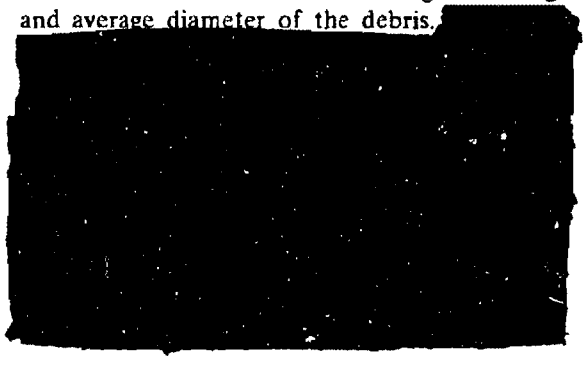

DN (b)

[redacted]

[redacted]

Figure 15-36. [redacted] Average Diameter of Stems Down, Comparison Between a Rain Forest and a Coniferous Forest, 1 kt [redacted]

[redacted] This distance is determined easily from photo reconnaissance, as are the debris zones described in Tables 15-3 and 15-4.

15-4 Vehicle Movement [redacted]

[redacted] The movement rates of various wheeled and tracked vehicles have been measured for both radial and circumferential traverses of various debris zones. Although quantitative data were obtained and can be used, correlations between vehicle movement and debris characteristics are incomplete and are not refined to the point of high reliability. Nevertheless, curves have been constructed that indicate in terms of the debris parameters (number of stem-feet per acre and diameter of debris) when a vehicle will not be able to move. These curves are presented in Figure 15-37 and 15-38 for radial movement from ground zero and circumferential movement, respectively. The general radial orientation of tree stems is significant in terms of movement, because selection of easier routes between stems is possible in some cases of radial movement, while all stems must be crossed in circumferential movement. The shaded areas on the graphs indicate debris characteristics where movement is difficult. The solid line indicates that movement is not possible. For example, from Figure 15-37, for debris characteristics of 10,000 stem-feet per acre with average diameters of 4, 6, and 8 inches, radial movement of wheeled vehicles would be possible, difficult, and not possible, respectively. Curves for wheeled vehicles are fairly well documented with data; however, the curves for the M113 and tank are not, because

[redacted]

[redacted]

DNA (b)(1)

Deleted

Figure 15-37. [redacted] Debris Characteristics Preventing Radial Movement of Vehicles [redacted]

[redacted]

[redacted]

DNA (b)(1)

Deleted

Figure 15-38. [redacted] Debris Characteristics Preventing Circumferential Movement of Vehicles [redacted]

[redacted] these vehicles were slowed but not stopped by the debris zones in which they were tested. Tracked vehicles can climb onto the debris and mat it down after a number of passes, with the result that wheeled vehicles might pass, although this technique was not tested.

15-5 Troop Movement [redacted]

[redacted] The effect of blowdown debris on the movement of troops is difficult to present quantitatively. Many factors other than the physical obstacle itself, such as visibility, leadership, size of force, mission, and what the troops are carrying are also influenced by the debris and indirectly affect movement. Movement of troops through a debris zone can be compared with moving through a thick jungle, although radial movement is generally easier than circumferential movement. Branch debris in a broadleaf forest blowdown area adds difficulties, particularly in visibility, that are not as severe in coniferous forest debris. Troop trials were conducted on both TNT detonations previously described.

[redacted] The troop tests conducted in conjunction with the rain forest detonation involved comparisons between preshot and postshot tests of day and night patrols, platoon exercises with a mortar squad, and tests with stretcher parties.

DNA (b)(1)

Deleted

[redacted]

[redacted]

[redacted]

DNA (b)(1)

Deleted

Deleted

[redacted] The night and day patrols were conducted over a route that was about 700 yards long, with one leg from virgin forest to the vicinity of ground zero, then back to the virgin forest on a different bearing.

[redacted] Tests with a loaded two-man stretcher indicated that passage through blowdown debris was very difficult. The stretcher bearers' attention was diverted from the patient as a result of the need to concentrate on locating suitable footing. Consequently, the simulated casualty had a very rough trip and was frequently struck by debris. The conclusion drawn from this trial was that the probability for survival of a casualty with a severe wound would be significantly reduced by transit through blowdown debris. If the casualty survived the carriage, it is almost certain that he would experience a marked degree of secondary shock.

[redacted] Troop trials conducted in the coniferous forest blowdown consisted of radial and circumferential platoon exercises, including a mortar squad, and a simulated casualty-moving test. Some movement rate data that were obtained are shown in Table 15-6.

DNA (b)(1)

Deleted

DNA (b) (1)

Deleted

[redacted] In the platoon attack trials, control problems were considerably eased in the blowdown area compared to the virgin forest, as a result of increased visibility.

DNA (b)(1)

Deleted

[redacted]

[redacted]

Table 15-5 [redacted] Comparison of Radial and Circumferential Movement Rates for Troops in a Rain Forest Blowdown Area, Scaled to a 1 kt Nuclear Explosion [redacted]

DNA (5)(1)

Deleted

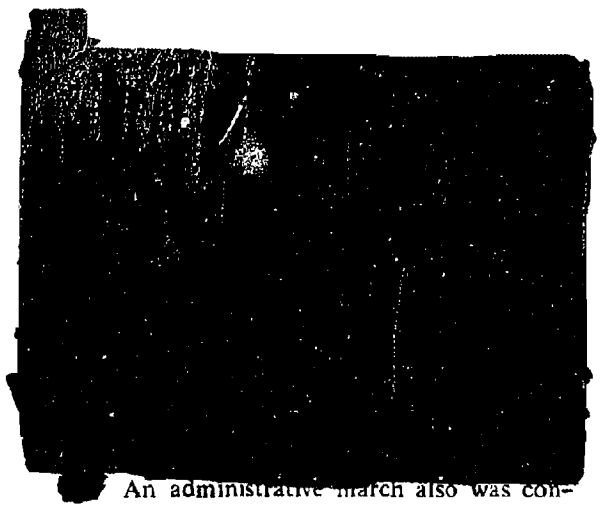

[redacted] An administrative march also was conducted over a radial–circumferential–radial route. The circumferential portion was in the area of maximum blowdown debris.

[redacted] A platoon night attack similar to the first circumferential trial described but in the opposite direction was performed. The platoon was organized as three attacking squad columns in line, except for the last 100 yards, where they deployed as a skirmish line. The 2-to-1 ratio in time was observed once again.

[redacted] The moving of a simulated casualty by two- and four-man stretcher bearer teams trav-

Table 15-6 [redacted] Comparison of Circumferential Movement Rates for Troops in a Coniferous Forest Blowdown Area, Scaled to a 1 kt Nuclear Explosion [redacted]

Deleted

DNA (5)(1)

[redacted]

[redacted]

eling circumferentially also was tested. Results were essentially the same as those from the rain forest trials.

15-6 Predicting Effects on Movement [redacted]

[redacted] The results of the tests conducted after the two TNT detonations, together with the forest descriptions in Section I and Table 15-1, and the forest damage definitions in paragraph 15-2, have been combined in Table 15-7 for use with Table 15-2 and Figures 15-1 through 15-34 to predict the ground distances at which movement will be affected to various degrees. The forest damage levels in Table 15-7 are restricted to Severe and Total, because Light and Moderate damage to forests have little influence on movement, except as a result of changes in visibility. Example problems will illustrate the use of Table 15-7 and will outline the limitations of the information presented.

Table 15-7 [redacted] Influence of Forest Damage on the Movement of Troops and Vehicles [redacted]

Deleted

DNA (b)(1)

[redacted]

[redacted]

Problem 15–2 Calculation of the Distance at Which Movement Will Be Impaired

[redacted] Table 15–7 together with Table 15–2 and Figures 15–1 through 15–34 provide the information necessary to estimate the area within which movement will be affected to various degrees as a result of tree blowdown. The information contained in these tables and figures allows determination of the affected area for movement of troops or vehicles as a function of weapon yield and forest stand type.

[redacted] *Example*

Given: A 2-Mt burst at 1,640 feet above a Type III forest stand.

Find: Will wheeled vehicles be stopped by the forest damage and at what maximum range?

[redacted]

DNA(b)(1)

[redacted]

[redacted]

Problem 15-3 Estimation of Movement Difficulty

DNA (b)(1)

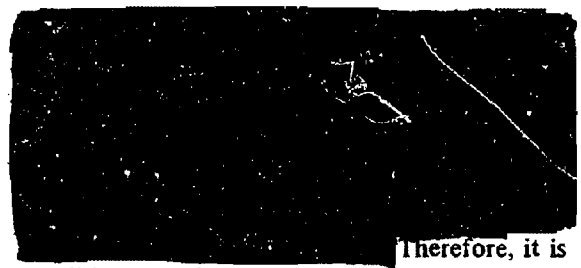

Therefore, it is possible to perform some evaluation of a forest using Figures 15-37 and 15-38 together with the forest characteristics. The forest characteristics required are tree density in trees per acre, average forest height in feet, average girth at breast height of the forest trees in either inches or centimeters, and tree type. The following parameters can then be determined:

Maximum Debris = (Forest density) (average height)

Average Debris Diameter in inches; girth, g, given in centimeters

DNA (b)(1)

[redacted]

Average Debris Diameter in inches; girth, g, in inches

DNA (b)(1)

[redacted]

With these two parameters, the potential obstacle of a forest can be estimated.

[redacted] *Example*

Given: A coniferous forest with a density of 200 trees per acre and average height of 50 feet. Girth at breast height averages 33 inches.

Find: What obstacle could be formed if the forest were damaged by a nuclear burst.

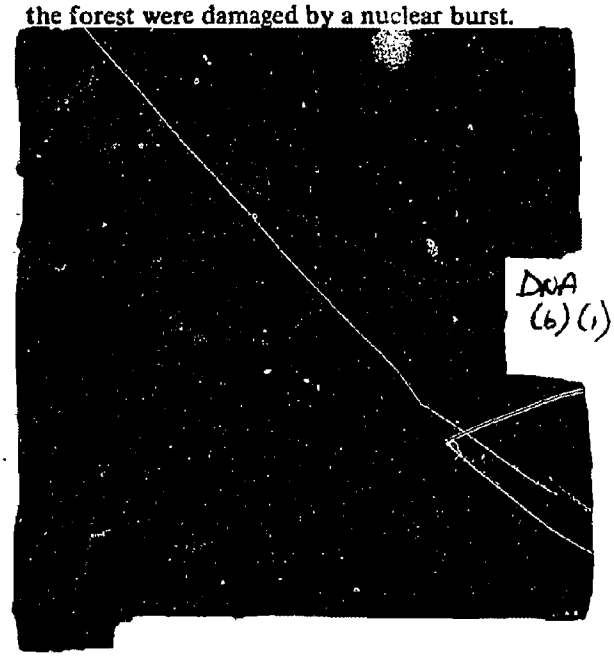

DNA (b)(1)

[redacted]

[redacted]

SECTION III
THERMAL RADIATION

[redacted] Under certain conditions, a nuclear weapon that is exploded over a forest or wildland area may cause fires. During the fire season, even when the burning potential (a measure of probable fire aggressiveness) is low, fires may spread. If fires are started in regions of sufficient fuel density when the burning potential is dangerously high, complete evacuation of personnel and equipment may be necessary. Organized control of the spread of the fire is virtually impossible until changes in weather or fuel availability reduce the burning potential.

15-7 Ignitions [redacted]

[redacted] Wildland fuels are typically a mixture of thin and heavy fuel components. Often, the thinner fuels will establish the limiting radiant exposure that will be required to start fires in the mixture.

[redacted] When fuels are dry, ignitions that have a reasonable chance of surviving the subsequent blast effects and of initiating fires that can represent a hazard to military personnel in the forest can be expected at quite low levels of radiant exposure. For example, broadleaf and coniferous litter (mixtures of fine grass, broken leaves and duff, and thin translucent broadleaf leaves) can be ignited by exposures of 2 to 3 cal/cm^2 from 1 kt low-altitude air burst, and heavier leaves (dead grass, conifer needles, and fallen, nearly opaque broadleaf leaves) can be ignited by exposures between 3 and 4 cal/cm^2, which correspond to distances at which 2 to 3 psi peak overpressures might occur, provided the full free-field radiant exposure falls on these fuels. As will be discussed subsequently, the likelihood of the full free-field exposure reaching these fuels in a forest area is quite low. Radiant exposure values required to ignite materials increase with moisture content and will be larger for the longer duration pulses of larger-yield weapons. The increase caused by moisture being absorbed from the air at high relative humidities ordinarily will not be more than a factor of 2 to 3. Wet or green leaves, however, may be impossible to ignite and, if ignited, they will not participate in the development of a persistent fire. The live foliage of conifers and many shrubs ignited by fire in associated dead fuel, however, burn vigorously and would add significantly to the intensity of spreading fire. This foliage is often the significant factor determining whether or not a crown fire develops.

15-8 Kindling Fuels [redacted]

[redacted] The majority of thin wildland fuels that serve as kindling material are typed into four classes as shown in Table 15-8. These classes correspond to different minimum exposures required for ignition. Since ignition generally occurs on surfaces that are most exposed to the atmosphere, ignition exposures are a function of relative humidity as shown in Figure 15-39. Fires may be blown out by the blast wave, depending on the time interval between ignition and arrival of the shock. Blowout is not expected to occur

Table 15-8 [redacted] Classes of Thin Wildland Kindling Fuels (Arranged in Order of Decreasing Flammability) [redacted]

Class	Description
I	Broadleaf and coniferous litter—mixture of fine grass, broken leaves and duff, and thin translucent broadleaf leaves.
II	Hardwood and softwood punk in various stages of decay.
III	Cured or dead grass.
IV	Conifer needles and thick, nearly opaque broadleaf leaves.

[redacted]

[redacted]

[redacted]

in overpressure regions below 5 psi or when the fuels are fully exposed. When fires are not blown out, they generally increase in intensity as a result of the blast wind.

[redacted]

[redacted]

Problem 15-4 Calculation of the Requirements for Wildland Kindling Fuel Ignition

[redacted] The curves of Figure 15-39 show the maximum radiant exposure as a function of relative humidity for ignition of wildland kindling fuels described in Table 15-8. The radiant exposures shown in Figure 15-39 apply to a 1 kiloton nuclear explosion.

[redacted] *Scaling.* For yields other than 1 kt, scale as follows:

$$\frac{Q}{Q_1} = W^{1/8}$$

where Q_1 is the radiant exposure for ignition of a particular class of wildland kindling fuel for 1 kt, and Q is the corresponding exposure for a yield of W kt.

[redacted] *Example* [redacted]

Given: A 40 kt weapon burst over a Class III wildland fuel when the relative humidity is 75 percent.

Find: The minimum radiant exposure required to ignite the fuel.

Solution: From Figure 15-39, the minimum radiant exposure for ignition of a Class III wildland fuel by a 1 kt explosion when the relative humidity is 75 percent is 4 cal/cm^2.

Answer: The corresponding exposure for 40 kt is

$$Q = Q_1 W^{1/8} = 4 \times (40)^{1/8} = 6.3 \text{ cal/cm}^2.$$

Reliability: Based upon observed results of limited full-scale tests and extensive laboratory experiments. The results are not considered reliable in the megaton range.

Related Material: See paragraphs 15-7, 15-8. For forest areas, see paragraphs 15-9 through 15-10. For determination of distances corresponding to a particular radiant exposure, see Chapter 3.

[redacted]

[redacted]

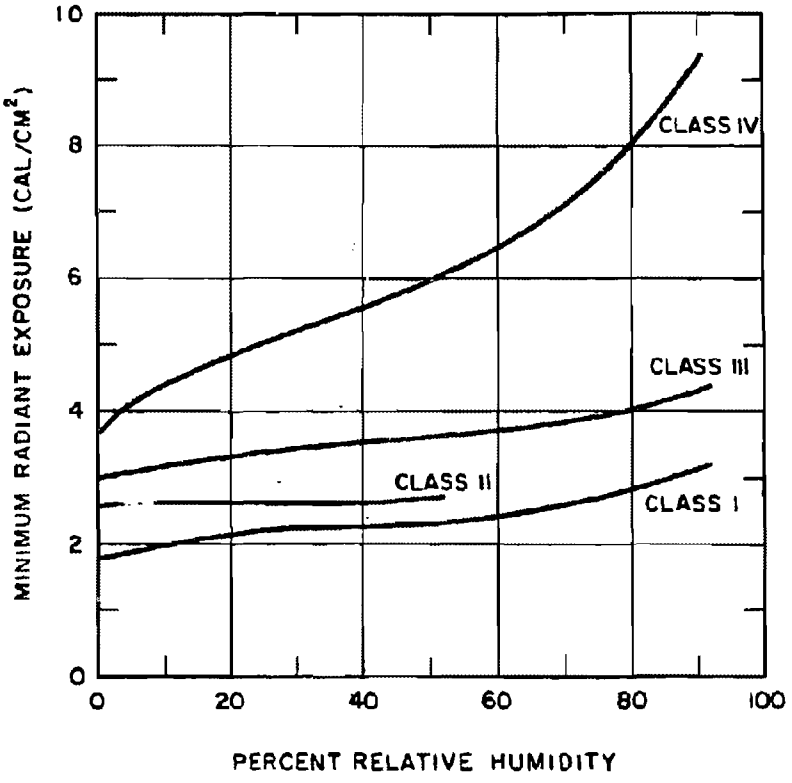

Figure 15-39. [redacted] Minimum Radiant Exposures of Wildland Kindling Fuels by a 1 Kiloton Explosion [redacted]

[redacted]

[redacted]

15-9 Thermal Radiation on Forests [redacted]

[redacted] Probably the largest uncertainty associated with thermal radiation on forested areas arises from a lack of information about the transmission of the radiation through the foliage and other obscuring features of forest stands for high-yield air bursts.

[redacted] Methods for approximating the fraction of the free-field thermal radiation exposure that is transmitted by the forest environment will be considered here. The methods for calculating the free-field exposure are discussed in Chapter 3.

[redacted] Both from the point of view of causing injury to exposed personnel and of starting fires, the primary interest is in assessing the exposure of the forest floor to thermal radiation from the nuclear fireball. The foliage making up the crowns of the trees, while it has a high probability of being exposed to the full free-field radiation environment from air bursts and may be severely dessicated, thermally (even explosively) decomposed, and, at high enough flux levels, flash ignited, is not likely to contribute to subsequent sustained fires. It may, however, materially reduce the exposure of the forest floor by generating quantities of smoke and steam as well as by direct shading.

[redacted] Neglecting these thermally-induced, self-protective screening effects (noting that "scattering in" may effectively offset "scattering out"), an approximation to attenuation by trees and associated vegetation may be obtained by assuming that the attenuation is proportional to the extent of coverage of the field of view of the fireball by the elements of the forest canopy, i.e., that the exposure of any spot on the ground is roughly proportional to the apparent area of the fireball seen by that spot. Hence, height of burst and yield are important geometrical parameters that must be considered.*

[redacted]

DNA (b)(1)

[redacted]

[redacted] Size of openings and tree height are other important determinants of the susceptibility of a forest to ignition from an air burst. This indicates the need for on-the-ground or from-the-air appraisal of forests and presumed explosion situations. This can be done with reasonable accuracy and much more rapidly from aerial observation or photographs than from surface measurements.

DNA (b)(1)

[redacted]

DNA (b)(1)

*Note that this assumes the source of thermal radiation to be above the tree tops. It will be seen in the subsequent discussion that thermal transmission is negligibly small for the low line-of-sight angles corresponding to burst heights less than tree heights, except perhaps for the short transmission paths that accompany bursts in the extreme low-end of the range of yields. Significant thermal exposures will never occur from these weapons, even in a sparsely vegetated forest environment, at distances corresponding to peak overpressures of 10 psi and less, because free-field exposure at these distances are only about 4 cal/cm^2 and less.

[redacted]

[redacted]

DNA (b)(1)

[redacted]

DNA (b)(1)

Table 15-9 [redacted] "Standard Northern European Forest" Data†

[redacted]

[redacted] The "standard Northern European forest" represents a composite of the characteristics of the forests of northern Europe obtained by averaging the features of 10 different forest stands chosen as representative of type (pine woods, spruce and deciduous forests, and mixtures of these) and tree density (range of about 200 to 1,000 trees/acre).

† [redacted] Sites were chosen on flat terrain in Northern Europe having uniform density distributions and generally uniform tree height (not more than 15% variation for not less than 90% of the trees in the stand). This uniformity is typical of the managed forests of Europe along with a general absence of undergrowth. These characteristics are not common to unmanaged (natural) forests. There is no reason to expect that information derived from these studies are in any way applicable to tropical hardwood forests.

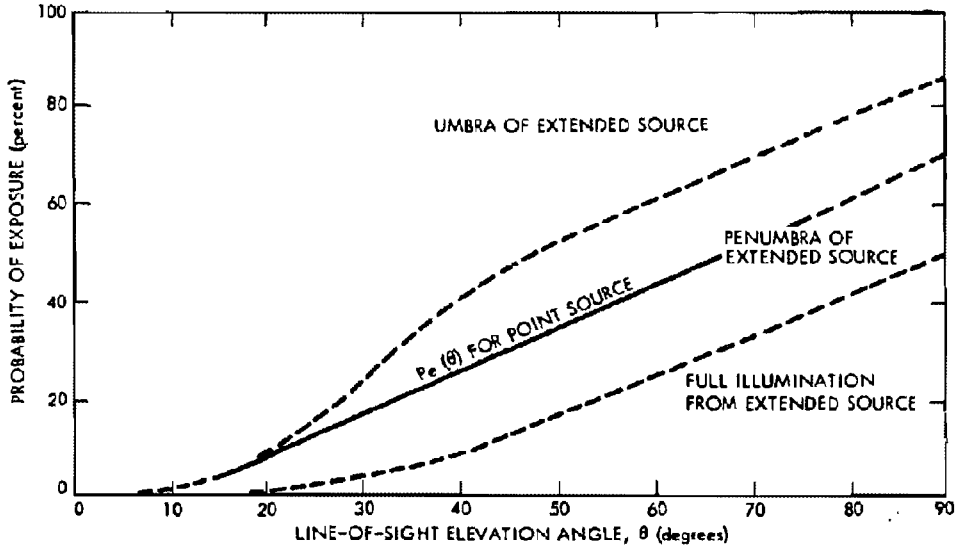

Figure 15-40. [redacted] Probability of Exposure of the Forest Floor ("Standard Northern European Forest") as a Function of Elevation Angle; Examples of a Point Source and a Spherical Source Subtending an Angle of 10 Degrees [redacted]

[redacted]

[redacted]

DNA (b)(1)

Obviously $Pe(\theta)$ functions, as illustrated by the "standard Northern European forest" in Figure 15–40, must depend on forest characteristics, notably tree density, with increased dispersion expected toward the larger angles of elevation. The data presently available do not reflect the degree of dispersion nor its dependence on forest characteristics adequately. Some idea of dispersion with tree density can be obtained from Figure 15–41, which displays the range of available results.

Although the current data base is quite poor, particularly as it applies to unmanaged forests and tropical or temperate-broad-leaf forests, it can be inferred that direct thermal effects in the forest environment do not contribute substantially to damage and casualties at distances where blast effects are not extreme, except, perhaps, in the least densely populated stands (less than 50 to 100 trees per acre). For most tactical situations where survival of blast effects can be expected, radiant exposures would be much less than half the free field over most of the floor of forests having densities of a few hundred or more trees per acre, and probabilities of exposure to the full free-field level would be negligibly small.

Declassified

15–10 Forest Fire Ignition and Spread

Under certain conditions, the explosion of a nuclear weapon over a forest or wildland area may cause fires. During the fire season, even when the burning potential is low, fires may spread. If fires are started in regions of high-fuel density when the fire potential is high, complete evacuation of personnel and equipment may be necessary. Organized control may be impossible until changes occur in the weather or the fire runs out of fuel.

An important exception to kindling fuel exposure to the full free-field radiant environment occurs in unmanaged forests of the temperate and cold regions. Many of these forests contain an abundance of dead and frequently punky

[redacted]

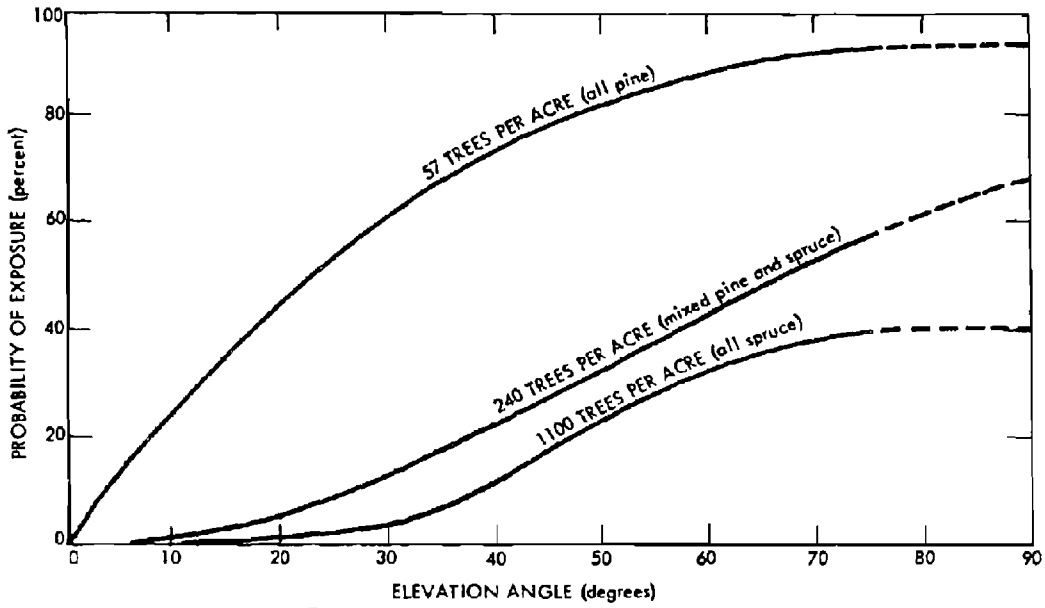

Figure 15-41. [redacted] Probability of Exposure of Forest Floor for Different Levels of Tree Density [redacted]

[redacted] wood exposed at or above the general canopy level. Of the common forest fuels, wood punk is probably the most susceptible to ignition by the thermal pulse. Moreover, since ignition is by charring or glowing combustion, these fuels are less susceptible to extinction by the blast wave than those that ignite with flame. These punky fuels, often easily detached from the parent tree, may be carried downwind for considerable distances and dropped to the forest floor as live embers. More rapid decomposition of dead wood makes this a less likely phenomenon in the moist tropics.

[redacted] As mentioned previously, the blast wave may extinguish fires at substantial overpressures, but the current state of the art does not permit quantitative evaluation of this phenomenon. On the other hand, at close-in distances where the blast wave arrives early during the thermal pulse (at times less than about 8 t_{max}) sufficient radiant exposure may follow the blast wave to re-ignite fuels and/or to ignite blast-created tinder.

[redacted] Current interpretations of the qualitative effects of blast on the persistence of incipient fires are based largely on experiments where kindling fuels were anchored in place. Had these fuels been free to move with the blast, many of them would have been translated for considerable distances as effective firebrands. Fire spread following ignitions by these brands would be influenced significantly by the return flow through the negative blast phase of the blast wave.

[redacted] The high degree of shading by tree crowns and stems for detonations at or below the canopy level often may be offset by scattering of burning debris ignited within the fireball. Many forest types contain large quantities of dead and rotten wood on and above the ground surface. If these materials are in flammable condition they may be expected to travel outward to the approximate limits of tree blowdown and provide plentiful ignition sources. Initial spread of fire from these

[redacted]

[redacted]

Table 15-10 [redacted] Condition of Wildland Fuels During Fire Season [redacted]

Fuel Type	Amount and Density of Fuel Required to Constitute a Fire Hazard	Condition During Fire Season
Grass or heath: Grassland; dry bracken ferns and other seasonal plants; dry regrowth in previously burned areas.	Uniform grass cover one-half ton or more per acre.	Vegetation nearly cured or dead.
Evergreen brush: Perennial evergreen shrubs and brush; chapparal; young evergreen growth.	75 percent or more covered.	15-25 percent by weight of leaves and associated twigs dead.
Deciduous broadleaf forest: Forest predominantly of trees such as oak, birch, maple, leaves of which die and fall every year.	Ground covered with more or less continuous layer of dead leaves.	Leaves off trees; ground vegetation dead or nonexistent.
Coniferous forest: Forest of evergreen pines, firs, spruces, etc.; generally the family of needle bearing trees.	Ground covered with more or less continuous layer of dead needles and twigs.	Needles and twigs dry enough to break easily when bent. Grass and other ground vegetation, if present, curing or dead.

[redacted]

sources would also respond to the inflow during the negative phase of the blast wave. Later behavior would depend on the degree of involvement of blowdown debris and the ambient weather.

[redacted] Times of the year during which the fire hazard is apt to be high are referred to as fire seasons. These are determined principally by the annual rainfall-temperature pattern and the amount and kinds of vegetation associated with it. Fire seasons vary widely from place to place throughout the world. Conditions associated with fire seasons in some typical wildland fuels are shown in Table 15-10. The more difficult problem is that of obtaining and systematically appraising local forest flammability data within a fire season on a day-to-day basis for fire spread predictions. No one formula will fit all situations.

[redacted] The main factors, aside from the fuels, that determine the fire hazard are: the nature of the terrain; the wind speed close to the ground; the relative humidity; and the precipitation history. Fuels seldom burn vigorously, regardless of wind conditions, when fuel moisture content exceeds about 16 percent. This corresponds to an equilibrium moisture content for a condition of 80 percent relative humidity. Rainfall of only a fraction of an inch will render most fuels temporarily nonflammable and may extinguish fires in thin fuels. The time required to restore the fire-danger condition may vary from hours to days depending on weather and soil conditions. Surface fuels in the interior of timber stands are exposed to reduced wind velocities; generally, these fuels retain their moisture as a result of

[redacted]

[redacted]

Table 15-11 [redacted] Criteria of "No-Spread" of Fires [redacted]

Fuel Type	Criteria
All forest fuels	Over 1 inch of snow on the ground at the nearest weather stations.
Grass	Relative humidity above 80 percent.
Brush or hardwoods	0.1 inch of precipitation or more within the past 7 days and: Wind 0-3 mph; relative humidity 60 percent or higher, or Wind 4-10 mph; relative humidity 75 percent or higher, or Wind 11-25 mph; relative humidity 85 percent or higher.
Conifer timber	1. One day or less since at least 0.25 inch of precipitation and: Wind 0-3 mph; relative humidity 50 percent higher, or Wind 4-10 mph; relative humidity 75 percent higher, or Wind 11-25 mph; relative humidity 85 percent or higher. 2. Two to three days since at least 0.25 inch of precipitation and: Wind 0-3 mph; relative humidity 60 percent or higher, or Wind 4-10 mph; relative humidity 80 percent or higher, or Wind 11-25 mph; relative humidity 90 percent or higher. 3. Four to five days since at least 0.25 inch of precipitation and wind 0-3 mph; relative humidity 80 percent or higher. 4. Six to seven days since at least 0.25 inch of precipitation and wind 0-3 mph; relative humidity 90 percent or higher.

[redacted]

shielding from the wind and shading from sunlight by the canopy. The spread or no-spread criteria are summarized in Table 15-11. This table lists the conditions under which fire would not be expected to spread.

[redacted] The criteria of Table 15-11 have been compared to the records of 4,378 wildland fires. Of the fires for which "no spread" would be predicted, 97.8 percent did not spread; only 40 percent of the fires that were predicted to spread actually did spread (at a rate of 0.005 mph or faster). This failure to spread often may be attributable to lack of fuel continuity around the point of origin.

[redacted] The criteria of Table 15-11 are considered to be reliable for American forests and suitably conservative to assure a low level of hazard to friendly forces. On the other hand, the criteria are probably not overly conservative to predict conditions for which enemy forces may be denied forested areas because of fire whenever the local weather history and conditions at the time of

[redacted]

[redacted]

Table 15-12 [redacted] Fire-Out Criteria [redacted]

Fuel Type	Criteria
Grass	"No-spread" conditions, or measurable precipitation.
Brush or hardwoods	0.1 inch of precipitation or more, or "no-spread" conditions for the next 12-hour period.
Conifer timber	1. 0.5 inch of precipitation or more; 2. 0.25 to 0.5 inch of precipitation and "no-spread" conditions for the following two 12-hour periods; 3. "No-spread" conditions for eight consecutive 12-hour periods and measurable precipitation during any two 12-hour periods; 4. "No-spread" conditions for 14 consecutive 12-hour periods.

[redacted]

detonation are known reliably, or whenever the initial fire is expected to be of substantial size.

[redacted] Weather conditions are subject to change, sometimes unpredictably, and fires that have been spreading may stop or go out. Conversely, fires that have not been spreading (other than on the microscale necessary to keep them dormantly alive) may flare up quite suddenly and spread rapidly as a result of a change in the weather. Whenever this threat of weather change cannot be tolerated, it is necessary to choose conditions for the employment of nuclear weapons so that dormant fires will not persist for times that are long compared to reliable weather-forecast periods. The "fire-out" criteria in Table 15-12 provide guidelines for this purpose. These criteria are derived from opinions of experienced fire personnel and should not, therefore, be considered to be as reliable as the "no-spread" criteria.

[redacted] Under identical weather conditions, concentrations of heavy fuels are more hazardous than thin fuels, even though they tend to reduce wind speeds locally and do not respond as rapidly to changes in relative humidity. This results from the fact that trees and heavy limbs on the forest floor may be ignited by an otherwise non-hazardous surface fire, and when heavy fuels are present near the borders of standing timber, the fire may travel into the tree crowns and spread from top to top even though ground fuel concentrations are low. Coniferous trees are most susceptible to crown fires. Hardwoods (deciduous trees) rarely, if ever, exhibit a true crown fire.

[redacted] Considerable information exists concerning rates of fire spread in American forests from historical records of major forest fires. Rates of spread rarely exceed 1 mile per hour except for brief periods of time during extreme burning conditions. Crown fires are capable of spreading at rapid rates, exceeding the rates of progress by men on foot attempting to out-run them. The high rate of progress of fire through crowns of trees probably results from the unimpeded wind-flow velocities above the forest canopy.

[redacted] Because of their potentially rapid rates of spread, crown fires represent a much higher level of hazard to personnel in forests than surface fires. Accordingly, it is desirable to be able to predict the occurrence of crown fires. Unfortunately, only qualitative criteria are available.

[redacted]

[redacted]

Table 15-13 [redacted] Burning Durations by Fuel Type [redacted]

Fuel Type	Violent Burning		Residual Burning		Total Burning Time
	Time (min)	Energy Release (percent)	Time (min)	Energy Release (percent)	
Grass	1.5	90	0.5	10	30 min
Light Brush (12 tons/acre)	2.	60	6.	40	16 hr
Medium Brush (25 tons/acre)	6.	50	24.	50	36 hr
Heavy Brush (40 tons/acre)	10.	40	70.	60	72 hr
Timber	24.	17	157.	83	7 days

[redacted] Surface fires exhibit brief "runs" at high speeds (a few miles per hour for several minutes, and a large fraction of a mile per hour for up to an hour or more), but average speeds over long periods of time range generally from 0.01 mile per hour to 0.5 mile per hour, with the most frequently noted values in the range of 0.1 to 0.5 mile per hour for 6- to 11-hour periods and in the range of 0.01 to 0.1 mile per hour for durations of 12 hours and more. These values are for American forests and should not be expected for managed forests (such as those of Europe) or tropical hardwood forests (such as those of some areas of Southeast Asia).

[redacted] An additional factor that affects the hazard of fire to military personnel and equipment is the burning duration of forest fuels. Examples of burning durations for fuels that are typical of American wildlands are summarized in Table 15-13.

[redacted] Table 15-13 refers to natural fuels in their undisturbed states. Experience shows that the highest fire intensities and fuel consumptions occur in the areas of greatest fuel accumulation. This fact has two implications with respect to nuclear detonations: if burning conditions are favorable, incipient fires from the thermal pulse falling on areas covered with a large amount of blast debris may build up rapidly; the blast debris accumulation may subsequently desiccate sufficiently to be a prime target for ignition by any means, either friendly or enemy.

[redacted]

[redacted]

BIBLIOGRAPHY

Bowe, T. W., et al., *Operation Blowdown, Scientific Observations and Analysis*, Commonwealth of Australia, July 1964, Report No. DSL 273 (3 volumes).

Chandler, C. C., et al., *Prediction of Fire Spread Following Nuclear Explosions*, Pacific Southwest Forest and Range Experiment Station, Berkeley, California, 1963, U.S. Forest Service Research Paper PSW-5.

Fons, W. L., F. M. Sauer, and W. Y. Pong, *Blast Effects on Forest Stands by Nuclear Weapons*, U.S. Department of Agriculture Forest Services, December 1957, AFSWP 971.

Kerr, J. W., et al., *Nuclear Weapons Effects in a Forest Environment—Thermal and Fire* [redacted] Panel N-2, TTCP, N2:TR 2-70, DASIAC Special Report No. 112, March 1971 [redacted]

Martin, S. and S. Holton, *Preliminary Computer Program for Calculating Ignition Ranges*, U.S. Naval Radiological Defense Laboratory, San Francisco, California, June 1965, USNRDL TR 866.

Nuclear Weapons Effects in a Forest Environment—Blowdown, Panel N-2, TTCP, August 1969, N2:TR 1-69, DASIAC Special Report No. 73.

Sauer, F. M., *Forest Blowdown in Comparison of the Results of High Explosive Experiments and Prediction Experiments*, Poulter Laboratory, Stanford Research Institute, Menlo Park, California, July 1969, DASA 2300.

Zaccor, J., et al., *Prediction and Significance of Forest Damage from a 50-Ton HE Surface Burst*, Project 7.01 Operation Distant Plane, Event 4, URS Research Company, June 1967, DASA 2065.

[redacted]

AD-A955 400

DTIC ELECTE 2 MAR 1989 S D E

Chapter 16

DAMAGE TO MISSILES

Missile systems are subject to damage by essentially all of the phenomena described separately in Chapters 2 through 8, Part I, of this manual, i.e., all or part of the system may be damaged by blast and shock (Chapter 2), by thermal radiation (Chapter 3), by X-ray radiation (Chapter 4), by nuclear radiation (Chapter 5) mainly in the form of transient radiation effects on electronics (TREE) phenomena (Chapter 6), or by the electromagnetic pulse (EMP (Chapter 7)). Communications and/or radar subsystems are also subject to degradation of their propagation characteristics as described in Chapter 8.

The damage that might result from several of the phenomena listed above is so dependent on specific system design that general methods for predicting specific missile system response cannot be provided. These phenomena include X-ray radiation, TREE, and EMP. Consequently, general descriptions of the damage mechanisms associated with these phenomena, applicable to missiles as well as other systems, are provided in Sections V, VII, and VIII, respectively, of Chapter 9. Additionally, some ambient nuclear radiation levels for "sure safe" and "sure kill" of missiles are given in Table 14-11, Chapter 14. Chapter 17 discusses the signal degradation of communications and radar systems. No further discussion of the damage or degradation from these phenomena is included herein.

This chapter is divided into two sections. Section I describes blast damage to tactical missiles. Section II describes the response of strategic systems to blast and thermal phenomena. Where appropriate, separate discussions are provided in Section II for antimissile systems (commonly called ABM) and reentry vehicles (*RV's*).

SECTION I

BLAST DAMAGE TO TACTICAL MISSILE SYSTEMS

The effects of air blast on three specific sample systems, the SERGEANT, the LANCE, and the HAWK, are described in this section. The vulnerability analysis of these missiles and their support equipment is intended to provide information from which the probable effects of air blast on other tactical missile systems may be estimated. An example of such an estimation for the HONEST JOHN missile is also provided. Outline drawings of the sample systems are shown in Figure 16-1 for comparison purposes.

In the case of each system, it is assumed that the system may be attacked from the time that the missiles are in stockpile until the missile warhead is detonated over the target. During any phase of this stockpile-to-target sequence, the system vulnerability is determined by the most susceptible component that is essential to completion of the mission. The vulnerability of all critical components is tabulated for each system. Vulnerability is expressed in terms of peak overpressure, assuming that the blast wave is from a contact surface burst with a yield between 1 kt and 300 kt. A range of values is given for the overpressure vulnerabilities, e.g., 12 to 19 psi. These numbers mean that either 12 psi from a 300 kt burst or 19 psi from a 1 kt burst is estimated to be sufficient to render the system component incapable of performing its necessary functions to complete the mission. Each vulnera-

DISTRIBUTION STATEMENT A
Approved for public release;
Distribution Unlimited

89 3 02 034

[redacted]

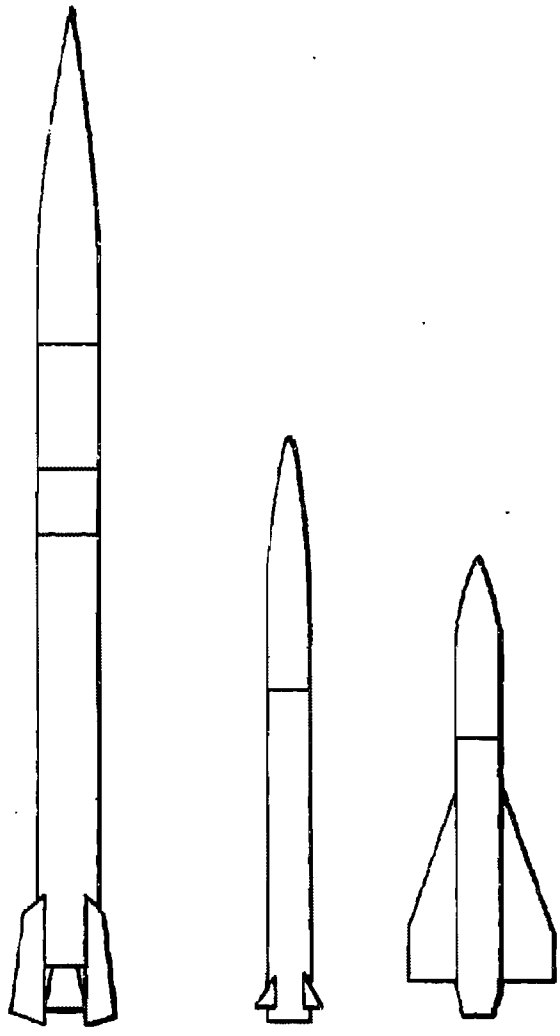

Missile	SERGEANT	LANCE	HAWK
Length ~ Ft.	34½	20	16
Diameter ~ In.	31	22	14
Weight ~ Lbs.	10,000	3100	1300
Application	Surface to Surface	Surface to Surface	Surface to Air
Range	46 to 137 NM.	5 to 75 NM.	to [redacted] Altitude with Horizontal Range
Warhead Section	1500 Lbs Nuclear	1000 Lbs Nuclear	73 Lbs. H.E.

Figure 16-1. [redacted] Missile Configurations, SERGEANT, LANCE, and HAWK [redacted]

QUALITY INSPECTED

Accession For
NTIS GRA&I
DTIC TAB
Unannounced
Justification
By
Distribution/
Availability Codes
Dist | Avail and/or Special
A-1

UNANNOUNCED

AMC (b)(1) (b)(1)

[redacted]

bility level is also shown in the form of a number curve, which allows critical values of range and overpressure to be determined as a function of weapon yield.

Many circumstances alter the vulnerability threshold of specific system components. For example, a truck that is carrying a missile to the launch site is less likely to be overturned by a blast wave if it is facing the burst than if it is hit from the side (see Table 14-5, Chapter 14). The velocity and orientation of a missile in flight both are important. If the terrain is conducive to the formation of a precursor, the truck may be subjected to a greatly enhanced dynamic pressure impulse, capable of overturning it much more easily than if it were exposed to the same burst at the same range under near-ideal conditions (paragraph 14-2, Chapter 14). The overpressure and dynamic pressure at the target depend on height of burst as well as distance. In order to reduce vulnerability data to a manageable set of numbers, the following conditions are assumed for the analysis in this section.

- The orientation of the system component with respect to the blast wave is such that the probability of serious damage is a maximum.
- Near-ideal surface conditions exist (no precursor).
- The blast wave is produced by a contact surface burst.

If radically different conditions are expected, appropriate changes in vulnerability levels must be made. In the case of a burst that produces a precursor, the dynamic pressure would be enhanced, and drag sensitive targets, i.e., those susceptible to toppling or overturning, probably would be damaged at an overpressure *lower* than predicted. Also, an air burst could produce a double shock on a target located in the regular reflection region; again this could lead to significant target damage at an overpressure lower than predicted. Thus, the numbers given should only be used as guides to the assessment of system blast damage.

Damage to targets that are primarily drag sensitive is determined by the dynamic pressure level. However, for near-ideal surface conditions, there is a known correspondence between peak overpressure and peak dynamic pressure (although the pulse durations can be somewhat different). Therefore, for the purpose of this chapter, all damage levels are expressed as overpressure levels, including the damage levels that apply to drag sensitive targets.

SERGEANT WEAPON SYSTEM

16-1 Description of the SERGEANT Weapon System

The SERGEANT weapon system is a second generation surface-to-surface missile system capable of being used under all terrain and weather conditions. Major items of the system are:

- *SERGEANT missile M15 and containers.* The SERGEANT missile body consists of four major assemblies:

  (1) rocket motor M53; (2) guidance section M38; (3) warhead section M65; and (4) control surface assemblies M58. Figure 16-1 shows a drawing of the missile. Figure 16-2 shows the missile parts in containers and ready for transport.
- *Four-wheel, semitrailer mounted guided missile launching station M504.* Figure 16-3 shows this unit in firing position. One component, the launching station firing set, is shown in more detail in Figure 16-4.
- *Four-wheel, 6 ton, low-bed semitrailer M527.*
- *Organizational Maintenance Test Station* (OMTS) *AN/MSM-35.* This trailer housed

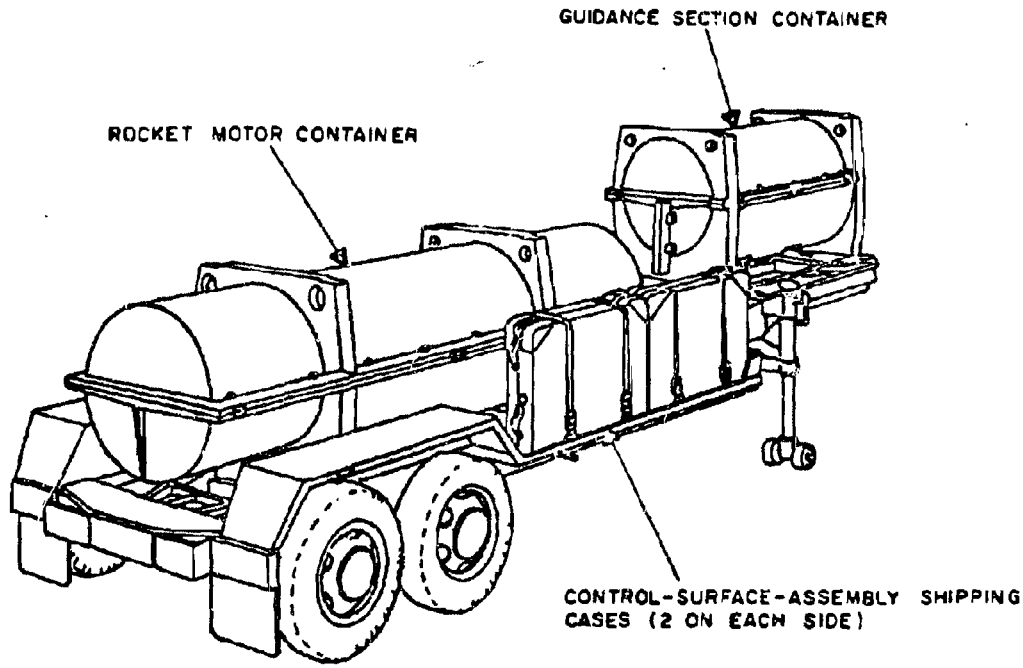

Figure 16-2. [redacted] SERGEANT System, Semitrailer Transporter with Missile Section Containers [redacted]

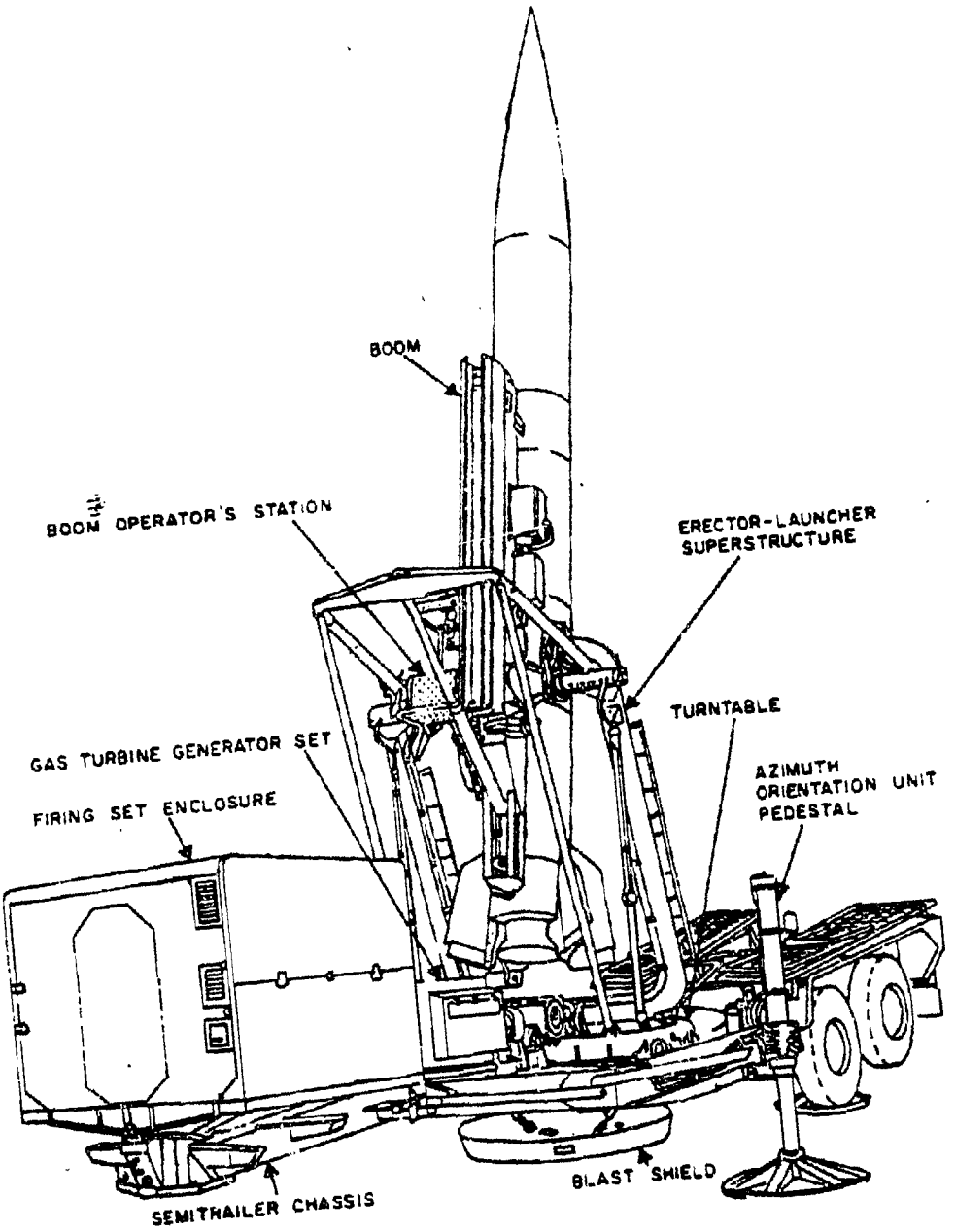

Figure 16-3. [redacted] SERGEANT System, Launching Station with Missile in Firing Position [redacted]

[redacted]

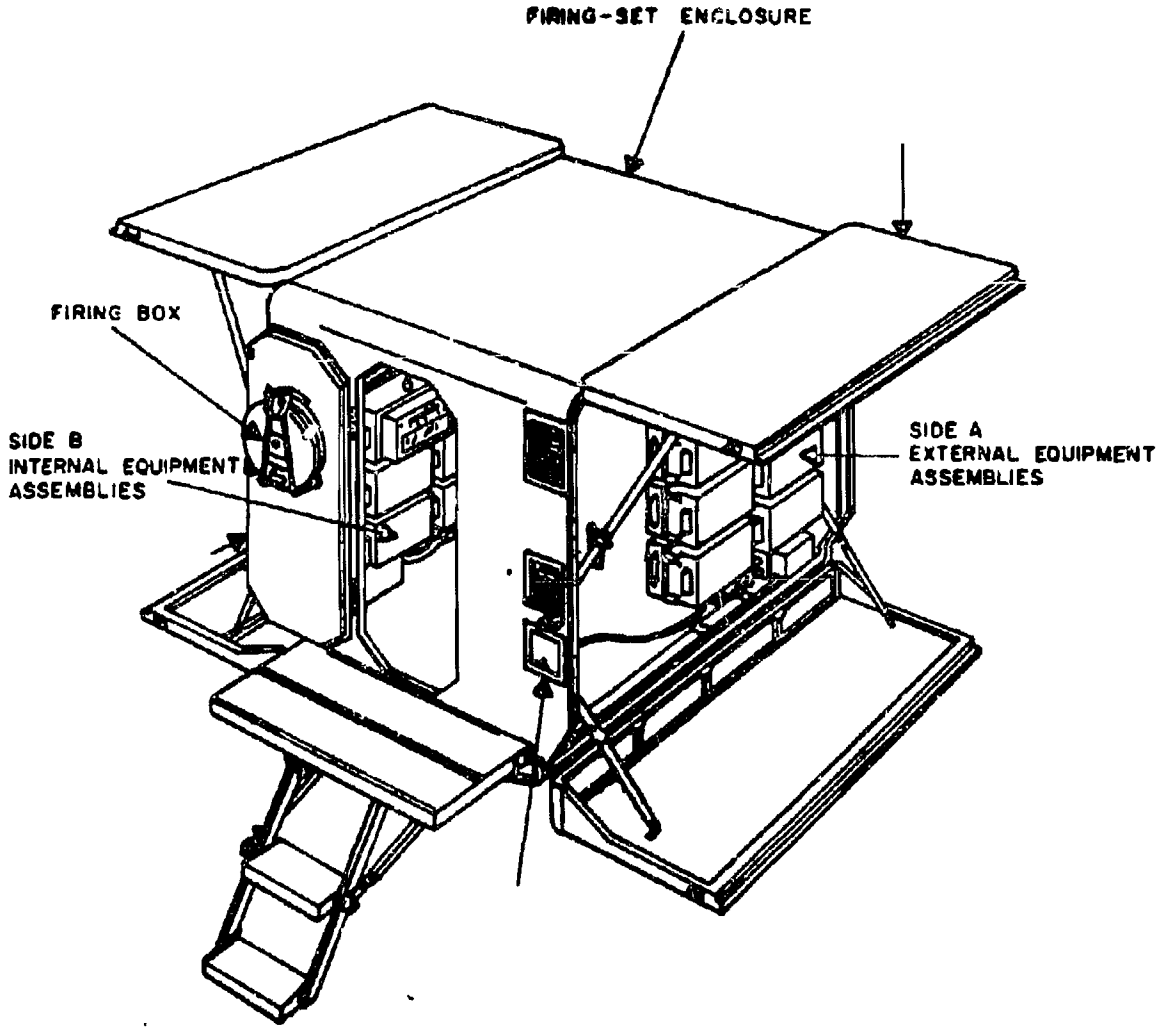

Figure 16-4. [redacted] SERGEANT System, Launching Station Firing Set [redacted]

[redacted]

unit, shown in Figure 16-5, is used for pre-launch testing and replacement of defective assemblies.

- *Field Maintenance Test Station (FMTS) AN/MSM-36.* This unit is similar to the OMTS. It can be used to perform many of the functions of the OMTS, and it is also used in situations that require more extensive testing and repair work than normally is done by the OMTS.
- *Warhead Section Container*
- *Truck, M35*

In addition to the equipment listed above, an M55 cargo truck is used to transport the rocket motor when the M527 is not available.

16-2 Vulnerability Levels of the SERGEANT Missile System

The vulnerability levels of the various components of the SERGEANT missile system are shown in Table 16-1.

The estimated vulnerability levels of the system in its various operational phases are described below. The most likely damage modes are also described.

- *Missiles in Containers at Storage Site (SERGEANT).* Figure 16-2 shows the type of containers used to store missile parts. The warhead section container, which is slightly longer than the guidance section container, is not shown.

DNA (6)(1)

DNA (6)(1)

- *Missiles in Containers in Transit (SERGEANT).* Since the transport vehicles afford partial protection for the containers, the vulnerability estimates were based on the pressure levels required to overturn the more vulnerable vehicle.

DNA (6)(1)

- *Equipment and Missile at the Firing Site (SERGEANT).*

DNA (6)(1)

- *Missile in Flight (SERGEANT).*

DNA (6)(1)

[redacted]

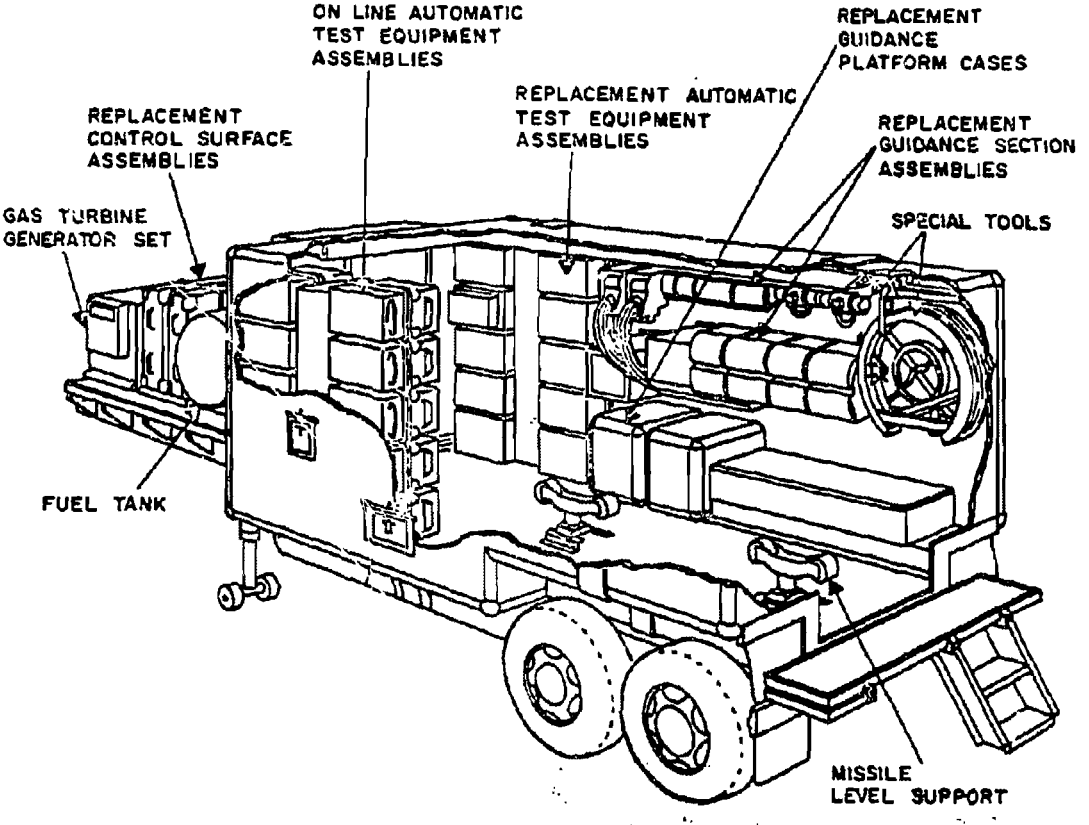

Figure 16-5. [redacted] SERGEANT System, Organizational Maintenance Test Station (OMTS) [redacted]

[redacted]

[redacted]

[redacted]

Table 16-1. [redacted] SERGEANT, Characteristics and Damage Levels for System Components [redacted]

USAMC
(b)(1)

Deleted

DAJA
(b)(3)
(b)(1)

[redacted]

[redacted]

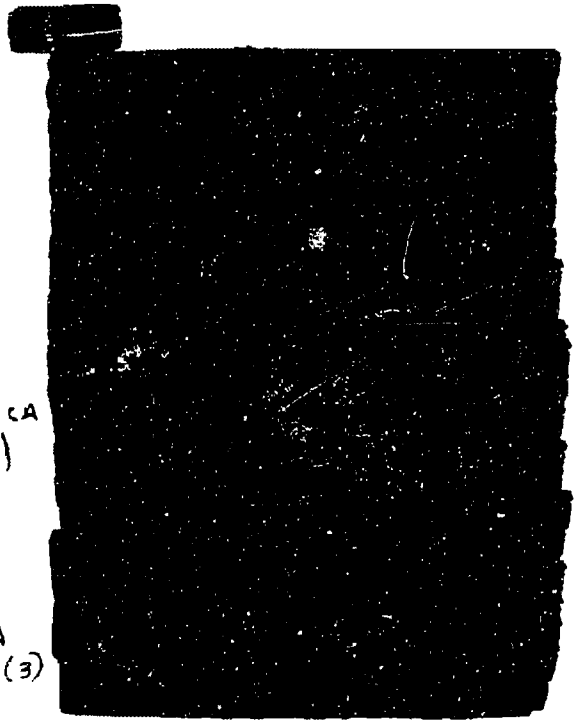

USAMICA (G)(1)

DNA (G)(3)

[redacted] The blast vulnerability of the principal components of the SERGEANT missile system can be determined by reference to Table 16-1 and Figure 16-6; the figure provides curves that allow the determination of pressure levels and distances for damage corresponding to various weapon yields. Table 16-2 shows a summary of the blast vulnerability of the susceptible subsystems in the various configurations of the SERGEANT missile system.

16-3 Reliability of SERGEANT Vulnerability Estimates [redacted]

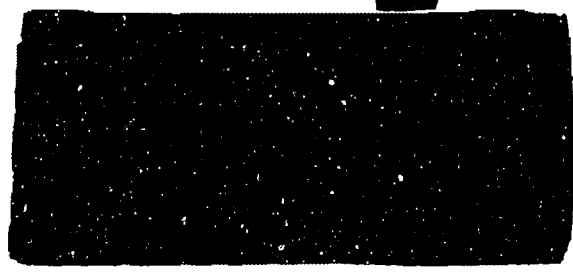

DNA (G)(1)

Table 16-2. [redacted] Blast Vulnerability Summary, SERGEANT Missile System [redacted]

DNA (G)(1) (G)(3)

USAMICA (G)(1)

Deleted

[redacted]

[redacted]

[redacted]

[redacted]

[redacted]

Figure 16-6. [redacted] SERGEANT, Major Item Blast Vulnerability [redacted]

[redacted]

[redacted]

[redacted]

DNA (L)(1)

DNA (L)(3)

[redacted] The sources of SERGEANT system damage data for the major items considered are:

DNA (L)(1)

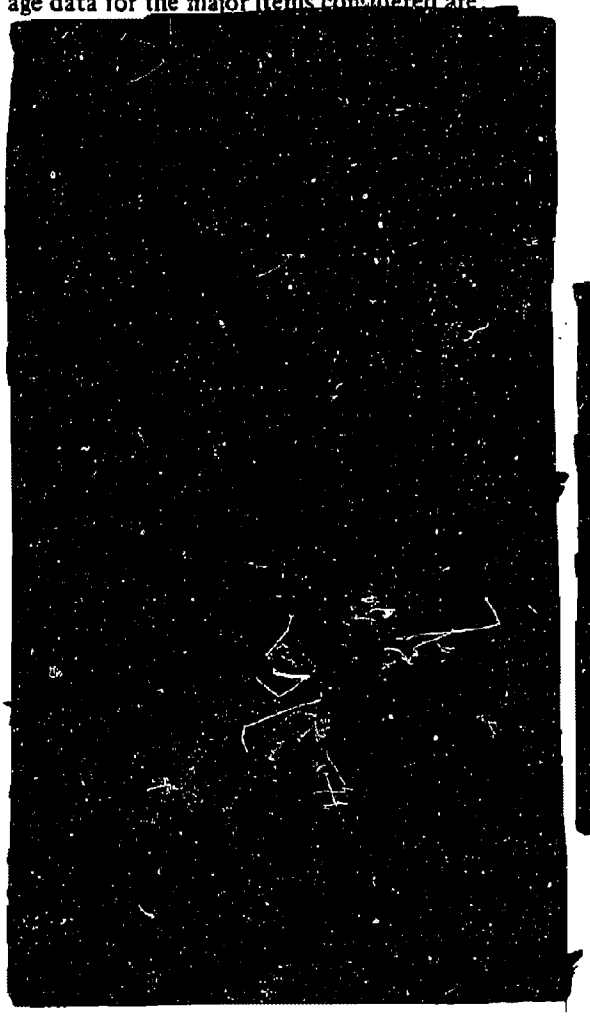

[redacted] LANCE WEAPON SYSTEM [redacted]

16-4 Description of the LANCE Weapon System [redacted]

[redacted] The LANCE is a surface-to-surface missile for general field artillery fire support of Army Divisions. The five major items of the LANCE system are:

- LANCE Missile Body, shown in Figure 16-1.
- Self-propelled Launcher (SPL), shown in Figure 16-7.
- Transporter Loader (TL), shown in Figure 16-7.
- Lightweight Launcher (LWL), shown in Figure 16-7.
- Other Ground Support Equipment, shown in Figure 16-8 (contact Support Test Set is not shown).

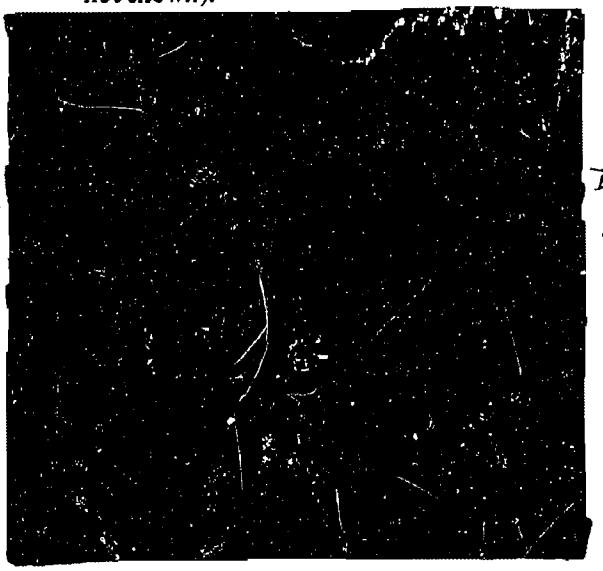

DNA (L)(1)

16-5 Vulnerability Levels for the LANCE Missile System [redacted]

[redacted] Blast vulnerability levels for the components of the LANCE missile system are shown in Table 16-3. Based on these values, the

[redacted]

[redacted]

[redacted]

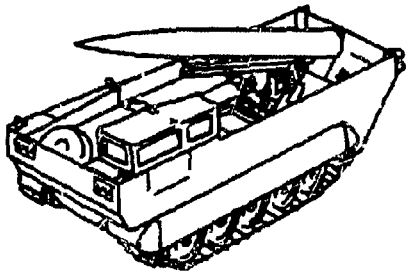

SELF-PROPELLED
LAUNCHER

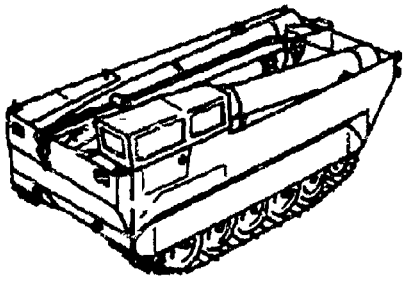

TRANSPORTER
LOADER

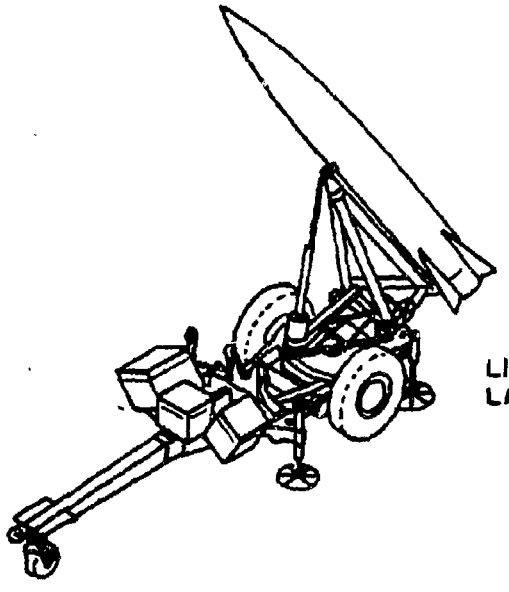

LIGHTWEIGHT
LAUNCHER

Figure 16-7. [redacted] LANCE System, Primary Units of the Missile System [redacted]

[redacted]

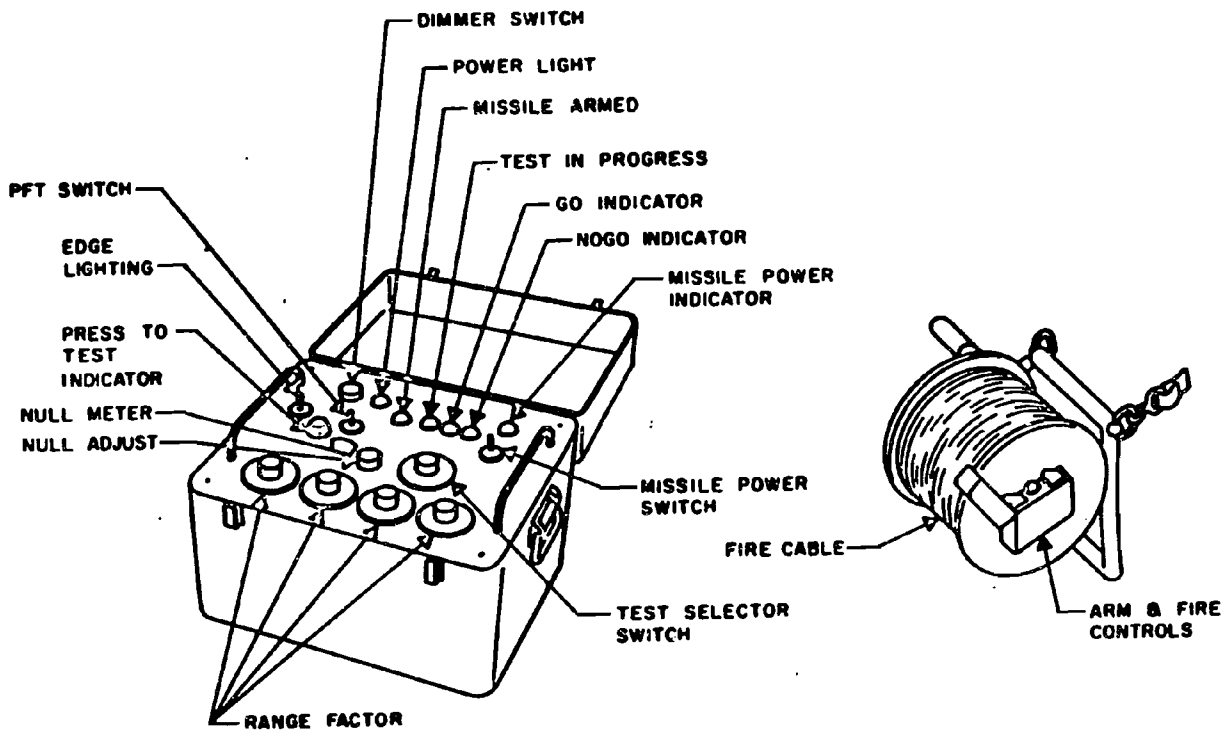

Missile Test Set (MTS) Firing Device (FD)

Figure 16-8. LANCE System, Prefire Tester and Fire Pack

[redacted]

Table 16-3. [redacted] LANCE, Characteristics and Damage Levels for System Components [redacted]

DNA (L)(1), (L)(3), USC (L)(1)

Deleted

[redacted]

susceptibility levels of the LANCE missile system during its various operational phases are estimated to be as follows:

- *Missile Parts in Containers at the Storage Site (LANCE).*

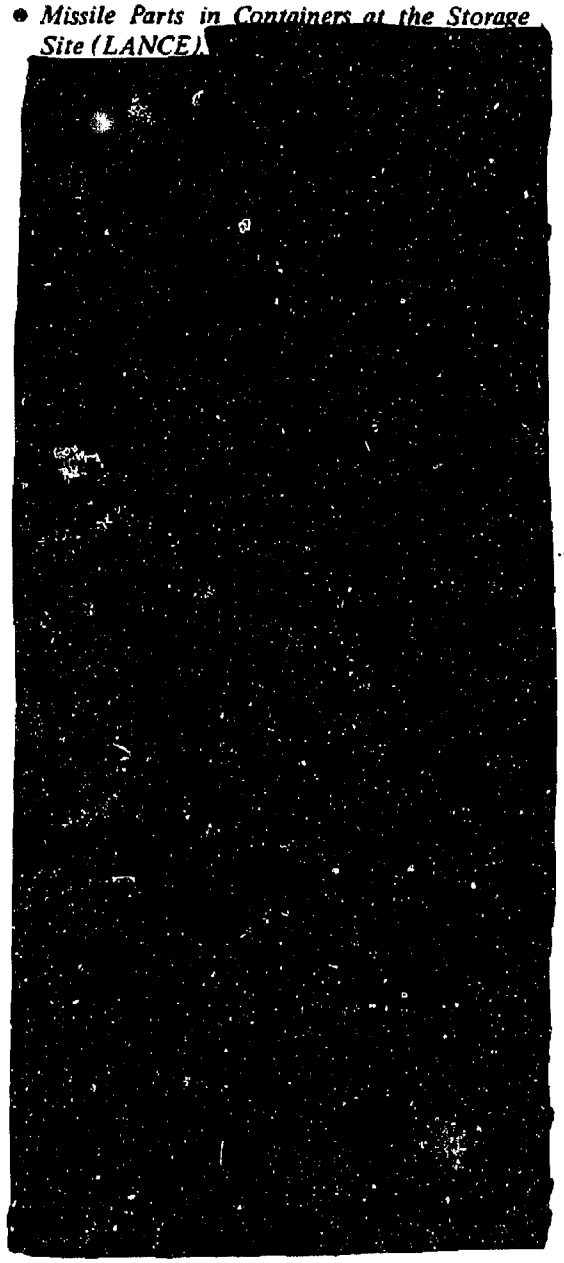

- *Missiles in Containers in Transit (LANCE).*

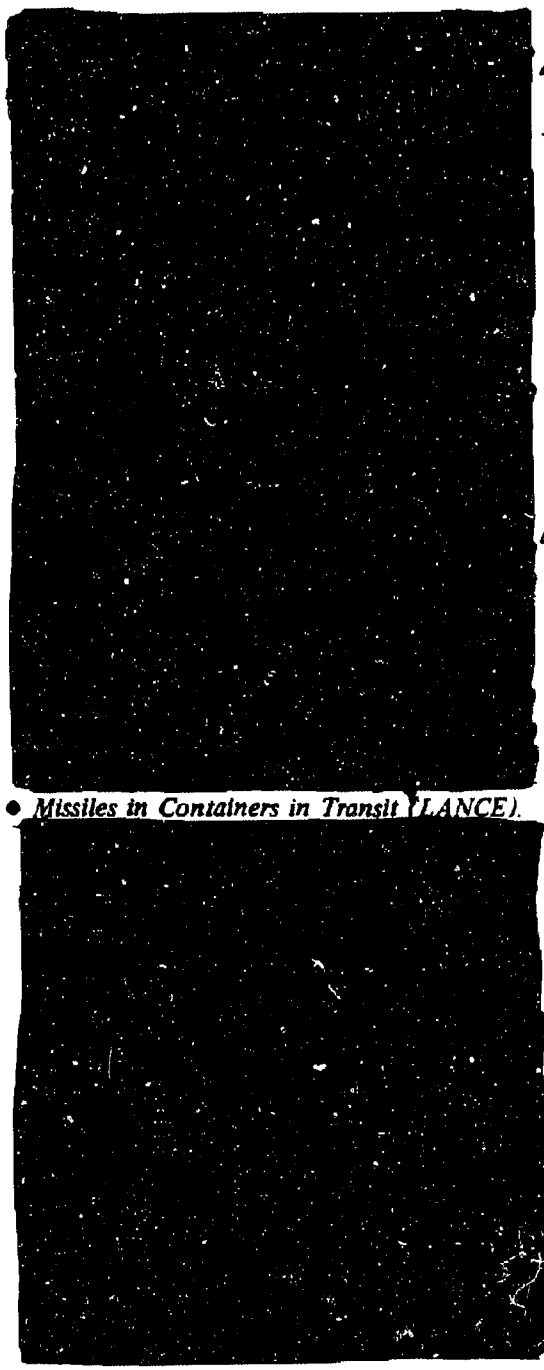

• *Missile System During Checkout, Prelaunch Phase, and Launching (LANCE).*

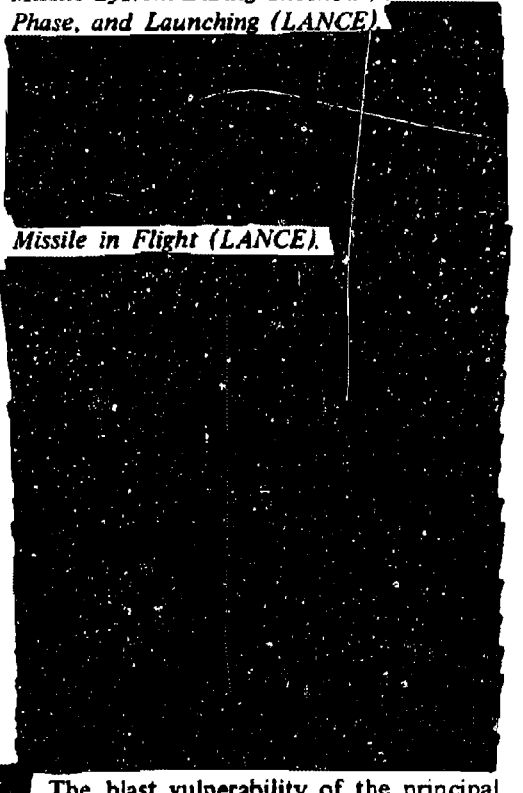

• *Missile in Flight (LANCE).*

The blast vulnerability of the principal configurations of the LANCE missile system can be obtained from Table 16-3 and Figure 16-9; the figure includes curves from which the pressure levels for damage corresponding to various weapon yields and ranges may be obtained. Table 16-4 shows a summary of the blast vulnerability of the susceptible subsystems in the various configurations of the LANCE missile system.

16-6 Reliability of LANCE Vulnerability Estimates

The source of the LANCE system damage data for the major items considered are:

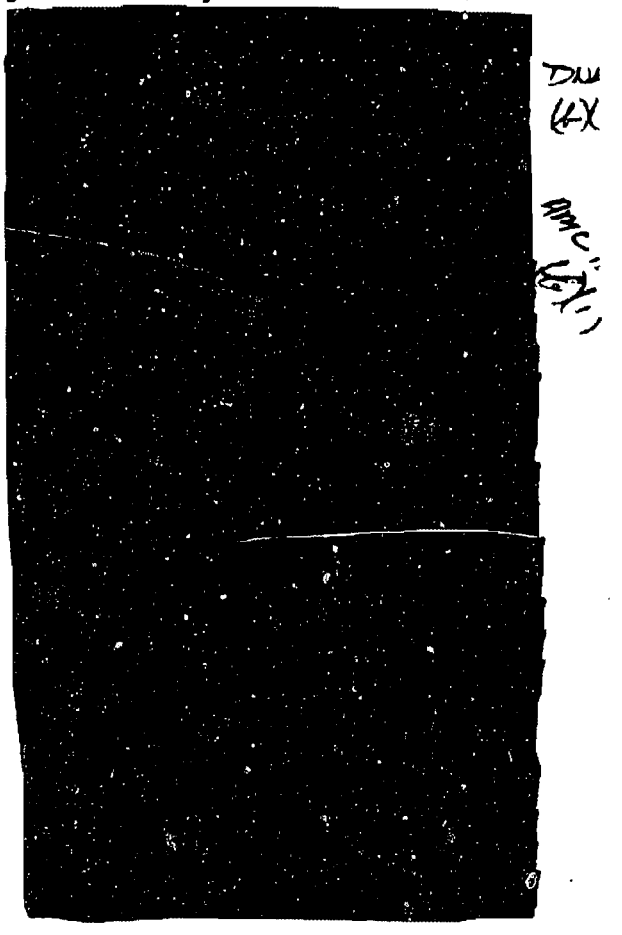

[redacted]

DNA
(L)(3)

Deleted

Figure 16-9. [redacted] LANCE, Major Item Blast Vulnerability [redacted]

[redacted]

[redacted]

Table 16-4. [redacted] Blast Vulnerability Summary, LANCE Missile System [redacted]

DNA (L-X3) (L)(1)

USAMC (L-X1)

Deleted

[redacted] These data were used for the missile structure vulnerability.

DNA (L)(1)

[redacted]

[redacted] HAWK WEAPON SYSTEM [redacted]

16-7 Description of the HAWK Weapon System [redacted]

[redacted] The HAWK is a surface-to-air, supersonic air defense system, designed to detect and identify airborne targets by means of radar, and to intercept and destroy those designated as hostile with homing guidance missiles.

[redacted] The major items of the HAWK system are:

- HAWK Missile Body, shown in Figure 16-1.
- Missile Loader, shown in Figure 16-10.
- Missile Launcher, shown in Figure 16-10.
- Assault Fire Command Console (AFCC) or Battery Control Central (BCC), shown in Figure 16-10.
- Radar Units, including
  (1) Range-only Radar (ROR), shown in Figure 16-11.
  (2) Pulse Acquisition Radar (PAR), shown in Figure 16-11.
  (3) CW Acquisition Radar (CWAR), shown in Figure 16-11.

[redacted]

[redacted]

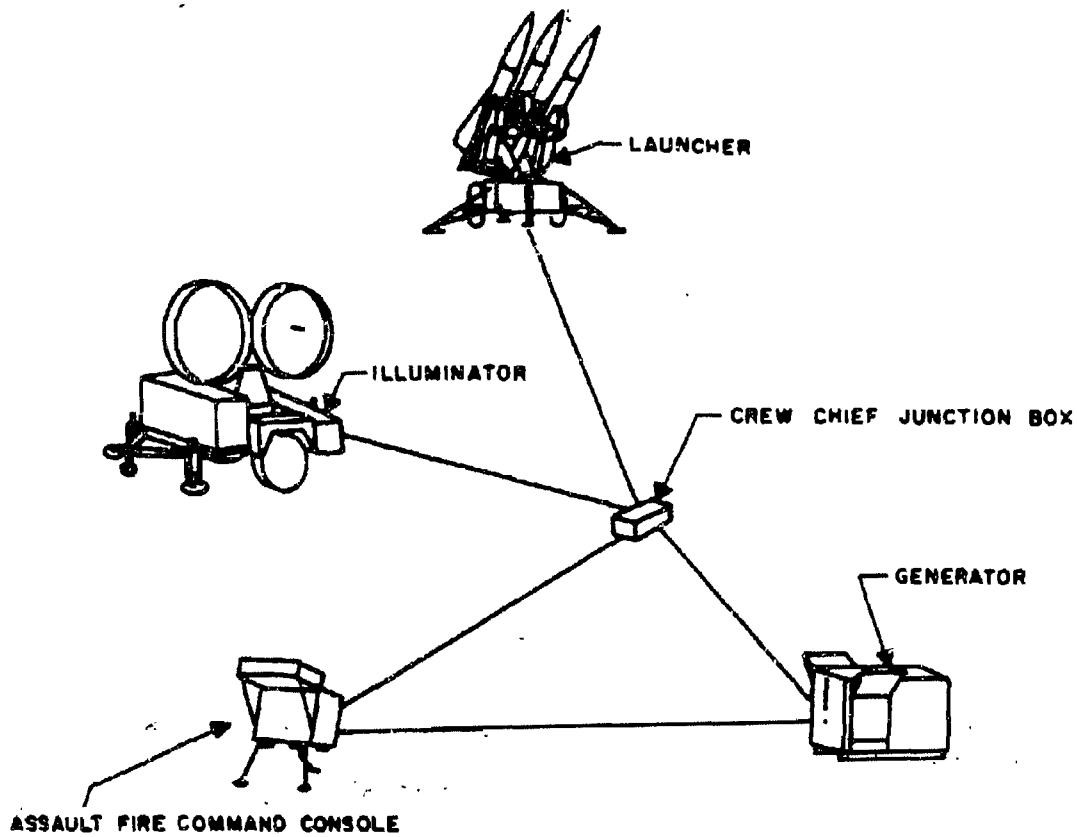

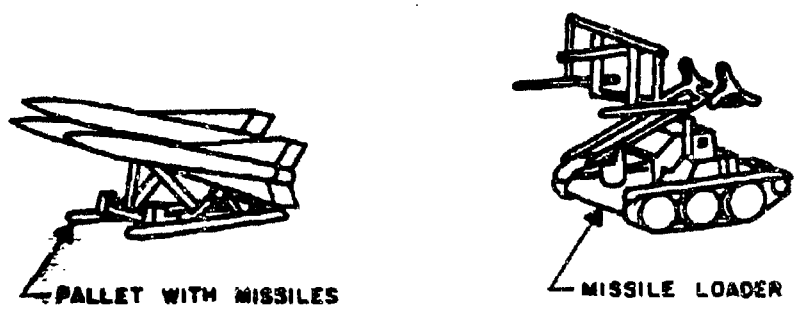

Figure 16-10. [redacted] HAWK System, Basic Assault Firing Unit [redacted]

[redacted]

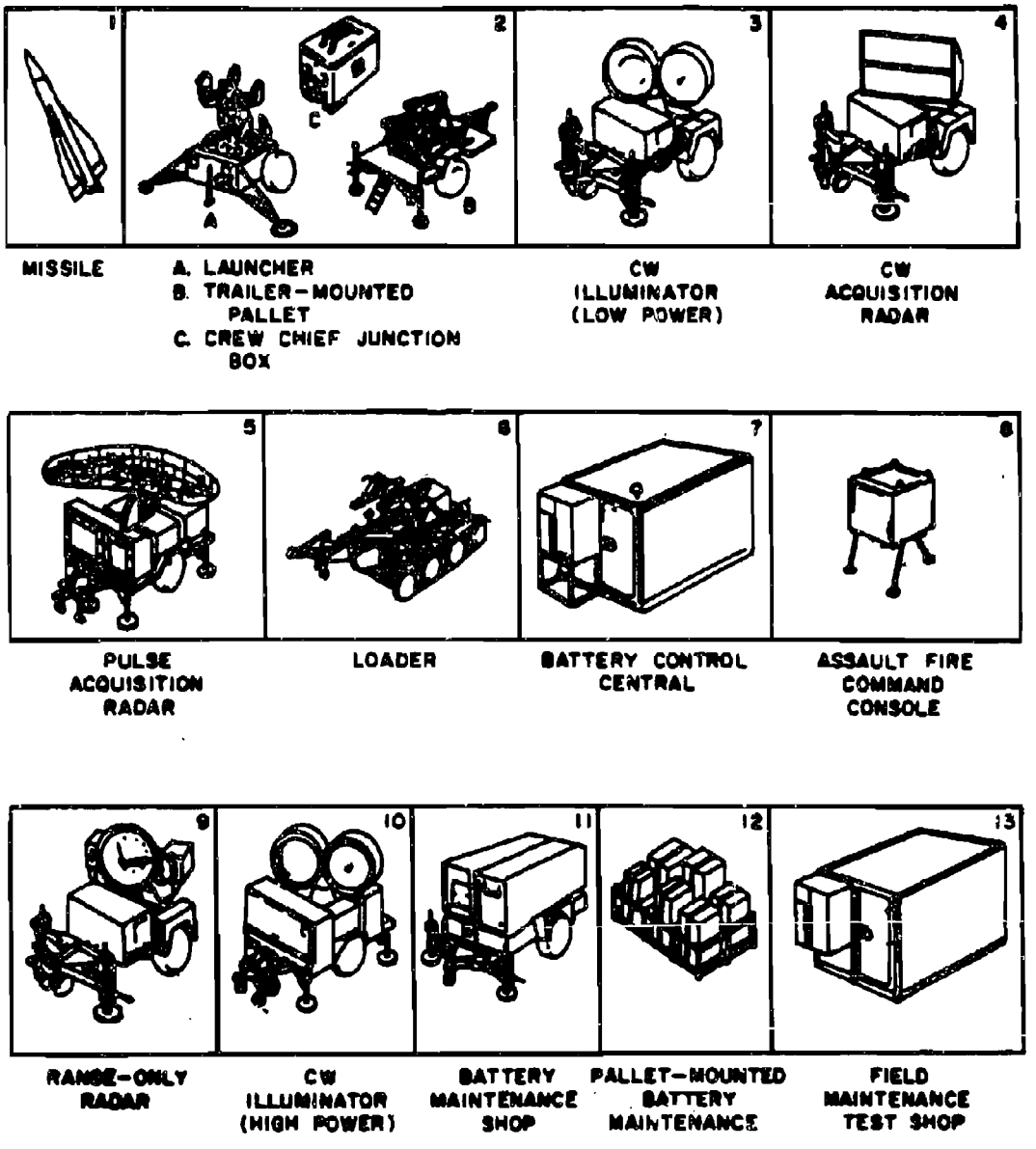

Figure 16-11. HAWK System, Auxiliary Components

[redacted]

Table 16-5. [redacted] HAWK, Characteristics and Damage Levels for System Components [redacted]

DNA
(L-X(1)

USANCA
(U-X(1)

Deleted

[redacted]

[redacted]

(4) CW Illumination Radar (CWIR), shown in Figure 16-10.

[redacted] Structurally, the missile body consists of four major sections: the warhead section; guidance components; rocket motor; and surface controls.

16-8 Vulnerability Levels for the HAWK Missile System [redacted]

[redacted] Blast vulnerability levels for the components of the HAWK missile system are shown in Table 16-5. Based on these values, the susceptibility levels of the HAWK missile system during its various operational phases are estimated to be as follows:

- *Missile Parts in Containers at Storage Site (HAWK).* [redacted]

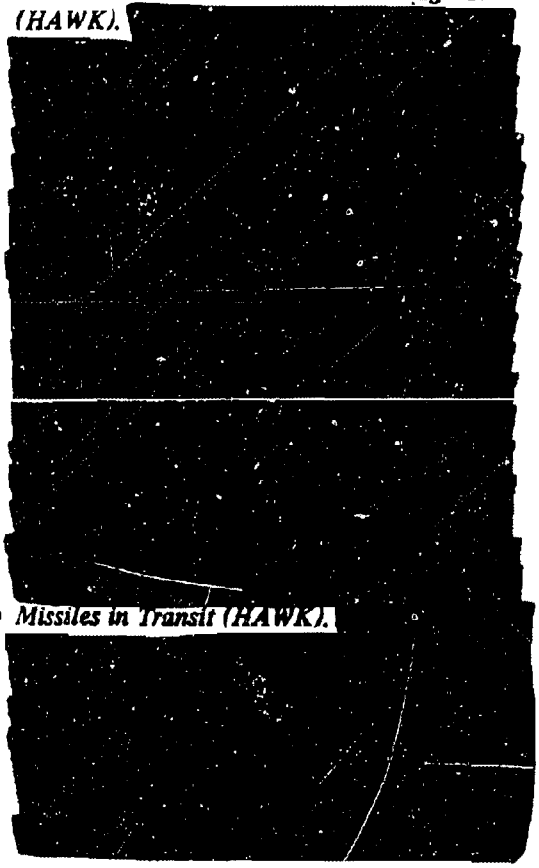

- *Missiles in Transit (HAWK).* [redacted]

- *Missile System During Checkout, Prelaunch, and Launch (HAWK).* [redacted]

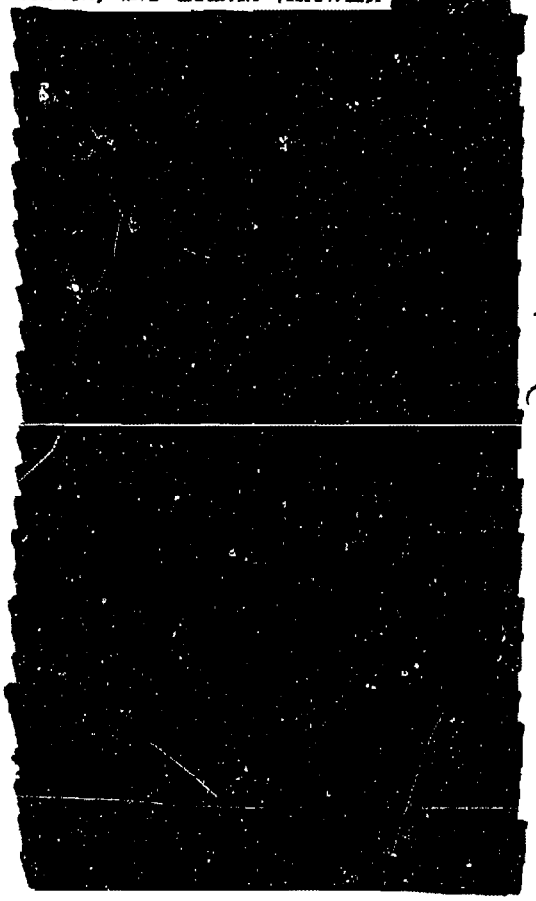

[redacted]

[redacted]

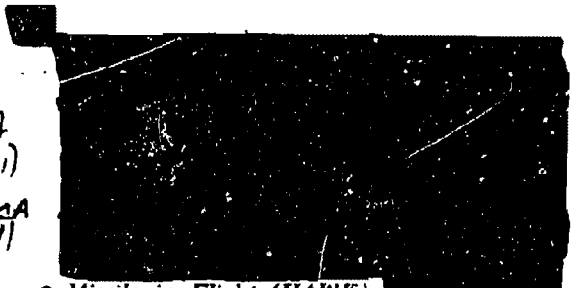

• *Missile in Flight (HAWK).*

[redacted] The blast vulnerability of the principal configurations of the HAWK missile system can be obtained from Table 16-5 and Figure 16-12; the figure includes curves from which pressure levels for damage corresponding to various weapon yields and ranges may be obtained. Table 16-6 shows a summary of the blast vulnerability of the susceptible subsystems in the various configurations of the HAWK missile system.

16-9 Reliability of HAWK Vulnerability Estimates [redacted]

[redacted] The sources of the HAWK system damage data for the major items considered are:

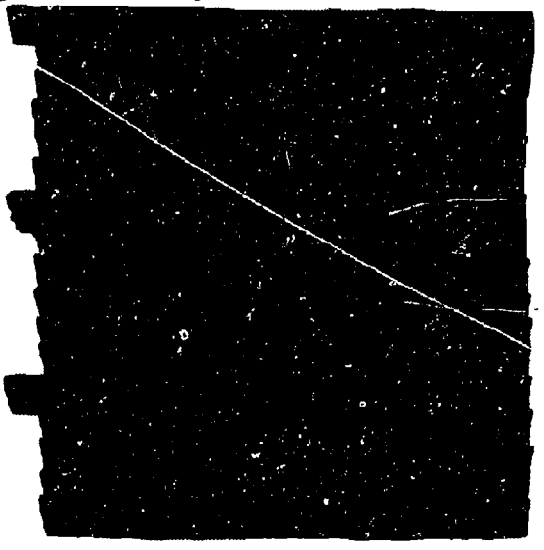

Table 16-6. [redacted] Blast Vulnerability Summary, HAWK Missile System [redacted]

[redacted]

Deleted

[redacted]

[redacted]

DNA
(b)(1)

USANCA
(b)(1)

Deleted

Figure 16-12. [redacted] HAWK, Major Item Blast Vulnerability [redacted]

[redacted]

[redacted]

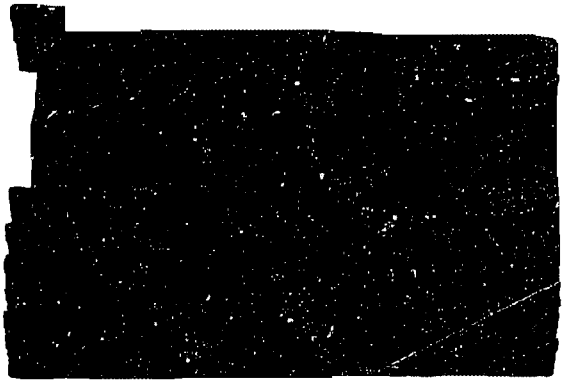

[redacted] SAMPLE PROBLEM: AIR BLAST DAMAGE TO A TACTICAL MISSILE SYSTEM [redacted]

[redacted] The material presented above concerning the SERGEANT, LANCE, and HAWK weapon systems is used to estimate the blast vulnerability of the HONEST JOHN weapon system as an illustration of the methods by which the vulnerability data may be applied.

16-10 Description of the HONEST JOHN System [redacted]

[redacted] The HONEST JOHN is a 762 nm, surface-to-surface, field artillery rocket designed to deliver warheads, weighing between 1,000 and 1,500 pounds, at horizontal ranges up to about 26 miles. It uses solid propellant, and it follows a ballistic trajectory after firing (no guidance).

[redacted] The HONEST JOHN system is mobile by both ground and air transport. The principal units of the system are the following:

- *Complete rocket.* The rocket includes a warhead section, motor assembly, and fins, for which containers are provided (see Figure 16-13).
- *Launcher, truck-or trailer-mounted.* The launcher includes the launching beam assembly, elevating and traverse mechanisms, and electrical controls (see Figures 16-14 and 16-15).
- *Other ground support equipment.* A wrecker, transporter trailer, generator, motor and warhead cradles, and handling beam make up the ground support equipment (see Figure 16-16).

[redacted] Table 16-7 lists the weight and size of the various HONEST JOHN components. The principal operational phases can be listed as follows:

- Storage at Storage Site,

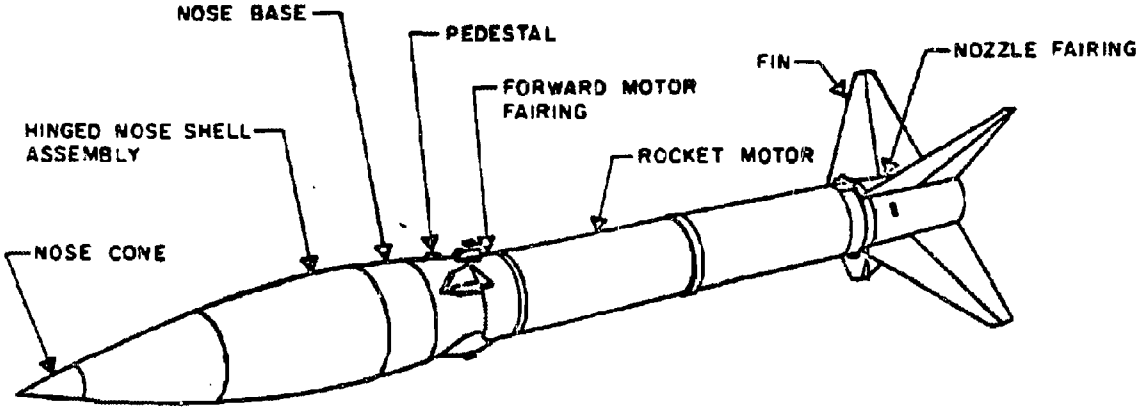

Figure 16-13. [redacted] HONEST JOHN, Major Components of Rocket [redacted]

[redacted]

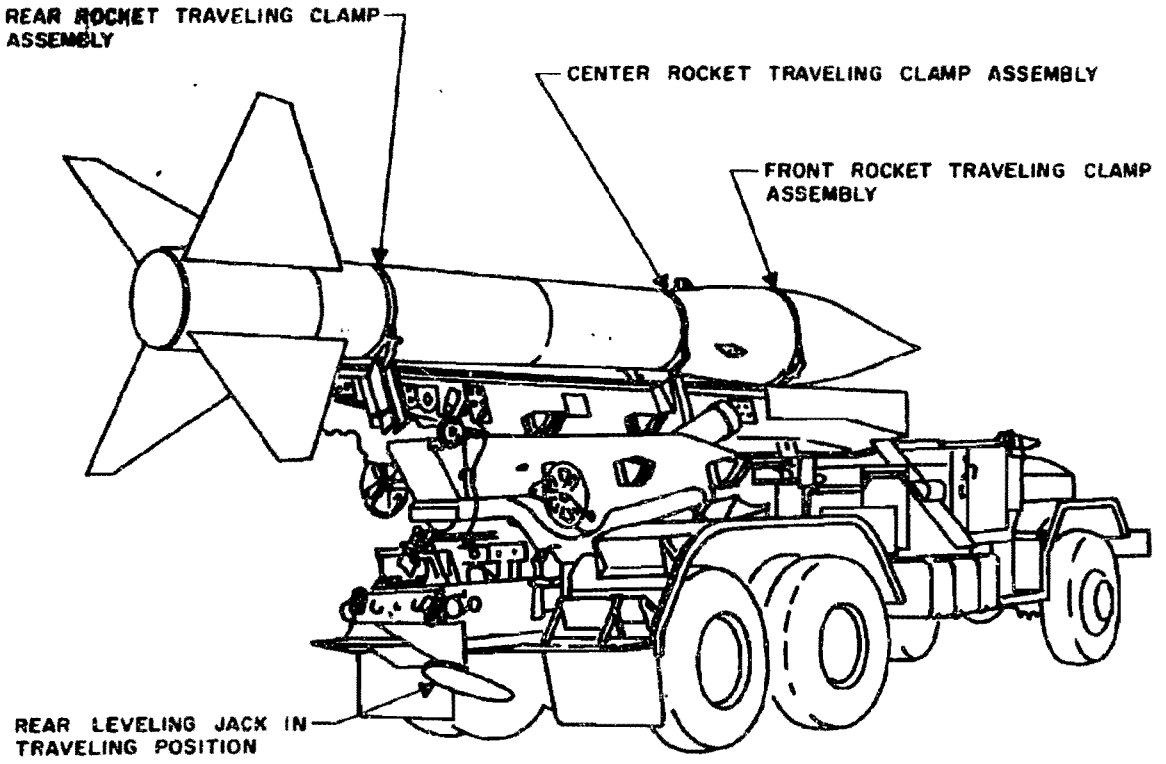
REAR ROCKET TRAVELING CLAMP ASSEMBLY
CENTER ROCKET TRAVELING CLAMP ASSEMBLY
FRONT ROCKET TRAVELING CLAMP ASSEMBLY
REAR LEVELING JACK IN TRAVELING POSITION

Figure 16-14. HONEST JOHN, Truck-Mounted Rocket Launcher in Traveling Position

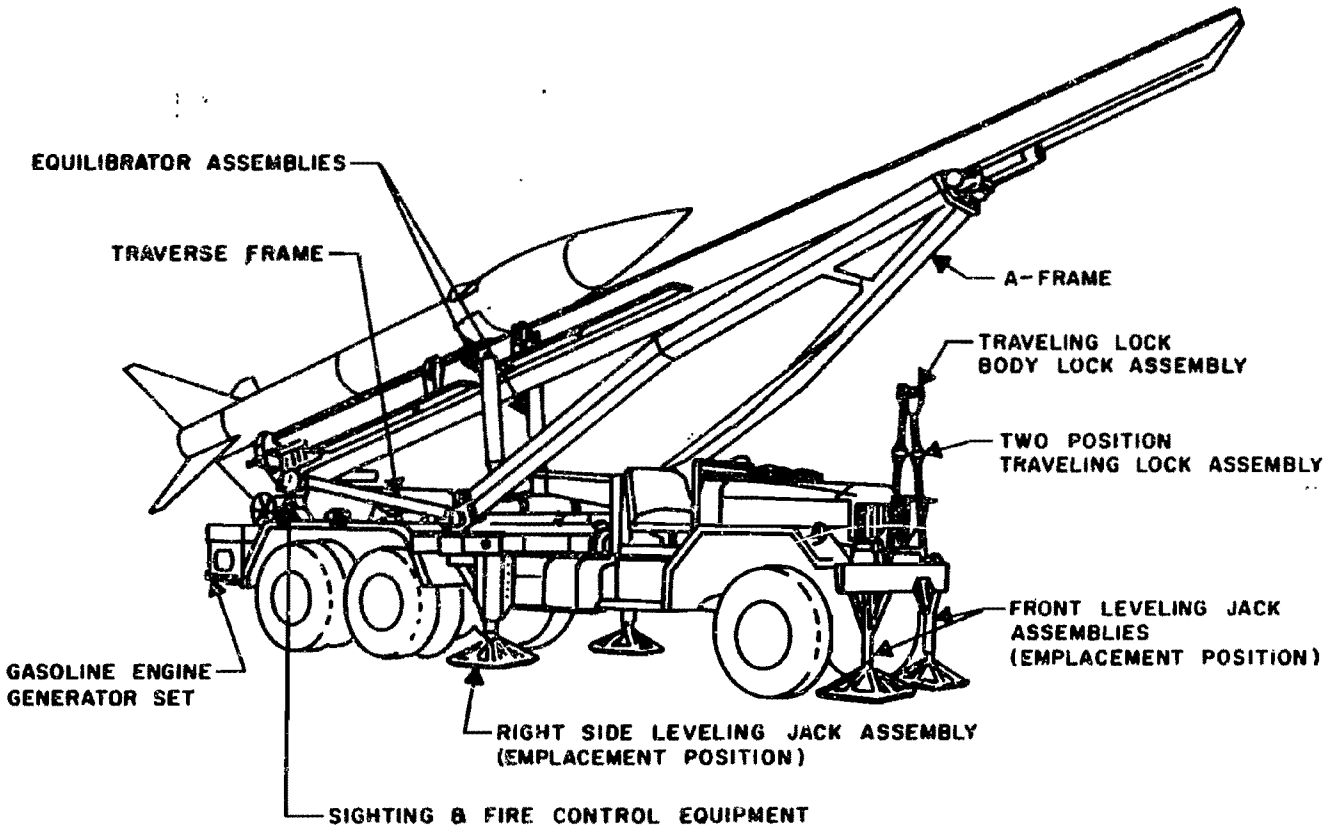
EQUILIBRATOR ASSEMBLIES
TRAVERSE FRAME
A-FRAME
TRAVELING LOCK BODY LOCK ASSEMBLY
TWO POSITION TRAVELING LOCK ASSEMBLY
FRONT LEVELING JACK ASSEMBLIES (EMPLACEMENT POSITION)
GASOLINE ENGINE GENERATOR SET
RIGHT SIDE LEVELING JACK ASSEMBLY (EMPLACEMENT POSITION)
SIGHTING & FIRE CONTROL EQUIPMENT

Figure 16-15. HONEST JOHN Rocket Launcher in Firing Position

[redacted]

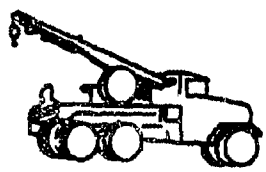

WRECKER
M62 OR M543

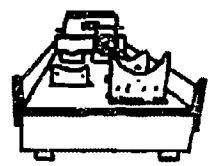

HEATING
& TIE-DOWN UNIT
XM78E1

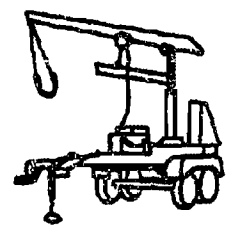

HANDLING UNIT
M40SE1

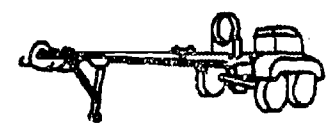

TRANSPORTER TRAILER
M329A1

TRANSPORT CART
ASSEMBLY
XM46S

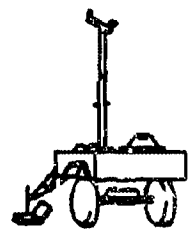

WIND MEASURING
SET

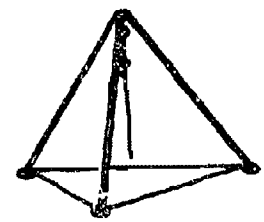

HOISTING UNIT TRIPOD
XM26

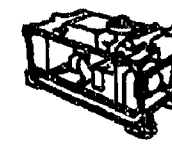

GENERATOR SET
M25C

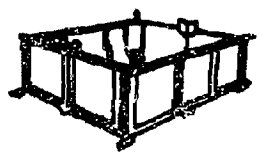

EQUIPMENT DELIVERY
BASKET M2

ELECTRIC BLANKET
M2E2

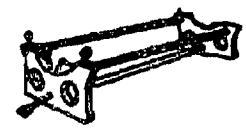

ROCKET MOTOR CRADLE
M5

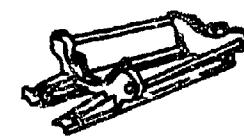

WARHEAD CRADLE
M4

HANDLING BEAM
XM4E2

WARHEAD HANDLING SLING
M6

Figure 16-16. [redacted] HONEST JOHN, Auxiliary Equipment [redacted]

[redacted]

[redacted]

Table 16-7. [redacted] Missile System Components – HONEST JOHN [redacted]

Item	Refer to Figure	Dimensions (in.) (Weight (lbs))	Remarks
1. Missile Components (in containers)			
(a) Warhead sections	–	144 x 50 x 45 (2,500)	Plywood containers
(b) Guidance sections	None	–	
(c) Rocket motor sections	–	235 x 44 x 38 (3,500)	Plywood containers
(d) Fins			
2. Missile Body (assembled)			
(a) Ready for launch	13	327 x 28 (3,750)	
(b) In-flight (near target)	13	327 x 28 (2,000)	Propellant burned
3. Transport Equipment			
(a) Semitrailers	16	315 x 97 x 48 (3,500)	w/o missile
(b) Trucks (M543 or M62)	16	310 x 97 x 103 (34,000)	
4. Launch Equipment			
(a) Lightweight launchers	–	346 x 83 x 61 (4,375)	w/o missile
(b) Self-propelled launchers	14, 15	508 x 121 x 151 (42,000)	w/o missile
(c) Loaders (handling unit on M62 truck)	16	310 x 97 x 210 (40,000)	w/o missile
5. Auxiliary Ground Equipment			
(a) Firing unit assembly	–	36 x 24 x 24 (300)	
(b) Sighting equipment	–	36 x 20 (175)	
(c) Generator set	16	60 x 30 x 30 (1,800)	On truck chassis

[redacted]

[redacted]

- Battalion Area Test and Repair,
- Transportation to Firing Site,
- Emplacement and Prefire Preparations,
- Flight.

16-11 Vulnerability Levels for HONEST JOHN Missile System [redacted]

[redacted] Blast vulnerability levels for the principal system configurations of the HONEST JOHN missile system are given in Table 16-8.

[redacted]

- *Missiles in Containers at Storage Site (HONEST JOHN).*

[redacted]

[redacted]

- *Missiles in Transit to Firing Site (HONEST JOHN).*

[redacted]

Table 16-8. [redacted] Summary – HONEST JOHN [redacted]

[redacted]

Deleted

[redacted]

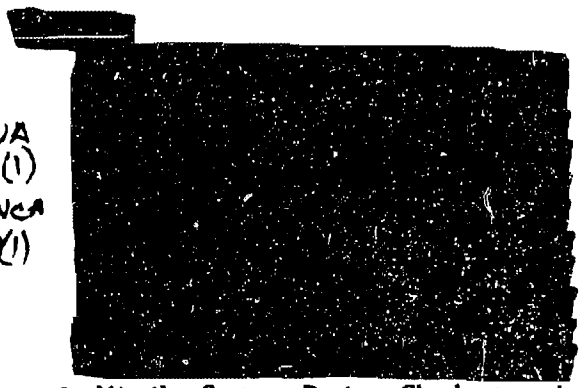

• *Missile System During Checkout and Launch Operations (HONEST JOHN).*

• *Missile in Flight (HONEST JOHN).*

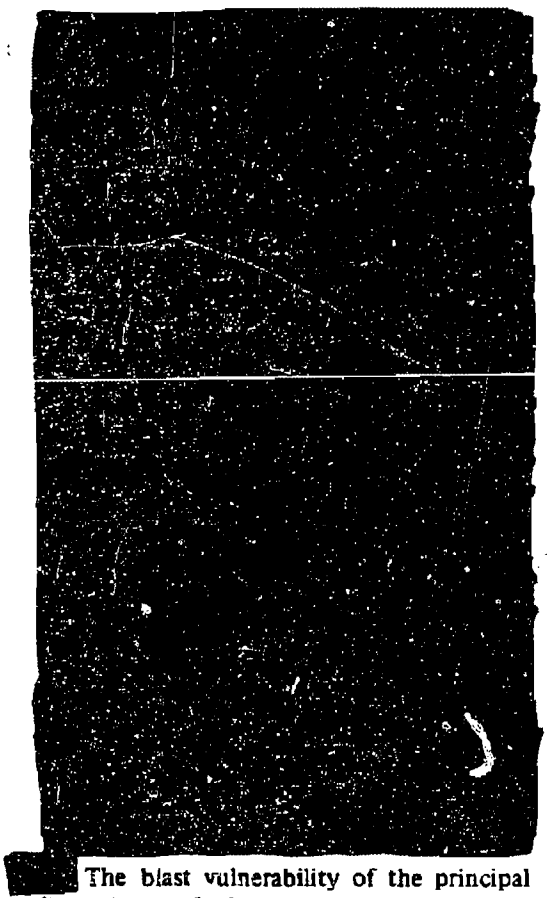

The blast vulnerability of the principal configurations of the sample missile system (HONEST JOHN) are described in Table 16-8 and Figure 16-17; the figure includes curves that allow the determination of pressure levels for damage corresponding to other weapon yields.

[redacted]

Deleted

Figure 16-17. [redacted] HONEST JOHN, Major Item Blast Vulnerability [redacted]

[redacted]

SECTION II

BLAST AND THERMAL VULNERABILITY OF IN-FLIGHT STRATEGIC SYSTEMS

INTRODUCTION

The blast and thermal damage to strategic systems are considered together since blast and thermal effects are closely associated in the physics of a nuclear explosion and also because the damage mechanisms of these two effects tend to interact and, at times, complement each other. It should be noted that this section only treats damage to in-flight aerospace systems; blast and thermal damage to surface and underground installations characteristic of the ground support portions of a strategic system are treated separately in Chapter 11.

Blast effects are important to in-flight strategic systems from sea level to altitudes of approximately 100,000 feet (about 30 kilometers). When a nuclear explosion occurs in this altitude region, the blast wave is formed by conventional hydrodynamic processes as the fireball expands. The details of these processes depend on the yield of the weapon, the altitude of burst, and the weapon design (see Chapter 2). The latter consideration (weapon design) is becoming increasingly important as warheads are tailored to [redacted] or to enhance specific elements of the output. The mechanisms of blast wave formation are reasonably well understood from a theoretical viewpoint for nuclear bursts up to altitudes as high as 50 kilometers but experimental verification is lacking (see paragraphs 2-42 through 2-44).

(U) Blast is important to in-flight strategic systems operating below about 100,000 feet, in terms of the following effects:

- Overpressure (static or dynamic) crushing or bending of the primary structure.
- Gust (or deceleration) loading on primary and/or secondary (internal) structures.
- Trajectory deviation (CEP degradation).
- Alteration of aerodynamic stability.

The thermal radiation (excluding X-ray effects*) associated with a nuclear burst must be considered from two main aspects:

- "Early" time thermal radiation emitted from a distant source that is incident on the missile surface; this radiation comes from the fireball and from the high-pressure shock front.
- Missile "fly-through" of the fireball region at "later" times, with the associated thermal radiation imposed on the body surface while it is inside the fireball region.

In addition to considering the effects of blast and thermal radiation on in-flight strategic systems separately, the possible coupling of these two effects in producing damage to the system should be considered. The magnitude of possible coupling effects probably will depend on the details of the system design; general statements are not valid.

The two major strategic systems of concern are defensive antimissile missiles (AMM), more commonly known as ABM, and offensive reentry vehicles (RV). Both systems respond to exposures to the environment produced by nuclear explosions in similar manners, despite significant differences in their configurations (Figure 16-18). The degree to which any system will respond depends on the flight characteristics of the specific vehicle involved, but, in general, there is considerable overlap between RV's and ABM's with respect to their velocity at different altitudes within the atmosphere. A comparison of operational regimes is shown in Figure 16-19.

* See Section V, Chapter 9 for a discussion of X-ray effects on aerospace vehicles.

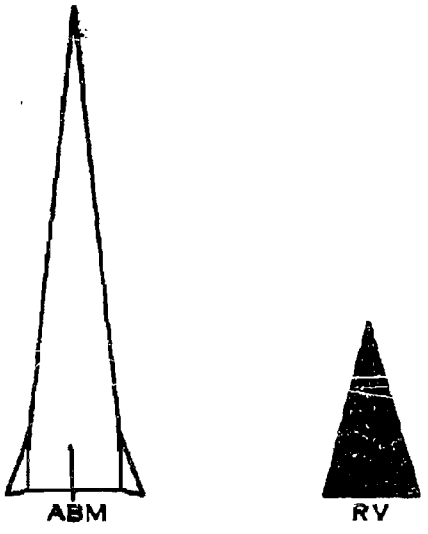

Figure 16-18. [redacted] ABM and RV Configuration Comparison [redacted]

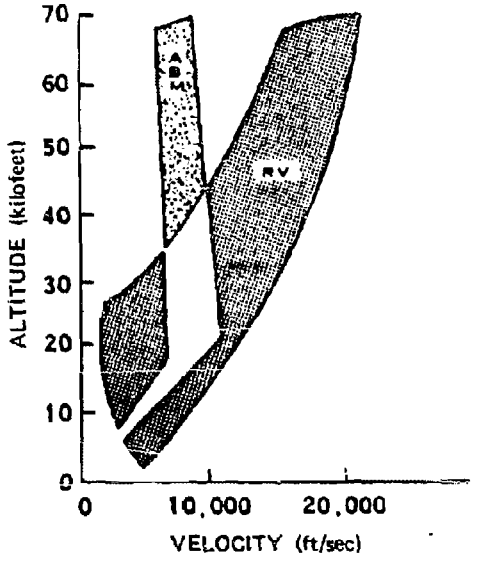

Figure 16-19. [redacted] ABM and RV Operating Envelope Comparison [redacted]

[redacted] The first two categories of blast effects listed above, static and dynamic overpressure crushing (or bending) and gust (acceleration) loading can damage the system physically, i.e., the blast wave from a nuclear explosion at altitudes up to 100,000 feet can cause permanent structural deformation to reentry vehicles, interceptor missiles, boosters, and aircraft. As the structure crosses the shock front, it is suddenly immersed in a "new," transient pressure field, hence, the term "pressure crushing." There is, of course, a complicated shock interaction when the bow shock surrounding a supersonic vehicle intersects the shock front of the blast wave. This interaction results in a high pressure transient ("shock-on-shock" load) that decays quickly to a quasi-steady loading behind the front. The duration of this transient or "spike" can be quite short (tens of microseconds) compared to the response time of the vehicle. At the same time, the vehicle structure is suddenly subjected to a gust loading or an additional aerodynamic loading that results from the particle velocity and the over-density behind the shock front that causes a jump in the dynamic pressure, which causes an abrupt deceleration of the whole vehicle body.

[redacted] The extent of physical damage or structural response from either pressure crushing or gust loading depends on the distance from the target to the burst point, the orientation of the target, the strength and duration of the blast wave, and the preblast flight loads imposed on the vehicle. These last loads depend on the speed, trajectory, and physical design characteristics of the vehicle. For an incoming reentry vehicle, the altitude of maximum deceleration from atmospheric drag depends on the ballistic coefficient, β. The ballistic coefficient is defined as $\beta = W/C_d A$, where W is the vehicle mass, C_d is the drag coefficient, and A is the body reference area. As the ballistic coefficient is increased, the

altitude at which the vehicle experiences maximum deceleration is decreased. The high performance, thin, cone-shaped vehicles have very high ballistic coefficients. Figure 16-20 shows the various response regimes for an interceptor missile including structural, e.g., shell buckling and beam bending, rigid body, and thermal response.

Rigid body response describes the gross whole body motion of an in-flight strategic vehicle that results from passing through the blast sphere and the fireball interior. It includes trajectory deviation (CEP degradation), aerodynamic stability changes, and the drag forces exerted on the overall vehicle; it should be noted that the deceleration forces imposed on the whole body also are transmitted, in a complex manner, to the internal components of the missile system. Trajectory deviation occurs when the blast wave deflects or displaces an in-flight vehicle from its preassigned (or benign environment) trajectory. Since this trajectory alteration results from the direction of the blast winds behind the shock front, this type of rigid body response depends on the relative geometry of the target and the explosion. If the system misses the target by an unacceptably wide margin, it will not be effective.

Passing through the hot fireball results in a thermal load on the system in addition to the thermal loads caused by the benign reentry heating or the supersonic flight of an ABM. Consequently, the impact of the *total* environment of a high altitude nuclear burst must be examined. Figure 16-21 shows the nuclear encounter sequence for RV and ABM systems. The loading and response of the vehicle at each point from 1 through 6 is a function of the local environment, the physical characteristics of the vehicle, and its flight profile.

After the vehicle enters the blast sphere, it may traverse a region of density lower than

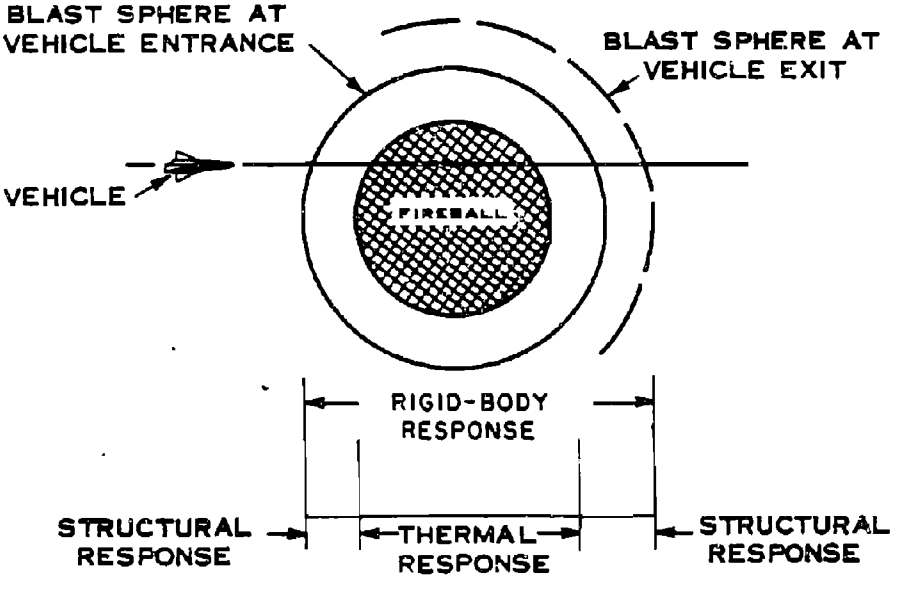

Figure 16-20. Response Regimes for Interceptor Missile

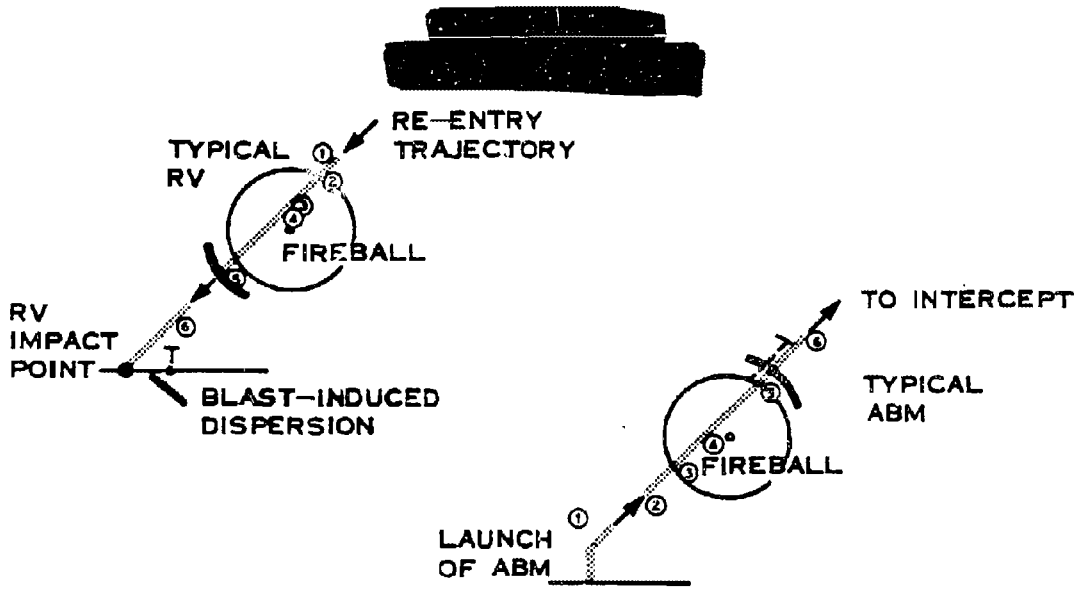

Figure 16-21. [redacted] Nuclear Encounter and Event Sequence for RV and ABM [redacted]

ambient before it exits the blast sphere. This may affect its flight stability, depending on the design characteristics, i.e., static margin and rate of damping. Under some conditions, a reentry vehicle on a ballistic trajectory may tumble in this region and/or subsequently emerge from the blast sphere with a large flight angle of attack, which may cause severe structural loading and may result in serious damage. Even if tumbling does not occur, exit loads imposed on a vehicle at a large angle of attack sometimes could be greater than initial entrance loads. Also, since the RV may exit the blast sphere at a large angle of attack, loss of accuracy and increased dispersion are likely. This is particularly true for advanced systems that use slender body configurations whose drag coefficients are very sensitive to changes in angle of attack.

[redacted] Maneuvering reentry vehicles are being considered with a view toward avoiding a nuclear encounter or reducing the exposure time by altering the usual ballistic trajectory on reentry. However, while the maneuverability of the reentry vehicle could increase its survivability, it could, under some circumstances, also increase its vulnerability to blast. The maneuvering vehicle would experience more severe aerodynamic preloads, to which the air blast induced loads would be added.

[redacted] These maneuver load effects also can be important for ABM systems. Since ABM's are required to maneuver within the atmosphere, control surfaces, which also are susceptible to damage from gust loading, are involved. For many situations, assuming a range of yields and warhead designs, spacing between interceptors is governed by blast fratricide. In a saturation attack, the stepdown firing doctrine for defense tactics depends directly on the hardness of the interceptor to all nuclear effects. Consequently, a complete description of the nuclear environment is necessary to predict the effects of a nuclear burst on in-flight strategic systems. With respect to the blast wave, the parameters of interest include overpressure, particle velocity, density and temperature, as a function of both time and distance.

[redacted]

[redacted]

[redacted] The propagation of the blast wave from the point of burst downward through a nonhomogeneous atmosphere must be considered. Atmospheric inhomogeneity is not a serious problem for small yields at moderate heights, although it does distort the blast sphere somewhat. Blast wave inhomogeneity becomes more severe as the altitude of burst is raised above about 100,000 feet; however, it is significant that at these higher altitudes, blast begins to be less severe as a damage mechanism than other competing effects.

16-12 Sources of Data [redacted]

[redacted] The blast effects on early RV's were expressed in terms of rigid body gust loading or "g" levels of deceleration. When these g loads were added to the normal "peaceful" reentry loads and then compared to design safety factors, it was found that the early RV designs were relatively soft and had large radii of blast vulnerability that outreached over nuclear effects. At these "vulnerable" ranges, overpressure levels were so low that local crushing or beam bending was not a problem.

[redacted] As better theoretical models of the nuclear environment have been developed, blast loading and structural response calculations have become more sophisticated. Progress has been made, from the early engineering analysis of simple spring-mass models subjected to idealized loading, to more complex computer codes that handle rings and shells subjected to loads more representative of the nuclear engagement, including local body pressures. Through the use of 6-degree-of-freedom trajectory codes, the trajectory dispersions induced by the blast wave can be computed and the tumbling within the blast sphere can be predicted using approximate values of environment levels. Theoretical analyses have been developed to treat the shock-on-shock interaction and these analyses have been confirmed at normal incidence by experiments. Test techniques have been developed to determine properties of materials at high strain rates.

[redacted] Early programs to determine blast and thermal vulnerability of in-flight strategic vehicles include HARTS, SPINE, and ABM Vulnerability and Hardening. These research programs were closely coordinated with the research requirements of systems designers. This coordination is shown by the following list of the various configurations of research vehicles that have been studied and their counterparts in terms of military systems.

Program	Research Vehicle	System Application
Air Force	HARTS A	Mark 12 (RV)
Air Force	HARTS B	Mark 11A (RV)
Army	AIRS I	SPRINT (ABM)
Army	AIRS II	SPARTAN (ABM)

This correlation permits use of physical data and the aerodynamic coefficients obtained during the development of the specific systems.

16-13 Limitations in Application of the Data [redacted]

[redacted] Since vulnerability (or damage) assessment of an in-flight strategic vehicle is such a strong function of the detailed characteristics of the specific vehicle, it is virtually impossible to devise a general method of vulnerability determination that could be applied to any vehicle. Some of the parameters that enter the problem are the details of the design of the primary structure of the vehicle (including all materials used, internal supports, field joint fixtures, etc.), the design features of the internal components and how they are supported on the primary structure, the detailed aerodynamic characteristics of the body and how it may fly (including the possible requirements for maneuvers). Therefore, it is obvious that an accurate definition of

[redacted]

[redacted]

the blast and thermal vulnerability of a *particular* in-flight strategic vehicle requires a great deal of analysis and the use of specialized computational models as well as experiments. Such analyses are beyond the scope of this manual.

[redacted] The following discussion will attempt to explain, in general terms, the technical aspects of the problem that appear to have the most important influence on the determination of nuclear weapon blast and thermal damage to in-flight strategic vehicles. The technical discussion will be presented under two main sections, one devoted to RV bodies and the other to ABM vehicles; some of the material appearing under the RV section will be applicable to the ABM and, where this is the case, it will be noted.

[redacted] BLAST LOADING ON REENTRY (RV) SYSTEMS [redacted]

[redacted] The general approach used herein to describe the important factors related to the determination of blast and thermal vulnerability of reentry vehicles was generated primarily under the Hardening Technology Study (HARTS). The HARTS vehicles that were studied are shown in Figure 16-22. Configuration A is a blunted cone and Configuration B is a sphere-cone-cylinder-flare. The dimensions and the ballistic coefficients are shown in the figure. Table 16-9 lists the range of parameters that were used in the HARTS studies. The term "hardness level" will be explained below.

16-14 Environment Scaling [redacted]

[redacted] The nomenclature used to describe RV/blast intercept conditions is shown schematically in Figure 16-23. The conditions pictured correspond to those where the RV does not traverse the center of the burst fireball ($\varphi \neq 0°$). As described in Chapter 2, blast scaling has been used extensively to predict air blast environments. Since RV intercept loads and traversal phenomena depend on the blast parameters, it is possible to scale RV intercept loads and traversal phenomena in a manner similar to the blast parameters.

Table 16-3. [redacted] Range of Basic Parameters for HARTS II [redacted]

Blast yield	30, 200, and 440 kt – blast environment from Hillendahl FIREBALL code
Intercept altitude	30,000 to 100,000 ft
Intercept angle (φ)	0 to 90 deg
Trajectory	Minimum energy trajectories for 2,000, 5,500, and 7,000 nm ranges
Hardness levels (axial acceleration for head-on intercept)	200 to 1,000 g
Configurations (see Figure 16-22)	A: β = 2,150 lb/ft^2 B: β = 680 lb/ft^2

[redacted] Figure 16-23 indicates that there are two important radii. First, the distance between the burst center and the vehicle at the time of detonation, denoted by RD, is significant for the comparison of *prompt* effects (e.g., neutrons, X-rays, etc.) as well as blast effects. Consideration of these RD values for various vehicle paths and orientations results in vulnerability envelopes referred to as *burst time* envelopes. Second, the distance between the burst center and the vehicle when the blast wave intercepts the vehicle, denoted by RB, results in envelopes referred to as *intercept time* envelopes. The reference time for which the envelope is constructed must be specified for each envelope.

[redacted] "Hardness Level" is a useful parameter to hold constant when studying blast phenomena. Hardness level is defined as that *axial* load

[redacted]

[redacted]

NOTE: ALL DIMENSIONS IN INCHES

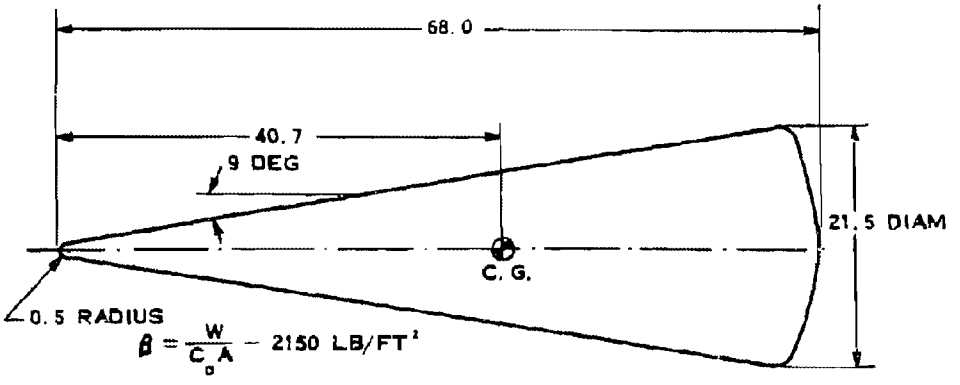

CONFIGURATION A

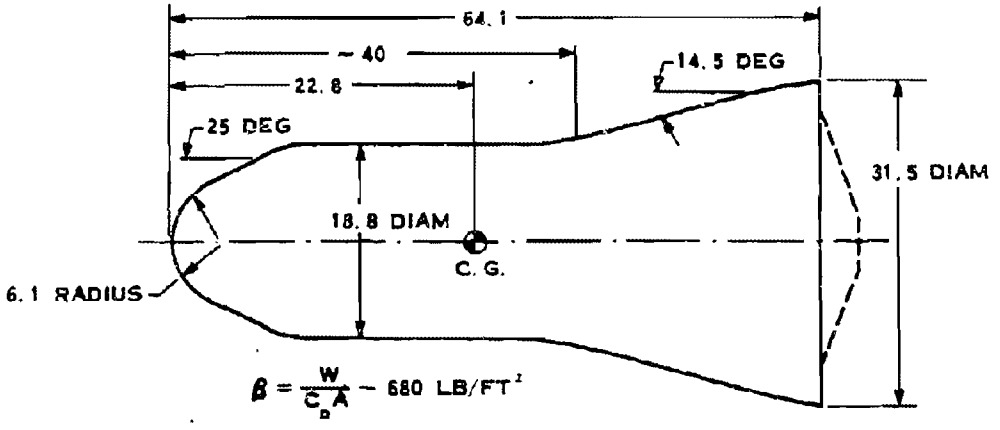

CONFIGURATION B

Figure 16-22. [redacted] HARTS Configuration [redacted]

[redacted]

[redacted]

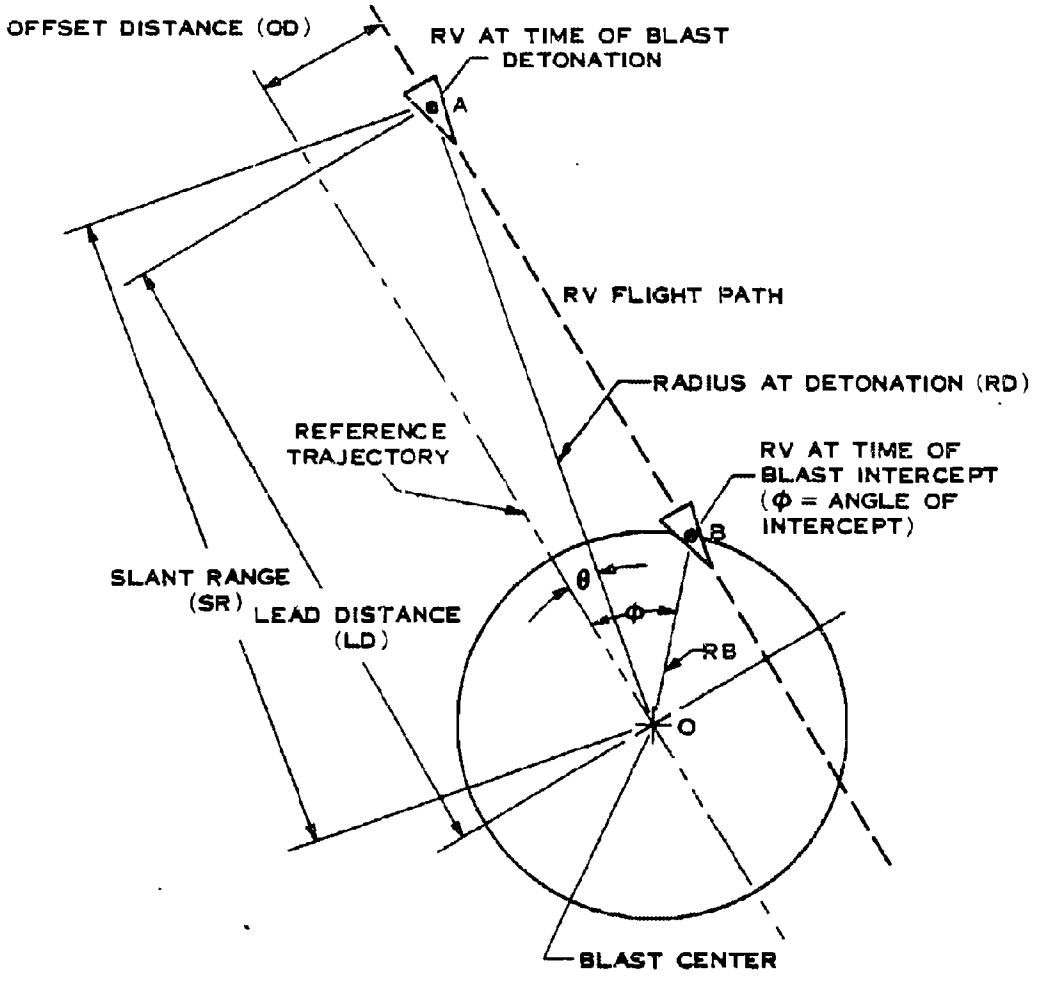

Figure 16-23. [redacted] Blast Intercept Conditions Nomenclature [redacted]

[redacted]

[redacted]

[redacted]

acceleration experienced by a vehicle intercepting a blast wave head on ($\varphi = 0°$) at zero angle-of-attack ($\alpha = 0$). For a given yield, burst altitude, and configuration combination, the specification of a blast intercept hardness level *determines the blast wave radius.* This in turn determines the blast *front* environment. Blast scaling laws indicate that these blast front conditions are identical to those at a different yield and radius where the new radius is equal to the old radius multiplied by the cube root of the ratio of the yields. For example:

$$RB_2 = RB_1 (W_2/W_1)^{1/3} \text{ (ft)},$$

where RB_2 and RB_1 are the blast intercept radii for yields of W_2 and W_1, respectively, and in general,

$$RS = RB/W^{1/3} \text{ (ft/kt}^{1/3}\text{)},$$

where RS is known as the scaled intercept radius. Values of scale radius, RS, at constant hardness level for varying altitude are shown in Figure 16-24. A similar presentation of scale time of blast intercept can be made, since time and radius are proportional. Thus, in general,

$$\tau_1 = t_1 W^{1/3} \text{ (sec/kt}^{1/3}\text{)},$$

where t_1 is the time after burst to intercept and τ_1 is the scaled time. Values of scaled time, τ_1, for constant hardness levels for varying altitude are shown in Figure 16-25.

[redacted] The hardness level, position-time relationships are defined in a manner that data for any yield can be derived over the given range of hardness levels and burst altitudes. System analysis parameters such as slant range SR, lead distance LD, and offset distance OD, from the burst at time of explosion also can be derived simply. For a given hardness level and burst altitude one RS and τ_1 combination exists. For specified yield,

$$RB = RS\ W^{1/3} \text{ (ft)}$$

$$t_1 = \tau_1 W^{1/3} \text{ (sec)}.$$

Referring to Figure 16-23, the following spacing relationships are apparent.

$$OD = RB \sin \varphi,$$

$$LD \approx RB \cos \varphi + Vt_1,$$

$$SR = (LD^2 + OD^2)^{1/2},$$

where V is the RV velocity, and the other symbols are defined in Figure 16-23.

[redacted] Determination of lead distance is illustrated in Problem 16-1. The variation of hardness level with altitude and slant range is shown in Figure 16-26[redacted]

DNA (1-)(3)

[redacted]

[redacted]

Problem 16-1. Calculation of Hardness Level

[redacted] Figures 16-24 and 16-25 show the scaled blast radius and scaled time of blast intercept, respectively, for a Configuration A vehicle on a 5,500 nautical mile flight path as a function of burst altitude for various hardness levels. Various system parameters may be determined from Figures 16-24 and 16-25 as discussed in paragraph 16-14.

[redacted] *Example*

Given: A HARTS Configuration A vehicle (Figure 16-22) is on a 5,500 nm trajectory. The RV hardness level is 500 g.

Find: The slant range at which the RV would experience a head on ($\varphi = 0°$) load equal to its hardness level if it were exposed to the blast wave [redacted]

DNA (L)(3)

[redacted]

DNA (L)(5)

[redacted]

Answer: If the *RV* is more than [redacted] away from the specified explosion at the time of burst, it will not be damaged by blast.

[redacted]

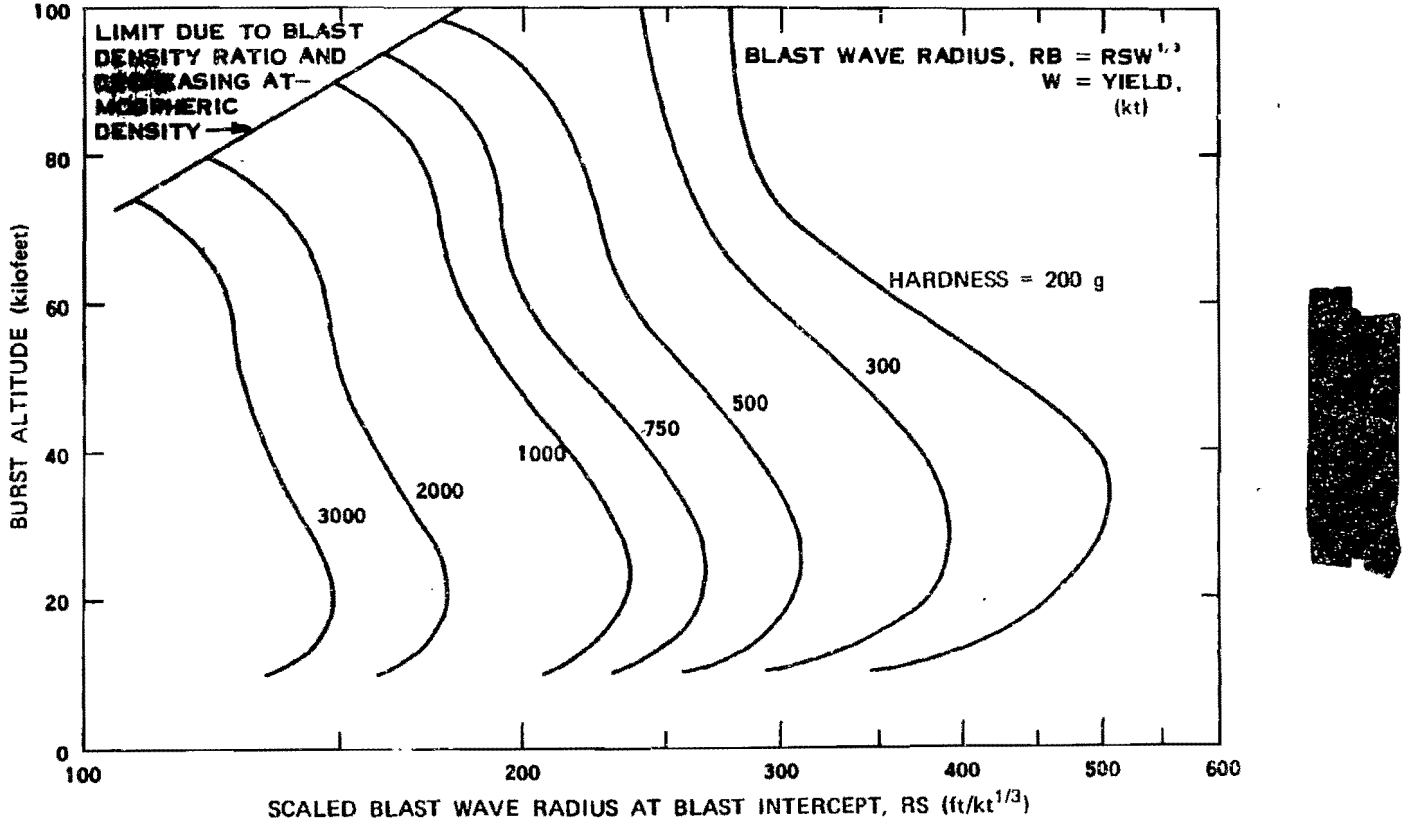

Figure 16-24. [redacted] Scaled Blast Wave Radius for Constant Hardness Level for Configuration A, 5,500 nm Range [redacted]

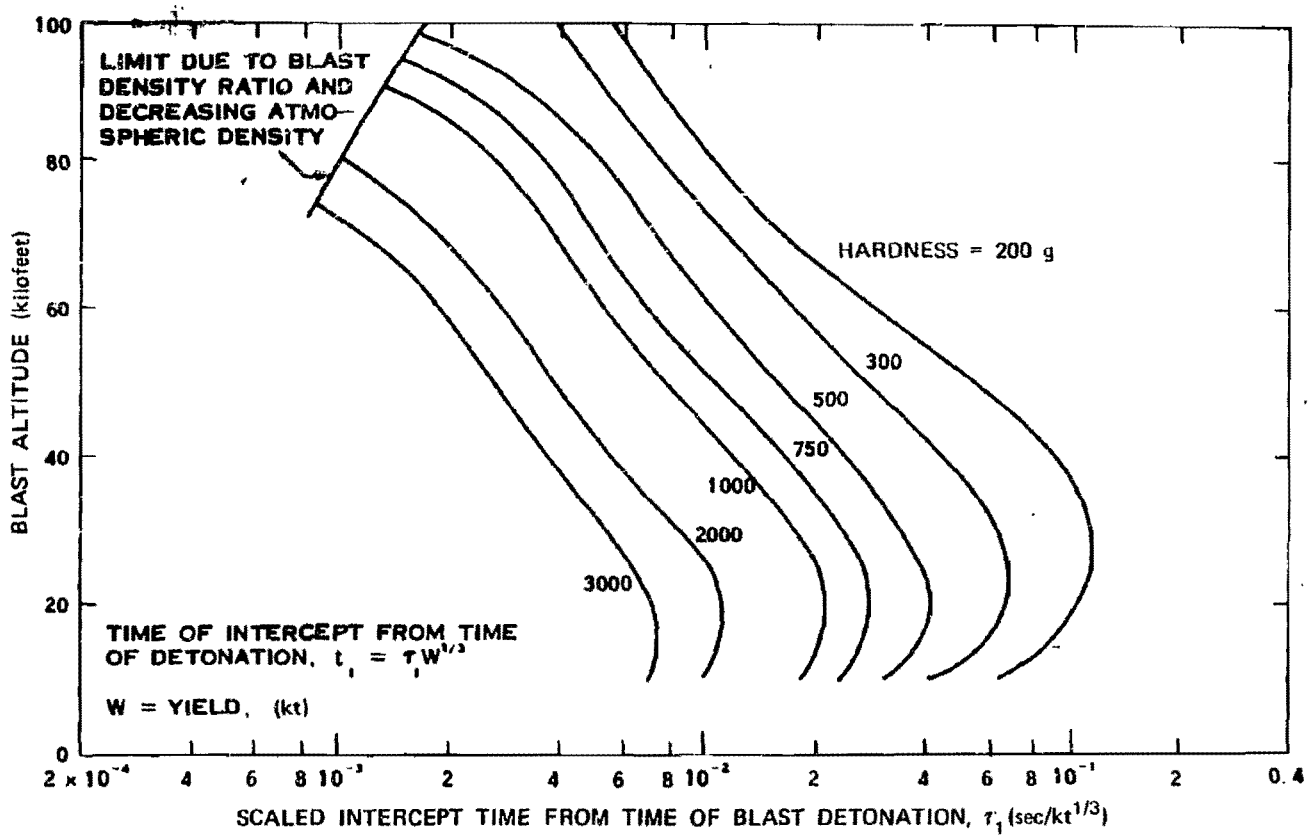

Figure 16-25. [redacted] Scaled Time of Blast Intercept for Constant Hardness Level for Configuration A, 5,500 nm Range [redacted]

DNA
(4)(3)

Deleted

Figure 16-26. [redacted] Variation of Hardness Level with Altitude and Slant Range for [redacted] Configuration A [redacted]

16-15 General Intercept Loads and Load Duration

The aerodynamic loading on hypersonic reentry vehicles can be divided into two general categories: steady state loading and transient loading. Steady state loading occurs when the pressure, density, particle velocity, and temperature do not change with time. Transient loading occurs when there is a time change in the environment surrounding the reentry body.

The vehicle experiences a continuing change in environment during normal reentry. However, since this change is relatively slow, steady state drag loading provides a good approximation for normal reentry conditions. For any type of flow over a body, the local pressure at any point on the surface can be found from the relation:

$$P_b = P_f + qc_p,$$

where

P_b = pressure at some point on the body surface,

P_f = free stream ambient pressure,

q = free stream dynamic pressure,

c_p = local pressure coefficient.

Classic Newtonian impact theory provides a simple closed-form solution for the local pressure coefficient, c_p. For steady state, hypersonic flow (above Mach 5) this theory provides adequate loading predictions. For any body of revolution the Newtonian theory predicts:

$$c_p = 2(\cos \alpha \sin \delta - \sin \alpha \cos \delta \sin \beta_r)^2,$$

where

α = angle between the vehicle longitudinal axis and the relative wind vector,

δ = vehicle semivertex angle,

β_r = rotational angle about axis of reentry vehicle.

A vehicle experiences axial and lateral decelerations and local pressure loading during normal reentry. The amount of deceleration and local pressure depends on the vehicle reentry angle, velocity, shape, weight, and altitude. Figures 16-27 through 16-29 show some nominal reentry trajectories. These graphs only include the combinations of reentry velocity and reentry angle that correspond to a ballistic missile having a nominal range of 5,500 nm. The reentry vehicle is characterized by the ballistic coefficient, which is varied over a range of values typical for reentry vehicle designs. Calculations for the parameters (velocity, altitude, and time) of the reentry trajectories were begun at an altitude of 400,000 feet, since this altitude is well above that of appreciable aerodynamic forces for the reentry vehicles considered. The reentry angles measured from the local horizontal at 400,000 feet were chosen arbitrarily as 20 and 30 degrees. The corresponding reentry velocities at 400,000 feet were determined from the basic equation for vacuum ballistic trajectories. The ballistic coefficients vary from 800 to 2,500 lb/ft^2. Below 100,000 feet the angle of attack is largely damped out, and the lateral force is very small.

The hardness level curves in Figure 16-24 represent one value on the intercept/load matrix of axial rigid body loads, G_A, for zero blast intercept angle ($\varphi = 0°$). It was determined that, at constant hardness level, the blast front environments for varying yields are essentially identical. The last variable to be accounted for in intercept loads is blast intercept angle. At constant hardness level and altitude, the intercept angle is the only factor that can affect intercept loads by changing the angle between the blast wind vector and the vehicle velocity vector, thereby causing a blast induced angle of attack at blast intercept.

(U) Blast yield scaling also can be applied to the scaling of intercept load duration, fireball

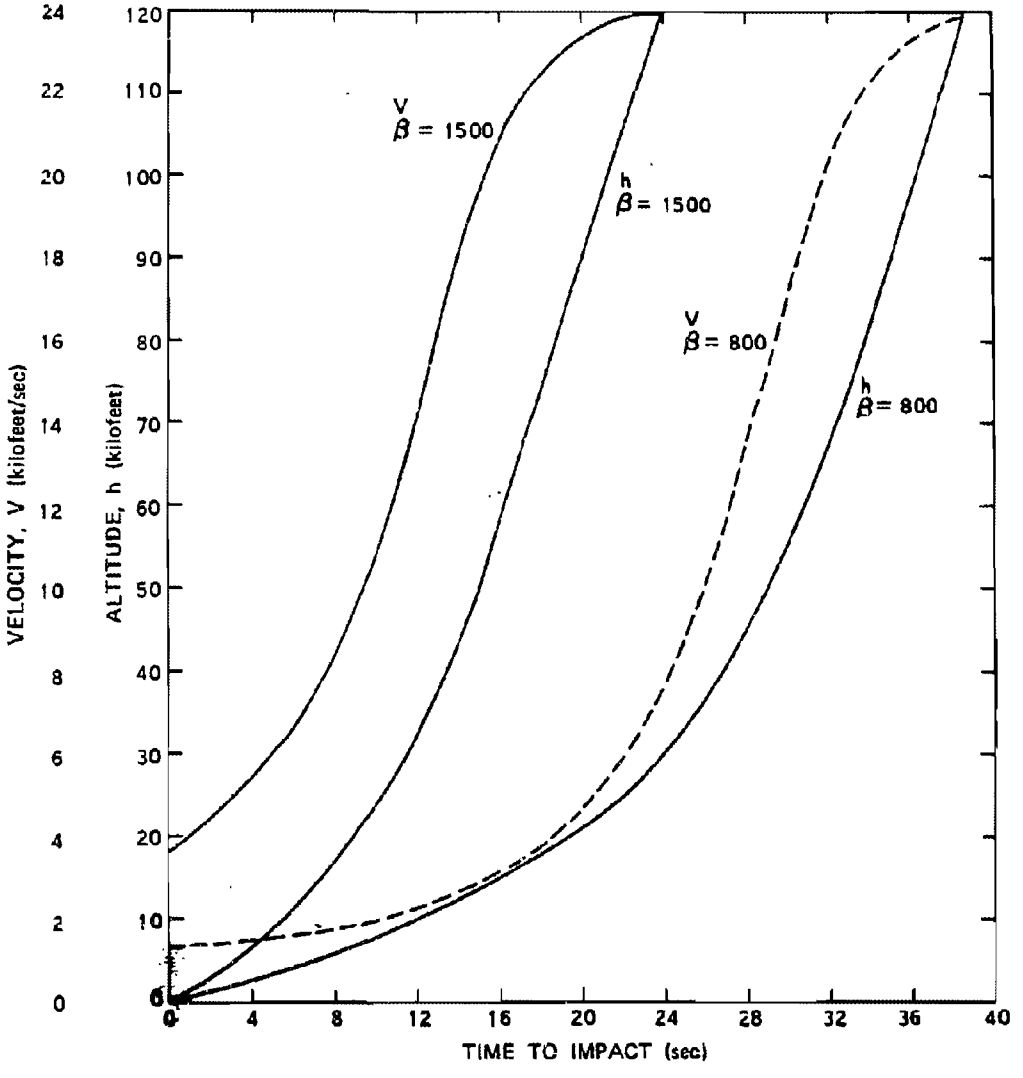

Figure 16-27. [redacted] Normal Reentry Trajectory; Initial Altitude = 400,000 ft, Initial Velocity (V_i) = 23,900 ft/sec, Initial Flight-Path Angle = 20°, Ballistic Coefficient $\beta = W/C_dA$ lb/ft^2 [redacted]

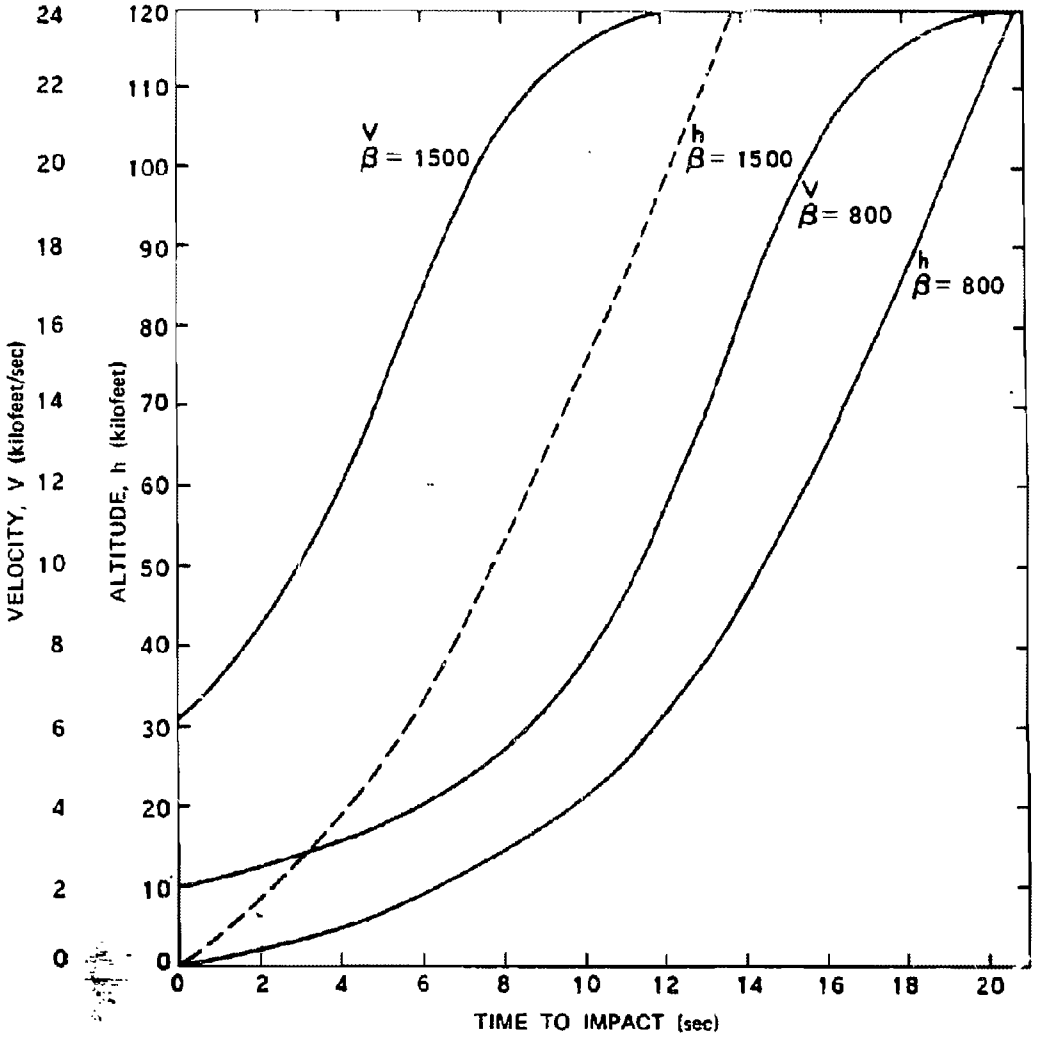

Figure 16-28. [redacted] Normal Reentry Trajectory; Initial Altitude = 400,000 ft, Initial Velocity (V_i) = 24,000 ft/sec, Initial Flight-Path Angle = 30°, Ballistic Coefficient $\beta = W/C_dA$ lb/ft^2 [redacted]

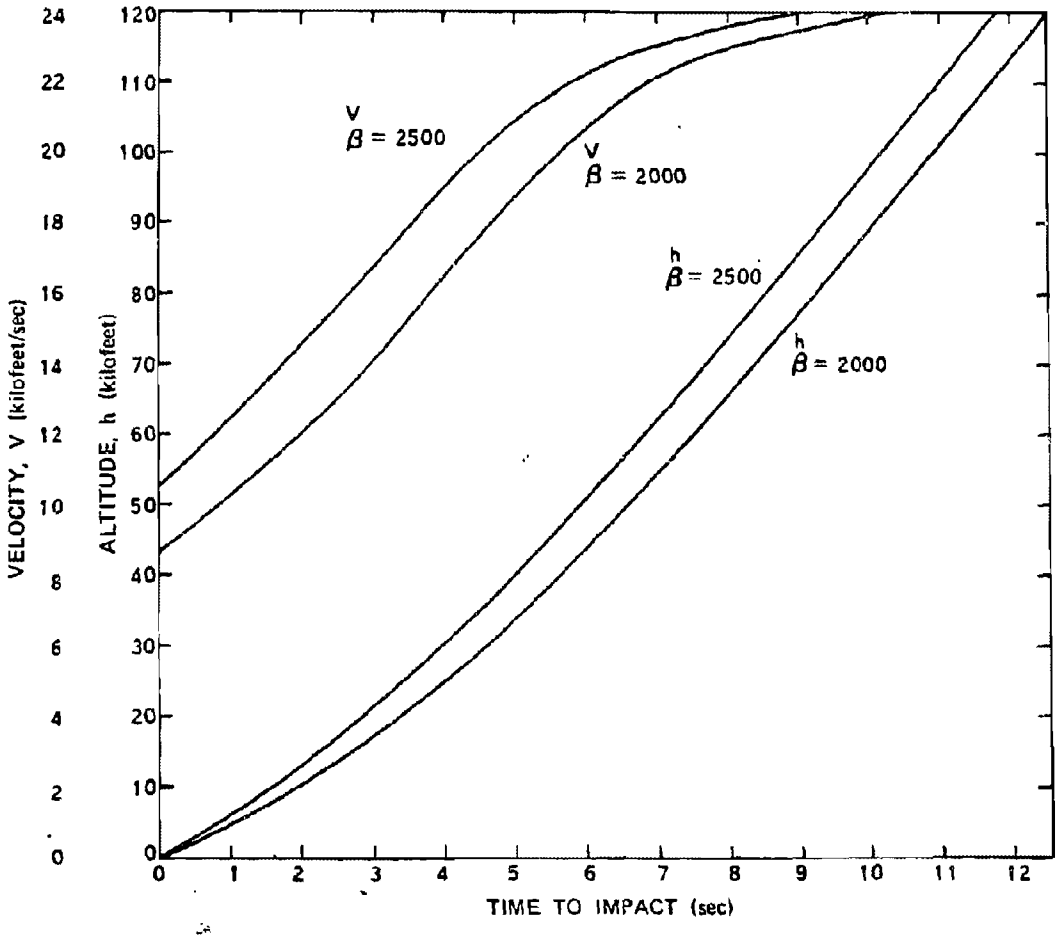

Figure 16-29. Normal Reentry Trajectory; Initial Altitude = 400,000 ft, Initial Velocity (V_i) = 24,000 ft/sec, Initial Flight-Path Angle = 30°, Ballistic Coefficient $\beta = W/C_d A$ lb/ft^2

traversal time, and total traversal time. Time and radial distances are scaled with the cube root of the yield. Interior blast phenomena can be assumed to scale with the cube root of the yield to obtain reduced radius or time. At any point in time the blast can be imagined to have a size of unity for 1 kt. The blast size for larger yields is unity times the cube root of yield in kilotons, on a relative basis. Since blast loading duration depends on the blast size, which can be scaled, the loading duration also can be scaled.

16-16 Intercept Load Duration

Intercept loads are a function of hardness level, blast intercept angle, and blast altitude. The duration of the load is necessary to describe the intercept loading phase adequately. Under most conditions, the intercept loading history can be approximated by a triangular shaped pulse, i.e., intercept impulse is essentially one-half the maximum load multiplied by the duration time.

$$I_I = \frac{G_I \Delta t_{ILP}}{2} \text{ g-sec.}$$

The intercept load time constant, Δt_{ILP}, is

$$\Delta t_{ILP} = t_I - t_{10\%} \text{ sec,}$$

where $t_{10\%}$ is the point at which the intercept load decays to 10 percent of its maximum value. The scaled intercept load duration time, τ_{ILP}, is

$$\tau_{ILP} = \frac{\Delta t_{ILP}}{W^{1/3}} \text{ sec/kt}^{1/3}.$$

Scaled intercept load duration times for a hardness level of 500 g are shown in Figure 16-30 for various intercept angles and altitudes. The intercept load duration times and intercept loads provide a usable set of data for estimating the intercept load impulse. The duration times apply to axial, normal, or total resultant loads. In general,

$$\Delta t_{ILP} = \tau_{ILP} W^{1/3} \text{ sec,}$$

and any load impulse is

$$I_I = \frac{1}{2} \Delta t_{ILP} G_I \text{ g-sec}$$

where I_I and G_I represent any intercept load impulse and maximum load, respectively.

16-17 Fireball Traversal Time

The time at which the intercept load has decayed to 10 percent of its maximum value (end of the intercept load pulse) corresponds approximately to the time when the vehicle enters the fireball (temperature ≈ 10,000 to 15,000° R). For practical considerations, the end of the intercept load pulse and initial fireball immersion can be considered as the same time. The time of fireball traversal is

$$\Delta t_{FB} = t_{EFB} - t_{10\%} \text{ sec,}$$

where t_{EFB} is the time of exiting the fireball, and the scaled time of fireball traversal is

$$\tau_{FB} = \Delta t_{FB} / W^{1/3} \text{ sec/kt}^{1/3}.$$

Scaled fireball traversal time for a hardness level of 500 g is shown in Figure 16-31 for various intercept angles and altitudes. The time of exiting the fireball, t_{EFB}, is that time during the exit phase when increasing dynamic pressure reaches the ambient level at the blast altitude. This time also is approximately when the temperature level drops below 10,000 to 15,000° R. It should be noted that the point during entry at which the decreasing dynamic pressure reaches

[redacted]

[redacted]

ambient level is about the same as the point of 10 percent load.

16-18 Total Traversal Time [redacted]

[redacted] Total blast traversal time is

$$\Delta t_t = t_E - t_i \text{ sec},$$

where t_E is the time of exit from the blast wave shell, and as before, t_i is the time of intercept. The scaled time of blast traversal is

$$\tau_t = \Delta t_t / W^{1/3} \text{ sec/kt}^{1/3}.$$

Scaled total blast traversal time for a hardness level of 500 g is shown in Figure 16-32 for various intercept angles and altitudes.

[redacted]

[redacted]

Problem 16-2. Calculation of Load Characteristics, Fireball Traversal Time and Total Traversal Time

[redacted] Figures 16-30 through 16-32 provide the information necessary to calculate the load characteristics, the fireball traversal time, and the total blast traversal time for a vehicle similar to Configuration A with a hardness level of 500 g that enters the blast front at various intercept angles.

[redacted] *Example* [redacted]

Given: An *RV* similar in design to HARTS Configuration A (see Figure 16-22) with a hardness level of 500 g that is traveling on a 5,500 nm trajectory.

Find: The intercept load characteristics, and traversal times if the *RV* is exposed [redacted]

[redacted]

DNA (1-)(3)

DNA (1-)(3)

[redacted]

[redacted]

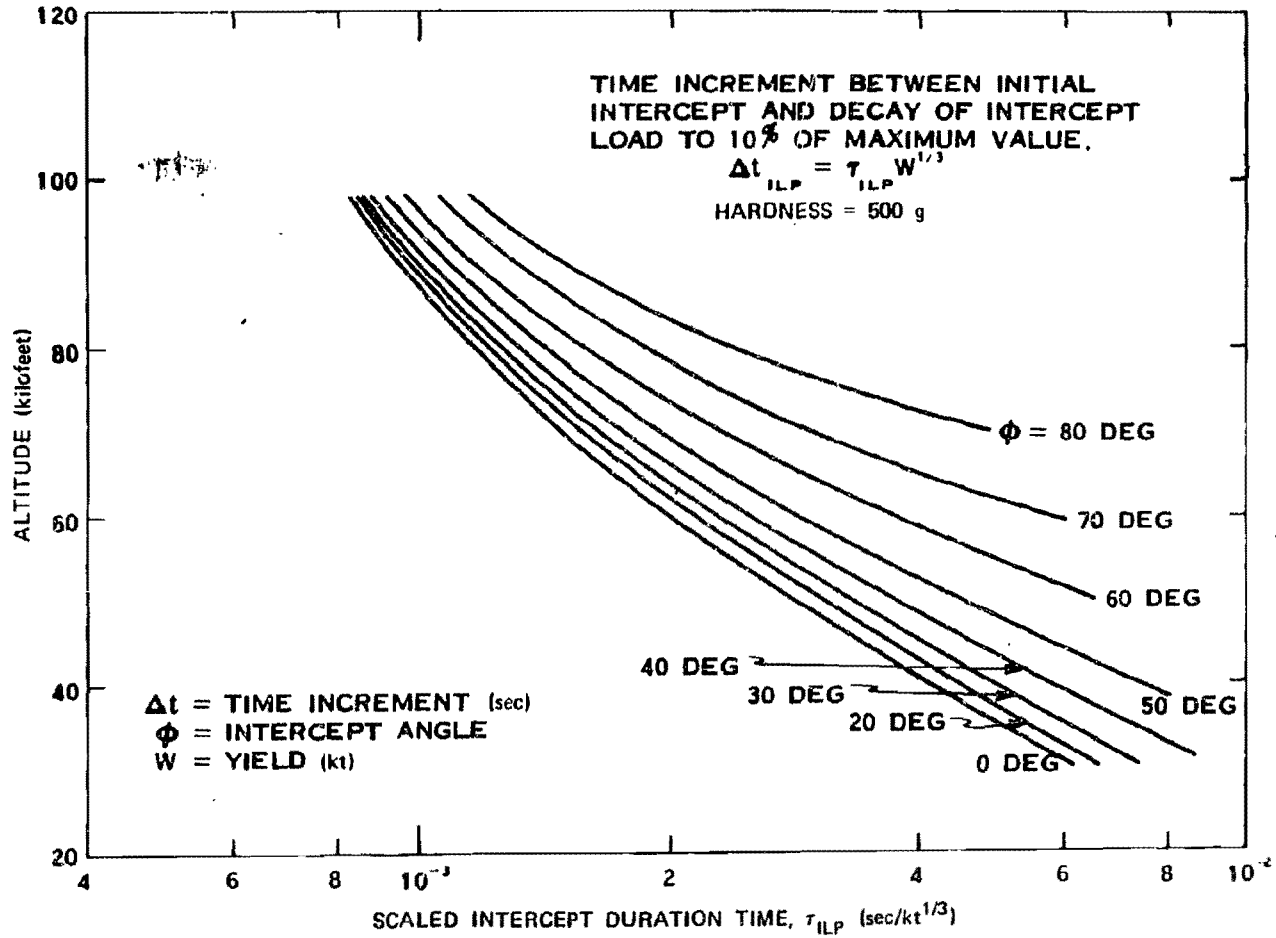

Figure 16-30. [redacted] Scaled Intercept Load Duration Time, 500 g Hardness, Configuration A [redacted]

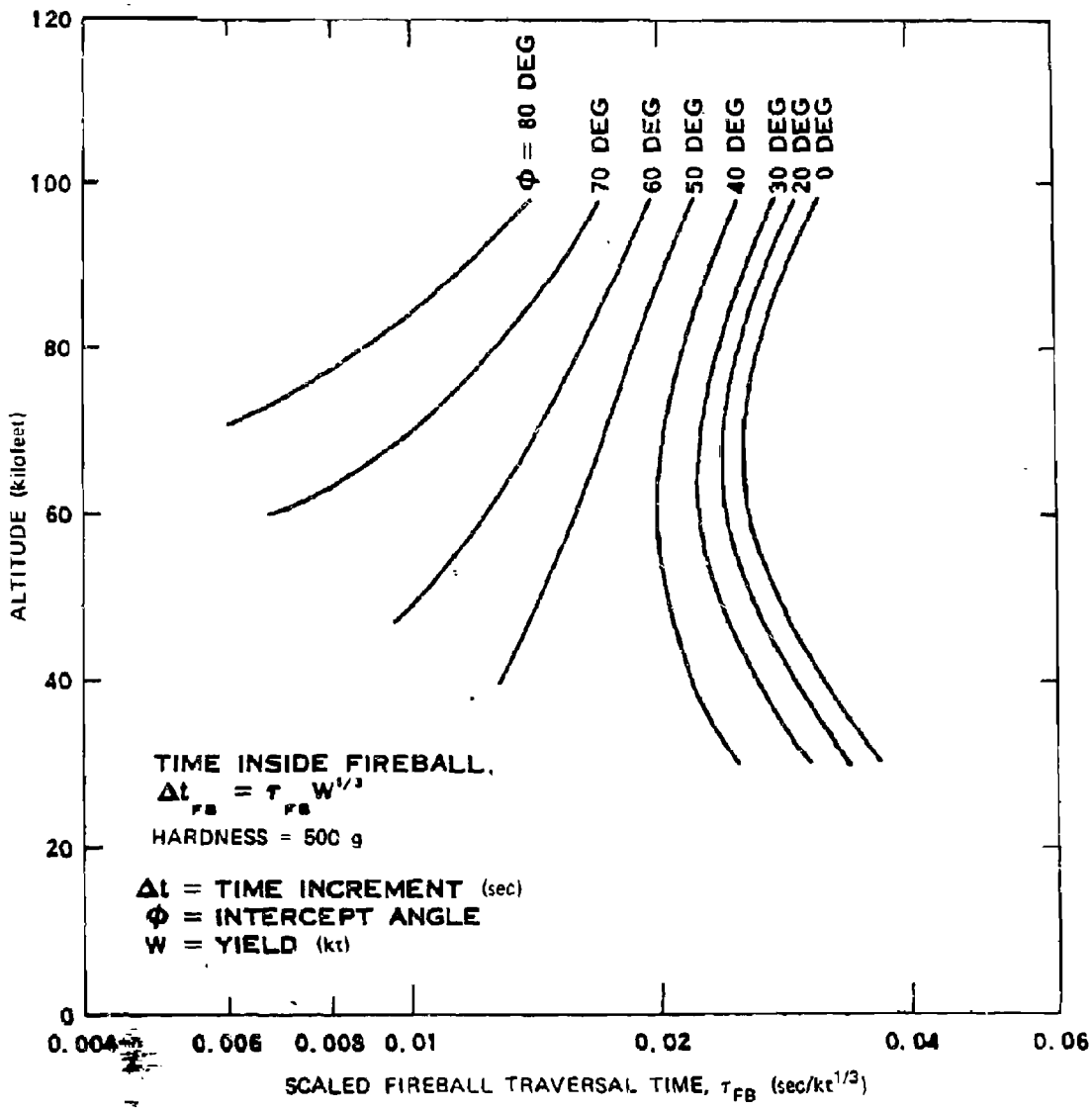

Figure 16-31. [redacted] Scaled Fireball Traversal Time, 500 g Hardness, Configuration A [redacted]

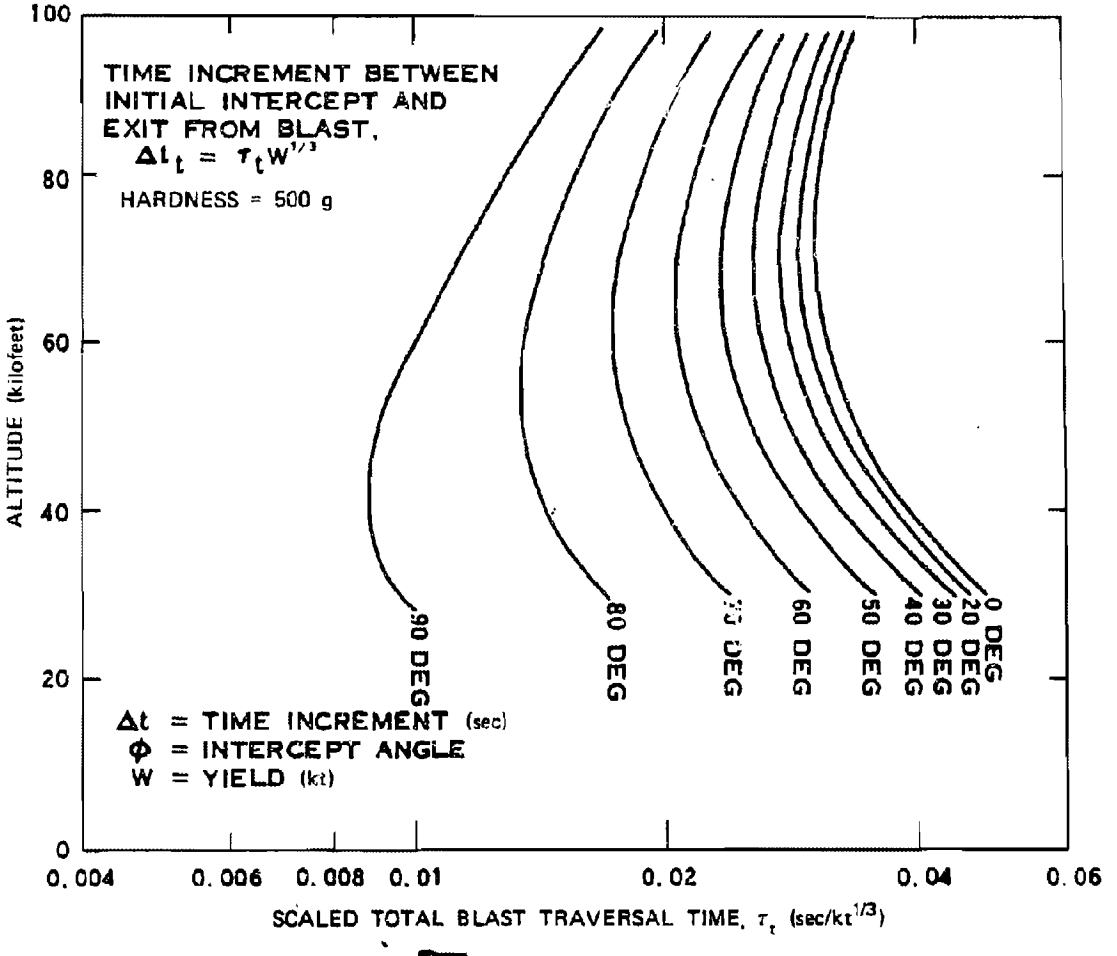

Figure 16-32. [redacted] Scaled Total Blast Traversal Time, 500 g Hardness, Configuration A [redacted]

16-19 Exit Loads

Intercept load, intercept load duration, fireball traversal time, and total traversal time are functions of hardness level, blast intercept angle, and blast altitude (on a scaled basis). Exit loads also depend on blast yield as well as the functions listed above. This precludes any universal scaling of exit loading: however, the following are generally true of exit loading conditions:

- The probability of obtaining higher exit than intercept loads is very low for vehicles similar to Configuration A.
- Exit loads decrease with decreasing intercept hardness level.

16-20 Blast Data Generalization

The data summarized in the preceding paragraphs were generated for Configuration A with a 5,500 nautical mile range minimum energy trajectory. Loading and duration scaling procedures applicable to the blast problem were demonstrated for this case. These specific data are *not* directly applicable to *any* configuration-range combination. However, by some simple relationships and approximations, the data can be applied to different configurations and ranges, or combinations of both, within limits.

Configuration Variations. For other configurations, *assume that the velocity, flight path angle, and intercept conditions at the same blast altitude are identical.* With these constraints, the intercept loads become a function of ballistic coefficient and lift characteristics. For axial loads,

$$\frac{G_{AI_1}}{G_{AI_2}} \approx \frac{\beta_2}{\beta_1}$$

and for normal loads,

$$\frac{G_{NI_1}}{G_{NI_2}} \approx \frac{\beta_{\alpha_2}}{\beta_{\alpha_1}}$$

where

$$\beta = \frac{W}{C_D A} \text{ lb/ft}^2$$

$$\beta_\alpha = \frac{W}{C_{N_\alpha} A} \frac{\text{lb-deg}}{\text{ft}^2}.$$

The term β_α is defined as the normal force ballistic coefficient.

16-21 Typical RV Aerodynamics

A body that is moving along a reentry trajectory at hypersonic velocities has a flow field associated with it. The flow field is composed of the following main regions or characteristics (see Figure 16-33): stagnation point,

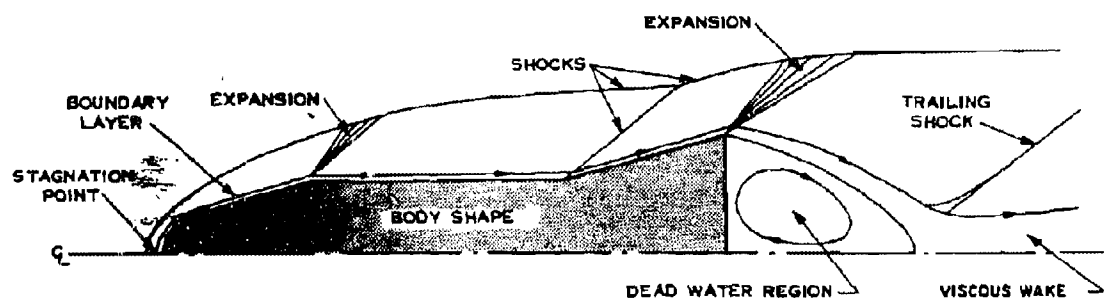

Figure 16-33. Flow Pattern Around an Axisymmetric Blunt-Nosed Body

shock layer, boundary layer, expansion shocks, pressure and density contours, wake, etc. The details of these flow regions are a strong function of the body shape, its velocity, and the properties of the air (i.e., altitude) through which the body is moving. Consequently, the flow field associated with even a single body is constantly changing during the reentry process.

Figure 16-34 shows the pressure distribution (in terms of pressure ratio) over the surface of a body similar to a HARTS Configuration B vehicle as a function of vehicle velocity. The pressure ratio is $(P_b - P)/P$, where P_b is the local pressure at any point along the surface and P is the ambient pressure. The overpressure $(P_b - P_o)$ are shown for sea level conditions (P_o is the ambient pressure at sea level) to provide some idea of the overpressures involved. It is evident that the overpressures near the stagnation region exceed all other pressures by a wide margin for this blunt body. It should be pointed out that these pressures do not take account of boundary layer perturbations, but the calculated pressures are indicative of actual flow field conditions: the overpressures associated with the flow field shock *front* are slightly higher than pressures on the surface. The curves in Figure 16-34 may be used to interpret the flow fields at altitude. For instance, the ambient pressure at 50 kilofeet is about one-tenth that at sea level. Thus, a vehicle at 50 kilofeet traveling at Mach 10 would have an overpressure on the flare of about 12 psi (i.e., 120/10) and stagnation value in excess of 150 psi. If the vehicle were traveling at Mach 20, the flare overpressure would be about 41 psi (410/10).

Another typical reentry flow field, which gives the pressure ratio distribution over a body similar to the HARTS Configuration A (i.e., cone-sphere shape), is shown in Figure 16-35. Figures 16-34 and 16-35 emphasize the differences caused by body shape. Depending on the bluntness of the nose section, there is a very small region over which high stagnation pressures exist. The pressures are virtually constant over the conical section. Figure 16-36 also shows sea level overpressure values for reference; the overpressures shown indicate that at altitudes near 50 kilofeet with the body traveling at Mach 20, the overpressure at the surface of the cone section is about 32 psi.

16-22 Initial Interaction of Vehicle Flow-Field and Blast Wave (Shock-Shock)

When the reentry vehicle bow wave and the blast wave contact each other a region of high pressure is generated. This region is characterized by a value of pressure that is larger than the value of pressure associated with either shock wave before the interaction. The HARTS results can be summarized by referring to a representative figure. Figure 16-36 shows the variation of maximum overpressure ratio (shock-shock maximum overpressure divided by quasi-steady maximum overpressure, *after interaction*) and duration with the nose surface angle for a hemispherical nose at typical intercept conditions (M_∞ = 15 to 22 and M_B = 5 to 8) assuming γ = 1.4. The general conclusion to be drawn from the upper curve of Figures 16-36 is that the shock-shock interaction peak overpressure will not exceed a factor of two larger than the quasi-steady overpressure (after interaction). Also, the lower curve on Figure 16-36 indicates that the duration of the shock-shock interaction is extremely short; as an example, if $\tau V_v/R$ is 0.2, then τ = 1 μsec (10^{-6} sec) for V_v = 20,000 ft/sec and R = 0.1 ft. However, it is evident that for the same nose radius (R), the value of τ increases as the vehicle speed (V_v) decreases.

16-23 Damage Envelopes

The culmination or end result of loading and response calculations is the damage envelope. The damage envelope defines a volume

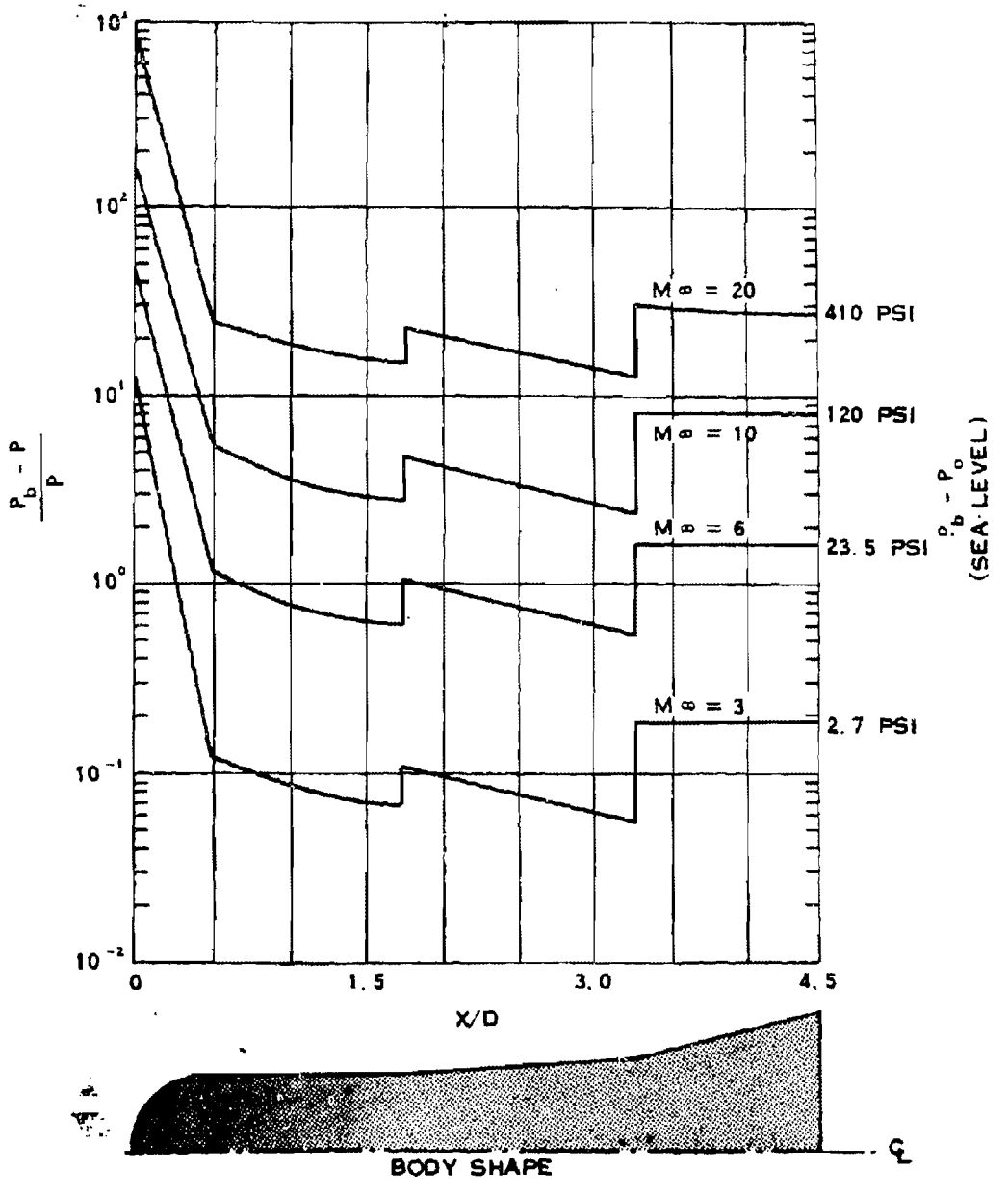

Figure 16-34. [redacted] Steady State Flow Field Surface Pressures, Sphere-Cone-Flare Body [redacted]

[redacted]

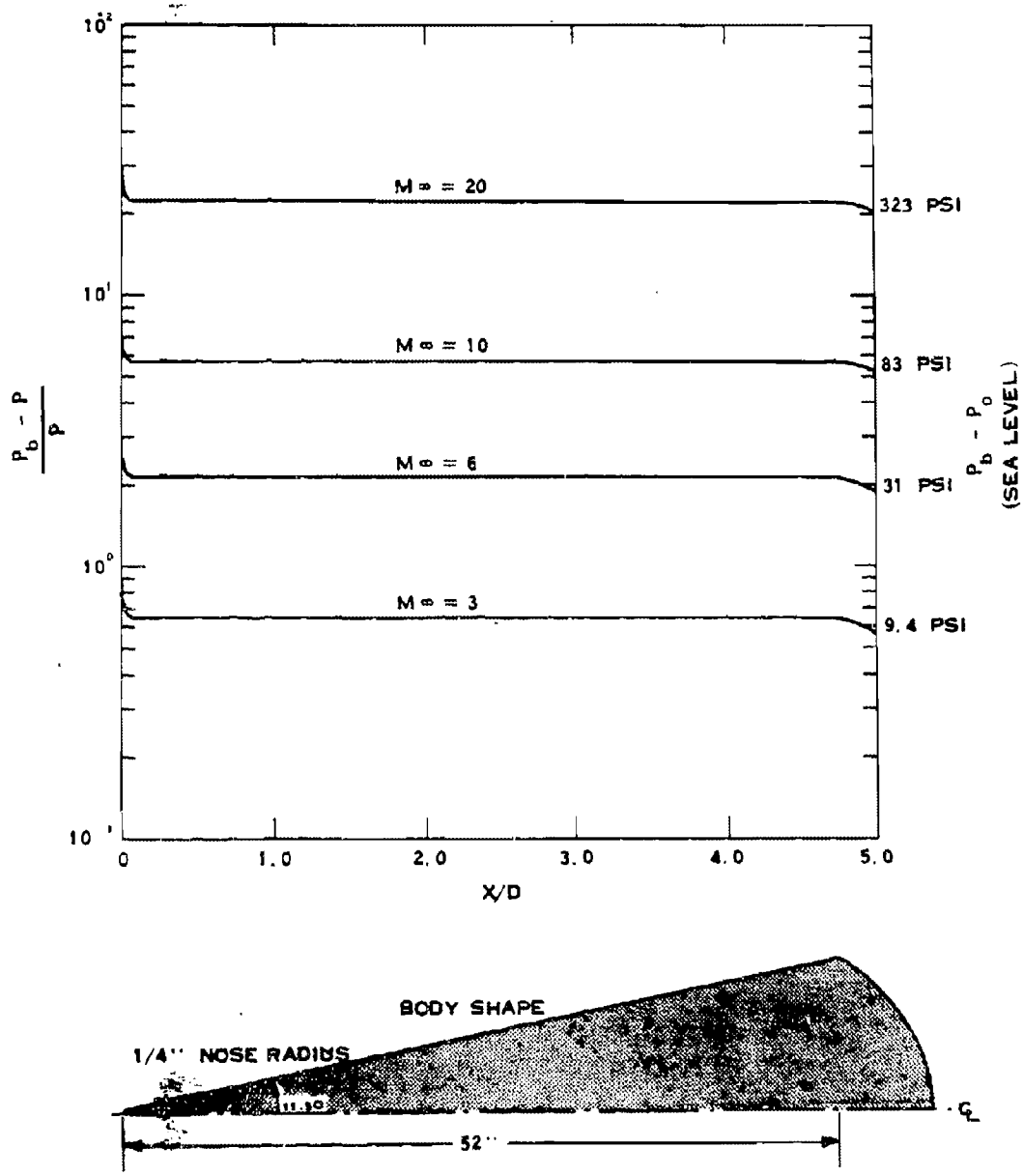

Figure 16-35. [redacted] Steady State Flow Field Surface Pressures, Cone Sphere Body [redacted]

[redacted]

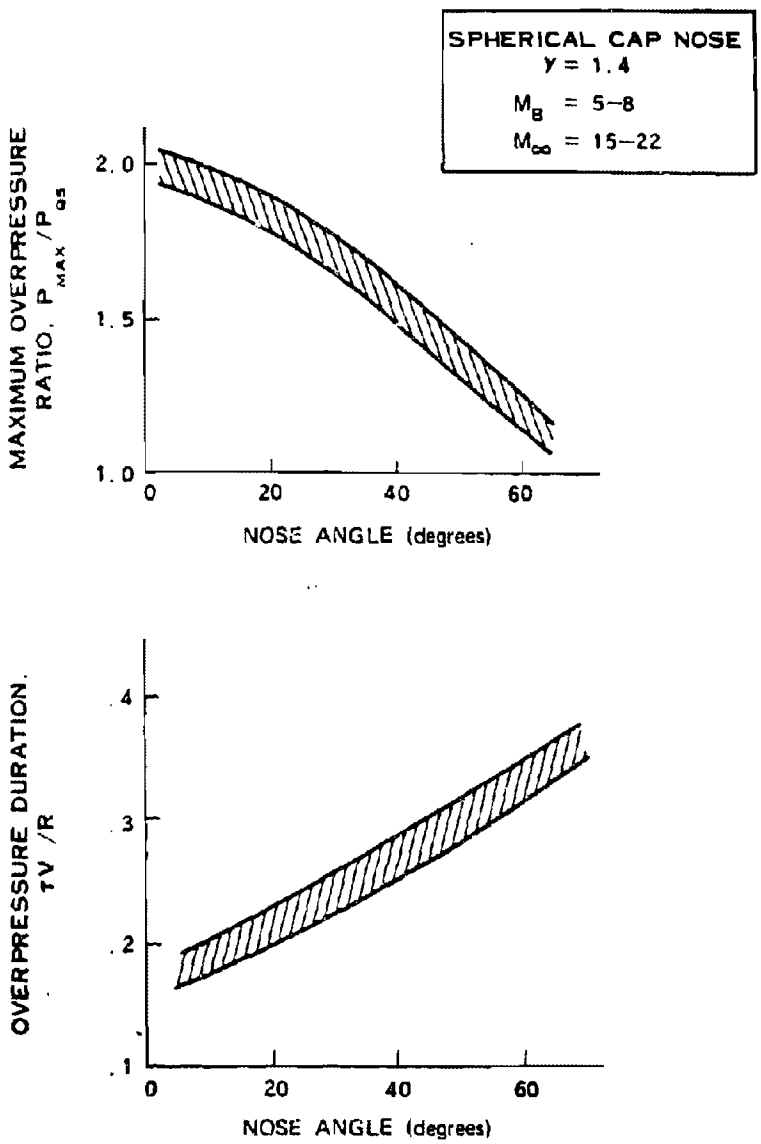

Figure 16-36. [redacted] Maximum Overpressure and Overpressure Duration for Typical Shock-Shock Interactions [redacted]

[redacted]

within which a burst of specific yield will cause axial or lateral forces greater than those for which the vehicle was designed. This envelope is required as part of the iterative processes in which tradeoffs involving weight penalties, yields, target damage criteria, defense capabilities, dispersion and booster capabilities must be considered. Two basic steps in determining the damage envelopes for an *RV* are: construction of the Locus of Escape (*LOE*); and location of points, relative to burst point, where the *RV* is subjected to forces equal to design loads.

[redacted] The nomenclature defined by Figure 16-23 will be used for simplicity and clarity. In this blast-intercept configuration, point A is the position of the *RV* at time of detonation; B is the point of intercept of the *RV* and the blast sphere; *OD* is the distance of closest approach of the *RV* to the burst center. The distance *LD* is called the lead distance, and *RB* is the radius of intercept.

[redacted] A reference trajectory is introduced to define a new coordinate system. This trajectory, which is one axis of the new coordinate system, is parallel to the *RV* trajectory and intersects the burst point (0) (see Figure 16-23). With the center of this coordinate system at 0, the other axis is perpendicular to the reference trajectory. This coordinate system locates the position of the vehicle at the time of detonation relative to the reference trajectory.

[redacted] The following procedure is used to construct the locus of escape (*LOE*). The *LOE* defines a volume, outside of which the reentry vehicle will not intercept the blast shock wave. Figure 16-37 illustrates a situation from which one point on the *LOE* is defined. During the time interval $(t_c - t_o)$ the shock front expands to point C. During the time interval $(t_c - t_x)$ the vehicle travels from point X to point C where it intersects the shock front. If $(t_c - t_x) = (t_c - t_o)$, X is a point on the *LOE*. The distance *XC* is the lead distance, while *OC* is the cross range. To determine another point on the *LOE*, pick another radius of intercept and find a distance *X'C'* such that $(t'_c - t'_x) = (t'_c - t_o)$. Determination of several points, both above and below the reference trajectory, will define the *LOE*.

[redacted] The next step in defining the damage envelope is to determine locations, with relation to the burst, at which the reentry vehicle would suffer lateral and axial forces equal to the design loads. Sufficient locations must be selected and g loads calculated for each point so that iso-g contours can be constructed. Correlation of design loads with these iso-g contours defines the damage envelope. In this case, a g level is specified as the damage criterion.

(U) Figure 16-38 is a qualitative example that shows the *LOE* and the lateral and axial iso-g contours. This figure is oriented with respect to a reference trajectory. Figure 16-39 shows the relation between Figure 16-38 and a real situation.

[redacted] It must be realized that the g loadings described in the above examples are those experienced by a rigid body vehicle. Since the forces are applied dynamically, dynamic amplification factors must be considered. Displacements that result from dynamic loading can be greater than those that result from static loading. Thus, the effective force experienced by the warhead or other internal components may be more than the rigid body g's.

[redacted] It should also be noted that the response of reentry vehicles depends not only on peak values of the force, but also on the rate of application and the rate of decay of the force. Having sustained the peak value of the force, which occurs at the shock front, the reentry vehicle suffers lesser forces and pressures as it penetrates the blast sphere. Complete and accurate definition of the damage envelope must include responses during the entire force-pressure time history. This will be discussed further in connection with the structural response analyses of

[redacted]

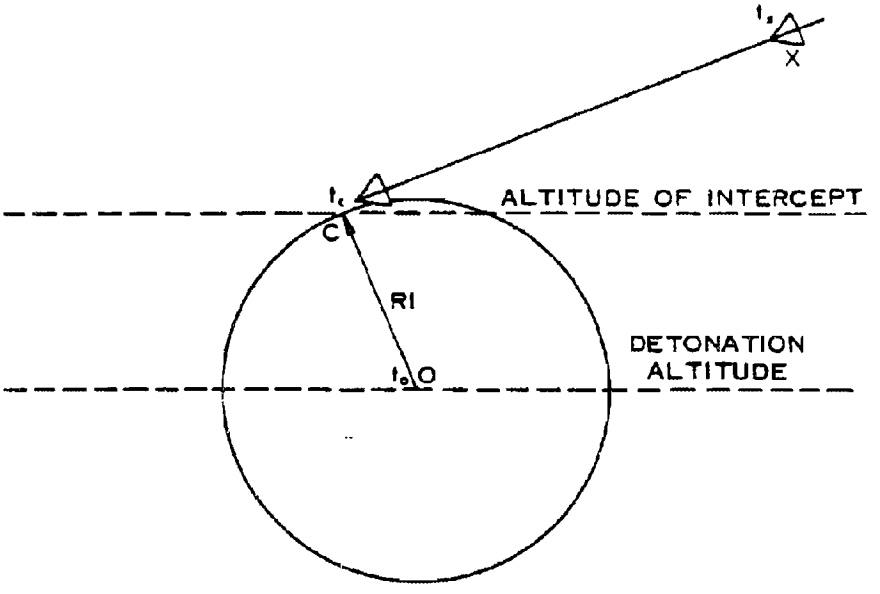

t_o = TIME OF DETONATION

t_c = TIME SHOCK FRONT AND RV ARE AT POINT C

t_x = TIME RV IS AT POINT X

Figure 16-37. [redacted] Determination of Locus of Escape [redacted]

[redacted]

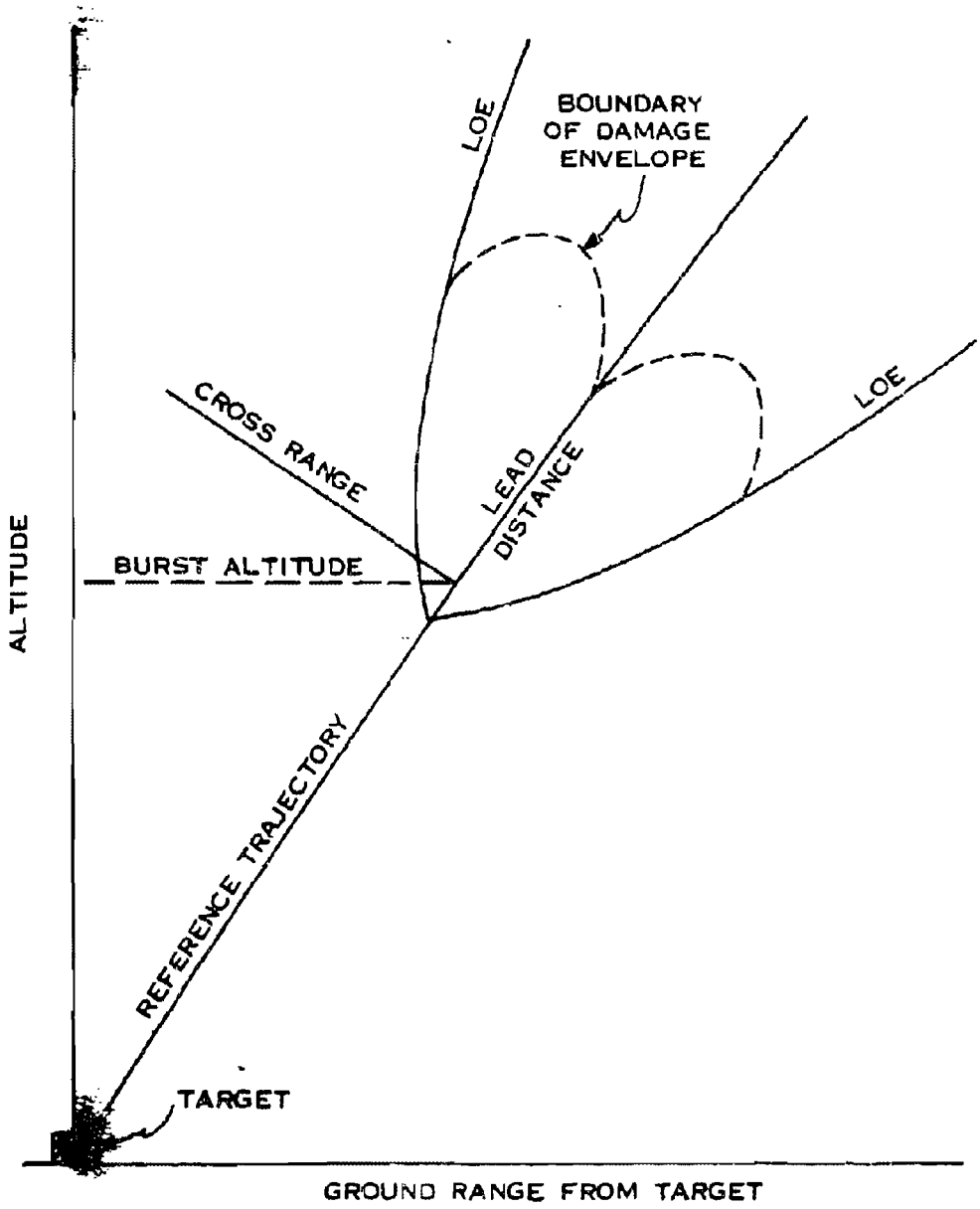

Figure 16-39. [redacted] In-Flight Intercept [redacted]

[redacted]

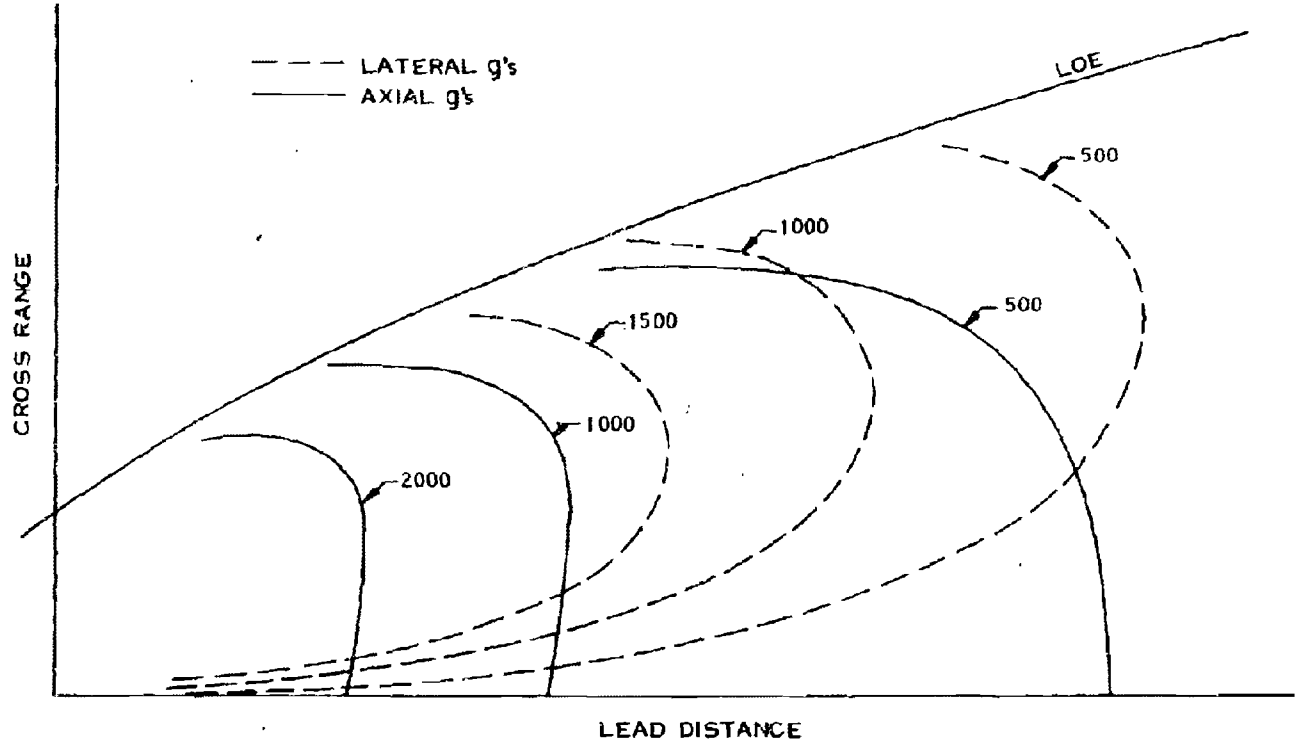

Figure 16-38. [redacted] Qualitative Iso-g Contours [redacted]

[redacted]

ABM vehicles (paragraph 16-32). It is evident that damage criteria other than rigid body g levels can be specified to define the damage envelope for a vehicle.

[redacted] RESULTS OF SOME RV BLAST AND THERMAL LOAD AND VULNERABILITY CALCULATIONS [redacted]

[redacted] As pointed out in paragraph 16-13, it is impossible to condense the determination of blast and thermal vulnerability into a generalized methodology suitable for hand computation. The computations are associated too intimately with the design details of the particular *RV* of interest. In order to provide the users of this manual with some understanding of the procedures involved in such computations, some typical calculations are described in the following paragraphs.

16-24 Blast Loads on the RV [redacted]

[redacted] Assume that a reentry vehicle is hardened to survive 200 cal/cm [redacted] incident X-ray environment. The information desired is whether or not the *RV* will be vulnerable to blast and/or thermal effects at any point along the trajectory. The sample vehicle is assumed to have the following parameters.

- It is a 6° sphere cone configuration.
- The ballistic coefficient is $\beta = 1{,}000$ lb/ft^2.
- Reentry altitude = 400,000 feet.
- Reentry angle = -35°.
- Reentry velocity = 17,000 ft/sec.

Two questions are examined separately to obtain the desired information.

- What blast load (axial and lateral accelerations) accompanies 200 cal/cm^2 incident X-ray exposure at the altitudes of interest from the standpoint of blast?
- What are the minimum axial and lateral rigid body accelerations that will allow blast survival through all altitudes for separation distances equal to the vacuum separation distance for 200 cal/cm^2 incident X-rays [redacted] (the minimum separation during exoatmospheric flight)?

[redacted] Figure 16-40 shows the results of calculation of the axial and lateral rigid body g loads as a function of intercept altitude that would result when the *RV* is initially separated from [redacted] burst so as not to receive more than 200 cal/cm^2 X-ray energy incident on the vehicle. The vacuum separation distance for this X-ray level is about 11,000 feet (Chapter 4), and if the vehicle maintains that separation between altitudes of 40 and 100 kilofeet it will attain maximum g loads at an altitude of 40 kilofeet. The axial load at this altitude is 230 g's and the lateral load is 280 g's. At intercept altitudes less than 40 kilofeet, the rigid body loads will be less for the same separation distance.

[redacted] The axial and lateral loads that would be sustained if the separation distance is such that 200 cal/cm^2 X-ray energy were deposited from [redacted] weapon are also shown in Figure 16-40. The approximate distances are shown as a function of intercept altitude in Figure 16-41.

[redacted] Figure 16-41 shows near *maximum* separation distance as a function of intercept altitude for the 230 g axial load and the 280 g lateral load. The approximate 200 cal/cm^2 separation distances also are shown as a function of intercept altitude for the [redacted] weapon.

[redacted] The maximum separation distances for the axial loads were obtained for the near head on interception of the *RV* by the blast wave. The maximum distances for the lateral loads were obtained from the near side on interception, i.e., 65 to 70° measured from the nose of the vehicle.

[redacted] The incident blast overpressures required to induce the g loads are shown in Figure 16-42 for the 230 g axial and 280 g lateral loads of

[redacted]

Pages 16-67 through 16-69
DELETED.
DNA (L)(3)

Figure 16-41. At 40 kilofeet intercept altitude, a minimum overpressure of 22 psi is required to attain the 230 g axial load. The overpressure required to attain 280 g's laterally is 18.5 psi at 40 kilofeet, and a minimum of 13.5 psi is required above 90 kilofeet altitude.

Figure 16-43 shows the curves of g load as a function of maximum separation distance for a 40 kilofeet altitude intercept by a blast wave from weapon. It should be noted, from this figure, that extremely large separation distances are indicated if the lateral hardening of an *RV* is less than 100 g's. For yields less than or greater than this separation range changes approximately as . The approximate nature of this ratio results from the change in the velocity of the vehicle between the points of initial separation and interception.

Based on this brief examination of the results of calculation of blast vulnerability, the main conclusion is that rigid body loads of 280 g's axially and 230 g's laterally are compatible with the 200 cal/cm^2 X-ray hardening of the *RV*. Moreover, if the *RV* rigid body response hardness level falls short of these g levels, the blast effects may predominate as a damage mechanism. More specific trajectory/blast cases must be studied to determine the required g loading criteria for balance with a 200 cal/cm^2 X-ray criterion.

16-25 Thermal Radiation Loads on the RV

A sample investigation has been made of the free field thermal radiation incident on the same *RV* described in paragraph 16-24 as it flies through a nuclear burst in the lower atmosphere. The basic trajectory considered in this study had a reentry velocity 17,000 ft/sec and a flight path angle of -35°. In addition, a limited study was performed for a 19,200 ft/sec/ -75° trajectory. Thermal radiation heat loads were computed for head on intercepts of burst at 40-, 60-, 80-, and 100-kilofeet burst altitudes. Burst yields of and were also considered at the 60 kilofeet altitude.

The thermal radiation heat flux produced by a nuclear burst can be obtained as a function of distance, direction and time from the radiation/hydrodynamic calculations of Hillendahl that were used to describe the thermal source in Chapter 3 together with the appropriate form factors. These are free field thermal radiation data and do not include any interaction between the vehicle and the radiation field, i.e., the possible attenuation of radiation resulting from an opaque layer of vaporized heat shield material in the flow field surrounding the vehicle was not included (see paragraph 16-31 for a discussion of these "blocking" effects). The total free field heat load to the stagnation point, cone, and base region of the *RV* was determined by integrating the heat flux as a function of time after detonation, assuming a straight line, constant velocity trajectory in the vicinity of the burst.

The total radiation heat load for this example is shown in Figures 16-44 through 16-46 as a function of the initial slant range of the vehicle, burst altitude, burst yield, and trajectory. For initial slant ranges less than about 3 to 5 kilofeet, the heat load is very large (35,000 Btu/ft^2) and is essentially independent of location on the vehicle. For a fixed burst yield and initial slant range, the heat load decreases with increasing altitude; conversely, for a fixed burst altitude and initial slant range, the heat load increases with increasing yield. Finally, a higher velocity trajectory increases the heat load for a fixed yield and altitude.

The thermal data shown in Figures 16-44 through 16-46 could be used in conjunction with the blast data of paragraph 16-24 to determine the total radiation heat loading as a function of blast loading (rigid body axial load

Page 16-71 Deleted.

[redacted]

DNA
CN(z)

Deleted

Figure 16-44. [redacted] Thermal Radiation Heat Load on the Cone as a Function of Initial Slant Range for Several Burst Altitudes [redacted]

[redacted]

[redacted]

[redacted]

DNA
H(3)

Deleted

Figure 16-45. [redacted] Thermal Radiation Heat Load on the Cone as a Function of Initial Slant Range for Several Burst Yields [redacted]

[redacted]

[redacted]

[redacted]

DNA
(6)(3)

Deleted

Figure 16-46. [redacted] Thermal Radiation Heat Load on the Cone as a Function of Initial Slant Range for Several Trajectories [redacted]

[redacted]

[redacted]

[redacted]

[redacted]

factors). As a particular example, these data show that, for a 350 kt burst at 40 kilofeet and the 17,000 ft/sec/-35° trajectory, the radiation heat load on the cone associated with a 200 g, head on intercept condition is only 530 Btu/ft^2, whereas for a 300 g intercept condition it is 5,400 Btu/ft^2. This particular example indicates that a 50 percent increase in blast hardness (as measured by the rigid body g criteria) produces an order of magnitude larger thermal environment.

16-26 Description of a Blast/Thermal Vulnerability Determination

[redacted] This paragraph continues the description of the sample computations that were described in paragraphs 16-24 and 16-25. The determination of the sample *RV* to blast and thermal effects produced by a nuclear weapon burst is described below.

[redacted] The blast vulnerability analysis of the *RV* is made under the following assumptions:

- 6° sphere cone vehicle with a ballistic coefficient of 1,000 lb/ft^2 (assumed constant for normal reentry).
- Point mass-zero lift trajectories were used in the computations.
- Reentry altitude = 400,000 ft.

[redacted] The blast model used in the computations is considered to be an upper bound to a conventional weapon blast output. Modified Sachs' scaling (see paragraph 2-14) was used in conjunction with curve fits to radius-time-overpressure data. The other peak blast parameters, such as density and particle velocity, are Rankine-Hugoniot values consistent with the scaled overpressures. The environment to which the vehicle is exposed in the interior of the shock front was simulated by assuming constant vehicle velocity during fly through and Sach's scaling curve fits to the interior profiles. It should be noted that, in actual practice, vehicle fly through loading calculations are performed on an electronic computer using the results of detailed radiation/hydrodynamic calculations corresponding to the nuclear device and burst altitude of interest.

[redacted] The vehicle reentry conditions used for this calculation are as follows:

- Case 1
  a. Reentry velocity = 17,000 ft/sec
  b. Reentry angle = -35°
- Case 2
  a. Reentry velocity = 19,200 ft/sec
  b. Reentry angle = -75°

[redacted] The temperature of the heat shield can be an important factor in determining the structural response of the *RV* to blast induced loading because of the possible temperature dependence of some of the structural properties, e.g., elastic modulus and yield stress, at elevated temperatures. For the study discussed here, predictions of the heat shield bulk temperature accounted for ascent heating, normal reentry heating to the burst altitude, and thermal radiation heating from the nuclear burst. The bulk temperature is symbolically related to the heat loads by

$$Q_{\text{ascent}} + Q_{\text{reentry}} + \alpha\, Q_{\text{radiation}} = \rho t \int_{T_{\text{launch}}}^{T_{\text{bulk}}} C_p\, dT \ (\text{Btu/ft}^2),$$

where it has been assumed that the temperature is uniform across the thin ablator skin and that heat losses are negligible compared to heat inputs. In general, considerable caution must be exercised in employing the thin skin-bulk temperature method.

[redacted] The thermal radiation heat flux produced by the nuclear burst was obtained as described in paragraph 16-25. The thermal radiation heat load incident on the vehicle was deter-

[redacted]

[redacted]

[redacted]

mined by numerically integrating the flux, as a function of time after detonation, assuming constant vehicle velocity at that altitude and no vehicle spin. It should be noted that, aside from the inherent uncertainties in the free field thermal radiation data, there are additional uncertainties in determining what fraction of the incident thermal radiation is actually absorbed by the ablative surface during the fireball fly through. This is due to a lack of knowledge of the spectral absorptivity of the vehicle surface under these conditions and of the possible attenuation of radiation as a result of an opaque layer of vaporized heat shield material in the flow field surrounding the vehicle.

[redacted] Two basic methods of structural analysis were employed for this sample calculation. The first method involves the application of a finite length, elastic cylinder response solution to determine the dynamic shell stresses resulting from head on intercept loadings. The second method, which was applied to the side on intercept, involved the evaluation of the dynamic response of a lumped parameter, free free beam model subjected to transient blast loadings. In actual practice, the analysis of the structural response of *RV* configurations should employ much more sophisticated and complex methods. The description of these relatively simple methods is included to indicate to the user the general analytical methods that could be used.

[redacted] The results of these two methods of structural analysis depend on assumptions made concerning the blast and thermal environment that the *RV* encounters. In this calculation, the transient aerodynamic loading was developed by using Newtonian theory for pressure magnitudes and distributions (see paragraphs 16-21 and 16-22) combined with a curve-fit exponential time decay obtained by flying an unperturbed trajectory through the blast model. To simplify the calculation, instantaneous engulfment was assumed and shock-on-shock interaction effects were ignored. In addition, the structural response was only examined for blast entrance and for normal reentry conditions. Blast traversal and exit of the vehicle from the blast region were not examined. Thermal loading from normal reentry and nuclear burst thermal radiation were considered for structural response through the bulk skin temperature rise. No attempt was made to evaluate resulting thermal stresses from this high temperature environment; however, the bulk temperature effect was accounted for when choosing material elastic properties and allowables.

[redacted] Three separate bays or ring-stiffened sections of the *RV* were investigated for the head on intercepts. After a few dynamic response calculations were made, it became apparent that Bay L-I (Station 37.5 to Station 49) was the most vulnerable to head on blast loadings; therefore, the results presented are for Bay L-I. The cylinder solution used is a closed form, elastic response code that computes all stresses at both the inside and outside shell fibers at any desired point on the shell.

[redacted] The side on intercept conditions were examined with a lump-parameter, free-free, "Timoshenko" beam model. The bending rigidity was supplied completely by the ablator shell, whereas the mass distribution was made up of both the main shell structure and all internal components. As in the head on studies, the thermal effects were included only in the evaluations of material elastic properties and allowables. Using this lumped-parameter mode, a normal mode solution was employed to determine the complete time history of bending stresses that developed at a number of stations along the missile length from the transient pressure loading that resulted from blast intercept. In all cases, the peak beam bending stresses occurred in a region bounded by Stations 20 and 25.

[redacted] In addition to these two basic tools of structural analysis, i.e., cylinder solution and

[redacted]

[redacted]

[redacted]

beam model, a check of shell buckling was made by using the semi-empirical results from the HARTS Program. This check calculation revealed that, if buckling did occur during blast intercept, it probably would be elastic; however, since rather thick walled shells were involved, the calculated critical buckling pressures are very high compared to pressures necessary to cause conditions leading to plastic deformation and rupture.

16-27 Results of the RV Vulnerability Determination [redacted]

[redacted] The results of the structural response study are shown in Figure 16-47 for head on intercept and Figure 16-48 for side on intercept. Figures 16-47 and 16-48 show the allowable stresses and the peak stresses developed from blast entrance loads (characterized by the plotted loads) as a function of initial slant range from a 350 kt burst at an altitude of 40 kilofeet. For the side on intercept cases (i.e., interception by the blast wave normal to the longitudinal axis of the vehicle), the loads are the total g's obtained by vectorially combining the axial and lateral values. For the head on intercept cases, the total loads are the same as the axial loads.

[redacted] The incipient structural damage is indicated in the figures by the intersection of the curve showing peak stress developed with the allowable stress curve. The curve labeled "Developed Stress" indicates the variation with slant range of the peak dynamic stresses developed in the vehicle during blast wave intercept. These curves are shown for both the nominal RV and the 1.2 nominal vehicle, which is the same vehicle with the skin thickness increased by 20 percent. The slant range, stress, and loads are tabulated for each of the points of incipient structural damage.

[redacted] It is apparent that the addition of 20 percent to the skin thickness reduces the vulnerability of the RV by decreasing the slant range for incipient structural damage markedly. It should be recognized that these values of slant range probably are minimum values for the onset of incipient structural damage as a result of the assumptions used in the stress calculations.

[redacted] The thermal response data are shown in Figure 16-49 in terms of the temperature at the aft end of the cone (X/R_N = 19.4) after burst exit as a function of the initial slant range of the vehicle from the burst. These data are the temperatures developed during normal reentry (including ascent heating) to the burst altitude plus the temperature rise caused by the fireball thermal radiation. Beyond initial slant ranges of 16 to 18 kilofeet, the temperatures shown are the normal reentry temperatures at the burst altitude, since the thermal radiation heat load is quite small at these large ranges. The 40-kilofeet burst altitude induces higher temperatures than the 60-kilofeet altitude because of increases in both reentry heating and thermal radiation heating.

[redacted] Two specific temperatures, 2,340°F and 1,750°F, are shown in Figure 16-49. The former is the ablator melt temperature, while the latter is the temperature at which the ablator has low structural strength. Since the bulk temperature generally lies somewhere in between the surface and backface temperatures, surface melting will commence before the bulk temperature reaches 2,340°F, but probably only in small amounts. Of more importance is the fact that if the vehicle emerges from the burst with a bulk temperature greater than 1,750°F at critical structural locations, it probably will not be able to survive the exit blast loads and/or the subsequent reentry loads as it descends through maximum dynamic pressure to impact, i.e., if the thermal radiation heat loads are sufficiently great to result in temperatures of 1,750°F at burst exit, "delayed" structural damage may occur subsequent to the blast entrance, even if the entrance loads are not sufficient to cause damage.

Pages 16-78 and 16-79
Deleted.
DNA (4)(3)

[redacted]

[redacted]

[redacted]

Deleted

Figure 16-49 [redacted] Cone Bulk Temperature after Fly Through as a Function of Initial Slant Range from Burst (Head On Intercept [redacted]

[redacted]

[redacted]

[redacted]

16-28 Summary and Conclusions Concerning RV Vulnerability Calculations [redacted]

[redacted] There are many different ways to summarize the blast/thermal vulnerability of an RV; this subsection employs a bar graph method, whereas the damage envelope method is used in the succeeding subsection to portray ABM Blast/Thermal Vulnerability. The minimum initial slant ranges for structural and thermal damage are summarized in Figure 16-50 for the 17,000 ft/sec/-35° trajectory and 40 kilofeet burst altitude. These data show that the RV is more vulnerable to the side on intercept/structural damage condition than any other condition. The 20 percent increase in ablator thickness reduces the initial slant ranges for damage considerably. The total "g" loading at the slant range for structural damage and the total free field radiation heat load at the slant range for thermal damage also are shown in the figure. It can be seen that there is *no unique* mechanical "g" load or thermal "Q" load that determines when damage occurs. This points out the requirement for more definitive information concerning damage criteria associated with actual RV designs.

[redacted] The separation distance at the burst altitude between two vehicles that were originally at the 130 and 200 cal/cm^2 X-ray separation distances apart in the exoatmospheric [redacted] also are shown in Figure 16-50. It can be seen that if two vehicles were spaced for these X-ray loadings from a 350 kt weapon in the exoatmosphere, and the lead vehicle encountered a direct hit from 350 kt at 40 kilofeet, the trailing vehicle definitely would incur damage if it encountered the blast wave.

(S) The foregoing description of the method and results of an RV blast/thermal vulnerability sample calculation was presented to give the user an indication of the important technical aspects that must be included in this type of analysis. Based upon the results, a few rather general conclusions can be drawn:

- It is apparent that the blast/thermal vulnerability of an RV cannot be uniquely expressed in terms of either rigid body "g" load levels or thermal radiation heat loads, but rather is a function of the particular reentry trajectory, intercept geometry, yield of the attacking weapon, and the specific damage mechanism considered.
- Vulnerability loads or damage criteria assigned to a particular RV corresponding to blast or thermal effects may not be compatible with the loads or criteria assigned for other nuclear weapon effects (e.g., X-rays).
- Thermal loads on the RV, resulting from a combination of reentry heating and radiation from the nuclear weapon, can have an important deleterious effect on the material properties (and in turn upon the structural response) of the RV ablator/substructure combination.
- The accurate assessment of RV vulnerability to nuclear weapon effects requires detailed analyses using advanced analytical tools and high-speed electronic computer facilities.

[redacted] ANTIMISSILE (ABM) SYSTEMS [redacted]

[redacted] The assessment of blast and thermal vulnerability of an antimissile (ABM) system presents many of the same problems that were discussed for reentry vehicles; however, ABM systems have some important characteristics that are unique, and these will form the basis for a large portion of the following discussion.

[redacted] There are fundamental differences between the views of the designers of RV's and ABM concerning blast and thermal vulnerability. The designer of an RV may be willing to have his vehicle sustain limited damage if the damage would not degrade the probability of mission success significantly. This willingness to sustain

[redacted]

[redacted]

DNH
(b)(3)

Deleted

Figure 16-50. [redacted] Minimum Initial Slant Range for Structural/Thermal Damage at 40 kft Burst Altitude, V_E/γ_E = 17,000 ft/sec/-35°

[redacted]

[redacted]

[redacted] some level of damage results from the fact that the RV designer usually deals with large numbers of vehicles directed against an array of targets with the objective of insuring that a fraction of the RV's penetrate the defense and reach the targets. The defense, on the other hand, attempts to deny all "leakage" of enemy RV's. Therefore, when considering blast and thermal fratricide damage, the ABM designer usually will not tolerate any degree of damage to the vehicle (i.e., it is designed to be "sure safe"). When assessing the ability of an ABM to defend a target and to kill an enemy RV, however, the objective dictates that the ABM designer achieve a "sure kill" miss distance relative to the incoming RV.

[redacted] Most of the following discussion results from a study to determine the probable damage modes and damage envelopes for the AIRS I and II vehicles (paragraph 16-12) when exposed to blast waves and thermal radiation from nuclear explosions.

[redacted] The scope of the discussion can be summarized as follows:

- Two vehicles are considered, AIRS I and AIRS II. These vehicles nominally represent interceptor vehicles of the SPRINT and SPARTAN class, respectively. Inboard profiles of these vehicles are shown in Figures 16-51 and 16-52.
- Four response modes are considered:
  (1) Shell breathing response to the blast wave.
  (2) Vehicle bending response to the blast wave.
  (3) Internal component damage due to rigid body acceleration produced by the blast wave.
  (4) Material damage produced by the thermal radiation.
- Coupling effects among the damage modes are neglected, except for the inclusion of degradation of material properties that results from heating the material.
- Control surface damage is not considered.
- Each vehicle is assumed to be in a steady state "n"-g maneuver (where n can be zero).

[redacted] The aerodynamic loads initiated by the blast wave must be defined to perform a blast vulnerability analysis. In the definition of the aerodynamic loads imposed on a vehicle traveling at hypersonic speeds when subjected to a strong blast wave, the initial shock-on-shock interactions during the vehicle engulfment by the blast wave present the most difficulty. Recent studies of the response of missile structures to blast loads indicate that the response to the shock-on-shock loads does not contribute significantly to the total response experienced by the missile structure.

[redacted] The response of the structure to blast is separated into shell breathing, vehicle bending, and rigid body acceleration responses. The separation of the total response into uncoupled breathing and bending responses is required since current methods cannot perform the coupled problem; however, this separation is justified to some extent by consideration of the types of damage associated with each response. In shell breathing response, segments of the shell between bulkheads are excited, and the damage is associated with high frequency local shell deformation. In vehicle bending, the damage results from relatively low frequency excitations of the overall structure.

[redacted] Criteria for the yielding and buckling response have been generated primarily from data generated in tests of simple cylindrical and conical bodies subjected to air blast from HE detonations. Studies of damage to the vehicle by bending have neglected the short-duration diffractive loading, which is of little consequence in exciting the long period oscillations associated with bending deformations (except possibly for very low yield weapons). The damage criteria for bending deformations, and the response analysis

[redacted]

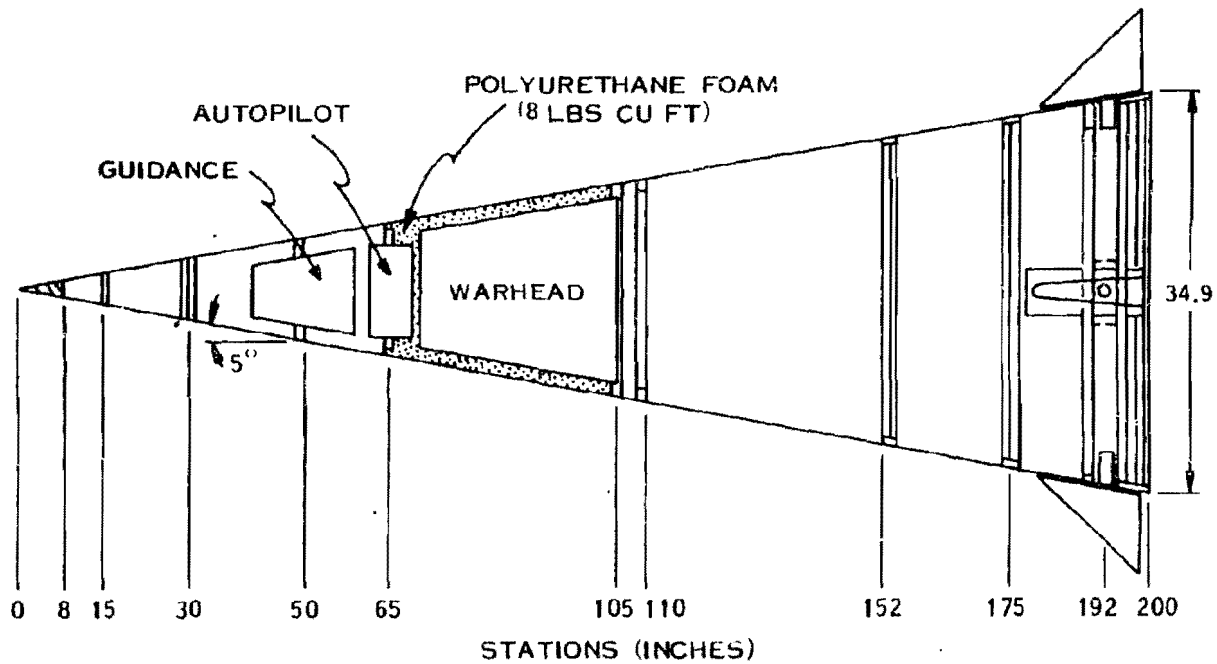

STATION	SKIN THICKNESS	MATERIAL
8 – 30	0.08	2014 – T6 AL
30 – 65	0.125	2014 – T6 AL
65 – 105	0.156	2014 – T6 AL
105 – 200	0.20	FILAMENT-WOUND FIBER GLASS

Figure 16-51. Inboard Profile of AIRS I Vehicle

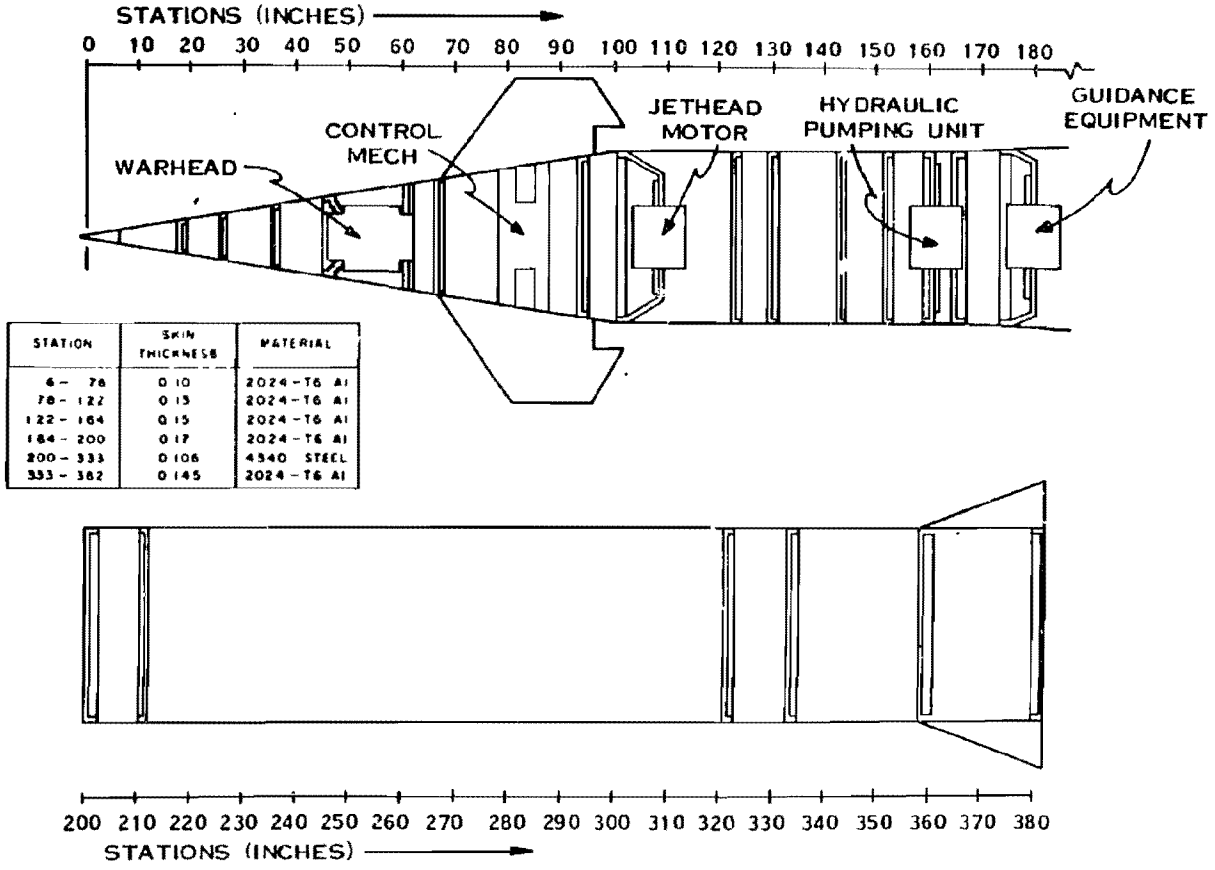

STATION	SKIN THICKNESS	MATERIAL
6 – 78	0.10	2024-T6 Al
78 – 122	0.15	2024-T6 Al
122 – 164	0.15	2024-T6 Al
164 – 200	0.17	2024-T6 Al
200 – 333	0.106	4340 STEEL
333 – 382	0.145	2024-T6 Al

Figure 16-52. [redacted] Inboard Profile of AIRS II Vehicle [redacted]

[redacted]

techniques, rely on knowledge developed in similar studies performed for aircraft and launch vehicles in the boost phase.

[redacted] Analysis of response to thermal radiation effects define the mechanisms by which heat is absorbed and distributed throughout the structure, both when the vehicle is outside and inside the fireball. Damage criteria from thermal radiation effects are selected on the basis of the loss of the insulative coverings over the substructure.

[redacted] Blast and thermal radiation effects damage envelopes for both AIRS I and II are presented below. The relative sizes of these envelopes for the various effects on the two representative vehicles and for the encounter condition variations (in yield and altitude) are discussed briefly.

16-29 Shell Breathing Response [redacted]

[redacted] Blast induced pressure loading causes the shell segments of the vehicle between the ring reinforcements to respond in what is usually termed the "breathing mode." Damage occurs in the form of permanent deformation of the skin through the formation of a dented area in the surface of the shell. The primary damage mechanism for the shells is an instability (buckling) of the shell that can occur either when the shell is all elastic or after portions of the shell have become plastic. This damage mechanism can be complicated by the presence of the ablator over the structural shell and by other states of stress and deformation imposed by bending of the vehicle as a result of blast and normal flight loads, or the thermal condition of the vehicle at blast intercept. These interaction problems are not considered.

[redacted] A complete determination of the blast damage to a shell segment that would be required to prevent the AIRS vehicles from performing a specified maneuver requires two separate analyses. The first analysis predicts response levels from threshold to severe post buckling damage, and a second analysis predicts the post damage response; the latter is the response of the "damaged" vehicle to the loads imposed by maneuver. Thus, it is not sufficient to calculate the shell response resulting from the blast loading. A sure-safe criterion also must be established for the actual in-flight conditions in the fratricide mode. The amount of damage that constitutes an "unsafe" level under a known set of environmental conditions must be determined eventually if vulnerability studies are to be considered useful to the military planner.

[redacted] The analyses of the response of critical shell segments of the AIRS I and II vehicles to blast that were selected for this example can only predict the threshold damage level caused by elastic buckling or initial material yielding. Analyses that calculate elastic-plastic response in the post buckling region have only been developed recently for shell response to blast, but experimental data are not sufficiently comprehensive to apply the results to various loading conditions and to different materials. Thus, rather arbitrary criteria must be postulated to relate computed damage levels to "unsafe" conditions for the ABM.

[redacted] The analyses discussed thus far primarily calculate the response of the shell up to threshold damage, i.e., sure-safe levels. These analyses are elastic in nature and cannot be used directly to determine response that includes severe damage. There are three additional elements required before lethality predictions can be made:

- Selection of the applicable analysis; that is, inelastic buckling or yielding (or possibly fracture).
- Definition of damage criteria, i.e., definition of the amount of damage that must occur in the selected damage mode to negate the intended mission of the vehicle.
- Selection of a means to apply the inelastic analysis to the determination of the load

[redacted]

[redacted]

level required to produce the amount of damage specified.

16-30 Vehicle Bending Response (U)

[redacted] Discussions of prediction techniques for the response of the AIRS I and AIRS II vehicles to blast in their rigid body and bending degrees of freedom are separated into two parts. First, a formulation of *damage criteria* for these vehicles in bending is discussed for damage to the primary structure and to the internal components. In the second part, analysis that predicts the *structural response* is discussed. The inclusion of critical damage criteria in a computer program for the response analysis results in the capability to determine sure safe envelopes for bending response to blast.

[redacted] A most difficult, but necessary, part of defining damage contours for interceptor missiles in a blast environment is the definition of the amount of damage that must be produced in the primary structure in bending or to internal components to constitute a positive failure of the mission. The approach adopted is to use a simple damage criterion available for interceptor vehicles.

[redacted] Selection of simple damage criteria for an interceptor vehicle undergoing bending deformations requires an understanding of the damage modes involved. The primary bending damage modes possible to the primary structure of a vehicle may be:

- Damage to the joints resulting from tensile stresses in excess of the stresses allowable for the joints.
- Buckling damage to the overall shell structure resulting from combined axial and bending induced normal stresses in the shell.

For this discussion, a damage condition in which the vehicle damage cannot support the loads associated with a specific "n"-g maneuver after buckling was selected tentatively as sufficient.

[redacted] Damage criteria for internal components should involve detailed investigations of the acceleration-time history environment that a component can withstand. In addition, the supports of internal components and the load-carrying ability of the supports must be considered in a comprehensive vulnerability analysis. It is the usual practice to consider an acceleration time-history and to assign a certain peak acceleration value to be critical.

[redacted] In view of a lack of fragility data for the internal components of the AIRS I and II, representative allowable peak acceleration values were selected from information available for design requirements for SPRINT and SPARTAN. These acceleration values are used to demonstrate the procedures involved in determining damage envelopes for internal component damage, but they are not necessarily representative of what the internal equipment mounted inside the vehicles can actually withstand.

[redacted] It is necessary to perform a comprehensive analysis of the blast loading and response of the entire missile structure (including primary and secondary structures) to determine the details of the blast loads imposed upon (and the response of) specific internal components when a missile body is exposed to a nuclear weapon environment. This analysis includes development of a detailed mathematical lumped-mass/spring model of the missile to determine the proper "transfer functions" between the primary structure and the internal component of interest. Calculations that use the mathematical model and the definition of the blast loads imposed on the missile structure during a real encounter lead to the determination of the loads imposed on the internal structures.

16-31 Thermal Radiation Effects [redacted]

[redacted] The establishment of thermal radiation damage criteria for AIRS I and AIRS II required an examination of the individual structures involved.

[redacted]

[redacted]

[redacted] In general, data concerning thermal radiation effects consists of a description of the temperature distribution through the ablator (and substructure material) and the mass ablation rate, both as a function of time and position on the missile. This fundamental information provides the thermal portion of the inputs for a realistic assessment of the overall vehicle performance during and after an encounter with a nuclear burst. The temperature distribution data can be used in a structural analysis to determine the magnitude of the allowable stresses (or strains), thermal stresses, etc. Furthermore, there are usually internal components in the guidance section, fuzing, arming and firing section (FAF), or warhead section that have a fairly low temperature tolerance. The ablation rates also affect the mass distribution and can affect the aerodynamic characteristics of the missile, which can affect its flight characteristics; however, the following discussion is limited to an examination of thermal effects in the ablator and substructure. No concurrent structural and/or trajectory analyses were performed.

[redacted] The principal type of ablation material used on the AIRS I missile is tape-wrapped silica phenolic, which is a silica cloth impregnated with phenolic resin. A detailed theoretical prediction of the thermal response of a charring, melting and vaporizing ablator such as silica phenolic on a high-speed missile that flies through (or near) a nuclear fireball during some portion of its mission involves simultaneous consideration of complex physical and chemical phenomena. The general situation is illustrated in a simplified fashion in Figure 16-53. During normal flight (i.e., preburst or post traversal), the vehicle is heated by forced convection ($\dot{q}_c$) caused by friction forces in the boundary layer on the vehicle (aerodynamic heating). During the fireball traversal phase, the predominant mode of heating is thermal radiation ($\dot{q}_R$) from the high temperature fireball air. In this case, the ablation rates generally are so high that the boundary layer is blown off, and the local flow field (which may be subsonic) is dominated by the ablation vapors. In either case, the heat transfer to the surface causes the ablator to heat, pyrolyze internally, and melt and vaporize at the surface.

[redacted] A realistic thermal analysis for a silica phenolic coated vehicle should consider the following effects:

- Internal heat conduction in the ablator and substructure.
- Pyrolysis of the phenolic resin in the ablator, with the attendant endothermic chemical reactions and pyrolysis gas flow through the char.
- Convective and radiative heat transfer at the ablator outer surface, and the accompanying surface recession that results from melting and vaporization of the silica cloth.
- The interaction of the injected ablation vapors with the local vehicle flow field, especially the absorption of thermal radiation by the vapors (radiation blocking).
- The time dependent nature of the fireball environment, as well as the transient nature of the temperature response of the ablator.
- Variation of all of the effects listed above with location on the body that result in differences in environment, type and/or thickness of ablator, etc.
- Variation of all of the effects with burst encounter conditions.

[redacted] It is convenient to separate the thermal analysis into several basic parts, each of which uses somewhat different techniques of analysis according to the most important physical processes that are treated. This concept can be visualized with the aid of Figure 16-53 and an energy balance at the outer surface of the ablator (denoted by a subscript w).

[redacted]

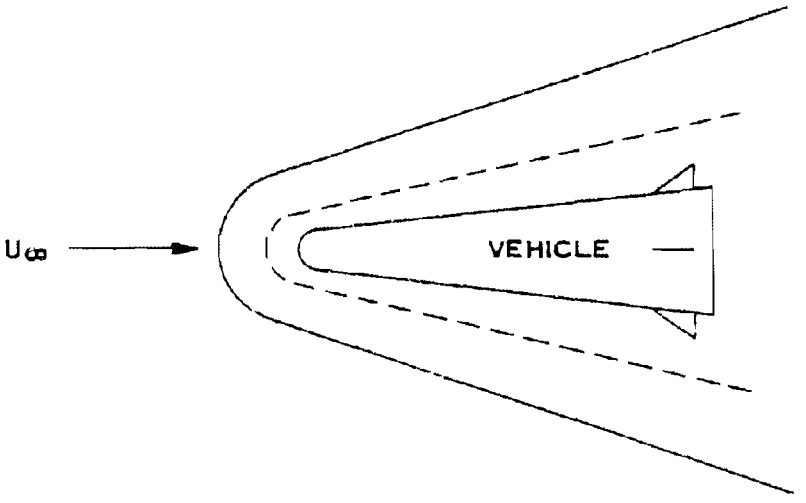

DEFINITION OF TERMS

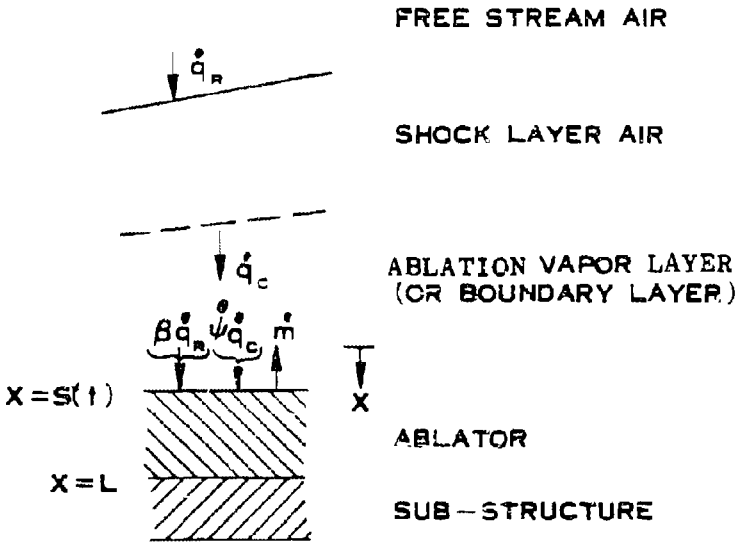

Figure 16-53. Illustration of Ablation Phenomena

[redacted]

$$\psi \dot{q}_c + \beta \dot{q}_R - \epsilon \sigma T_w^4 - \dot{m} \Delta H = \left(-K \frac{\partial T}{\partial x}\right)_w$$

where $\dot{q}_c$ and $\dot{q}_R$ are the free field convective and radiant heating rates, respectively. The term "free field" heating rate denotes that the quantity is computed without regard to ablation effects. Thus, the free field convective heating is computed on the basis of nonblowing boundary layer solutions, while the free field radiative heating is computed on the basis of the fireball flow field being unperturbed by the presence of the vehicle. Therefore, by definition, the free field thermal environment depends only on time and body position for a particular trajectory and encounter condition, and not on the type of ablation material used.

[redacted] The quantities ψ and β are the convective and radiative blocking functions, respectively. They denote the fraction of the free field heating rate that exists at the ablator surface during the actual ablation process. The blocking functions must be obtained from a solution for the local vehicle flow field that accounts for the effects of the injected ablation vapors on the flow field. In general, their values will depend on the level of the free field environment and on the particular ablation material. The quantity $\epsilon \sigma T_w^4$ represents the energy reradiated from the surface, while the term $\dot{m} \Delta H$ represents the energy absorbed in surface melting and vaporization. Finally,

$$\left(-K \frac{\partial T}{\partial x}\right)_w$$

is the heat conducted into the surface of the solid ablator, which in general must be obtained from a solution of the temperature profile in the ablator.

[redacted] The equation simply states that the net convective and radiative heating at the surface, less the energy reradiated and absorbed in melting and vaporization, equals the energy conducted into the ablator. When the net heating rate is sufficiently high to produce surface melting and vaporization, the equation relates the mass ablation rate ($\dot{m}$) to the free field environment and the temperature distribution in the ablator.

[redacted] For the purpose of the present discussion, which is primarily concerned with the thermal effects of a nuclear environment, the overall analysis is separated into two basic parts: fireball radiation and ablation, and the internal temperature and ablation response. The former is essentially multidimensional (around the body) and quasi-steady in nature, since it deals with high temperature flow about a high speed missile, whereas the latter is primarily one dimensional (through-the-thickness) and transient in nature since it deals with heat conduction. The coupling condition (boundary condition) that relates the free field environment and local flow field to the internal response is the energy balance at the surface, i.e., the equation given above.

[redacted] When the results of various theoretical methods are compared there is about a ±50 percent uncertainty in the predictions of the total silica phenolic mass ablated during a nuclear fireball traversal, even among theoretical models that assume full vaporization. If only melting is assumed, the results are at least a factor of five higher, and typically a factor of ten.

[redacted] The condition for thermal damage to the ATRS vehicles was taken to be the time at which 50 percent of the ablator mass was gone; this condition is probably on the conservative side, leading to an upper limit in the size of the vulnerability envelopes.

16-32 ABM Blast/Thermal Vulnerability Envelopes [redacted]

[redacted] The previous paragraphs described techniques of analysis that can be employed to de-

[redacted]

[redacted]

fine vulnerability envelopes for the AIRS I and AIRS II vehicles exposed to blast and thermal radiation from nuclear explosions. The vulnerability envelopes for the AIRS vehicles and for two typical encounter conditions are shown in Figures 16-54 through 16-57. In each figure, the vehicle under attack is at the origin (0, 0) flying from left to right. If the attacking weapon is burst inside the envelope, the load on the vehicle will exceed the critical level. Thus, the largest envelope on the graph identifies the "most" critical damage mechanism for the vehicle and the burst condition considered.

[redacted] Figures 16-54 and 16-55 correspond to the AIRS I vehicle in a typical fratricide situation; it is obvious that the size of the critical damage envelopes are very sensitive to the maneuver (or nonmaneuver) condition of the AIRS I. The AIRS II curves in Figures 16-56 and 16-57, indicate envelopes of somewhat different shapes, but the general behavior is similar to AIRS I.

16-33 Conclusions [redacted]

[redacted] The AIRS I and AIRS II vulnerability study produced the following main conclusions:

- The internal component acceleration envelopes are the largest for both AIRS I and AIRS II, but this predominance must be regarded cautiously as a result of the arbitrary nature by which acceleration damage levels were selected for the AIRS internal components.
- Thermal radiation effects appear to be more important for AIRS I than for AIRS II; however, blast effects produce the larger envelopes for both vehicles.
- Thermal radiation effects tend to increase in relative importance for the larger yields and lower intercept altitudes.
- Shell response and bending response damage are of comparable importance for the nonmaneuver condition for both vehicles. For the maneuver condition, however, the shell damage mode is more important than the bending damage mode in defining vulnerability envelopes for both vehicles.
- The maneuver condition modifies the acceleration, bending and shell damage vulnerability envelopes appreciably. In general, the overall areas (or volumes) of these envelopes increase significantly for the maneuver condition.

[redacted] It should be emphasized that the conclusions only apply to the AIRS I and AIRS II vehicles. The foregoing discussion was presented to indicate the types of analyses that must be performed to assess the vulnerability of ABM vehicles to blast and thermal effects. The conclusions could well be significantly different for vehicles of different design.

Pages 16-92 through 16-95
DELETED. DNA (L)(3)

[redacted]

[redacted]

[redacted] BLAST AND THERMAL LETHALITY [redacted]

[redacted] Previous subsections of this section have concentrated on concerns relative to the blast and thermal vulnerability of friendly RV's and ABM's. This subsection will discuss the concern of the defense in the effectiveness of ABM in "killing" an RV. The emphasis shifts from "sure safe" criteria to "sure kill" criteria.

[redacted] The definition of the threat RV vehicles and the details of the free field blast and thermal environments of the ABM are the two primary factors that influence the determination of the kill effectiveness of an ABM system. Calculations of blast kill radii have been performed by various groups for the SPRINT ABM against some representative RV threats. The results of these calculations are described in the following paragraphs.

16-34 Blast and Thermal Free Field Environments [redacted]

DNA (L)(3)

[redacted]

16-96

[redacted]

[redacted] Some of the results of these calculations are shown in Figures 16-58 through 16-61 in the form of blast wave parameters at one altitude, e.g., temperature and flow field profile data, at one typical time. These data are essentially self explanatory. They are useful to provide an overview of the environments; however, for detailed vehicle response studies, the principal output of a radiation-hydrodynamics code calculation consists of the radiation-hydrodynamic and field data as a function of radius at a large number of times after burst. These basic data are stored on magnetic tapes (called Usertapes), which allows dissemination of the principal results for use in many studies. This is necessary since blast/thermal effects studies often require that the vehicle be flown through the environment as a function of time, and it is impossible to present environmental data at the vehicle position as a function of time graphically for all possible combinations of vehicles, trajectories, and intercept conditions.

DNA (L-Y)

16-35 ABM Blast Loads on Threat Vehicles (Point Mass) [redacted]

[redacted] The study of ABM blast loads on threat vehicles consisted of computer analyses using a generalized trajectory code, with capabilities of including the free field blast environment provided by the radiation-hydrodynamics Usertapes. A nonrotating spherical earth model with a 1962 atmosphere was used for this calculation. The aerodynamics were computed by Newtonian mechanics, based on the input size and shape data defining a sphere-cone for each vehicle. The reentry conditions for the RV nominal-trajectories were defined in terms of altitude, flight path angle, and reentry velocity. Having computed a flight profile with the specified reentry conditions, the blast fly through runs included trajectory computations that started

[redacted]

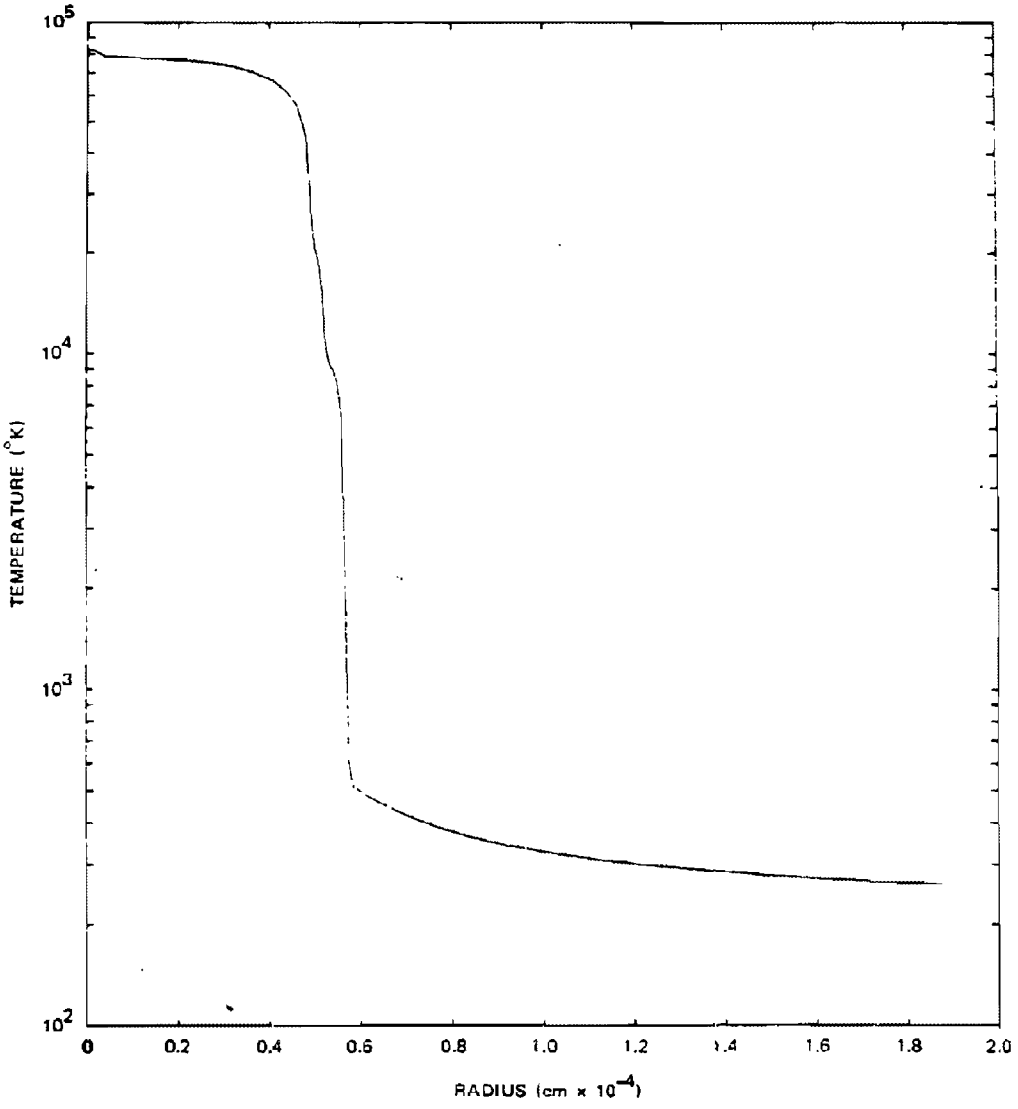

Figure 16-58. [redacted] Computed Temperature Profile, t = 4.64 msec, 30 kilofeet Altitude [redacted]

[redacted]

[redacted]

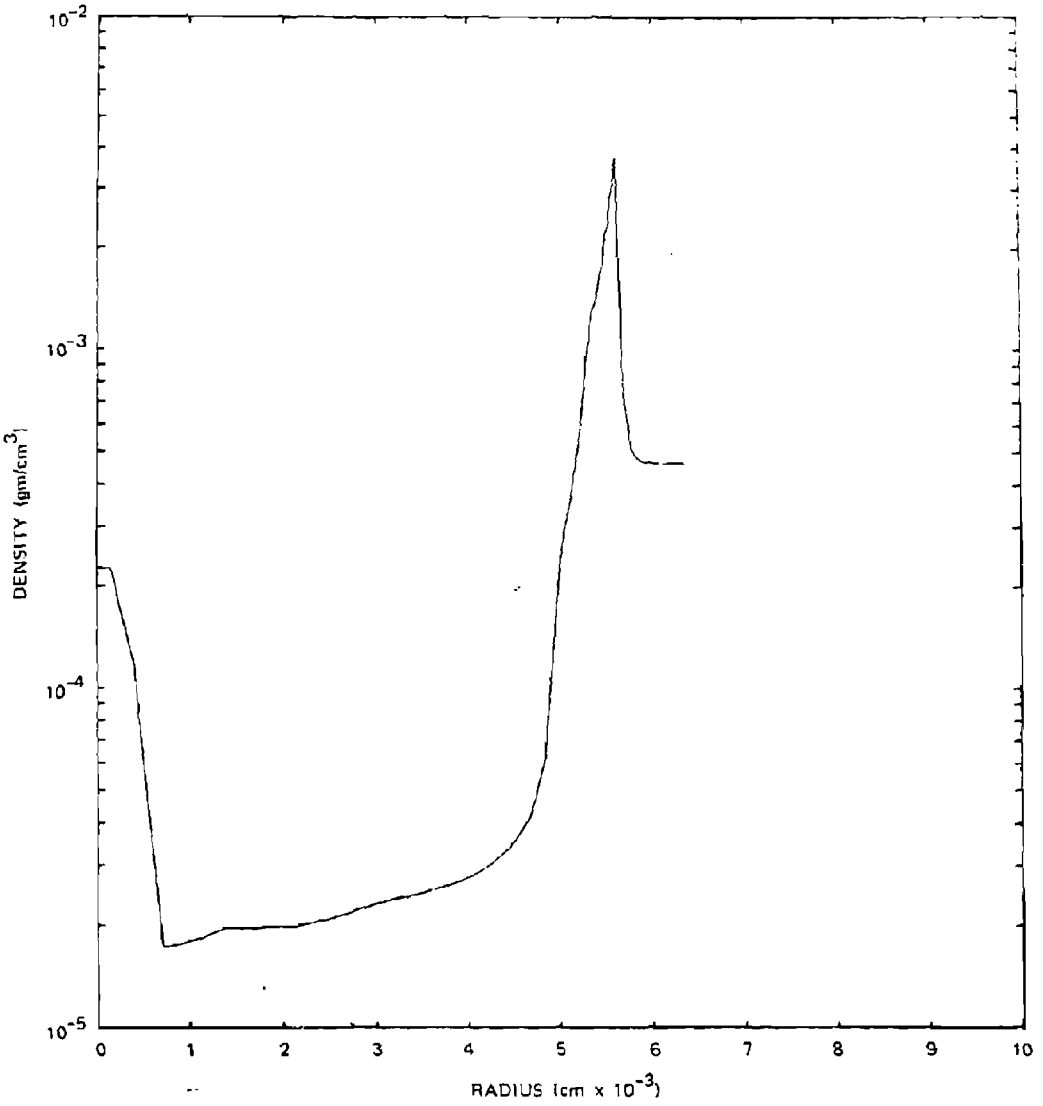

Figure 16-59. [redacted] Computed Density Profile, t = 4.64 msec, 30 kilofeet Altitude [redacted]

[redacted]

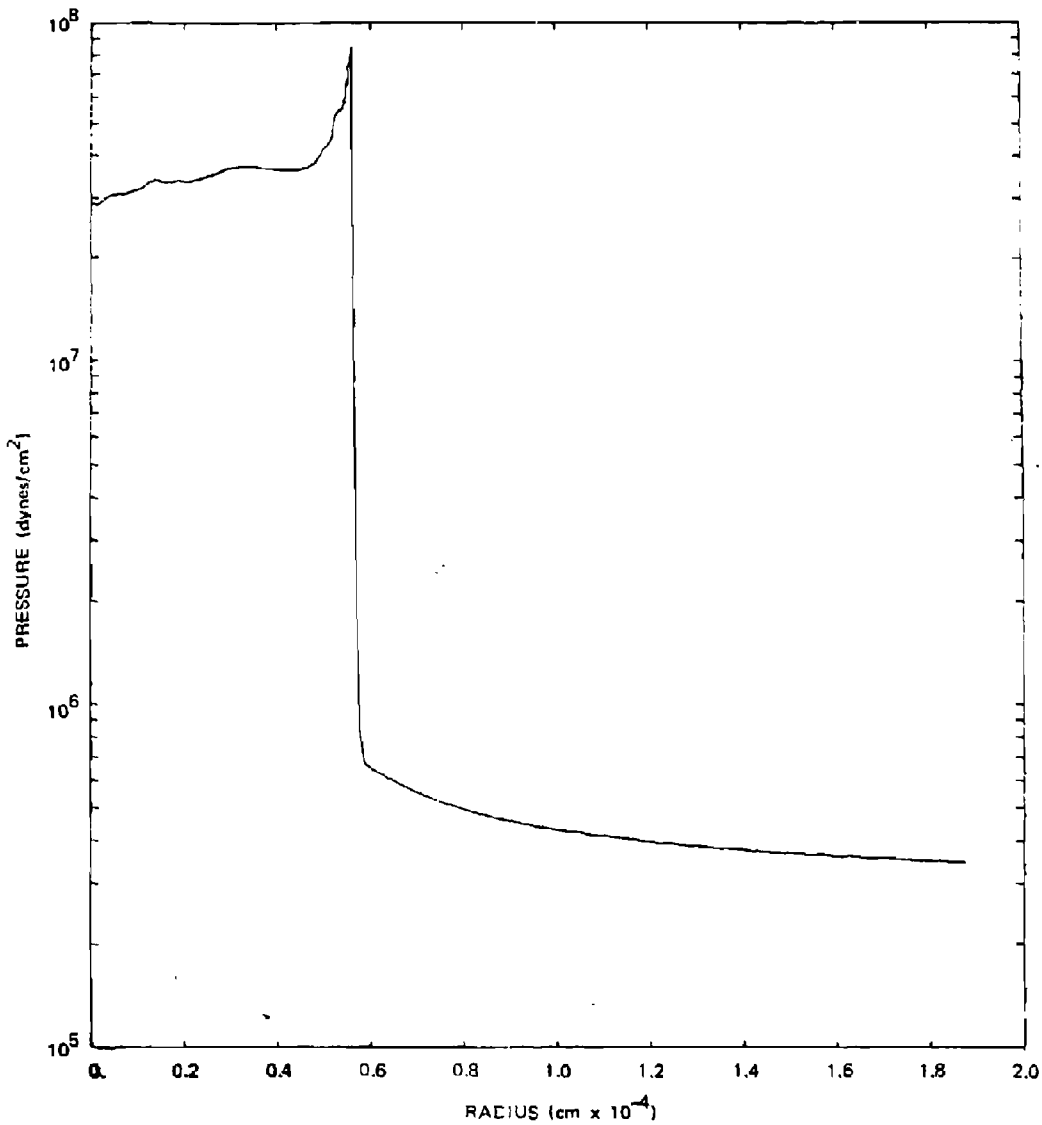

Figure 16-60. [redacted] Computed Static Pressure Profile, t = 4.64 msec, 30 kilofeet Altitude [redacted]

[redacted]

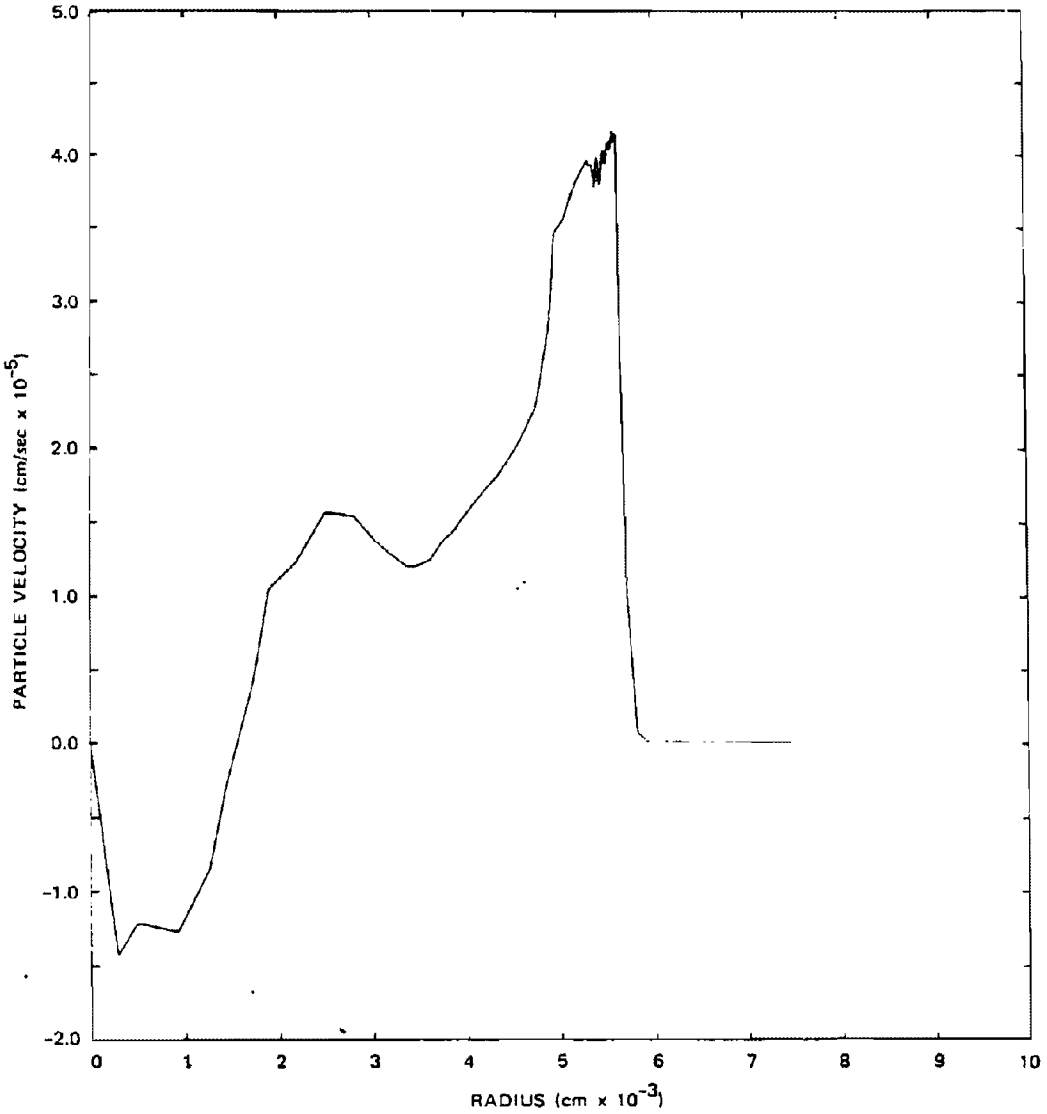

Figure 16-61. [redacted] Computed Particle Velocity Profile, t = 4.64 msec, 30 kilofeet Altitude [redacted]

[redacted]

[redacted]

just prior to shock front intercept and terminated within one second. In the dynamic simulation involving interaction between the rapidly changing blast environment and the vehicle trajectory, the environment changes rapidly; changes are measured in microseconds and in inches. The computed dynamic response, nevertheless, is considered to be a valid model.

[redacted] Figures 16-62 through 16-65 provide a graphic portrayal of a sample blast intercept condition. For this one intercept case, four curves are shown: static overpressure, dynamic pressure, static overpressure impulse, and dynamic pressure impulse. All times indicated are measured from the time of blast wave intercept. Twenty-five milliseconds of data are shown in Figure 16-62 while only the first millisecond is shown in Figures 16-63 through 16-65. The values of dynamic pressure impulse are the results of continuous summation from prior trajectory restart conditions, and the measurements must be read relative to a baseline value at time of intercept.

[redacted] The two impulse curves (Figures 16-64 and 16-65) show the relative importance of the dynamic pressure impulse compared to overpressure impulse at early times. The former builds up and levels off extremely quickly while the latter continues to increase. This characteristic is due to the rapid drop in dynamic pressure, whereas the overpressure, plotted for 25 msec, illustrates a considerably slower decay rate.

16-36 Blast Loads on the RV Threat Vehicle [redacted]

[redacted] The time history of surface loading on a threat reentry vehicles were computed from knowledge of the fly through environments (overpressure, dynamic pressure, relative wind angle of attack) and local vehicle aerodynamics.

[redacted] The time history of loading on any part of the RV is found to be the sum of a very short duration dynamic pressure or drag loading, superimposed on a longer duration overpressure loading. (See Figures 16-62 through 16-65 for typical pressure-time histories.)

[redacted] The spatial distributions of these two types of loads on the vehicle surface generally will differ considerably. Blast overpressure results in uniform pressure being applied over the complete vehicle surface, whereas dynamic pressure loadings vary over the vehicle surface, depending on the structural configuration and intercept geometry. These various relationships can be expressed in the following functional form.

$$P(t) = q(t,\alpha,\theta,\psi,\beta) + \Delta p(t)$$

where

- q = dynamic pressure
- Δp = static overpressure
- α = relative wind intercept angle
- ψ,θ = local angles defining structural geometry
- β = circumferential angle on structure measured from windward ray of intercept.

Newtonian aerodynamics were used to determine the peak values of surface pressure resulting from the dynamic pressure environment for all the reentry vehicles that were studied. The structural configurations all were made up of some combination of a sphere nose cap and a conical body. Most of the early structural lethality studies were concentrated on the aft (or weakest) conical shell bay. Shock-on-shock loads were neglected in the analysis.

[redacted] The surface pressure loading on the conical shell elements is computed from the equation on page 16-106.

[redacted]

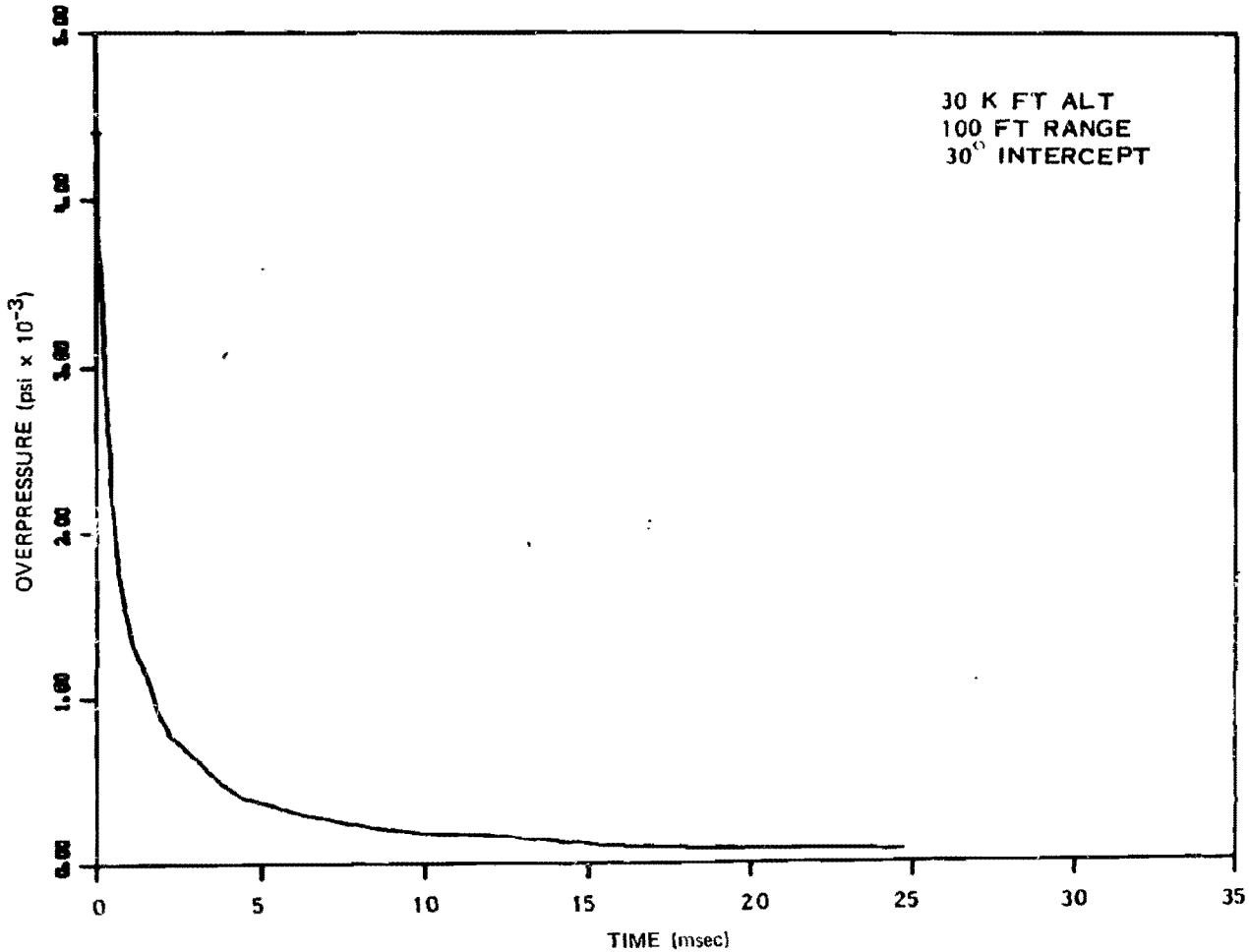

Figure 16-62. [redacted] RV Target A, Static Overpressure as a Function of Time, 30° Intercept [redacted]

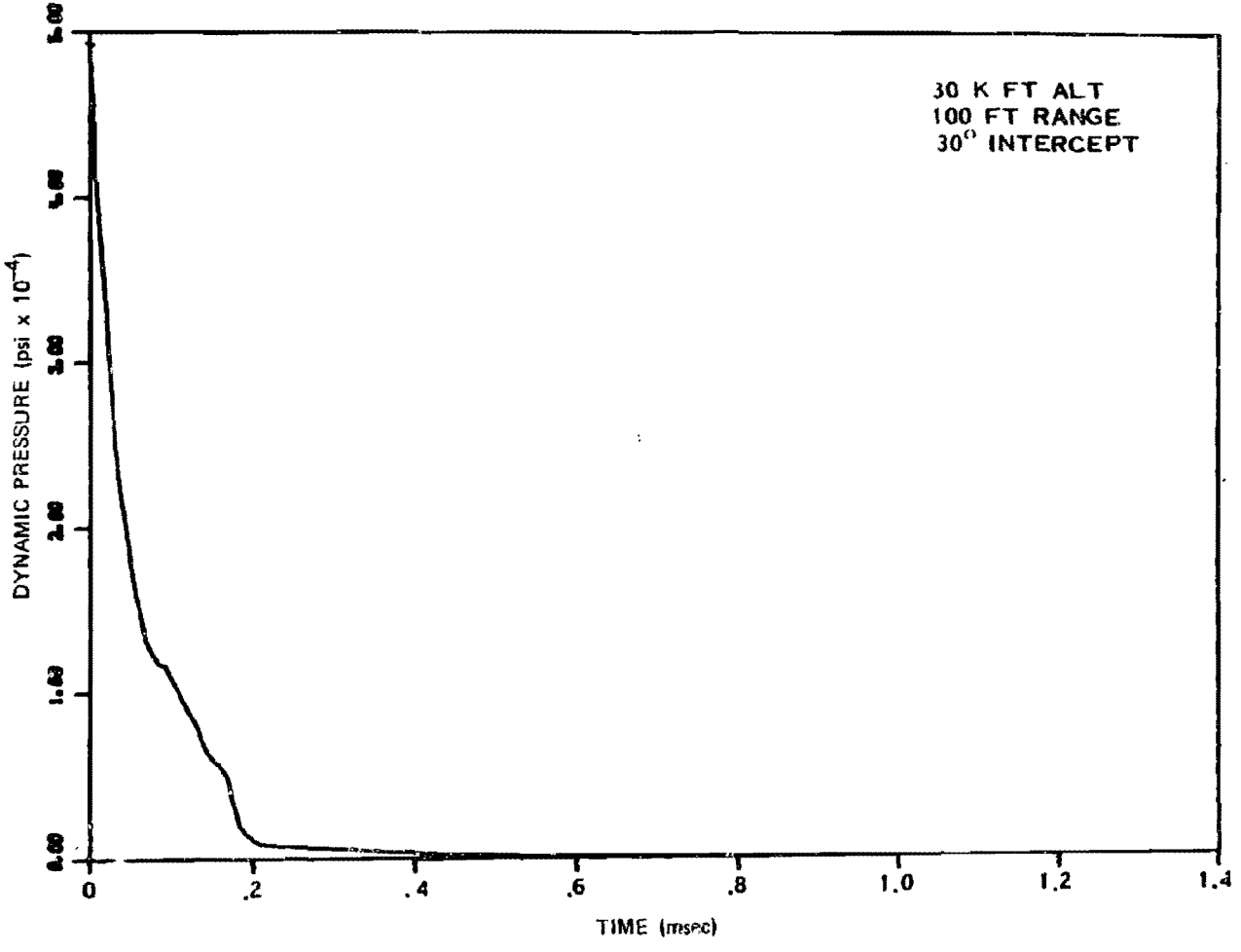

Figure 16-63. [redacted] RV Target A, Dynamic Pressure as a Function of Time, 30° Intercept [redacted]

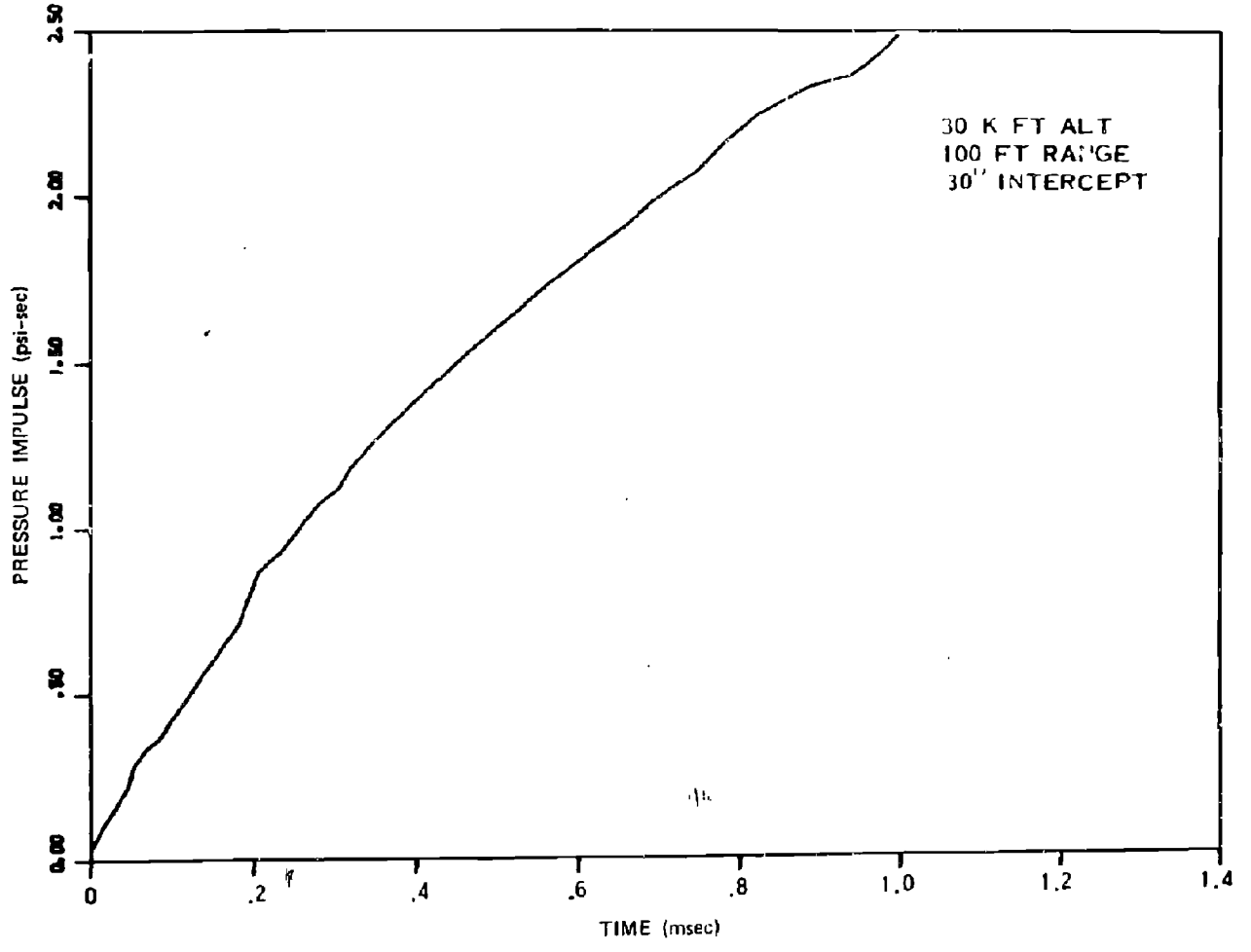

Figure 16-64. [redacted] RV Target [redacted] tatic Overpressure Impulse as a Function of Time, 30° Intercept [redacted]

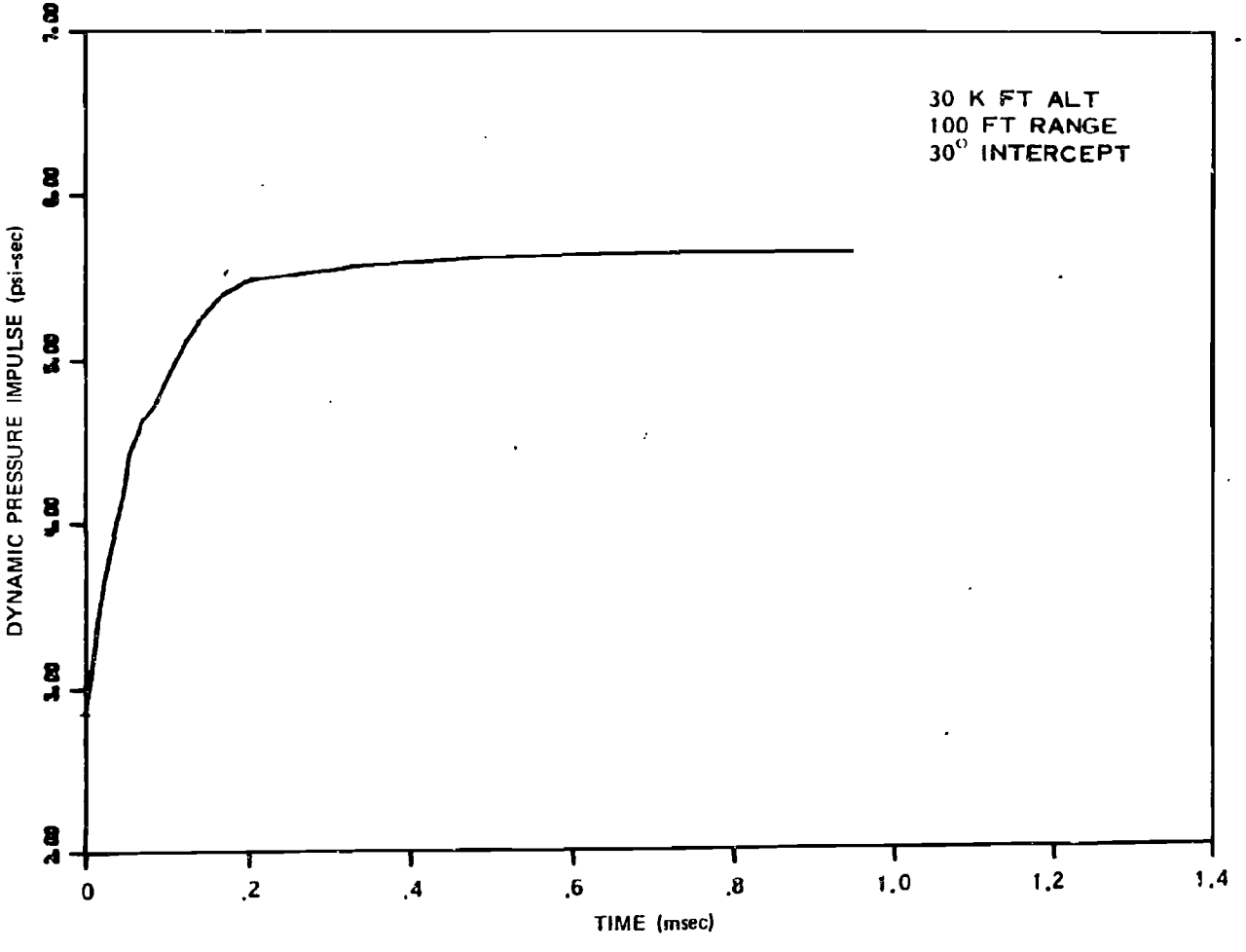

Figure 16-65. [redacted] RV Target [redacted], Dynamic Pressure Impulse as a Function of Time, 30° Intercept [redacted]

$$P(t) = 2q(t)\,(\cos\alpha \sin\theta + \sin\alpha \cos\theta \cos\beta)^2 + \Delta p(t);$$

$$-\beta_{max} \leq \beta \leq \beta_{max}$$

$$P(t) = \Delta p(t) \qquad \beta_{max} \leq \beta \leq -\beta_{max}$$

where

$$\beta_{max} = \cos^{-1}\left\{1 - \left(\frac{\tan\theta}{\tan\alpha}\right)^2\right\}^{1/2}$$

θ = cone half angle

at the windward ray $\beta = 0$, therefore maximum surface pressure is

$$P(t) = 2q(t)\,\sin^2\,(\theta + \alpha) + \Delta p(t),$$

and the impulse at any time, T, at $\beta = 0$ on the cone is

$$I(t) = \int_0^T \left\{2q(t)\,\sin^2\,(\theta + \alpha) + \Delta p(t)\right\} dt,$$

where it is noted that $q(t)$ and $\Delta p(t)$ will not, in general, have the same time dependency.

16-37 ABM Blast Kill Radii

Structural lethality levels of the threat reentry vehicles are evaluated in terms of the blast loadings on the primary structure of the vehicle. In the calculations described here, two categories of lethal loadings were evaluated: (1) Immediate kill, Category 6* and (2) Delayed kill, Category 4. Immediate kill corresponds to load levels sufficient to cause some degree of structural breakup of the metallic subshell. This usually will be accompanied by removal of the ablative covering and severe structural deformation of the remaining subshell. Delayed kill refers to removal of the ablative covering over large portions of the loaded side of the vehicle. In general, this load level also will be sufficient to cause considerable plastic deformation in the vehicle subshell. These definitions of damage are consistent with those recommended by Stanford Research Institute following participation in the HARTS and SPINE experimental programs.

One approach used to relate these damage levels to the computed applied loading involves the establishment of a given damage level in terms of the pressure and impulse of the applied surface loading. The equation for a given damage level in the P-I plane is then defined by the following hyperbolic form:

$$\left(\frac{I}{I_o} - 1\right)\left(\frac{P}{P_o} - 1\right) = 1.0.$$

In this equation I_o and P_o are asymptotes corresponding to values of impulsive loading and static pressure loading necessary to induce the specified damage level. Thus, I_o and P_o must be determined for each structure to be studied and for both damage categories, i.e., immediate kill and delayed kill. Although much of the data are consistent with the value 1.0 on the right-hand side of the equation, some data indicate that a value near 3.0 would be more appropriate.

For a given structural element, the I_o and P_o asymptotes for a given damage level can be related to computed values of impulse and pressure based on some very simplistic structural analysis techniques. For example, modeling the two layered aft bay shell element as a rigid, perfectly plastic cylinder, the uniform externally applied impulse necessary to cause a permanent

* Sometimes referred to as "catastrophic damage."

[redacted]

strain, ϵ, in the shell wall is found to be:

$$I = \left\{2\epsilon(\rho_s h_s + \rho_c h_c)(\sigma_{ys} h_s + \sigma_{yc} h_c)\right\}^{1/2},$$

where

ρ_s, ρ_c = mass densities of shell and ablative cover materials,

σ_{ys}, σ_{yc} = yield stress values of shell and ablative cover materials,

h_s = shell thickness,

h_c = ablator thickness.

Under similar assumptions, the value of uniform static pressure necessary to cause material yielding in the shell wall is

$$P_y = \frac{1}{a}\left\{\sigma_{ys} h_s + \sigma_{yc} h_c\right\}$$

where a = average radius of cylinder. The well-known I_{05} parameter for impulsively loaded shells can be obtained by setting $\epsilon = 0.05$.

$$I_{05} = \left\{0.1(\rho_s h_s + \rho_c h_c)(\sigma_{ys} h_s + \sigma_{yc} h_c)\right\}^{1/2}.$$

[redacted] The next step in lethality evaluation is to relate the I_{05} and P_y load levels to load levels corresponding to the Category 6 and Category 4 damage. For the cylindrical or slightly conical shells representative or the aft bay of most threat RV's, these relationships are empirically established based on results obtained from a large number of experimental tests performed during the HARTS, SPINE, and DRIS Programs. Based on the results of these correlations, the following relations were selected to establish the impulsive and quasistatic load level asymptotes for damage Categories 6 and 4.

IMPULSE ASYMPTOTE

Category 4: $I_4 = I_{05}$

Category 6: $I_6 = 2.5\ I_{05}$

QUASISTATIC PRESSURE ASYMPTOTE

Category 4: $P_4 = 0.7\ \frac{a}{L}\ P_{05}$

Category 6: $P_6 = 1.56\ \frac{a}{L}\ P_{05}$

It should be noted that, in the definition of the quasistatic pressure asymptote, the effect of shell length has been included empirically by including the radius-to-length ratio (a/L).

[redacted] Based on the structural lethality estimates described above and the blast environment loading for the various encounter geometries, lethality estimates of the threat RV's can be made. A sample plot is shown in Figure 16-66; the I_{05} and P_{05} (P_y) asymptotes have been determined, and the curves corresponding to the damage asymptotes I_6, P_6 (immediate kill) and I_4, P_4 (delayed kill) are shown. The dashed line shows the damage curve for immediate kill corresponding to the constant in the pressure-impulse equation being equal to 3.0 instead of 1.0.

[redacted] By combining the loads calculated for the various encounters, in terms of pressure and impulse of peak surface loading, with the damage level plot (Figure 16-66), estimates of loads (in terms of slant range and intercept angle) necessary to incur lethal damage can be made for each vehicle. An example of the superposition of the structure load pressures and impulses on the damage definition curves is shown in Figure 16-67. In the figure, different symbols correspond to loads for various intercept angles, and the number adjacent to each symbol defines the value of slant range *at burst time* to which that particular load calculation corresponds.

[redacted]

[redacted]

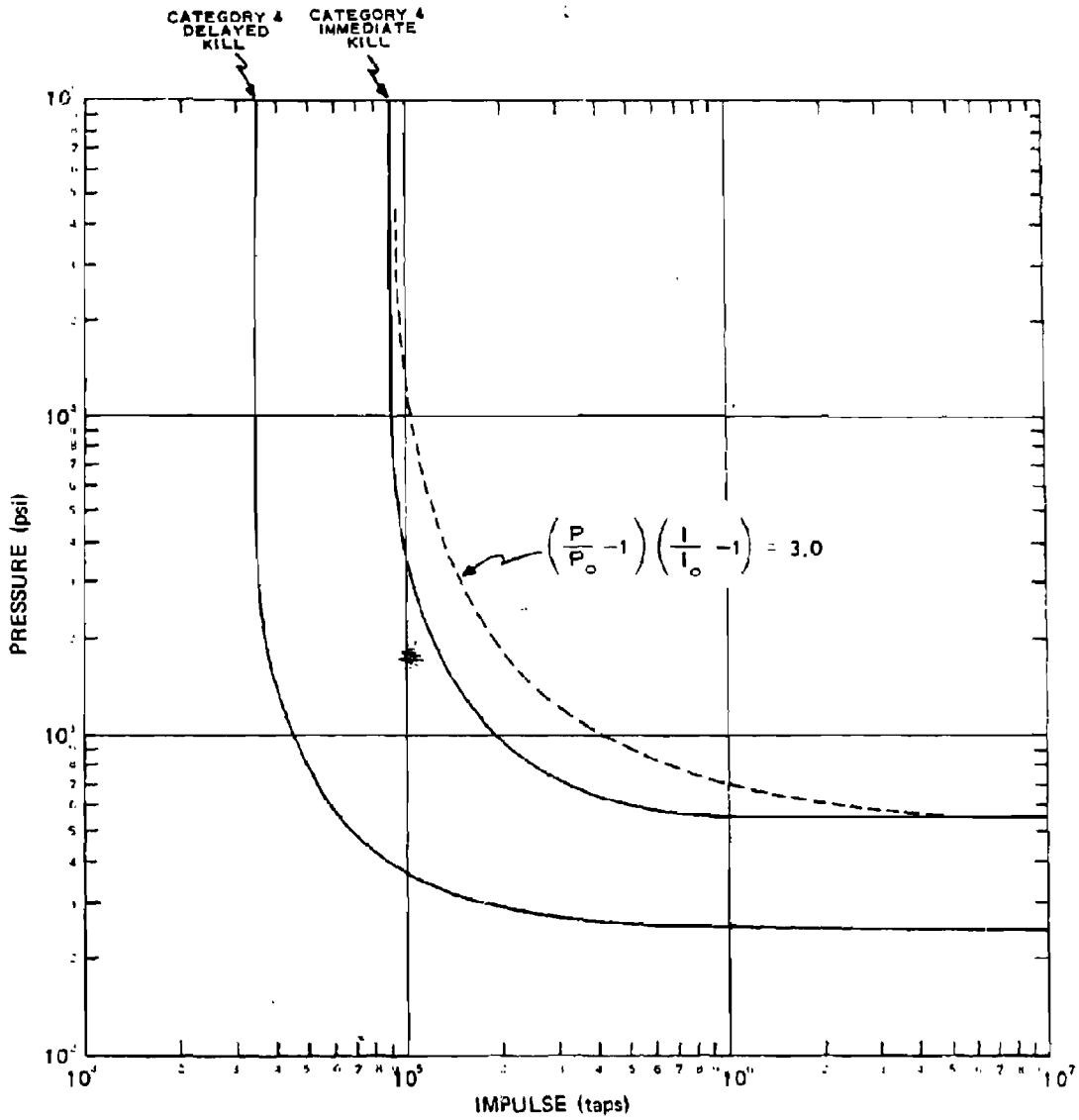

Figure 16-66. [redacted] Pressure-Impulse Damage Levels, RV Target A Configuration, Aft Bay [redacted]

[redacted]

[redacted]

[redacted] By noting where the blast loading points cross the damage level lines in the *P-I* plane, estimates of burst time slant range can be made, for a given intercept angle, that will result in Category 6 immediate kill and Category 4 delayed kill. The following RV kill slant ranges (at burst time) are obtained from the example (Figure 16-67).

DNA (E)(3)

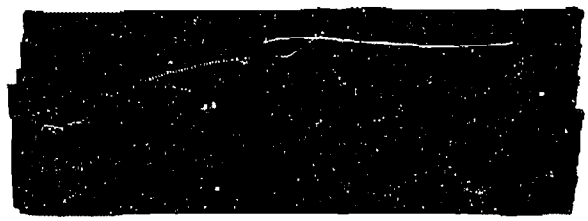

[redacted] It should not be inferred that the *P-I* plot method described above is the only method of analysis that is used to determine blast lethality radii. Some investigators have been successful in computing the structural response of RV's to the derived blast load inputs; however, here experimental data must be used to relate the computed response to damage level, e.g., immediate kill.

16-38 Fireball Thermal Effects on Threat RV's [redacted]

[redacted] Whenever a vehicle intercepts an early time blast wave, it subsequently traverses through (or very near) a high temperature nuclear fireball. Therefore, as one part of a lethality investigation, the thermal effects that would be expected on a threat RV flying through an ABM nuclear fireball would be examined. The calculations for the following example employed the RAD ABLE code. This code uses the free field fireball thermal environment data as read off of a rad-hydro Usertape. The RAD ABLE code formalism assumes that the vehicle flies a constant velocity-straight line trajectory in the vicinity of the burst point. A simplified method is used that accounts for radiation blocking effects in an approximate manner based on detailed stagnation point (rad-hydro) flow field solutions.

[redacted] Figure 16-68 shows a typical history of the ablation rate ($\dot{m}$) and the amount of material ablated

$$\left(m = \int_0^t \dot{m}\, dt \right)$$

for a head on traversal of an ABM explosion at 30 kilofeet altitude. The burst time standoff distance (X_o) of the vehicle was 100 feet in this case.

[redacted] Figure 16-69 summarizes the results of a number of fireball traversal calculations (similar to those illustrated in Figure 16-67) in the form of total mass ablated at fireball exit as a function of initial standoff distance (X_o) and burst altitude. All of these results are for head on ($X_o > 0$) or tail on ($X_o < 0$) intercepts with

[redacted]

[redacted]

DNA
(L)(3)

Deleted

Figure 16-67. [redacted] SPRINT Blast Loads, RV Target A, 30 kilofeet Altitude, Aft Bay [redacted]

[redacted]

[redacted]

DOE
(A)(3)

Deleted

Figure 16-68. [redacted] Ablation Rate and Mass Ablated as a Function of Time for Target A Threat RV [redacted]

[redacted]

[redacted]

[redacted]

Deleted

Figure 16-69. [redacted] Mass Ablated as a Function of Burst Time Standoff Distance for Target A Threat RV [redacted]

[redacted]

[redacted]

[redacted]

no lateral offset (i.e., 0° or 180° intercept angles).

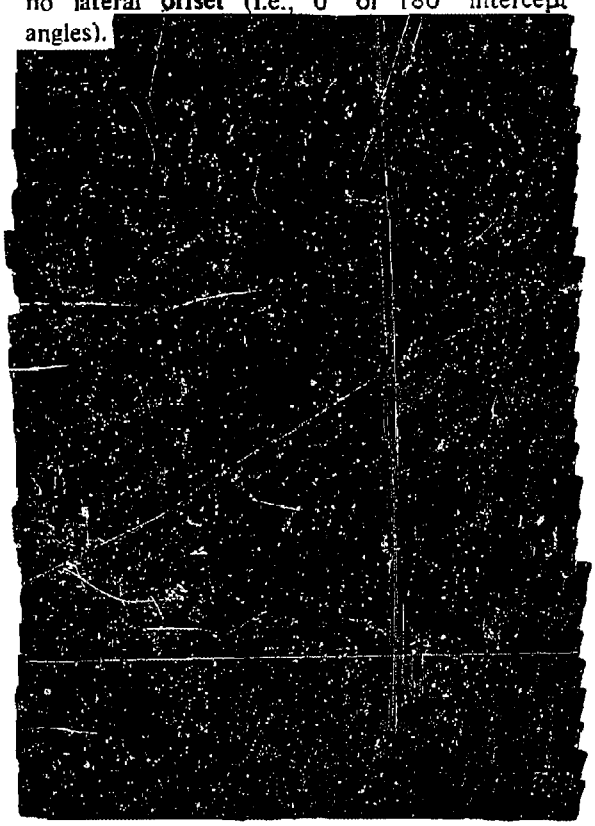

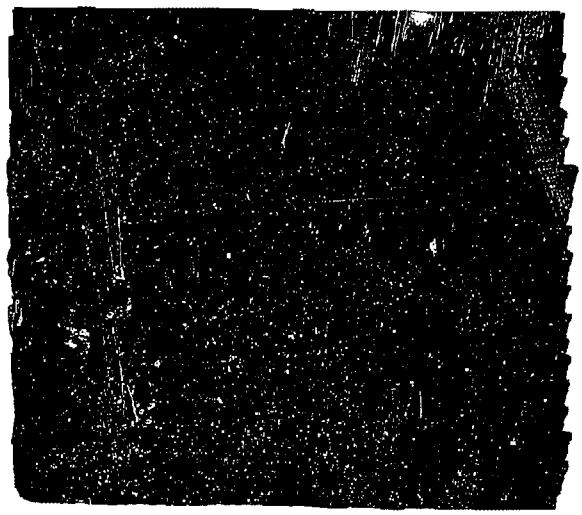

[redacted]

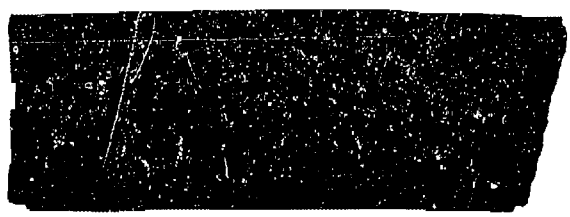

DNA
(b)(3)

[redacted]

[redacted]

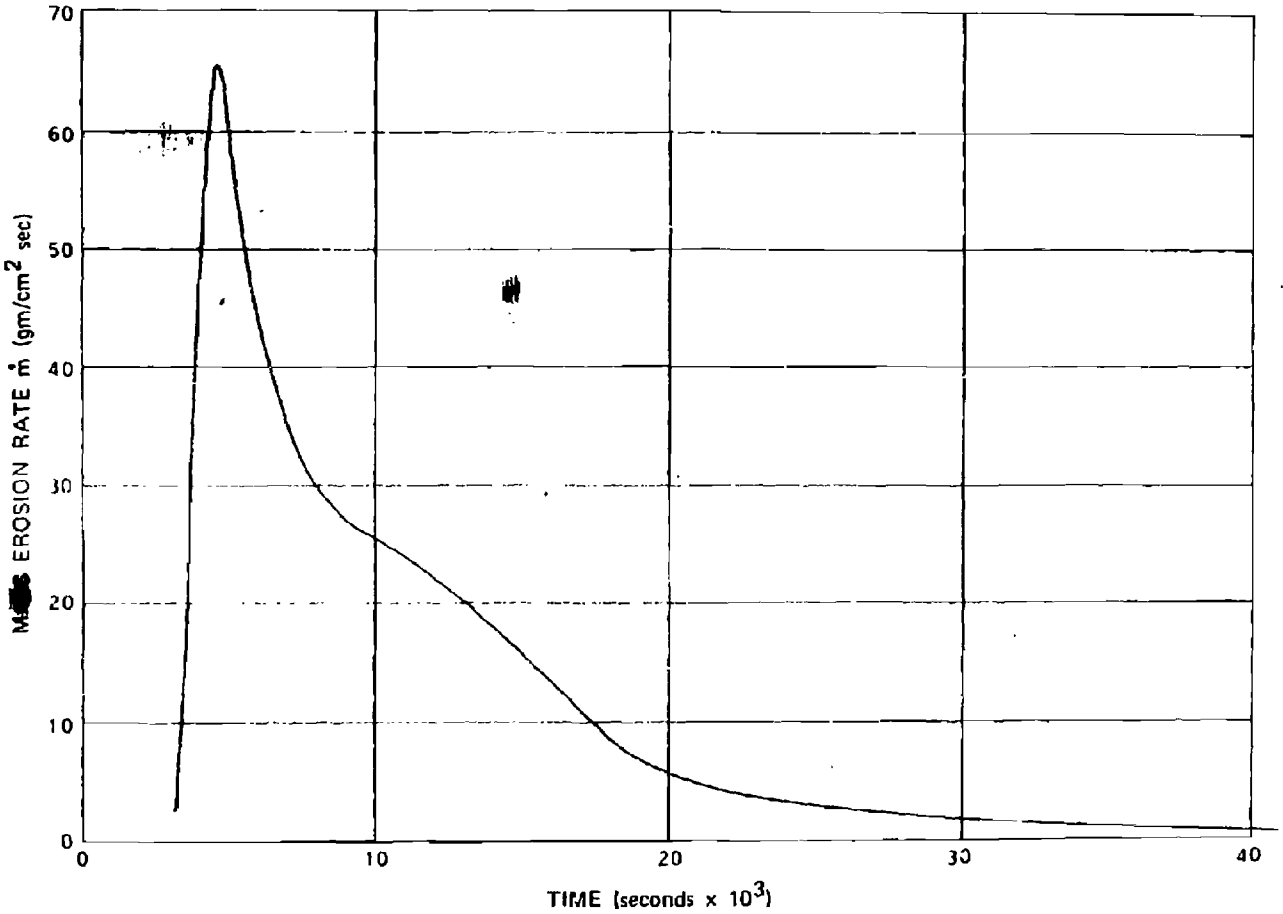

Figure 16-70. [redacted] Typical Traverse-Mass Erosion Rate History [redacted]

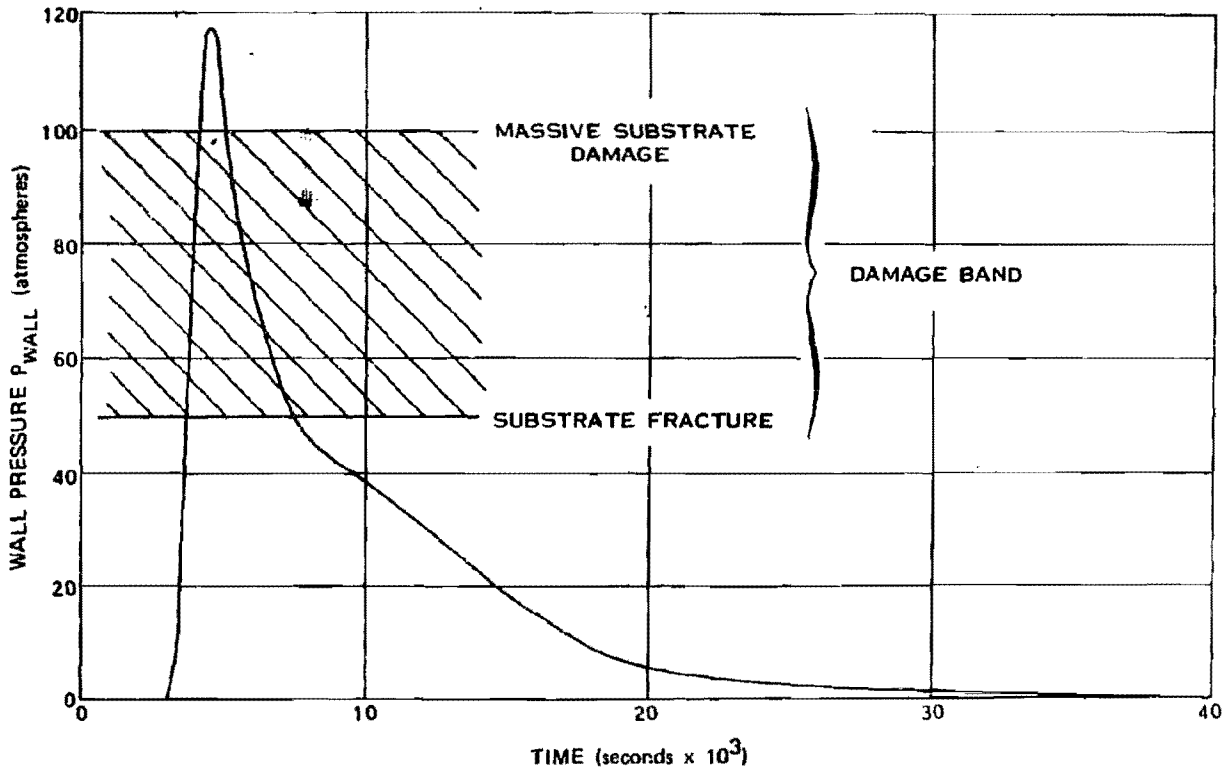

Figure 16-71. [redacted] Typical Traverse-TML History [redacted]

BIBLIOGRAPHY

Baker, W. E., P. A. Westine, and S. Silverman, *Feasibility Study on Simulating the Structural Response of High Altitude Missiles to Blast Loading*, Final Technical Report AMC-66-8, Southwest Research Institute, San Antonio, Texas, 21 January 1966

Barry, Jr., J. M., *Supplementary Data for the AIRS-II Vehicle*, Kaman AviDyne TM-25, AMC-66-15, Kaman AviDyne, Burlington, Massachusetts, July 1966

Bryant, E. J., N. H. Ethridge, and M. R. Johnson, *Response of Drag Type Equipment Targets in the Precursor Zone*, WT1123, Ballistic Research Laboratories, Aberdeen Proving Ground, Maryland, August 1956

Bryant, E. J., and J. D. Day, *Effects of Rough Terrain on Drag-Sensitive Targets*, WT1408, Ballistic Research Laboratories, Aberdeen Proving Ground, Maryland, 9 November 1959

Criscione, E. S., L. J. Mente, N. P. Hobbs, *Vulnerability of Standard Army Interceptor Systems (AIRS I and II) to Nuclear Weapon Blast and Thermal Radiation Effects*, AMC-67-18, Kaman AviDyne, Burlington, Massachusetts, April 1967

Eppes, R., Jr., *Review of Experimental Programs for Blast Intercept and Traversal, and Feasibility of Using a Large Bore Gun Facility for Launching Vehicles for Blast Intercept*, AMSMI-RS-TR-66-12, AMC-66-8, U.S. Army Missile Command, October 1966

Field and Depot Maintenance Manual: Description and Theory of Air Defense Guided Missile XM3E1, TM 9-1410-500-35, June 1960

Field and Depot Maintenance Manual: Description and Theory: Guided Missile System Components Organizational Maintenance Test Station AN/MSM-35 (SERGEANT Artillery Guided Missile System), Notes on Material NOM 9-4935-303-35/2, November 1961.

Field and Depot Maintenance Manual: Schematics: SERGEANT Artillery Guided Missile XM 15 (SERGEANT Artillery Guided Missile System), TM 9-1410-302-35/1, August 1963.

Fraser, W. A., *A Comparison of Experimentally and Theoretically Determined Pressure Distributions on a Blast-Loaded Missile Body*, AMC-67-30, Kaman Nuclear, Colorado Springs, Colorado, June 1968

Hardening Technology Studies – I, LMSC-B130200, Volumes I-IV, Lockheed Missiles and Space Company, Sunnyvale, California, 30 September 1965

Hardening Technology Studies – II [redacted] LMSC-B130391, Volumes I-IV, Lockheed Missiles and Space Company, Sunnyvale, California, 30 September 1966 [redacted]

Hillendahl, R. W., *Theoretical Models for Nuclear Fireballs* [redacted], DASA 1589-1 through 1589-39, Lockheed Missiles and Space Company, Sunnyvale, California, 1965-1966 [redacted]

Joint Engineer/Service Test SERGEANT Guided Missile System [redacted], Volume I, U.S. Army Test and Evaluation Command Technical Report 143, November 1963 [redacted]

Johnson, O. T., R. D. Mayerhofer, and W. J. Schuman, Jr., *Effect of Blast Upon Simulated and Actual Missiles (Project 1.4 Operation Snow Ball)* [redacted] Memorandum Report No. 1655, U.S. Army Ballistic Research Laboratories, Aberdeen Proving Ground, Maryland, May 1965 [redacted]

Johnson, O. T., and R. D. Mayerhofer, *Susceptibility and Vulnerability of the Lance Missile System to Nuclear Effects (Blast)* [redacted] BRL-MR-1862, U.S. Army Materiel Command, Ballistic Research Laboratories, Aberdeen Proving Ground, Maryland, August 1967 [redacted]

Johnson, O. T., R. D. Mayerhofer, *Susceptibility and Vulnerability of the SERGEANT Weapon System to Nuclear Effects (Blast)* [redacted], BRL-R-1324, U.S. Army Materiel Command, Ballistic Research Laboratories, Aberdeen Proving Ground, Maryland, June 1966 [redacted]

Kelley, B. E., *LANCE Automet Control System* [redacted], RG-TR-64-3, U.S. Army Missile Command, Redstone Arsenal, Alabama, 25 June 1964 [redacted]

Lindberg, H. E., et al., *Response of Reentry Vehicle-Type Shells to Blast Loads*, LMSC-B130200, Volume IV-C, Stanford Research Institute, Menlo Park, California, for Lockheed Missiles and Space Company, Sunnyvale, California, 30 September 1965 [redacted]

Lindberg, H. E., and G. E. Sliter, *Response of Reentry Vehicle-Type Shells to Transient Surface Pressures*, AFWL-TR-68-56, Stanford Research Institute, Menlo Park, California, June 1969 [redacted]

Logistic Support Plan for the LANCE Missile System [redacted], (Second Revision), U.S. Army Missile Command, Redstone Arsenal, Alabama [redacted]

Mente, K. J., *Standard Research Systems for Army Interceptors* [redacted] TR-35, Kaman AviDyne, Burlington, Massachusetts, July 1965 [redacted]

Mente, K. J., *Supplementary Data for the AIRS-I Vehicle* [redacted] TM-24, Kaman AviDyne, Burlington, Massachusetts, June 1966 [redacted]

[redacted]

Mikami, K., R. D'Amato, *Criteria for the Effect of Damage on the Operational Capabilities of U.S. Army Missile Systems Volume 2, Lance Missile System*, TR-38, Kaman AviDyne, Burlington, Massachusetts, February 1966

Mikami, K., L. J. Mente, R. D'Amato, *Criteria for the Effect of Damage on the Operational Capabilities of U.S. Army Missile Systems Volume 5, Hawk Missile System*, TR-38, Kaman AviDyne, Burlington, Massachusetts, July 1966

Muller, J. and D. L. Blank, *SLEDGE Program: Phase I, Feasibility Study*, DASA-1988, Martin Marietta Corporation (Orlando Division), Orlando, Florida, September 1967

Nicholson, J. E., and J. J. Rossi, *Pressure-Time Histories of Blast Wave Interactions with a Re-Entry Body*, MC-65-163-R1, Mithras, Inc., February 1966

Nicholson, J. E., E. F. Kent, N. Zessoules, and P. H. McIngvale, *A Ballistic Wind Tunnel Test Technique for Measuring Shock-on-Shock Interactions*, MC-66-142-R31, Mithras, Inc., 4 October 1966

Nuclear Radiation Effects Study on LANCE Directional Control Electronics, RG-TR-64-14, U.S. Army Missile Command, Redstone Arsenal, Alabama, September 1964

Nuclear Weapons Blast Phenomena, Volume I, Source and Development of Blast Waves in Air, DASA 1200-I, DASIAC, Santa Barbara, California, 1 March 1971

Nuclear Weapons Blast Phenomena, Volume II, Blast Wave Interaction, DASA 1200-II, DASIAC, Santa Barbara, California, 1 December 1970

Nuclear Weapons Blast Phenomena, Volume III, Air and Subsurface Explosions, DASA 1200-III, DASIAC, Santa Barbara, California, 1 March 1970

Organizational Maintenance Manual: SERGEANT Artillery Missile XM 15 (SERGEANT Artillery Guided Missile System), Notes on Material NOM 9-1410-302-20, May 1962.

Operation and Field Maintenance Manual: General Support Shop Set (GSSS) (SERGEANT Field Artillery Guided Missile System), Technical Manual TM 9-4935-305-40/1, July 1963.

Operator and Organizational Maintenance Manual: Guided Missile System. Components Organizational Maintenance Test Station AN/MSM-35 (SERGEANT Artillery Guided Missile System), Notes on Material NOM 9-4935-303-12, October 1961.

Operator's Manual: Guided Missile System Components Field Maintenance Test Station AN/MSM-36 (SERGEANT Artillery Guided Missile System) [redacted]. Notes on Material NOM 9-4935-304-10, October 1963.

Operator's Manual, SERGEANT Artillery Guided Missile System [redacted]. Notes on Material NOM 9-1400-300-10, December 1960 [redacted]

Operator and Organizational Maintenance Manual: Air Defense Guided Missile XM3E1 [redacted]. TM 9-1410-500-12, July 1962 [redacted]

Operator and Organizational Maintenance Manual: Emplacement of Hawk Air Defense Guided Missile System [redacted]. TM 9-1400-500-12/1, August 1961 [redacted]

Operator's Manual: Description for Hawk Air Defense Guided Missile System [redacted]. TM 9-1400-500-10, June 1960 [redacted]

Operator and Organizational Maintenance Manual: SERGEANT Missile Trainer, Device 3G52 (SERGEANT Artillery Guided Missile System) [redacted]. Technical Manual TM 9-6920-130-12, January 1963.

Operator and Organizational Maintenance Manual: Four-Wheel Semitrailer-Mounted Guided Missile Launching Station XM 504 (SERGEANT Artillery Guided Missile System) [redacted]. Notes on Material NOM 9-1440-301-12, October 1961.

Parechanian, H. S., et al., *Dynamic Response Investigation of Simulated R/V Structure – Volume II Impulse and Blast Tests* [redacted]. SAMSO TR-69-144, Volume II, McDonnell Douglas Astronautics Company, Santa Monica, California, September 1969 [redacted]

Proceedings: DASA/RAND Hydrodynamic Code Conference [redacted]. DASA-1553, DASA Data Central, General Electric Company, Tempo, Santa Barbara, California, September 1964 [redacted]

Proceedings: DASA Conference on Nuclear Weapons Effects on Re-Entry Vehicles and Interceptor Missiles [redacted]. DASA-1651, DASA Data Center, General Electric Company, Tempo, Santa Barbara, California, September 1965 [redacted]

Proceedings: DASA/AFFDL Shock-on-Shock Interaction Conference [redacted]. DASA-1674, DASA Data Center, General Electric Company, Tempo, Santa Barbara, California, May 196[redacted]

Proceedings: DASA Anti-Ballistic Missile Blast Vulnerability Conference [redacted]. DASA-1744, DASA Data Center, General Electric Company, Tempo, Santa Barbara, California, April 1966 [redacted]

Reck, R. J., and H. E. Lindberg, *Structural Response of the SPINE Reentry Vehicle Models to Blast and Impulsive Loads*, AFWL-TR-67-118, Stanford Research Institute, Menlo Park, California and Douglas Aircraft Company, Santa Monica, California, January 1968

Sachs, D. C. and R. E. Keeffe, *An Investigation of Static Blast/Vehicle Intercept Simulation Methods*, AMC-67-30, Kaman Nuclear, Colorado Springs, Colorado, November 1967

Sachs, D. C., et al., *An Investigation of Dynamic Blast/Vehicle Intercept Simulation Methods*, AMC-67-28, Kaman Nuclear, Colorado Springs, Colorado, August 1967

Schuman, W. J., Jr., *The Response of Cylindrical Shells to External Blast Loading*, BRL Memorandum Report No. 1461, U.S. Army Ballistic Research Laboratories, Aberdeen Proving Ground, Maryland, March 1963

Schuman, W. J., Jr., *The Response of Cylindrical Shells to External Blast Loading, Part II*, BRL Memorandum Report No. 1560, U.S. Army Ballistic Research Laboratories, Aberdeen Proving Ground, Maryland, May 1964

SERGEANT Missile System Operation and Environment Test Program, White Sands Missile Range Technical Memorandum 874, White Sands, New Mexico, June 1961

Sieck, D. W., *Stress Analysis of the Hawk I Missile*, NA 1-55-10, Volumes I & II, Northrop Aircraft, Inc.,

Sliter, G. E., et al., *Warhead Optimization for Structural Kill of Re-Entry Vehicles, Lethality Tests of SPINE Vehicles*, DASA-2215, Stanford Research Institute, Menlo Park, California, July 1969

Sliter, G. E., et al., *Warhead Optimization for Structural Kill of Re-Entry Vehicles*, DASA-2281, Stanford Research Institute, Menlo Park, California, July 1969

SPRINT Blast Survivability Program-Interim Report, AMC-4-69(T), Kaman Sciences Corporation, Colorado Springs, Colorado, June 1969

Studies of Blast Simulation Techniques on Re-Entry Vehicles, AFSWC TDR 62-129, Sandia Corp., Albuquerque, New Mexico, November 1962

Transportation Data for the U.S. Army Hawk Missile System, AR-150, Raytheon Company Aero/Weapons Division, Andover Plant, Andover, Massachusetts, June 1961.

[redacted]

Wells, P. B. and E. A. Bathke, *Theoretical Methods and Computer Codes for Fireball Ablation Effects* [redacted] KN-70-220(R), Kaman Nuclear, Colorado Springs, Colorado, 14 April 1970 [redacted]

Wells, P. B., E. A. Bathke, and D. C. Sachs, *SPRINT Blast and Thermal Environment Calculations* [redacted] KN-70-754(R), Kaman Nuclear, Colorado Springs, Colorado, 2 October 1970 [redacted]

Whitaker, W. A., et al., *Theoretical Calculations of Early Phenomenology – 200 kt at 32 kilometers* [redacted] AFWL-TR-67-68, Air Force Weapons Laboratory, Kirtland Air Force Base, Albuquerque, New Mexico, October 1967 [redacted]

Zvara, J., R. D'Amato, *Criteria for the Effect of Damage on the Operational Capabilities of U.S. Army Missile Systems, Volume I, SERGEANT Guided Missile System* [redacted] TR-38, Kaman AviDyne, Burlington, Massachusetts, February 1966 [redacted]

[redacted]

[redacted]

(This page intentionally left blank)

[redacted]

AD-A955 401

DTIC ELECTE S 2 MAR 1989 D E

Chapter 17

RADIO FREQUENCY SIGNAL DEGRADATION RELEVANT TO COMMUNICATIONS AND RADAR SYSTEMS [redacted]*

[redacted] INTRODUCTION [redacted]

[redacted] Nuclear detonations can affect the performance of radio communication, radar, and other electronic systems that rely on electromagnetic-wave propagation. Usually, the effects will be deleterious although performance may occasionally be enhanced. Applicable nuclear-weapon-induced phenomena are discussed in Chapters 3, 5, and 8. Generally, each system and environmental situation of interest must be examined to determine whether nuclear weapons effects will be important and to what extent they will be important.

[redacted] Electromagnetic waves propagating along paths entirely below 25 kilometers are not likely to be affected by nuclear-produced disturbances. When a detonation occurs below 25 kilometers, the major degradation region is the fireball, which is limited in extent. When a detonation occurs above 25 kilometers, very little of the weapon radiation penetrates below 25 kilometers and the effects that are produced are short-lived.

[redacted] Electromagnetic waves propagating along paths above 25 kilometers can be affected severely by nuclear detonations. If the detonation occurs below 25 kilometers, the effects will be minimal, unless the weapon yield is so large that the fission debris is carried well above 25 kilometers. As the detonation altitude is raised above 25 kilometers, propagation disturbances can cover a major portion of a hemisphere; they may last for hours, and they may interfere with systems that depend on the natural ionosphere to reflect or scatter energy, such as HF systems, seriously. The size of the region affected and the duration of the effects on the system decrease with increasing wave frequency for frequencies above a few megahertz. Effects on wave frequencies above a few gigahertz are limited to the fireball region (a few tens to a few hundred kilometers in diameter).

[redacted] As a result of the very large number of possible interactions between the effects caused by a nuclear burst and the electronic system in its operating environment, problems deriving from the degradation of signals in a nuclear environment are so complex that techniques for calculating signal degradation in nuclear environments are not appropriate for the subject material of this chapter. Such problems are performed most effectively with the aid of computers, using codes such as RANC 4 (see bibliography). Methods for computation of system performance by hand have been devised, but, in general, they are lengthy, even though many simplifications must be included. Some such computations for determining absorption are described in Chapter 8. Analyses of generic systems for selected burst conditions are useful for determining the nature and order of magnitude of effects; however, generalizations from such analyses are not warranted.

* [redacted] Although the English system of units for measuring distance is given priority throughout most chapters of this manual, wavelengths and other dimensions dealing with electromagnetic wave propagation usually are given in the metric system. Therefore, in this chapter and in Chapter 8, the metric system is used for distance dimensions. Conversion factors from the metric system to the English system are provided in Appendix B.

[redacted]

89 3 02 033

This document has been approved for public release and sale; its distribution is unlimited.

[redacted]

As discussed in Chapter 8, considerable uncertainty exists in the prediction of the effects of nuclear weapon bursts on electromagnetic propagation, particularly for burst or propagation conditions different from those for which test data have been obtained. While in general the prediction of weapon effects is more difficult in a multiple-burst environment than for a single burst, system performance may be relatively insensitive to burst parameters; for such cases simple models of the disturbed environment can be used for analysis.

SECTION I
DEGRADATION MECHANISMS

Nuclear weapon effects on electromagnetic propagation are grouped into three degradation mechanisms in this section: attenuation, which defines the change in the amount of electromagnetic energy reaching a given location; interference, which defines the level of noise competing with a received signal; and distortion, which defines the change in information content of a received signal.

ATTENUATION

Attenuation of signals in a nuclear environment derives principally from the phenomena of absorption, scattering, and beam spreading (small angle scattering, i.e., differential refraction or defocusing). In some instances, generally at times after detonation in excess of a few minutes, scattering and beam spreading can be the more important phenomena. For most cases, however, attenuation caused by absorption is regarded as one of the most important effects caused by nuclear detonations (see ELECTROMAGNETIC PROPAGATION IN IONIZED REGIONS in Chapter 8), and it is one of the best understood and most predictable of the effects. There are three principal atmospheric absorption regions caused by a nuclear detonation: the fireball, a region around the fireball, and the D-region of the ionosphere (approximately 50 to 80 km altitude). Figure 17-1 illustrates the absorption regions for several burst altitudes and times after burst.

17-1 Fireball Absorption

The fireball is generally the most intensely absorbing region. Significant absorption within the fireball can last tens of seconds for frequencies less than about 10 GHz (see paragraph 8-6). Fireball sizes vary from less than a kilometer for small-yield surface bursts to several hundred kilometers for large-yield, high-altitude bursts. The fireball size and location as a function of burst parameters can be determined from Table 8-2 and Figures 8-16 and 8-38. The amount of signal attenuation caused by absorption of signals propagating through the fireball can be determined from Tables 8-3 through 8-7. For many cases of interest in analyzing a system, the duration of attenuation due to fireball absorption is determined by the rise rate of the rising fireball rather than the length of time the fireball remains absorbing.

17-2 Absorption in the Region Around the Fireball

When the fireball is below the D-region, delayed gamma rays emitted from fission debris in the fireball cause ionization and thus absorption in a small region surrounding the fireball (see paragraph 8-8). The size of the region depends on the burst and propagation parameters; it can extend beyond the fireball for tens of kilometers for frequencies below a few gigahertz. Estimates of signal attenuation can be obtained from Figures 8-42 through 8-48 (Problem 8-6).

When the fireball is above the D-region, most of the absorption outside the fireball occurs in the D-region as discussed below.

QUALITY INSPECTED 4

[redacted]

UNANNOUNCED

For
ed
tion
By
Distribution/
Availability Codes
Dist | Avail and/or Special
A-1

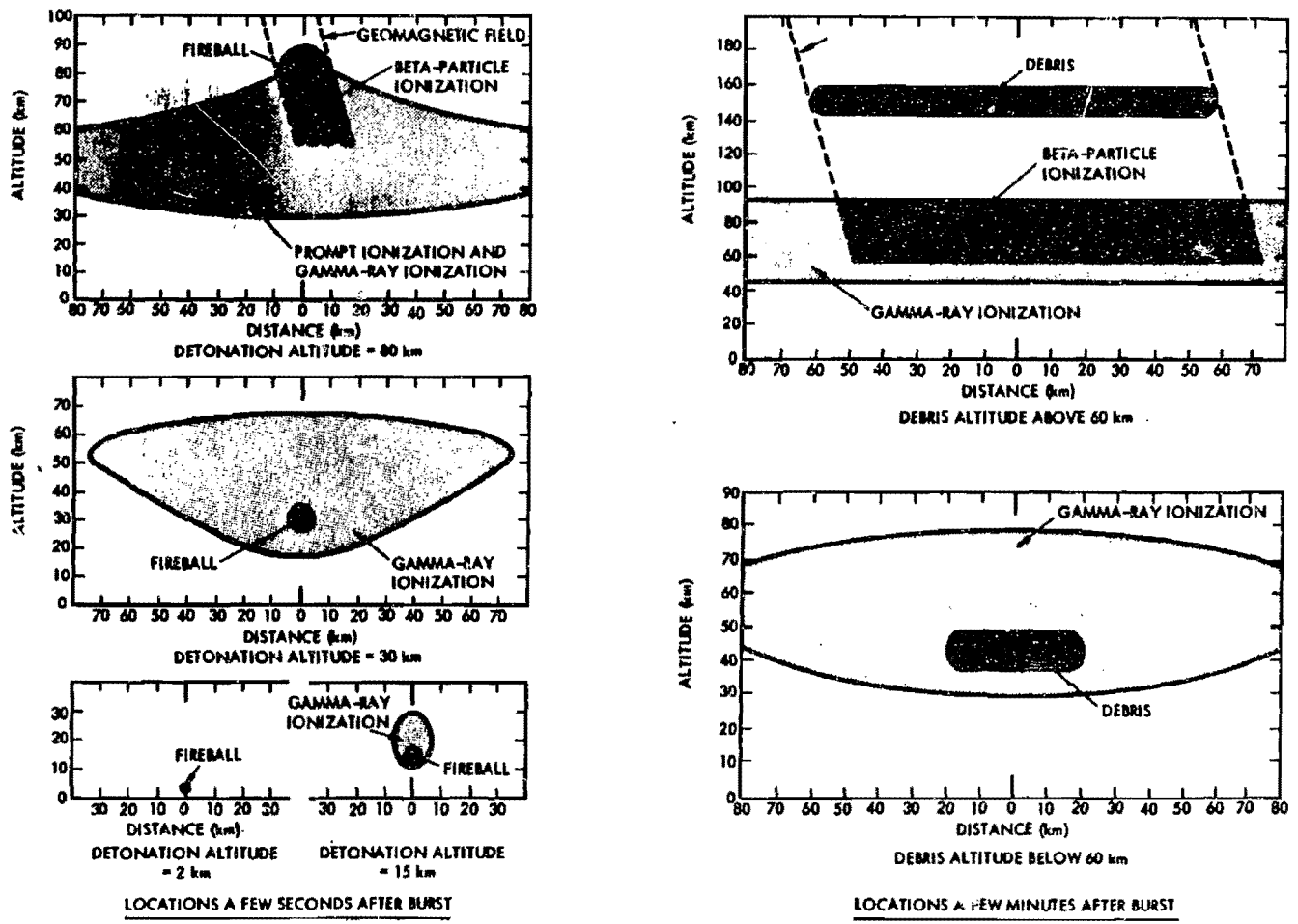

Figure 17-1. Approximate Locations of Ionization Causing Absorption

17-3 D-Region Absorption

The largest and most persistent absorption region caused by nuclear detonations generally occurs in the D-region. Depending on detonation altitude and weapon yield, both prompt radiation (X-rays and neutrons) and delayed radiation (beta particles and gamma rays) can ionize the D-region and cause absorption (see paragraphs 8-2 through 8-8). For frequencies above a few megahertz, absorption in the D-region is related inversely to the square of the frequency at which the system operates. The extent of D-region ionization caused by prompt radiation depends on the detonation altitude. The size of the ionized region increases from a few tens of kilometers for detonations below the D-region to thousands of kilometers for detonations above several hundred kilometers. The duration of significant absorption caused by ionization resulting from prompt radiation varies from less than a second for 1 GHz and nighttime conditions to tens of minutes for 10 MHz and daytime conditions.

Delayed gamma rays are an important D-region ionization source when the fission debris is above about 25 kilometers. The extent of the ionization increases with debris altitude. Large regions (thousands of kilometers in diameter) are affected when the debris is above several hundred kilometers in altitude. The larger ionization regions are primarily of importance for frequencies below a few hundred megahertz. Some of the Compton electrons produced in the burst region by gamma rays are guided by the geomagnetic field and produce ionization in the D-region on the opposite side of the magnetic equator (see paragraph 8-3). The resulting absorption is less intense than that due to gamma ray ionization in the burst region, but it can be important for frequencies in and below the HF band.

Beta particles ionize the D-region when the fission debris is above about 60 kilometers. As illustrated in Figure 17-1 and discussed in paragraph 8-3, the size and location of the region ionized by beta-particles depend on the size and location of the debris region and the direction of the geomagnetic field. For each debris region above 60 kilometers there are two beta-particle absorption regions; one in the burst locale and one on the opposite side of the geomagnetic equator. At early times after burst when the debris region is relatively small (less than a few hundred kilometers in radius), beta-particle ionization can cause significant absorption for frequencies below a few gigahertz. At later times, when the debris is dispersed over large regions, the ionization is primarily important in causing absorption for frequencies below a few hundred megahertz.

Estimates of D-region absorption caused by prompt and delayed radiation can be obtained from Figures 8-40 through 8-51.

17-4 Absorption of Noise

Receiving system performance also may be affected if noise normally reaching the system via the ionosphere is absorbed. The noise level of some systems is determined by external sources (atmospheric noise, cosmic noise, or interfering signals from other sources) that propagate energy through the atmosphere. Both the desired signal and the undesired signal may be attenuated. The resulting signal-to-noise ratio depends upon the exact location of terminals, noise source, and weapon-produced ionization.

17-5 Attenuation by Scattering and Beam Spreading

Attenuation by absorption results when energy from a radio wave is deposited in the propagation medium in the form of heat. A different class of attenuation is that due to scattering of radio energy from the desired direction to other (possibly widely different) directions. A fundamental requirement for scattering is that

[redacted]

the refractive index of the medium be structured. Thus, regions of high electron-density gradient (e.g., fireball boundaries and various regions containing plasma striations) are of prime concern.

[redacted] Characteristics of the electron-density structure that are important are its strength (i.e., the magnitude of spatial variation) and its size or scale. Generally, the greater the variation (especially in the integral of electron density along the line of sight), the greater the portion of energy scattered, and, the smaller the structure, the wider the scatter cone. The scale, relative to two parameters of the operating system, the wavelength and the Fresnel-zone radius, determine the nature of the attenuation effects associated with this scattering.

[redacted] As a practical matter, the environments of concern seem to divide naturally, leading to a useful separation of effects into attenuation by scattering and attenuation by signal reduction through beam spreading. The former, loss by scattering, implies scattering at angles that are substantially larger than the system beamwidth. The latter, beam spreading, implies scattering, defocusing, or diffraction at angles comparable to or less than the system beamwidth.

[redacted] The simplest effects to visualize are those due to structure that is large compared with both the wavelength and the Fresnel zone. These effects are refractive in nature and can be understood on the basis of ray optics. Simple ray bending may apparently displace a radio source from an antenna beam, resulting in attenuation, unless the beam is made to track the source. A patch of enhanced plasma will cause such ray bending in its border regions. In the mid-region of such a patch, the ray bending is minimum, but the radio energy density is actually decreased by defocusing, even if the source is kept in beam center. In effect, the plasma patch acts as a radio-frequency diverging lens. A region of lower-than-average electron density, on the other hand, will act as a converging lens.

[redacted] A region of plasma-density irregularities (e.g., fireball striations) may act as an ensemble of diverging and converging lenses, producing both attenuation and enhancement of signals. If the scale of the irregularities is small enough to be comparable with the system Fresnel zone at the range of the plasma, then they are too small to produce lenslike focuses, and the propagation must be treated by diffraction theory. The result regarding signal strength, however, still is to produce positive and negative fluctuations. This diffractive scatter can occur even if the irregularities are too weak to produce significant focuses or defocuses; the situation may be viewed intuitively as multipath propagation.

[redacted] As the irregularity scale becomes smaller, the scatter cone becomes wider and can exceed the system beamwidth. In this case, not only will there be fluctuations in signal strength but also a net attenuation on the average. This net attenuation will occur whether the antenna achieves its directivity by employing a reflecting aperture (e.g., a dish antenna) or from phased elements distributed on the aperture (i.e., a phased array).

[redacted] In the extreme, when the plasma structure becomes comparable in scale to the system wavelength, the radio energy is backscattered and lost to any receiver on the opposite side of the structured plasma, regardless of its antenna beamwidth. In this case, the attenuation effect is virtually indistinguishable from that due to absorption. Usually, the intensity of very small scale size fluctuations is small so that, although backscatter does occur — leading to radar clutter (paragraph 8-12) — such a small fraction of the energy goes into this phenomenon that the resulting attenuation of the primary beam is quite small. The presence of radar clutter does not necessarily imply that targets cannot be seen on the other side of the scattering region.

[redacted]

17-6 Effects of Reflection

In addition to absorption, another important cause of signal attenuation in the HF band is loss of reflection from the E- and F-regions of the ionosphere (see TRAVELING DISTURBANCE in Chapter 8). Signals that normally would be returned to the receiver continue on into space. Conversely, burst-induced ionization in the E- and F-regions of the ionosphere may increase the electron density and allow reflection of signals at higher frequencies than normal.

INTERFERENCE

17-7 Noise

Thermal noise radiated by the hot fireball can produce receiving-antenna noise temperatures of several thousand degrees Kelvin for tens of seconds to several hundred seconds, depending upon the fireball altitude. A system normally will not experience problems from fireball noise unless the fireball is large enough that the antenna beam is essentially filled by the fireball and that absorption outside the fireball is significant at the frequency of interest.

Synchrotron noise may be associated with nuclear bursts that take place at very high altitudes or if the weapon debris rises to very high altitudes. The effect is noticeable only if a large number of electrons are trapped in the geomagnetic field outside the atmosphere. Only very sensitive HF receiving systems with upward-pointing antennas are likely even to detect synchrotron noise, but it may persist for weeks.

17-8 Reflection, Refraction, and Scatter

Reflection and refraction of electromagnetic (EM) waves can cause unwanted signals to reach the receiver. These signals can mask and distort desired signals. Multipath interference occurs when a desired signal travels two or more paths. The result is severe fading and distortion. HF and VHF systems operating in a nuclear-burst environment may experience unusual multipath conditions due to E- and F-region ionization, causing highly anomalous propagation modes with consequent signal distortion. Reflection from fireball surfaces may, under certain conditions, cause multipath in the UHF band.

Signal scattering can occur as a result of irregularities in electron density. A radar signal scattered back to the receiver may mask desired target returns or may produce a false target. Signals from other transmitters may scatter into a receiver, increase the noise level, and mask desired signals. In general, scatter in and above the HF band is caused by fireballs and by beta-particle ionization regions.

SIGNAL DISTORTION

Propagation media disturbances may change the characteristics of a signal and degrade system performance. Frequency shifts, time delays, angle-of-arrival deflection, and polarization rotation are all possible effects (see PHASE EFFECTS in Chapter 8). The results may include reduction of effective system bandwidth and increased error rates when the signal is processed by the system.

Range and angular errors may be induced in radar systems by time delay and bending of the propagation direction. Generally, D-region ionization sufficient to produce signal distortion also will produce large absorption levels. At altitudes above the D-region, signal distortion (particularly range and angular errors) may occur at low or moderate absorption levels. Irregularities in electron density in and above the upper part of the D-region can change the direction of propagation and cause fluctuations in the angle of arrival of received signals (scintillation).

The significance of a change in signal characteristics depends critically on the signal

processing employed and on the system mission. The effects are most likely to be significant in systems that feature extreme accuracy and sensitivity, and depend upon sophisticated waveform processing.

SECTION II
SYSTEM CHARACTERISTICS AND EFFECTS

Nuclear environments related to the various types of military engagements affect the propagation medium and noise production differently. A detailed analysis of nuclear effects depends on specifying all of the nuclear burst and system parameters, and is beyond the scope of this chapter. However, the kinds of effects and their spatial and temporal extent can be illustrated with a limited number of examples. These examples suggest the general nature of the nuclear effects for most practical cases and will assist in identifying critical system parameters.

VLF AND LF SYSTEMS

17-9 VLF and LF Propagation

Propagation at frequencies below about 1 MHz, i.e., in the VLF, LF, and part of the MF bands, is controlled by the D-region of the ionosphere. Under natural conditions, there is a distinct difference between propagation of VLF (10 to 30 kHz) and LF (30 to 300 kHz). At VLF, the distance between the earth and the ionosphere is only a few wavelengths, and it is natural to think of these two boundaries as the walls of a waveguide. The received field is then the sum of the normal modes that have propagated to the observation point. The quantities of interest are the excitation factor (the relative energy supplied to the mode by the transmitter), the attenuation rate (loss of energy per unit distance), and the phase velocity of each mode. If the ionosphere is less than about three wavelengths from the ground, the modes are almost equally excited, and the most important mode is always the mode of least attenuation. Lowering the ionosphere (which results from weapon-produced ionization) will usually increase the attenuation rate, and will increase the energy in the propagating modes. The effect on the total field strength depends on the trade off of these two effects. The different modes have different phase velocities, so if two modes are of almost equal strength, their sum will vary as a function of distance. The sum will be large where the two components are in phase and small where they are out of phase.

At frequencies above 30 kHz, the distance between the earth and the ionosphere is many wavelengths, and it is more convenient to think of the total field strength as the sum of the direct (or ground) wave, the first-hop skywave (energy reflected once from the ionosphere), the second-hop skywave (energy reflected twice from the ionosphere), etc. This is the same concept used at HF, but there is an important additional consideration. At LF, the downcoming skywaves diffract significantly around the curvature of the earth, so it is necessary to include them at distances that would be considered geometrically impossible at HF.

In the VLF and LF bands, the noise at the receiver is assumed to have an atmospheric source. It therefore depends upon season, time, and geographic location.

17-10 Effects of Nuclear Bursts on VLF and LF Systems

The effects on propagation of VLF and LF signals caused by nuclear detonations result from ionization produced in and below the D-region (see IONIZATION AND DEIONIZATION, Chapter 8). Usually the effects are caused by free electrons, but significant absorption also may result from ions. Depending on weapon type and burst location, prompt radiation (neutrons and X-rays) can produce D-region ioniza-

[redacted]

[redacted] tion in the general vicinity of the burst. Significant D-region ionization also can be produced in the burst region by delayed gamma rays from fission debris if the debris is above 25 kilometers altitude and by beta particles if the debris is above 60 kilometers altitude. Beta particles and Compton electrons (produced by gamma rays) can cause significant ionization in the region magnetically conjugate to the debris location. Under certain circumstances, ionization at locations very distant from the burst may result from neutron-decay betas and the dumping of trapped radiation.

[redacted] Blackout or complete disruption, of VLF and LF communication systems usually requires burst-produced ionization to affect a large portion of the propagation path. Since the propagation paths are typically many thousands of kilometers long, high-altitude detonations or multiple detonations dispersed over the propagation path are required to produce the necessary ionization. Degradation can be caused by reduction of signal amplitude and rapid changes in signal phase. The significance of phase changes to system performance depends critically upon the system characteristics.

[redacted] Usually the greatest change in signal amplitude and phase from preburst conditions occurs for nighttime conditions; however, there are little day-night differences for large weapon yields. Effects are not uniform over the frequency band. When there is sufficient ionization to cause low reflection altitudes, propagation near the lower end of the LF band appears to suffer the least degradation. When the reflection boundary is near normal height but diffuse, propagation near the lower end of the VLF band appears to be affected least. In some cases the ionization distribution along the propagation path is such that low reflection altitudes occur over part of the path and a diffuse reflection boundary over the remainder.

[redacted] In general, the longer the path length, the greater the probability of circuit degradation. Although there is a small probability that the signal-to-noise ratio may be increased, it will generally be reduced. Severe signal reductions can persist for hours, depending on the extent and kind of weapon-produced ionization. Equal reduction of signal and atmospheric noise may not influence system performance until the reduction in noise is so great as to render local receiver noise a determining factor.

[redacted] Phase shifts up to about 1,000 degrees per burst at rates as high as 1 degree per microsecond may occur for each burst. The rate of recovery is usually a few degrees per second. Systems that cannot follow these phase shifts will lose synchronization. Time to reestablish synchronization is very difficult to estimate, but may require tens of minutes or longer.

[redacted] The general effects of nuclear bursts on VLF and LF systems may be summarized as follows:

1. The most severe signal degradation and system outages of longest duration occur for widespread debris environments. This environment may be caused by a large-yield weapon detonated at high altitudes or by multiple detonations distributed over a large area.
2. An ionization impulse resulting from a very-high-altitude (even though low yield) detonation affects a wide area and may degrade LF system performance for tens of minutes. The propagation effects are greater at night than during the day.
3. Single detonations at altitudes below several hundred kilometers produce less severe signal degradation, unless the burst is close to the propagation path. Detonations near the surface (below about 30 km) have the least effect on VLF and LF propagation.

[redacted]

[redacted]

17-11 Spread-Debris Environment [redacted]

[redacted] Following nuclear bursts, debris can be spread over a large area if weapons are detonated above about 50 kilometers at dispersed locations. By assuming the debris to be uniformly distributed, a relatively simple model that provides useful estimates of propagation effects resulting from several bursts is obtained. The ionization affecting VLF and LF propagation is caused by beta and gamma radiation from the fission debris. This ionization can be characterized by the fission yield per unit area and the average age of the debris. Assuming the detonations occur within a few minutes of each other, a parameter w can be defined by

$$w = \frac{W_F}{A} \frac{1}{t^{1.2}},$$

where W_F/A is megatons of fission yield per square kilometer, and t is time after attack in seconds. A value for w of 10^{-7} represents a very severe attack environment. Values of w between 10^{-9} and 10^{-11} are representative of a wide range of attack conditions, and can apply over a considerable area even for relatively light attacks.

[redacted] Figure 17-2 shows the signal attenuation for a 4000 km path. For large values of w, the reflection altitude is low and propagation near the low end of the LF band is least affected. In the range of the more likely w value of 10^{-11} to 10^{-9}, the reflection boundary becomes more diffuse and propagation in the VLF band shows minimum effects. For daytime conditions the LF signal attenuations are somewhat smaller than for nighttime conditions when w is less than about 10^{-11}. Effects similar to those described for propagation beneath the debris occur on the opposite side of the geomagnetic equator as a result of beta-particle and Compton electron ionization (see paragraph 8-3).

[redacted] While the results shown are for that portion of a path under the debris, it should be noted that degradation effects will not be limited to this region. Gamma radiation will increase the size of the ionization region up to several thousand kilometers from the debris boundary. Propagation effects outside the debris region, while significant, depend on the details of the debris-path geometry.

17-12 Effect of a [redacted] 6300-km Burst

[redacted] Prompt radiation from [redacted] burst at 6300-km altitude (one earth radius) produces an impulse of ionization over a very large region. The extent of ionization is determined by the X-ray horizon, [redacted]

[redacted] Figure 17-3 shows the signal attenuation for nighttime conditions on a 4000-km path. The ionization impulse produces a diffuse reflection boundary, and propagation near the lower end of the VLF band is affected less than at the higher end. [redacted] Attenuation caused by prompt radiation is much less in the daytime than at night.

[redacted] The phase advance caused by the ionization impulse (for times greater than 1 second after burst) is shown in Figure 17-4. At the time of the burst, the phase advance is much larger, on the order of thousands of degrees occurring in a few milliseconds.

[redacted]

[redacted]

[redacted]

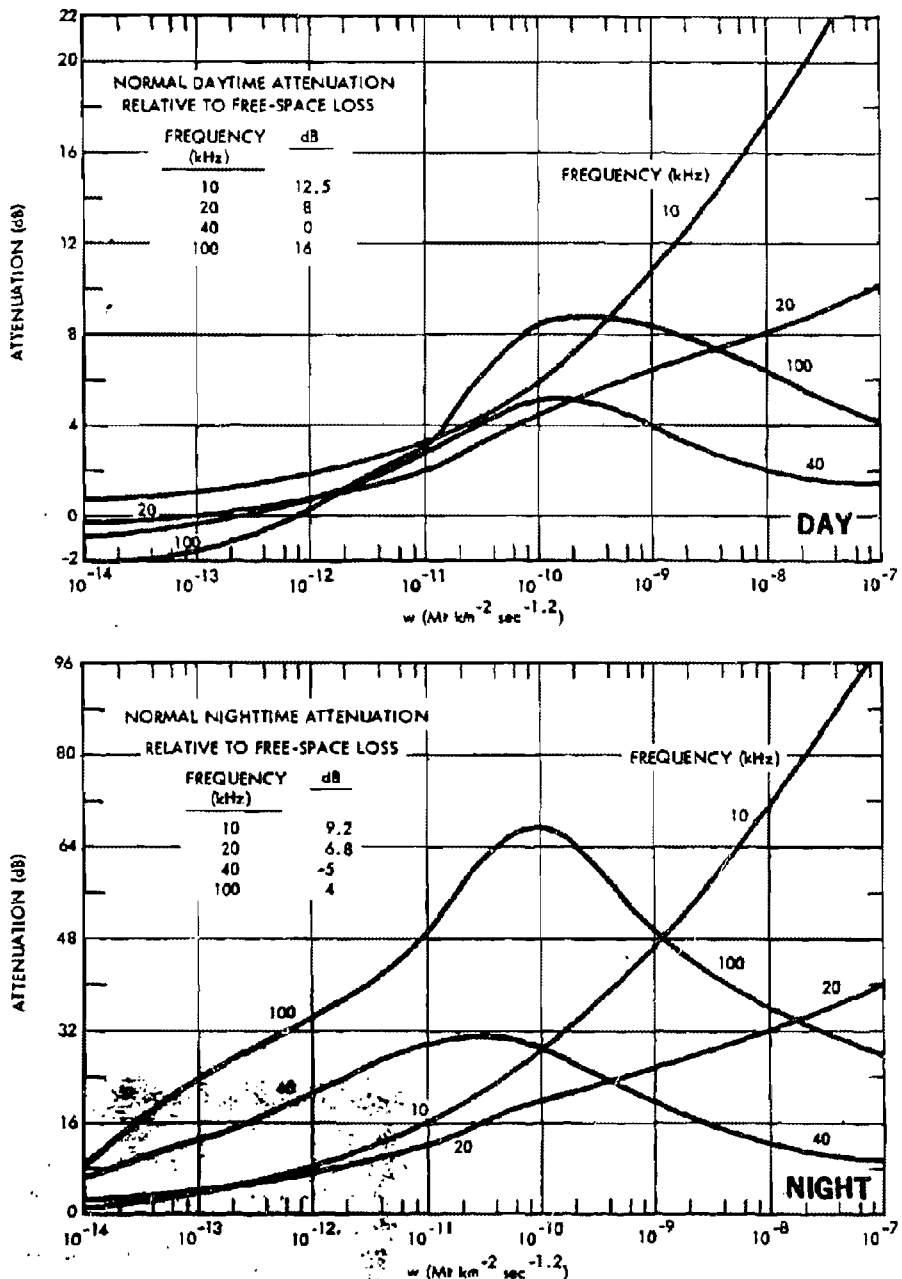

Figure 17-2. [redacted] Attenuation Related to Normal Loss Due to Spread-Debris Environment, 4000-km Path Length [redacted]

PAGES 17-11 THRU 17-12 DELETED DNA(4)(1)

[redacted]

[redacted]

17-13 Effect of Detonations Below About 300 km [redacted]

[redacted] If a nuclear burst occurs below 300 km, the portion of a propagation path that is affected is generally small unless the burst is close to the path. Depending on burst location and detonation altitude, there can be two degradation periods. The first period occurs at or within few minutes of burst time and is caused by prompt radiation and gamma radiation from the fission debris. The second period occurs when the fission debris has spread sufficiently that beta particles produce ionization along the path. In general, degradation is more severe in the LF band than the VLF band. An exception to this rule occurs during the first few minutes after a large-yield burst, which can produce intense ionization along the path that will cause low reflection altitudes.

[redacted] When a nuclear weapon is burst on the surface, ionization is limited essentially to the fireball region until the debris reaches altitudes above about 25 kilometers, where gamma radiation can penetrate the atmosphere. Even then, the extent of ionization affecting propagation is only a few hundred kilometers, and the effects are minimal. A large number of surface bursts, such as might occur during a nuclear war, could produce widespread ionization. Propagation effects similar to those described above for the case where the fission debris has spread to large distances would be expected for such conditions.

[redacted] HF SYSTEMS [redacted]

17-14 HF Propagation [redacted]

[redacted] Propagation at frequencies between about 1 and 60 MHz is supported by the F-region of the ionosphere. Generally speaking, the HF signal is a composite of many signals propagated along ray paths with different geometries. Figure 17-5 is an example of the ray-path geometry of a 4000-km path during the daytime at a single frequency. This multiple ray-path characteristic of HF is very important in any analysis of the susceptibility of a circuit to degradation from nuclear effects. Natural variations in the ionosphere affect the exact ray-path geometry at any specific time.

[redacted] Noise at HF comes from a variety of sources. Noise power in this frequency range has been conventionally calculated as a combination of propagated noise from thunderstorm centers (concentrated mostly in tropical areas) and man-made local noise. Atmospheric noise tends to be dominant at night when ionospheric absorption is less, whereas man-made noise may set the daytime level. Very often, however, the noise level is determined by other interfering signals because of congestion of the HF band. No means have been devised for quantitatively treating this latter and perhaps most important source of noise.

17-15 Effect of Nuclear Bursts on HF Systems [redacted]

[redacted] The most important phenomenon produced by nuclear bursts that affects HF systems is absorption resulting from D-region ionization. The ionization of the D-region is produced by prompt and delayed radiation. The amount of ionization depends on the altitude and the yield of the detonation (see IONIZATION AND DEIONIZATION in Chapter 8). Persistent absorption results from delayed gamma radiation when the debris is above 25 kilometers, and from beta particles when the debris is above 60 kilometers. Beta particles and Compton electrons can produce significant absorption in the region magnetically conjugate to the debris location. D-region absorption can extend over several thousand kilometers and can be important for hours after burst. For detonations above about 100 kilometers, there are often two distinguishable absorption periods: one, which starts at burst time,

[redacted]

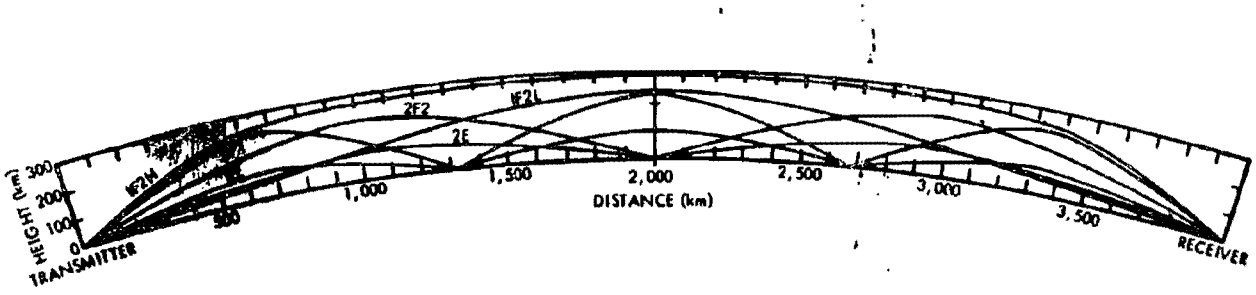

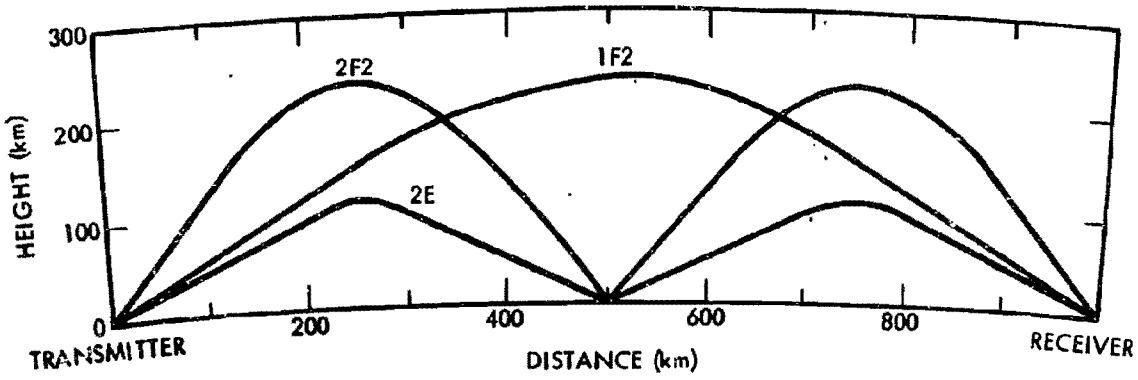

Figure 17-6. Examples of Daytime HF Ray-Path Geometry

[redacted]

results from ionization caused by prompt radiation and delayed gamma rays; a second results from ionization caused by beta particles. This latter starts when the fission debris has spread sufficiently that beta particles can ionize the D-region at the location of the propagation path. The duration of absorption depends on weapon yield and design, frequency, and time of day. The duration may vary from a few minutes for a small-yield weapon burst at night to several hours or more for a large-yield weapon burst during the day.

[redacted] Detailed calculations of signal attenuation due to D-region absorption require the determination of the absorption for each ray path connecting transmitter and receiver. The procedures given in Chapter 8 (see Problems 8-5 through 8-7) can be used to determine the absorption when the ray path geometries are specified. Since D-region ionization does not alter ray-path geometry appreciably (see paragraph 8-10, Chapter 8), the pre-burst ray-path geometry can often be used in determining absorption. However, as discussed below, changes produced by the burst in the E- and F-region electron density can alter the number and location of ray paths, and thus can affect absorption calculations.

[redacted] Ionization produced by a nuclear burst and traveling disturbances in the E- and F-regions of the ionosphere can produce significant changes in the E- and F-region electron densities that can last for hours (see TRAVELING DISTURBANCES IN E- AND F-REGIONS OF THE ATMOSPHERE in Chapter 8). Changes in the E- and F-region electron density can result in significant multipath effects by increasing the available ray paths and by introducing off-great-circle propagation paths. The maximum usable frequency (MUF) may be much lower than normal after nighttime detonations for ray paths that pass within several thousand kilometers of the detonation. For certain geometries and burst conditions the MUF may be higher, perhaps up to 60 MHz. Current theoretical models do not provide reliable prediction of the MUF as a function of burst and system parameters. Oblique, frequency-sweep ionospheric sounders may allow determination of usable frequencies during disturbed conditions.

[redacted] While HF system performance usually will be degraded by nuclear bursts (often resulting in complete circuit outage for significant periods of time), there may be factors that tend to minimize the degradation. For example, a reduction in noise or interference may accompany a reduction in signal strength, thus tending to preserve the preburst signal-to-noise ratio. Higher frequency propagation may be possible because of increased E- and F-region ionization, and the higher frequency will be less susceptible to absorption.

[redacted] The general effects of nuclear bursts on HF systems are summarized below:

1. The higher the altitude of detonation, the greater and more widespread are the effects.
2. HF systems can recover from a nuclear attack, with nighttime recovery being much more rapid than daytime.
3. Intermittent propagation may occur even under severe circumstances, but the frequency range is not always predictable.
4. When ionization produced by weapon debris is not widespread (less than about 500 km) and the circuit is longer than a few thousand kilometers, the chances are good that continuous communication can be maintained after recovery from the prompt effects.
5. Multiple bursts occurring at dispersed locations and times can increase the degradation greatly and can reduce the sensitivity of the system to burst location.

The variations in the effects of nuclear bursts on

[redacted]

[redacted]

HF systems are illustrated by the descriptions of several specific examples in the following paragraphs.

17-16 Effect of Surface or Near-Surface Bursts

[redacted] Single or closely spaced bursts may occur during attacks against ground targets. Weapon radiation initially is confined to a volume of space near the detonation point, and a fireball is produced that subsequently rises (see paragraph 1-12 and 1-20). Ionization produced by the burst is essentially confined to the fireball region until the fireball carries the fission debris above about 25 kilometers, where gamma radiation can penetrate the atmosphere and produce D-region ionization. The extent of this ionization is a sensitive function of debris altitude. Gamma rays produce ionization over about 200 km horizontal extent for a 1-Mt surface burst, and over about 400 km for a 10-Mt surface burst. Because the area of high absorption is small, multiple rays will be affected only if they have a common D-region intersection. In any situation where the signal propagates over multiple ray paths that are sufficiently separated in the vicinity of the absorbing area, there will be little if any effect. Calculations for long and intermediate path lengths show that it is very difficult to eliminate all propagating frequencies. In some cases it would be necessary to switch to lower rather than higher frequencies to avoid outage, but communications could be maintained.

[redacted] Signal attenuation caused by surface bursts can be severe for short paths since the D-region intersections of the ray paths are close together (see Figure 17-5). Communications on certain frequencies can be disrupted for a period of hours, especially during the day.

17-17 Effect of a [redacted] 30-km Burst

DNA (EX)

[redacted] A [redacted] device detonated near an altitude of 30 kilometers has potential as a possible penetration aid. The detonation point is sufficiently high that gamma rays will produce moderately widespread ionization even at early times. By 5 minutes after detonation, the debris will have risen [redacted] and beta particles can escape the debris region. Therefore, both gamma rays and beta particles are important ionization sources. [redacted]

DNA (EX1)

[redacted] For a typical burst location, there would be two periods of pronounced absorption; the first would occur during the initial debris rise, and the second would occur when the radiation from the spreading debris reaches critical D-region points. [redacted]

DNA (EX1)

[redacted] Because the region of increased ionization for this example is comparable to the D-region spacing between ray paths, the sensitivity to exact burst position is less critical than it is for surface bursts. The effects are still relatively limited, however, and the communication degradation does depend upon the burst location and the propagation path length. [redacted]

DNA (EX1)

[redacted]

[redacted]

17-18 Effects of a [redacted] 50-km Burst

DNA (G)(1)

[redacted] The effects of an extremely large yield weapon can be illustrated by describing the effects of [redacted] at 50 kilometers. Ionospheric effects are widespread and severe in both the burst and the conjugate regions. The debris rises to approximately 150 kilometers in less than 10 minutes, and it spreads to nearly 600 kilometers radius within 15 minutes. Thereafter, the debris radius continues to increase slowly as a result of winds.

[redacted] The relatively high altitude and large yield of such a burst produce immediate and severe effects.

DNA (G)(1)

[redacted] The size of the absorbing region is large enough that nearly all rays along a given propagation path will be affected simultaneously, causing path orientation and path length within the region to be unimportant. Absorption effects of a similar nature also can be expected in a region on the opposite side of the magnetic equator from the burst centered at the conjugate of the burst point.

[redacted] The shock wave from a nighttime explosion [redacted] can be expected to reduce the critical frequency of the reflection region [redacted] This condition will probably persist [redacted] after sunrise.

DNA (R)(1)

[redacted] If the propagation path is offset from the burst, there can be an initial period of absorption as a result of prompt and delayed gamma radiation. This period might be followed by a period of recovery to near normal conditions, and then a second period of absorption would occur as the debris expands and beta particles affect the path.

[redacted]

DNA (G)(1)

17-19 Effect of Multiple Multimegaton 150-km Bursts [redacted]

[redacted] Multiple multimegaton high altitude bursts represent conditions that may result from the employment of a ballistic missile defense system. The most significant effects on HF circuits are widespread prompt ionization, widespread and intense delayed radiation, and F-region modifications. The debris will be distributed over a large altitude region, with some debris reaching altitudes above 1000 kilometers. The geomagnetic field plays an important role in determining late-time debris location (see Problem 8-7, Chapter 8).

[redacted] If multiple multimegaton high altitude bursts occur, HF circuits will be interrupted over a very substantial area, essentially at burst time.

[redacted]

The duration of the outage for paths at these extreme ranges will be brief.

DNA (G)(1)

[redacted]

[redacted] The particularly large radius of effects at early times results from the high altitude to

[redacted]

[redacted]

which the debris rises. Gamma radiation from the debris has a horizon of about 4000 kilometers from the burst points. Eventual expansion of the debris results in secondary outages when beta-particle ionization reaches a given path. In the region around the conjugate of the burst points beta-particle ionization is similar to that produced in the burst region. Compton electrons cause ionization which is less intense than that produced by gamma rays in the burst locale (see paragraph 8-3).

[redacted] The critical frequency of the reflection region probably will be affected out to about 1000 kilometers after many large yield high altitude bursts. Significant electron density enhancement may occur near the detonation points, and electron density depletion may occur at more remote locations [redacted]

DNA (6)(1)

[redacted]

17-20 Effect of a 1-Mt, 250-km Burst [redacted]

[redacted] A 1-Mt weapon burst at an altitude of 250 kilometers will result in significant propagation effects from prompt radiation, delayed radiation, and changes in the F-region. Debris will be distributed over a large altitude region; the geomagnetic field will affect the late-time debris location, with some debris being transported across the geomagnetic equator. Very intense and widespread effects will be produced on the ionosphere; hence there will be degradation of HF communication systems. However, because of the lower yield and somewhat shorter debris rise than in the case discussed in paragraph 17-18, the effects are more dependent on the location and length of the communication path. [redacted] Ionization caused by the betas emitted by the spreading debris from such a burst will result in prolonged outage of HF systems. The lowest frequencies will be out for the longest period of time. [redacted]

DNA (6)(1)

[redacted] During the nighttime, the rapid decay of D-region ionization results in rapid recovery of all HF communication circuits that are not affected by beta ionization. [redacted]

DNA (6)(1)

[redacted] Circuits within several thousand kilometers of the conjugate of the burst point will also experience significant degradation. The absorption caused by beta-particle ionization is similar to that described for the burst region.

[redacted] For this type of high-altitude burst, the E- and F-region electron densities may be increased in the region near the burst. [redacted]

DNA (6)(1)

[redacted]

reduced below the MUF at distances beyond 500 kilometers from the burst.

17-21 Effect of a 1000-km Burst

DNA (G)(1)

weapon burst at an altitude of 1000 kilometers would be primarily an anticommunication event. In spite of the small yield, the X-ray output is sufficiently large that even from an altitude of 1000 kilometers, significant ionization would be produced in the lower ionosphere.

The radius of effects from such a burst is much greater than individual mode separation distances; thus, the exact ray path position, path length, and orientation are not important for distances less than approximately 2000 kilometers.

DNA (G)(1)

SATELLITE COMMUNICATION SYSTEMS

The basic elements of a satellite communication system consist of a ground-terminal transmitter, a satellite-borne repeater, and a ground-terminal receiver. Typically, the satellite-borne equipment provides only the functions of frequency translation and amplification; signal processing and demodulation take place at the ground terminals. Gigahertz frequencies and large bandwidths are typical of satellite communication systems, but some systems may operate in the VHF and lower UHF bands.

17-22 Effects of Nuclear Bursts on Satellite Systems

The nuclear bursts of primary importance to military satellite communication systems are those that produce an intense ionization region which is intersected by the propagation paths of the relay circuit. One of the principal effects of this ionization is absorption of the propagating signal. The region of significant ray-path absorption for communication satellites operating at several gigahertz is usually confined to the fireball; however, other important absorption regions may exist for some combinations of yield and burst altitude. (See Chapter 8 for a discussion of ionization and absorption regions produced by nuclear detonations.)

DNA (G)(1)

D-region ionization produced by prompt and delayed radiation (beta particles and gamma rays) produces absorption that depending on propagation frequency, burst altitude, and fission yield. Delayed gamma rays can affect propagation in the VHF band The extent of D-region absorption caused by beta particles is determined by the debris expansion, and this absorption can affect propagation in the VHF and UHF bands

DNA (G)(1)

In modern low-noise receivers, it is often the noise appearing at the terminals of the receiving antenna that will set the limit on the overall performance of the system. As a result, fireball thermal noise can be significant in degrading the performance of satellite communication systems (see ELECTROMAGNETIC RADI-

[redacted]

ATIONS in Chapter 8). The amount of electromagentic thermal radiation reaching the receiver antenna depends on the effective fireball temperature at the frequency of interest (a function of temperature and emissivity) and on the amount of attenuation between the fireball and the antenna. Antenna temperature generally will be less than the effective fireball temperature as a result of absorption that occurs outside the fireball and the effect of antenna gain in the direction of the fireball.

DNA (L)(1)

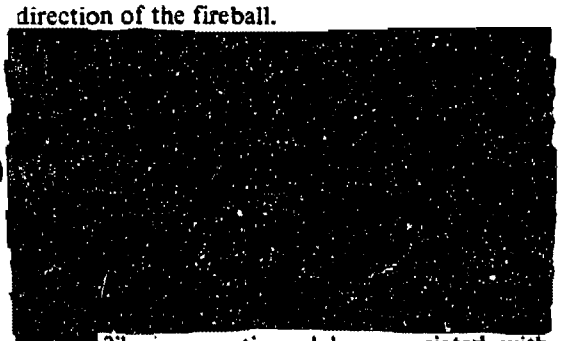

[redacted] The group time delay associated with signal propagation through a plasma usually is frequency dependent. This causes phase distortion of angle-modulated signals (frequency and phase modulation are forms of angle modulation), resulting in what is termed intermodulation noise. This frequency-dependent time delay, or dispersion, also results in envelope distortion for pulse transmission through a plasma. Hence, another effect of burst-produced ionization that may be of importance to angle-modulated multichannel satellite systems of large channel capacities is the intermodulation distortion noise. The strength of this intermodulation noise is determined largely by the integrated electron density along the ray path and the modulation parameters. Typically, it is the late-time, high-altitude fireball ionization that may give rise to this dispersion effect. Similarly, satellite digital-communication systems may encounter pulse distortion when propagating through burst-produced ionization, which in turn may result in large decoding error rates. The dispersive medium may affect pulse amplitude systems because of envelope distortion. The magnitude of the pulse distortion is determined by the integrated electron density along the ray path, the carrier frequency, and the pulse width.

[redacted] Time-variant time delays due to the structured and filament-like behavior of high-altitude fireball striations may be a possible source of degradation to satellite communication systems; no estimate has been made of these effects because of the lack of data from which to scale results. The effects of time-variant time delays would be to introduce channel noise of a nature similar to intermodulation noise or adjacent-channel interference.

17-23 Nuclear Effects on Two Typical Satellite Systems [redacted]

[redacted] Two hypothetical but typical satellite systems have been selected to illustrate many of the problems of satellite communication in a nuclear warfare environment. System A (see Table 17-1) represents a high-volume military communication system. The mission requires continuous coverage between virtually every pair of points on the earth's surface. The system provides a tactical quality of voice communications.

[redacted] System B (see Table 17-2) operates in the UHF band at 400 MHz. It employs an 8-hour circular communications orbit. The power requirements, antenna size, channel capacity, and grade of service provided represent a tactical, transportable communication system.

[redacted] The systems considered employ Frequency Division Multiplex-FM (FDM-FM) as a means of carrier modulation. Voice channels are frequency multiplexed onto a single baseband using subcarriers. This baseband is then applied to a linear frequency modulator to modulate the transmitter RF carrier.

[redacted]

[redacted]

Table 17-1. [redacted] Satellite Communications Link Description, System A [redacted]

System Parameters	Description
Frequency	4 GHz
Channel capacity	300 duplex channels
Baseband	60 to 1300 kHz
Modulation format	FDM-FM
RMS frequency deviation	0.9 MHz
FM threshold	12 dB
Ground antenna	80-foot dish
Ground transmitter power	10 kw
Ground receiver I-F bandwidth	15 MHz
Ground receiver system noise temperature	100°K
Satellite receiver noise figure	10 dB
Satellite antenna (toroidal pattern)	5 dB gain
Satellite transmitter power	25 watts
Satellite altitude (synchronous)	35,788 km

Table 17-2. [redacted] Satellite Communications Link Description, System B [redacted]

System Parameters	Description
Frequency	400 MHz
Channel capacity	12 duplex channels
Baseband	0 to 60 kHz
Modulation format	FDM-FM
RMS frequency deviation	27.4 kHz
FM threshold	12 dB
Ground antenna	30-foot dish
Ground transmitter power	10 kw
Ground receiver I-F bandwidth	0.672 MHz
Ground receiver system noise temperature	250°K
Satellite receiver noise figure	10 dB
Satellite I-F bandwidth	1 MHz
Satellite antenna (toroidal pattern)	-3 dB
Satellite transmitter power	20 watts
Satellite altitude (8-hour circular orbit)	13,896 km

[redacted] Table 17-3 summarizes outage times for the two systems [redacted]

DNA (G)(1)

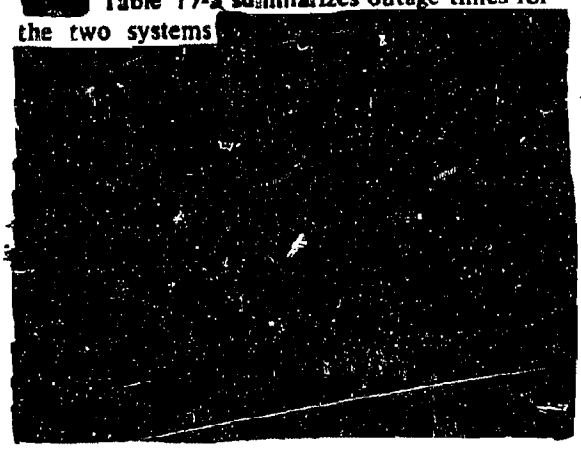

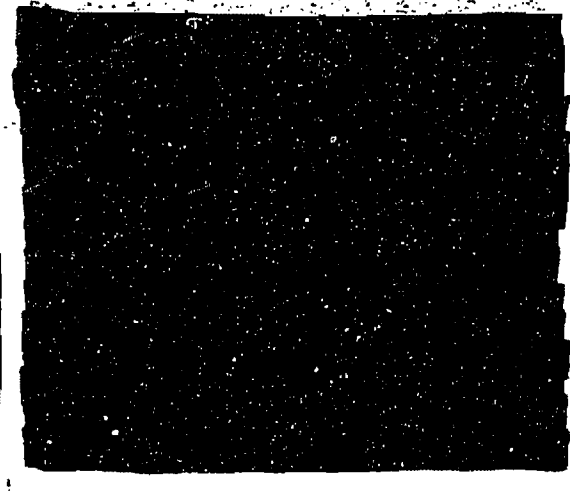

DNA (G)(1)

[redacted]

[redacted]

Table 17-3. [redacted] Estimated Outage Times for Fireball Intersection of the Propagation Path [redacted]

Deleted

DNA (L-X1)

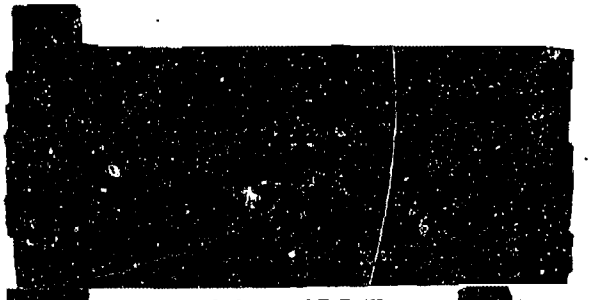

DNA (L)(1)

Figures 17-6 and 17-7 illustrate [redacted] two [redacted] degradation mechanisms: fireball absorption and fireball noise. Figure 17-6 shows signal-to-noise ratio for Systems A and B [redacted] The fireball is located such that the ray path traverses the fireball when it has stabilized in altitude. Figure 17-6 also shows, for reference, the absorption along the ray path.

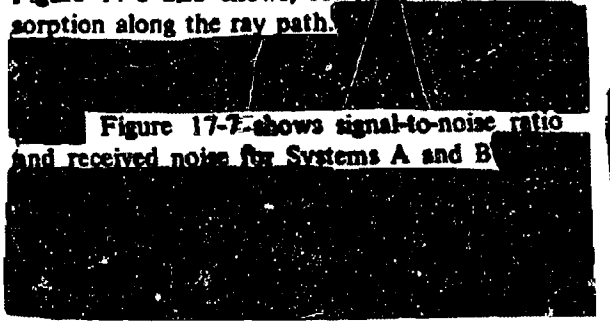

Figure 17-7 shows signal-to-noise ratio and received noise for Systems A and B [redacted]

[redacted] TROPOSCATTER COMMUNICATION SYSTEMS [redacted]

[redacted] Tropospheric forward-scatter communications are used for communications and military purposes in locations where the nature of the terrain makes other means of highly reliable communication difficult.

[redacted] Figure 17-8 shows the geometry for a troposcatter link. Propagation from transmitter to receiver is via scatter in the common volume in the troposphere.

17-24 Effects of Nuclear Bursts on Troposcatter Systems [redacted]

[redacted] Three potential sources of degradation of troposcatter communication systems are signal absorption, fireball thermal noise, and multipath interference via fireball scattering. [redacted]

DNA (L)(1)

Since troposcatter systems typically operate between a few hundred MHz and a few GHz, only the regions of intense ionization will produce appreciable signal absorption. The ionization resulting

PAGES 17-23 THRU 17-24 DELETED
DNA (L)(1)

[redacted]

[redacted]

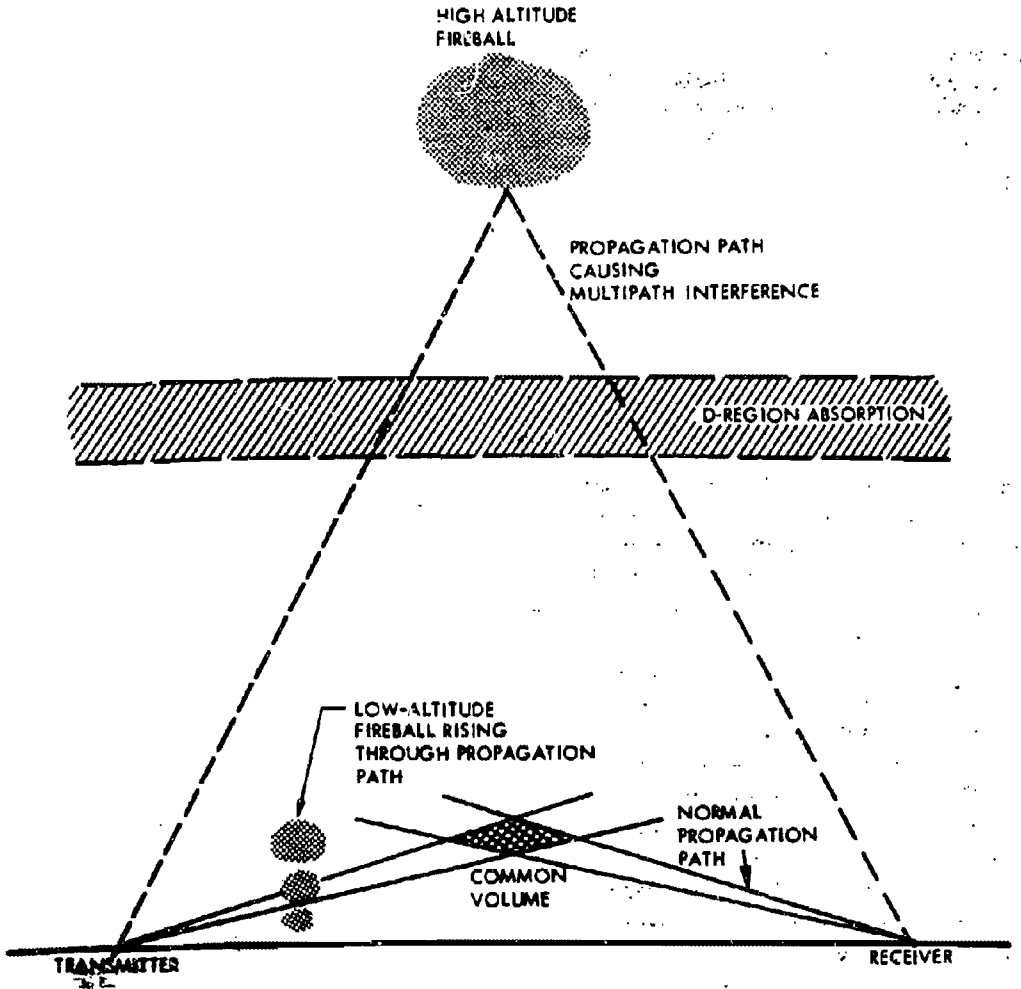

Figure 17-8. [redacted] Illustration of Troposcatter Geometry [redacted]

[redacted]

from a low-altitude nuclear burst is largely confined to the immediate vicinity of the fireball; consequently, in order to obstruct troposcatter communications as a result of ray-path absorption, the fireball must be within the scatter path.

DNA (EX)

In low-noise receivers, fireball thermal noise may degrade the performance of troposcatter communication systems significantly. The amount of electromagnetic thermal radiation reaching the receiver antenna depends on the effective fireball temperature at the frequency of interest (a function of temperature and emissivity) and on the amount of attenuation between the fireball and antenna.

DNA (EX)

There are no significant differences between day and night effects for troposcatter systems.

17-25 Nuclear Effects on Three Typical Troposcatter Systems

Three typical troposcatter communication systems have been selected to illustrate propagation effects for selected weapon environments. System A is representative of a high-quality commercial scatter system; System B is representative of a tactical system; and System C is representative of a long-distance system. The system characteristics are summarized in Table 17-4.

Table 17-5 summarizes the effects on the typical systems for several burst environments. There are essentially no differences between day and night effects. The amount of degradation depends on the fireball/debris geometry, which is variable with regard to size, shape, and location. The magnitude of multipath attenuation also depends on the antenna pattern (in the examples, the side-lobe gain was taken to be that of an isotropic antenna).

IONOSCATTER COMMUNICATION SYSTEMS

Ionoscatter systems provide intermediate-distance radio service of 4 to 16 channels of teleprinter and/or a single voice channel. Figure 17-9 shows the geometry for an ionoscatter link. Propagation between transmitter and receiver occurs via scattering from a common volume in the D-region.

The ionoscatter system considered here transmits at a continuous low data rate via a scatter signal that is always present, although weak and variable. The ionospheric scatter mode is fundamentally most suitable for low-data-rate teleprinter operations. High-quality voice communications via ionospheric scatter cannot be

[redacted]

Table 17-4. [redacted] Troposcatter Communication Link Description [redacted]

System Parameter	System A	System B	System C
Frequency	2 GHz	900 MHz	400 MHz
Path length	300 km average per hop, 6 hops	150 km, 1 hop	600 km, 1 hop
Channel capacity	120 channels	24 channels	12 channels
Power	10 kw	1 kw	100 kw
Antennas	80-foot dish	18-foot dish	120-foot dish
Antenna height	30 meters	30 meters	30 meters
Diversity	Quad, space	Dual, space	Quad, space
FM threshold	12 dB	8 dB	12 dB
Receiver noise figure	9 dB	9 dB	2.5 dB
Baseband	60-552 kHz	12-108 kHz	12-60 kHz
Modulation format	FDM-FM	FDM-FM	FDM-FM
RMS frequency deviation	362 kHz	63.5 kHz	35.3 kHz
I-F bandwidth	6 MHz	1.3 MHz	775 kHz

[redacted]

achieved with reasonable transmitter power.

[redacted] Ionoscatter systems typically operate at frequencies just above the E- and F-layer MUFs to eliminate multipath reflections and HF interference.

17-28 Effects of Nuclear Bursts on Ionoscatter Systems [redacted]

[redacted] As a result of their reliance on D-layer scattering mechanisms, ionoscatter systems are very susceptible to low-level residual ionization from a nuclear explosion. In view of the very small margin of operation above receiver threshold, usually limited by galactic noise, such systems are vulnerable to abnormal absorption along the scatter path and/or within the scattering volume. Prediction of effects in a nuclear environment is very difficult, because the ionospheric scatter phenomena in the natural environment are not well understood.

[redacted] The low frequencies employed by ionoscatter systems (about 35 to 50 MHz) allow appreciable absorption, even at low levels of residual ionization. Prompt radiation, delayed gammas from fission debris if the debris is above 25 km, and beta particles if the debris is above 60 km can all cause significant D-region ionization. If the debris is above 60 km, the betas will usually be more important than the gammas, and about one-half of the betas will be deposited in the region magnetically conjugate to where the debris is located. [redacted] DNA (6)(

[redacted]

[redacted]

Table 17-6. [redacted] Approximate Extent and Duration of Effects on Troposcatter Communications, Assuming Proper Burst Placement [redacted]

Deleted

DNA (6)(1)

DNA (6)(1) [redacted] Increased E- and F-region ionization caused by prompt radiation and traveling disturbances from a nuclear detonation may result in multipath effects, which decrease the effective bandwidth of ionoscatter circuits.

DNA (6)(1) [redacted] Electromagnetic thermal radiation from fireballs is usually not important to ionoscatter systems because of the high ambient-noise environment.

17-27 Nuclear Effects on Typical Ionoscatter Systems

[redacted] The ionoscatter system selected as an example uses two-frequency operation: 35 MHz for low transmission loss, and 60 MHz to avoid multipath interference at times of high solar activity.

[redacted] The system parameters are summarized in Table 17-6. For digital communication, the encryption and order of diversity are perhaps the most important parameters that influence system performance. Because of the large variations in system performance with path length, results for 1000-, 1500-, and 2000-km links are considered. The antennas of the system consid-

[redacted]

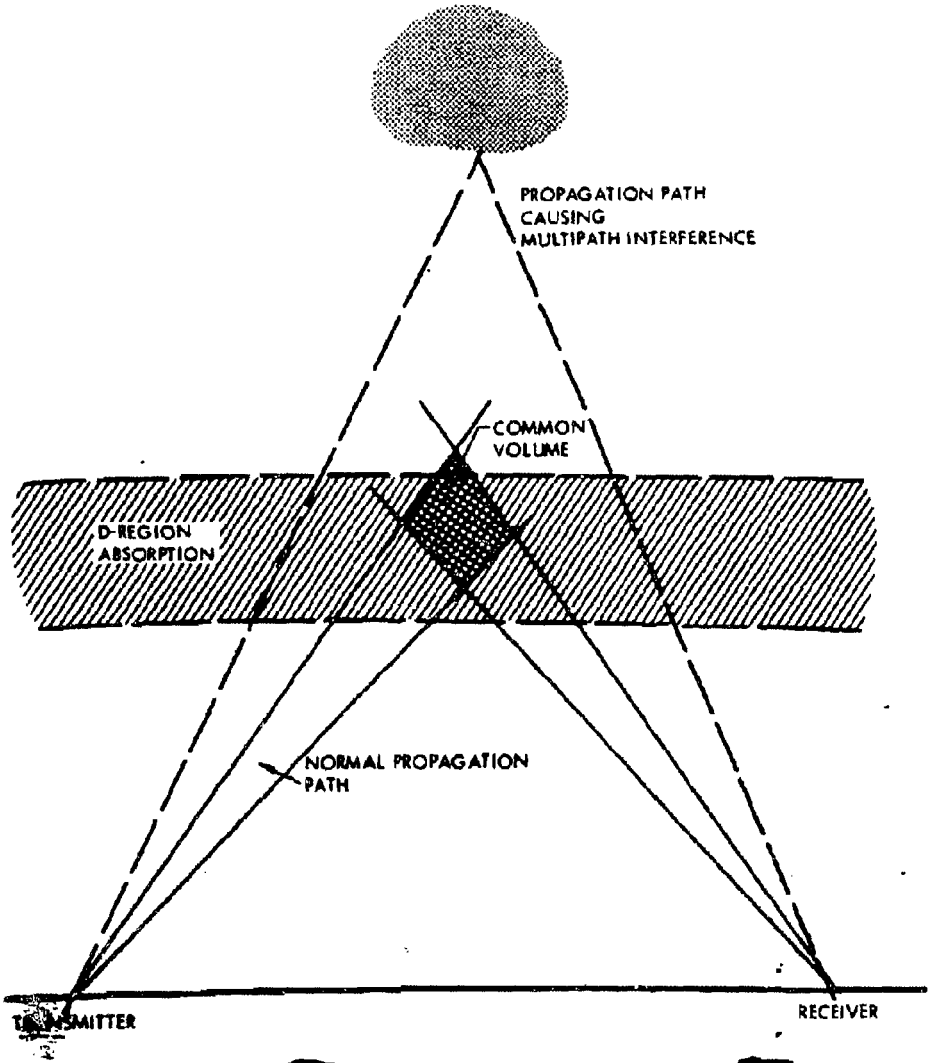

Figure 17-9. Illustration of Ionoscatter Geometry

[redacted]

Table 17-6. [redacted] Ionoscatter Communications Link Description [redacted]

System Parameters	Description
Frequency	35 or 60 MHz
Path lengths	1,000, 1,500, 2,000 km (three systems)
Channel capacity	16 channels, teletype
Power	60 kw
Antenna gain	19 dB
Antenna 3-dB beamwidths	45 degrees vertical, 11 degrees horizontal
Polarization	Horizontal
Diversity	Dual, space
Receiver noise temperature	450°K
Receiver noise bandwidth	1.2 kHz
Modulation format	TDM-FSK
Frequency shift	6 kHz mark-space
Demodulator	Dual filter, optimal without Doppler spread
Radiated signal element length	1.7 milliseconds
Transmission rate	600 bauds
Coding and synchronization	Standard 5-unit, start-stop neutral code

[redacted]

ered here are aligned along a great-circle path. Each terminal of an ionoscatter link is capable of duplex transmission.

[redacted] Table 17-7 summarizes the effects of several burst environments on the system described in Table 17-6. These effects show a strong dependence on the location of the burst with respect to the [redacted] scatter path and on the scatter path length.

[redacted] Thermal noise from the fireball has negligible effect on this system because of the high cosmic noise levels. Effects of scattering from high-altitude fireballs, field-aligned ionization, or enhanced E- and F-region electron densities that may produce multipath interference are not included in Table 17-7 because the phenomena are not sufficiently understood.

[redacted] The most serious difficulty in predicting ionoscatter propagation characteristics in a nuclear environment is lack of understanding of the mechanisms involved in normal propagation.

[redacted] RADAR SYSTEMS [redacted]

[redacted] Radars are used in a wide variety of missions, including surveillance, target acquisition, navigation, tracking, fire control, discrimination between true targets and decoys, guidance and control, and fuzing. The radars may be ground-based or airborne. Their frequency usually is above the HF band with line-of-sight propaga-

[redacted]

[redacted]

Table 17-7. [redacted] Approximate Outage Times 1000-, 1500-, and 2000-km Ionoscatter Links, Assuming Proper Burst Placement [redacted]

Deleted

DNA (6-X(1)

[redacted]

tion paths. An exception is over-the-horizon radar (OTH or OHR), which operates in the HF band and uses E- and F-region refraction to detect objects at long ranges. Nuclear-weapon effects on over-the-horizon radars correspond to effects on [redacted] systems, described earlier in this section. OTH radars may be used for early detection of targets before detonation of nuclear weapons, and to provide supplementary information to ballistic missile defense radars at later times.

[redacted] The choice of parameters to be used (frequency, radiated power, antenna beam shape, pulse waveforms, etc.) depends on the function intended for the system. Acquisition radars are designed to maximize the initial detection range and angular coverage. These radars generally use lower frequencies than tracking systems and have less stringent requirements for measurement accuracy. Tracking and discrimination radars require high measurement accuracy, and they generally use as high a frequency as

[redacted]

possible. Discrimination radars may use complex waveforms and signal processing to estimate the nature of the incoming object. An important parameter related to radar susceptibility to nuclear-weapon effects is the altitude of the region of space (sometimes called the battle space) from which target echoes are to be received.

In view of the different parameters and accuracy requirements for the different types of systems, the significance of weapon effects depends on the radar function. For example, fairly low levels of D-region ionization can cause sufficient absorption to reduce the initial detection range of an acquisition radar without affecting track radars. Levels of clutter, scintillation, and dispersion effects that are too small to affect acquisition radars may degrade discrimination radars seriously.

Radars associated with detection of aircraft or surface targets usually will not experience signal degradation, since the propagation paths are below altitudes where persistent or widespread effects are caused by nuclear weapons (about 25 km). Fireballs from surface or air bursts may interdict the propagation path, but the small size of low-altitude fireballs and the relative motion between the rising fireball and the propagation path will usually limit outage to a few seconds. Blast, thermal, and nuclear radiation damage generally will be more significant for such systems when weapons are detonated close enough to interdict the propagation path.

17-28 Ballistic Missile Defense Systems

Ballistic missile defense (BMD) systems can be categorized conveniently according to the size of the region defended. Area and regional defense systems are designed to protect a large area, such as one or more cities. The functions of detection, tracking, and discrimination of incoming objects are performed at as great a range as possible to allow the area to be defended with a minimum number of radars and interceptor missile sites, and to minimize the damage to the defended area from detonation of intercept weapons. Initial detection ranges are typically a few thousand kilometers (approximately 10 minutes before impact of the incoming object). Intercept of those objects designed as threatening usually is above about 50 kilometers.

Hardsite defensive systems are designed to protect a small area, usually hardened against direct damage effects (blast, thermal, etc.). Information concerning threatening objects may be transferred to the system from area defense radars. Since the defended site is hardened, intercept altitudes usually are below 30 kilometers and may be as low as a few kilometers. The system typically is designed to be able to perform acquisition, tracking, and discrimination functions after incoming objects are below 100 kilometers. High-performance interceptor missiles and data handling systems are used.

17-29 Nuclear Effects on Area Defense Systems

Nuclear weapon effects on area-defense radars may be caused by interceptor weapons (self-blackout) or by penetration aid weapons used by the offense. Although interceptor weapons are designed to minimize propagation effects on defensive radars, the use of a number of interceptor weapons in certain locations can cause significant problems. In the cases of area and regional defense systems, where interceptor detonation altitudes are high, the degradation mechanisms include absorption in the fireball and the D-region, scattering in the fireball and the E- and F-regions, noise, and clutter interference. Scattering and beam spreading can produce attenuation even in the absence of absorption; these propagation effects also produce scintillation of various kinds (amplitude, phase, angle, etc.). Receiver response to these effects will be similar to that associated with multipath. Absorption and scattering appear to be the most significant of the effects.

[redacted]

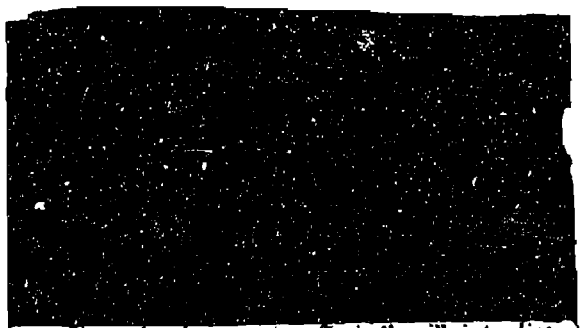

DNA (b)(1)

Whether the interceptor fireball will interdict the radar propagation path depends on the spacing of incoming objects, the interceptor weapon yield and detonation altitude, and the geometrical relation between the radar and the threat approach azimuth[redacted]

DNA (b)(1)

[redacted] D-region ionization caused by prompt and delayed radiation can be a significant cause of absorption, because for typical geometries the propagation path must traverse the D-region. D-region absorption scales inversely with frequency squared and is essentially negligible for frequencies above a few gigahertz. At a few seconds after burst, the most intense D-region absorption is caused by beta particles. As discussed in paragraph 8-4, the beta-particle ionization region is offset horizontally from the debris region by an amount that is determined by the orientation of the geomagnetic field and the height of the debris above the D-region. Intercept altitudes that place the beta-particle ionization region along the propagation path to successive objects can produce significant signal attenuation as a result of absorption after each intercept burst. Both the location of the ionization region and the propagation path are moving, and the duration of absorption is determined by the length of time the propagation path remains in the beta-particle ionization region. Refraction effects from D-region ionization are generally negligible, unless the level of ionization is large enough to also cause large signal attenuation.

[redacted] Prompt radiation from bursts detonated above about 100 kilometers increases the electron density in the E- and F-regions. The horizontal extent of the affected region depends on the burst altitude, weapon yield, and weapon design. While absorption resulting from E- and F-region ionization outside the fireball is small for radar frequencies, refraction or bending of the propagation path will cause angular errors. Even very small elevation and azimuth errors can result in significant interceptor miss distances.

[redacted] Interference and signal distortion also may be caused by noise (fireball thermal radiation), clutter, dispersion, and scintillation. While noise from fireball thermal radiation does not appear to be a significant problem for military radar systems, the conclusion should be reviewed for specific systems, particularly if low-noise receivers are used. Clutter returns can be orders of magnitude larger than target echoes and may mask the desired echo or appear as false targets. While it appears that antenna side-lobe rejection and doppler discrimination techniques can be used to reject clutter returns, these techniques may increase the data processing required by a substantial amount. Signal distortion caused by dispersion appears to be a secondary effect for acquisition and track radars, but it may degrade the performance of discrimination radars. Scintillation may cause pulse-to-pulse fluctuation in the apparent direction of the target. Computational models for scintillation are currently incomplete.

[redacted] The computational models given in Chapter 8 can be used to estimate fireball absorption for ray paths traversing the fireball or D-region. While effects other than absorption are discussed in Chapter 8, computational models are not given because of the complexity of the scaling. Analysis of radar performance in a nuclear environment usually is done with computer

[redacted]

codes to facilitate the large number of computations required.

An example of the results of code calculations is provided below to illustrate the types of effects and the sensitivity of the effects to radar and burst parameters. The example is not intended to model an actual engagement, but it provides representative nuclear environments that might be produced by penetration aid or interceptor weapons. The geometry chosen for the example is shown in Figure 17-10. The threat trajectory (path of an incoming object) is in the direction of the geomagnetic field. One radar is located at the defended target and another is offset from the target to view the incoming object from the side.

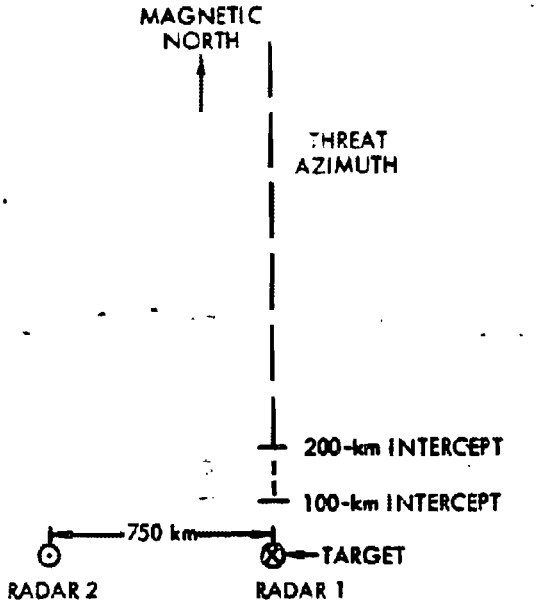

Figure 17-10. (U) Plan View of Radar and Target Geometry (U)

As the incoming object approaches the target a series of nuclear bursts are assumed to occur at a fixed altitude on the trajectory.

Figure 17-11 shows the signal-to-noise ratio and the elevation errors calculated for the radar located at the target. Results are shown for bursts occurring at two detonation altitudes. The propagation path from the radar to the incoming object traverses beta-particle ionization regions.

As previously mentioned, refraction due to E- and F-region ionization can cause angular errors that affect the defense's ability to predict the location of incoming objects and perform intercepts. Figure 17-11 shows the elevation errors computed for the radar located at the target

PAGE 17-35 DELETED DNA (6)(1)

[redacted]

DNA (L)(1)

[redacted] Figure 17-12 shows the signal-to-noise ratios and elevation errors calculated for the offset radar. Because of the offset, the propagation path does not traverse beta-particle ionization regions or fireball regions, and signal attenuation is due to ionization caused by prompt radiation and delayed gamma radiation.

DNA (L)(1)

[redacted] The above example does not show the dependence of system performance on the type of burst, the spacing and number of incoming objects, or the location of the threat azimuth with respect to the geomagnetic field, all of which can be significant. Further, the calculations for the example were based on the assumption that the phenomenology for each weapon was independent of previous weapons.

DNA (L)(1)

[redacted] it is expected that modifications of burst phenomenology in a sequential-burst environment will be important. Models for such environment are under development (see Appendix E for code listings).

[redacted] some field simulation has been performed by releasing barium in the ionosphere (at altitudes between 100 and 200 km) in order to produce structured plasmas. The resulting plasma does not produce significant absorption, but it does tend to striate along the geomagnetic field to produce structure [redacted] This permits at least qualitative simulation of scattering effects.

DNA (L)(1)

[redacted]

[redacted]

DNA (L)(1)

[redacted] The angular extent of the region obscured by the fireball is shown in Figure 17-13 as a function of detonation altitude for a typical sight line. The solid angle subtended varies as a function of time due to rise and expansion of the fireball (see Problem 8-1, Chapter 8). The magnitude of the variation is not great, however, and the values of solid angle shown in Figure 17-13 are representative of those occurring for the first few tens of seconds after detonation.

[redacted]

DNA (L)(1)

[redacted]

PAGE 17-37 DELETED
DNA (L)(1)

[redacted]

Deleted

DNA (L)(1)

Figure 17-13. [redacted] Solid Angle Obscured by 10-kt Intercept [redacted]

DNA (L)(1)

[redacted] Clutter returns and thermal noise from the fireball are potential degradation mechanisms for area defense systems. The use of narrowbeam antennas and signal processing will generally prevent degradation, but detailed analyses of system performance for specific scenarios and radar geometries are required.

[redacted] Penetration-sid weapons (precursors) detonated between about 20 and 50 kilometers can interfere with detection, track, and discrimination functions, and can reduce the reaction time available to the defense.

DNA (L)(1)

[redacted]

Denial of all information to the defense

is very difficult

[redacted]

PAGE 17-39 DELETED
DNA (L)(1)

BIBLIOGRAPHY

Atmospheric Ionization and Effects on Radar and Communications, A Bibliography, DASA 2069, Defense Atomic Support Agency, Washington, D.C., January 1968

Electromagnetic Blackout Handbook (U), Second Edition, Volume I: *Guide to System Effects* DASA 1580, Defense Atomic Support Agency, Washington, D.C., December 1964

Electromagnetic Blackout Handbook Second Edition, Volume II: *Nuclear Weapons Effects* DASA 1580-1, Defense Atomic Support Agency, Washington, D.C., February 1965

Knapp, W. S., and P. G. Fischer, *Aids for the Study of Electromagnetic Blackout*, DASA 2499, General Electric, TEMPO, Santa Barbara, Calif., July 1970

Nuclear Effects on HF Communications Systems *Selected Examples*, DASA 1955-1, October 1967; *General Prediction Techniques*, DASA 1955-2, April 1968; Defense Atomic Support Agency, Washington, D.C.

Nuclear Effects on VLF and LF Communications Systems *Selected Examples*, DASA 1954-1, June 1968; *General Prediction Techniques*, DASA 1954-2, September 1968; Defense Atomic Support Agency, Washington, D.C.

Nuclear Effects on Satellite and Scatter Communication Systems *Selected Examples*, DASA 1956-1, October 1967; *General Prediction Techniques for Satellite Systems*, Vol. 1, DASA 1956-2, July 1968; *General Prediction Techniques for Scatter Systems*, Vol. 2, DASA 1956-2, October 1968; Defense Atomic Support Agency, Washington, D.C.

RANC IV, Computer Simulation of Radar in a Nuclear Environment, Volume I, *Computational Models*, DASA 2497-1; Volume II, *Operational Data*, DASA 2497-2; Volume III, *Appendices*, DASA 2497-3; Defense Atomic Support Agency, Washington, D.C., prepared by General Electric Company-TEMPO, Center for Advanced Studies, Santa Barbara, California, July 1970

Weapon Effects Computer Code Directory, DASA 1727, Special Report 43, DASIAC, Santa Barbara, California, April 1969

Younker, E. L., et al., *VLF/LF Communications During a Major Nuclear Attack* SRI 7045, DASA 2369, Stanford Research Institute, Menlo Park, California, September 1969

ADA955402

[redacted]

DTIC
ELECTE
2 MAR 1989
S D
E

AD-A955 402

APPENDIX A

SUPPLEMENTARY BLAST DATA [redacted]

[redacted] This appendix consists of two sections. Section I is a collection of equations and data useful in the study of shock waves. Section II contains a description of certain shock wave properties in a way that is intended to convey an understanding of these topics. None of the information in this appendix is required to solve the problems in Chapter 2 concerning blast phenomena or the blast related problems in the chapters of Part II of this manual. This appendix provides supplementary information, useful for solving special problems or for developing a better physical understanding of the phenomena described in Chapter 2.

[redacted] The shock wave equations presented in this appendix are those that are most likely to be encountered in the study of air blast phenomena, and the concepts that are discussed are those that are most likely to be troublesome to the person who is studying shock wave theory for the first time.

[redacted] This appendix presupposes a reasonable familiarity with the laws of mechanics and some understanding of how these laws apply to energy and momentum exchange in gases in motion.

SECTION I

[redacted] MATHEMATICAL DESCRIPTION OF THE SHOCK FRONT [redacted]

[redacted] Most mathematical descriptions of shock wave phenomena are focused on the shock front itself since shock front conditions are fairly easy to treat mathematically, but the characteristics of the waveforms that follow the front are not. This limitation is not serious for many types of calculations, because the strength of the shock front is usually the best indicator of the severity of the entire shock wave.

[redacted] In the absence of direct, simple mathematical techniques, analysis of the shock waveform usually depends on empirical data such as the predetermined shock waveforms shown in paragraph 2-12, Chapter 2. Numerical integration of shock wave problems on a computer provides an alternate method. The computer codes for blast waves from nuclear weapons incorporate the details of weapon configuration, radiation transport, and hydrodynamics; these codes are complex and their characteristics will not be discussed here.

A-1 The Rankine-Hugoniot Equations [redacted]

[redacted] A set of three equations governing shock front behavior may be derived from the laws of mechanics. These equations (or any set of three independent equations derived from them) are called the Rankine-Hugoniot equations. They do not completely specify shock front behavior; a fourth equation, the equation of state of the material, is necessary to specify the complete behavior of the shock front. However, these equations have the advantage of being valid for all conditions under which a shock front can occur. They apply equally well to shock waves in solids and in gases.

[redacted] The equations given below outline the conventional derivation of the Rankine-Hugoniot equations. The same set of equations are derived in Section II in a manner that requires less algebra but more physical reasoning. The three conservation equations that lead to the Rankine-Hugoniot equations involve the so-called jump conditions across a shock front. The parameters involved are illustrated in Figure A-1.

[redacted]

REPRODUCED BY
U.S. DEPARTMENT OF COMMERCE
NATIONAL TECHNICAL
INFORMATION SERVICE
SPRINGFIELD, VA 22161

QUALITY INSPECTED 4

Accession For
NTIS GRA&I
DTIC TAB
Unannounced
Justification
By
Distribution/
Availability Codes
Dist | Avail and/or Special
A-1

[redacted]

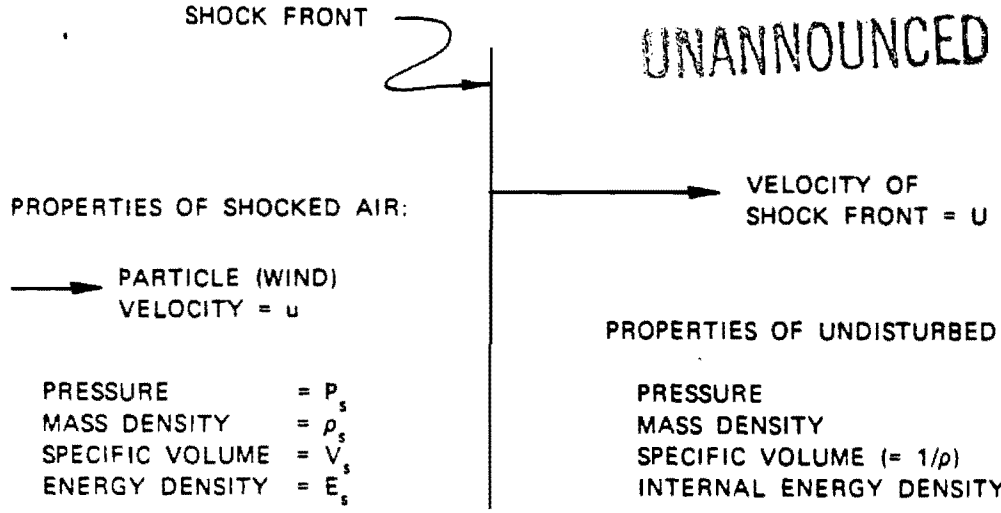

Figure A-1. (U) Change in Air Properties Across a Shock Front [redacted]

[redacted] An equation for the conservation of mass states that the mass of air per unit time overtaken by a unit area of the shock front is equal to the mass of air per unit area per unit time added behind the shock front.

$$\rho U = \rho_s(U - u),$$

where ρ is the ambient air density, U is the shock velocity, ρ_s is the density of the air behind the shock front, and u is the peak velocity of the air behind the shock front.

[redacted] Newton's second law states that force is equal to the rate of change of momentum. The force per unit area acting to accelerate the air entering the shock front is the overpressure, $\Delta p = P_s - P$, where P_s is the absolute pressure behind the shock front and P is the ambient pressure. The mass per unit time that enters a unit area of the shock front is ρU. The change of velocity of the air is u. Thus,

$$\Delta p = P_s - P = \rho U u.$$

[redacted] Conservation of energy requires that the work done while the shock front moves through a unit mass of air, $P_s\,(V - V_s)$, must equal the kinetic energy imparted to the unit mass of air, $u^2/2$, plus the change in internal energy, $E_s - E$, where the various symbols are defined in Figure A-1. Thus,

$$P_s \Delta V = (u^2/2) + (E_s - E),$$

or

$$P_s(V - V_s) = (u^2/2) + (E_s - E).$$

Using the relations $V = 1/\rho$ and $V_s = 1/\rho_s$, a simultaneous solution of these three equations leads to the Rankine-Hugoniot equations in their usual form:

$$E_s - E = \frac{1}{2}(P_s + P)(V - V_s),$$

$$u = \left((P_s - P)(V - V_s)\right)^{1/2},$$

$$U = V\left(\frac{P_s - P}{V - V_s}\right)^{1/2}.$$

[redacted]

A-2 Equation of State of an Ideal Gas

[redacted] A gas that is heated at constant volume does not do external work; therefore, all of the thermal energy added to the gas is converted to internal energy. This amount of energy is

$$\Delta E = C_V \Delta T$$

where ΔE is the change in internal energy per unit mass, C_V is the specific heat of the gas at constant volume, and ΔT is the temperature change. By definition, the specific heats of an ideal gas are constant; and the internal energy per unit mass is

$$E = C_V T,$$

where T is absolute temperature.

[redacted] Using the thermodynamic identities $PV = RT$, and $C_P - C_V = R$ (where C_P is specific heat at constant pressure, and R is the universal gas constant) the following equation follows:

$$E = \frac{C_V PV}{C_P - C_V} = \frac{PV}{\gamma - 1}$$

where

$$\gamma = \frac{C_P}{C_V}.$$

Eliminating the variables E_s and E makes it possible to use the Rankine-Hugoniot equations to determine the conditions across a shock front in an ideal gas uniquely.

[redacted] The significance of the quantity γ as it appears in the shock wave equations deserves some explanation. In thermodynamics, γ appears most frequently in equations that involve isentropic compression. For example, γ appears in the equation for sound speed because sound wave pressure fluctuations are isentropic. The presence of γ in shock wave equations is sometimes incorrectly interpreted as implying a relationship between shock wave compression and isentropic compression; actually, γ is a convenient constant relating energy content of a gas to pressure and volume. This fact becomes important in paragraph A-6 where strong shock waves are discussed. Variations in the value of γ must then be considered, and the equations

$$\Delta E = C_V \Delta T, \text{ and}$$

$$E = C_V T$$

cannot hold simultaneously. Conveniently, γ is redefined, so the equation

$$\Delta E = C_V \Delta T$$

still may be used. The meaning of γ as a specific heat ratio is lost, and γ becomes simply a constant in the energy equation.

A-3 Shock Wave Equations for an Ideal Gas (U)

[redacted] From the relation for the speed of sound in ambient air,

$$c = (\gamma P/\rho)^{1/2}$$

and the equation for overpressure,

$$\Delta p = P_s - P$$

the set of shock wave equations shown in Table A-1 can be derived. The equations in the right hand column were obtained by assigning to γ the value 1.4, the value for air at moderate temperatures and pressures.

[redacted] These ideal gas equations apply to shock

[redacted]

[redacted]

Table A-1. [redacted] Shock Wave Equations for an Ideal Gas [redacted]

Equations in General Form:	Equations for $\gamma = 1.4$
Velocity of the Shock Front	
$U = c\left(1 + \frac{\gamma + 1}{2\gamma} \cdot \frac{\Delta p}{P}\right)^{1/2}$	$U = c\left(1 + \frac{6\Delta p}{7P}\right)^{1/2}$
Particle Velocity Behind the Shock Front	
$u = \frac{\Delta p}{\gamma P} \cdot \frac{c}{\left(1 + \frac{\gamma + 1}{2\gamma} \cdot \frac{\Delta p}{P}\right)^{1/2}}$	$u = \frac{5\Delta p}{7P} \cdot \frac{c}{(1 + 6\Delta p/7P)^{1/2}}$
Density Ratio Across the Shock Front	
$\frac{\rho_s}{\rho} = \frac{2\gamma + (\gamma + 1)\Delta p/P}{2\gamma + (\gamma - 1)\Delta p/P}$	$\frac{\rho_s}{\rho} = \frac{7 + 6\Delta p/P}{7 + \Delta p/P}$
Dynamic Pressure Behind the Shock Front	
by definition, $q = \frac{1}{2}\rho_s u^2$	
$q_s = \frac{(\Delta p)^2}{2\gamma P + (\gamma - 1)\Delta p}$	$q_s = \frac{5}{2} \cdot \frac{(\Delta p)^2}{7P + \Delta p}$
Temperature Behind the Shock Front	
$T_s = T\left(1 + \frac{\Delta p}{P}\right)\frac{2\gamma + (\gamma - 1)\Delta p/P}{2\gamma + (\gamma + 1)\Delta p/P}$	$T_s = T\left(1 + \frac{\Delta p}{P}\right)\frac{7 + \Delta p/P}{7 + 6\Delta p/P}$
Peak Reflected Overpressure at Normal Incidence	
$\Delta p_r = 2\Delta p + (\gamma + 1)q$	$\Delta p_r = 2\Delta p \frac{7 + 4\Delta p/P}{7 + \Delta p/P}$

[redacted]

waves in air provided the shock strength, $\xi = (\Delta p + P)/P = P_s/P$, is not too large. Usually these equations are assumed to hold for shock strengths of about 10 (132 psi overpressure at sea level) or less; note that at high altitudes this limit corresponds to relatively low overpressures, e.g., about 25 psi at 40,000 ft. The equations for high pressure shock waves are given in paragraph A-6.

As shown in Figure A-1, the subscript s denotes conditions behind the shock front; the absence of a subscript denotes ambient conditions (the subscript o is reserved for ambient conditions at sea level as in Chapter 2). The overpressure is $\Delta p = P_s - P$; c is the speed of sound in undisturbed air; and γ is the ratio of specific heats C_p/C_v. Other quantities are defined by subheadings in the table.

A-4 Units, Constants, and Conversion Factors

Since the most commonly used shock wave equations are written in terms of dimensionless ratios, the choice of units is purely a matter of convenience; therefore, there is an inclination to ignore the fact that certain equations must be handled more carefully. Examples of these equations are the Rankine-Hugoniot equations and the dynamic pressure equation. Three consistent sets of units in common use are shown in Table A-2. Conversion factors and sea level values of various parameters are given in the various units in Appendix B.

A-5 Equation of State of Air

As air is heated by the compression of strong shock waves, the specific heat ratio γ decreases. Therefore, the equation that gives γ in terms of the ratios of the specific heats, which is based on the assumption of a constant γ, is no longer valid. The means of avoiding this problem has already been stated in paragraph A-2: γ_s customarily is *redefined* as that number which gives the correct value for internal energy. Since γ appears frequently in shock wave equations to replace an energy term, the new definition is a convenient one. Note, however, that (except in undisturbed air, where the new and old definitions of γ agree) γ is no longer the specific heat ratio. Therefore, γ should not be used (for example) to calculate sound speed in strongly shocked air.

Table A-2. English and Metric Systems of Units

Unit	mks	cgs	English
length	meter	centimeter	foot
mass	kilogram	gram	pound
force	newton	dyne	slug
time	second	second	second
pressure	newtons/m^2	dynes/cm^2	pounds/ft^2
density	kg/m^3	g/cm^3	slugs/ft^3
velocity	m/sec	cm/sec	ft/sec
energy	joule	erg	ft-lb

Figure A-2 shows the equation of state of air for altitudes up to 240,000 feet. The nearly vertical curves are the Hugoniot curves for air at the indicated altitudes. The Hugoniot curve for a given altitude shows the combinations of peak pressure and peak density that are possible behind a shock front moving into undisturbed air, i.e., into air that is initially at the ambient pressure and density corresponding to that altitude. Curves that show the value of γ assigned to the air just behind the shock front cross the graph as nearly horizontal lines. The curves that cut diagonally across the graph show absolute pressure (not overpressure) just behind the shock front. The ordinate of the graph is shock strength, which was defined in paragraph A-3.

A-6 Equations for Strong Shock Waves in Air

For shock strengths of 10 or more, accurate calculations must use the nonideal equation

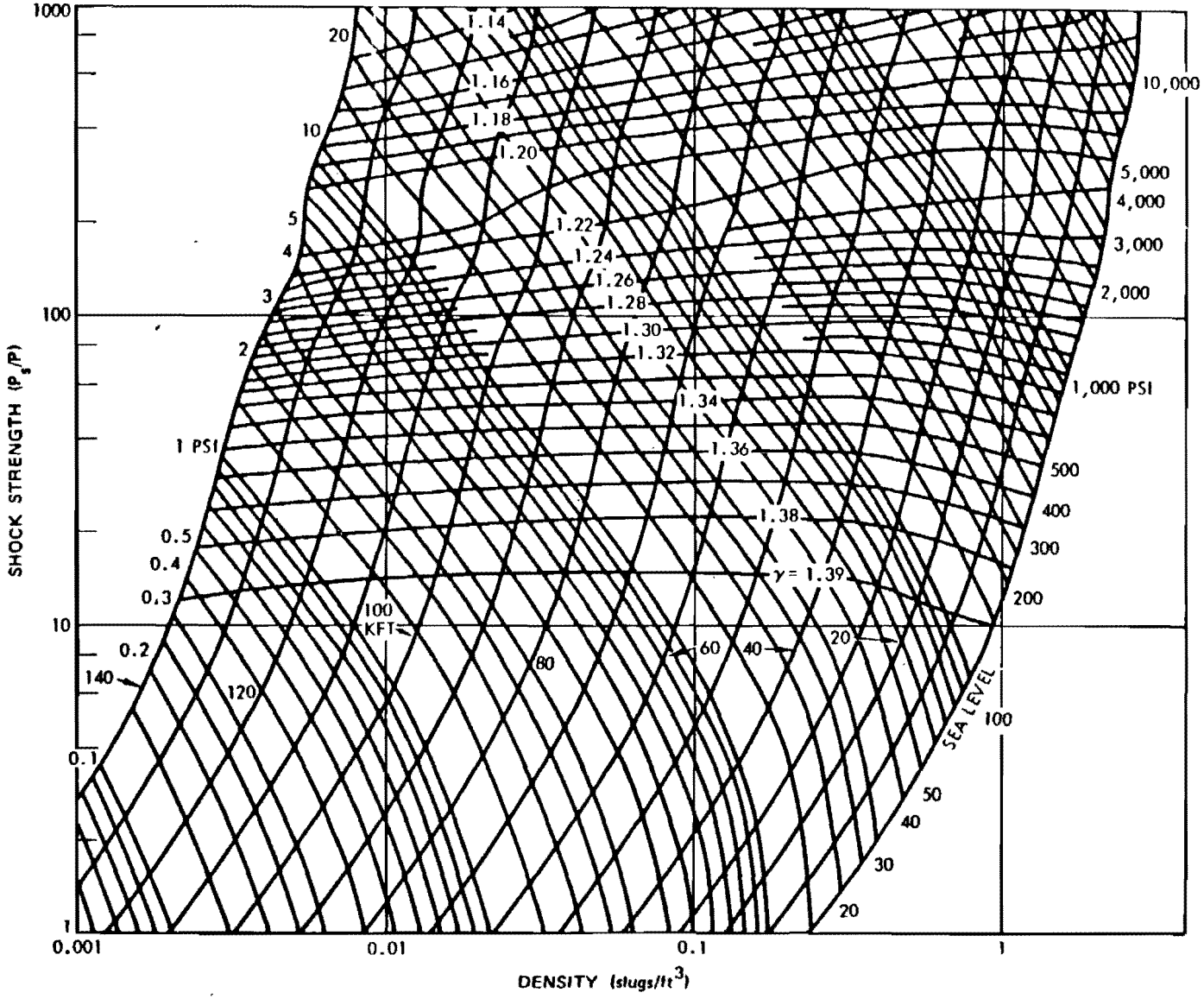

Figure A-2. [redacted] Equation of State Data for Air [redacted]

[redacted]

of state data from Figure A-2. The appropriate shock wave equations are derived in the same manner as those shown in Table A-1. The principal difference is that two values of γ appear, γ for the air ahead of the shock and γ_s for the air just behind the shock front; the values in general are not equal. The shock wave equations for strong shock waves in air are listed in Table A-3. Two approximate velocity equations, accurate to within about 5 percent for shock strengths greater than 5, are shown on the right. As in Table A-1, the subscript s refers to parameters behind the shock front, and symbols with no subscript refer to ambient conditions.

[redacted] Note that shock strength ξ is a direct function of the absolute pressure P_s behind the shock front, rather than of Δp, the overpressure.* A shock strength of 1 therefore represents a vanishingly weak shock wave: and, at sea level, a shock strength of 2 represents an *overpressure* of 14.7 psi. Values for γ_s must be obtained from the equation of state data in Figure A-2.

* [redacted] This definition is not universal; shock strength is defined in some reports as $\Delta p/P$.

Table A-3. [redacted] Equations for Strong Shock Waves [redacted]

Complete Equation:	High-Shock-Strength Approximation:
Velocity of the Shock Front	
$U = c\left(\frac{(\xi - 1)(1 + \mu_s\xi)}{\gamma[\xi(\mu_s - 1) - (\mu - 1)]}\right)^{1/2}$	$U = c\left(\frac{\xi(\gamma_s + 1)}{2\gamma}\right)^{1/2}$
Particle Velocity Behind the Shock Front	
$u = c\left(\frac{(\xi - 1)[\xi(\mu_s - 1) - (\mu - 1)]}{\gamma_o(1 + \mu_s\xi)}\right)^{1/2}$	$u = c\left(\frac{2\xi}{\gamma(\gamma_s + 1)}\right)^{1/2}$
Density Ratio Across the Shock Front	
$\frac{\rho_s}{\rho} = \frac{1 + \mu_s\xi}{\mu + \xi}$	
Dynamic Pressure Behind the Shock Front	
$q_s = \frac{1}{2}P(\xi - 1)\left(\frac{1 + \mu_s\xi}{\mu + \xi} - 1\right)$	

where

$$\mu_s = \frac{\gamma_s + 1}{\gamma_s - 1}, \quad \mu = \frac{\gamma + 1}{\gamma - 1}, \quad \xi = \frac{P_s}{P} = \left(\frac{\Delta p + P}{P}\right), \quad \gamma = 1.4$$

[redacted]

SECTION II

PHYSICAL DESCRIPTION OF SHOCK WAVE BEHAVIOR

Newton's second law, which relates force to the change in momentum that it produces, provides straightforward explanations of many shock wave phenomena. In particular, it explains certain reflection phenomena and the way in which these phenomena determine the forces produced by a blast wave when it strikes a surface or a small object.

Acoustic theory also provides explanations of blast phenomena. These explanations are important because they appear frequently in discussions of shock wave reflection. The following discussion relates the acoustic theory explanations with those that are based on Newton's second law.

A-7 Step Function Shock Wave

In most respects, the properties of the shock front are independent of the shape of the pressure waveform that follows the front. Shock wave phenomena, therefore, can be explained in terms of the simplest possible waveform: a region of completely uniform pressure, density, and particle velocity behind a planar shock front. In such a wave, the shock front usually is considered a mathematical discontinuity, in which the pressure, velocity and other parameters are step functions of position and time.

This type of simple shock wave may be generated by the mechanism shown in Figure A-3. A piston moves at constant velocity in a frictionless cylinder (a piston velocity of 431 ft/sec, a number that will be used later for purposes of illustration, produces a shock wave with

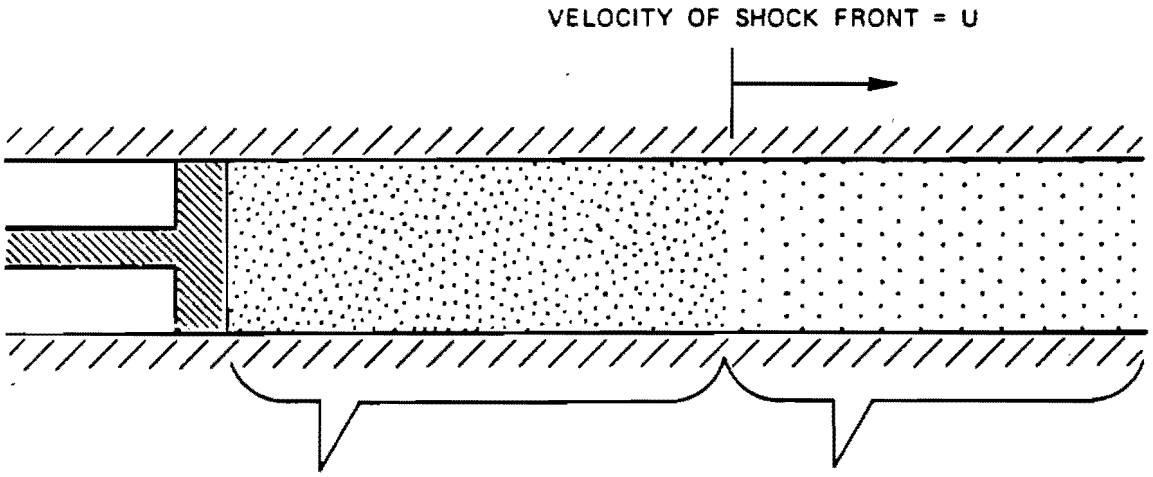
VELOCITY OF SHOCK FRONT = U
CONDITIONS BEHIND SHOCK FRONT:
PARTICLE (WIND) VELOCITY = u
DENSITY = ρ_s
PRESSURE = P_s
ENERGY PER UNIT MASS = E_s
CONDITIONS IN AMBIENT AIR:
PARTICLE VELOCITY = 0
DENSITY = ρ
PRESSURE = P
ENERGY PER UNIT MASS = E

Figure A-3. Idealized Shock Wave

[redacted]

an overpressure of 10 psi). The compressed air that constitutes the shock wave is uniform in density, pressure, and velocity.

[redacted] The step function shock wave differs from the blast wave from a nuclear burst in that the latter: (1) becomes weaker as it propagates away from the burst; (2) produces a decaying rather than a constant overpressure after the shock front passes a given point; and (3) has a spherical rather than a planar shock front. However, these differences are unimportant in the development of most of the concepts that apply to the shock front. As a result of its long overpressure duration, the blast wave from a high yield nuclear weapon is in many respects comparable to the idealized shock wave of Figure A-3.

A-8 Shock-Front Formation [redacted]

[redacted] The piston shown in Figure A-3 will require an interval of time to reach its final velocity. While it is accelerating, the pressure at the face of the piston will increase steadily. The pressure wave that the piston generates during this time lacks the abrupt pressure rise characteristic of a shock; however, differences in the velocities of different parts of the pressure wave ultimately will cause a shock front to form. Small pressure disturbances travel at the local speed of sound. In the air compressed by the piston, two factors cause this speed to differ from the speed of sound in ambient air; (1) compression of the air raises the air temperature, thereby increasing the speed of sound; (2) in moving air, pressure disturbances move with a velocity that is the vector sum of the air and sound velocities.

[redacted] As the piston starts to move, it creates an initial pressure disturbance that propagates ahead of the piston (to the right in Figure A-3) with a velocity equal to the velocity of sound in ambient air. By the time the piston reaches its final velocity, it will have produced a pressure wave that can propagate considerably faster than the ambient speed of sound. The wave produced by the high pressure just ahead of the piston soon overtakes the lower pressure wave, and a shock front is formed.

[redacted] After steady-state conditions are reached, the shock front moves at supersonic velocity with respect to the undisturbed air but at subsonic velocity with respect to the air behind the shock front. Ahead of the shock front, there is no early pressure increase to indicate the impending arrival of the shock wave. If such an early pressure wave were present, the shock front would overtake it. Behind the shock front, whatever pressure irregularities that may form can overtake the front and merge with it. The tendency for all pressure gradients to concentrate at the shock front is so strong that moderately strong shock waves in air generate shock fronts that are only a few atomic mean free paths (mfp) thick (at sea level, 1 mfp is about 10^{-5} cm).

A-9 Pressure-Momentum Interaction at a Shock Front [redacted]

[redacted] Before applying Newton's second law to a reflection problem, it will be examined with respect to a step function shock wave shown in Figure A-4. This is a simple problem that requires little more than a sample calculation. It is, however, useful as a preparation for the reflection problem that is discussed below. Numerical values of pressure, density, and velocity, calculated from the equations in Table A-1, appear in the figure.

[redacted] To evaluate Newton's second law, it is necessary to determine the momentum change per unit time and the force that produces the change. If a unit area of the shock front is considered, the force is numerically equal to the shock wave overpressure Δp, which in this example is 10 psi. To obtain a consistent set of units, this pressure must be expressed as 1,440 lbs/ft^2.

[redacted]

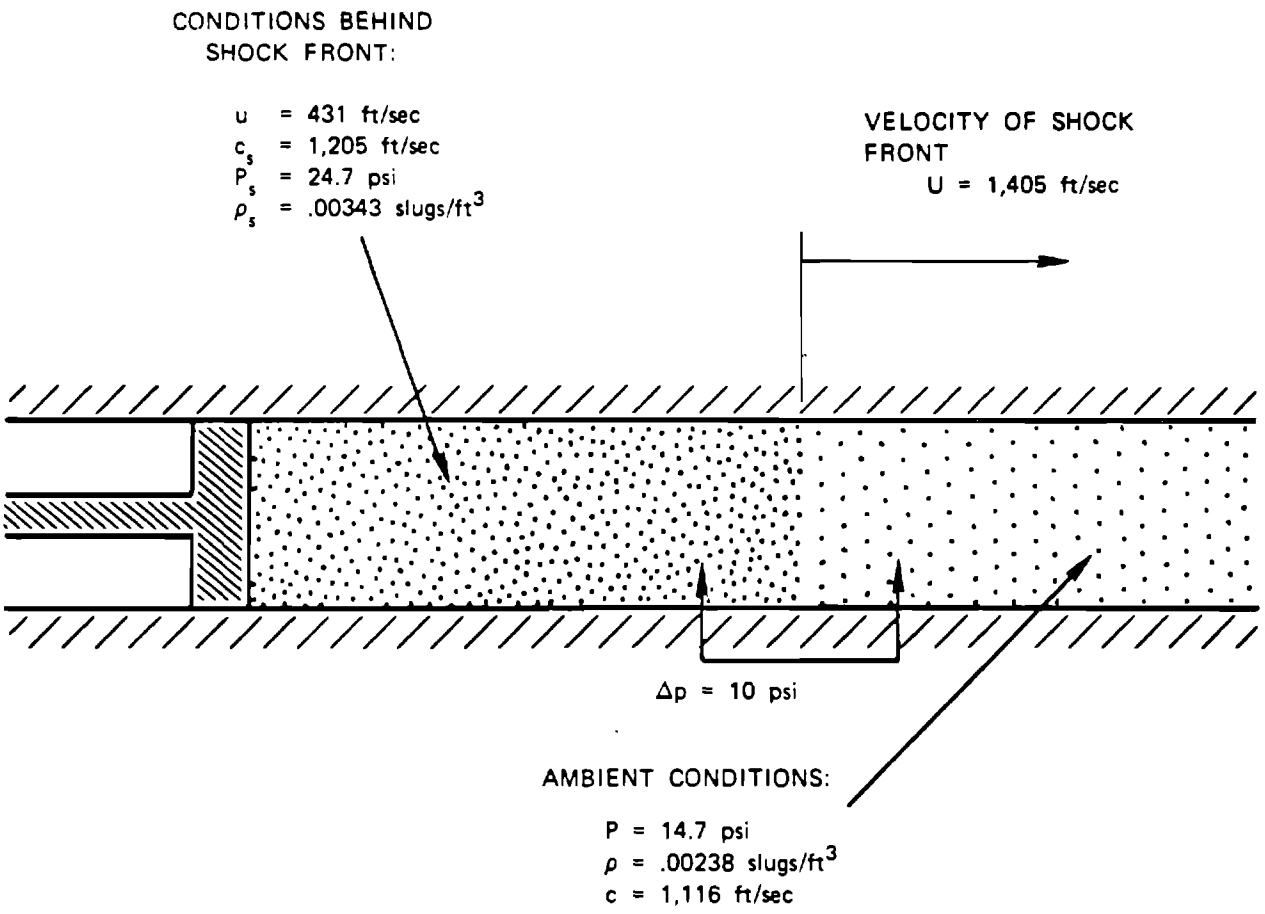

Figure A-4. [redacted] Parameters of a 10 psi Shock Wave [redacted]

[redacted] The mass of air that enters one square foot of shock front area each second is the ambient density, .00238 slugs/ft^3, times the shock front velocity of 1,405 ft/sec. This air is given a velocity of 431 ft/sec as it enters the shock wave. Thus,

$$\Delta p = \rho U u, \text{ or}$$

$$1{,}440 = .00238 \times 1{,}405 \times 431$$

A-10 Normal Reflection at a Solid Barrier [redacted]

[redacted] Figure A-5 shows a 10-psi shock wave that has struck the end of the cylinder and has formed a receding shock wave. Behind the receding shock front, the air is stationary. The velocity change at the reflected shock front has the same magnitude (but the opposite direction) as the velocity change of 431 ft/sec at the incident shock front. However, the pressure jump Δp_1 across the reflected shock front is greater than Δp because more mass per second is involved (see Figure A-5). The difference results principally from the higher density of the air entering the shock wave, but also results from the greater relative velocity, 1,491 ft/sec, between the shock front and the incoming air.

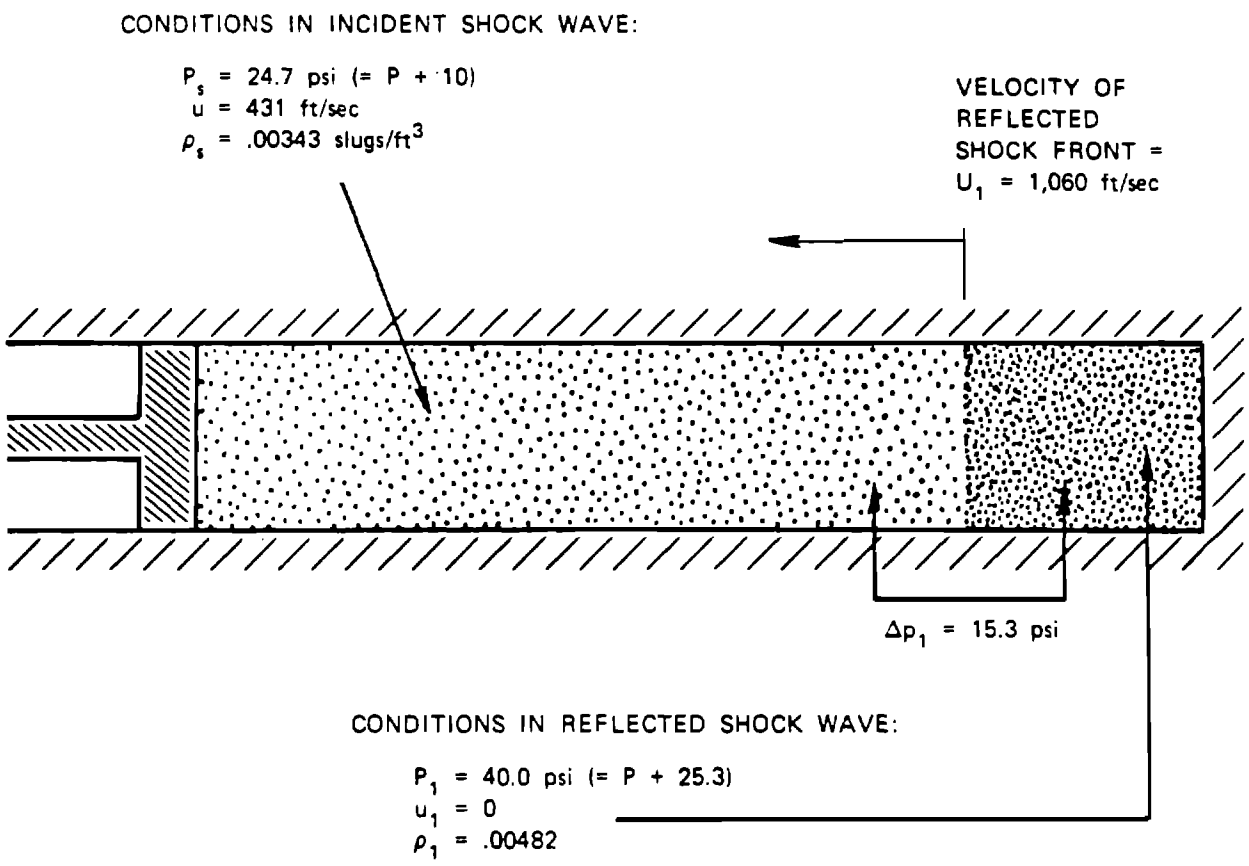
CONDITIONS IN INCIDENT SHOCK WAVE:
P_s = 24.7 psi (= P + 10)
u = 431 ft/sec
ρ_s = .00343 slugs/ft^3
VELOCITY OF REFLECTED SHOCK FRONT = U_1 = 1,060 ft/sec
Δp_1 = 15.3 psi
CONDITIONS IN REFLECTED SHOCK WAVE:
P_1 = 40.0 psi (= P + 25.3)
u_1 = 0
ρ_1 = .00482

Figure A-5. [redacted] Reflection of a 10 psi Shock Wave from a Solid Barrier [redacted]

[redacted] The equation expressing Newton's second law may be obtained from basic physical principles, or it may be obtained from equations given in Section I by changing the frame of reference to one that is stationary with respect to the air ahead of the reflected shock front.

$$\Delta p = \rho U u,$$

$$15.3 \times 144 = .00343\ (1{,}060 + 431)\ 431,$$

$$2{,}220 = .00343 \times 1{,}491 \times 431$$

[redacted] The reflected overpressure, Δp_r, is the amount by which the pressure at the reflecting surface exceeds ambient pressure. It is the sum of the pressure jumps across the incident and the reflected shock fronts, or 25.3 psi.

[redacted] Acoustic theory often draws on the useful concept of images to explain the shock wave patterns produced at a reflecting surface. The reflecting surface is equivalent to a plane of symmetry. In the foregoing example, the image created by the reflecting surface would be a second piston, moving to the left with a velocity of 431 ft/sec, and located as far to the right of the reflecting surface as the real piston is to the left of it. As the two shock waves of equal strength collide, they produce conditions equivalent to those shown in Figure A-5.

[redacted]

[redacted] Explanation of the strength of the reflected shock front does not follow as readily from acoustic theory as does the basic shock wave pattern. Acoustic theory began with the study of sound waves, which have such low amplitudes that air acts as a linear medium. In such a medium, pressures are additive, and the wave reflected by a perfect reflector has the same amplitude as the incident wave. Shock wave effects are decidedly nonlinear, as is shown in the preceding example.

[redacted] Acoustic theory explains that the pressure jump of 15.3 psi instead of 10 psi at the reflected shock front is caused by the effect of dynamic pressure. Mathematically, this is a convenient explanation. For shock strengths less than about 10, the equations

$$\Delta p_1 = \Delta p + 2.4\ q$$

and

$$\Delta p_r = 2\Delta p + 2.4\ q$$

give correct values for Δp_1, the pressure jump at the reflected shock front and Δp_r, the reflected overpressure. The constant 2.4 is valid for air subjected to low shock strengths. In general, the constant has the value $\gamma + 1$.

[redacted] Physically, however, the explanation is artificial. In the sense that dynamic pressure effects are the effects caused by the momentum of air in motion, Δp_1 is produced entirely by dynamic pressure. The basic acoustic theory fails to predict shock wave phenomena. Predictions are possible only from a modified theory, tailored to fix experimental facts, and experience in using this theory is necessary to use it successfully.

A-11 Pressures on Simple Shapes[redacted]

[redacted] Two examples will be used to illustrate the phenomena that occur when a blast wave interacts with a target.

[redacted] The first example is the steady-state pressure pattern around a sphere placed in the path of the shock wave. Figure A-6 shows the nature of this pattern after the shock front has passed, and equilibrium conditions apply.

[redacted] This problem is more complex than the one discussed in paragraph A-10. The air particles directed exactly toward the center of the sphere reach the stagnation point, a point on the sphere at which the air is brought to rest, and the momentum that these particles give up may be calculated readily. All of the other air particles affected by the sphere behave in a more complicated way. They are slowed down and deflected, but they are not stopped.

[redacted] An order-of-magnitude equation for force may be obtained by assuming that all of the air directed toward the sphere is stopped. The momentum per unit area per unit time di-

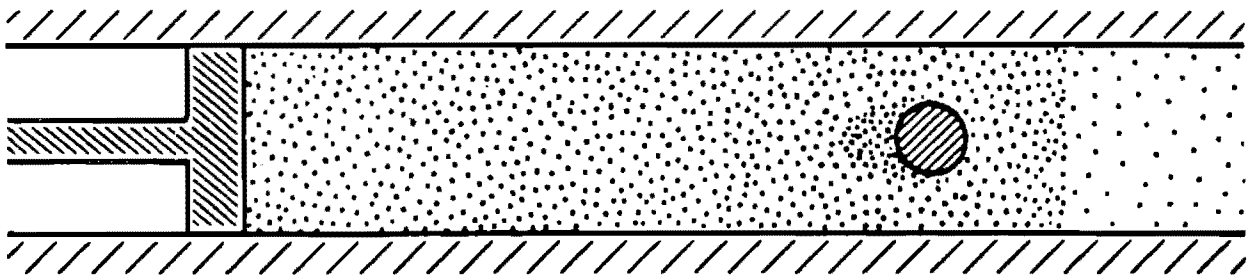

Figure A-6. [redacted] Reflection of a Shock Wave by a Small Object [redacted]

[redacted]

[redacted]

rected toward the sphere is $\rho_s u$ (the mass flow per unit area per unit time). Application of Newton's second law shows that the wind pressure is about

$$F/A = \rho_s u^2.$$

A detailed analysis would show that the pressure produced at the stagnation point of a sphere in a moderately strong wind is more closely approximated by dynamic pressure, which has a value that is just half of that given by the previous equation

$$q = \frac{1}{2} \rho_s u^2.$$

[redacted] Therefore, the wind pressure at the stagnation point on the sphere is roughly

$$q = \frac{1}{2} \times .00343 \times (431)^2,$$

$$= 318.58 \text{ lbs/ft}^2,$$

$$= 2.2 \text{ psi}.$$

Total pressure at the stagnation point is about 12.2 psi, the sum of the static overpressure and the dynamic pressure.

[redacted] The important point in this example is that the high pressure region around the object is stationary, not moving forward to meet the oncoming air as was the receding shock wave shown in Figure A-5. Consequently, the rate at which air enters the high pressure region is lower. The rate at which momentum is extracted from incoming air is correspondingly lower. By Newton's second law, the pressure developed is smaller.

[redacted] Acoustically, no reflection is considered to occur in this example. The problem is simply one of an object in an airstream.

[redacted] The second illustration is the transient interaction between a blast wave and a small cube. This type of interaction is largely a combination of those already discussed. For simplicity, the blast wave is assumed to strike one side of the cube head-on. Shortly after the shock front strikes the cube, the reflection process is much like that produced at the closed end of a piston (Figure A-5). A receding shock wave is formed, the mass flow rate into this shock wave is high, and the front face of the cube is subjected to a high reflected overpressure (25.3 psi for a 10 psi incident shock wave).

[redacted] At the edges of the front face of the cube, the layer of compressed air in the receding shock wave is unconfined. It flows outward, around the edges of the cube. This outward flow relieves the high pressure behind the receding shock front. As a result of this pressure relief, the receding shock front loses velocity; consequently, the incoming air gives up its momentum at a decreasing rate. A steady-state flow pattern develops, and the pressure at the front surface of the cube drops to roughly the incident overpressure plus the incident dynamic pressure. The situation is now similar to that shown in Figure A-6.

[redacted] Part of the acoustic explanation is very descriptive. Pressure relief waves form at the edge of the front surface of the cube and propagate inward. Reflections that occur when these relief waves meet increase the rate of flow over the front face and around the edges of the cube. The time required for the steady-state flow pattern to develop is about two or three times that required for a shock wave to travel from the edge of the cube to the center of the front face.

[redacted] The remainder of the acoustic explanation is evident only to a person familiar with acoustic theory or to a person who has previously encountered this particular explanation. It involves understanding: (1) the reflection coefficient of an object becomes small as the wave-

[redacted]

length of the incident sound wave becomes large compared with the dimensions of the object; and (2) a pressure waveform has an equivalent spectrum of sound waves of different wavelengths (strictly speaking, the equivalent spectrum requires a linear medium and is only an approximation in strongly shocked air).

These acoustic concepts, applied to the problem of reflection from a small cube, predict that the cube will reflect the shock front strongly, but that the reflection coefficient of the cube will decrease rapidly after the shock front passes. The reflected wave weakens by spherical divergence as it propagates away from the cube, and the pressure on the front face of the cube decreases to its steady-state value.

A-12 The Rankine-Hugoniot Equations (Alternate Analysis)

In the conventional derivation of the Rankine-Hugoniot equations (paragraph A-1), the algebra tends to obscure the physical picture associated with the derivation. The following analysis provides a more intuitive introduction to the subject.

The interaction at the shock front is basically an inelastic collision. The truth of this statement is evident from the definition of an inelastic collision. It is a collision in which the colliding bodies stick together and move with a common velocity after they collide.

The statement given above provides a method to account for the energy exchanges that occur at the shock front. It may be applied most readily if the collision is considered to occur between a very thin layer of unshocked air and the mass of air behind the shock front. The following statement may then be confirmed readily.

The inelastic collision at the shock front is 50 percent efficient in transferring kinetic energy to the incoming air. A change to the center-of-mass frame of reference is the first step necessary to demonstrate this fact. Since the mass of air being picked up at any instant is infinitesimal, this frame of reference moves with the air behind the shock front. The initial kinetic energy per unit area of the shock front is, in this frame of reference, that of the thin layer of unshocked air approaching the shock front with a relative velocity of u. If its mass is dm, its initial kinetic energy is*

$$d(KE) = \frac{1}{2} u^2 dm.$$

After a completely inelastic collision, the kinetic energy in the center-of-mass frame of reference is zero.† In other words, the amount of energy that is converted from kinetic energy to internal energy in the collision is equal to $d(KE)$.

In the original frame of reference (stationary with respect to the unshocked air), $d(KE)$ is equal to the kinetic energy of the thin layer of air after it has become a part of the shock wave. Thus, the kinetic energy imparted to the air and the kinetic energy converted to internal energy by the inelastic collision are equal, i.e., this method of transferring kinetic energy is 50 percent efficient.‡

Accounting for all of the work done at the shock front is complicated by an energy ex-

* A rigorous derivation of the equations governing the inelastic collision of two bodies requires the simultaneous solution of the energy and momentum equations of the system. If a large mass and a very small mass are approaching one another with equal and opposite momenta, the kinetic energy of the larger mass is negligible compared to the kinetic energy of the smaller mass.

† By definition, total momentum in the center-of-mass frame of reference is zero. Since momentum is conserved in the collision of two bodies, the total momentum remains zero after any collision. After a completely inelastic collision, neither of the colliding bodies is moving with respect to the center of mass; therefore, their final kinetic energy in this frame of reference is zero.

‡ Although kinetic energy changes with changes in the frame of reference, the energy loss in an inelastic collision does not.

change that is independent of the exchange produced by the inelastic collision. The total work done on a unit mass of incoming air results from the pressure P_s that is behind the shock front moving through the distance required to compress this mass of air from its initial volume V to its final volume V_s.

$$W'_{total} = P_s(V - V_s).$$

One portion of this work is done by the ambient pressure P in displacing the volume $V - V_s$. Since the ambient pressure does not produce a force that has directional characteristics, it has no function in setting the air in motion. This portion of the work only contributes to compression.

$$W'_{comp} = P(V - V_s)$$

The remainder of the work is done by the overpressure $\Delta p = P_s - P$, displacing the volume $V - V_s$. At the shock front, the effect of overpressure is completely directional, and overpressure creates the force that accelerates the air that is overtaken by the shock front. This is the portion of the work that is required to produce kinetic energy by a collision process,

$$W'_{coll} = (P_s - P)(V - V_s).$$

As already demonstrated, half of this work appears as kinetic energy and half as internal energy of the unit mass of air added to the shock front. Note that the work converted to internal energy by the collision process is closely related to W'_{comp} in that both contribute to compressing the gas to the volume V_s and, in this way, both increase the internal energy of the air.

The energy exchange equations for a unit mass of air entering the shock front follow directly from the discussion in the preceding paragraph. The kinetic energy added to the unit mass of air is

$$\frac{1}{2}u^2 = \frac{1}{2}W'_{coll},$$

$$= \frac{1}{2}(P_s - P)(V - V_s),$$

and the particle (wind) velocity is

$$u = \left((P_s - P)(V - V_s)\right)^{1/2}.$$

The change in internal energy of the unit mass of air is

$$E_s - E = W'_{comp} + \frac{1}{2}W'_{coll}$$

$$= P(V - V_s) + \frac{1}{2}(P_s - P)(V - V_s)$$

$$= \frac{1}{2}(P_s + P)(V - V_s).$$

To obtain the equation for shock front velocity, note that while the air in the shock wave moves into a volume $V - V_s$, the shock front has advanced through a volume V. The ratio of shock front velocity to particle velocity is therefore

$$\frac{U}{u} = \frac{V}{V - V_s}$$

$$U = \left(\frac{V}{V - V_s}\right)\left((P_s - P)(V - V_s)\right)^{1/2}$$

$$U = V\left(\frac{P_s - P}{V - V_s}\right)^{1/2}.$$

The equations for u, $(E_s - E)$, and U are the Rankine-Hugoniot equations given previously in paragraph A-1.

[redacted]

Note: Although the interaction at the shock front is completely inelastic, the overall reaction of a blast wave in free air is partially elastic. In such a blast wave, the pressure behind the shock front is not constant, but decays with time. The air behind the front expands and returns energy that helps to propagate the shock wave (see footnote to paragraph 2-33, Chapter 2). This fact does not alter the validity of the argument presented above. It simply points out that the inelastic collision at the shock front only describes part of the mechanism of blast wave propagation.

A-13 Dynamic Pressure [redacted]

[redacted] Dynamic pressure is frequently equated to the wind force produced on a target by the high velocity winds in a blast wave, but the relation between force and dynamic pressure is not this simple.

[redacted] One source of confusion is the name which implies a meaning that differs from the correct one. In a compressible fluid, the true meaning of dynamic pressure is limited to the mathematical definition

$$q = \frac{1}{2}\rho_s u^2$$

where ρ_s is mass per unit volume and u is particle velocity behind the shock front. Strictly speaking, q is not a pressure. A body moving along with moving air will not feel a force that is attributable to dynamic pressure. Dynamic pressure is kinetic energy per unit volume. Reasons for calling it a pressure are: (1) it has the dimensions of pressure; and (2) this energy can be used to develop a pressure.

[redacted] A stationary body exposed to a wind will experience pressures that differ at different points on its surface. The highest pressure on the body is the stagnation pressure, which occurs wherever the air is completely stopped by impact with the body. For example, if the body is a sphere, the stagnation pressure occurs at the point on the surface that faces directly into the wind. For an incompressible fluid, stagnation pressure is simply the sum of the free-stream static pressure and the free-stream dynamic pressure. However, for a compressible fluid, such as air, stagnation pressure is the sum of the free-stream static pressure and a quantity called the free-stream *impact pressure.* At low velocities, impact pressure and dynamic pressure are essentially equal, but at velocities that are appreciable compared with sound speed, impact pressure rises above dynamic pressure. When wind speed is equal to sound speed, impact pressure exceeds dynamic pressure by about 28 percent.

[redacted] The forces exerted by strong winds correspond more directly to impact pressures than to dynamic pressure. This suggests that weapons effects calculations should be based on impact pressures rather than on dynamic pressures; but, both in this field and in aerodynamics, dynamic pressures are employed more commonly. The choice is based on conventional practice. In aerodynamic problems, dynamic pressure is used because it may be calculated readily. Wind force on an object is calculated from the equation

$$F_w = C_D q A$$

where C_D is drag coefficient and A is an area related to the size of the object. The drag coefficient is not constant. It is a function of velocity, and its variation absorbs not only the discrepancy between dynamic pressure and impact pressure, but also accounts for the net effect of the complex pressure pattern that forms around an object in an airstream. The product qA, although it has the dimensions of a force, has no direct physical relation to any force exerted by the wind.

[redacted] In weapons effects calculations, dynamic pressure often is as convenient as it is in aerody-

[redacted]

[redacted]

[redacted]

namics: damage criteria for such objects as buildings are established in terms of conventional shock wave parameters, such as overpressure, dynamic pressure, or impulse. Consequently, the stagnation pressure or other actual pressures found at various points on specific structures usually are not calculated unless specific blast loading information is desired. In some cases, the choice of dynamic pressure may not be appropriate for damage criteria. For example, when the air in the blast wave is dust laden (as it is for certain combinations of yield, burst height, ground range, and surface properties), a measurement with a conventional dynamic pressure gauge often is ambiguous. The dust is not necessarily in velocity equilibrium with the air, and the amount of dust is not known. As a result, it is often difficult to calculate the dynamic pressure of air alone from such experimental measurements.

[redacted]

[redacted]

APPENDIX B

USEFUL RELATIONSHIPS[redacted]

B-1 General Equivalents [redacted]

[redacted] One kiloton (kt) is defined to be 10^{12} calories of energy release.* This amount of energy will be released by the complete fission of 0.057 kg (57 grams or 2 ounces) of fissionable material.† Equivalents to this amount of energy in other units are:

- 2.61×10^{25} million electron volts (MeV),
- 4.18×10^{19} ergs,
- 1.16×10^{6} kilowatt-hours,
- 3.97×10^{9} British thermal units.

[redacted] Some equivalents of the complete conversion of mass to energy are:

1 gram mass = 5.61×10^{26} MeV
= 8.99×10^{20} ergs
= 2.15×10^{13} calories

[redacted] The temperature associated with one electron volt is 11,605.9 degrees Kelvin.

B-2 Constants [redacted]

[redacted] Velocity of light: 3×10^{8} m/sec = 3×10^{10} cm/sec.

[redacted] Avagadro's number: 6.023×10^{23} molecules per mole (gram molecular weight).

[redacted] Planck's constant: 6.625×10^{-27} erg-sec.

[redacted] Boltzmann constant: 1.38×10^{-16} erg/°K.

[redacted] ‡Mass of electron: 9.1085×10^{-28} gm.

[redacted] ‡Mass of proton: 1.672×10^{-24} gm.

[redacted] ‡Mass of neutron: 1.675×10^{-24} gm.

[redacted] ‡Mass of alpha particle: 6.64×10^{-24} gm.

[redacted] Loschmidt number: 2.687×10^{19} molecules of ideal gas per cubic centimeter at °C.

[redacted] Electron charge:

4.803×10^{-10} esu = 1.602×10^{-20} emu
= 1.602×10^{-19} coulombs.

B-3 Standard Sea Level Atmosphere [redacted]

[redacted] Pressure = 14.696 psi
= 2,116.22 lb/ft^2
= 1,013.25 millibars
= 101,325. newtons/m^2
= 1,013,250. dynes/cm^2

[redacted] Temperature = 59°F
= 15°C
= 288.15°K
= 518.4°R

[redacted] Density = 2.38×10^{-3} slug/ft^3
= 7.65×10^{-2} lb/ft^3
= 1.225×10^{-3} gm/cm^3
= 1.225 kg/m^3

[redacted] Speed of sound = 1,116.45 ft/sec
= 340.29 m/sec
= 34,029 cm/sec

[redacted] See footnote on page 1-3 for the origin of the definition.

† [redacted] This is the energy released by the *fission* of 57 grams of fissionable material. It is *not* the energy that would be released by the conversion of 57 grams mass to energy.

‡ [redacted] Classical rest mass.

[redacted]

[redacted]

[redacted] Gravitational acceleration
= 9.8067 m/sec^2
= 32.1741 ft/sec^2

B-4 Conversions [redacted]

[redacted] Length:

1 ft = 0.3048 m
= 30.48 cm

1 m = 3.281 ft

1 kft = 0.3048 km
= 0.1894 mi
= 0.1645 nm

1 km = 1,000 m
= 3,281 ft
= 3.281 kft
= 0.6214 mi
= 0.5396 nm

1 mi = 5,280 ft
= 1,760 yds
= 5.280 kft
= 1.609 km
= 0.8684 nm

[redacted] Force:

1 dyne = 1.0197 x 10^{-3} gm (weight)
= 2.2481 x 10^{-6} lb (weight)

1 gm (weight) = 980.665 dynes
= 2.2046 x 10^{-3} lb (weight)
= 1 x 10^{-3} kg (weight)

1 lb (weight) = 4.4482 x 10^5 dynes
= 453.59 gm (weight)
= 0.45359 kg (weight)

[redacted] Pressure:

1 dyne/cm^2 = 1.0197 x 10^{-3} gm/cm^2
= 1 x 10^{-1} newtons/m^2
= 7.5 x 10^{-4} mm mercury (0°C)
= 4.015 x 10^{-4} in. water (4°C)
= 2.089 x 10^{-3} lb/ft^2
= 1.451 x 10^{-5} lb/in.^{2} (psi)
= 1.02 x 10^{-2} kg/m^2
= 1 x 10^{-3} millibars

1 gm (wt)/cm^2 = 980.665 dynes/cm^2
= 980.665 x 10^{-1} newtons/m^2
= 10.0 kg/m^2
= 2.048 lb/ft^2
= 1.422 x 10^{-2} lb/in.^{2} (psi)
= 7.35 x 10^{-1} mm mercury (0°C)
= 0.394 in. water (4°C)
= 980.665 x 10^{-3} millibars

1 lb (wt)/in.^{2} (psi) = 6.895 x 10^4 dynes/cm^2
= 6.895 x 10^3 newtons/m^2
= 703.07 kg/m^2
= 70.307 gm/cm^2
= 51.715 mm mercury (0°C)
= 27.673 in. water (4°C)
= 68.947 millibars

1 millibar = 100 newtons/m^2
= 1,000 dynes/cm^2
= 1.45 x 10^{-2} lb/in.^{2}
= 2.089 lb/ft^2

[redacted] Density:

1 gm/cm^3 = 1,000 kg/m^3
= 3.613 x 10^{-2} lb/in.^{3}
= 62.43 lb/ft^3
= 1.94 slugs/ft^3

1 kg/m^3 = 1 x 10^{-3} gm/cm^3
= 3.613 x 10^{-5} lb/in.^{3}

[redacted]

[redacted]

[redacted]

= 6.243×10^{-2} lb/ft^3
= 1.94×10^{-3} slugs/ft^3

1 lb/ft^3 = 1.6018×10^{-2} gm/cm^3
= 16.018 kg/m^3
= 5.787×10^{-4} lb/in.^{3}
= 3.108×10^{-2} slugs/ft^3

1 slug/ft^3 = 0.5154 gm/cm^3
= 515.4 kg/m^3
= 1.862×10^{-2} lb/in.^{3}
= 32.174 lb/ft^3

[redacted] Energy:

1 gm-cal = 4.184 joules
= 4.184×10^7 ergs
= 3.086 ft-lb
= 3.966×10^{-3} Btu

1 joule = 1×10^7 ergs
= 0.239 gm-cal
= 0.738 ft-lb
= 9.480×10^{-4} Btu

1 erg = 1×10^{-7} joules
= 2.39×10^{-8} gm-cal
= 7.38×10^{-8} ft-lb
= 9.48×10^{-11} Btu

1 ft-lb = 1.356 joules
= 1.356×10^7 ergs
= 3.240×10^{-1} gm-cal
= 1.285×10^{-3} Btu

1 Btu = 252 gm-cal
= 1,054 joules
= 1.054×10^{10} ergs
= 778 ft-lb

[redacted] Velocity:

1 cm/sec = 1×10^{-2} m/sec
= 3.281×10^{-2} ft/sec
= 2.237×10^{-2} mi/hr
= 1.942×10^{-2} knots

1 m/sec = 100 cm/sec
= 3.281 ft/sec
= 2.237 mi/hr
= 1.942 knots

1 ft/sec = 30.48 cm/sec
= 3.048×10^{-1} m/sec
= 6.818×10^{-1} mi/hr
= 5.921×10^{-1} knots

1 mi/hr = 44.70 cm/sec
= 0.4470 m/sec
= 1.4667 ft/sec
= 0.8684 knots

1 knot = 51.48 cm/sec
= 0.5148 m/sec
= 1.689 ft/sec
= 1.152 mi/hr

[redacted] Temperature:

°K = °C + 273.15
°R = °F + 459.4
°C = 5/9 (°F - 32)
°F = 9/5 °C + 32

[redacted] Wavelength:

1 Å = 10^{-8} cm
= 10^{-10} m
= $10^{-4}\mu$

1μ = 10^{-4} cm
= 10^{-6} m
= 10^4 Å

[redacted]

B-5 Fractional Powers and Dimension Scaling

Figures B-1 and B-2 provide the information necessary to perform many of the fractional power scaling operations required by equations presented in this manual. The use of these figures is demonstrated in Problem B-1. Figure B-3 is a nomogram that shows the relationships among the height of burst, the horizontal distance, and the slant range. A straight line through any two (known) of these quantities (on the appropriate scale) will pass through the third (unknown) quantity on its scale. The three dimensions must, of course, be in the same units. The diagram accompanying this nomogram should make its use obvious, and no example is provided. While Figures B-1 through B-3 are plotted accurately, visual interpolation on these figures cannot provide accurate results. If tools such as a slide rule, logarithm tables, or a calculator that can perform fractional power operations are available, users of this manual are encouraged to make use of those tools. Figures B-1 through B-3 are provided for those who desire a reasonable answer in the absence of such tools.

[redacted]

Problem B-1. Use of Fractional Power Curves and Dimension Scaling Nomogram

[redacted] Figure B-1 shows several fractional powers of numbers between 1 and 100,000. The fractional powers are those that are necessary to apply various scaling procedures presented elsewhere.

[redacted] Figure B-2 is a nomogram from which actual dimensions may be obtained from various scaled dimensions for yields from 0.1 kt to 100 Mt. The scaling power for which the scaled dimensions are applicable is indicated at the top of the scale in each case. A straight line connecting a yield with any scaled dimension will cross the actual dimension scale at the proper value according to the scaling which is being used. The dimensions may be in any units for which scaling is given, but the scaled dimension and the actual dimension will always be in the same units.

[redacted] *Example 1* [redacted]

Given: A 500 kt weapon is to be burst at the minimum height of burst at which fallout is not expected. A conservative height of burst is desired.

Find: The actual height of burst at which the weapon is to be detonated.

Solution: From paragraph 5-22, the minimum conservative height of burst for a 500 kt weapon at which fallout is not expected is 180 $W^{0.4}$ ft.

Answer a: From B-1

$$(500)^{0.4} = 12$$

$$180 \times 12 = 2{,}160 \text{ ft.}$$

Answer b: From Figure B-2, a straight line connecting 500 on the yield scale with 180 on the 0.4 power scaled dimension scale crosses the actual dimension scale at 2,160. The desired height of burst is thus 2,160 feet. (*Note.* Conversion from one scaling procedure to another is particularly easy with the nomogram. The line mentioned above crosses the cube root scaled dimension scale at 270. Thus 180 $W^{0.4}$ ft corresponds to 270 $W^{1/3}$ ft for 500 kt.)

[redacted] *Example 2* [redacted]

Given: A ground distance of 2,580 yd from an 80 kt surface burst.

Find: The proper distance to determine overpressure from the 1 kt curves.

Solution: The applicable scaling is (Problem 2-9).

$$\frac{d}{d^1} = W^{1/3}.$$

Answer a: From Figure B-1

$$(80)^{1/3} = 4.3,$$

$$d_1 = \frac{d}{W^{1/3}} = \frac{2{,}580}{4.3} = 600 \text{ yd}$$

$$= 1{,}800 \text{ ft.}$$

Answer b: From Figure B-2, a straight line from 80 on the yield scale through 2,580 on the actual dimension scale intersects the cube root scaled dimension scale at 600. The scaled distance is 600 yards. The proper distance to enter the overpressure charts is 1,800 feet.

[redacted]

[redacted]

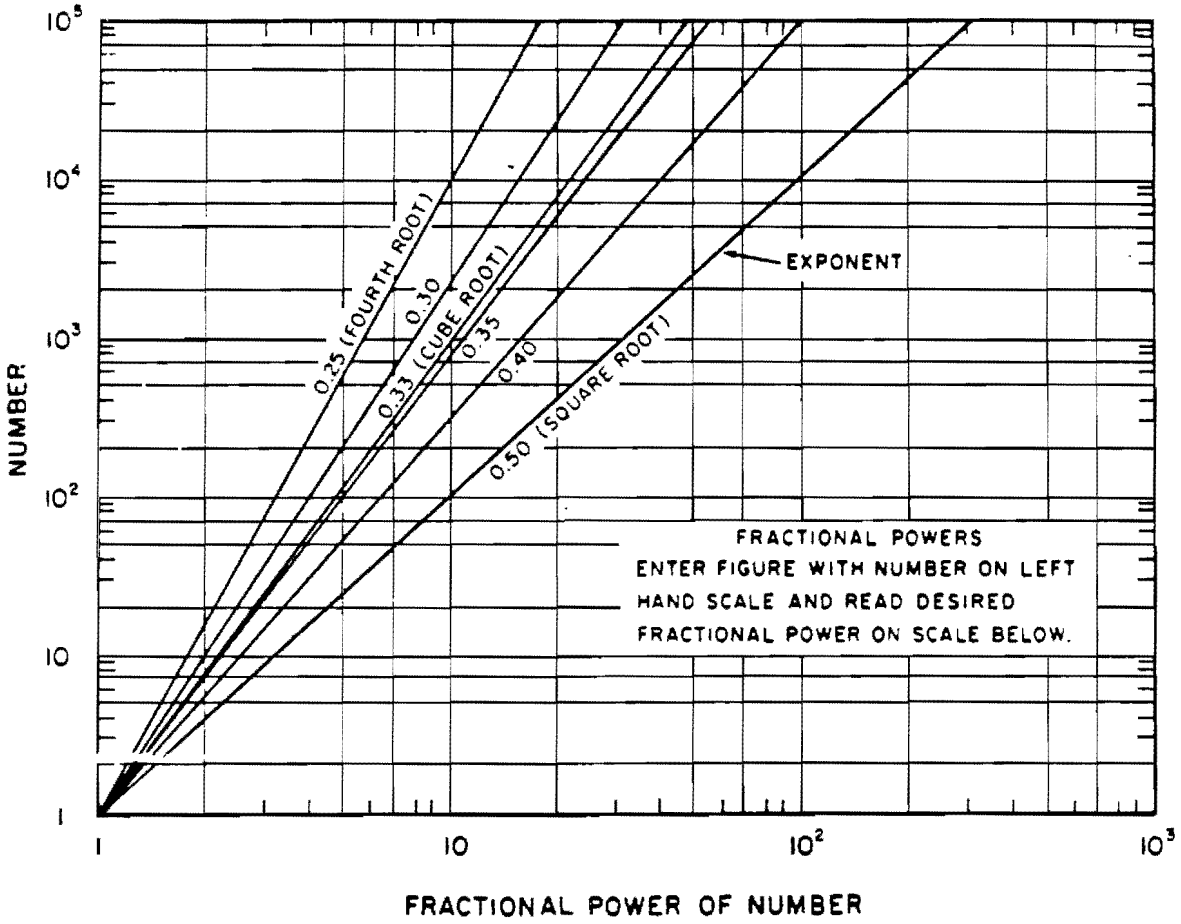

Figure B-1. [redacted] Various Fractional Powers of Numbers [redacted]

[redacted]

[redacted]

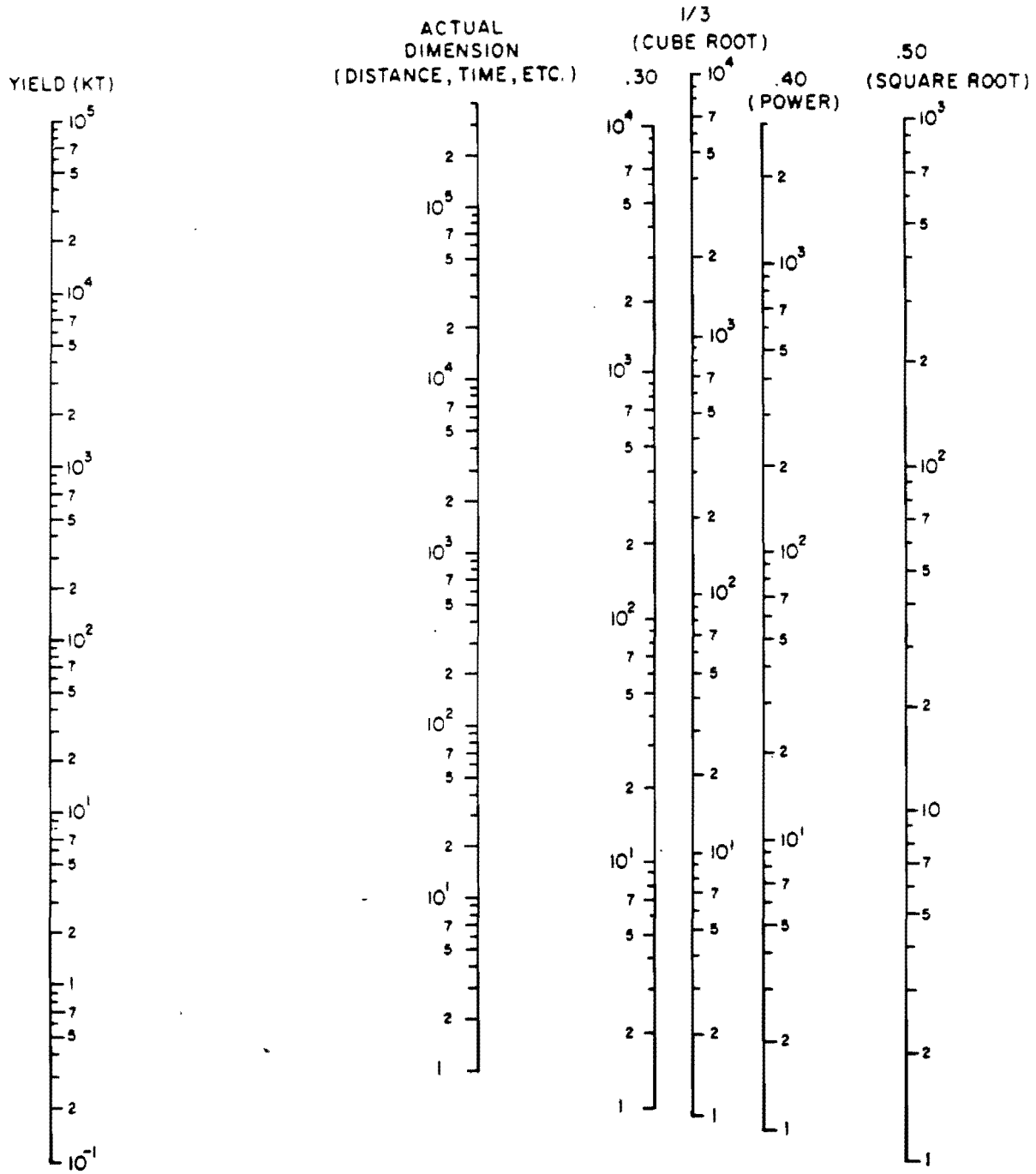

Figure B-2. [redacted] Dimension Scaling Nomogram [redacted]

[redacted]

[redacted]

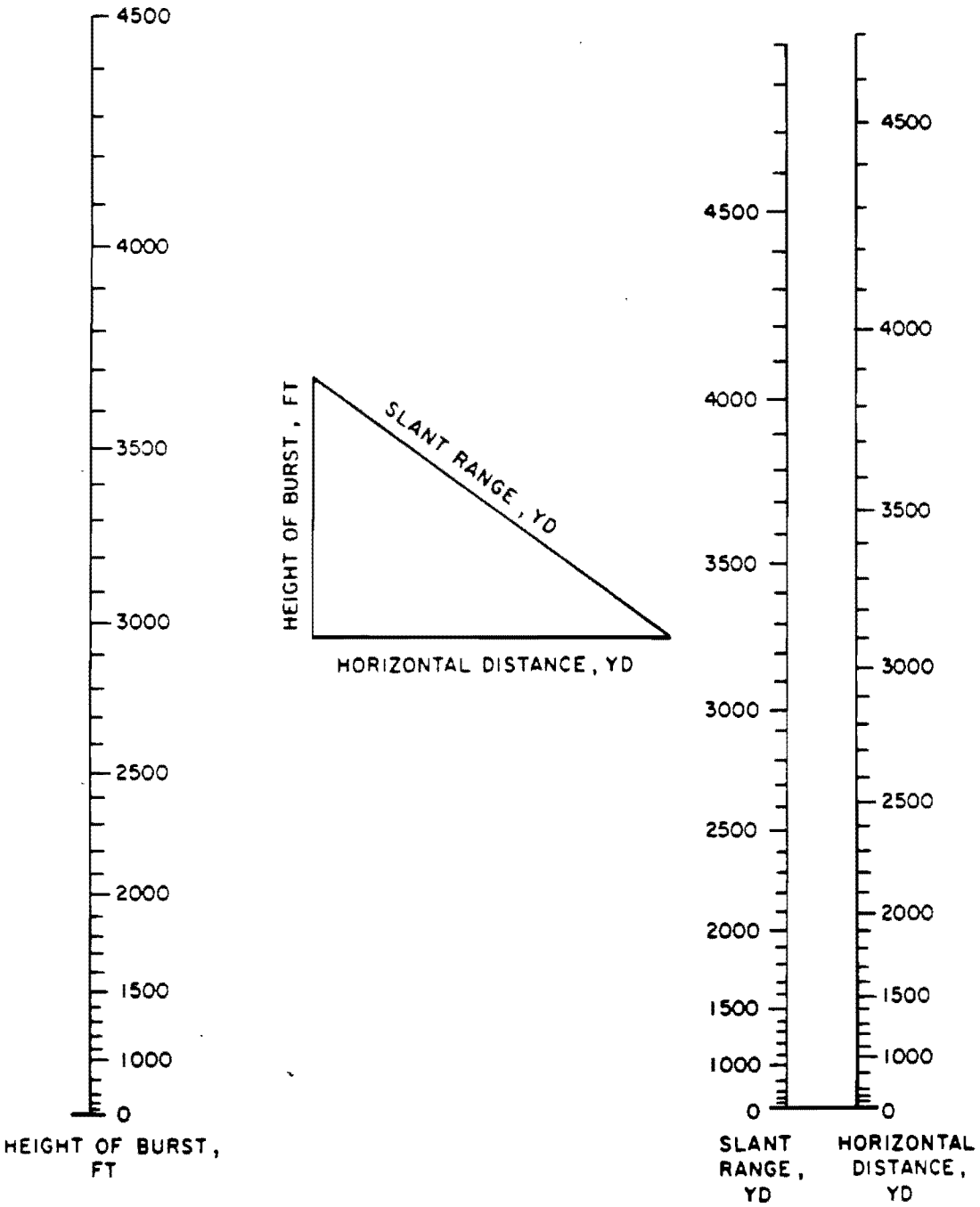

Figure B-3. [redacted] Height of Burst—Horizontal Distance—Slant Range Nomogram [redacted]

[redacted]

APPENDIX C

PROBABILITY CONSIDERATIONS

The procedures described in Sections I through III of Chapter 11 permit independent calculations of the 50 percent probability of damage to structures, equipment and personnel. Section I of this appendix provides a method for determining the probability of failure for conditions other than those considered in Chapter 11, i.e., where the median or 50 percent probability level of vulnerability differs from the median or 50 percent probability level of input motions or pressures. Section II provides the derivation of some equations used in Section I. Familiarity with Section III, Chapter 2 and Sections I through III, Chapter 11 is presupposed.

The discussion herein is related to the intensity of motion (either displacement, velocity, or acceleration) that is required to produce severe damage to equipment or personnel, and to the intensity of input pressures produced by the air shock that will cause severe or moderate damage to both aboveground and belowground structures. The failure of rock openings is also treated in terms of slant range. Either free field values, or values within the structure at the point of support of the equipment, or the response spectrum values, may be used interchangeably as input. In general, the response spectrum values of motion will be used. Different probabilities will be obtained for shock effects depending on the knowledge available pertaining to the type and design of the shock mount.

In all cases, the parameters that are dealt with are the intensity of motion, the intensity of overpressures, or the slant range. For motion vulnerability, one of the three elements of motion (displacement, velocity, or acceleration) can be used, depending on which region of the spectrum is involved, without otherwise distinguishing among them. By comparing the median value of input (motion, pressure, or slant range) with the median value of vulnerability, respectively, to motion, overpressure, or slant range as appropriate, the probability of failure or survival of the particular piece of equipment or structure can be obtained directly. When these two levels are equal, the probability of failure is, of course, 50 percent. However, when they are different, the tables and figures provided in this appendix may be used to obtain the probability of failure or of survival.

C-1 Protective Design and Weapon Selection

In general, all of the parameters governing the response of a structure, including the loading and the structural parameters, are subject to variation and uncertainty. In making a design of a structure to resist certain overpressures, or other inputs, for a particular yield of weapon, the designer ordinarily makes assumptions on the conservative side in all or nearly all of the cases where he has a choice of parameter values. The designer desires to state, with a high degree of confidence, that his structure will withstand an overpressure (the "design" overpressure), or other inputs, specified to him. He will, therefore, choose parameter values sufficiently conservative to assign a high confidence value to his statement, e.g., 90 percent or better.

The weapon analyst who is estimating the vulnerability of a structure, on the other hand, can work with an overall variation, which reflects the variation of the individual parameters. The weapon analyst is not bound to the selection of single values for these parameters,

because he is not solely interested in being able to state the probability that a single specified input will cause the desired damage, or that a certain input will cause damage with a high degree of confidence. Instead, he must answer the question, given a specified combination of weapon yield and height of burst, and considering the possible variations associated with the structural and weapon parameters, what is the probability that the specified damage will occur.

SECTION I
DAMAGE PROBABILITIES

DAMAGE CAUSED BY MOTION INPUT

C-2 Description of Charts for Damage Caused by Motion Input

Values of the standard deviation σ, stated in terms of a percentage of the mean value m of intensity of motion, are shown in Item 1 of Table C-1. These values represent the combination of variabilities and uncertainties relative to the shock motions as well as to the vulnerability of structures or equipment and personnel. The values apply equally for input displacement in the constant displacement region, of velocity in the constant velocity region and acceleration in the constant acceleration region (see Figures 2-90 and 11-51).

Separate values are given for equipment that is not shock mounted and for equipment that is shock mounted. Different values are given for shock mounted equipment to distinguish between equipment where the design of the mount is known, and for two different situations for shock mounted equipment where the design is unknown. In the case where the design is unknown, the type of equipment may be known and therefore some better measure of the vulnerability level can be assessed; alternately, the type of equipment also may be unknown, and major uncertainties must be considered to exist in the data. The values of σ/m given in Items 1a through 1d reflect these degrees of uncertainties.

The distributions of the combined vulnerabilities can be considered to be logarithmic normal, and to have the shape corresponding to the typical lognormal curve for the particular values of σ/m listed in Table C-1. The parameters of the lognormal probability distribution and its properties are summarized in Section II of this appendix.

Figure C-1 shows the probability distributions for failure or for survival for the various combined values of σ/m stated in Table C-1, plotted as a function of the ratio of the median value of input motion (or input pressure or slant range), b_i, to the median value of vulnerability level of motion (or of pressure vulnerability or of slant range), for the equipment or structure, b_v. Figure C-2 is similar to Figure C-1, except that the ratio σ/m is shown as a function of b_i/b_v for different probability values. Where $b_i = b_v$, i.e., the ratio is unity, the probability of failure is 50 percent. These curves are used to obtain the probability of failure for any other ratio of b_i/b_v; as shown in Section II, these same curves give the probability of survival if the ordinates are taken as b_v/b_i in place of b_i/b_v. Therefore, the probability of failure or of survival can be determined by using the appropriate curve in Figure C-1 or C-2. For example, if a situation exists in which velocity governs the response (in the constant velocity region) and where the equipment is shock mounted (design known) with the mounting being the item in which failure is to be produced, the appropriate σ/m of 100 percent is obtained from Item 1b of Table C-1. With this value, it can be seen that if the median value of input velocity is 2.0 times the vulnerability velocity level, either Figure C-1 or Figure C-2 shows that the probability of failure is about 79 percent.

[redacted]

If, however, the acceleration bound governs, and the shock mounting design is unknown but the type is known, Item 1c of Table C-1 shows σ/m to be 150 percent. With this value, if the median input acceleration is 2.0 times the vulnerability level of acceleration, the probability of failure is only 74 percent. To achieve an 85 percent probability of failure for this condition would require that the median value of acceleration be 3.1 times the vulnerability level of acceleration, as shown in Figure C-2.

C-3 Instructions for Motion Input Analyses [redacted]

[redacted] A step-by-step procedure for motion input analysis is given below. Illustrative examples for specific analyses are given in paragraph C-4. It is assumed that b_v is known and b_i for the particular weapon and conditions is assumed for motion inputs and vulnerability. The steps are:

1. Determine the value of σ/m from Table C-1 depending on whether or not an element is shock mounted and on the knowledge of the type and design of the mount.

2. If information other than that given in Table C-1 is available in the form of coefficients of variations of the input motions and of the vulnerabilities, the following equation can be used to obtain the combined σ/m:

$$\frac{\sigma}{m} = \left\{ \left(\frac{\sigma_i}{m_i}\right)^2 + \left(\frac{\sigma_v}{m_v}\right)^2 + \left(\frac{\sigma_i}{m_i}\right)^2 \left(\frac{\sigma_v}{m_v}\right)^2 \right\}^{1/2}.$$

If the parameters are different from those tabulated, and a value of σ/m computed from the above equation is different from any of those shown in Table C-1, enter Figure C-2 with the value of σ/m as abscissa, and read the value of b_i/b_v for a chosen probability of failure P_f (suggest P_f = 90 percent or 95 percent). With this value of b_i/b_v, a line can be plotted on Figure C-1 appropriate to the particular value of σ/m. The value of b_i/b_v is plotted on Figure C-1 as the ordinate at the chosen probability, P_f = 90 percent or 95 percent as the case may be. A line from the plotted point through the 50 percent point (where the other lines intersect) gives the entire curve. Alternately, if the combined value of σ/m is not given in Table C-1 or Figure C-1, Figure C-2 may be used in place of Figure C-1.

3. For the particular value of σ/m determined, read the probability of failure from Figure C-1 using the abscissa at the bottom of the figure, or the probability of survival using the abscissa at the top of the figure for the particular value of b_i/b_v.

4. For the given ratios of σ/m, and for any value of b_i/b_v, the probabilities of failure or of survival are determined as described above; however, Figures C-1 and C-2 also can be used with a ratio of b_v/b_i to give the same probabilities by interchanging P_f, the probability of failure, with P_s, the probability of survival.

5. If a particular probability of failure or survival is desired, the value of b_i/b_v is obtained from Figure C-1 or C-2 for the particular combined value of σ/m, and the desired value of b_i is obtained by trial-and-error for the particular given value of b_v.

C-4 Illustrative Examples for Motion Inputs [redacted]

Example 1 [redacted]

[redacted] Consider the vulnerability of non-shock mounted equipment. The value of b_v is assumed to be 10g at approximately 20 cycles per second. Consider the case in which the spectrum intersection is along a line parallel to a line of constant acceleration.

[redacted] From Table C-1, Item 1a indicates a value of σ/m of 100 percent.

[redacted] For a particular explosion, the acceleration level is determined to be b_i = 7g (by the

[redacted]

[redacted]

methods of Section III, Chapter 2). Therefore, the ratio of b_i to b_v is 7/10 = 0.7. From Figure C-1, with b_i/b_v = 0.7 and σ/m = 100 percent, the probability of failure is 33 percent, or the probability of survival is 67 percent. Alternately, b_v/b_i = 1.43. Using this value of b_v/b_i and σ/m = 100 percent, the survival probability is read directly from Figure C-1 or C-2 to be 67 percent.

Example 2

[redacted] For the same conditions as example 1, determine the input acceleration that would be required to produce a 90 percent probability of failure.

[redacted] From Figure C-1 or C-2, a 90 percent probability of failure occurs for σ/m = 100 percent if b_i/b_v = 2.9. This means that an acceleration of 29g will be required to produce 90 percent probability of failure.

Example 3

[redacted] For the same equipment, consider a condition in which the equipment is shock mounted, with a velocity vulnerability of 1,000 in./sec at approximately 4 cycles. Failure is desired in the mounting for a known design of the mount.

[redacted] From Table C-1, Item 1b, σ/m = 100 percent.

[redacted] If the velocity level for the explosion conditions is determined to be 1,500 in./sec, the probability of failure from Figure C-1 or C-2 is 69 percent for b_i/b_v = 1.5 and σ/m = 100 percent.

[redacted] For the same conditions, a 95 percent probability of failure requires a value of b_i/b_v of 4.00, or a value of velocity of approximately 4,000 in./sec.

Table C-1. [redacted] Standard Deviations for Use in Probability Analyses [redacted]

Item	σ/m (percent of mean of reference parameter)	Reference Parameter
1. Shock effects on personnel and equipment		
a. Not shock mounted	100	Shock motion
b. Shock mounted, design of mount known	100	Shock motion
c. Shock mounted, type of mount known, design unknown	150	Shock motion
d. Shock mounted, type of mount and design unknown	200	Shock motion
2. Aboveground structures or elements flush with ground surface	35	Overpressure
3. Underground structural elements subjected to vertical pressure	65	Overpressure
4. Underground structural elements subjected to horizontal pressure	80	Overpressure
5. Openings in rock	50	Slant range

[redacted]

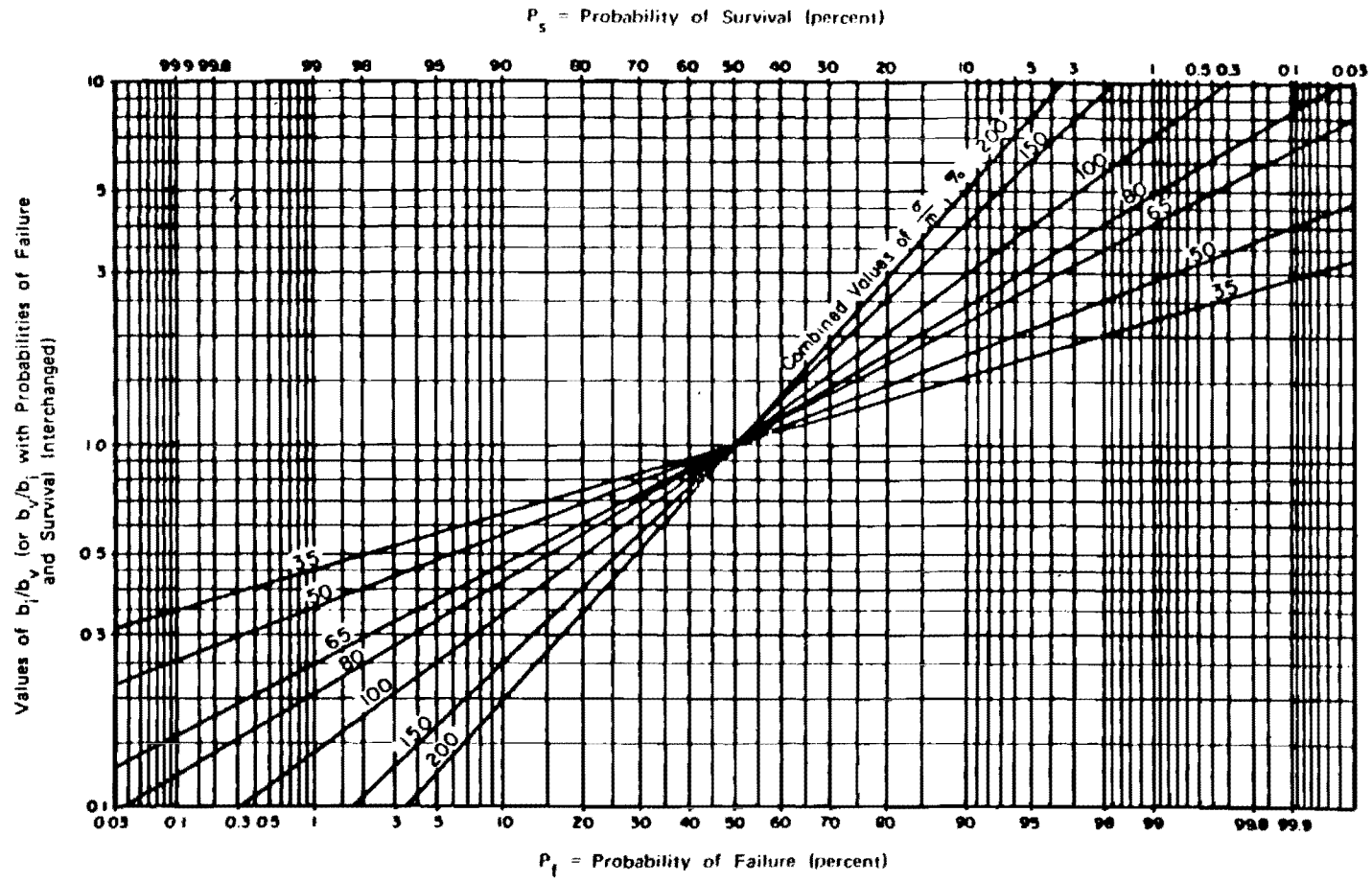

Figure C-1. [redacted] Probability Distributions for Failure or for Survival as Function of Ratio of Median Input Motion b_i to Median Vulnerability Level of Motion b_v [redacted]

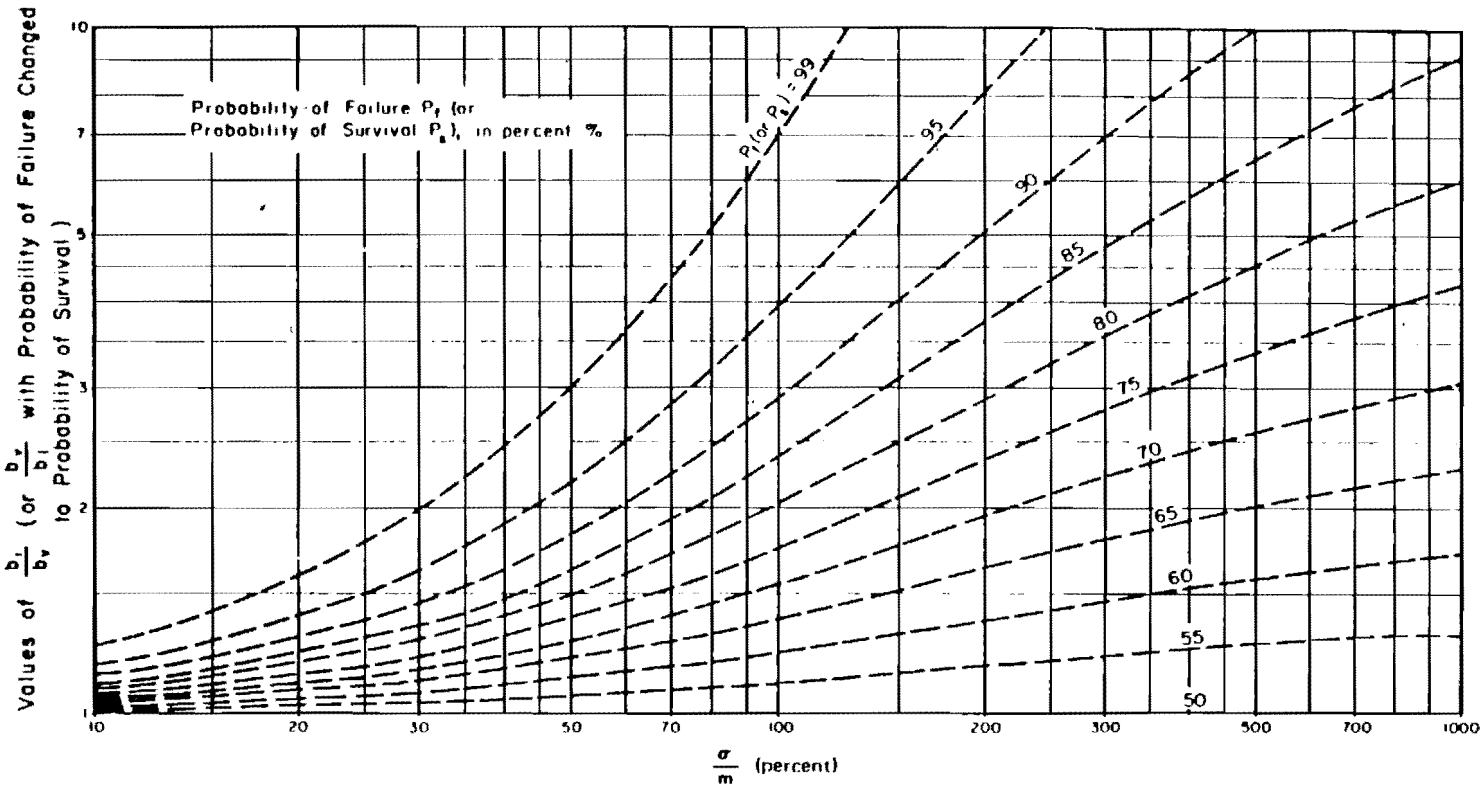

Figure C-2. [redacted] Coefficient of Variation σ/m as Function of b_i/b_v Ratio for Specified Probability of Failure (or of b_v/b_i for Specified Probability of Survival) [redacted]

DAMAGE CAUSED BY PRESSURE

C-5 Description of Charts for Damage to Surface Structures Caused by Pressure Input

The probability graphs presented in Figures C-1 and C-2 also apply to failure of surface structures that are sensitive to overpressures or dynamic pressures. In these cases, b_i is the median of the overpressure or dynamic pressure, and b_v is the median vulnerability to overpressure or dynamic pressure. Values of b_i, as a function yield, height of burst, and distance from ground zero may be obtained from the overpressure and dynamic pressure height of burst curves in Section I, Chapter 2.

Tables C-2 and C-3 show the median values of overpressure and dynamic pressure respectively, b_v, that correspond to severe damage to the 22 types of structures for which isodamage curves are presented in Figure 11-2 through 11-23. The structures and the types of damage that are considered severe, moderate, or light for each structure are described by number in Table 11-1. Tables C-4 and C-5 show the corresponding overpressures and dynamic pressures, respectively, that provide moderate damage to the same family of structures. Even though the pressure required to produce a stated level of damage to a given structure with a given yield varies somewhat, as shown in the isodamage curves of Chapter 11, the median values presented in the tables are considered to be sufficiently reliable for the calculation of damage probabilities.

The ratio σ_i/m_i for the input pressure is assumed to be 20 percent for both overpressure and dynamic pressures, and σ_v/m_v for pressure vulnerability is assigned a value of 30 percent. The combined value may be obtained from the equation given in paragraph C-3:

$$\sigma/m = \left\{\left(\frac{\sigma_i}{m_i}\right)^2 + \left(\frac{\sigma_v}{m_v}\right)^2 + \left(\frac{\sigma_i}{m_i}\right)^2 \left(\frac{\sigma_v}{m_v}\right)^2\right\}^{1/2},$$

$$\sigma/m = \left\{(0.2)^2 + (0.3)^2 + (0.2)^2 \quad (0.3)^2\right\}^{1/2},$$

$\sigma/m \approx 35$ percent.

With this combined value of σ/m, the probability of failure of a given structure subjected to a specified overpressure or dynamic pressure from a known weapon yield can be determined from Figure C-1 or C-2. For example, consider a diffraction sensitive structure similar to type 11-3 that is subjected to an overpressure of 20 psi from a 3 kt explosion. From Table C-2, the median overpressure vulnerability corresponding to a 3 kt yield is 15 psi. The ratio b_i/b_v is, therefore, 1.333. Using $b_i/b_v = 1.333$, and σ/m = 35 percent, P_f = 80 percent as the probability of severe structural damage from either Figure C-1 or Figure C-2. The corresponding probability of failure for light to moderate damage of the same structure may be obtained similarly by using the appropriate overpressure vulnerability obtained from Table C-4.

To design for a given probability of survival from severe damage from a specified overpressure or dynamic pressure, b_i, and weapon yield, W, enter Figure C-2 with the given P_s to obtain the value of b_v/b_i corresponding to σ/m = 35 percent. The structure should have a median vulnerability equal to the calculated b_v. For example, if the median overpressure from a 30 kt weapon is 10 psi, the design of a structure corresponding to structure type 11-5 with a 70 percent probability of survival from severe damage is determined from Figure C-2, with σ/m = 35 percent and P_s = 70 percent, to be b_v/b_i = 1.25. Hence, the structure must have a median vulnerability of 1.25 b_i = 12.5 psi to achieve a 70 percent probability of survival.

[redacted]

[redacted] To inflict severe damage to a surface structure of known type with a given probability of failure, Figure C-1 or C-2 is entered with this probability to obtain a ratio b_i/b_v corresponding to σ/m = 35 percent. The required median overpressure or dynamic pressure, b_i, is then obtained in terms of b_v from Table C-2 for diffraction sensitive structures or from Table C-3 for drag sensitive structures. A yield that will provide the required pressure input is then selected with the aid of the height of burst curves in Section 1, Chapter 2.

C-6 Description of Charts for Damage to Underground Structures Caused by Pressure Input [redacted]

[redacted] Failure due to vertical overpressures or horizontal pressures must be distinguished for underground structures that are sensitive to soil pressures. Again, b_i is the median of the applied pressure. In this case, the median vulnerability, b_v, to vertical or horizontal pressure is obtained by the procedures discussed in Section II and III, Chapter 11.

[redacted] When using the probability charts, a value of σ/m = 65 percent should be used for structures and structural elements subjected to vertical pressures; however, for structures and structural elements subjected to horizontal pressures, a value of σ/m = 80 percent should be used with appropriate b_i/b_v or b_v/b_i. The procedure for the analysis of the probability of failure or of survival is the same as for aboveground structures. Therefore, the illustrations presented for aboveground structures may be followed.

[redacted] For deep underground openings in rocks that are sensitive to slant range, the quantities b_i and b_v must be expressed in terms of slant range. Similarly, the value of σ/m = 50 percent given in Table C-1 for openings also is expressed in the same term. The computation of probabilities of failure or of survival is again performed with Figure C-1 or Figure C-2. The procedure is the same as described above except that the ratio b_i/b_v or b_v/b_i is the ratio of the slant ranges, and a value of σ/m = 50 percent should be used (Table C-1).

C-7 Instructions for Pressure Input Analyses [redacted]

[redacted] The instructions given in paragraph C-3 pertaining to the use of Figures C-1 and C-2 for motion inputs also apply for pressure inputs. The only difference is in the determination of b_i/b_v and values of σ/m = 65 percent or 80 percent for underground structures sensitive to vertical and horizontal pressures, respectively or 35 percent for aboveground structures. In the case of pressure inputs, the pressure vulnerabilities of a structure are determined from one of the Tables C-2 through C-5 for aboveground structures. For underground structures, these vulnerabilities must be computed as described in Sections II and III of Chapter 11.

1. For a given surface structural type subjected to a specified weapon yield, determine the pressure vulnerability from Table C-2 or C-3 for severe damage, and from Table C-4 or C-5 for light to moderate damage. Tables C-2 and C-4 give the overpressure vulnerability for diffraction sensitive structures, while Tables C-3 and C-5 give the dynamic pressure vulnerabilities for drag sensitive structures. Comparable values for underground structures must be computed by the methods described in Chapter 11.

2. Using appropriate values of σ/m as given in Items 2, 3, and 4 of Table C-1 for aboveground and underground structures, the probabilities of failure or survival can be determined from Figure C-1 or Figure C-2.

C-8 Illustrative Examples for Pressure Inputs [redacted]

Example 1 [redacted]

[redacted] Consider a 5-story conventional reinforced concrete office building of the type de-

[redacted]

scribed as Type 11-3 in Chapter 11. Assume that an explosion of 100 kt yield occurs at a height of burst of 1,100 ft. If the building is located at a distance of 4,200 ft from ground zero, the corresponding height of burst and ground distance from a 1 kt explosion would be

$$h_1 = \frac{h}{W^{1/3}} = \frac{1{,}100}{(100)^{1/3}} = 237 \text{ ft},$$

$$d_1 = \frac{d}{W^{1/3}} = \frac{4{,}200}{(100)^{1/3}} = 905 \text{ ft}.$$

From Figure 2-18, the overpressure is 15 psi. From Table C-2, the median vulnerability is 11 psi. Thus $b_i/b_v = 15/11 = 1.36$. With this value of b_i/b_v, and $\sigma/m = 35$ percent, the probability of severe damage is determined from Figure C-1 or Figure C-2 to be approximately 80 percent. To determine the probability of moderate damage, Table C-4 shows the median vulnerability to be 7 psi, and, therefore, $b_i/b_v = 15/7 = 2.14$. From Figure C-1 or Figure C-2, the probability of moderate damage is 98 percent.

Example 2

For the same structure, yield, and height of burst that were used in Example 1, the distance corresponding to 20 percent probability of severe damage may be determined as follows. With $\sigma/m = 35$ percent and the probability of survival equal to (1-0.2) = 80 percent, Figure C-2 shows a ratio $b_v/b_i = 1.35$. Thus $b_i = 11/1.35 = 8.15$. The median overpressure, therefore, is 8.15 psi. From Figure 2-19, the distance from ground zero corresponding to a height of burst of 237 feet for a 1 kt explosion and 8.15 psi is 1,220 feet. The corresponding distance from a 100 kt explosion is 5,660 feet. The distance for 20 percent probability of moderate damage corresponds to an overpressure of 7/1.35 (Table C-3 and Figure C-2) = 5.18 psi. From Figure 2-19, the distance from ground zero corresponding to a height of burst of 237 feet for a 1 kt explosion and 5.18 psi is 1,650 feet. The corresponding distance from a 100 kt explosion is 7,660 feet.

C-9 System Consideration

The calculation of probabilities described in the preceding paragraphs pertains to the failure or survival of a single item or component. If the survival or proper performance of a complete piece of equipment or a system requires the survival of every component in the system, the components can be considered to be in series. An example is that of a shock mounted equipment; the satisfactory performance of the equipment requires the survival of the shock mount as well as of the equipment itself. In determining the failure probability or survival probability of a system the two points of view, the designer's and the weapon analyst's, must be distinguished in arriving at conservative estimates of the actual survival probabilities.

From the designer's (defensive) point of view, a conservative estimate of the system failure probability is obtained if the failure of the components are assumed to be statistically independent. The probability of failure of the system is:

$$P_f = 1 - (1 - P_{f1})(1 - P_{f2}) \ldots$$

$$(1 - P_{f(n-1)})(1 - P_{fn})$$

where P_{f1}, P_{f2} . . . P_{fn} are the probabilities of failure of the individual components, which can be determined with the procedure described in the preceding paragraphs.

For example, in the case of the shock mounted equipment, if the probability of failure of the shock mount is 30 percent and that of the equipment is 40 percent, the probability of failure of the system is 1 - (0.70)(0.60) = 58 percent.

[redacted]

Table C-2. [redacted] Median Vulnerability to Overpressures Corresponding to Severe Damage of Diffraction Sensitive Structures [redacted]

Weapon Yield	Type of Structure				
	11-2	11-3	11-4	11-5	11-6
	(Median Vulnerability Overpressure, psi)				
30 mt	28	10	5.0	9.0	3.4
10 mt	29	10	5.0	9.0	3.4
3 mt	30	10	5.0	9.0	3.4
1 mt	30	11	5.0	9.0	3.5
300 kt	30	11	5.0	9.0	3.5
100 kt	32	11	5.0	9.5	3.5
30 kt	34	12	5.0	9.5	3.6
10 kt	34	13	5.5	10.0	3.6
3 kt	36	15	5.5	10.0	3.8
1 kt	48	17	5.5	11.0	4.0
[illegible] kt	–	20	6.0	12.0	4.4
0.1 kt	–	22	6.5	12.0	4.8
0.03 kt	–	24	7.0	13.0	5.2
0.01 kt	–	28	7.5	14.0	5.8

[redacted]

Table C-3. [redacted] Median Vulnerability to Dynamic Pressures Corresponding to Severe Damage of Drag Sensitive Structures [redacted]

Weapon Yield	Type of Structure																
	II-7	II-8	II-9	II-10	II-11	II-12	II-13	II-14	II-15	II-16	II-17	II-18	II-19	II-20	II-21	II-22	II-23
	(Median Vulnerability of Dynamic Pressure, psi)																
30 mt	0.8	1.6	2.6	5.0	2.4	5.0	2.6	2.4	2.0	2.0	9.6	5.0	2.8	3.3	2.0	1.4	0.6
10 mt	0.8	1.6	2.6	6.0	2.6	5.0	2.8	2.4	2.0	2.0	10.0	5.0	2.8	3.3	2.0	1.4	0.6
3 mt	0.9	1.8	2.8	7.0	3.0	6.0	3.0	2.6	2.0	2.0	13.0	5.2	2.8	3.3	2.0	1.4	1.0
1 mt	1.0	2.0	3.2	8.5	3.6	7.0	3.4	3.0	2.0	2.0	20.0	6.0	2.8	3.4	2.0	1.4	1.6
300 kt	1.2	2.2	3.6	12.0	4.8	9.0	4.2	3.8	2.5	2.0	48.0	8.0	3.0	4.0	2.0	1.4	2.8
100 kt	1.4	2.6	4.4	18.0	6.0	11.0	5.2	5.0	3.0	2.2		12.0	3.4	5.2	2.2	1.4	4.5
30 kt	2.0	3.6	5.8	34.0	10.0	16.0	7.0	10.0	4.0	2.6	-	20.0	4.0	10.0	2.6	1.4	7.5
10 kt	3.2	5.2	7.5	--	16.0	26.0	10.0	24.0	7.0	3.5	-	40.0	5.2	24.0	3.4	1.6	12.0
3 kt	5.4	7.5	12.0	--	36.0	-	18.0		15.0	5.0			7.0		4.6	2.0	20.0
1 kt	9.5	13.0	20.0	-	60.0	-	28.0	-	35.0	12.0			12.0	-	8.0	2.2	32.0
0.3 kt	18.0	26.0	38.0	-	--	--							22.0		18.0	3.0	55.0
0.1 kt	--	--	--	-				-	--				--	--		4.0	85.0
0.03 kt	--	--	-	--	--		-	-					--	--	--	6.0	
0.01 kt	-	--	-	--		--	-				--		-	-	-	9.0	

[redacted]

Table C-4. [redacted] Median Vulnerability to Overpressures Corresponding to Moderate Damage of Diffraction Sensitive Structures [redacted]

Weapon Yield	Type of Structure				
	11-2	11-3	11-4	11-5	11-6
	(Median Vulnerability Overpressure, psi)				
30 mt	20	6.5	3.4	6.5	2.2
10 mt	20	6.5	3.4	6.5	2.2
3 mt	20	6.5	3.4	6.5	2.2
1 mt	20	6.5	3.4	6.5	2.2
300 kt	20	6.5	3.4	6.5	2.2
100 kt	20	7.0	3.4	6.5	2.2
30 kt	20	7.0	3.4	6.5	2.2
10 kt	20	7.0	3.6	6.5	2.2
3 kt	22	7.5	3.6	6.5	2.2
1 kt	24	8.0	3.6	6.5	2.2
0.3 kt	28	9.0	3.8	7.0	2.4
0.1 kt	–	10.0	4.0	7.5	2.6
0.03 kt	–	11.0	4.2	7.5	2.8
0.01 kt	–	12.0	4.4	8.0	3.0

[redacted]

Table C-5. [redacted] Median Vulnerability to Dynamic Pressures Corresponding to Moderate Damage of Drag Sensitive Structures [redacted]

Weapon Yield	Type of Structure																
	II-7	II-8	II-9	II-10	II-11	II-12	II-13	II-14	II-15	II-16	II-17	II-18	II-19	II-20	II-21	II-22	II-23
	(Median Vulnerability of Dynamic Pressure, psi)																
30 mt	0.6	1.2	2.0	3.4	1.6	3.6	2.0	2.4	2.0	2.0	9.6	5.0	2.8	3.2	2.0	1.4	0.2
10 mt	0.6	1.2	2.0	3.4	1.6	3.6	2.0	2.4	2.0	2.0	10.6	5.0	2.8	3.2	2.0	1.4	0.2
3 mt	0.6	1.2	2.0	3.4	1.6	3.6	2.0	2.4	2.0	2.0	12.0	5.2	2.8	3.2	2.0	1.4	0.4
1 mt	0.6	1.2	2.0	3.6	1.8	3.8	2.0	2.6	2.0	2.0	16.0	5.8	2.8	3.2	2.0	1.4	0.6
300 kt	0.6	1.2	2.0	4.0	2.0	4.0	2.2	2.8	2.0	2.0	26.0	7.4	2.8	3.4	2.0	1.4	1.0
100 kt	0.6	1.2	2.2	4.4	2.0	4.4	2.4	3.2	2.2	2.0	46.0	9.0	3.0	4.0	2.0	1.4	2.0
30 kt	0.6	1.4	2.4	5.4	2.4	5.2	2.6	4.0	2.8	2.2	88.0	14.0	3.4	5.0	2.2	1.4	3.0
10 kt	0.8	1.4	2.6	7.5	3.0	6.0	3.0	6.0	3.6	2.8	–	22.0	4.0	8.4	2.4	1.4	5.0
3 kt	0.8	1.6	3.2	12.0	4.4	9.0	3.6	12.0	6.4	4.2	–	40.0	5.4	18.0	3.4	1.6	8.0
1 kt	1.0	2.0	4.0	20.0	7.5	12.0	5.0	30.0	12.0	6.2	–	–	7.4	36.0	4.6	1.8	13.0
0.3 kt	1.2	3.0	6.0	40.0	13.0	22.0	9.0	–	–	16.0	–	–	10.0	–	6.4	2.2	22.0
0.1 kt	2.2	5.0	10.0	–	20.0	–	16.0	–	–	–	–	–	15.0	–	14.0	2.6	60.0
0.03 kt	–	–	–	–	–	–	–	–	–	–	–	–	–	–	–	3.4	100.0
0.01 kt	–	–	–	–	–	–	–	–	–	–	–	–	–	–	–	4.2	–

[redacted]

However, from the weapon analyst's (offensive) standpoint, a conservative estimate of the system failure probability may be obtained if the failure or survival of the components are assumed to be perfectly correlated. In this case, the probability of failure of the system is equal to the largest value among the failure probabilities of the components, or

$$P_f = \max\ (P_{f1}, P_{f2}, \ldots, P_{fn}).$$

In the example given above for shock mounted equipment, the system failure probability would be 40 percent.

SECTION II

DERIVATION OF EQUATIONS USED IN SECTION I

The treatment used herein is based on the logarithmic normal distribution that was used in Section I. Values were given for the ratio of the standard deviation to the mean of a lognormal distribution, obtained by combining the corresponding quantities for individual parameters governing the distribution.

Consider a logarithmic normal distribution for vulnerability, characterized by the parameter σ_v for standard deviation, m_v for [redacted] for median. Now consider also a logarithmic normal distribution for input having similar parameters, but with the subscript i instead of v. Each case is designated by d_v and β_v or d_i and β_i, respectively, the mean value and standard deviation of the logarithm of the corresponding variate.

C-10 Properties of Lognormal Variates

For logarithmic normal random variables, the relationships between the above parameters are as follows:

$$m = e^{\alpha + \frac{\beta^2}{2}},$$

$$\sigma^2 = m^2 \left(e^{\beta^2} - 1\right), \quad \text{or} \quad \left(\frac{\sigma}{m}\right)^2 = e^{\beta^2} - 1.$$

Thus,

$$\beta^2 = \ln\left[\left(\frac{\sigma}{m}\right)^2 + 1\right]$$

Also,

$$\alpha = \ln\ b$$

where b is the median of the lognormal variable.

C-11 Probability of Failure or Survival

Assume that the input I and vulnerability V are both logarithmic normal variates with mean and standard deviations m_i, σ_i and m_v, σ_v, respectively, and hence corresponding medians b_i and b_v. The logarithms of the input and vulnerability are therefore individually normal random variables.

Failure occurs whenever the vulnerability is less than or equal to the input; or $I/V \geq 1.0$. If

$$X = \frac{I}{V},$$

then failure means $X \geq 1.0$, or $\ln X = (\ln I - \ln V) \geq 0$. Therefore, $\ln X$ is also normal with parameters

$$\alpha = \alpha_i - \alpha_v,$$

and

$$\beta = \left(\beta_v^2 + \beta_i^2\right)^{1/2}.$$

Therefore, the probability of failure P_f is

$$P_f = \frac{1}{\sqrt{2\pi}\,\beta} \int_0^\infty e^{-\frac{1}{2}\left(\frac{\ln X - \alpha}{\beta}\right)^2} d(\ln X).$$

[redacted]

[redacted]

Let

$$y = \frac{\ell n\ X - \alpha}{\beta}.$$

Then

$$dy = \frac{d(\ell n\ X)}{\beta},$$

and

$$P_f = \frac{1}{\sqrt{2\pi}} \int_{-\frac{\alpha}{\beta}}^{\infty} e^{-\frac{1}{2} y^2}\ dy$$

= area of standard normal curve from $-\frac{\alpha}{\beta}$ to ∞.

But

$$\alpha = \alpha_i - \alpha_v = \ell n\ b_i - \ell n\ b_v.$$

Hence,

$$\alpha = \ell n \frac{b_i}{b_v},$$

and,

$$\beta = \left(\ell n\left[\left(\frac{\sigma}{m}\right)^2 + 1\right]\right)^{1/2} = \left(\beta_v^2 + \beta_i^2\right)^{1/2}.$$

Therefore,

$$\ell n\left[\left(\frac{\sigma}{m}\right)^2 + 1\right] = \ell n\left[\left(\frac{\sigma_v}{m_v}\right)^2 + 1\right]\left[\left(\frac{\sigma_i}{m_i}\right)^2 + 1\right],$$

and

$$\left(\frac{\sigma}{m}\right) = \left(\left(\frac{\sigma_v}{m_v}\right)^2 + \left(\frac{\sigma_i}{m_i}\right)^2 + \left(\frac{\sigma_v}{m_v}\right)^2 \left(\frac{\sigma_i}{m_i}\right)^2\right)^{1/2}.$$

This is the equation given in paragraph C-3. Therefore, for specified (σ/m), β is a non-negative constant, and

$$P_f = \frac{1}{\sqrt{2\pi}} \int_{\frac{\alpha}{\beta}}^{\infty} e^{-\frac{1}{2} y^2}\ dy$$

$$= \frac{1}{\sqrt{2\pi}} \int_{-\frac{1}{\beta}\ell n\left(\frac{b_i}{b_v}\right)}^{\infty} e^{-\frac{1}{2} y^2}\ dy,$$

which gives a linear plot of b_i/b_v with P_f on lognormal probability paper, as shown in Figure C-1.

[redacted] If the ordinates in Figures C-1 and C-2 are expressed in b_v/b_i, it can be shown that the probability of failure in these curves becomes the probability of survival. From the equations given above,

$$P_s = 1 - \frac{1}{\sqrt{2\pi}} \int_{-\frac{1}{\beta}\ell n\left(\frac{b_i}{b_v}\right)}^{\infty} e^{-\frac{1}{2} y^2}\ dy$$

$$= \frac{1}{\sqrt{2\pi}} \int_{-\infty}^{\infty} e^{-\frac{1}{2} y^2}\ dy -$$

[redacted]

[redacted]

$$= \frac{1}{\sqrt{2\pi}} \int_{-\frac{1}{\beta}\ln\left(\frac{b_1}{b_v}\right)}^{\infty} e^{-\frac{1}{2}y^2}\, dy$$

$$= \int_{-\infty}^{-\frac{1}{\beta}\ln\left(\frac{b_1}{b_v}\right)} e^{-\frac{1}{2}y^2}\, dy$$

$$= \int_{-\infty}^{\frac{1}{\beta}\ln\left(\frac{b_v}{b_1}\right)} e^{-\frac{1}{2}y^2}\, dy.$$

Since the standard normal distribution is symmetric about the origin, this integral is equal to the integral for P_f. Therefore, the probabilities in Figures C-1 and C-2 become probabilities of survival if the ordinates are replaced by b_v/b_1.

[redacted]

[redacted]

APPENDIX D

[redacted] ABSTRACTS OF DNA HANDBOOKS [redacted]

[redacted] NUCLEAR WEAPONS BLAST PHENOMENA [redacted]

[redacted] *DASA 1200 (Vols. I-V)* (Vol. I, SRD; Vol. II, CRD; Vol. III, SFRD; Vol. IV, to be published; Vol. V, CFRD).

[redacted] *Prepared by:* DASIAC, Santa Barbara, California. Major contributors: Defense Atomic Support Agency, Kaman Nuclear, URS Research Company, Bolt, Beranek, and Newman, and Dikewood Corporation.

[redacted] *Availability:* Volumes I through III through Defense Documentation Center on request through Defense Nuclear Agency, Washington, D.C. 20305. Volume V, limited distribution.

[redacted] DASA 1200 is a source book of air blast data and theory applicable to nuclear explosions occurring in free air, on or near the surface, and beneath the surface. Volume I begins with a detailed description of the nuclear explosion energy source, and presents the theoretical background associated with the formation and propagation of the blast wave in free air. The long range propagation of shock waves is treated in detail. Volume II presents a discussion of blast wave interaction phenomena, including ideal reflection and refraction, ideal diffraction, and nonideal effects. A discussion of topography and shock wave shielding and a section on air blast measurements in the high pressure region also are included. Volume III contains an analysis of and methods for the prediction of the blast phenomena from nuclear weapons burst at moderate altitudes, on the surface, underwater, and underground. Volume IV contains a discussion of the simulation of nuclear air blast phenomena with high explosives. Volume V is a compilation of the measurements of the various blast parameters associated with nuclear weapons at the various nuclear operations. It is planned for limited distribution to scientists and agencies who are working in the field of nuclear weapons blast phenomena.

[redacted] HANDBOOK OF UNDERWATER NUCLEAR EXPLOSIONS [redacted]

[redacted] *DASA 1240* [redacted]

[redacted] *Prepared by:* DASIAC, Santa Barbara, California. Major contributors include NOL, DTMB, Waterways Experiment Station, Naval Civil Engineering Laboratory and the U.S. Naval Radiological Defense Laboratory.

[redacted] *Availability:* Qualified requestors may obtain these documents from the Defense Documentation Center. Each transmittal outside the agencies of the U.S. Government must have prior approval of the Defense Nuclear Agency.

[redacted] The Handbook of Underwater Nuclear Explosions is divided into two parts: Part I, Phenomena, consists of 11 chapters, and Part II, Effects, consists of 13 chapters. Individual chapters and in some cases sections of chapters have been previously published separately.

[redacted] The entire handbook is undergoing revision and will be published in three volumes. The revised Handbook of Underwater Nuclear Explosions will be an authoritative presentation of current knowledge and a reliable source of useful data concerning the phenomena of underwater nuclear explosions. The presentation will include the phenomena of shock wave propaga-

[redacted]

[redacted]

[redacted]

tion, surface waves, underwater cratering, and radioactive debris. The effects of underwater explosions on surface ships, submarines, harbors, and structural installations also will be described.

[redacted] NUCLEAR GEOPLOSICS (A Sourcebook of Underground Phenomena and Effects of Nuclear Explosions [redacted]

[redacted] DASA 1285 (Volumes I-V) [redacted]

[redacted] *Prepared by:* Stanford Research Institute, Menlo Park, California.

[redacted] *Availability:* This document is not approved for open publication or distribution to the Office of Technical Services, Department of Commerce. Qualified requestors may obtain copies of this report from Defense Documentation Center. Foreign announcement and dissemination of this report is not authorized.

[redacted] The Nuclear Geoplosics Handbook contains five volumes: Part I, Theory of Directly Induced Ground Motions; Part II, Mechanical Properties of Earth Materials; Part III, Test Sites and Instrumentation; Part IV, Empirical Analysis of Ground Motion and Cratering; and Part V, Effects on Underground Structures and Equipment.

[redacted] The theory of directly induced ground motion is presented in Part I. The tools and elements required for the study of ground motion effects are discussed. Two analytical solutions of shock propagations are presented. Theoretical predictions (obtained by numerical and analytical methods) are compared with field measurements. The mechanical properties of earth materials are described in Part II. It consists of a preparation of a clear and systematic, but largely qualitative, description of the resistance of earth materials to compression and shear. A summary on stress-strain behavior with very short load durations is included. The basic concepts regarding the mechanical behavior of soil and experimental methods of determining the mechanical properties of soil are described. The physical characteristics of test sites and instrumentation of nuclear and high explosive detonations on which ground motion has been measured are presented in Part III. The discussion of air blast induced ground motion in Part IV relies primarily on experimental evidence. A knowledge of the effects induced in the free field ground motion, the factors influencing these effects, the structure-medium interaction, and the factors influencing interaction is implicit in the study of behavior of underground structures. Part V summarizes these various phenomena as they apply to understanding structures in general and discusses the behavior of equipment mounted within a structure.

[redacted] The book is meant to be an authoritative sourcebook. It is not meant to be a handbook of design specifications.

[redacted] Part II and Part IV are currently under revision. Publication is expected during calendar year 1973.

[redacted] TREE (Transient-Radiation Effects on Electronics) HANDBOOK [redacted]

[redacted] DNA 1420 H-1 (edition 3), DNA 1420 H-2 (edition 3), (1420 H-1, [redacted] 1420 H-2, [redacted]

[redacted] *Prepared by:* Battelle Memorial Institute, Columbus, Ohio

[redacted] *Availability:* Qualified requestors may obtain this document from the Defense Documentation Center. Foreign announcement and dissemination is not authorized.

[redacted] The TREE Handbook consists of two volumes which present information that will be useful to a design engineer who is designing electronic systems for survival in a nuclear-burst environment. The information that is presented covers those areas directly related to electronic parts, circuits, and systems. The

[redacted]

[redacted]

nuclear-burst environment that is covered includes both transient and steady state. It also includes all radiation effects except external EMP. Major areas covered in DNA 1420 H-1 are: the simulated versus burst environment, interaction of transient radiation with matter, discrete semiconductor devices, integrated circuits, capacitors, resistors, miscellaneous electronic materials and devices, circuit hardening, and network analysis techniques. DNA 1420 H-2 discusses the nuclear weapon-burst environment, interaction of transient radiation with matter, system hardening, and internal EMP.

[redacted] The TREE Handbook is updated on a continuing basis.

[redacted] THEORETICAL MODELS FOR NUCLEAR FIREBALLS [redacted]

[redacted] *DASA 1589-A, 1589-B, 1589-1 through 1589-39* (1589-A, [redacted] 1589-B, [redacted] 1589-1 through 1589-39, [redacted]

[redacted] *Prepared by:* Lockheed Missiles and Space Company, Sunnyvale, California.

[redacted] The first volume, with parts A and B, describes a radiation hydrodynamic code appropriate for calculation of nuclear fireball phenomenology in the lower atmosphere. Part A describes the code, and part B discusses the results. The FIREBALL code is a one dimensional, spherical, Lagrangian, radiation-hydrodynamics code, which employs a non-grey transport equation to describe the radiation field. The code is used to compute 39 theoretical models for bombs of various explosion yields at various altitudes. These graphical descriptions are the 39 volumes (DASA 1589-1 through 1589-39). Results are compared to experimental measurements made in U.S. field tests.

[redacted] WEAPONS RADIATION SHIELDING HANDBOOK [redacted]

[redacted] *DASA 1892-1 through 1892-6* (DASA 1892-1, -2, -3, and -5 [redacted] DASA 1892-4, [redacted] DASA 1892-6, [redacted]

[redacted] *Prepared by:* Oak Ridge National Laboratory, Oak Ridge, Tennessee. Major contributors: Radiation Research Associates and the University of Tennessee.

[redacted] *Availability:* Qualified requestors may obtain these documents from the Defense Documentation Center. Requests for DASA 1892-4 must be on request through Headquarters, Defense Nuclear Agency, Washington, D.C. 20305.

[redacted] DASA 1892-5 (Chapter 2 of the handbook) describes the basic concepts underlying the methods used for weapon radiation shield analyses. These concepts include the quantities used to describe particle populations and the quantities used to describe radiation interactions with materials. The characteristics of the particular radiations produced by weapons, neutrons and gamma rays, are discussed in detail, including their physical properties and their important interactions. The processes by which neutrons and gamma rays are produced also are described. The chapter also discusses the various response functions that are used to convert a radiation field to a biological effect.

[redacted] DASA 1892-3 (Chapter 3 of the handbook) surveys the methods used most frequently to calculate the attenuation of neutrons and gamma rays. Summaries of computer codes based on the various methods also are provided. All of the techniques are either approximate solutions to the Boltzmann equation or are based on kernels obtained from solutions to the equation.

[redacted] DASA 1892-2 (Chapter 4 of the handbook) surveys the work performed to date on

[redacted]

[redacted]

the various types of nuclear radiation albedos, particularly as they relate to penetration of air filled openings through radiation shields (ducts, passageways, etc.). This topic is important in that the primary increase in the radiation that penetrates a shield results from such openings and enters primarily as a result of the successive scattering of the radiation from the walls of the openings. Most of the techniques for estimating the transmission through such openings depend on the use of albedos.

[redacted] DASA 1892-1 (Chapter 5 of the handbook) describes effective methods for designing air filled holes in protective structures (access ways, ventillation ducts, other utility pipes, distributed voids resulting from the use of non-homogeneous material in the structure, etc.) to reduce the amount of radiation that enters the structure.

[redacted] DASA 1892-4 (Chapter 6 of the handbook) describes the various sources of radiation produced by a nuclear explosion and presents techniques for calculating the transport of the radiations from the point of burst to the surface of a shield, i.e., it presents methods for determining source terms for shield attenuation calculations. The emphasis is on initial radiation, i.e., that produced within the first minute following the explosion.

[redacted] DASA 1892-6 (Chapter 7 of the handbook) presents a simplified method for designing (or evaluating) shield covers on single compartment underground structures that will protect against the neutrons and initial gamma rays. Emphasis is given to neutrons. The method is limited to surface or near surface bursts, to weapon yields between 1 kiloton and 20 megatons, and to distances from the burst at which overpressures are between 5 and 100 psi, but no closer than 500 meters.

[redacted] THERMAL RADIATION PHENOMENA

[redacted] *DASA 1917 (Volumes 1-6)* (Vols. I-V, [redacted] Vol. VI, [redacted]

[redacted] *Prepared by:* Lockheed Missiles and Space Company, Palo Alto Research Laboratory, Palo Alto, California. Major contributor: The Rand Corporation.

[redacted] *Availability:* Qualified requestors may obtain these documents from the Defense Documentation Center. Volumes I through V are approved for open publication. Volume VI is available only by request through Headquarters, Defense Nuclear Agency, Washington, D.C. 20305.

[redacted] Volume I of the six volume handbook describes the equilibrium thermodynamic properties of high temperature air. The report contains information on air and a mixture of ideal gases in chemical equilibrium: ideal gas properties for monatomic gases, diatomic gases, and polyatomic gases. The effects of interparticle forces on the thermodynamic properties of air, effects of coulomb forces on the thermodynamic properties of air, and equilibrium calculations and results for air are discussed. Tables and graphs of the composition and properties of the atmosphere are included.

[redacted] Volume II presents the theoretical aspects of the equilibrium radiative properties of air. The theory of radiation in hot gases (elementary radiative transfer, theory of radiation, theory of molecular absorption) is described. Spectral and mean absorption coefficients of heated air and spectroscopic properties of six important band systems that contribute to opacity of heated air are included.

[redacted] Tables of the equilibrium radiative properties of air and its constituents are presented in Volume III for a wide range of temperatures and densities. The information contained in the tables is a combination of experimental data and theoretical computation.

[redacted]

[redacted]

[redacted] Volume IV describes the excitation and nonequilibrium phenomena of air that has been subjected to a large amount of radiation. Topics include: absorption and scattering of X-rays and gamma rays; collisions of ions and electrons with air molecules; secondary processes following this excitation (including the creation of various chemical species); X-ray heating and shock heating of air, with special reference to very high energy densities; the approach to composition equilibrium in low and high temperature air; adiabatic, near equilibrium cooling of air and the formulation of a criterion for local thermodynamic equilibrium; nonequilibrium radiative transport and its effect on the total amount and the spectrum of emitted radiation; radiation in tenuous air at high temperatures, and radiation in tenuous air with contaminants at low temperatures.

[redacted] Volume V provides an introduction to radiation hydrodynamics (RH). It contains a discussion of the application of RH to fireballs in the atmosphere. After formulating the basic equations of RH, special attention is given to the radiative transfer problem. Several methods for solving the equations of transfer are touched upon, but special emphasis is placed on the two stream method with a frequency averaging procedure, which is specifically designed for use with finite zone sizes. A version of the fireball code, which uses this approach, is described.

[redacted] Volume VI provides data concerning the interaction of nuclear weapon radiation and debris with the atmosphere. The theoretical analysis of fireball development uses computations based on the equations of radiation hydrodynamics (RH). Various models for simplifying these equations are described, and a summary of codes and calculations based on these models is included. The emphasis of the theoretical discussion is on the status of understanding rather than a detailed quantitative treatment. Yield and altitude scaling laws are developed.

[redacted] **DASA REACTION RATE HANDBOOK**

[redacted] DNA 1948H [redacted]

[redacted] *Prepared by*: General Electric Company, Missile and Space Division, Philadelphia, Pennsylvania. Major contributors: General Electric TEMPO, University of Pittsburgh, Air Force Cambridge Laboratory, Geophysics Corporation of America, The Rand Corporation, G C Dewey Corporation, University of Colorado, General Atomic, Westinghouse Research Laboratories, NASA Ames Research Center, and Air Force Weapons Laboratory.

[redacted] *Availability*: Qualified requestors may obtain this handbook from the Defense Documentation Center.

[redacted] This handbook contains useful, accurate, and reliable information on upper atmospheric chemical and physical processes. Such information is required for the solution of various problems involving military radar and communication blackout. Periodic additions to, and revisions of, this handbook are planned to accomodate new information, revisions of older data, corrections, etc. The material is presented in 19 separate chapters covering pertinent aspects of reaction rate science. Appropriate appendices and illustrations are included.

[redacted] This handbook was issued in March 1973 and is still in process of being completed according to original plans. Several revisions have been made to update the original contents.

[redacted] **NUCLEAR EFFECTS ON VLF AND LF COMMUNICATION SYSTEMS** [redacted]

[redacted] *DASA 1954 (Volumes I and II)* (Vol. I, [redacted] Vol. II, [redacted]

[redacted] *Prepared by*: Institute for Telecommunications Sciences, Boulder, Colorado. Major contributors: General Electric/TEMPO, Illinois Institute of Technology Research Institute.

[redacted]

[redacted]

[redacted] *Availability:* Qualified requestors may obtain these documents from the Defense Documentation Center through Headquarters, Defense Nuclear Agency, Washington, D.C. 20305.

[redacted] This handbook is published in two volumes that describe the effects of nuclear bursts on the propagation of LF and VLF communication systems.

[redacted] The examples presented in Volume I illustrate the approximate duration and extent over which typical systems may experience difficulty. In addition to specific results, a brief tutorial description of the effects of nuclear bursts on radio wave propagation and VLF and LF propagation in natural environments is given.

[redacted] Volume II presents techniques for modeling a relatively wide range of nuclear situations and for predicting how these situations would degrade LF and VLF communications system performance. This volume is intended to be used with Volume I. Together, they provide a basic understanding of nuclear phenomenology and its interrelation with LF and VLF propagation.

[redacted] NUCLEAR EFFECTS ON HF COMMUNICATION SYSTEMS [redacted]

[redacted] *DASA 1955 (Volumes I and II)* [redacted]

[redacted] *Prepared by:* Stanford Research Institute, Menlo Park, California. Major contributors: General Electric/TEMPO, Illinois Institute of Technology Research Institute.

[redacted] *Availability:* Qualified requestors may obtain these documents from the Defense Documentation Center through Headquarters, Defense Nuclear Agency, Washington, D.C. 20305.

[redacted] This handbook is published in two volumes that describe propagation effects of nuclear bursts on HF communication systems.

[redacted] The examples presented in Volume I illustrate the approximate duration and extent over which typical systems may experience difficulty. In addition to specific results, a brief tutorial description of the effects of nuclear bursts on radio wave propagation and HF propagation in natural environments is given.

[redacted] Volume II presents techniques for modeling a relatively wide range of nuclear situations and for predicting how these situations would degrade HF communication system performance. This volume is intended to be used with Volume I. Together they provide a basic understanding of nuclear phenomenology and its interrelation with HF propagation.

[redacted] NUCLEAR EFFECTS ON SATELLITE AND SCATTER COMMUNICATION SYSTEMS [redacted]

[redacted] *DASA 1956-1, 1956-2 Vol. I, 1956-2 Vol. II* [redacted]

[redacted] *Prepared by:* Electromagnetic Systems Laboratories, Sunnyvale, California. Major contributors: General Electric/TEMPO, Illinois Institute of Technology Research Institute.

[redacted] *Availability:* Qualified requestors may obtain these documents from the Defense Documentation Center through Headquarters, Defense Nuclear Agency, Washington, D.C. 20305.

[redacted] This handbook contains two parts. Part 1 describes the propagation effects of selected nuclear bursts on satellite and scatter communication systems. The examples presented illustrate the approximate duration and extent over which typical systems may experience difficulty. In addition to specific results, a brief tutorial description of the effects of nuclear bursts on radio wave propagation and satellite and scatter propagation in natural environments is given.

[redacted] Part 2, consisting of two volumes, describes the effects of nuclear bursts on the propagation of satellite communication systems

[redacted]

[redacted]

(Vol. I) and troposcatter and ionoscatter communication systems (Vol. II). Techniques to model a relatively wide range of nuclear situations and to predict how these situations would degrade the communication systems performance are presented. These volumes are intended to be used with DASA 1956-1. Together, they provide a basic understanding of nuclear phenomenology and its interrelation with propagation to satellites.

[redacted] TREE PREFERRED PROCEDURES (Selected Electronic Parts)

[redacted] *DNA 2028H* [redacted]

Prepared by: Battelle Columbus Laboratories, Columbus, Ohio.

[redacted] *Availability:* Qualified requestors may obtain this document from the Defense Documentation Center.

[redacted] This document provides persons conducting TREE (transient radiation effects on electronics) experiments with recommended procedures which experience has shown to be efficient for determining transient radiation effects on electronic parts. Areas that are covered in detail include, experimental design, experimental documentation, dosimetry and environmental correlation, and preferred measurement procedures for diodes, transistors, capacitors, and microcircuits.

[redacted] HANDBOOK FOR ANALYSIS OF NUCLEAR WEAPON EFFECTS ON AIRCRAFT [redacted]

[redacted] DNA 2048 (Revised March 1976) (DNA 2048 H-[redacted] DNA 2048 H-2. [redacted]

[redacted] *Prepared by:* Kaman Avidyne, Burlington, Massachusetts

[redacted] *Availability:* Qualified requestors may obtain this handbook from the Defense Documentation Center.

[redacted] This handbook and its supplement are designed for use in analyzing conventional nuclear weapon effects on aircraft. DNA 2048 contains a comprehensive review of a large body of available literature pertinent to vulnerability and safety analysis of aircraft subjected to the effects of nuclear explosions. The handbook describes methods for analyzing material velocity, overpressure, thermal radiation and nuclear radiation effects on airplanes and helicopters, including the crew. Sure-safe and sure-kill criteria pertinent to the various weapon effects are presented, as well as the methods to be employed in constructing aircraft sure-safe and sure-kill burst-time volumes. The supplement to DNA 2048 is a handbook of computer programs designed to analyze nuclear weapon effects on aircraft. Detailed methodology for anlyzing material velocity (gust), overpressure, thermal radiation and nuclear radiation effects on airplanes and helicopters, including crew, are presented. Only the computer programs corresponding to the methods of analyzing of DNA 2048 are included, and a full understanding of the programs will require access to DNA 2048.

[redacted] A MANAGEMENT GUIDE TO TREE [redacted]

[redacted] *DNA 2051H* [redacted]

Prepared by: Batelle Columbus Laboratories, Columbus, Ohio.

[redacted] *Availability:* Qualified requestors may obtain this document from the Defense Documentation Center through Headquarters, Defense Nuclear Agency, Washington, D.C. 20305.

[redacted] This guide is intended primarily for management personnel associated with the development of electronic systems that must survive the transient radiation environment generated by a nuclear explosion. The document is intended to be useful to the manager, whether his background and responsibilities are wholly technical, technically oriented, or wholly administrative. The guide is also a satisfactory primer for engineering and scientific personnel.

[redacted]

[redacted]

[redacted] SUMMARY OF COMMUNICATION SYSTEMS DEGRADATION IN A NUCLEAR ENVIRONMENT [redacted]

[redacted] *DASA 2090* [redacted]

[redacted] *Prepared by:* General Electric/TEMPO, Santa Barbara, California. Major contributor: Illinois Institute of Technology Research Institute.

[redacted] *Availability:* Qualified requestors may obtain this document from the Defense Documentation Center through Headquarters, Defense Nuclear Agency, Washington, D.C. 20305.

[redacted] This report summarizes the degradation of communication systems in a nuclear environment. It is based on the results of a three year program to determine the effects of nuclear detonations on communication systems. The report provides information that will aid in determining whether sophisticated analyses are required to predict degradation.

[redacted] DNA EMP (ELECTROMAGNETIC PULSE) HANDBOOK [redacted]

[redacted] *DNA 2114H-1 (Volume 1), DNA 2114H-2 (Volume 2), DNA 2114H-3 (Volume 3), DNA 2114H-4 (Volume 4),* (Volumes 1, 2, and 4 [redacted] Volume 3, [redacted] Volume 3 will be issued early in calendar year 1973.

[redacted] *Prepared by:* DASIAC, Santa Barbara, California. Major contributors: Illinois Institute of Technology Research Institute, Mission Research Corporation, American Nucleonics Corporation, Lawrence Livermore Laboratory, U.S. Army Harry Diamond Laboratories, Braddock, Dunn and McDonald, Incorporated, Hughes Aircraft Corporation, Procedyne Corporation, Stanford Research Institute, Sandia Corporation, Air Force Weapons Laboratory, Massachusetts Institute of Technology, Defense Nuclear Agency, General Electric/TEMPO.

[redacted] *Availability:* Qualified requestors may obtain this document from the Defense Documentation Center. Volume 3 must be obtained on request through Headquarters, Defense Nuclear Agency, Washington, D.C. 20305.

[redacted] Volume 1 is designed for the practical electrical engineer. It contains information concerning an overall system evaluation and the practices that should be followed in circuit layout, shielding, grounding, and the use of protective devices for systems that are hardened to EMP. Volume 2 is designed for the theoretical or experimental analyst. It includes an analytic treatment of EMP problems in shielding, antennas, cables, and filters, experimental and analytic information on component degradation, and survey information on test methods and hardware. Volume 3 develops EMP threat criteria and provides an assessment of real system effects. The EMP environment information is presented from a system standpoint. Volume IV contains bibliographic and computer code information. Over 1,000 citations are given for such topics as theoretical calculations and nuclear test data related to the EMP environment and detection, EMP vulnerability analysis for systems and components, EMP protection, internal EMP, test direction and planning, and EMP simulators, sensors, and instrumentation. Current EMP computer codes are described and compared for the topics of environment, internal EMP, and circuit analysis.

[redacted] CORRECTIONS FOR DASA COMMUNICATION HANDBOOK (DASA 1954, 1955, 1956) [redacted]

[redacted] *DASA 2313* [redacted]

[redacted] *Prepared by:* General Electric/TEMPO, Santa Barbara, California.

[redacted] *Availability:* Qualified requestors may obtain this document from the Defense Documentation Center. No foreign dissemination is allowed without approval of Headquarters,

[redacted]

[redacted]

Defense Nuclear Agency, Washington, D.C. 20305.

[redacted] This handbook provides a set of corrections to the DASA Communications Handbooks, DASA 1954, 1955 and 1956 (see abstracts of these handbooks above).

[redacted] TREE SIMULATION FACILITIE[redacted]

[redacted] DNA 2432H (Edition 1)[redacted]

[redacted] *Prepared by:* Battelle Memorial Institute, Columbus, Ohio

[redacted] *Availability:* Qualified requestors may obtain this document from the Defense Documentation Center.

[redacted] This handbook characterizes individual pulse reactors, flash x-ray and LINAC facilities on a technical basis for those persons working in the area of transient radiation effects on electronics (TREE). DNA 2432H is arranged to provide the persons who perform TREE experiments with the information concerning facilities which they would require in order to perform an experiment at one of the facilities.

[redacted] X-RAY CROSS SECTION COMPILATION [redacted]

[redacted] *DNA 2433F-1 and -2 and DNA 2433F Supplement*[redacted]

[redacted] *Prepared by:* Kaman Sciences Corporation, Colorado Springs, Colorado.

[redacted] *Availability:* Qualified requestors may obtain this document from the Defense Documentation Center. Requests from other than U.S. government agencies must be made through Headquarters, Defense Nuclear Agency, Washington, D.C. 20305.

[redacted] The experimental X-ray attenuation cross sections for 94 elements between 0.1 keV and 1 MeV, which were obtained for the period from 1920 through 1970, together with exact photoelectric absorption values for hydrogen, are presented in this compilation.

[redacted] Scattering cross sections were calculated by relativistic SCF methods. These were subtracted from the total attenuation data, and the resulting photoelectric and measured photoelectric absorption cross sections from 1 keV to 1 MeV were fit by a least squares procedure to obtain best values. Interpolations were made for elements and energy ranges for which there were no experimental data. From 0.1 keV to between 1 keV and 10 keV nonrelativistic, self-consistent, independent electron theory was used to calculate photoelectric absorption cross sections. Scattering values were added to all photoelectric cross sections to obtain a best set of attenuation cross sections.

[redacted] NUCLEAR ENVIRONMENT DESCRIPTIONS [redacted]

[redacted] *DASA 2491* (CONFIDENTIAL).

[redacted] *Prepared by:* Boeing Company, Seattle, Washington.

[redacted] *Availability:* Qualified requestors may obtain this document from the Defense Documentation Center.

[redacted] The phrase "Nuclear Environment Descriptions" includes: (1) nuclear environment criteria; (2) nuclear effects design specifications; and (3) nuclear effects test specifications. This volume provides an introductory discussion of the three types of nuclear environment descriptions, but it is concerned primarily with the first of these descriptions.

[redacted] The major considerations and procedures required for the development of nuclear environment criteria within a logical system development process are described and illustrated. A standard, comprehensive, understandable format for expressing this description is specified. The material presented is not predicated on the administrative procedures of any one military service and is, therefore, of general applicability.

[redacted]

[redacted]

[redacted] NUCLEAR WEAPON THERMAL RADIATION PHENOMENA [redacted]

[redacted] DNA 2500H [redacted]

[redacted] *Prepared by*: Kaman Sciences Corporation, Colorado Springs, Colorado

[redacted] *Availability*: Volumes 2 and 3 were published in July 1974 and February 1974 respectively. Parts of Volume 1 were completed and published separately in February 1974 as DNA 3220Z, "New Thermal Scaling Laws for Low Altitude Nuclear Bursts (U)," and DNA 3223Z, "Atmospheric Transmission of Nuclear Weapon Thermal Radiation (U)." In November 1977, a draft version of Volume 1 was completed. It is expected to be incorporated into one document and published by mid 1978 under the title *New Thermal Scaling Laws for Bursts Below 30 Kilometers*. All published portions are available for qualified users from the Defense Documentation Center.

[redacted] The DNA Thermal Sourcebook is being prepared as a comprehensive summary of theoretical and experimental information on the prompt thermal radiation environment produced by atmospheric nuclear weapons. This book is designed to provide the latest and most reliable information on thermal environments, including both fireball source characteristics and the transport of the fireball radiation through great distances in the atmosphere. The book does not include the numerous considerations relating to target response, although a short appendix on thermal damage effects will be provided.

[redacted] Volume 1 of this sourcebook will treat the following subjects: nuclear weapon outputs, energy deposition in the atmosphere, the physics of fireballs, radiation-hydrodynamics codes, atmospheric transmission phenomena, weapons test data, comparisons of theory and experiment, and environment prediction methods. Volume 2 provides a complete tabulation of all thermal environment measurements made at all U.S. atmospheric nuclear tests through Operation DOMINIC in 1962. Volume 3 is an extensive bibliography of reports, papers, etc., on the subject of nuclear weapons thermal radiation phenomena.

[redacted] TRAPPED RADIATION HANDBOOK

[redacted] DNA 2524H (Unclassified)

[redacted] *Prepared by*: Lockheed Palo Alto Research Laboratory

[redacted] *Availability*: This document has been approved for public release and sale; its distribution is unlimited.

[redacted] The Trapped Radiation Handbook provides useful information and design data for scientists and engineers engaged in the design of spacecraft systems that must operate in the trapped radiation environment. It contains a compilation of useful charts and graphs and abbreviated derivations of equations and developments of concepts in a wide range of subject matter pertinent to the radiation belts. The handbook is intended to be helpful to scientists who are beginning studies or research in this field as well as to scientists who are actively engaged in magnetospheric research. The following subjects are discussed: the magnetosphere; features and mathematical models of the earth's magnetic field; the motion of charged particles in the field; the properties of the particles in the natural radiation belts; source and loss mechanisms; the artificial radiation belts that have resulted from tests of nuclear devices conducted at high altitudes; the phenomenology of nuclear detonations and beta injection processes; the effects of trapped particles (both natural and fission betas) on materials and devices; the irradiation of circular orbit satellites by trapped particles of the natural environment as well as the environment produced by weapon tests L-values, and an estimated wartime environment; the synchrotron radiation emitted by the trapped electrons; and the vulnerability of oper-

[redacted]

ational systems in the environments mentioned previously.

This handbook is updated on a periodic basis. As of September 1977, five changes have been issued.

STATUS OF NEUTRON AND GAMMA OUTPUT FROM NUCLEAR WEAPONS

DASA 2567

Prepared by: Science Applications Incorporated, La Jolla, California.

Availability: Qualified requestors may obtain this document from the Defense Documentation Center on request through Headquarters, Defense Nuclear Agency, Washington, D.C. 20305.

This report presents a review and evaluation of existing experiments and calculations of neutron and gamma output spectra and intensities. Comparisons of calculated and measured results for a number of devices are described together with possible explanations for some deviations between the experiment and numerical results. In addition, detailed gamma output calculations were performed for Tambourine, using up-to-date neutron and gamma production cross section data.

IMPROVED MODELS FOR PREDICTING NUCLEAR WEAPON INITIAL RADIATION ENVIRONMENTS

DASA 2615

Prepared by: Radiation Research Associates, Inc., Fort Worth, Texas.

Availability: Qualified requestors may obtain this document from the Defense Documentation Center on request through Headquarters, Defense Nuclear Agency, Washington, D.C. 20305.

DASA 2615 presents a review and evaluation of current data and techniques for predicting the initial radiation exposure at or near the ground surface resulting from a nuclear explosion. State-of-art models were then developed for neutron dose, secondary gamma exposure from neutron interactions in the air and ground, and fission product gamma ray exposure occurring during the first minute following a detonation. The neutron and secondary gamma model, based on Straker's discrete ordinates calculations of neutron transport in an air-over-ground geometry and French's first-last collision method for source height effects, yield results for slant ranges up to 4,800 meters from each of 8 different types of weapons. The results may be adjusted for the desired burst height and air density. The fission-product gamma ray model is based on Monte Carlo air transport calculations by Marshall and Wells. It incorporates source spectra, source decay rates, cloud rise approximations, and hydrodynamic enhancement treatments based on the work of a number of previous investigators. The model provides for a wide variety of burst heights and air densities and provides for slant ranges up to 4,800 meters. The models and the incorporated data were validated through extensive comparison with weapon test results and with other calculated and semi-empirical data.

THE MODELING OF NUCLEAR CLOUDS

DASA 2626

Prepared by: General Research Corporation, Arlington, VA

Availability: This document is available to qualified users from the Defense Documentation Center.

This modeling was performed in response to the need for a systems program to describe the dust particle environment in a nuclear cloud from a detonation on or near the surface. The flowfield during cloud rise was parameterized using a spherical vortex model empirically

[redacted]

fit to data from nuclear tests. This work is supplemental to DASA-2304T [redacted] Volume I, "Nuclear Surface Burst Debris [redacted]" as is also the determination of the lofted mass. The cloud dust loading depends on the height-of-burst in a nonlinear manner which is analyzed and modeled empirically. The particle size distribution of the dust in the cloud is that of the crater ejecta and sweep-up modified by the drag forces exerted by the buoyant and convective air flow. Both during rise and after stabilization, the cloud and dust are translated with the ambient wind. The speed and directional shears cause a time dependent cloud shape, which is important to the systems analyst, for whom the model was developed.

[redacted] The spherical model was completed and reported in DNA 2940T [redacted] "Vortex Dust Model for Rising Nuclear Cloud." Some modifications of the post stabilization model was reported in DNA 2745T [redacted] "New Measurements of Visible Cloud Diameter," and DNA 3158F-1 [redacted] "Post-Stabilization Nuclear Dust Cloud," and have been incorporated in the programming of the vortex model.

[redacted] HANDBOOK OF NUCLEAR WEAPONS AS X-RAY SOURCES [redacted]

DNA 2866H [redacted]

[redacted] *Prepared by*: Kaman Sciences Corporation, Colorado Springs, Colorado.

[redacted] *Availability*: Qualified requestors may obtain this document from the Defense Documentation Center.

[redacted] This handbook contains a chronological tabulation of most of the X-ray effects tests that have been conducted by the Department of Defense and the Atomic Energy Commission, as well as a general description of the X-ray spectra and the fluence levels available for experiments on each event. Six illustrative X-ray tests are discussed in some detail. Their X-ray spectra are presented as curves and tabulations and some discussion of their radiation times is given. There is some discussion of the outputs from underground X-ray tests simulating tactical ABM environments.

[redacted] The handbook is not intended to provide all the information required by a person who is not familiar with X-ray effects testing, nor is it for a person whose full time occupation is analysis of X-ray spectra from nuclear weapons. The information is useful to the large majority of the community associated with military effects of X-rays from nuclear weapons. Whether or not this is a "handbook" depends more on the user's definitions than on the author's.

[redacted]

DNA (b)(3)

[redacted] INSTRUMENTS FOR MEASURING NEUTRON AND GAMMA RADIATION FROM NUCLEAR-WEAPON TESTS [redacted]

DNA 2888F [redacted]

[redacted] *Prepared by*: Science Applications Incorporated, La Jolla, California.

[redacted] *Availability*: To be issued during calendar year 1972.

[redacted] DNA 2888 reviews the methods to obtain neutron and gamma ray fluence and spectral data in a nuclear test environment. Approximately forty instruments of those surveyed during this study are described. A complete outline of the experimental techniques employed in these types of measurements is provided, with a description of device input and typical radiation environments encountered during a nuclear test.

[redacted] With few exceptions, only those instruments that have been used in past tests are con-

[redacted]

[redacted]

sidered in this report. Instruments to provide neutron and gamma ray dose as a function of time, dose or fluence as a function of energy, and integrated dose were considered. A summary of the relative merits of each instrument is included.

[redacted] THE EFFECTS OF NUCLEAR WEAPONS [redacted]

[redacted] *Prepared and published by*: The U.S. Department of Defense and the U.S. Department of Energy. S. Glasstone and P. J. Dolan, editors.

[redacted] *Availability*: This document may be obtained by contacting the Superintendent of Documents, U.S. Government Printing Office, Washington, D.C.

[redacted] This book presents as accurately as possible, within the limits of national security, a comprehensive summary of information concerning nuclear weapons effects in an unclassified form. The phenomena of air blast, ground and water shock, thermal radiation, and nuclear radiations associated with nuclear explosions are very complex, and descriptions of these phenomena and their related effects are somewhat technical in nature. However, this handbook has been arranged in such a manner as to serve the [redacted] possible range of readers. Most of the chapters are presented in two parts, the first consisting of a general treatment of a particular topic in a less technical manner and the second discussing some of the more technical aspects. The material is so arranged that the reader will experience no loss of continuity by the omission of any or all of the more highly technical sections, but the technical material is available for the use of those who may have need of such information.

[redacted] The third edition of this book was published in December 1977.

[redacted] VORTEX DUST MODEL FOR RISING NUCLEAR CLOUDS [redacted]

[redacted] DNA 2940T [redacted]

[redacted] *Prepared by*: Science Applications, Incorporated, Arlington, VA

[redacted] *Availability*: Qualified users may obtain this document from the Defense Documentation Center.

[redacted] The transport of soil particles after a nuclear detonation on or near the surface is modeled by the vortex flowfield which has a simple mathematical form. By including appropriate particle drag relations and empirically fitting the vortex parameters to both experimental and hydrocode data, a simpler hydrodynamic model (VORDUM) was obtained to predict the soil particle environment. The boundary condition of zero vertical flow velocity at the surface is obtained by using an image vortex moving downward. The VORDUM results are similar to those obtained using the SHELL hydrocode (developed at AFWL). The model has been applied to yields from less than 1 MT to greater than 10 MT. The pancake geometry of the post stabilization model, reported in DASA 2304T [redacted] Volume I, "Nuclear Surface Burst Debris [redacted] was superseded by this description.

[redacted] The post stabilization cloud geometry was improved by the modeling of the late time cloud reported in DNA 3158 F-1 [redacted] "Post-Stabilization Nuclear Dust Cloud."

[redacted] COMMUNICATION SATELLITE SYSTEMS VULNERABILITY TO NUCLEAR EFFECTS – SELECTED EXAMPLES BY FREQUENCY BAND [redacted]

[redacted] DNA 3185H-1 [redacted]

Prepared by: ESL Incorporated

Availability: Qualified requestors may obtain these documents from the Defense Documentation Center. Each transmittal outside the

[redacted]

[redacted]

[redacted] agencies of the U.S. Government must have prior approval of the Defense Nuclear Agency.

[redacted] This document describes communication satellite system vulnerability to propagation disturbance induced by nuclear explosions. Examples of the effects of selected nuclear burst on communication satellite system performance are given by frequency band. The satellite systems analyzed are representative of existing, planned, or proposed systems in seven bands extending from 150 MHz to 14 GHz. The examples presented illustrate the approximate duration and extent over which typical systems may experience difficulty. In addition to specific results, the nuclear effects from the selected weapon environments have been parameterized so that these results can be extended to other systems.

[redacted] Among the effects considered are radio wave absorption, thermal noise, signal dispersion, and propagation time delays. The effect of signal dispersion is considered on systems employing frequency division multiplex-frequency modulation (FDM-FM), and digital systems employing phase shift keying (PSK). While not modeled for the selected examples, the potential effects of phase scintillations on systems employing PSK modulation are shown. Potential effects on systems employing Time Division Multiple Access (TDMA) and Code Division Multiple Access (CDMA) using spread spectrum techniques are discussed.

[redacted] ELECTROMAGNETIC BLACKOUT HANDBOOK [redacted]

[redacted] DNA 3380 H-1, 2, 3 (DNA 3380 H-1, [redacted] DNA 3380 H-2, [redacted] DNA 3380 H-[redacted]

[redacted] *Prepared by:* General Electric Company – [redacted]PO.

[redacted] *Availability:* Qualified requestors may obtain these documents from the Defense Documentation Center. Each transmittal outside the agencies of the U.S. Government must have prior approval of the Defense Nuclear Agency.

[redacted] This handbook provides source material on nuclear weapon phenomenology, atmospheric processes, and effects of disturbed atmospheric environments on electromagnetic propagation for use in analysis of radar and communications systems. This edition of the handbook is a revision of DASA 1580 and DASA 1580-1 (same title) and replaces those documents. The handbook is divided into seven chapters plus appendices and is published in three volumes. Chapter 1 provides an introduction to nuclear weapon effects on electromagnetic propagation and a summary of communication and radar system performance in nuclear environments. Chapters 2, 3, and 4 present detailed descriptions of weapon radiations and energy deposition in the atmosphere, the phenomenology of heated regions, and atmospheric processes that affect nuclear weapon-induced atmospheric ionization. Chapters 5, 6, and 7 describe electromagnetic propagation effects and weapon-produced noise sources that can have effect on radar and communication systems. The several appendices include material on the properties of the atmosphere and earth's magnetic field, reference material on electromagnetic propagation and thermal radiation, and parametric scaling for weapon-produced regions and effects.

[redacted] ELECTROMAGNETIC PULSE HANDBOOK FOR ELECTRIC POWER SYSTEMS [redacted] December 1974

[redacted] DNA 3466F [redacted]

[redacted] *Prepared by:* Stanford Research Institute, Menlo Park, California

[redacted] *Availability:* Qualified users may obtain this handbook from the Defense Documentation Center.

[redacted] This handbook has been prepared primarily for the power, communications, and systems engineer who must be concerned with the

[redacted]

[redacted]

effects of the nuclear electromagnetic pulse on his system. The power engineer should be aware of the effects of EMP on his transmission and distribution system, and the power users must protect their equipment from the pulse conducted into their facilities on the power lines. The commercial power system can be a major path for coupling the EMP into ground-based systems. The power distribution system forms a very large, completely exposed antenna system that is hard-wired into the customer's facility. Thus, extremely high voltages may be developed on the power conductors, and even if the commercial power is not relied on for system survival, these voltages may be delivered to the system either before commercial power is lost, or by the ground or neutral system after transferring to auxiliary power.

[redacted] Considerable research has been performed on EMP coupling to commercial power systems in an effort to characterize the power distribution lines as EMP collectors, and to determine the effects of major components, such as transformers, lightning arresters, and low-voltage wiring, on the penetration of the received signal into ground-based facilities. This research has entailed development and experimental verification of the theory of coupling to transmission lines. This handbook on the interaction of EMP with commercial power systems has been prepared so that designers and systems engineers can benefit from the results of extensive data already accumulated.

[redacted] **A POCKET MANUAL OF THE PHYSICAL AND CHEMICAL CHARACTERISTICS OF THE EARTH'S ATMOSPHERE**

[redacted] DNA 3467H[redacted]

Prepared by: General Electric Co., Space Sciences Laboratory, P. O. Box 8555, Philadelphia, Pa. based upon information provided by the Bell Telephone Laboratory, the Lockheed Palo Alto Research Laboratory, and the Santa Barbara Research Center. Information was also obtained from "Aid for the Study of Electromagnetic Blackout," DASA 2499 (1970), the DNA "Reaction Rate Handbook, Second Edition," DNA 1948H (1972), and "The Trapped Radiation Handbook" (1971), DNA 2542H.

[redacted] *Availability:* Qualified requestors may obtain the handbook from the Defense Documentation Center or from the National Technical Information Service (NTIS).

[redacted] This pocket manual provides a pocket size compendium of current available knowledge concerning the physical and chemical properties of the earth's ionosphere. It is based principally upon data contained in greater detail in DNA Reaction Rate Handbook, Second Edition (1972), DNA 1948H, as well as the other sources mentioned above. A circular slide rule is normally inserted in the flap of the front cover for convenient calculational use.

[redacted] It is anticipated that as important changes occur in relevant information they will be issued to recipients for inclusion in this pocket manual.

[redacted] **AID FOR THE STUDY OF ELECTROMAGNETIC BLACKOUT**

[redacted] DNA 3499H[redacted]

Prepared by: General Electric Company – TEMPO

[redacted] *Availability:* Qualified requestors may obtain this document from the Defense Documentation Center.

[redacted] This report is a revision of DASA 2499 (same title) and replaces that document. The report is a compendium of selected graphs, charts, equations, and relations useful in the analysis of electromagnetic blackout caused by nuclear explosions. Information is provided concerning weapon outputs, ionization source functions, deionization, absorption, phase effects, and noise. The report also contains sections listing atmospheric properties, physical constants, definition of symbols, and a glossary of frequently used terms.

[redacted]

APPENDIX E

GLOSSARY

Absorption – The irreversible conversion of the energy of an electromagnetic wave into another form of energy as a result of its interaction with matter.

Absorption coefficient – A number characterizing a given material with respect to its ability to absorb radiation. The linear absorption coefficient refers to the ability of a given material to absorb radiation per unit thickness, it is expressed in reciprocal units of thickness. The mass absorption coefficient refers to the ability of a given material to absorb radiation per unit mass; it is expressed in units of area per unit mass, and it is equal to the linear absorption coefficient divided by the density of the absorbing material.

Acceleration – Time rate of change of velocity. The acceleration due to gravity (g) is 32.2 ft/sec^2.

Activity – The rate of decay of radioactive material expressed as the number of nuclear disintegrations per second.

Adiabatic – Occurring without change in heat content, i.e., without gain or loss of heat by the system involved.

Air burst – See *Burst types.*

Albedo – The fraction of the incident radiation reflected by a material in any manner.

Alpha particle – A particle ejected spontaneously from the nuclei of some radioactive elements. It is identical to the helium nucleus, which has an atomic weight of four and an electric charge of plus two atomic mass and charge units, respectively, i.e., two protons and two neutrons.

Amorphous – Lacking in ordered crystalline structure.

Amplitude – The maximum displacement of an oscillating particle or wave from its position of equilibrium.

Angle of incidence – The angle between the perpendicular to a surface and the direction of propagation of a wave.

Annealing – The process of displacement damage reduction with time, temperature, electrical conditions, etc.

Annealing factor – The ratio of the maximum displacement damage to the displacement damage at a certain time after irradiation. It is a function of time.

Apparent crater – The visible crater remaining after a nuclear detonation. See *Crater.*

Atmospheric transmissivity – The fraction of the radiant exposure received at a given distance after passing through the atmosphere relative to that which would have been received at the same distance if no atmosphere were present.

[redacted]

[redacted]

Atomic cloud – An all-inclusive term, identified as the hot gases, liquid and solid particles, and vapors produced by a nuclear explosion. Clouds resulting from large yield weapons may penetrate the tropopause and deposit debris in the stratosphere. The cloud contains radioactive fission products. See *Fireball*.

Atomic weapon – See *Nuclear weapon*.

Attenuation – Reduction of the intensity of radiation or a blast or shock wave as a result of passing through any medium.

Base surge – A cloud that rolls out from the bottom of the column produced by a subsurface burst of a nuclear weapon. For underwater bursts, the surge is a cloud of liquid droplets, which has the property of flowing almost as if it were a homogeneous fluid. For subsurface land bursts the surge is made up of small solid particles, but it still behaves like a fluid.

Beta aurora – Fluorescence caused by deposition of beta particle energy in the atmosphere. See *Beta particle*.

Beta particle – A small particle ejected spontaneously from a nucleus of either natural or artificially radioactive elements. It carries a negative charge of one electronic unit and has an atomic weight of 1/1840. See *Electron*.

Bipolar transistor – A transistor that utilizes both minority and majority carriers. Presently, the most common type of transistor.

Black body – A perfect radiator (emitter) of electromagnetic energy. The radiating characteristics of a black body are completely specified by its temperature.

Black body radiation – See *Planckian radiation*.

Blast wave – The shock wave transmitted through the air as the result of an explosion is referred to as a blast wave or air blast. See *Shock wave*.

Blowin – The movement of air into the column of an underwater explosion if the column walls rupture when the enclosed explosion bubble contents are below atmospheric pressure. See *Bubble* and *Column*.

Blowoff – Fragments of material separating from the surface of a material.

Blowout – The escape of underwater explosion bubble contents to the atmosphere at high pressure leading to the formation of a cauliflower cloud considerably wider than the column. See *Bubble* and *Cauliflower cloud*.

Breakaway – The onset of a condition in which the shock front moves away from the periphery of the expanding fireball.

Breaking wave – A wave of such steep slope that it is unable to maintain its shape and loses height by tumbling or falling over.

Breakdown voltage – In semiconductor-junction devices, that voltage that causes appreciable conduction in the reverse direction.

Breakover voltage – The voltage in silicon PNPN devices at which the device switches. That is, the device switches from a high voltage-low current state to a low voltage-high current state.

[redacted]

[redacted]

Bubble – The globe of gas, vapor, and explosion products that forms when an explosion occurs under water.

Bulk conductivity – A measure of the ability of a material to conduct electric current.

Burst geometry – The location of a nuclear detonation with respect to the ground surface, water surface, or bottom.

Burst types:

Air burst – The explosion of a nuclear weapon at such a height that the weapon phenomenon of interest is not significantly modified by the earth's surface. For example, these heights are such that for –

Blast – The reflected wave passing through the fireball does not overtake the incident wave above the fireball ($\sim 160\ W'^{1/3}$ ±15 percent).

Thermal radiation – The apparent thermal yield viewed from the ground is not affected by heat transfer to the earth's surface nor by distortion of the fireball by the reflected shock wave ($\sim 180\ W'^{0.4}$ ±20 percent for 10 to 100 kt and ±30 percent for other yields).

Fallout – Militarily significant local fallout of radioactive material will not occur. This height generally can be taken to be $100\ W'^{0.35}$; however a more conservative estimate of $180\ W'^{0.4}$ feet may be desirable for use under some circumstances. See paragraph 5-22, Chapter 5.

Surface burst – The explosion of a nuclear (or atomic) weapon at the surface of the land or water or at a height above the surface less than the radius of the fireball at maximum luminosity (in the second thermal pulse). An explosion in which the weapon is detonated actually on the surface (or within $5\ W'^{0.3}$ feet, where W' is the explosion yield in kilotons, above or below the surface) is called a contact surface burst.

Subsurface burst – The explosion of a nuclear weapon in which the center of the detonation lies at any point beneath the earth's surface (either ground or water surface).

Calorie – The amount of heat required to raise the temperature of 1 gram of water from 15°C to 16°C at 760 mm Hg pressure.

Camouflet – The cavity resulting from an underground explosion when no rupture of the surface of the earth occurs. See also *Crater*, *True Crater*, and *Apparent Crater*.

Cauliflower cloud – The roughly spherical turbulent cloud which is formed above the column on a very shallow nuclear burst.

Cavitation – The separation of the water particles and the forming of cavities, as a result of the inability of water to withstand the tensional wave reflected from the water surface.

Charge carrier – Any particle possessing a net positive or negative electric charge.

Charge transfer – The movement of electric charge from one material to another. Charge transfer often results in undesirable transient currents, electromagnetic fields, and steady-state voltages.

Circuit saturation – That process in which a circuit is locked in a stable state that often remains after the radiation pulse has subsided (not latchup).

Circuit upset – A circuit response which causes some electrical subsystem or system to malfunction temporarily.

[redacted]

[redacted]

[redacted]

Circumvention – A general term applied to techniques that allow the circuits in a system to be temporarily perturbed by an ionizing-radiation pulse, but that enable the system to recognize the cause of the perturbations and to ignore any spurious signals or misinformation generated by them.

Cloud chamber effect – See *Condensation cloud.*

Collector junction – One of two junctions in a bipolar transistor. Typically the collector junction is the largest junction and generates the most photocurrent.

Collision frequency – The average number of collisions (involving momentum transfer) per second of a particle of a given species with particles of another or the same species.

Column – The visible column of particulate matter, which may extend to the tropopause (the boundary between the troposphere and the stratosphere) subsequent to the explosion of a nuclear weapon. Also, the hollow cylinder of material thrown up from a subsurface nuclear detonation.

Column jets – Plumes that form on an expanding water column.

Combat ineffective – An individual whose injuries are of such nature that he is no longer capable of carrying out his assigned task.

Component part (component) – A device that performs a function and is not manufactured from other devices (e.g., transistor, integrated circuit, capacitor, resistor).

Component damage – Permanent change in the characteristics of a device due to electromagnetic coupling. See *Coupling.*

Compton current – Electron current generated as a result of Compton processes. See *Compton effect.*

Compton effect – Elastic interaction of gamma rays or X-rays with matter, resulting in the emission of secondary electrons that contain part of the energy of the incident radiation. See *Photoelectric effect*

Compton electrons – Secondary electrons generated by the gamma rays or X-rays from a nuclear burst absorbed through Compton collisions. See *Compton effect.*

Compton scattering – Scattering photons through their interaction by means of the Compton effect. See *Compton effect.*

Condensation cloud – A mist or fog which temporarily surrounds the fireball after a nuclear explosion in a comparatively humid atmosphere. Since it is similar to the cloud observed by physicists in the Wilson cloud chamber, it is also called the "Wilson cloud." Rapid cooling of the previously heated air surrounding the fireball during the negative pressure phase of the shock wave causes the moisture in the air to condense temporarily, forming a cloud. The cloud is dispelled within a second or so upon return of the air pressure to normal.

Conjugate points – Points at the north and south ends of a geomagnetic field line which are either at corresponding altitudes or at corresponding field strength.

Contamination – The deposit of radioactive material on the surfaces of structures, areas, objects, or personnel, following a nuclear explosion. This material generally consists of fallout in which fission products and other weapon debris have become incorporated with particles of dirt, etc. Contamination can also arise from the radioactivity induced in certain substances by the action of neutrons from a nuclear explosion. See *Decontamination, Fallout, Induced radioactivity, Weapon debris.*

[redacted]

[redacted]

[redacted]

Contour method – The representation of the degree of contamination resulting from a nuclear burst by the use of contour lines to connect points of equal radiation dose or dose rate. See *Isodose lines.*

Conventional current flow – Electric current assumed to flow from the most positive point of the circuit to the most negative point in the circuit relative to ground.

Counterpoise – An electrically continuous conductive material usually installed around the perimeter of a building to reduce the apparent ground resistance.

Coupling – Interaction of electromagnetic fields with electrical systems whereby part of the energy of the field is transferred to the system. Also the energy transfer of a shock wave traveling in one medium, which produces a shock wave in a second medium at their common interface. Also the absorption of radiant energy by a material by conversion to internal energy resulting in a shock wave being developed in the material.

Crack – A rapidly expanding white disc on the water surface whose leading edge follows closely behind the intersection of the underwater shock wave with the surface. The whiteness is believed to be the cavitated region caused by the rarefaction wave, which forms and moves downward when the primary shock is reflected from the surface.

Crater – The pit, depression, or cavity formed in the surface of the earth by an explosion. It may range from saucer shaped to conical, depending largely on the depth of burst. See also *True crater, Apparent crater,* and *Camouflet.*

Crater depth – The maximum depth of the crater measured from the deepest point of the pit to the original level.

Crater radius – The average radius of the crater measured at the level corresponding to the original surface of the ground.

Critical radiant exposure – The thermal radiant exposure required for a particular effect on a material. The unit of critical radiant exposure is the cal/cm^2.

Cross section – A measure of the probability that a nuclear reaction will occur. It is the apparent or effective area presented by a target (e.g., atomic nucleus or other particle) to an oncoming particle or radiation (e.g., X-ray or gamma ray).

Crystalline – Refers to a material (e.g., a semiconductor) possessing an ordered lattice structure.

Curie – The quantity of any radioactive nuclide in which the number of disintegrations per second is 3.7×10^{10}.

Dazzle – See *Flashblindness.*

Debris radiation – Radiation emitted after the first few hundred microseconds after the burst. It is primarily gamma ray and beta radiation.

Decontamination – The process of removing contaminating radioactive material from an object, a structure, or an area. See *Contamination.*

Delamination – Separation of bulk material (see Figure 6-5).

Diffraction – The bending of waves around the edges of objects.

[redacted]

[redacted]

Diffraction loading – The forces exerted upon an object or structure by the blast wave overpressures as the shock front strikes and engulfs it.

Diffusion – That process in which particles (e.g., charge carriers) move from a region of high concentration toward a region of lower concentration.

Direct shock wave – A shock wave traveling through the medium in which the explosion occurred, without having encountered an interface, is referred to as the direct shock wave.

Dispersion – Effects on an electromagnetic wave traversing a region in which the propagation characteristics are frequency dependent.

Displacement – A type of transient and permanent damage in crystalline materials in which atoms are moved from their normal lattice positions.

Dose – See *Radiation dose.*

Dose rate – See *Radiation dose rate.*

Dosimeter – An instrument for measuring the amount of radiation received.

Dosimetry – The process of measuring and providing a quantitative description of a radiation environment, preferably in terms relevant to the radiation effect being studied (e.g., neutron fluence, dose etc.).

Drag loading – The forces exerted upon an object or structure by the dynamic pressures from the blast wave of an explosion, influenced by certain characteristics (primarily the shape) of the object or structure.

D-Region – The region of the ionosphere between about 40 and 90 kilometers altitude. See *Ionosphere.*

Drift – That process in which charge carriers move along the line of action of an electric field.

Ductility – The ability of a material or object to undergo large permanent deformations without rupture.

Dynamic pressure (q) – $q = 1/2\ \rho_s u^2$, where ρ_s is the density of the medium behind the shock front, and u is the particle velocity behind the shock front. The drag force on an object is proportional to the dynamic pressure.

Dynamic pressure impulse – See *Impulse.*

Early transient incapacitation – A temporary inability of a person to perform a required task properly. Onset is shortly after exposure to insult or stress. The incapacitation will be followed by partial or complete recovery of performance ability, frequently temporary in nature.

Eddy current – Current created on the building shielding by the impinging magnetic and electric fields.

E field – Electric field associated with an electromagnetic wave or created by a charge distribution.

Ejecta (throw-out) – Original material dissociated and ejected to the area surrounding a crater. The ejecta creates missile hazards.

[redacted]

[redacted]

Electric surge arrestor (ESA) – Hybrid device which provides protection across the frequency spectrum and voltage spectrum.

Electromagnetic pulse (EMP) – The time-varying electromagnetic radiation that results from a nuclear detonation.

Electromagnetic radiation – Radiation made up of oscillating electric and magnetic fields and propagated with the speed of light. It includes gamma radiation, X-rays, ultraviolet, visible and infrared radiation, and radar and radio waves.

Electromagnetic spectrum – The frequencies (or wave lengths) present in a given electromagnetic radiation. A particular spectrum could include a single frequency or a wide range of frequencies.

Electron – Classically, a unit negatively charged particle usually bound to an atom and orbiting about its nucleus.

Electron volt – The amount of kinetic energy gained by an electron when accelerated through a potential of one volt. (1.6×10^{-12} ergs).

Electrostatic coupling – Capacitive coupling between two parallel lines. See *Coupling.*

Emitter junction – One of two junctions in a bipolar transistor. Typically the emitter junction is the smaller junction and many times the photocurrent generated in it is neglected.

EMP – See *Electromagnetic pulse.*

Energy flux density – The energy of any radiation incident upon or flowing through a unit area, perpendicular to a radiation beam, in unit time.

Energy partition – The distribution of the total energy released by a nuclear detonation among the various phenomena, e.g., nuclear radiation, thermal radiation, and blast. The exact distribution is a function of time, weapon yield, and the medium in which the weapon is detonated.

Energy spectrum – A description of the relative magnitudes of various energy components or energy ranges of electromagnetic radiation or particles.

Epitaxial – The formation of single crystalline material upon a single crystalline substrate by chemical reduction from the vapor or liquid phase. The grown material assumes the same crystal orientation as the substrate.

E-Region – The region of the ionosphere between about 90 to 160 kilometers altitude. See *Ionosphere.*

Exposure – A measure of the radiation energy available (the dose in air). Exposure generally is specified in roentgens.

Exposure rate – A measure of the radiation energy available per unit time (the dose rate in air). Exposure rate generally is specified in roentgens per second or roentgens per hour.

Factor – A multiplier, frequently used to indicate range of coverage. For example, "correct within a factor of two" means correct within a possible range of values between twice and one-half the stated value.

Failure threshold – That exposure which changes one or more material (device) properties to such an extent that the material (device) becomes unsuitable for a specified application.

[redacted]

[redacted]

[redacted]

Fallback – Original material dissociated but not completely removed from the true crater. Upon impact, the fallback and ejecta assist in the development of the hazardous base surge dust cloud.

Fallout – The process or phenomenon of the fallback to the surface of the earth of particles contaminated with radioactive material from the radioactive cloud. The term is also applied in a collective sense to the contaminated particulate matter itself. The early (or local) fallout is defined, somewhat arbitrarily, as those particles which reach the earth within 24 hours after a nuclear explosion. The delayed (or world-wide) fallout consists of the smaller particles which ascend into the upper troposphere and into the stratosphere and are carried to all parts of the earth. The delayed fallout falls to earth, over extended periods of time ranging from months to years.

Fast neutron – Typically, a neutron with energy exceeding 10 keV (this energy threshold has not been standardized). See *Neutrons, fast.*

Film badge – A photographic film packet in the form of a badge, carried by personnel, for obtaining a measure of gamma and also in some cases, beta and neutron dose. See *Dosimeter.*

Fireball – The visible luminous sphere of hot gases formed by a nuclear explosion.

Fission – The splitting of a heavy nucleus into two (or rarely more) nuclei of lighter elements – the fission products. Fission is accompanied by the emission of neutrons and the release of energy. It can be spontaneous or it can be caused by the impact of a neutron, a fast charged particle, or a photon. The most important fissionable materials for weapons are uranium-235 and plutonium-239.

Fission products – A general term for the complex mixture of substances produced as a result of nuclear fission. A distinction should be made between these and the direct fission products or fission fragments that are formed by the actual splitting of the heavy element nuclei. The fission fragments, being radioactive, immediately begin to decay, forming additional (daughter) products, which are included in the complex mixture of isotopes that is observed at some time after the fission event.

Flashblindness (Dazzle) – Temporary impairment of vision resulting from an intense flash of light. See *Retinal burn.*

Fluence – The number of particles or photons or the amount of energy that enters an imaginary sphere of unit cross-sectional area. It is the time-integrated flux.

Fluorescence – The reemission of absorbed energy by molecules and atoms at the same or longer wavelengths than those that were absorbed.

Flux – The flow of photons, particles, or energy per unit time through an imaginary sphere of unit cross-sectional area.

Forward bias – Voltage applied across a PN junction in such a direction as to cause conduction through the junction i.e., the most positive potential is connected to the P side of the junction.

Forward resistance – The value of the ratio of the forward voltage to the current flowing through the PN junction when that same forward voltage is applied to it. The value varies with forward voltage.

Forward voltage – The voltage applied to a PN junction which forward biases the junction.

Fractionation – The phenomenon which results in a fallout sample being nonrepresentative of the total amount of radioactivity produced by a nuclear explosion. For example a bomb may produce x

[redacted]

[redacted]

[redacted]

atoms of one fission product and y atoms of another. Any fallout sample (airborne or on the ground) for which the ratio of the number of these two products is different from x/y is said to be fractionated.

Free air – A region of homogeneous air sufficiently remote from reflecting surfaces or other objects that the characteristics of the direct shock are not modified in any way by reflected shocks or other disturbances arising from scattering objects.

Free air overpressure (sometimes called free air pressure) – The unreflected pressure in excess of atmospheric or ambient pressure created in the air by the incident shock of any explosion.

Free charge – The charge carriers that are capable of moving (i.e., those which are not bound to atoms).

F-Region – The region of the ionosphere above about 160 kilometers.

Fusion – The process by which nuclei of light elements, especially the hydrogen isotopes deuterium and tritium, combine to form the nucleus of a heavier element with a substantial exothermic release of energy.

Gain – With reference to an electronic circuit or device, the ratio of output response to input signal. Gain is a measure of amplification.

Gamma rays – Highly penetrating, high-frequency electromagnetic radiation from the nuclei of radioactive substances. They are of the same nature as X-rays, but of nuclear rather than atomic origin, and are emitted with discrete, definite energies.

Ground zero (GZ) – The point on the surface of land or water vertically below or above the center of a burst of a nuclear weapon; also called surface zero.

Hardening – The process of decreasing vulnerability to a nuclear explosion by design.

Height of burst – The height above the surface of the earth at which a weapon is burst. Altitude, by contrast, is the height above mean sea level.

H field – Magnetic field associated with an electromagnetic wave or created by an electric current.

Hole – With reference to electronic valence structure of a semiconductor that acts as a positive electronic charge with a positive mass.

Hot spots – Regions in a contaminated area in which the level of radioactive contamination is considerably higher than in neighboring regions.

Impedance – The total opposing force to current flow, a factor of energy dissipation.

Impulse – The product of the average force and the time during which it acts at a given point, or the integral of the curve representing variation of force with time, with integration over the time of interest. In considering the effectiveness of a shock wave in producing damage, it is generally more convenient to employ the concepts of overpressure impulse and dynamic pressure impulse. The overpressure impulse of the positive phase of a blast wave is the integral of the curve representing the variation of overpressure with time, the integration being performed from $t = 0$, the time of arrival of the shock front at a given location, to $t = t_p^+$, the *end* of the positive phase. The dynamic pressure impulse is a similar integral of the dynamic pressure-time curve.

[redacted]

[redacted]

Incapacitation – The inability to perform a required task as the result of a physical or mental disability. See also *Permanent Complete Incapacitation* and *Early Transient Incapacitation.*

Induced radioactivity – Radioactivity that results from certain nuclear reactions in which exposure to radiation results in the production of unstable nuclei. Many materials near a nuclear explosion enter into this type of reaction, primarily as a result of neutron interactions.

Induced shock wave – The shock wave that is induced in a medium when a shock wave traveling in another medium crosses the interface between the two media.

Ineffective – See *Combat ineffective.*

Inelastic scattering – Scattering in which the total kinetic energy of a two-particle system is decreased, and one or both of the particles is or are left in an excited state.

Infrared – That portion of the electromagnetic spectrum occurring between the wavelengths 0.7 and 12 microns.

Initial nuclear radiation – Radiation produced by a nuclear explosion within 1 minute following the burst. It includes neutrons and gamma rays given off at the instant of the explosion, gamma rays produced by the interaction of neutrons with weapon components and the surrounding medium, and the alpha, beta, and gamma rays emitted by the fission products and other weapon debris during the first minute following the burst. See *Residual radiation.*

Internal EMP – A term commonly applied to the electric and magnetic fields generated within an enclosure by the interaction of high energy nuclear radiation (gamma rays, X-rays, neutrons) with the walls.

Interstitial – An atom of a crystalline material located at some point other than a normal lattice position. Interstitials are created during the displacement process. See *Displacement.*

Inversion (atmospheric temperature inversion) – A region in the atmosphere in which the temperature rises with increasing altitude instead of dropping, as it does in the more general case.

Ion – An atom with a net electric charge.

Ionization – The separation of a normally electrically neutral atom or molecule into electrically charged components.

Ionizing radiation – Electromagnetic radiation (gamma rays or X-rays) or particle radiation (neutrons, electrons, etc.) capable of producing ions, i.e., electrically charged atoms or molecules, during its passage through matter.

Ionosphere – That part of the atmosphere where ions and electrons are present in quantities sufficient to affect the propagation of radio waves.

I_{pp} – Primary photocurrent. See *Primary photocurrent.*

Irradiance – The incident thermal energy per unit time per unit area. The unit of irradiance is the cal/cm^2/sec.

Isobaric – Constant pressure condition.

Isodose lines – A term applied to imaginary contours in a radioactive field on which the total accumulated radiation dose is the same.

[redacted]

[redacted]

[redacted]

Jitter effect – Instability of the signal on the radar indicator.

Kelvin scale – The absolute temperature scale for which the zero is -273°C. Conversion from centigrade to Kelvin is made by adding 273 to the centigrade reading.

Kiloton (kt) – The energy release of one thousand tons of TNT, where 1 ton equals 2,000 pounds and where the energy content of TNT is defined as 1,102 calories per gram.

Latchup – Regenerative device action in transistors or circuits in which an undesired stable condition is attained.

Lattice – The pattern defined by an orderly crystalline structure in a material.

Leakage current – An undesirable reverse current across a semiconductor junction.

Lethal gust envelope – The boundary of the area in any given plane within which the gust loading effects from an explosion inflict sufficient structural damage to destroy a given aircraft.

Linear circuit – An electronic circuit in which voltages and currents can be continuously variable.

Lip height – The height above the original surface to which earth is piled around the crater formed by an explosion.

Loading – The forces imposed upon an object.

Loop – A closed path or circuit over which an electric signal can circulate.

Lossy devices – Devices that convert portions of the input energy into heat, which is lost to the surrounding medium.

Lossy field coupling – Coupling of an electromagnetic field into an electrical system so that part of the energy is lost due to radiation. See *Coupling.*

Mach stem – The shock formed by the fusion of the incident and reflected shocks from an explosion. The term usually is used with reference to an air-propagated wave reflected from the surface of the earth, generally nearly vertical to the reflecting surface. See *Shock front.*

Magnetic coupling – Energy departed to (or voltage induced in) a loop of finite area due to a change in flux linkages within the loop.

Magnetic conjugate points – Points at the north and south ends of a geomagnetic field line that are either at corresponding altitudes or at corresponding magnetic field strengths.

Majority carrier – In semiconductors, the type of carrier that constitutes more than half the total number of carriers. The majority carriers are electrons in an N-type semiconductor and holes in a P-type semiconductor.

Mean free path – Average distance traveled by particles before interaction or average distance a single particle travels between interactions.

Median lethal dose – The amount of radiation received over the whole body which would be fatal to about 50 percent of a specified animal. The median lethal dose for humans is not well established, but for the purpose of this manual it is assumed to be 450 rads, if the total dose is delivered within a period of 24 hours or less. Sometimes abbreviated as MLD or LD-50.

Megaton (Mt) – The energy release of a million tons of TNT (10^{15} calories). See *Kiloton.*

[redacted]

[redacted]

[redacted]

Metal-oxide-semiconductor (MOS) transistor – A field-effect transistor consisting of a silicon chip, a silicon oxide, and a metal contact.

Micron (μ) – A unit of length equal to 10^{-6} meters, 10^{-3} meters, 10^{-3} millimeter, or 10^{4} Angstrom units.

Millibar – One thousand dynes per square centimeter, a unit of measure of atmospheric pressure.

Minority carrier – The type of carrier that constitutes less than half the total number of carriers in a semiconductor. The minority carriers are holes in an N-type semiconductor and electrons in a P-type semiconductor.

Minority-carrier lifetime – The time period starting with the creation of a minority carrier and ending with its being recombined.

Mobility – The ease with which carriers move through a semiconductor either through random motion or when they are subjected to electric forces.

Monte Carlo method – A method of solution of a group of physical problems by means of a series of statistical experiments which are performed by applying mathematical operations to random numbers.

MOS – Metal-oxide-semiconductor.

Negative phase – That portion of the blast wave in which pressures are below ambient atmospheric pressure.

Neutron – An electrically neutral particle which is one of the fundamental particles making up the nucleus of all atoms except hydrogen. It has nearly the same weight as the hydrogen nucleus (atomic weight 1). The neutron under appropriate conditions is capable of causing fission of U^{235} or Pu^{239} and certain other radionuclides. In the fission process other neutrons are produced, which can cause fission in additional U^{235} or Pu^{239} atoms. This multiplication process, triggered by neutrons, gives rise to the chain reaction which makes nuclear explosions possible.

Neutron capture – A basic interaction of neutrons with matter. Neutron capture can result in the generation of gamma rays and/or charged particles.

Neutron fluence – The number of neutrons entering an imaginary sphere of unit cross-sectional area. It is equal to the time integrated neutron flux. It is generally expressed as n/cm^2. If expressed as Nvt, N is the neutron density (n/cm^3) in the beam v is the average speed (cm/sec), and t is the time duration. The spectrum should be specified with the fluence, e.g., n/cm^2 (fission spectrum).

Neutron flux – The flow of neutrons into an imaginary sphere of unit cross-sectional area. It is generally expressed as $n/cm^2/sec$. If expressed as Nv, N is the neutron density in the beam (n/cm^3), and v is the average speed (cm/sec). The spectrum should be specified with the flux, e.g., $n/cm^2/sec$ (fission spectrum).

Neutrons, fast – Neutrons with energies exceeding 10 keV, although sometimes different energy limits are given. See *Fast neutrons.*

Neutrons, thermal – Neutrons in thermal equilibrium with their surroundings. At room temperature their mean energy is about 0.025 electron volts (eV).

Nonlinear zone – A wedge-shaped zone in water, which increases in depth as the range from the burst point increases, and within which anomalous reflections affect the underwater pressure history.

[redacted]

[redacted]

[redacted]

N type – This term refers to semiconductor material which has had certain impurities added so that there are excess electrons available for conduction.

Nuclear radiation – Any or all of the radiations emitted as a result of the radioactive decay of a nucleus. The radiations include gamma radiation (of electromagnetic character) and particle radiation (alpha particles, positive and negative beta particles, and neutrons).

Nuclear Weapon – Means the same as "Atomic Weapon" as that term is defined in Section 11d, Public Law 703, 83rd Congress, viz: any device utilizing atomic energy, exclusive of the means for transporting or propelling the device (where such means is a separable and divisible part of the device), the principal purpose of which is for use as, or for development of, a weapon, weapon prototype, or a weapon test device.

Nuclide – A general term referring to all nuclear species, both stable and unstable, of the chemical elements as distinguished from the two or more nuclear species of a single chemical element, which are called isotopes.

Overpressure – The transient pressure, usually expressed in pounds per square inch, exceeding existing atmospheric pressure manifested in the blast wave from the explosion. During some period of the passage of the wave past a point, the overpressure is negative.

Overpressure impulse – See *Impulse.*

Pair production – A basic interaction of photons with matter (see Figure 6-1c).

Passive elements – Mainly filter devices and circuits which remove portions of the energy spectrum not needed by system operation.

Performance decrement (personnel) – Reduction of efficiency in performance of a required task, such as increased reaction time, increased performance time, and/or increased error rate.

Period of vibration (period) – The time for one complete cycle of oscillation or vibration.

Permanent complete incapacitation (personnel) – The inability to perform any task as the result of a physical or mental disability that will not improve subsequently.

Permanent effects – Changes in material properties that persist for a time long compared with the normal response time of the system of which the material is a part.

Photocurrent – A flow of excess charge carriers generated in a material or device by ionizing radiation.

Photoelectric effect – The process whereby a gamma ray or X-ray photo, with energy somewhat greater than that of the binding energy of an electron in an atom, transfers all of its energy to the electron, which is removed from the atom.

PIN junction – This type of diode has intrinsic (undoped) semiconductor material between the P and N-doped materials. See *N type* and *P type.*

Planar diffused – A technique for manufacturing semiconductor devices by introducing dopant elements into the semiconductor wafers by selective diffusion from the surface. All junction-surface intersections are protected from the ambient atmosphere by a passivation layer, typically silicon oxide, grown on the device structure.

[redacted]

[redacted]

[redacted]

Planckian radiation – The energy distribution of the radiation emitted by a black body radiator. The spectrum is determined by the temperature and is given by Planck's radiation law (see paragraph 4-2, Chapter 4). See *Black body*.

Plastic deformation – That deformation from which a deformed object does not recover upon removal of the deforming forces.

PNP – A three-layer semiconductor structure that constitutes a bipolar transistor. See *N type* and *P type*.

Popcorning – The ejection of dust particles from certain types of surface upon absorption of the thermal radiation emitted by a nuclear detonation.

Potting – The complete immersion of encapsulation of devices or circuitry in an insulating compound. Potting typically is used in TREE work to reduce the effects of leakage currents caused by radiation induced air ionization.

Positive phase – That portion of the blast wave in which pressures are above ambient atmospheric pressure.

Precursor -- A pressure wave which precedes the main blast wave of a nuclear explosion.

Primary photocurrent (I_{pp}) – Current which flows across a semiconductor junction as a result of ionization.

Prompt conductivity – Conductivity resulting from exposure to prompt gamma radiation.

Prompt gamma rays – Gamma rays produced in fission and fusion reactions and as a result of nuclear excitation of the weapon materials.

Prompt neutrons – Neutrons generated by the fission and fusion reactions of a nuclear weapon burst.

Proton – A positively charged particle with a mass approximately the same as that of a neutron. In nature, protons are bound in the nuclei of atoms.

P type – Semiconductor material which has had certain impurities added so that there is an excess of holes available for conduction.

Punch through – Breakdown mechanism in transistors caused by an arc discharge at the junction.

Rad – A unit of absorbed dose of radiation; it represents the absorption of 100 ergs of nuclear (or ionizing) radiation per gram of the absorbing material or tissue. When specifying dose, the absorbing material must be indicated, e.g., C, Si, tissue.

Radiant energy – See *Thermal radiation.*

Radiant exposure – The incident radiant energy per unit area, generally expressed in cal/cm^2.

Radiant power – Time rate of radiant energy emission. The useful units of radiant power are kt/sec or cal/sec.

Radiation dose – The total amount of radiation absorbed by material or tissue, commonly expressed in rads. In the case of materials, the radiation dose may be expressed in cal/gm (material) or ergs/gm (material).

[redacted]

[redacted]

[redacted]

Radiation dose rate – The time rate of absorbing radiation, commonly expressed in rads/sec or rads/hr. In the case of materials the radiation dose rate may be expressed in cal/gm/sec (material) or ergs/gm/sec (material).

Radioactivity – The property of certain nuclides of undergoing a spontaneous nuclear transformation in which the nucleus emits particles and/or gamma rays, or undergoes spontaneous fission, or in which the atom emits X-rays or Auger electrons following orbital electron capture or internal conversion. As a result of the emission of particles, the radioactive isotope is converted (or decays) into the isotope of a different (daughter) element which may or may not also be radioactive. Ultimately, as a result of one or more stages of radioactive decay, a stable (non-radioactive) end product is formed.

Rarefaction wave – When a shock wave in a medium strikes the interface between this medium and a less dense medium, part of the energy of the shock wave induces a shock wave in the less dense medium. The remainder of the energy forms a rarefaction or tensile wave which travels back through the denser medium.

Reaction rate – In chemical kinetics, the time derivative of the concentration of a given species is called the reaction rate of that species; it is also called the velocity or speed of the reaction.

Recombination – A process by which a hole-electron pair is annihilated, usually by direct combination of a free electron with a free hole, by capture of a free electron by an excited center containing a hole, or by capture of a free hole by an excited center containing an electron. Recombination transistions of these types may be radiative.

Recombination center – In some electron-hole recombinations the electron (hole) in the conduction band does not make a direct transition to the valence band but first occupies an intermediate state in the forbidden gap called a recombination center, which is associated with lattice imperfections or chemical impurities.

Reflected pressure – The pressure along a surface at the instant a blast wave strikes the surface.

Reflected shock wave – When a shock wave traveling in a medium strikes the interface between this medium and a denser medium, part of the energy of the shock wave induces a shock wave in the denser medium and the remainder of the energy results in the formation of a reflected shock wave which travels back through the less dense medium.

Refraction – Bending of an electromagnetic wave path when it traverses a region whose propagation characteristics are a function of position.

Relative air density – The ratio of air density under a specified condition to the air density of the standard atmosphere at sea level (see Tables 2-1 and 2-2, Chapter 2).

Residual nuclear radiation – Nuclear radiation, chiefly beta particles and gamma rays, which persists for some time following a nuclear explosion. The radiation is emitted mainly by the fission products and other bomb residues in the fallout, and to some extent by earth and water constituents, and other materials, in which radioactivity has been induced by the capture of neutrons.

Response – The action of an object under the applied loading.

Retinal burn – A permanent eye injury caused when the retinal tissue of the eye is excessively heated by the focused image of the fireball.

[redacted]

[redacted]

Rise time – The time interval from blast wave arrival to the time of peak overpressure in the blast wave.

Roentgen – A unit of exposure to gamma rays or X-rays. It is defined precisely as the quantity of gamma ray or X-ray radiations such that the associated corpuscular emission per 0.001293 gram of air produces, in air, ions carrying one electrostatic unit quantity of electricity of either sign. It is approximately equivalent to a dose of 87.7 ergs/gm in air [0.877 rads (air)] and 97 ergs/gm in tissue [0.97 rads (tissue)]. For the purposes of this manual, an exposure of 1 roentgen is equivalent to a radiation dose of 1 rad (tissue).

Rupture zone – Zone extending from the earth media-rubble interface in which stresses created by the detonation cause fracture and crushing of the material. The rupture zone enhances the use of cratering for the demolition of certain hard targets and for quarrying operations.

Scattering – Change in direction of propagation of radiation caused by collision with particles.

Scavenging – That process by which fission products are removed from the radioactive cloud by becoming attached to earth, rain, or other particles.

Scintillation – Random fluctuations in the magnitude and direction of an electromagnetic wave as it traverses an inhomogeneous medium.

Secondary electron – An electron that is emitted as a result of bombardment of a material by high energy radiation.

Secondary EMP – Same as internal EMP.

Secondary photocurrent – The primary photocurrent in a transistor can be of sufficient magnitude to forward bias the base-emitter junction and hence cause "normal" current to flow. The collector current thus produced is called the secondary photocurrent.

Semiconductor devices – Devices that use material that has a conductivity between that of a good conductor and a good insulator. Transistors, diodes, and integrated circuits belong to this class of devices.

Semiconductor junction – Two adjacent semiconductor materials that differ in the polarities of their majority carriers.

Shake – A nonstandard unit of time used in nuclear physics, equal to 10^{-8} second.

Shielding – 1. Material of suitable thickness and physical characteristics used to protect personnel from radiation during the manufacture, handling and transportation of fissionable and radioactive materials.

2. Obstructions that protect personnel or materials from the effects of a nuclear explosion.

3. Electrically continuous housing for a facility, area, or component, used to attenuate impinging electric and magnetic fields both by absorption and reflection.

Shock front – The boundary at which the medium being traversed by a shock or blast wave undergoes abrupt changes in velocity, pressure, and temperature.

Shock strength – The ratio of the peak blast wave overpressure plus the ambient pressure to the ambient pressure.

[redacted]

[redacted]

[redacted]

Shock wave – The steep frontal compression or pressure discontinuity that advances through a medium rapidly as the consequence of a sudden application of pressure to the medium. Its form depends on the magnitude of the pressure and the displacement of the medium as the wave progresses. In soil the shock wave is commonly referred to as the ground shock; in water, the water shock; and in air, the air blast.

Slant range – The direct distance between an explosion and a point.

Simulation – To produce the effect of a nuclear burst on a particular material or device by means other than a full scale explosion.

Space charge – The electric charge carried by a cloud or stream of electrons or ions in a vacuum or a region of low gas pressure, when the charge is sufficient to produce local change in the potential distribution.

Spallation – The removal of fragments from the back surface of a material (see Figures 6-5 and 9-43, Chapters 6 and 9, respectively).

Spectral distribution – The distribution of energy by wave length over the electromagnetic spectrum.

Steady state – Constant with time.

Steady state primary photocurrent – The constant primary photocurrent that would be observed to flow across a semiconductor junction under continuous irradiation.

Subsurface burst – See *Burst types.*

Sure-kill level – A set of environmental conditions under which it is 100 percent certain that the system mission cannot be executed.

Sure-safe level – A set of environmental conditions under which it is 100 percent certain that the system mission can be completed.

Surface burst – See *Burst types.*

Synchrontron radiation – Electromagnetic radiation emitted by a high-energy electron moving in a magnetic field.

Tensile wave – See *Rarefaction wave.*

Thermal energy – See *Thermal radiation.*

Thermal pulse – The radiant power vs time pulse from a nuclear weapon. See *Radiant power.*

Thermal radiation – Electromagnetic radiation from a nuclear weapon, which is emitted in the wavelength range from 0.2 micron in the ultraviolet, through the visible, to 12 microns in the infrared. Also called *Thermal energy* and *Radiant energy*.

Thermonuclear – An adjective referring to the process involving the fusion of light nuclei such as those of deuterium and tritium.

TNT effects equivalence – The expressing of the effect of a particular phenomenon of a nuclear detonation in terms of the amount of TNT that would produce the same effect.

TNT energy equivalent – Total energy of a nuclear detonation expressed in terms of the amount of TNT required to produce an equivalent energy.

[redacted]

[redacted]

[redacted]

Transient effects – Changes in material properties that persist for a time shorter than, or comparable to, the normal response time of the system of which the material is a part.

Transient radiation – A pulse or burst of radiation whose pulse width at half-maximum intensity generally ranges from nanoseconds to a few milliseconds.

Transistor – A semiconductor device that uses a small current to control a much larger current.

Transition zone (region) – A zone extending above the earth's surface in which the weapon phenomenon of interest from a burst in the zone will be modified by the presence of the earth's surface. See *Burst types: Air burst.*

Transmissivity - See *Atmospheric transmissivity.*

Trapping – That process in which a free charge carrier is captured, and once captured, has a greater probability of being reexcited to a free state than of recombining with a carrier of the opposite polarity.

Trapping center – A site in a solid at which a free electron or hole may be captured, and in which the charge carrier, once captured, has a greater probability of being thermally reexcited to a free state than of recombining with a carrier of the opposite sign. See *Trapping.*

TREE – Transient-radiation effects on electronics.

TREES – Transient-radiation effects on electronic systems.

Triple point – The intersection of the incident, reflected and fused shock fronts produced by an explosion in the air. Because of the variation of the angle of incidence as the blast wave expands, and because the reflected wave, in a heated, denser medium, travels faster than the incident wave, the height of the triple point increases with the distance from the explosion. See *Mach stem.*

True crater – The crater excluding fallback material. See *Crater.*

Ultraviolet – That portion of the electromagnetic spectrum occurring between the wavelengths 0.2 and 0.4 micron.

Underground burst – See *Burst types.*

Underwater burst – See *Burst types.*

Upthrust – Deformation material pushed up around a crater, but not dissociated from the earth media by a nuclear blast.

Vacancy – An empty lattice site in a crystalline material.

Visible – That portion of the electromagnetic spectrum occurring between 0.4 and 0.7 micron. The term luminous also is applied to radiation in this region.

Visibility – The horizontal distance at which a large, dark object can just be seen in daylight near the horizon.

Wave length – The distance between two similar and successive points on an alternating wave, as between maxima.

Wave train – A series of alternating crests and troughs of a wave system resulting from a surface disturbance.

[redacted]

[redacted]

[redacted]

Weapon debris – The residue of a nuclear weapon after it has exploded; that is, the materials used for the casing and other components of the weapon, plus unexpended plutonium or uranium, together with fission products.

Wilson cloud – See *Condensation cloud.*

Wind shear – A relatively abrupt change with altitude of wind direction or magnitude.

X-rays – High frequency electromagnetic radiation produced by any of three processes: radiation from a heated mass (e.g., a black body); deceleration of a charged particle; electron transitions between atomic energy levels, usually excited by incident beams of high-energy particles, resulting in characteristic, discrete energy levels.

Yield – The energy released in a nuclear explosion, usually measured by the estimated equivalent amount of TNT required to produce the same energy release. See *TNT energy equivalence.*

[redacted]

[redacted]

APPENDIX F

LIST OF SYMBOLS [redacted]

[redacted] This manual covers a wide variety of subject matter. Consequently, it has been necessary to use a large number of symbols to represent quantities of interest. In many cases, one symbol has different meanings in different parts of the manual. This was done for two reasons:

- the large quantity of symbols;
- the desire to use accepted symbols for specific quantities; e.g., the symbol σ is used for the Stefan-Boltzmann constant, conductivity, stress, radiation interaction cross section, and for the standard deviation in probability equations, for each of which σ is the usual symbol.

If a symbol has one meaning throughout the manual, that meaning is shown without indication of location. If a symbol has one meaning in several chapters and other meanings in isolated cases, the most frequent meaning is listed without indication of location, and other meanings are listed as exceptions, with the location of the exceptions being indicated by chapter and, in some cases by section of a chapter. When a symbol has different meanings in several isolated locations, each location is indicated by chapter.

[redacted] Except where specifically indicated in the text, the subscript 1 is reserved for burst parameters (overpressure, height of burst, distance, etc.) for a 1 kiloton explosion, and the subscript 0 is reserved for standard sea level atmospheric properties (pressure, temperature, density, etc.). Symbols with these subscripts having these meanings are not listed separately below. Exceptions are listed.

[redacted] One further convention should be noted. Many logarithmic and semi-logarithmic graphs are used in the manual. In most cases, either a full logarithmic grid is shown or tick marks are provided for each digit within a decade. In a few cases, unmarked tick marks are not shown for all digits (e.g., Figure 8-7). In all such cases, the tick marks are shown for the digits 2, 4, 6, and 8 (times the indicated power of ten for that decade).

Symbol	*Designation*
A	Area of fission debris from a high altitude explosion (Chapter 8; Chapter 17).
A	Area of an object exposed to the air blast wave of a nuclear explosion (Section II, Chapter 9; Chapter 14; Appendix A).
A	Thermal absorption coefficient (Section III, Chapter 9).
A	Area of transistor PN junction (Section VII, Chapter 9).
A_1	Cross-sectional steel area per inch of width of a deeply buried horizontal steel arch (Chapter 11).

[redacted]

[redacted]

Symbol	*Designation*
A	Reference area for determination of a missile ballistic coefficient (Chapter 16).
A_e	Effective thermal absorption coefficient (Section IV, Chapter 9).
A_{dw}	Energy absorbed in a material as the result of X-ray interactions (Section V, Chapter 9).
A_{fb}	Absorption of electromagnetic signals propagating through a fireball (Chapter 8).
A'_{fb}	Absorption of a 1,000 MHz signal propagating through a fireball (Chapter 8).
A_{max}	Maximum radius of the bubble created by an underwater explosion (See A_n, A_1, A_2, A_3) (Chapter 2).
A_n	Maximum radius of a migrating and pulsating underwater bubble during its nth period.
A_p	One-way absorption due to ionization from prompt nuclear radiation of an electromagnetic signal propagating on an oblique path outside of the fireball (Chapter 8).
A'_p	One-way absorption due to ionization from prompt nuclear radiation of an electromagnetic signal propagating on a vertical path outside of the fireball (Chapter 8).
A_1	Radius of the bubble from an underwater nuclear explosion at the first maximum expansion (equal to A_{max}).
A_2	Radius of the bubble from an underwater nuclear explosion at the second maximum expansion.
A_3	Radius of the bubble from an underwater nuclear explosion at the third maximum expansion.
A_β	One-way absorption of an electromagnetic signal propagating on an oblique path outside of the fireball caused by beta particles and their ionization.
A'_β	One-way absorption of an electromagnetic signal propagating on a vertical path outside of the fireball caused by beta particles and their ionization.
A_γ	One-way absorption of an electromagnetic signal propagating on an oblique path outside of the fireball caused by ionization from delayed gamma rays.
A'_γ	One-way absorption of an electromagnetic signal propagating on a vertical path outside of the fireball caused by ionization from delayed gamma rays.
Ag	Maximum acceleration of ground particles from a near surface (air) burst, surface burst, or subsurface burst.

[redacted]

Symbol	*Designation*
AR	Aspect ratio* of aircraft wing or horizontal tail or of an isolated vertical tail.
AR_B	Aspect ratio of the vertical tail of an aircraft in the presence of the fuselage.
AR_{eff}	Effective aspects ratio of the vertical tail of an aircraft.
AR_{HB}	Aspect ratio of the vertical tail of an aircraft in the presence of both the horizontal tail and the fuselage.
B	Brightness of an object relative to its background. May be positive if the object is lighter than the background, or negative if the object is darker than the background (Chapter 3).
B	Buildup factor. The increase in flux (or fluence) at a point relative to that that would be present without scattered photons or particles (Chapter 4).
B	Parameter that describes the overpressure contribution to the total impluse delivered by the air blast wave to an object (Chapter 14).
B'	Brightness of the background surrounding an object (Chapter 3). (See paragraph 3-7 for the relationship between B and B' as used in Chapter 3 to define "contrast.")
B_φ	Azimuthal magnetic field of the electromagnetic pulse (EMP).
BH_i	Burst height parameters for the calculation of overpressure effects on aircraft in-flight or parked (Chapter 13).
C	Contrast between brightness of an object and its background (Chapter 3).
C	Parameter that describes the dynamic pressure contribution to total impulse (Chapter 14).
C	Point of intersection of a missile with the shock front (Chapter 16).
C_d	Drag coefficient, which relates the force on an object to the incident dynamic pressure or atmospheric pressure in the case of a missile.
C_{db}	Drag coefficient for the back side of an object, i.e., the side away from the explosion.
C_{df}	Drag coefficient for the front side of an object, i.e., the side facing the explosion.
$C_{L\alpha}$	Aerodynamic coefficient for aircraft wings and/or horizontal tails.

*Aspect ratio of an isolated aircraft component (wing, horizontal tail, or vertical tail) is the ratio of the square of the span (tip to center of fuselage) of the component to the area of the component.

[redacted]

Symbol	*Designation*
$\overline{C}_{L\alpha}$	Lift coefficient for a vertical tail on an aircraft.
$C_{L\alpha}^{MR}$	Lift curve slope for the main rotor of a helicopter.
$C_{L\alpha}^{W}$	Lift coefficient for a helicopter wing.
C_M	Correction factor for material properties of deeply buried horizontal reinforced concrete arches (Chapter 11).
$C_{N\alpha}$	Normal force coefficient (missiles or aircraft).
C_p	Specific heat at constant pressure.
C_{tp}	Correction factor to obtain an equivalent triangular waveform for overpressure (Chapter 2).
C_{tq}	Correction factor to obtain an equivalent triangular waveform for dynamic pressure (Chapter 2).
C_V	Specific heat at constant volume.
C_α^p	Aspect ratio correction factor for the strength of two-way slabs (Chapter 11).
C_γ	Correction factor to obtain the gamma ray intensity parameter for high altitude weapon debris (Chapter 8).
C.G.	Center of gravity.
CI	Combat ineffectiveness.
D	Maximum displacement of a buried structure or piece of equipment that results from ground shock (Chapter 2).
D	Distance from an explosion or from high altitude debris to the point of interest along a path parallel to the surface of the earth (Chapter 8).
D_a	Depth of the apparent crater, which is the distance from the bottom of the visible portion of the crater to the original ground surface (see Figure 2-70).
$D_{a\ell}$	Height of the crest of a crater lip measured from the bottom of the visible portion of the crater (see Figure 2-70).
D_c	Thickness of roof or wall of a buried structure (Chapter 11).
D_d	Maximum offset of the debris from an explosion above 200 kilometers altitude, which is the distance between lines through the center of the burst and the center of the debris after it travels down the magnetic field lines and stabilizes each line being perpendicular to the surface of the earth (see Figure 8-18).

[redacted]

[redacted]

Symbol	*Designation*
D_{max}	Maximum radius of the water column formed by an underwater explosion.
D_N	The neutron dose from a nuclear explosion at some specified location on or near the surface of the earth.
D_s	Depth of the section of a structural member (see Figure 11-33).
$D_{\gamma f}$	That portion of the initial nuclear radiation dose received at a specified location on or near the surface of the earth that results from gamma rays that are produced by fission product decay.
$D_{\gamma s}$	That portion of the initial nuclear radiation dose received at a specified location on or near the surface of the earth that results from gamma rays that are produced by neutron interactions.
DF	Dynamic factor – a parameter used in the determination of incremental lift of aircraft by the air blast wave.
DOB	Depth of burst.
D-Region	See Glossary.
$\dot{D}$	Gamma radiation exposure rate (Section VI, Chapter 9).
$\dot{D}_t$	Residual gamma radiation dose rate at time *t* after the explosion (Chapter 5).
$\dot{D}_1$	Residual radiation dose rate one hour after an explosion.
$\dot{D}_{\gamma p}$	Peak gamma ray dose rate.
E	Young's modulus of elasticity (Chapter 2 and Chapter 11).
E	Water shock energy flux from an underwater explosion (Chapter 2).
E	Energy of a photon (Chapter 4).
E	Hydrodynamic enhancement factor, which is the factor by which the initial gamma dose is increased as a result of the reduced air density behind the shock front (Chapter 5).
E	Peak value of the electric field of the radiated electromagnetic pulse (EMP) (Chapter 7).
E	Internal energy per unit mass of material (Section V, Chapter 9; Appendix A).
E_c	Potential energy of a cavity created by an underwater explosion.
E_{itan}	Tangential component of an incident electromagnetic field.

[redacted]

[redacted]

Symbol	*Designation*
E_o	Explosive yield of an underwater charge (Section IV, Chapter 2).
E_o	X-ray yield of a weapon (Chapter 4).
E_r	Peak radial electric field of the electromagnetic pulse (EMP).
E_s	Heat of sublimation of a material (Section V, Chapter 9).
E_s	Energy density of air behind a shock front (Appendix A).
E_{so}	Heat of sublimation at absolute zero, i.e., the energy required to form the saturated vapor from the solid at a temperature of absolute zero.
E_θ	Peak transverse electric field of the electromagnetic pulse (EMP).
EMP	Electromagnetic Pulse. The time varying electromagnetic radiation resulting from a nuclear explosion.
$E(m)$	The specific energy deposited by X-rays corresponding to a depth for which the integrated mass is m.
E-Region	See Glossary.
$\bar{E}$	Restrained modulus of a medium transmitting a shock wave.
$\bar{E}_g$	Electric field of an electromagnetic pulse that is refracted into the ground.
$\bar{E}_i$	Incident electric field of the electromagnetic pulse (EMP).
F	Force (Appendix A).
F_N	Neutron dose function (yards^2 rads/kt) (Section I, Chapter 5).
$F_{..}$	Force exerted on an object by the winds accompanying a blast wave (Appendix A).
$F_{\gamma f}$	Fission product gamma ray dose function (rads/kt) (Section I, Chapter 5).
$F_{\gamma s}$	Secondary gamma ray dose function (yards^2 rads/kt) (Section I, Chapter 5).
FF	Fraction of total weapon debris that is deposited in one of three regions subsequent to a high altitude nuclear explosion (*FF*1, *FF*2, and *FF*3 are deposited in regions 1, 2, and 3 respectively, as defined in Chapter 8).
F-Region	See Glossary.
$F(t)$	Time dependent gain degradation of a transistor that is exposed to radiation (Section VII, Chapter 9).
$F(u)$	Density function of the normalized Planck distribution (Chapter IV).

[redacted]

[redacted]

Symbol	*Designation*
G	Grüneisen ratio of a material (Section V, Chapter 9).
G_A	One value on the intercept/load matrix of axial rigid body loads on missiles (Chapter 16).
G_I	Maximum load on a missile at blast wave intercept (Chapter 16).
G_N	One value on the intercept/load matrix of normal rigid body loads on missiles (Chapter 16).
G_T	One value on the intercept/load matrix of total rigid body loads on missiles (Chapter 16).
$G(u)$	Cumulative distribution function of the normalized Planck distribution (Chapter 4).
GW	Gross weight of an aircraft (Chapter 13).
GZ	Ground zero. That point on the surface of the earth that is directly below, directly above, or at the point of an explosion (**see SGZ, SZ**).
H	Height of the Mach stem (Section I, Chapter 2).
H	Depth to which the air-induced shock wave extends into the earth during the effective duration of the shock (Section III, Chapter 2).
H	Amplitude of the maximum of the first envelope, trough to crest, of a water wave generated by underwater explosions (Section IV, Chapter 2).
H	Time of an explosion, i.e., H + 1 hour indicates a time of one hour after an explosion (Chapter 5 and Chapter 14).
H	Heat of fusion (Chapter 13).
$H_{a\ell}$	Apparent height of a crater lip.
H_{av}	Average cover over a structure that is buried in soil (Chapter 11).
H_c	Depth of cover over the crown of a structure that is buried in soil (Chapter 11).
H_{max}	Limiting height of a water wave that can propagate over deep water in a stable manner (Michell limit).
H_R	Range dependent burst height adjustment factor for the fission product gamma ray component of the initial nuclear radiation dose.
H_W	Yield dependent burst height adjustment factor for the fission product gamma ray component of the initial nuclear radiation dose.

[redacted]

[redacted]

Symbol	*Designation*
H_1	Detonation height correction factor for the neutron and secondary gamma ray components of the initial nuclear radiation dose (Chapter 5).
H.E.	High explosive.
HOB	Height of burst.
$\overline{H}$	Magnetic field of the electromagnetic pulse (EMP).
$\overline{H}_i$	Incident magnetic field of the electromagnetic pulse (EMP).
$\overline{H}_r$	Reflected magnetic field of the electromagnetic pulse (EMP).
$\overline{HR}_i$	Horizontal range parameters for the determination of the vulnerability of aircraft to overpressure (i = 1, 2, 3).
I	Either overpressure or dynamic pressure impulse.
I	Current produced in a conductor as a result of coupling of energy from the electromagnetic pulse (EMP) (Section VIII, Chapter 9).
I_B	Air blast impulse on the back face of an object.
I_F	Air blast impulse on the front face of an object.
I_i	Impulse corresponding to categories of lethal loading to reentry vehicles (i = 4, 5, 6) (Chapter 16).
I_I	Impulse from the blast intercept loading of a reentry vehicle (Chapter 16).
I_N	Net overpressure impulse on an object.
I_p	Positive phase overpressure impulse.
I_{PP}	Primary photocurrent induced in a PN junction of a transistor by transient radiation.
I_q	Dynamic pressure impulse.
I_T	Total impulse.
I_γ	Fission debris radiation intensity parameter for determination of electromagnetic signal attenuation caused by gamma rays outside of the fireball.
I'_γ	Parameter used to determine I_γ ($I_\gamma = C_\gamma I'_\gamma$, where C_γ is the debris height correction factor) (Chapter 8).
$I'_{\gamma i}$	Same as I'_γ when there are more than one debris region (i = 1, 2, 3 for bursts above 120 kilometers) (Chapter 8).

[redacted]

[redacted]

Symbol	*Designation*
J	One-half of the plastic moment arm of a structural member.
J'	Empirical constant that relates the bubble radius of an underwater explosion at its first maximum to the weapon yield and the hydrostatic head. J' is generally taken to be 1,500 when the yield is in kilotons, and the hydrostatic head and the bubble radius are in feet.
$\bar{J}$	Electric current density.
K	Water depth and yield dependent parameter that relates the shock wave duration of an underwater explosion to the shock wave impulse and the peak shock pressure (Section IV, Chapter 2).
K	Semiconductor lifetime damage constant (Chapter 6; Section VII, Chapter 9).
K	The bulk modulus (modulus of volume elasticity) (Section V, Chapter 9).
K	Parameter used in analysis of structural damage to belowground structures (see Table 11-10) (Section II, Chapter 11).
K_g	Energy-dependent free-charge-carrier-generation constant for semiconductors (Section VII, Chapter 9).
K_H	Factor that accounts for the relative size of horizontal tails in the vulnerability analysis of aircraft (Chapter 13).
K_o	Ratio of horizontal to vertical soil pressures (Section II, Chapter 11).
$K.E.$	Kinetic energy.
$K(t)$	Semiconductor time dependent damage constant after a fast burst of nuclear radiation (Section VII, Chapter 9).
$K(\infty)$	Steady-state value of a semiconductor damage constant (Section VII, Chapter 9).
L	Length of a row crater formed by simultaneous or near simultaneous explosions (Section II, Chapter 2).
L	Length of the peak wave formed by an underwater explosion (Section IV, Chapter 2).
L	Thickness of a layer of material exposed to thermal radiation (Section III, Chapter 9).
L	Diffusion length for minority carriers on the side of a transistor junction with the longer diffusion length (Section VII, Chapter 9).

[redacted]

[redacted]

Symbol	*Designation*
L	Span length of a buried structure (Section II, Chapter 11).
L	Preblast value of lift of an aircraft in flight (Chapter 13).
L_{down}	Length of a tube fireball measured from the burst point down the magnetic field lines (see Figure 8-16, Chapter 8).
L_n	Diffusion length in the N region of a transistor (Section VII, Chapter 9).
L_p	Diffusion length in the P region of a transistor (Section VII, Chapter 9).
L_{up}	Length of a tube fireball measured from the burst point up the magnetic field lines (see Figure 8-16, Chapter 8).
LD	Lead distance. The distance, parallel to the line of flight of a reentry vehicle (RV), between the RV and a line perpendicular to the line of flight through the burst center (see Figure 16-23, Chapter 16).
LOE	Locus of escape. The surface of a volume around a burst outside of which a reentry vehicle will not intercept the blast wave (see Figures 16-37 and 16-38, Chapter 16).
LR	Lethal ratio. A parameter dependent on yield and aircraft class that is used in determination of the vulnerability of airplanes in flight to the gust effects of the air blast wave.
L'	A parameter that determines L_{down} for bursts between 85 and 120 kilometers under certain circumstances (see Problem 8-2, Chapter 8).
L'_a	A parameter used in the determination of the absorption of electromagnetic signals propagating through a fireball at altitudes below 60 kilometers and times greater than 300 seconds after burst (Chapter 8).
M	Mass of a neutron (Chapter 5).
M	Mach number. The ratio of the velocity of an object to the ambient speed of sound (Chapters 13 and 16).
M	The dynamic constrained modulus of deformation of a medium sustaining a stress (Chapter 11).
M_p	Total capacity of a structural member under pure bending (Chapter 11).
N	Total number of photons emitted by a source per unit time (Chapter 4).
N	Generic symbol for aircraft load factor. Used for critical load factor for failure in determining intercept time sure-safe and sure-kill envelopes and the maneuver normal load factor in determining burst-time gust effect envelopes (Chapter 13).

[redacted]

[redacted]

Symbol	*Designation*
N^+	Up-loading aircraft limit load factor (Chapter 13).
N^-	Down-loading aircraft limit load factor (Chapter 13).
N_e	Density of free electrons at a point of interest.
N_o	Total number of neutrons emitted by a source (e.g., total number of neutrons emitted during a nuclear explosion).
N_{oi}	Total number of neutrons of energy i emitted by a source.
N_β	Beta radiation intensity parameter used in determining the ion-pair production rate and electron density caused by fission product beta particles.
$N_{\beta i}$	Same as N_β; used when there are more than one debris region (i = 1, 2, 3).
N-type	See Glossary.
OD	Offset distance. The distance measured perpendicular to the line of flight of a reentry vehicle (RV) between the RV and a line parallel to the line of flight that passes through the burst center (see Figure 16-23, Chapter 16).
P	Ambient air pressure at the altitude of interest, except as noted below.
P	Radiant power (Chapter 3).
P	Pressure induced in a material by internally deposited energy (Section V, Chapter 9).
P	A parameter used in vulnerability evaluation or design of shallow buried arches (Section II, Chapter 11).
P_b	Local pressure at some desired point on a hypersonic reentry vehicle (Chapter 16).
P_f	Free stream ambient pressure around a hypersonic reentry vehicle (Chapter 16).
P_f	Probability of failure of a system or structure (Appendix C).
P_{fn}	Probability of failure of a component of a system (Appendix C).
P_{GAS}	Local pressure within a fireball (Chapter 16).
P_{max}	Radiant power at the time of the final maximum of the thermal pulse.
P_{min}	Radiant power at the time of the principal minimum of the thermal pulse.

[redacted]

[redacted]

Symbol	*Designation*
P_o	Asymptote corresponding to the value of static pressure loading necessary to produce a specified damage level to a reentry vehicle (Chapter 16; otherwise P_o represents ambient sea level atmospheric pressure – see introductory paragraphs to this appendix).
P_s	Absolute pressure behind the shock front in air (Appendix A).
P_s	Probability of survival of a system (Appendix C).
P_u	Total capacity of a buried structure under pure thrust (Section II, Chapter 11).
P_{WALL}	Wall pressure induced by mass removal blowoff during transit of a reentry vehicle through a fireball (Chapter 16).
P_y	Uniform static pressure necessary to cause material yielding in a shell wall (Chapter 16).
$Pe(\theta)$	Probability of exposure of a point on a forest floor by a point source of thermal radiation (Chapter 15).
Pr	Prandtl number. A dimensionless quantity which is equal to the specific heat at constant pressure times the viscosity divided by the thermal conductivity. Its significance is momentum diffusivity (thermal diffusivity) (Section IV, Chapter 9).
P-type	See Glossary.
Q	Radiant exposure, i.e., thermal energy incident per unit area (generally expressed as cal/cm^2).
Q_a	Thermal energy absorbed per unit area.
Q_c	Critical heat; thermal energy per unit area required to produce a specified effect.
Q_o	Radiant exposure required to ignite dry fuels.
Q_r	Radiative heat loss from a material.
Q_{ascent}	Heat load on a reentry vehicle during ascent.
Q_{cone}	Total heat load on the cone of a reentry vehicle.
$Q_{radiation}$	Thermal radiation heating of a reentry vehicle from a nuclear burst.
$Q_{reentry}$	Normal heating of a reentry vehicle during reentry.
R	Slant range, except as noted below (generally measured from the burst to the point of interest).

[redacted]

[redacted]

Symbol	*Designation*
R	Reentry vehicle nose radius (Chapter 16).
R	Universal gas constant (Appendix A).
R_a	Radius of the apparent crater (Chapter 2).
R_a	Critical range that determines the sure-safe or sure-kill distance from a burst above an aircraft (Chapter 13).
$R_{a\ell}$	Radius of the apparent crater lip crest.
R_{av}	Radius of a volume, centered on an aircraft, that determines the sure-safe or sure-kill locations of bursts for thermal radiation damage (Chapter 13).
R_b	Critical range that determines the sure-safe or sure-kill distance from a burst below an aircraft (Chapter 13).
R_d	Radius of the debris region from air bursts.
R_e	Radius of the outer boundary of the continuous ejecta from a crater (Chapter 2).
R_{eq}	Magnetic equilibrium radius of the fireball for high altitude bursts (Chapter 8).
R_f	Radius of the visible fireball (Chapter 3).
R_{fb}	Fireball radius for communications interference calculations (Chapter 8).
R_{inner}	Inner radius of the debris once it becomes a toroid (Chapter 8).
R_m	Maximum range of missiles thrown from a crater of a surface or near-surface burst (Chapter 2).
R_{min}	Radius of the fireball at the time of the principal minimum of thermal radiation.
R_{MR}	Radius of the main rotor blade of a helicopter (Chapter 13).
R_o	Initial fireball radius (Chapter 8).
R_s	Radius of the base surge from a water surface or subsurface burst (Chapter 2).
R_s	Critical range that determines the sure-safe or sure-kill distance from a burst at the side of an aircraft (Chapter 13).
R_{tube}	Radius of the fireball tube, measured perpendicular to the magnetic field lines, from a high altitude burst once the fireball (debris) is aligned with the geomagnetic field.
RB	Radius from the burst center to a reentry vehicle at the time of intercept of the vehicle by the blast wave (Chapter 16).

[redacted]

[redacted]

Symbol	*Designation*
RD	Slant range from a burst to a reentry vehicle at the time of the explosion (Chapter 16).
Re	Reynolds number. A dimensionless quantity equal to the inertia force of an object divided by the viscous force on the object.
RS	Scaled radius from the burst center to a reentry vehicle at the time of intercept of the vehicle by the blast wave (RB scaled to 1 kt).
S	Clearing distance; the shortest distance from the stagnation point of a blast wave interacting with a structure to a clear edge on the structure (Chapter 11).
S	Area of the wing or horizontal tail of an aircraft including the extensions of the leading and trailing edges to the aircraft centerline (Chapter 13).
S_d	Altitude scaling factor used to scale distance for various blast parameters to different ambient air pressures.
S_p	Altitude scaling factor used to scale overpressure or dynamic pressure to different ambient air pressures.
S_t	Altitude scaling factor used to scale the time of arrival of the air blast wave to different ambient air pressures.
S_w	Total area of the wings of a helicopter (if there are wings). Measured by the extension of the leading and trailing edges of both wings to the aircraft centerline.
*S**	The shear modulus of a material (Section V, Chapter 9).
SGZ	Surface ground zero. Used mainly in measuring crater dimensions from surface or near surface bursts. That point on the earth which is directly below, directly above or at the point of the explosion (see *GZ, SZ*).
SH	Semi-height of a pancake shaped fireball. This is the shape that the fireball formed by bursts below 85 kilometers ultimately assumes (Chapter 8).
SZ	Surface zero. Used mainly for water surface or subsurface bursts. That point on the earth that is directly below, directly above, or at the point of the explosion (see *GZ, SGZ*).
T	Transmittance factor. That fraction of thermal energy emitted from a nuclear explosion that reaches a target (Chapter 3).
T	Absolute temperature (Section I, Chapter 2, Chapter 4, Appendix A).
T	Period of vibration of a structure (Chapter 11).

[redacted]

[redacted]

Symbol	*Designation*
T	Duration of a shock wave in water (Section IV, Chapter 2).
T_c	Critical temperature of aircraft skin panels. For sure-safe conditions, it is the temperature at which the modulus of elasticity of the thinnest structural skin on the fuselage is reduced by 20 percent. For sure-kill conditions, it is the temperature at which the thickest structural skin on the fuselage will melt.
T_d	Transmission coefficient for the direct flux of thermal energy.
T_e	Effective radiating temperature (Chapter 4).
T_e	Equilibrium temperature of the skin of an aircraft prior to exposure to thermal radiation (Chapter 13).
T_m	Melting temperature of a material of interest (Section IV, Chapter 9).
T_o	Absolute temperature of the air surrounding an object of interest that is exposed to thermal radiation (Section IV, Chapter 9). (Otherwise, T_o refers to ambient air temperature at sea level – see introductory remarks to this appendix).
T_r	Strain or velocity rise time for direct-transmitted ground shock from a buried explosion.
T_s	Surface temperature of the radiating volume of a nuclear explosion.
T_w	Absolute temperature at the outer surface of the ablator of a reentry vehicle (Chapter 16).
U	Velocity of propagation of the shock front.
V	Maximum value of ground motion velocity (Chapter 2).
V	Visual range (Chapter 3).
V	Velocity of an aircraft or missile (Chapters 9, 13, and 16).
V	Specific volume of undisturbed air (Appendix A).
V_a	Volume of the apparent crater produced by a nuclear explosion.
V_o	Initial spray velocity from an underwater explosion.
V_E	Reentry velocity (Chapter 16).
W	Weapon yield, except as noted below (generally in kilotons, but, where specified, may be in megatons).
W	Reentry vehicle mass (Chapter 16).

[redacted]

[redacted]

Symbol	*Designation*
W'_{coll}	Work performed by the air blast overpressure to produce kinetic energy in the air.
W'_{comp}	Work done by the ambient pressure in compressing the air during passage of a blast wave.
W'_{eff}	Effective blast yield (Chapter 2).
W'_{eff}	Effective thermal yield (Chapter 3).
W'_{F}	That portion of the weapon yield that is derived from fission.
W''_{F}	Debris region fission yield (Chapter 8).
W'_{HE}	Weight of a high explosive charge (given in equivalent pounds of TNT).
W_{T}	Thermal energy radiated by a nuclear explosion.
W'_{total}	Total work done on a unit mass of air as it is engulfed by the blast wave.
W'_{x}	The X-ray yield of a weapon.
W_{γ}	The gamma-ray yield of a weapon.
X	Fraction of the debris from an explosion above 120 kilometers that goes to debris region 3 (the conjugate region) (Chapter 8).
X	Arching factor for a roof of a buried structure (Chapter 11).
X	Length, measured along the center line, from the nose tip to a point on a reentry vehicle body (Chapter 16).
X_{d}	Closest point of approach of a communication system ray path to the center of the debris region. Used in calculation of absorption by the region of space that is ionized by gamma rays emitted by the debris.
X_{o}	Distance (measured head-on or tail-on) between a reentry vehicle and a nuclear burst at the time of the explosion (Chapter 16).
Y_{o}	Yield strength of a material (compressive yield strength if that is different from its yield strength in simple tension) (Section V, Chapter 9).
Z	Hydrostatic head for an underwater burst (taken to be equal to the depth of burst plus 33 feet) (Chapter 2).
Z	Atomic number of an element (Chapter 4, Section V, Chapter 9).
a	Incremental path absorption of an electromagnetic signal (absorption per unit distance traveled) (Chapter 8).

[redacted]

[redacted]

Symbol	*Designation*
a	Acceleration of a buried structure resulting from ground shock (Chapter 11).
a_r	Peak acceleration in the radial direction from direct transmitted ground shock (Section III, Chapter 2).
a_s	Maximum acceleration of the ground at the surface resulting from air-induced ground shock.
a_n	Peak horizontal component of acceleration at a point below the earth's surface resulting from ground shock (Section III, Chapter 2).
a_y	Peak vertical component of acceleration at a point below the earth's surface resulting from ground shock (Section III, Chapter 2).
b	Thickness of a metal plate exposed to thermal radiation and air blast (Section IV, Chapter 9).
b	Span, tip to tip, of the wing or horizontal tail of an aircraft (Chapter 13).
b	Median of a lognormal variable (Appendix C).
b_L	Clear span of the long side of a rectangular buried structure (Section II, Chapter 11).
b_s	Clear span of the short side of a rectangular buried structure (Section II, Chapter 11).
c	Ambient speed of sound in air (Chapter 2, Chapter 13, Appendix A).
c	Velocity of light (Chapter 4).
	Seismic velocity of structural material (Chapter 11).
c_E	Elastic velocity of a shock wave traveling through a material (Section V, Chapter 9).
c_m	Seismic velocity of a particular structural type (Chapter 11).
c_{MR}	Helicopter main rotor blade chord length (Chapter 13).
c_o	Bulk sound speed in a material (Section V, Chapter 9, otherwise ambient speed of sound in air at sea level).
c_p	Local pressure coefficient for aerodynamic loading on hypersonic reentry vehicles (Chapter 16).
c_p	Seismic velocity of a medium in which a structure is buried (Chapter 11).

[redacted]

[redacted]

Symbol	*Designation*
c_r	Wing/horizontal tail root chord, i.e., the length along the fuselage centerline subtended by extensions of the leading and trailing edges (Chapter 13).
c_t	Wing/horizontal tail tip chord, i.e., the length along the fuselage centerline subtended by the wing/horizontal tail tip (Chapter 13).
d	Horizontal distance from ground zero, or surface zero for underwater bursts, except as noted below.
d	Distance at which the case shock arrives at the hydrodynamic shock front, which marks the beginning of a scalable shock wave (Section I, Chapter 2).
d	Horizontal distance between two points at different altitudes (Chapter 4).
d	Displacement of a buried structure by ground shock (Chapter 11).
d	Fuselage depth at the intersection of the leading edge of the vertical tail with the fuselage (Chapter 13).
d_{ac}	Depth of the apparent crater from an underwater burst (Section IV, Chapter 2).
d_b	Depth of burst.
d_r	Maximum radial displacement of the earth caused by ground shock (Chapter 2).
d_r	Damage reduction distance; the amount by which the horizontal distance from ground zero at which a specified level of damage to a surface target is less for a subsurface burst than for a surface burst (Chapter 11).
d_s	Differential displacement of the earth at the surface caused by ground shock (Chapter 2).
d_{se}	Differential transient elastic displacement of the earth at the surface caused by ground shock (Chapter 2).
d_{sp}	Permanent displacement of the earth at the surface caused by ground shock (Chapter 2).
d_w	Depth of the water where an underwater explosion occurs.
d_x	Horizontal displacement of the earth at a point below the surface caused by ground shock (Chapter 2).
d_y	Vertical displacement of the earth at a depth "y" caused by ground shock (Chapter 2).
d_{ye}	Differential elastic transient vertical displacement of the earth at a depth "y" caused by ground shock (Chapter 2).

[redacted]

[redacted]

Symbol	*Designation*
d_{yp}	Permanent vertical displacement of the earth at a depth "y" caused by ground shock (Chapter 2).
d_2	Depth of the bubble from an underwater burst at the second maximum radius (Chapter 2).
d_3	Depth of the bubble from an underwater burst at the third maximum radius (Chapter 2).
e_c	Compton electron (Chapter 7).
e_o	Hydrodynamic yield. Used primarily for underwater high explosive bursts (Chapter 2).
f	Natural frequency of an oscillator (Section III, Chapter 2).
f	Retardation factor of the spray from an underwater burst (Section IV, Chapter 2).
f	Thermal partition of the total yield (Chapter 3 and Chapter 13).
f	Fraction of total weapon energy emitted as prompt gamma rays (Chapter 5).
f	Frequency of an electromagnetic signal in megahertz (Chapter 8).
f_h	Factor to correct the fireball height as a function of time when the maximum altitude to which the fireball rises is greater than 200 kilometers (Chapter 8).
f_o	Factor to correct the debris offset when the maximum fireball rise exceeds 200 kilometers (Chapter 8).
f_y	Yield strength of reinforcement in an underground concrete structure (Chapter 11).
f_c'	Strength of the concrete in an underground structure (Chapter 11).
h	Height of burst, except as noted below.
h	Maximum spray dome height from an underwater burst (Section IV, Chapter 2).
h	Planck's constant (6.625×10^{-27} erg-sec) (Chapter 4, Section V, Chapter 9).
h	Relative humidity (Section III, Chapter 9).
h	Height of a buried arch type structure (Section II, Chapter 11).
h	Aircraft flight altitude (Chapter 13).
h	Altitude along a reentry vehicle flight path (Section II, Chapter 16).

[redacted]

[redacted]

Symbol	*Designation*
h_b	Altitude of the base of the fireball tube once the fireball from a high altitude burst forms a tube along the geomagnetic field lines.(Chapter 8 – see Figure 8-16).
h_c	Height of the visible base surge cloud from an underwater explosion (Section IV, Chapter 2).
h_c	Reentry vehicle or defensive missile ablator thickness (Chapter 16).
h_{cv}	Convective heat loss for turbulent flow (Section IV, Chapter 9).
h_d	Altitude of the weapon debris (Chapter 8).
h_{di}	Same as h_d when there are more than one debris region (i = 1,2,3 for bursts above 120 kilometers) (Chapter 8).
h_{fb}	Altitude of the fireball (Chapter 8).
h_ℓ	Height of the apparent crater lip from an underwater burst (Section IV, Chapter 2).
h_m	Maximum altitude to which the fireball rises (Chapter 8).
h_{mi}	Maximum altitude to which the weapon debris rises when there are more than one debris region (i = 1,2,3 for bursts above 120 kilometers) (Chapter 8).
h_N	Normalizing factor to obtain fireball height at times before the fireball reaches its maximum altitude (Chapter 8).
h_o	Detonation altitude – used as the starting altitude to determine the location of the fireball at various times after burst (Chapter 8).
h_r	Distance that a fireball will rise above the detonation point (Chapter 8).
h_1, h_2	Altitudes of two points of interest in the determination of the mass integral of air between them (Chapters 4 and 5).
h'_{cv}	Convective heat loss for laminar flow (Section IV, Chapter 9).
k	Linear spring constant (Section III, Chapter 2).
k	Boltzmann constant (1.38×10^{-16} erg/°K) (Chapter 4).
k	Thermal conductivity (Section III, Chapter 9).
k	Factor for the calculation of the aerodynamic coefficient of vertical tails of aircraft (function of the vertical tail span, and the fuselage depth) (Chapter 13).

[redacted]

[redacted]

Symbol	*Designation*
m	Mass attached to a linear spring (Section III, Chapter 2).
m	Mass of a body into which energy has been deposited (Section V, Chapter 9).
m	Mean value of the intensity of motion used in the calculation of damage probabilities (Appendix C).
m_i	Median value of input motion used in the calculation of damage probabilities (Appendix C).
m_o	Rest mass of an electron (Chapter 4).
m_v	Median value of the vulnerability level of motion (Appendix C).
$\dot{m}$	Rate of mass removal from a missile ablator material (Chapter 16).
n	Number of explosive charges in a row crater (Section II, Chapter 2).
n	Period of an oscillating underwater bubble (Section IV, Chapter 2).
n	Preblast load factor on an aircraft (Chapter 13).
p_b	Pressure on the back face (face away from the burst) of an object exposed to an air blast wave (Section II, Chapter 9).
p_d	Peak value of stress applied to a buried structure (Section II, Chapter 11).
p_f	Pressure on the front face (face nearest the burst) of an object exposed to an air blast wave (Section II, Chapter 9).
p_f	Percentage of reinforcement in a reinforced concrete buried structure (Section II, Chapter 11).
p_H	Static radial soil pressure on a buried structure (Section II, Chapter 11).
p_h	Horizontal component of stress at a point below the surface in soil (Chapter 11).
p_i	Stress at the interface between two media through which a shock wave is traveling (Section III, Chapter 2).
p_m	Peak shock pressure in water (Section IV, Chapter 2).
p_r	Reflected stress at the interface between two media through which a shock wave is traveling (Section III, Chapter 2).
p_{so}	Peak side-on overpressure. Generally used to represent the overpressure at the surface of the earth in the calculation of air-induced ground shock (Section III, Chapter 2, and Section II, Chapter 11).

[redacted]

[redacted]

Symbol	*Designation*
$(p_{so})_a$	Component of overpressure at the surface that produces thrust in a buried arch (Section II, Chapter 11).
$(p_{so})_b$	Component of overpressure at the surface that produces flexure.
p_t	Transmitted stress at the interface between two media through which a shock wave is traveling (Section III, Chapter 2).
p_v	Vertical component of stress at a point below the surface in soil (Chapter 11).
q	Peak value of the dynamic pressure of the air blast wave, except as noted below.
q	Charge of an electron (1.6×10^{-19} coulombs) (Section VI, Chapter 9).
$q(h)$	Mass integral of air above a point at altitude "h" (Chapter 4).
$q(R)$	Mass integral of air between two points separated by a slant range "R" (Chapter 4).
q_{eq}	That dynamic pressure under nonideal surface conditions from which the dynamic pressure impulse would cause a particular level of damage for a particular yield and height of burst (Chapter 14).
q_u	Ultimate bearing strength of soil (Chapter 11).
q_y	Yield resistance of a buried structure (Chapter 11).
$\dot{q}_c$	Forced convection caused by friction forces at the boundary layer around a missile that produces aerodynamic heating during flight (Chapter 16).
$\dot{q}_R$	Heating rate of a missile during traversal through a fireball (Chapter 16).
	Radius of a high temperature black body source of electromagnetic radiation emission (Chapter 4).
r	Radius of a buried dome or arch (Chapter 11).
r	Radius of turn of a maneuvering aircraft (Chapter 13).
r_{ac}	Radius of the apparent crater from an underwater explosion (Section IV, Chapter 2).
r_q	Radius of gyration of an element of a buried structure (Section II, Chapter 11).
r_n	Parameter that relates the energy of the bubble from an underwater burst to the energy of the preceding (n-1) bubble (Section IV, Chapter 2).
r_{su}	Horizontal extent of the spray dome from an underwater burst (Section IV, Chapter 2).

[redacted]

[redacted]

Symbol	*Designation*
s	Space between charges in row of explosive charges emplaced to produce a row crater (Section II, Chapter 2).
s	Support condition for an element of a buried structure (Section II, Chapter 11, see Table 11-10).
t	Time after burst that the shock front of an air blast wave reaches a point of interest; also, the instantaneous value of time subsequent to shock front arrival (Chapter 2).
t	Time after burst (Chapter 5 and Chapter 8).
t	Aircraft skin thickness (Chapter 13).
t_a	Time of arrival of the blast wave at a point of intercept with an aircraft (Chapter 13).
t_{bky}	Time of breakaway, the time at which the shock front becomes detached from the fireball (Chapter 2 and Chapter 3).
t_c	Time of intersection of a reentry vehicle with a blast wave (see Figure 16-37) (Chapter 16).
t_{csa}	The time of case-shock arrival at the hydrodynamic shock front (Chapter 2).
t_d	Effective duration of the loading on a buried structure (Chapter 11).
t_d	Transistor switching delay time (Section VII, Chapter 9).
t_e	Thickness of the ejecta from a surface or near surface burst (Chapter 2).
t_E	Time of exit of a reentry vehicle from the blast shell (Chapter 16).
t_{EFB}	Time of exit of a reentry vehicle from the fireball (Chapter 16).
t_f	The fall time portion of the switching time of a transistor (Section VII, Chapter 9).
t_i	Effective duration of the air-induced ground shock (Section III, Chapter 2).
t_I	Time of intercept of a reentry vehicle by a blast wave (Chapter 16).
t_{max}	Time to final maximum on the fireball power-time curve.
t_{min}	Time to the principal minimum on the fireball power-time curve.
t_o	Time of detonation (used in determining the locus of escape of a reentry vehicle from the air blast – see Figure 16-37) (Chapter 16).

[redacted]

[redacted]

Symbol	*Designation*
t_r	Effective velocity pulse rise time for air-induced ground shock (Section III, Chapter 2).
t_r	Time for weapon debris to reach its maximum altitude (Chapter 8).
t_r	The storage time portion of a transistor switching time (Section VII, Chapter 9).
t_s	Time after burst for computation of underwater burst phenomena (Section IV, Chapter 2).
t_s	Charge storage time for an electronic device of interest (Section VII, Chapter 9).
t_{sf}	Shock formation time (Section I, Chapter 2).
t_{sr}	Reduced time after burst for computation of underwater burst phenomena (Section IV, Chapter 2).
t_{sr}	Radiation storage time for an electronic device of interest (Section VII, Chapter 9).
t_{toroid}	Time at which the fireball forms a toroid (Chapter 8).
t_x	Time for a reentry vehicle to travel from its location at burst time to intercept with the blast wave (see Figure 16-37) (Chapter 16).
$t_{1\ max}$	Time to reach the first (traditional first – see paragraph 3-11) maximum of the fireball power-time curve.
$t_{10\%}$	Time at which the blast intercept load on a reentry vehicle decays to ten percent of its maximum value (Chapter 16).
t_Δ	Effective duration of the pressure pulse of an air blast wave when it is represented as a simple triangular pulse (Section I, Chapter 2).
t_p^+	Duration of the positive phase of the overpressure of an air blast wave.
t_q^+	Duration of the positive phase of the dynamic pressure of an air blast wave.
t'	Time required for the fireball to reach its equilibrium radius (applies to bursts between 85 and 120 kilometers) (Chapter 8).
u	Particle (wind) velocity behind the shock front, except as noted below.
u	Maximum relative displacement of a simple linear oscillator (mass on a spring) (Section III, Chapter 2).
u	Normalized photon energy (a dimensionless quantity) (Chapter 4).
$\dot{u}$	Velocity of a simple linear oscillator (mass on a spring) (Section III, Chapter 2).

[redacted]

[redacted]

Symbol	*Designation*
$\dot{u}_{max}$	Maximum of $\dot{u}$.
v	Particle velocity in a particle in a soil medium that is transmitting a ground shock (Section III, Chapter 2; Section III, Chapter 11).
v	Velocity of a neutron (Chapter 5).
v_i	Radial velocity of a particle in a soil medium that is transmitting ground shock (Section III, Chapter 2).
v_s	Maximum velocity of a particle in a soil medium that is transmitting ground shock (Section III, Chapter 2).
v_x	Horizontal velocity of a particle in a soil medium that is transmitting ground shock (Section III, Chapter 2).
v_y	Vertical velocity of a particle in a soil medium that is transmitting ground shock (Section III, Chapter 2).
w	Width of the depletion layer between N and P sections of a semiconductor (Section VII, Chapter 9).
w	Component of aircraft velocity normal to the wing (Chapter 13).
w	A parameter used in characterizing the ionization caused by beta and gamma radiation from several high altitude bursts (Chapter 17).
x	Transient displacement induced by ground shock (used in the representation of ground shock induced motion by a simple oscillator) (Section III, Chapter 2).
x	Penetration distance of a beam of particles or electromagentic radiation into a material (Chapters 4 and 5).
x	Semithickness of the fireball once it has assumed a pancake shape (see Figure 8-16) (Chapter 8).
x	Spacing between members of a structure (Section III, Chapter 11).
x_s	Deflection of a system mounted in a buried structure when subjected to ground shock (Section III, Chapter 11).
$\dot{x}$	Velocity of the base of a simple oscillator used to represent ground shock induced motion (Section III, Chapter 2).
$\ddot{x}$	Acceleration of the base of a simple oscillator used to represent ground shock induced motion (Section III, Chapter 2).
y	Depth below the surface of the earth (Section III, Chapter 2).

[redacted]

[redacted]

Symbol	*Designation*
y	Coordinate of motion of the mass of a simple oscillator used to represent ground shock induced motion (Section III, Chapter 2).
$\dot{y}$	Velocity of the mass of a simple oscillator used to represent ground shock induced motion (Section III, Chapter 2).
$\ddot{y}$	Acceleration of the mass of a simple oscillator used to represent ground shock induced motion (Section III, Chapter 2).
z	Depth from the ground surface at which the radial load on a buried vertical cylinder is desired (Section II, Chapter 11).
Γ	Parameter used in the analysis of damage to buried structures. The parameter is defined by structural type and dimensions in Table 11-10.
Δ_d	Distance by which the weapon debris is offset from ground zero toward the nearest magnetic pole (Chapter 8).
Δ_β	Distance by which the beta particle absorption region is offset from ground zero (or from the conjugate ground zero, see Figure 8-53) toward the nearest magnetic pole (Chapter 8).
$\Delta\beta_i$ (i = 1,2,3)	Distances by which the beta particle absorption regions are offset from ground zero (or from the conjugate ground zero) when there are three debris regions (see Figure 8-18) (Chapter 8).
ΔE	Energy density deposited by X-rays within a given volume of air (Chapters 2 and 3).
ΔE	Change of internal energy per unit mass of an ideal gas when the gas is heated at constant volume (Appendix A).
Δh	Absolute value of the difference in burst altitude and target altitude (targets above the surface) (Chapter 3).
ΔL	Incremental lift on an aircraft resulting from the air blast wave (Chapter 13).
Δp	Peak overpressure of an air blast wave.
$\Delta p(t)$	Instantaneous value of the overpressure as a blast wave passes a point of interest.
Δp_{eq}	Equivalent overpressure under near-ideal surface conditions at which the dynamic pressure impulse for a particular yield and height of burst would cause a particular level of damage (Chapter 14).
Δp_r	Peak reflected overpressure.

[redacted]

[redacted]

Symbol	*Designation*
ΔR	Change in fireball radius at times later than seven minutes after burst (Chapter 8).
ΔT	Critical temperature rise of an aircraft skin for sure-safe or sure-kill conditions (Chapter 13).
Δt_{FB}	Traversal time of a missile through a fireball (Chapter 16).
Δt_{ILP}	Missile intercept time load constant (equals the time of intercept by a blast wave minus the time at which the blast load decreases to ten percent of the intercept value) (Chapter 16).
Δt_t	Total time for a missile to traverse through a blast wave shell (Chapter 16).
ΔZ_i	Distance of upward migration of an underwater bubble during the ith period (i = 1,2,3) (Section IV, Chapter 2).
$\Lambda_{c/2}$	Sweepback angle of the mid-chord line of an aircraft wing or horizontal tail (Chapter 13).
Λ_{LE}	Sweepback angle of the leading edge of an aircraft wing or horizontal tail (Chapter 13).
Φ	Angle between the direction of propagation of a shock wave and the line of steepest ascent or descent of a slope that the shock wave encounters (Chapter 2).
Φ	Particle, photon, or energy flux (Chapters 4 and 5).
Φ	Angular change in an aircraft's flight path between burst time and blast intercept time (Chapter 13).
Φ_s	X-ray energy flux at the source; the total power emitted per unit area of the source per unit time (Chapter 4).
$\Phi_{\gamma P}$	Prompt gamma output energy rate (Chapter 5).
Ψ	Energy density radiated by a black body between wavelengths λ and $\lambda + d\lambda$ (Planck spectrum) (Chapter 4).
Ω_{MR}	Angular velocity of the main rotor of a helicopter (Chapter 13).
α	Coefficient for determination of attenuation of ground shock with depth (see note on page 2-180 for description of differences in attenuation coefficients in Section III, Chapter 2 and Section II, Chapter 11) (Section III, Chapter 2).
α	Thermal diffusivity of a material (Section III, Chapter 9).

[redacted]

[redacted]

Symbol	*Designation*
α	Parameter used to determine the reciprocal of the ground shock depth attenuation coefficient (see Figure 11-29; not equal to depth attenuation of Chapter 2, see note on page 2-180) (Chapter 11).
α	Thermal absorptivity coefficient of an aircraft surface (Chapter 13).
α	Reentry vehicle angle-of-attack; the angle between the longitudinal axis of the vehicle and the relative wind vector (wind from either an air blast wave or normal atmospheric forces) (Chapter 16).
α_e	Coefficient of thermal expansion of a material (Section IV, Chapter 9).
β	Elevation angle of electromagnetic signal propagation (Chapter 8).
β	Reciprocal of the ground shock attenuation coefficient (not equivalent to $1/\alpha$ of Section III, Chapter 2; see note on page 2-180) (Section II, Chapter 11).
β	Radiative heat blocking function of the surface of a reentry vehicle (Chapter 16).
β	Circumferential angle on the structure of a reentry vehicle measured from the windward ray of intercept with a blast wave (Chapter 16).
β	Reentry vehicle ballistic coefficient (Chapter 16).
β	Standard deviation of the logarithm of a variate in a logarithmic normal distribution (Appendix C).
β_i	Standard deviation of the logarithm of the input function (Appendix C).
β_v	Standard deviation of the logarithm of the vulnerability function (Appendix C).
β_r	Rotational angle about the axis of a reentry vehicle (Chapter 16).
β_o	Gain of a transistor prior to irradiation (Section VII, Chapter 9).
$\beta_\varphi(t)$	Gain of a transistor as a function of time after irradiation (Section VII, Chapter 9).
$\beta_\varphi(\infty)$	Steady state value of the gain of a transistor that is reached after irradiation and annealing (Section VII, Chapter 9).
γ	Ratio of the specific heat of air at constant pressure to the specific heat of air at constant volume at moderate temperatures and pressures; for strong shocks, γ simply becomes a constant in the energy equation of an ideal gas (see paragraph A-2, Appendix A) (Section I, Chapter 2; Chapter 16; and Appendix A).
γ	Unit weight of a medium that is transmitting ground shock (Section III, Chapter 2).

[redacted]

[redacted]

Symbol	*Designation*
γ	Parameter used in determining the effective shock pulse duration on buried structures (Section III, Chapter 11).
γ_E	Terminal flight path angle of a reentry vehicle (Chapter 16).
γ'	Effective shock pulse duration on buried structures (Section III, Chapter 11).
δ	Underwater burst spray dome angle (see sketch in Problem 2-32) (Section IV, Chapter 2).
δ	Characteristic thermal thickness of a material. If a thick slab of material is exposed to a rectangular thermal pulse, the temperature at the surface would be about the same as would be produced by uniformly distributing the absorbed thermal energy in a slab of thickness δ, and the peak temperature rise at depth δ in the thick slab is about half as great as the peak temperature rise at the surface (Section III, Chapter 9).
δ	Parameter used in analysis of vulnerability of buried structures (defined in Table 11-10) (Section II, Chapter 11).
δ	Semivertex angle of a reentry vehicle (Chapter 16).
ϵ	Strain; the deformation resulting from stress measured by the ratio of the change to the total dimension in which the change occurred (Section III, Chapter 2; Section IV, Chapter 9; Chapter 16).
ϵ	Thermal efficiency; the fraction of energy absorbed by air that is reradiated (Chapter 3).
ϵ	Internal energy per unit volume (Section V, Chapter 9).
ϵ	Emissivity of a heated system (Section IV, Chapter 9).
η	Ratio of the time of arrival of the blast wave to the time to final thermal maximum (Section IV, Chapter 9).
η	Ratio of the density of a material at pressures above ambient to the density of the same material at ambient pressures (Section V, Chapter 9).
η	Parameter used in the calculation of blast intercept time envelopes for helicopters (Chapter 13).
θ	Effective slope angle for the interaction of a blast wave with a rising or falling slope (θ is equal to the actual slope angle, θ_s, if the direction of propagation of the blast wave is perpendicular to the foot of the slope) (Section I, Chapter 2).

[redacted]

[redacted]

Symbol	*Designation*
θ	Time constant of an underwater shock wave (Section IV, Chapter 2).
θ	Angle that the direction of propagation of a Compton scattered photon makes with direction of the original photon (Chapter 4).
θ	Angle of incidence of an electromagnetic signal ray path with an imaginary shell 65 kilometers above the surface of the earth (Chapter 8).
θ	Angle formed by two lines through the burst point – one line parallel to a reentry vehicle's flight path and the other through the reentry vehicle at burst time (see Figure 16-23) (Chapter 16).
θ_{cone}	Angle from the longitudinal axis of a cone shaped reentry vehicle to the edge of the vehicle (Chapter 16).
θ_d	Angle between a horizontal plane through the debris center and the geomagnetic field lines that pass through the debris (Chapter 8).
θ_i	Angle of incidence of a blast wave as it strikes a reflecting surface; the angle that the *shock front* (not the direction of propagation of the blast wave) makes with the surface (see footnote on page 2-38) (Section II, Chapter 2).
θ_s	Actual angle of a rising or falling slope that a blast wave encounters – measured perpendicular to the foot of the slope.
κ	Mass attenuation coefficient (Chapter 4 and 5).
λ	Photon wavelength (Chapter 4).
λ	Taper ratio of an aircraft wing, horizontal tail or vertical tail (length along the fuselage centerline subtended by the wing/tail tip divided by the length along the fuselage centerline subtended by the leading and trailing edges) (Chapter 13).
λ'	Wavelength of a scattered photon (Chapter 4).
μ	Linear attenuation coefficient; the probability of interaction per unit distance traveled by particulate or electromagnetic radiation, except as noted below.
μ	Viscosity of air (Section IV, Chapter 9).
μ_a	Linear absorption coefficient; the probability, per unit distance traveled, of an interaction in which energy is absorbed by the medium being traversed (in this manual the symbol is only used for photon (X-ray or gamma ray) interactions) ($\mu_a + \mu_s = \mu$).
μ_{ce}	Rayleigh scattering (coherent elastic scattering) linear attenuation coefficient (for photons $\mu_{ce} + \mu_{ie} = \mu_s$).

[redacted]

Symbol	*Designation*
μ_{ie}	Compton elastic (incoherent elastic scattering) linear attenuation coefficient (for photons $\mu_{ce} + \mu_{ie} = \mu_s$).
μ_{is}	Compton inelastic scattering linear attenuation coefficient (for photons $\mu_{is} + \mu_p = \mu_a$).
μ_p	Photoelectric linear attenuation coefficient (for photons $\mu_p + \mu_{is} = \mu_a$).
μ_s	Linear scattering coefficient; the probability of interaction, per unit distance traveled, that removes radiation from the direct beam (in this manual the symbol is only used for photon (X-ray or gamma ray) interactions) ($\mu_a + \mu_a = \mu$).
ν	Poisson's ratio (Section III, Chapter 2; Section II, Chapter 11).
ν	Photon frequency (Chapter 4; Section V, Chapter 9).
ν	Electron collision frequency (Chapter 8).
ξ	Shock strength ($\xi = \Delta p/P + 1$, where Δp is the peak overpressure and P is the absolute ambient pressure).
ρ	Mass density.
ρ_c	Mass density of reentry vehicle ablative cover materials (Chapter 16).
ρ_e	Density of electrons in a medium through which X-rays are penetrating (Chapter 4).
ρ_{GAS}	Local density within a fireball (Chapter 16).
ρ_m	Weight density of the material of the skin of an aircraft (Chapter 13).
ρ_o	Normal density of a material prior to absorption of energy (Section V, Chapter 9); otherwise, mass density of air at ambient sea level conditions.
ρ_s	Mass density of the shell of a reentry vehicle (Chapter 16) otherwise, mass density of air behind a shock front.
ρ_w	Density of water in which an underwater explosion takes place (Section IV, Chapter 2).
ρ_1	Density of shocked air after reflection from a solid barrier (Appendix A).
$\bar{\rho}$	Relative air density ($\bar{\rho} = \rho/\rho_o$, where ρ is the air density at the altitude of interest and ρ_o is the air density at sea level).
σ	Stefan-Boltzmann constant (Chapter 4; Section IV, Chapter 9).

[redacted]

Symbol	*Designation*
σ	Cross section for a given nuclear reaction (see Glossary for definition of cross section) (Chapters 4 and 5).
σ	Conductivity (σ_{air}, air conductivity; σ_g, ground conductivity) (Chapter 7).
σ	Stress; the force per unit area tending to produce deformation in a body (Section IV, Chapter 9; Section II, Chapter 11; Section II, Chapter 16).
σ	Standard deviation for damage probability calculations (Appendix C).
σ_A	Allowable stress on a reentry vehicle (Chapter 16).
σ_D	Stress developed on a reentry vehicle for prescribed flight conditions and loads (Chapter 16).
σ_{yc}	Yield stress of a reentry vehicle ablative cover material (Chapter 16).
σ_{ys}	Yield stress of a reentry vehicle shell (Chapter 16).
$\tau(h)$	Effective optical height of the burst height for specifying thermal transmittance (Chapter 3).
τ	Emission time of prompt gamma rays (Section I, Chapter 5).
τ	Semiconductor minority-carrier lifetime (Chapter 6).
τ_{eff}	Effective semiconductor lifetime (Section VII, Chapter 9).
τ_{FB}	Scaled time of fireball traversal by a reentry vehicle (Chapter 16).
τ_I	Scaled time of intercept of a reentry vehicle by a blast wave (Chapter 16).
τ_{ILP}	Scaled duration of the intercept load of a blast wave on a reentry vehicle (Chapter 16).
τ_o	Pre-irradiation semiconductor minority-carrier lifetime (Chapter 6; Section VII, Chapter 9).
τ_o	Characteristic thermal response time that relates the response of a material to the thermal pulse (Section III, Chapter 9).
τ_{surf}	Semiconductor surface lifetime (Section VII, Chapter 9).
τ_t	Scaled time of blast traversal by a reentry vehicle (Chapter 16).
τ_φ	Semiconductor minority-carrier lifetime at fluence φ (Chapter 6; Section VII, Chapter 9).

[redacted]

[redacted]

Symbol	*Designation*
φ	Total energy, particle, or photon fluence at a point of interest, except as noted below.
φ	Angle formed by the geomagnetic field line and a vertical line through the main debris location once a tube fireball has been formed from bursts between 85 and 120 kilometers. It is the magnetic dip angle at the location of the debris (see Figure 8-16) (Chapter 8).
φ	Angle of internal friction for nongranular soils (Section II, Chapter 11).
φ	Angle between a line through the burst point and a reentry vehicle at burst time and a line between the burst point and the reentry vehicle at blast intercept time (see Figure 16-23) (Chapter 16).
φ_{dir}	Energy, particle, or photon fluence that arrives in a direct line from the source to a point of interest, i.e., the total fluence minus the scattered fluence.
φ_o	Incident X-ray fluence that arrives normal (perpendicular) to a surface of interest (Section V, Chapter 9).
ψ	Ratio of impedances of two media where a ground shock wave is crossing the interface between the media (Section III, Chapter 2).
ψ	Parameter used in analysis of damage to underground structures. ψ depends on structural type, dimensions and seismic velocity. Relations are given in Table 11-10 (Section II, Chapter 11).
ψ	Convective heat blocking function that helps determine the fraction of free field heating rate that exists at an ablator surface (Chapter 16).
$\sim$	Circular frequency of a simple oscillator (Section III, Chapter 2).
ω	Electromagnetic wave frequency in radians per second (Chapter 8).

[redacted]